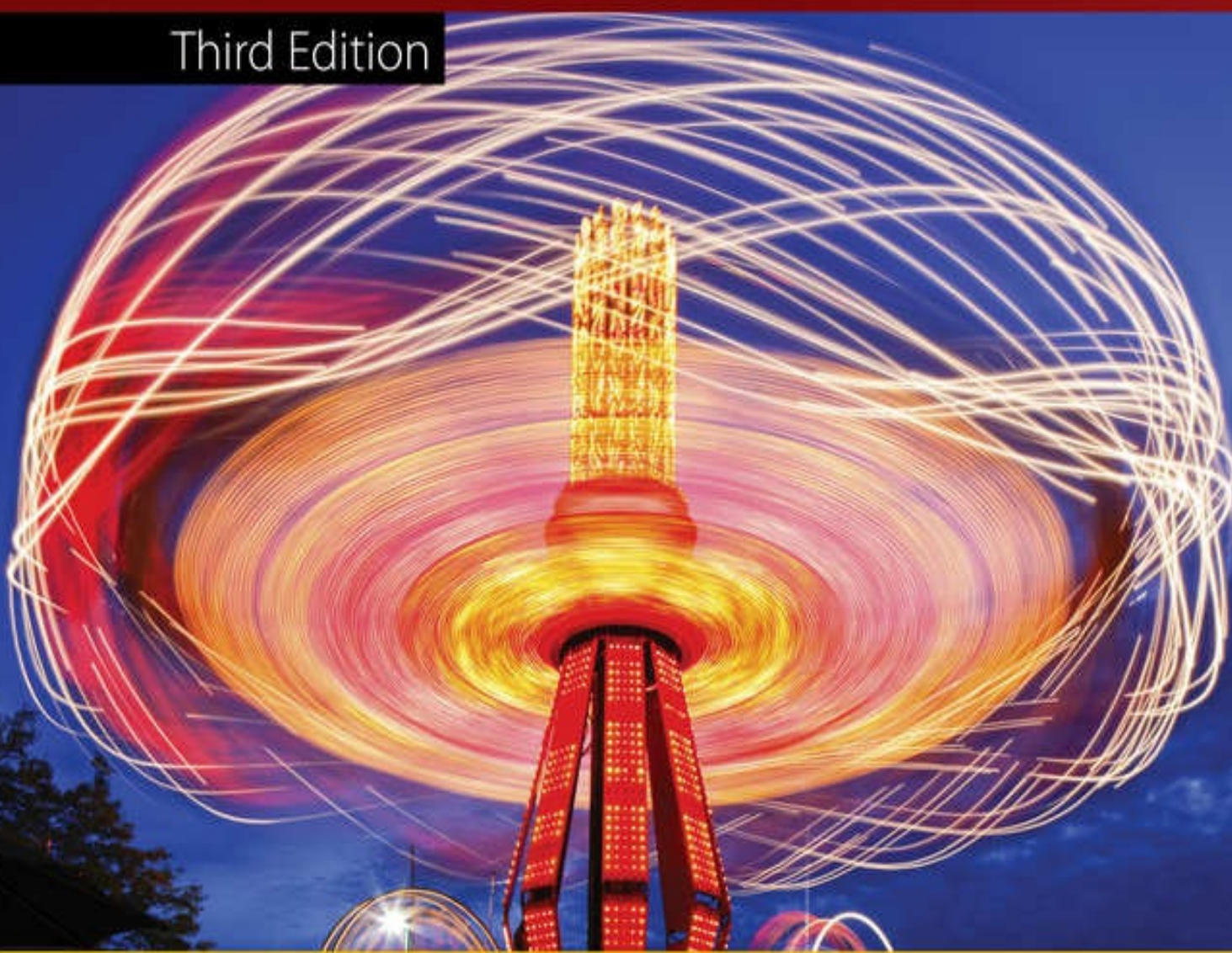


Kinematics, Dynamics, and Design of Machinery

Third Edition



Kenneth J. Waldron • Gary L. Kinzel • Sunil K. Agrawal



WILEY

CONTENTS

[Cover](#)

[About the Companion Website](#)

[Title Page](#)

[Copyright](#)

[Preface](#)

[Chapter 1: Introduction](#)

[1.1 Historical Perspective](#)

[1.2 Kinematics](#)

[1.3 Design: Analysis and Synthesis](#)

[1.4 Mechanisms](#)

[1.5 Planar Linkages](#)

[1.6 Visualization](#)

[1.7 Constraint Analysis](#)

[1.8 Constraint Analysis of Spatial Linkages](#)

[1.9 Idle Degrees of Freedom](#)

[1.10 Overconstrained Linkages](#)

[1.11 Uses of the Mobility Criterion](#)

[1.12 Inversion](#)

[1.13 Reference Frames](#)

[1.14 Motion Limits](#)

[1.15 Continuously Rotatable Joints](#)

[1.16 Coupler-Driven Linkages](#)

[1.17 Motion Limits for Slider-Crank Mechanisms](#)

[1.18 Interference](#)

[1.19 Practical Design Considerations](#)

[References](#)

[Problems](#)

[Chapter 2: Techniques in Geometric Constraint Programming](#)

[2.1 Introduction](#)

[2.2 Geometric Constraint Programming](#)

[2.3 Constraints and Program Structure](#)

[2.4 Initial Setup for a GCP Session](#)

[2.5 Drawing a Basic Linkage Using GCP](#)

[2.6 Troubleshooting Graphical Programs Developed Using GCP](#)

[References](#)

[Problems](#)

[Appendix 2A Drawing Slider Lines, Pin Bushings, and Ground Pivots](#)

[Appendix 2B Useful Constructions When Equation Constraints are Not Available](#)

[Chapter 3: Planar Linkage Design](#)

[3.1 Introduction](#)

[3.2 Two-Position Double-Rocker Design](#)

[3.3 Synthesis of Crank-Rocker Linkages for Specified Rocker Amplitude](#)

[3.4 Motion Generation](#)

[3.5 Path Synthesis](#)

[References](#)

[Problems](#)

[Chapter 4: Graphical Position, Velocity, and Acceleration Analysis for Mechanisms with Revolute Joints or Fixed Slides](#)

[4.1 Introduction](#)

[4.2 Graphical Position Analysis](#)

[4.3 Planar Velocity Polygons](#)

[4.4 Graphical Acceleration Analysis](#)

[4.5 Graphical Analysis of a Four-Bar Mechanism](#)

[4.6 Graphical Analysis of a Slider-Crank Mechanism](#)

[4.7 Velocity Image Theorem](#)

[4.8 Acceleration Image Theorem](#)

[4.9 Solution by Geometric Constraint Programming](#)

[References](#)

[Problems](#)

[Chapter 5: Linkages with Rolling and Sliding Contacts, and Joints on Moving Sliders](#)

[5.1 Introduction](#)

[5.2 Reference Frames](#)

[5.3 General Velocity and Acceleration Equations](#)

[5.4 Special Cases for the Velocity and Acceleration Equations](#)

[5.5 Linkages with Rotating Sliding Joints](#)

[5.6 Rolling Contact](#)

[5.7 Cam Contact](#)

[5.8 General Coincident Points](#)

[5.9 Solution by Geometric Constraint Programming](#)

[Problems](#)

[Chapter 6: Instant Centers of Velocity](#)

[6.1 Introduction](#)

[6.2 Definition](#)

[6.3 Existence Proof](#)

[6.4 Location of an Instant Center from the Directions of Two Velocities](#)

[6.5 Instant Center at a Revolute Joint](#)

[6.6 Instant Center of a Curved Slider](#)

[6.7 Instant Center of a Prismatic Joint](#)

[6.8 Instant Center of a Rolling Contact Pair](#)

[6.9 Instant Center of a General Cam-Pair Contact](#)

[6.10 Centrodes](#)

[6.11 The Kennedy-Aronhold Theorem](#)

[6.12 Circle Diagram as a Strategy for Finding Instant Centers](#)

[6.13 Using Instant Centers to Find Velocities: The Rotating-Radius Method](#)

[6.14 Finding Instant Centers Using Geometric Constraint Programming](#)

[References](#)

[Problems](#)

[Chapter 7: Computational Analysis of Linkages](#)

[7.1 Introduction](#)

[7.2 Position, Velocity, and Acceleration Representations](#)

[7.3 Analytical Closure Equations for Four-Bar Linkages](#)

[7.4 Analytical Equations for a Rigid Body After the Kinematic Properties of Two Points are Known](#)

[7.5 Analytical Equations for Slider-Crank Mechanisms](#)

[7.6 Other Four-Bar Mechanisms with Revolute and Prismatic Joints](#)

[7.7 Closure or Loop Equation Approach for Compound Mechanisms](#)

[7.8 Closure Equations for Mechanisms with Higher Pairs](#)

[7.9 Notational Differences: Vectors and Complex Numbers](#)

[Problems](#)

[Chapter 8: Special Mechanisms](#)

[8.1 Special Planar Mechanisms](#)

[8.2 Spherical Mechanisms](#)

[8.3 Constant-Velocity Couplings](#)

[8.4 Automotive Steering and Suspension Mechanisms](#)

[8.5 Indexing Mechanisms](#)

[References](#)

[Problems](#)

[Chapter 9: Computational Analysis of Spatial Linkages](#)

[9.1 Spatial Mechanisms](#)

[9.2 Robotic Mechanisms](#)

[9.3 Direct Position Kinematics of Serial Chains](#)

[9.4 Inverse Position Kinematics](#)

[9.5 Rate Kinematics](#)

[9.6 Closed-Loop Linkages](#)

[9.7 Lower-Pair Joints](#)

[9.8 Motion Platforms](#)

[References](#)

[Problems](#)

[Chapter 10: Profile Cam Design](#)

[10.1 Introduction](#)

[10.2 Cam-Follower Systems](#)

[10.3 Synthesis of Motion Programs](#)

[10.4 Analysis of Different Types of Follower-Displacement Functions](#)

[10.5 Determining the Cam Profile](#)

[References](#)

[Problems](#)

[Chapter 11: Spur Gears](#)

[11.1 Introduction](#)

[11.2 Spur Gears](#)

[11.3 Condition for Constant-Velocity Ratio](#)

[11.4 Involutes](#)

[11.5 Gear Terminology and Standards](#)

[11.6 Contact Ratio](#)

[11.7 Involutometry](#)

[11.8 Internal Gears](#)

[11.9 Gear Manufacturing](#)

[11.10 Interference and Undercutting](#)

[11.11 Nonstandard Gearing](#)

[11.12 Cartesian Coordinates of an Involute Tooth Generated with a Rack](#)

[References](#)

[Problems](#)

[Chapter 12: Helical, Bevel, and Worm Gears](#)

[12.1 Helical Gears](#)

[12.2 Worm Gears](#)

[12.3 Involute Bevel Gears](#)

[References](#)

[Problems](#)

[Chapter 13: Gear Trains](#)

[13.1 General Gear Trains](#)

[13.2 Direction of Rotation](#)

[13.3 Simple Gear Trains](#)

[13.4 Compound Gear Trains](#)

[13.5 Planetary Gear Trains](#)

[13.6 Harmonic Drive Speed Reducers](#)

[References](#)

[Problems](#)

[Chapter 14: Static Force Analysis of Mechanisms](#)

[14.1 Introduction](#)

[14.2 Forces, Moments, and Couples](#)

[14.3 Static Equilibrium](#)

[14.4 Free-Body Diagrams](#)

[14.5 Solution of Static Equilibrium Problems](#)

[14.6 Transmission Angle in a Four-Bar Linkage](#)

[14.7 Friction Considerations](#)

[14.8 In-Plane and Out-of-Plane Force Systems](#)

[14.9 Conservation of Energy and Power](#)

[14.10 Virtual Work](#)

[14.11 Gear Loads](#)

[Problems](#)

[Chapter 15: Dynamic Force Analysis of Mechanisms](#)

[15.1 Introduction](#)

[15.2 Problems Solvable Using Particle Kinetics](#)

[15.3 Dynamic Equilibrium of Systems of Rigid Bodies](#)

[15.4 Flywheels](#)

[Problems](#)

[Chapter 16: Static and Dynamic Balancing](#)

[16.1 Introduction](#)

[16.2 Single-Plane \(Static\) Balancing](#)

[16.3 Multi-Plane \(Dynamic\) Balancing](#)

[16.4 Balancing Reciprocating Masses](#)

[16.5 Expressions for Inertial Forces](#)

[16.6 Balancing Multi-Cylinder Machines](#)

[16.7 Static Balancing of Mechanisms](#)

[16.8 Reactionless Mechanisms](#)

[References](#)

[Problems](#)

[Chapter 17: Integration of Computer Controlled Actuators](#)

[17.1 Introduction](#)

[17.2 Computer Control of the Linkage Motion](#)

[17.3 The Basics of Feedback Control](#)

[17.4 Actuator Selection and Types](#)

[17.5 Hands-On Machine-Design Laboratory](#)

[References](#)

[Problems](#)

[Index](#)

[End User License Agreement](#)

List of Tables

[Table 1.1](#)

[Table 1.2](#)

[Table 1.3](#)

[Table 1.4](#)

[Table 2.1](#)

[Table 2.2](#)

[Table 3.1](#)

[Table 7.1](#)

[Table 7.2](#)

[Table 7.3](#)

[Table 7.4](#)

[Table 7.5](#)

[Table 8.1](#)

[Table 9.1](#)

[Table 9.2](#)

[Table 9.3](#)

[Table 9.4](#)

[Table 10.1](#)

[Table 10.2](#)

[Table 10.3](#)

[Table 10.4](#)

[Table 10.5](#)

[Table 10.6](#)

[Table 10.7](#)

[Table 10.8](#)

[Table 10.9](#)

[Table 10.10](#)

[Table 10.11](#)

[Table 10.12](#)

[Table 11.1](#)

[Table 11.2](#)

[Table 11.3](#)

[Table 11.4](#)

[Table 12.1](#)

[Table 12.2](#)

[Table 12.3](#)

[Table 12.4](#)

[Table 12.5](#)

[Table 13.1](#)

[Table 13.2](#)

[Table 13.3](#)

[Table 16.1](#)

List of Illustrations

[Figure 1.1](#)

[Figure 1.2](#)

[Figure 1.3](#)

[Figure 1.4](#)

[Figure 1.5](#)

[Figure 1.6](#)

[Figure 1.7](#)

[Figure 1.8](#)

[Figure 1.9](#)

[Figure 1.10](#)

[Figure 1.11](#)

[Figure 1.12](#)

[Figure 1.13](#)

[Figure 1.14](#)

[Figure 1.15](#)

[Figure 1.16](#)

[Figure 1.17](#)

[Figure 1.18](#)

[Figure 1.19](#)

[Figure 1.20](#)

[Figure 1.21](#)

[Figure 1.22](#)

[Figure 1.23](#)

[Figure 1.24](#)

[Figure 1.25](#)

[Figure 1.26](#)

[Figure 1.27](#)

[Figure 1.28](#)

[Figure 1.29](#)

[Figure 1.30](#)

[Figure 1.31](#)

[Figure 1.32](#)

[Figure 1.33](#)

[Figure 1.34](#)

[Figure 1.35](#)

[Figure 1.36](#)

[Figure 1.37](#)

[Figure 1.38](#)

[Figure 1.39](#)

[Figure 1.40](#)

[Figure 1.41](#)

[Figure 1.42](#)

[Figure 1.43](#)

[Figure 1.44](#)

[Figure 1.45](#)

[Figure 1.46](#)

[Figure 1.47](#)

[Figure 1.48](#)

[Figure 1.49](#)

[Figure 1.50](#)

[Figure 1.51](#)

[Figure 1.52](#)

[Figure 1.53](#)

[Figure 1.54](#)

[Figure 1.55](#)

[Figure 1.56](#)

[Figure 1.57](#)

[Figure 1.58](#)

[Figure 1.59](#)

[Figure P1.3](#)

[Figure P1.6](#)

[Figure P1.7](#)

[Figure P1.8](#)

[Figure P1.9](#)

[Figure P1.10](#)

[Figure P1.13](#)

[Figure P1.14](#)

[Figure P1.15](#)

[Figure P1.16](#)

[Figure P1.17](#)

[Figure P1.18](#)

[Figure P1.19](#)

[Figure P1.20](#)

[Figure P1.21](#)

[Figure P1.22](#)

[Figure P1.23](#)

[Figure P1.24](#)

[Figure P1.25](#)

[Figure P1.26](#)

[Figure P1.27](#)

[Figure P1.28](#)

[Figure P1.29](#)

[Figure P1.30](#)

[Figure P1.31](#)

[Figure P1.32](#)

[Figure P1.33](#)

[Figure P1.34](#)

[Figure P1.35](#)

[Figure P1.36](#)

[Figure P1.39](#)

[Figure P1.42](#)

[Figure P1.45](#)

[Figure 2.1](#)

[Figure 2.2](#)

[Figure 2.3](#)

[Figure 2.4](#)

[Figure 2.5](#)

[Figure 2.6](#)

[Figure 2.7](#)

[Figure 2.8](#)

[Figure 2.9](#)

[Figure 2.10](#)

[Figure 2.11](#)

[Figure 2.12](#)

[Figure 2.13](#)

[Figure 2.14](#)

[Figure 2.15](#)

[Figure 2.16](#)

[Figure 2.17](#)

[Figure 2.18](#)

[Figure P2.1](#)

[Figure P2.2](#)

[Figure P2.5](#)

[Figure P2.6](#)

[Figure P2.7](#)

[Figure P2.8](#)

[Figure P2.9](#)

[Figure P2.10](#)

[Figure P2.11](#)

[Figure P2.12](#)

[Figure 2A.1](#)

[Figure 2A.2](#)

[Figure 2A.3](#)

[Figure 2A.4](#)

[Figure 2A.5](#)

[Figure 2A.6](#)

[Figure 2B.1](#)

[Figure 2B.2](#)

[Figure 2B.3](#)

[Figure 2B.4](#)

[Figure 2B.5](#)

[Figure 2B.6](#)

[Figure 3.1](#)

[Figure 3.2](#)

[Figure 3.3](#)

[Figure 3.4](#)

[Figure 3.5](#)

[Figure 3.6](#)

[Figure 3.7](#)

[Figure 3.8](#)

[Figure 3.9](#)

[Figure 3.10](#)

[Figure 3.11](#)

[Figure 3.12](#)

[Figure 3.13](#)

[Figure 3.14](#)

[Figure 3.15](#)

[Figure 3.16](#)

[Figure 3.17](#)

[Figure 3.18](#)

[Figure 3.19](#)

[Figure 3.20](#)

[Figure 3.21](#)

[Figure 3.22](#)

[Figure 3.23](#)

[Figure 3.24](#)

[Figure 3.25](#)

[Figure 3.26](#)

[Figure 3.27](#)

[Figure 3.28](#)

[Figure 3.29](#)

[Figure 3.30](#)

[Figure 3.31](#)

[Figure 3.32](#)

[Figure 3.33](#)

[Figure 3.34](#)

[Figure 3.35](#)

[Figure 3.36](#)

[Figure 3.37](#)

[Figure 3.38](#)

[Figure 3.39](#)

[Figure 3.40](#)

[Figure 3.41](#)

[Figure 3.42](#)

[Figure 3.43](#)

[Figure 3.44](#)

[Figure 3.45](#)

[Figure 3.46](#)

[Figure 3.47](#)

[Figure 3.48](#)

[Figure 3.49](#)

[Figure 3.50](#)

[Figure 3.51](#)

[Figure 3.52](#)

[Figure 3.53](#)

[Figure 3.54](#)

[Figure 3.55](#)

[Figure 3.56](#)

[Figure 3.57](#)

[Figure 3.58](#)

[Figure 3.59](#)

[Figure 3.60](#)

[Figure 3.61](#)

[Figure 3.62](#)

[Figure 3.63](#)

[Figure 3.64](#)

[Figure 3.65](#)

[Figure 3.66](#)

[Figure 3.67](#)

[Figure 3.68](#)

[Figure 3.69](#)

[Figure 3.70](#)

[Figure 3.71](#)

[Figure 3.72](#)

[Figure 3.73](#)

[Figure 3.74](#)

[Figure 3.75](#)

[Figure 3.76](#)

[Figure 3.77](#)

[Figure 3.78](#)

[Figure 3.79](#)

[Figure 3.80](#)

[Figure 3.81](#)

[Figure 3.82](#)

[Figure P3.1](#)

[Figure P3.2](#)

[Figure P3.3](#)

[Figure P3.4](#)

[Figure P3.5](#)

[Figure P3.11](#)

[Figure P3.12](#)

[Figure P3.13](#)

[Figure P3.14](#)

[Figure P3.15](#)

[Figure P3.16](#)

[Figure P3.17](#)

[Figure P3.18](#)

[Figure P3.19](#)

[Figure P3.20](#)

[Figure P3.21](#)

[Figure P3.22](#)

[Figure P3.23](#)

[Figure P3.24](#)

[Figure P3.25](#)

[Figure P3.26](#)

[Figure P3.45](#)

[Figure P3.50](#)

[Figure P3.51](#)

[Figure P3.52](#)

[Figure P3.53](#)

[Figure P3.54](#)

[Figure P3.55](#)

[Figure P3.72](#)

[Figure P3.73](#)

[Figure P3.74](#)

[Figure P3.75](#)

[Figure P3.76](#)

[Figure P3.85](#)

[Figure P3.87](#)

[Figure P3.89](#)

[Figure P3.91](#)

[Figure P3.119](#)

[Figure P3.120](#)

[Figure 4.1](#)

[Figure 4.2](#)

[Figure 4.3](#)

[Figure 4.4](#)

[Figure 4.5](#)

[Figure 4.6](#)

[Figure 4.7](#)

[Figure 4.8](#)

[Figure 4.9](#)

[Figure 4.10](#)

[Figure 4.11](#)

[Figure 4.12](#)

[Figure 4.13](#)

[Figure 4.14](#)

[Figure 4.15](#)

[Figure 4.16](#)

[Figure 4.17](#)

[Figure 4.18](#)

[Figure 4.19](#)

[Figure 4.20](#)

[Figure 4.21](#)

[Figure 4.22](#)

[Figure 4.23](#)

[Figure 4.24](#)

[Figure 4.25](#)

[Figure 4.26](#)

[Figure P4.1](#)

[Figure P4.2](#)

[Figure P4.3](#)

[Figure P4.4](#)

[Figure P4.5](#)

[Figure P4.6](#)

[Figure P4.7](#)

[Figure P4.8](#)

[Figure P4.9](#)

[Figure P4.10](#)

[Figure P4.11](#)

[Figure P4.13](#)

[Figure P4.14](#)

[Figure P4.15](#)

[Figure P4.16](#)

[Figure P4.17](#)

[Figure P4.18](#)

[Figure P4.19](#)

[Figure P4.20](#)

[Figure P4.21](#)

[Figure P4.22](#)

[Figure P4.23](#)

[Figure P4.24](#)

[Figure P4.25](#)

[Figure P4.26](#)

[Figure P4.27](#)

[Figure P4.28](#)

[Figure P4.29](#)

[Figure P4.30](#)

[Figure P4.31](#)

[Figure P4.32](#)

[Figure P4.33](#)

[Figure P4.34](#)

[Figure P4.35](#)

[Figure P4.36](#)

[Figure P4.38](#)

[Figure P4.39](#)

[Figure P4.40](#)

[Figure P4.41](#)

[Figure P4.42](#)

[Figure P4.43](#)

[Figure P4.44](#)

[Figure P4.45](#)

[Figure P4.46](#)

[Figure P4.47](#)

[Figure 5.1](#)

[Figure 5.2](#)

[Figure 5.3](#)

[Figure 5.4](#)

[Figure 5.5](#)

[Figure 5.6](#)

[Figure 5.7](#)

[Figure 5.8](#)

[Figure 5.9](#)

[Figure 5.10](#)

[Figure 5.11](#)

[Figure 5.12](#)

[Figure 5.13](#)

[Figure 5.14](#)

[Figure 5.15](#)

[Figure 5.16](#)

[Figure 5.17](#)

[Figure 5.18](#)

[Figure 5.19](#)

[Figure 5.20](#)

[Figure 5.21](#)

[Figure 5.22](#)

[Figure 5.23](#)

[Figure 5.24](#)

[Figure 5.25](#)

[Figure 5.26](#)

[Figure 5.27](#)

[Figure 5.28](#)

[Figure 5.29](#)

[Figure 5.30](#)

[Figure 5.31](#)

[Figure 5.32](#)

[Figure 5.33](#)

[Figure 5.34](#)

[Figure 5.35](#)

[Figure 5.36](#)

[Figure 5.37](#)

[Figure 5.38](#)

[Figure 5.39](#)

[Figure P5.1](#)

[Figure P5.2](#)

[Figure P5.3](#)

[Figure P5.4](#)

[Figure P5.5](#)

[Figure P5.6](#)

[Figure P5.7](#)

[Figure P5.8](#)

[Figure P5.9](#)

[Figure P5.10](#)

[Figure P5.11](#)

[Figure P5.12](#)

[Figure P5.13](#)

[Figure P5.15](#)

[Figure P5.16](#)

[Figure P5.17](#)

[Figure P5.18](#)

[Figure P5.19](#)

[Figure P5.20](#)

[Figure P5.21](#)

[Figure P5.22](#)

[Figure P5.23](#)

[Figure P5.24](#)

[Figure P5.25](#)

[Figure P5.26](#)

[Figure P5.27](#)

[Figure P5.28](#)

[Figure P5.29](#)

[Figure P5.30](#)

[Figure P5.31](#)

[Figure P5.32](#)

[Figure P5.33](#)

[Figure P5.34](#)

[Figure P5.35](#)

[Figure P5.36](#)

[Figure P5.37](#)

[Figure P5.38](#)

[Figure P5.39](#)

[Figure P5.40](#)

[Figure P5.41](#)

[Figure P5.42](#)

[Figure P5.43](#)

[Figure P5.44](#)

[Figure P5.45](#)

[Figure P5.46](#)

[Figure P5.47](#)

[Figure 6.1](#)

[Figure 6.2](#)

[Figure 6.3](#)

[Figure 6.4](#)

[Figure 6.5](#)

[Figure 6.6](#)

[Figure 6.7](#)

[Figure 6.8](#)

[Figure 6.9](#)

[Figure 6.10](#)

[Figure 6.11](#)

[Figure 6.12](#)

[Figure 6.13](#)

[Figure 6.14](#)

[Figure 6.15](#)

[Figure 6.16](#)

[Figure 6.17](#)

[Figure 6.18](#)

[Figure 6.19](#)

[Figure 6.20](#)

[Figure 6.21](#)

[Figure 6.22](#)

[Figure 6.23](#)

[Figure 6.24](#)

[Figure 6.25](#)

[Figure 6.26](#)

[Figure 6.27](#)

[Figure 6.28](#)

[Figure 6.29](#)

[Figure 6.30](#)

[Figure 6.31](#)

[Figure 6.32](#)

[Figure 6.33](#)

[Figure 6.34](#)

[Figure 6.35](#)

[Figure 6.36](#)

[Figure 6.37](#)

[Figure 6.38](#)

[Figure P6.1](#)

[Figure P6.2](#)

[Figure P6.3](#)

[Figure P6.4](#)

[Figure P6.5](#)

[Figure P6.6](#)

[Figure P6.7](#)

[Figure P6.8](#)

[Figure P6.9](#)

[Figure P6.10](#)

[Figure P6.11](#)

[Figure P6.12](#)

[Figure P6.13](#)

[Figure P6.14](#)

[Figure P6.15](#)

[Figure P6.16](#)

[Figure P6.17](#)

[Figure P6.18](#)

[Figure P6.19](#)

[Figure P6.20](#)

[Figure P6.21](#)

[Figure P6.22](#)

[Figure P6.23](#)

[Figure P6.24](#)

[Figure P6.25](#)

[Figure P6.26](#)

[Figure P6.27](#)

[Figure P6.28](#)

[Figure P6.29](#)

[Figure P6.30](#)

[Figure P6.31](#)

[Figure P6.32](#)

[Figure P6.33](#)

[Figure 7.1](#)

[Figure 7.2](#)

[Figure 7.3](#)

[Figure 7.4](#)

[Figure 7.5](#)

[Figure 7.6](#)

[Figure 7.7](#)

[Figure 7.8](#)

[Figure 7.9](#)

[Figure 7.10](#)

[Figure 7.11](#)

[Figure 7.12](#)

[Figure 7.13](#)

[Figure 7.14](#)

[Figure 7.15](#)

[Figure 7.16](#)

[Figure 7.17](#)

[Figure 7.18](#)

[Figure 7.19](#)

[Figure 7.20](#)

[Figure 7.21](#)

[Figure 7.22](#)

[Figure 7.23](#)

[Figure 7.24](#)

[Figure 7.25](#)

[Figure 7.26](#)

[Figure 7.27](#)

[Figure 7.28](#)

[Figure 7.29](#)

[Figure 7.30](#)

[Figure 7.31](#)

[Figure 7.32](#)

[Figure 7.33](#)

[Figure 7.34](#)

[Figure 7.35](#)

[Figure 7.36](#)

[Figure 7.37](#)

[Figure 7.38](#)

[Figure 7.39](#)

[Figure 7.40](#)

[Figure 7.41](#)

[Figure P7.1](#)

[Figure P7.3](#)

[Figure P7.5](#)

[Figure P7.7](#)

[Figure P7.8](#)

[Figure P7.9](#)

[Figure P7.11](#)

[Figure P7.12](#)

[Figure P7.13](#)

[Figure P7.14](#)

[Figure P7.15](#)

[Figure P7.16](#)

[Figure P7.17](#)

[Figure P7.18](#)

[Figure P7.19](#)

[Figure P7.20](#)

[Figure P7.21](#)

[Figure P7.22](#)

[Figure P7.23](#)

[Figure P7.24](#)

[Figure P7.25](#)

[Figure P7.26](#)

[Figure 8.1](#)

[Figure 8.2](#)

[Figure 8.3](#)

[Figure 8.4](#)

[Figure 8.5](#)

[Figure 8.6](#)

[Figure 8.7](#)

[Figure 8.8](#)

[Figure 8.9](#)

[Figure 8.10](#)

[Figure 8.11](#)

[Figure 8.12](#)

[Figure 8.13](#)

[Figure 8.14](#)

[Figure 8.15](#)

[Figure 8.16](#)

[Figure 8.17](#)

[Figure 8.18](#)

[Figure 8.19](#)

[Figure 8.20](#)

[Figure 8.21](#)

[Figure 8.22](#)

[Figure 8.23](#)

[Figure 8.24](#)

[Figure 8.25](#)

[Figure 8.26](#)

[Figure 8.27](#)

[Figure 8.28](#)

[Figure 8.29](#)

[Figure 8.31](#)

[Figure 8.30](#)

[Figure 8.32](#)

[Figure 8.33](#)

[Figure 8.34](#)

[Figure 8.35](#)

[Figure 8.36](#)

[Figure P8.1](#)

[Figure P8.3](#)

[Figure P8.4](#)

[Figure P8.5](#)

[Figure P8.7](#)

[Figure 9.1](#)

[Figure 9.2](#)

[Figure 9.3](#)

[Figure 9.4](#)

[Figure 9.5](#)

[Figure 9.6](#)

[Figure 9.7](#)

[Figure 9.8](#)

[Figure 9.9](#)

[Figure 9.10](#)

[Figure 9.11](#)

[Figure 9.12](#)

[Figure 9.13](#)

[Figure 9.14](#)

[Figure 9.15](#)

[Figure 9.16](#)

[Figure 9.17](#)

[Figure 9.18](#)

[Figure 9.19](#)

[Figure P9.1](#)

[Figure P9.2](#)

[Figure P9.3](#)

[Figure P9.4](#)

[Figure P9.5](#)

[Figure P9.6](#)

[Figure P9.8](#)

[Figure P9.10](#)

[Figure P9.11](#)

[Figure P9.14](#)

[Figure P9.15](#)

[Figure P9.16](#)

[Figure P9.17](#)

[Figure P9.18](#)

[Figure P9.19](#)

[Figure P9.20](#)

[Figure P9.21](#)

[Figure 10.1](#)

[Figure 10.2](#)

[Figure 10.3](#)

[Figure 10.4](#)

[Figure 10.5](#)

[Figure 10.6](#)

[Figure 10.7](#)

[Figure 10.8](#)

[Figure 10.9](#)

[Figure 10.10](#)

[Figure 10.11](#)

[Figure 10.12](#)

[Figure 10.13](#)

[Figure 10.14](#)

[Figure 10.15](#)

[Figure 10.16](#)

[Figure 10.17](#)

[Figure 10.18](#)

[Figure 10.19](#)

[Figure 10.20](#)

[Figure 10.21](#)

[Figure 10.22](#)

[Figure 10.23](#)

[Figure 10.24](#)

[Figure 10.25](#)

[Figure 10.26](#)

[Figure 10.27](#)

[Figure 10.28](#)

[Figure 10.29](#)

[Figure 10.30](#)

[Figure 10.31](#)

[Figure 10.32](#)

[Figure 10.33](#)

[Figure 10.34](#)

[Figure 10.35](#)

[Figure 10.36](#)

[Figure 10.37](#)

[Figure 10.38](#)

[Figure 10.39](#)

[Figure 10.40](#)

[Figure 10.41](#)

[Figure 10.42](#)

[Figure 10.43](#)

[Figure 10.44](#)

[Figure 10.45](#)

[Figure 10.46](#)

[Figure P10.8](#)

[Figure P10.9](#)

[Figure P10.11](#)

[Figure P10.14](#)

[Figure P10.16](#)

[Figure P10.17](#)

[Figure P10.18](#)

[Figure P10.23](#)

[Figure 11.1](#)

[Figure 11.2](#)

[Figure 11.3](#)

[Figure 11.4](#)

[Figure 11.5](#)

[Figure 11.6](#)

[Figure 11.7](#)

[Figure 11.8](#)

[Figure 11.9](#)

[Figure 11.10](#)

[Figure 11.11](#)

[Figure 11.12](#)

[Figure 11.13](#)

[Figure 11.14](#)

[Figure 11.15](#)

[Figure 11.16](#)

[Figure 11.17](#)

[Figure 11.18](#)

[Figure 11.19](#)

[Figure 11.20](#)

[Figure 11.21](#)

[Figure 11.22](#)

[Figure 11.23](#)

[Figure 11.24](#)

[Figure 11.25](#)

[Figure 11.26](#)

[Figure 11.27](#)

[Figure 11.28](#)

[Figure 11.29](#)

[Figure 11.30](#)

[Figure 11.31](#)

[Figure 11.32](#)

[Figure 11.33](#)

[Figure 11.34](#)

[Figure 11.35](#)

[Figure 11.36](#)

[Figure 11.37](#)

[Figure 11.38](#)

[Figure 12.1](#)

[Figure 12.2](#)

[Figure 12.3](#)

[Figure 12.4](#)

[Figure 12.5](#)

[Figure 12.6](#)

[Figure 12.7](#)

[Figure 12.8](#)

[Figure 12.9](#)

[Figure 12.10](#)

[Figure 12.11](#)

[Figure 12.12](#)

[Figure 12.13](#)

[Figure 12.14](#)

[Figure 12.15](#)

[Figure 12.16](#)

[Figure 12.17](#)

[Figure 12.18](#)

[Figure 12.19](#)

[Figure 12.20](#)

[Figure 12.21](#)

[Figure 12.22](#)

[Figure 12.23](#)

[Figure 12.24](#)

[Figure 12.25](#)

[Figure 12.26](#)

[Figure 12.27](#)

[Figure 12.28](#)

[Figure 12.29](#)

[Figure 12.30](#)

[Figure 12.31](#)

[Figure 12.32](#)

[Figure 12.33](#)

[Figure 12.34](#)

[Figure 13.1](#)

[Figure 13.2](#)

[Figure 13.3](#)

[Figure 13.4](#)

[Figure 13.5](#)

[Figure 13.6](#)

[Figure 13.7](#)

[Figure 13.8](#)

[Figure 13.9](#)

[Figure 13.10](#)

[Figure 13.11](#)

[Figure 13.12](#)

[Figure 13.13](#)

[Figure 13.14](#)

[Figure 13.15](#)

[Figure 13.16](#)

[Figure 13.17](#)

[Figure 13.18](#)

[Figure 13.19](#)

[Figure 13.20](#)

[Figure 13.21](#)

[Figure 13.22](#)

[Figure 13.23](#)

[Figure 13.24](#)

[Figure 13.25](#)

[Figure 13.26](#)

[Figure 13.27](#)

[Figure P13.1](#)

[Figure P13.3](#)

[Figure P13.4](#)

[Figure P13.5](#)

[Figure P13.10](#)

[Figure P13.13](#)

[Figure P13.20](#)

[Figure P13.22](#)

[Figure P13.25](#)

[Figure P13.28](#)

[Figure P13.31](#)

[Figure P13.34](#)

[Figure P13.36](#)

[Figure P13.38](#)

[Figure 14.1](#)

[Figure 14.2](#)

[Figure 14.3](#)

[Figure 14.4](#)

[Figure 14.5](#)

[Figure 14.6](#)

[Figure 14.7](#)

[Figure 14.8](#)

[Figure 14.9](#)

[Figure 14.10](#)

[Figure 14.11](#)

[Figure 14.12](#)

[Figure 14.13](#)

[Figure 14.14](#)

[Figure 14.15](#)

[Figure 14.16](#)

[Figure 14.17](#)

[Figure 14.18](#)

[Figure 14.19](#)

[Figure 14.20](#)

[Figure 14.21](#)

[Figure 14.22](#)

[Figure 14.23](#)

[Figure 14.24](#)

[Figure 14.25](#)

[Figure 14.26](#)

[Figure 14.27](#)

[Figure 14.28](#)

[Figure 14.29](#)

[Figure 14.30](#)

[Figure 14.31](#)

[Figure 14.32](#)

[Figure 14.33](#)

[Figure 14.34](#)

[Figure 14.35](#)

[Figure 14.36](#)

[Figure 14.37](#)

[Figure 14.38](#)

[Figure P14.1](#)

[Figure P14.2](#)

[Figure P14.3](#)

[Figure P14.4](#)

[Figure P14.5](#)

[Figure P14.6](#)

[Figure P14.7](#)

[Figure P14.8](#)

[Figure P14.9](#)

[Figure P14.10](#)

[Figure P14.11](#)

[Figure P14.12](#)

[Figure P14.13](#)

[Figure P14.14](#)

[Figure P14.15](#)

[Figure P14.16](#)

[Figure P14.17](#)

[Figure P14.18](#)

[Figure P14.19](#)

[Figure P14.20](#)

[Figure P14.21](#)

[Figure P14.25](#)

[Figure 15.1](#)

[Figure 15.2](#)

[Figure 15.3](#)

[Figure 15.4](#)

[Figure 15.5](#)

[Figure 15.6](#)

[Figure 15.7](#)

[Figure 15.8](#)

[Figure 15.9](#)

[Figure 15.10](#)

[Figure 15.11](#)

[Figure 15.12](#)

[Figure P15.1](#)

[Figure P15.2](#)

[Figure P15.4](#)

[Figure P15.5](#)

[Figure P15.6](#)

[Figure P15.7](#)

[Figure P15.8](#)

[Figure P15.9](#)

[Figure P15.11](#)

[Figure 16.1](#)

[Figure 16.2](#)

[Figure 16.3](#)

[Figure 16.4](#)

[Figure 16.5](#)

[Figure 16.6](#)

[Figure 16.7](#)

[Figure 16.8](#)

[Figure 16.9](#)

[Figure 16.10](#)

[Figure 16.11](#)

[Figure 16.12](#)

[Figure 16.13](#)

[Figure 16.14](#)

[Figure 16.15](#)

[Figure 16.16](#)

[Figure 16.17](#)

[Figure 16.18](#)

[Figure 16.19](#)

[Figure 16.20](#)

[Figure P16.1](#)

[Figure P16.2](#)

[Figure P16.3](#)

[Figure P16.5](#)

[Figure P16.7](#)

[Figure P16.8](#)

[Figure P16.9](#)

[Figure P16.10](#)

[Figure P16.11](#)

[Figure P16.13](#)

[Figure P16.16](#)

[Figure P16.18](#)

[Figure P16.21](#)

[Figure P16.23](#)

[Figure P16.25](#)

[Figure P16.27](#)

[Figure 17.1](#)

[Figure 17.2](#)

[Figure 17.3](#)

[Figure 17.4](#)

[Figure 17.5](#)

[Figure 17.6](#)

[Figure 17.7](#)

[Figure 17.8](#)

[Figure 17.9](#)

[Figure 17.10](#)

ABOUT THE COMPANION WEBSITE

This book is accompanied by two companion websites: one for students and one for certified instructors.

www.wiley.com/go/waldron/kinematics

The student website includes:

- Movie files for selected linkage animations
- Sample Solidworks files illustrating the use of GCP
- MATLAB® programs
- The instructor website (password protected) includes:
 - Solutions manual
 - PowerPoint teaching slides
 - Textbook figures
 - Material in student website



Kinematics, Dynamics, and Design of Machinery

Third Edition

Kenneth J. Waldron

Professor Emeritus, Stanford University, USA

Professor, University of Technology, Sydney, Australia

Gary L. Kinzel

Professor Emeritus, The Ohio State University, USA

Sunil K. Agrawal

Professor, Columbia University, USA

WILEY

© 2016, John Wiley & Sons, Ltd.

Registered office

John Wiley & Sons Ltd, The Atrium, Southern Gate, Chichester, West Sussex, PO19 8SQ, United Kingdom

For details of our global editorial offices, for customer services and for information about how to apply for permission to reuse the copyright material in this book please see our website at www.wiley.com.

The right of the author to be identified as the author of this work has been asserted in accordance with the Copyright, Designs and Patents Act 1988.

All rights reserved. No part of this publication may be reproduced, stored in a retrieval system, or transmitted, in any form or by any means, electronic, mechanical, photocopying, recording or otherwise, except as permitted by the UK Copyright, Designs and Patents Act 1988, without the prior permission of the publisher.

Wiley also publishes its books in a variety of electronic formats. Some content that appears in print may not be available in electronic books.

Designations used by companies to distinguish their products are often claimed as trademarks. All brand names and product names used in this book are trade names, service marks, trademarks or registered trademarks of their respective owners. The publisher is not associated with any product or vendor mentioned in this book.

Limit of Liability/Disclaimer of Warranty: While the publisher and author have used their best efforts in preparing this book, they make no representations or warranties with respect to the accuracy or completeness of the contents of this book and specifically disclaim any implied warranties of merchantability or fitness for a particular purpose. It is sold on the understanding that the publisher is not engaged in rendering professional services and neither the publisher nor the author shall be liable for damages arising herefrom. If professional advice or other expert assistance is required, the services of a competent professional should be sought.

MATLAB® is a trademark of The MathWorks, Inc. and is used with permission. The MathWorks does not warrant the accuracy of the text or exercises in this book. This book's use or discussion of MATLAB® software or related products does not constitute endorsement or sponsorship by The MathWorks of a particular pedagogical approach or particular use of the MATLAB® software.

Library of Congress Cataloging-in-Publication Data is available:

ISBN: 978-1-118-93328-2

A catalogue record for this book is available from the British Library.

PREFACE

One of the most amazing aspects of the preparation of this new edition of *Kinematics, Dynamics, and Design of Machinery* is the radical nature of the changes we found to be necessary. The first edition of this work appeared in September 1998, and it is appropriate to reflect on the changes that have occurred during the intervening eighteen years. Although this is a core subject in the mechanical engineering curriculum that has been taught in one form or another throughout the period in which it has been recognized as a technical discipline, there have been many recent changes. In 1998, most production machines were still driven by a single prime mover with their various functions mechanically coordinated. It is true that industrial robots were well established in some industries, notably the manufacture of automobiles, but they were still the exception rather than the rule in utilizing digital coordination of multiple actuators. The first edition of this work broke new ground as an undergraduate text by including chapters on robots and spatial mechanisms. Of course, this picture has totally changed with embedded controllers ubiquitous in our appliances, automobiles, and production machinery. Multiple functions are now much more likely to be coordinated digitally. We have recognized this reality by expanding the material on actuation and creating a new [Chapter 17](#). We have, in that chapter, created an interface to courses on control, and particularly digital control.

It is even truer that the tools available to the machine designer are completely different from what was available in 1998. At that time, computer-aided engineering software was certainly well established, but modern solid modeling packages were not well developed. The constraint management capabilities built into these tools provide a very powerful new capability that renders special purpose mechanism design software—such as that we, ourselves, developed—obsolete. In recognition of this new reality, we have introduced a chapter on Geometric Constraint Programming as [Chapter 2](#), and examples of solving mechanism design problems by this means in [Chapters 3, 4, 5, and 6](#). In addition, [Chapter 10](#) on cam design has been completely revised to base it on methods employing instant centers that are much simpler than the methods we used in the earlier editions. For this reason, although this text covers the same technological territory that the first edition did, it is a very different presentation that takes full advantage of new design technologies.

It is also true that the way in which the subject matter is taught has changed. In the years preceding 1998, this material most often formed the content of a separate course in the mechanical engineering curriculum. Since that time, it has become one element in an overarching discipline of mechanical systems, or *mechatronics*. As such, this material is often interleaved with material from control systems engineering and other related disciplines. To facilitate the use of our material as a component of a mechanical systems course, or in machine design courses, we have attempted to make each chapter as modular as possible. There is a box at the beginning of each chapter stating which material from elsewhere in the book is a prerequisite for successful study of that chapter. It is intended that, if the instructor so desires, he or she can place before their students only the material they intend to cover.

In addition to updating even those sections that are similar to those of Editions 1 and 2, we have added a significant number of new problems, including some open-ended design problems. Supporting material that was included on a CD with Editions 1 and 2 is now available on the companion website maintained by John Wiley & Sons: www.wiley.com/go/waldron/kinematics. It has also been updated as necessary.

We trust that this new presentation will be welcomed as an up-to-the-minute teaching tool and a useful reference for instructors and practitioners in this field. Yes, the new approaches are likely to take instructors who have taught the material for a number of years out of their comfort zone, but we believe the required extra effort to become familiar with the new techniques will prove to be very worthwhile.

In order to take advantage of the Geometric Constraint Programming (GCP) techniques, it is necessary for students to have access to parametric design software that incorporates constraint managers. We believe that tomorrow's students will increasingly be working with solid modeling packages throughout the curriculum. If this should prove not to be true, inexpensive drawing packages that have constraint managers are readily available.

We would like to express our sincere thanks to the colleagues and students who have contributed to the success of the three editions of this book. For the third edition, we especially acknowledge the help of Profs. James

Schmiedeler and Edward Kinzel who co-developed the GCP procedure. Both provided assistance on writing [Chapter 2](#) and parts of [Chapter 3](#), and Jim in particular generously provided his tutorial notes to facilitate the development of the teaching material. We would also like to thank Dr. Matthew Detrick who rewrote the GUI-based kinematic programs for the new versions of MATLAB®. The programs for both the previous and current versions of MATLAB are included in the supplementary material for the book.

Kenneth J. Waldron

Professor Emeritus, Stanford University

Professor, University of Technology, Sydney

Gary L. Kinzel

Professor Emeritus, The Ohio State University

Sunil K. Agrawal

Professor, Columbia University

1

INTRODUCTION

Prerequisite Knowledge Needed for Chapter 1

No prior knowledge is required for this chapter. It is an advantage to have completed undergraduate courses in statics and dynamics, but is certainly not essential.



1.1 Historical Perspective

A mechanism is a machine composed of rigid members that are joined together. Joints permit the members to interact with one another. Portions of the surfaces of the members that contact one another form the joints. The geometries of the contacting surface segments determine the properties of each joint.

Mechanisms are used for diverse purposes. Some are incorporated into items we use every day. [Figure 1.1](#) shows a mechanism whose function is to magnify the force generated by a user squeezing the handles to a very large force exerted by the jaws. It is also designed to lock in place while generating that force, so the handles can be released while the jaws remain clamped on a work piece. This is an example of a planar mechanism because the members of the mechanism all move parallel to a single plane of motion. Many familiar mechanisms have this characteristic. Planar mechanisms are the primary focus of [Chapters 3](#) through [7](#) of this book. Mechanisms whose primary function is transmitting force, like this one, are discussed in [Chapter 14](#).



[Figure 1.1](#) A pair of vice-grip pliers. A planar mechanism that multiplies the force applied by a user to the handles to apply a much greater force at the jaws. The mechanism is also designed to be locked in the closed position.

Other mechanisms are characterized by points in their members following paths that are curves in space. In [Figure 1.2](#), the leg mechanisms allow the feet to be placed anywhere within a volume of space. Each mechanism is primarily used to generate a straight-line foot trajectory relative to the body, so that the machine can walk at a constant height with uniform speed. Notice that the critical function here is the ability to have a designated point generate a path of specified geometry (a straight line). This is known as a path generation problem. The leg mechanisms used here are called pantographs. A pantograph is a special kind of planar mechanism discussed in Section 8.1.3.



[Figure 1.2](#) The Adaptive Suspension Vehicle [7]. Each leg is a planar pantograph mechanism hinged to the body about an axis parallel to the longitudinal axis of the vehicle. The feet can be placed anywhere within a volume of space, so this is, overall, a spatial mechanism. The pantograph mechanism allows the ankle joint to be moved in a straight line relative to the vehicle body by a single hydraulic cylinder.

[Figure 1.3](#) is the drive mechanism of an ornithopter, a vehicle that flies by flapping its wings like a bird. Here a spatial trajectory of the entire wing must be generated relative to the body, not just the path of a point, as was the case with [Figure 1.2](#). The wings must flap relative to the body, but they must also rotate about the long axis of the wing at the top of the flap to allow the wing to generate lift. The wing must rotate back (feathering) at the bottom of the flap to minimize air resistance to the upstroke. This is an example of using a mechanism to generate a specified path in space of a whole body (the wing). We call this a motion-generation problem. There are many other ways in which mechanisms are used. Here the wings are flapped by two planar four-bar mechanisms that are geared together. The rotation about the wing axis is accomplished by a cam-and-follower mechanism. Cam mechanisms are discussed in [Chapter 10](#).

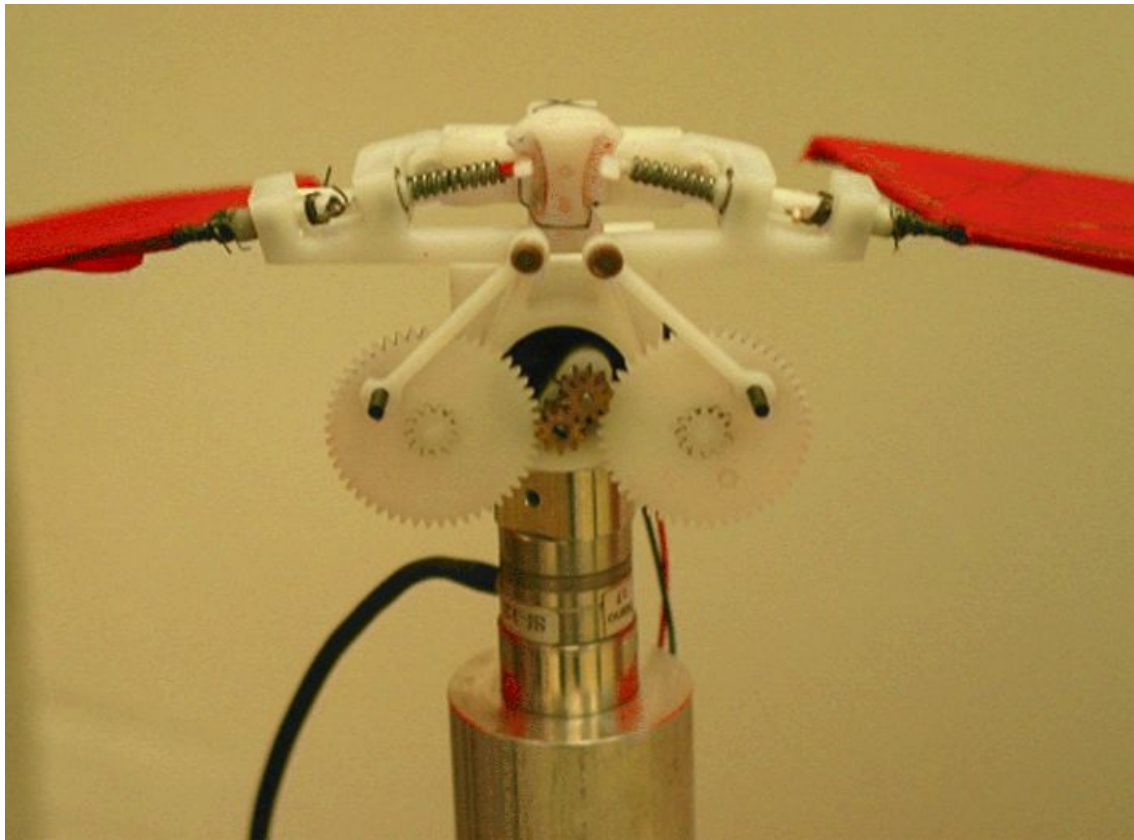


[Figure 1.3](#) The drive mechanism of an ornithopter [1]. The mechanism must both flap the wings and rotate them about their long axes at the top and bottom of the flapping motion. A pair of four-bar mechanisms that are geared together accomplish the flapping motion. Cam and follower mechanisms are used to accomplish rotation of the wing at the top and bottom of the flapping motion.

Other common examples of ways in which mechanisms are used include the suspension of an automobile. A mechanism is used to maintain the wheels in a proper relationship with the body of the vehicle while allowing them to move to accommodate variations in the profile of the road. The suspension functions as a mechanical filter isolating the body of the vehicle and its occupants from bumps in the road.

Yet another example is the mechanism of an excavator, like the one shown in [Figure 1.4](#), in which multiple hydraulic actuators are used to provide versatile paths of the bucket under direct control of the human operator to accomplish varied digging tasks.



Figure 1.4 Several hydraulic cylinders control a mechanical excavator.

The design of mechanisms is a technical area that is unique to mechanical engineering. Its history stretches back to prehistoric times. Artisans such as blacksmiths and carpenters also functioned as designers of mechanisms. One of the original functions of engineers was the design of mechanisms for both warfare and peaceful uses. During the Renaissance, Leonardo da Vinci [9] depicted a sophisticated variety of mechanisms, mostly for military purposes. Sometime thereafter, civil engineering and military engineering became distinct entities.

The modern era in mechanism design, along with the history of mechanical engineering as a distinct discipline, can be viewed as starting with James Watt [4]. However, the subject has not remained static. In fact, there have been dramatic changes in the practice of mechanism design in recent years.

Traditionally, machines were designed to be powered by a single “prime mover,” with all functions mechanically coordinated—a tradition that predates Watt. Developments in computer technology starting in the early 1970s, coupled with improvements in electric motors and other actuators, have made it possible to use a different approach. In this approach, machines are powered by multiple actuators coordinated electronically. The resulting machines are simpler, less expensive, more easily maintained, and more reliable. Another major change is in the techniques used in mechanism design. The use of interactive computer graphics has had a dramatic impact on design practice. One of our motivations in producing this book is to provide a treatment that reflects these changes in practice.

The functions for which mechanisms are used have changed with time, as have the methods used in designing them. Mechanisms were earlier used to generate irregular motion patterns. The Norden bombsight of World War II was a mechanical analog computer with dozens of mechanisms generating special functions mechanically [10]. Not only can those calculations now be performed more accurately and flexibly by a digital computer, but any desired motion can be generated easily and inexpensively with a computer-controlled electric motor, so there is little interest in using mechanisms in this way anymore.



1.2 Kinematics

Kinematics is the study of position and its time derivatives. Specifically, we are concerned with the positions, velocities, and accelerations of points and with the angular positions, angular velocities, and angular accelerations of solid bodies. The position of a body can be defined by the position of a nominated point of that body combined with the angular position of the body. In some circumstances, we are also interested in the higher time derivatives of position and angular position.

The subject of kinematics is a study of the geometry of motion—geometry with the element of time added. The bulk of the subject matter of this book can be referred to as the kinematics of mechanisms. Kinetics brings in the relationship between force and acceleration embodied in Newton's laws of motion is another important topic. Together, kinematics and kinetics constitute the subject known as dynamics. The subject matter is approached from a mechanical designer's perspective to present techniques that can be used to design mechanisms to meet specific motion requirements.



1.3 Design: Analysis and Synthesis

The material in this book falls into two sections. The first comprises methods for mathematically determining the geometry of a mechanism to produce a desired set of positions and/or velocities or accelerations. These are rational synthesis techniques. The second section discusses techniques to determine the positions, velocities, and accelerations of points in the members of mechanisms and the angular positions, velocities, and accelerations of those members. These are kinematic analysis techniques.

The creative activity that distinguishes engineering from science is design or, more formally, synthesis. Science is the study of what is; engineering is the creation of what is to be. The classical rational synthesis techniques developed by kinematicians offer a rather direct route to mechanism design that lends itself well to automation using computer-graphics workstations. However, these techniques represent only one way to design mechanisms, and they are relatively restrictive. Rational synthesis techniques exist only for specific types of mechanism design problems, and many practical mechanism design problems do not fit within the available class of solutions.

A new set of techniques that depend on the computational capabilities of modern graphical modeling software, in combination with a knowledge of motion geometry, are presented in [Chapter 2](#) of this book. Yet another alternative is to use informal synthesis. This is a methodology used by engineers to solve design problems in many technical areas, not just in mechanism design. The basic procedure is to “guess” a set of dimensions and use analysis to check the resulting performance. The dimensions are then adjusted to attempt to match more closely the performance specifications and the mechanism is analyzed again. The process is repeated until an acceptably close match to the specifications is achieved. Thus, a primary use of the analysis material is also in mechanism design.

From an engineering point of view, it is not possible to treat mechanism design solely in terms of kinematics. The motivation for performing an acceleration analysis is often to enable inertia forces on the links to be calculated, allowing, in turn, computation of the forces transferred between links and the internal forces, or stresses, within the links. Mechanisms must usually drive loads, as well as generate motions. As soon as we introduce the concept of force, we leave the domain of pure kinematics and enter that of kinetics. Insofar as the largest forces in many mechanisms are inertia forces created by motion, it is convenient to study them within the general framework of kinematic techniques. There is also an important symmetry between the geometry of the force distribution and that of the velocity distribution that is particularly useful when working with spatial mechanisms. Thus, it is entirely appropriate to treat mechanism statics or kinetics within the general geometry of motion framework constructed to study mechanism kinematics. This treatment is presented in the later chapters of this book.



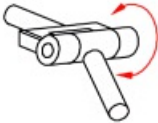
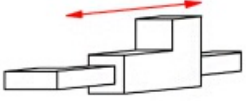
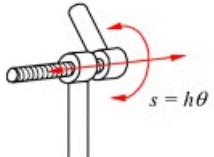
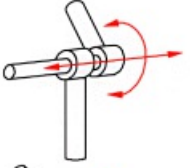
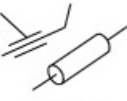
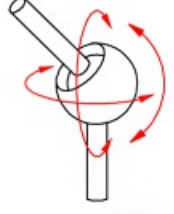
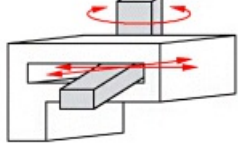
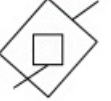
1.4 Mechanisms

Mechanisms are assemblages of solid members connected by joints. Mechanisms transfer motion and mechanical work from one or more actuators to one or more “output” members. For the purposes of kinematic design, we idealize a mechanism to a kinematic linkage in which all the members are assumed to be perfectly rigid and are connected by kinematic joints. A kinematic joint is formed by direct contact between the surfaces of two members. One of the earliest codifications of mechanism kinematics was that of Reuleaux [8], and some of the basic terminology we use originated with him. He called a kinematic joint a “pair.” He further divided joints into “lower pairs” and “higher pairs.” A lower-pair joint is one in which contact between two rigid members occurs over geometrically congruent surfaces. The surface contact between lower pairs results in relatively low-contact stresses. A higher-pair joint is one in which contact occurs only at isolated points or along line segments. All other things being equal, a higher-pair joint will produce much higher stresses than will a lower-pair joint.

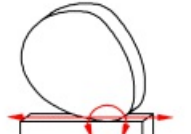
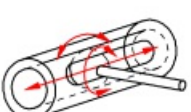
Joints are the most important aspect of a mechanism to examine during an analysis. They permit motion in some directions while constraining motion in others. The types of motion permitted are related to the number of degrees of freedom (dof) of the joint. The number of degrees of freedom of the joint is equal to the number of independent coordinates needed to specify uniquely the position of one link relative to the other, as constrained by the joint.

Lower-pair joints are necessarily restricted to a relatively small number of geometric types, because the requirement that surface contact be maintained constrains the geometry of the contacting surfaces. There are only six fundamentally different types of lower-pair joints, classified by the types of relative motion that they permit. There are, in contrast, an infinite number of possible higher-pair geometries. The lower-pair joint types are shown in [Table 1.1](#). Some important examples of higher-pair joints are shown in [Table 1.2](#).

[Table 1.1](#) Lower-Pair Joints

Connectivity (Number of Degrees of Freedom)	Names	Letter Symbol	Typical Form	Sketch Symbol
1	Revolute Hinge Turning pair	R		(Planar)  (Spatial) 
1	Prismatic joint Slider Sliding pair	P		(Planar)  (Spatial) 
1	Screw joint Helical joint Helical pair	H		(Spatial) 
2	Cylindric joint Cylindric pair	C		
3	Spherical joint Ball joint Spherical pair	S		(Spatial) 
3	Planar joint Planar pair	P _L		

[Table 1.2](#) Examples of Higher-Pair Joints

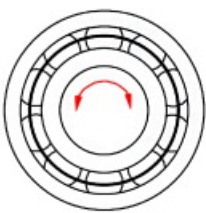
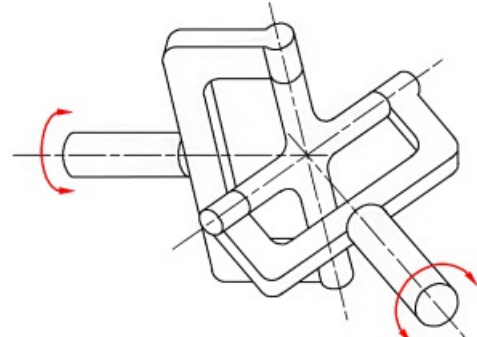
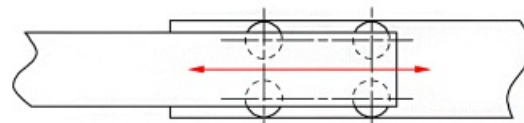
Connectivity (Number of Degrees of Freedom)	Names	Typical Form	Comments
1	Cylindrical roller		Roller rotates about this line at this instant in its motion. Roller does not slip on the surface on which it rolls.
2	Cam pair		Cam rolls and slides on follower
3	Rolling ball		Ball rolls without slipping
4	Ball in cylinder		Ball can rotate about any axis through its center and slide along the cylinder axis
5	Spatial point contact		Body can rotate about any axis through the contact point and slide in any direction in the tangent plane

Lower-pair joints are frequently used in mechanism design practice. They give good service because wear is spread out over the contact surface and because the narrow clearance between the surfaces provides good conditions for lubrication and a tight constraint on the motion. The change in the geometric properties of the joint with wear is slow for a lower pair. At least as important are the simple geometries of the relative motions that these joints permit. The simple geometries of the contacting surfaces also make them easy to manufacture.

Higher-pair joints that involve pure rolling contact, or that approximate that condition, are also used frequently. In pure rolling contact, the points in one of the two joint surfaces that are actually in contact with the other surface at any instant are at rest relative to that surface. Hence there is no relative sliding of the surfaces and joint friction and wear are minimized. Physically, the limitation of this kind of joint is the stress intensity that the material of the contacting bodies can support. Stresses are necessarily high because of the very small contact areas. If the bodies were perfectly rigid, contact would occur only at discrete points or along a line, the contact area would be zero, and the stresses would be locally infinite!

Lower-pair joints such as revolute joints and cylindrical joints are also often simulated by systems such as ball or roller bearings in which there are many elements acting in parallel. The actual contact joints in a ball bearing are rolling contacts, which are higher pairs. In this way, the low-friction properties of rolling contacts are exploited to obtain a joint with lower friction and higher load and relative speed capabilities than would be possible with a plain revolute joint. At the same time, the simple overall relative motion geometry of the revolute joint is retained. This is one example of a compound joint in which the joint is actually a complex mechanism but is regarded as kinematically equivalent to a simple revolute. Several examples of compound joints are shown in [Table 1.3](#).

[Table 1.3](#) Examples of Compound Joints

Connectivity	Names	Form
1	Ball bearing Anti-friction bearing Rolling contact bearing	
2	Universal joint Hooke joint Cardan joint	
1	Roller slide Roller guide	

Single higher-pair joints are sometimes replaced by a series of lower-pair joints that permit equivalent motion ([Figure 1.5](#)). For example, the function of a pin-in-a-slot joint can be replaced by a combination of a revolute joint and a prismatic joint. Note that this involves adding extra members to the mechanism. When a rolling contact bearing or compound joint replaces a lower-pair joint, the two mechanisms are said to be *kinematically equivalent*. This means that the relative motions that are permitted between the bodies in the two cases are the same, even though the joint is physically quite different.

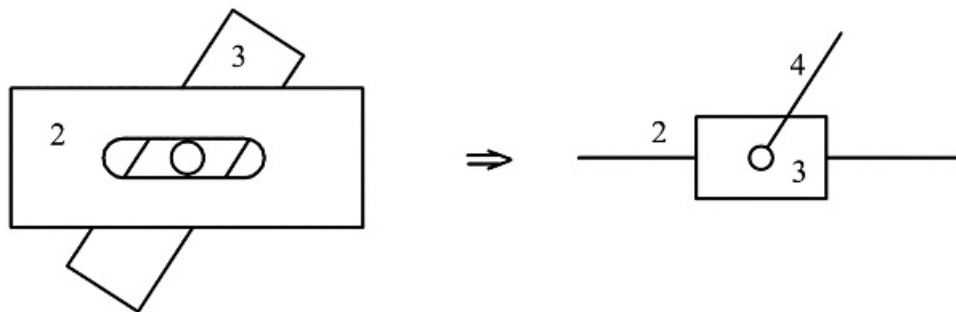


[Figure 1.5](#) Replacement of a higher-pair joint by a kinematically equivalent combination of lower-pair joints.

The number of degrees of freedom (connectivity) of a joint is the minimum number of independent parameters required to define the positions of all points in one of the bodies it connects relative to a reference frame fixed to the other. The term *connectivity* is used to denote this freedom of the body, even though the joint may be something very elaborate such as the antifriction bearing shown in [Table 1.3](#) and [Figure 1.6](#). If motion is restricted to a plane, the maximum number of degrees of freedom is three. In general spatial motion, the maximum number is six. The number of degrees of freedom permitted by each joint is listed in [Tables 1.1](#), [1.2](#) and [1.3](#) in the first column.



[Figure 1.6](#) Various rolling-element and plain bearings. As discussed in the text, rolling-element bearings are compound joints that replace kinematically equivalent plain joints.



1.5 Planar Linkages

A planar linkage is one in which the velocities of all points in all members are directed parallel to a plane, called the plane of motion. The only lower-pair joints that are properly compatible with planar motion are revolute and prismatic joints. The axes of rotation of all revolute joints must be normal to the plane of motion because points would not otherwise move in parallel planes. The directions of sliding of all prismatic joints must be parallel to the plane of motion, since all points in a member connected to another by a prismatic joint move on lines parallel to the sliding direction relative to the second member. Occasionally other lower-pair joints will appear in what is otherwise a planar linkage. However, they then function only as revolute or prismatic joints. For example, a spherical joint may be substituted for a revolute joint, but if the linkage is functionally planar, that spherical joint will operate as a revolute with rotation occurring only about the axis normal to the plane of motion. This type of situation will be discussed in more detail in the context of degrees of freedom and mobility.

A common schematic method of representing planar linkages is to represent revolute joints by small circles as shown in [Table 1.1](#). Binary links, those that have two joints mounted on them, are represented as lines joining those joints. Ternary links, those that have three joints mounted on them, are represented as triangles with the joints at the vertices, and so on. Examples of the resulting representation are shown in [Figures 1.7](#) through [1.9](#). The link geometries may then be easily reproduced, giving an accurate view of the linkage in a specified position. Alternatively, the schematic may be used conceptually without accurate geometric data, to indicate the topology of the linkage. *Topology* is the branch of geometry that deals with issues of connectedness without regard to shape. Links with three or more joints should be shaded or crosshatched. Otherwise, the schematic for a quaternary link, one with four joints, cannot be distinguished from the schematic for a four-bar linkage loop.

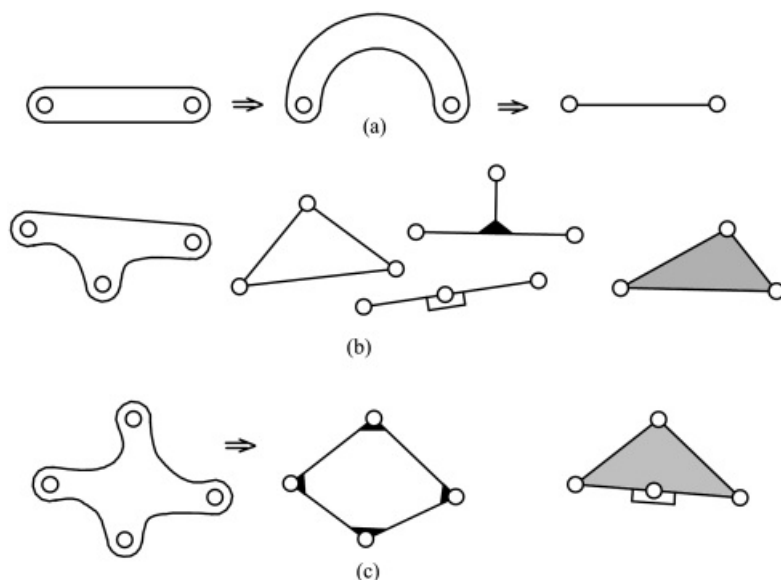


[Figure 1.7](#) Representations of links in linkages: (a) Binary links: those to which two joints are mounted; (b) ternary links; and (c) quaternary links. These have three and four joints, respectively.

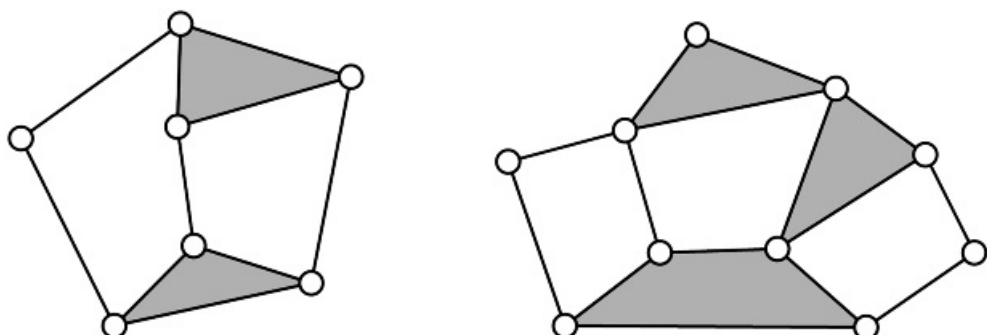


Figure 1.8 Conventional representations of planar linkages. Circles indicate revolute joints. Binary links, those with two joints mounted on them, are represented by line segments. Ternary links, with three joints, are represented by triangles, and so on.

A kinematic chain is any assemblage of rigid links connected by kinematic joints. A closed chain is one in which the links and joints form one or more closed circuits. Each closed circuit is a loop in which each link is attached to other links by at least two joints.

Prismatic joints are represented by means of a line in the direction of sliding, representing a slide, with a rectangular block placed on it. This produces linkage representations such as those shown in [Figure 1.9](#). A *frame* or base member is a link that is fixed. That is, it has zero degrees of freedom relative to the fixed coordinate system. A *linkage* is a closed kinematic chain with one link selected as the frame.

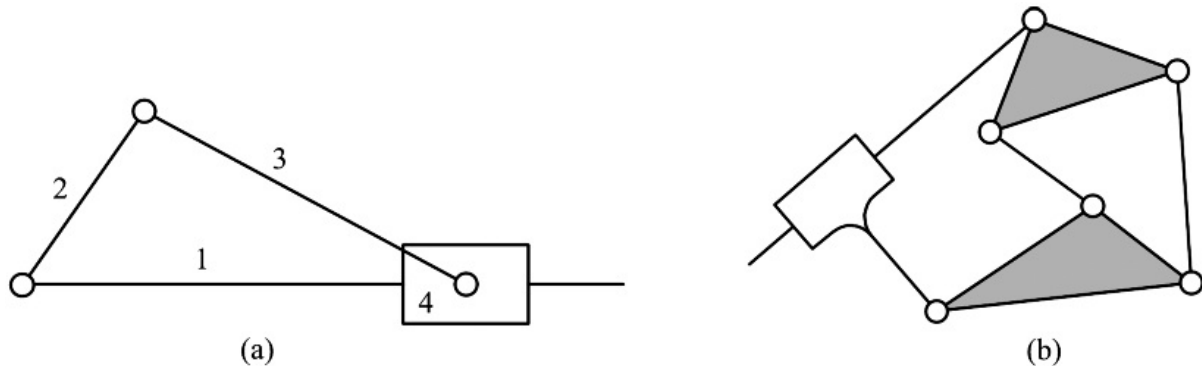


Figure 1.9 Representations of planar linkages with prismatic joints. (a) A four-bar slider-crank mechanism. Note that the sliding “block” is a binary member of the mechanism with a revolute joint and a prismatic joint providing the connections to adjacent members in the loop. The fillets connecting the block to a binary member represented by a line in (b) represent a rigid connection. Thus, the combination is, in this case, a binary member of the linkage.

In cases in which it is necessary to distinguish the base member of a linkage, it is customary not to show the base as a link in the normal manner but to indicate joints to base by “mounts,” as shown in [Figures 1.10](#) and [1.11](#).

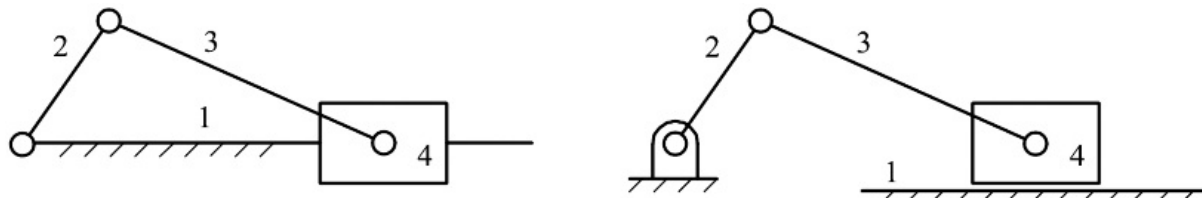


Figure 1.10 Selection of a frame member converts the chain of [Figure 1.9\(a\)](#) into a linkage. This linkage is known as a slider-crank linkage.

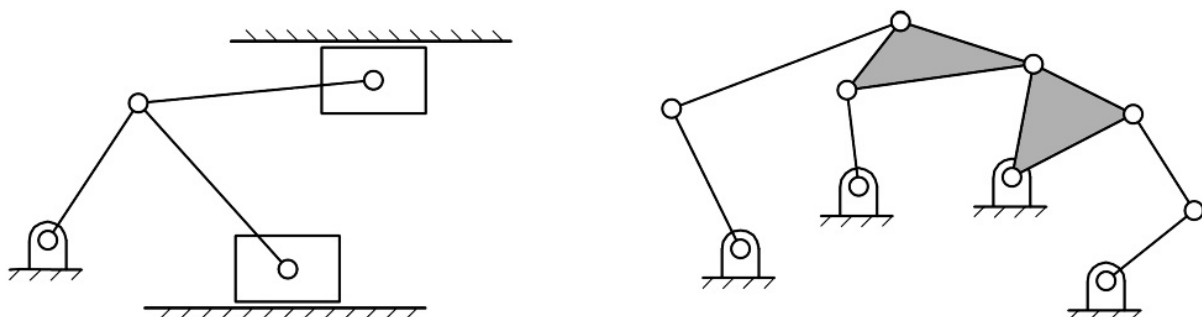
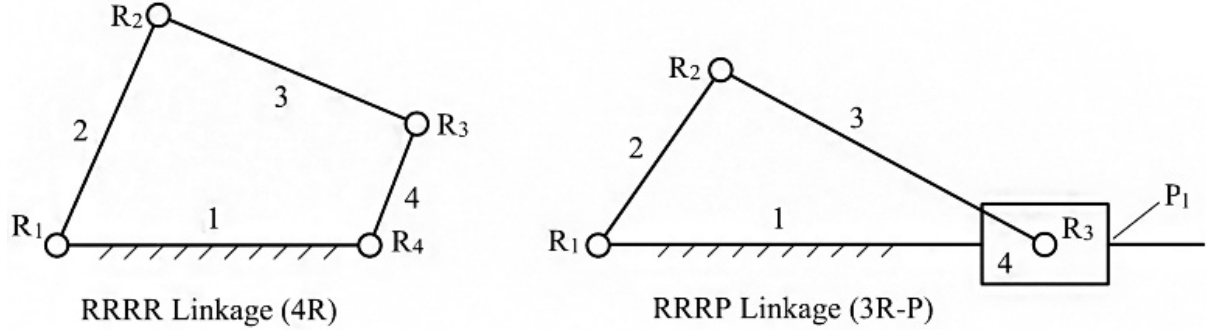


Figure 1.11 Representations of planar linkages with the base link not shown in the same form as the other links. The page can be thought of as representing the base link. Hatched “mounts” indicate the joints to the base link.

The term *mechanism* is somewhat interchangeable with *linkage*. In normal usage, it is a somewhat more generic term encompassing systems with higher pairs, or combinations of lower- and higher-pair joints, whereas the term linkage tends to be restricted to systems that have only lower-pair joints. The links are numbered with the frame link usually taken as link 1.

Simple, single-loop linkages are given a symbolic designation by a sequence of letters denoting joint types written in clockwise order beginning and ending with the joints mounted to the frame link as shown in [Figure 1.12](#). The letter designations for the different joints are given in [Table 1.1](#).



[Figure 1.12](#) Designation of single loop linkages by means of their joints. The joints are taken in clockwise order around the loop, starting and finishing with a joint to frame.

The profiles of the contacting surfaces of higher pairs, such as cams and followers, are drawn in planar linkages producing representations such as that shown in [Figure 1.13](#). Those surfaces must be general (not necessarily circular) cylinders whose straight-line generators are normal to the plane of motion. The profile drawn is, therefore, the generating curve of the cylinder shown in [Figure 1.14](#). The cylinder is generated by translating that curve along a straight line in the direction normal to its plane. The familiar cylinder with a circular generating curve is called a right-circular cylinder.

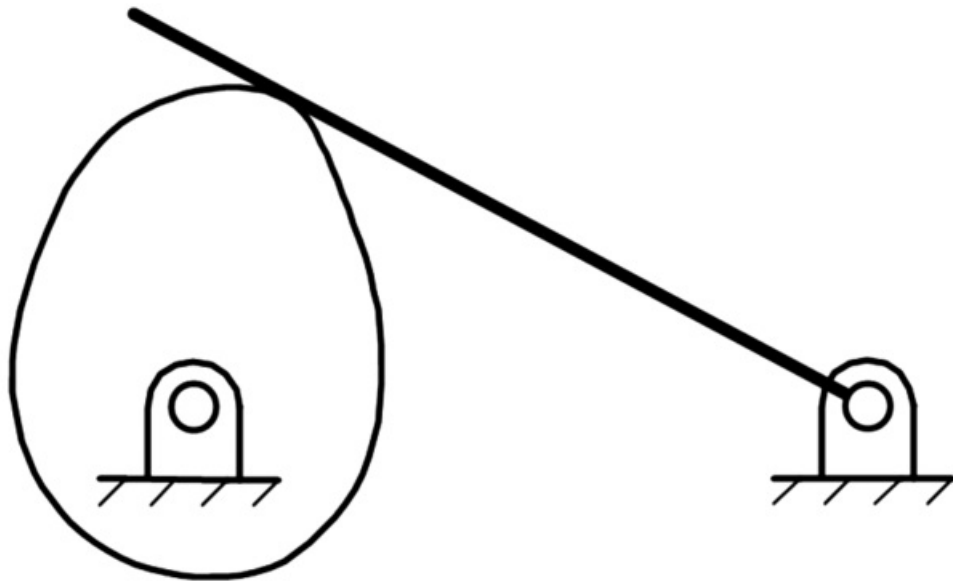


[Figure 1.13](#) Representation of a plate cam with a rocker follower. The face of the follower is a plane, so it is represented by a line. The cam is represented by its profile curve.

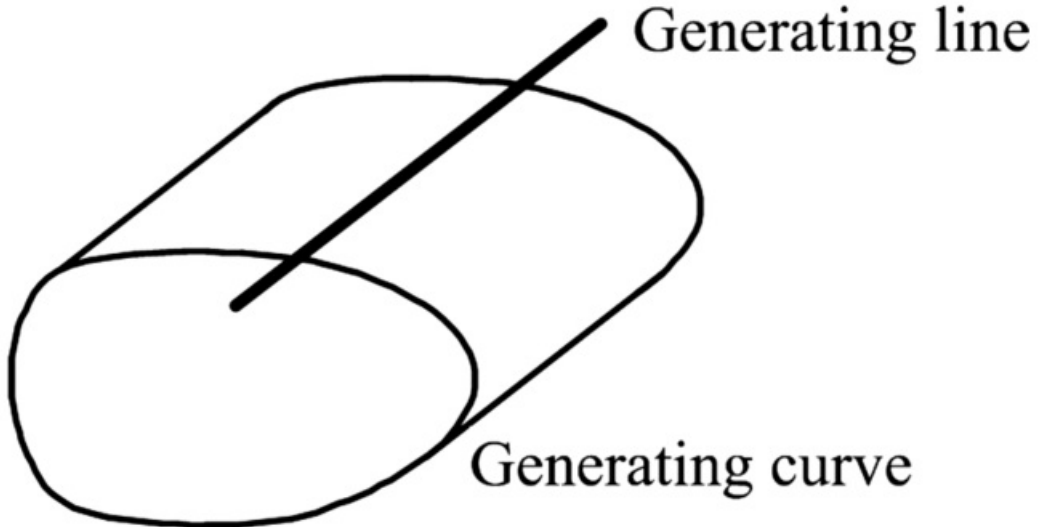


[Figure 1.14](#) General cylinder. The generating curve is a plane curve. Its plane is normal to the generating line. The surface may be generated by moving the generating curve so that a point on it moves along the generating line. Alternatively, the surface may be generated by moving the generating line so that a point on it traverses the generating curve.



1.6 Visualization

Because linkage motion is inextricably intertwined with geometry, it is always important to the designer to visualize the motion. In this respect, planar linkages are relatively easy to work with because their geometry and loci representing their motion can be drawn on a two-dimensional surface. Nevertheless, it can be very difficult to visualize successive positions of the links of a planar linkage from a drawing of that linkage in a representative position. Yet this succession of positions and the relative locations of all the links in each of the positions are very important when trying to predict effects such as interference with each other and with other machine parts.

Mechanism designers have traditionally solved this problem by constructing simple physical models with the links cut from cardboard (e.g., a manila folder) and revolute joints formed by pins (e.g., thumbtacks) or grommets.

Prototyping kits or even children's construction toys ([Figure 1.15](#)) provide an alternative that requires more construction time but gives a more functional model.

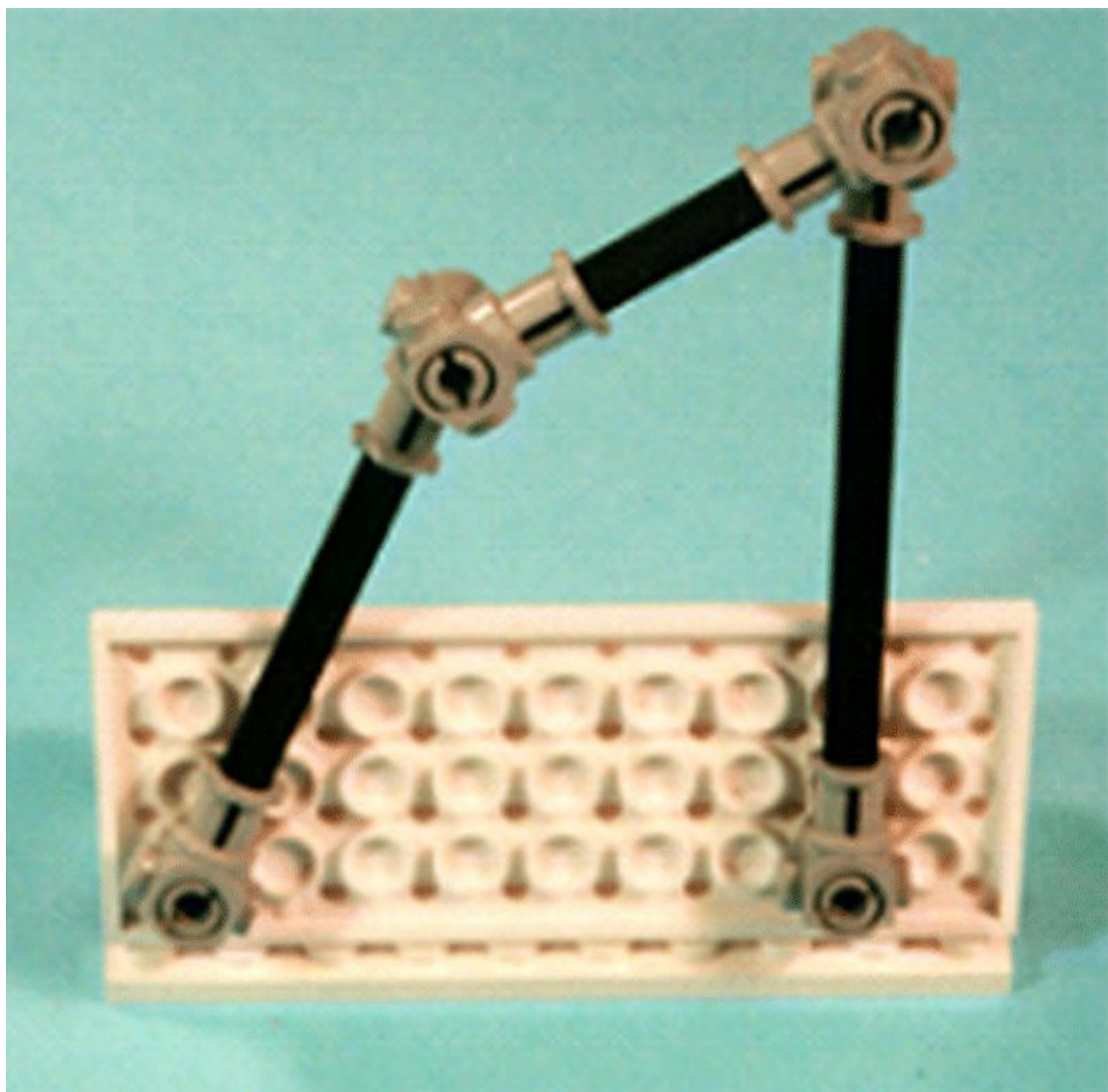


[Figure 1.15](#) Planar four-bar linkage model made with LEGO Technics [6].

When mechanisms are designed using computer graphics systems, animation on a computer can be used to visualize the motion of the mechanism, rather than construction of a physical model. Animation should be used with caution, however. As will be seen in a later section of this chapter, there are important interference effects that do not lend themselves to planar representation but which become immediately apparent in a physical model. Furthermore, adding realistic boundary profiles to the representations of links on computer graphic systems is often time consuming and simply not worth the effort when trying a variety of different alternative linkage

configurations. Instead, quick physical visualization models may be a more efficient alternative. The reader is urged to get into the habit of constructing simple models to visualize the motions of linkages that are being designed or analyzed, and to make use of computer animation when it is available. If the appropriate resources are available, physical models can be produced from solid models on the computer by means of 3D printing techniques. [Figure 1.16](#) shows such a physical model.



[Figure 1.16](#) A spatial mechanism model manufactured using a 3D printing system.



1.7 Constraint Analysis

The number of degrees of freedom (dof) of a body is the number of independent coordinates needed to specify uniquely the position of that body relative to a given reference frame. Similarly, we call the minimum number of coordinates needed to specify uniquely the positions of all of the members of a system of rigid bodies the number of degrees of freedom of that system. We will use the concept of the number of degrees of freedom in three distinct but closely related ways. The first is the number of degrees of freedom of a body relative to a specified reference frame, which is defined as above. The second is the number of degrees of freedom of a kinematic joint. The third is the number of degrees of freedom of the entire linkage or mechanism.

Both because “number of degrees of freedom” is such a mouthful and because we are using a distinct concept, we will refer to the number of degrees of freedom of a joint as its *connectivity*. In addition, the term connectivity will apply to the number of relative freedoms between two bodies. Likewise, we will refer to the number of degrees of freedom of a linkage as the *mobility* of that linkage. These terms may be formally defined as follows:

If a kinematic joint is formed between two rigid bodies that are not otherwise connected, the *connectivity* of that joint is the number of degrees of freedom of motion of (either) one of the two bodies joined relative to the other.

The *mobility* of a mechanism is the minimum number of coordinates needed to specify the positions of all members of the mechanism relative to a particular member chosen as the base or frame.

The mobility, or number of degrees of freedom of a linkage, is used to determine how many pair variables must be specified before the positions of all of the points on all of the members of the linkage can be located as a function of time. A linkage has a mobility of one or more. Traditionally, almost all linkages had one degree of freedom. However, in modern design practice, linkages with two or more degrees of freedom are becoming very common. Coordination to achieve a desired motion is then done using actuators that are digitally controlled. How this is done is discussed in [Chapter 17](#). If the mobility is zero or is negative, as determined by the constraint equations developed below, the assemblage is a structure. If the mobility is zero, the structure is statically determinate. If the mobility is negative, the structure is statically indeterminate.

To compute the mobility, let us consider the planar case first and then extend the results to the spatial case. As indicated in [Figure 1.17](#), in the plane, a body moving freely has three degrees of freedom. Suppose that in a given linkage, there are n links. If they are all free to move independently, the system has mobility $3n$. If one link is chosen as the frame link, it is fixed to the base reference frame and loses all of its degrees of freedom. Therefore the total mobility of the system is $3(n - 1)$ with no joints formed between the members.

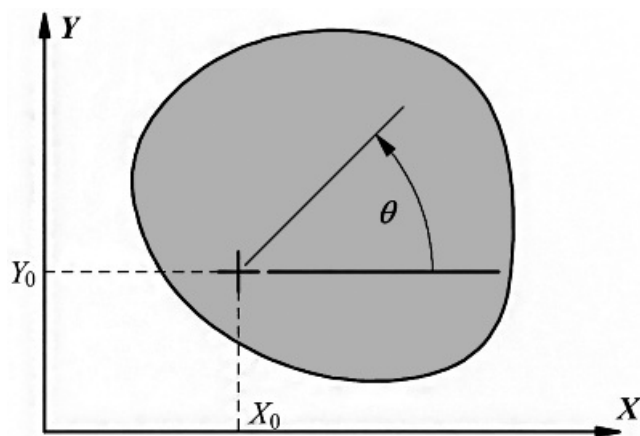


[Figure 1.17](#) One set of three coordinates that can be used to describe planar motion. The number of degrees of freedom of a body is the number of independent coordinates needed to specify its position. Therefore, a body moving freely in a plane has three degrees of freedom.

If a joint with connectivity f_i (f_i degrees of freedom) is formed between two bodies, the mobility of the system is diminished since those two bodies originally had three degrees of freedom of motion relative to one another. After

formation of the joint, they have only f_i degrees of freedom of relative motion. Hence the reduction in the system mobility is $3 - f_i$. If joints continue to be formed until there are j joints, the loss of system mobility is

$$(3 - f_1) + (3 - f_2) + \dots + (3 - f_j) = \sum_{i=1}^j (3 - f_i) = 3j - \sum_{i=1}^j f_i$$

Then the total mobility of the linkage will be

$$M = 3(n - 1) - \left(3j - \sum_{i=1}^j f_i\right) = 3(n - j - 1) + \sum_{i=1}^j f_i \quad (1.1)$$

[Equation 1.1](#) is called a constraint criterion. There are many different-appearing versions of this relationship to be found in the literature. They all, in fact, are equivalent to one another, except that some are restricted to a subset of the cases covered by [Equation 1.1](#).

A problem arises in some cases in which the same joint apparently connects more than two members. Typically, three or more members are pinned together by the same shaft and are free to rotate relative to one another about the same revolute axis. This difficulty is readily resolved if we recall that a kinematic joint is formed by contact between the surfaces of *two* rigid bodies. This is the reason for Reuleaux's name "pair" for what we here call a "joint." Considering the present case, we see that there is not one joint but several between the bodies. In fact, if p members are connected at a "common" joint, the connection is equivalent to $p - 1$ joints all of the same type. Inclusion of this number in j , and $(p - 1)f$ in the connectivity sum of [Equation 1.1](#) will ensure correct results. This is illustrated in Example 1.3.



Example 1.1

Degrees of Freedom in a Simple Four-Bar Linkage

Determine the mobility of the planar four-bar linkage shown in [Figure 1.18](#).

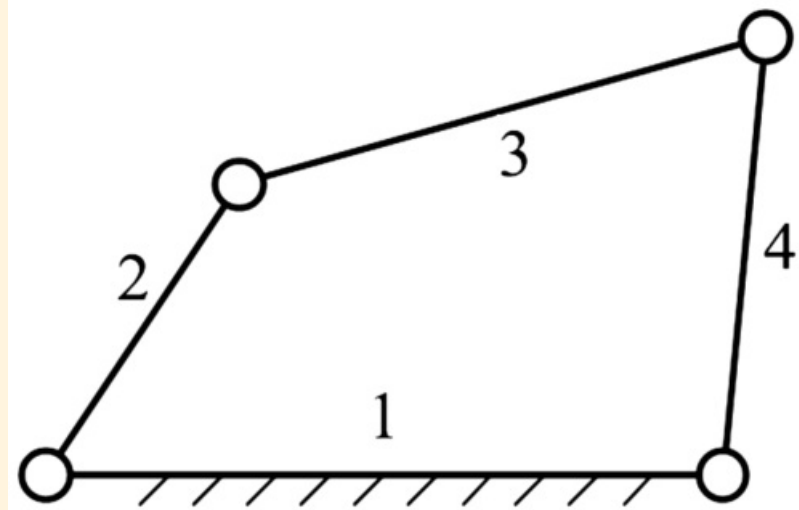


[Figure 1.18](#) Mechanism for Example 1.1.

Solution:

$$n = j = 4$$

$$\sum_{i=1}^j f_i = j \times 1 = 4$$

$$M = 3(n - j - 1) + \sum_{i=1}^j f_i = 3(4 - 4 - 1) + 4 = 1$$

A special case that deserves attention occurs when the mobility in [Equation 1.1](#) is set to one and all joints have connectivity one ($f_i = 1$). Then, [Equation 1.1](#) gives

$$M = 3(n - j - 1) + \sum_{i=1}^j f_i = 3(n - j - 1) + j = 1$$



Example 1.2

Degrees of Freedom in a Complex Mechanism

Determine the mobility of the linkage shown in [Figure 1.19](#). The linkage is planar and all joints have connectivity one.

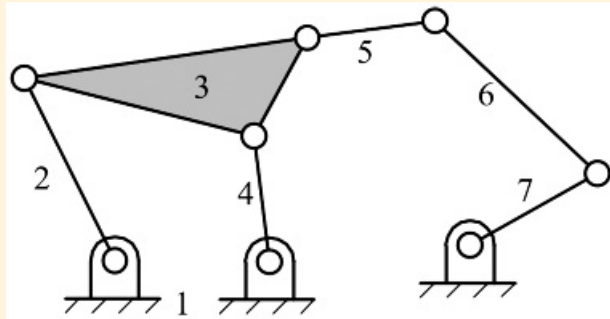


[Figure 1.19](#) Two-loop planar linkage model for Example 1.2.

Solution:

Notice that the base member must always be counted even when it is not shown in the same way as the other members but just by a set of “bearing mounts.” The solution is

$$\begin{aligned}n &= 7; j = 3 \\ \sum_{i=1}^j f_i &= j \times 1 = 3 \\ M &= 3(n - j - 1) + \sum_{i=1}^j f_i = 3(7 - 3 - 1) + 3 = 2\end{aligned}$$



Example 1.3

Degrees of Freedom When Joints Are Coincident

Determine the mobility of the linkage shown in [Figure 1.20](#). The linkage is planar and all joints have connectivity one. Links 3, 4, and 5 are connected at the same revolute joint axis.

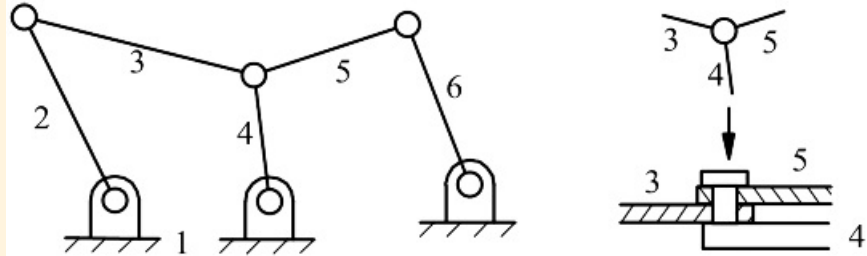


[Figure 1.20](#) Mobility analysis of a linkage when more than two members come together at a single point location.

Solution:

When p members are connected at the same joint axis, then $p - 1$ joints are associated with the same axis. Hence the location where links 3, 4, and 5 come together counts as two revolute joints. As indicated in [Figure 1.20](#), members 3 and 5 can be thought of as being connected to link 4 by two separate revolute joints that have the same axis of rotation. The solution to the problem is

$$n = 6; j = 7$$

$$\sum_{i=1}^j f_i = j \times 1 = 7$$

$$M = 3(n - j - 1) + \sum_{i=1}^j f_i = 3(6 - 7 - 1) + 7 = 1$$



Example 1.4

Degrees of Freedom for a Mechanism Containing a Higher Pair

Determine the mobility of the linkage shown in [Figure 1.21](#). The linkage is planar and not all of the joints have connectivity one.

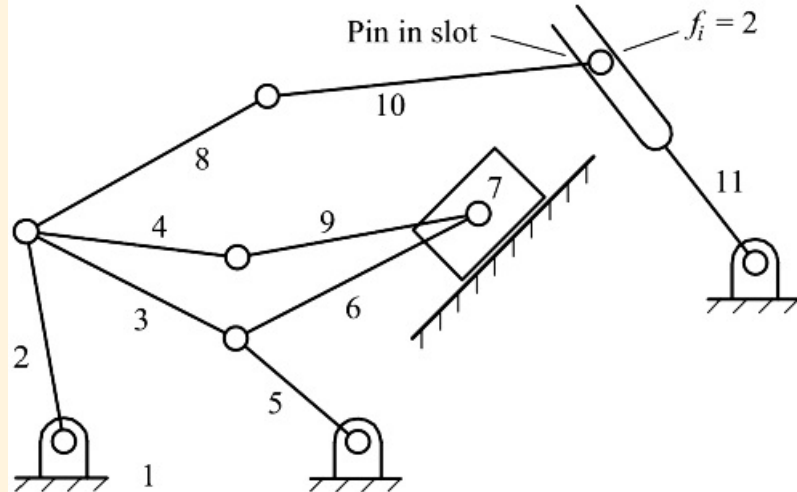


[Figure 1.21](#) Mobility analysis of a linkage with various types of joints.

Solution:

In this mechanism, there are three places where more than two links come together at the same revolute joint location. In addition, there is a pin-in-a-slot joint that permits two degrees of freedom (connectivity equals 2). Therefore, the joints must be counted carefully. When this is done, we find n and j to be

$$n = 11, j = 14$$

and

$$\sum_{i=1}^j f_i = 13 \times 1 + 1 \times 2 = 15$$

Then

$$M = 3(n - j - 1) + \sum_{i=1}^j f_i = 3(11 - 14 - 1) + 15 = 3$$

or

$$3n - 2j = 4 \quad (1.2)$$

Because n and j are integers, n must be even because 4 and $2j$ are both even numbers. This is an example of a

Diophantine equation. That is, one that admits only integral solutions. Written as an expression for j in terms of n , the equation becomes

$$j = 3n/2 - 2$$

Some of the possible solutions are listed in [Table 1.4](#). In each case, the joints may be either revolute or prismatic joints, since they are the only lower-pair joints that can properly be included in planar linkages.

[Table 1.4](#) Different Integer Solutions to [Equation 1.2](#) for Mobility of One

Solution Number	n	j	Number of Configurations
1	2	1	1
2	4	4	1
3	6	7	2
4	8	10	16
5	10	13	230
6	12	16	6856

Solution 1 gives the rather trivial case of two bodies connected by a single revolute or slider joint. This is shown in [Figure 1.22\(a\)](#). Actually, this mechanism is very common. For example, a door, its hinges, and the doorframe form an open kinematic chain and a mechanism of this type.

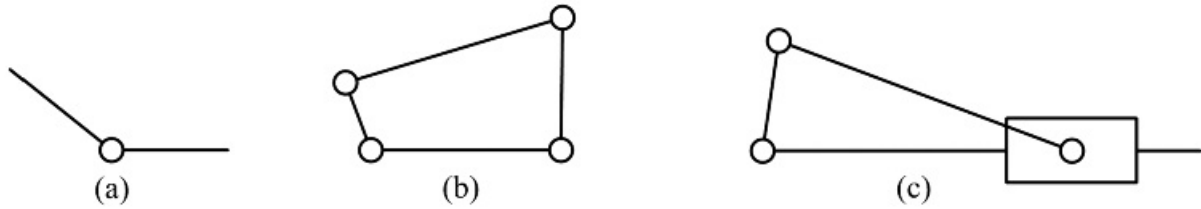


[Figure 1.22](#) Solutions of the planar mobility equation for $M = 1$ when $n = 2$ and $n = 4$.

Solution 2 gives a single, closed loop of four members with four joints. Two forms are shown in [Figure 1.22\(b\)](#) and [1.22\(c\)](#). The one in [Figure 1.22\(b\)](#) is the planar four-bar linkage that forms a major element in planar linkage theory. The one in [Figure 1.22\(c\)](#) is the slider-crank linkage, which has also been extensively studied.

Solution 3 presents two new features: First members with more than two joints mounted on them appear. Second, even when only revolute joints are included, there are two possible, topologically distinct, configurations of six members with seven joints. These are respectively named the Watt and Stephenson six-bar chains and are shown in [Figure 1.23](#).

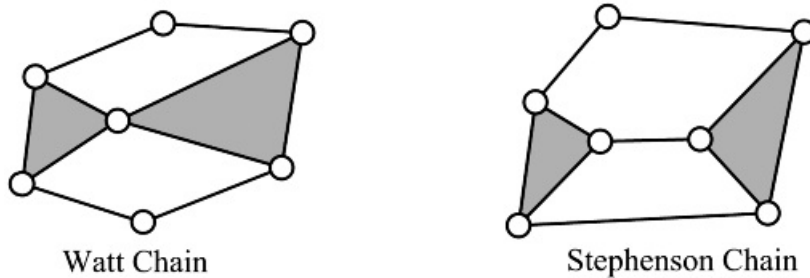


[Figure 1.23](#) The two solutions of the planar mobility equation for seven revolute joints. $M = 1$ and each kinematic chain has six members.

Solution 4 gives 16 possible different topological configurations (shown in [Figure 1.24](#)), and solution 5 gives 230. The number increases very rapidly with larger numbers of members. For example, solution 6 gives 6856

configurations [5].

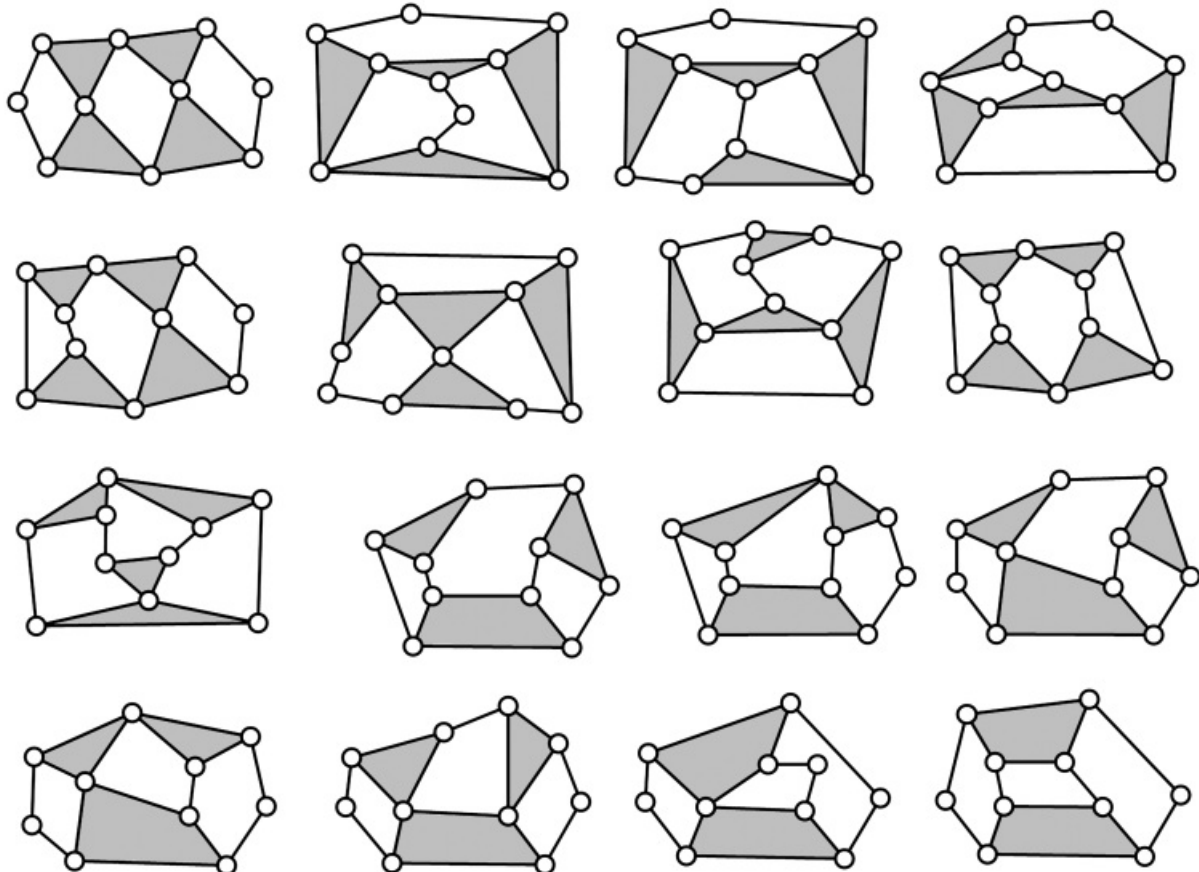


[Figure 1.24](#) The 16 solutions of the planar mobility equation for 10 revolute joints. $M = 1$ and each kinematic chain has eight members.

From the above, it should be apparent why we spend so much effort on the design of four-link mechanisms. The four-link arrangement is the simplest possible nontrivial linkage. It turns out that most design requirements can be met by four- or six-link mechanisms.

Note that, in the previous discussion, the type of the joints was not specified. All that was specified was that the joints have connectivity one and that the linkage is planar and has mobility one. Although the joints pictured in Figures. [1.22–1.24](#) are all revolute, rolling contact joints could be substituted for any of the joints, and prismatic joints could be substituted for some of them. Thus, even if the joints are confined to lower pairs, the four-link, four-joint solution represents the four different chains shown in [Figure 1.25](#). The scotch yoke, based on the 2R-2P chain, is shown in [Figure 1.26](#).

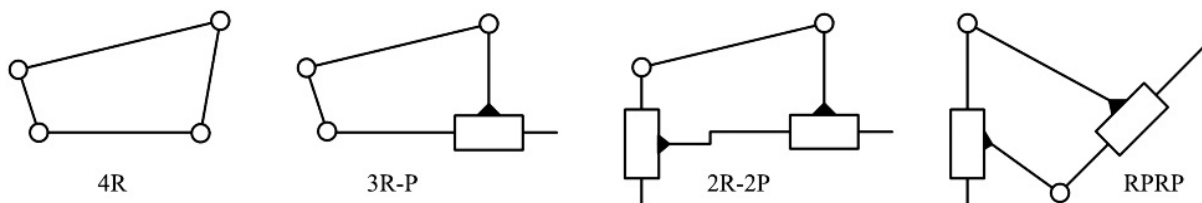


[Figure 1.25](#) Four different forms of four-bar chains with combinations of revolute and prismatic joints.

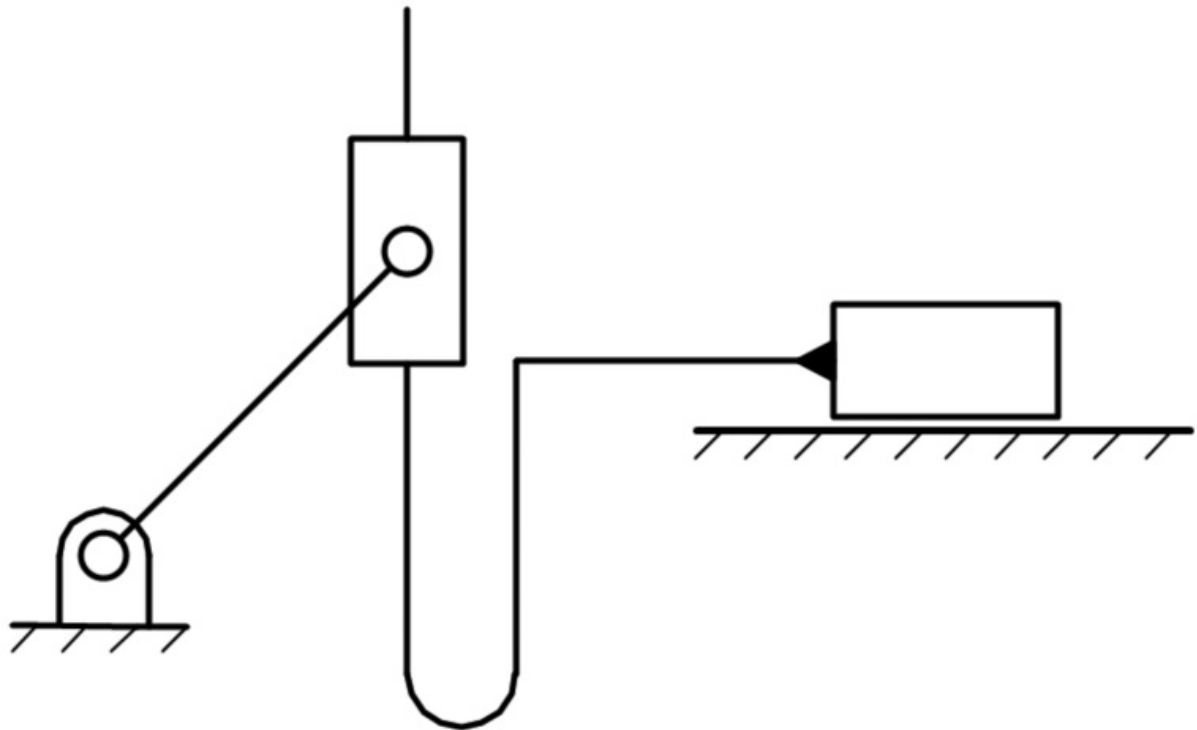


[Figure 1.26](#) The 2R-2P chain as a scotch-yoke mechanism.

Furthermore, as discussed later in this chapter, the important concept of inversion generates several different linkages from any mechanism based on the 3R-P and 2R-2P chains. An inversion is a different mechanism derived from a given mechanism or linkage. “Different” means that the motion relative to the frame that can be produced by the inversion is different from that provided in the original mechanism, that is, the inversion produces a different general form for the paths of points on the different links or a different input-output function.



1.8 Constraint Analysis of Spatial Linkages

In spatial motion, each body that moves freely has six degrees of freedom rather than three. Using exactly the same reasoning as was used in the planar case, the constraint criterion equation becomes

$$M = 6(n - j - 1) + \sum_{i=1}^j f_i \quad (1.3)$$

This is called the Kutzbach criterion. If only lower pair joints are involved, each with connectivity one, the equation becomes

$$M = 6(n - j - 1) + j = 6n - 5j - 6$$

If the linkage is required to have mobility one, this gives

$$6n = 7 + 5j \quad (1.4)$$

[Equation 1.4](#) corresponds to [Equation 1.2](#) derived in the case of planar motion. Like that equation, it is a Diophantine equation that admits only integral values of the variables. Evidently, j must be odd because $5j$ must be odd to combine with the odd number 7 to produce the even number $6n$. The sum $7 + 5j$ must also be divisible by three. Solutions to [Equation 1.4](#) are a little harder to generate than those of [Equation 1.2](#). The simplest solution is given by $j = 1$ and $n = 2$. This is exactly the same as the simplest solution in the planar case depicted in [Figure 1.22\(a\)](#). The next allowable solution is $j = 7$ and $n = 7$. This is a single, closed loop with seven members and seven joints. It bears the same relationship to general spatial linkage topologies that the planar four-bar linkage does to planar ones. The next order solution is $j = 13$, $n = 12$. There are three distinct topological forms in this case. For spatial mechanisms, the complexity increases with the number of members and joints even more rapidly than it does for planar mechanisms.



Example 1.5

Degrees of Freedom in a Spatial Mechanism

Determine the mobility of the linkage shown in [Figure 1.27](#). The linkage is spatial. The joints are lower pairs of the types labeled.

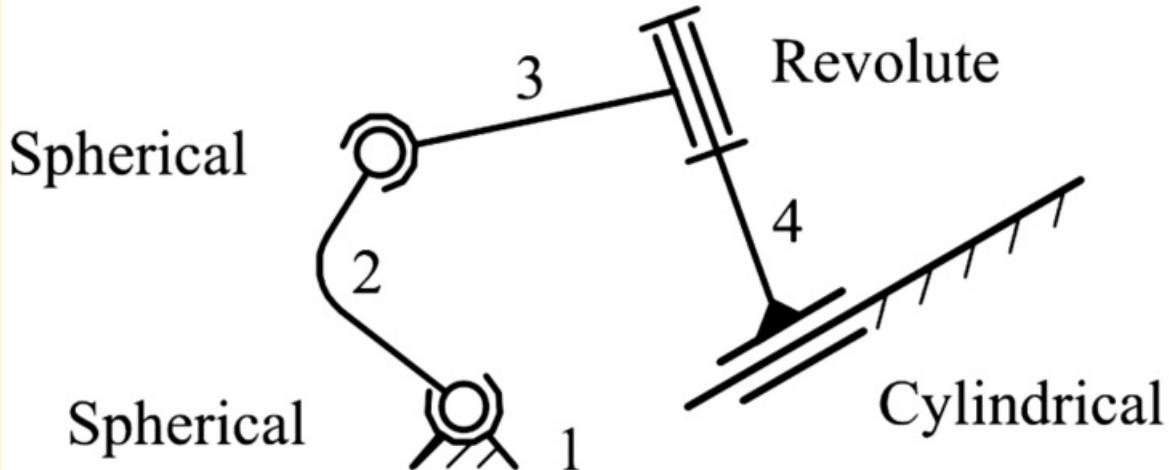


[Figure 1.27](#) A four-member, single loop, spatial linkage.

Note how the three-dimensional joints are drawn. There is no formalism that is more or less universally recognized for representing spatial mechanisms as there is for planar linkages; however, we will follow the symbols shown in [Table 1.1](#).

Solution:

$$n = j = 4$$

$$\sum_{i=1}^j f_i = 2 \times 3 + 1 \times 1 + 1 \times 2 = 9$$

$$M = 6(n - j - 1) + \sum_{i=1}^j f_i = 6(4 - 4 - 1) + 9 = 3$$

Another way of looking at the constraint criterion is in terms of closures. Imagine building up the linkage by starting with the base link and successively adding members and joints. If a joint connects an additional member to the system, the number of degrees of freedom is increased by f_i , if f_i is the connectivity of that joint, and the numbers of members and joints are both increased by one. If a joint is made between two members that are already part of the linkage, the total number of degrees of freedom is decreased by the number of constraints imposed by that joint. The number of constraints imposed by a joint is the number of degrees of freedom lost by the system when that joint is formed. For a spatial mechanism, it is $6 - f_i$ since two bodies have six degrees of freedom of motion relative to one another when they are free of each other and only f_i degrees of freedom of relative motion after the joint is formed. Also, in this case, the formation of the joint results in the formation of a

closed loop of members and joints within the linkage. This is called a closure. Proceeding in this manner, the mobility of the linkage can be expressed as

$$M = \sum_{i=1}^j f_i - 6c$$

where c is the number of closures. Now, when a closure is formed, the number of members does not increase, whereas the number of joints increases by one. If there are no closures (open kinematic chains), the number of link members is given by

$$m = i - 1$$

the additional member being the base member. Therefore, if there are c closures in the linkage

$$z = s + 1 - \eta$$

Thus, substitution for c in the expression for the mobility leads to [Figure 1.28](#). The relationship among c , j , and n is illustrated in the figure.

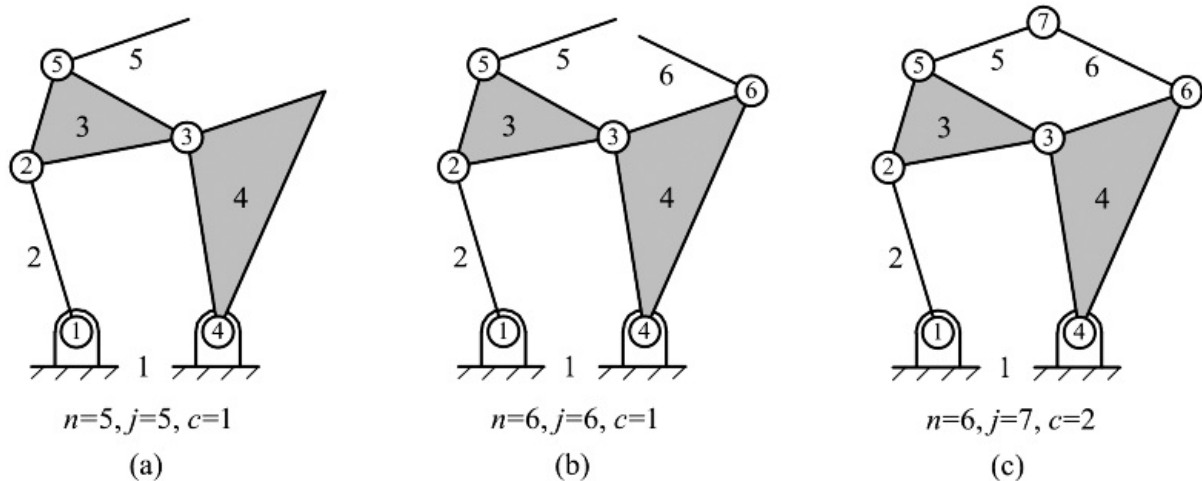


[Figure 1.28](#) The effect of adding a member to a linkage together with a joint (b) and of adding a joint without an additional member (c). Adding a joint without a member always closes a loop within the linkage.

The reason for looking at the constraint criterion from this viewpoint is that it relates to the position analysis of a spatial linkage. When a closure is formed, a set of six algebraic equations called *closure* equations can be written. The formulation of these equations will be briefly treated in [Chapter 9](#), although their study is largely beyond the scope of this book. The quantity $6c = 6(j + 1 - n)$ is therefore the number of equations available for position analysis of the mechanism. The variables in those equations are the joint parameters, the variables needed to fix the relative positions of the bodies connected by each joint. There are f_i of these joint parameters for joint i . Therefore the total number of variables in the linkage is

$$\sum_{i=1}^s f_i$$

In this way, it may be seen that Equation 1.3 expresses the mobility of the linkage as the number of variables less

the number of equations for the system.

Yet another viewpoint on the constraint criterion that is productive to pursue is that of static force analysis. Free body diagrams can be drawn for all members except the base. Six static equilibrium equations can be written for each free body. Hence there are $6(n - 1)$ equations describing the system. At each joint there is a number of reaction force and torque components that is equal to the number of constraints of that joint. These force components are the variables in a static force analysis. Since the number of constraints at joint i is $6 - f_i$, the number of variables is

$$\sum_{i=1}^j (6 - f_i) = 6j - \sum_{i=1}^j f_i$$

Therefore, the difference between the number of variables and the number of equations is

$$6j - \sum_{i=1}^j f_i - 6(n - 1) = -M$$

Thus, the mobility is meaningful from the point of view of static force analysis also. If $M = 0$, the linkage is not movable and is a structure. The position problem can be solved to obtain the joint positions that cannot vary. The static equilibrium problem can be solved for all of the reaction force and torque components. The structure is statically determinate since there is a unique solution to the static equilibrium problem.

If the mobility is -1 , the number of equations for the position problem exceeds the number of variables. Therefore, in general there is no solution to the position problem. For a solution to exist, it is necessary for the equations to be dependent. This means that the geometry of the mechanism must satisfy the conditions needed for the equations to be dependent. Physically, this means that, in general, it is not possible to assemble the linkage. One or more of the closures cannot be made. However, if the link geometry is changed to bring the surfaces for the closing joint into alignment, the linkage may be assembled.

From the viewpoint of force analysis, the mobility is the number of static equilibrium equations less the number of force variables: the converse of the situation for position analysis. Thus, if $M = -1$ there is one more force variable than the number of force equations. Therefore, in this case, solutions of the system exist, but there is no unique solution. The force problem cannot be solved without additional information relating the forces in the system. The linkage is a statically indeterminate structure. If the links are modeled as elastic, rather than rigid solids, compatibility of their deflections under load provides the necessary additional relationships.

Conversely, if the mobility is one or more, the number of position variables is greater than the number of position equations. Solutions to the system exist, but there is no unique solution. The number of force equations is greater than the number of force variables, so, in general, no solution to the static force problem exists. In practice, application of an arbitrary set of loads to the linkage would lead to rapid, uncontrolled acceleration, and the system behavior could not be described without writing dynamic equations. However, this invalidates the assumption of a static model.

Specification of the value of a joint parameter is equivalent to fixing that joint. Physically, putting an actuator on that joint which would hold it in position might do it. The joint can now support a force, or torque. The effect is to increase the number of unknown force variables by one. If a linkage has mobility one, fixing the position of a joint with connectivity one converts it into a structure. It also converts the static force problem from one in which there is one more equation than there are variables to one in which the number of variables is the same as the number of equations. That is, it is statically determinate.

Fixing the torque applied about a revolute joint, or the force applied by an actuator at a prismatic joint, has a quite different effect. It does not change the number of variables or the number of equations in either the position or the force problem. This is because having a passive joint is already equivalent to fixing the force or torque variable

about that joint. The torque applied at a passive revolute joint is fixed to zero. Changing it to any other value does not affect the number of unknown variables. It does, however, affect the values of the unknown force variables.

This is important in practical applications of multiply actuated mechanisms. Consider the manipulator arm shown in [Figure 1.29](#). It has seven members (italic numbers) and six joints. The red dashed lines with bold numbers indicate the joint axes. Joints 1, 2, 4, 5, and 6 are revolute joints. Joint 3 is a prismatic joint. The axes of joints 3 and 4 are the same. Member one is the base member.

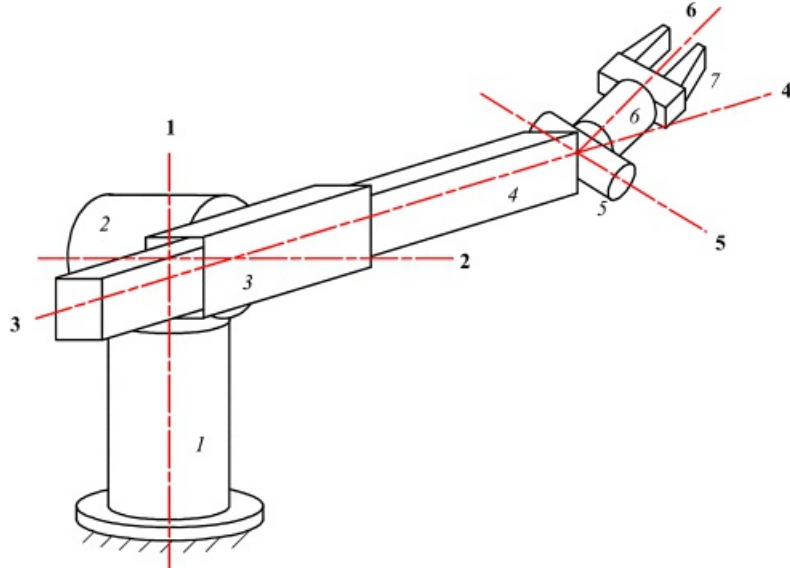


[Figure 1.29](#) A robotic manipulator that is used to produce general spatial motions of its gripper.

Applying the constraint criterion to this mechanism, we have: $n = 7, j = 6, \sum_{i=1}^j f_i = 6$ so

$$M = 5(n - j - 1) + \sum_{i=1}^j f_i = 5(7 - 6 - 1) + 6 = 6$$

If we actuate all of the joints so that we can specify their positions, the position of the mechanism is uniquely specified.

Consider now what happens if the manipulator grips an object that is fixed relative to the base member, as is shown in [Figure 1.30](#). It is assumed that the gripper grasps the object tightly so that no relative motion is possible. The effect is to make link 7 a part of link 1. Therefore, application of the constraint equation gives $n = 6, j = 6$,

$$\sum_{i=1}^j f_i = 6 \text{ so}$$

$$M = 5(n - j - 1) + \sum_{i=1}^j f_i = 5(6 - 6 - 1) + 6 = 0$$

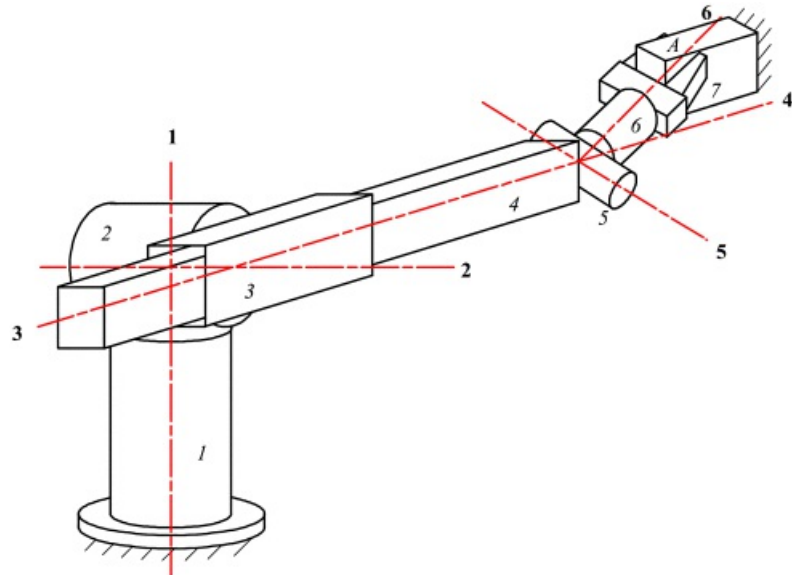


[Figure 1.29](#) The robotic manipulator of [Figure 1.29](#) gripping a fixed object. If the gripper grasps the object so that no relative motion is possible, the gripper becomes fixed to member one. This reduces the number of members in the system to six and closes a loop.

The mechanism is now a structure, and we do not have the liberty of setting the joint variables to any value we wish. Attempting to control the mechanism by commanding joint positions, as is done when the manipulator is moving freely, is not effective in this case. Since most manipulator structures are very stiff, a small position error results in very large forces on the actuators. The usual result is that the actuator controllers become unstable, producing violent vibratory behavior. However, if the actuators are commanded to produce specified forces or torques, there is no problem. The actuator torques and forces can be set to any desired set of values. In this way it is possible to apply a specified force system to the fixed object *A* by means of the manipulator. Notice that commanding forces and torques all the time is not a solution. If actuator forces are commanded when the manipulator is moving freely, the number of static equilibrium equations exceeds the number of variables by six and the manipulator will perform rapid uncontrolled movements, violating the assumption of static stability.



1.9 Idle Degrees of Freedom

Equation 1.4 sometimes gives misleading results. There are several reasons for this. One is the phenomenon of idle degrees of freedom. Consider the linkage shown in Figure 1.31. This linkage has four members and four joints. Two of the joints are revolutes. The other two are spherical joints. This mechanism is quite often used in situations such as the steering mechanisms of automobiles. Applying the constraint criterion, we have $n = 4$, $j = 4$ so

$$\sum_{i=1}^j f_i = 2 \times 1 + 2 \times 3 = 8$$

Therefore

$$M = 5(n - j - 1) + \sum_{i=1}^j f_i = 5(4 - 4 - 1) + 8 = 2$$

Nevertheless, practical experience with this mechanism shows that there is a unique value of the output joint angle, ϕ , for any given value of the input angle, θ . How can this be explained?

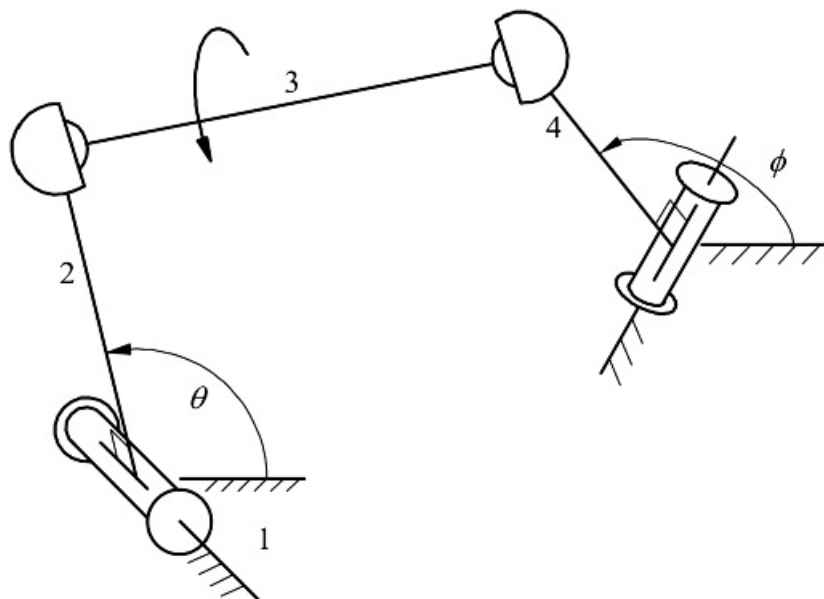


Figure 1.31 A spatial four-member, four-joint linkage. Two of the joints are revolutes. The other two are spherical joints. θ is the input joint angle and ϕ is the output joint angle. The linkage has an idle degree of freedom since member 3 can spin about the line joining the centers of the spherical joints without affecting the relationship between θ and ϕ .

Examination of the mechanism reveals that the coupler member is free to spin about the line through the centers of the two spherical joints. This motion can take place in any position of the linkage without affecting the values of the input and output joint angles. It is what is termed an idle degree of freedom. That is, it is a degree of freedom that does not affect the input-output relationship of the linkage.

The real problem here is that usually we are not really interested in the mobility of the entire linkage, that is, of all of its links. Rather, we are interested in the connectivity that the linkage provides as a joint between two of its members. This is a new use of the term *connectivity*. Previously we applied it only to simple joints at which the members contact each other directly. However, a mechanism constrains the number of degrees of freedom of

relative motion of any two of its members. Therefore it can be regarded as forming a kinematic joint between any two of its members. We can define its connectivity as a joint between those members and as the number of degrees of freedom of relative motion that it permits between the members.

In the example of [Figure 1.31](#), the connectivity of the linkage as a joint between the input and output members is one, even though the mobility of the linkage is two, and the connectivity between links 3 and 1 is two. The mobility places an upper bound on the connectivity of the mechanism as a joint between any two of its members. There is no simple method of directly determining connectivity, so the mobility equation is used. If the mobility is one and the linkage is predictable by means of [Equation 1.3](#), there is no problem. The connectivity of the linkage as a joint between any two of its members is also one. If the mobility is greater than one, strictly speaking, all that can be said is that the connectivity between any given pair of members may be equal to the mobility or may be less than that number. Fortunately, idle degrees of freedom can usually be identified by inspection.

Another example is shown in [Figure 1.32](#). This is one form of the Stewart-Gough platform mechanism, discussed in detail in [Chapter 9](#). This mechanism is commonly used to produce general spatial motions in aircraft simulators for training pilots. The output member is connected to the base by six “limbs,” each of which has an actuated prismatic joint in the middle and two spherical joints at either end. There are 14 members: 2 in each of the limbs plus the base and output members. There are 18 joints: 6 prismatic joints and 12 spherical joints. Hence

$$\sum_{i=1}^j f_i = 6 \times 1 + 12 \times 3 = 42$$

Therefore

$$M = 6(n - j - 1) + \sum_{i=1}^j f_i = 6(14 - 18 - 1) + 42 = 12$$

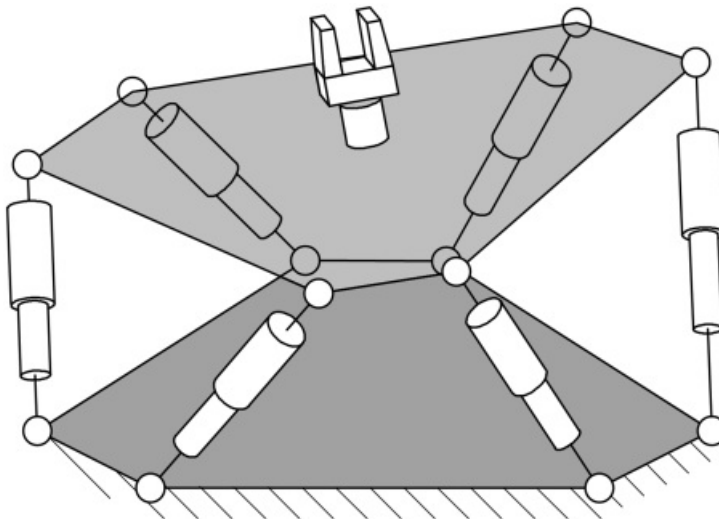


[Figure 1.32](#) A Stewart-Gough platform. The upper and lower members are plane hexagons connected by six limbs, each having an actuated prismatic joint. The limbs are connected to the upper and lower hexagons by spherical joints.

However, it is easily seen that each limb is free to spin about the line joining the centers of its spherical joints without affecting the position of the output member relative to the base. Therefore, the mechanism has six idle degrees of freedom, and its connectivity as a joint between base and output member is

$$C = M - \delta = \delta$$

By positioning the actuated prismatic joints, the output member can be placed in any position within its working volume.

While idle degrees of freedom are most common in spatial linkages, they can also occur in planar linkages. Typically, this occurs when cam roller followers are involved. For example, if the mobility of the linkage in [Figure 1.33](#) is computed, it will be found to be 1 if there is rolling contact between the roller (link 5) and the cam (link 6) at point *B*. However, if there is cam contact at *B*, the mobility will be 2. The extra degree of freedom is associated with the free rotation of link 5 relative to the frame. Usually, this rotation will be of no interest because the motion of all of the other links in the mechanism will be unaffected by this rotation.

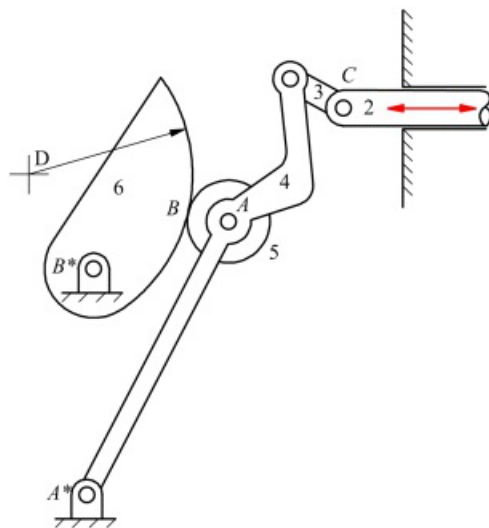


[Figure 1.33](#) A planar mechanism with an idle degree of freedom. The roller follower can rotate without affecting the relative positions of the other members.

To locate the idle degrees of freedom, it is first necessary to identify the input link and output link. Then check to determine if a single link or a combination of connected links can move without altering the relative position of the input and output links. Idle degrees of freedom are dependent both on geometry and on the choice of the input and output links. In some cases, idle degrees of freedom will exist for one choice of input/output but not for a different choice.



1.10 Overconstrained Linkages

A second reason why the constraint criteria—[Equations 1.1](#) and [1.3](#)—sometimes give misleading results is the phenomenon of *overconstraint*. A mechanism can be overconstrained either locally or generally. If the mechanism is overconstrained locally, a portion of the system may be a structure, but the entire mechanism can move. When this happens, we must replace that portion of the linkage with a single rigid body and recompute the mobility of the mechanism. An example is shown in the planar system of [Figure 1.34\(a\)](#).

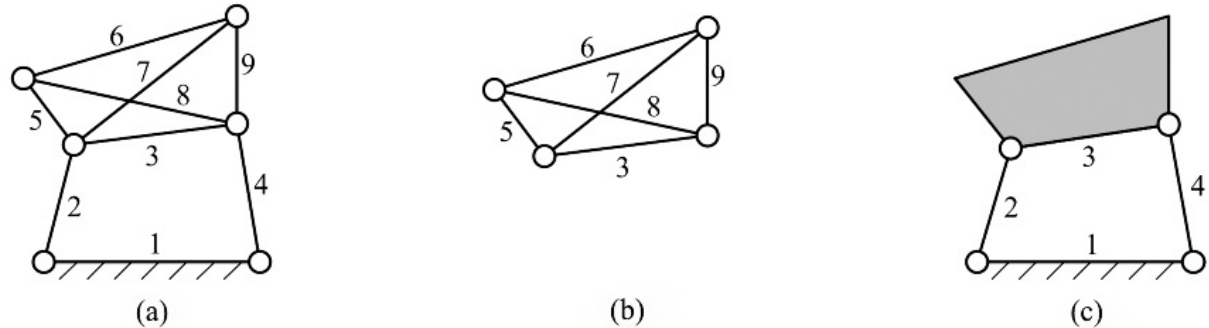


[Figure 1.34](#) (a) A planar mechanism in which part of the mechanism is a structure, leading to a misleading value of mobility. All joints are revolutes. (b) The part of the mechanism that is a statically indeterminate structure. (c) A modified model of the linkage that gives the correct mobility value.

Here $n = 9$ and $j = 2 \times 1 + 2 \times 2 + 2 \times 3 = 12$. Note that there are two joints at which three members are connected and two at which four members are connected

$$\sum_{i=1}^j f_i = j = 12$$

Hence

$$M = 3(n - j - 1) + \sum_{i=1}^j f_i = 3(9 - 12 - 1) + 12 = 0$$

However, it is obvious that the portion of the linkage consisting of members 3, 5, 6, 7, 8, and 9 is a statically indeterminate structure. This portion is shown in [Figure 1.34\(b\)](#). Here $n = 6$ and, because three members are connected at each joint location, $j = 4 \times 2 = 8$. Also

$$\sum_{i=1}^j f_i = j = 8$$

Therefore

$$M = 3(n - j - 1) + \sum_{i=1}^j f_i = 3(9 - 12 - 1) + 12 = 0$$

This reveals the statically indeterminate nature of the structure and the source of the error in the mobility value. A portion of the linkage that is a statically *determinate* structure does not cause an error in calculating mobility.

To compute a correct value of mobility, the linkage is remodeled as shown in [Figure 1.34\(c\)](#) with the portion that is a structure replaced by a single, rigid member. The linkage is now revealed to be a planar four-bar linkage for which the mobility is one.

Mechanisms, and especially spatial mechanisms, can also be generally overconstrained. [Figure 1.35](#) shows a spatial linkage with four members and four revolute joints. It has a special geometry. The opposite members are identical, and the normals to the pairs of axes in the links intersect at the joint axes. The lengths of those normals (a and b) are related to the angles between successive axes (α and β) by the relationship

$$a \sin \beta = b \sin \alpha$$

As was demonstrated over a hundred years ago by Bennett [4], this linkage has mobility one. However, if we apply the constraint criterion with $n = j = 4$ and $\sum_{i=1}^j f_i = 4$, the result is

$$M = 6(n - j - 1) + \sum_{i=1}^j f_i = 6(4 - 4 - 1) + 4 = -2$$

In this case, because of the special geometry, the position equations of the linkage turn out to be dependent in all positions. For this reason, the effective number of equations is only three, rather than the six that would be expected for a single closed spatial loop. Because the constraint criterion calculates the difference between the number of position variables and the number of available equations, it miscounts the mobility by three degrees of freedom. It turns out that a rather large number of linkages have anomalous mobility like the Bennett mechanism. Another example is the linkage shown on [Figure 1.16](#). Here $n = 6$ and $j = 6$, so M should be 0, yet the mechanism is movable with one degree of freedom. Such linkages are called overconstrained linkages. Many of these are largely curiosities. However, there are several very important families of overconstrained linkages that are exceedingly common in engineering practice.

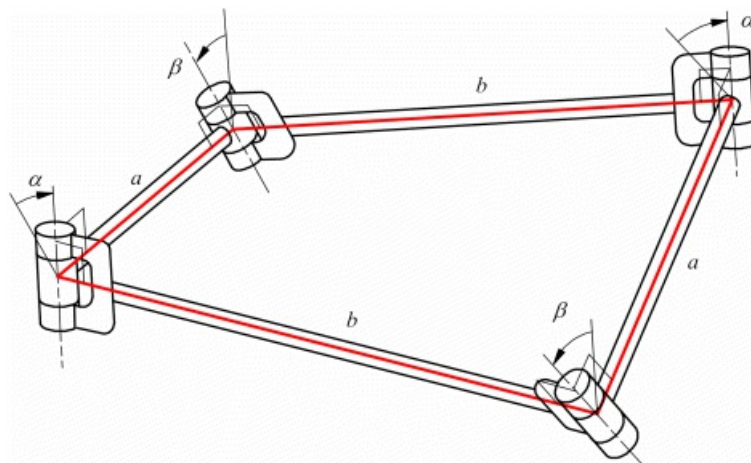


[Figure 1.35](#) The Bennett mechanism is a spatial four-bar linkage that is movable despite violating the constraint criterion. The side lengths and twist angles obey the relationship $a \sin \beta = b \sin \alpha$.

The most common example of overconstraint is the family of planar linkages. There is no *a priori* reason why planar linkages should not obey the general spatial mobility criterion. Nevertheless, as we saw in Section 1.7, they do not. [Equation 1.3](#) gives a value for M that is always $3c$ less than the correct value, where c is the number of independent closure equations for the linkage. The fact that planar linkages obey [Equation 1.1](#), that has the same form as [Equation 1.3](#) but with the coefficient 6 replaced by 3, indicates that only three of the six equations produced by any closure are independent for a planar linkage.

Another common family of overconstrained linkages is the family of spherical linkages. These are linkages whose

joints are all revolutes. The axes of those joints all pass through a single point. [Figure 1.36](#) shows a spherical four-bar linkage.

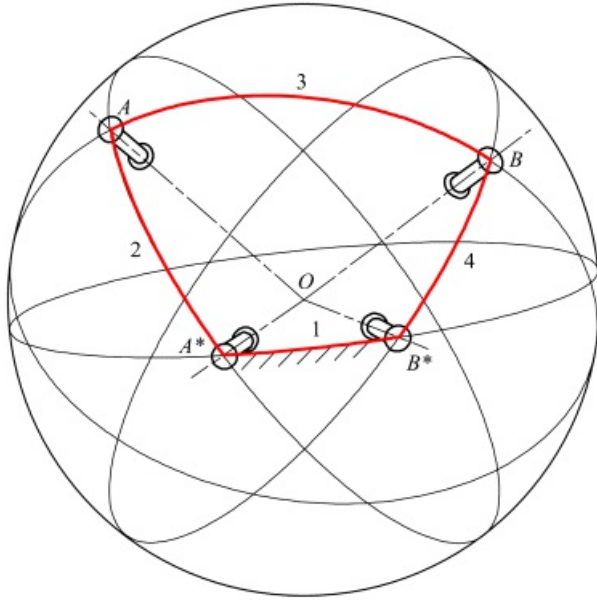


[Figure 1.36](#) A spherical four-bar linkage. Here the axes of the four revolute joints intersect at a single point, O .

Spherical linkages obey the same form of constraint criterion as planar linkages and the Bennett linkage. Thus, three of the equations resulting from each closure in a spherical linkage are always dependent.

Compared with properly constrained linkages (those that obey [Equation 1.3](#)) overconstrained linkages have properties that are different in important and practical ways. They tend to be much stiffer and stronger in supporting loads, particularly those orthogonal to the direction of motion at the point of application. However, they are sensitive to dimensional accuracy in their members. This requires manufacture to relatively tight tolerances, which can increase cost. Conversely, properly constrained linkages are completely insensitive to link geometry, as far as mobility is concerned. This means that, in lightly loaded situations, they can absorb abuse that deforms links and still function, at least after a fashion. This is an important property in situations such as the control linkages of agricultural machinery. In heavily loaded situations, the design engineer will often deliberately increase the degree of overconstraint to improve stiffness and strength. An example is the bucket support linkage of a front-end loader. A photograph of the loader is shown in [Figure 1.37](#), and one of the bucket support linkages is identified in [Figure 1.38](#).



[Figure 1.37](#) A front-end loader. If analyzed using the planar mobility equations, the mechanism will be found to have less than one degree of freedom. Parallel actuators are used on both sides of the machine to balance the load and increase stiffness. The loader part of the machine has two degrees of freedom.

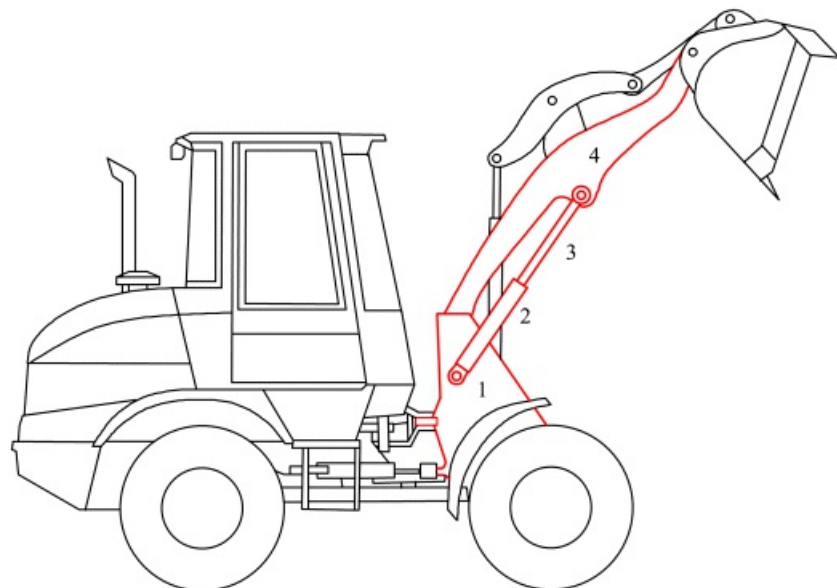


[Figure 1.38](#) Schematic drawing of the bucket-support linkage for a front-end loader similar to that shown in [Figure 1.37](#).

In principle, only one of the two planar-inverted, slider-crank linkages is needed to lift/support the bucket. In this case, we would have

$$n_s = j = \sum_{i=1}^j f_i = 4$$

and

$$M = 6(n - j - 1) + \sum_{i=1}^j f_i = 6(4 - 4 - 1) + 4 = -2$$

Since the true mobility is 1, the degree of overconstraint is $1 - (-2) = 3$. However, the mechanism is doubled up with identical linkages supporting each end of the bucket. This gives $n = 7$ and $j = \sum_{i=1}^j f_i = 8$. Thus

$$M = 6(n - j - 1) + \sum_{i=1}^j f_i = 6(7 - 8 - 1) + 8 = -4.$$

Therefore, for the doubled linkage the degree of overconstraint is $1 - (-4) = 5$. The result is a much stronger mechanism since the individual planar loops do not have to support the large out-of-plane moments that a single linkage would have to support. The cost is that the axes of the corresponding joints on both sides must be collinear to a high degree of accuracy, requiring careful manufacturing.



1.11 Uses of the Mobility Criterion

The mobility criterion is most useful to the engineer when examining an unfamiliar mechanical system. It allows a quick check to determine whether the links, joints, and actuators identified are consistent with system function. Inconsistency may indicate that some elements have been mis-identified or that passive degrees of freedom are present. As already discussed, overconstraint may also need to be considered. In particular, if the linkage is planar or spherical, the appropriate form of the constraint equation should be used in place of the general form.

It is possible to formulate expressions for the mobility that accommodate overconstrained closures of arbitrary type. These expressions are equivalent to the form

$$M = \sum_{k=1}^c b_k + \sum_{i=1}^j f_i \quad (1.5)$$

where $c = n - j - 1$ is the number of closures of the linkage.

Unfortunately, unless the values of b_k associated with the different closures can be identified by inspection, such expressions have no value. The reason is that the mobility equation gives a quick check of the number of position variables and independent equations without the need to develop those equations. However, the only way to verify an overconstrained closure of a type not identifiable by inspection is to develop the closure equations and analyze them for dependency. Therefore the quick-check advantage of the mobility equation disappears, and there is no way to derive information about the linkage without performing a complete position analysis.



1.12 Inversion

A commonly used tactic in studying mechanism kinematics is *inversion*. This is a change of the fixed reference frame from one link to another that causes different characteristics of the motion relative to the frame to become evident. For example, [Figure 1.39](#) shows the different inversions of a slider-crank linkage, and [Figure 1.40](#) shows the inversions of a pin-in-a-slot mechanism. The pin-in-a-slot inversions are often used as inexpensive substitutes for the slider-crank inversions. The motion characteristics of the coupler links for each of the mechanisms are all very different. Nevertheless, the linkage topology and the relative angular relationships among the links are the same in all cases. Therefore, useful information obtained from the study of the linkage in one inversion can be transferred to the study of other inversions. Note that in [Figure 1.39](#), the relative positions of all of the joints are the same for the position chosen. It is only when the mechanisms move that the different motion characteristics are revealed. To determine the inversions of a mechanism, it is convenient to start with the chain from which the mechanism is formed. A different linkage results whenever a different link is selected as the frame.

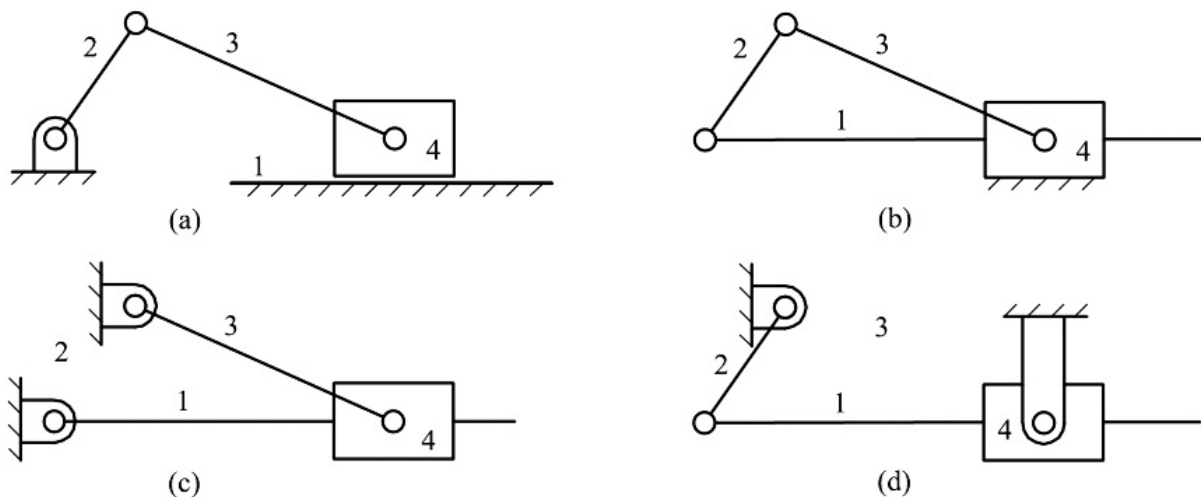


[Figure 1.39](#) Inversions of the slider-crank linkage. The linkage in (a) is the original linkage and those in (b), (c), and (d) are the inversions. Note that the motion properties of the inversions are quite different from those of the original linkage, and from each other, but yet are related in useful ways.

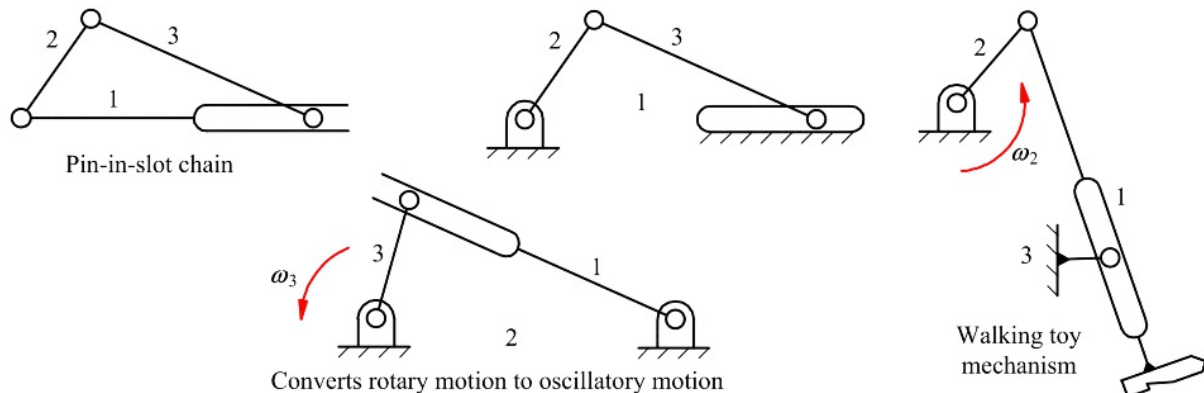


[Figure 1.40](#) Uses of inversions of a pin-in-a-slot linkage.



1.13 Reference Frames

It is necessary to be careful about reference frames when working with systems of many bodies. A reference frame can be attached to each body, and we can express positions, velocities, and accelerations relative to any or all of them.

As far as kinematics is concerned, there is no restriction on the use of reference frames. All frames are equally viable. We can invert from one frame to another without restriction.

It is only when we introduce forces and enter the realm of kinetics that a restriction appears. It is then that Newton's first and second laws, that relate motion properties to force, are true only if all motion properties are referred to a common reference frame. This common reference frame must be of a special type, called an *inertial reference frame*. For the purposes of mechanism design, the inertial reference frame is almost always fixed to the earth. There are, however, engineering problems, such as the design of mechanisms to be carried on spacecraft, for which the primary inertial reference frame must be used. The primary inertial reference frame of Newtonian mechanics is fixed relative to the fixed stars. A more complete discussion of inertial reference frames can be found in most texts on rigid-body dynamics. Einstein showed that in a space-time framework all reference frames are equally valid, thereby removing the Newtonian distinction between inertial reference frames and others. However, in the domain in which mechanical engineers usually operate, Newtonian mechanics provides a very accurate simplification of relativistic mechanics that is of great practical utility.

It is important to remember that position and motion properties can be expressed only relative to a reference frame. A habit has grown up in this subject of referring to a velocity or acceleration of a point relative to another point. This convention will be found to be convenient in some types of problems, particularly in graphical analysis, and there is no harm in using it provided that it is clearly understood that it is a shorthand expression for the velocity or acceleration of the first point relative to a *reference frame* in which the second point is fixed. The identity of that reference frame should always be kept in mind.

In some discussions in the following, it will be convenient to have a notation that explicitly states the reference frame in which a particular vector is expressed. A method that is often used is to indicate the reference frame by means of a superscript placed in front of the symbol for the vector. For example, ${}_1v_A$ indicates the velocity of point A relative to reference frame 1, and ${}_2\omega_3$ indicates the angular velocity of member 3 relative to reference frame 2.

Usually, we will associate one reference frame with each member of a linkage and will number it to agree with the number of the member. Reference frame 1 will usually refer to the fixed link. Unfortunately, the use of superscripts to indicate reference frames complicates expressions and makes them more difficult to read. For this reason, the superscripts will be dropped whenever the reference frame to which motions are referred is evident.



1.14 Motion Limits

A member of a linkage that is connected to the base by a revolute joint and that rotates completely as the linkage moves through its motion cycle is called a crank. Usually, there will also be members in the linkage that look exactly like cranks because they are connected to the base by a revolute joint, but which cannot rotate completely.

Consider the four-bar linkage shown in [Figure 1.41\(a\)](#) in which the link A^*A is a crank rotating fully about the revolute joint A^* . It will be assumed to rotate continuously in the counterclockwise direction. Complete revolution of this link requires that it pass through the positions shown in [Figure 1.41\(b\)](#) and [1.41\(c\)](#). Now consider the motion of the revolute joint B^* . Prior to reaching the position of [Figure 1.41b](#), link B^*B was rotating counterclockwise about joint B^* . In the position of [Figure 1.41\(b\)](#), further rotation of B^*B about B^* in the counterclockwise direction is not possible. B^*B comes to rest and reverses its direction of motion. Similarly, before entering the position of [Figure 1.41\(c\)](#), the link B^*B is rotating clockwise about the joint B^* . In this position, further rotation in this direction is not possible and the link comes to rest and then reverses direction. The positions shown in [Figure 1.41\(b\)](#) and [1.41\(c\)](#) are called motion limit positions for the joint B^* . The link B^*B does not perform a full rotation but simply oscillates between these positions. That is, it is not a crank, it is a rocker.

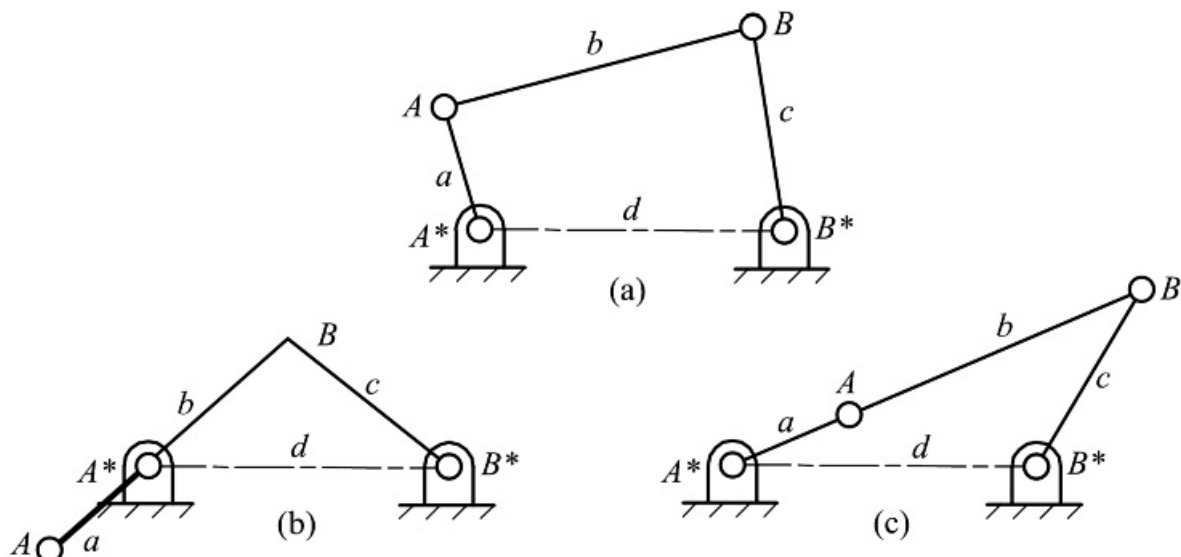


[Figure 1.41](#) The limiting positions of joint B of a four-bar linkage.

In [Figure 1.41](#), we have introduced a joint nomenclature that we will generally use throughout this book. Both rockers and cranks will contain joints that rotate about joints fixed to the frame. When possible, we will represent the moving joint and fixed joint as a set where the moving joint or pivot is designated by a letter (e.g., A), and the fixed joint or pivot is designated by the same letter with an asterisk (e.g., A^*). This nomenclature is especially useful when discussing mechanism synthesis.



1.15 Continuously Rotatable Joints

At this point it is necessary to introduce some terminology to describe the different members of a four-bar linkage. The fixed link, that is, the member to which the frame of reference is attached, is called the base or frame. The two members that are connected to the base by revolute joints are called turning links. The link that is jointed to both turning links and has no direct connection to the base is called the coupler. The turning links may be further distinguished by the terms crank, for a link capable of complete revolution relative to the base, and rocker, for a link that is only capable of oscillating between motion limits.

A linkage is actuated, or driven, by applying a force to one of its moving links or a torque about one of the axes. This may be done in a variety of ways, as is evident from the number of different types of commercial actuators ([Figure 1.42](#)). Actuators are more fully discussed in [Chapter 17](#). It is frequently convenient for the powered link to be connected to the base by a revolute joint. The linkage may then be actuated by applying a torque to that link, or, more precisely, applying a torque between the base and that link. In this case it is usually also preferable that the link be continuously rotatable since it may then be actuated by means of a continuously rotating motor. For this reason, it is important to be able to identify four-bar linkages that have continuously rotatable joints and to locate those joints. This may be done by means of a simple set of rules called Grashof's rules [2].



[Figure 1.42](#) Photographs of a variety of actuators.

Grashof distinguished two fundamentally different types of four-bar linkage by means of the inequality

$$s + l < p + q \quad (1.6)$$

where, as shown in [Figure 1.43](#), s is the length of the shortest side, l is the length of the longest side, and p and q are the lengths of the other two sides. Linkages that obey this inequality (Grashof type 1 linkages) have two joints that perform complete rotations and two that oscillate between motion limits. The two fully rotatable joints are those on the ends of the shortest link. Linkages that do not obey the inequality (Grashof type 2 linkages) have no

fully rotatable joints. All four joints then oscillate between motion limits.

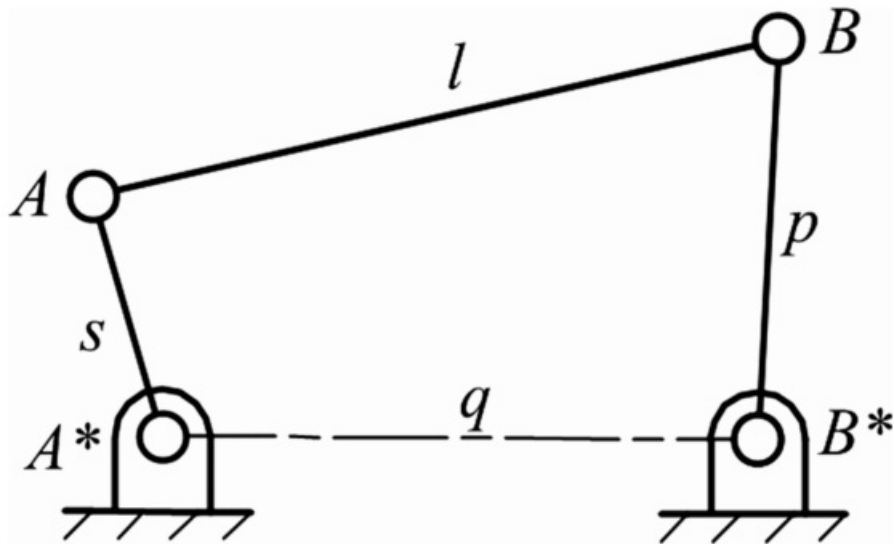


[Figure 1.43](#) The nomenclature used when discussing Grashof's inequality.

The behavior of a linkage that obeys the Grashof inequality is strongly dependent on the locations of the fully rotatable joints relative to the base link. That is, it is dependent on the inversion of the linkage. The following additional rules distinguish three subtypes that have different behavior:

1. If the shortest link is jointed to the base, the linkage is a crank-rocker ([Figure 1.44](#)). The joint between the shortest link and the base is fully rotatable. Hence, that link is a crank. The other fully rotatable joint connects that crank to the coupler. Hence, the other joint connected to the base is not fully rotatable, and the link it connects to the base oscillates. It is the rocker. A crank-rocker can be conveniently driven about the joint connecting the crank to the base.
2. If the shortest link is the base, both joints at the base are fully rotatable, and so both links connected to the base are cranks ([Figure 1.45](#)). The linkage is a double-crank, also known as a drag-link. It may be conveniently actuated at either of the base joints.
3. If the shortest link is the coupler, neither base joint is fully rotatable ([Figure 1.46](#)). The linkage is a type 1 double-rocker. Its behavior is different from that of type 2 double-rockers, those that do not satisfy the inequality, because in the type 1 linkage the two floating joints can rotate completely. The result is that the coupler performs a complete rotation relative to the base while the two frame mounted links simply rock. The angular motion of the coupler of a type 2 double-rocker is an oscillation relative to the base.

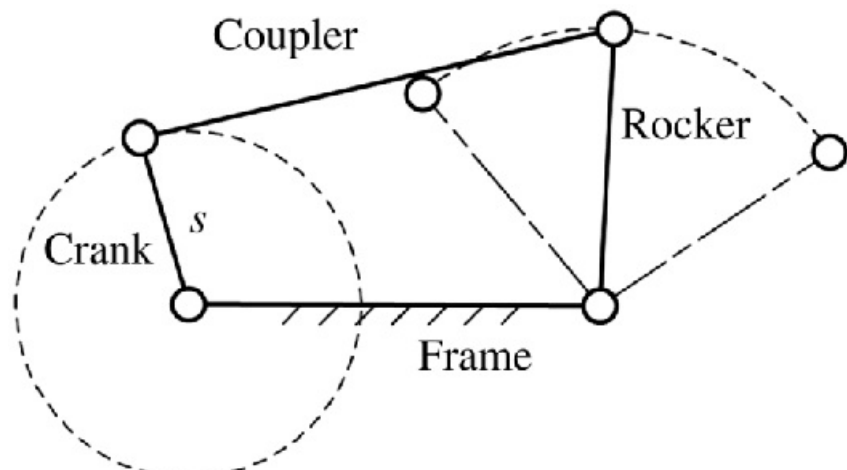


[Figure 1.44](#) Crank-rocker subtype of Grashof type 1 linkage. This linkage type occurs when the shortest

link is jointed to the base of the linkage.

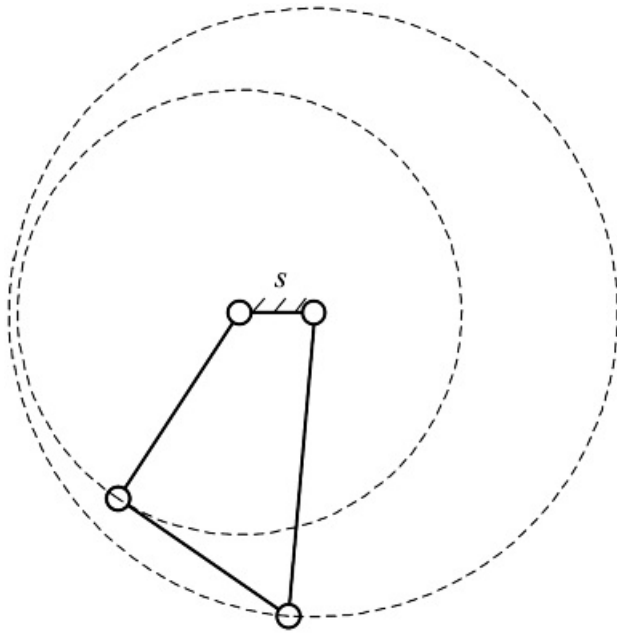


[Figure 1.45](#) The double-crank subtype of Grashof type 1 linkage. This linkage type is also called a drag-link. It occurs when the shortest link is the base.

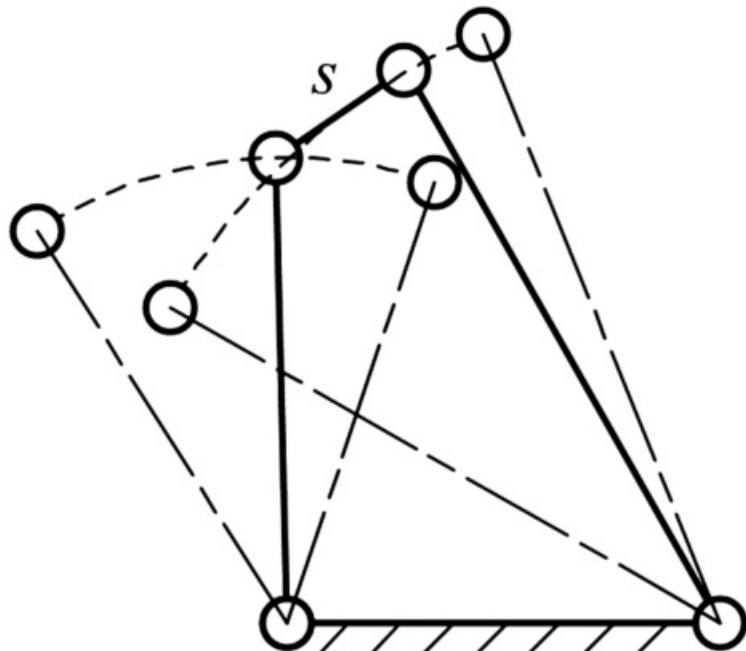


[Figure 1.46](#) The type 1 double-rocker. This subtype occurs when the shortest link is the coupler.

The Grashof inequality may be proved as follows: Consider the linkage shown in [Figure 1.47\(a\)](#). In order to perform a complete rotation it must pass through the positions shown in [Figure 1.47\(b\)](#) and [1.47\(c\)](#). Let a be the length A^*A , b the length AB , c the length B^*B , and d the length A^*B^* . It is assumed that

$$a < c$$

The triangle inequality states that the sum of the lengths of any two sides of a triangle is greater than that of the third. It may be applied three times to [Figure 1.47\(b\)](#) to give

$$a + d < b + c \quad (a)$$

$$b < c - a - d \quad (b)$$

$$c < b - a - d \quad (c)$$

The triangle inequality may also be applied three times to [Figure 1.47\(c\)](#) to give

$$d - a < b + c \quad (d)$$

$$b < c + d - a \quad (e)$$

$$c < b + d - a \quad (f)$$

Examination of these inequalities reveals that if (e) is true then (b) is certainly true, because the right-hand side of (b) is that of (e) plus $2a$. We say that inequality (e) is stronger than inequality (b). Hence inequality (b) can be eliminated. By adding a to both sides, inequality (e) can be written in the form

$$a + b < c + d \quad (e')$$

Similarly, inequality (c) is certainly true if inequality (f) is true. Once again, the right-hand side of inequality (c) is larger by $2a$. If a is added to both sides, inequality (f) assumes the form

$$a + c < b + d \quad (f')$$

Inequality (d) is certainly true if inequality (a) is true, since its left-hand side is less than that of inequality (a) by $2a$. Hence, the six inequalities are reduced to three: (a), (e') and (f'). Addition of both sides of inequalities (a) and (e') gives

$$2a + b + d < 2c + b + d$$

so that

$$a < c$$

Likewise, addition of both sides of inequalities (a) and (f') gives

$$2a + c + d < 2b + c + d$$

so that

$$s < b$$

Since a has also been assumed to be less than d , it follows that a is the shortest link length. Now, whichever of the inequalities (a), (e'), and (f') has the longest link length on the left added to a will be the strongest. That is, the left-hand side is largest and the right-hand side is smallest. Whichever one this is assumes the form

$$s + l < p + q$$

where $s = a$ is the shortest link length, l is the longest link length, and p and q are the two remaining link lengths.

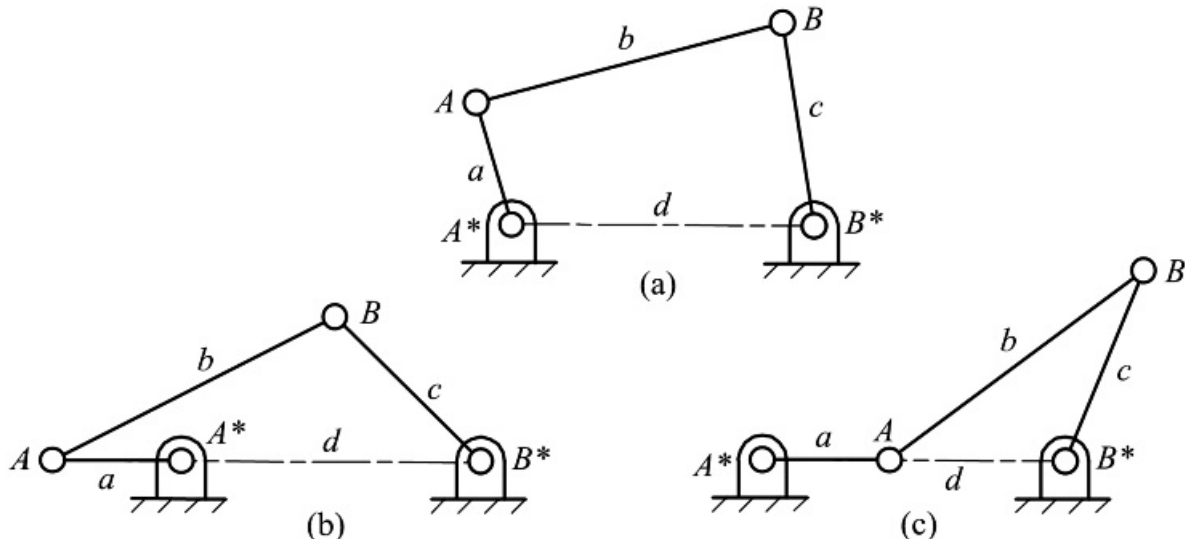


Figure 1.47 (b) and (c) are the extreme positions during the motion of the four-bar linkage (a). The triangle inequality is applied to these positions during the proof of the Grashof inequality.

It must be remembered that we assumed that a was less than d . It is also necessary to deal with the case in which a is larger than d . This can be handled by inverting the linkage so that AB becomes the base link and A^*B^* becomes the link jointed to it by the continuously rotatable joint. Pursuing the application of the triangle inequality then results in d being the shortest link length, and the Grashof inequality again results.

What we have shown so far is that the Grashof inequality is a necessary condition for the presence of a fully rotatable joint, and that joint is always at one end of the shortest link. Now, there can never be just one fully rotatable joint in a four-bar linkage. There must always be at least two. If there were just one fully rotatable joint, a topological contradiction would result when the rotation of A^*A relative to the other links after one cycle were to be considered. If that link were to perform a complete rotation about joint A^* , and joints A , B , and B^* were to oscillate back to their initial positions, A^*A would have performed a complete rotation relative to each of the other links. That is, it would have performed a complete revolution relative to AB . However, joint A has not performed a complete revolution but, rather, has performed zero net rotation. Hence there cannot be just one completely rotatable joint. Since we have shown that any completely rotatable joint must be at one end of the shortest link, it follows that there are two completely rotatable joints, and they are at either end of the shortest link. This completes the proof of Grashof's rules.

The shortest link of a type 1 linkage performs a complete revolution in each motion cycle relative to the other members. The net rotations of the fully rotatable joints on both ends of that link cancel one another so that the net rotations of the remaining links relative to one another are zero for a complete motion cycle.

Sometimes it is not necessary for the mechanism to perform a complete motion cycle. A restricted range of driving joint motion may be adequate. In that case, linear actuators, such as hydraulic or pneumatic cylinders acting across the driving joint, may be used. However, it is still necessary that the driving joint not pass through a motion limit within the necessary range of motion. Grashof's rules are often useful in ensuring that this does not happen.

Occasionally it is necessary to drive a crank-rocker linkage by oscillating the rocker through a part of its motion range. In this case the linkage is usually referred to as a rocker-crank.

The reasons associated with the use of type 2 double-rocker linkages, or with the use of type 1 linkages driven by rockers rather than cranks, will be better understood after a discussion of linkage synthesis. Often, a linkage that is synthesized to produce a specific motion cannot be driven through that motion without the driving joint passing through a motion limit position. In that case, a solution might be to drive the other base joint.

A special case arises when

$$s + l = p + q$$

This is called a transition linkage or Grashof neutral linkage. In this case, the linkage can assume a “flattened” configuration as shown in [Figure 1.48](#). When passing through this position, it can change from one to the other of the two configurations in which the linkage can be assembled for a given driving crank angle. In practice, this is often undesirable because it leads to unpredictable behavior and possibly large loads on the members and joints.

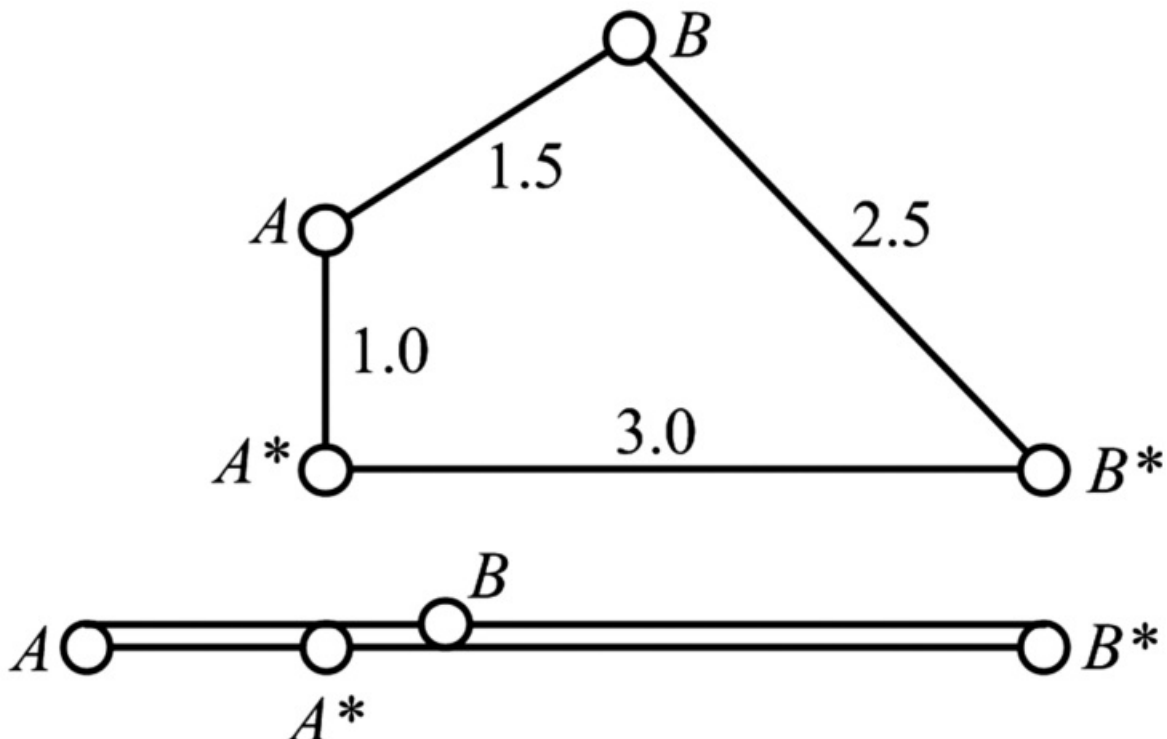


[Figure 1.48](#) A Grashof neutral linkage. A characteristic of such linkages is the ability to assume the flattened position shown.



1.16 Coupler-Driven Linkages

In some applications, linkages are actuated not by applying a force or torque to one of the links jointed to the base but rather by applying a force or torque to the coupler, the member that has no direct connection to the base. Everyday examples are not uncommon (e.g., polycentric hinges for heavy doors or for automotive hood and trunk lids and oscillating fans).

It is still important for a coupler-driven mechanism not to pass through a motion limit within the desired motion range. The motion limit positions for a coupler drive are quite different from those for a crank drive. They are the positions in which the two rotating links become parallel, as shown in [Figure 1.49](#). In these positions the angular motion of the coupler ceases and must reverse if motion is to continue. Elimination of these motion limits produces a linkage whose coupler performs a complete revolution relative to the base link. Because in a type 1 linkage the shortest link rotates completely relative to the remaining links, that link must be either the coupler or the base. It follows that the Grashof subtypes for which complete rotation of the coupler relative to the base is possible are the type 1 double-rocker and drag-link subtypes.

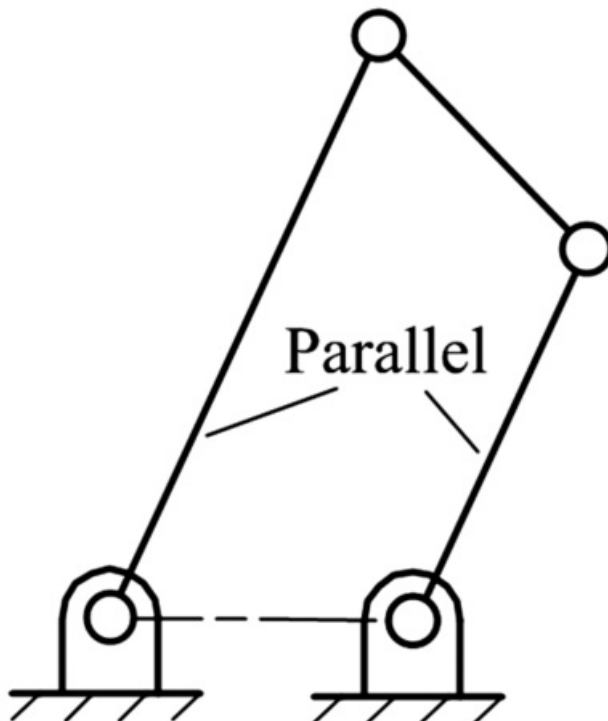


[Figure 1.49](#) The motion limit for the coupler of a coupler-driven four-bar linkage.



1.17 Motion Limits for Slider-Crank Mechanisms

The limits for a slider-crank mechanism can be determined by considering the combinations of link lengths that will cause the linkage to lock up. A typical slider-crank is shown in [Figure 1.50](#).

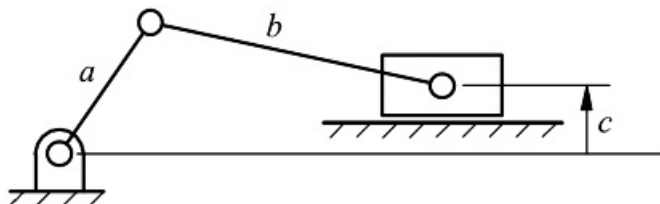


[Figure 1.50](#) General slider-crank mechanism with offset dimension c .

The limit positions of the rotating link a of [Figure 1.50](#) are determined when the coupler link is perpendicular to the direction of slider travel. The limiting assembly position occurs for one of the four geometries shown in [Figure 1.51](#).

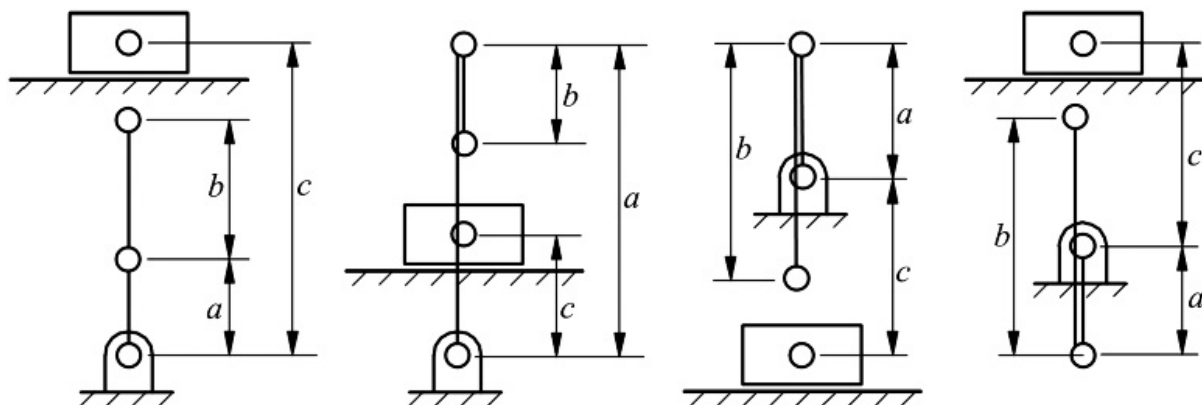


[Figure 1.51](#) Positions for which the slider-crank mechanism represented in [Figure 1.50](#) cannot be assembled.

From the four limit positions shown in [Figure 1.51](#), it is apparent that the following relationships must be maintained if it is to be possible to drive the slider-crank for a full 360° rotation of the crank

$$b > a$$

and

$$b - a > c$$

where

a = length of the crank

b = length of the coupler

c = offset distance from crank-ground pivot to slider pin (measured positive upward)



Example 1.6 Using Grashof's Equation

In the Watt six-bar linkage shown in [Figure 1.52](#), the joint between links 5 and 6 must be placed on the arc indicated. Using Grashof's rule, determine the region for joint *D* that will allow the full rotation of link 6. The critical dimensions are

$A^*A = 1.14$ in	$AB = 2.26$ in	$A^*C = 1.74$ in	$EF = 1.2$ in	$FG = 0.57$ in
$A^*E = 2.00$ in	$CD = 2.68$ in	$b = 0.8$ in	$c = 1.09$ in	

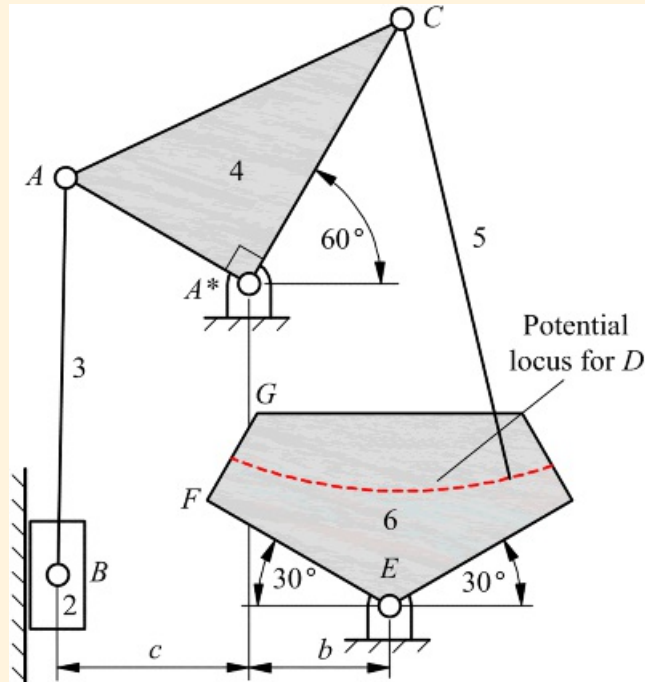


[Figure 1.52](#) Mechanism for which range for point *D* is to be determined.

In the position shown, link 6 is symmetric about the vertical axis through *E*

Solution

Consider first the slider-crank mechanism (A^*AB) even though the crank A^*A does not rotate 360° . Clearly, if the crank A^*A can rotate through 360° , it will not lock up in any intermediate position. Based on the dimensions given

$$AB > A^*A$$

and

$$AB - A^*A = 1.12,$$

Therefore

$$AB - A^*A > c$$

and the crank of the slider-crank mechanism can rotate a full 360° .

Next consider the crank-rocker mechanism (A^*CDE). For a crank rocker, link 6 must be the crank, which means that DE must be the shortest link. The longest link is CD . Therefore, based on [Equation 1.6](#), for A^*CDE to be a crank-rocker mechanism

$$DE + CD < A^*E + AC$$

or

$$DE + 2.63 < 2.00 + 1.74$$

or

$$DE < 1.06 \text{ in}$$

The allowable range for D is shown on the [Figure 1.53](#).

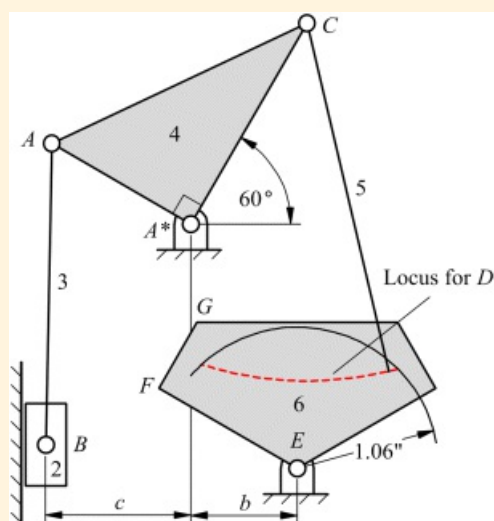


[Figure 1.53](#) Allowable range for point D .



1.18 Interference

This is a topic that is often ignored in courses and texts on mechanism design. That is unfortunate since a full-cycle motion capability can be prevented by topological interference even when Grashof's rules indicate that it is possible. An understanding of topological interference is particularly important at the present time, when linkages are often designed using CAD systems and their functioning checked by animation rather than by construction of physical models. It is very difficult to represent topological interference adequately on a planar display. For this reason, the reader is urged to construct models using cardboard and thumbtacks, or whatever other appropriate materials are available, when reading this section. That is the best way to gain an understanding of the nature of topological interference. There is also a tendency to regard interference as a result of the physical shape of the links and as something that can be avoided if enough care is given to the design of the physical link geometry. That is not what we are talking about here. Topological interference is a fundamental property of a linkage configuration in the same way that Grashof type is. It cannot be avoided by simply reshaping the links.

Topological interference really affects only the capability of executing a complete motion cycle using a rotary input. If oscillatory motion over a partial cycle is all that is required, topological interference can usually be circumvented.

The topological and physical limitation that the links cannot pass through each other creates difficulties in arranging for input and output motion transfer to and from type 1 linkages. When a simple, type 1 four-bar linkage is viewed as a three-dimensional structure with revolute joint axes of finite length, there is only one way in which it can be assembled to avoid any of the links or joint axes having to pass through each other. This is shown in [Figure 1.54](#). The problem is the fully rotatable joints.

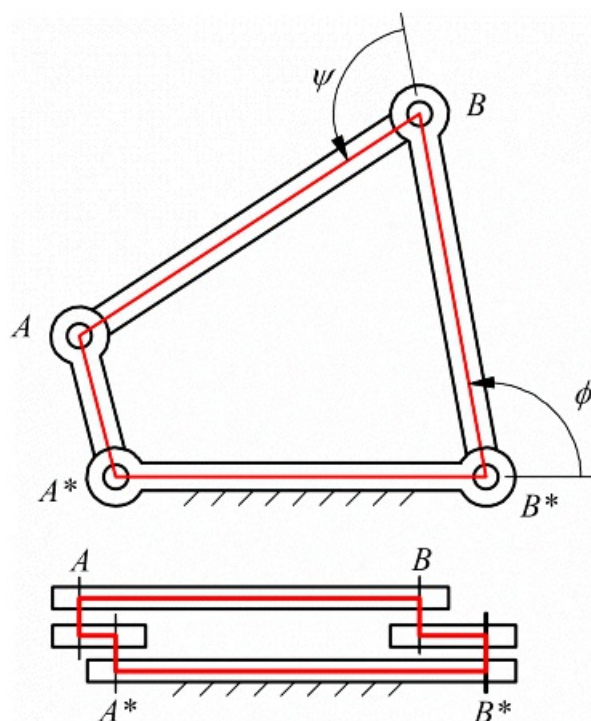


[Figure 1.54](#) Assembly order of type 1 linkage needed to avoid topological interference. Notice that here the vital information is about the order in which the links are placed *along the joint axes*.

The oscillatory joints of a type 1 linkage never pass through positions in which their joint angles ϕ and ψ , shown in [Figure 1.54](#), become either zero or π . If either one did so, the joint diagonally opposite it would be at a motion limit, preventing it from performing a complete rotation. Consequently, the axes of these joints never cross the lines of the links AB and A^*B^* , so there is no interference. However, when joint A^* is fully rotated, the axis of joint A must cross the line A^*B^* and, since A^*A is the shortest link, it must cross between B^* and A^* . Likewise, when joint A is fully rotated, the axis of joint A^* will cross the line AB between A and B . Viewing the linkage from

a direction normal to the joint axes, it can be seen that, if joint A is on one side of the link A^*A , the link A^*B^* must be on the other side, otherwise the link will cut the joint axis. Similarly, joint A^* must be on the opposite side of A^*A to link AB . It follows that, in the direction along the link axes, AB and A^*B^* are on opposite sides of A^*A and B^*B . This may seem to be dependent on the physical realization of the links, but it is, in fact, a fundamental topological property of the loop.

The simplest situation for motion transfer is when both input and output motions are rotary. Motion can then be transferred into and out of the linkage by means of shafts attached to the turning links. Interference constrains the arrangement of the input and output shafts, as shown in [Figure 1.55](#). If the linkage is a *crank-rocker* both shafts must enter from the same side in order to avoid interference between the shafts and the coupler link [[Figure 1.55\(a\)](#)]. Notice that the shafts must pass through the base link to get to the turning links, which are on the inside of the linkage in this inversion. Physically, the shafts are supported in bearings mounted in the base link.

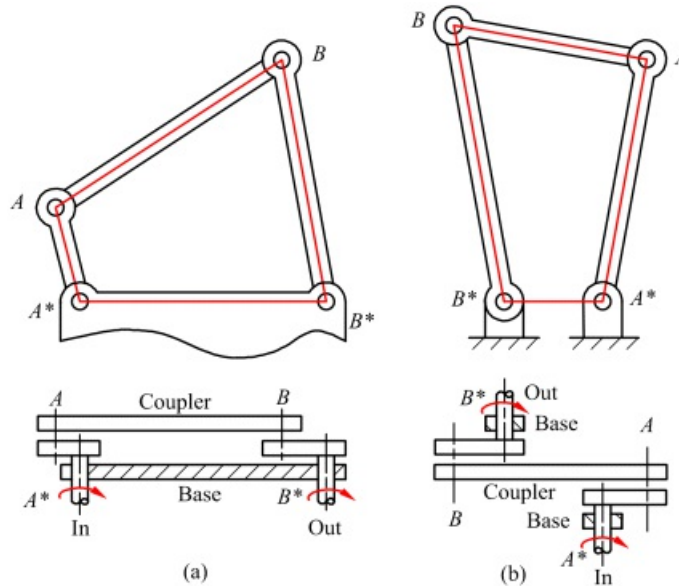


[Figure 1.55](#) Drive shaft configurations needed for crank-rocker (a) and drag-link (b) linkages.

If the linkage is a *drag-link*, the shafts may be attached directly to the turning links, one on either side, since those links are on the outside of the linkage in this inversion. If this is done, the fixed bearings may be moved to the outside, essentially turning the base link inside out. The base link becomes a pair of fixed bearing mounts on either side of the linkage, as is shown in [Figure 1.55\(b\)](#). A *drag-link* linkage must always be mounted in this manner to achieve full cycle motion, regardless of the means of input or output, since otherwise the coupler must pass through the base.

The discussion of rotary input and output to *type 1 double-rocker* linkage will be left until later because it is not possible to achieve full-cycle motion with a crank drive in this type of linkage.

A more complex case is that in which the input is rotary and motion must be transferred from a point on the coupler link. This is easy enough to arrange in the *crank-rocker* case, as shown in [Figure 1.56](#), because the base and coupler are on the outside of the linkage.

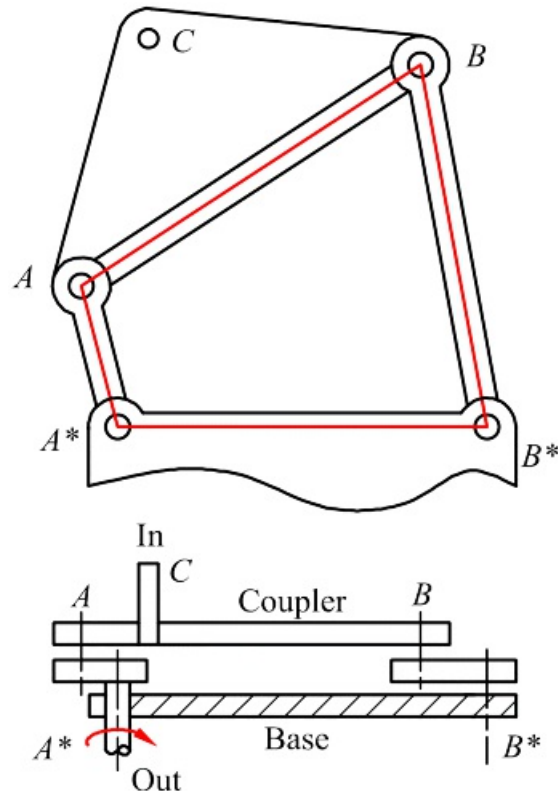


[Figure 1.56](#) Configuration necessary for transfer of motion from a point on the coupler of a crank-rocker mechanism.

Much more difficult is the case in which motion must be transferred from a point on a crank or on the coupler of a *drag-link*. Because the coupler moves between the cranks there is no way to avoid interference of a shaft coming off the coupler with those cranks in full-cycle motion. Furthermore, because the two parts of the base are outside the cranks, there is also a problem of interference with the base. This latter problem also affects the transfer of motion to or from points on the cranks.

It is possible to circumvent the interference problem for motion transfer from points on a crank by “doubling” the crank. This is shown in [Figure 1.57\(a\)](#). If the transfer point is reasonably close to the base joint of the crank, the result in [Figure 1.57\(a\)](#) can be achieved by using a bearing of sufficiently large diameter to encompass the transfer point. This is shown in [Figure 1.57\(b\)](#). The crank is essentially duplicated on the outside of the base bearing. A shaft rigidly fixed to both the crank and the duplicate passes through the bearing forming the base joint and ensures that both move together. This effectively makes points on the crank available outside the base, where additional links can be attached at motion transfer joints. In this way, multiloop linkages such as that shown in [Figure 1.58](#) can be built up and driven by the driving crank of the master *drag-link* loop.

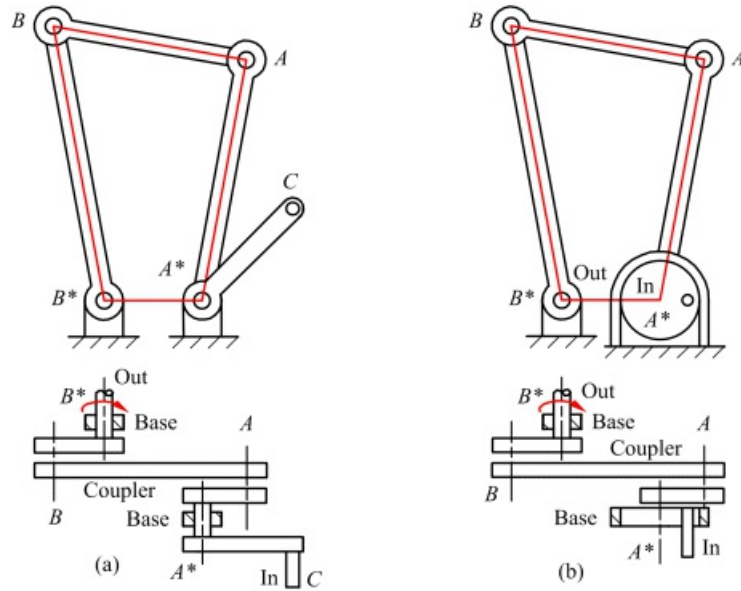


[Figure 1.57](#) Alternative arrangements for motion transfer from a point on the crank of a drag-link.

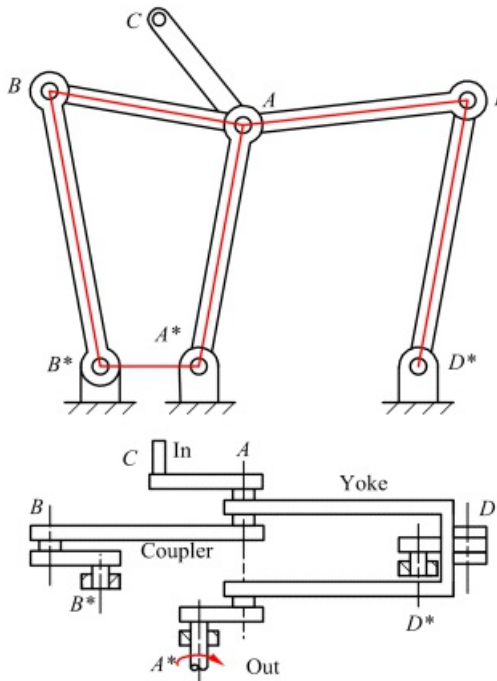


[Figure 1.58](#) Six-bar modification necessary to achieve motion transfer from the coupler of a drag-link linkage.

There is no simple way to transfer motion from a point on the coupler of the *drag-link* without preventing full-cycle mobility. It can be done by splitting one of the joints between crank and coupler, allowing the linkage loop to pass through itself. This requires the addition of at least one auxiliary link, so the mechanism, strictly speaking, is no longer a four-bar. The yoke shown in [Figure 1.58](#) carries the two bearings that replace the simple joint of the original linkage. It is undesirable to leave this link unconstrained, so it is usual to add a second link connecting it to base, as shown in the figure. This allows the coupler to be moved outside the crank. However, it is still not possible to transfer motion directly from a point on the coupler because of interference with the yoke. For this reason, the coupler is doubled in the same way that the crank was in [Figure 1.57](#), producing the six-bar arrangement shown. As can be seen, this is quite an extensive modification.

The situation for coupler drive, in which the driving torque is applied to the coupler link and the output motion is taken off that same link, is quite similar. The two linkage types that can, in principle, perform complete motion

cycles in the coupler drive mode are the *type 1 double-rocker* and *drag-link* types. Both present a problem because the base and coupler are inside the cranks in the basic loop. The *type 1 double-rocker* can be made to allow full cycle motion, without interference, by doubling the coupler.

Once again, the *drag-link* presents additional problems because of the necessity of splitting the base, resulting in the base joints being outside the cranks. Coupler-driven full-cycle motion of a simple *drag-link* is not possible because of interference. The six-bar arrangement of [Figure 1.58](#) can be used for full-cycle motion that is identical to that of the *drag-link* with coupler drive.

All of the foregoing discussion relates only to full-cycle motion, that is, to motion in which the driving link performs a complete rotation. If oscillation through a partial motion cycle is adequate for the application, interference can always be avoided by modifying the physical shapes of the links. This is true even for the *drag-link* type. Type 2 linkages can also be used in this mode. One only has to ensure that it is not necessary for such linkages to pass through motion limit positions of the driving link when traversing the desired segment of the motion cycle.



1.19 Practical Design Considerations

1.19.1 Revolute Joints

A rubbing contact between two members, here called a kinematic joint, is also known as a bearing. Design of bearings to perform satisfactorily for long periods under a load is a focus of the subject of tribology. Although an in-depth treatment of tribology is beyond the scope of this book, it is necessary for the mechanism designer to be aware of the limitations that may be placed on the design by the necessity of having bearings.

Revolute joints perform well under many conditions. As with all the lower pairs, the distribution of contact over a surface distributes and normally slows wear. The closed geometry of the joint provides good conditions for trapping lubricant between the joint surfaces.

A revolute joint that is in continuous, unidirectional rotation at relatively high speeds can enter a regime called hydrodynamic lubrication in which the relative movement of the bearing elements acts to entrain lubricant and maintain a separation between the solid journal elements. The entrainment action creates an area of elevated pressure in the lubricant that supports the load on the bearing. The establishment of hydrodynamic action is often assisted by pumping lubricant into the bearing. In principal, once hydrodynamic action is established, there is no contact between the solid bearing elements, and hence there is no wear. The effective friction is solely due to viscous resistance in the lubricant and is, therefore, low. Typically wear occurs only when the machine is started up and shut down. The crankshaft support bearings, and the bearings between the crankshaft and the connecting rods of an automotive engine are good examples of hydrodynamic bearings.

Another type of bearing that has some of the characteristics of a hydrodynamic bearing, but is free of some of its limitations, is a hydrostatic bearing. Here the objective remains the same, to carry the bearing load by a pressure differential in the lubricant, and maintain separation between solid bearing journals at all times. However, in this case, the pressure to support the bearing load is provided by pumping the lubricant into the bearing on the loaded side at an elevated pressure. Hydrostatic bearings do not rely on continuous rotation to maintain bearing action. Therefore, they can be used when the rotation speeds are low, or when the direction of rotation reverses. They do tend to be expensive, due to a need for close tolerances to minimize lubricant leakage out of the bearing, and because of the need for a relatively high capacity lubricant pump. Hydrostatic bearings are usually used for the main rotor bearings on large turbo-generator sets.

When the speed of rotation is slow, or reverses, a greased bushing or a solid contact bearing may be used. These bearing types are geometrically similar, and differ only in the use of a liquid lubricant. Usually that lubricant will be a viscous grease. The high viscosity both promotes some hydrostatic action and diminishes leakage out the sides of the bearing. Frequent lubrication is, nevertheless, necessary for this type of bearing. The materials should also be chosen to provide adequate performance and wear resistance even in the absence of lubricant.

Solid contact bearings rely on the choice of contacting materials to provide both low friction and wear resistance. Teflon has a low coefficient of friction with most metals. It is also relatively hard and highly temperature resistant for a plastic material. Consequently it is frequently chosen for one element of a bearing pair. Other plastic materials such as nylon and delrin are also used. Note that the same material should never be used for both journal members of a solid bearing pair. The reason is that journals with similar materials can weld together at small asperities when driven under load, resulting in high friction and rapid wear. This is why bronze bushings are frequently partnered with steel journals for greased bearings. Generally harder materials wear better than softer ones. Hence steel is preferred to aluminum for bearing journals. One final caution is that some materials should never be lubricated with petroleum-based lubricants. Nylon tends to absorb oil and swell and fail. Solid lubricants such as graphite or molybdenum disulphide can be used when petroleum based lubricants are not an option because of material or other constraints.

Rolling element bearings provide another alternative for the support of rotary motion. Here the load is transferred between the journals by hardened steel balls or rollers trapped between the journals. The contact between one of these rolling elements and the journal is, of course, a higher-pair joint. However, the combined effect of all the balls or rollers rolling on the journals is kinematically equivalent to a revolute joint. Lubricants are used, but the

way in which they work is somewhat different from that of the lubricants in other types of joints. This kind of action is called *boundary lubrication*. The lubricant is squeezed to very high pressures between the rolling element and journal and plays a role in distributing the load over both elements. The contact between a ball and journal is a point, if both are perfectly rigid, and that between a roller and journal is a line. In either case, the stress is ideally locally infinite. Of course, elastic deformation of the elements acts to distribute the load over a finite area. The boundary lubrication mechanism assists in this load distribution.

Because pure rolling contact does not involve sliding of one member over another, wear, of the type found in other bearings, is not an issue for rolling contact bearings. Also, the effective friction can be very low, and rolling element bearings work well with motion cycles that stop or reverse. However, the very high contact stresses in the elements require very hard and very accurately manufactured rolling elements and journals. Consequently, rolling element bearings can be relatively expensive. They are also relatively bulky and are not well suited to situations where space is limited. The principal failure mode of a rolling element bearing is basically fatigue due to the high contact, or Hertzian stresses, in the rolling elements and journals. This leads to subsurface cracking and eventual spalling, or breaking out of pieces from the surface of a rolling element. Once this process starts, the bearing tends to fail quite rapidly. The nature of the failure mode is such that all rolling elements have finite life. Unfortunately that life is statistically distributed over a significant range, making it relatively difficult to predict failure and apply preventive maintenance procedures to change bearings before failure occurs.

1.19.2 Prismatic Joints

As compared to revolute joints, prismatic joints are much more problematic in their application. As will be shown next, they are sensitive to the direction and manner of load application. Also, a prismatic joint cannot be infinite in length so all prismatic joints experience motion reversals which precludes the use of fully established hydrodynamic lubrication.

If a sliding joint is loaded by a connecting rod, as in a slider crank mechanism, the loading force is applied along the line through the bearing center, as shown in [Figure 1.59\(a\)](#). The friction force along the joint direction is proportional to the normal force. If the friction force exceeds the component of the applied force along the slide direction the joint will jam. That is, if the angle between the axis of the connecting rod and the normal to the joint direction is less than the friction angle

$$\phi = \tan^{-1} \mu$$

where μ is the coefficient of friction, the joint will jam.

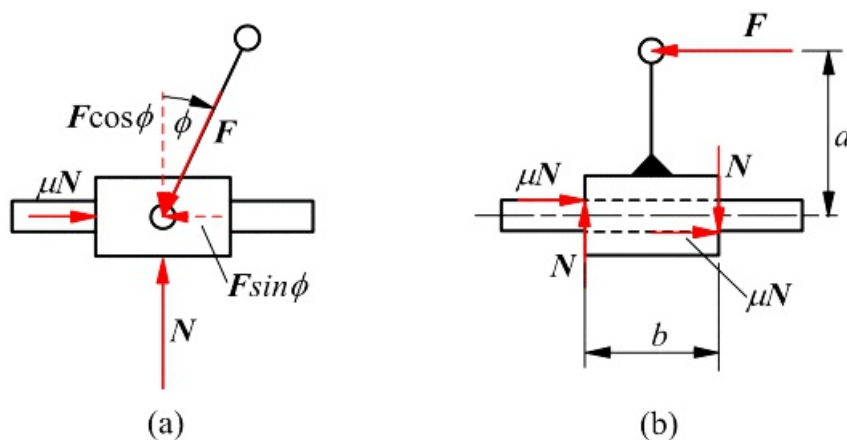


[Figure 1.59](#) Jamming in sliding joints. In (a), the slide will jam if the angle between the applied force F and the direction of sliding becomes too great. The slider will jam when the angle ϕ is less than $\tan^{-1} \mu$. In (b), the slider will jam due to the offset force if $2\mu a > b$.

[Figure 1.59\(b\)](#) shows another effect that may lead to jamming of the slider. Applying a load offset from the slider

surfaces results in an applied moment that must be resisted by a couple composed of normal forces, as shown in the figure. In a real prismatic joint, there must be a small clearance between the members. The application of the offset force, F , causes the block to angulate slightly relative to the shaft so that contact actually occurs only at the ends of the joint. Thus, the block is subject to normal and friction forces at the locations shown in the figure. The joint will jam if

$$F \leq 2\mu N$$

However, for horizontal force and moment equilibrium

$$2\mu bN = F \text{ and } aF = bN$$

Therefore, the joint will jam if

$$b < 2\mu a$$

Offset loads and loading directions at large angles to the joint direction also combine to produce jamming.

Jamming is best avoided by shunning designs that have sliding joints with poor loading geometries. If such a geometry cannot be avoided, jamming due to offset loading may be alleviated by increasing the length of the prismatic joint, if space allows. Increasing b until it is greater than any expected value of $2\mu a$ should avoid the problem. Reducing the effective coefficient of friction is effective in either case. That might be done by lubrication, or by choice of a low-friction material combination. Lubrication, as a solution, may be problematic if jamming is a catastrophic failure mode. Sooner or later, the joint is likely to have too little lubricant.

The best solution, in many cases, is to use a rolling contact joint to minimize the effective coefficient of friction. Roller on rail configurations that are kinematically equivalent to a prismatic joint are available. A ball bushing is a relatively inexpensive and compact device. It must roll on a smooth, hardened steel shaft. A ball bushing does not provide any restraint on twisting about the shaft axis. For this reason, when ball bushings are used, the bushings and shafts are usually configured in parallel pairs.

1.19.3 Higher Pairs

Pure rolling contact may not require any lubrication, or special attention, as is the case of the contact between a vehicle tire and the ground. Sliding contacts, however, can result in very rapid wear, jamming, and failure unless carefully designed and lubricated. Combined rolling and sliding, as in a gear mesh, also requires careful attention to lubrication at any but the lowest loads and speeds. Gears that carry significant loads and power flows are normally enclosed in gearboxes to allow lubricant to be actively splashed or pumped over them. The gearbox allows lubricant to run off the gears and collect in the bottom of the box, or sump, for recycling.

Cam and follower pairs are particularly demanding with respect to lubrication, particularly if flat-faced followers are used. The valve timing cams in an automotive engine are housed in a sealed chamber so they can be bathed in lubricant. Oil is often pumped through the rocker shaft to ports in the faces of the followers to ensure lubrication, and some hydrodynamic action, over the rubbing surfaces.

1.19.4 Cams versus Linkages

As will be seen, both cams and linkages are used to generate desired irregular motions. As solutions to design problems requiring irregular motions, they each have their strengths and weaknesses. Cams are usually easier to design geometrically, but much harder to make work satisfactorily. The lubrication issues involved in rubbing contact are referred to above. In low volume, cams are expensive to manufacture. However, if the volume of parts needed is high enough to justify manufacture of a die, and production of the cams by near net shape methods such as injection molding, die casting, or powder metallurgy becomes feasible, cam mechanisms can be very

economical. Cams are particularly convenient for timing mechanisms, such as valve lifters. They are easily designed to dwell in a set position for a set portion of the motion cycle.

Linkages are robust and inexpensive, particularly if only revolute joints are needed. They are economical to manufacture in either large or small volumes. Lubrication is, relatively speaking, very easy. However, they do not allow as much freedom to the designer as cams. It is quite difficult to design a high quality dwell mechanism using only linkages. Also, linkages often consume more space than cam mechanisms. Given an irregular motion generation problem, most experienced machine designers will seek a linkage solution first, unless the problem is clearly better suited to a cam.

Notes

1. Problem courtesy of Joseph Davidson, Arizona State University.
2. Problem courtesy of Joseph Davidson, Arizona State University
3. Problem based on [3].



References

1. Agrawal, Sunil K., Madangopal, Rajkiran, and Khan, Zaeem A. (2004). " Biologically Inspired Design of Small Flapping Wing Air Vehicles Using Four-Bar Mechanisms and Quasi-Steady Aerodynamics." *Journal of Mechanical Design*, pp. 1–8.
2. Grashof, Franz. (1883). *Theoretische Maschinenlehre*, Vol. 2, Leipzig; L. Voss.
3. Harrisberger, Lee. (1965). " A Number Synthesis Survey of Three-Dimensional Mechanisms." *Trans. ASME, J. of Eng. for Ind.*, May, pp. 213–220.
4. Hartenberg, R. S., and Denavit, J. (1964). *Kinematic Synthesis of Linkages*, New York, NY: McGraw-Hill.
5. Hunt, K. H. (1978). *Kinematic Geometry of Mechanisms*. Oxford, UK: Oxford University Press, p. 40.
6. LEGO Systems, Inc., 555 Taylor Road, Enfield, CT.
7. McGhee, R. B., and Waldron, K. J. (1985). " The Adaptive Suspension Vehicle Project: A Case Study in the Development of an Advanced Concept for Land Locomotion." *Unmanned Systems*, Vol. 4, No. 1, Summer, pp. 34–43.
8. Reuleaux, Franz. (1963). *The Kinematics of Machinery* (Transl. and ed. by Alexander B. W. Kennedy). New York, NY: Dover Publications, Inc.
9. Richter, Irma A. (1952). *Leonardo Da Vinci Notebooks*. New York, NY: Oxford University Press, Inc.
10. U.S. War Department. (1944). Bombardiers' Information File, AAF Form 24B, Washington, DC.



Problems

Linkage Structure

- 1.1 Find a mechanism as an isolated device or in a machine and make a realistic sketch of the mechanism. Then make a freehand sketch of the kinematic schematics for the mechanism chosen.
- 1.2 Cabinet hinges use various types of linkages for the folding mechanism. Identify three types of cabinet hinges and make a freehand sketch of the kinematic mechanism used.
- 1.3 The drawings shown in [Figure P1.3](#) are pictorial representations of real mechanisms that are commonly encountered. Make a freehand sketch of the kinematic schematic representation of each mechanism.

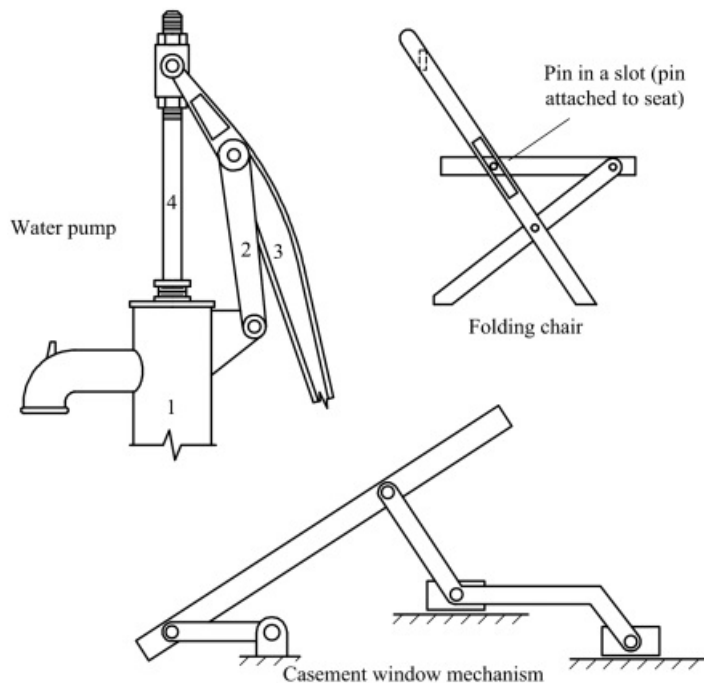


[Figure P1.3](#) Linkages for Problem 1.3.

- 1.4 Linkages are often used to guide devices such as computer keyboards in and out of cabinets. Find three such devices, and make a freehand sketch of the kinematic mechanisms used for the devices.
- 1.5 Four-bar linkages are used in common devices around the home and businesses. Locate six such devices and make a freehand sketch of the device and describe its function.
- 1.6 [Figure P1.6](#) is an elliptical trainer machine. The mechanism is a planar linkage. There are linkages on both sides of the machine. The linkage on the right is a mirror image of the one on the left and the linkages are connected together so that they are always 180° out of phase with each other. For the left side linkage identify the moving joints and links. There is a handle that rotates about a fixed pivot. There is also a foot pedal that floats in that it is not connected to the frame of the machine. Sketch the topology of the linkage. How many links and joints are there? How many binary links? How many ternary links? How many four-bar loops can you identify? Which linkage topology in [Figure 1.23](#) or [1.24](#) does the topology match? Identify any joints that perform complete rotations as the mechanism is cycled.



[Figure P1.6](#) Linkage for Problem 1.6.

[1.7](#) [Figure P1.7](#) shows another type of elliptical trainer machine. The mechanism is a planar linkage that includes a slider joint. There are linkages on both sides of the machine. The linkage on the right is a mirror image of the one on the left and the linkages are connected together so that they are always 180° out of phase with each other. For the left side linkage identify the moving joints and links. There is a handle that rotates about a fixed pivot. There is also a foot pedal that floats in that it is not connected to the frame of the machine. Sketch the topology of the linkage. How many links and joints are there? How many binary links? How many ternary links? Identify any joints that perform complete rotations as the mechanism is cycled.



[Figure P1.7](#) Linkage for Problem 1.7.

1.8 [Figure P1.8](#) shows a bicycle suspension linkage. If the shock absorber is considered, the linkage can be represented as a six bar mechanism. Draw the back suspension linkage and identify the chain in [Figure 1.23](#) to which the topography corresponds.



[Figure P1.8](#) Bicycle for Problem 1.8.

1.9 A small excavator is shown in [Figure P1.9](#). The machine has a swing linkage but the main mechanism is planar. Draw the planar excavation linkage. Treat each hydraulic cylinder as a slider in a tube.



[Figure P1.9](#) Excavator linkage for Problem 1.9.

1.10 Since the mid-1940s, modern tractors used for farming, construction, and landscape work have used a three-point hitch to attach implements to the rear of the tractor. This allows the operator to control the height and orientation of the implement using the tractor hydraulic system. A three-point hitch is shown in [Figure P1.10](#) along with a schematic of the linkage. The kinematics of the system can be studied using a planar schematic as shown. In the schematic, link 2 is rotated using a hydraulic motor, and the implement being controlled is link 6. Characterize the linkage as a Watt's or Stephenson's six-bar linkage.



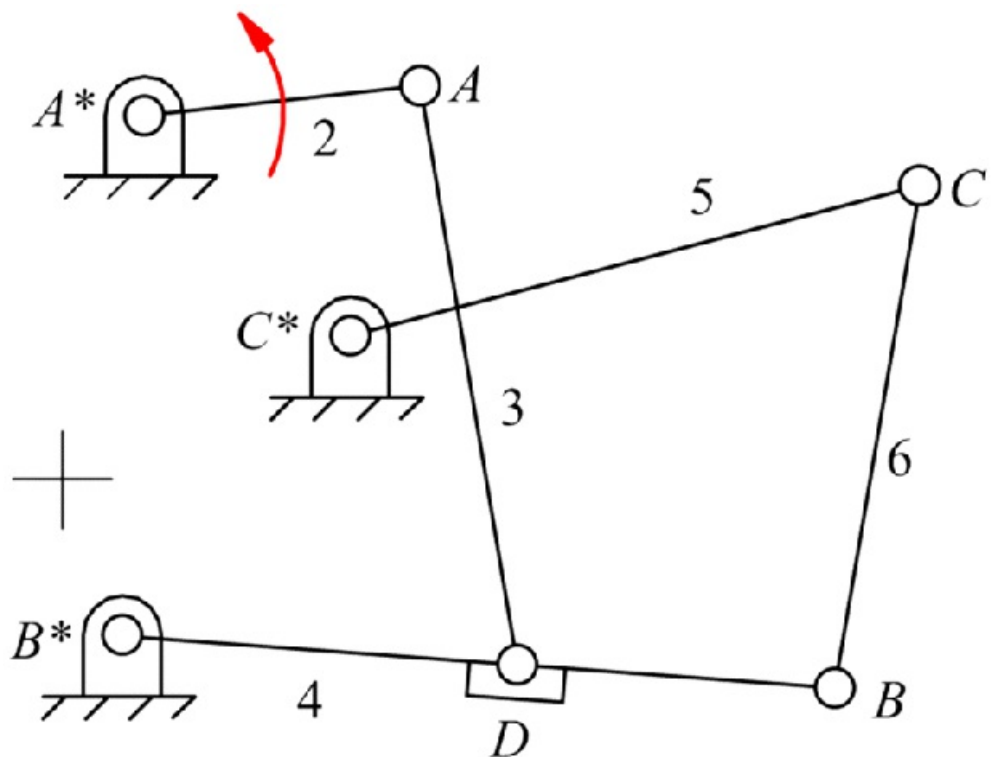


[Figure P1.10](#) Tractor three-point hitch linkage for Problem 1.10.

Mechanism Mobility for Planar Mechanisms

1.11 Calculate the mobility, or number of degrees of freedom, of each of the mechanisms in Problem 1.3.

1.12 What is the number of members, number of joints, and mobility of each of the planar linkages shown in [Figure 1.12](#).

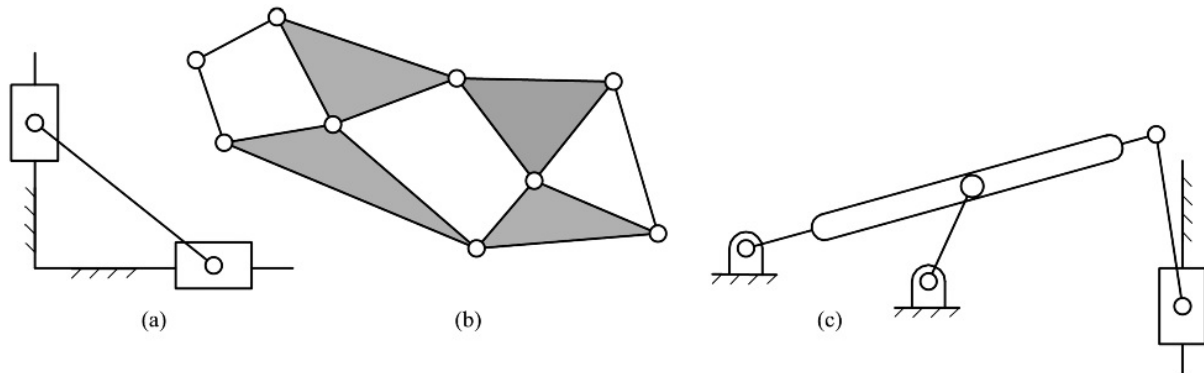


[Figure P1.12](#) Linkages for Problem 1.12.

1.13 What are the number of members, number of joints, and mobility of each of the planar linkages shown in [Figure P1.13](#)?

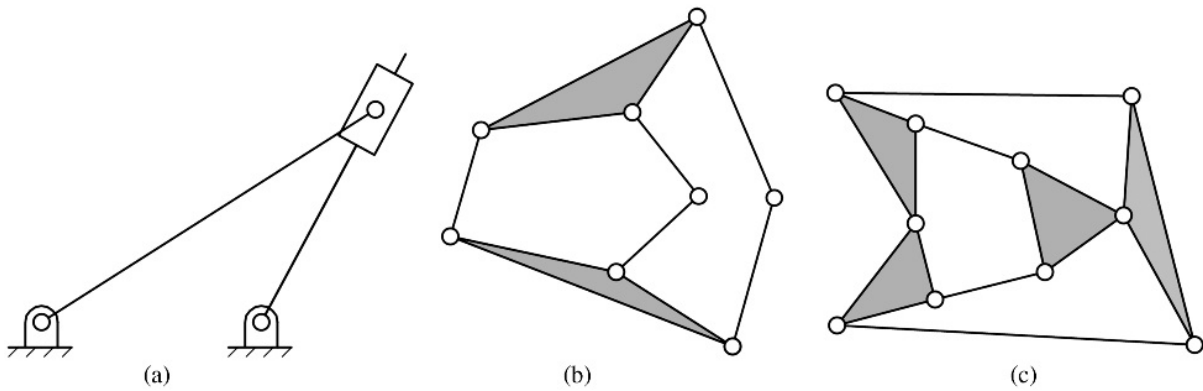


[Figure P1.13](#) Linkages for Problem 1.13.

1.14 Determine the mobility and the number of idle degrees of freedom of each of the planar linkages shown in [Figure P1.14](#). Show the equations used and identify the input and output links assumed when determining your answers.

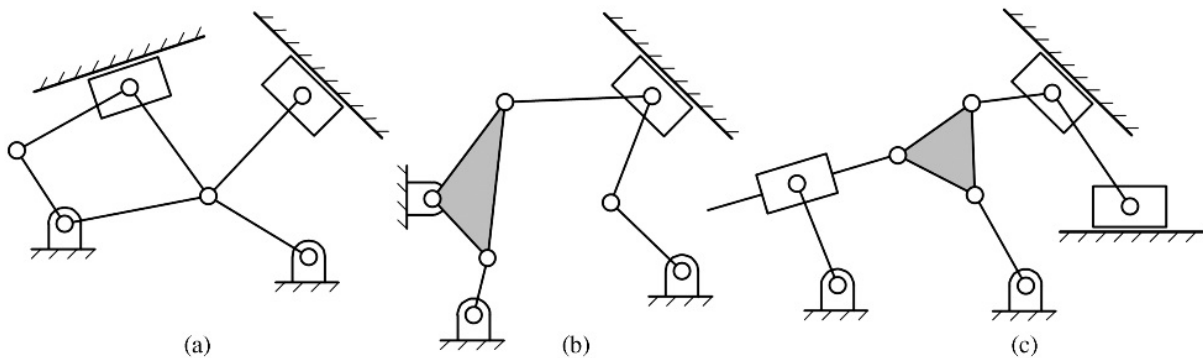


[Figure P1.14](#) Linkages for Problem 1.14.

1.15 Determine the mobility and the number of idle degrees of freedom of the linkages in [Figure P1.15](#). Show the equations used and identify any assumptions made when determining your answers.

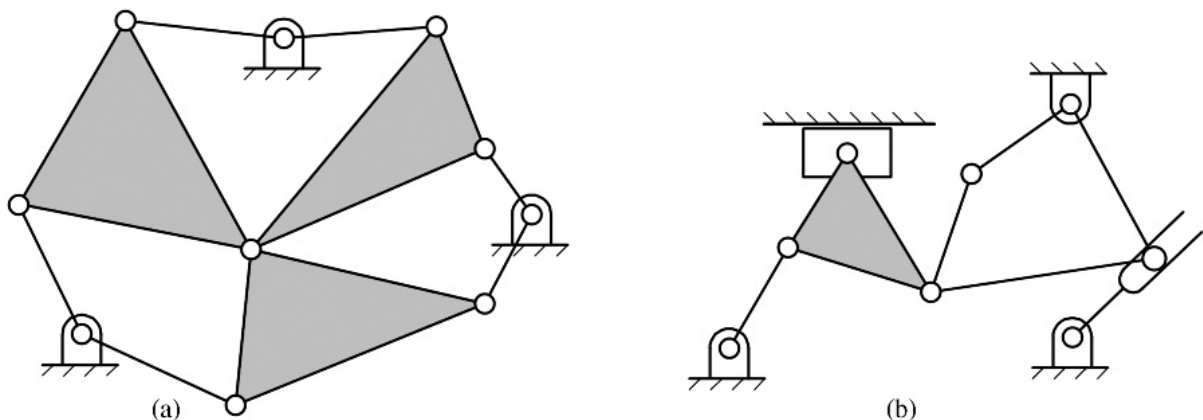


[Figure P1.15](#) Linkages for Problem 1.15.

1.16 Determine the mobility and the number of idle degrees of freedom associated with the mechanism in [Figure P1.16](#). Show the equations used and identify any assumptions made when determining your answers.

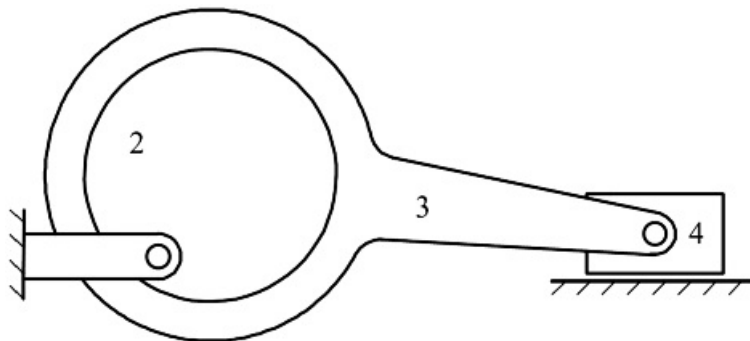


[Figure P1.16](#) Linkage for Problem 1.16.

1.17 Determine the mobility of each of the planar linkages shown in [Figure P1.17](#). Show the equations used to determine your answers.

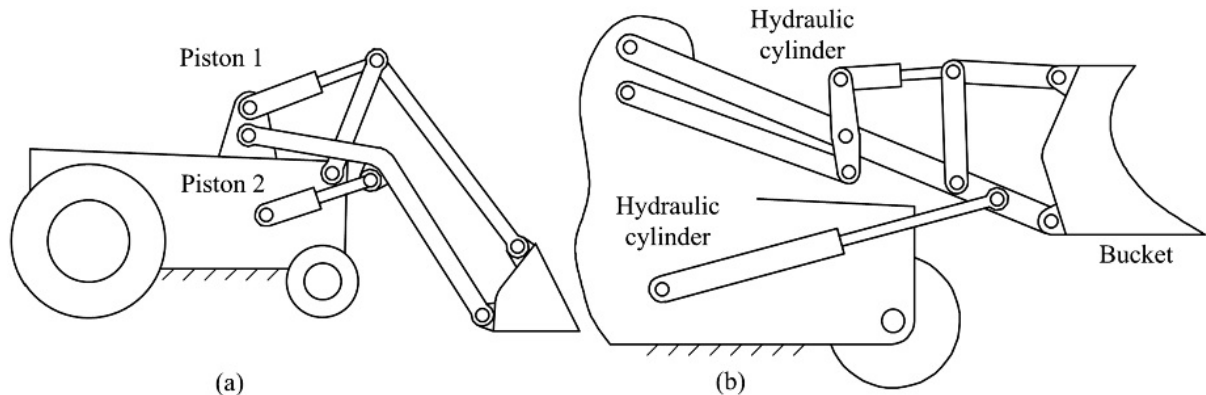


[Figure P1.17](#) Linkages for Problem 1.17.

1.18 Determine the mobility and the number of idle degrees of freedom of each of the planar linkages shown in [Figure P1.18](#). Show the equations used and identify any assumptions made when determining your answers.

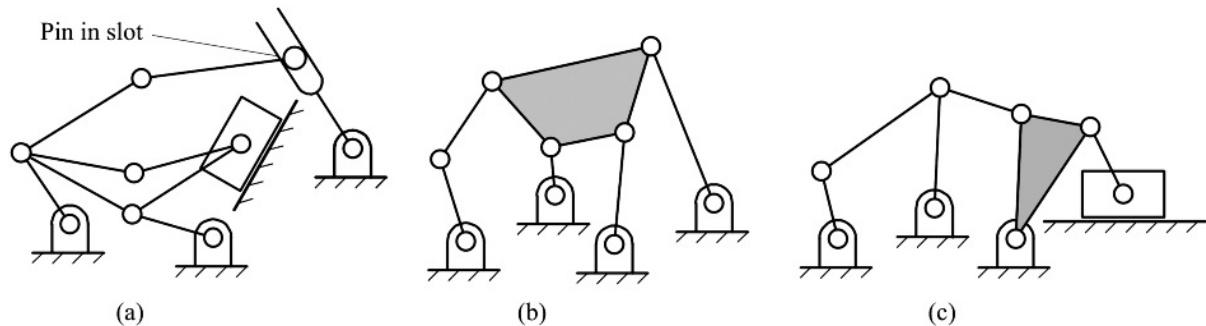


[Figure P1.18](#) Linkages for Problem 1.18.

1.19 Determine the mobility and the number of idle degrees of freedom of each of the planar linkages shown in [Figure P1.19](#). Show the equations used to determine your answers.

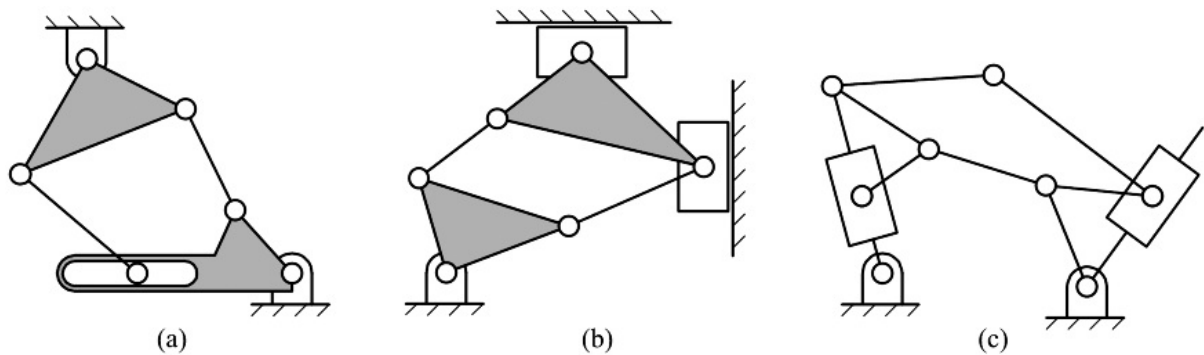


[Figure P1.19](#) Linkages for Problem 1.19.

1.20 Determine the mobility and the number of idle degrees of freedom of each of the planar linkages shown in [Figure P1.20](#). Show the equations used and identify any assumptions made when determining your answers.

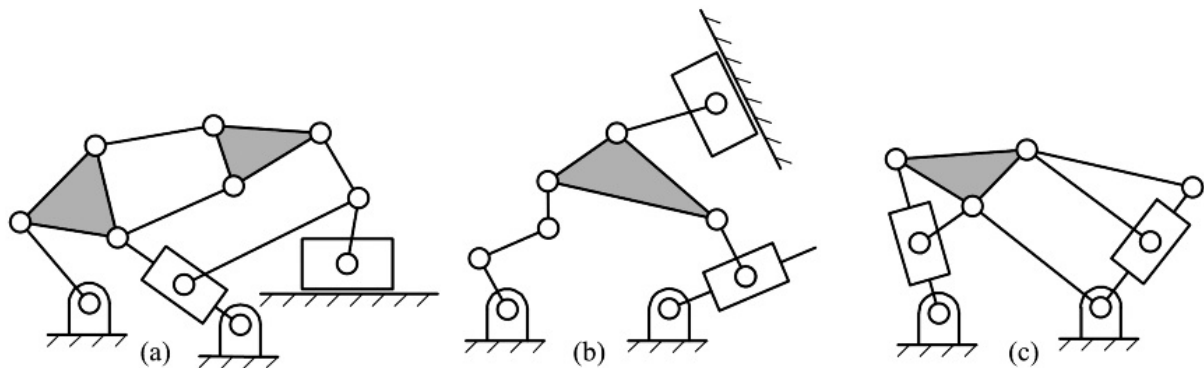


[Figure P1.20](#) Linkages for Problem 1.20.

1.21 If position information is available for all points in the planar linkage shown in [Figure P1.21](#), can all of the velocities be determined uniquely if the value of ω is given? Explain your answer.

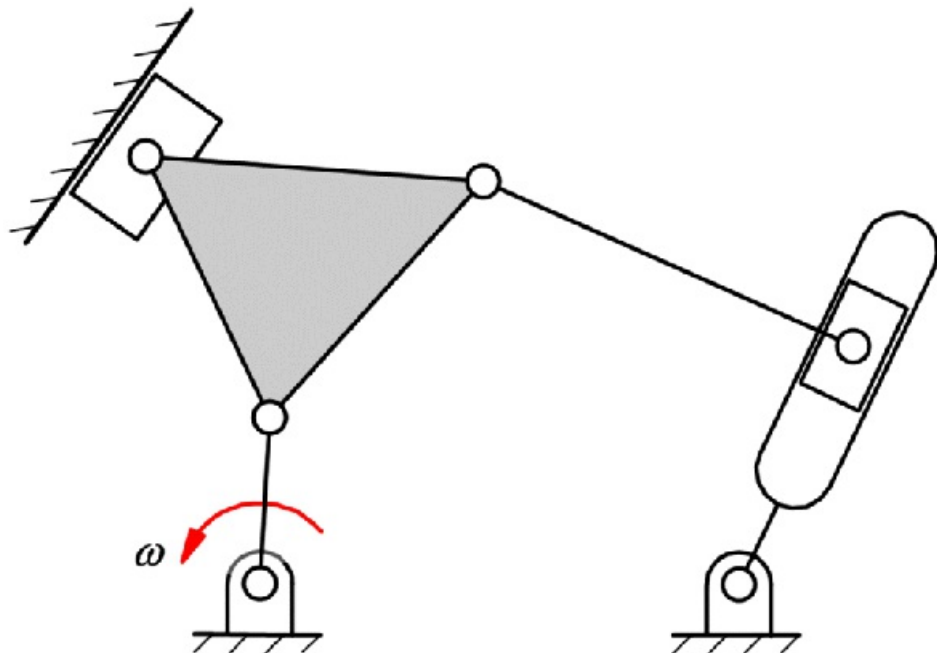


[Figure P1.21](#) Linkage for Problem 1.21.

1.22 Determine the mobility and the number of idle degrees of freedom associated with each mechanism in [Figure P1.22](#). Show the equations used and identify any assumptions made when determining your answers.

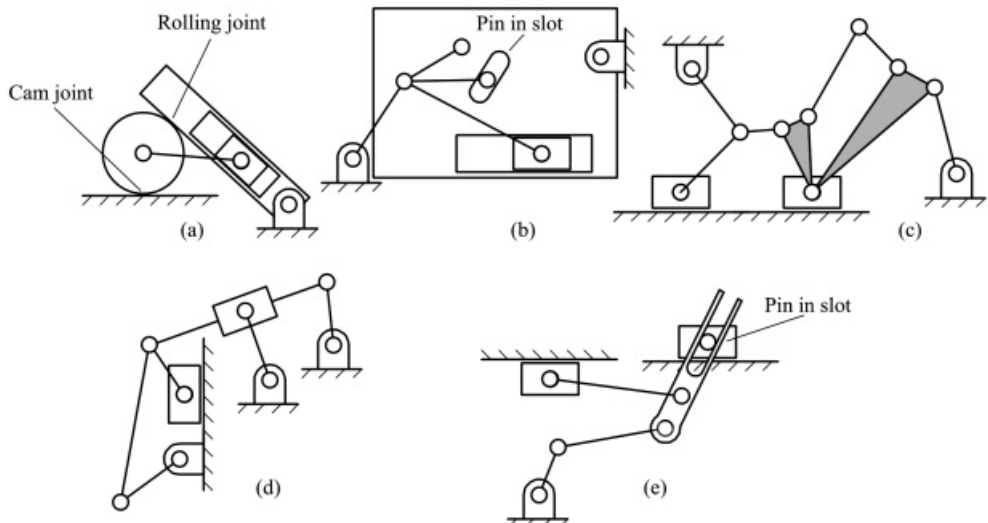


[Figure P1.22](#) Linkages for Problem 1.22.

1.23 Determine the mobility and the number of idle degrees of freedom for each of the mechanisms shown in [Figure P1.23](#). Show the equations used and identify any assumptions made when determining your answers.

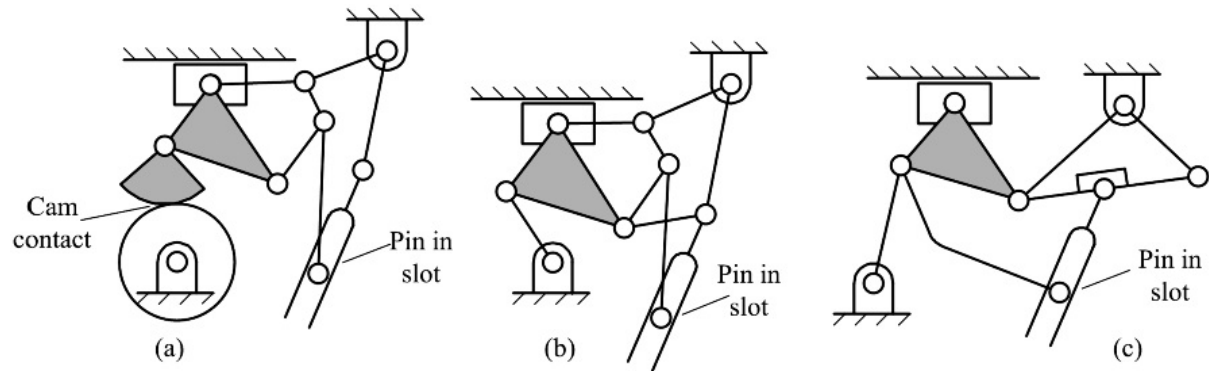


[Figure P1.23](#) Linkages for Problem 1.23.

1.24¹ Determine the mobility and the number of idle degrees of freedom associated with the mechanism shown in [Figure P1.24](#). The mechanism is a side-dumping car that consists of body 2 and truck 3 connected together by two six-bar linkages, $ABCDEF$ and $AGHJKLMN$. Link NM is designed as a latch on its free end (see left drawing). When jack 1 is operated, body 3 is lifted to the dumping position shown in the right-hand drawing. Simultaneously, the six-bar linkage $AGHJKLMN$ opens the latch on link NM and raises link GH . Linkage $ABCDEF$ swings open side BC and the load can be dumped at some distance from the car (see right-hand drawing). Show the equations used to determine your answers.

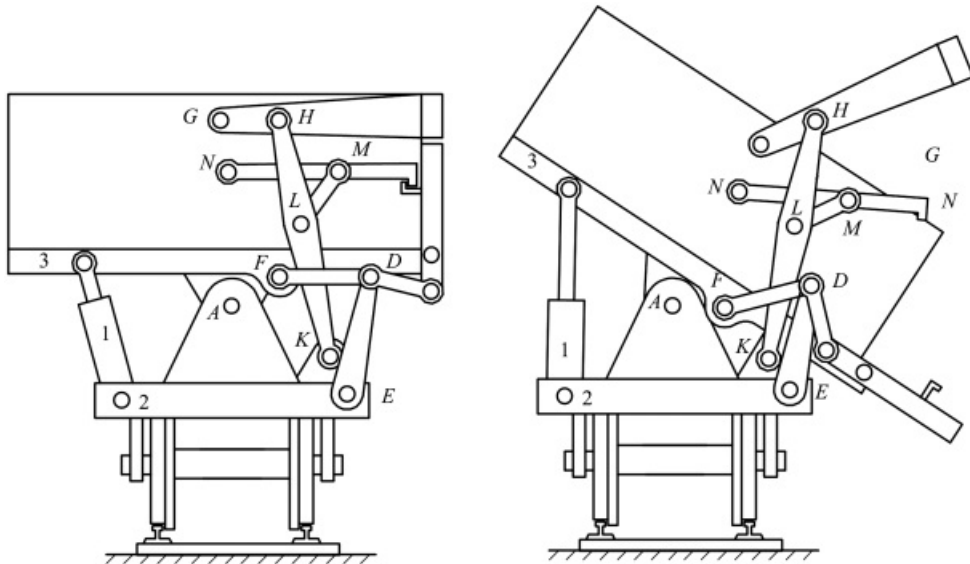


Figure P1.24 Linkage for Problem 1.24.

1.25 Determine the mobility and the number of idle degrees of freedom associated with the mechanism in [Figure P1.25](#). The round part rolls without slipping on the pieces in contact with it.

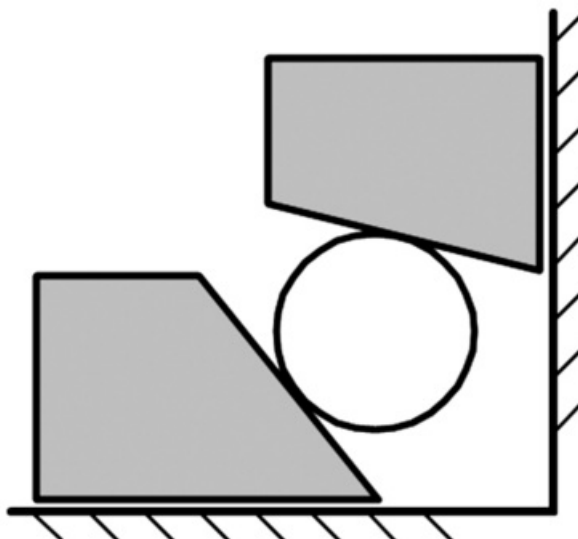


Figure P1.25 Linkage for Problem 1.25.

1.26 Determine the mobility and the number of idle degrees of freedom for each of the mechanisms shown in Figure P1.26. Show the equations used and identify any assumptions made when determining your answers.

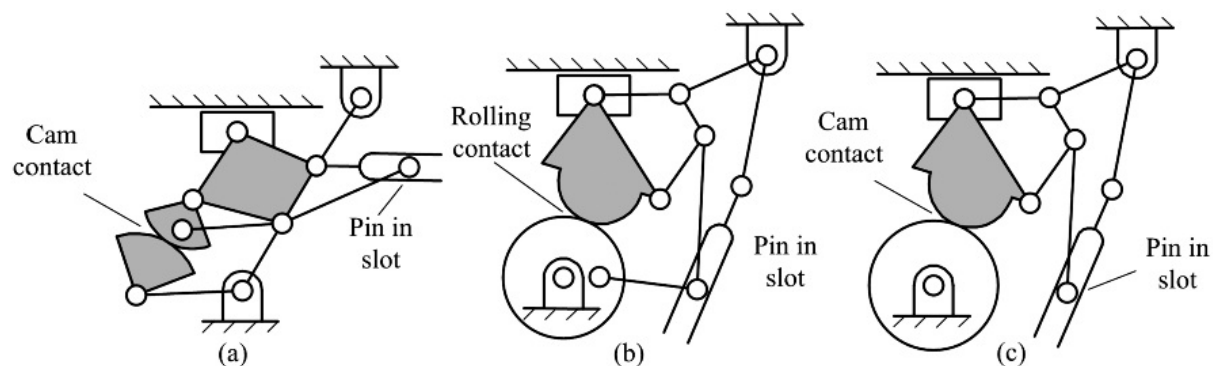
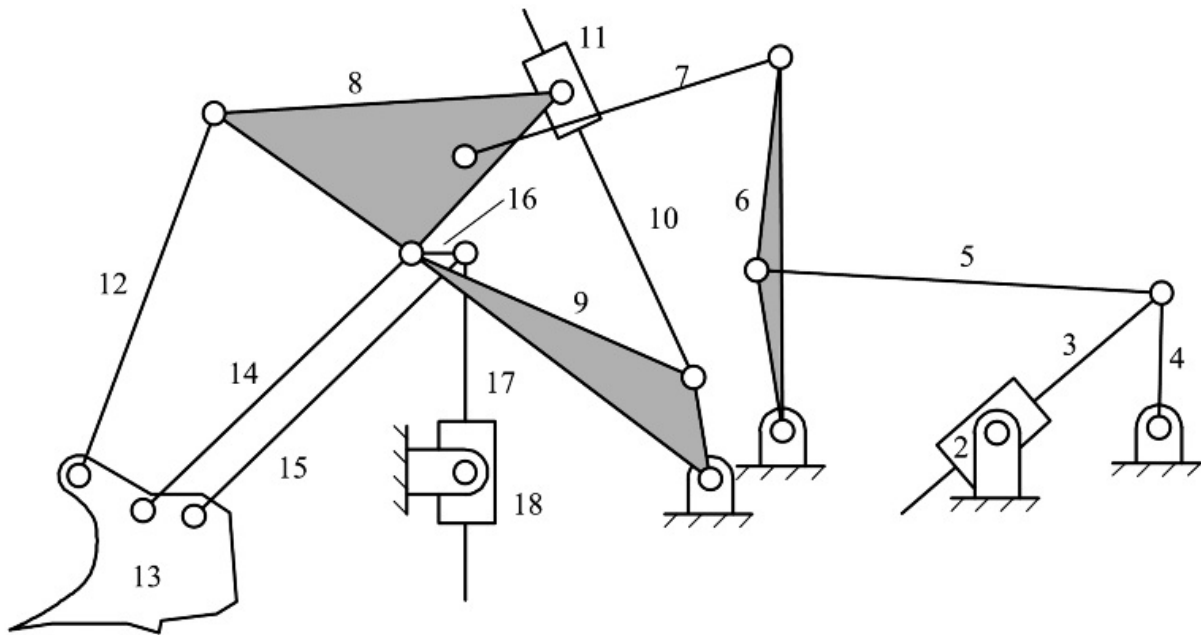


Figure P1.26 Linkages for Problem 1.26.

1.27² Determine the mobility and the number of idle degrees of freedom associated with the mechanism in [Figure P1.27](#). The figure is a schematic of the entire linkage for a large power shovel used in strip mining. It can cut into a bank 20 m high and can dump to a height of 14.5 m. Link 7 is connected to link 8 with a revolute joint. Show the equations used and identify any assumptions made when determining your answers.



[Figure P1.27](#) Linkage for Problem 1.27.

1.28 In [Figure P1.28](#) is a portion of the support mechanism for the dipper on a large earth-moving machine used in removing overburden in strip mining operations. The fixed centers for the portion of the mechanism shown really move, but useful information can be obtained by observing the dipper motion relative to the “frame” as shown in the sketch. Both links 4 and 5 are mounted at B^* . Links 4 and 6 are parallel and of equal length. The dipper is moved by a hydraulic cylinder-driving crank 5 about its fixed axis. Determine the mobility of the mechanism.

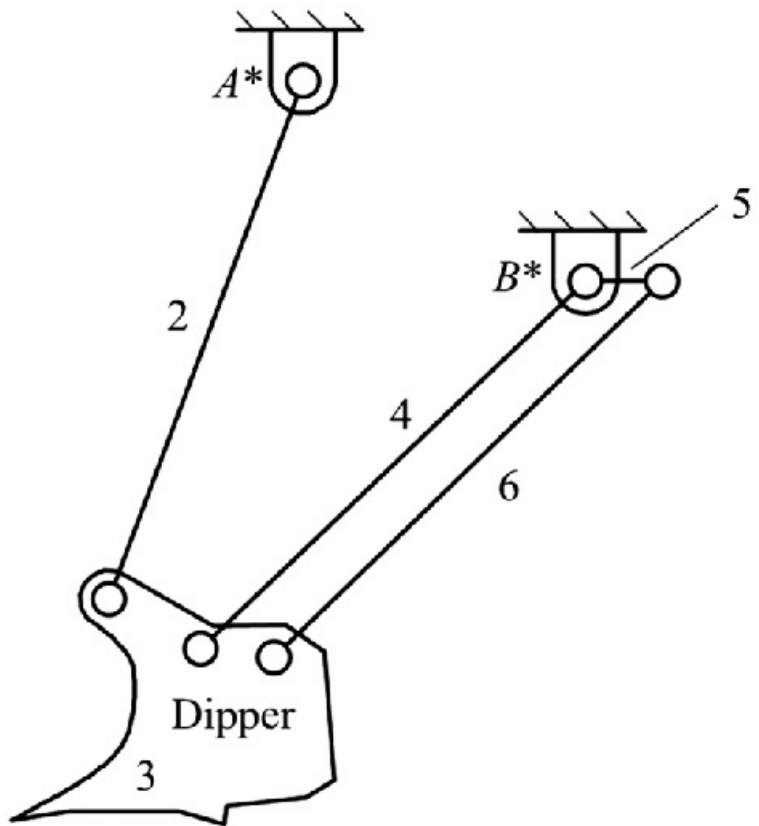


[Figure P1.28](#) Linkage for Problem 1.28.

Mechanism Mobility for Spatial Mechanisms

1.29 What are the number of members, number of joints, mobility, and the number of idle degrees of freedom of each of the spatial linkages shown in [Figure P1.29](#)? For the idle degrees of freedom, identify the input and output links assumed.

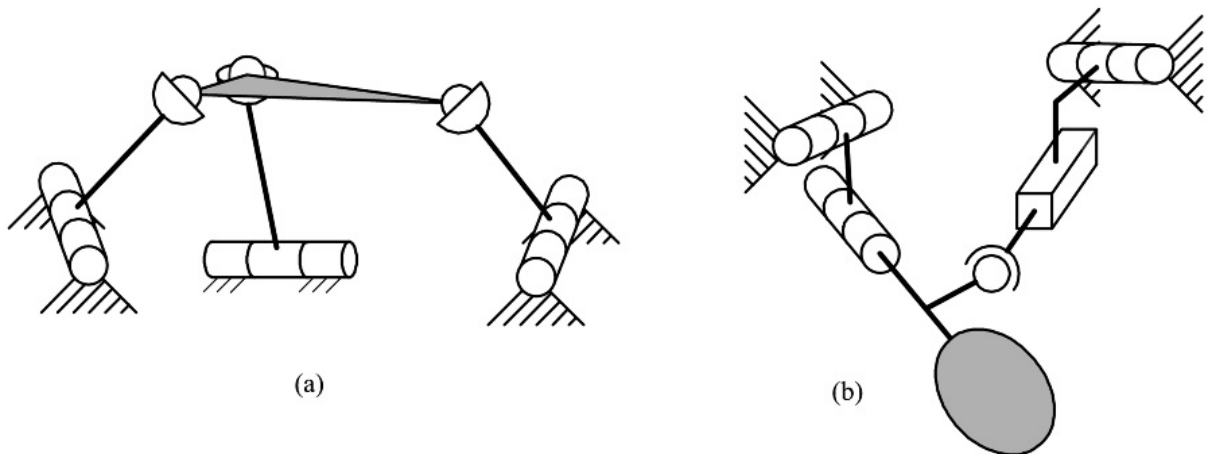


[Figure P1.29](#) Linkages for Problem 1.29.

1.30 Determine the mobility and the number of idle degrees of freedom of the spatial linkages in [Figure P1.30](#). Show the equations used to determine your answers. For the idle degrees of freedom, identify the input and output links assumed.

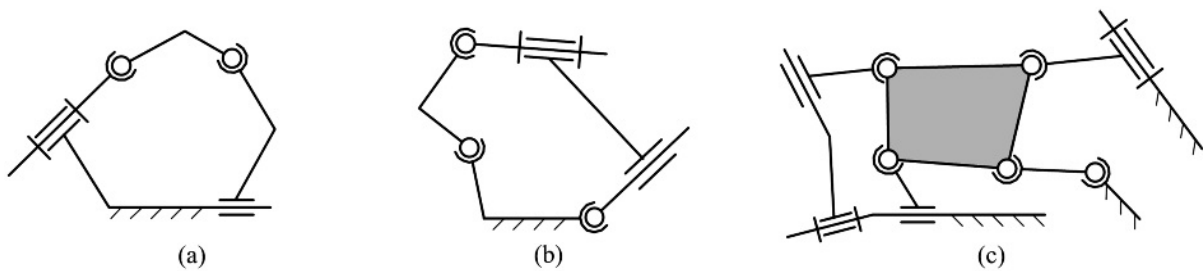


[Figure P1.30](#) Linkages for Problem 1.30.

1.31 Determine the mobility and the number of idle degrees of freedom of the spatial linkages shown in [Figure P1.31](#). Show the equations used to determine your answers. For the idle degrees of freedom, identify the input and output links assumed.

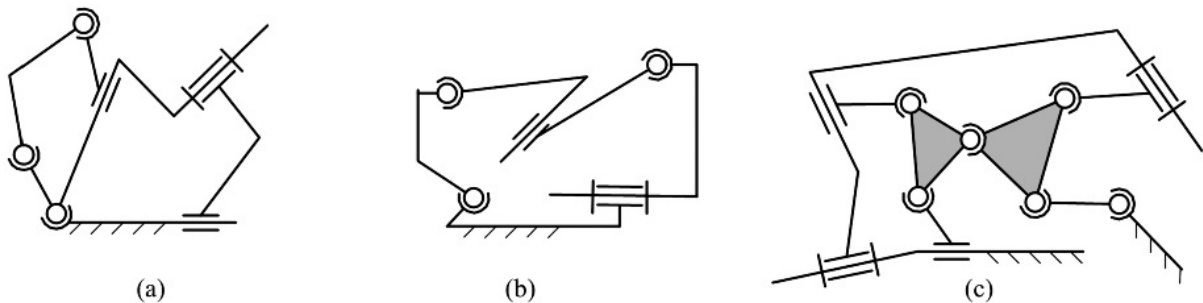


[Figure P1.31](#) Linkages for Problem 1.31.

1.32 Determine the mobility and the number of idle degrees of freedom for each of the mechanisms shown in [Figure P1.32](#). Show the equations used to determine your answers. For the idle degrees of freedom, identify the input and output links assumed.

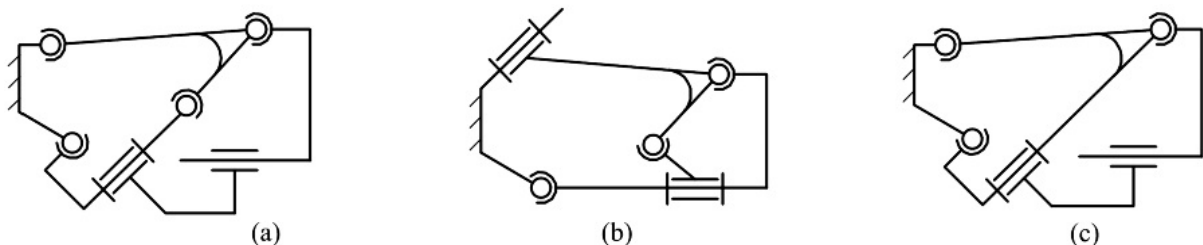


[Figure P1.32](#) Linkages for Problem 1.32.

1.33 Determine the mobility and the number of idle degrees of freedom for each of the mechanisms shown in [Figure P1.33](#). Show the equations used to determine your answers. For the idle degrees of freedom, identify the input and output links assumed.

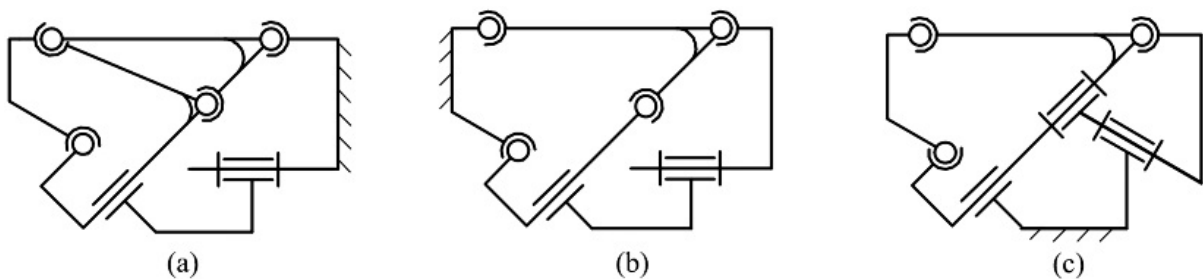


[Figure P1.33](#) Linkages for Problem 1.33.

1.34³ Determine the mobility and the number of idle degrees of freedom associated with each mechanism in [Figure P1.34](#). Show the equations used to determine your answers.

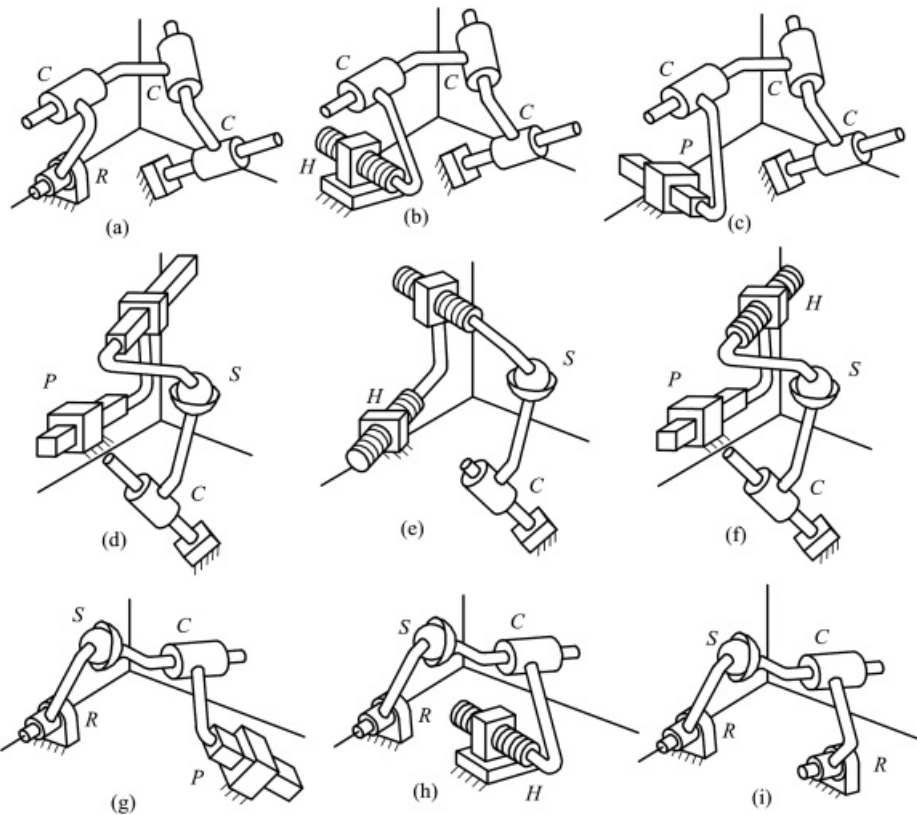


[Figure P1.34](#) Linkages for Problem 1.34.

[1.35](#) In the spatial linkages shown in [Figure P1.35](#), (a) through (d) are all known to have mobility 1. The joints are revolutes in all cases except for one spherical joint in each of (c) and (d). In each case, determine if the linkage is properly constrained or overconstrained. Justify your answers. If the linkage is overconstrained, what geometrical specializations can you see that might result in mobility.

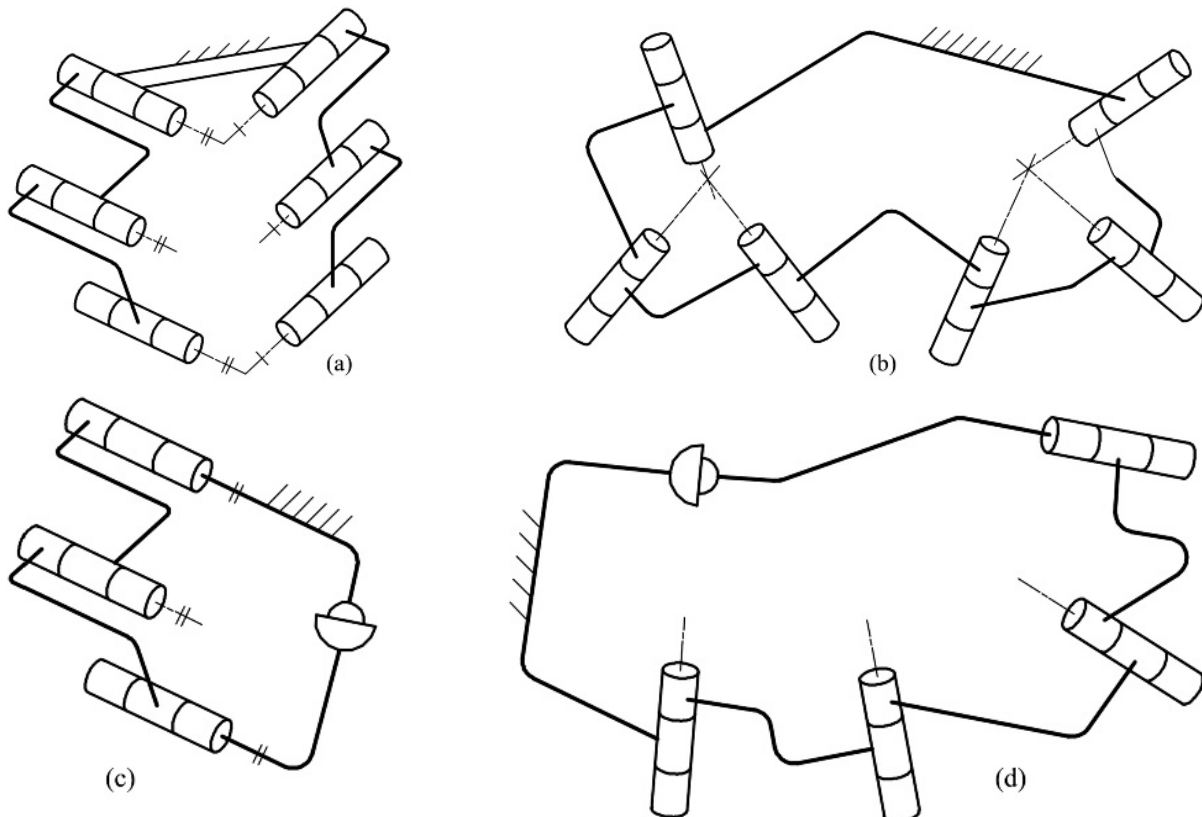


[Figure P1.35](#) Linkages for Problem 1.35.

Four-Bar Linkage Type (Grashof's Equation)

1.36 Determine which (if either) of the following linkages can be driven by a constant-velocity motor. For the linkage(s) that can be driven by the motor, indicate the driver link.

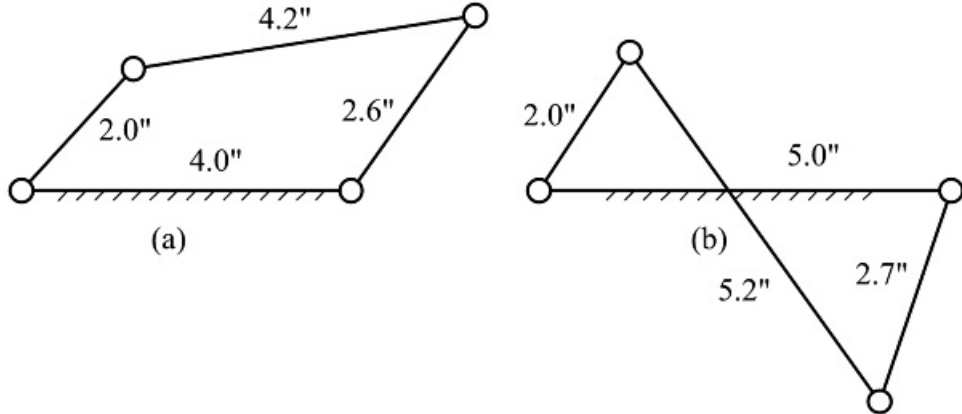


[Figure P1.36](#) Linkages for Problem 1.36.

1.37 Assume that you have a set of links of the following lengths: 2 in, 4 in, 5 in, 6 in, 9 in. Design a four-bar linkage that can be driven with a continuously rotating electric motor. Justify your answer with appropriate equations, and make a scaled drawing of the linkage. Label the crank, frame, coupler, and rocker (follower).

1.38 Assume that you have a set of links of the following lengths: 20 mm, 30 mm, 45 mm, 56 mm, 73 mm. Design a four-bar linkage that can be driven with a continuous-rotation electric motor. Justify your answer with appropriate equations, and make a freehand sketch (labeled) of the resulting linkage. Label the crank, frame, coupler, and rocker (follower).

1.39 For the four-bar linkages in [Figure P1.39](#), indicate whether they are Grashof type 1 or 2 and whether they are crank-rocker, double-crank, or double-rocker mechanisms.

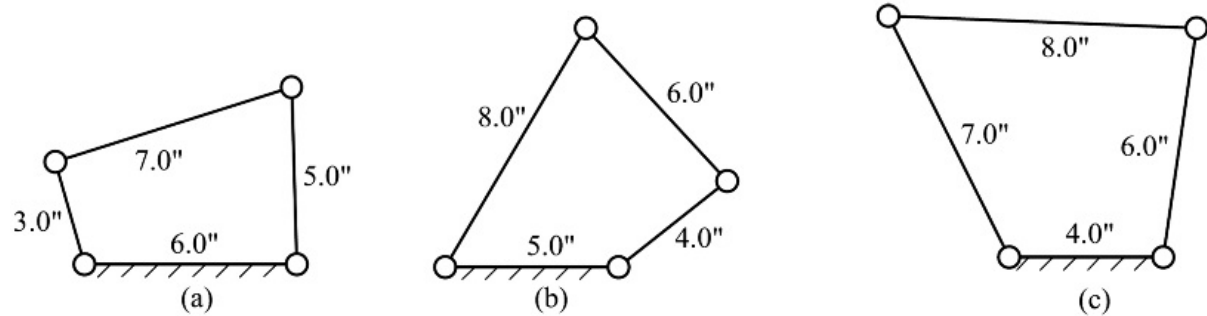


[Figure P1.39](#) Linkages for Problem 1.39.

1.40 You are given a set of three links with lengths 2.4 in, 7.2 in, and 3.4 in. Select the length of a fourth link and assemble a linkage that can be driven by a continuously rotating motor. Is your linkage a Grashof type 1 or Grashof type 2 linkage? (Show your work.) Is it a crank-rocker, double-rocker, or double-crank linkage? Why?

1.41 You have available a set of eight links from which you are to design a four-bar linkage. Choose the links such that the linkage can be driven by a continuous-rotation motor. Sketch the linkage and identify the type of four-bar mechanism resulting.

$$L_1 = 2", L_2 = 3", L_3 = 4", L_4 = 6", L_5 = 7", L_6 = 9.3", L_7 = 13", \text{ and } L_8 = 9"$$

1.42 Determine the number of fully rotating cranks in the planar mechanisms shown in [Figure P1.42](#). Show your

calculations.

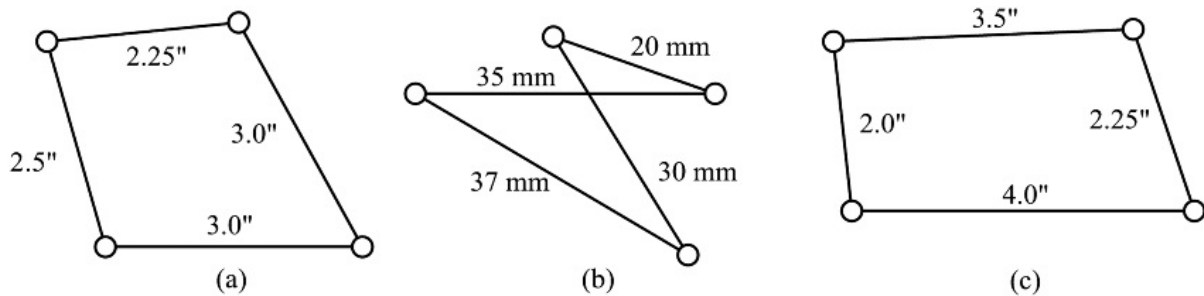


[Figure P1.42](#) Linkages for Problem 1.42.

1.43 If the link lengths of a four-bar linkage are $L_1 = 1$ mm, $L_2 = 3$ mm, $L_3 = 4$ mm, and $L_4 = 5$ mm and link 1 is fixed, what type of four-bar linkage is it? Also, is the linkage a Grashof type 1 or 2 linkage? Answer the same questions if $L_1 = 2$ mm.

1.44 You are given two sets of links. Select four links from each set such that the coupler can rotate fully with respect to the others. Sketch the linkage and identify the type of four-bar mechanism.

- $L_1 = 5''$, $L_2 = 8''$, $L_3 = 15''$, $L_4 = 19''$, and $L_5 = 28''$
- $L_1 = 5''$, $L_2 = 2''$, $L_3 = 4''$, $L_4 = 3.5''$, and $L_5 = 2.5''$

1.45 The mechanisms shown in [Figure P1.45](#) are drawn to scale.

- Sketch kinematic schematics showing the relationships between the members and joints.
- Determine the Grashof type of each four-bar linkage in each mechanism.

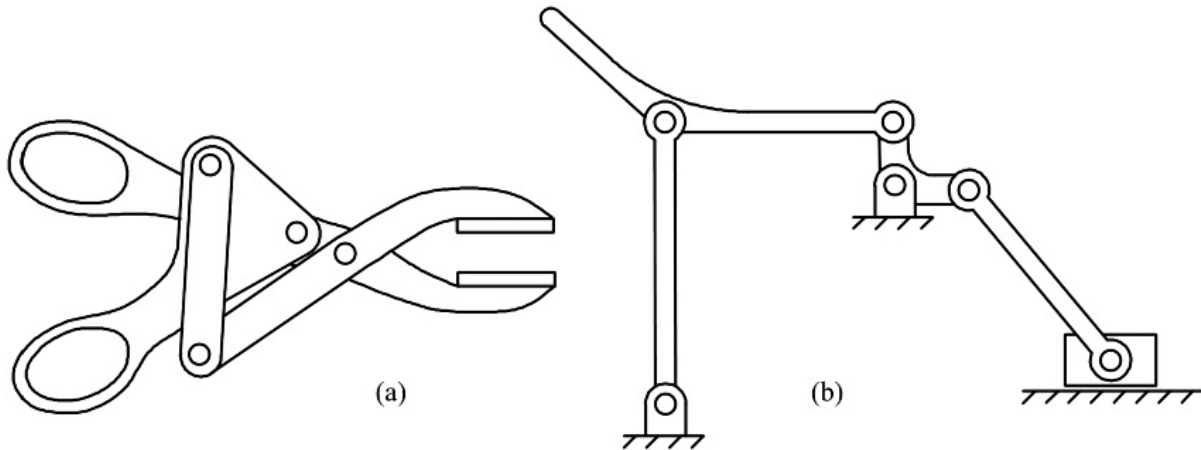


[Figure P1.45](#) Linkages for Problem 1.45.

2

TECHNIQUES IN GEOMETRIC CONSTRAINT PROGRAMMING

Prerequisite Knowledge Needed for Chapter 2

A basic knowledge of two-dimensional drawing in a parametric design program is assumed. This knowledge can be achieved by going through the tutorials available directly from the program vendor or from the tutorials available on the web. Some familiarity with the types of simple linkages discussed in [Chapter 1](#) would be helpful but is not essential.

A knowledge of the kinematic entities links, joints, and linkage chains and loops described in [Chapter 1](#) is necessary. A particle dynamics course providing an understanding of the vector nature of positions, velocities, and accelerations would be helpful.



2.1 Introduction

When solving a kinematic analysis problem, as will be described in [Chapters 4](#) and [5](#), the mantra is position, then velocity, then acceleration. The most efficient way to find the position of a linkage has been to construct it graphically, since the trigonometric equations needed to find it analytically are nastily nonlinear. All of that has changed with the advent of modern CAD software that solves those nonlinear equations without the user being aware of what it is doing. There is no point in manually constructing the right bisector of the line through a pair of points when any modern CAD program will draw it with the touch of a cursor. Consequently, it is highly desirable for the student to have the use of such a program, and to become sufficiently expert in its use to efficiently construct solutions to simple kinematic problems. The ways in which this can be done form the subject of this chapter. It is recommended that the student select a suitable software tool and use it to follow through the simple examples presented here step by step.

Prior to the 1950s, kinematic design and analysis was accomplished almost exclusively using graphical techniques supplemented by labor-intensive calculations. Sandor and Freudenstein [7] published the first paper on kinematic synthesis using a digital computer in 1959, and thereafter, a large number of programs were developed for the design and analysis of mechanisms. The analysis programs tended to be general, and today there are general purpose programs such as ADAMS [9], WorkingModel [3], and Analytix [13], as well as modules in most solid-modeling programs such as Solidworks [2], Solidedge [15,16], Autodesk Inventor [25], and PTC Creo (formerly ProEngineer) [11]. Kinematic synthesis tends to be more difficult than analysis because of the nonlinearities associated with different problems. Therefore, synthesis has generally been approached by developing special purpose programs for specific types of kinematic problems. Examples of such programs are KINSYN [12], LINCAGES [6], and RECSYN [19–24] for rigid-body guidance, and the WATT [4] suite for other problems such as path generation, and SAM [1] for multiple problems such as path generation and rigid body guidance. Erdman [5] wrote a survey article that gave a fairly long and comprehensive list of mechanism synthesis software in 1995. In addition, a number of universities have developed special computer programs based on general-purpose software platforms. Examples of this are the Matlab modules provided with this textbook and programs based on TK Solver [18] developed by Norton [10].

As solid-modeling software packages and kinematic analysis packages have improved both in the user interface and computational speed, it has been possible for the designer to use trial and error to solve many of the simple kinematic design problems that once required specific programs to solve efficiently. One effect of this has been that the market for kinematic synthesis programs has greatly reduced, making it difficult for software companies to justify the resources to maintain sophisticated kinematic design programs. As a result, many of the programs developed earlier are no longer supported. In 2015, the authors were able to find only one program (SAM) that is being actively marketed.

Fortunately, modern solid-modeling programs now provide an infrastructure where an engineer with an undergraduate understanding of kinematics can develop relatively sophisticated graphical “programs” for solving a wide range of kinematic design and analysis problems. In fact, most of the linkage design and analysis problems discussed in this textbook can be solved using standard solid-modeling software.

When computer-aided drafting programs were originally developed, the drawings were represented internally by the coordinates of points and tables indicating which points were connected by lines or polygons. In modern solid-modeling programs based on parametric technology, the point coordinates are represented by variables, and the geometric features defined by the points are represented by homogeneous equations. Additional constraint equations are used to locate and orient various features relative to each other and to define how the features combine. Each time a change is made, the system solves a large system of mostly nonlinear equations to determine the boundary elements of the entire solid model. Because of the speed of modern computers, highly efficient nonlinear equation solvers, and constraint managers [17] that identify what equations can be solved and the most efficient order for doing so, very comprehensive solid-modeling programs are now available as a design tool for most engineers. The user typically has no access to the constraint manager nor does he/she need to be aware of how it is functioning behind the user interface. This solid-modeling environment can be used efficiently for both kinematic design and analysis.

The use of parametric, solid-modeling programs to solve kinematic problems was first developed by Kinzel, Schmiedeler, and Pennock [8]. They refer to the technique as Geometric Constraint Programming (GCP), and they developed the original concepts using the drafting module in SolidEdge that currently offers a free version of the two-dimensional (2D) module from their general solid-modeling program [16]. This 2D module is adequate for performing all of the design work presented in this book. However, the original approach developed for GCP can be implemented in any of the parametric, solid-modeling programs currently available. We have used SolidWorks for the drawings in this book. The overall concepts are the same for any parametric-design program, but the implementation details will vary slightly with different programs.



2.2 Geometric Constraint Programming

In GCP, the user works in the 2D drawing mode available in all parametric-based programs. Depending on the program, the appropriate 2D drawing mode to use for GCP will be available through two avenues. All of the programs will have a sketch mode where the geometry is defined prior to solid-modeling operations such as extrusion or revolving. Typically, the sketch mode will have the maximum number of constraint features available; however, drawing features such as line type and color and polygon fills may be limited. In addition, each of the programs will have a drawing mode whereby 2D drawings can be produced. However, in the drawing mode, constraint features may be more limited than in the sketch mode. Therefore, the user should review the features available in both the sketch mode and drawing mode to determine which mode is more appropriate for the specific problem being addressed. The minimum number of constraint types required is discussed in the next section.

When solving a problem using the 2D module, the user can draw a mechanism very accurately without performing a single calculation. In addition, a basic position, velocity, acceleration, and instant-center analysis can be performed without making any calculations, although the vector equations programmed should be written down to guide the analysis. The kinematic figures and polygons are drawn by enforcing the geometric constraints that define the problem. The process can be used in two similar ways. In the first instance, the process can be used for a specific problem by dimensioning the mechanism and specifying all positions so that that the problem is unique. By simply measuring the dependent variables, the problem can be solved. In the second instance, the user identifies what variables can be changed and treats them as design inputs. These variables are almost always dimensions. If the constraints are specified properly, the mechanism will adjust visually as the dimensions are changed. One or more of the input variables can be left unspecified, which allows the mechanism model to be moved to determine visually the effect of parameter changes on position or on other variables. This flexibility allows the geometric figure to be evaluated for a variety of inputs so that it, in essence, becomes a graphical program. This is the basis for the term Geometric Constraint Programming or GCP.



2.3 Constraints and Program Structure

2.3.1 Required Constraints

In CGP, the user specifies the desired constraints, and the software constructs and solves the mathematical equations defined by the constraints. While more may be useful, only nine types of constraints are necessary, and all modern parametric-design programs will have these available in either the sketch or drawing mode. The programs will also have a “snapping” feature where the constraint can be applied automatically if the two entities are close enough to approximate the constraint. This feature may be turned on or off. Generally, it is desired to leave the snapping feature turned on until the final design is developed and then to turn it off when exploring variations in the final design. It should be noted that the solid-modelling program used might not refer to constraints as such. For example, SolidWorks designates as *relations* many of the constraints listed below, and it constrains a line length to a fixed value (dimension lock) by dimensioning the line and designating the resulting dimension as a *driving dimension*. The basic constraint types needed for GCP are [14,26]:

Merge: A single point is required to coincide with another point. If the snapping feature is turned on, the program will apply this constraint automatically when a line is drawn from the end point of one line near to the start, mid, or end point another line. A revolute joint is represented by this constraint.

Coincidence: A single point is required to lie on a line or a curve. If the snapping feature is turned on, most programs will apply this constraint whenever a line is drawn to a point near a curve or line. That is, the program will constrain the point to lie on the line or curve if a point near the line or curve is selected. A pin-in-slot joint is represented by this constraint.

Dimension Lock: A linear dimension or an angular dimension is constrained to have a fixed quantity. Note that dimensions can be specified to be either *driving* or *driven*. This constraint refers to a *driving dimension*. A *driven* dimension is not constrained to have a specified value and is used only to report the current value. The value of a *driving dimension* is constant and constitutes a constraint while a *driven dimension* can vary with the linkage position and is not a constraint.

Position Lock (Fix): A point, line, or curve is constrained to be fixed to the ground. Fixed pivots or fixed slider lines are constrained in this manner.

Equality: Two or more lines (or arcs) are constrained to be of equal length (or radius). This constraint equates the magnitudes only. There is no sense of direction in most 2D drafting programs.

Parallelism: A line is constrained to be parallel to another line.

Perpendicularity: A line is constrained to be perpendicular to another line.

Tangency: A curve or a line is constrained to be tangent to a specified curve. The joint between a cam and follower is defined by this constraint.

Equation: A functional relationship is defined between two or more dimensions. This constraint is required only when the length of one line is a scalar product of that of another line, or is related to another line length in a nonlinear manner. Most problems involving only positions or velocities do not require this type of constraint. However, the solution of acceleration problems will be simplified if equation constraints are available.

2.3.2 Other Constraint Options

Depending on the parametric-design program, other constraints may be available. Some of these may be achieved by a combination of two or more of the basic constraints above but are available directly for simplicity. Examples are:

Vertical: A line is constrained to be vertical or parallel to the *y* axis of the implied coordinate system, or two or more points are required to lie on a virtual vertical line

Horizontal: A line is constrained to be horizontal or parallel to the *x* axis of the implied coordinate system, or

two or more points are required to lie on a virtual horizontal line.

Collinear: Two or more lines are constrained to be collinear.

Midpoint: The endpoint of one line is constrained to be coincident with the midpoint of another line.

Parametric programs will have all of the above constraints available in the sketch mode; however, some may not be available in the drawing mode. For example, SolidWorks does not have the equation constraint available in the drawing mode. On the other hand, the drawing mode usually has enhanced drawing features that make this mode easier to use. When preparing this textbook, we used the drawing mode because of the enhanced drawing features. When equation constraints were required, we performed the calculations external to the program.

2.3.3 Annotations

All programs will have some way to print text on the drawing so that points can be labeled; however, generally subscripts and superscripts will not be directly available. Subscripts and superscripts can be drawn by creating them separately; however, this takes considerable effort and generally is not required for legibility. Therefore, for simplicity it is generally preferable to use $A1$ rather than A_1 . Also, the text will usually be static (fixed) and not attached to points, lines, or polygons. This is not an issue if the lines and polygons are static; however, if they move (which is the usual case when GCP is used in the programming mode), static text annotations are not useful. In that case, it is preferable to rely on other means such as color or line types to identify different quantities as they move. Once a static configuration is established, the text can be easily moved to its proper position. This is the technique employed in most of the examples used in this text.

2.3.4 Use of Drawing Layers

The entire process associated with solving a problem using GCP involves drawing lines and curves and applying dimensions and other constraints. If all of the work is done on a single, visible drawing space, the drawing will become too cluttered to be readable. For this reason, it is desirable to set up the solution process on drawing layers that can be selectively hidden. All solid-modeling programs will have a layer structure available in some form. In the sketch mode, layers may not be designated as such, but new sketches can be defined and others hidden. Therefore, different sketches can function as layers in the drafting sense and, in the following, we will use sketches and layers interchangeably. In the 2D drafting/drawing mode, traditional layers can be defined directly. However, depending on the settings, the layers may behave differently in different programs. In particular, it may or may not be possible to edit the entities in one layer when another layer is active. It is important for the user to determine the properties of the layers before setting up the solution process. If all layers can be edited from any other layer, it is possible to make unwanted changes inadvertently. In this text, the only feature of layers that we will use is visibility and invisibility.

To illustrate the organization of a GCP program with the use of layers, assume that we would like to analyze a linkage for position and velocity. The layers we might use are:

Layer for the basic linkage

Layer for miscellaneous dimensions such as those required to draw ground pivots and joints

Layer for linkage dimensions

Layer for velocity polygon

Layer to dimension the velocity polygon to identify the individual velocities

Layer showing velocity “vectors” attached to specific points on the linkage

Here, “vector” is used in quotes because only the magnitude and line of action of the true vector can be represented in GCP. Therefore, the line drawn may appear to be in the direction opposite to the correct one defined by a true vector. This means that the user must infer which end of the line contains the arrowhead from the context of the problem and solution process. Although GCP is a powerful design technique, the user must have a basic engineering understanding of the problem to use it effectively.

The reason for this choice of layers is that during the solution process, it may be desirable to hide certain

information in one or more layers. For example, we may not be interested in seeing any of the dimensions at the end of the solution process while they will be of great interest at intermediate steps. Similarly, we may be interested in only the velocity magnitude lines as the linkage moves and not in the velocity polygon itself. Conversely, we may be interested in only the velocity polygon and not in the velocity magnitudes as the linkage moves.

A different set of layers may be useful for each class of problem. Therefore, the user should give some thought to the layer setup before starting the drawing. Layers can be added (or deleted) at any stage of the solution process, and information can be moved from one layer to another through cut-and-paste operations. However, this may require additional work that can be avoided with preplanning.

2.3.5 Limitations of GCP

As will be illustrated throughout this book, GCP is a powerful tool for solving a large range of kinematic problems. Kinematic synthesis can be accomplished only with a good understanding of geometry; however, to use GCP effectively for velocity and acceleration problems, the user needs to have an undergraduate level of understanding of kinematics. While no calculations need to be made for solving velocity problems, the user must know the vector relationships in order to draw and/or interpret the lines appropriately. More importantly, the user needs to be able to estimate the proper directions for the velocity vectors since, as the linkage moves, the lines representing the velocity vectors for selected points may appear to be in the wrong direction if the end with the arrow head is not interpreted correctly. This will be illustrated later when the procedure is used to solve velocity problems using both polygons and instant centers of velocity.

In addition, the procedure can be used to solve specific acceleration problems, but either some external calculations will be needed or functional (equation) constraints must be a program option. Without functional constraints, it is not possible to develop general graphical programs for acceleration analyses because it is not practical to construct directly the acceleration components that are nonlinear functions of the link angular velocities.¹ However, these components can be easily defined using functional constraints.



2.4 Initial Setup for a GCP Session

Commercial parametric-design programs are capable of developing and analyzing very complex models and assemblies. It typically takes months of training to become proficient with all aspects of the programs. Fortunately, GCP requires only a small subset of the capabilities of such programs. Therefore, in this section, we will describe only the essential features required to solve kinematics problems. The drawings shown to illustrate the process were developed using SolidWorks; however, similar results can be obtained using any of the full-function, parametric, solid-modeling programs.

To begin, we will assume that the program has been properly installed on the computer being used, and the user has some familiarity with the program in general. Such a familiarity can be achieved by studying the basic tutorials available under the program *Help* or through tutorials available within the program or on the web.

To begin a design session, open the program and create a new document. If all of the required constraint types are available in the drafting mode, select it because of the richer set of drawing options than are available in the sketch mode. Otherwise, select the sketch mode. Next use available page setup options to format the drawing sheet for a white background and with no extraneous lines such as borders, title boxes, or other similar information.

Ensure that the general snap feature is activated. This means that when any two entities are close to any of the constraint conditions listed above, the entities will snap to the constraint condition. This is usually desired during the initial phase of the solution process. However, once the linkage is designed or the analysis problem solved, it is usually desirable to turn off (deactivate) automatic constraints to avoid automatic snapping to unwanted constraints.

In each solid modeling program, it will be possible to deactivate individual constraints. This feature is necessary because unwanted constraints may be established through the snapping operation. This operation may involve nothing more than selecting an icon corresponding to the constraint and deleting it. As part of the initial setup procedure for GCP, the user must determine the process for deactivating unwanted constraints.

Next select the default colors desired for lines and polygons. Also select the units desired for the specific problem. Explore the program's procedure for labeling or annotating the drawing. Make sure that it is possible to move the annotations on the drawing because the labels typically will not move with lines and polygons, and it is desirable to move the labels to their correct positions when the linkage is in its final position. Save the generic, formatted file with all of the default values set. We will typically start with this blank page for various exercises in this book.

2.4.1 Effect of Typical Constraints

In GCP, the main entities used for solving problems are points, straight lines, and circles (or circular arcs). Therefore, here we will limit our discussion to the relations available for these three types of entities. The relations for splines and ellipses will be natural extensions of those for lines, points, and circles. Typically, the solid-modeling program used will indicate the valid relations available when one or more entities are selected. For example, when a single line is selected, typical constraints available might be:

1. Fix
2. Constrain to be vertical
3. Constrain to be horizontal

When two lines are selected, typical constraints available might be:

1. Fix both lines
2. Constrain both lines to be vertical
3. Constrain both lines to be horizontal
4. Constrain both lines to be collinear
5. Constrain the lines to be perpendicular

6. Constrain the lines to be parallel
7. Constrain the lines to be of equal length

Generally, one of the entities must be moved or changed to apply a constraint. If both entities can be moved or changed, the constraint manager in the program determines the entity that is moved or changed. If it is necessary for one line to be moved instead of the other, the line that cannot be moved should be fixed prior to applying the constraint. It is important to be able to delete the constraint and start over if the wrong line is moved or changed when the constraint is applied.

When a single line is drawn or selected, at least three points can be identified. These are the two end points and the midpoint. These individual points can be selected either alone or in conjunction with other entities and constraints applied.

If a line and point are selected, typical constraints available might be:

1. Fix both the point and the line
2. Constrain the point to lie on the line (coincident)
3. Constrain the point to snap to the midpoint of the line
4. Constrain the point to snap to one of the endpoints of the line

Depending on the program, if a point snaps to another point (endpoint or midpoint), the operation might be equivalent to merging the two points. In that case, the operation cannot be undone by deleting the constraint because the merged points become a single point. Again, operations 2–4 above will generally require one of the entities to move, and the entity that moves will depend on the constraint manager unless one of the entities is fixed first.

If two points are selected, typical constraints available might be:

1. Fix both points
2. Constrain both points to be on a vertical line
3. Constrain both points to be on a horizontal line
4. Merge both points. Typically, this constraint cannot be undone by deleting the constraint

If one of the points must move to satisfy the constraint and only one point can move, it is necessary to fix the other point to ensure that the proper point moves. If this is done and if the fixed point is not supposed to be permanently fixed, the fix constraint can be deleted after the operation.

When a circle and a line are selected, typical constraints that might be applied are:

1. Fix both the line and circle
2. Constrain the line and circle to be tangent

Which entity moves to satisfy the tangency constraint will again depend on the constraint manager, and one of the objects should be temporarily fixed if the order is important. Also, the line can be tangent to the circle on either side. If the side is important, the line should be moved close to the desired side of the circle prior to enforcing the constraint.

If a point and a circle are selected, typical constraints that might be applied are:

1. Fix both the point and circle
2. Constrain the point to be coincident with the center of the circle
3. Constrain the point to be coincident with the circle circumference

Depending on the program, constraining the point to be coincident with the center of the circle may retain the identity of the two points and the constraint can be deleted. If the point is constrained to be coincident with the circle circumference, the point can move along the circumference and is not constrained to any single point on the circumference. Again, whether the point or the circle is moved to satisfy the last two constraints will depend on

the program. If one of the entities should not be moved, it should be temporarily fixed.

If two circles are selected, typical constraints available will be:

1. Fix both circles
2. Constrain the circles to be tangent to each other
3. Constrain the circles to be concentric
4. Constrain the circles to have equal radii

When one of the circles must move or change size to enforce a constraint, the circle that is moved or changed will depend on the program unless one of the circles is fixed.

2.4.2 Unintended Constraints

When the setup procedure was discussed, we suggested allowing the program to snap to constraints during the initial part of process. When this is done, the program will snap to any constraints that are close. However, this may fix degrees of freedom that the user wants to be free. For example, when drawing two lines, the user may unintentionally draw one end of the second line so close to the first that an endpoint of one line is made coincident with the first line. If the constraint is undesired, it can be deleted by identifying the constraint and pressing the delete key. The manner in which the constraint is identified will depend on the program; however, it is typical for each constraint to be represented by an icon. Removing the constraint is therefore as simple as selecting the icon and deleting it. An unintended perpendicular constraint may also be imposed when a second line is moved relative to the first one, and the user momentarily pauses when the two lines are almost perpendicular. Again when this happens, it is only necessary to identify the constraint and delete it. After the linkage is designed and automatic constraints are no longer useful, the user should deselect the option to snap to constraints. However, it is important to remember when doing this that none of the constraints will be applied automatically afterward. Therefore, any desired constraints such as merging two points must be applied directly.

2.4.3 Layers, Line Type, and Line Color

The basic process in using GCP to solve problems is quite simple; however, the readability of the results can be greatly improved by the judicious use of layers, line types, and line colors. We can also use notes to annotate the drawings; however, it is difficult to make the notes follow the lines when they are animated. Therefore, it is better to use color and line type to differentiate among different points and lines if at all possible. This is often an issue between using the sketch mode and 2D drafting mode in a given program. In particular, the sketch mode may have very limited options associated with line colors and line types because the sketch mode is typically used only in a preliminary step in defining solid modeling extrusions or cutouts. Therefore, if the drafting mode has all of the types of constraints required, it is preferred over the sketch mode. If, however, required constraints are available only in the sketch mode, it is often possible to create uncluttered GCP programs by the judicious use of more hidden sketches (layers) than would be required if the program were used for traditional solid modeling.



2.5 Drawing a Basic Linkage Using GCP

Much of the process in using GCP consists of drawing arbitrary linkages of the same type in selected positions and then constraining the link lengths to be equal. Therefore, we will illustrate the procedure for drawing both a four-bar linkage and a slider-crank linkage. The basic procedures are extremely simple and easy to follow if we use layers.

2.5.1 Drawing a Four-Bar Linkage Using GCP

To begin the procedure for drawing a four-bar linkage, open the generic, blank drawing sheet, and set the program so that it automatically snaps to constraints. In the drawing window, draw three connected lines, as shown in [Figure 2.1](#). There are four points and three lines. Except for the automatic Merge constraint at the ends of the first and second lines, no constraints have been set, and it should be possible to move any of the entities (points or lines) arbitrarily. To gradually constrain the linkage, click on the first point of the first line drawn and apply the Fix constraint. Next constrain the first and last points to be on a horizontal line (Horizontal constraint). The link lengths can still be changed, and the second ground pivot can still be moved on a horizontal line. Use the annotation or text feature in the program to label the drawing. Place the letters *A* and *B* at the two coupler points and *A** and *B** at the corresponding locations of the ground pivots.

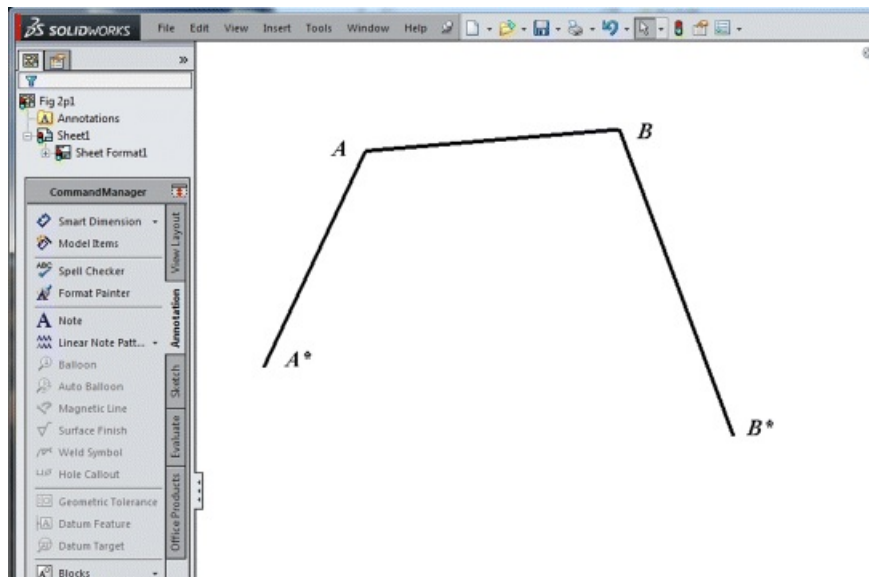


[Figure 2.1](#) Initial three lines drawn to define a four-bar linkage with annotations.

Next construct a coupler triangle by starting at the coupler point at *B* and drawing to an arbitrary point. Complete the triangle by drawing a line to the coupler point at *A*. Label the third coupler point as *C*. If the program will allow a polygon fill, fill the coupler triangle with a solid fill color. Also color the triangle lines a different color (for example red) from the color of the two cranks. The final result is shown in [Figure 2.2](#) with the coupler triangle outlined in red. It should be possible to move any of the linkage points (other than the previously fixed point at *A**) or any of the link lengths. However, when this is done, the annotations *A*, *B*, *B**, and *C* do not move automatically. Once the linkage is set, however, we can move the letters to the proper locations manually.

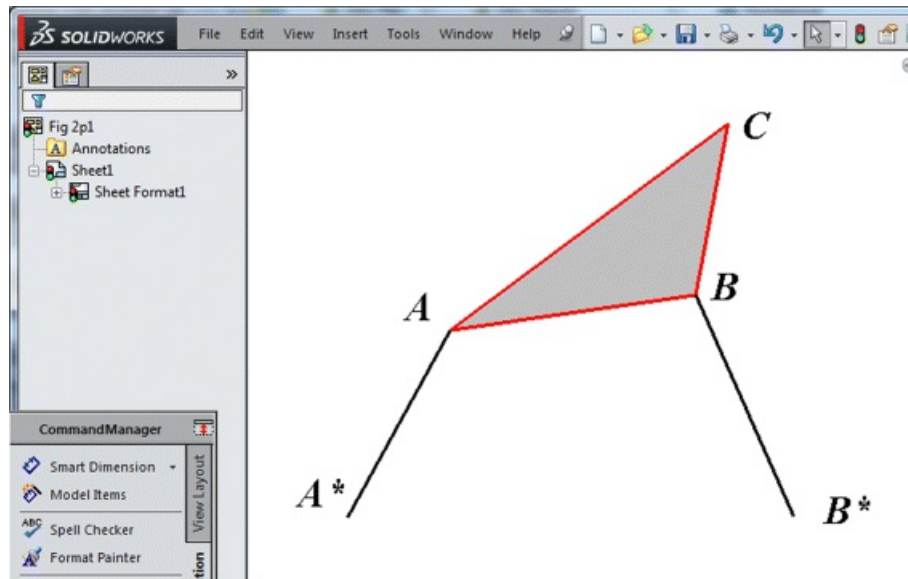
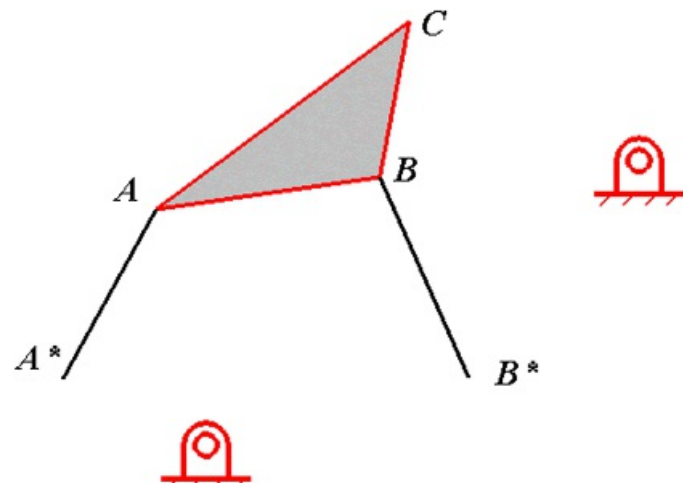


[Figure 2.2](#) A linkage with the coupler triangle shaded and labeled.

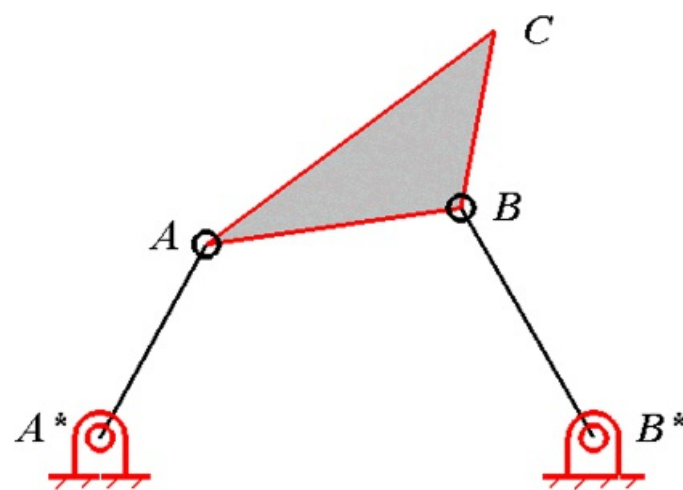
2.5.2 Including Ground Pivots and Bushings

To make the linkage drawings in [Figure 2.2](#) look more like a traditional mechanical linkage, we can add pin bushings and ground pivots. For pin bushings, we can draw a simple circle and merge the center point of the circle with the end point of a given link. However, ground pivots are somewhat more involved. A procedure for drawing ground pivots is presented in Appendix 2A. We will assume that a file has been created with a scaled version of the ground pivot, and we will simply use the results from that procedure.²

To begin the procedure, copy the ground pivot drawing and ALL of its constraints and dimensions and paste two instances of the ground pivot drawing into the drawing area for the four-bar linkage. Hide the dimensions for the ground pivots in a separate layer. The drawing should appear as shown in [Figure 2.3](#). Next select the center of the small circle for one ground pivot and simultaneously select the point on the line next to A^* . Merge the center of the circle with the endpoint point at A^* . Repeat the procedure for the second ground pivot and the point at B^* . Because point B^* is not fixed, it may move on a horizontal line through A^* to merge with the ground pivot. If this happens, we could drag the pivot to near the original position of B^* and move the letter B^* if necessary, or we could temporarily fix the location of the point at B^* before constraining the center of the ground pivot to lie at B^* . To draw bushings at the locations of A and B , we can draw a small circle and dimension it to be the same diameter as the inner circle of the ground pivot (0.1 in). Copy and paste the circle once to create a pivot for each location. Select each circle and constrain their diameters to be equal. Next merge the center of one circle and the point at A . Repeat the process for the other circle and B . The final result is shown in [Figure 2.4](#). Because of how the constraints were applied, the ground pivots and circles at A and B will move as the points and lines are moved to new locations either by dragging or by setting additional constraints.



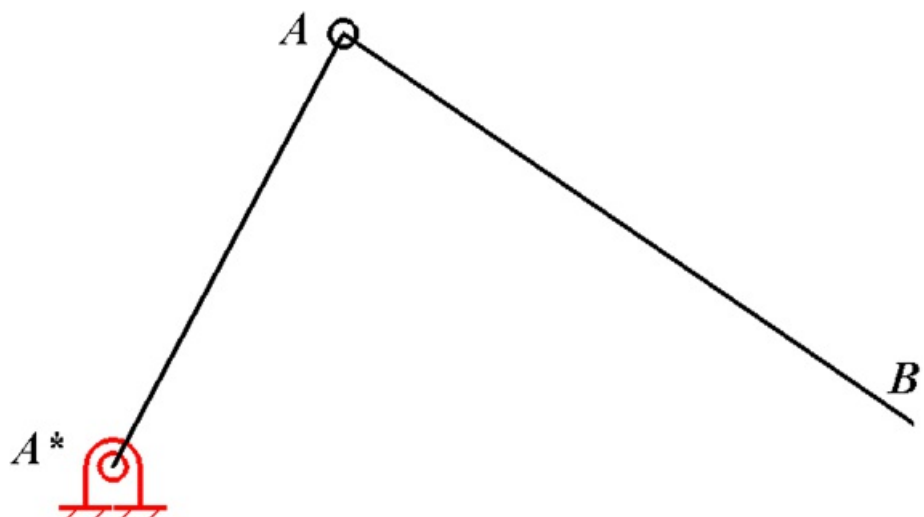
[Figure 2.3](#) Linkage with ground pivots copied to drawing.



[Figure 2.4](#) Final linkage with ground pivots and bushings properly placed.

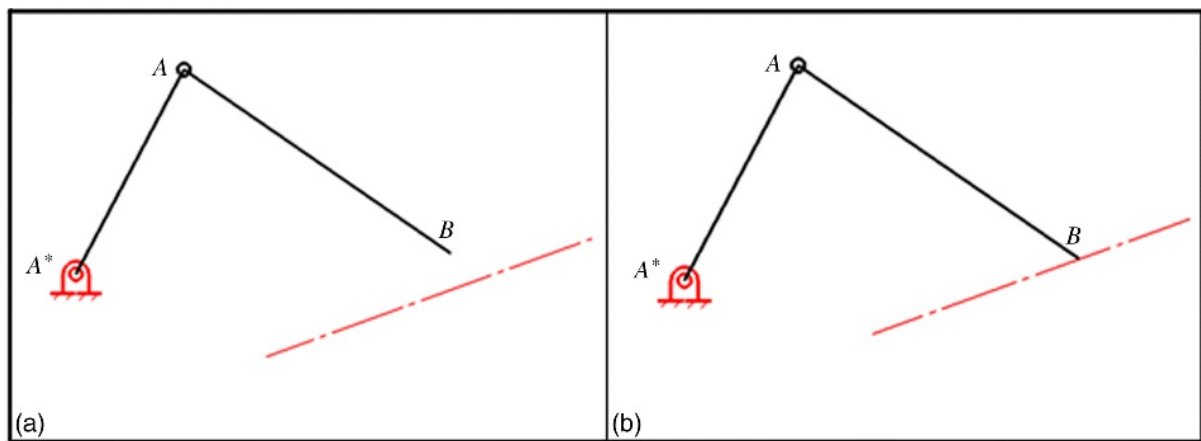
2.5.3 Drawing a Slider-Crank Linkage

Drawing a slider-crank linkage initially follows the same procedure as for the four-bar linkage. To begin the procedure for the drawing, open the blank drawing sheet and draw two lines to represent the crank and coupler for the slider-crank mechanism. Copy and paste the ground pivot in the drawing and merge the center of the ground pivot with the fixed pivot at the crank location. Label the points as shown in [Figure 2.5](#).



[Figure 2.5](#) Initial part of slider-crank mechanism.

Drawing the slider requires several steps ([Figure 2.6](#)) if a general slider crank is to be represented. First draw a construction line in the direction of the slider motion and temporarily fix the line (a). To be general, we will assume that the line is not horizontal. Select both the point at *B* and the construction line and make them coincident (b). Draw a rectangle centered at *B* and along the construction line (c). Draw a second construction line along the bottom of the rectangle and constrain the new construction line to be parallel to the first one (d). Fix the second construction line. The procedure for developing an inclined slider line is also included in Appendix 2A. Create a generic slider line using the procedure shown in Appendix 2A because it will be used numerous times throughout the exercises in this book.³ Copy the slider line along with all of its constraints and dimensions and paste it into the slider crank drawing (e). Hide the dimensions by copying them to a hidden layer. Select both the lower construction line and the bottom point of the baseline of the slider line and make them coincident (f). Repeat the process for the topmost point on the slider line and the lower construction line (g). Delete both construction lines. Next select both the top and bottom lines of the rectangle and one of the base lines of the slider line and constrain them to be parallel. Then select the bottom line on the rectangle and one of the base lines of the slider line and make them collinear. Finally draw a circle, dimension it the same as the other bushings, and merge the center of the circle with the link point at *B*.



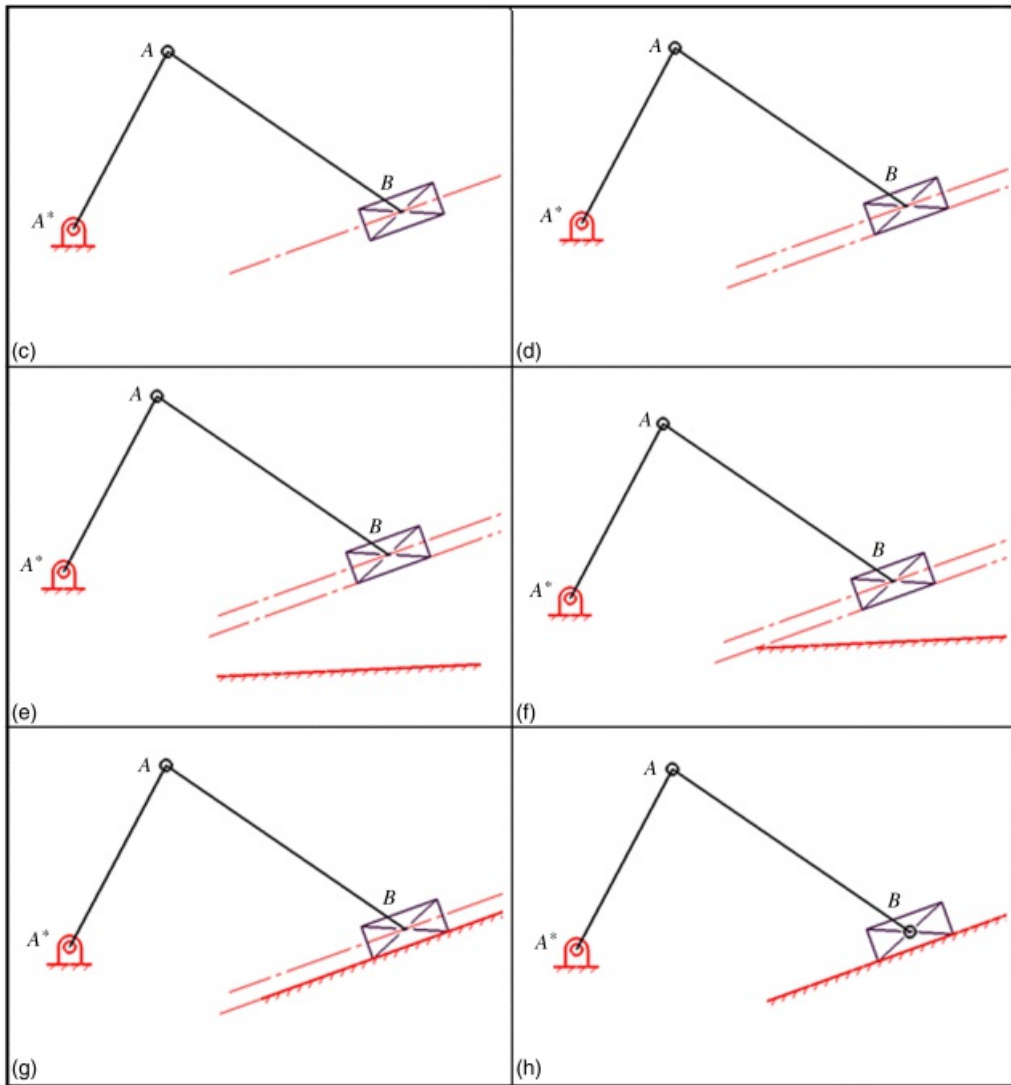


Figure 2.6 Steps in adding slider to slider-crank mechanism: (a) Draw fixed construction line; (b) constrain point at B to be coincident with construction line; Steps in adding slider to slider-crank mechanism: (c) draw slider; (d) draw second, fixed construction line at bottom of slider and parallel to first line; (e) copy and paste slider line into drawing; (f) make bottom end of slider line coincident with second construction line; (g) make top end of slider line coincident with second construction line; (h) delete construction lines and add bushing to point at B and constrain the bottom of the slider to remain parallel with the top and coincident with the slider line.

The final linkage in [Figure 2.6](#), (h) is generally unconstrained. The linkage points near A and B can be moved and both links can be stretched or compressed. The slider line can move in only a parallel direction; however, the orientation of the line can be changed by drawing a horizontal construction line and constraining by dimensioning the angle between the construction line and the slider line.

We can also add a coupler triangle to the coupler line (A-B) to locate a coupler point as was done with the four-bar linkage. The procedure is exactly the same as that for the four-bar linkage, and the result is shown in [Figure 2.7](#). Note that the coupler point location can be changed by dragging the point at C or by dimensioning the sides of the coupler triangle.



Example 2.1

Using GCP to Design a Double-Rocker Mechanism

To illustrate the use of GCP for mechanism design, we will use the procedure to design a double-rocker four-bar linkage. This design problem will be covered theoretically in [Chapter 3](#); however, it is simple enough that we can develop a graphical program by applying constraints in a systematic manner. We will start with a specific design problem and then show how different design specifications can be accommodated simply by changing the dimensional constraints on the input and output links.

The initial problem statement is shown in [Figure 2.8](#). The output link is to move through an angle of 80° while the input link moves through an angle of 40° . The fixed pivots are assumed to lie on a horizontal line. The motion of the output link is to start from an angle of 25° from the horizontal, and the motion of the input link is to start from an angle of 20° . The distance between fixed pivots is to be 4 in, and the output link is to be 2 in long. If the fixed pivots lie on a horizontal line, the problem is defined by a total of eight variables, six of which are independent. We can represent the variables as shown in [Table 2.1](#).

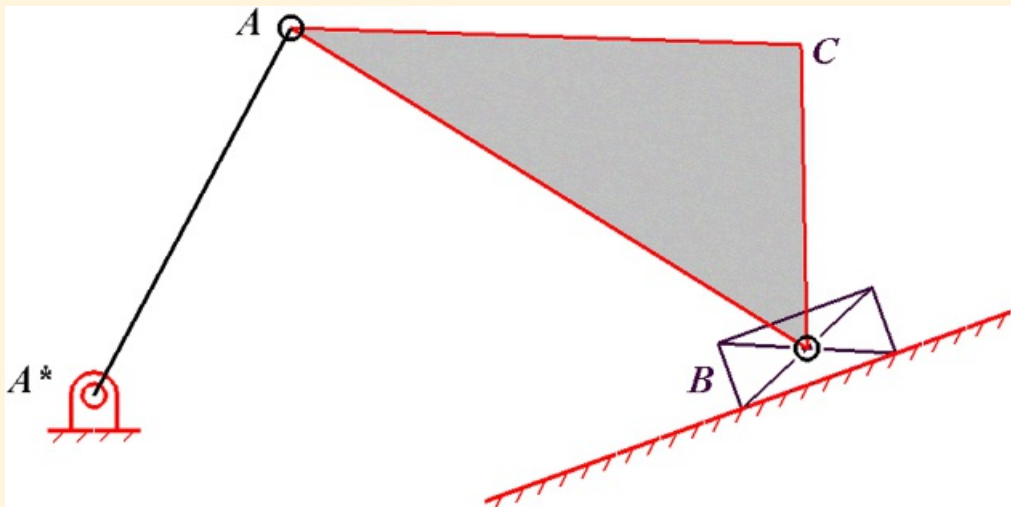


[Figure 2.7](#) Final version of slider-crank mechanism with coupler point identified.

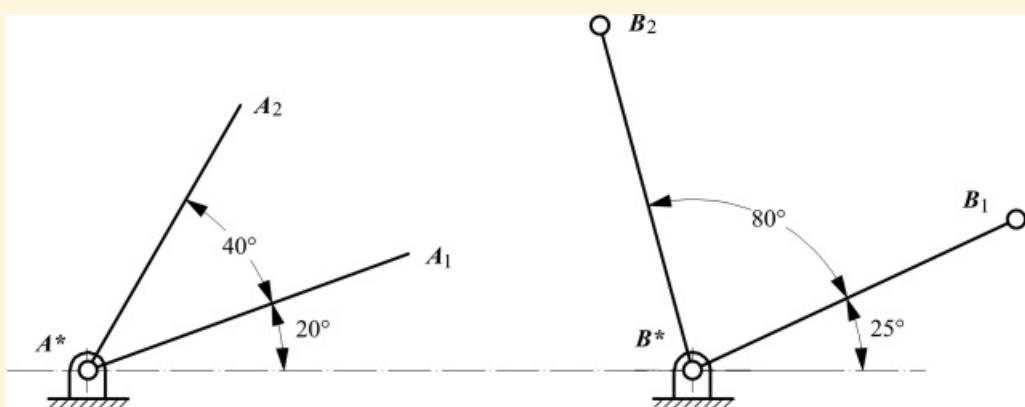


[Figure 2.8](#) Problem statement for double-rocker problem.

[Table 2.1](#) Input Variables for Double-Rocker Problem

Variable	Type	Description	Initial Value
x_1	Driving	Initial angle for input link	20°

x ₂	Driving	Displacement angle for input link	40°
x ₃	Driving	Initial angle for output link	25°
x ₄	Driving	Displacement angle for output link	80°
x ₅	Driving	Length of base	4 in
x ₆	Driving	Length of output link	2 in
x ₇	Driven	Length of input link	
x ₈	Driven	Length of coupler	

To begin the solution procedure, open the blank drawing and set up the following layers: *ProblemDrawing*, *InputVariables*, *SolutionConstruction*, *SolutionDimensions*, *FinalLinkage*, *TransmissionAngle*, and *Dimensions*. These layers were selected because they separately contain information that we might want to hide during different phases of the design process. Note that we are using four separate layers for the dimensions.

InputVariables contains only the input dimensions that will be used as input variables for the graphical program we will develop. *SolutionDimensions* contains only the dimensions for the two link lengths that were not specified. *Dimensions* contains miscellaneous dimensions such as those associated with pin bushings and ground pivots.

TransmissionAngle contains only the dimension for the transmission angle, the significance of which will be discussed later. At various times throughout this book, we will want different classes of dimensions to be visible while the others are hidden.

Prior to starting the drawing process, set the solid modeling program to automatically snap to constraints. Even though this may result in isolated unwanted constraints being imposed and which need to be deleted, it will ultimately simplify the drawing process. Set *ProblemDrawing* as the active layer, and draw a horizontal construction line of arbitrary length, and fix the left end. Label the ends of the line as *A** and *B**. From the *A** end of the line, draw two lines at arbitrary angles. Select the two lines and constrain them to be equal.

Repeat the process for the end of the horizontal construction line at *B**. Label the approximate locations of the input link as *A₁* and *A₂* and of the output link as *B₁* and *B₂*. Note that in the GCP drawing and in the description of the drawing process, we are not using subscripts because the solid-modeling program does not easily accommodate subscripts. As the lines are drawn, be sure that the solid-modeling program does not assign unwanted constraints, such as making two lines perpendicular. If an unwanted constraint is assigned, delete it.

Make the *InputVariables* layer active, and dimension the drawing with the input information. The dimensioned drawing is shown in [Figure 2.9](#). All of the dimensions are driving dimensions and represent constraints. Set *SolutionConstruction* as the active layer and hide the input dimensions shown in [Figure 2.9](#) by hiding the *InputVariables* layer. Next, draw two four-bar linkages to represent the two extreme positions of the solution linkage. If possible, distinguish between the two instances of the linkage by coloring the lines such that the first position is red. The lines for the second position can be black. [Figure 2.10a](#) shows an example of two positions of the approximate instances of the linkage. Because both of these sketches of the solution linkage will ultimately represent the two extreme positions of the same linkage, the following conditions/constraints must be satisfied:

1. The instances of the input links must be of equal length.
2. The instances of the output links must be of equal length and must be equal to $B^* - B_1$ and $B^* - B_2$.
3. The instances of the coupler links must be of equal length.
4. The first position (red) of the input link must be collinear with line $A^* - A_1$.
5. The second position (black) of the input link must be collinear with line $A^* - A_2$.
6. The first position (red) of the output link must be collinear with line $B^* - B_1$.
7. The first position (red) of the output link must be collinear with line $B^* - B_2$.

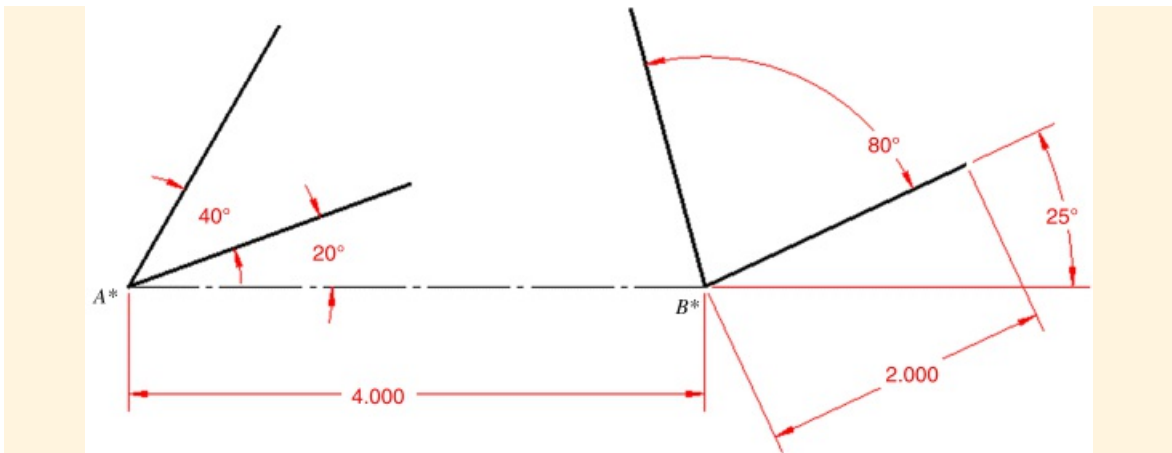


Figure 2.9 Dimensions corresponding to the variables in [Table 2.1](#).

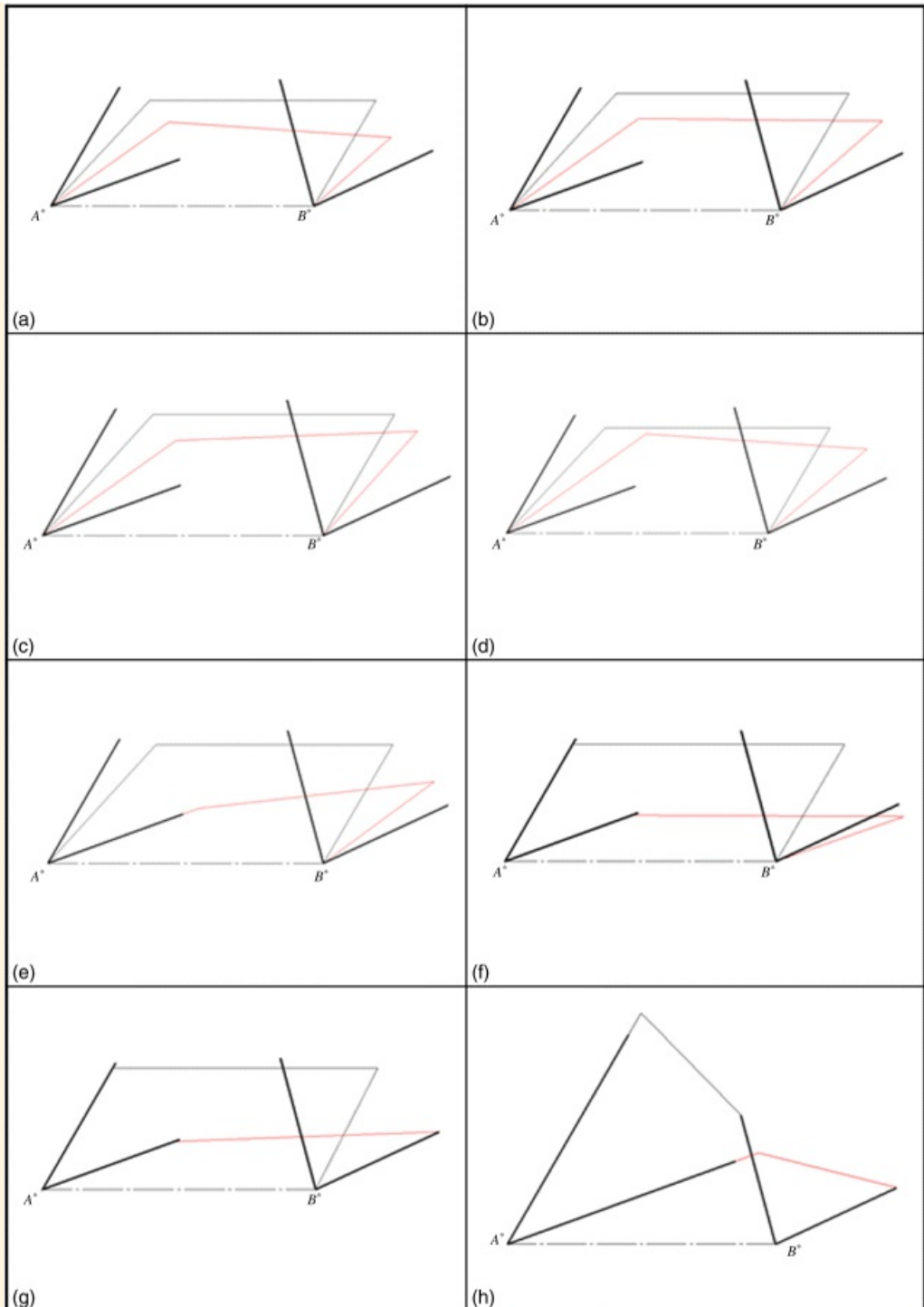
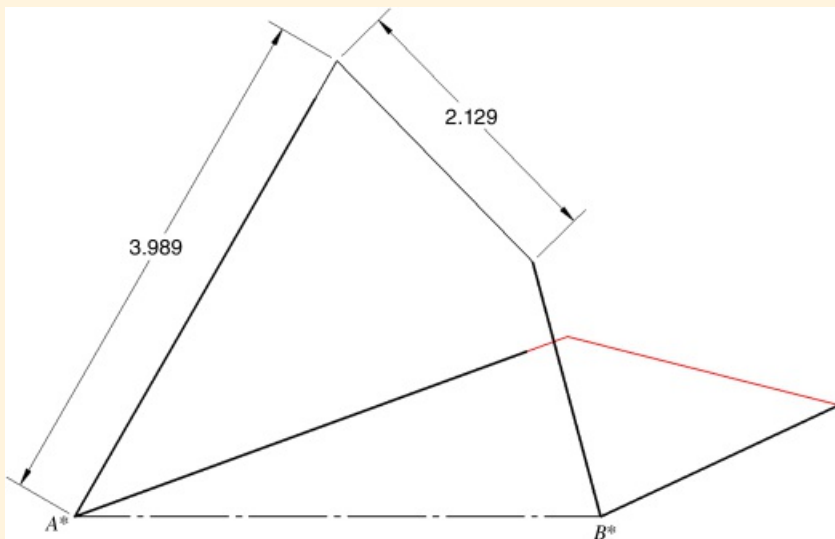


Figure 2.10 Steps in solving a double-level problem: (a) Draw two arbitrary four-bar linkages; (b) constrain instances of input links to be equal; (c) constrain instances of output links to be equal to each other and to the assigned value; (d) constrain instances of couplers to be equal; (e) constrain first position of input link to be collinear with specified position; (f) constrain second position of input link to be collinear with specified position; (g) constrain first position of output link to be collinear with specified position; (h) delete unwanted horizontal constraint for second position of coupler and constrain second position of output link to be collinear with specified position.

These seven conditions can be enforced by selecting the entities involved and enforcing the proper constraints. In general, the relations can be applied in any order, but for simplicity, we will apply them in the order listed. The results are shown in [Figure 2.10](#). Note that when the linkage was drawn in the second

position (a), the coupler became approximately horizontal because the program snapped to the horizontal constraint. This relation is undesired, and totally constrains the drawing after step (g) in [Figure 2.10](#). Therefore, this constraint must be deleted. In general with GCP, if the solution becomes unexpectedly constrained, the user should look for unwanted constraints that have been automatically applied by the program. After the horizontal constraint is deleted, the last constraint can be applied to determine the solution linkage that is shown in the two extreme positions in [Figure 2.10\(h\)](#).

The unknown dimensions for the linkage are the driver link length and the coupler length. Before measuring using the dimension tool, make *SolutionDimensions* the active layer. Dimensioning the lines normally would involve setting constraints. However, the drawing is already fully constrained so the added dimensions as driving dimensions would overconstrain the drawing. Therefore, when the dimensions are applied, they should be set as driven rather than driving dimensions. Different parametric-design programs may use different terms for the type of dimension used; however, a driven dimension simply reports the current length and does not set it as a constraint. The measurements are shown in [Figure 2.11](#).



[Figure 2.11](#) Dimensions for input link and coupler of solution linkage in second extreme position.

The drawing in [Figure 2.11](#) is fully constrained. It is not possible to move the linkage instances from either the first or second position. To investigate the movement of the linkage from one position to the other, we can redraw the final linkage in an intermediate position. We can also insert the fixed pivots and pin bushings to make the linkage look more realistic.

Before drawing the final linkage, set the active layer to *FinalLinkage* and hide the *SolutionDimensions* layer. To draw the final linkage, draw three lines starting from A^* and ending at B^* as before. Next, constrain the three links of the linkage to be equal to the corresponding lengths of the linkage instances in the extreme positions. Open the file containing the ground pivot geometry, copy the ground pivot (with all of its dimensions and constraints), and paste two instances of it into the linkage drawing. If the dimensions for the ground pivots are not automatically placed in the *Dimensions* layer, move them to that layer. Merge the two centers of the ground pivot bushings with the linkage points at A^* and B^* . For the pin bushings, draw two circles and constrain them to be equal to the circles used for the ground pivot. Then merge the centers of the circles with the points at the two ends of the coupler. Before moving the linkage, turn off the feature to automatically snap to constraints. This will allow the linkage to be moved without snapping to the nearest constraint. The final linkage design is shown in [Figure 2.12](#). It is possible to move the linkage throughout (and beyond) the range of interest defined by the original problem statement.

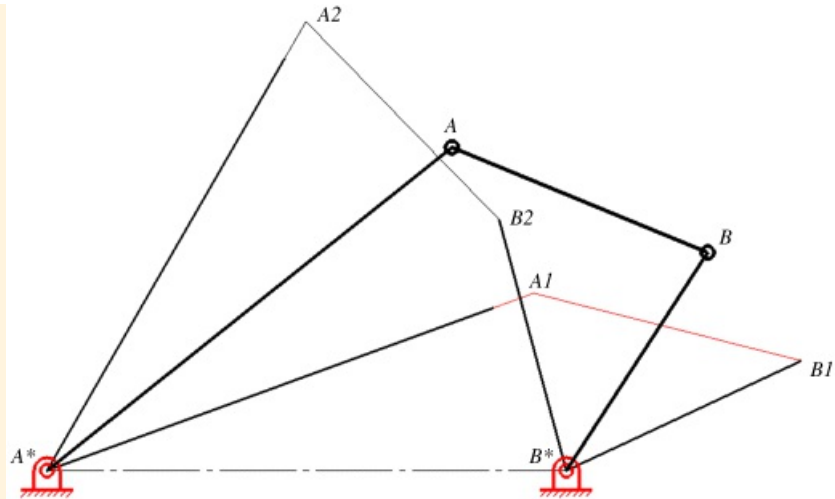


[Figure 2.12](#) The solution linkage in an intermediate position.

Displaying the Transmission Angle

One metric for the quality of the linkage is the transmission angle. This is the internal angle between the output link and the coupler. As discussed in [Chapters 3](#) and [14](#), this angle directly affects the input torque required to drive the linkage. Ideally, we would like this angle to be as near to 90° as possible throughout the range of motion of the mechanism. The linkage cannot transmit torque when the transmission angle is either 0° or 180° . We can measure this angle using the dimension tool in the parametric-design program and display the value for intermediate positions of the mechanism as it moves. Prior to doing this, set *TransmissionAngle* as the active layer. Then use the dimension tool to measure the angle. Adding this dimension as a constraint will fully constrain the linkage, and it cannot move. Therefore, make the transmission angle a driven dimension with the dimension tool. The transmission angle is shown in [Figure 2.13](#). As the linkage moves, the transmission angle is monitored and displayed each time the motion is stopped. For the solution linkage in [Figure 2.13](#), the transmission angle varies between 39° and 151° .

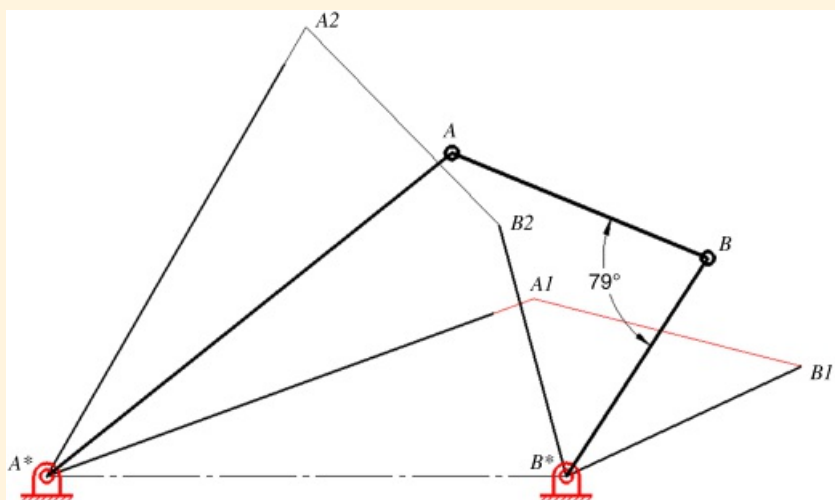


[Figure 2.13](#) Using the dimension feature to measure and display transmission angles.

Using a Final Drawing as a Graphical Program

We solved the double-lever problem using the specific values for the variables listed in [Table 2.1](#). However, once the solution drawing is developed, we may change any of the values by simply changing the dimensions in [Figure 2.9](#). Therefore, the constraint-based drawing becomes a graphical program. To use different inputs for the problem, make the *InputVariables* layer visible and active, and change any of the dimensions. Four examples of changes are shown in [Figure 2.14](#). For these examples, the labels (*A1*, *A2*, *B1*, *B2*) have been moved manually after the changes were made. We can also simply delete one of the dimensions and move

the link involved to observe continuous changes. And finally, we can switch the role of the dependent and independent variables in [Table 2.1](#). To do this, we simply change the dimensions for the original dependent variables to driving dimensions and change the corresponding dimensions of the original independent variables to driven dimensions. An example of this is shown in [Figure 2.15](#)

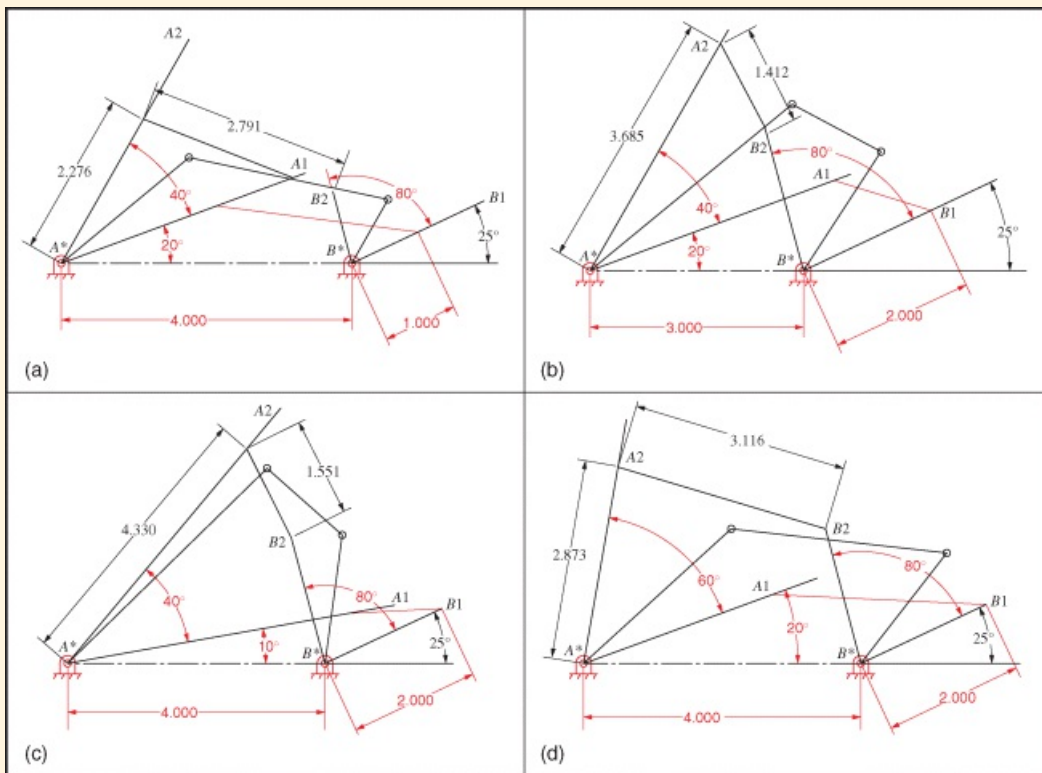


[Figure 2.14](#) Results for input changes in the double-rocker graphical program: (a) Change in length of output link; (b) change in base link length; (c) change in initial angle for input; and (d) change in angle range for input link.

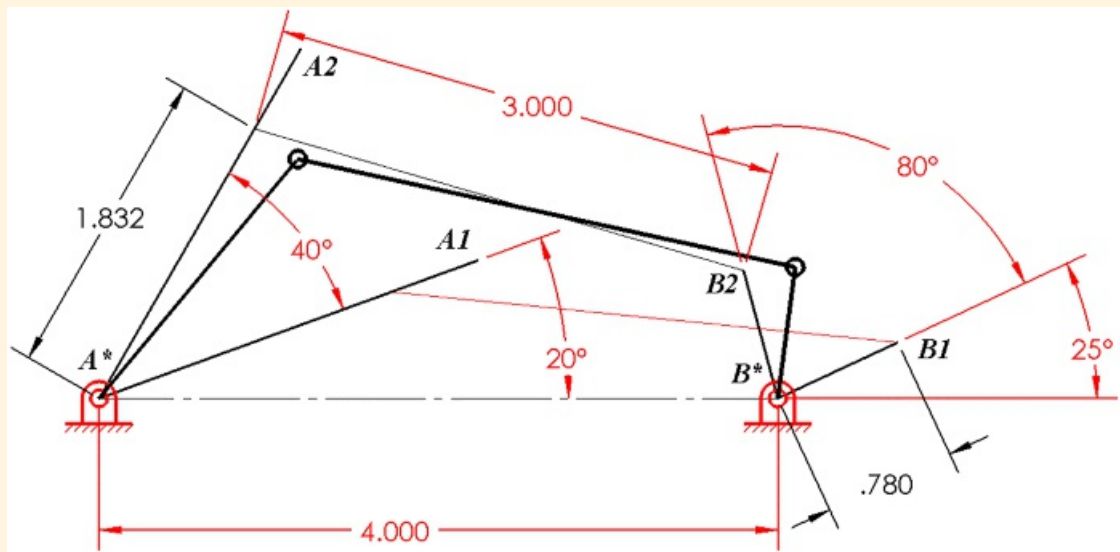


[Figure 2.15](#) Results for the graphical program when the coupler length is made a driving dimension and the initial angle of the output link is made a driven dimension.



Example 2.2

Using GCP to Model a Cam Mechanism

GCP can be used to analyze cam mechanisms for position and velocity as long as the cams are defined by closed curves that can be represented by circles, ellipses, or splines. We will illustrate the procedure on a simple circular cam with an oscillating flat-faced follower. Both the design and analysis of complex cams will be covered extensively in [Chapter 2](#).

The initial problem geometry is shown in [Figure 2.16](#). The cam rotates 360° , and the flat-faced follower oscillates. The fixed pivots are assumed to lie on a horizontal line. The distance between the fixed pivots is to be 2.75 in, and the follower length is 4 in. Actually, the length of the follower does not affect the kinematics as long as the follower is long enough to stay tangent to the cam. If the fixed pivots lie on a horizontal line, the problem is defined by a total of 6 variables, five of which are independent (driving). We can represent the variables as shown in [Table 2.2](#).

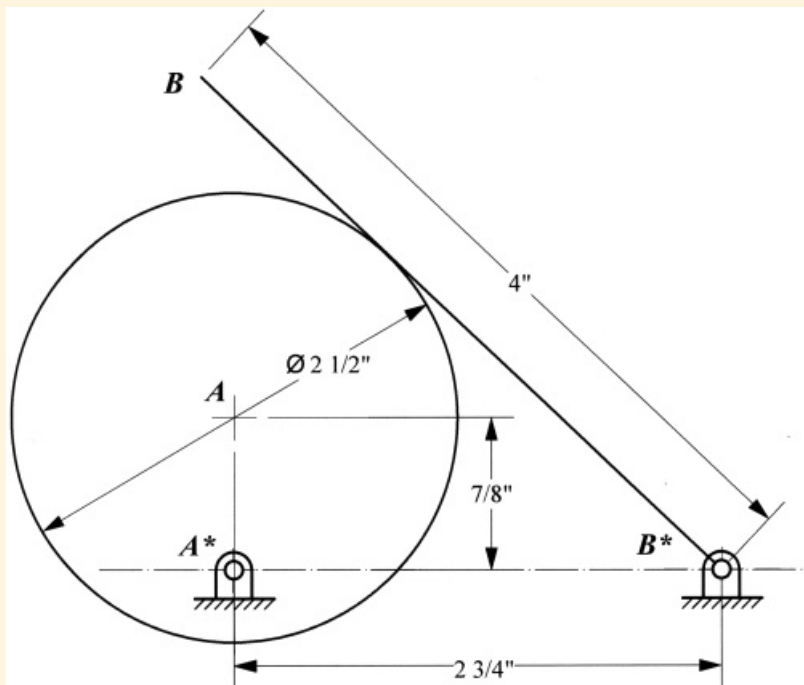


[Figure 2.16](#) Circular cam mechanism.

[Table 2.2](#) Variables for Cam Mechanism

Variable	Type	Description	Initial Value
x_1	Driving	Diameter of cam	1 1/2"
x_2	Driving	Cam center offset	7/8"
x_3	Driving	Center distance	2 3/4"
x_4	Driving	Length of follower	4"
x_5	Driving	Cam rotation angle	$0-2\pi$
x_6	Driven	Angle between follower and frame	

To begin the solution procedure, open the blank drawing sheet and set up the following layers:

ProblemDrawing, InputVariables, SolutionConstruction, SolutionDimensions, CamLinkage, and Dimensions.

The logic for selecting these layers is similar to that used in Example 2.1. If possible, use red for the line color in the *SolutionDimensions* and *SolutionConstruction* layers. Use black for the other layers.

The steps for constructing the mechanism are shown in [Figure 2.17](#). First set *ProblemDrawing* as the active layer and make sure that the program will snap to constraints. Draw a horizontal construction line of arbitrary length, and fix the left end. Label the ends of the line as A^* and B^* . Draw a circle with its center above point A^* but ensure that A^* lies within the circle. It will be convenient to identify the center of the circle visually throughout the solution process. To do this, draw a small cross at the center location. Constrain the legs of the cross to be equal and perpendicular, and dimension one of the legs. Also label the center as A . Draw an arbitrary line from B^* to represent the follower. Label the other end of the line as B .

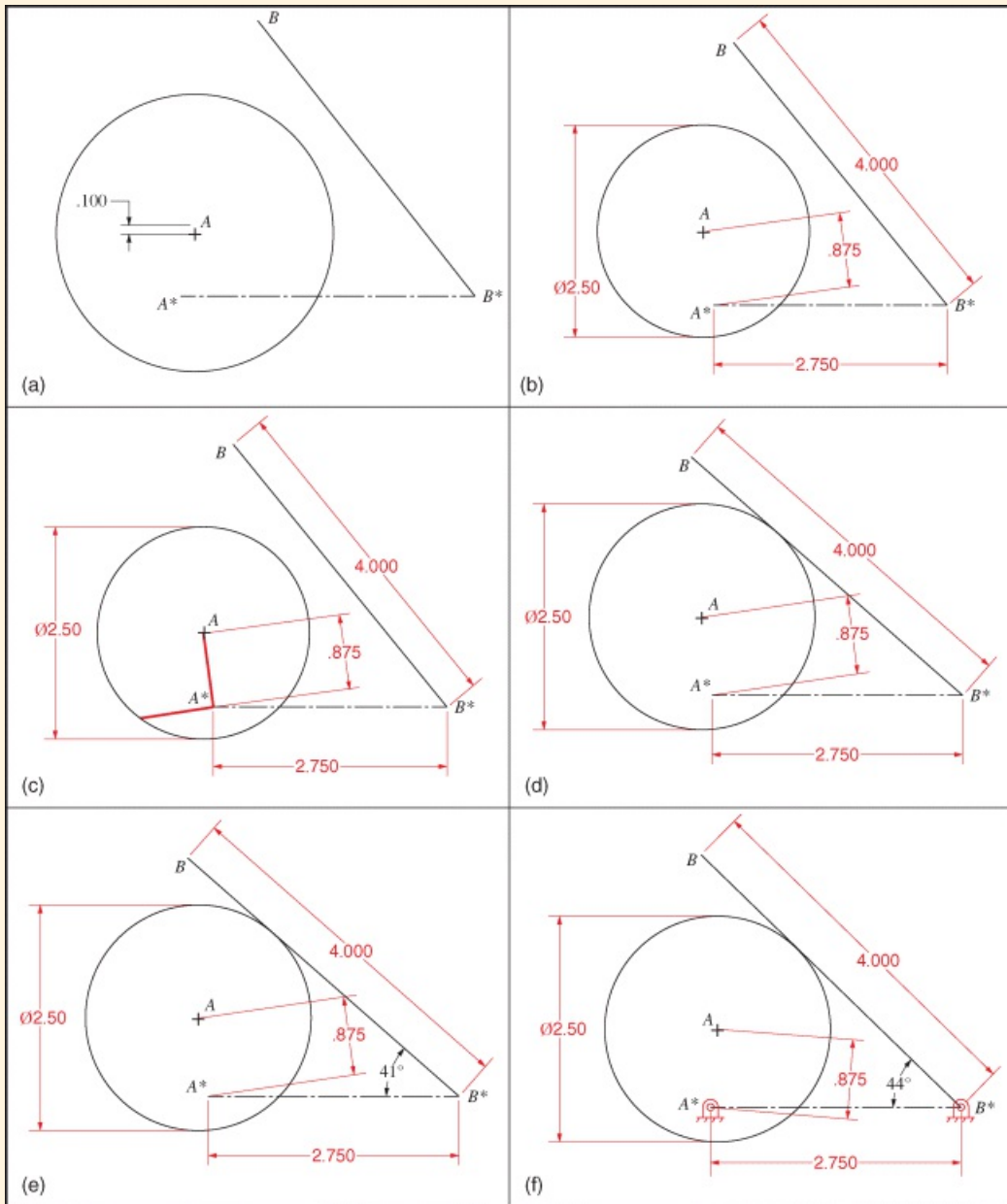


[Figure 2.17](#) Possible steps in solving cam-follower problem: (a) Horizontal construction line, circle, circle center, and follower line; (b) dimension the entities from previous step; (c) draw two lines and make them perpendicular to constrain the circle to move about A^* ; (d) hide the two lines from step c and constrain the follower line to be tangent to the circle; (e) measure the follower angle with a driven dimension; and (f) the final mechanism with pivots shown.

Make the *InputVariables* layer active, and use the dimension tool to constrain the distance A^*B^* , the

diameter of the circle, and the length of the follower. Also constrain the distance from the center of the circle to the fixed point at A^* .

We now need to constrain the circle to rotate about A^* . This will require constructing two lines to fix the pivot location. Ultimately, we will want to hide these lines, so make the layer *SolutionConstructions* active. Draw the first line from the center of the circle to A^* . The ends of the line are automatically merged with the points at A^* and A if the snap-to-constraints feature is activated. Draw a second line from A^* and constrain it to be coincident with the perimeter of the circle. Select both lines and constrain them to be perpendicular. It should now be possible to rotate the circle about A^* by clicking on either A or the line A^*A and dragging it with the pointer. Hide the *SolutionConstructions* layer.

Make the *ProblemDrawing* layer active again. Select the circle and the follower line and constrain them to be tangent. The follower is now constrained to stay tangent with the circle as the circle rotates. To record the follower angle, first make the *SolutionDimensions* layer active. Next, measure the angle between the follower and the horizontal line using the dimension tool. To avoid fully constraining the linkage, make the dimension a driven dimension so that the program simply reports the current angle.

To improve the appearance of the drawing, open the file containing the ground pivot geometry and dimensions, and copy the ground pivot with all of its constraints and dimensions. Set the active layer to *ProblemDrawing* and paste two instances of the ground pivot into the cam-follower drawing. Move the dimensions of the ground pivots to the *Dimensions* layer and merge the centers of the bushings with points A^* and B^* . To simplify the drawing as the cam rotates, hide the input dimensions, and rotate the cam.

The cam mechanism can now be used as a graphical program by changing any of the independent variables. One set of changes is indicated in [Figure 2.18](#).

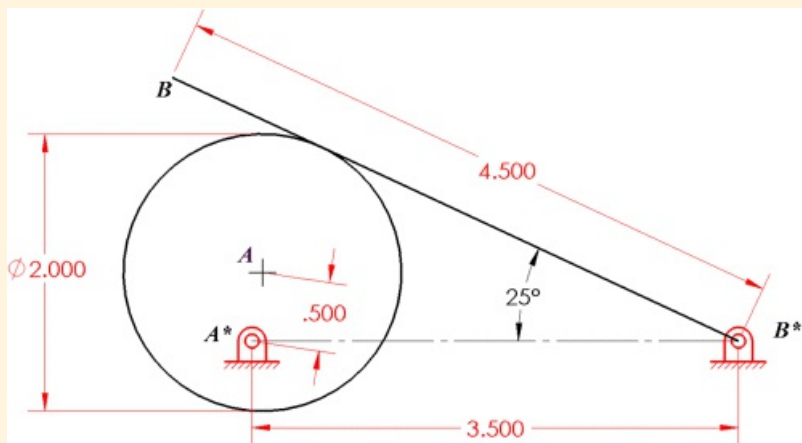


[Figure 2.18](#) Results from changing input variable values in [Figure 2.17\(f\)](#).



2.6 Troubleshooting Graphical Programs Developed Using GCP

GCP relies on the constraint manager and nonlinear equation solver in the parametric-design program used. While these are extremely robust, they can sometimes fail to generate a useful solution. This may be because no solution exists or because the nonlinear equation solver is unable to solve the underlying geometric equations. If the program indicates that no solution is available, it may be because the problem is overconstrained. Typically this problem can be resolved by deleting the offending constraints. If the original problem is not expected to be over constrained with the relations assigned, it is important to check that the program has not assigned unwanted constraints. It is often convenient to reverse the steps in making the drawing by using the Undo command. Using this procedure, it is sometimes possible to determine the step when the unwanted constraint was added.

Some of the problems we will consider later are highly nonlinear and have multiple solutions. Therefore, the nonlinear equation solver can converge to an undesired solution. The procedure uses the current position information along with the constraint equations to iterate to a solution. The chances of converging to the desired solution are enhanced if the initial position of the mechanism is reasonably close to the final solution. If the user has no idea what the final design dimensions will be and the procedure cannot determine an acceptable solution, it may be advantageous to draw the initial instances of the linkage in a variety of different positions. For very complex problems, it may also be necessary to reduce the number of positions that the user is trying to match. Ultimately, there may not be a physical solution to the problem being posed. In that case, neither GCP nor any other procedure will give an exact solution.



References

1. Artas Engineering Software, Het Puyven 162, NL-5672 RJ Nuenen, The Netherlands. (2014). SAM (Synthesis and Analysis of Mechanisms) software. <http://www.artas.nl/en/sam/>.
2. Dassault Systèmes SolidWorks Corp, 175 Wyman Street, Waltham, MA 02451. (2014). SolidWorks Solid Modeling Software. <http://www.solidworks.com/>.
3. Design Simulation Technologies, Inc., 43311 Joy Road #237, Canton, MI 48187. (2014). Working Model 2D, 2D Dynamic Motion Simulation. <http://www.design-simulation.com/WM2D/index.php/>.
4. Draijer, Harry, and Kokkeler, Frans. (2002). "Heron's Synthesis Engine Applied to Linkage Design." *Proceedings of the 2002 ASME Design Technology Conference*, Montreal, Quebec, Canada, Sept 29–Oct 2, Paper No. DETC2002/MECH-34373.
5. Erdman, A. G., and Chase, T. R. (1985). "New Software Synthesizes Complex Mechanisms." *Machine Design*, Vol. 57, No. 19, pp. 107–113.
6. Erdman, A. G., and Gustafson, J. E. (1977). "LINCAGES: Linkage Interactive Computer Analysis and Graphically Enhanced Synthesis Package." ASME Paper No. 77-DET-5, presented at the Design Engineering Technical Conference, Chicago, IL, USA, September 1977.
7. Freudenstein, F., and Sandor, G. N. (1959). "Synthesis of Path-Generating Mechanisms by Means of a Programmed Digital Computer." *ASME Journal of Engineering for Industry*, Vol. 81, Series B, No. 2, pp. 159–167.
8. Kinzel, E. C., Schmiedeler, J. P., and Pennock, G. R. (2006). "Kinematic Synthesis for Finitely Separated Positions Using Geometric Constraint Programming." *ASME Journal of Mechanical Design*, Vol. 128, no. 5, pp. 1070–1079.
9. MSC Software Corp. 4675 MacArthur Court, Suite 900, Newport Beach, CA 92660, (2014). ADAMS, Multibody Dynamics Simulation, <http://www.mscsoftware.com/product/adams/>.
10. Norton, R.L. (2012). *Design of Machinery: An Introduction to the Synthesis and Analysis of Mechanism and Machines*, 5th Ed. New York, NY: McGraw-Hill.
11. PTC, 140 Kendrick Street, Needham, MA 02494. (2014). PTC Creo Design Software (formerly Pro/Engineer). <http://www.ptc.com/product/creo/>.
12. Rubel, A. J., and Kaufman, R. E. (1977). "KINSYN III: A New Human-Engineered System for Interactive Computer-Aided Design of Planar Linkages." *ASME Journal of Engineering for Industry*, Vol. 99, No. 2, pp. 440–448.
13. Saltire Software, 12700 SW Hall Blvd, Tigard, OR, 97223. (2014). Analytix 21 and Mechanical Expressions. <http://www.saltire.com/analytix/>.
14. Schmiedeler, J. P. (2008). "Workshop: Planar, Rigid-Body Mechanism Synthesis Using Geometric Constraint Programming." *ASME 2008 Design Engineering Technical Conferences and Computer and Information in Engineering Conference*, New York, NY, August 3, 2008.
15. Siemens PLM Software, 5800 Granite Parkway, Suite 600, Plano, TX 75024. (2014). Solid Edge Solid Modeling Software. http://www.plm.automation.siemens.com/en_us/products/velocity/solidedge/.
16. Siemens PLM Software, 5800 Granite Parkway, Suite 600, Plano, TX 75024. (2014). Solid Edge 2D Drafting software. http://www.plm.automation.siemens.com/en_us/products/velocity/solidedge/free2d/.
17. Sridhar, N., Agrawal, R., and Kinzel, G. L. (1996). "Algorithms for the Structural Diagnosis and Decomposition of Sparse, Underconstrained Design Systems." *Computer-Aided Design*, 28 (4), pp. 237–249.

18. Universal Technical Systems, Inc., 4053 North Perryville Road, Loves Park, IL 61111I. (2014). TK Solver 5.0. <http://www.uts.com/>.
19. Waldron, K. J. (1974). "Range of Joint Rotation in Planar Four-Bar Synthesis for Finitely Separated Positions: Part I—The Multiple Branch Problem." ASME Paper No. 74-DET-108, presented at the Design Engineering Technical Conference, New York, NY.
20. Waldron, K. J. (1974). "Range of Joint Rotation in Planar Four-Bar Synthesis for Finitely Separated Positions: Part II—Elimination of Unwanted Grashof Configurations." ASME Paper No. 74-DET-109, presented at the Design Engineering Technical Conference, New York, NY.
21. Waldron, K. J. (1975). "The Order Problem of Burmester Linkage Synthesis." *ASME Journal of Engineering for Industry*, Vol. 97, No. 4, pp. 1405–1406.
22. Waldron, K. J. (1976). "Elimination of the Branch Problem in Graphical Burmester Mechanism Synthesis for Four Finitely Separated Positions." *ASME Journal of Engineering for Industry*, Vol. 98, No. 1, pp. 176–182.
23. Waldron, K. J. (1977). "Graphical Solution of the Branch and Order Problems of Linkage Synthesis for Multiply Separated Positions." *ASME Journal of Engineering for Industry*, Vol. 99, No. 3, pp. 591–597.
24. Waldron, K. J. (1978). "Location of Burmester Synthesis Solutions with Fully Rotatable Cranks." *Mechanism and Machine Theory*, Vol. 13, No. 2, pp. 125–137.
25. Autodesk, Inc., 111 McInnis Parkway, San Rafael, CA, 94903. Autocad Inventor 2015. www.autodesk.com/products/inventor/.
26. Mirth, John A. (2014). "A GCP Design Approach for Infinitesimally and Multiply Separated Positions Based on the Use of Velocity and Acceleration Vector Diagrams." DETC2014-34074, Proceedings of the ASME 2014. International Design Engineering Technical Conferences & Computers and Information in Engineering Conference, August 17–20, 2014.



Problems

2.1 A slider-crank mechanism is to move the slider 1 in for 40° of rotation of the crank as shown in [Figure P2.1](#). Using GCP methods, develop a graphical solution to determine the necessary crank and coupler lengths. Explicitly identify the layer structure used, and make a separate layer for all possible input dimensions. Also, explicitly list the driving and driven variables. Use your graphical program to resolve the problem when the slider distance is 1.5 in and the crank rotates through an angle of 60° .

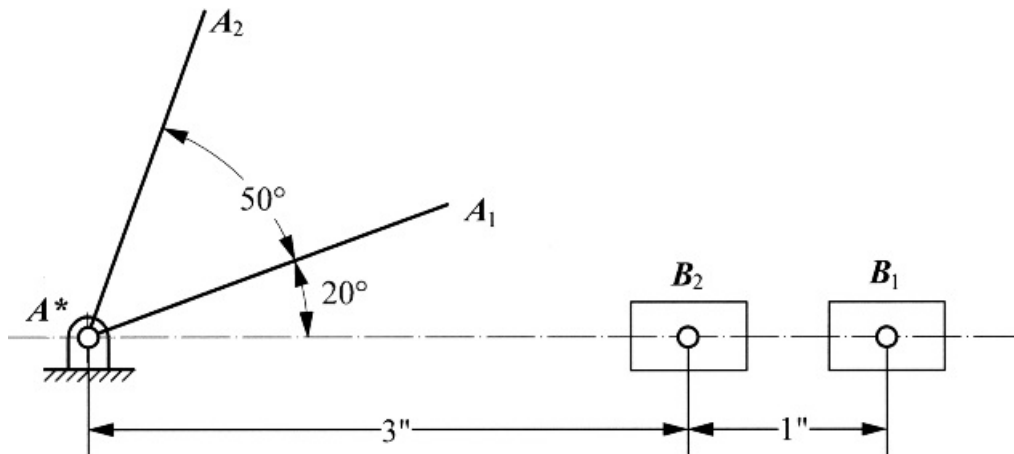


[Figure P2.1](#) Slider and crank positions for Problem 2.1.

2.2 An inverted slider-crank mechanism is to move the slider 0.4 in for 45° of rotation of the slide as shown in [Figure P2.2](#). Using GCP methods, develop a graphical solution to determine the necessary crank (B^*B) and base (A^*B^*) lengths. Explicitly identify the layer structure used, and make a separate layer for all possible input dimensions. Also, explicitly list the driving and driven variables. Use your graphical program to resolve the problem when the slider displacement is 0.8 in and the slide rotates through an angle of 55° .

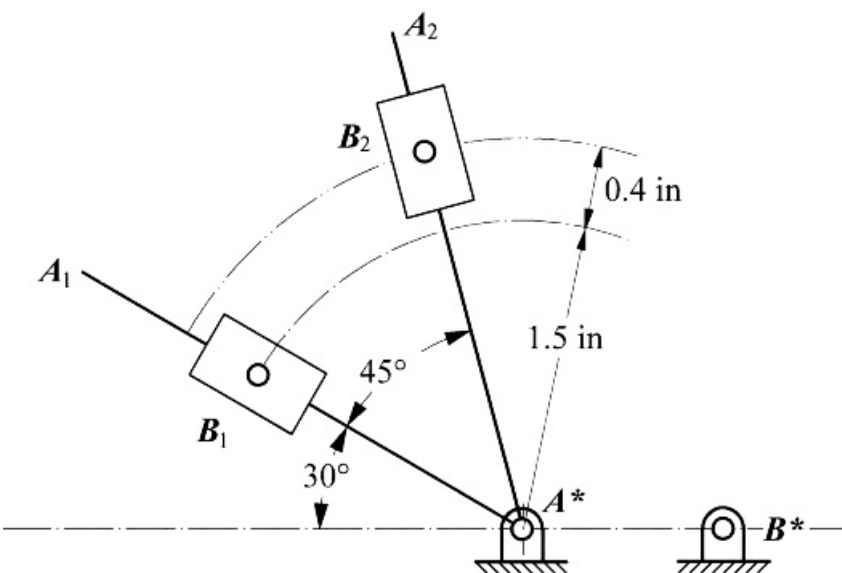


[Figure P2.2](#) Slider and crank positions for Problem 2.2.

2.3 An elliptic trammel is a mechanism where two sliders are connected by a binary link. In the case considered in this problem, the slides are perpendicular to each other. As indicated in the drawing, one slider is to move 0.4 in when the other slider moves 0.5 in. Using GCP methods, develop a graphical solution to determine the necessary link length between A and B and the starting position for point A_1 . Explicitly identify the layer structure used, and make a separate layer for all possible input dimensions. Also, explicitly list the driving and driven variables. Use

your graphical program to resolve the problem when the slider distance for the horizontal slider is 0.6 in and the slider distance for the vertical slider is 0.4 in.

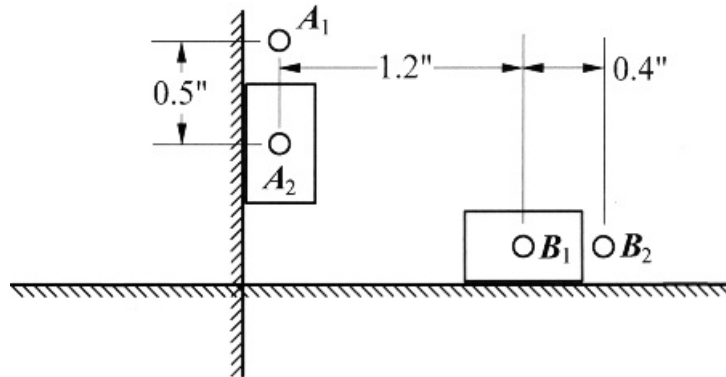


Figure P2.3 Slider positions for Problem 2.3.

2.4 Using GCP methods, develop a graphical program that will let you animate the Scotch-yoke mechanism with the crank (A^*A) as the input. Explicitly identify the layer structure used and the driving and driven variables.

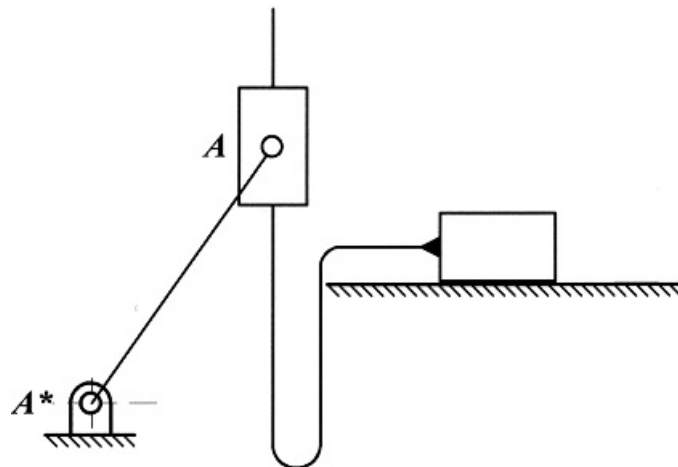


Figure P2.4 Scotch-yoke mechanism for Problem 2.4.

2.5 Using GCP methods, develop a graphical program that will let you animate the elliptical cam mechanism in [Figure P2.5](#) with the cam rotation as the input. Explicitly identify the layer structure used and the driving and driven variables. Change the base length to 2 in and the minor diameter to 1 in and show the results.

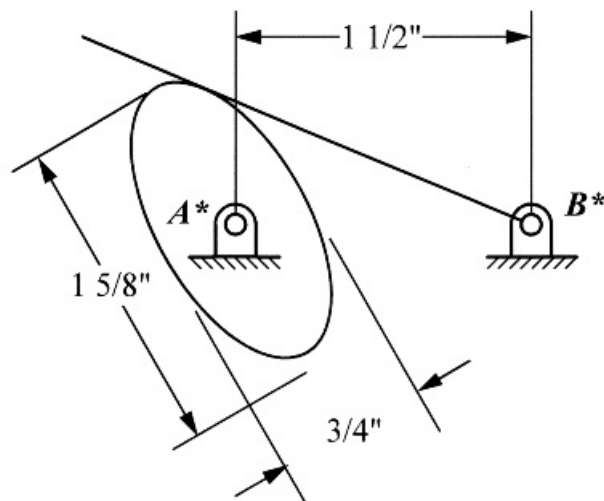


Figure P2.5 Elliptical cam for Problem 2.5.

2.6 The inversion of the slider crank shown in the figure is used extensively for walking toys. Using GCP methods, develop a graphical program that will let you animate the mechanism with the crank (A^*A) as the input so that you can observe the path of the “foot.” Explicitly identify the layer structure used and make a separate layer for all possible input dimensions. Also, explicitly list the driving and driven variables.

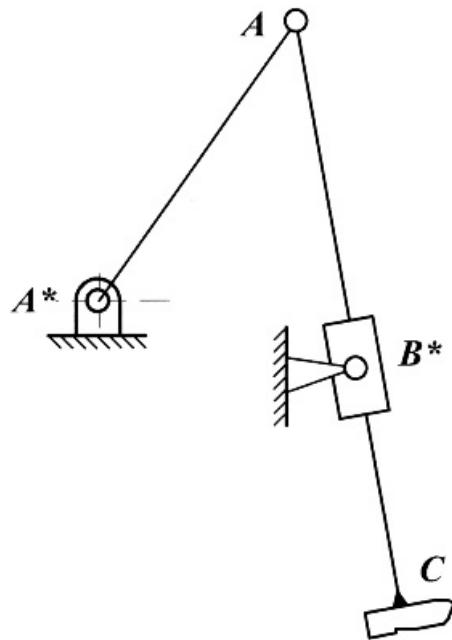


Figure P2.6 Walking linkage for Problem 2.6.

2.7 The mechanism shown in [Figure P2.7](#) is used to change rotary motion into oscillating motion. Using GCP methods, develop a graphical program that will let you animate the mechanism with the crank (A^*A) as the input. Explicitly identify the layer structure used, and make a separate layer for all possible input dimensions. Also, explicitly list the driving and driven variables.

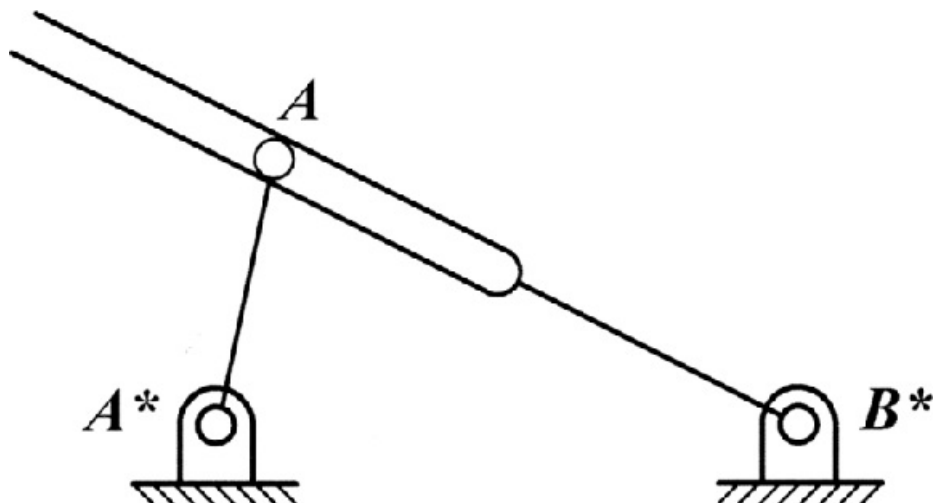
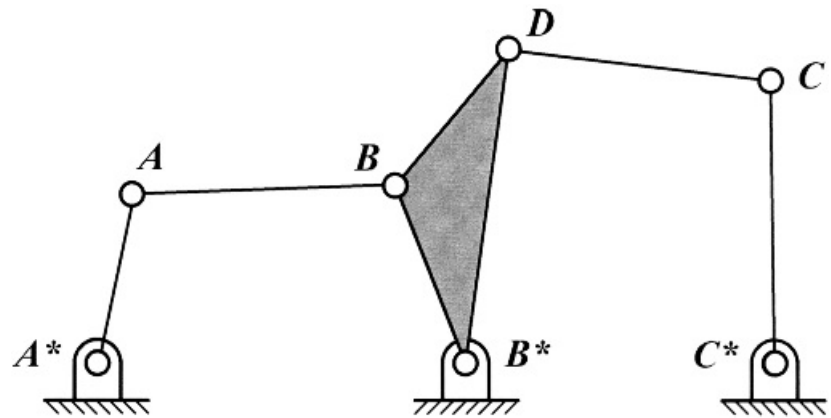


Figure P2.7 Mechanism for Problem 2.7.

2.8 The mechanism shown in [Figure P2.8](#) is one inversion of the Watt mechanism. Using GCP methods, develop a graphical program that will let you animate the mechanism with the crank (A^*A) as the input. Explicitly identify the layer structure used, and make a separate layer for all possible input dimensions. Also, explicitly list the driving and driven variables.



[Figure P2.8](#) Linkage for Problem 2.8.

2.9 The mechanism in [Figure P2.9](#) is a second inversion of the Watt mechanism. Using GCP methods, develop a graphical program that will let you animate the mechanism with the crank (A^*A) as the input. Explicitly identify the layer structure used, and make a separate layer for all possible input dimensions. Also, explicitly list the driving and driven variables.

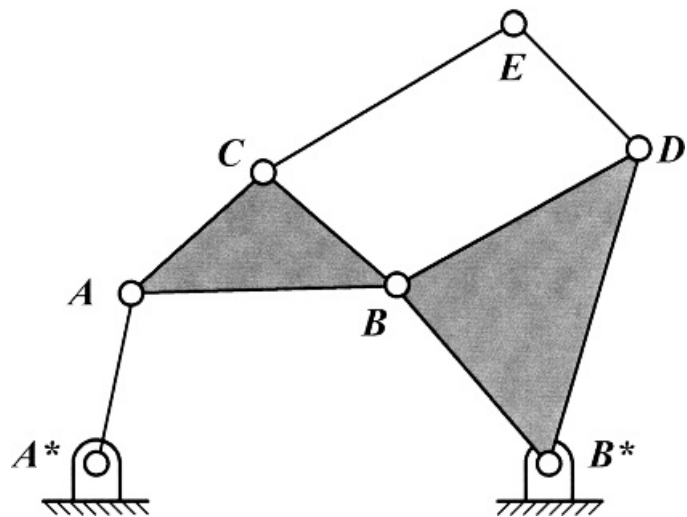


[Figure P2.9](#) Linkage for Problem 2.9.

2.10 The mechanism shown in [Figure P2.10](#) is an inversion of the Stephenson mechanism. Using GCP methods, develop a graphical program that will let you animate the mechanism with the crank (A^*A) as the input. Explicitly identify the layer structure used, and make a separate layer for all possible input dimensions. Also, explicitly list the driving and driven variables.

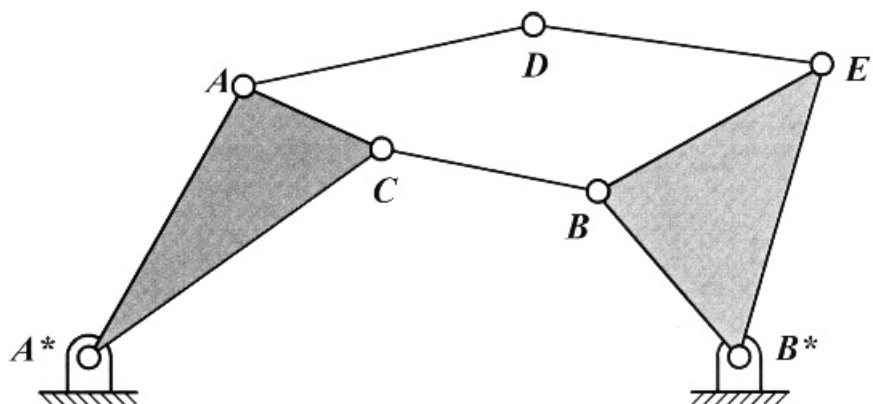


[Figure P2.10](#) Linkage for Problem 2.10.

2.11 The mechanism in [Figure P2.11](#) is a second inversion of the Stephenson mechanism. Using GCP methods, develop a graphical program that will let you animate the mechanism with the crank (A^*A) as the input. Explicitly identify the layer structure used, and make a separate layer for all possible input dimensions. Also, explicitly list the driving and driven variables.

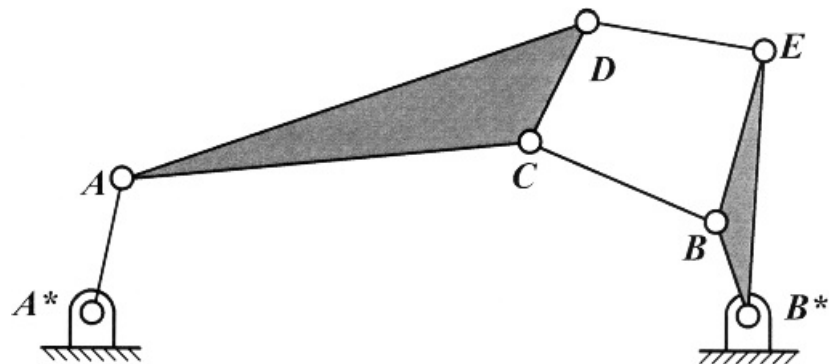


[Figure P2.11](#) Linkage for Problem 2.11.

2.12 The mechanism in [Figure P2.12](#) is a third inversion of the Stephenson mechanism. Using GCP methods, develop a graphical program that will let you animate the mechanism with the crank (A^*A) as the input. Explicitly identify the layer structure used, and make a separate layer for all possible input dimensions. Also, explicitly list the driving and driven variables.

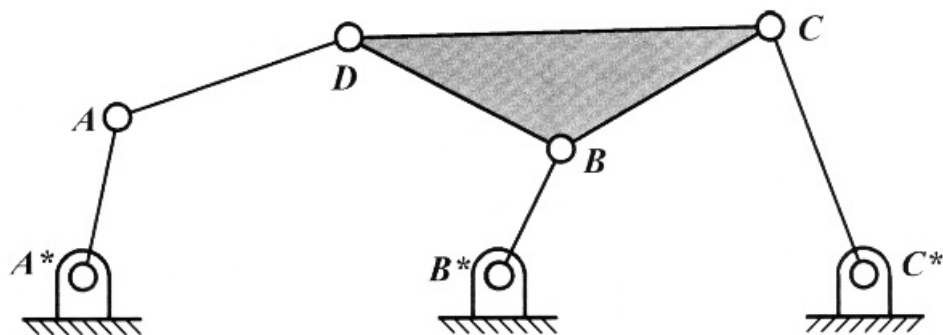


[Figure P2.12](#) Linkage for Problem 2.12.



Appendix 2A Drawing Slider Lines, Pin Bushings, and Ground Pivots

2A.1 Slider Lines

Much of the effort in GCP consists of drawing arbitrary linkages of the same type in selected positions and then introducing constraints so that the corresponding links in all instances of the linkage have the same lengths. To make the linkage drawings look more like a traditional mechanical linkage, we can add slider lines, pin bushings, and ground pivots. For pin bushings, we can draw a simple circle, dimension it, and merge the centerpoint of the circle with the endpoint of a given link. However, slider lines and ground pivots are somewhat more involved. For slider lines and ground pivots, it is convenient to create a separate file for each and then copy them when needed into the final drawing. When doing this, it is necessary to copy ALL constraints and dimensions, too. Once copied into the final drawing, the entities can be re-dimensioned to size them properly for the final drawing. Also the dimensions can be moved to the proper layer to hide them.

The slider line routine is also used to create the ground pivot so the slider line will be considered first. Start by creating a blank drawing file and save it as *SliderLine*. Create two layers: *SliderLine*, and *Dimensions*. If possible, set the color to red in each layer and set the line thickness in the *SliderLine* layer to a medium thickness. We can ultimately create several slider lines of different lengths for use in various problems.

To begin the procedure, create a slider-line element that can be duplicated and combined with others to make longer slider lines. The element is shown in [Figure 2A.1](#). First make the *SliderLine* layer active, and draw two short, inclined lines of arbitrary length. Draw the lines inclined so that the slider line can be oriented at any angle. If it is drawn either horizontally or vertically, an automatic constraint will be imposed, and it will be difficult to incline the line later. Merge the ends of the two lines and constrain them to be parallel. Use the dimension tool, and make the length of one inclined line be three times that of the other. From the intersection of the two inclined lines, draw a diagonal line at an angle of approximately 45°. Select the line thickness for the diagonal line to be about half of that for the two inclined lines. Use the dimension tool to constrain the acute angle between the diagonal line and inclined lines to be 45°. Next use the dimension tool and constrain the distance from the end of the diagonal line to the inclined lines to be half the sum of the lengths of the two inclined lines. Typical dimensions are shown in [Figure 2A.1](#). The linear dimensions used are somewhat arbitrary, but it is useful to make them close to the actual sizes that will be used in the linkage drawings. For the drawings in this book, we used mainly the dimensions in [Figure 2A.1](#).

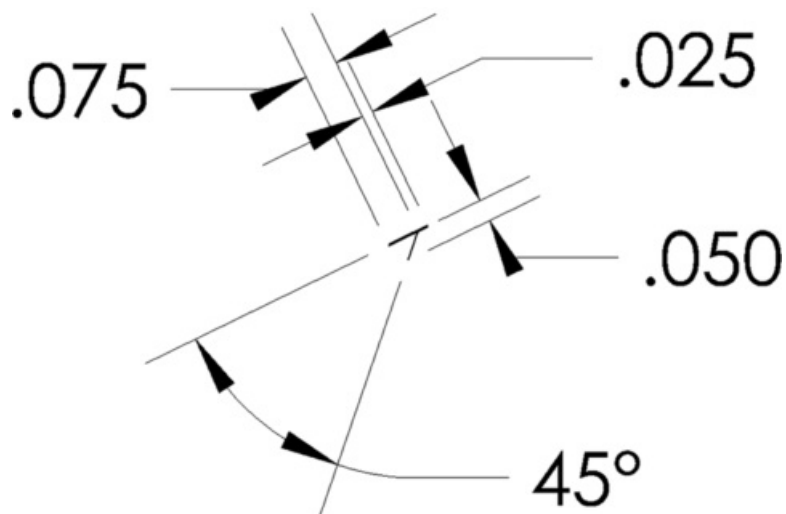


[Figure 2A.1](#) Basic slider line element.

The steps for creating a four-element line are shown in [Figure 2A.2](#). First copy and paste the basic elements with all of their constraints and dimensions four times [[Figure 2A.2\(b\)](#)]. Then merge the point at the end of one element with the beginning of the other element and constrain the baselines to be parallel [[Figure 2A.2\(c\)](#)]. The drawing in [Figure 2A.2\(c\)](#) is very cluttered and hard to read. To simplify the drawing and improve readability, we

can reduce the number of dimensions by using constraints. To do this, delete all but one of the same linear dimensions on the top line and all but one of the linear dimensions defining the height of the diagonal lines. Also, delete all but one of the angle dimensions. Then select each segment of the baseline with the same dimension and constrain them to be equal and collinear. Next select all of the diagonal lines and constrain them to be equal and parallel. The slider line is now fully constrained with only four dimensions. The result is shown in [Figure 2A.2\(d\)](#). When the four-element line is used, the dimensions can be copied to a hidden layer so that they do not appear. If we ever draw lines or create dimensions in the wrong layer, we can easily move the entities to the proper layer by first selecting all of the entities to be moved and using the copy and paste commands.

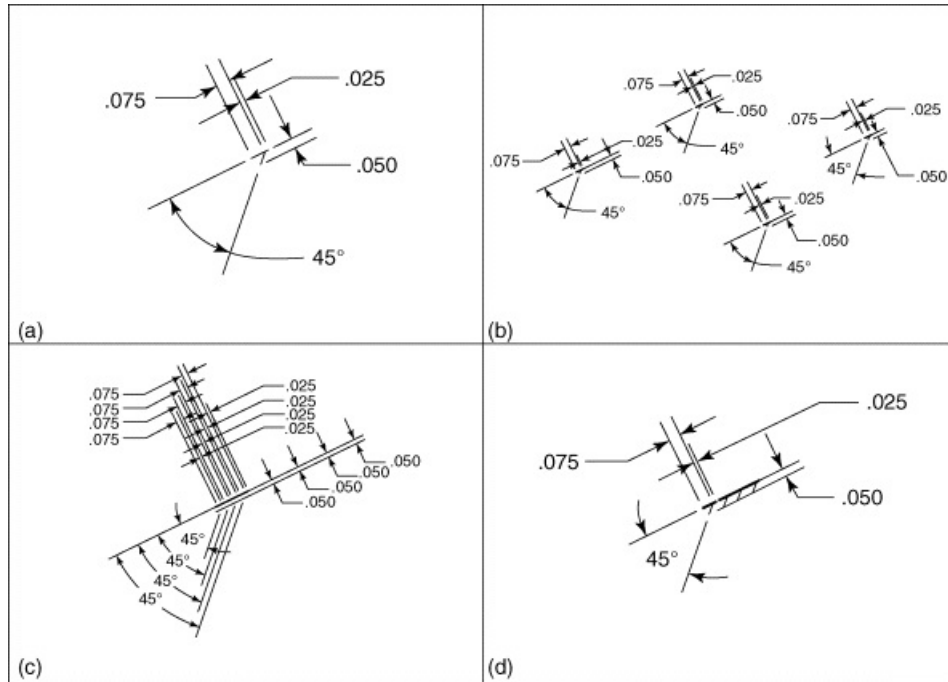


[Figure 2A.2](#) Creation of a four-element slider line:.. (a) Basic slider line element; (b) four copies of basic element; (c) merging the beginning of the base line of one element with the end of the baseline for the previous element and; (d) replacing the duplicate dimensions by the use of constraints.

We may now use the four-element line as a new element to create longer slider lines. First duplicate (copy and paste) the new four-element line with ALL of its constraints and dimensions as many times as necessary to create the length line desired. Then merge the elements together as was done above. Organize the four types of dimensions into groups, and delete all but one of the dimensions in each group as was done in [Figure 2A.2\(d\)](#). Then use the constraints to ensure that the line segments from each line type in each four-element segment are equal and parallel. [Figure 2A.3](#) shows how six of the four-element lines can be used to create a relatively long (24 single elements) slider line with only four dimensions. Using this procedure, a slider line of any length can be created. However, when the final line is copied and pasted into a linkage drawing, it is necessary to ensure that all dimensions and constraints were copied correctly.

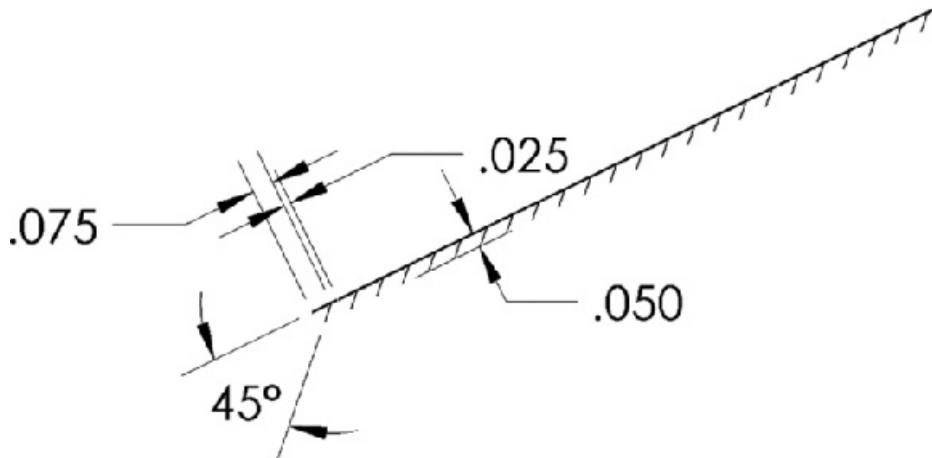


[Figure 2A.3](#) 24-element slider line.

To constrain the slider-line inclination to be a specific angle, draw a temporary horizontal construction line and constrain it to be fixed. Use the dimension tool to define the angle between the baseline of the slider line and the horizontal line. If the slider line is to be horizontal or vertical, these constraints can be set directly without the need for the horizontal construction line. To make the results more readable, hide the dimensions by copying them to the *Dimension* layer and hiding it.

2A.2 Pin Bushings and Ground Pivots

For the ground pivot, open the blank drawing file and save it as *GroundPivot*. Next set up two layers: *GroundPivot* and *Dimensions*. It is useful to use the same relationships among the dimensions so that the ground pivots will appear consistent from drawing to drawing. For this, the basic dimension chosen is the diameter (d) of the bushing of the ground pivot as shown in [Figure 2A.4](#). All other dimensions are made proportional to d . Pin bushings are made by drawing a circle of diameter d and merging the center point of the circle with the end point of a given link.

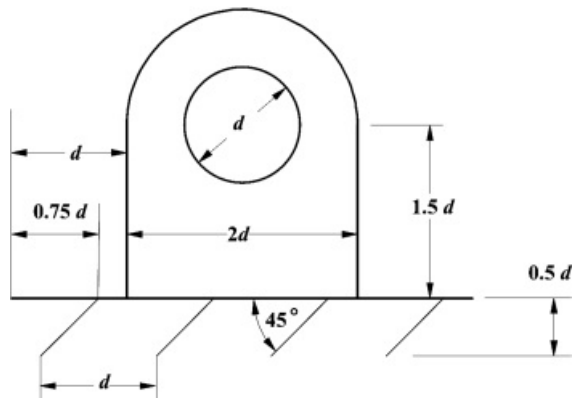


[Figure 2A.4](#) Proportions used for ground pivots.

The steps for drawing the ground pivot are shown in [Figure 2A.5](#). Start the figure by drawing the bushing circle [[Figure 2A.5\(a\)](#)]. Next draw a second larger circle concentric with the first [[Figure 2A.5\(b\)](#)]. Then draw two vertical lines tangent to each side of the second circle [[Figure 2A.5\(c\)](#)]. Select both vertical lines and constrain them to be equal [[Figure 2A.5\(d\)](#)]. Delete the bottom half of the larger concentric circle [[Figure 2A.5\(e\)](#)]. Draw a horizontal line from the bottom of the left vertical line [[Figure 2A.5\(f\)](#)]. Now constrain the model by setting the dimensions according the ratios indicated in [Figure 2A.4](#). Dimension the bushing circle to be the selected value for d . The value used is somewhat arbitrary, but it is best to use a value that will be compatible with the size of the linkage figures for which the ground pivot will be used. Here we have selected 0.1 in. Dimension the radius of the larger circle arc to be 0.1 in. Set the vertical lines to be 1.5 times the bushing diameter (0.15 in). If necessary zoom in on the drawing to make it easier to see. Next, dimension the horizontal line to be equal to the bushing diameter [[Figure 2A.5\(f\)](#)]. The drawing is now ready for the baseline.

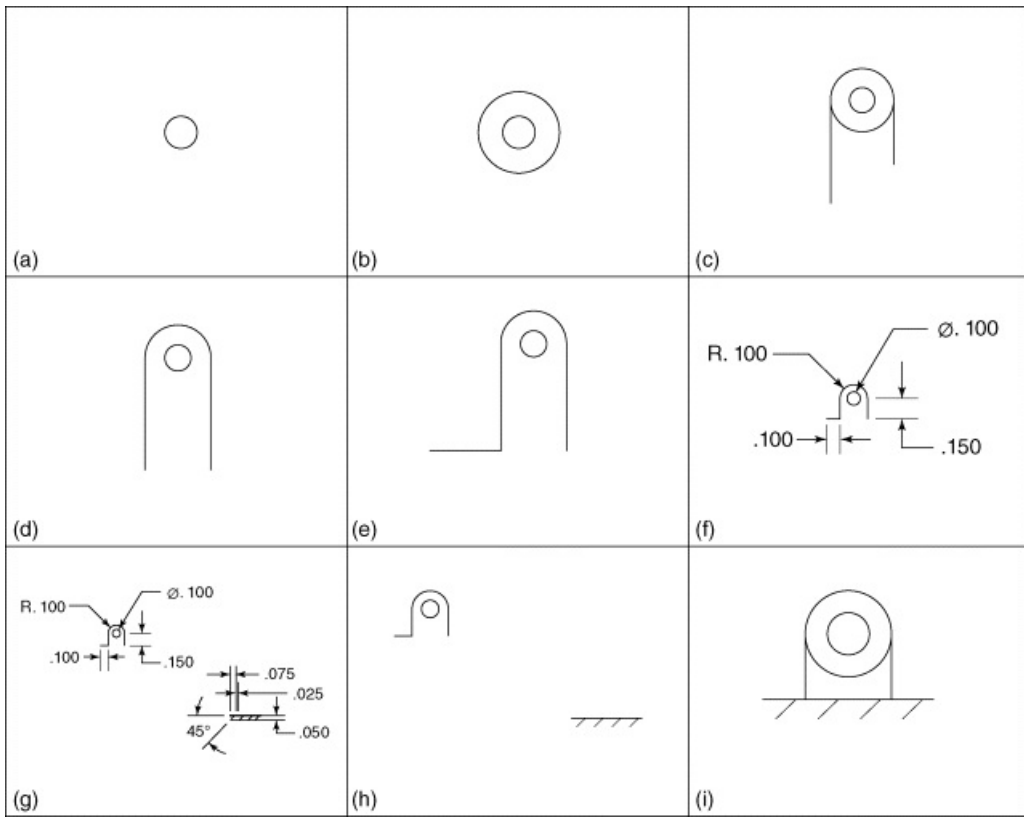


[Figure 2A.5](#) Steps in drawing ground pivot: (a) Draw bushing circle; (b) draw outer circle; (c) draw two vertical tangent lines tangent to outer circle; (d) constrain tangent lines to be equal and delete/trim lower half of outside circle; (e) draw horizontal line at base; (f) dimension bushing circle, outer circle arc, vertical lines, and horizontal line; (g) copy and paste a four-element slider line and constrain to be horizontal; (h) hide dimensions; and (i) select the left endpoint of slider line and the left endpoint of the horizontal line on the bushing and merge them. This gives the final bushing.

Open the four-element slider line and constrain the baseline to be horizontal. Then copy the line drawing, constraints, and dimensions, and paste the results into the *GroundPivot* drawing [[Figure 2A.5\(g\)](#)]. The dimensions from both the ground pivot drawing and the slider line should be hidden next [[Figure 2A.5\(h\)](#)]. Also notice that the slider line is dimensioned consistently with the ground pivot so we need to simply merge the two images. To merge the two entities, select the left-most point on the horizontal line for the ground pivot and the left-most point on the slider line and select the merge constraint. The result is shown in the last frame of [Figure 2A.5](#) with the dimensions and constraint icons hidden. The ground pivot model can now be copied into linkage drawings.

In most instances, we will want the baseline for the ground pivots to be horizontal; however, occasionally, we may wish to have them inclined. This may be done by copying the horizontal ground pivot and setting the constraints to incline it. First draw a fixed construction line at an arbitrary angle as was done with the single element case. Next delete all vertical and horizontal constraints in the horizontal model. Constrain the base elements as was done for the slider line in Section 2A.1. Use the angle dimension tool to set the inclination angle between the construction line and the baseline to be something other than zero. Delete the construction line. Now set the constraints so that the ground pivot looks like that in [Figure 2A.6](#). Typically, this will mean constraining the two lines that were originally vertical to be parallel and equal to each other and perpendicular to the baseline. Also constrain the bottom points of these two lines to be coincident with the baseline. To incline the ground pivot to be at a specific angle with the horizontal, draw a fixed, horizontal construction line, and use the dimension tool to set the angle between the horizontal construction line and the baseline of the ground pivot.

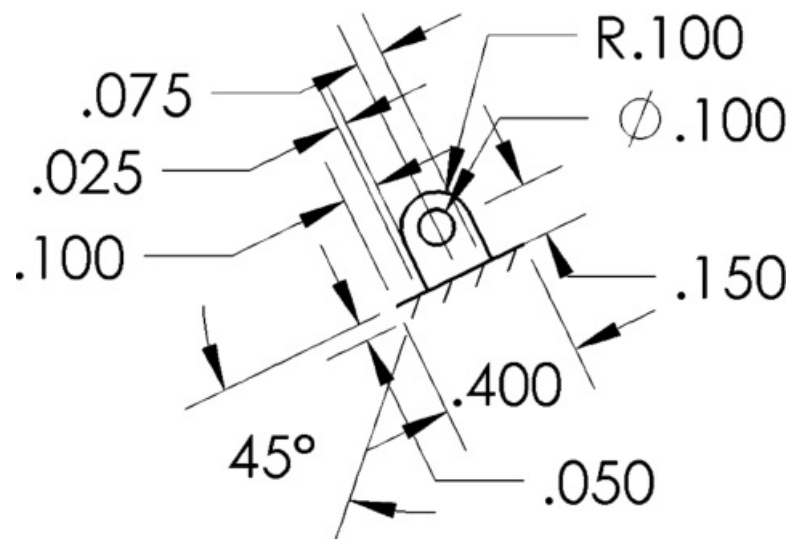


[Figure 2A.6](#) Inclined ground pivot with dimensions shown.



Appendix 2B Useful Constructions When Equation Constraints are Not Available

While equation constraints are the preferred way to implement constraints that treat dimensions as functional variables in nonlinear relationships, some parametric-design programs do not always have reliable functional constraints in the mode that the designer is using. In that case, it is useful to develop alternative graphical constructions that can be used to impose the same constraints. There are five constructions that are useful if functional constraints are not available:

1. Constrain two angles to be equal or to make one angle an integral multiple of another angle.
2. Define a line to be half the length of another line.
3. Construct a line to represent $x = ky$ where y is a known vector magnitude and k is a scaling factor. This construction can be used to develop a scaled polygon after an unscaled polygon is developed.
4. Construct a line to represent the function $a_r = v^2/r$ where v and r are known length variables. This construction is required for representing the radial components of acceleration.
5. Construct a line to represent the function $x = yz/r$ where y , z , and r are known length variables. This construction represents the Coriolis component of acceleration.

Constructions 1 and 2 are useful for crank-rocker designs ([Chapter 3](#)), and constructions 3, 4, 5 are useful for velocity and acceleration analyses ([Chapters 4 and 5](#)).

2B.1 Constrain Two Angles to Be Integral Multiples of Another Angle

Assume that we have four lines that define two angles and label the lines as a , b , c , d [[Figure 2B.1\(a\)](#)]. Construct a triangle inside each of the angles and merge one corner of each triangle with the apex of each of the angles [[Figure 2B.1\(b\)](#)]. Select each side of the triangles next to the apex angles and constrain them to be equal. Similarly, select the two triangle bases and constrain them to be equal. The result is two congruent isosceles triangles shown [[Figure 2B.1\(c\)](#)]. Next, constrain the two sides of each triangle to be collinear with the adjacent line defining each angle. The two angles are now constrained to be equal [[Figure 2B.1\(d\)](#)]. If we want to make one angle twice the size of another (or vice versa), we can construct one congruent triangle within one angle and two within the other. Two steps of this process are shown in [Figures 2B.2\(a\)](#) and [2B.2\(b\)](#).

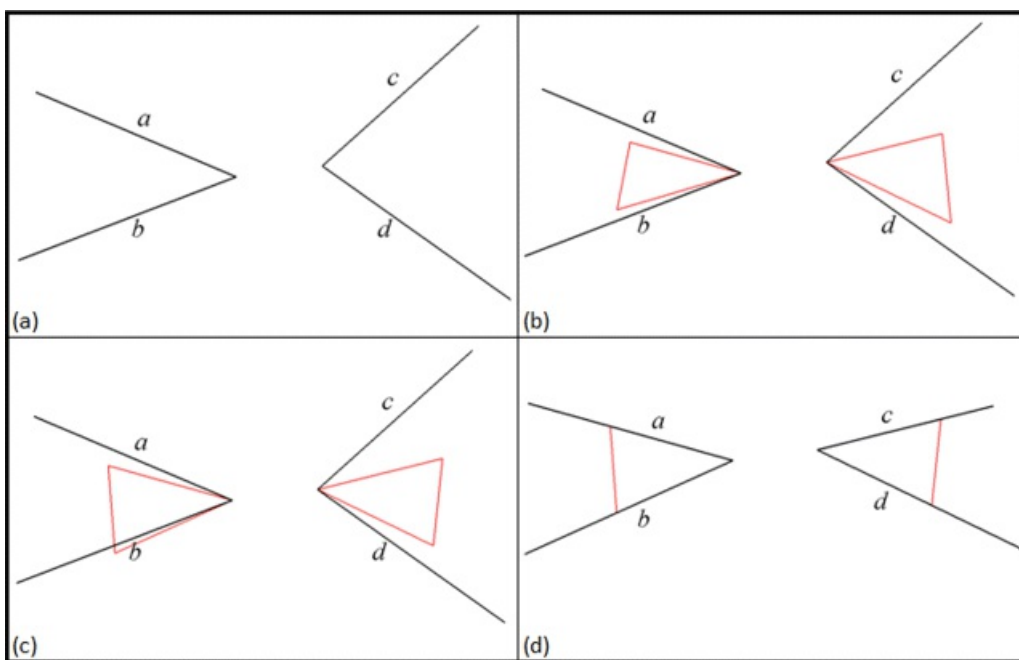


[Figure 2B.1](#) Procedure for constraining two angles to be equal: (a) Original angles; (b) draw two triangles

that share apexes with the angles; (c) constrain the sides of the triangles to be equal and the bases to be equal; and (d) constrain the sides of the triangles to be collinear with the adjacent sides of the angles.

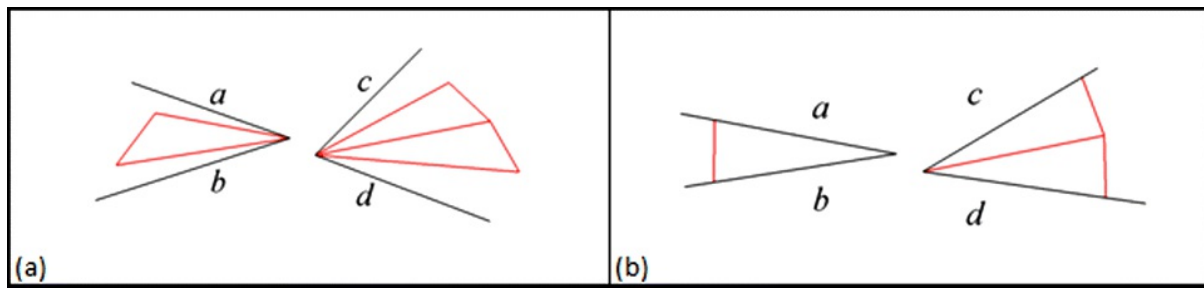


[Figure 2B.2](#) Procedure for constraining one angle to be half (or twice) the other: (a) Original angles and (b) constrain the sides of the triangles to be equal and the bases to be equal. Also, constrain the sides outside of the triangles to be coincident with the sides of the angles.

2B.2 Constrain a Line to Be Half the Length of Another Line

If the midpoint of a line is available, it is only necessary to construct a line from the midpoint of the line to the end and constrain the desired line to be equal to the constructed line. If the midpoint is not available for whatever reason, draw an isosceles triangle on the line as shown in [Figure 2B.3\(a\)](#). Next constrain the apex angle of the triangle to be coincident with the line. Each leg of the triangle will be half the length of the line as shown in [Figure 2B.3\(b\)](#).

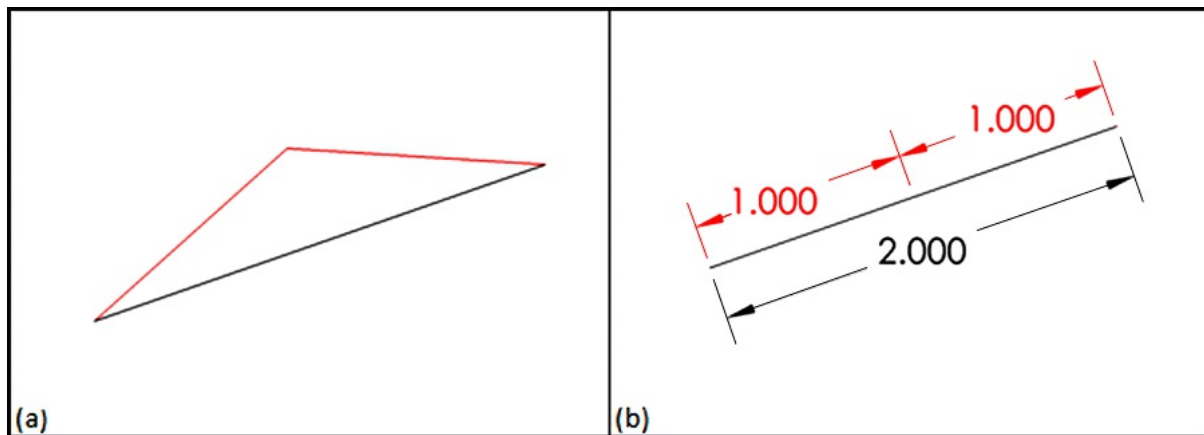


[Figure 2B.3](#) Procedure for constructing a line that is half the length of another line: (a) Original line as base of isosceles triangle and (b) constrain apex of triangle to be coincident with line. Each leg of the triangle is half the length of the line.

2B.3 Construction for Scaling

The construction for scaling is represented in [Figure 2B.4](#).

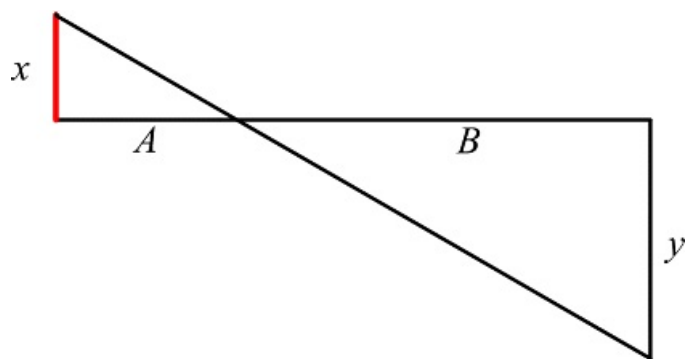


[Figure 2B.4](#) Geometry representing scaling.

From [Figure 2B.4](#)

$$\frac{x}{A} = \frac{y}{B}$$

and

$$x = \left(\frac{A}{B}\right)y = ky$$

By adjusting the distances A and B , any scaling value for k can be represented graphically. This construction can be used in either a velocity or acceleration analysis to develop a scaled polygon.

2B.4 Construction for Square Ratio v^2/r

The construction for the square ratio is shown in [Figure 2B.5](#). From the figure

$$\frac{\omega_r}{v} = \frac{v}{r}$$

and

$$\omega_r = \frac{v^2}{r}$$

For this construction to give a result that is numerically correct, the lengths of the lines corresponding to ω_r , v , and r must all be plotted full scale. Because of the relative sizes of the lines, the size of the resulting figure may be vastly different from that of the position diagram. This makes it difficult to display the results in a single drawing. The velocity diagrams can be scaled arbitrarily as discussed above; however, to display the acceleration polygon, the construction in [Figure 2B.4](#) must be used to scale any vector corresponding to the radial components of acceleration. This can be tedious and not worth the effort unless a relatively large number of input positions is of interest. For one position, it is simpler to compute the radial components of acceleration externally and draw them directly in a scaled polygon.

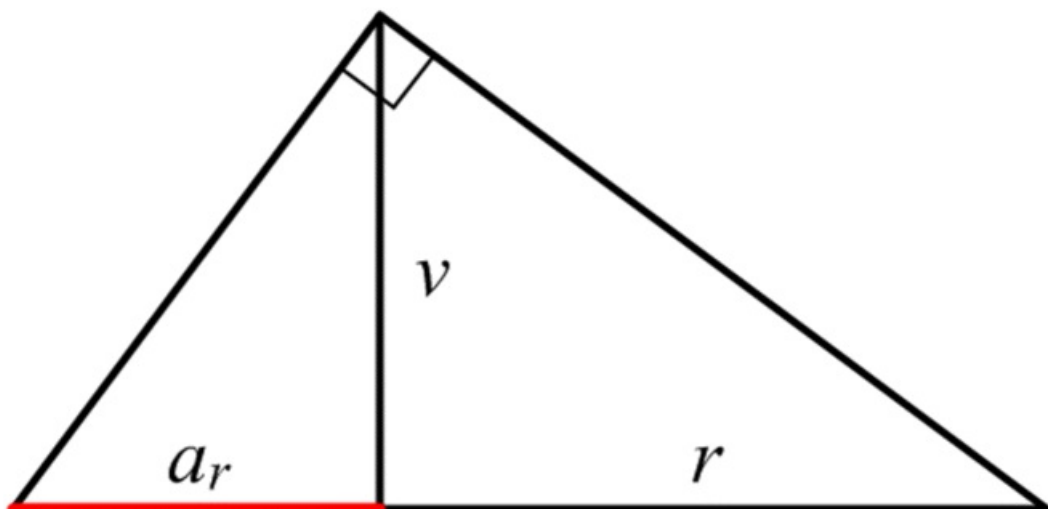


[Figure 2B.5](#) Geometry representing square ratio.

2B.5 Construction for Function $x = yz/r$

To use GCP for accelerations when moving sliders are involved, it is necessary to be able to determine a product ratio to represent the function $x = yz/r$ where y , z , and r are known variables. This construction is required for representing the Coriolis acceleration. The construction is shown in [Figure 2B.6](#) and is the same as in [Figure 2B.4](#) except that the lengths of the sides corresponding to A and B are specific values in [Figure 2B.4](#). From [Figure 2B.6](#)

$$\frac{x}{z} = \frac{y}{r}$$

and

$$x = \frac{yz}{r}$$

In an acceleration analysis, x would be the Coriolis acceleration, and y and z would correspond to velocities from the velocity polygon, and r would correspond to a radial distance from the position polygon. Again, because of the amount of work involved, it is usually only worth doing the constructions for accelerations when a graphical program for a range of positions is needed. If it is necessary to analyze only one position, it is simpler to make the necessary calculations for the normal and Coriolis components of acceleration external to the program.

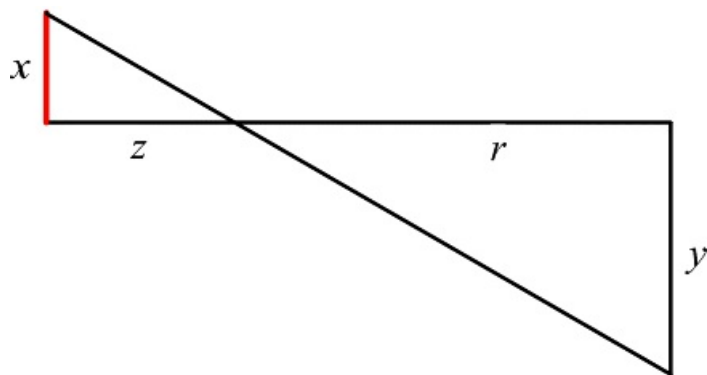


[Figure 2B.6](#) Geometry representing product-ratio.

Notes

1. It is possible to develop a graphical construction for the nonlinear components of acceleration; however, this is usually too complex to be practical.
2. A scaled ground pivot is saved in the SolidWorks file *GroundPivot.SLDDRW* included in the supplemental material for this book.
3. A SolidWorks file for a generic inclined slider line is included with the supplementary material for this book in the file *Long_Inclined_SliderLine.SLDDRW*.

3

PLANAR LINKAGE DESIGN

Prerequisite Knowledge Needed for Chapter 3

Knowledge of linkage structure, degrees of freedom, linkage inversion, and Grashof inequality from [Chapter 1](#). A thorough knowledge of Geometric Constraint Programming (GCP) from [Chapter 2](#), and a familiarity with basic linear algebra and matrices.



3.1 Introduction

The machine designer is often called upon to provide a means of generating an irregular motion. For our purposes, an irregular motion can be regarded as anything other than uniform rotation about a fixed axis or uniform rectilinear translation. The means of generating irregular motions can vary from using electromechanical systems, involving servomotors or robotics, to purely mechanical systems involving linkages, noncircular gears, and/or cams. The decision on what type of system to use falls under the general topic of type synthesis. Before starting dimensional synthesis, the engineer must decide on the type of device to use. Cost and reliability are two of the primary criteria for choosing one particular system over another. The cost of computer-controlled electromechanical devices is decreasing each year and the reliability is improving. However, when large numbers are required or high power must be transmitted, mechanical systems currently tend to have a significant advantage, and the designer should always consider them as viable choices in such circumstances.

Once the designer has chosen to use a system that is primarily mechanical, there are still many choices for the type of device to use. A number of books have cataloged different ways of solving mechanical problems. For example, Artobolevsky [3] has compiled five volumes on various mechanical devices, and Jones, Horton, and Newell [14,16,19] have edited four volumes with significant explanations. Chironis and Slater [4] have edited an encyclopedic collection of drawings and articles on mechanisms and mechanical devices for various applications in one volume, and Parmley [20] has edited a similar sourcebook of mechanical components. It is highly recommended that the designer consult books such as these when beginning a design project. Although information on the Internet is improving, these sources still provide more options and detailed information on mechanical devices than is currently available directly on the web.

When considering the type of mechanical device to use for irregular motions, one-degree-of-freedom (dof) mechanisms are attractive because they require only a single actuator and can transmit a large amount of power. The two main types of one-degree-of-freedom mechanisms are cams and linkages. As irregular motion generators, they each have advantages and disadvantages. In general, cams are easily designed but are relatively difficult, and therefore expensive, to manufacture, especially if high speeds must be accommodated. They are also relatively unreliable in uncontrolled environments due to wear problems. Linkages are more difficult to design but are relatively inexpensive to manufacture and very reliable. Both types of mechanism are important, and we will consider the design of linkages in this chapter and the design of cams in [Chapter 10](#).

We naturally attempt to use the simplest mechanism capable of performing the desired function. For this reason, four-link mechanisms are by far the most widely used. This is clearly evident in most of the references [3,14,16,19] identified here. The techniques used for the design of six- and eight-bar mechanisms are basically extensions of those used for four-link mechanisms. Thus, while we will discuss six- and eight-bar mechanisms, the primary emphasis in this chapter will be on four-bar mechanism synthesis.

The joints most commonly used in mechanisms are those in which the joint constraints are provided by two surfaces in contact. This is an important difference from the point or line contact that occurs in cams and gears. Surface contact is desirable from the point of view of lubrication and wear resistance. As was indicated in [Chapter 1](#), the only surface-contact or lower-pair joints that are available for use in planar mechanisms are revolute joints or hinges and prismatic slides. There are four basic types of four-link mechanisms with surface contact joints:

1. The four-revolute four-bar linkage: This linkage is typically referred to as a four-bar linkage. In this linkage, all four joints are hinges as shown in [Figure 3.1](#). This is by far the most widely used linkage for irregular motion generation.

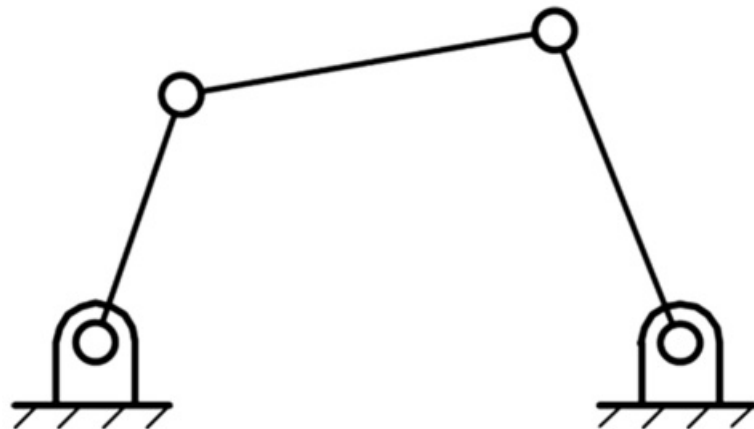


[Figure 3.1](#) The four-revolute, four-bar linkage. This is one of four basic planar single-loop linkages.

2. The slider-crank (and its inversions): The slider-crank linkage is shown schematically in [Figure 3.2](#). Mechanisms based on this linkage or its inversions are very commonly used to convert translation to rotary motion and vice versa. It is little used when neither a translating input nor a translating output is needed.

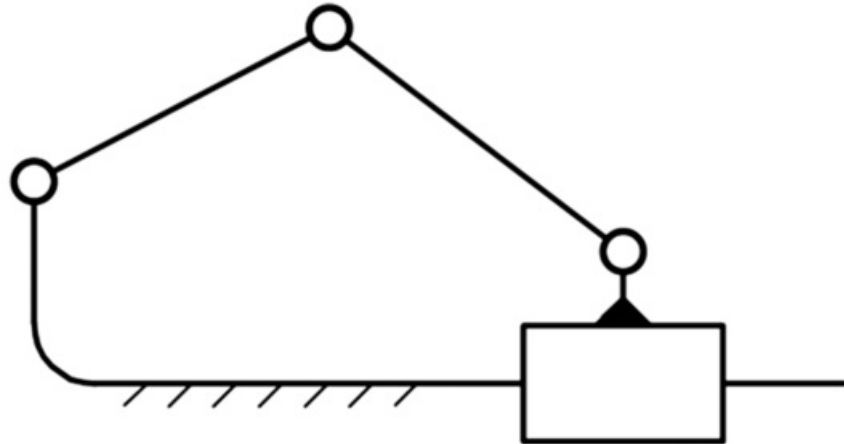


[Figure 3.2](#) The slider-crank linkage is obtained by replacing one revolute joint in a four-bar linkage with a prismatic joint. When inverted onto the crank, or the coupler, so that the slide rotates, the linkage becomes a turning block linkage.

3. The elliptic-trammel linkage (and its inversions): A schematic drawing for the elliptic-trammel is shown in [Figure 3.3](#). Except for the scotch-yoke [3,20] and Oldham [3,20] inversions, the elliptic-trammel is little used because of slip-stick friction problems in the two slides.

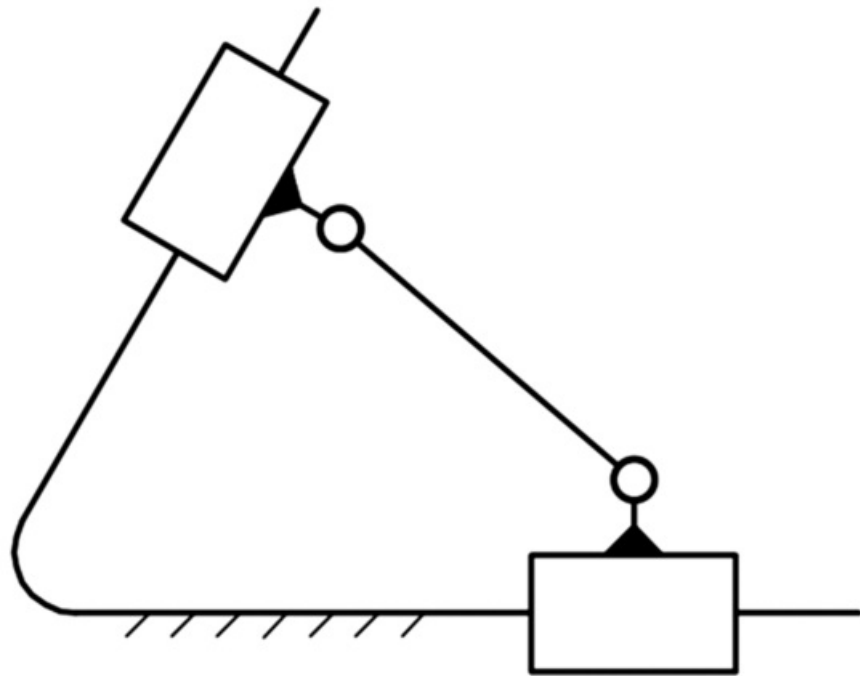


[Figure 3.3](#) Elliptic-trammel linkage. The paths of all points in the coupler are ellipses. When inverted onto one of the revolute-prismatic members, this becomes a scotch-yoke linkage. The scotch-yoke is sometimes used as a harmonic motion generator. The other possible inversion, onto the coupler, is used in practice as the Oldham coupling. This is a simple mechanism for accommodating misalignment between shafts.

4. Rapson-slide: A schematic diagram of the Rapson-slide is shown in [Figure 3.4](#). There are two sliders that must be carefully designed if mechanisms based on this chain are to work properly. In practice, the Rapson-slide is much less used than the four-bar linkage or slider-crank mechanism because neither rotary joint can be made to rotate 360° and because of slip-stick friction in the two slides.

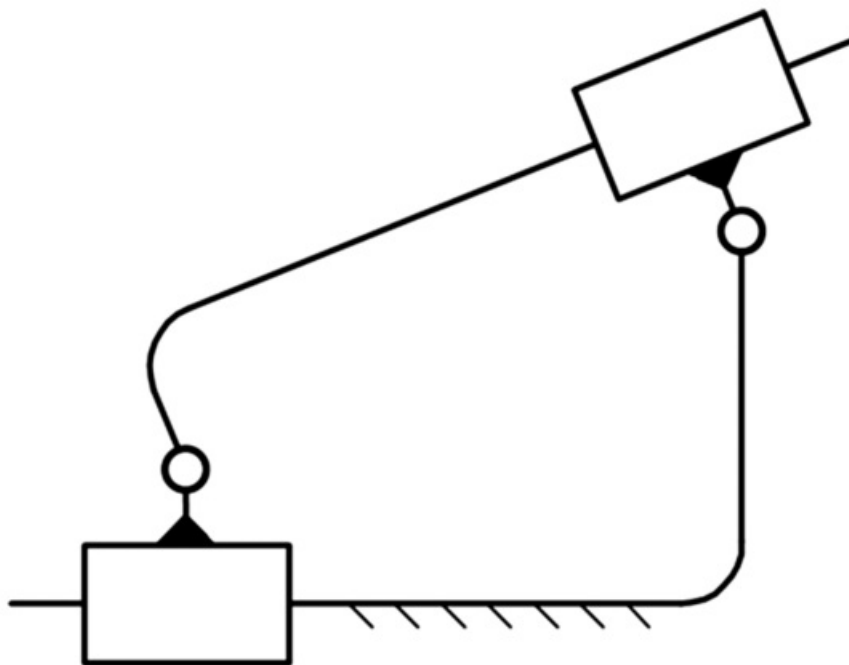


[Figure 3.4](#) The Rapson-slide linkage. Its inversions are also Rapson-slide linkages.

The majority of the techniques discussed in this book are intended for four-bar linkage synthesis. This is primarily

because of the relatively large number of dimensions that can be varied, allowing for flexibility in design. Unfortunately, it also results in somewhat complicated design techniques. When the techniques are applied to linkages having one or more slider joints, the results are somewhat simpler.

It is very rare for the desired motion to be exactly producible by a four-bar linkage. Thus, we can typically only approximate the desired motion. One approach is to select a number of positions (precision points) along the desired path and compel the linkage to move exactly through those positions. Using this method, one has no direct control over the behavior of the linkage between the design positions. One works in the (sometimes pious) hope that the linkage movement will not deviate too far from that desired between the design positions. It is, in fact, remarkable how accurate this method can be in favorable circumstances. For example, it is possible to design a four-bar linkage for which the path of a point on the coupler deviates no more than one-thousandth of an inch from a straight line over a 10-inch line length.

The types of problems most usually tackled using the precision-position approach permit graphical solutions. This is straightforward for problems with two and three design positions but becomes complex and laborious for four or five design positions. In theory, five positions are possible for most four-bar precision-position problem types, but most do not, in practice, admit as many as four or five design positions.

The second basic approach to linkage synthesis is to select a rather large number of design positions and, instead of requiring the mechanism to pass through them exactly, minimize the sum of the squares of the deviations of the mechanism positions from those positions. Thus, the linkage motion approaches the design positions but may not exactly pass through any of them. This method makes use of numerical optimization techniques to produce solution linkages. Used directly, this type of approach requires the user to manipulate the mathematical constraints to obtain control over the type and properties of the solution linkage.

In a given problem, either of these approaches may yield good results. The choice is most often decided by the techniques with which the designer is most familiar and what aids, such as drawing or synthesis programs, he or she has available.

The range of synthesis problems that arise in engineering design is infinite. The classes of problems that are most commonly treated, because of a combination of practical importance and a well-developed theory, are:

1. The double-rocker problem: This is one of the simplest linkage design problems and is very common in industry. The problem is to design a four-bar linkage that will move its output link through an angle ϕ while the input link moves through the angle θ .
2. The rocker-amplitude problem: The output link is to oscillate through a specified angular amplitude while the input rotates a full revolution. The required linkage is a crank-rocker with continuously rotating driving crank. The oscillatory output motion is specified as part of the input information.
3. The motion-generation problem: A linkage is to be synthesized where the coupler, as a whole, is to follow a desired trajectory. That is, the movement of the coupler as a whole is specified, not just that of a point lying on it. In the development here, we will concentrate on graphical procedures for motion generation with a particular emphasis on the use of Geometric Constraint Programming (GCP) that can be used to solve all of the motion-generation problems considered in this book. Analytical approaches to this problem have been developed [22,28,34]. However, these have been largely superseded by GCP methods and are generally beyond the scope of this book.
4. The function-generation problem: In function generation, normally the angles of the two cranks are to be coordinated. Historically, the name *function generation* originated in the days in which mechanical analog computers were used to perform complex mathematical calculations in devices such as naval gun sights and carburetor linkages. Linkages were used to generate angular relationships approximating logarithms, trigonometric functions, and so forth [10]. In practice, computer-controlled actuators have largely superseded the use of linkages for function generation. For this reason, we will not treat function generation as a major topic in the current edition of this book. Interested readers are referred to earlier editions of this book or to Hall [12] for a thorough treatment.
5. The path-generation problem: In path generation, a single point on the coupler is to follow a nominated curve. In this form, the problem does not admit of a direct graphical solution. However, this class of problem

is important from a practical point of view, and we will present design methods. These are trial-and-error techniques starting with the selection of an approximate coupler-point path from an atlas of coupler curves or from curves generated with a computer program. Simple computer programs can be important aids in the trial-and-error process.

A modified type of point path problem in which the progression of the coupler point between design positions is coordinated with the corresponding angular displacements of the driving crank does permit direct graphical solution. This is referred to as the path-angle problem. The techniques required for solution of this type of problem are related to solution methods for motion-generation problems, but are beyond the scope of this book. They are covered in a number of references, for example Hain [11] and Erdman et al. [9].

After individual computer workstations became common in the 1980s, a number of special purpose programs were developed to facilitate linkage design for complex problems. These include KINSYN [21], RECSYN [32–37], LINCAGES [8], WATT [7], and SAM [2]. However, with the advent of powerful general-purpose solid-modeling programs with kinematic analysis modules, modern personal computers, and good user interfaces, many traditional kinematic design problems can be solved in the context of these solid-modeling programs. As a result, it is no longer financially attractive for software companies to market and support special purpose, yet powerful kinematic design programs. Fortunately, the 2D drafting features in parametric-design programs such as SolidWorks [5] and Solidedge [24,25] can be used with GCP to solve most of the problems that once required special purpose programs. In fact, it is possible to use the GCP techniques discussed in [Chapter 2](#) to develop graphical programs to aid in the solution of all of the kinematic design problems presented in most textbooks, and the graphical programs can be developed with little more effort than is required to solve a single problem using traditional graphical techniques.

In this chapter, we will usually address the design of linkages with two approaches. The first will be the classical graphical approach. Designers will rarely use this approach in practice, but it identifies the geometric issues and provides insight into the second approach using Geometric Constraint Programming that is most attractive for everyday use. In some instances, the graphical approaches will be augmented by analytical approaches that are easy to program and can be used for specialized processes unique to mechanism design problems. The equations are usually based on models for the graphical techniques presented. The design programs supplied with the supplementary material for this book are based on these hybrid graphical-numerical methods.



3.2 Two-Position Double-Rocker Design

One of the most common problems in kinematics is the design of a double-lever or double-rocker mechanism. The design situation is shown in [Figure 3.5\(a\)](#). The problem is to design a four-bar linkage for which the output link will rotate through an angle ϕ when the input link rotates through an angle θ . For the problem we will consider here, the design variables are the distance between the fixed pivots A^* and B^* , the length of the output link B^*B , the starting angle (θ_1) for link 2, the starting angle (ϕ_1) for link 4, the length of the input link A^*A , and the length of the coupler AB . Overall, there are eight variables, and we can solve for two of them. In the graphical solution procedure discussed in the following section, we will assume that values for all of the variables are known except for the lengths of the input link (A^*A) and of the coupler (AB).

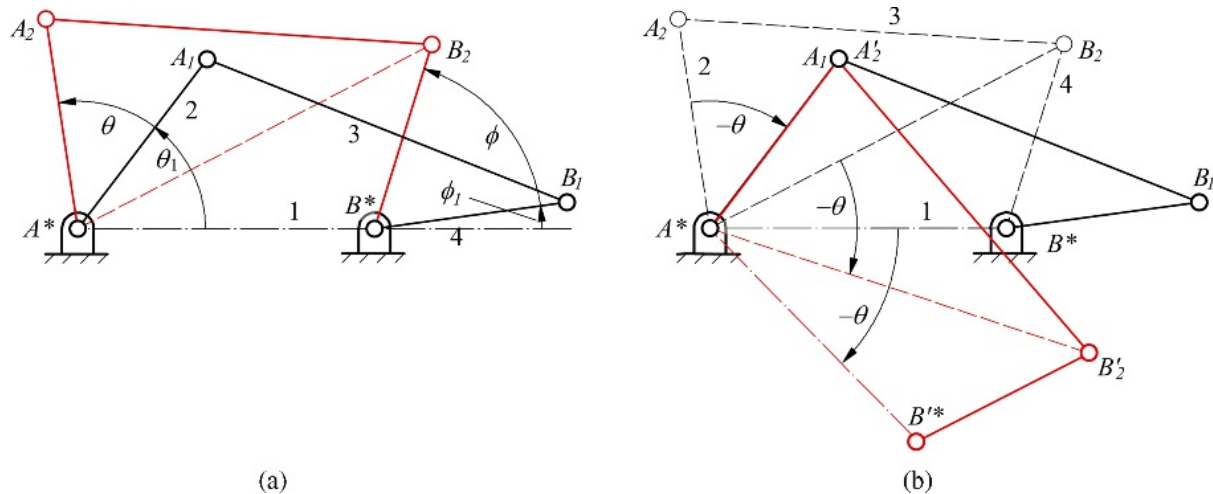


[Figure 3.5](#) Two positions of the rockers of a four-bar linkage. (a) Positions relative to the frame, and (b) positions relative to the input rocker in position 1.

3.2.1 Graphical Solution Procedure

The basis for solving the problem is to invert the mechanism onto the input link and visualize the motion of the mechanism when the observer is fixed to that link. This apparent motion is shown in [Figure 3.5\(b\)](#). Observed from the ground, or link 1, points A and B appear to move from Position 1 to Position 2 through their respective angles, θ and ϕ . However, if link 2 is the reference, then link 2 appears to be stationary, and the other links, including the frame, appear to move relative to link 2 in the direction of $-\theta$. In a given position, the relative geometry is the same regardless of which link is the reference link. Therefore, the quadrilateral $A^*A_2B_2B^*$ is the same whether link 1 is the reference or link 2 is the reference. To show the apparent position of the links relative to Link 2, we need only rotate the quadrilateral $A^*A_2B_2B^*$ through an angle of $-\theta$ about pivot A^* . When this is done, lines A^*B^* and A^*B_2 are both rotated by the angle $-\theta$. This observation is the basis for the graphical design procedure given next.

The design procedure is illustrated in [Figure 3.6](#). We begin knowing the distance between the frame pivots A^* and B^* and the length of the output link, B^*B . We must also draw rays corresponding to A^*A_1 and A^*A_2 as shown in [Figure 3.6\(a\)](#). First draw the line A^*B_2 and rotate it by the angle $-\theta$ about the pivot A^* . This will locate B'_2 , which is where B_2 would appear to be if the observer were on link 2. Relative to the input link in position 1, point B appears to rotate on a circular arc about A_1 as B travels from B_1 to B'_2 . Therefore, A_1 must lie on the perpendicular bisector of the line segment $B_1B'_2$. Also, A_1 will lie on the ray through A^* shown in [Figure 3.6\(a\)](#).

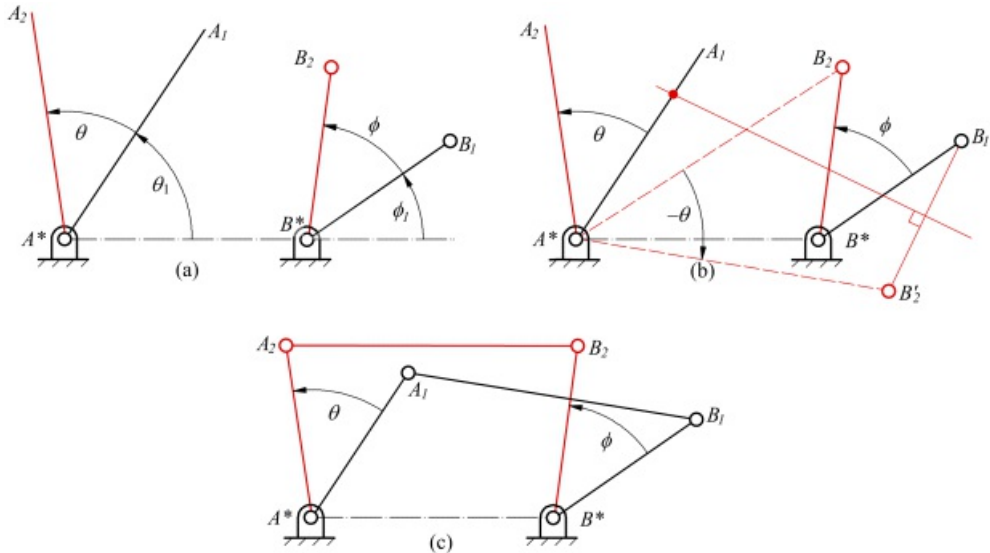


Figure 3.6 Locating point A_1 that in turn determines the length of the coupler and the input rocker.

Once A_1 is determined, the lengths of the input rocker and of the coupler will be known. The input rocker length is A^*A_1 and the coupler length is A_1B_1 (or $A_1B'_2$). Note that the solution to this problem makes use of the idea of inversion. We will use inversion again when we consider the design of linkages for motion-generation or rigid-body guidance.

If we wanted to specify the input-crank length rather than the output-link length, we could use the same procedure by inverting onto the output link, rather than the input link.

3.2.2 Solution Using Geometric Constraint Programming

Using GCP to solve the double-rocker problem was discussed in detail in Example 2.1 in [Chapter 2](#). To summarize the CGP procedure for the double-rocker problem, we begin by drawing two arbitrary four-bar linkages with a common base link. We then constrain the two input links, the two couplers, and the two output links to be equal. We also constrain the input links of the two linkages to coincide with the rays A^*A_1 and A^*A_2 . Similarly, we constrain the output links of the two linkages to coincide with the rays B^*B_1 and B^*B_2 . The resulting figure is the basic graphical program. Of the eight variables identified above, we must designate six of them as driving (independent) dimensions and two of the variables as driven (dependent) dimensions. We can use the dimension tool in the solid-modeling program to specify dimension values for six of the eight variables. The final “program” for the double-rocker problem from [Figure 2.15](#) is repeated here as [Figure 3.7](#). The figure shows three instances of the linkage. Two of the instances are in the extreme positions, and they are the instances used when developing the solution. The third instance (drawn with heavier lines) represents the final linkage that can be moved. By using the mouse to drag the joint at either A or B , it is possible to observe the motion of the linkage as it moves between the limits for the input and output links. In the figure, the driving dimensions (independent variables) are shown in red and the driven dimensions (dependent variables) are shown in black. The choice of which six variables are driving is somewhat arbitrary. To change the roles of any two variables, designate one of the black variables as driving and one of the red variables as driven. After values for six driving variables are specified through dimensioning, the constraint manager in the solid-modeling program will compute the remaining unknowns and adjust the drawings of the three instances of the linkage accordingly.

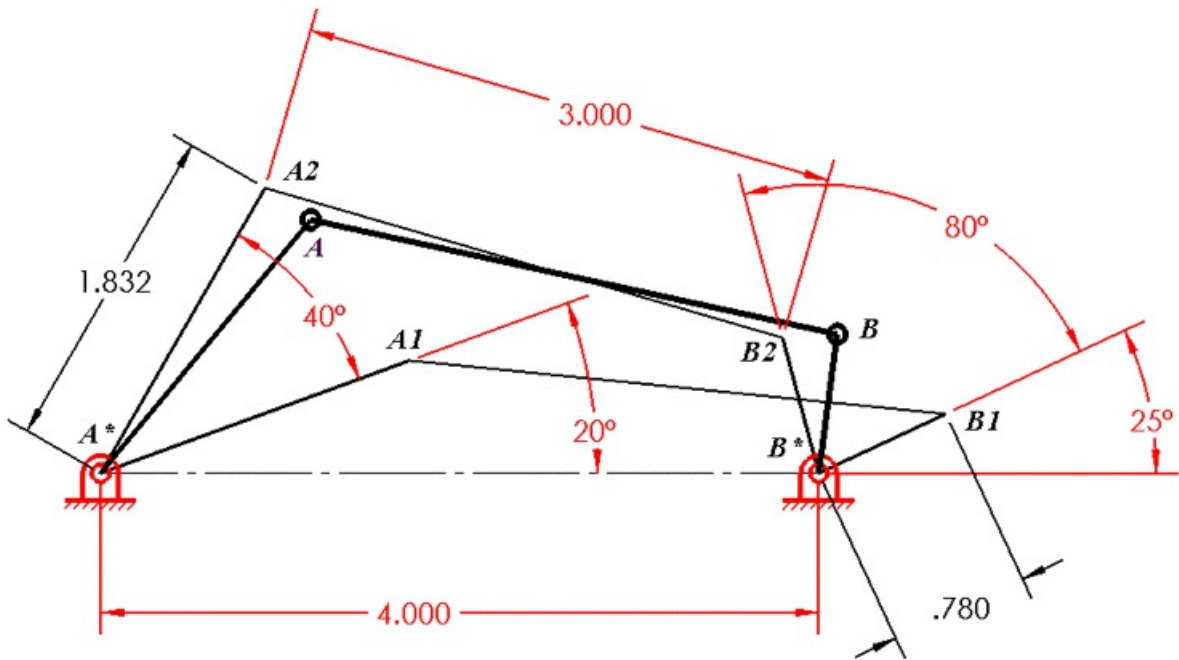


[Figure 3.7](#) Graphical program developed using GCP. The red variables are the driving variables (independent) and the black variables are the driven variables (dependent). The roles of any two variables can be easily changed in the solid-modeling program used for GCP.

3.2.3 Numerical Solution Procedure

The double-rocker problem can be solved analytically so that the design procedure can be easily programmed in MATLAB or another programming language. To begin, locate the origin of the coordinate system at A^* and orient the x axis through B^* as shown in [Figure 3.8](#). We have assumed that the direction of rotation is counterclockwise. This is consistent with the standard positive sign convention for angles using the right-hand rule. Using the variables represented in [Figure 3.8](#), we can compute the (x, y) coordinates of B_1 and B_2 .

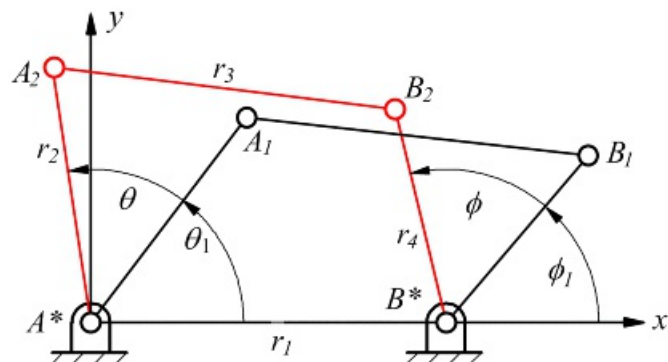


[Figure 3.8](#) Variables for numerical solution procedure.

For B_1

$$\begin{aligned} x_{B_1} &= r_1 + r_4 \cos \phi_I \\ y_{B_1} &= r_4 \sin \phi_I \end{aligned} \quad (3.1)$$

To simplify the resulting expression, let

$$\begin{aligned}\theta_2 &= \theta_1 + \phi \\ \phi_2 &= \phi_1 + \dot{\phi}\end{aligned}$$

Then for B_2

$$\begin{aligned}x_{B_2} &= r_1 + r_4 \cos \phi_2 \\ y_{B_2} &= r_4 \sin \phi_2\end{aligned}\quad (3.2)$$

Similarly, the coordinates of A_1 and A_2 can be written in terms of the input crank length r_2 . For A_1

$$\begin{aligned}x_{A_1} &= r_2 \cos \theta_1 \\ y_{A_1} &= r_2 \sin \theta_1\end{aligned}\quad (3.3)$$

and for A_2

$$\begin{aligned}x_{A_2} &= r_2 \cos \theta_2 \\ y_{A_2} &= r_2 \sin \theta_2\end{aligned}\quad (3.4)$$

The distance between A and B is a constant (r_3) for all positions of A and B . Therefore, we can write

$$r_3 = \sqrt{(x_{A_1} - x_{B_1})^2 + (y_{A_1} - y_{B_1})^2} = \sqrt{(x_{A_2} - x_{B_2})^2 + (y_{A_2} - y_{B_2})^2}\quad (3.5)$$

or

$$(x_{A_1} - x_{B_1})^2 + (y_{A_1} - y_{B_1})^2 = (x_{A_2} - x_{B_2})^2 + (y_{A_2} - y_{B_2})^2$$

Substituting values for the x 's and y 's from [Equations 3.1–3.4](#),

$$(r_2 \cos \theta_1 - r_1 - r_4 \cos \phi_1)^2 + (r_2 \sin \theta_1 - r_4 \sin \phi_1)^2 = (r_2 \cos \theta_2 - r_1 - r_4 \cos \phi_2)^2 + (r_2 \sin \theta_2 - r_4 \sin \phi_2)^2$$

Expanding and simplifying using $\sin^2 \theta + \cos^2 \theta = 1$, we get

$$\begin{aligned}-r_1 r_2 \cos \theta_1 - r_2 r_4 \cos \theta_1 \cos \phi_1 + r_1 r_4 \cos \phi_1 - r_2 r_4 \sin \theta_1 \sin \phi_1 \\ = -r_1 r_2 \cos \theta_2 - r_2 r_4 \cos \theta_2 \cos \phi_2 + r_1 r_4 \cos \phi_2 - r_2 r_4 \sin \theta_2 \sin \phi_2\end{aligned}$$

In this equation, the only unknown is r_2 . The equation is linear in the unknown, and can be easily solved for r_2 . Collecting terms

$$r_1 r_2 \cos \phi_2 - r_1 r_4 \cos \phi_1 = r_2 [-r_1 \cos \theta_1 - r_4 \cos \theta_1 \cos \phi_1 - r_4 \sin \theta_1 \sin \phi_1 + r_1 \cos \theta_2 + r_4 \cos \theta_2 \cos \phi_2 + r_4 \sin \theta_2 \sin \phi_2]$$

Then using the identity $\cos(a - b) = \cos a \cos b + \sin a \sin b$, and solving for r_2 we get

$$r_2 = \frac{r_1 r_4 |\cos \phi_2 - \cos \phi_1|}{-r_4 |\cos(\theta_1 - \phi_1)| + r_1 [\cos \theta_2 - \cos \theta_1] + r_4 |\cos(\theta_2 - \phi_2)|}$$

Knowing r_2 , we can compute r_3 from [Equation 3.5](#) as

$$r_3 = \sqrt{(r_2 \cos \theta_1 - r_1 - r_4 \cos \phi_1)^2 + (r_2 \sin \theta_1 - r_4 \sin \phi_1)^2}$$

These equations are programmed in the MATLAB m-file called *Doublerockerdesign* included in the supplemental material with this book.



3.3 Synthesis of Crank-Rocker Linkages for Specified Rocker Amplitude

The crank-rocker design problem might be thought of as the extreme case of the double-rocker design problem in which the input crank rotates through 360° and the rocker oscillates through a specified angle θ . We also introduce the additional constraint of a time ratio, the ratio of the time for the forward stroke of the rocker to that for the return stroke. This is a very common linkage for driving an oscillating link with a continuously rotating motor. This mechanism is often used interchangeably with cam mechanisms for the same function. However, there are many cases in which a crank-rocker mechanism is superior to a cam-follower mechanism. Among the advantages over cam systems are the smaller contact forces involved, the elimination of the retaining spring, and the closer clearances achieved because of the use of revolute joints.

3.3.1 The Rocker-Amplitude Problem: Graphical Approach

As the crank in a crank-rocker mechanism rotates through 360° , the output link or rocker will oscillate through an angle θ . The limiting positions of the rocker occur when the crank and coupler are collinear as shown in [Figure 3.9](#). In general, the time required for the rocker oscillation in one direction will be different from the time required for the other direction. As indicated above, the ratio of the times required for the forward and return motions is called the time ratio. An expression for the time ratio can be developed by using the nomenclature defined in [Figure 3.9](#).

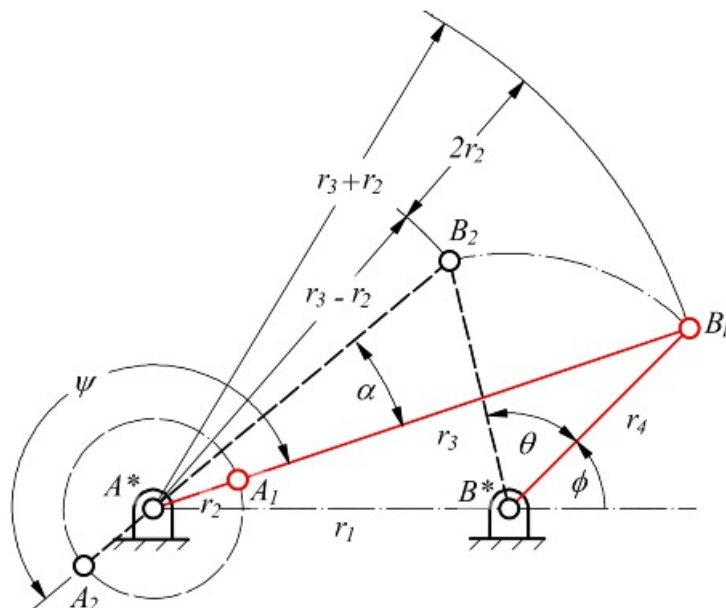


[Figure 3.9](#) Crank-rocker mechanism in extreme positions.

In the crank-rocker mechanism, the crank moves through the angle ψ while the rocker moves from B_1 to B_2 through the angle θ . On the return stroke, the crank moves through the angle $360^\circ - \psi$, and the rocker moves from B_2 to B_1 through the angle $-\theta$.

Assuming that the crank moves with constant angular velocity, the ratio of the times for the forward and reverse strokes of the follower can be related directly to the angles in [Figure 3.9](#). The crank angle for the forward stroke is ψ or $180^\circ + \alpha$. The crank angle for the return stroke is $360^\circ - \psi$ or $180^\circ - \alpha$. Therefore, the time ratio, Q , can be written as

$$Q = \frac{18\psi^\circ + \alpha}{180^\circ - \alpha} \quad (3.6)$$

where α is given in degrees.

The most common problem associated with the synthesis of crank-rocker mechanisms is that of designing the linkage for a given oscillation angle and a given time ratio. For the discussion here, assume that the time ratio, Q , has been given. The first step in the synthesis is to compute the angle α . This can be done by solving [Equation 3.6](#) for Q . Then

$$\alpha = \frac{Q - 1}{Q + 1} 180^\circ \quad (3.7)$$

Note that α is positive when Q is greater than 1 and negative when Q is less than 1. Examples of positive and negative α 's are shown in [Figure 3.10](#).

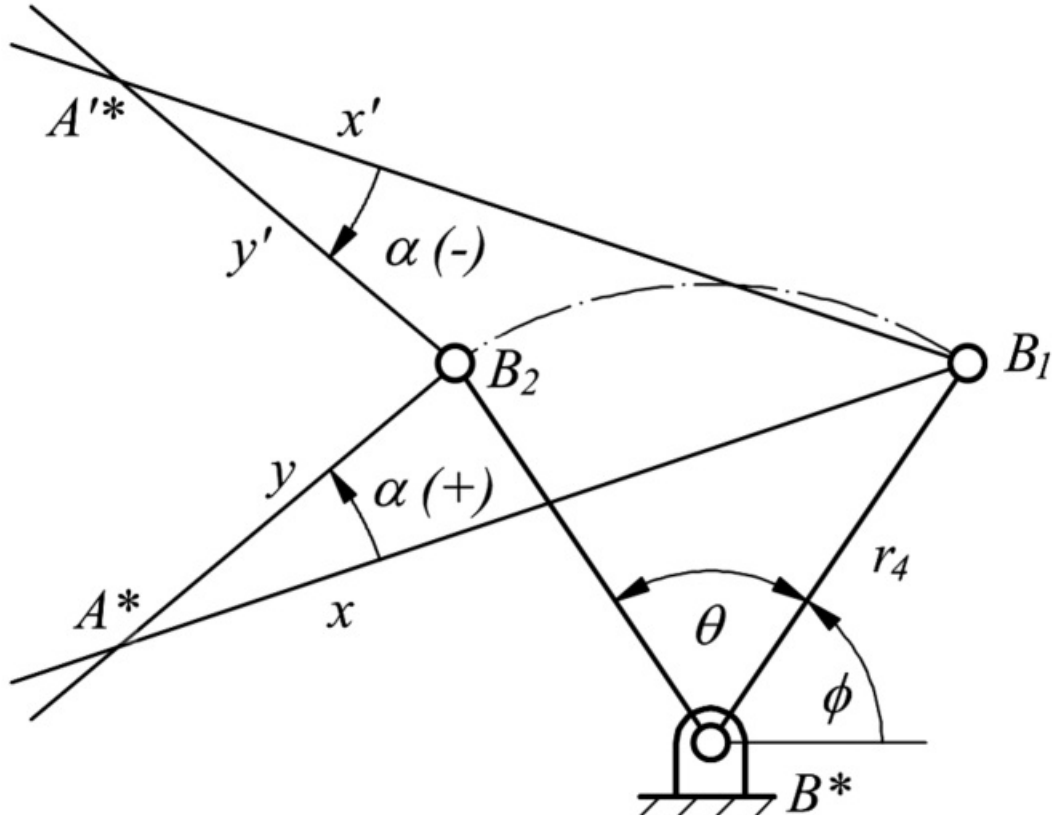


[Figure 3.10](#) Locations of A^* given θ and $\pm\alpha$.

Once α is known, there are a number of ways to proceed with the design. The simplest way to proceed is based on [Figure 3.10](#). To start, choose a location for B^* , select ϕ , and draw the two positions of the rocker (r_4) separated by the angle θ . Draw any line x through the moving pivot at B_1 , and construct a second line at an angle of α to the line x and through the moving pivot at B_2 . Call the second line y . The intersection of lines x and y defines the location of the second fixed pivot (A^*).

Next compute the values of r_2 and r_3 . This is done by using the geometric relationships shown in [Figure 3.9](#). That is

$$r_2 + r_3 = A^* B_1$$

and

$$r_3 - r_2 = A^* B_2$$

Therefore

$$r_2 = \frac{A^*B_1 - A^*B_2}{2} \quad (3.8)$$

and

$$r_3 = \frac{A^*B_1 + A^*B_2}{2} \quad (3.9)$$

Note that during the design procedure, several choices were made. Among these were the starting angle ϕ for the line B^*B_1 and the slope of the line x in [Figure 3.10](#). There are an infinite number of possible choices for each, and each choice will give a different linkage.

Note also, that not all solutions are valid. In particular, the pivots B_1 and B_2 may not cross the line of centers through the fixed pivots A^* and B^* . Referring to [Figure 3.9](#), if this happens, the linkage must be disassembled to reach the two positions, and the desired oscillation angle will not be achieved. As was indicated by Hall [12], once α and θ are known, the locus of acceptable positions for A^* must lie on circular arcs represented by the red sections of the circles shown in [Figure 3.11](#). The locus of A^* must be on a circular arc, according to a classical theorem of Euclid, because the triangle $B_2B_1A^*$ has a fixed base and a constant apex angle (α). If A^* is chosen in the black part of the circles, the two positions of B will be on opposite sides of the line of centers.

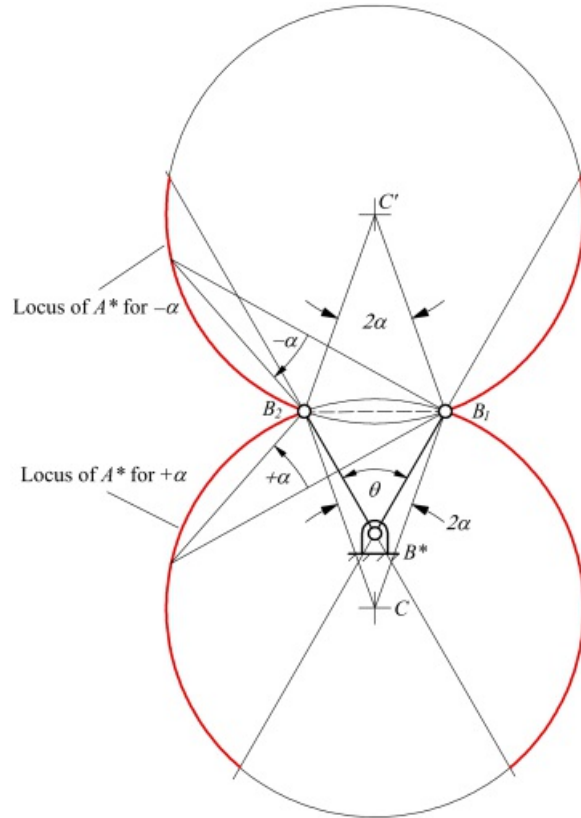


[Figure 3.11](#) Possible locations for A^* given θ and α .

Transmission Angle

Based on [Figure 3.9](#), the crank-rocker problem is characterized by seven variables ($\alpha, \phi, \theta, r_1, r_2, r_3, r_4$). Before we can solve the problem, we need to specify five of the seven variables. For each value chosen for one of the input

variables, we will compute different values for r_2 and r_3 . Therefore, we need to establish criteria by which we can compare different designs with the goal of identifying the optimum design. A common criterion to use is the transmission angle. For a crank-driven linkage, the transmission angle (η) is the internal angle between the coupler and the output link. When $\eta = \pm\pi/2$, a force from the coupler on link 4 will produce the maximum output torque. When $\eta = 0^\circ$ or $\eta = \pi$, the coupler force will produce zero torque on link 4 regardless of the size of the force from the coupler. Therefore, for optimum force transmissibility, we would like the transmission angle to be as close to $\pi/2$ as possible for all positions of the linkage. The positions for the linkage when the maximum (η_{\max}) and minimum (η_{\min}) transmission angles occur are shown in [Figure 3.12](#). Typically, a poor transmission angle corresponds to a large value of $\pi/2 - \eta_{\max/\min}$. Note that the maximum and minimum values for the transmission angle do not occur at the extreme positions of r_4 , but η_{\max} and η_{\min} can be easily computed using the geometry in [Figure 3.12](#). The equations are

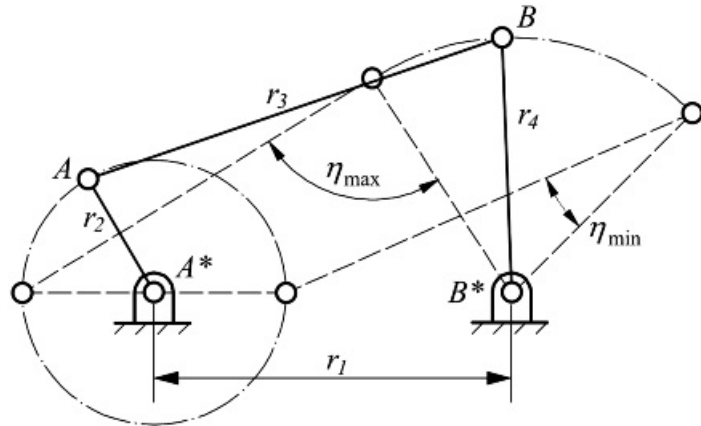


[Figure 3.12](#) Positions corresponding to the maximum and minimum transmission angles.

$$\eta'_{\max} = \cos^{-1} \left| \frac{r_4^2 - (r_1 + r_2)^2 + r_3^2}{2r_3r_4} \right| \quad (3.10)$$

$$\eta'_{\min} = \cos^{-1} \left| \frac{r_4^2 - (r_1 - r_2)^2 + r_3^2}{2r_3r_4} \right| \quad (3.11)$$

If η'_{\max} is negative, then $\eta_{\max} = \pi + \eta'_{\max}$. Otherwise, $\eta_{\max} = \eta'_{\max}$. Similar conditions apply to η_{\min} .

Unscaling the Solution

In the previous derivation, it is assumed that the rocker link (r_4) is specified. This is not always the case. However, to determine the true size of the links, it is necessary to know the size of just one of the links initially. Through a scaling factor, we can determine the sizes of the other links.

Assume that the actual link lengths are R_1, R_2, R_3, R_4 , and the R 's are related to the computed r 's through the following

$$\left. \begin{array}{l} R_1 = K r_1 \\ R_2 = K r_2 \\ R_3 = K r_3 \\ R_4 = K r_4 \end{array} \right\} \quad (3.12)$$

where K is the scale factor for the linkage. From [Equation 3.12](#)

$$K = R_1/r_1 = R_2/r_2 = R_3/r_3 = R_4/r_4 \quad (3.13)$$

After the design procedure is completed, we will know r_1 , r_2 , r_3 , and r_4 . Therefore, we need to specify only *one* of R_1 , R_2 , R_3 , or R_4 to find K using [Equation 3.13](#). Knowing K , we can compute the actual link lengths using [Equation 3.12](#).

Range for α

A study of [Figure 3.11](#) will indicate the extreme values for the angle α . When the time ratio is 1, $\alpha = 0$. This case is shown in [Figure 3.13](#). When $\alpha = 0$, the centers of the limiting circles shown in [Figure 3.11](#) approach infinity and the circles become straight lines through B_1 and B_2 . Any point outside the span between B_1 and B_2 may be chosen as the fixed pivot for the crank. Note that for this case, the distance between B_1 and B_2 is equal to $2r_2$. (See [Equation 3.8](#).)

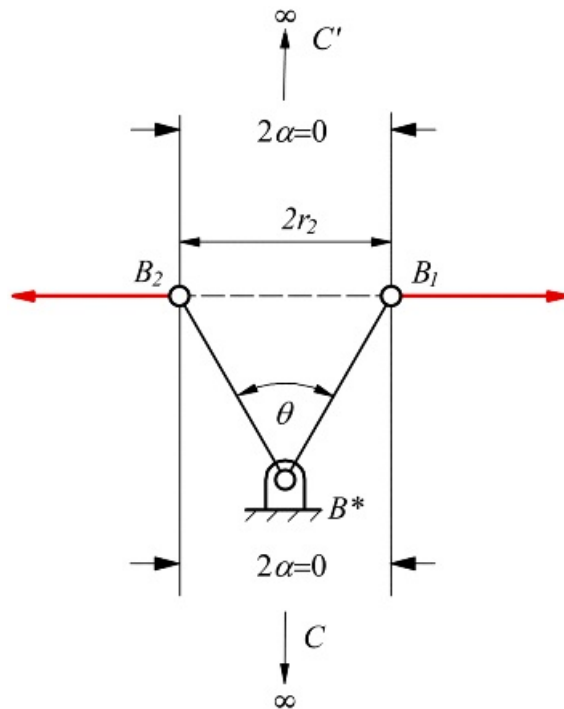


[Figure 3.13](#) Limiting case when $\alpha = 0$ and $Q = 1$.

As $+\alpha$ increases from 0, the center C of the bottom circle in [Figure 3.11](#) will move from $-\infty$ toward the pivot B^* . The highest location possible for the circle is when it is tangent to lines B^*B_1 and B^*B_2 at the two extreme locations of r_4 . This is shown in [Figure 3.14](#). In this position, there are no solutions possible, but if C is only slightly lower than the location C_m shown in [Figure 3.14](#), solutions exist for A^* for positive α . When C moves above the line between B_1 and B_2 , the angle 2α is the larger angle shown in [Figure 3.14](#). From the geometry shown, the maximum value for α will be $\pi/2 + \theta/2$.

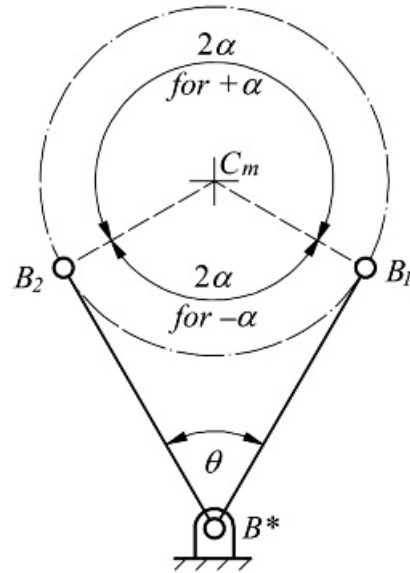


[Figure 3.14](#) Limiting values for $\pm\alpha$. The maximum value when α is positive is $\pi/2 + \theta/2$. The minimum value when α is negative is $-(\pi/2 - \theta/2)$.

As α decreases from 0 (i.e., α becomes more negative), the center C' of the top circle in [Figure 3.11](#) will move from $+\infty$ towards the pivot B^* . The lowest location possible for the circle is again when it is tangent to B^*B_1 and B^*B_2 for the two extreme locations of r_4 . Again, in this position, no solutions are possible, but if C' is moved only slightly *higher* than the location C_m shown in [Figure 3.14](#), solutions will exist for A^* . When C' moves above C_m , the angle -2α is the smaller angle at C_m as shown. From the geometry shown in [Figure 3.14](#), the minimum value for α will be $-(\pi/2 - \theta/2)$. Note that while the linkage will move when values for α are chosen near the extreme limits, the transmission angle characteristics will be poor regardless of the values chosen for the other independent variables. Therefore, regions near the extreme limits for α should always be avoided.



Example 3.1

Crank-Rocker Design (Graphical)

A crank-rocker is to be used in the transmission of an automatic washing machine to drive the agitator. The rocker link is attached to a gear sector that drives a pinion gear attached to the agitator shaft. The radius of the pitch circle (the effective radius, see [Chapter 11](#)) of the sector gear is 3 in, and the pinion radius is 1 in. The pivot for the output link is at B^* . The sector gear is to oscillate 90° . The times for the forward and return stroke of the sector are to be the same. If the base link (R_1) of the mechanism is to be 10 cm long, determine the lengths of the other links (R_2 , R_3 , and R_4).

Solution

A sketch of the mechanism is shown in [Figure 3.15](#). We must determine the four-bar linkage defined by A^* , B^* , A , and B . The sector gear is attached to the output link that rotates through an angle θ of 90° . The time ratio is 1 so

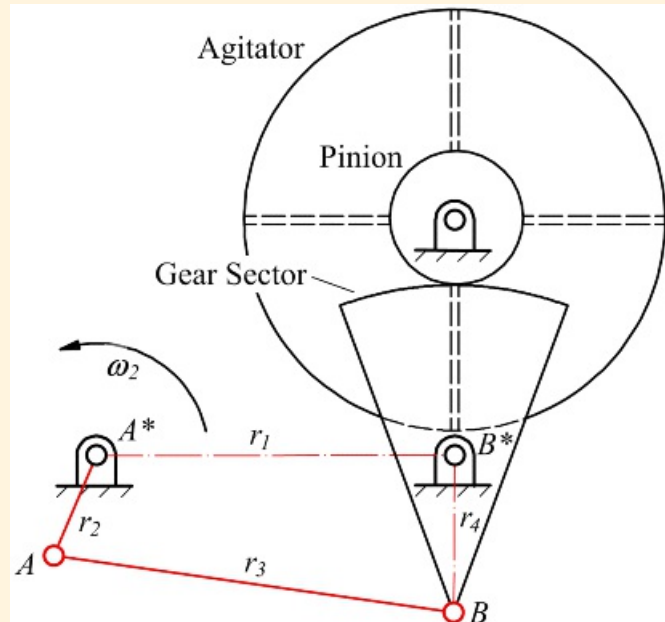


[Figure 3.15](#) Sketch of linkage for Example 3.1.

$$\alpha = 180 \left[\frac{2-1}{2+1} \right] = 180 \left[\frac{1}{2} \right] = 90^\circ$$

Therefore, the locus for A^* corresponds to that shown in [Figure 3.13](#). For the construction, let r_4 be 1 in. Then a solution for the linkage can be constructed as shown in [Figure 3.16](#).

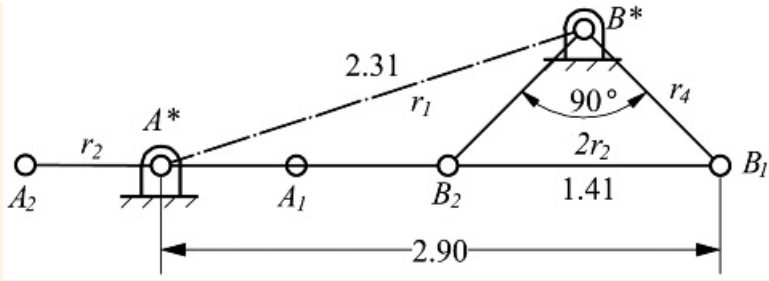


[Figure 3.16](#) A solution to Example 3.1.

The location of A^* along the line through B_1B_2 is arbitrary. Here we selected the distance A^*B_1 to be 2.9 in. Referring to [Figure 3.16](#)

$$r_4 = 1 \text{ in}$$

$$A^*B_1 = 2.9 \text{ in}$$

And

$$2r_2 = 2r_4 \sin 45^\circ = 2 \sin 45^\circ = 1.41 \Rightarrow r_2 = 0.705 \text{ in}$$

Then,

$$r_2 + r_3 = A^*B_1 = 2.90 \Rightarrow r_3 = A^*B_1 - r_2 = 2.90 - 0.705 = 2.20 \text{ in}$$

We can measure r_1 directly to be 2.31 in.

Determining the scaling factor

$$K = \frac{r_1}{r_2} = \frac{10}{2.31} = 4.329 = \frac{r_2}{r_3} = \frac{r_3}{r_4} = \frac{r_4}{r_1}$$

Unscaling the other link lengths gives

$$r_2 = 4.329 r_2 = 4.329(0.705) = 3.05 \text{ cm}$$

$$r_3 = 4.329 r_3 = 4.329(2.20) = 9.52 \text{ cm}$$

$$r_4 = 4.329 r_4 = 4.329(1) = 4.33 \text{ cm}$$

The mechanism is drawn to scale in [Figure 3.17](#).

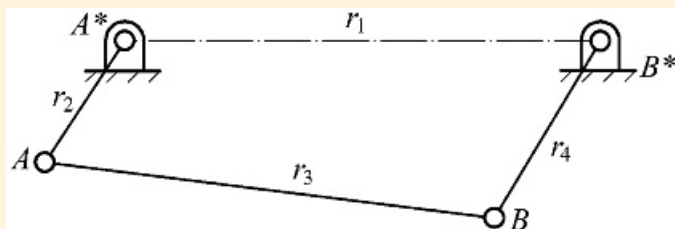


[Figure 3.17](#) Final linkage design for Example 3.1.

3.3.2 Alternative Graphical Design Procedure Based on Specification of A^*B^*

The graphical procedure developed earlier could be programmed if desired. However, it has the undesirable characteristic of a variable length for the frame. An approach presented by Hall [12] is easier to program, although the theoretical basis for the procedure is more complicated. The procedure will be presented here without the theoretical background. Readers are referred to Hall for those details. In this procedure, we will select the length of the frame link initially (instead of r_4). This approach reduces the design problem to a one-dimensional problem in which well-defined limits are known for the design variable. This makes the problem especially suitable for optimization using one-dimensional search routines [1].

Assuming θ and α are known, the following procedure, represented in [Figure 3.18](#), provides a means for determining all of the linkages satisfying the design requirements. The approach is to determine the locus for all possible positions of B_2 relative to the frame. To construct the locus, do the following:

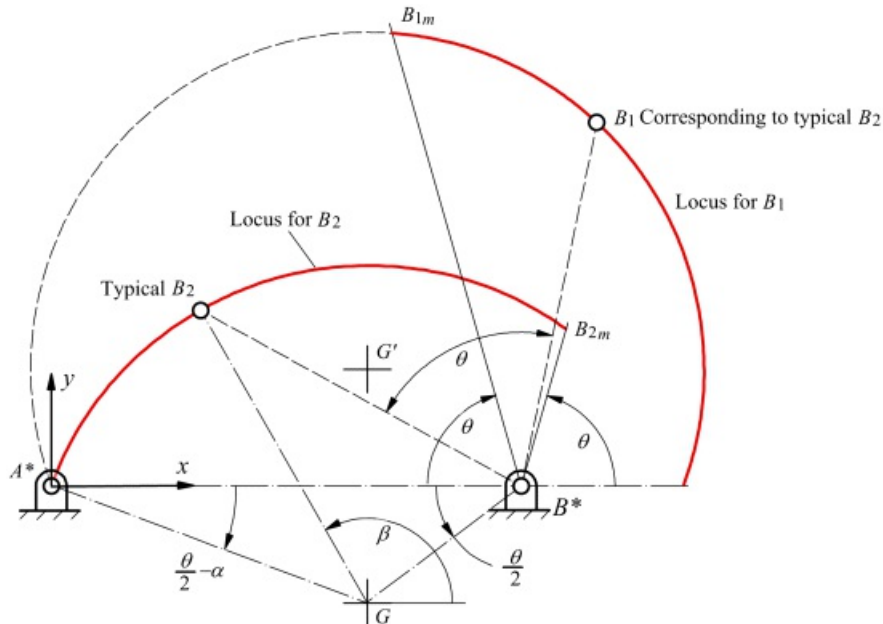


[Figure 3.18](#) Construction of the circle arc giving the loci for B_2 and B_1 .

1. Pick the base link and locate the ground pivots A^* and B^* . The distance A^*B^* determines the scale for the linkage.
2. Draw the line A^*G at an angle $\theta/2 - \alpha$ (positive clockwise) relative to A^*B^* .
3. Draw the line B^*G at an angle of $\beta/2$ (positive counterclockwise) relative to A^*B^* .
4. Draw the circle arc of radius GA^* centered at G .
5. Draw a line (B^*B_{2m}) through B^* at an angle of θ (positive counterclockwise) relative to A^*B^* .
6. The circular arc starting at A^* and ending at the intersection with either B^*B_{2m} or A^*B^* (whichever occurs first) gives the locus of the point B in the second extreme position of the rocker. The line B^*B_1 is located at an angle θ relative to the line B^*B_2 for every location of B_2 . The locus of B_1 will be a second circle arc that has the same radius as the B_2 circle arc, and the center for the B_1 circle arc will be the reflection of point G about the A^*B^* axis. The length r_4 is equal to both B^*B_2 and B^*B_1 .

After B_2 is chosen and B_1 is located, the remaining link lengths (r_2 and r_3) can then be computed by solving [Equations 3.8](#) and [3.9](#). The transmission angle limits can be measured after drawing the linkage in the extreme positions shown in [Figure 3.12](#). They may also be calculated using the cosine rule from trigonometry.



Example 3.2

Crank-Rocker Design Using Alternative Graphical Procedure

A crank-rocker mechanism is to have an oscillation angle of 80° and a time ratio of 1.3. The base length is to be 2 in. Design a linkage that will satisfy these conditions.

Solution

The time ratio is 1.3 so

$$\alpha = \left[\frac{\varnothing - 1}{\varnothing + 1} \right] 180^\circ = \left[\frac{1.3 - 1}{1.3 + 1} \right] 180^\circ = 23.47^\circ$$

We will begin the design procedure by drawing the two fixed pivots, locating point G , and drawing the arc corresponding to the locus for B_2 . The angles needed to locate G are

$$\frac{\varnothing}{2} = 40^\circ$$

and

$$\frac{\varnothing}{2} - \alpha = 40^\circ - 23.47 = 16.53^\circ$$

The construction is shown in [Figure 3.19](#).

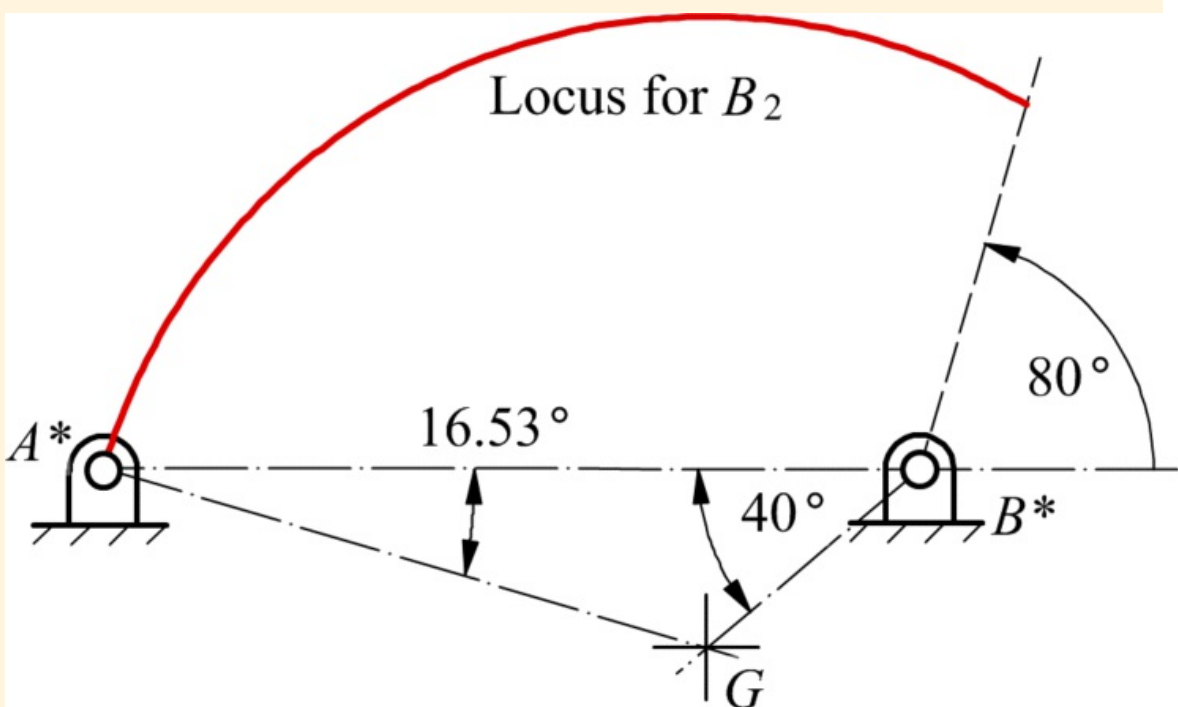


[Figure 3.19](#) Construction showing the locus of B_2 for Example 3.2.

We can select any point on the locus for B_2 to define r_4 . Once B_2 is selected, B_1 can be found. This is shown in [Figure 3.20](#). Given B_1 and B_2 , the other link lengths can be found using [Equations 3.8](#) and [3.9](#).

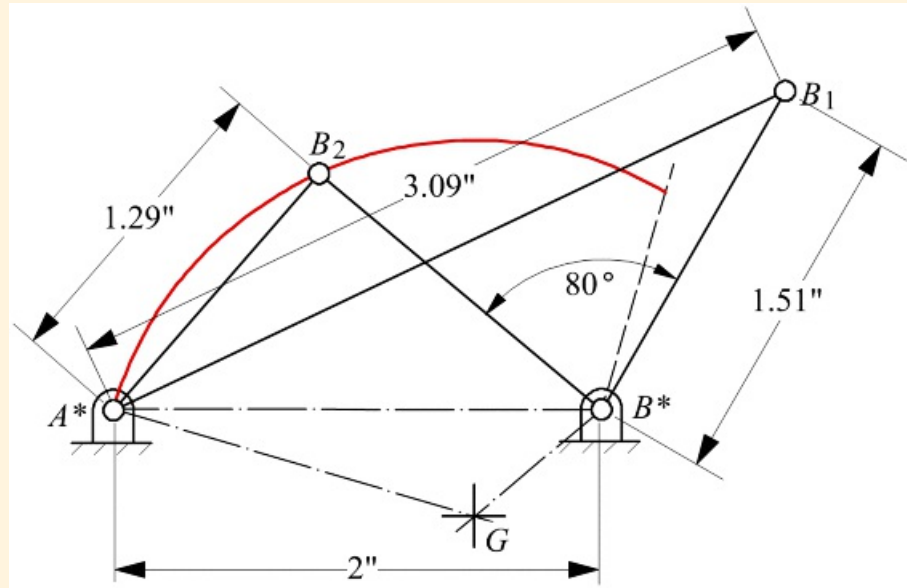


[Figure 3.20](#) Construction of B_2 and B_1 for Example 3.2.

From [Figure 3.20](#)

$$r_3 = 1.51 \text{ in}$$

$$r_4 = 2 \text{ in}$$

$$r_2 + r_3 = A^* B_1$$

$$r_3 - r_2 = A^* B_2$$

or

$$r_2 = (A^* B_1 - A^* B_2)/2 = (3.09 - 1.29)/2 = 0.90 \text{ in}$$

$$r_3 = (A^* B_1 + A^* B_2)/2 = (3.09 + 1.29)/2 = 2.19 \text{ in}$$

The mechanism is drawn to scale in [Figure 3.21](#).

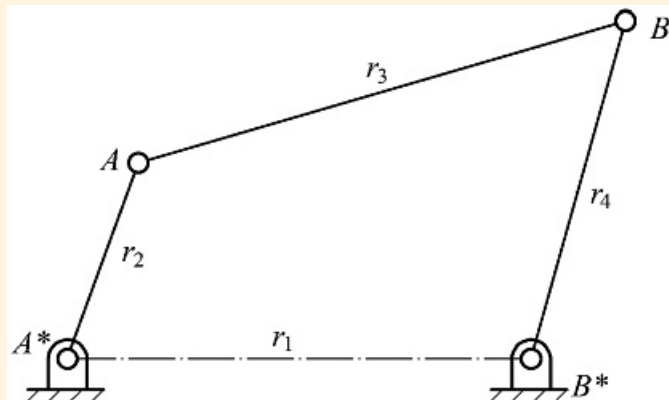


[Figure 3.21](#) Final linkage for Example 3.2.

3.3.3 Using GCP to Design Crank-Rocker and Crank-Shaper Mechanisms

Reviewing the graphical procedure represented in [Figure 3.18](#), it is apparent that once θ and a are known, the arc defining the locus for B_2 is defined. Locating a point on the arc requires the specification of only one additional parameter (β). Therefore, different designs can be developed by adjusting this single variable. Furthermore, because the locus for B_2 is the circle arc between A^* and B_{2m} , the limits for β can be established at the beginning of the design procedure.

The geometry shown in [Figure 3.18](#) is the general geometry for the design procedure. However, depending on the values of θ and a , four cases need to be considered. These are represented in [Figure 3.22\(a\)–\(d\)](#). The four cases are characterized by the following:

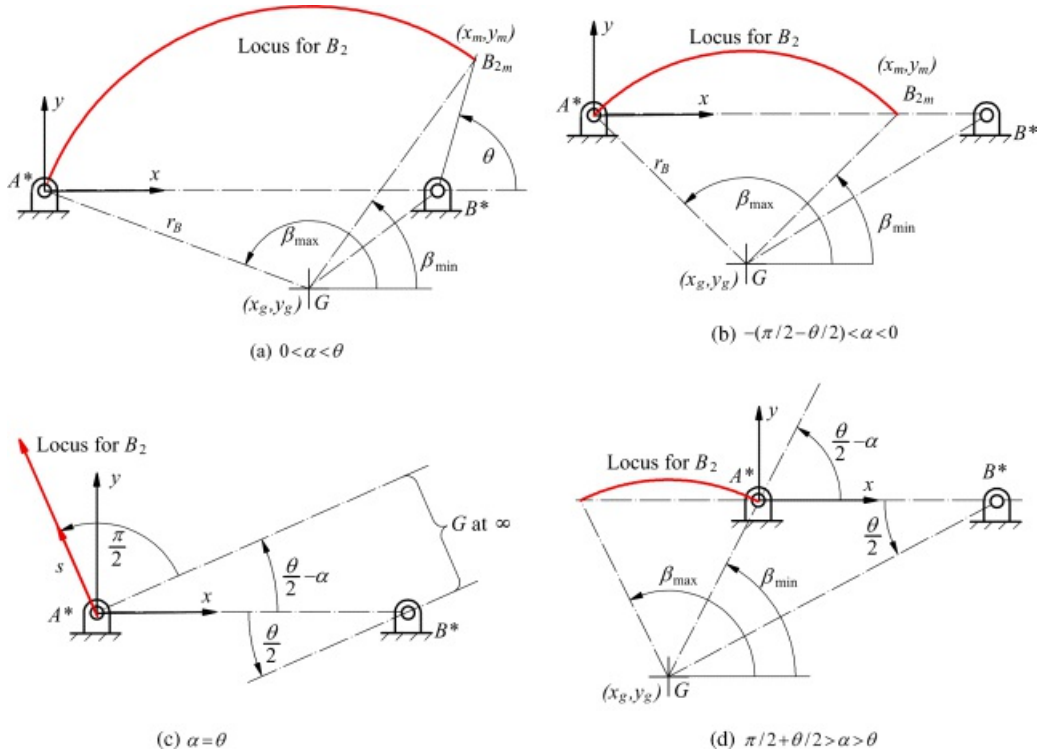


[Figure 3.22](#) Different geometries based on the relative values of θ and α .

$0 < \alpha < \theta$ This is the general case and the one represented in [Figures 3.18](#) and [3.22\(a\)](#).

$-(\pi/2 - \theta/2) < \alpha < 0$ [Figure 3.22\(b\)](#)

$\alpha = \theta$ [Figure 3.22\(c\)](#)

$\pi/2 + \theta/2 > \alpha > \theta$ [Figure 3.22\(d\)](#)

Case c in [Figure 3.22](#) is especially interesting because B_2 can be selected at any location along the locus given including at infinity. When B_2 is placed at any finite location, a crank-rocker mechanism results. When B_2 is located at infinity, the coupler becomes a slider and the mechanism becomes an inverted slider-crank mechanism commonly called a crank-shaper mechanism (see Hall [12]) because it is used in quick-return shaper machines. This mechanism is shown in [Figure 3.23](#). The time ratio for all mechanisms from this class is given by [Equation 3.6](#) using

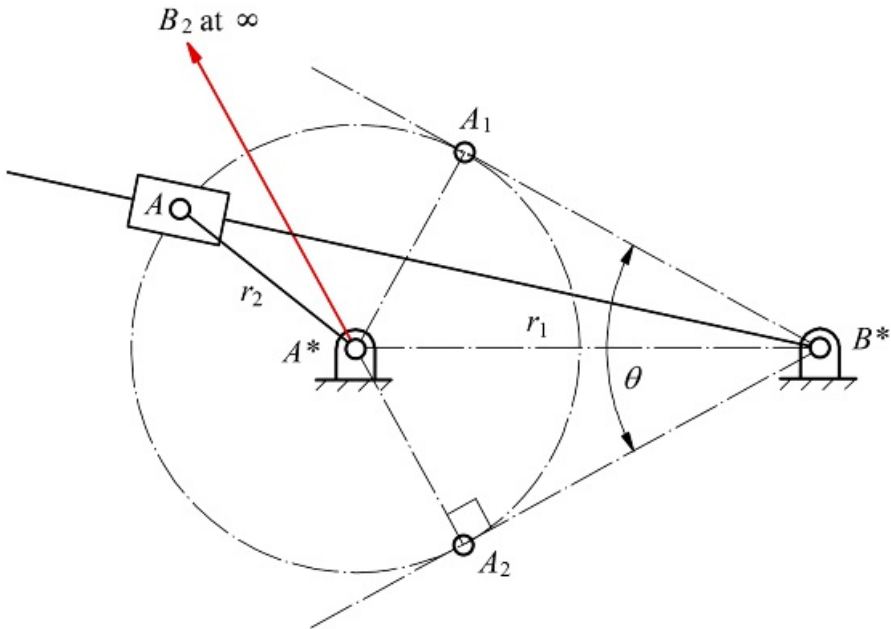


[Figure 3.23](#) Design of a crank-shaper mechanism when $\alpha = \theta$ and B_2 is selected at infinity.

$$Q = \frac{s + \theta}{s - \theta}$$

When a crank-shaper mechanism is designed, large values of θ can be used which will result in large values for Q . For example, if θ is $3\pi/4$, the time ratio is 7. Friction between the slider and slide must be addressed, but the pressure angle *per se* is not an issue.

The use of GCP is well suited to solving all of the different cases for the crank-rocker design problems. However, before demonstrating the procedure, it is important to recognize that GCP is based purely on geometric constructions, and therefore, the programming must be done in this context. In particular, it is not possible to use logical constructs such as *If-Then* statements. In addition, we need to recognize that we must depend on the constraint manager and the nonlinear equation solver available in the parametric-design program being used. The constraint manager identifies the optimum sequence in which to solve the geometric equations associated with our program based on our inputs, and we can often improve the efficiency of the process by selecting alternate variables for inputs when there is a choice of which variables are chosen as driving (independent) and which are driven (dependent). In addition, all nonlinear equation solvers can have difficulties near singular positions. In mechanisms, these positions typically occur when the transmission angles become especially poor. When problems occur, it is usually when attempting to drag a link to simulate an animation. In such cases, choosing to drive another link for the animation may give better results.

In the supplementary material with this book, we have provided GCP programs in SolidWorks for all of the cases in [Figure 3.22](#) in addition to the special case when $\alpha = 0$ and for case c in [Figure 3.22](#) when a shaper mechanism is to be designed. We have also provided a MATLAB program for all of the crank-rocker cases. It is to be noted that a single MATLAB program can be written because it allows logical constructs and equations which make it relatively simple to handle special cases within a single program. However, even though a different program must be developed in GCP for each special case, the use of GCP is much faster than programming in MATLAB, and GCP requires no formal programming experience. In addition, GCP works directly in a graphics environment so it is simple to include (i.e., draw) boundary and space constraints and observe how the resulting mechanism will interact with its environment. Furthermore, by simply changing dimensions, we can make changes directly to the mechanism and observe the effects on all of the other components.

We will illustrate the development of programs using GCP on Case a from [Figure 3.22](#) and for a crank-shaper design. Case a is the most complicated of the cases in [Figure 3.22](#), and the other cases can be easily solved in a

similar manner. The details of using GCP were covered in [Chapter 2](#) so the steps will be described here without the details.

Using GCP to Solve Case α ($0 < \alpha < \theta$)

We will develop the program by solving Example 3.2 where $\theta = 80^\circ$ and $\alpha = 23.47^\circ$. We can then change any of the dimensions used to solve other problems. We could base the GCP procedure on either of the two graphical procedures discussed above. However, an alternative procedure makes it easier to select locations for B_2 that are in an appropriate range. To begin the process, open a general blank worksheet and set the units appropriately. Also, make sure that the program will automatically snap to constraints. However, as the design progresses, if the program indicates that the model is unexpectedly overconstrained, check for unwanted constraints that have been automatically applied. Delete any unwanted constraints.

Set up the following five layers:

1. *Linkage*: Contains the final linkage that can be animated.
2. *Dimensions*: Contains the dimensions for the link lengths and other variables.
3. *Main Const*: Contains most of the geometric constructions for solving the problem.
4. *Trans Angle*: Contains the constructions for the maximum and minimum transmission angles.
5. *Pivot Dimensions*: Contains the dimensions associated with the ground pivots and any other features that should be hidden when the final program is developed.

Before beginning the construction, we need to know the angles to locate G in [Figure 3.18](#). These are

$$\frac{\theta}{2} = \frac{80^\circ}{2} = 40^\circ$$

and

$$\frac{\theta}{2} - \alpha = 40^\circ - 23.47^\circ = 16.53^\circ$$

For the crank-rocker problem, start by making the layer *Main Const* active and drawing a horizontal construction line to represent the line between the pivot points. Dimension the line to be 2-in long. Label the two ends as A^* and B^* and fix the point at B^* . Starting from B^* , draw an inclined line above the horizontal line between the pivots and constrain the inclined line to be at an angle of 80° relative to the horizontal line. This will be the boundary for acceptable values of B_2 . Starting from B^* , draw an inclined line below the centerline and constrain the angle between that line and the pivot centerline to be half (40°) of that between the B_2 boundary line and the horizontal. Establish this constraint using either a functional constraint or construct the angle to be half the angle defining the limit for the B_2 circle arc. This simple construction is shown in Appendix 2B of [Chapter 2](#). Next draw an inclined line from A^* and dimension it to be 16.53° below the pivot centerline. This locates G . Draw an arc with center at G and starting from A^* to the limit line for B_2 . The point at the left end of the arc should be merged with the point at A^* , and the point at the right end of the arc should be coincident with the limit line for B_2 . This establishes the range of valid locations for B_2 . The initial construction lines are shown in [Figure 3.24\(a\)](#).

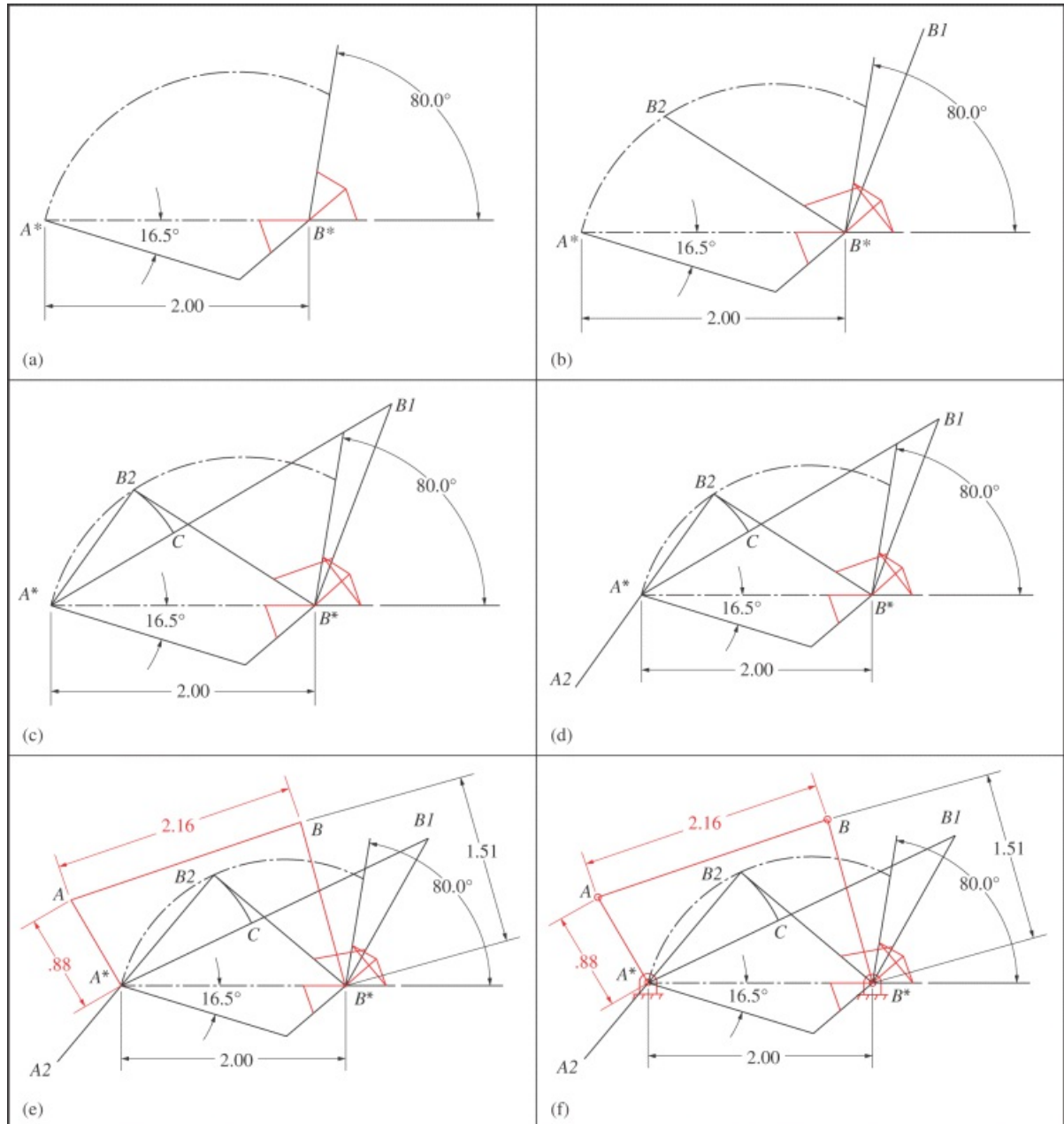


Figure 3.24 Procedure for designing a Case *a* crank-rocker mechanism: (a) Locating loci for B_2 and setting oscillation angle; (b) locating B_2 and B_1 ; (c) Locating lines for $r_3 + r_2$ and $r_3 - r_2$; (d) locating extreme position for A_2 ; (e) drawing final linkage and determining link lengths; and (f) including fixed pivots and pin bushings.

Identify a point on the circle arc as B_2 and draw a line from B_2 to B^* . This line gives the length of r_4 . Draw a second line from B^* , and constrain it to be at an angle of 80° relative to the line from B_2 to B^* ; however, do not use the dimension tool to constrain the angle. Use either a functional constraint to set this angle equal to the angle set in [Figure 3.24\(a\)](#) or use the construction in Appendix 2B of [Chapter 2](#). The reason we are using this procedure to set the angle constraint rather than using the dimension tool is so that we need to specify the rocker angle only once when we use the final figure as a graphical program. Next constrain the length of the second line to be equal to that of the first. The end of the second line identifies the location of B_1 . The construction of the two lines is shown in [Figure 3.24\(b\)](#).

Draw a line from A^* to B_1 and a second line from A^* to B_2 . The first line is equal to $r_3 + r_2$ and the second line is equal to $r_3 - r_2$. Starting from B_2 , draw an arc centered at A^* to the line from A^* to B_1 . Let the intersection of the

arc with the line A^*B_1 be point C . The distance CB_1 is equal to $2r_2$ as indicated in [Figure 3.9](#). The construction thus far is indicated in [Figure 3.24\(c\)](#).

Half of the distance CB_1 gives the length of r_2 . Starting at A^* , draw a line below the pivot centerline and constrain the line to be collinear with A^*B_2 . Constrain the length of the line to be equal to half the distance between C and B_1 . Set the constraint with either a functional constraint or use the construction shown in Appendix 2B of [Chapter 2](#). This locates A_2 in one extreme position. Next, draw a new line from A_2 to point B_2 . As indicated in [Figure 3.24\(d\)](#), this line corresponds to r_3 . With this construction, shown in [Figure 3.24\(d\)](#), the length of each link is known, and we can draw the final linkage in a general position.

Before drawing the linkage in an arbitrary position, make *Linkage* the active layer. Draw an arbitrary four-bar linkage starting from A^* and ending at B^* . Constrain the input link to be equal to the line corresponding to r_2 and the coupler link to be equal to the line corresponding to r_3 . Note that the r_3 line may be under the lines A^*B_2 and A^*A_2 . If this happens, right click the mouse and select *other*. Finally constrain the output link to be equal to the line B^*B_2 . If an attempt is made to move the input crank of the linkage, it will be apparent that the linkage is not fully constrained. We can constrain the linkage in a variety of ways such as fixing the point corresponding to either B_1 or B_2 . However, a more useable way to constrain the linkage is to dimension the length of one of the links. In Example 3.2, B_2 was fixed and r_4 was measured to be 1.51 in. Before setting the length constraint, make *Dimensions* the active layer. We can dimension the length of either A^*B_1 , A^*A , or A^*B_2 . Here we will choose to constrain the length of B^*B . The linkage is now fully constrained except for the positions of the moveable links. To finish the design, dimension the lengths of r_2 and r_3 . However, when doing this, set the dimensions to be *driven* to eliminate overconstraining the linkage. The final linkage is shown in red in [Figure 3.24\(e\)](#). The driving link lengths are shown in black and the driven link lengths are shown in red. The link lengths shown are more accurate than those computed by the manual graphical construction in Example 3.2.

While not strictly necessary, the appearance of the final linkage can be improved by representing ground pivots and joint bushings. If a file has been established with a ground-pivot drawing prepared, open it and copy the drawing information for the ground pivot including all dimensions and constraints. Otherwise, the bushings can be drawn directly. Select all of the dimensions for the two ground pivots, make the *Pivot Dims* layer active, and move the pivot dimensions to the *Pivot Dims* layer. Hide the *Pivot Dims* layer and make the *Linkage* layer active again. For the joint bushings, draw two circles and constrain the diameter of the circles to be equal to the diameter of the circles in the ground pivots. Merge the center of one circle with the linkage point at A and the center of the other circle with the linkage point at B . The result is shown in [Figure 3.24\(f\)](#).

An optional step in developing the graphical program is to compute the maximum and minimum transmission angles. Before making the drawings, set the active layer to *Trans Angle*, and hide the *Main Constraint* and *Dimensions* layers to simplify the drawing. Begin by drawing two four-bar linkages with A^* and B^* as the fixed pivots. Draw one linkage with its driver to the left of A^* and the other with its driver to the right of A^* as shown in [Figure 3.25\(a\)](#). In [Figure 3.25\(a\)](#), the crank-rocker linkage from [Figure 3.24](#) is shown in red and the two general linkages are shown in black. Next, select the three driver links and set them to be equal. Do the same thing with the couplers and output links. Finally, constrain the driver links of the black linkages to be horizontal. This constrains the two instances of the linkage to be in the configurations identified in [Figure 3.12](#). Measure the maximum and minimum transmission angles with the dimension tool. When dimensioning the transmission angles, make them *driven* dimensions so that the linkage is not overconstrained. The final result is shown in [Figure 3.25\(b\)](#).

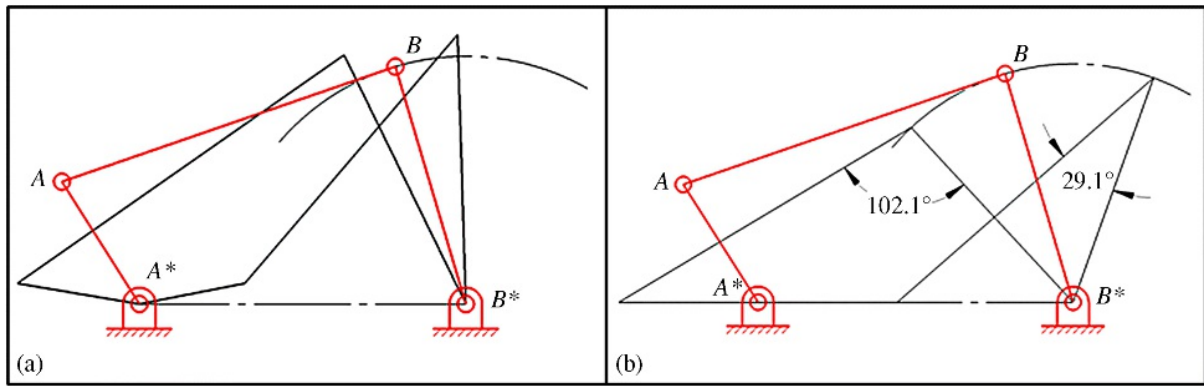


Figure 3.25 Procedure for determining the transmission angles: (a) Drawing two arbitrary four-bar linkages; (b) constraining the link lengths to be equal to the corresponding link lengths in the final linkage and constraining the two instances of the driver link to be horizontal.

The graphical program is now complete. The motion can be illustrated by using the mouse to drag the red linkage through its cycle. The other instances of the linkage cannot be moved. By selectively hiding and showing different layers, various information can be displayed. Any of the driving dimensions can be changed and the other information is automatically updated, as are all of the line drawings. The labels are not moved automatically; however, they can be easily moved by dragging with the mouse after the position is stabilized. Also, if information appears in the wrong layer, it is only necessary to select the item and move it to the correct layer.

Using GCP to Design a Crank-Shaper Mechanism

To design a crank-shaper mechanism, we can use GCP and [Figure 3.23](#) directly. We can begin the program by solving a specific problem. The dimensions in the graphical program can then be changed to solve any similar problem. The problem is to design a crank-shaper mechanism with a time ratio of 5 and a pivot length of 10 in. Recognizing that $\beta = \alpha$ and using [Equation 3.7](#)

$$\theta = \alpha = 180 \frac{Q-1}{Q+1} = 180 \frac{5-1}{5+1} = 120^\circ$$

In the following, only an overview of the process will be given. Most of the details are similar to those in the crank-rocker design, and the reader can choose layers that are appropriate for selected information as desired. However, set up at least two layers, one for the drawing and one where miscellaneous dimensions such as the ground pivot dimensions can be moved and hidden. The overall construction is shown in [Figure 3.26](#).

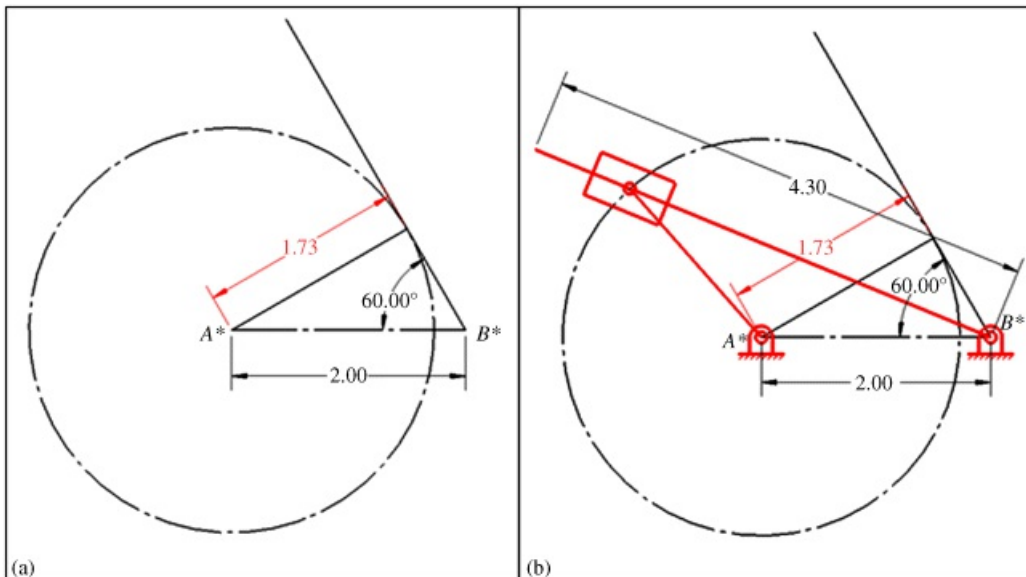


[Figure 3.26](#) Procedure for designing a crank-shaper mechanism: (a) Drawing path of the slider pin and extreme limit for the slide; (b) final linkage with fixed pivots and sliding block included.

Begin the process by drawing a horizontal line and dimensioning it to be 2 in long as shown in [Figure 3.26\(a\)](#). This corresponds to r_1 . Label one end as A^* and the other end as B^* . Draw a circle with its center at A^* . Starting from B^* , draw a line above the circle and constrain it to be tangent to the circle. Using the dimension tool, constrain the angle between the tangent line and the horizontal line to be 60° (half of 120°). Draw a line from A^* to the point of tangency between the inclined line and the circle. The length of this line is r_2 . Use the dimension tool to measure the length of r_2 . Treat the dimension as a *driven* dimension. All of the critical dimensions for the mechanism are now established.

To construct the mechanism in an intermediate position, first draw the slider line starting from B^* and intersecting the circle somewhere below the tangency point established above. The length of this line is arbitrary; however, to ensure that the slider point stays in contact with the line, use the dimension tool to constrain the line to be about 2.5 times the length of r_2 or about 4.3 in long. Draw a second line from A^* . Constrain the line to be equal to the line from A^* to the tangency point and constrain the end of the line to be coincident with the slider line. This line corresponds to the crank of the shaper mechanism.

The mechanism is now designed, and the mouse can be used to drag the crank to show the mechanism motion. However, the drawing will look more like an actual mechanism if we add a slider and ground pivots. These can either be drawn directly or the information can be copied from generic drawings made earlier. The final drawing is shown in [Figure 3.26\(b\)](#). The two critical driving dimensions that can be changed for other designs are the distance between pivots (2.00) and the angle (60.00°) between the tangent line and the horizontal. For example, if the time ratio is 3, $\theta = 90^\circ$ and $\theta/2 = 45^\circ$. The new design developed by simply changing dimensions in [Figure 3.26\(b\)](#) is shown in [Figure 3.27](#).

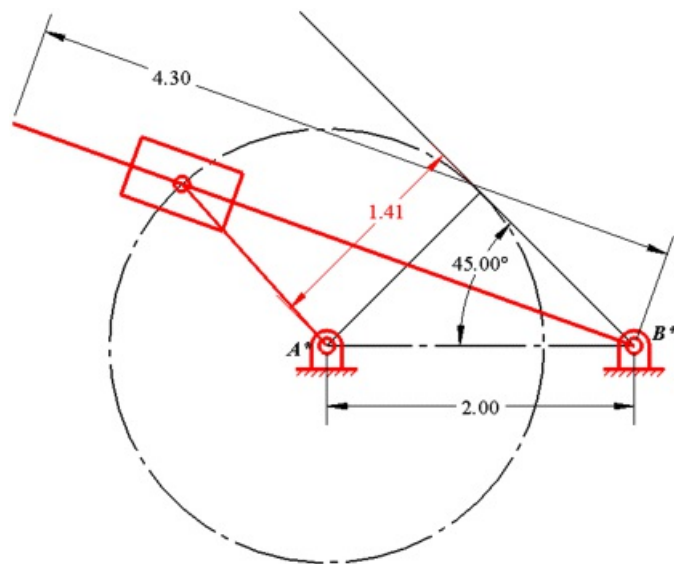


[Figure 3.27](#) Crank-slider mechanism with a time ratio of 3.



3.4 Motion Generation

3.4.1 Introduction

[Figure 3.28](#) shows the path of a moving lamina as described by the paths of three points (A, B, C) embedded in it. That is, A_1 is the first position of point A , A_2 is its second position, and A_3 is its third position, and similarly for points B and C . We will use this notation extensively in the following. As viewed from the moving lamina, there is only one point, A . As seen from the fixed reference frame, this point assumes three different positions, A_1, A_2, A_3 , as the moving lamina moves through the three positions shown.

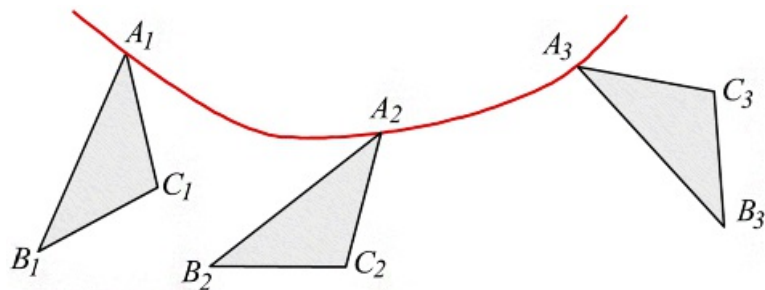


[Figure 3.28](#) Motion of a lamina along a continuous trajectory. Each point in the lamina moves along a continuous curve. The triangle ABC drawn on the lamina is shown in three different positions along the trajectory: $A_1B_1C_1$, $A_2B_2C_2$, and $A_3B_3C_3$.

Actually, only the path of one point and the changes in the orientation of a line drawn on the moving lamina are needed to describe its motion. To synthesize a four-bar linkage whose coupler will approximate the given motion, we choose a number of positions on the trajectory, such as $A_1B_1C_1$, $A_2B_2C_2$, and $A_3B_3C_3$ as design positions. This is shown in [Figure 3.28](#). The coupler will be made to pass through these positions precisely. Depending on the degree of accuracy required, a larger or smaller number of design positions can be chosen. Synthesis of the linkage is easier and the flexibility available to the designer is greater if fewer positions are used. Five is the theoretical upper limit for the number of design positions that can be used. However, from a practical standpoint, a maximum of four positions is usually specified.

Geometrically, a crank has the effect of constraining the center of its moving pivot to move on a circle. The fixed pivot is at the center of that circle and is sometimes called a center point. Consequently, the problem of synthesizing a four-bar linkage to move its coupler through the design positions is basically the problem of locating two circle points in the moving lamina. Successive positions of each point in the moving lamina all lay on the same circle. These points are sometimes called circle points. These points are taken as the locations of the moving pivots of the two cranks. The centers of the two circles on which their successive positions lie become the fixed pivots of the cranks.

3.4.2 Two Positions

Because an infinite number of circles can be drawn through any two points, any point in the moving lamina can be chosen as a moving pivot when two positions are of interest. In the example shown in [Figure 3.29](#), the two positions of the lamina are defined relative to the fixed frame by the line segments A_1B_1 and A_2B_2 that are two positions of the line segment AB drawn on the moving lamina. Because any point in the lamina can be a moving pivot or circle point, we might as well choose A and B . In each case, we then have an infinite number of points that can be chosen as the fixed pivots or center points, namely all points on the perpendicular bisector of A_1A_2 can be selected for the fixed pivot A^* corresponding to A and all points on the perpendicular bisector of B_1B_2 can be selected for the fixed pivot B^* corresponding to B .

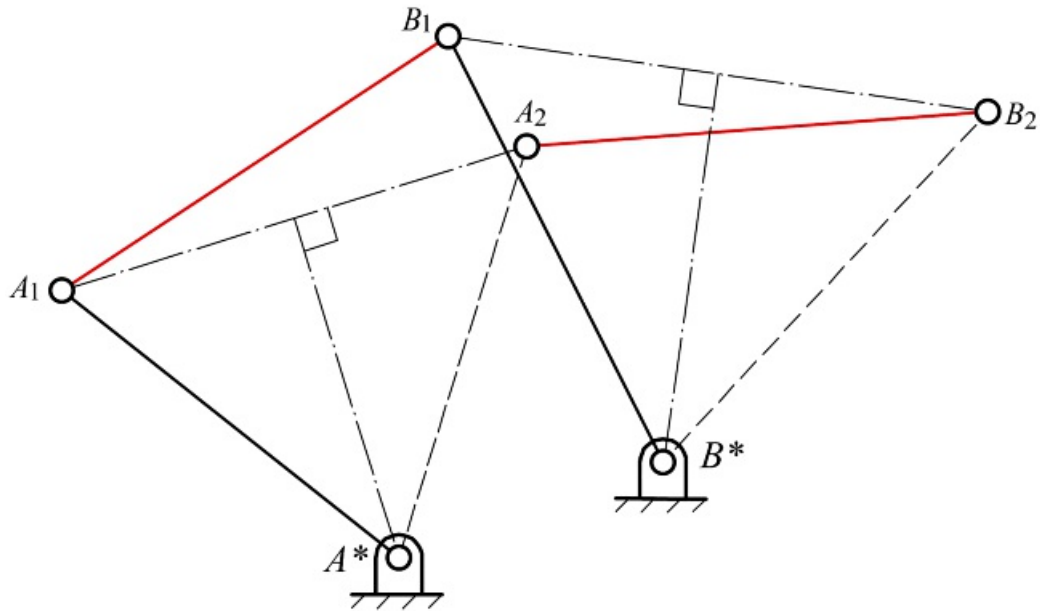


[Figure 3.29](#) Construction of a four-bar linkage that moves its coupler plane through the positions A_1B_1 and A_2B_2 .

The four-bar linkage that results from this construction is, in its first position, $A^*A_1B_1B^*$. The base link is A^*B^* . The coupler is A_1B_1 . That is, in this case, the coupler is simply the line segment used to define the positions of the moving lamina. However, this is often not where the circle points are chosen.

Any point in the moving lamina, not just A or B , can be chosen as a moving pivot. This is shown in [Figure 3.30](#), in which point C is chosen as the second moving pivot, rather than point B . We normally define the location of C in position 1 and locate it by construction in subsequent positions. To locate point C_2 , we note that ABC is a triangle drawn on the rigid, moving lamina, and it does not change shape as the lamina moves. Therefore triangle $A_2B_2C_2$ is congruent to triangle $A_1B_1C_1$. Consequently, C_2 can be located by completing triangle $A_2B_2C_2$ given A_2B_2 .

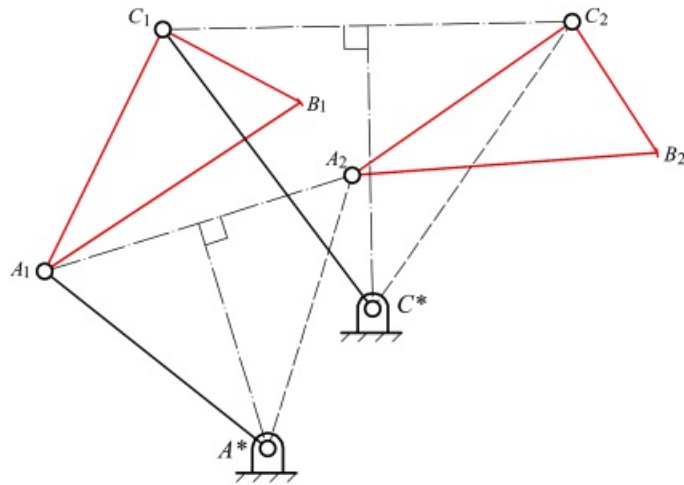


[Figure 3.30](#) Solution of the same two-position problem shown in [Figure 3.29](#) with a different point C_1 chosen as the second moving pivot.

When constructing triangle $A_2B_2C_2$ it is important to ensure that the triangle is congruent with triangle $A_1B_1C_1$ and not its mirror image. The orientation of the congruent triangle is obtained by simply translating and rotating triangle $A_1B_1C_1$ and not flipping it over. A simple check is to count off the vertices A_1, B_1, C_1 when proceeding in a counterclockwise direction around the triangle. Counting off A_2, B_2, C_2 when proceeding around $A_2B_2C_2$ in the

same direction will give the same order. If the order is $A_2C_2B_2$, the triangle is the mirror image, and the solution is incorrect.

The problem can now be solved in exactly the same manner as it was before, except that C_1 and C_2 are used instead of B_1 and B_2 . That is, the perpendicular bisector of A_1A_2 is constructed, and any point A^* is selected on that perpendicular bisector to be the fixed pivot corresponding to the moving pivot A . The perpendicular bisector of C_1C_2 is then constructed, and any point C^* on that bisector is chosen to be the fixed pivot corresponding to the moving pivot C . The resulting four-bar linkage is, in its first position, $A^*A_1C_1C^*$. In its second position it is $A^*A_2C_2C^*$.

Actually, for two positions, it is possible to locate a unique point such that the moving lamina can be attached to a single, fixed pivot at that point and will rotate through the two design positions. This is shown in [Figure 3.31](#). This point, P_{12} , is called the displacement pole for the two positions. One position can be reached from the other by means of a pure rotation about the pole.

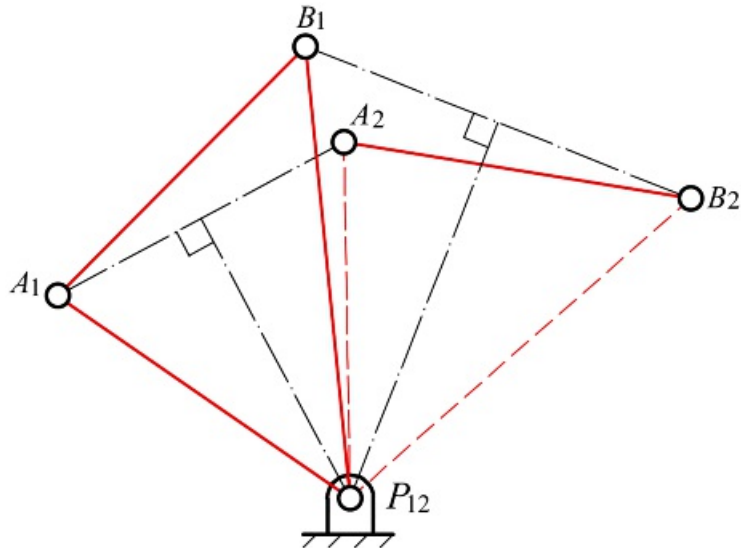


[Figure 3.31](#) Location of the displacement pole, P_{12} , of the moving lamina from position 1 to position 2. P_{12} is located at the intersection of the perpendicular bisectors of A_1A_2 and B_1B_2 . The moving lamina can be displaced from position 1 to position 2 by a pure rotation about P_{12} .

The construction for locating the pole is as shown in [Figure 3.31](#). Since P_{12} lies on the perpendicular bisector of A_1A_2 , it is equidistant from A_1 and A_2 . Similarly, it is equidistant from B_1 and B_2 . Thus position 2 can be reached from position 1 by a pure rotation about P_{12} . Note that the pole is unique for the two positions, and we can use the two positions of *any* two points on the moving body to locate the pole. For example, we could also have used points A and C or C and B .

If more than two positions are involved, as is the case in the next section, there will be a displacement pole for every two positions. For example, for three positions, there will be three poles P_{12} , P_{13} , and P_{23} . In each case, the poles will be located using the procedure shown in [Figure 3.31](#).

3.4.3 Three Positions with Selected Moving Pivots

Because a circle can be drawn through any three points, any point on the moving lamina can be a moving pivot for three positions. The corresponding fixed pivot is at the center of the circle on which the three positions of the point lie. Taking A as one moving pivot, the corresponding fixed pivot A^* is located at the center of the circle upon which A_1 , A_2 , and A_3 , the three positions of point A , lie. Notice that A_1 , A_2 , and A_3 represent the three positions of *a single point*, A , in the moving plane. They are the positions of that point *as seen from the fixed plane*. The positions of points and lines in the moving plane are, by convention, drawn on the first position of the moving plane. Thus, points A and A_1 can be regarded as being identical, as can B and B_1 .

The center of the circle, A^* , can be found at the intersection of the perpendicular bisectors of A_1A_2 and A_2A_3 . Similarly, B^* is located at the center of the circle on which B_1 , B_2 , and B_3 lie. That is, B^* is at the intersection of the perpendicular bisectors of B_1B_2 and B_2B_3 . The solution linkage is then the four-bar $A^*A_1B_1B^*$ as shown in position 1. This construction is shown in [Figure 3.32](#).

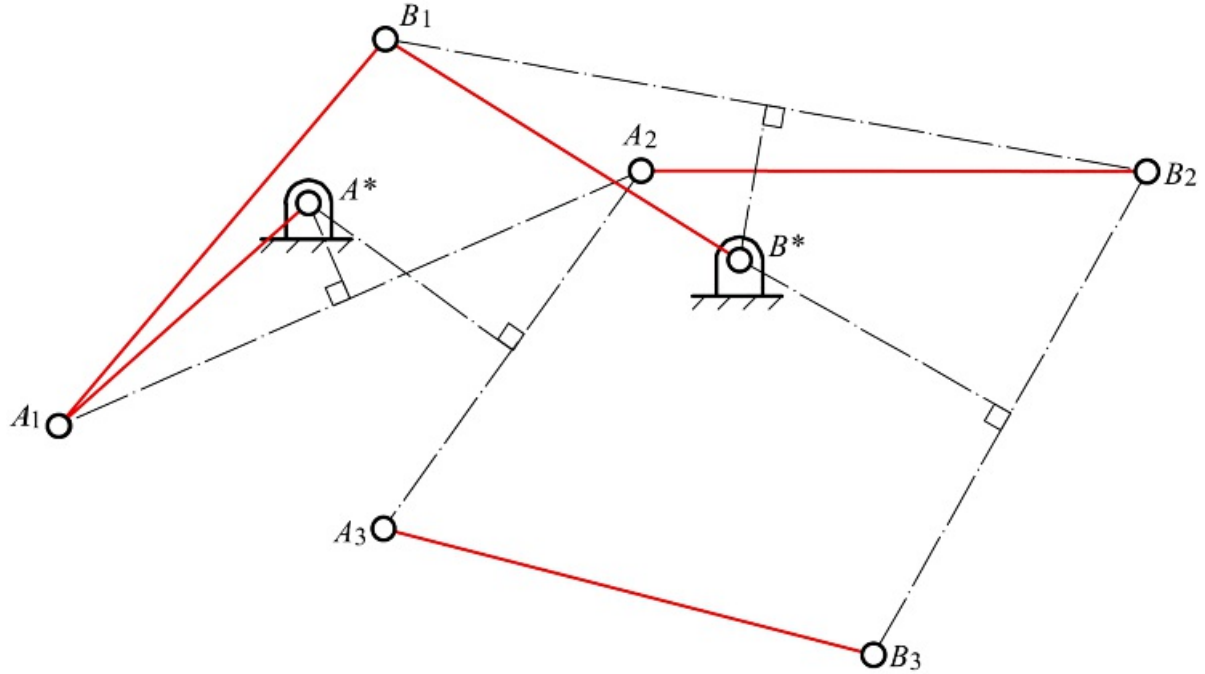


[Figure 3.32](#) Synthesis of a four-bar linkage that moves its coupler plane through three positions. The line segment AB defines the three positions of the moving plane. The points A and B are also chosen as the moving pivots of the two cranks. A^* and B^* are the fixed pivots of those cranks.

As was pointed out in the two-position case, it is not necessary for A and B to be chosen as the moving pivots. If a third point, C ($\equiv C_1$), is chosen as a moving pivot, its second and third positions may be found by constructing triangles $A_2B_2C_2$ and $A_3B_3C_3$ congruent to triangle $A_1B_1C_1$. [Figure 3.33](#) shows the synthesis of a four-bar linkage that moves its coupler through the three positions in [Figure 3.32](#). The points C and D that do not lie on the line AB are chosen as the moving pivots. Points C_2 and C_3 are located by constructing congruent triangles. Likewise, points D_2 and D_3 are located by constructing triangles $A_2B_2D_2$ and $A_3B_3D_3$ congruent to triangle $A_1B_1D_1$. Notice that, although we represent the moving lamina by means of the line segment AB , the moving lamina is a *plane*, not a line, and we are at liberty to draw on the lamina points and lines that do not lie on AB .

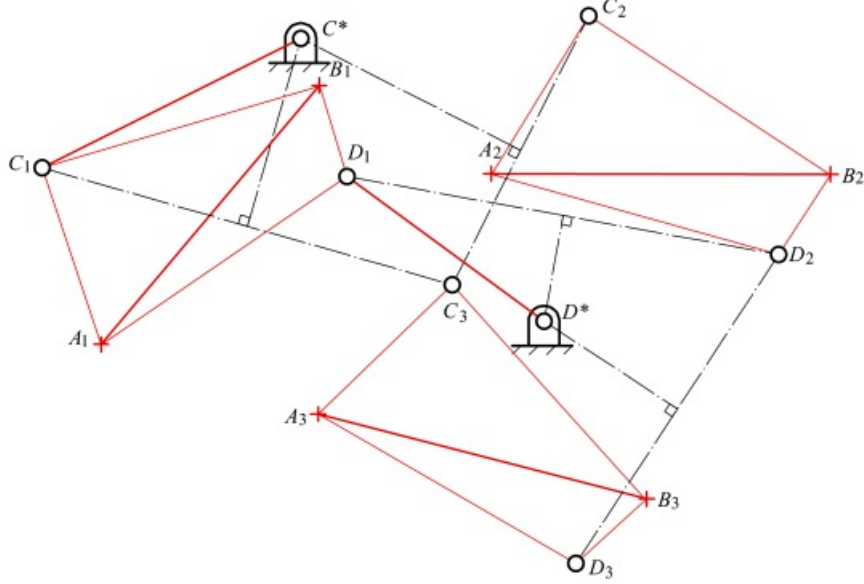


[Figure 3.33](#) The same problem as that of [Figure 3.32](#) solved with points C and D selected as moving pivots, rather than A and B . Triangles $A_2B_2D_2$ and $A_3B_3D_3$ are congruent to $A_1B_1D_1$. The solution linkage, shown in its first position, is $C^*C_1D_1D^*$.

3.4.4 Synthesis of a Crank with Chosen Fixed Pivots

The procedure given above allows us to synthesize a crank with any chosen moving pivot. If we wish to choose the fixed pivot rather than the moving pivot, the linkage must be inverted such that the coupler rather than the mechanism frame becomes the reference frame. The observer is then fixed to the coupler rather than to the frame link. When this is done, the chosen fixed pivot is observed to move through three apparent positions as seen by the observer on the coupler. The resulting construction is shown in [Figure 3.34](#).

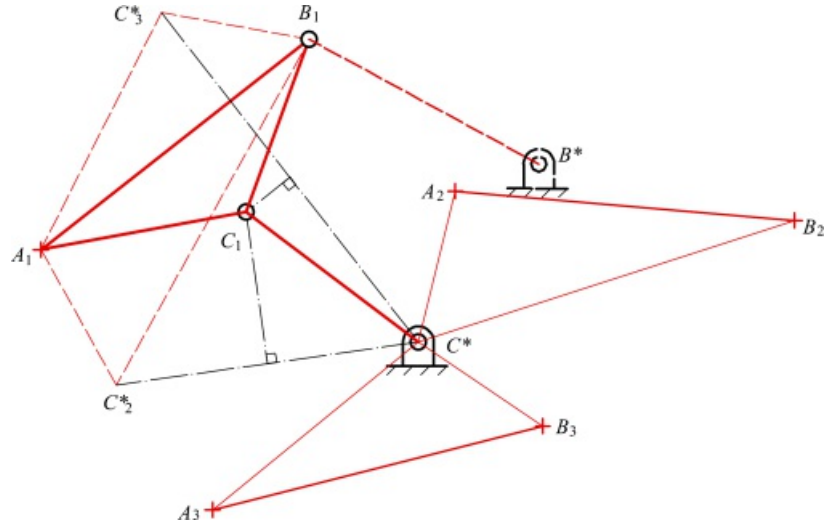


[Figure 3.34](#) Synthesis of a crank with a selected fixed pivot C^* . C^*_2 and C^*_3 are, respectively, the second and third positions of point C^* as seen from the moving lamina. C_1 is the center of the circle passing through C^* , C^*_2 , and C^*_3 . After the crank C^*C_1 has been synthesized, the linkage may be completed by designing a second crank by any method. The dashed crank is the result of choosing B_1 as the moving pivot of the second crank.

The three positions assumed by the chosen fixed pivot C^* relative to the moving lamina are plotted on the first position of that lamina. The apparent position of C^* when the lamina is in the first position is then its true position. Its apparent positions C^*_2 and C^*_3 when the lamina is in its second and third positions are obtained by

constructing triangle $A_1B_1C^*_2$ congruent to $A_2B_2C^*$ and triangle $A_1B_1C^*_3$ congruent to triangle $A_3B_3C^*$. The location, C_1 , of the moving pivot in the first position is obtained as the center of the circle on which C^* , C^*_2 , and C^*_3 lie. This defines the crank C^*C_1 in its first position. If needed, the second and third positions (C_2 , C_3) of the moving pivot can be located by constructing triangle $A_2B_2C_2$ congruent to triangle $A_1B_1C_1$ and triangle $A_3B_3C_3$ congruent to triangle $A_1B_1C_1$.

This technique gives only one crank. If both cranks are to have preselected fixed pivots, the construction must be repeated for the second crank. If the moving pivot of the second crank is to be chosen, then the earlier construction is used.

3.4.5 Design of Slider-Cranks and Elliptic-Trammels

Motion generation or rigid-body guidance is not limited to four-bar linkages with revolute joints. Any mechanism with a link that is not directly connected to the ground link can be used. Two four-link mechanisms that are commonly used are the slider-crank mechanism and the elliptic-trammel. Both involve sliders that move on slides fixed to the frame. Examples are shown in [Figure 3.35](#).

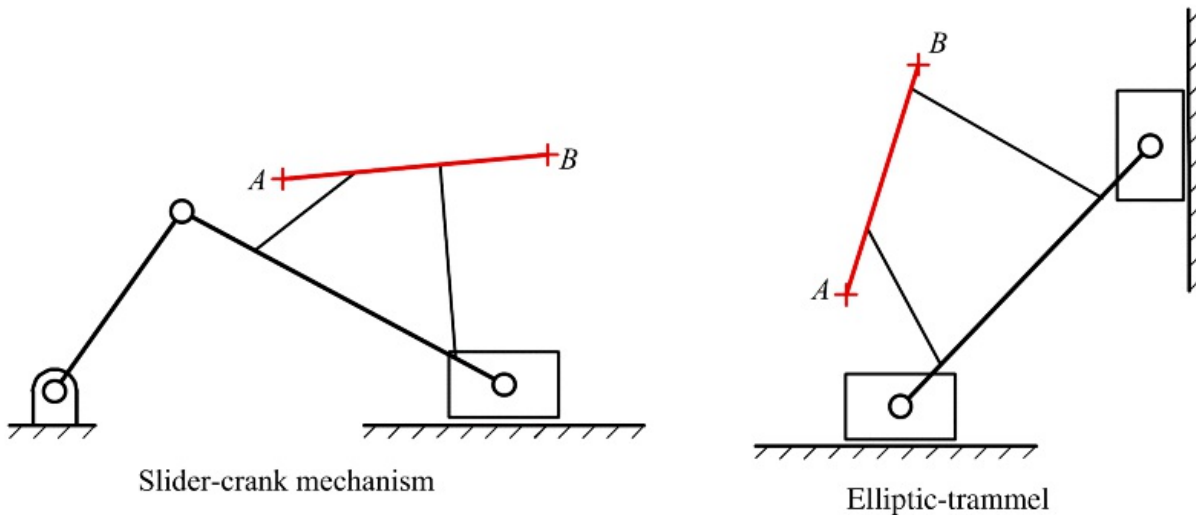


[Figure 3.35](#) Slider-crank and elliptic-trammel mechanisms used for motion generation.

To design a linkage that has a slider moving on a straight line, we must find a coupler point that has three positions on a straight line. This is shown in [Figure 3.36](#). The points having three positions on a straight line are those special circle points that move on a circle of infinite radius. Therefore, the points satisfying this condition are a very select set of points. The procedure for finding these special points is described in the following. Hall [12] gives the proof of the construction.

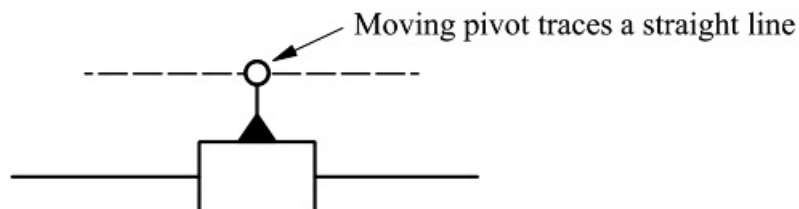


[Figure 3.36](#) Geometric effect of replacing the fixed revolute of a crank by a prismatic joint.

1. Locate the poles P_{12} , P_{13} , and P_{23} for positions 1 and 2, 1 and 3, and 2 and 3, respectively.
2. Locate the point \bar{P}_{22} called an image pole by making triangle $\bar{P}_{12}\bar{P}_{13}\bar{P}_{22}$ the mirror image of triangle $P_{12}P_{13}P_{23}$ about the line through poles P_{12} and P_{13} . The image pole \bar{P}_{22} is the point in the coupler about which the frame appears to pivot as the coupler moves from position i to position j . Poles P_{12} and P_{13} are both poles and image poles.

3. Locate the center of the circle circumscribing the image pole triangle $P_{12}P_{13}P_{23}$ by drawing the perpendicular bisectors of $P_{12}P_{13}$ and $P_{13}P_{23}$ or $P_{12}P_{23}$.
4. Draw the circle through P_{12} , P_{13} , and P_{23} . This circle is fixed to the coupler and is called the circle of sliders. Any point on this circle has all three of its positions collinear. Hence, any point on this circle can be used as the moving pivot of a slider-hinge link.
5. Select a point on the circle of sliders and construct the three positions of that point (the moving pivot). These three positions will be collinear. The slide direction is parallel to the line on which all three positions lie. Actually, in this construction, one needs to construct only two of the three positions since any two positions will determine the slider line. However, constructing all three positions give a graphical check on the accuracy of the construction. Three positions of the coupler triangle (ABC) are shown in [Figure 3.37](#). Note that the three triangles $A_1B_1C_1$, $A_2B_2C_2$, and $A_3B_3C_3$ are congruent.

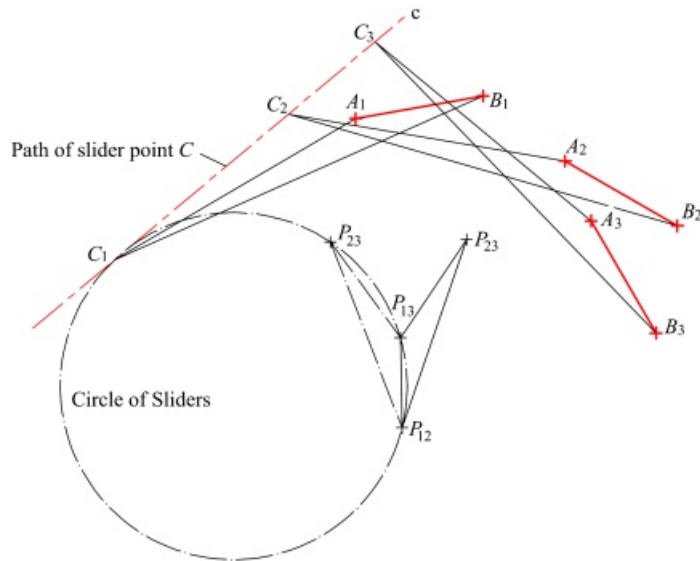


[Figure 3.37](#) Construction of slider link and slider line. The three design positions are A_1B_1 , A_2B_2 , and A_3B_3 . The slider point, C_1 , is chosen from the circle that passes through the points P_{12} , P_{13} , and P_{23} . C_2 and C_3 are the second and third positions of the slider point. c is the line in the direction of sliding.

3.4.6 Change of Branch

Note that the preceding techniques really only guarantee that the mechanism can be assembled in the design positions; *they do not guarantee that the mechanism will move correctly from one design position to the next*. It is confusing, but it is quite possible for the simple graphical procedures developed above to produce spurious solutions. These are solutions that do not physically pass through the design positions or they pass through the design positions in the wrong order. Thus, two problems can occur that may make the design unacceptable. For two and three design positions of a four-revolute linkage only the change-of-branch problem is important. The order in which the design positions are passed can be an issue if the linkage is a slider-crank or elliptic-trammel.

The first problem is due to the fact that there are two possible assembly modes for a four-bar linkage of given link lengths corresponding to a given value of the driving-crank angle. These are termed *assembly modes*, *assembly configurations*, or *solution branches*. Typical assembly modes are shown in [Figure 3.38](#). If the solution linkage for a motion generation problem is such that some of the design positions lie on one assembly configuration and others on the other assembly configuration, it will not be possible to move the linkage with a continuous motion of the input link through all design positions without physically disassembling it and reassembling it in the other assembly configuration. Fortunately, there are two simple ways to identify this problem.

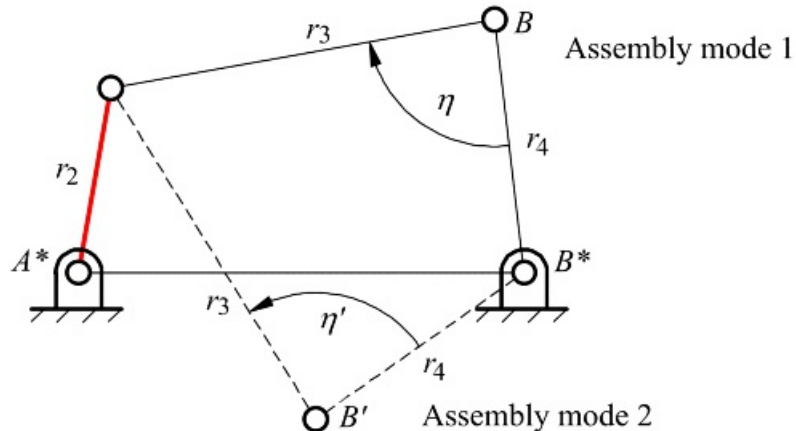


Figure 3.38 Typical assembly modes for a four-bar linkage. A crank-rocker mechanism must be disassembled and reassembled to reach one assembly mode from the other. The magnitudes of the transmission angles η and η' are the same in both assembly modes but the signs are opposite.

To detect whether a mechanism must change branches to pass through all of the positions, it is necessary only to assemble the mechanism in one position and determine whether it can be moved through the other two positions. This can be done conveniently if the linkage can be animated on a computer screen. If one position is missed, then a change of branch is indicated.

Another way to determine if a change of branch is indicated is to examine the angle, η , between the coupler and the output link. This angle corresponds to the transmission angle η discussed earlier. As shown in [Figure 3.38](#), η has a different sign in the two assembly configurations, and the key to determining the branch change is the sign of the angle η . A convenient method is to construct the cranks and coupler in all design positions and inspect the sign or direction of the angle η between the driven crank (the longer of the two cranks) and the coupler. A change in direction of this angle indicates a change of branch in a crank-rocker or drag-link type of mechanism and a drive failure in a double-rocker type of linkage. In either case, the solution linkage is not usable. An example of this condition is shown in [Figure 3.39](#). There the direction of the angle $D^*D_1C_1$ is opposite to that of angles $D^*D_2C_2$ and $D^*D_3C_3$. Hence the linkage must be disassembled to reach all of the design positions, and it is not an acceptable design. The reader may find it useful to construct a model using cardboard and thumbtacks to verify this effect.

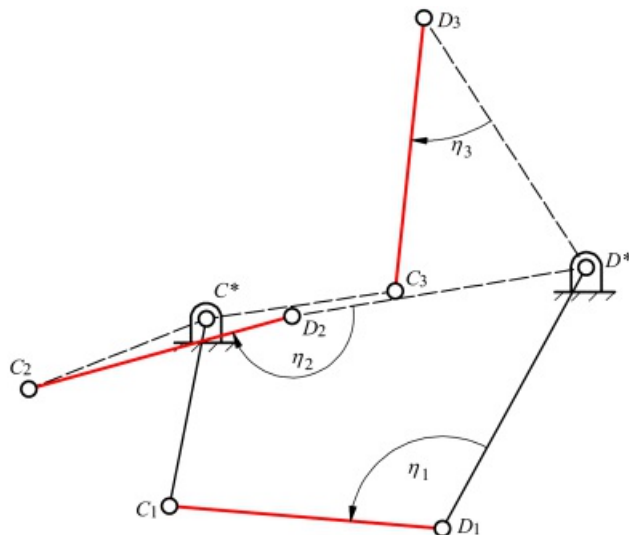


Figure 3.39 An example in which the solution linkage is not capable of moving through the design positions without being disconnected and reassembled. The solution linkage is shown in all three design positions as $C^*C_1D_1D^*$, $C^*C_2D_2D^*$, and $C^*C_3D_3D^*$, respectively. The angles between the driven (longer) crank and the coupler are examined in all three positions. These are the angles $D^*D_1C_1 = \eta_1$, $D^*D_2C_2 =$

η_2 , and $D^*D_3C_3 = \eta_3$, respectively. η_1 is counterclockwise, and η_2 and η_3 are clockwise. Thus the angle η changes sign, indicating a change of branch in the solution.



Example 3.3

Position Synthesis of Four-Bar Linkage

Design a four-bar linkage whose coupler moves through the three positions indicated by the line segment AB in [Figure 3.40](#). Point A is to be one moving pivot, and point X^* is to be one fixed pivot. The three positions are defined by the following where θ is measured in the counterclockwise direction from a horizontal line, and A in position 1 is the origin of the coordinate system.

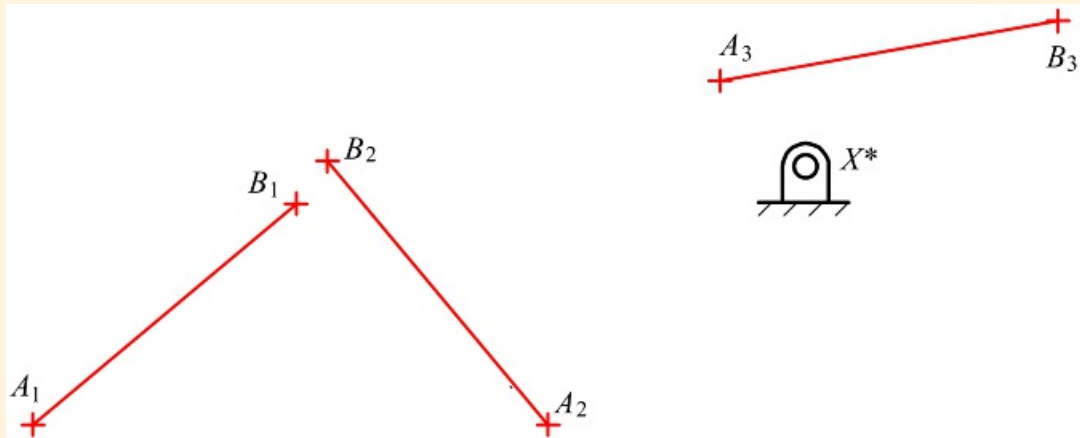


[Figure 3.40](#) The problem of Example 3.3.

Position 1:	$x_A = 0$	$y_A = 0$	$\theta_A = 40^\circ$
Position 2:	$x_A = 3$	$y_A = 0$	$\theta_A = 130^\circ$
Position 3:	$x_A = 4$	$y_A = 2$	$\theta_A = 10^\circ$

Position of center point X^* : $x = 4.5$ $y = 1.5$

The problem does not depend on units as long as consistent units are used for all linear dimensions.

Solution

1. The procedure for locating the fixed pivot A^* is shown in [Figure 3.41](#). The construction used is that of [Figure 3.32](#).

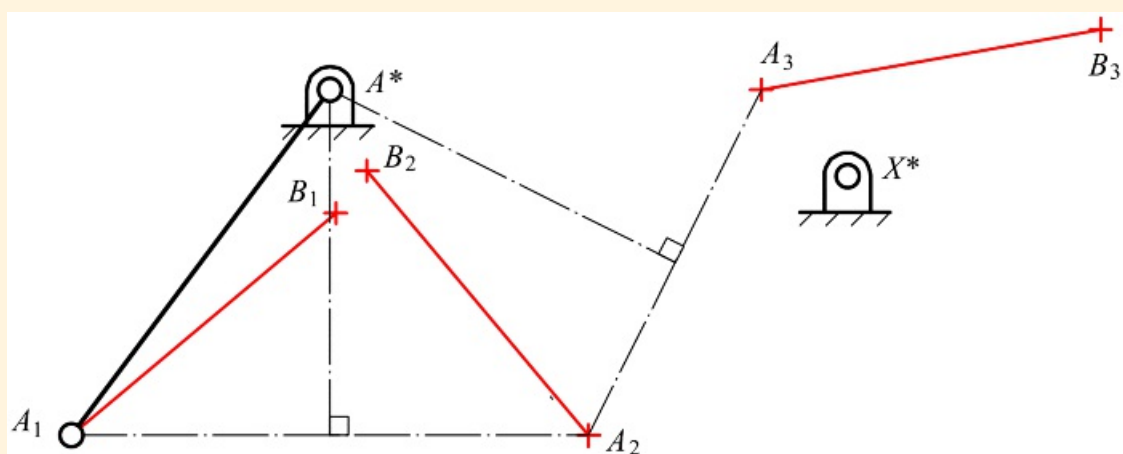


[Figure 3.41](#) Location of the fixed pivot, A^* , given the moving pivot, A .

2. The procedure for the location of moving pivot X is shown in [Figure 3.42](#). The construction used is that

of Figure 3.34.

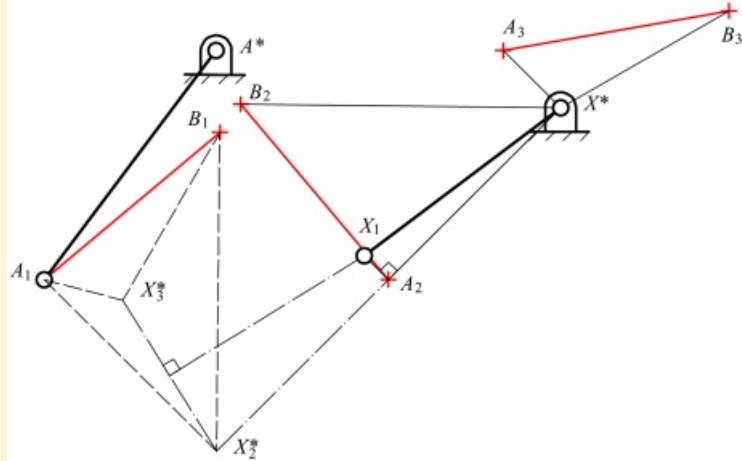


[Figure 3.42](#) Location of moving pivot, X_1 , given the location of the fixed pivot, X^* . Triangles $A_1B_1X_2^*$ and $A_2B_2X^*$ are congruent, as are triangles $A_1B_1X_3^*$ and $A_3B_3X^*$.

Triangle $A_1B_1X_2^*$ is congruent to triangle $A_2B_2X^*$, and triangle $A_1B_1X_3^*$ is congruent to triangle $A_3B_3X^*$.

X_1 is located at the center of the circle $X^*X_2^*X_3^*$.

The other two positions of point X , (X_2 and X_3) can then be located by constructing triangles $A_2B_2X_2$ and $A_3B_3X_3$ congruent to triangle $A_1B_1X_1$.

3. Check solution. The complete mechanism is shown in [Figure 3.43](#).

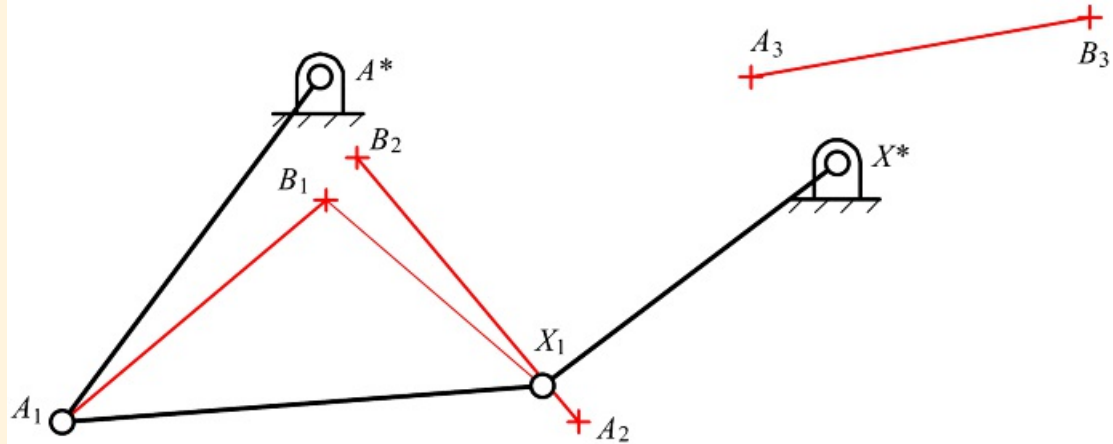


[Figure 3.43](#) Final linkage for Example 3.3.

We first check the Grashof type of the linkage by measuring the length of each link

$$X^*A^* = 3.04 = l$$

$$A_1X_1 = 2.80 = p$$

$$A^*A_1 = 2.50 = q$$

$$X^*X_1 = 2.14 = s$$

$$l + s = 5.18, p + q = 5.30$$

so

$$l + s < p + q$$

The shortest link, s , is a crank so the linkage is a crank rocker if X^*X_1 is the driver.

To check for change of branch, we need to draw the linkage in all three of the design positions, as shown in [Figure 3.44](#). All of the information necessary to do this has already been generated in previous stages of the construction procedure.

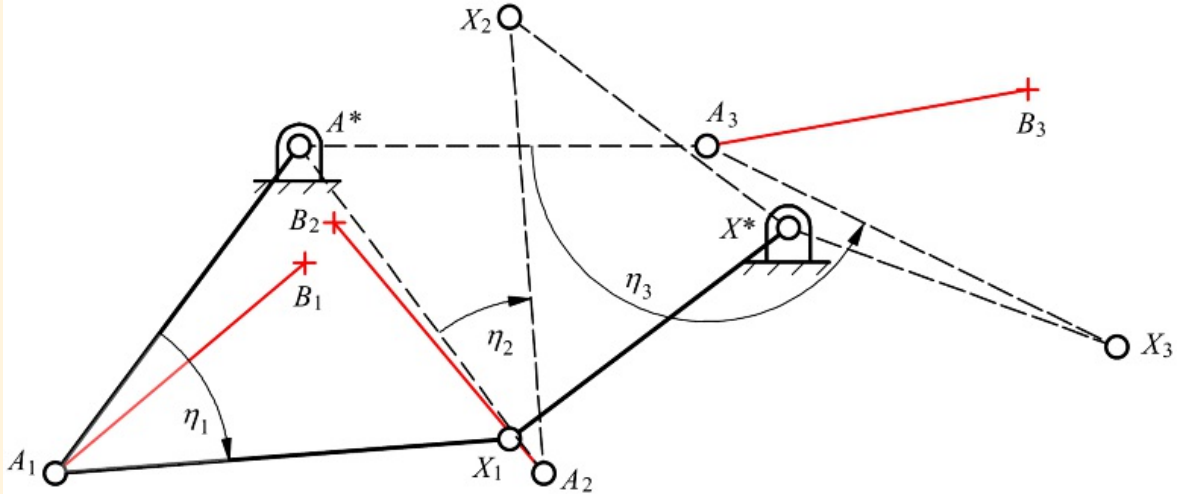


[Figure 3.44](#) Construction of solution linkage and check if it satisfies the design positions without disconnection. In this case, the linkage fails the test because η_1 and η_2 are clockwise while η_3 is counterclockwise. Hence, the linkage cannot be moved through all of the design positions by a continuous rotation of the crank X^*X without disassembling and reassembling the linkage.

Because A^*A is the longer of the two cranks, assume that it is the driven link and X^*X is the driver link. We can then check the signs of the angles $A^*A_1X_1$, $A^*A_2X_2$, and $A^*A_3X_3$ to check for branching. $\angle A^*A_1X_1$ and $\angle A^*A_2X_2$ are clockwise while $\angle A^*A_3X_3$ is counterclockwise. Hence a change of branch must occur.



Example 3.4

Position Synthesis of Slider-Crank Mechanism

Design a slider-crank mechanism to move a coupler containing the line AB through the three positions shown in [Figure 3.45](#). Use point A as a circle point. The three positions are defined by the following, where θ is measured in the counterclockwise direction from a horizontal line:

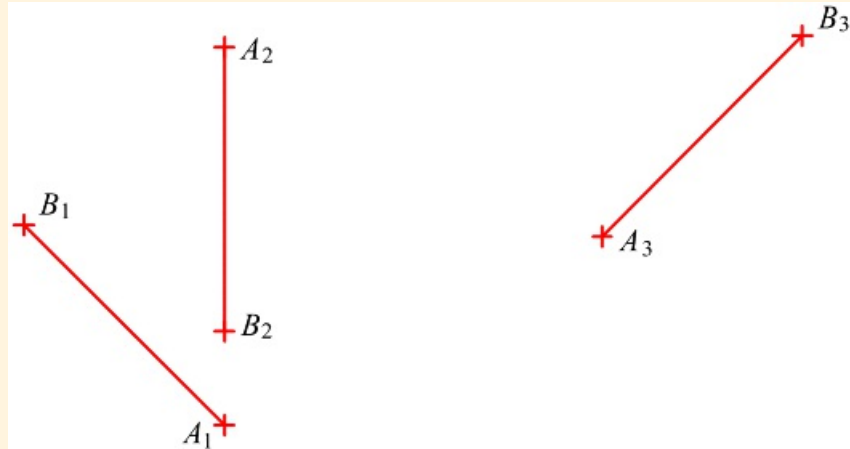


[Figure 3.45](#) Design positions for Example 3.4.

Position 1:	$x_A = 0$	$y_A = 0$	$\theta_A = 135^\circ$
Position 2:	$x_A = 0$	$y_A = 2$	$\theta_A = -90^\circ$
Position 3:	$x_A = 2$	$y_A = 1$	$\theta_A = 45^\circ$

Solution

To design a slider-crank mechanism, it is necessary to identify a circle point and the corresponding center point (or vice versa) and a slider point. We must also locate the direction for the slider line. In this problem, point A has been identified as the circle point for the crank. Therefore, to locate the center point, we need only find the center of the circle on which the three positions of A lie. The construction for finding the center point (A^*) and the crank in position 1 is shown in [Figure 3.46](#).

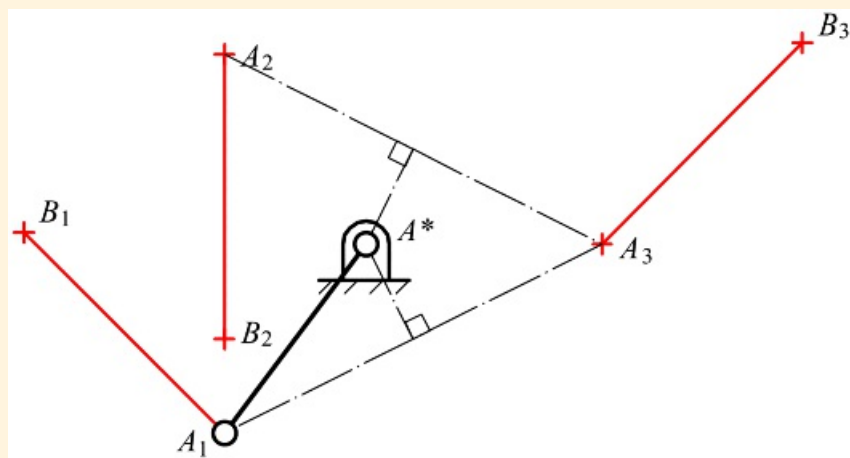


[Figure 3.46](#) Construction of crank of slider-crank mechanism for Example 3.4.

To locate the slider point, we must locate the poles, the image pole \bar{z}_2 , and the circle of sliders in position 1.

This circle is attached to the coupler. The construction of the poles is shown in [Figure 3.47](#), and the locations of the image pole and circle of sliders are shown in [Figure 3.48](#). We can select any point on the slider circle as a slider point. The point chosen is C . To complete the design, we need to locate the slider point in positions 2 and 3. The three positions, C_1 , C_2 , and C_3 , will be collinear on the slider line. The construction of the slider line is also shown in [Figure 3.48](#).

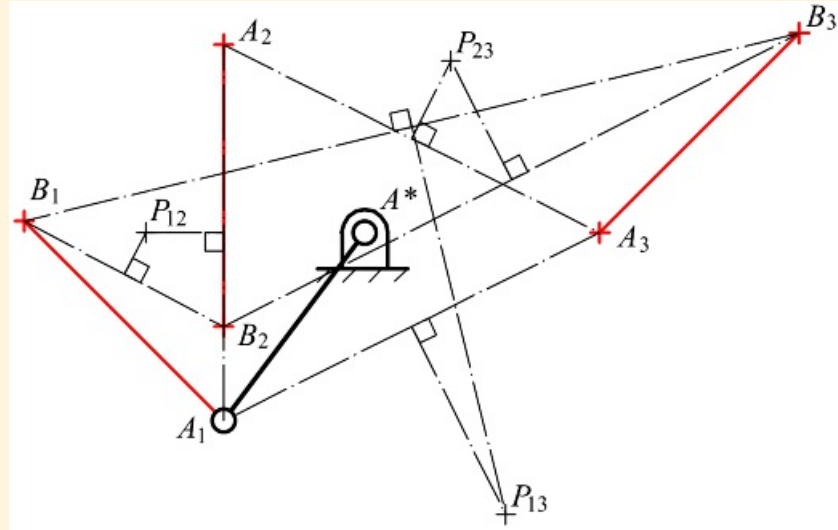


[Figure 3.47](#) Construction of the poles for Example 3.4.

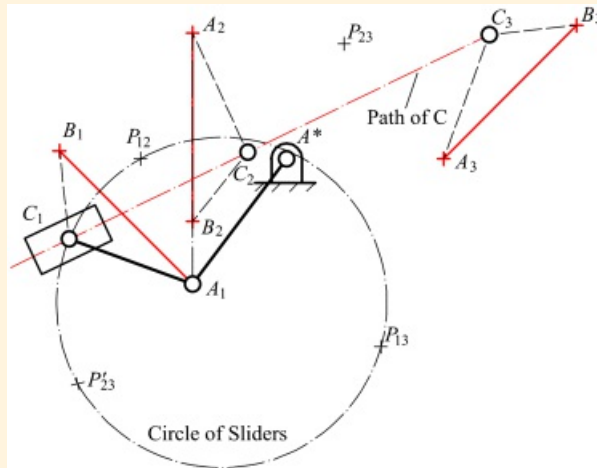


[Figure 3.48](#) Circle of sliders and final linkage for Example 3.4.

From the three positions of C shown in [Figure 3.48](#), it is clear that the linkage can be assembled in the three positions in the correct order; however, because of the orientation of the triangle $A_2B_2C_2$ for position 2, the linkage will not pass through position 2 without being disassembled and reassembled in the other configuration (i.e., there is a branch problem). In general, it is necessary to check both for order and branch problems, and this is typically most easily done by using a computer to animate the linkage. Unfortunately, it is often difficult to find an acceptable linkage without the aid of a computer program that will permit the designer to explore a large part of the design space quickly. A design program has been included as part of a MATLAB program (*KinDAP*) supplied with the supplementary material for this book. It should be recognized, however, that sometimes no valid solution exists and so no solution can be found with even the most sophisticated computer program. When this is the case, it is necessary to change the location or orientation of one or more positions. Often only the first and/or last position must be maintained precisely and there is considerable latitude in locating the intermediate position.

3.4.7 Using GCP for Rigid-Body Guidance

It is fairly simple to use GCP to implement the graphical procedure in Section 3.4.3; however, a better approach is to use constraints directly to enforce the relationships between circle points and center points. In particular, each position of a given circle point lies on (i.e., is coincident with) the circle with its center at the center point. This is the procedure originally proposed by Kinzel, Schmiedeler, and Pennock [17], and it has the advantage of being applicable directly to 2, 3, 4, and 5 positions. The details for four-position synthesis are given by Schmiedeler [23]. We will develop the procedure using three positions to be consistent with the discussions in the previous section on this topic. However, we will also illustrate the procedure in an example for four positions. This is significant, because the kinematic theory for solving a four-position problem using classical methods is well beyond the scope of this book. However, using GCP, we can design a trial solution linkage for four positions, explore issues such as branch and order problems, and animate the final linkage to study its general motion characteristics without a need to know any more kinematic theory than is needed for three position synthesis.

Using GCP for Three Positions to Design a Four-Bar Linkage

We will explain the procedure within the context of a specific problem. The dimensions used to specify the positions become the input for a graphical program that can be used to solve a wide range of problems. Three positions for a line in the coupler are shown in [Figure 3.49](#). The line is designated by CD , and the origin of the coordinate frame is located at C_1 . In the first position, C_1D_1 is horizontal. The length of the line is arbitrarily taken to be 1.25 in.

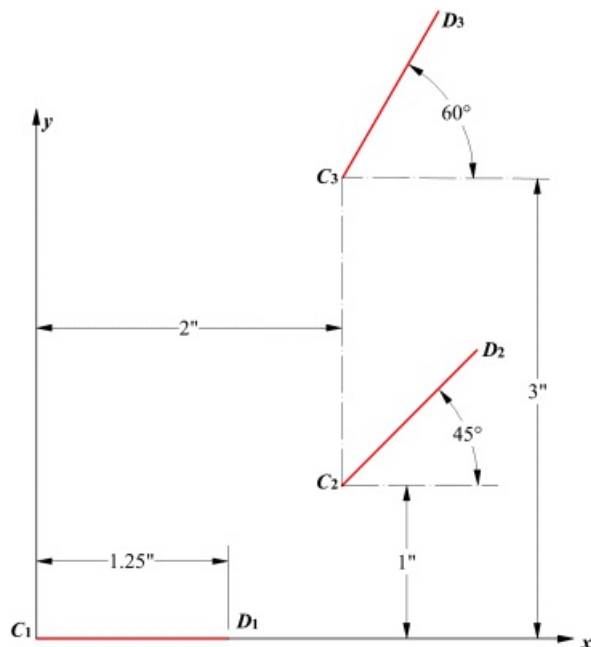


[Figure 3.49](#) Positions of coupler line for GCP discussions.

In the procedure, we will identify three positions of the circle point for each crank by means of congruent triangles in the coupler. We will constrain the three positions of each circle point to lie on the same circle. The radii of the two circles (one for each crank) will be the lengths of the cranks. The distance between the circle points in any one position is equal to the length of the coupler. We can locate the line, CD , in the coupler by two triangles, and animate a trial linkage to determine if it will travel through all of the positions in the correct order. If there is a branch or order problem, we can change either the circle point or center point for each crank until a satisfactory linkage is designed. If no satisfactory linkage can be designed by this procedure, we can consider changing the coordinates of one or more of the design positions. All of the changes are made within the context of the graphical program.

To begin the procedure, open a blank worksheet in the parametric-design program. Because of the number of constraints that will ultimately be involved, it will be difficult to discover unwanted constraints that might be applied automatically. Therefore, turn off the process that allows the program to automatically snap to constraints. Next set up the following layers:

Positions: Contains the drawings for the three specified positions

Dimensions: Contains the position dimensions (x, y coordinates of C and angles for CD in each position)

First Crank: Contains the constructions for the circle and center points for the first crank

Second Crank: Contains the constructions for the circle and center points for the second crank

Final Linkage: Contains an instance of the final linkage that can be animated

Pivot Dimensions: Contains dimensions for the ground pivots and bushings

Make the *Positions* layer active, and then draw three lines to represent the positions of the line on the coupler and constrain the line segments to be equal. Next make the *Dimensions* layer active and use the dimension tool to set the dimensions shown in [Figure 3.49](#). The positions will not change for the rest of the problem so we can label the ends of the lines as shown in [Figure 3.49](#). Also, fix the end of the line at C_1 . The result is shown in [Figure 3.50\(a\)](#). We can now hide the *Dimensions* layer to simplify the drawing window. These dimensions will not change and need not be visible for the rest of the procedure. To define a different problem, we need only show the *Dimensions* layer and change values as desired.

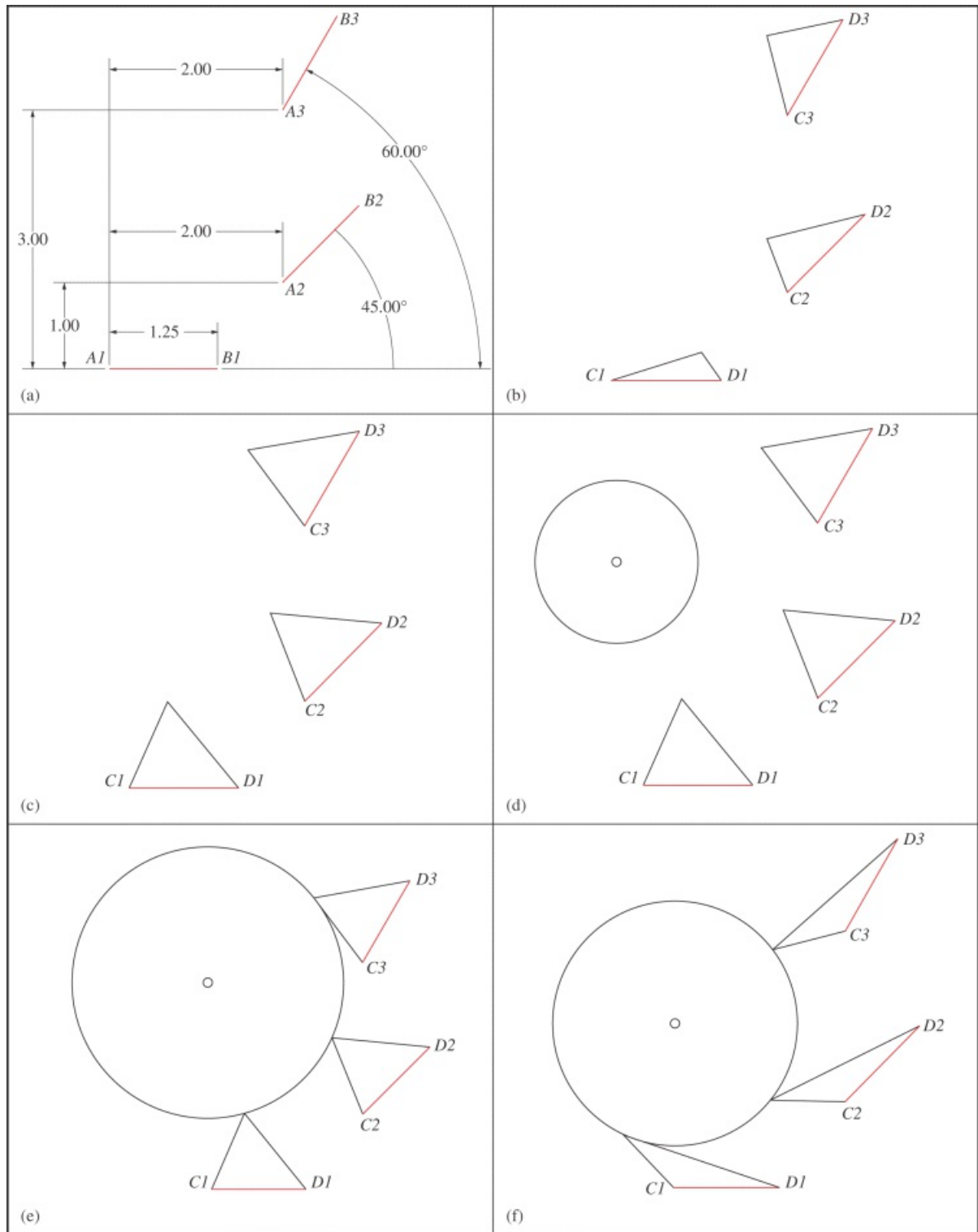


Figure 3.50 Procedure for designing a four-bar mechanism for rigid-body guidance through three positions: (a) original positions; (b) initial triangles for locating first circle points; (c) constraining the triangles to be congruent; (d) initial circle for locating crank length and center point; (e) constraining coupler point to be coincident with circle in three positions; and (f) identifying alternative circle and center points by dragging one of the triangle apexes.

Now make the *First Crank* layer active, and draw a triangle at each position of the line *CD*. This is shown in [Figure 3.50\(b\)](#). These triangles will be used to define the relative position of the circle point in each position, and they need to be congruent. Select the sides next to the three positions of *C* and make them equal. Repeat the

process for the sides next to the three positions of D . When defining the triangles, it is important to make them truly congruent. During the construction process, it is easy for one of the triangles to flip over so that it becomes the mirror image of the triangle desired. If this happens, delete the mirror image and redraw it on the correct side of the coupler line. The result is shown in [Figure 3.50\(c\)](#). Now draw a circle of arbitrary diameter in the general areas of the three triangles. Both the size and location of the circle will be determined by the constraints. To make it easy to locate the center of the circle, draw a second small circle and merge the centers of the two circles. The result is shown in [Figure 3.50\(d\)](#). Select the circle and the apex point of the triangle at C_1D_1 and constrain the point to be coincident with the circle. Repeat the process for the apex points at C_2D_2 and C_3D_3 . The center of the circle is the center point for the first crank, and the apexes of the triangles give the three positions of the circle point. The result is shown in [Figure 3.50\(e\)](#).

Note that either the center point or circle point can be changed by simply using the mouse to drag either the center of the circle or one of the apex points. Alternative center and circle points are shown in [Figure 3.50\(f\)](#). The constraint manager in the parametric-design program maintains all of the constraints as the points are moved.

To design the second crank, hide the *First Crank* layer and make the *Second Crank* layer active. Repeat the process used to design the first crank. In particular, draw three triangles using the three positions of the coupler line as the bases and use the equal constraint to make the three triangles congruent. Next draw an arbitrary circle and draw a second smaller circle to easily locate the center of the larger circle. Merge the centers of the two circles. Then select both the apex of any triangle and the larger circle and constrain the point to be coincident with the circle. Repeat the process for the other two apexes. The result is shown in [Figure 3.51\(a\)](#). Again, we can select other circle points or center points by dragging any of the apexes of the triangles or the center of the circle, respectively.

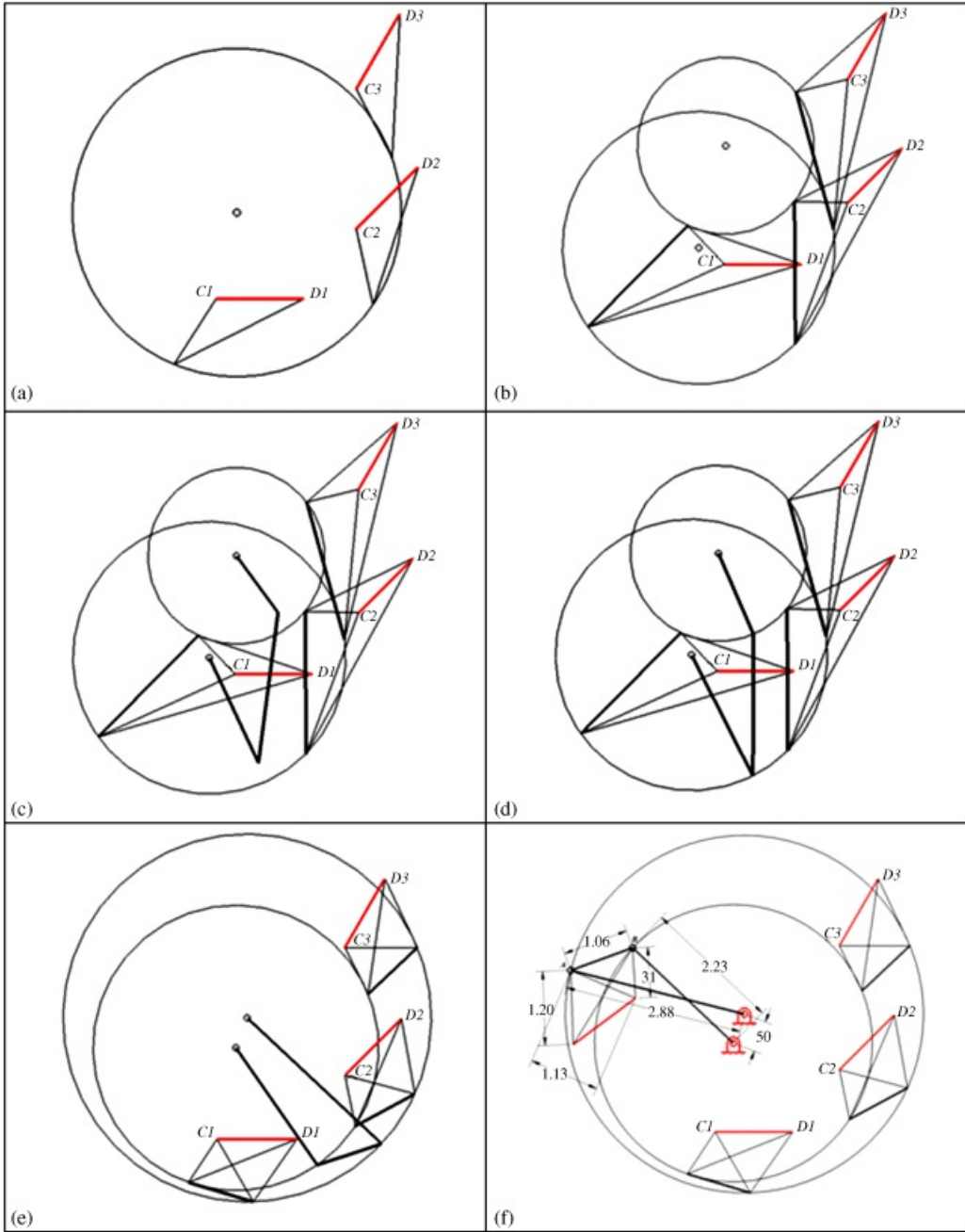


[Figure 3.51](#) Continuation of procedure for designing a four-bar mechanism for rigid-body guidance through three positions: (a) triangles to locate second circle point; (b) locating the coupler line between two circle points; (c) drawing initial linkage with pivots at two center points; (d) constraining ends of cranks to be on circle-point circles; (e) linkage after new circle points have been selected; and (f) final linkage with fixed pivots, pin bushings, dimensions, and original coupler line shown.

To define the coupler, unhide the *First Crank* layer and draw a line from the circle point for the first crank to the circle point for the second crank in each position. The coupler is shown by the heavy black lines in [Figure 3.51\(b\)](#). To check the design, make the *Final Linkage* layer active. Starting from the center point of the first crank and ending with the center point of the second crank, draw an arbitrary four-bar linkage. This is shown in [Figure 3.51\(c\)](#). To constrain the linkage, select the coupler of the linkage and one of the coupler lines shown in [Figure 3.51\(c\)](#) and constrain them to be equal. Next select the end point of the first crank and the circle for the first crank and constrain the point to be coincident with the circle.

Finally, select the end point of the second crank and the circle for the second crank and constrain the point to be

coincident with the circle. The four-bar linkage should then appear in a general position as shown in [Figure 3.51\(d\)](#). We can animate the linkage by simply dragging one of the cranks with the mouse. However, when we attempt to do this, we will find that the drawing is under constrained, and the circle and center points will tend to move. To constrain the drawing so that we can animate the linkage, select both center points and fix them. We can then check to ensure that the coupler passes through the three positions without the need for disassembly. When we check the linkage in [Figure 3.51\(d\)](#), we will find that disassembly is required for it to pass through all three positions. Therefore, we must change the design. To do this, unfix the two center points and drag either the center points or circle points until a satisfactory solution is achieved. When doing this, some of the triangles can flip over. This will result in a design that will not go through all of the positions even if the linkage is disassembled. Therefore, if a triangle does flip over, it is necessary to move the center points or circle points to those regions where all of the triangles remain congruent. In practice, this is easy to do.

Finding an acceptable linkage can be challenging in many cases. One technique that sometimes works is to first place the linkage near the position that is missed during the animation. Then move the center points around until the coupler line associated with that position appears to line up with the coupler line on the linkage. An acceptable linkage for the positions chosen is shown in [Figure 3.51\(e\)](#). Note that we do not have to actually draw line CD to check the linkage. If the coupler line between the two circle points passes through the positions properly, the line CD will also move properly from position to position.

The appearance of the final linkage can be improved by adding fixed pivots and bushings at the joints. We can also add the coupler line CD . To add the fixed pivots and bushings, use the procedure outlined in previous examples.

To show the line CD on the coupler, create two triangles with the coupler line as the base as shown in [Figure 3.51\(f\)](#). The apex of one triangle will be C and the apex of the other triangle will be D . In [Figure 3.51\(f\)](#), the circle points are labeled as A and B , and the corresponding center points are labeled as A^* and B^* . This is done to illustrate the procedure for finding the coupler line CD only. The points A, B, C, D , will not move with the mechanism when it is animated. Using the equal constraint, the triangle ABC is made congruent to the corresponding triangles in the different positions of the coupler. Similarly, triangle ABD is also made congruent to the corresponding triangles in the different positions of the coupler. The mechanism can now be animated to show the motion of all lines on the coupler plate as it moves through the three positions.

[Using GCP for Three Positions to Design a Slider-Crank Mechanism](#)

Designing a slider-crank mechanism is the same as designing a four-bar linkage except that we use a straight line instead of a circle for the second “crank.” We will illustrate the procedure again using the positions indicated in [Figure 3.49](#). The design of the crank is exactly the same as the design of the first crank for the four-bar linkage so the steps described previously and summarized in [Figure 3.50](#) apply directly. A slider will be used instead of the second crank.

To design the slider, hide the *First Crank* layer and create a layer entitled *Slider* and make it active. Draw three triangles using the three positions of the coupler line as the bases and use the equal constraint to make the three triangles congruent. These triangles will be used to define the slider point. Next draw an arbitrary line somewhere near the triangles. This is shown in [Figure 3.52\(a\)](#). Select the apex of one of the triangles and the line and constrain the apex to be coincident with the line. Repeat the process for the other two apexes. The drawing will adjust so that all of the apexes lie on the same straight line. The line can be moved to change the relative locations and order of the slider points. Adjust the orientation of the line so that the slider points appear in the proper order (1, 2, 3). An acceptable location is shown in [Figure 3.52\(b\)](#). As the slider line is moved, note that the individual positions of the slider points appear to move on invisible circles. These invisible circles are the different positions of the circle of sliders that is attached to the coupler, as was described in Section 3.4.5.

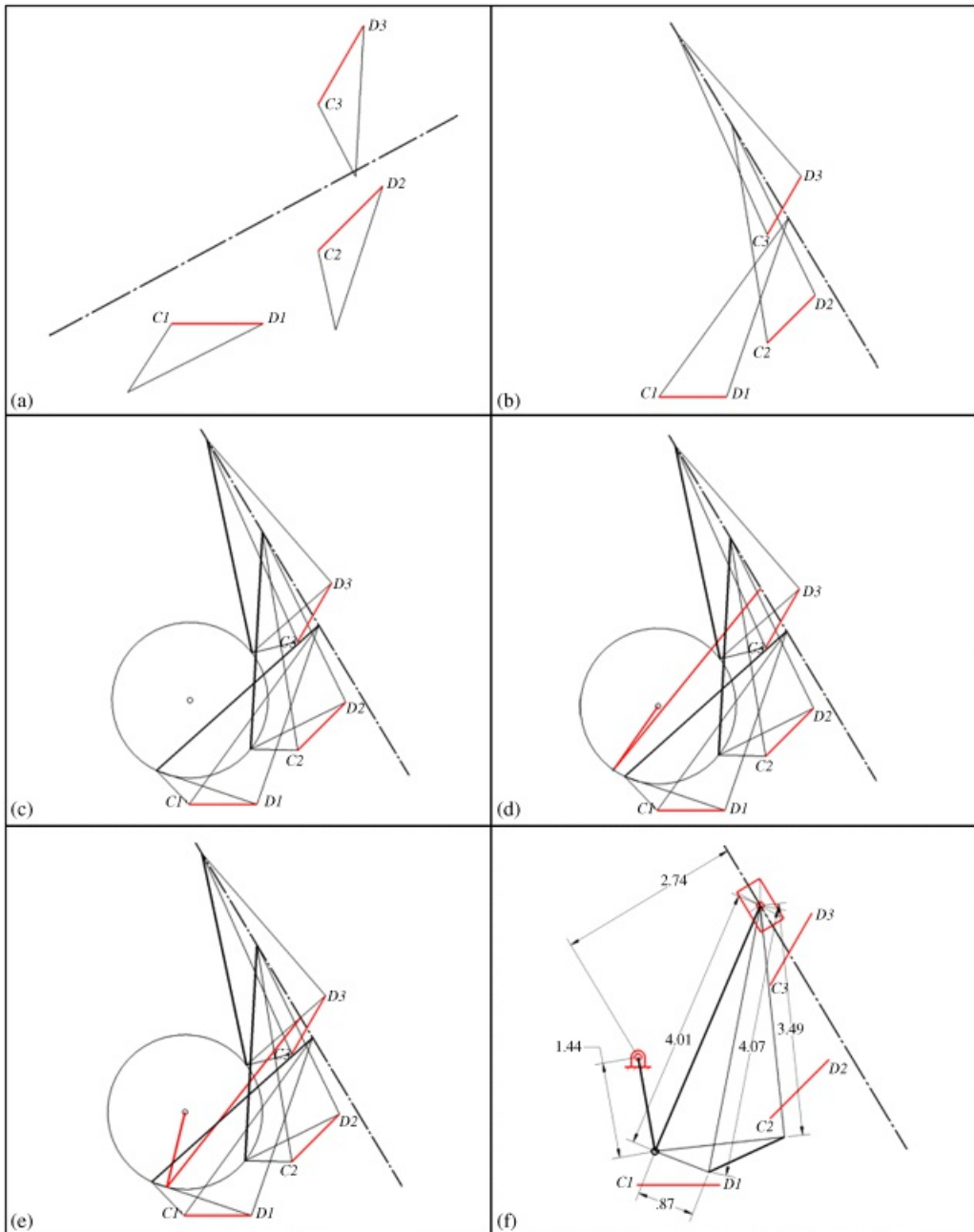


[Figure 3.52](#) Design of a slider-crank mechanism for rigid-body guidance through three positions. This figure is a continuation of [Figure 3.50](#): (a) triangles to locate slider point; (b) constraining the slider-point positions to lie on a straight line; (c) drawing the coupler in three positions; (d) drawing a general slider-crank linkage and constraining the end of the crank to be on the circle point circle and the slider point to be on the slider line; (e) constraining the coupler of the linkage to be equal to the coupler lines in the various positions; and (f) final linkage with fixed pivot and joint bushings represented.

Make the *First Crank* layer visible, and draw a line from the slider point to the circle point for each position. These lines represent the coupler of the slider-crank mechanism in the three positions. The coupler lines are shown in [Figure 3.52\(c\)](#).

Starting from the center of the circle, draw two lines to represent the slider-crank mechanism. Select the end of the crank and the crank circle and constrain the point to be coincident with the circle. Select the end of the coupler line corresponding to the slider and the slider line and constrain the point to be coincident with the line. The result is shown in red in [Figure 3.52\(d\)](#). Before trying to animate the linkage, select the coupler of the red linkage and the coupler line in one of the three positions and constrain them to be equal. The result is shown in [Figure](#)

[3.52\(e\)](#). Before animating the linkage to check for a branching issue, fix the center point and one end of the slider line. Then animate the mechanism by using the mouse to drag either the slider point or the circle point. The coupler of the mechanism in [Figure 3.52\(e\)](#) passes through all of the positions in the correct order without disassembly.

To improve the appearance of the slider-crank linkage, we can add a ground pivot at the center point and bushings at the two ends of the coupler. We can also add a block to represent the slider. And finally, we can construct two triangles using the coupler as the base to locate the two ends of the original slider line CD represented in [Figure 3.49](#). After the two triangles are constrained to be congruent with the corresponding triangles for each of the original three positions of the coupler, we can draw a line representing the coupler line CD . This is shown in [Figure 3.52\(f\)](#). The linkage can now be animated to illustrate that it does satisfy the design requirements.

Using GCP to Design a Four-Bar Linkage for Four Positions

While the kinematic theory for four-position synthesis is beyond the scope of this book, the use of GCP for designing four-bar linkages for four positions is a simple extension of that for three positions. The main difference between synthesis for three and four positions is that with three positions, any point in the coupler plane can be chosen as a circle point because three positions of a point define a unique circle. With four positions, there is a unique set of points in the coupler plane that will have four positions on a circle. These points lie on a cubic curve drawn in the coupler. However, there is still an infinite number of points on this curve that can be chosen as circle points. More importantly, GCP automatically identifies points on the curve, so the location and shape of the curve is transparent to the user. The only issue the user will notice is that as the mouse is used to drag the circle points in the coupler, the points will be constrained to move along a path rather than freely moving throughout the plane as is the case for three positions.

More so than was the case for three positions, there may not be any acceptable solution to the problem when four arbitrary positions are chosen. While GCP can identify linkages that can be assembled in all of the positions, branch and order problems may make it impossible for those linkages to move continuously from position to position. The solution space can be explored by dragging the circle points and center points. It is often the case that no acceptable solution exists. In that case, it may be necessary to adjust the original positions and re-explore the solution space. This is easily done using GCP because all that is required to change the original positions is to change the dimensions used to define them.

To illustrate the use of GCP for four positions, assume that we wish to design a four-bar linkage to move a line on the coupler through the positions identified in [Figure 3.53](#). The length of the line is 2 in. Because the design process is so similar to that for three positions, we will only outline the procedure here. The same layer structure will be used as for three positions, and the layers will be made active and hidden in the same manner. To begin the design process, open a blank worksheet and draw the four positions. Add the dimensions and fix the point at C_1 . The positions with labels should be associated with the *Positions* layer and the dimensions with the *Dimensions* layer. The positions are shown in [Figure 3.54\(a\)](#).

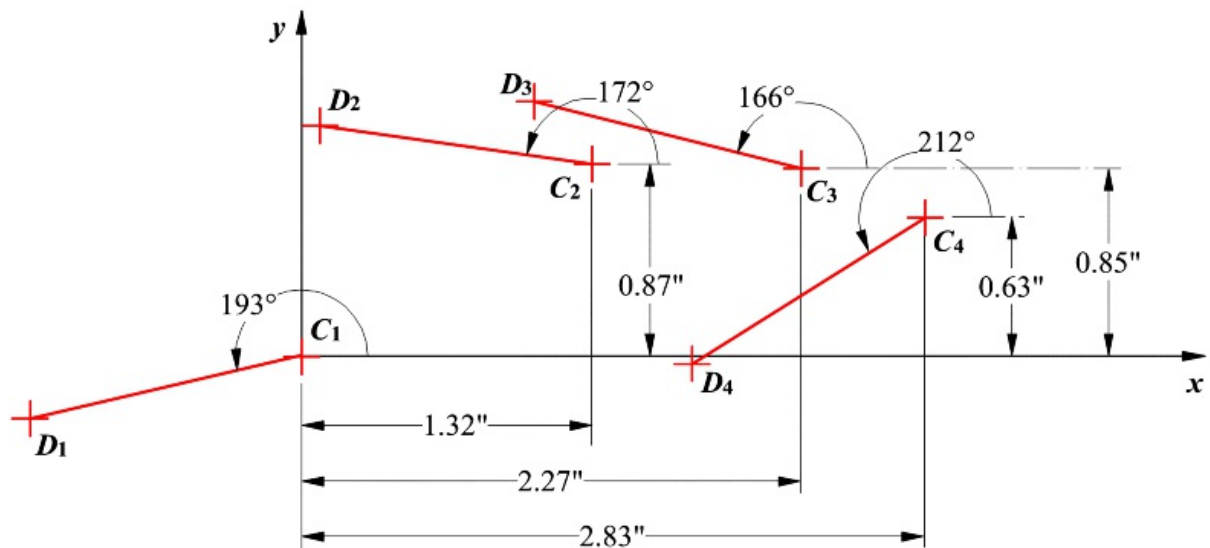


Figure 3.53 Position information for four-position synthesis example.

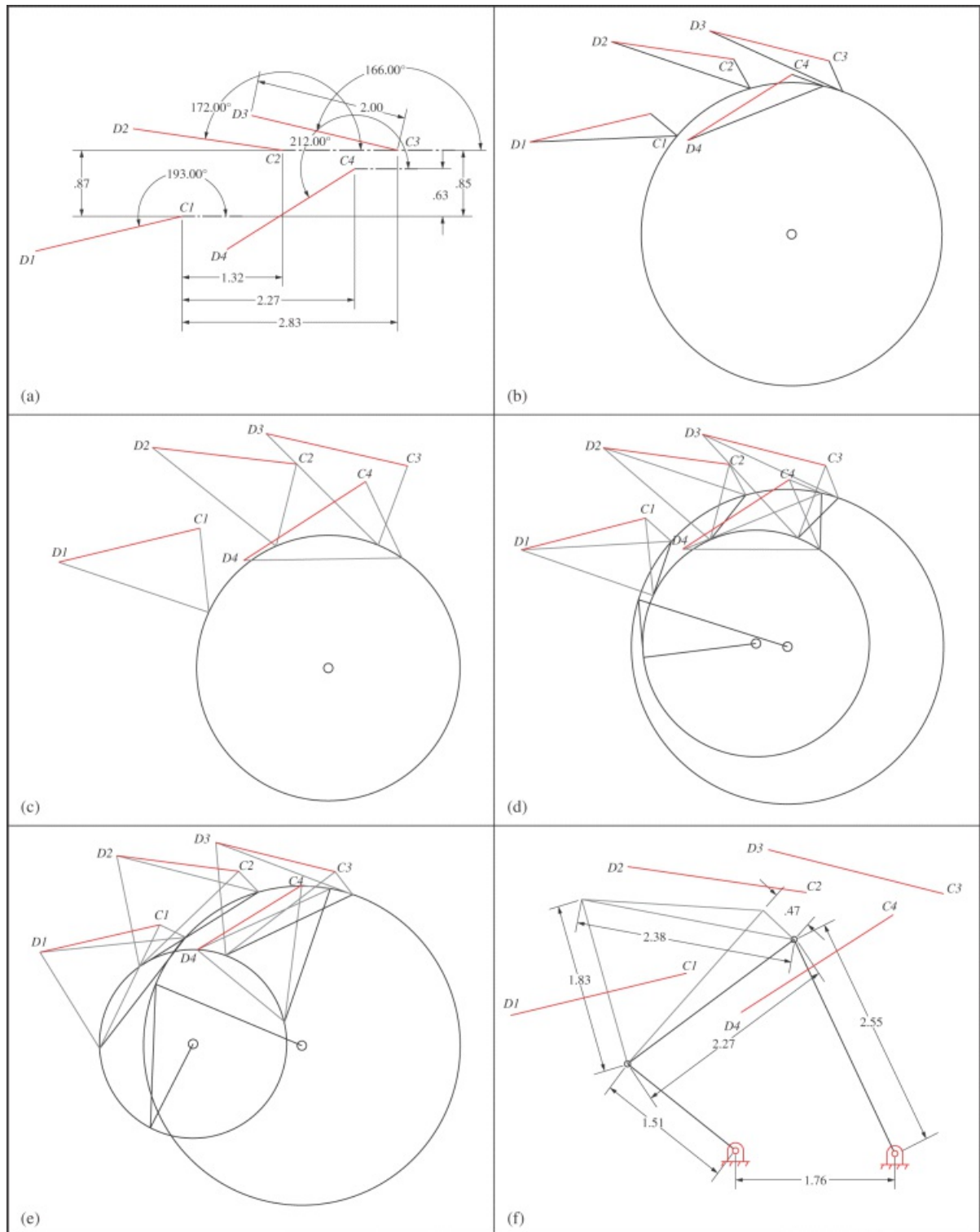


Figure 3.54 Design of a four-bar mechanism for rigid-body guidance through four positions: (a) original positions; (b) locating first circle point; (c) locating second circle point; (d) drawing trial linkage and checking for branch and order problems; (e) linkage after new circle points have been selected; and (f) final linkage with fixed pivots, pin bushings, and original coupler line shown.

Make the *First Crank* layer active, and draw a triangle at each position using the designated line as the base. Make the triangles congruent. Next draw an arbitrary circle, and constrain the apex of each triangle to lie on the circle. Identify the center of the circle by a small concentric circle. The center point and the triangles identifying the four positions of the first circle point are shown in [Figure 3.54\(b\)](#). The apexes of the triangles locate the four positions

of the circle point A , and the center of the circle locates A^* . Do not label the points yet because the labels will not move if different locations for the circle points are chosen later in the design process.

Hide the *First Crank* layer, make the *Second Crank* layer active, and draw a second triangle at each position again using the designated line as the base. Make the triangles congruent. Draw a second arbitrary circle, and constrain the apex of each triangle to lie on the circle. The second center point and the triangles identifying the four positions of the second circle point are shown in [Figure 3.54\(c\)](#). The apexes of the triangles locate the four positions of the circle point B , and the center of the circle locates B^* .

Make the *First Crank* layer visible, and draw a line from the apex of the triangle for the first crank to that of the triangle for the second crank for each position. This gives the locations of the coupler line AB in the four positions.

Make the *Final Linkage* layer active, and draw a general four-bar linkage beginning at the center point A^* and ending at the center point B^* . Select the end of one of the cranks and one of the circle-point circles, and constrain the point to lie on the circle. Similarly, make the end of the second crank coincident with the second circle. Select the coupler of the general linkage and one of the lines corresponding to the positions of AB and constrain them to be equal. This is shown in [Figure 3.54\(d\)](#).

It is now possible to animate the linkage; however, to keep the other dimensions from changing during the animation, first fix the centers of the two circles. Drag the end point of the linkage through the range corresponding to the four positions to determine if there are branch or order issues. This is the case with the linkage chosen in [Figure 3.54\(d\)](#) so the design is not acceptable.

If there are branch or order problems, delete the fixed constraints at the centers of the two circles and move either of the centers of the circles by dragging them with the mouse or move one of the circle points. The constraint manager in the parametric-design program should maintain all of the constraints established so far. It will also ensure that we drag the center points along the center-point curve even though the curve is not visible. Similarly, If we drag the circle points, the constraint manager will allow us to choose only those points on the invisible circle-point curve. For each selection of circle points and center points, we can fix the center points and animate the linkage. The shape of the linkage will change as we move the points so we can also visually evaluate the linkage during the process. Again, it is important to check the triangles defining the positions of each circle point to ensure that they stay congruent. If one of the triangles flips over, we need to move the corresponding circle point to a different region. Using this guided trial-and-error process, we can usually find an acceptable solution to the problem if one exists. A solution that does not have either branch or order issues for this problem is shown in [Figure 3.54\(e\)](#).

As in the three-position case, we can check for branch and order issues by observing that AB moves through the positions properly. If AB moves properly, so will the original line CD .

To improve the appearance of the final linkage, we can add ground pivots at the center points and bushings at the circle points. We can also construct two triangles to properly locate CD on the moving coupler as was done in the three-position example. The final linkage is shown in [Figure 3.54\(f\)](#).

The advantage of GCP is evident in the four-position synthesis case. We were able to extend the three-position synthesis process based on a fundamental understanding of the relationship between center points and circle points. Except for being required to select circle points along an invisible but specific curve, no other knowledge of the kinematic geometry is required.

In principle, the procedure can also be extended to five positions using the same process. However, this is usually of little practical interest because there are a maximum of four discrete solutions possible for circle-center point pairs, and two, or all four, may be imaginary. Even when there are real solutions, there is often a branch or order issue with all of them. Therefore, in most instances, we are limited to four positions.



3.5 Path Synthesis

The path-synthesis problem is that of specifying the path taken by a single point fixed in a coupler link of a mechanism where a coupler is any link that does not share a joint directly with the ground link. There may also be a requirement for faster or slower speeds along different portions of the path. Although many research papers have been written on the subject of path synthesis, designers usually use a trial-and-error approach in practice. The traditional resource for this purpose has been the Hrones and Nelson coupler-curve atlas [15]. This is a large book containing plots of four-bar linkage coupler curves for a large variety of points located in the coupler plane and a large range of link length variations. The approach is to search through the coupler-curve atlas and select a curve that has more or less the right shape and then refine it by trial and error, testing the effect of small variations in the position of the coupler point or small variations in the link lengths. One limitation of the Hrones and Nelson atlas is that it is limited to Grashof type mechanisms that have a fully rotating crank such as a crank-rocker mechanism. There are problems where coupler points on double-rocker mechanisms are adequate.

Fortunately, programs that generate coupler curves are easily written and readily available. Several programs are also available on the web, for example Thompson [31]. In addition, most textbooks written on kinematics, including this one, will include a program to generate coupler curves. Coupler curve programs written in MATLAB for both four-bar linkages and slider-crank mechanisms are included with the supplementary material for this book. These programs use the same nomenclature as the Hrones and Nelson atlas. Using these programs, it is possible to review quickly the coupler curves available and to determine the link lengths and coupler point that will generate the curve. In addition, a general four-bar linkage analysis program is included. This program will display the coupler curve for a specific point, and the four-bar linkage can be either a Grashof or non-Grashof linkage. Another option is to draw the trial linkage using a CAD program and use GCP procedures to observe the effects of different variations.

3.5.1 Design of Six-Bar Linkages Using Coupler Curves

Coupler curves from four-bar linkages and slider-crank mechanisms are used in two main ways. The first is to use the motion of the coupler in the area of the curve to perform some function. A common use for such points is in packaging and conveying equipment. [Figure 3.55](#) shows a coupler mechanism design for an animated tiger used in movie productions [30]. Coupler curves are used extensively for walking machines or even kinetic sculptures [13]. [Figure 3.56](#) shows a mechanism that has been used to feed film in a motion picture projector [13]. The coupler point traces a D-shaped curve, and similar mechanisms are used in transport machinery [13].

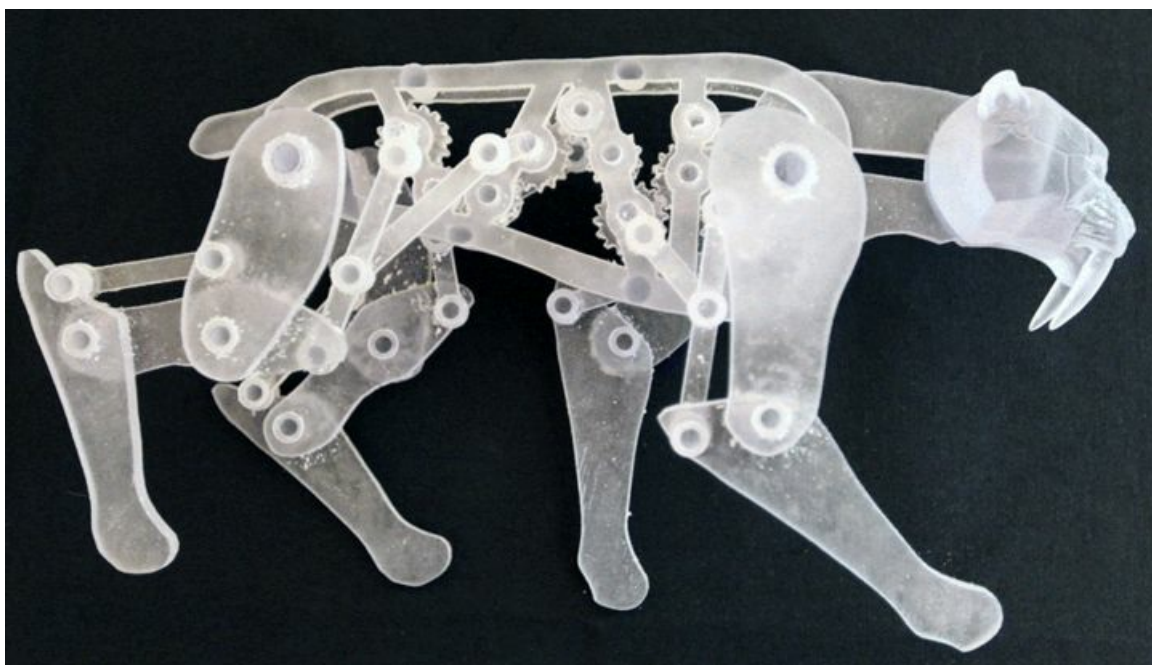


[Figure 3.55](#) Cyber tiger. Animated walking saber-toothed tiger based on a coupler curve at the middle of each foot Courtesy of Disney Enterprises, Inc., Burbank, CA.

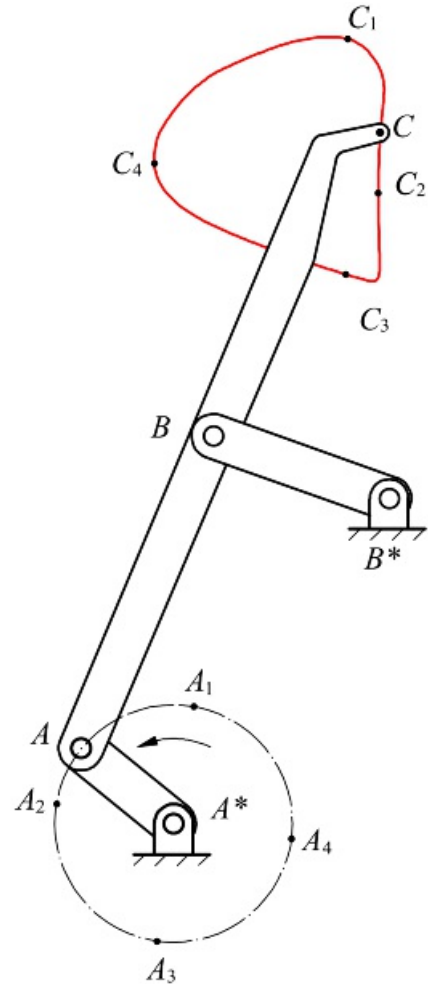


[Figure 3.56](#) Coupler point used in film feed and material transport mechanisms.

A second use for coupler curves is to facilitate the design of six- and eight-link mechanisms where the output link is to have a prescribed motion relative to the input link. A six-link mechanism is represented schematically in [Figure 3.57](#), where link 2 is the input and link 6 is the output. The output dyad (links 5 and 6) is driven by the coupler point (*C*) of the four-bar linkage. By properly selecting the coupler curve, different functional relationships between ϕ and θ can be achieved. The design of six-link mechanisms using coupler curves is discussed extensively by Soni [27]. The design procedure is illustrated in the following two examples.

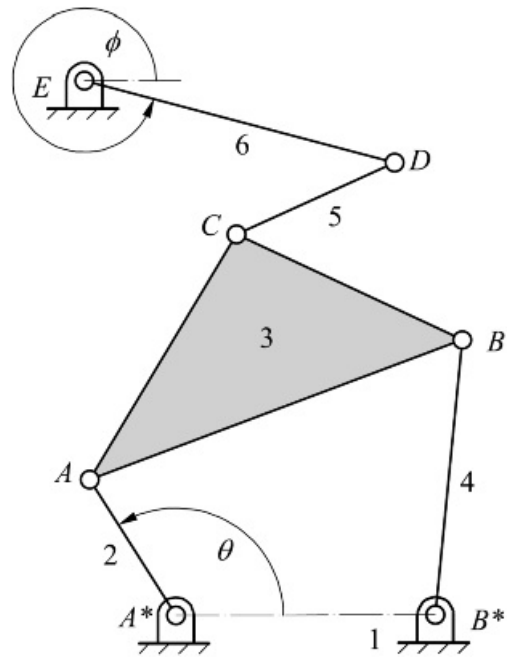


[Figure 3.57](#) Six-link Stephenson mechanism that can be designed using coupler curves.

A procedure is necessary to locate the coupler point relative to the traditional coupler line between the moving pivots (points A and B in [Figure 3.57](#)) if the points are to be used in a subsequent linkage design. The procedure we will use is shown in [Figure 3.58](#). If C is the coupler point, we can locate C relative to AB by specifying the radial distance AC and the angle β measured in the CCW direction from AB . All couplers will have at least two points corresponding to A and B that can be located directly; therefore, this procedure gives a convenient way to locate coupler points on coupler links in even the most complicated linkages.

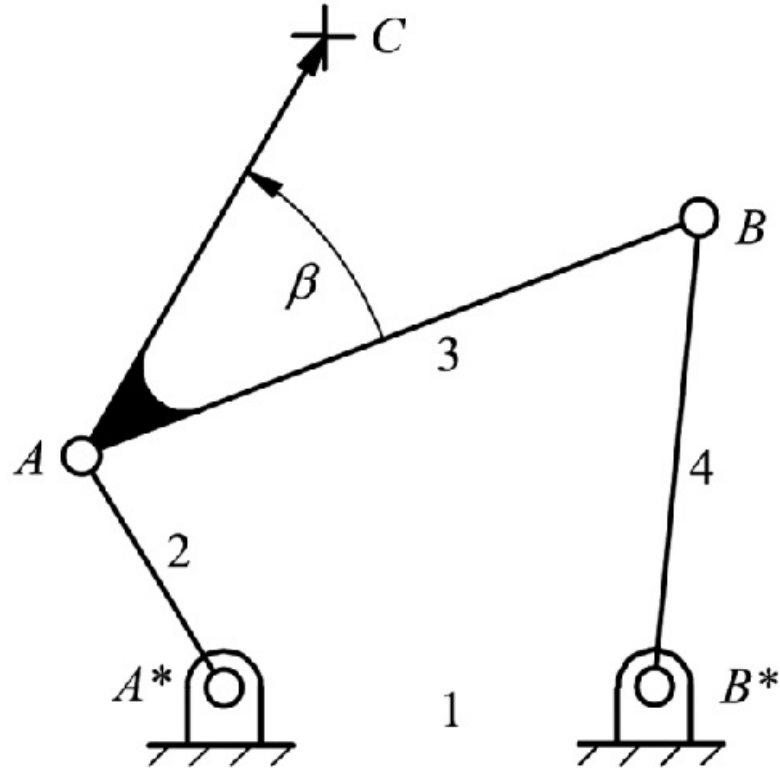


[Figure 3.58](#) Procedure for locating a coupler point relative to moving pivots A and B .



Example 3.5

Design of a Six-Link Dwell Mechanism Using Coupler Curve

A mechanism of the type shown in [Figure 3.57](#) is to be designed such that link 6 is an oscillating lever and link 2 rotates a full 360° . The output link is to oscillate through a range of 30° during the first 120° of crank rotation. Link 6 is then to dwell for 90° of crank rotation, and return during the remaining 150° of crank rotation.

Solution

To solve this problem, it is necessary to have access to an atlas of coupler curves or to use a program that can generate the coupler curves. Regardless of the procedure used, we must be able to determine the geometry of the curve and the travel distance along the curve as a function of input rotation. In the Hrones and Nelson atlas, and in the programs *hr_crankrocker.m* and *hr_slidercrank.m* provided with the supplementary material for this book, a dashed line is used for each 5° of crank rotation. For this example, we will use the four-bar program *hr_crankrocker.m* to generate candidate coupler curves. The first step is to visualize the shape of coupler curve that can be used to drive links 5 and 6. Several different geometries might be used, but the simplest is a curve of roughly elliptical shape. The coupler curves used are displayed in [Figures 3.59](#) and [3.60](#), and the design procedure is shown in [Figure 3.61](#). The procedure is described in the following:

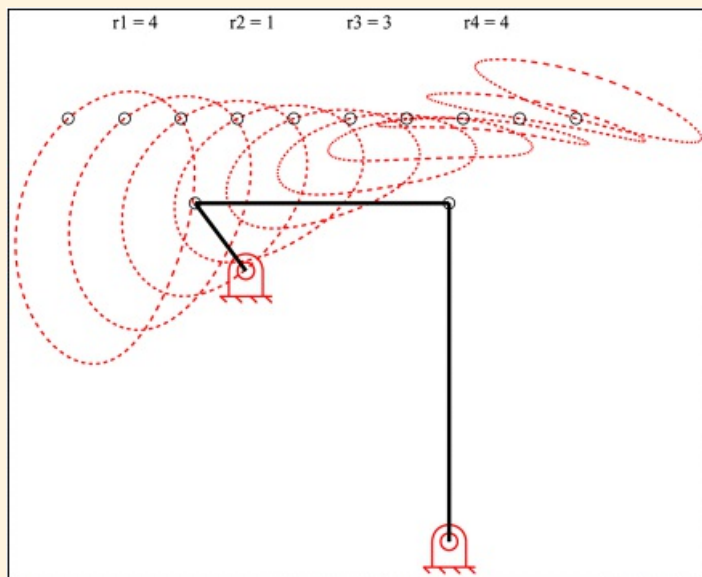


[Figure 3.59](#) Coupler curves for Example 3.5—each dash corresponds to 5° of crank rotation.

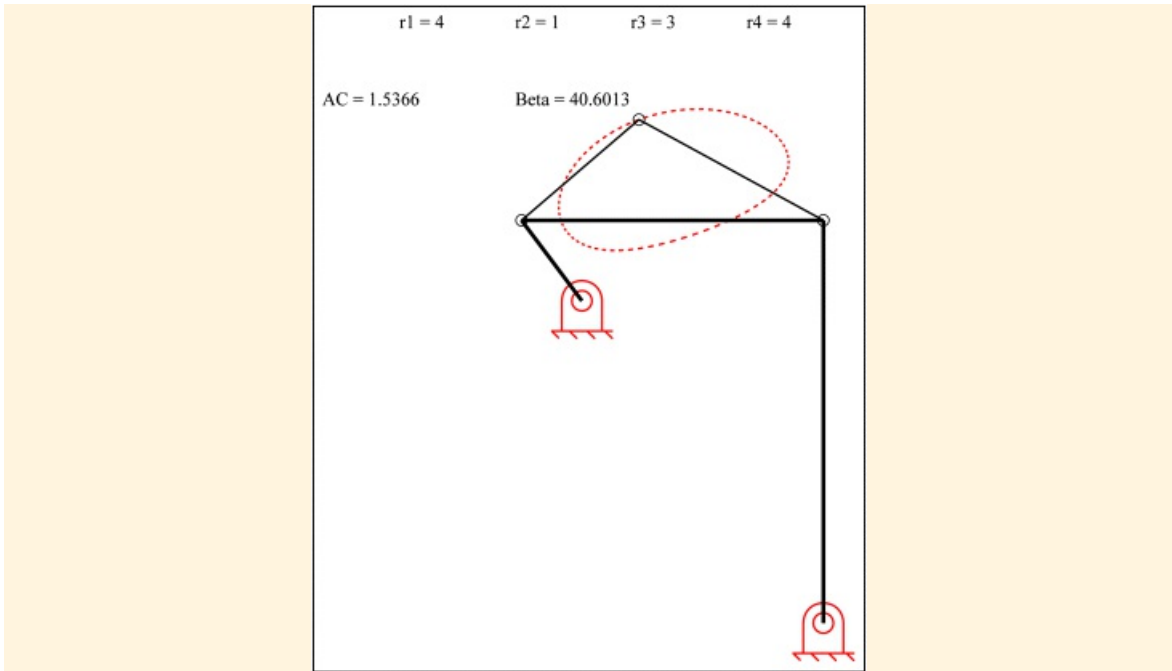


[Figure 3.60](#) Coupler curve chosen for design in Example 3.5.

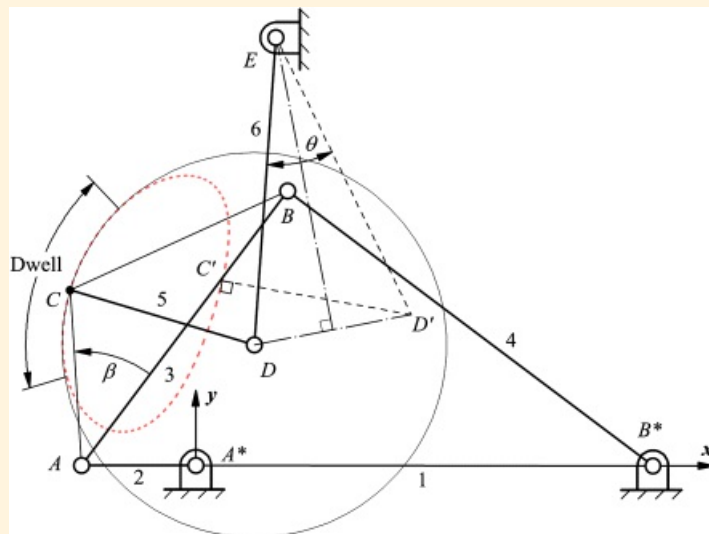


[Figure 3.61](#) Design procedure for mechanism in Example 3.5.

1. Test different coupler curves to determine whether a portion of the curve in the vicinity of the minor axis is roughly circular in shape for the desired dwell period (90° or 18 dashes). [Figure 3.59](#) gives a set of curves generated with the program *hr_crankrocker.m* when $r_1 = 4$, $r_2 = 1$, $r_3 = 3$, and $r_4 = 4$. From the curves displayed, we will select the curve shown in [Figure 3.60](#).
2. After a coupler curve is identified, find the center of the circle that best fits the circular region identified in step 1. The radius of the circle will be the length of link 5. Identify explicitly the beginning and end of the circular portion of the curve. The center of the circle arc will be one extreme position for point D. This is shown in [Figure 3.61](#), where the mechanism has been redrawn so that the frame link (r_1) is horizontal.
3. Point D' corresponds to the second extreme position of D. To locate D' , identify the point on the coupler curve corresponding to 120° (24 dashes) of crank rotation beyond the dwell. Locate a perpendicular line to the coupler curve at this point, and locate D' on this line. Note that when link 5 is in an extreme position, it will be perpendicular to the coupler curve.

4. The pivot E must be located on the perpendicular bisector of the line DD' . Locate E such that the angle $\angle DED'$ is 30° . If A^* is the origin of the x, y coordinate system used to locate pivot E , the parameters corresponding to the solution are

$r_1 = 4$	$r_5 = 1.682$	$AC = 1.537$
$r_2 = 1$	$r_6 = 2.694$	$\beta = 40.6^\circ$
$r_3 = 3$	$E_x = 0.697$	
$r_4 = 4$	$E_y = 3.740$	

5. Compute and plot the motion of link 6 relative to link 2 to evaluate the design. This can be most easily done in either MATLAB or a parametric design program. The resulting mechanism is simply a four-bar linkage with the addition of two more links (Stephenson's six-bar mechanism). The two additional links are called a dyad and can be easily analyzed using the procedures developed in subsequent chapters. A MATLAB routine (*sixbar.m*) for a six-bar linkage analysis is provided with the supplementary material for this book. Part of the analysis from this program is given in [Figure 3.62](#). The results are close to the design specifications, and the basic design is acceptable.

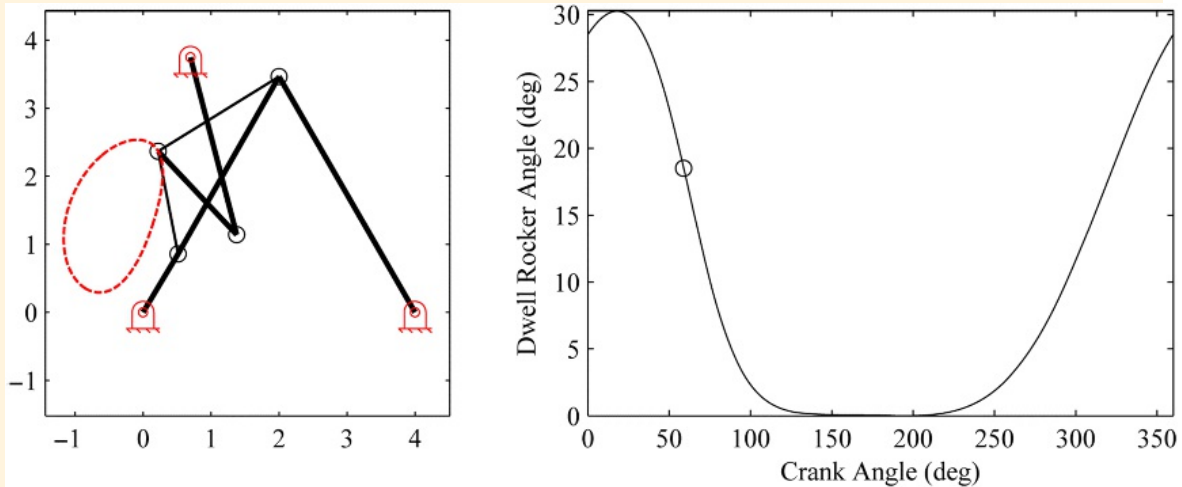


[Figure 3.62](#) Analysis of linkage designed in Example 3.5.

This design procedure can yield a large number of candidate designs. The best design can be chosen by using an appropriate evaluation criterion. Typical criteria are linkage size, force transmission characteristics, and acceleration characteristics.



Example 3.6

Design of a Six-Link Mechanism for a Double Oscillation

A mechanism of the type shown in [Figure 3.57](#) is to be designed such that link 6 will make two complete 30° oscillations for each revolution of the driving link.

Solution

For this problem, no timing information is required. Therefore, we need only ensure that the output link makes two complete oscillations for one oscillation of the input crank. Again, we will use the four-bar program (*hr_crankrocker.m*) to generate candidate coupler curves. The first step is to visualize the shape of coupler curve that can be used to drive links 5 and 6. One curve that will work for this type of problem is a figure-8 curve. Once the curve is found, the design procedure is shown in [Figure 3.63](#) and described in the following:

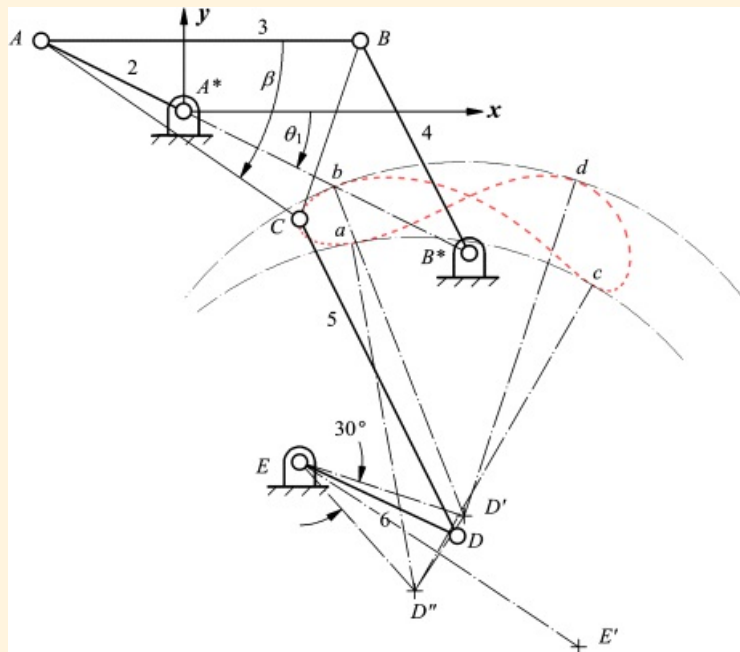


[Figure 3.63](#) Procedure for designing linkage for Example 3.6.

1. Select a coupler curve that is a figure-8 curve with roughly equal lobes. The coupler curve selected is displayed in [Figure 3.64](#).

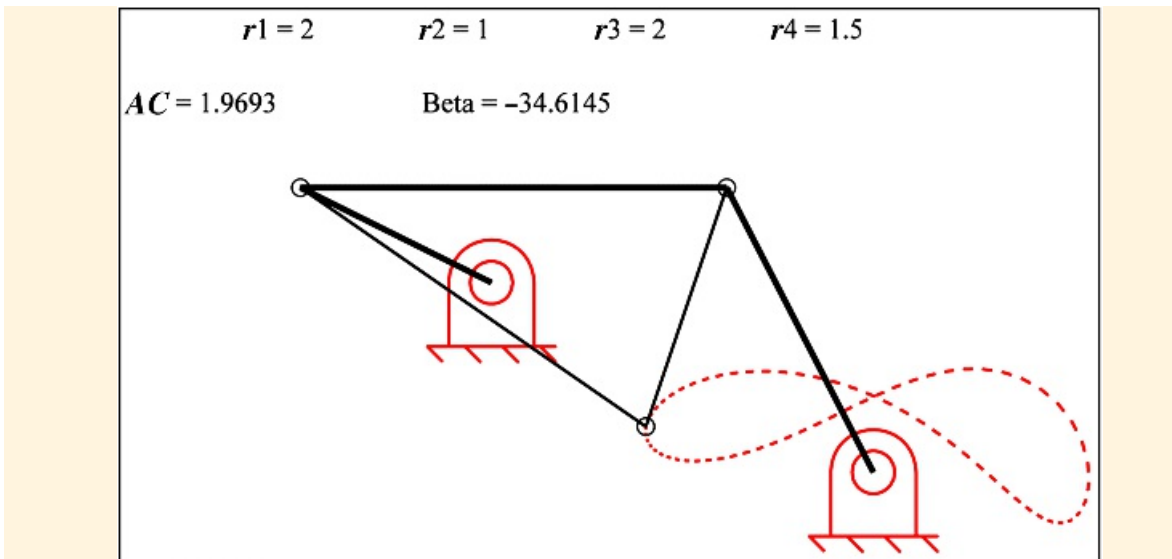


[Figure 3.64](#) Curve that can be used for Example 3.6.

2. After the coupler curve is identified, select the length of link 5 and draw a circle or circle arc with a radius equal to the length of link 5 and tangent to the coupler curve at the two points b and d . The center, D' , of this circle is one extreme position of point D . Draw another circle or circle arc of the same radius tangent to the coupler curve at points a and c . The center, D'' , of this circle is the second extreme position of D .
3. The pivot point, E , must be located on the perpendicular bisector of the line $D'D''$. Locate E such that the angle $D'ED''$ is 30° . The length of link 6 is the distance from D' to E (or from D'' to E). Note that there are two possible locations for the point E . The location E is chosen in this example over E' because E will result in better force transmission characteristics. If point E' is chosen, links r_5 and r_6 will become nearly parallel during periods of their travel, resulting in a very poor transmission angle. The parameter values corresponding to the solution are

$r_1 = 2$	$r_5 = 2.218$	$AC = 1.969$
$r_2 = 1$	$r_6 = 1.088$	$\beta = -34.61$
$r_3 = 2$	$E_x = 0.724$	$\theta_1 = -26.05$
$r_4 = 1.5$	$E_y = -2.198$	

4. Compute and plot the motion of link 6 relative to link 2 to evaluate the design. This is done in [Figure 3.65](#) based on the program (*sixbar.m*) provided with the supplementary material for this book. The results given in [Figure 3.65](#) are very close to the design specifications. If more accurate results are desired, the location of E or the lengths of r_5 or r_6 could be adjusted slightly. This can be done manually or by using an optimization program that minimizes the error created by the linkage. However, even if an optimization program is used, the graphical procedure, which is very simple and quick to apply, is a good means of generating an initial estimate of the optimum solution.

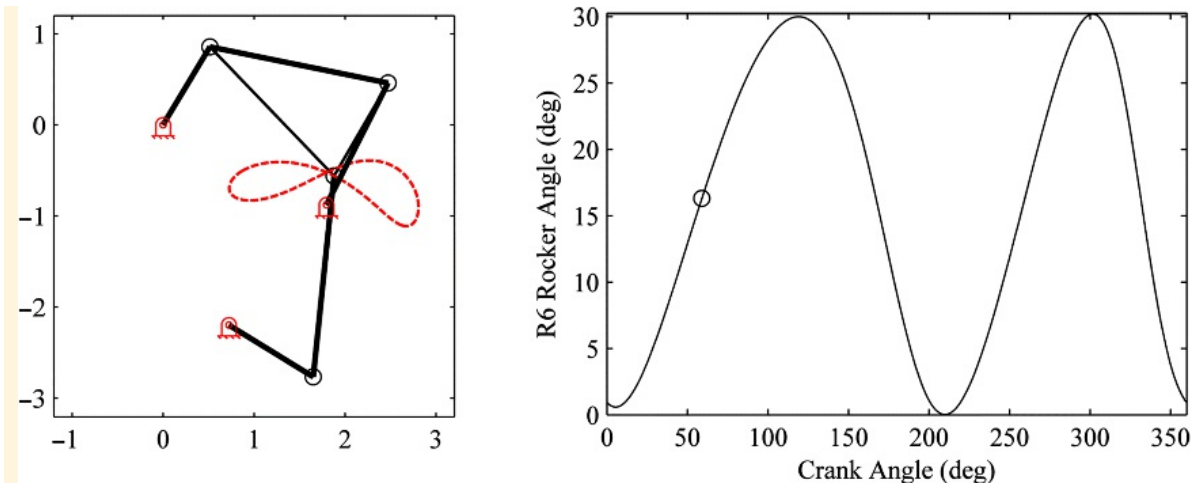


[Figure 3.65](#) Analysis of mechanism designed for Example 3.6.

3.5.2 Motion Generation for Parallel Motion Using Coupler Curves

In industrial applications, it is sometimes necessary to move a rigid body along a curved path in such a way that its angular orientation does not change. This situation, shown in [Figure 3.66](#), is a special case of rigid-body guidance when all of the positions are parallel. If we attempt to use a four-bar linkage for this problem, only a parallelogram linkage can guide a linkage through more than two parallel positions in general [26], and the design constraints for parallelogram linkages are severely restricted. Therefore, guiding a linkage in parallel motion along a complex path generally requires more than four links.

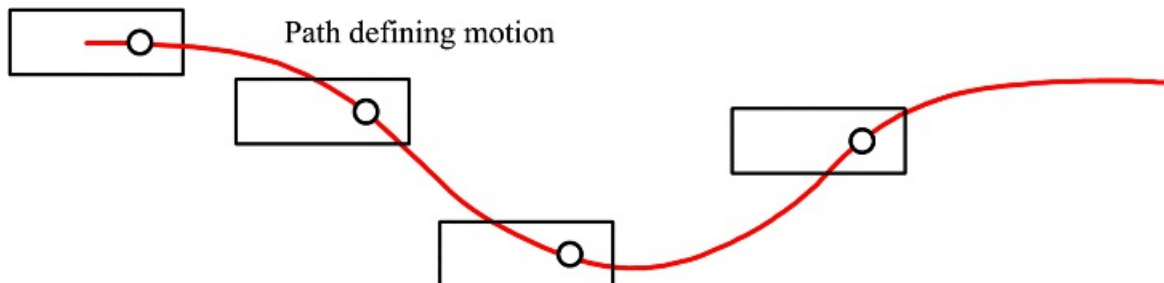


[Figure 3.66](#) General parallel motion along a curved path.

A relatively simple solution to parallel motion synthesis is to use a four-bar linkage and two parallelogram linkages in parallel to form an eight-link mechanism. The four-bar linkage defines a coupler path along which one point of the rigid body is guided, and the parallelogram linkages maintain the orientation of the rigid body relative to the ground. This configuration is shown in [Figure 3.67](#).

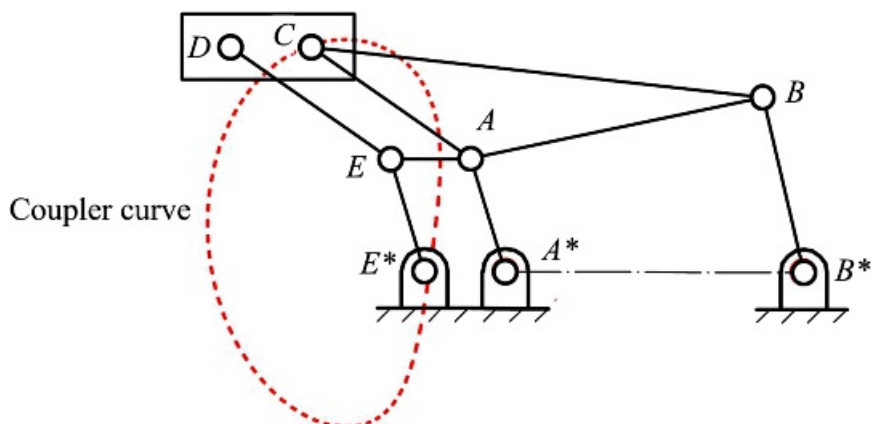


[Figure 3.67](#) Eight-link mechanism to guide parallel motion along a curved path.

To design the eight-link mechanism, we need only find a coupler curve that will approximate the curve that the linkage must follow. This defines linkage A^*B^*BAC in [Figure 3.67](#). Next the parallelogram linkages are added to maintain the orientation of the rigid body. Referring to [Figure 3.67](#), link EE^* is equal in length to AA^* , and link ED is equal in length to AC . Lengths E^*A^* , EA , and DC are equal, but the actual length is arbitrary from the standpoint of kinematics. Note that the parallelograms could also have been used with lengths B^*B and BC . The side of the linkage used depends on the design constraints.

In practical situations, the parallelograms may not work for the full range of motion of the four-bar linkage either because of a need to change branch or because of a mechanical interference among the links. If a full range of motion is required, the parallelogram linkages can be replaced by two cable, belt, or chain drives. This is shown in [Figure 3.68](#). The motion of link 2 relative to link 4 is equivalent in both cases if the two pulley or sprocket diameters are equal. Any kind of timing belt, chain, or cable drive can be used as long as there is no slipping at the pulleys.

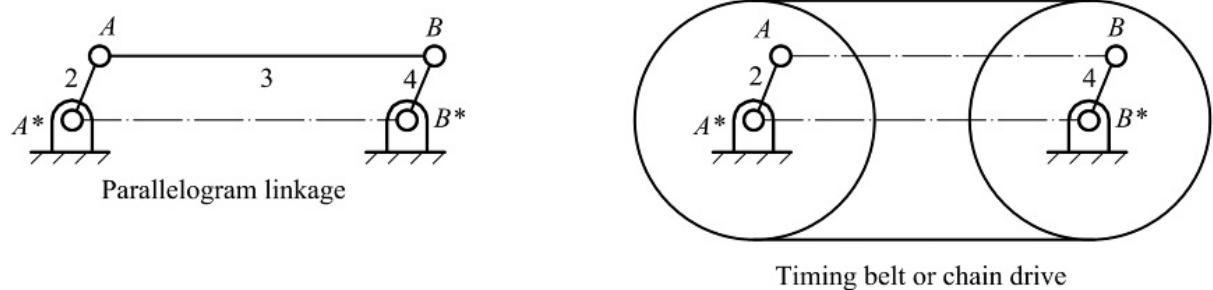


[Figure 3.68](#) The motion of a parallelogram linkage can be duplicated by a timing belt or chain drive if the pulleys are of equal diameter.

The equivalent system corresponding to [Figure 3.67](#) is shown in [Figure 3.69](#). Different pulley diameters are used for the two equivalent parallelogram-linkage drives to illustrate that the two drives are separate. However, the two pulleys pivoting about point A must be fixed together.

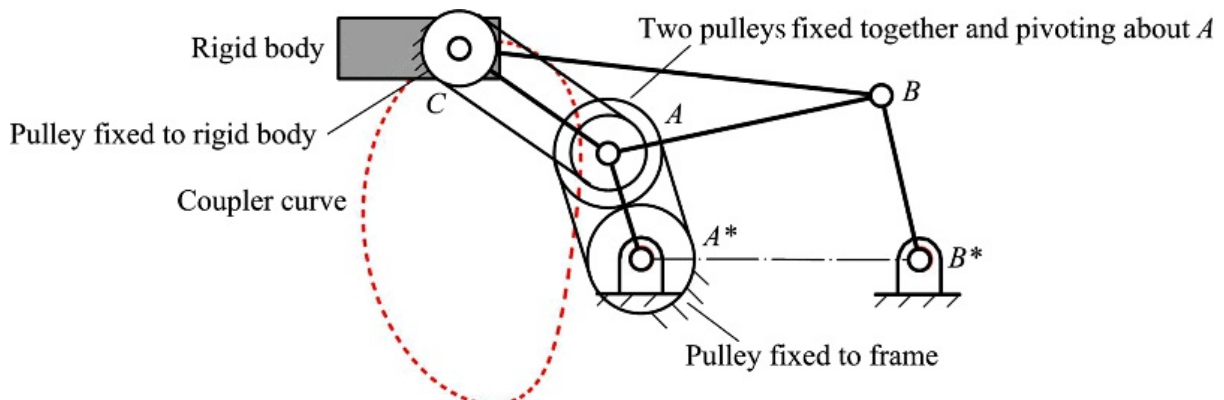


[Figure 3.69](#) Replacement of the parallelogram linkages in [Figure 3.67](#) by timing belt drives.



Example 3.7

Design of an Eight-Link Mechanism for Parallel Motion Generation

A test fixture must be removed from a hot hydraulic fluid bath. The fixture must be lifted vertically 6 inches and then carried horizontally 25 inches along the approximate path shown in [Figure 3.70](#). The test fixture must remain horizontal at all times. Design a linkage system that will move the fixture.

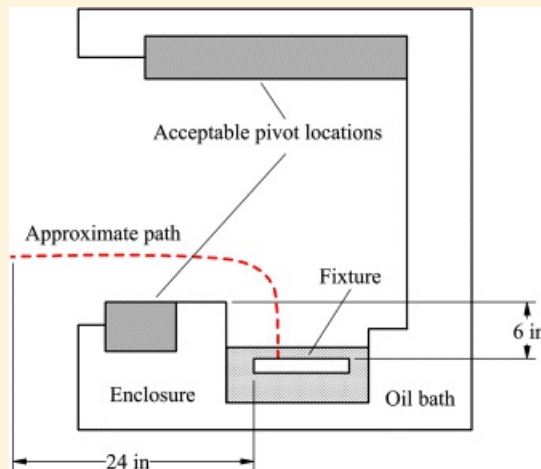


[Figure 3.70](#) General geometry for fixture and enclosure.

Solution

To solve the problem, it is necessary to identify a four-bar linkage coupler curve that will match approximately the curve represented in [Figure 3.70](#). The important features of the linkage are the allowable regions for the pivot locations, the 6-in rise in the coupler curve, and the lateral motion of approximately 25 in.

Two programs (*FourbarAnalysis* and *HRCrankRockerAnalysis*) for generating four-bar linkage coupler curves are in the *KinDAP* suite of programs available with the supplementary material for this book. The first program will generate coupler curves for both Grashof Type I and Type II linkages while the second program is limited to crank-rocker mechanisms. For this problem, a crank-rocker linkage is not necessary so the first program was used. The linkage was designed by trial and error, and the result is shown in [Figure 3.71](#). The linkage is shown with the fixture in [Figure 3.72](#). Because of the range of motion required for the linkage, cable driven pulleys are suggested for the final design rather than parallelogram linkages.

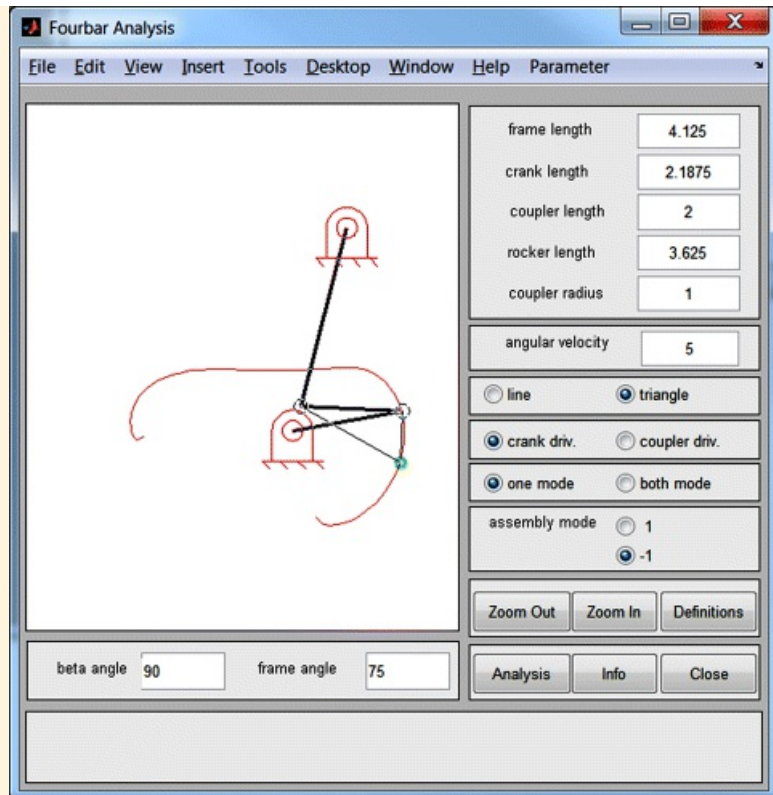


[Figure 3.71](#) Screen capture from *FourBar Analysis* program showing solution coupler curve.

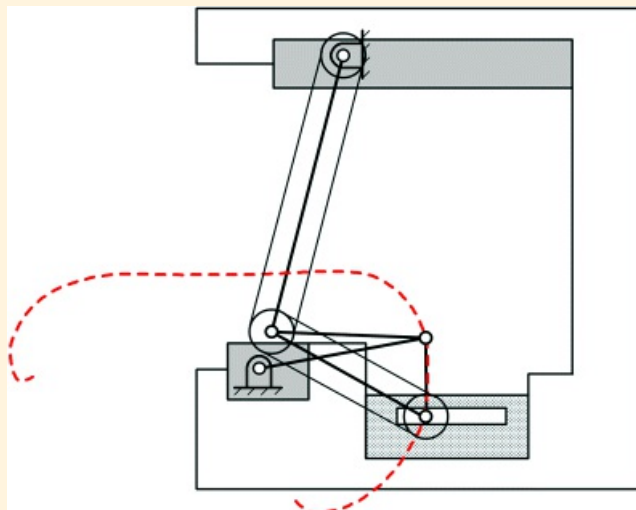


[Figure 3.72](#) The mechanism located in the chamber.

3.5.3 Cognate Linkages

A given four-bar linkage with coupler point C will generate a unique coupler curve. There are two other four-bar linkages that will generate exactly the same coupler curve. There are also three five-bar linkages that will generate the same coupler curve if the two cranks of the five-bar linkage are driven at the same speed and in the same direction. The three four-bar and three five-bar linkages that will generate the same coupler curve are called cognates. From a design standpoint, one of the linkages may have more desirable motion characteristics than the others. Therefore, it is useful to identify all six linkages once the coupler curve is defined so that the best one can be selected.

Four-Bar Cognate Linkages

The existence of the three cognate linkages was originally discovered by Roberts [12,22]. A general discussion of cognate linkages and a proof for Roberts' theorem that identifies the geometric relationships among cognates are given in [Chapter 8](#). Therefore, in this chapter, we will limit our discussion to a procedure for finding cognates.

The geometry of the four-bar cognate linkages can be determined by considering extreme versions of the three linkages. The resulting diagram shown in [Figure 3.73](#) is called Roberts' linkage [12] and the nomenclature used in [Figure 3.73](#) is based on that used by Hall [12]. The mechanisms in this diagram will not move; however, the diagram shows the relationships that must exist among the three cognate linkages. These relationships are maintained when triangle MQO is shrunk while maintaining similarity, thereby permitting the linkages to move. In particular, triangles MQO , ABC , GCF , and CDE are similar. Also, figures $MACG$, $BQDC$, and $FCEO$ are parallelograms. The coupler point is C , and two cognate linkages share each of the fixed pivots. The couplers of each of the cognates are geometrically similar to each other and to the triangle formed by the fixed pivots. If we identify the fixed pivots as M , Q , and O , we can identify the three four-bar linkages by their pivots. That is, one four-bar is the MQ four-bar, one is the MO four-bar, and the third is the QO four-bar.

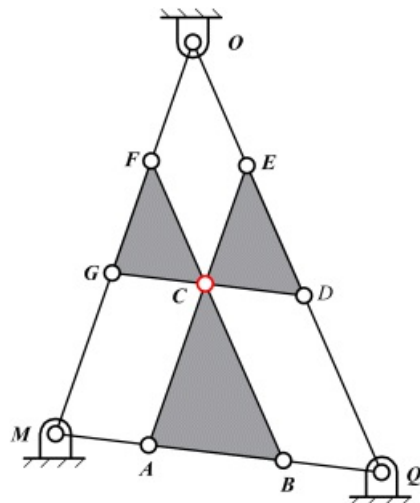


[Figure 3.73](#) Roberts' linkage.

The geometric relationships among the three general cognate linkages are shown in [Figure 3.74](#). When determining the cognate linkages, it is assumed that the MQ linkage is known along with the coupler point C . The cognate linkages can be identified with the aid of Roberts' linkage, which reveals the geometric relationships among the three linkages. Given the positions of M , Q , and C and the lengths r_1 , r_2 , r_3 , r_4 , and r_5 , the equations for the location of pivot O and the corresponding angles and lengths of the other cognate linkages are shown in [Table 3.1](#). When the location of the coupler point is specified, the coordinates of A , B , and C must be given, or alternatively, the coordinates of A and B can be given along with the angle β and length r_5 . The equations in [Table 3.1](#) can be easily programmed to determine the geometry of the cognate linkages, and this is done in a program (*cognates.m*) provided with the supplementary material for book. [Figure 3.75](#) shows the cognate linkages for the mechanism shown in [Figure 3.60](#).

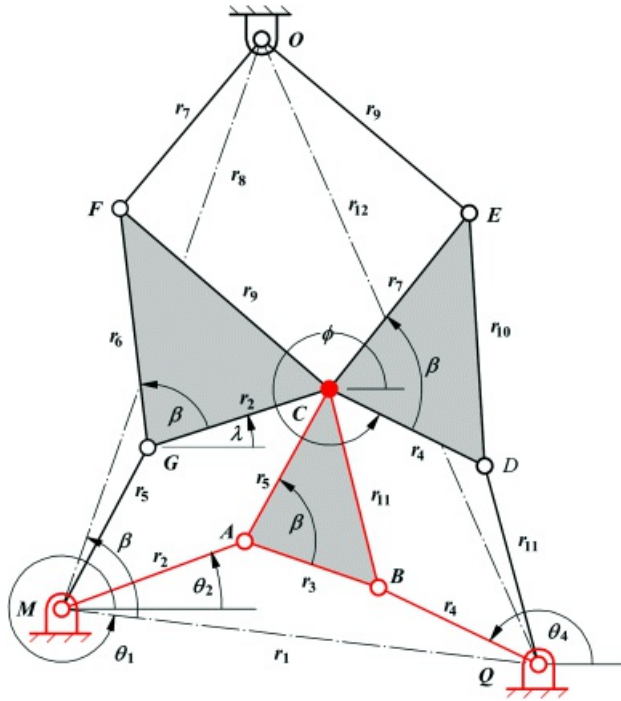


[Figure 3.74](#) Three four-bar cognate linkages will generate the same coupler curve.

[Table 3.1](#) Angle and link relationships permitting the cognate linkages to be determined. The variables refer to the diagram in [Figure 3.74](#). The coordinates (x_A, y_A) , (x_B, y_B) , and (x_C, y_C) are assumed to be known from the analysis of the MQ linkage. Alternatively, β , ϕ , and λ can be given separately.

$r_5 = r_2 \frac{r_3}{r_2}$	$r_7 = r_4 \frac{r_3}{r_2}$	$r_8 = r_1 \frac{r_3}{r_2}$
$\beta = \tan^{-1} \left \frac{y_C - y_A}{x_C - x_A} \right - \tan^{-1} \left \frac{y_A - y_G}{x_A - x_G} \right $		
$x_G = x_{G1} + r_8 \cos(\theta_1 + \beta)$	$y_D = y_{G2} + r_8 \sin(\theta_1 + \beta)$	
$x_G = x_{G1} + (x_C - x_A)$	$y_G = y_{G2} + (y_C - y_A)$	
$x_G = x_{G1} + (x_C - x_B)$	$y_D = y_G + (y_C - y_B)$	
$\phi = \tan^{-1} \left \frac{y_B - y_C}{x_B - x_C} \right $	$\lambda = \tan^{-1} \left \frac{y_C - y_E}{x_C - x_E} \right $	
$x_S = x_C + r_7 \cos(\beta + \phi)$	$y_S = y_C + r_7 \sin(\beta + \phi)$	
$x_F = x_C + r_5 \cos(\lambda + \beta)$	$y_F = y_C + r_6 \sin(\lambda + \beta)$	
$r_9 = \sqrt{(x_F - x_C)^2 + (y_F - y_C)^2}$	$r_{10} = \sqrt{(x_E - x_D)^2 + (y_E - y_D)^2}$	

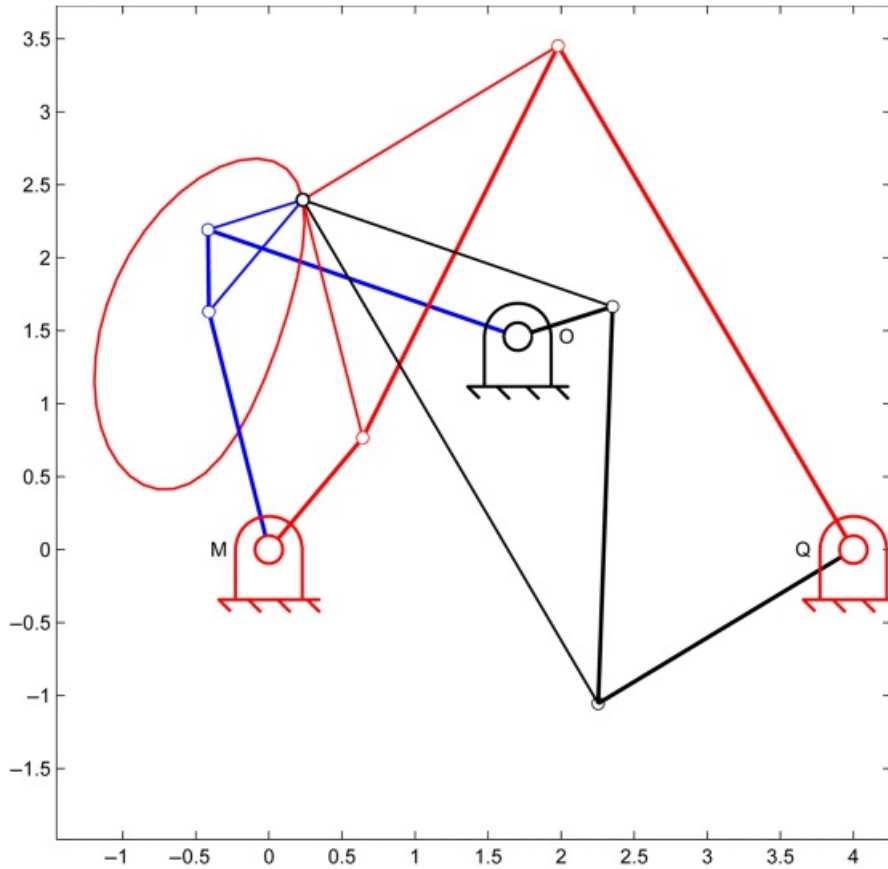


[Figure 3.75](#) Three cognate linkages for the coupler curve in [Figure 3.60](#).

Note that the cognates will all be of the same Grashof type; however, if the original linkage is a crank-rocker, the cognates may be type I double rockers. Therefore, to trace the entire curve, it will be necessary to drive the coupler point directly with some of the cognates.

Five-Bar Cognate Linkages

Chebyshev [12] appears to have been the first to discover that any coupler curve that can be traced by the coupler point of a four-bar linkage can also be traced by a five-bar linkage if the two cranks are driven in the same direction and at the same velocity. The five-bar linkage is identified by constructing two parallelograms as shown in [Figure 3.76](#). The original four-bar linkage is shown in black and the five-bar cognate is shown in red. The cranks of the five-bar linkage are D^*D and E^*E .

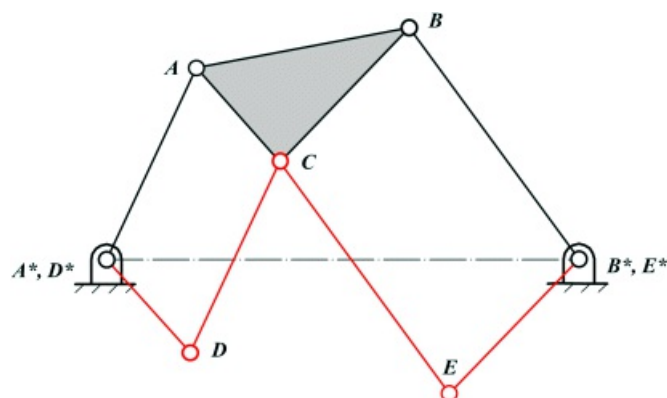


[Figure 3.76](#) Five-bar cognate for four-bar linkage. The five-bar linkage is shown in red. If cranks D^*D and E^*E are driven at the same speed and in the same direction, the five-bar linkage will trace the same coupler curve at C as does the four bar linkage.

There are a number of ways to drive D^*D and E^*E in the same direction and at the same speed. Three methods are shown in [Figure 3.77](#). The first is based on a six-bar linkage by forming a triangle using E^*E as one side and a second link that is parallel and of the same length as D^*D as a second side. A link equal in length to D^*E^* is connected to the apex of the triangle and to D . The second method rigidly connects two equal-diameter pulleys to the two cranks and connects the pulleys with a timing belt. The third method rigidly connects two equal-diameter gears to the two cranks and connects the gears via an idler gear. Note that if the gears were meshed directly without the idler, they would rotate at the same speed, but in opposite directions.

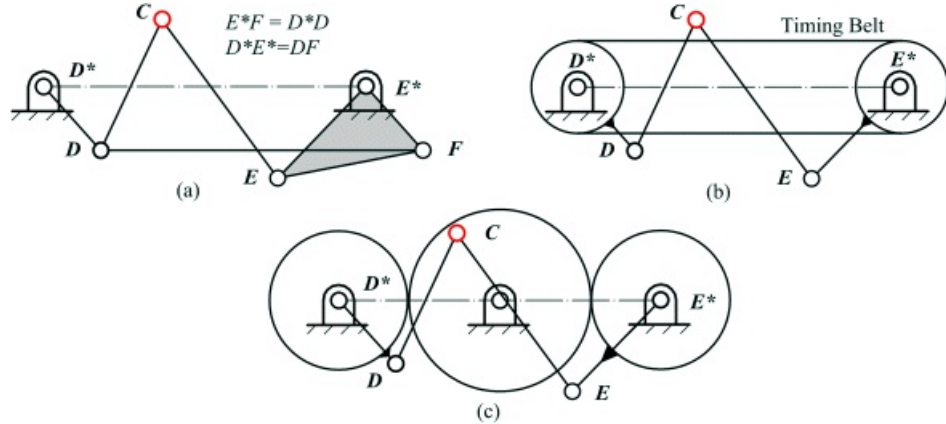


[Figure 3.77](#) Methods of driving D^*D and E^*E at the same speed and in the same direction: (a) six-bar linkage with D^*E^*FD as a parallelogram; (b) timing belt with equal-diameter pulleys; and (c) equal-diameter gears connected by an idler gear.

3.5.4 Using GCP for Path Synthesis

Geometric Constraint Programming (GCP) is especially useful in path synthesis because the constraint based graphics approach is directly applicable for all of the constructions discussed in this section. In particular, it is possible to check out quickly the gross motion of all of the linkages associated with coupler curves. Also, the construction of dwell mechanisms is much simpler with GCP than with conventional drawing programs. We will illustrate the use of GCP with two examples. The first will be for the design of a double-dwell mechanism, and the second will be to find cognate linkages.



Example 3.8

Using GCP to Design a Double-Dwell Mechanism

The problem is to design a mechanism where the input angle θ and the output angle ϕ have the following relationship:

ϕ dwells
ϕ rotates 55°
ϕ dwells
ϕ rotates 55° to return to the original position

Solution

Hrones and Nelson [15] illustrate the use of coupler curves for dwell mechanisms in two ways. The first uses a coupler curve with a segment that approximates a circular arc, as was used in Example 3.5. The second uses a coupler curve with an approximate straight-line segment. The resulting mechanism is still a six-bar linkage, but one of the joints is a slider attached to the coupler point as shown in [Figure 3.78](#). For a double-dwell mechanism of the type shown in Example 3.7, we need to find a coupler curve with two circular segments with the same radius. Such a coupler curve would have a “kidney-bean” shape. For a double-dwell mechanism of the type shown in [Figure 3.78](#), we need to find a coupler curve with two straight-line segments where the straight lines are separated by an angle of 55° . Such a coupler curve would have an “ice cream cone” appearance.

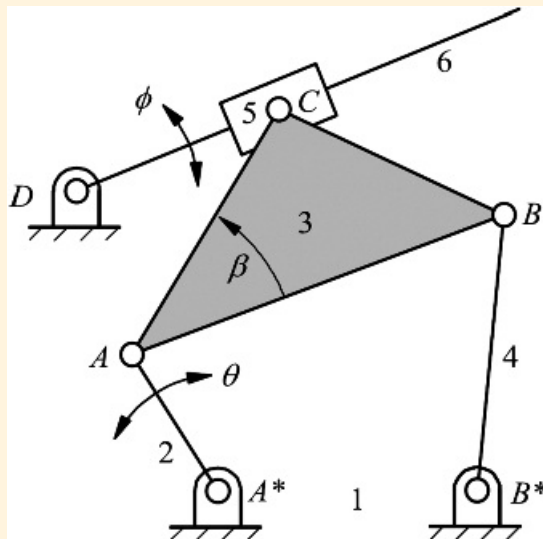


[Figure 3.78](#) Six-bar linkage that can be used as dwell mechanism.

For this problem, we will design a mechanism similar to that shown in [Figure 3.78](#). We can find an appropriate coupler curve from a catalog such as that developed by Hrones and Nelson [15], or we can use a program that will generate coupler curves. Here the program *hr_crankrocker* employed for Examples 3.6 and 3.7 was used. To find an appropriate coupler curve, we need to convert the angles given in the problem statement to dashes where one dash on the coupler curve corresponds to 5° of crank rotation. Therefore, we need to find a curve that has two approximate straight line segments of 14 dashes in length and the segments need to be separated by an angle of 55° . The straight-line segments need to be separated by 14 dashes on one end and 30 dashes on the other. The coupler curve found together with the solution linkage is shown in [Figure 3.79](#). Using the nomenclature in [Figure 3.78](#), the dimensions corresponding to the four-bar linkage

in [Figure 3.79](#) are

$A^*B^* = 3.2$	$A^*A = 1$	$AB = 3$	$B^*B = 3.2$	$AC = 4.44$	$\beta = -38.38^\circ$
----------------	------------	----------	--------------	-------------	------------------------

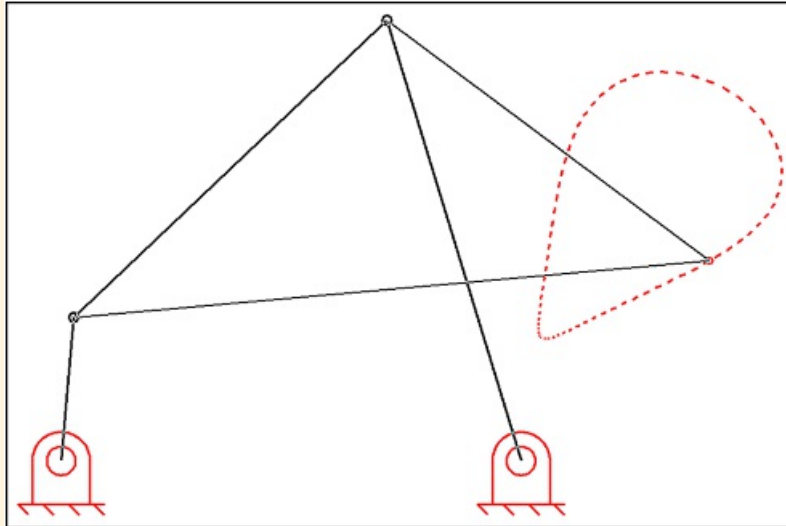


[Figure 3.79](#) Coupler curve from *hr_crankrocker* satisfying requirements in problem statement.

To begin the process using GCP, open a blank document and set up the following layers:

Basic Construction: Contains geometric constructions for finding pivot location for link 6

Linkage: Contains the drawing of the final linkage

Linkage Dimensions: Contains the dimensions for the final linkage

Pivot Dimensions: Contains the dimensions for the ground pivots, bushings, and slider block

Create a TIF file corresponding to [Figure 3.79](#) and insert it into the parametric-design program used and move the picture to the center of the drawing area. Make the *Linkage* layer active, and carefully draw a linkage that duplicates the linkage in the picture. Fix the points at the pivot locations. Make the *Linkage Dimensions* layer active and visible, and use the dimension tool to constrain the length of each line drawn to define the linkage. Note that these dimensions are unlikely to be the same as those listed above; however, they should be proportional. Determine the proportionality factor by dividing the actual distance (3.2) for A^*B^* by the dimension in the drawing. Check each of the other dimensions in the drawing and correct them if necessary. Animate the linkage to ensure that the coupler point follows the coupler curve. If the drawing was done carefully, any corrections should be minor. The dimensions in the drawing are shown in [Figure 3.80\(a\)](#). Hide the *Linkage Dimensions* layer.

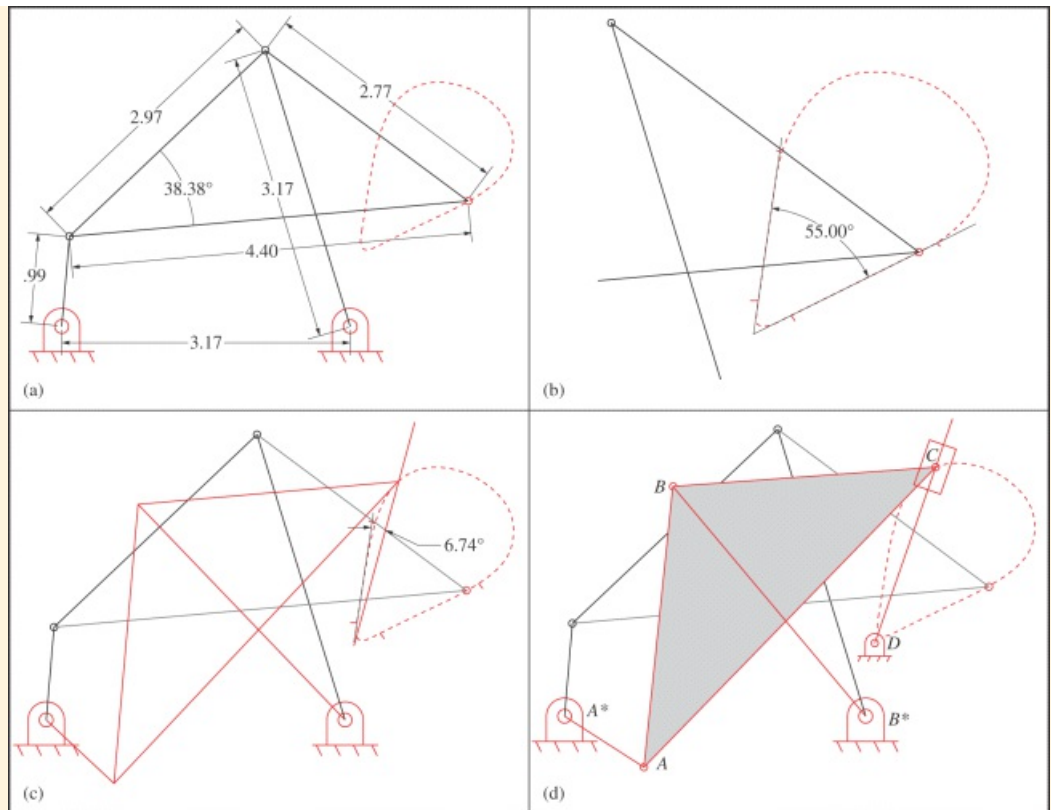


Figure 3.80 Design of a double-dwell mechanism using GCP: (a) original linkage with coupler curve; (b) identifying dwell regions and slide pivot; (c) basic linkage with slider line; and (d) final linkage with shading, ground pivots, and bushings added.

Make the *Basic Construction* layer active and locate the beginning and end of each dwell line with a tick mark on the drawing. Draw lines through these tick marks and along the coupler curve. The intersection of these lines will give the pivot location corresponding to *D* in [Figure 3.78](#). Trim the construction lines so that they do not extend beyond the intersection point. Fix the intersection point. Check the angle between the two construction lines to ensure that the angle is approximately 55° . The construction is shown in [Figure 3.80\(b\)](#). As indicated, the coupler point is in the dwell region in the drawing. Therefore, we can use the construction line as the actual output link. To unconstrain the line, make the angle dimension between the two construction lines to be driven. Fix the top dwell line to use as a reference as the linkage is animated. Next select the coupler point at the apex of the coupler triangle and the bottom dwell line and constrain the coupler point to be coincident with the dwell line. To make the linkage easier to distinguish from the original picture, select all of the links, including the slider line, and make them a color such as red. To check the design, animate the linkage by dragging link 2 with the mouse. The linkage in an intermediate position is shown in [Figure 3.80\(c\)](#).

While not necessary from a functional standpoint, the appearance of the linkage can be improved by adding a ground pivot at the pivot location for the output link, bushings, and a slider at the coupler point. We can also shade the coupler triangle. The result is shown in [Figure 3.80\(d\)](#).

While the constructions in [Figure 3.80](#) could be done with any good drawing program, the advantage of GCP is that the constructions can be made easily, and the final linkage can be checked by animation within the context of the same program. Also, the user can see the effect of any slight alterations of the dimensions immediately.



Example 3.9

Using GCP to Find Cognate Linkages

Find the cognate linkages for Watt's straight-line mechanism shown in [Figure 3.81](#). This mechanism is one of several four-bar linkages that have coupler points that trace approximate straight-line paths.

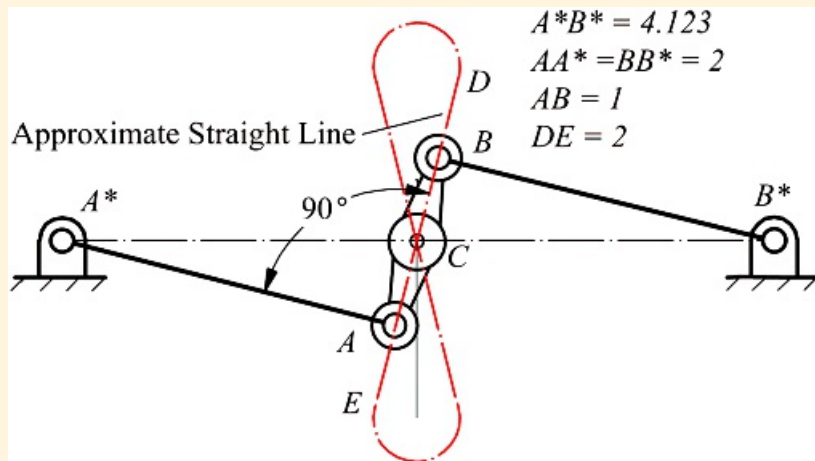


[Figure 3.81](#) Watt's approximate straight-line mechanism.

Solution

Begin the process by opening a blank document and set up the following layers:

MQ Linkage: Contains the original linkage in [Figure 3.81](#)

MQ Dimensions: Contains the dimensions for the *MQ* linkage

MO Linkage: Contains *MO* cognate based on Roberts' linkage in [Figure 3.73](#)

QO Linkage: Contains *QO* cognate based on Roberts' linkage in [Figure 3.73](#)

Pivot Dimensions: Contains the dimensions for the ground pivots and bushings

Make the *MQ Linkage* layer active, and draw an arbitrary four-bar linkage with an arbitrary coupler point as shown in [Figure 3.82\(a\)](#). We have labeled the points to explain the procedure, but this is not necessary in most cases. Fix point *M* and constrain *Q* to be on a horizontal line through *M*. Next select *MA* and *BQ* and constrain them to be equal. Select *AC* and *CB* and constrain them to be equal. Select point *C* and the line *AB* and constrain *C* to lie on line *AB*. Draw a small circle centered at *C* to make the coupler point evident. To improve the appearance of the drawing, add fixed pivots at *M* and *Q* and bushings at *A* and *B*. Use the dimension tool to constrain the dimensions given in [Figure 3.81](#). Move the dimensions to the *MQ Dimensions* layer. Draw a construction line between *M* and *Q*. Draw the straight-line portion of the coupler curve based on the geometry in [Figure 3.81](#). Make the coupler point and coupler curve line red if possible. The dimensioned linkage is shown in [Figure 3.82\(b\)](#). Move the linkage by dragging the point at *A* with the mouse. Point *C* should follow the coupler curve. If the linkage will not move, check for and delete any unintended constraints that might have been applied.

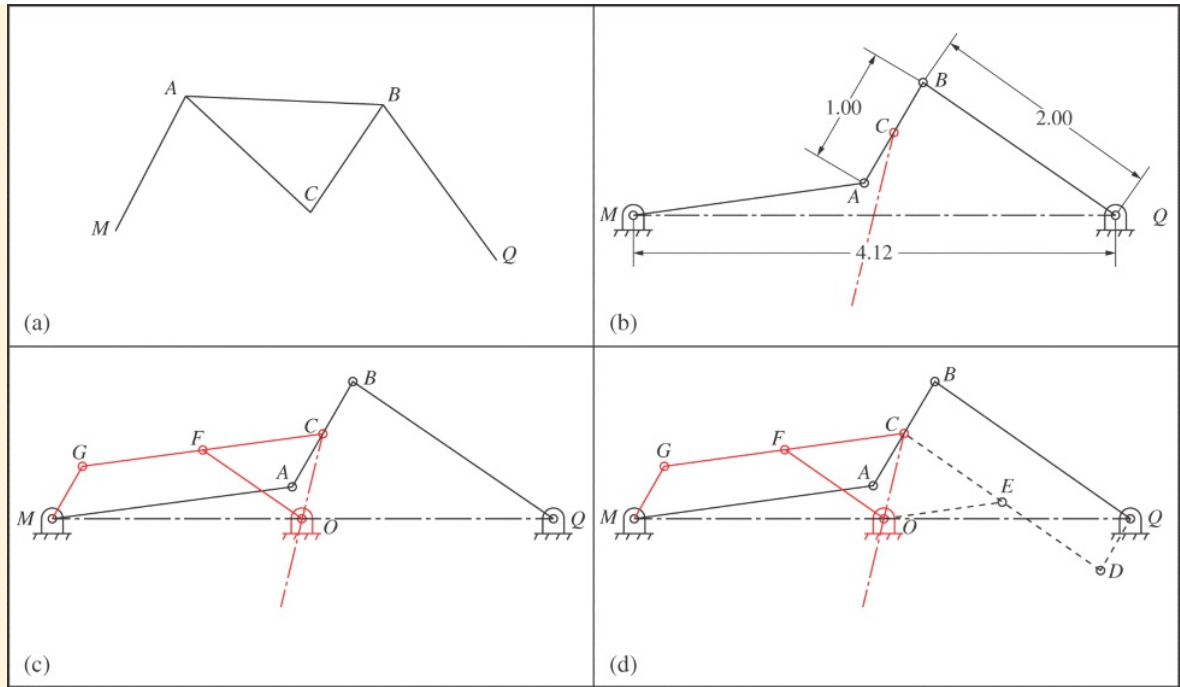


Figure 3.82 Finding cognates for Watt's straight-line linkage using GCP: (a) generic linkage with coupler; (b) *MQ* cognate; (c) *MO* cognate; and (d) all linkages combined on one drawing.

Hide the *MQ Dimensions* layer and make the *MO Linkage* layer active. The *ACB* “triangle” is collapsed to a straight line so the *MOQ* similar “triangle” is a straight line also. Because *C* is in the center of the *AB* line, point *O* will be in the center of line *MQ*. Draw a small circle anywhere on the diagram. Select the center of the circle and the line *MQ* and constrain the center of the circle to be coincident with the midpoint of *MQ*. Draw two lines with the first starting from *M* and the second ending at *C*. Label the endpoint of the line starting from *M* as *G*. Constrain the line *MG* to be parallel and equal to *AC*. This will automatically constrain *GC* to be equal and parallel to *MA*. “Triangle” *GFC* is similar to *ACB*; therefore, point *F* must lie in the center of *GC*. Again, draw a small circle anywhere in the diagram. Select the center of the circle and the line *GC* and constrain the center of the circle to be coincident with the midpoint of *GC*. Draw a line from point *F* to *O*. Add bushings at *G* and *F* and a ground pivot at *O*. This completes the *MO* linkage. The linkage is shown in red in [Figure 3.82\(c\)](#). Again, move the linkage by dragging on the point at *A* with the mouse, and remove any unintended constraints if the linkage will not move.

Make the *QO Linkage* layer active. Draw lines to represent *DC* and *QD*, and set *DC* to be parallel and equal to *QB*. “Triangle” *CED* is similar to *ACB*; therefore, point *E* is in the center of the line *DC*. Again, draw a small circle anywhere in the diagram. Select the center of the circle and the line *DC* and constrain the center of the circle to be coincident with the midpoint of *DC*. Draw a line from point *E* to *O*. This completes the *QO* linkage. The *QO* linkage is shown by dashed lines in [Figure 3.81\(d\)](#) along with the other cognates. Note that the *MO* and *QO* linkages are the same except for the crank's being out of phase. By dragging the coupler point in [Figure 3.82\(d\)](#) with the mouse, the motion of all of the cognates can be studied. As in the previous example, the use of GCP not only provides an environment that makes it relatively easy to draw the cognates, but GCP also allows the engineer to study the motion after the models are generated. By varying the dimensions, the effect of changes in the designs can also be studied.



References

1. Arora, J. S. (1989). *Introduction to Optimal Design*. New York, NY: McGraw-Hill.
2. Artas Engineering Software, Het Puyven 162, NL-5672 RJ Nuenen, The Netherlands. (2014). SAM (Synthesis and Analysis of Mechanisms) software. <http://www.artas.nl/en/sam/>.
3. Artobolevsky, Ivan I. (1975). *Mechanisms in Modern Engineering Design*. Moscow, USSR: MIR Publishers.
4. Chironis, Nicholas P., and Slater, Neil, Eds. (1991). *Mechanisms and Mechanical Devices Sourcebook*. New York, NY: McGraw-Hill.
5. Dassault Systèmes SolidWorks Corp. 175 Wyman Street, Waltham, MA 02451. (2014). SolidWorks Solid Modeling Software. <http://www.solidworks.com/>.
6. Delana. (2014). “Moving Art: Unbelievable Kinetic Sculptures of Theo Jansen.” <http://weburbanist.com/2008/10/11/unbelievable-kinetic-sculptures-of-theo-jansen/>.
7. Draijer, Harry, and Kokkeler, Frans. (2002). “Heron’s Synthesis Engine Applied to Linkage Design.” *Proceedings of the 2002 ASME Design Technology Conference*, Montreal, Quebec, Canada, Sept 29–Oct 2, Paper No. DETC2002/MECH-34373.
8. Erdman, A. G., and Gustafson, J. E. (1977). “LINCAGES: Linkage Interactive Computer Analysis and Graphically Enhanced Synthesis Package.” ASME Paper No. 77-DET-5, presented at the Design Engineering Technical Conference, Chicago, IL, USA, September 1977.
9. Erdman, Arthur G., Sandor, George N., and Sridhar, Kota. (2001). *Mechanism Design, Analysis and Synthesis, Volume 1, 4th Ed.* Upper Saddle River, NJ: Prentice Hall.
10. Freudenstein, F. (1959). “Approximate Synthesis of Four-Bar Linkages.” *Transactions of ASME*, Vol. 77, pp. 853–861, August.
11. Hain, Kurt. (1967), *Applied Kinematics, 2nd Ed.* Translated by D. P. Adams, F. R. E. Crossley, F. Freudenstein, T. P. Goodman, B. L. Harding, and D. R. Raichel. New York, NY: McGraw-Hill.
12. Hall, A. S. (1961). *Kinematics and Linkage Design*. West Lafayette, IN: Balt Publishers.
13. Hartenberg, R.S., and Denavit, J. (1964). *Kinematic Synthesis of Linkages*. New York, NY: McGraw-Hill.
14. Horton, Holbrook L., Ed. (1951). *Ingenious Mechanisms for Designers and Inventors, Volume 3*. New York, NY: Industrial Press, Inc.
15. Hrones, J. A., and Nelson, G. L. (1951). *Analysis of the Four-Bar linkage*, Cambridge, MA: The Technology Press of M.I.T. and New York, NY: John Wiley & Sons.
16. Jones, Franklin, Ed. (1936). *Ingenious Mechanisms for Designers and Inventors, Volumes 1 & 2*. New York, NY: Industrial Press, Inc.
17. Kinzel, E. C., Schmiedeler, J. P., and Pennock, G. R. (2006). “Kinematic Synthesis for Finitely Separated Positions Using Geometric Constraint Programming.” *ASME Journal of Mechanical Design*, Vol. 128, No. 5, pp. 1070–1079.
18. Mallik, A. K., Ghosh, A., and Dittrich, G. (1994). *Kinematic Analysis and Synthesis of Mechanisms*. Boca Raton, FL: CRC Press, Inc.
19. Newell, John A., and Horton, Holbrook L., Eds. (1967). *Ingenious Mechanisms for Designers and Inventors, Volume 4*. Industrial Press, Inc. New York, NY: Industrial Press, Inc.
20. Parmley, R. O., Ed. (2000). *Illustrated Sourcebook of Mechanical Components*. New York, NY: McGraw-Hill.

21. Rubel, A. J., and Kaufman, R. E. (1977). "KINSYN III: A New Human-Engineered System for Interactive Computer-Aided Design of Planar Linkages." *ASME Journal of Engineering for Industry*, Vol. 99, No. 2, pp. 440–448.
22. Sandor, G. N., and Erdman, A. G. (1984). *Advanced Mechanism Design: Analysis and Synthesis*. Englewood Cliffs, NJ: Prentice Hall.
23. Schmiedeler, J. P. (2008). "Workshop: Planar, Rigid-Body Mechanism Synthesis Using Geometric Constraint Programming." ASME 2008 Design Engineering Technical Conferences and Computer and Information in Engineering Conference, New York, NY, August 3, 2008.
24. Siemens PLM Software, 5800 Granite Parkway, Suite 600, Plano, TX 75024. (2014). Solid Edge Solid Modeling Software. http://www.plm.automation.siemens.com/en_us/products/velocity/solidedge/.
25. Siemens PLM Software, 5800 Granite Parkway, Suite 600, Plano, TX 75024. (2014). Solid Edge 2D Drafting software. http://www.plm.automation.siemens.com/en_us/products/velocity/solidedge/free2d/.
26. Song, S.-M. (1981). *Theoretical and Numerical Improvements to Computer-Aided Linkage Design*. Ph.D. Dissertation, The Ohio State University.
27. Soni, A. H. (1974). *Mechanism Synthesis and Analysis*. New York, NY: McGraw-Hill.
28. Suh, C. H., and Radcliffe, C. W. (1978). *Kinematics and Mechanisms Design*. New York, NY: John Wiley & Sons, Inc.
29. Sumitomo Heavy Industries Material Handling Systems Co., Ltd. (2014). <http://www.shi.co.jp/shi-mh/english/product/jibcrane.html>.
30. Thomaszewski, B. et al. (2013). "Computational Design of Mechanical Characters." ACM transactions on Graphics (TOG) – SIGGRAPH 2013 Conference Proceedings, Vol. 32, Issue 4, Article No. 83, July 2013.
31. Thompson, T. (2014). "Four-bar Coupler Curve and Centrode Atlas." Centerville University. <http://www.cedarville.edu/cf/engineering/kinematics/ccapdf/fccca.htm>.
32. Waldron, K. J. (1974). "Range of Joint Rotation in Planar Four-Bar Synthesis for Finitely Separated Positions: Part I-The Multiple Branch Problem." ASME Paper No. 74-DET-108, presented at the Design Engineering Technical Conference, New York, NY.
33. Waldron, K. J. (1974). "Range of Joint Rotation in Planar Four-Bar Synthesis for Finitely Separated Positions: Part II-Elimination of Unwanted Grashof Configurations." ASME Paper No. 74-DET-109, presented at the Design Engineering Technical Conference, New York, NY.
34. Waldron, K. J. (1975). "The Order Problem of Burmester Linkage Synthesis." *ASME Journal of Engineering for Industry*, Vol. 97, No. 4, pp. 1405–1406.
35. Waldron, K. J. (1976). "Elimination of the Branch Problem in Graphical Burmester Mechanism Synthesis for Four Finitely Separated Positions." *ASME Journal of Engineering for Industry*, Vol. 98, No. 1, pp. 176–182.
36. Waldron, K. J. (1977). "Graphical Solution of the Branch and Order Problems of Linkage Synthesis for Multiply Separated Positions." *ASME Journal of Engineering for Industry*, Vol. 99, No. 3, pp. 591–597.
37. Waldron, K. J. (1978). "Location of Burmester Synthesis Solutions with Fully Rotatable Cranks." *Mechanism and Machine Theory*, Vol. 13, No. 2, pp. 125–137.



Problems

Double-Rocker Linkages

- 3.1 Design a double-rocker, four-bar linkage so that the base link is 2 in and the output rocker is 1 in long. The input link turns counterclockwise 60° when the output link turns clockwise through 90° . The initial angle for the input link is 30° counterclockwise from the horizontal, and the initial angle for the output link is -45° . The geometry is indicated in [Figure P3.1](#).

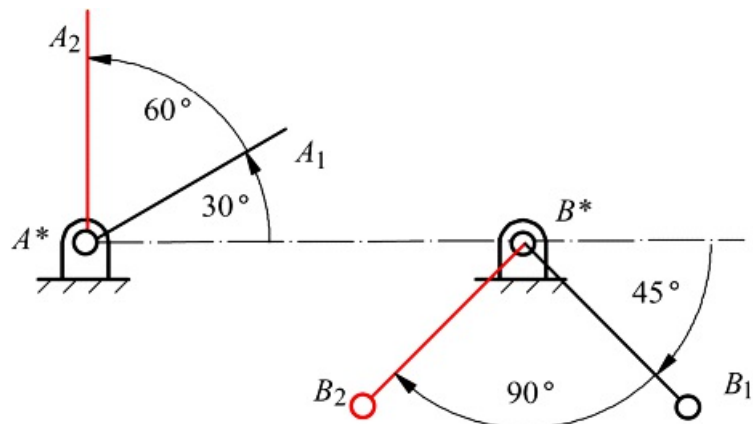


[Figure P3.1](#) Positions for Problem 3.1.

- 3.2 Design a double-rocker, four-bar linkage so that the base link is 4 in and the output rocker is 2 in long. The input link turns counterclockwise 40° when the output link turns counterclockwise through 80° . The initial angle for the input link is 20° counterclockwise from the horizontal, and the initial angle for the output link is 25° . The geometry is indicated in [Figure P3.2](#).

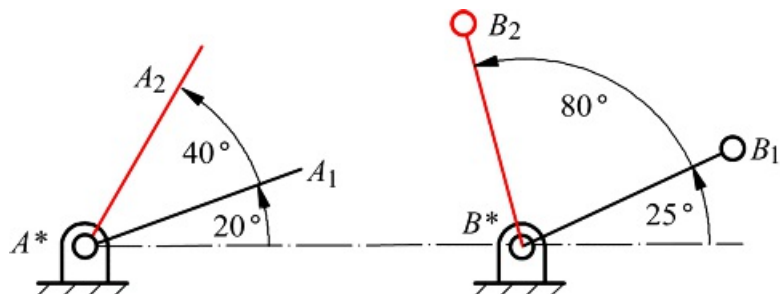


[Figure P3.2](#) Positions for Problem 3.2.

- 3.3 In a backhoe, a four-bar linkage is added at the bucket, in part to amplify the motion that can be achieved by the hydraulic cylinder attached to the pin of the link that rotates the bucket, as shown in the figure. The link attached to the bucket and the input link is the frame link. It is 8 in long, and the input link is 12 in long. The input link driven by the hydraulic cylinder rotates through an angle of 80° and the output link (the bucket) rotates through an angle of 120° . From [Figure P3.3](#), estimate reasonable values for the starting angles (θ_0 and ϕ_0) for both of the rockers and determine lengths for the coupler and output link to which the bucket is attached.



[Figure P3.3](#) Backhoe linkage for Problem 3.3.

3.4 The lid of the bin, B^*B , shown in [Figure P3.4](#), is to be opened by means of the foot pedal, A^*A . With A^* and B^* located as shown, find suitable positions for A and B so that B rotates through 90° about B^* when A^*A rotates through 15° . The lines A^*A and B^*B are to be horizontal when the lid is closed.

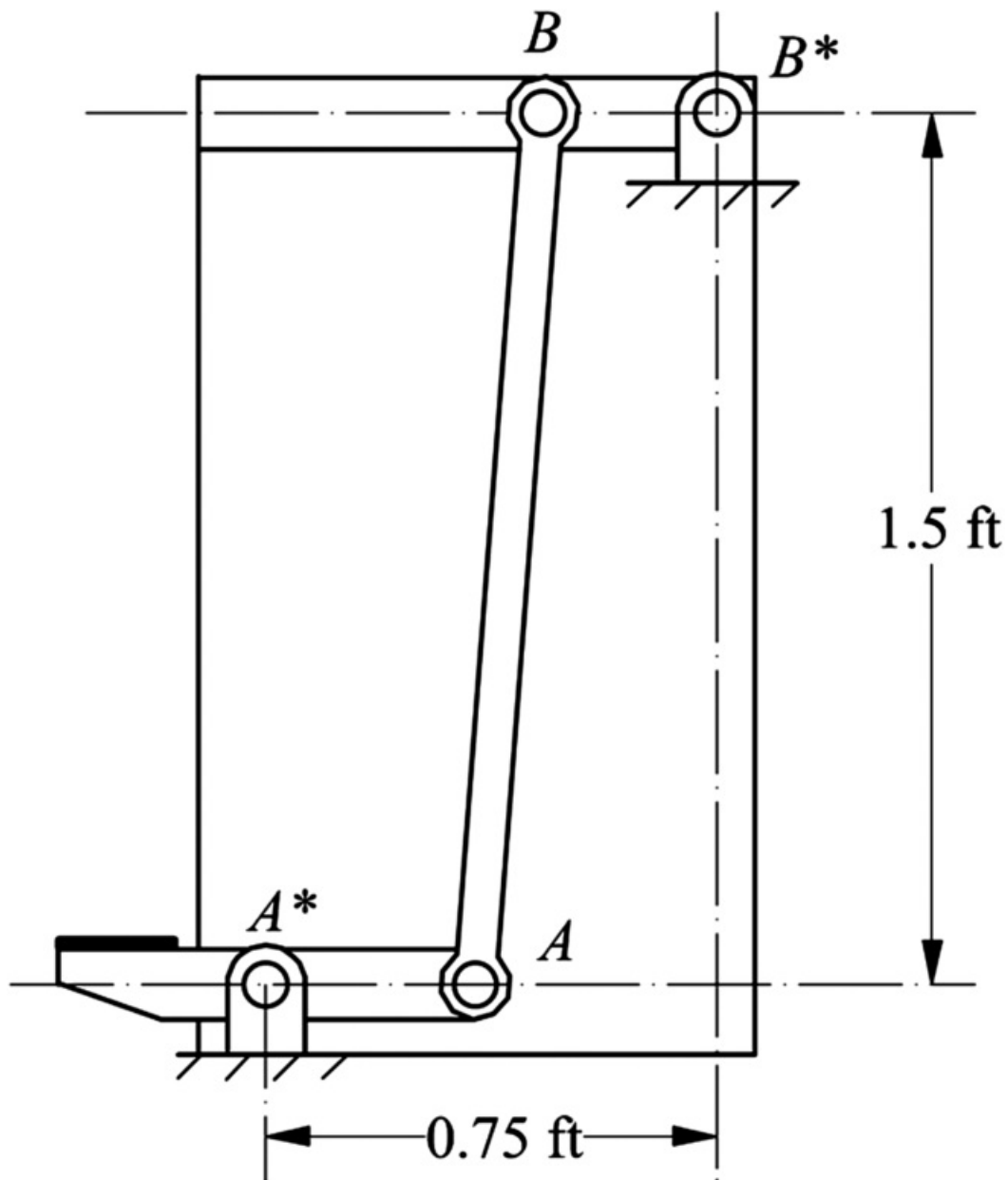


[Figure P3.4](#) Bin linkage for Problem 3.4.

3.5 A four-bar linkage is often used to retract the saw guard on a cutoff saw as the saw is moved into a piece of wood. A typical saw is shown in its lowest position in [Figure P3.5](#). If r_2 rotates 47° when r_4 rotates 52° , design an appropriate linkage to rotate the blade guard. Assume that r_1 is $2''$ and r_4 is $9 \frac{1}{2}''$. What is the total rotation of link 3 relative to the frame for your design?



[Figure P3.5](#) Positions for Problem 3.5.

- 3.6 Use GCP to develop a graphical design program and solve Problem 3.1.
- 3.7 Use GCP to develop a graphical design program and solve Problem 3.2.
- 3.8 Use GCP to develop a graphical design program and solve Problem 3.3.
- 3.9 Use GCP to develop a graphical design program and solve Problem 3.4.
- 3.10 Use GCP to develop a graphical design program and solve Problem 3.5.

Rigid-Body Guidance Linkages

- 3.11 In [Figure P3.11](#), $AB = 1.25$ cm. Use A and B as circle points, and design a four-bar linkage to move its coupler through the three positions shown. Use Grashof's equation to identify the type of four-bar linkage designed.

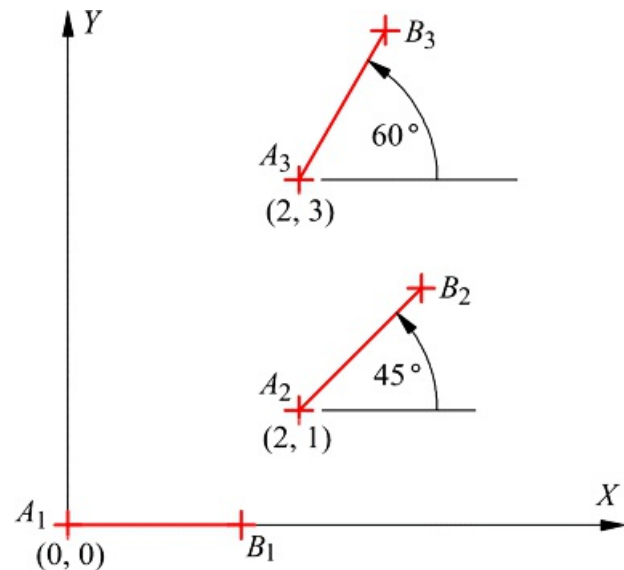


[Figure P3.11](#) Positions for Problem 3.11.

- 3.12 Using points A and B as circle points, design a four-bar linkage that will position the body defined by AB in the three positions shown in [Figure P3.12](#). Draw the linkage in position 1, and use Grashof's equation to identify the type of four-bar linkage designed. Position A_1B_1 is horizontal, and position A_2B_2 is vertical. $AB = 1.5$ in.

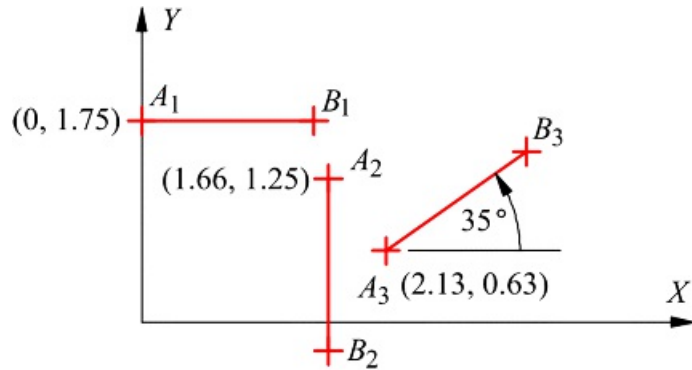


[Figure P3.12](#) Positions for Problem 3.12.

3.13 Design a four-bar linkage to move its coupler through the three positions shown in [Figure P3.13](#) using points A and B as moving pivots. $AB = 4$ cm. What is the Grashof type of the linkage generated?

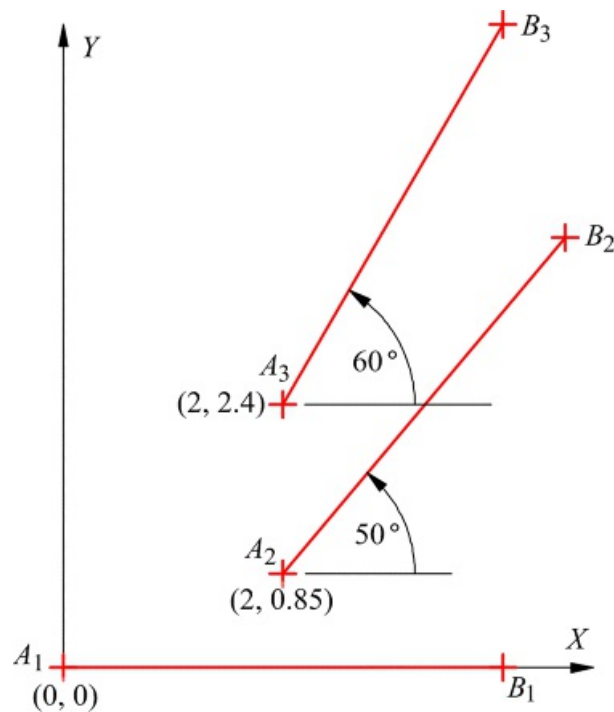


[Figure P3.13](#) Positions for Problem 3.13.

3.14 A four-bar linkage is to be designed to move its coupler plane through the three positions shown in [Figure P3.14](#). The moving pivot (circle point) of one crank is at A and the fixed pivot (center point) of the other crank is at C^* . Draw the linkage in position 1 and use Grashof's equation to identify the type of four-bar linkage designed. Also determine whether the linkage changes branch in traversing the design positions. Positions A_1B_1 and A_2B_2 are horizontal, and position A_3B_3 is vertical. $AB = 3$ in.

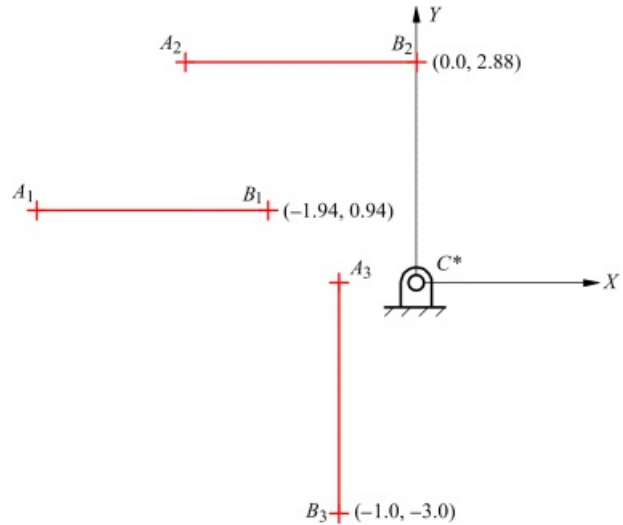


[Figure P3.14](#) Positions for Problem 3.14.

3.15 Design a four-bar linkage to move a coupler containing the line AB through the three positions shown in [Figure P3.15](#). The moving pivot (circle point) of one crank is at A and the fixed pivot (center point) of the other crank is at C^* . Draw the linkage in position 1 and use Grashof's equation to identify the type of four-bar linkage designed. Position A_1B_1 is horizontal, and positions A_2B_2 and A_3B_3 are vertical. $AB = 4$ in.

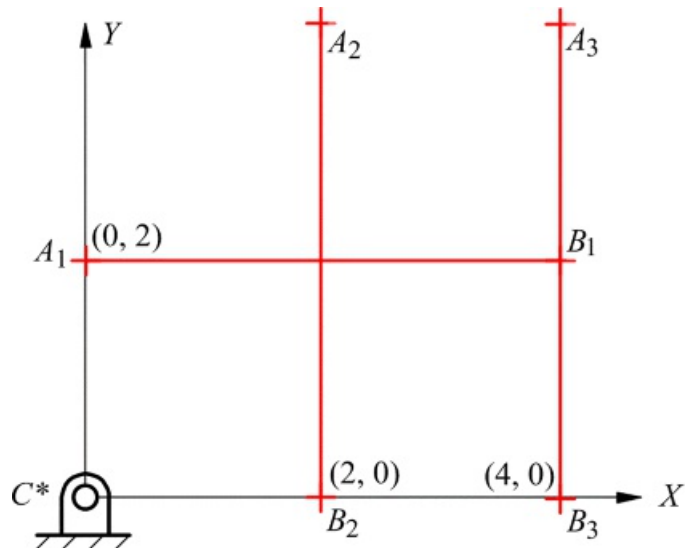


[Figure P3.15](#) Positions for Problem 3.15.

3.16 A mechanism must be designed to move a computer terminal from under the desk to top level, as shown in [Figure P3.16](#). The system will be guided by a linkage, and the use of a four-bar linkage will be tried first. As a first attempt at the design, do the following:

- a. Use C^* as a center point and find the corresponding circle point C in position 1.
- b. Use A as a circle point and find the corresponding center point A^* .
- c. Draw the linkage in position 1.
- d. Determine the type of linkage (crank-rocker, double-rocker, etc.) resulting.
- e. Evaluate the linkage to determine whether you would recommend that it be manufactured.

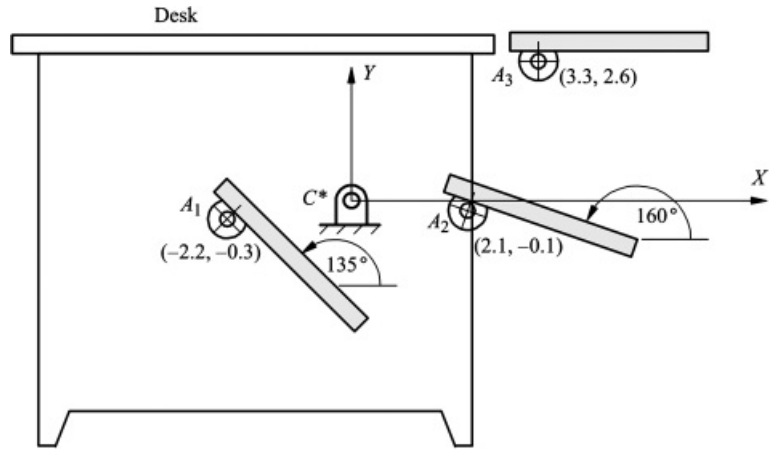


[Figure P3.16](#) Positions for Problem 3.16.

3.17 Design a four-bar linkage to move the coupler containing line segment AB through the three positions shown in [Figure P3.17](#). The moving pivot for one crank is to be at A , and the fixed pivot for the other crank is to be at C^* . Draw the linkage in position 1 and determine the classification of the resulting linkage (e.g., crank-rocker, double-crank). Positions A_2B_2 and A_3B_3 are horizontal, and position A_1B_1 is vertical. $AB = 3.5$ in.

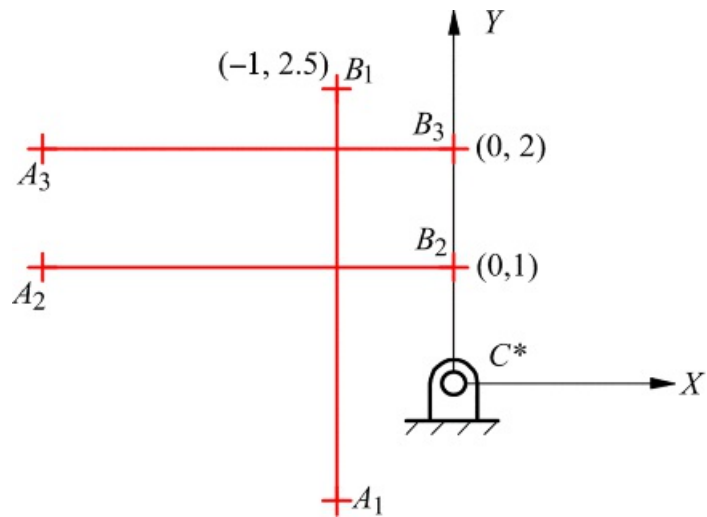


[Figure P3.17](#) Positions for Problem 3.17.

3.18 Design a four-bar linkage to move a coupler containing the line AB through the three positions shown in [Figure P3.18](#). The moving pivot (circle point) of one crank is at A and the fixed pivot (center point) of the other crank is at C^* . Draw the linkage in position 1, and use Grashof's equation to identify the type of four-bar linkage designed. Position A_1B_1 is horizontal, and positions A_2B_2 and A_3B_3 are vertical. $AB = 6$ cm.

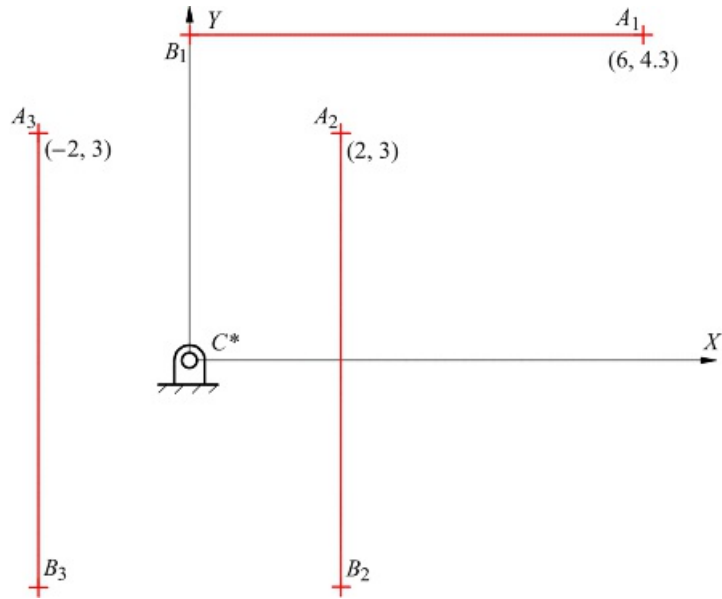


[Figure P3.18](#) Positions for Problem 3.18.

3.19 Design a four-bar linkage to move the coupler containing line segment AB through the three positions shown in [Figure P3.19](#). The moving pivot for one crank is to be at A , and the fixed pivot for the other crank is to be at C^* . Draw the linkage in position 1 and determine the classification of the resulting linkage (e.g., crank rocker, double crank). Also check to determine whether the linkage will change branch as it moves from one position to another. Position A_1B_1 is horizontal, and position A_3B_3 is vertical. $AB = 5.1$ cm.

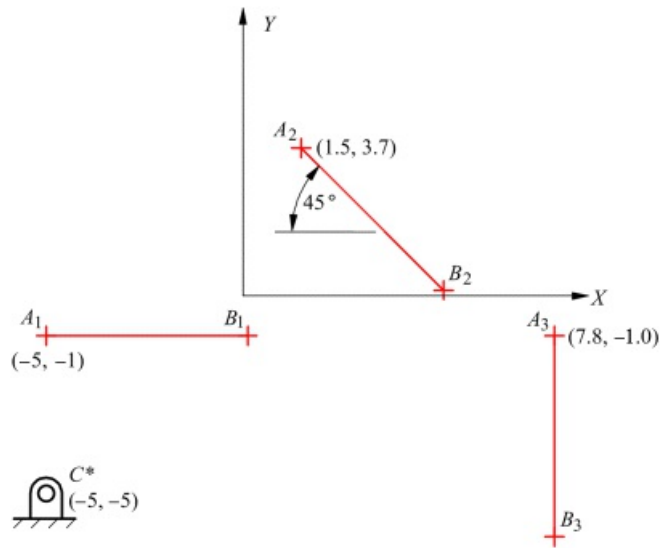


[Figure P3.19](#) Positions for Problem 3.19.

3.20 Synthesize a four-bar mechanism in position 2 that moves its coupler through the three positions shown in [Figure P3.20](#) if points C^* and D^* are center points. Position A_1B_1 and position A_3B_3 are horizontal. $AB = 4$ cm.

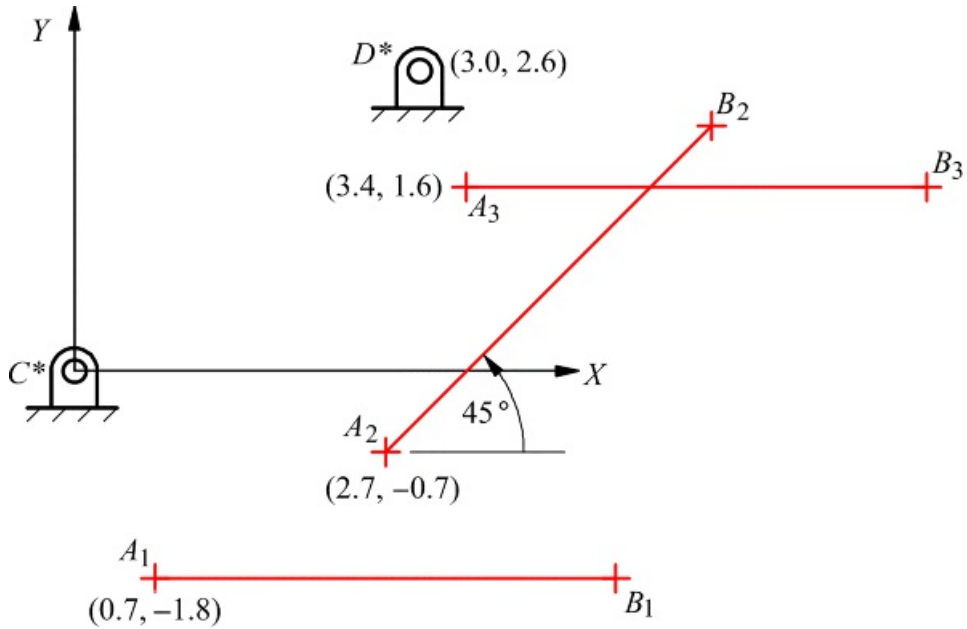


[Figure P3.20](#) Positions for Problem 3.20.

3.21 Synthesize a four-bar mechanism in position 2 that moves its coupler through the three positions shown in [Figure P3.21](#). Point A is a circle point, and point C^* is a center point. Position A_1B_1 and position A_3B_3 are horizontal. $AB = 4$ cm.

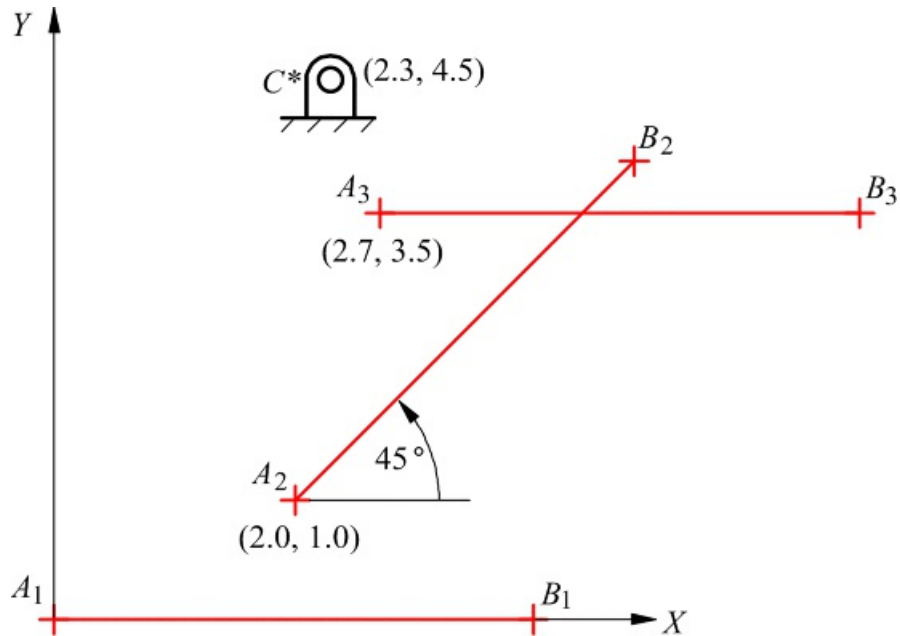


[Figure P3.21](#) Positions for Problem 3.21.

3.22 A hardware designer wants to use a four-bar linkage to guide a door through the three positions shown in [Figure P3.22](#). Position 1 is horizontal, and position 3 is vertical. As a tentative design, she selects point B^* as a center point and A as a circle point. For the three positions shown, determine the location of the circle point B corresponding to the center point B^* and the center point A^* corresponding to the circle point A . Draw the linkage in position 1 and determine the Grashof type for the linkage. Indicate whether you think that this linkage should be put into production.

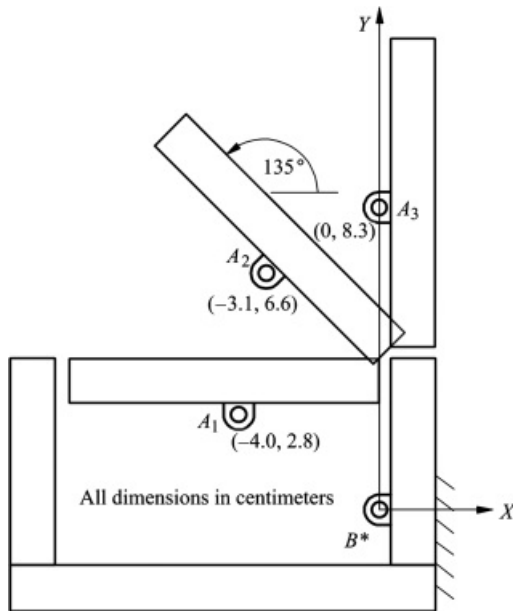


Figure P3.22 Positions for Problem 3.22.

3.23 Design a slider-crank mechanism to move the coupler containing line segment AB through the three positions shown in Figure P3.23. The moving pivot for the crank is to be at A. Determine the slider point, and draw the linkage in position 1. Also check to determine whether the linkage will move from one position to another without being disassembled. Position A₁B₁ is horizontal, and position A₃B₃ is vertical. AB = 2.0 in.

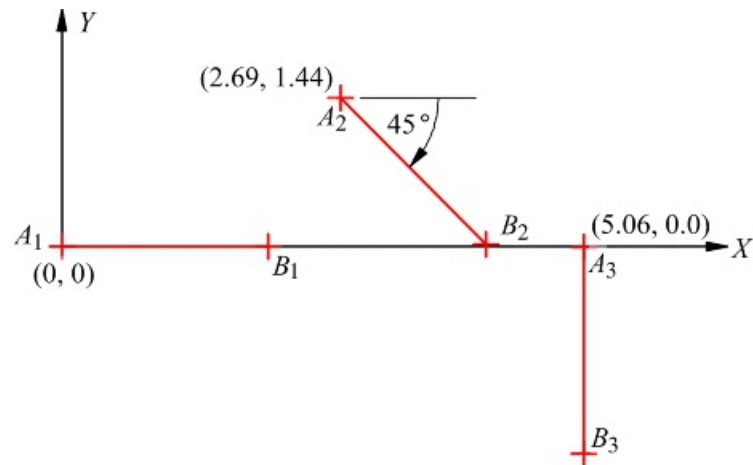
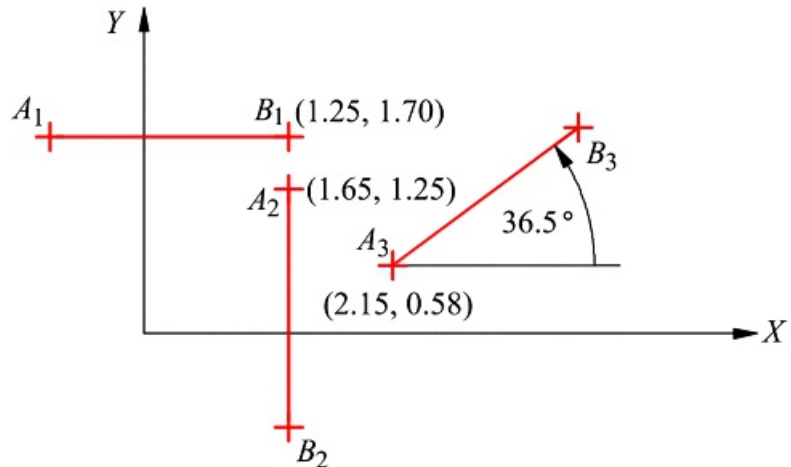


Figure P3.23 Positions for Problem 3.23.

3.24 Design a slider-crank mechanism to move a coupler containing the line AB through the three positions shown in Figure P3.24. The moving pivot (circle point) of the crank is at A. Find A* and the slider point that lies above B₁ on a vertical line through B₁, and draw the linkage in position 1.



[Figure P3.24](#) Positions for Problem 3.24.

3.25 Design a slider-crank linkage to move a coupler containing the line AB through the three positions shown in [Figure P3.25](#). The fixed pivot (center point) of the other crank is at C^* . Draw the linkage (including the slider line) in Position 1. Position A_1B_1 is horizontal, and positions A_2B_2 and A_3B_3 are vertical. $AB = 4$ in.

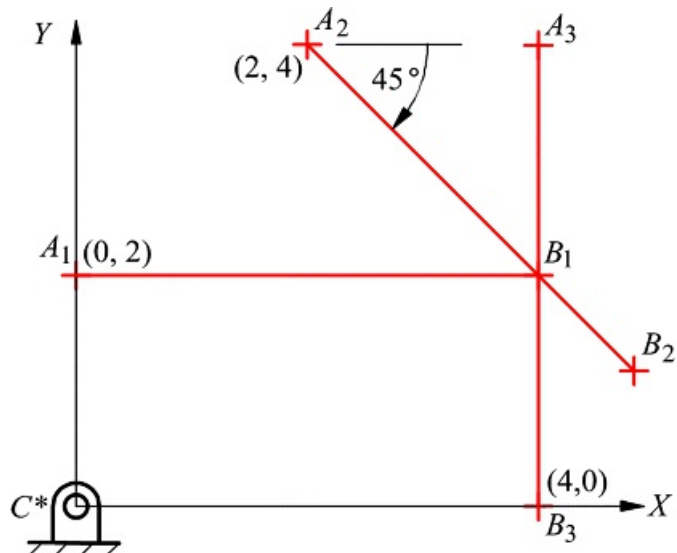


[Figure P3.25](#) Positions for Problem 3.25.

3.26 Design a slider-crank mechanism to move a coupler containing the line AB through the three positions shown in [Figure P3.26](#). The moving pivot (circle point) of the crank is at A . Find the slider point that lies on Line BC and draw the linkage (including the slider line) in position 1. Note that Line BC is NOT the line on which the slider moves.

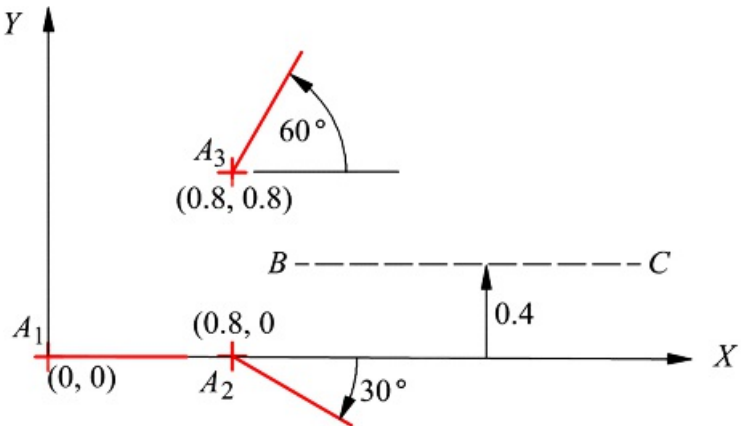


Figure P3.26 Positions for Problem 3.26.

- 3.27** Use GCP to develop a graphical design program and solve Problem 3.11. Animate the linkage and check if a branch problem exists.
- 3.28** Use GCP to develop a graphical design program and solve Problem 3.12. Animate the linkage and check if a branch problem exists.
- 3.29** Use GCP to develop a graphical design program and solve Problem 3.13. Animate the linkage and check if a branch problem exists.
- 3.30** Use GCP to develop a graphical design program and solve Problem 3.14. Animate the linkage and check if a branch problem exists.
- 3.31** Use GCP to develop a graphical design program and solve Problem 3.15. Animate the linkage and check if a branch problem exists.
- 3.32** Use GCP to develop a graphical design program and solve Problem 3.16. Animate the linkage and check if a branch problem exists.
- 3.33** Use GCP to develop a graphical design program and solve Problem 3.17. Animate the linkage and check if a branch problem exists.
- 3.34** Use GCP to develop a graphical design program and solve Problem 3.18. Animate the linkage and check if a branch problem exists.
- 3.35** Use GCP to develop a graphical design program and solve Problem 3.19. Animate the linkage and check if a branch problem exists.
- 3.36** Use GCP to develop a graphical design program and solve Problem 3.20. Animate the linkage and check if a branch problem exists.
- 3.37** Use GCP to develop a graphical design program and solve Problem 3.21. Animate the linkage and check if a branch problem exists.
- 3.38** Use GCP to develop a graphical design program and solve Problem 3.22. Animate the linkage and check if a branch problem exists.
- 3.39** Use GCP to develop a graphical design program and solve Problem 3.23. Animate the linkage and check if a branch problem exists.
- 3.40** Use GCP to develop a graphical design program and solve Problem 3.24. Animate the linkage and check if a branch problem exists.
- 3.41** Use GCP to develop a graphical design program and solve Problem 3.25. Animate the linkage and check if a branch problem exists.
- 3.42** Use GCP to develop a graphical design program and solve Problem 3.27. Animate the linkage and check if a branch problem exists.

Crank-Rocker Mechanisms

3.43 The output arm of a lawn sprinkler is to rotate through an angle of 90° , and the ratio of the times for the forward and reverse rotations is to be 1 to 1. Design the crank-rocker mechanism for the sprinkler. If the crank is to be 1 in long, give the lengths of the other links.

3.44 Design a crank-rocker mechanism such that with the crank turning at constant speed, the oscillating lever will have a time ratio of advance to return of 3:2. The lever is to oscillate through an angle of 80° , and the length of the base link is to be 2 in.

3.45 A packing mechanism, shown in [Figure P3.45](#), requires that the crank (r_2) rotate at a constant velocity. The advance part of the cycle is to take twice as long as the return to give a quick-return mechanism. The distance between fixed pivots must be 0.5 m. Determine the lengths for r_2 , r_3 , and r_4 .

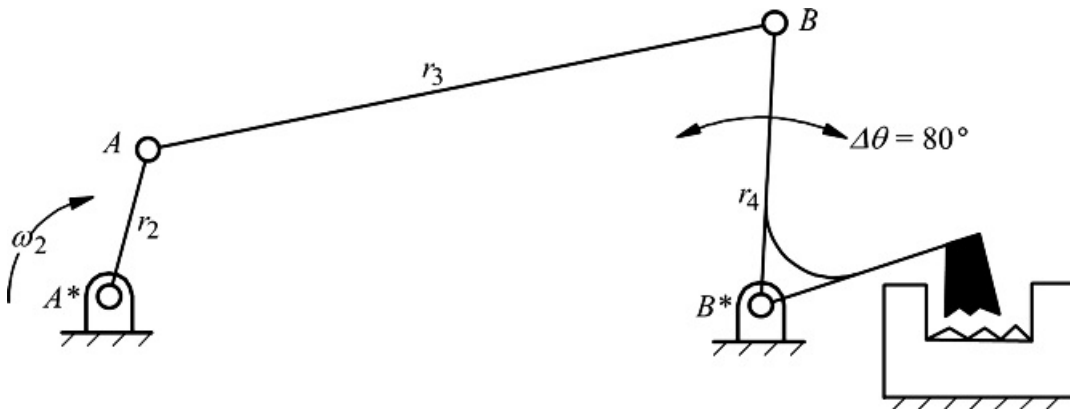


[Figure P3.45](#) Crank-rocker linkage for Problem 3.45.

3.46 The rocker B^*B of a crank-rocker linkage swings symmetrically about the vertical through a total angle of 70° . The return motion should take 0.75 the time that the forward motion takes. Assuming that the two ground pivots are 2.5 in apart, find the length of each of the links.

3.47 A crank-rocker is to be designed such that with the crank turning at a constant speed, the rocker will have a time ratio of advance to return of 1.25. The rocking angle is to be 40° , and it rocks symmetrically about a vertical line through B^* . Assume that the two pivots are on the same horizontal line, 3 in apart.

3.48 Design a crank-rocker mechanism that has a base length of 2.0 in, a time ratio of 1.3, and a rocker oscillation angle of 100° . The oscillation is to be symmetric about a vertical line through B^* . Specify the length of each of the links.

3.49 A crank-rocker mechanism with a time ratio of $\frac{2}{3}$ and a rocker oscillation angle of 72° is to be designed. The oscillation is to be symmetric about a vertical line through B^* . Draw the mechanism in any position. If the length of the base link is 2 in, give the lengths of the other three links. Also show the transmission angle in the position in which the linkage is drawn.

3.50 The mechanism shown in [Figure P3.50](#) is used to drive an oscillating, sanding drum. The drum is rotated by a splined shaft that is cycled vertically. The vertical motion is driven by a four-bar linkage through a rack-and-pinion gear set (model as a rolling contact joint). The total vertical travel for the sander drum is 3 in, and the pinion has a 2 in radius. The sander mechanism requires that the crank (r_2) rotate at a constant velocity, and the advance part of the cycle is to take the same amount of time as the return part. The distance between fixed pivots must be 4 in. Determine the lengths for r_2 , r_3 , and r_4 .

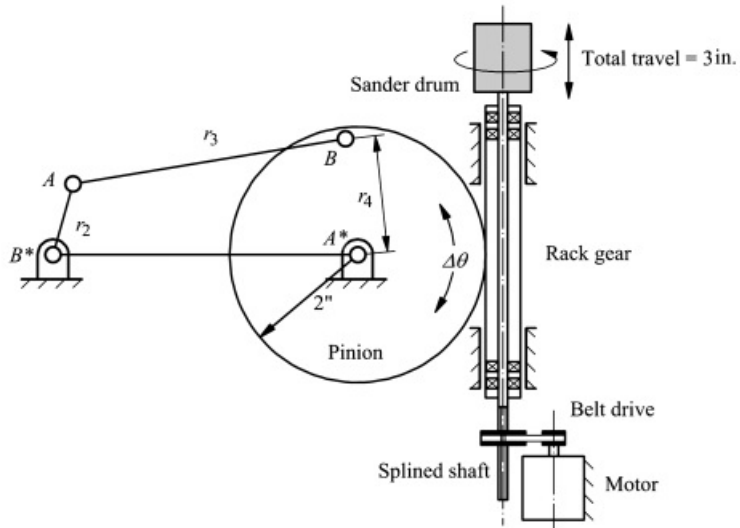


[Figure P3.50](#) Crank-rocker linkage for Problem 3.50.

3.51 The mechanism shown schematically in [Figure P3.51](#) is proposed for a rock crusher. The crusher hammer rotates through an angle of 20° , and the gear ratio R_G/R_p is 4:1, that is, the radius r_G is four times the radius r_p . Contact between the two gears can be treated as rolling contact. The crusher mechanism requires that the crank (r_2) rotate at a constant velocity, and the advance part of the cycle is to take 1.5 times as much as the return part. The distance between fixed pivots A^* and B^* must be 4 ft. Determine the lengths for r_2 , r_3 , and r_4 .

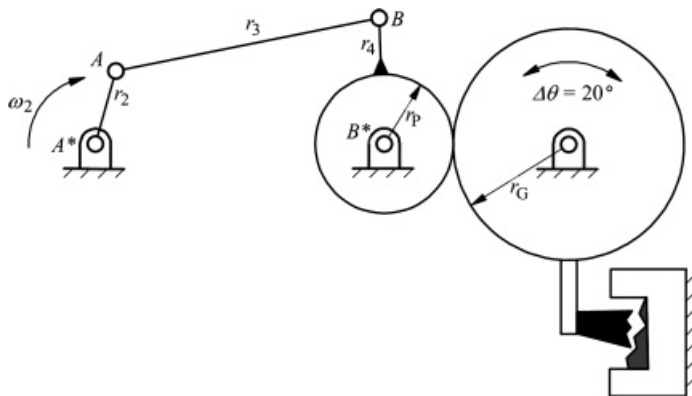


[Figure P3.51](#) Crank-rocker linkage for Problem 3.51.

3.52 The mechanism shown in [Figure P3.52](#) is proposed for a shaper mechanism. The shaper cutter moves back and forth such that the forward (cutting) stroke takes twice as much time as the return stroke. The crank (r_2) rotates at a constant velocity. The follower link (r_4) is to be 4 in and to oscillate through an angle of 80° . Determine the lengths for r_1 , r_2 , and r_3 .

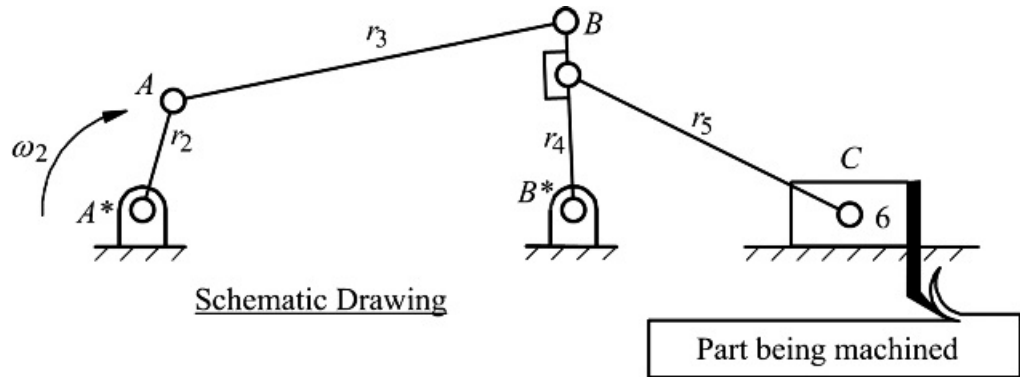


[Figure P3.52](#) Shaper linkage for Problem 3.52.

3.53 A crank-rocker is to be used in the door-closing mechanism shown in [Figure P3.53](#). The door must open 100°. The crank motor is controlled by a timer mechanism such that it pauses when the door is fully open. Because of this, the mechanism can open and close the door in the same amount of time. If the crank (r_2) of the mechanism is to be 10 cm long, determine the lengths of the other links (r_1 , r_3 , and r_4). Sketch the mechanism to scale.

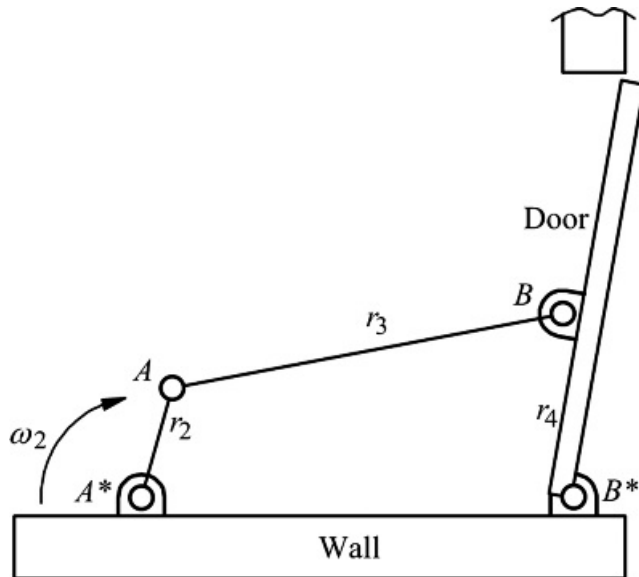


[Figure P3.53](#) Crank-rocker linkage for Problem 3.53.

3.54 A crank-rocker is to be used for the rock crusher mechanism shown in [Figure P3.54](#). The oscillation angle for the rocker is to be 80°, and the working (crushing) stroke for the rocker is to be 1.1 times the return stroke. If the frame link (r_1) of the mechanism is to be 10 ft long, determine the lengths of the other links (r_2 , r_3 , and r_4). Sketch the mechanism to scale.

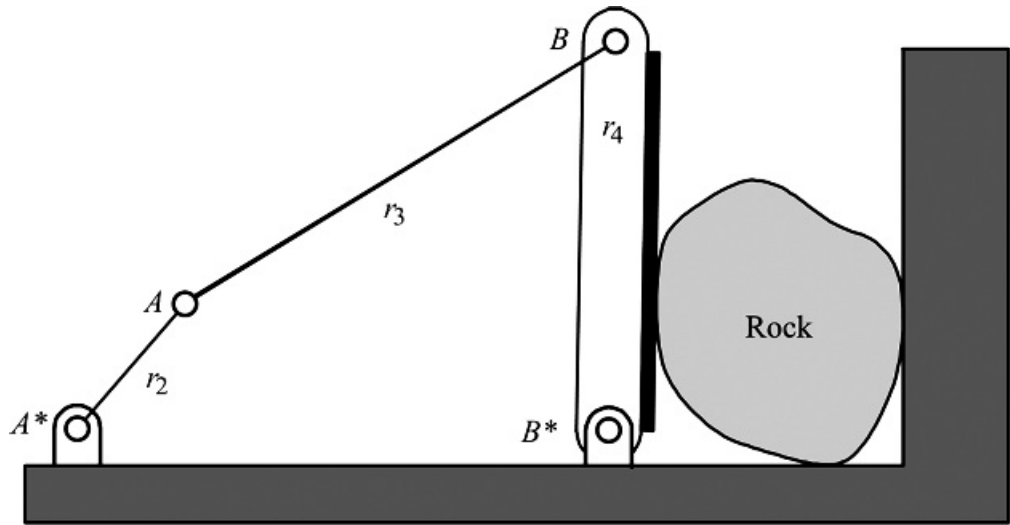


[Figure P3.54](#) Crank-rocker linkage for Problem 3.54.

3.55 A crank-rocker is to be used in the windshield-wiping mechanism shown in [Figure P3.55](#). The wiper must oscillate 80° . The times for the forward and return strokes for the wiper are the same. If the base link (r_1) of the mechanism is to be 10 cm long, determine the lengths of the other links (r_2 , r_3 , and r_4). Sketch the mechanism to scale.

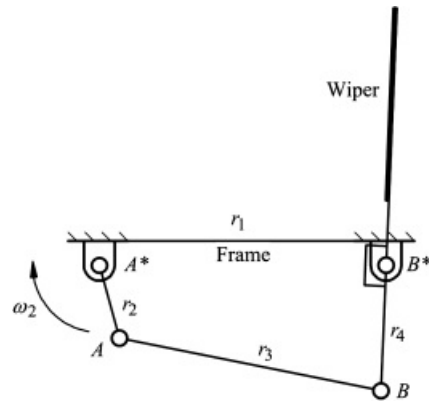


[Figure P3.55](#) Crank-rocker linkage for Problem 3.55.

3.56 Use GCP to develop a graphical design program and solve Problem 3.43. Also determine the maximum and minimum transmission angle and animate the linkage.

3.57 Use GCP to develop a graphical design program and solve Problem 3.44. Also determine the maximum and minimum transmission angle and animate the linkage.

3.58 Use GCP to develop a graphical design program and solve Problem 3.45. Also determine the maximum and minimum transmission angle and animate the linkage.

3.59 Use GCP to develop a graphical design program and solve Problem 3.46. Also determine the maximum and minimum transmission angle and animate the linkage.

3.60 Use GCP to develop a graphical design program and solve Problem 3.47. Also determine the maximum and minimum transmission angle and animate the linkage.

3.61 Use GCP to develop a graphical design program and solve Problem 3.48. Also determine the maximum and minimum transmission angle and animate the linkage.

3.62 Use GCP to develop a graphical design program and solve Problem 3.49. Also determine the maximum and minimum transmission angle and animate the linkage.

3.63 Use GCP to develop a graphical design program and solve Problem 3.50. Also determine the maximum

and minimum transmission angle and animate the linkage.

3.64 Use GCP to develop a graphical design program and solve Problem 3.51. Also determine the maximum and minimum transmission angle and animate the linkage.

3.65 Use GCP to develop a graphical design program and solve Problem 3.52. Also determine the maximum and minimum transmission angle and animate the linkage.

3.66 Use GCP to develop a graphical design program and solve Problem 3.53. Also determine the maximum and minimum transmission angle and animate the linkage.

3.67 Use GCP to develop a graphical design program and solve Problem 3.54. Also determine the maximum and minimum transmission angle and animate the linkage.

3.68 Use GCP to develop a graphical design program and solve Problem 3.55. Also determine the maximum and minimum transmission angle and animate the linkage.

Path-Generation Linkages

3.69 Design a six-bar linkage like that shown in [Figure 3.57](#) such that the output link will do the following for one complete revolution of the input crank:

1. Rotate clockwise by 30° for a clockwise rotation of 210° of the input crank.
2. Rotate counterclockwise by 30° for a clockwise rotation of 150° of the input crank.

3.70 Design a six-bar linkage like that shown in [Figure 3.57](#) such that the output link will make two complete 35° oscillations for each revolution of the driving link. (Hint: Select a coupler curve that is shaped like a figure 8.)

3.71 Design a six-bar linkage like that shown in [Figure 3.57](#) such that the output link will do the following for one complete revolution of the input crank:

1. Rotate clockwise by 40°
2. Rotate counterclockwise by 35°
3. Rotate clockwise by 30°
4. Rotate counterclockwise by 35°

(Hint: Select a figure 8- or kidney bean-shaped coupler curve.)

3.72 Design a six-bar linkage like that shown in [Figure 3.57](#) such that the displacement of the output link (link 6) is the given function of the input link rotation. The output displacement reaches maximum values of 30° and 60° at input rotations of 60° and 240° , respectively. The rotation of the output link is zero when the input rotation angle is 0° , 120° , and 360° .

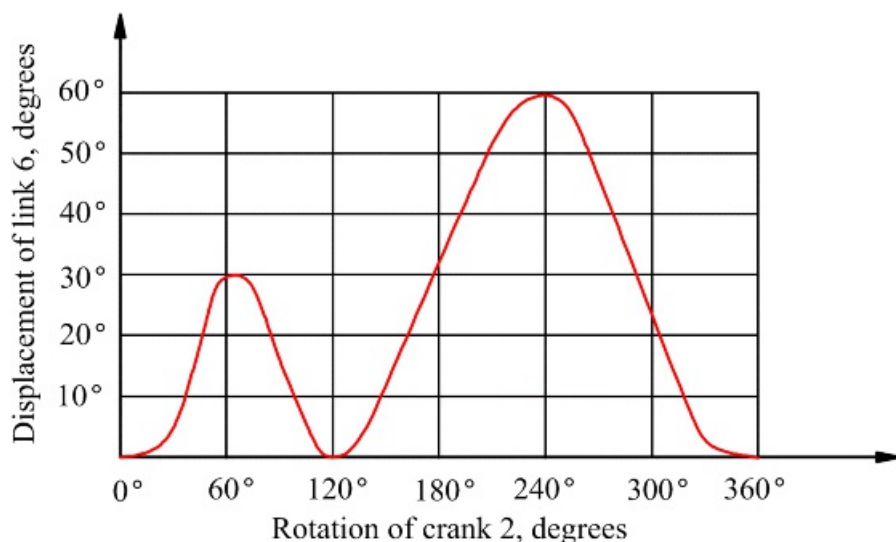


Figure P3.72 Motion profile for Problem 3.72.

3.73 Design a six-bar linkage like that shown in [Figure 3.57](#) such that the displacement of the output link (link 6) is the given function of the input link rotation. The output link dwells for 90° of input rotation starting at 0° and 180°. The maximum rotation angle for link 6 is 15°.

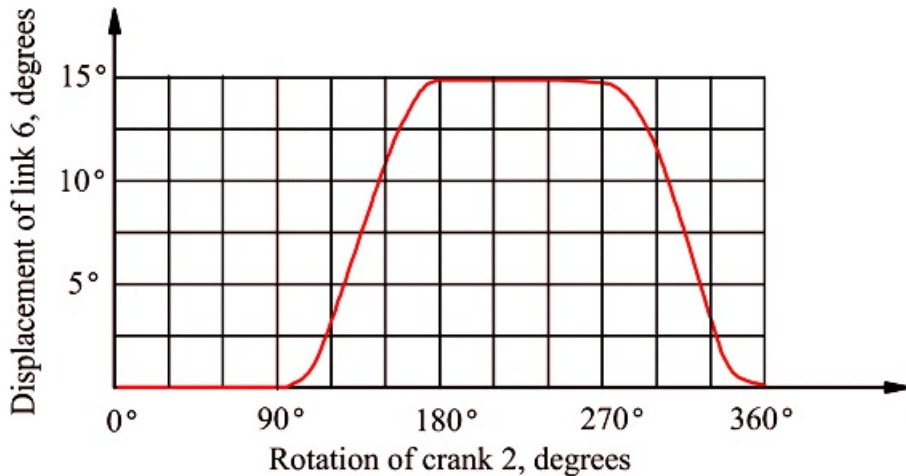


Figure P3.73 Motion profile for Problem 3.73.

3.74 Design an eight-bar linkage like that shown in [Figure 3.67](#) such the coupler remains horizontal while the given point on the coupler moves approximately along the path given.

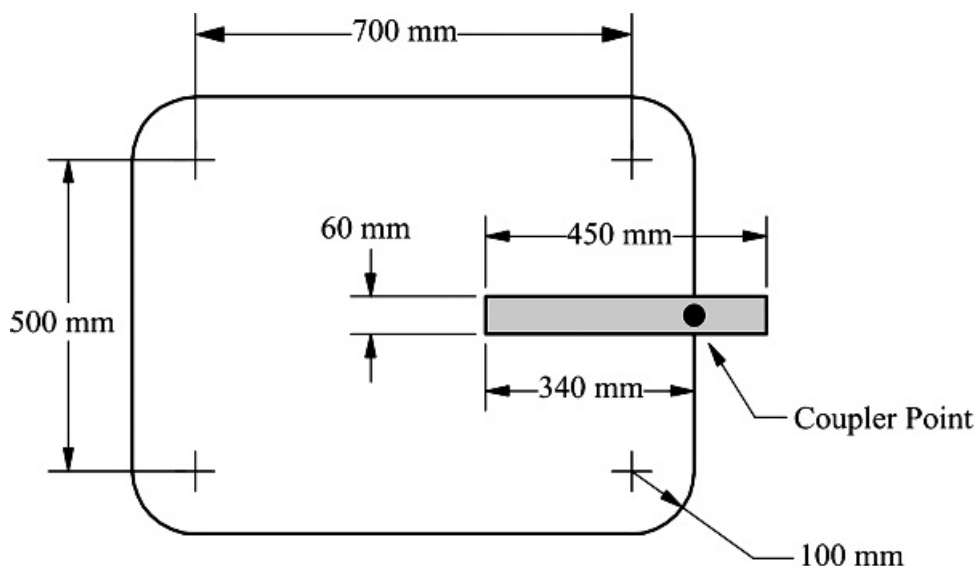


Figure P3.74 Coupler curve for Problem 3.74.

3.75 Resolve Problem 3.75 if the coupler is inclined at an angle of 45°.

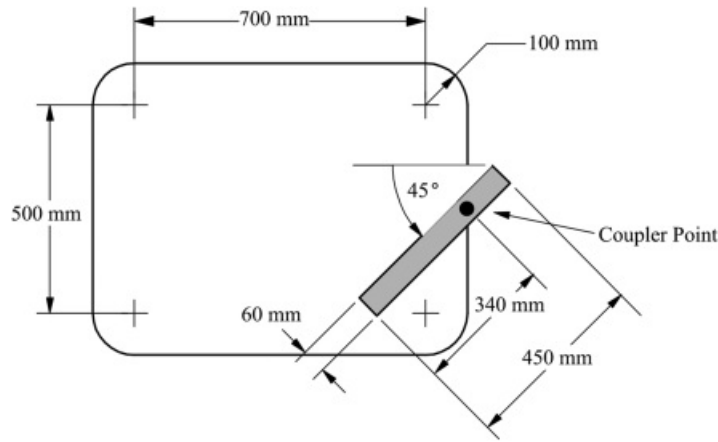


Figure P3.75 Coupler curve for Problem 3.75.

3.76 Design an eight-bar linkage like that shown in [Figure 3.67](#) such that the coupler remains horizontal while the given point on the coupler moves *approximately* along the path from *A* to *B* to *C*. The coupler can return either by retracing the path from *C* to *B* to *A* or by going directly from *C* to *A*. This means that the basic four-bar linkage need not be a crank-rocker.

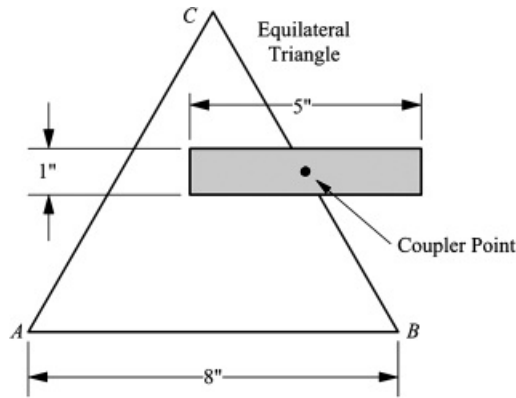


Figure P3.76 Coupler curve for Problem 3.76.

3.77 Use GCP to solve Problem 3.69 and to animate the linkage.

3.78 Use GCP to solve Problem 3.70 and to animate the linkage.

3.79 Use GCP to solve Problem 3.71 and to animate the linkage.

3.80 Use GCP to solve Problem 3.72 and to animate the linkage.

3.81 Use GCP to solve Problem 3.73 and to animate the linkage.

3.82 Use GCP to solve Problem 3.74 and to animate the linkage.

3.83 Use GCP to solve Problem 3.75 and to animate the linkage.

3.84 Use GCP to solve Problem 3.76 and to animate the linkage.

Cognate Linkage Exercise Problems

3.85 Determine the two four-bar linkages cognate to the one shown in [Figure P3.85](#). The dimensions are $A^*A = 10$ cm, $AB = 16$ cm, $AC = 32$ cm, $B^*B = 21$ cm, and $A^*B^* = 24$ cm. Draw the cognates in the position for $\theta = 90^\circ$.

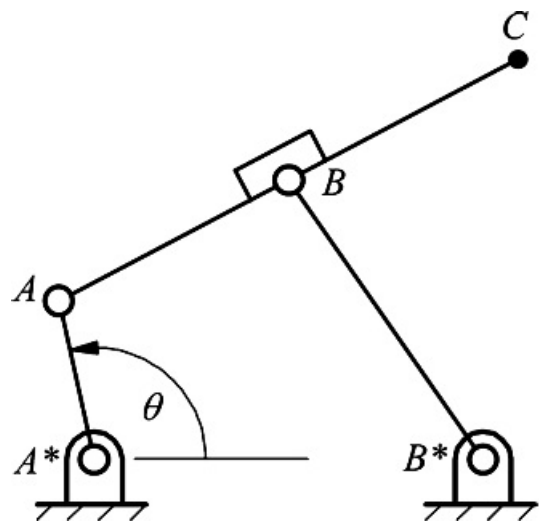


[Figure P3.85](#) Coupler point and linkage for Problem 3.85.

3.86 Determine the three five-bar linkages cognate to the one shown in [Figure P3.85](#).

3.87 Determine the two four-bar linkages cognate to the one shown in [Figure P3.87](#). The dimensions are $A^*B^* = 1.5$ in, $AB = BC = B^*B = AC = 1$ in, and $A^*A = 0.5$ in. Draw the cognates in the position for $\theta = 90^\circ$.

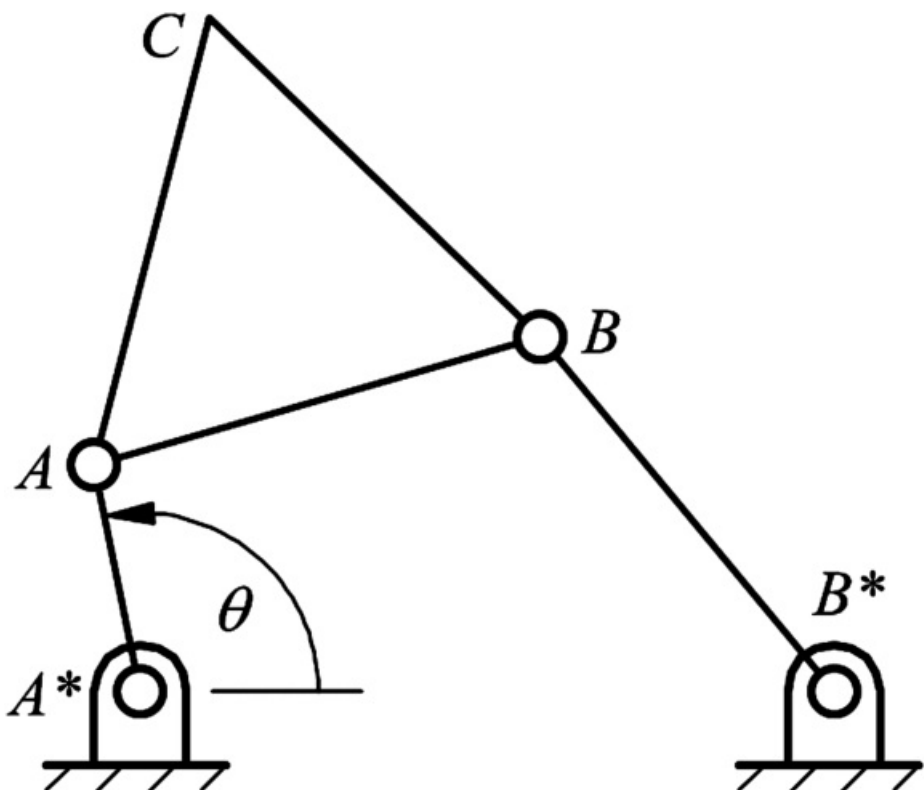


[Figure P3.87](#) Coupler point and linkage for Problem 3.87.

3.88 Determine the three five-bar linkages cognate to the one shown in [Figure P3.87](#).

3.89 Determine the two four-bar linkages cognate to the one shown in [Figure P3.89](#). The dimensions are $A^*B^* = 2$ in, $AB = BC = B^*B = 1$ in, and $A^*A = 0.5$ in, $AC = 0.75$ in. Draw the cognates in the position for $\theta = 45^\circ$.

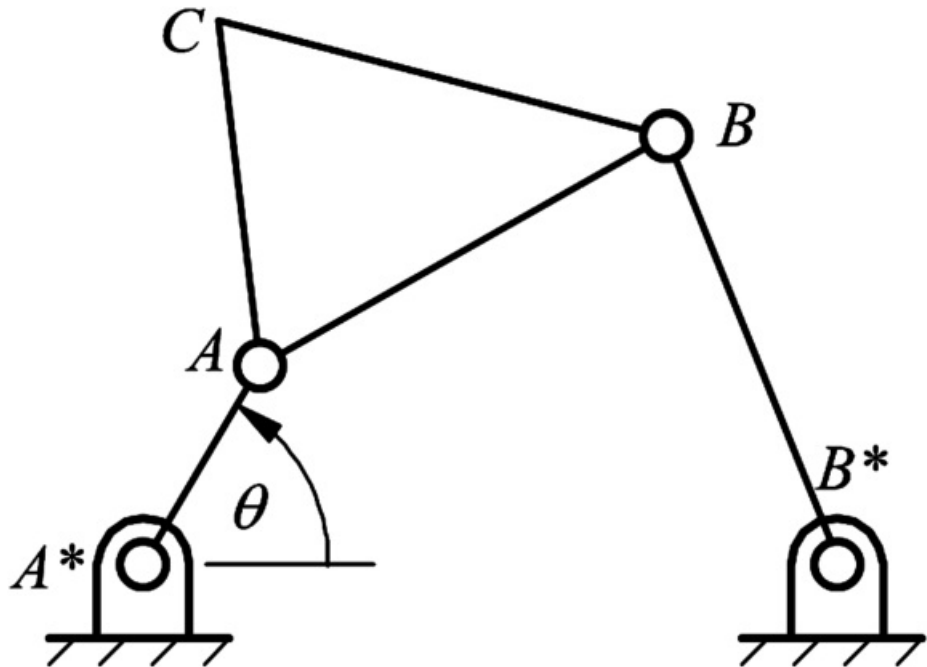


[Figure P3.89](#) Coupler point and linkage for Problem 3.89.

3.90 Determine the three five-bar linkages cognate to the one shown in [Figure P3.89](#).

3.91 Determine the two four-bar linkages cognate for the drag-link mechanism shown in [Figure P3.91](#). The dimensions are $A^*B^* = 1$, $A^*A = B^*B = 4$ m, $AB = 2$ m, and angles CAB and CBA both equal 45° . Notice that the cognates will also be Grashof mechanisms. Draw the cognates in the position for $\theta = 180^\circ$.

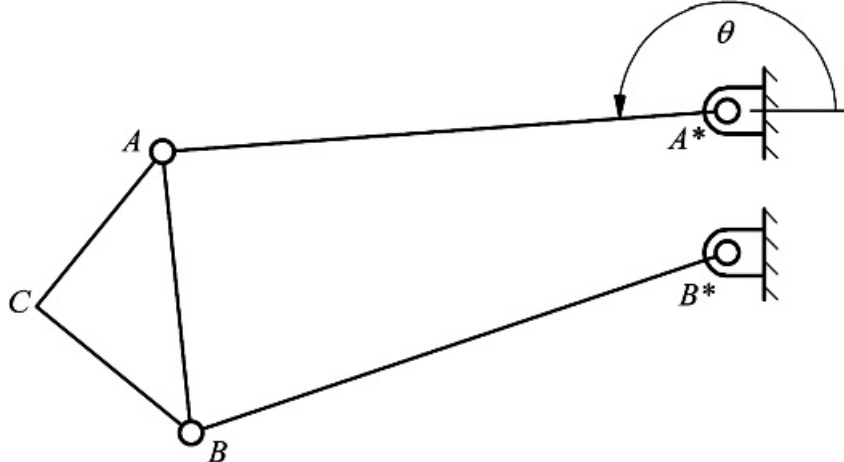


[Figure P3.91](#) Coupler point and linkage for Problem 3.91.

3.92 Scale the drawing in [Figure 3.56](#) and determine the two four-bar linkages cognates.

3.93 Determine the two four-bar linkages cognate for the linkage shown in [Figure 3.60](#).

3.94 Determine the two four-bar linkages cognate for the linkage shown in [Figure 3.64](#).

3.95 Determine the two four-bar linkages cognate for the linkage shown in [Figure 3.71](#).

3.96 Determine the two four-bar linkages cognate for the linkage shown in [Figure 3.80\(a\)](#).

3.97 Determine the three five-bar linkages cognates to the one shown in [Figure 3.60](#).

3.98 Determine the three five-bar linkages cognates to the one shown in [Figure 3.64](#).

3.99 Determine the three five-bar linkages cognates to the one shown in [Figure 3.71](#).

3.100 Use GCP to develop a cognate program and solve Problem 3.85. Animate the linkage by moving the coupler point with the computer mouse.

3.101 Use GCP to develop a cognate program and solve Problem 3.87. Animate the linkage by moving the coupler point with the computer mouse.

3.102 Use GCP to develop a cognate program and solve Problem 3.89. Animate the linkage by moving the coupler point with the computer mouse.

3.103 Use GCP to develop a cognate program and solve Problem 3.91. Animate the linkage by moving the coupler point with the computer mouse.

3.104 Use GCP to develop a cognate program and solve Problem 3.92. Animate the linkage by moving the coupler point with the computer mouse.

3.105 Use GCP to develop a cognate program and solve Problem 3.93. Animate the linkage by moving the coupler point with the computer mouse.

3.106 Use GCP to develop a cognate program and solve Problem 3.94. Animate the linkage by moving the coupler point with the computer mouse.

3.107 Use GCP to develop a cognate program and solve Problem 3.95. Animate the linkage by moving the coupler point with the computer mouse.

3.108 Use GCP to develop a cognate program and solve Problem 3.96. Animate the linkage by moving the coupler point with the computer mouse.

Design Projects

3.109 Walking machine: Design a mechanism to serve as the leg of a walking machine such that it drives the foot through a typical walking stride. This will include periods of support where the foot is on ground and periods of return where the foot is in the air. Determine an appropriate sequence of foot movements, and design the mechanism to achieve these. Explain how your design could be scaled for different walking machines. See www.strandbeest.com for inspiration.

3.110 Vehicle roof rack assist: Design a mechanism to assist an individual in loading objects such as luggage, canoes, skis, etc. onto the roof of a vehicle. An “ideal” design could be attached to a standard roof rack, lowered flat to the ground, loaded with equipment, raised back up to be flat on the roof, and locked into place. A “practical” design would likely have a smaller working envelope and not necessarily achieve all of those characteristics. Explain how the design would be scaled for use on an actual vehicle and on vehicles of different size.

3.111 Design of trenching attachment for a farm tractor: Trenching machines are used to dig narrow trenches for pipe and cable. This permits the pipe or cable to be buried without damaging a large ground area. Design a trenching device that will attach to the three-point hitch on a tractor and can be powered using the power takeoff. The device must be able to dig a trench that is from 0 to 2 ft deep and 6 in wide. The kinematic design problem is to design the system so that the digging depth can be controlled by the three-point hitch. Choose a nominal tractor size for your design, but explain how the design can be changed for other tractor sizes. To get dimensions of the three-point hitch, either measure a tractor directly or look on the web.

3.112 Rocking-chair simulator: Design a rocking-chair simulator that takes up the same floor space as a normal Boston Rocker and moves with the same motion. The simulator should be supported from a framework involving only pin or revolute joints. For this, you must first determine the exact motion of the Boston Rocker and then design a linkage that will duplicate the motion. The linkage must be driven by a continuous rotation motor so that the user simply sits in the chair and does not have to power it. There should also be the option to deactivate the motor and move the chair as you would in a real rocker. Assume that it will be used by an elderly person.

3.113 Efficient windshield wiper: On a typical small car, the windshield wipers move on relatively small arcs such that a considerable percentage of the windshield is not cleaned by the wiper motion. Design a new wiper

system that can be retrofit on existing cars and will clean at least 95 percent of the windshield. You may design your system for a specific car model; however, explain how the system can be modified to adjust to other car models. The mechanism must have all revolute joints, that is, no sliders.

3.114 Shoe tester: Design a machine that will wear test shoe soles for a typical walking cycle. For this, you must determine what the typical walking cycle will be and then design a device that will simulate the walking cycle as closely as possible.

3.115 Spring-linkage counterbalance: Design a mechanism to counterbalance a tool that weights 50 pounds over a length of 2 ft in the vertical direction so that an assembly line worker does not have to strain him/herself to use the tool. The mechanism must weight significantly less than the tool, and friction in the joints should be negligible. The counterbalance should not involve movement of the tool in any direction other than vertical. Some type of spring is to be incorporated into the mechanism to achieve the counterbalancing. Explain how your design could be scaled for different assembly line tasks.

3.116 Solar panel tracking mechanism for north-south direction: Design a linkage that will change the angle of a solar panel so that it tracks the sun (in the north and south direction at noon) throughout the year from the summer solstice to the winter solstice and has a constant velocity input.

3.117 Solar panel tracking mechanism for daytime and seasons: Design a solar panel tracking system that will change the angle of a solar panel so that it tracks the sun (in the north and south direction at noon) throughout the year from the summer solstice to the winter solstice and has a constant velocity input. Also move the solar panel so that it follows the sun from sunup to sunset during the day. Estimate the error in the motion for both the seasons and the daylight hours.

3.118 Laptop computer mechanism: Design a mechanism that will lift a laptop computer from a cavity in a desk. The linkage must be driven by a lid covering the cavity. When the lid is opened, the computer must be lifted from the cavity and the lid of the laptop computer must open. As part of the design process, identify all of the functions that the linkage must do. You may design the linkage for a specific laptop computer, but explain how you can change the linkage to accommodate other brands of laptops.

3.119 Toy chicken: Design a mechanism that will open and close the beak on a toy chicken, as shown in [Figure P3.119](#). Currently, the bird has a single gear (G_1) with a peg on it that pushes against a lever on the leg. When this peg reaches the end of the lever, it releases and a spring rapidly causes the leg to accelerate creating the hop. Use a four-bar linkage with lengths L_1 to L_4 . L_1 is on a gear, G_2 , which is actuated by G_1 . For the purposes of this problem, consider the centers of gears G_1 , G_2 , and the top portion of the beak, denoted by the black triangle, to be initially fixed. The goal is to open and close the beak, denoted by lower red triangle. Assume that the beak is closed completely at its nominal configuration.

- a. If the beak is to open 45° , select reasonable values of L_1 to L_4 to produce this motion.
- b. If the beak needs to open three times per hop, how would this be achieved? Are there any potential issues with your proposed solution? How would this affect the overall function of the toy?
- c. Identify another mechanism that could be used to move the beak and sketch a diagram showing how it would be implemented.

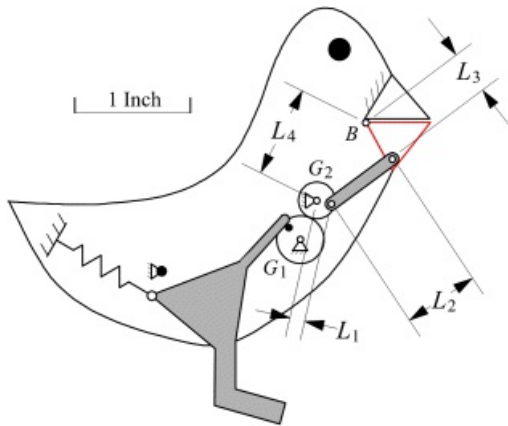


Figure P3.119 Linkage for Problem 3.119.

3.120 Toy iguana: [Figure P3.120](#) represents the head of a toy iguana. Design a mechanism that will extend the tongue of the iguana as the mouth opens. The tongue is part of a slide. The crank, driven by a motor rotating CW, has an extension that pushes the tongue slide. The crank has a length of L_4 from the center of rotation, and the pushing edge extends radially from the center. The tongue slider has a length L_3 and connects to a link that opens the jaw. The tongue itself has the length L_T and a thickness T_T (not shown). The link that opens the jaw has a length L_2 and connects to the jaw at a distance of L_1 from the jaw hinge. The vertical distance from the jaw hinge to the crank pin is L_6 . The slider has a backstop that prevents the tongue from being pulled further back. This is also L_5 from the axis of the crank. Use reasonable dimensions, and design the following:

- Determine appropriate dimensions for the head and the rest of the iguana so that it would be a desirable toy. If the tongue tip starts at a distance of $L_T/4$ behind the lips, how thick can the tongue be before it hits the lips before they open enough?
- Determine the distance the tongue should extend to simulate that of a real iguana based on the size you have chosen for the head. Based on the maximum extension of the tongue, what is the maximum opening of the jaw?
- How must you arrange the joints so that the jaw and tongue reach their maximum motions at the same time?
- How could you change the design to increase the length of the tongue while keeping the head the same size?
- Currently the tongue extends slowly and retracts quickly because of the spring. How can you modify the design so that the tongue also extends quickly? You may need to select another mechanism for this.

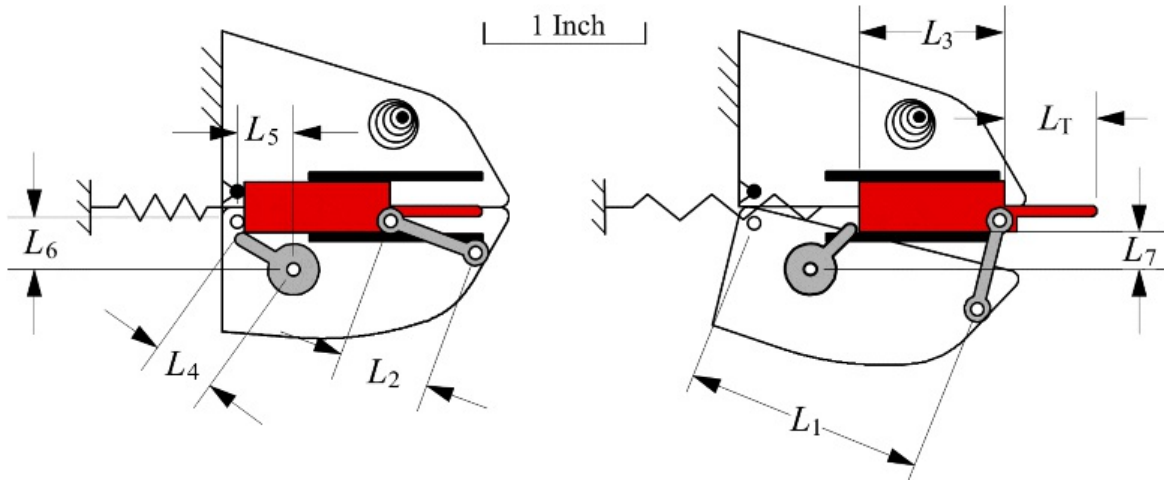


Figure P3.120 Linkage for Problem 3.120.

4

GRAPHICAL POSITION, VELOCITY, AND ACCELERATION ANALYSIS FOR MECHANISMS WITH REVOLUTE JOINTS OR FIXED SLIDES

Prerequisite Knowledge Needed for Chapter 4

Knowledge of linkage structure from [Chapter 1](#) and of general dynamics from basic mechanics courses. A knowledge of Geometric Constraint Programming (GCP) from [Chapter 2](#), and a familiarity with vector mechanics.



4.1 Introduction

Historically, planar linkage analysis problems were solved graphically using drafting equipment. Currently computer techniques offer a viable and attractive alternative, and some teachers of the subject now prefer to concentrate their time on analytical approaches. Nevertheless, there are still many situations in which graphical techniques offer the most efficient solution, and the insight into the problem obtained by an understanding of the graphical approach is, we feel, essential. For this reason, we have chosen to present both approaches. In this and each of the following two chapters, we first consider the traditional graphical approach followed by the graphical approach based on Geometric Constraint Programming (GCP). In [Chapter 7](#), we will present a completely analytical approach to planar linkage analysis.

We have separated the presentation of graphical analyses into three chapters. In this chapter, we present the analysis of mechanisms with only revolute joints or sliders on fixed slides. Such mechanisms constitute the majority of mechanisms found in the real world. These mechanisms can also be analyzed using relatively simple equations derived from basic physics. In [Chapter 5](#), mechanisms involving higher pairs and moving slides will be addressed. The approach to analyzing these mechanisms is more involved than that required in this chapter because moving coordinate systems must be considered directly.

In [Chapter 6](#), we present a special graphical procedure based on instant centers of velocity. When two laminas or links are moving relative to one another, there exists, at every instant, a point in one lamina that is at rest relative to the other, and vice versa. This is the instant center of relative motion of those laminas. The technique of velocity analysis based on instant centers presents advantages when solving certain types of problems. Therefore, it is advantageous for the engineer to be familiar with this technique, as well as the vector polygon technique. This is a very powerful procedure if only velocities are important, and the graphical approach gives considerable insight into the design of planar mechanisms. The approach is also simple to implement using GCP.

A purely analytical approach to kinematic analysis based on vector-loop equations will be presented in [Chapter 7](#). This procedure can be easily programmed, but, unless a program is readily available, it is typically much more time consuming than a graphical analysis when only one position of the mechanism is of interest.

There is a tendency to discard traditional graphical techniques in favor of numerical solutions. However, there are many situations in which graphical techniques are useful. For example, it is always necessary to check and debug computer programs, and this is done most effectively by comparing the numerical solutions of sample problems with solutions to the same problems obtained using completely different techniques. Graphical techniques are ideal for providing these alternative solutions. At other times, a quick answer to a problem is needed, and no suitable program is available. Rather than writing and debugging a program specifically to solve the problem, it is often more efficient to use the graphical approach especially when it can be done using a CAD program. Most importantly, insight into the kinematic geometry that governs all mechanism behavior is obtained by an understanding of the graphical approach.

The graphical approach using GCP is a new approach that allows us to develop a graphical program for a given mechanism and then use that program for all mechanisms of the same class with much less effort than is required in the traditional graphical approach. The velocity polygon changes as we change the dimensions of the linkage, and the output results are determined by simple scaling. Therefore, we can see directly the effect on velocities of dimensional changes in the linkage. The acceleration results require more than simple scaling, but the level of effort to obtain a solution is still considerably less than with the traditional graphical approach. The GCP environment is also an excellent environment for solving all of the graphical exercises contained in [Chapters 4, 5, and 6](#), even if a graphical program is not of interest. Because of the way that the constraints are applied, the accuracy of the graphical solutions obtained using GCP will rival those obtained from regular computer programs.



4.2 Graphical Position Analysis

Regardless of what procedure is used for a linkage analysis, it is *always* necessary to determine the positions of the links before it is possible to perform a velocity analysis. Likewise, it is necessary to know the link velocities before an acceleration analysis can be performed. That is, the kinematic analysis of a linkage must *always* proceed in this sequence: position analysis, then velocity analysis, then acceleration analysis. If the linkage has one degree of freedom and the driver is a crank, it is necessary that the angular position, angular velocity, and angular acceleration of a driving link be specified for a solution to be possible. If the driving member is connected to the base by a prismatic joint, the linear position, linear velocity, and linear acceleration of some point in that link must be specified.

When working graphically, the position analysis consists of simply drawing the linkage to scale. Usually this is so straightforward that it tends to be forgotten as an important step in the solution process. The representation used is a geometric skeleton of the linkage: links with revolute joints are represented by the line, or lines, joining the joint axes. Prismatic joints are represented by sliders on lines in the direction of sliding. Revolute joints are usually represented only by the points that are the intersections of their axes with the plane of motion. The way the method works in the analysis of a simple linkage is illustrated in the examples. Note that this is different from the linkage skeleton representation used in [Chapter 1](#). However, it is sometimes useful to indicate revolute joints by small circles centered on the joint axes and prismatic joints by sliding blocks. If this is done, the present representation becomes a geometrically accurate equivalent of the linkage skeleton.

The position equations for mechanisms are inherently nonlinear. In many cases, the mechanism can be assembled (or drawn) in two possible configurations after the position of the driving link is known. These configurations correspond to the assembly modes discussed in [Chapter 3](#). It is necessary to know before the analysis is conducted which solution is desired. This will be illustrated in the examples that will be discussed after the equations for velocity and acceleration are developed.

We will begin the analysis of velocities and accelerations with a relatively simple case involving two points fixed to the same rigid link. The equations for this case are commonly developed in courses in mechanics using the procedure we shall use here. The equations developed will be directly applicable to mechanisms with revolute joints and/or sliders on fixed (non-rotating) lines. We will illustrate the use of the procedure with several examples.

For more complex joints, a more rigorous and general approach will be used to develop the velocity and acceleration equations. This will entail identifying the coordinate systems relative to which each of the vectors is described and relative to which the time derivatives are desired. It will be shown that the velocity and acceleration equations developed for the case of two points on a rigid link are special cases of the more general equations. This procedure will be given in [Chapter 5](#).



4.3 Planar Velocity Polygons

A velocity analysis is the determination of the angular velocities of different links in a mechanism and of the velocities of points on the links, given either the angular velocity of some member or the velocity of some point on the link designated as the input. The vector-polygon technique will be used here to solve the velocity and acceleration equations. The method facilitates the solution of a large variety of velocity and acceleration problems and also has the advantage that the acceleration polygon solution has a strong similarity to that of the velocity polygon solution. This makes it relatively straightforward to learn and remember the equations to use for the acceleration analysis once the velocity analysis is conducted successfully. Almost all practical problems can be solved by this approach.

In theory, however, the technique is not general. It is possible to formulate problems that cannot be solved by the methods presented here. Special techniques have been developed that allow treatment of some of the simpler cases that are not amenable to the vector-polygon method; however, it is possible to formulate problems that cannot be solved by even these embellished techniques. The reader is referred to books by Hirschhorn [1], Hall [2], and Holowenko [3] for the auxiliary-point technique and other methods of handling more general mechanisms. It should be emphasized, however, that problems that can be solved by the methods presented in this chapter are the ones most commonly encountered in practice.

The key to the graphical velocity analysis of most linkages is the relationship between the velocities of any two points embedded in a rigid body. This relationship can be derived by considering the two points A and B fixed to a moving link as shown in [Figure 4.1](#). The position of A relative to the coordinate system fixed to the frame is r_A and the position of B is given by r_B . The vector from A to B is given by $r_{B/A}$, and the angular orientation of $r_{A/B}$ relative to the fixed X axis is given by θ . Then

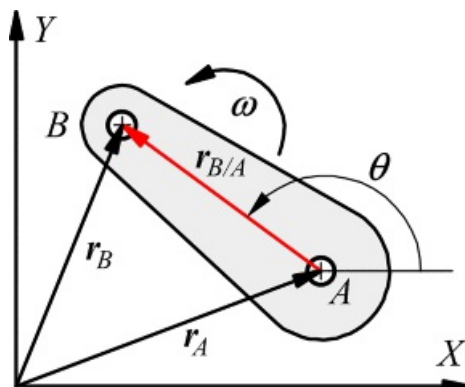


[Figure 4.1](#) Position relationships for two points embedded in a moving link.

$$\vec{r}_B = \vec{r}_A + \vec{r}_{B/A} \quad (4.1)$$

The link rotates with the angular velocity ω relative to the frame where

$$\omega = \frac{d\theta}{dt}$$

Differentiating the position equation with respect to time and recognizing that in general,

$$v = \frac{dr}{dt}$$

we get

$$v_B = r_A + \frac{\omega r_{B/A}}{\delta t} \quad (4.2)$$

Because points A and B are fixed in the moving link, the vector $r_{A/B}$ is fixed in that link and moves with it. It has a constant length so only its direction can change with time. Let the change in direction in a small but finite time interval δt be $\delta\theta$ as shown in [Figure 4.2](#). The magnitude of the change in $r_{A/B}$ during the time interval δt is

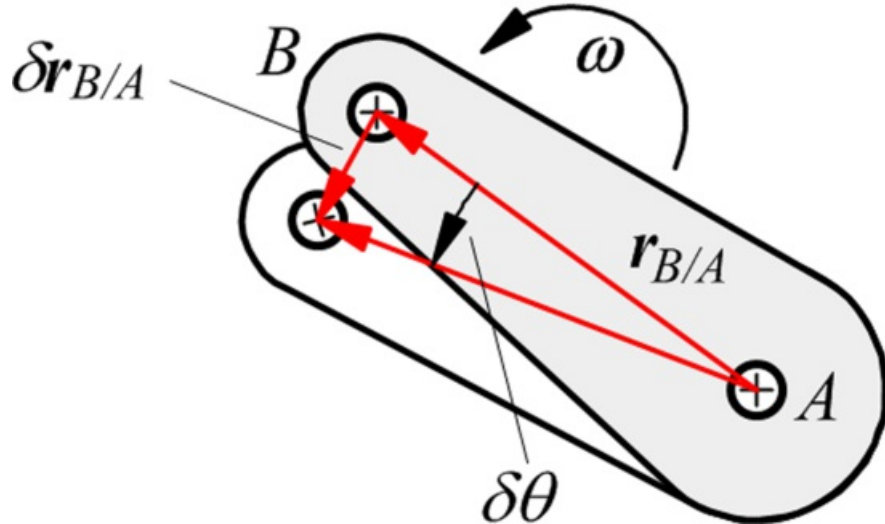


[Figure 4.2](#) Successive positions of the link separated by a small time interval, δt .

$$\delta r_{B/A} = r_{B/A} \delta\theta$$

As δt and $\delta\theta$ approach zero, the angle between $\delta r_{B/A}$ and $r_{B/A}$ approaches 90° . If ω is the magnitude of the angular velocity of the link

$$\delta\theta = \omega \delta t$$

and

$$\delta r_{B/A} = r_{B/A} \omega \delta t$$

Therefore

$$\frac{\delta r_{B/A}}{\delta t} = r_{B/A} \omega$$

and in the limit as δt approaches zero

$$\left| \frac{\delta r_{B/A}}{\delta t} \right| \xrightarrow{\delta t \rightarrow 0} \left| \frac{dr_{B/A}}{dt} \right| = r_{B/A} \omega$$

If ω is considered to be a vector perpendicular to the plane of motion, clockwise (CW) if directed away from the observer and counterclockwise (CCW) if directed toward the observer, the direction of $\dot{r}_{B/A}/dt$ is perpendicular to both ω and to $r_{B/A}$ and obeys the right-hand screw rule with respect to those vectors. Therefore $\dot{r}_{B/A}/dt$ can be represented by the expression

$$\dot{r}_{B/A}/dt = \omega \times r_{B/A} \quad (4.3)$$

What we have actually derived here is a general expression for the derivative of a vector of constant magnitude ($r_{B/A}$) embedded in a link in planar motion, for which ω is the angular velocity relative to a fixed reference frame. We will make use of this expression in [Chapter 5](#) and elsewhere. Thus, [Equation 4.2](#) can finally be written as

$$v_B = v_A + \omega \times r_{B/A} \quad (4.4)$$

As will be shown in [Chapter 5](#), this expression is actually valid for general, spatial motion, although the derivation above applies only to planar motion.

It is convenient to write [Equation 4.4](#) in the form

$$v_B = v_A + v_{B/A} \quad (4.5)$$

where

$$v_{B/A} = \omega \times r_{B/A} \quad (4.6)$$

The vector $v_{B/A}$ is usually called the velocity of B relative to A , although, strictly speaking, it is meaningless to talk of a velocity relative to a point. Velocities are vectors and are measured relative to reference frames. Therefore, $v_{B/A}$ would be the velocity of point B relative to a reference frame that has its origin at point A and which moves so as to be always parallel to the fixed frame.

It should be emphasized that for [Equation 4.6](#) to be valid, it is essential that points A and B be fixed to the same rigid link. If one of the points is attached to a different link, the equation is incomplete. This case is covered in [Chapter 5](#). When the link is not obvious, we will use subscripts on the letters (e.g., A_2) for points to identify the link to which each point is attached to ensure that the proper points are being considered when using the equation. When developing the equations here, however, subscripts will not be used because only one link is being considered and the appropriate link will be obvious.

If only one letter is used as a subscript (e.g., v_B), the resulting velocity is called an absolute velocity. This means that it is the derivative of a position vector that has its tail fixed to a point that has zero velocity. From [Equation 4.5](#) it is clear that $v_B = v_{B/A}$ if $v_A = 0$. Note that point A need not be *absolutely* fixed because it might have a velocity that is only momentarily zero.

The basic technique used in a graphical linkage analysis is to work from one or more points with known velocity to one of unknown velocity using the relationship in [Equation 4.4](#) between the velocities of two points fixed in the same link. The intersections of the axes of revolute joints with the plane of motion form transfer points because they are actually the locations of coincident points fixed in two different links. Thus, the velocity of a revolute point can be obtained by considering it to be a point in one of the links it connects. That information can then be used by considering it to apply to the coincident point fixed in the other link as well.

[Equation 4.5](#) can be represented graphically as the vector triangle shown in [Figure 4.3](#). This triangle can always be solved given the direction and magnitude of one of the three vectors and the directions of the remaining two. This is the normal situation in planar velocity analysis. Again, the way in which this works will be illustrated in several

examples after all of the necessary equations have been developed.

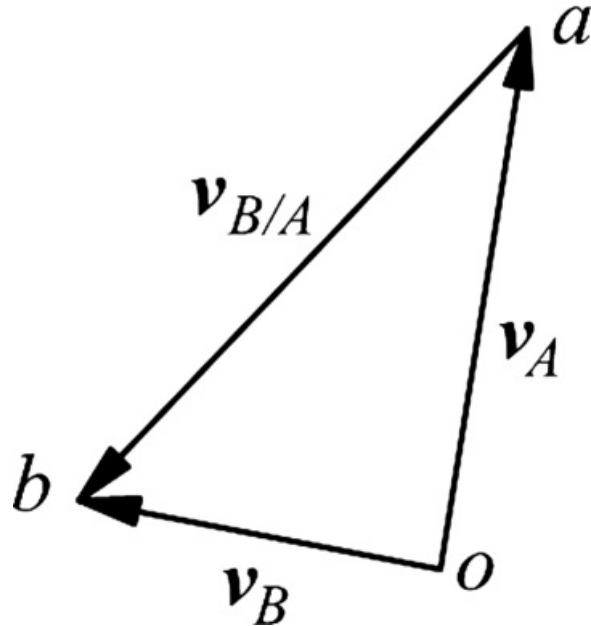


[Figure 4.3](#) Velocities of two points embedded in a moving link.

In [Figure 4.3](#), we have used lowercase letters to designate the velocities of the points identified by uppercase letters on the position diagram. The origin of the velocity-vector polygon is designated by the lowercase letter *o*. This corresponds to any point that has zero velocity in the position diagram. By using the lowercase letters, it is simple to determine at a glance the absolute and relative velocities for selected points. Absolute velocity vectors always have their tails starting from the origin at *o*. Relative velocity vectors correspond to the vectors between the lowercase letters. For example, the relative velocity, $v_{B/A}$ is the vector from *a* to *b* on the velocity diagram.

Based on [Equation 4.6](#), to find the angular velocity, ω , for a given link, we must know the relative velocity between two points on that link, and the relative position between the two points on the position diagram. The vectors in [Equation 4.6](#) will be mutually orthogonal as indicated schematically in [Figure 4.4](#). Because we will know the lines along which each of the vectors must lie from the position diagram, the main problem is which way the vectors point along the lines and the magnitudes of each of the vectors. Given any two of the vector directions, we can find the direction of the third by observing the directions given by the right-hand screw rule. Two examples are shown in [Figure 4.4](#).

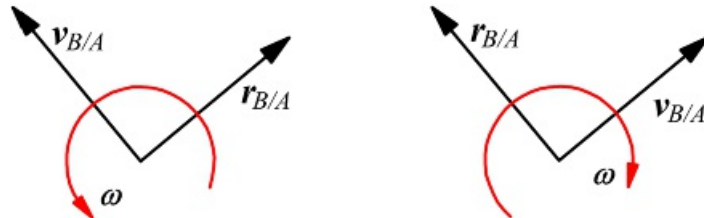


[Figure 4.4](#) The direction relationship among the vectors $v_{B/A}$, ω , and $r_{B/A}$ for planar motion.

Notice that $v_{B/A}$ and $r_{B/A}$ are always perpendicular to each other. Also, visually, we can determine the direction of $v_{B/A}$ by rotating $r_{B/A}$ 90° in the direction of ω . Similarly, if we know the directions of $v_{B/A}$ and $r_{B/A}$, we can determine the direction of ω by visualizing the direction in which we must rotate $r_{B/A}$ to obtain the direction of $v_{B/A}$.

Because the three vectors in [Equation 4.6](#) are orthogonal, their magnitudes are related by

$$|v_{B/A}| = |\omega| |r_{B/A}| \quad (4.7)$$

Given any two of the three magnitudes in [Equation 4.7](#), we can easily solve for the third magnitude.



4.4 Graphical Acceleration Analysis

Just as was the case for a velocity analysis, the key to most graphical acceleration analyses is the relationship between the accelerations of two points fixed in the same rigid link. This relationship can be derived by differentiating the velocity relationship with respect to time. Rewriting [Equation 4.4](#)

$$\ddot{r}_B = \ddot{r}_A + \omega \times \dot{r}_{B/A} \quad (4.4)$$

Differentiating

$$\ddot{a}_B = \ddot{a}_A + \frac{d\omega}{dt} \times r_{B/A} + \omega \times \frac{d\dot{r}_{B/A}}{dt}$$

From [Equation 4.3](#)

$$\frac{d\dot{r}_{B/A}}{dt} = \omega \times \dot{r}_{B/A}$$

The angular acceleration (α) of the link is defined as

$$\alpha = \frac{d\omega}{dt}$$

Therefore, [Equation 4.8](#) can be rewritten as

$$\ddot{a}_B = \ddot{a}_A + \alpha \times \dot{r}_{B/A} + \omega \times (\omega \times \dot{r}_{B/A}) \quad (4.8)$$

As will be demonstrated in [Chapter 5](#), this expression is generally valid for three-dimensional motion, although it has been derived here only in the planar motion context. For planar motion, it is possible to simplify the expression by noting that, in this case, ω and $\dot{r}_{B/A}$ are orthogonal, as shown in [Figure 4.5](#). Also, $\omega \times \dot{r}_{B/A}$ has the magnitude $\omega \dot{r}_{B/A}$ and is perpendicular to both ω and $\dot{r}_{B/A}$ in the sense given by the right-hand screw rule. Then, $\omega \times (\omega \times \dot{r}_{B/A})$ has the magnitude $\omega^2 \dot{r}_{B/A}$ and is perpendicular to both ω and $\omega \times \dot{r}_{B/A}$. Applying the right-hand screw rule again, it can be seen that the vector $\omega \times (\omega \times \dot{r}_{B/A})$ is always in the negative $\dot{r}_{B/A}$ direction. Therefore, it can be written as $-\omega^2 \dot{r}_{B/A}$, and the relationship between the accelerations of points A and B is

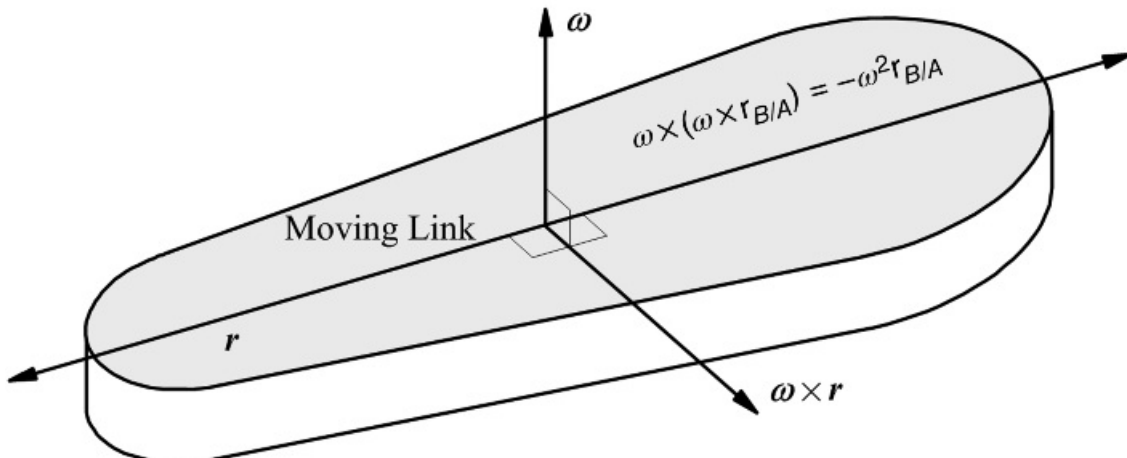


Figure 4.5 The derivation of the relationship $\omega \times (\omega \times r_{B/A}) = -\omega^2 r_{B/A}$ that is valid for planar motion.

$$\omega_S = \omega_A + \omega_{B/A} = \omega_A + \omega \times r_{S/A} - \omega \times (\omega \times r_{B/A}) \quad (4.9)$$

It is usual to write

$$\omega_{B/A} = \omega_{B/A}^r + \omega_{B/A}^t$$

where

$$\omega_{B/A}^r = -\omega^2 r_{B/A} \text{ and } \omega_{B/A}^t = \omega \times r_{B/A} \quad (4.10)$$

with $\omega_{B/A}^r$ called the radial component of the acceleration of *B* relative to *A* and $\omega_{B/A}^t$ called the tangential component of the acceleration of *B* relative to *A*. As was noted in the case of velocities, it is not really proper to talk about the velocity or acceleration of one point relative to another point. As in the case of relative velocities, the vector $\omega_{B/A}$ is really the acceleration of point *B* relative to a reference frame with origin at *A* and moves so that it is always parallel to the fixed frame.

The vector polygon corresponding to [Equation 4.10](#) is shown schematically in [Figure 4.6](#). If a velocity analysis of the linkage has been performed, the angular velocities of all the links will be known, and so the radial component $\omega_{B/A}^r = \omega^2 r_{B/A}$ can always be calculated and plotted. Hence, if one of the other vectors is also known, and the directions of the remaining two are also known, the polygon can be solved in very much the same way as the vector triangle was used in velocity analysis. This is the normal procedure for a graphical acceleration analysis.

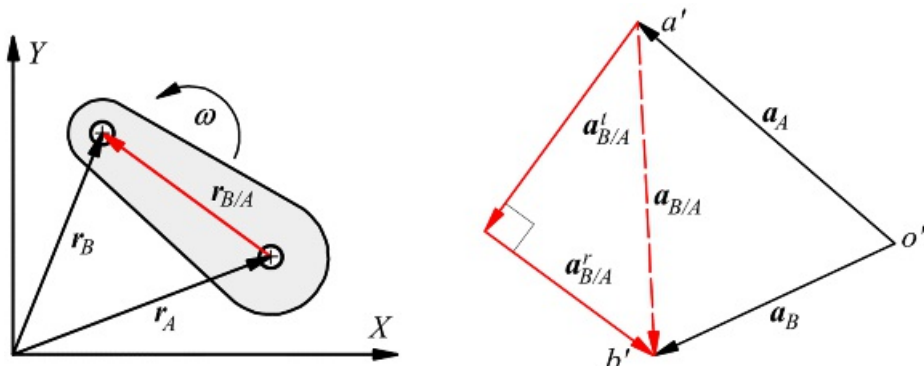


[Figure 4.6](#) Accelerations of two points embedded in a moving link.

In the acceleration polygon in [Figure 4.6](#), we have designated the origin by o' . This is the location in the polygon for all points that have zero acceleration. The other points in the acceleration polygon are designated by lowercase letters with a prime superscript. Absolute accelerations are designated by vectors from o' to the point of interest as shown in the polygon. Relative accelerations are given by vectors from one point to another.

The angular acceleration for a given link is obtained in the same manner as the angular velocity except that the *tangential* component of relative acceleration is used instead of the linear velocity. To find a value of α , we must know the tangential component of the relative acceleration between any two points on the link. That tangential component of acceleration must be given relative to the desired reference frame. For example, the relative tangential acceleration relationship for points B and A as written in [Equation 4.10](#) is

$$\alpha_{B/A}^t = \omega \times r_{B/A}$$

Because we will know the lines along which the vectors must lie, the main problem again is to determine the directions along the lines and the magnitude of each of the vectors. Given any two of the vector directions, we can find the direction of the third by observing the directions given by the right-hand screw rule. Two examples are shown schematically in [Figure 4.7](#).

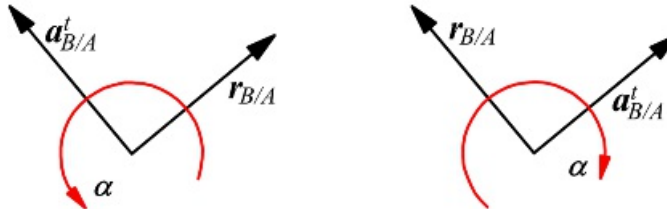


[Figure 4.7](#) The direction relationship among the vectors $\alpha_{B/A}^t$, ω , $r_{B/A}$ for planar motion. Note the similarities with angular velocities.

Notice that these relationships are exactly the same as for the velocity expressions if ω is replaced by $\dot{\theta}$ and $r_{B/A}$ is replaced by $\dot{r}_{B/A}$. In particular, notice that $\alpha_{B/A}^t$ and $r_{B/A}$ are always perpendicular to each other. Also, we can determine the direction of $\alpha_{B/A}^t$ by visually rotating $r_{B/A}$ 90° in the direction of ω . Similarly, if we know the directions of $r_{B/A}$ and $\alpha_{B/A}^t$ we can determine the direction of ω by visualizing the direction in which we must rotate $r_{B/A}$ to obtain the direction of $\alpha_{B/A}^t$.

Because the three vectors in [Equation 4.10](#) are orthogonal, their magnitudes are related by

$$|\alpha_{B/A}^t| = |\omega| |r_{B/A}| \quad (4.11)$$

Therefore, given any two of the three magnitudes in [Equation 4.11](#), we can easily solve for the third magnitude.



4.5 Graphical Analysis of a Four-Bar Mechanism

Having derived the basic equations for relative velocities and accelerations between two points on a rigid link, we will illustrate the use of the equations for the graphical analysis of several mechanisms. The first example involves the position, velocity, and acceleration analysis of the four-bar mechanism given in [Figure 4.8](#). The analysis for this example will be conducted in detail, but in subsequent examples, less detail will be given. In all of the examples, subscripts will be used to identify the links to which the points are attached. This is necessary because the equations derived in Sections 4.3 and 4.4 apply only when the points (A and B) are fixed to the same link.

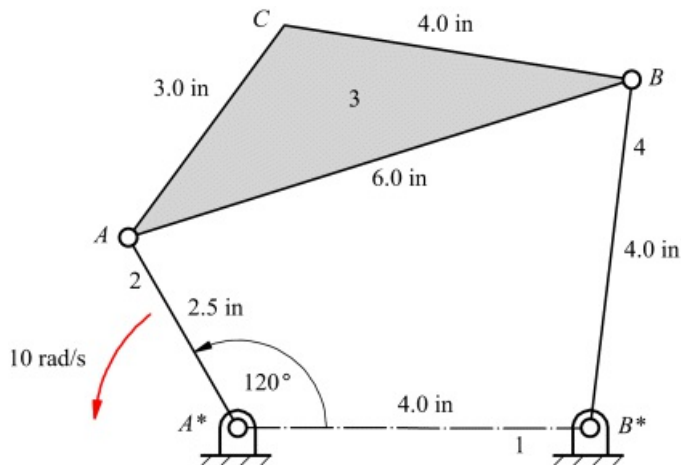


[Figure 4.8](#) The four-bar linkage of Example 4.1.



Example 4.1

Graphical Analysis of a Four-Bar Mechanism

Determine the angular positions, angular velocities, and angular accelerations of all members of the linkage shown when link A^*A is at 120° to the horizontal as shown in [Figure 4.8](#). Also find the position, velocity, and acceleration of point C in the coupler member of the linkage. Link A^*A is driven at a constant angular velocity of 10 rad/s counterclockwise (CCW).

Solution

(a) Position Analysis

We will begin by addressing the graphical determination of the link positions. The first step is to choose a scale. The larger the scale, the more accurate the results. A CAD system that supports the construction of lines and arcs and locates intersections of lines and arcs is preferred, and ultimate accuracy will be achieved by using GCP. In the present case, we want to fit the figure onto a regular book page, so the construction will be described when it is drawn at half-scale (1 in on the drawing corresponds to 2 in on the actual mechanism). If using standard letter-sized paper, full scale can be used. We will describe the construction as if the drawing were made with a ruler and triangles, but similar ideas will apply if a CAD or parametric-design program is used.

The construction is shown in the position diagram in [Figure 4.9](#). A horizontal line representing the base link is drawn first, and the two points bounding an interval of 2 in (half-scale) are marked to represent A^* and B^* . Next locate point A , which is where the driver link (link 2) is joined to the coupler (link 3). A line through point A^* at an angle of 120° to A^*B^* is drawn, and a point on that line at a distance of 1.25 in is marked to represent point A . Next locate point B , which is where the coupler is joined to the rocker (link 4).

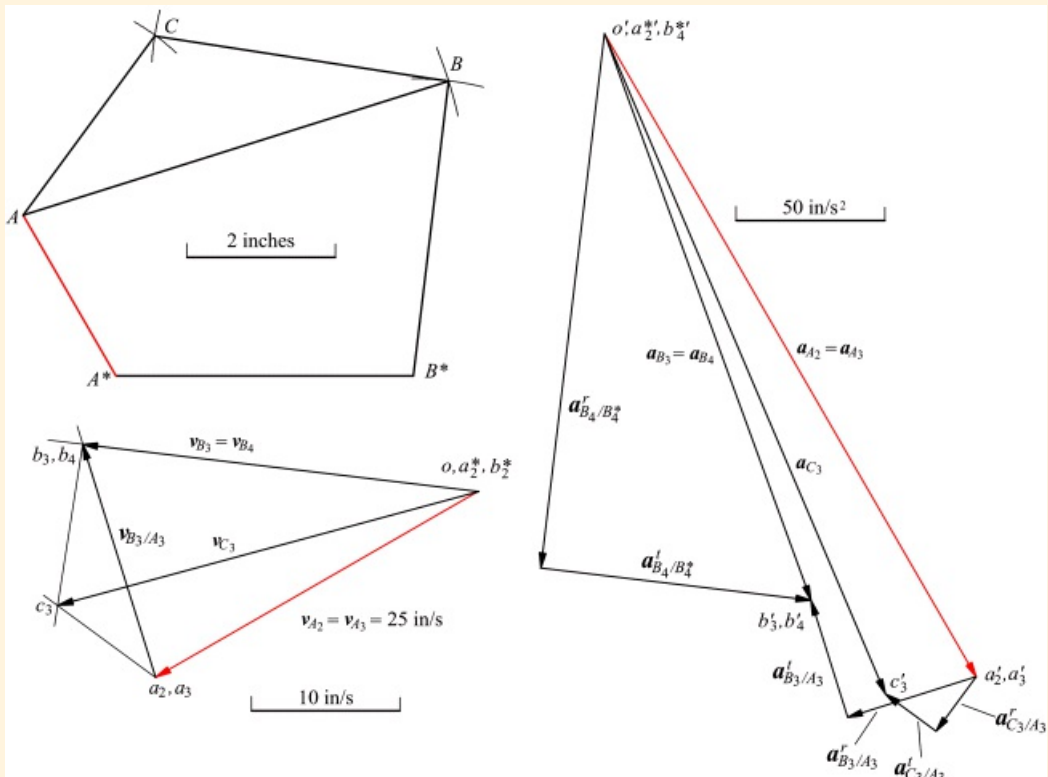


[Figure 4.9](#) Position, velocity, and acceleration polygons for the four-bar linkage in [Figure 4.8](#). Note that the position solution is needed before the velocity polygon can be drawn, and the velocity

polygon is needed before the acceleration polygon can be drawn.

To locate point B , draw a circle centered at A and with a radius of 3.0 in. Next draw a second circle centered at A^* and with a radius of 2.0 in. B is at the intersection of the two circles. Actually, there are two possible intersection points corresponding to the two assembly modes of the mechanism. The second intersection is below the line defined by A^*B^* . This is a common situation with many mechanisms, and it is necessary for the designer to know which assembly mode is desired. In the present case, the correct one is easily located by referring to [Figure 4.8](#).

Point C can now be located in a similar manner to that used for B because we know the distance from point C to point A and to point B . First draw a circle arc centered at A and with a radius of 1.5 in (the scaled distance from C to A). Next draw a second circle arc centered at B and with a radius of 2.0 in (the scaled distance from C to B). C is at an intersection of the two circles. Once again two intersections are possible (one below AB and one above AB), and the correct intersection can be identified by referring to [Figure 4.8](#).

This completes the construction of the scale drawing of the linkage and hence completes the solution of the position analysis problem. The resulting construction is shown in [Figure 4.9](#). The angular positions of the links may be measured from the drawing. Likewise, the position of point C can be measured and the coordinates multiplied by the scale factor of 2. In practice, if the position analysis is being performed solely as a preliminary step to a velocity analysis, the angular positions of the links and the position of point B would not need to be measured directly. Rather, the angular information would be transferred directly to the velocity diagram by constructing perpendicular or parallel lines. For the acceleration analysis, however, the linear distances would be required.

(b) Velocity Analysis

In the velocity analysis, we will typically use the same points in the same order that we used for the position analysis. We will first compute the velocity of point A , then the velocity of B , and finally the velocity of C . Location A is the position of two points, A_2 and A_3 , and to be rigorous, we need to identify which of the points we are considering. Start with A_2 , that is, the point on the driver link 2. We want to compute \dot{v}_{A_2} , that is, the absolute velocity of point A_2 .

This absolute velocity can be expressed as the relative velocity between A_2 and any point that has zero velocity. The point we shall use is A_1^* . It has zero velocity because it is always coincident with A_1^* , which is fixed to frame 1. All points in frame 1 have zero velocity. Then the velocity expression in [Equation 4.4](#) can be written as

$$\dot{v}_{A_2} = \dot{v}_{A_1^*} + \dot{v}_{A_2/A_1^*} = \omega_2 \times r_{A_2/A_1^*}$$

because points A_2 and A_1^* are both on the same link (link 2). Note that we do not need to identify the link associated with A and A^* in \dot{v}_{A/A^*} because all of the A s have the same coordinates, and all of the A^* s also have the same coordinates.

Note also that we know the direction and magnitude for both ω_2 and r_{A_2/A_1^*} , and we know that the two vectors are orthogonal to each other. Therefore, because of the cross-product, the velocity \dot{v}_{A_2/A_1^*} will be orthogonal to ω_2 and r_{A_2/A_1^*} , and the direction will be given by the right-hand screw rule. The relationship among the three vectors is represented by a diagram similar to that shown in [Figure 4.5](#). We can compute the magnitude of the velocity of A_2 from an equation similar to [Equation 4.7](#). The magnitude is given by

$$|\dot{v}_{A_2/A_1^*}| = |\omega_2| |r_{A_2/A_1^*}| = (10 \text{ rad/s})(2.5 \text{ in}) = 25 \text{ in/s}$$

The direction for \dot{v}_{A_2/A_1^*} is given by using the right hand rule or by rotating r_{A/A^*} 90° in the direction of ω_2 .

It is now necessary to select a scale to plot \dot{v}_{A_2/A_1^*} . We used a scale of 10 in/s to 1 in in the velocity diagram

shown in [Figure 4.9](#). This scale is based on the input velocity. We are assuming that all of the vectors will be of about the same order of magnitude. If the polygon began to move off of the page, we would need to select a new scale and redraw the vectors.

We must also select a starting point for drawing the velocity polygon. This starting point is labeled with a lowercase o for origin. The origin o is also called the velocity pole. Obviously, this starting point will also influence whether or not the velocity polygon will fit on the page. Therefore, the velocity pole and polygon scale are selected together.

On paper, the direction of \dot{v}_{A_2/A_3} may be obtained by placing one of the edges of a triangle along AA^* and drawing a line along the orthogonal edge, since \dot{v}_{A_2/A_3} is perpendicular to \dot{v}_{A/A^*} or AA^* . Two points, o and a_2 , separated by an interval of 4.5 in, are marked as shown in [Figure 4.9](#). On the polygon, the line $o\alpha_2$ may be labeled as the vector \dot{v}_{A_2/A_3} . Here we are again using the convention of labeling points on the velocity polygon with *lowercase* letters and the corresponding points on the position polygon with *uppercase* letters. Thus, the absolute velocity of point A_2 given above by \dot{v}_{A_2/A_3} would be represented on the velocity polygon by the line from o to α_2 or from α_2^* to α_2 .

Next we want to compute the velocity of point B . We know that A_2 and A_3 are permanently pinned together so that

$$\dot{v}_{A_2} = \dot{v}_{A_3} = 25 \text{ in/s}$$

in the direction shown in [Figure 4.9](#). Similarly, B_3 and B_4 are permanently pinned together. Therefore

$$\dot{v}_{B_3} = \dot{v}_{B_4}$$

Because A_3 and B_3 are both fixed to link 3, we can write a relative velocity equation similar to [Equation 4.5](#). That is

$$\dot{v}_{B_3} = \dot{v}_{A_3} + \dot{v}_{B_3/A_3} \quad (4.13)$$

In [Equation 4.13](#), the vector \dot{v}_{A_3} is entirely known. Also, because A_3 and B_3 are on the same rigid link, we know that \dot{v}_{B_3/A_3} is given by

$$\dot{v}_{B_3/A_3} = \omega_3 \times \dot{r}_{B/A}$$

Therefore, we know that the vector \dot{v}_{B_3/A_3} is perpendicular to $\dot{r}_{B/A}$ or line AB . We can then construct a line through point a_3 on the velocity polygon in a direction perpendicular to AB on the position diagram. On paper, this is easily done with the help of drafting triangles. This defines one locus of b_3 . To find another locus for b_3 , we need to find the direction of the vector \dot{v}_{B_3} . We know that $\dot{v}_{B_3} = \dot{v}_{B_4}$, and we can identify the direction of the velocity of B_4 by inspection (B can only move on a circle about point B^* , and therefore, \dot{v}_{B_4} must be perpendicular to the line BB^*) or we can write a relative velocity equation for \dot{v}_{B_4} . Again, the velocity \dot{v}_{B_4} is an absolute velocity, and it can be expressed as the relative velocity between B_4 and any point that has zero velocity. If we choose B^* as that point, the velocity equation becomes

$$\dot{v}_{B_4} = \dot{v}_{B_4^*} - \dot{v}_{S_4/B_4^*} = \dot{v}_{S_4/B_4^*} = \dot{\omega}_4 \times \dot{r}_{B/S_4} \quad (4.14)$$

Because of the cross-product, it is clear that \dot{v}_{B_4} must be perpendicular to \dot{r}_{S_4/B_4^*} or the line BB^* . To locate b_4

on the velocity polygon, draw a line through the origin point o in a direction perpendicular to BB^* on the position diagram. Once again, on paper this is most easily done with drafting triangles. Because b_3 and b_4 are permanently located at the same point, this gives a second locus for b_3 that can be determined as shown in [Figure 4.9](#). The vectors v_{A_3} , v_{B_3} , and v_{B_3/A_3} are as shown. The magnitude of ω_3 may be found from the expression for the relative velocity v_{B_3/A_3} . Then

$$|v_{B_3/A_3}| = |\omega_3| |v_{B/A}|$$

or

$$|\omega_3| = |v_{B_3/A_3}| / |v_{B/A}|$$

To determine v_{B_3/A_3} , measure the length of $\overline{a_3b_3}$ on the velocity polygon and multiply by the scale factor (10). In the present case, $a_3b_3 = 1.65$ in, so $v_{B_3/A_3} = 1.65 \times 10 = 16.5$ in/s. Then

$$|\omega_3| = |v_{B_3/A_3}| / |v_{B/A}| = 16.5 / 6.0 = 2.75 \text{ rad/s}$$

To identify the direction, visualize the direction in which we would have to rotate $v_{B/A}$ to obtain the direction of v_{B_3/A_3} . This is the counterclockwise (CCW) direction.

Next compute the angular velocity ω_4 from [Equation 4.7](#). The magnitude can be found from an expression for the relative velocity v_{B_4/E_4} . Then

$$|v_{B_4/E_4}| = |\omega_4| |v_{B/E_4}|$$

or

$$|\omega_4| = |v_{B_4/E_4}| / |v_{B/E_4}|$$

To obtain the velocity v_{B_4/E_4} , measure the distance $\overline{b_4e_4}$ on the velocity polygon and multiply by the scale factor. In the present case, $\overline{b_4e_4} = 2.69$ in, so $v_{B_4/E_4} = 2.69 \times 10 = 26.9$ in/s. Then

$$|\omega_4| = |v_{B_4/E_4}| / |v_{B/E_4}| = 26.9 / 4.0 = 6.73 \text{ rad/s}$$

To identify the direction, visualize the direction in which we would have to rotate v_{B/E_4} to obtain the direction of v_{B_4/E_4} . The direction is CCW.

The velocity of point C_3 may be obtained by considering first the point pair C_3 and A_3 and then the pair C_3 and B_3 . Both pairs of points are fixed to member 3. The relative velocity expressions are

$$v_{C_3} = v_{A_3} - v_{C_3/A_3} = v_{B_3} - \omega_3 \times r_{C/A} \quad (4.15)$$

and

$$v_{C_3} = v_{B_3} + v_{C_3/B_3} = v_{B_3} + \omega_2 \times r_{C/B} \quad (4.16)$$

The velocities v_{A_3} and v_{B_3} are known and have been plotted as oa_3 and ob_3 on the velocity polygon. We can compute v_{C_3} two different ways as implied by Equations 4.15 and 4.16. One way is to compute the cross-product in Equation 4.15 and add the resulting vector to v_{A_3} . We could make similar calculations using Equation 4.16. A second way is to solve both equations simultaneously. Using Equation 4.15, we know that v_{C_3} lies on a line through a_3 on the velocity diagram and perpendicular to CA on the position diagram. Similarly, v_{C_3} lies on a second line through b_3 on the velocity diagram and perpendicular to CB on the position diagram. The point c_3 lies on the intersection of the two lines, and v_{C_3} is the vector from o to the point c_3 .

The magnitude of v_{C_3} can be obtained by measuring oc_3 and multiplying by the scale factor. The distance oc_3 = 2.93 in, so $|v_{C_3}| = 29.3 \text{ in/s}$. Its direction may be measured from the diagram with a protractor. The direction is at an angle of -164.9° with the zero-angle reference being horizontal and positive to the right. This completes the velocity analysis for the linkage.

(c) Acceleration Analysis

The acceleration analysis can be conducted using the same points in the same order that were used in the velocity analysis. In fact, usually the acceleration analysis can be conducted simply by differentiating the velocity equations. We will first compute the acceleration of point A_2 (and A_3), then the acceleration of B_3 (and B_4), and finally the acceleration of C_3 . The acceleration of A_2 can be expressed as the absolute acceleration between A_2 and A_2^* . Because two points on the same rigid link are involved, an acceleration expression similar to Equation 4.8 can be written as

$$\ddot{a}_{A_2} = \ddot{a}_{A_2^*} + \ddot{a}_{A_2/A_2^*} = \ddot{a}_{A_2/A_2^*} = \ddot{\omega}_2 \times r_{A/A^*} + \ddot{\omega}_2 \times (\ddot{\omega}_2 \times r_{A/A^*}) = \ddot{a}_{A_2/A_2^*} = \ddot{a}_{A_2/A_2^*}$$

Note that we know the directions and magnitudes for $\ddot{\omega}_2$, $\ddot{a}_{A_2^*}$, and r_{A/A^*} , and therefore we can compute each of the vectors in the equation. Because of the cross-product, the acceleration \ddot{a}_{A_2/A_2^*} will be orthogonal to $\ddot{a}_{A_2^*}$ and r_{A/A^*} , and the direction will be given by the right-hand screw rule. The direction of \ddot{a}_{A_2/A_2^*} will be opposite to the direction of r_{A/A^*} . We can compute the magnitude of \ddot{a}_{A_2/A_2^*} from an equation similar to Equation 4.11. The magnitude is given by

$$|\ddot{a}_{A_2/A_2^*}| = |\ddot{\omega}_2| |r_{A/A^*}| = (3)(2.5) = 0$$

The magnitude of the radial component can be computed by using Equation 4.10. Then

$$\ddot{a}_{A_2/A_2^*} = \ddot{\omega}_2 \times (\ddot{\omega}_2 \times r_{A/A^*}) = |\ddot{\omega}_2|^2 |r_{A/A^*}| = 10^2 (2.5) = 250 \text{ in/s}^2$$

and the direction is opposite r_{A/A^*} . The direction of \ddot{a}_{A_2/A_2^*} is therefore 60° below the horizontal (down and to the right). It is now necessary to choose a scale and starting point (acceleration pole) and plot the acceleration of point A_2 . We will use a scale of 50 in/s^2 to 1 in to ensure that the diagram will fit on a quarter-sized page. The acceleration $\ddot{a}_{A_2/A_2^*} = \ddot{a}_{A_2/A_2^*}$ is plotted in Figure 4.9 as \ddot{a}_{A_2/A_2^*} . Here, we are again using the convention that a lowercase letter with a prime ('') indicates the acceleration of the corresponding point on the position diagram. On paper, the most convenient way to plot a line parallel to AA^* is to place a drafting triangle with one of the two orthogonal sides along ob_2 on the velocity diagram, and draw a line through o' along the other orthogonal side of the triangle. Since ob_2 is perpendicular to AA^* , this results in a

line parallel to AA^* . Once again, $\ddot{\omega}_{B_2}$ is directed down and to the right because it is in the minus \dot{r}_{A/A^*} direction.

Next we want to compute the acceleration of point B . Recall that A_2 and A_3 are permanently pinned together. Therefore

$$\ddot{\omega}_{A_2} = \ddot{\omega}_{A_3} = 250 \text{ in/s}^2$$

in the direction shown in [Figure 4.9](#). Similarly, B_3 and B_4 are permanently pinned together. Therefore

$$\ddot{\omega}_{B_3} = \ddot{\omega}_{B_4}$$

Because A_3 and B_3 are both fixed to link 3, we can write the following relative acceleration equation

$$\ddot{\omega}_{S_2} = \ddot{\omega}_{B_3} + \ddot{\omega}_{B_3/A_3} = \ddot{\omega}_{A_3} + \ddot{\omega}_{B_3/B_3} + \ddot{\omega}_{B_3/A_3} \quad (4.17)$$

In [Equation 4.17](#), the vector $\ddot{\omega}_{A_3}$ is entirely known. Also, the radial component of the acceleration that is a function of position and velocity only can be computed directly from the following

$$\ddot{\omega}_{S_2/A_3} = \ddot{\omega}_3 \times (\ddot{\omega}_3 \times \dot{r}_{B/A})$$

From the velocity analysis, we computed the magnitude of the angular velocity to be $\ddot{\omega}_3 = 2.75 \text{ rad/s}$. The radial component of acceleration is a vector from B to A on the position diagram (opposite $r_{B/A}$), and the magnitude is given by

$$|\ddot{\omega}_{S_2/A_3}| = |\ddot{\omega}_3 \times (\ddot{\omega}_3 \times \dot{r}_{B/A})| = |\ddot{\omega}_3|^2 |\dot{r}_{B/A}| = 2.75^2 (3) = 45.4 \text{ in/s}^2$$

On paper, a convenient way to draw a line parallel to AB is, again, to place a triangle with one of the orthogonal sides along $\ddot{\omega}_3$ on the velocity polygon and draw a line along the other orthogonal side through point $\ddot{\omega}_3$. The direction is down and to the left because this component is in the minus $\dot{r}_{B/A}$ direction.

The tangential component $\ddot{\omega}_{B_3/A_3}$ is given by

$$\ddot{\omega}_{S_2/A_3} = \ddot{\omega}_3 \times \dot{r}_{B/A}$$

The magnitude of $\ddot{\omega}_{B_3/A_3}$ is unknown because $\ddot{\omega}_3$ is unknown. However, this vector will be perpendicular to AB . Hence a line is drawn through the tip of the $\ddot{\omega}_{B_3/A_3}$ vector to represent this direction. This defines one locus of $\ddot{\omega}_3$. To find another locus for $\ddot{\omega}_3$, we need to find another equation for the vector $\ddot{\omega}_{B_3}$. We know that $\ddot{\omega}_{B_3} = \ddot{\omega}_{B_4}$, and we can write an equation for the acceleration of B_4 . Again, the acceleration $\ddot{\omega}_{B_4}$ is an absolute acceleration, and it can be expressed as the relative acceleration between B_4 and any point that has zero acceleration. If we choose B_5^* as that point, the acceleration equation becomes

$$\ddot{\omega}_{S_4} = \ddot{\omega}_{B_5^*} + \ddot{\omega}_{B_5/B_4^*} = \ddot{\omega}_{B_4/B_4^*} = \ddot{\omega}_{B_4/B_4^*} + \ddot{\omega}_{S_4/B_4^*}$$

The radial component of the acceleration is a function of position and velocity only and can be computed directly from the following

$$\ddot{\omega}_{B_4/B_3}^r = \omega_4 \times (\omega_4 \times r_{B/B_4})$$

From the velocity analysis, we computed the magnitude of the angular velocity to be $|\omega_4| = 6.73 \text{ rad/s}$. The radial acceleration is a vector from B to B^* on the position diagram (opposite r_{B/B^*}), and the magnitude is given by

$$|\ddot{\omega}_{B_4/B_3}^r| = |\omega_4|^2 |r_{B/B^*}| = 6.73^2(4) = 181.2 \text{ in/s}^2$$

This vector is plotted from o' in [Figure 4.9](#).

The tangential component $\ddot{\omega}_{B_4/B_3}^t$ is given by

$$\ddot{\omega}_{B_4/B_3}^t = \omega_4 \times r_{B/B_3}$$

The magnitude of $\ddot{\omega}_{B_4/B_3}^t$ is unknown because ω_4 is unknown. However, this vector will be perpendicular to BB^* . Hence a line is drawn through the tip of the $\ddot{\omega}_{B_4/B_3}^r$ vector to represent this direction. This defines a second locus for B'_3 and B'_4 . The points B'_3 and B'_4 are located where the two loci intersect as shown in [Figure 4.9](#). The vectors $\ddot{\omega}_{B_3/A_3}^t$, $\ddot{\omega}_{B_4/B_3}^t$, and $\ddot{\omega}_{B_4/A_3}^r$ are as shown. The magnitude of $\ddot{\omega}_3$ may be found from the expression for the tangential component of the relative acceleration between B_3 and A_3 . Then

$$|\ddot{\omega}_{B_3/A_3}^t| = |\omega_3| |r_{B/A}|$$

or

$$|\omega_3| = |\ddot{\omega}_{B_3/A_3}^t| / |r_{B/A}|$$

To get $|\ddot{\omega}_{B_3/A_3}^t|$, measure the length of the vector on the acceleration polygon and multiply by the scale factor.

On the acceleration polygon, the length of the line corresponding to $\ddot{\omega}_{B_3/A_3}^t$ is 0.847 in. Therefore,

$$|\ddot{\omega}_{B_3/A_3}^t| = 0.847 \times 50 = 42.2 \text{ in/s}^2. \text{ Then}$$

$$|\omega_3| = |\ddot{\omega}_{B_3/A_3}^t| / |r_{B/A}| = 42.2 / 6.0 = 7.06 \text{ rad/s}^2$$

To get the direction, visualize the direction in which we would have to rotate $r_{B/A}$ to obtain the direction of $\ddot{\omega}_{B_3/A_3}^t$. The direction is CCW.

Next compute the angular acceleration $\ddot{\omega}_4$. The magnitude can be found from an expression for the tangential component of the relative acceleration $\ddot{\omega}_{B_4/B_3}^t$. Then

$$|\ddot{\omega}_{B_4/B_3}^t| = |\omega_4| |r_{B/B_3}|$$

or

$$|\omega_3| = \left| \dot{\theta}_{B_4/B_3}^r \right| / |r_{B_4/B_3}|$$

To obtain the magnitude of the tangential component of acceleration, measure $\ddot{\theta}_{B_4/B_3}^t$ on the acceleration diagram and multiply by the scale factor. From [Figure 4.9](#), $|\ddot{\theta}_{B_4/B_3}^t| = 1.816 \times 50 = 90.8 \text{ in}/\text{s}^2$. Then

$$|\omega_3| = \left| \dot{\theta}_{B_4/B_3}^r \right| / |r_{B_4/B_3}| = 90.8 / 4.0 = 22.7 \text{ rad/s}$$

To get the direction, visualize the direction that we would have to rotate r_{B_4/B_3} to obtain the direction of $\dot{\theta}_{B_4/B_3}^r$. The direction is CW.

The acceleration of point C_3 may be obtained by considering first the point pair C_3 and A_3 and then the pair C_3 and B_3 . Both pairs are fixed to member 3. The relative acceleration expressions are

$$\ddot{a}_{C_3} = \ddot{a}_{A_3} + \ddot{a}_{C_3/A_3} = \ddot{a}_{A_3} + \ddot{a}_{C_3/A_3}^r + \ddot{a}_{C_3/A_3}^t = \ddot{a}_{A_3} + \omega_3 \times r_{C/A} + \omega_3 \times (\omega_3 \times r_{C/A}) \quad (4.18)$$

and

$$\ddot{a}_{C_3} = \ddot{a}_{B_3} + \ddot{a}_{C_3/B_3} = \ddot{a}_{B_3} + \ddot{a}_{C_3/B_3}^r + \ddot{a}_{C_3/B_3}^t = \ddot{a}_{B_3} + \omega_3 \times r_{C/B} + \omega_3 \times (\omega_3 \times r_{C/B}) \quad (4.19)$$

The accelerations \ddot{a}_{A_3} and \ddot{a}_{B_3} are known and have been plotted as $\sigma' a_3$ and $\sigma' b_3$ on the acceleration polygon. As in the corresponding case of velocities, we can compute \ddot{a}_{C_3} two different ways as implied by [Equations 4.18](#) and [4.19](#). One way is to compute the cross-products in [Equation 4.18](#) and add the resulting vectors to \ddot{a}_{A_3} . We could also make similar calculations using [Equation 4.19](#). A second way is to solve both equations simultaneously as was done in the velocity analysis. We will use the first procedure here. To determine \ddot{a}_{C_3} using [Equation 4.18](#), we must compute \ddot{a}_{C_3/A_3}^r and \ddot{a}_{C_3/A_3}^t . The direction of the radial component is opposite $r_{C/A}$, and the magnitude is given by

$$|\ddot{a}_{C_3/A_3}^r| = |\omega_3|^2 |r_{C/A}| = 2.78^2(3) = 22.7 \text{ in}/\text{s}^2$$

This vector is added to \ddot{a}_{A_3} in [Figure 4.9](#).

The direction of \ddot{a}_{C_3/A_3}^t is found using the right-hand screw rule or by turning $r_{C/A}$ 90° in the direction of ω_3 . Recall that ω_3 is CCW. The magnitude of \ddot{a}_{C_3/A_3}^t is given by

$$|\ddot{a}_{C_3/A_3}^t| = |\omega_3| |r_{C/A}| = 7.06(3) = 21.2 \text{ in}/\text{s}^2$$

This vector is plotted in [Figure 4.9](#). The point c'_3 is located at the tip of \ddot{a}_{C_3/A_3}^t . The acceleration of C_3 is located by the vector from a' to c'_3 on the acceleration diagram. To determine the magnitude, measure $\sigma' c'_3$ and multiply by the scale factor. The result is

$$|\mathbf{a}_{C_2}| = 4.33(30) = 242 \text{ in/s}^2$$

The vector is pointed in a direction that is 67° below the horizontal and to the right. A more efficient way to locate point C_2 using acceleration images will be presented later in this chapter.



4.6 Graphical Analysis of a Slider-Crank Mechanism

The analysis of a slider-crank mechanism depends on whether the crank or the slider is the driver. If the crank is the driver, we need to know the angular position, velocity, and acceleration of the crank. If the slider is the driver, we need to know the position, velocity, and acceleration of some point on the slider. Note that each point on the slider will have a unique position, but all points will have the same velocity and the same acceleration.

We will analyze the slider-crank mechanism shown in [Figure 4.10](#), where the crank is the driver. As was the case for the four-bar linkage, the key to the acceleration analysis of this mechanism is the relationship between the velocities and accelerations of two points on the same rigid body. Note that the equations for the analyses are very similar to those for the four-bar linkage. This is due in part to the fact that the slider-crank mechanism is a special case of the four-bar linkage (i.e., because link 4 is of infinite length, it is represented as a slider.)

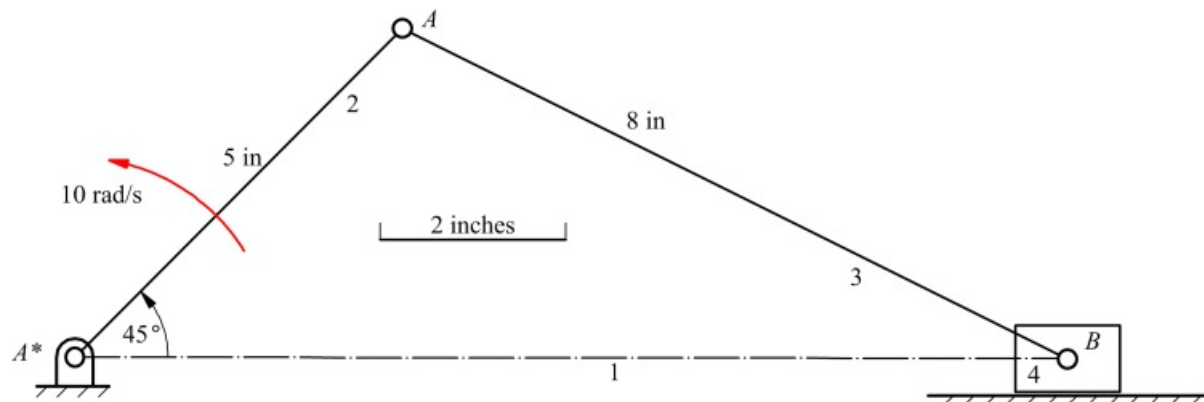


[Figure 4.10](#) The slider-crank linkage to be analyzed in Example 4.2.



Example 4.2

Graphical Analysis of a Slider-Crank Mechanism

Find α_B and $\ddot{\theta}_2$ for the slider-crank linkage in the position shown in [Figure 4.10](#). The crank AA^* (link 2) is driven at a constant angular velocity of 10 rad/s CCW. Point B is the axis of the revolute joint connecting the connecting rod, link 3, to the slider, link 4. In the position shown, AA^* is at 45° to A^*B , and the link lengths are shown on the drawing. The angular velocity of link 2 is 10 rad/s (CCW) and constant (the angular acceleration is zero). Because the analysis is similar to that for the four-bar linkage, the procedure will be given in less detail than was given in the previous example.

Solution

(a) Position Analysis

The linkage is first drawn to scale to establish the direction of member AB . To do this, first locate the horizontal line through A^* and on which B lies. Next, draw member A^*A to scale. Then draw a circle scaled to represent 8 in and centered at A . The circle intersects the horizontal line through A^* at two locations. The desired location is to the right of A^* as indicated in [Figure 4.10](#). The scaled drawing is shown in [Figure 4.11](#).

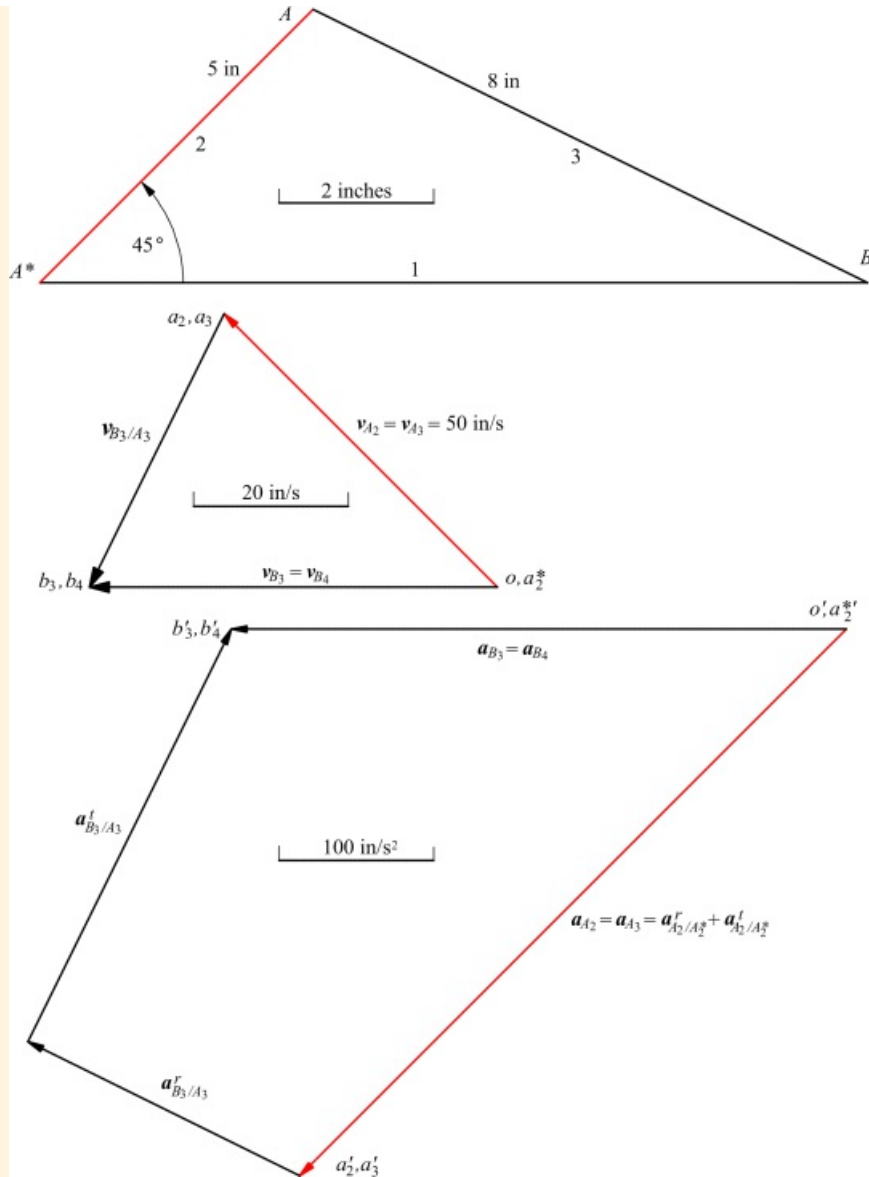


Figure 4.11 Velocity and acceleration polygons for Example 4.2.

(b) Velocity Analysis

In the velocity analysis, we will again use the same points in the same order that we used for the position analysis. We will first compute the velocity of point A_2 and then the velocity of B_3 . Start with A_2 , that is, the point on the driver link 2. We want to compute v_{A_2} which is the absolute velocity of point A_2 .

This absolute velocity can again be expressed as the relative velocity between A_2 and A_2^* . Then the velocity expression in [Equation 4.4](#) can be written as

$$v_{A_2} = v_{A_2^*} + v_{A_2/A_2^*} = v_{A_2/A_2^*} = \omega_2 \times r_{A_2/A_2^*}$$

because points A_2 and A_2^* are both on the same link (link 2). From the given data

$$|v_{A_2/A_2^*}| = |\omega_2| |r_{A_2/A_2^*}| = (10 \text{ rad/s})(3 \text{ in}) = 30 \text{ in/s (normal to } r_{A_2/A_2^*})$$

The direction for \dot{v}_{A_3/B_3} is given by using the right-hand rule or by rotating $r_{A/A}$ 90° in the direction of ω_2 .

To find the velocity of point B_3 , the basic equation to be solved is

$$v_{B_3} = v_{A_3} - v_{B_2/A_3} = v_{A_2} - v_{B_2/A_3} = v_{A_2/A_2^*} - v_{B_3/A_3} = v_{A_2/A_2^*} + \omega_3 \times r_{B/A}$$

The direction for the velocity of B_3 must be horizontal because B_3 and B_4 are pinned together. This lets us solve the basic velocity equation as shown in [Figure 4.11](#). The length of a_3b_3 in [Figure 4.11](#) is 1.98 in. Therefore

$$|v_{B_3/A_3}| = 1.98(20) = 39.6 \text{ in/s}$$

Then

$$|\omega_3| = |v_{B_3/A_3}| / r_{B/A} = 39.6 / 8.0 = 4.95 \text{ rad/s (CCW)}$$

(c) Acceleration Analysis

Following the points used in the velocity analysis, the basic acceleration equation to be solved is

$$\ddot{v}_{B_3} = \ddot{v}_{A_3} + \ddot{v}_{B_3/A_3} = \ddot{v}_{A_2/A_2^*} - \ddot{v}_{B_2/A_2^*} + \ddot{v}_{B_3/A_2} + \ddot{v}_{B_3/A_2}$$

From the given data

$$\begin{aligned} \ddot{v}_{A_2/A_2^*} &= |\omega_2|^2 r_{A/A} = 10^2(3) = 300 \text{ in/s}^2 \\ \ddot{v}_{B_2/A_2^*} &= |\omega_2| r_{B/A} = 0(3) = 0 \end{aligned}$$

Using information from the velocity analysis

$$|\ddot{v}_{B_3/A_3}| = |\omega_3|^2 r_{B/A} = 4.95^2(3) = 120 \text{ in/s}^2$$

The direction for the acceleration of B_3 must be horizontal, and the basic acceleration equation can now be solved for the acceleration of B_3 as shown in [Figure 4.11](#). The length of a_3b_3 in [Figure 4.11](#) is 3.98 in. Therefore

$$|\ddot{v}_{B_3}| = 3.98(100) = 398 \text{ in/s}^2$$

And the length of \ddot{v}_{B_3/A_3} in [Figure 4.11](#) is 2.98 in. Therefore

$$|\ddot{v}_{B_3/A_3}| = 2.98(100) = 298 \text{ in/s}^2$$

Then

$$|\alpha_3| = |\omega_{B_3/A_3}^t| / |r_{B/A}| = 296/6.0 = 37.3 \text{ rad/s}^2 (\text{CCW})$$

The steps for the total analysis are summarized in the following, and the results are shown in [Figure 4.11](#):

1. Draw the linkage to scale.
2. Construct the velocity polygon and compute ω_3 .
3. Compute the magnitudes of $\omega_{A_2/A_2^*}^t$, $\omega_{A_2/A_2^*}^i$, and ω_{B_3/A_2}^t , and identify their directions.
4. Choose a suitable scale and plot $\omega_{A_2/A_2^*}^t$ opposite to the direction of r_{A/A^*} . Put the tail of the vector at the acceleration pole, o' .
5. Plot $\omega_{A_2/A_2^*}^i$ (zero in this case) perpendicular to r_{A/A^*} and through the tip of $\omega_{A_2/A_2^*}^t$. The tip of $\omega_{A_2/A_2^*}^i$ gives the point B'_2 . Here, the direction for $\omega_{A_2/A_2^*}^i$ is in the direction of $-r_{A/A^*}$.
6. Plot the vector ω_{B_3/A_2}^t opposite to the direction of $r_{B/A}$ with its tail at point B'_2 .
7. Draw a line through the tip of vector ω_{B_3/A_2}^t perpendicular to line AB .
8. Draw a line through o' parallel to line A^*B . The intersection of the lines drawn in steps 7 and 8 gives point B'_3 .
9. Measure the magnitude of α_{B_3} as $B'_3 B_3$ and note its direction.
10. Measure ω_{B_3/A_3}^t and compute $|\alpha_3| = |\omega_{B_3/A_3}^t| / |r_{B/A}|$. Note that the sense of α_3 is found by visualizing rotating B about A so that B moves in the ω_{B_3/A_3}^t direction.



4.7 Velocity Image Theorem

To conduct a graphical analysis of a linkage with more than one loop, it is necessary to obtain the velocities of additional points on a rigid link once the kinematic properties of the first two points are known. After the velocity and acceleration of two points on the same link are known, the angular velocity of the body can be determined. Knowing the velocity of a point and the angular velocity of the body, the velocity of any other point on the rigid body can be computed using [Equations 4.4](#) and [4.5](#). Similarly, if the velocity analysis has been conducted, and the acceleration of a point and the angular acceleration of the body are known, the acceleration of any other point on the body can be found using [Equation 4.9](#). An alternative method for determining the velocity and acceleration of a third point on a rigid body is to use the concept of velocity and acceleration image. The velocity image theorem will be discussed first.

As indicated previously, a convenient means of labeling the velocity polygon is to use a lowercase letter to identify the absolute velocity of each point from the position diagram. Then a vector from the velocity pole to the point will represent the absolute velocity of the point. A vector between any two points will correspond to the relative velocity between the points. For example, in [Figure 4.12](#), $v_{A/S} = \dot{\theta}a$.

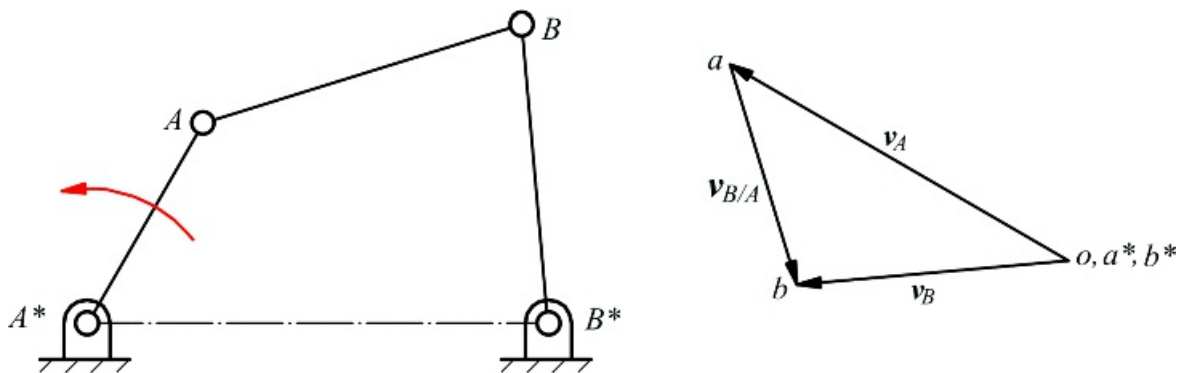


[Figure 4.12](#) Notation used on velocity polygon to facilitate velocity image. The lowercase letters on the velocity polygon correspond to the uppercase letters on the linkage. $v_A = \dot{\theta}a$ and $v_B = \dot{\theta}b$. The point o corresponds to all points with zero velocity. That is, A^* and B^* both map into point o .

Consider the triangle PQR formed by three points (P , Q , and R) all fixed to the same rigid body. The velocity image theorem states that given the triangle PQR in a rigid body, the triangle pqr will be similar to triangle PQR , rotated from PQR by 90° in the positive ω direction, and magnified by the factor ω if both diagrams are drawn to scale. This theorem, stated here for triangles, can be extended to apply to any polygon, because any polygon can be approximated by a series of triangles. We can extend the idea still further to any shape, since any shape can be approximated by a polygon to any desired degree of accuracy. Thus, the unscaled velocity image of any geometric shape is similar to that geometric shape, rotated relative to that shape through 90° in the positive ω direction, and is magnified by a factor ω .

The proof of the theorem can be developed using [Figure 4.13](#). In that figure, the position diagram for the rigid link is PQR and the velocity diagram is pqr . Using $v_{Q/P}$ as an example

$$v_{Q/P} = \omega \times v_{Q/P}$$

Therefore, $v_{Q/P}$ is perpendicular to PQ and has the magnitude ωPQ . Hence, pq has magnitude ωPQ and is rotated 90° in the ω direction relative to PQ . Similarly $qr = \omega RP$ and is rotated 90° in the ω direction relative to RP . Hence, triangle pqr is similar to triangle PQR , is rotated from triangle PQR through 90° in the ω direction, and is magnified over triangle PQR by a factor ω .

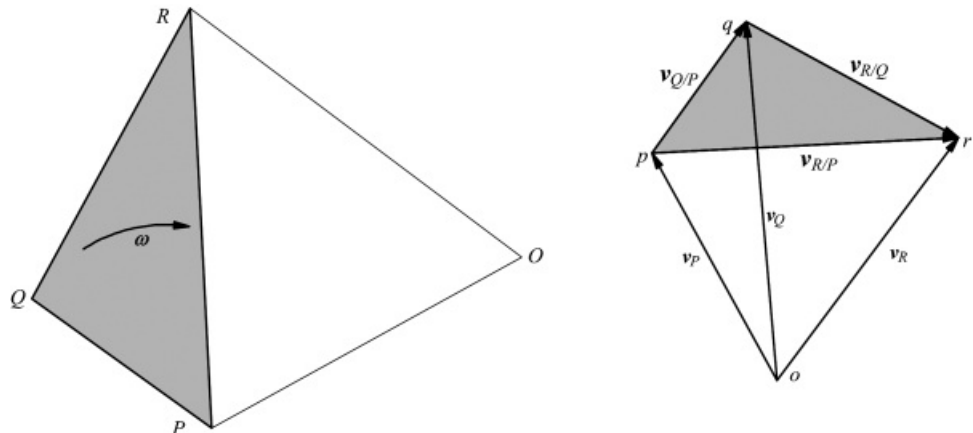


Figure 4.13 Link PQR and its velocity image in the velocity polygon. Triangle pqr is similar to triangle PQR and is rotated from it by 90° in the ω direction. Point O in the position diagram corresponds to point o in the velocity diagram (i.e., point O is the point in the link defined by PQR that has zero velocity).

Note that the velocity image can be used to determine directly the velocity of any point in the rigid body given the position of the point and the velocity diagram. Conversely, the location of a point with a given velocity can be found by mapping points in the velocity diagram to points in the position diagram. For example, in [Figure 4.13](#), point o in the velocity diagram has been mapped to point O in the position diagram to locate the point in PQR that has zero velocity.

The manner in which the velocity image is used to analyze multi-loop linkages is illustrated in Example 4.3 involving a six-bar linkage.



Example 4.3

Graphical Velocity Analysis of Six-Bar Linkage

Develop a procedure for finding the angular velocities of links 3, 5, and 6 and the velocity of point *B* of the linkage shown in [Figure 4.14](#) if the angular velocity of link 2 is given.

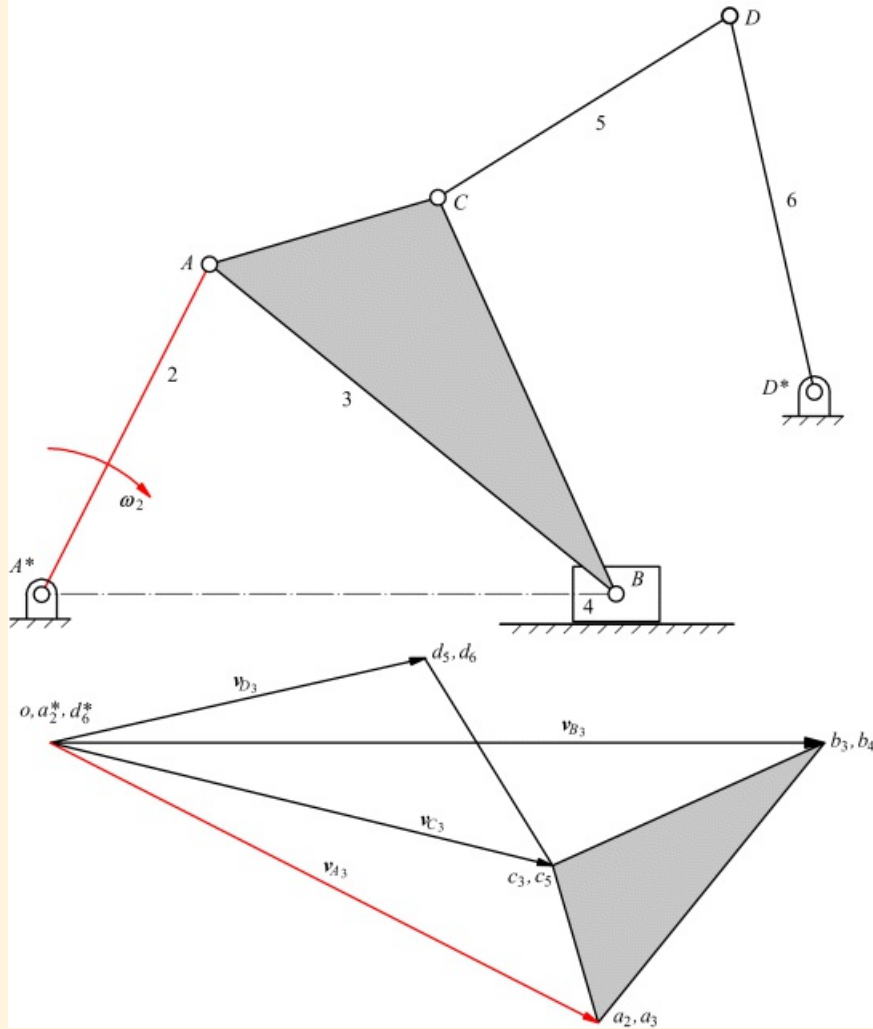


[Figure 4.14](#) The linkage and velocity polygon of Example 4.3. The velocity image theorem is used to locate point c_3 (and c_5).

Solution

The polygons for the analysis are shown in [Figure 4.14](#). The angular velocity ω_2 is assumed to be known. The velocity analysis starts with the slider-crank part of the mechanism. The equations involved and the order in which they are solved are given in the following

$$v_{A_2} = v_{A_3} = v_{A_2/A_2^*} = \omega_2 \times r_{A_2/A_2^*}$$

and

$$v_{B_3} = v_{B_4} = v_{A_3} + v_{B_3/A_3}$$

Next we will find the velocity of point C_3 by image. Then the dyad (links 5 and 6) can be analyzed using

$$\begin{aligned} v_{B_3} &= v_{B_5} \\ v_{B_3} &= v_{C_3} + v_{B_3/C_3} = v_{C_3} + \omega_3 \times r_{B/C} \\ v_{B_5} &= v_{B_6} + v_{B_6/B_5} = \omega_5 \times r_{B/D} \end{aligned}$$

Steps

1. Draw the linkage to scale in the nominated position.
2. Select a suitable scale and plot $v_{A_2} = v_{A_3} = v_{A_2/A_3} = \omega_3$ perpendicular to line AA^* . Point o represents the points on the fixed frame and all other points with zero velocity. That is, *all* points with zero velocity in the linkage map into point o , and all points at o map to the linkage as points with zero velocity.
3. Draw a line from point o parallel to line A^*B . The velocity of B_3 must lie on this line.
4. Draw a line from point a_3 perpendicular to line AB . The intersection of the lines drawn in steps 3 and 4 gives point b_3 .
5. Now find the velocity image of C_3 . Start by drawing a line from point a_3 perpendicular to line AC .
6. Draw a line from point b_3 perpendicular to line BC . The intersection of the lines drawn in steps 5 and 6 is point c_3 (and c_5).
7. Next locate d_5 (and d_6). Start by drawing a line from point c_5 perpendicular to line CD .
8. Draw a line from point o perpendicular to line DD^* . The intersection of the lines drawn in steps 7 and 8 is point d_5 .
9. Compute ω_3 from $[\omega_3] = [v_{B_3/A_3}] / [r_{B/A}]$. Note that the sense is CCW. This is inferred by noting that B_3 must rotate CCW about A_3 to move in the direction of v_{B_3/A_3} .
10. Compute ω_5 from $[\omega_5] = [v_{D_5/C_5}] / [r_{D/C}]$. The sense is CCW, since D_5 must rotate CCW about C_5 to move in the direction of v_{D_5/C_5} .
11. Compute ω_6 from $[\omega_6] = [v_{D_6/B_5}] / [r_{D/B}]$. The sense is CW, since D_6 must move CW about B_5 to move in the direction of v_{D_6/B_5} .

The velocity image theorem is very useful for finding the velocity of a point on the coupler of a linkage at which an additional joint is placed. It is important to notice that the *shape* of any velocity polygon (i.e., all angles in it) is determined by only the shape of the linkage in a given position. See, for instance, [Figure 4.14](#). Further, the speed at which the linkage is operated can affect only the *size*, or scale, of the velocity polygon and not the shape. If the input velocity is doubled, the magnitude of all vectors in the velocity diagram will be doubled.



4.8 Acceleration Image Theorem

As was the case in the velocity analysis, an acceleration image theorem provides an easy way to obtain accelerations of additional points on a rigid body when the accelerations of two points are already known. This is useful when multiple loops are involved in the linkage. In the acceleration diagram, we will again use primed lowercase letters to indicate the absolute accelerations of various points. Thus $\alpha_{Q/P} = \ddot{y}'q'$, $\alpha_{S/A} = \ddot{a}'b'$ and so on. Once again, o' on the acceleration diagram corresponds to the pole where all points with zero acceleration map.

The acceleration image theorem states that, if PQR is a triangle fixed in a rigid link in motion relative to the fixed frame, then triangle $p'q'r'$ is similar to triangle PQR .

Triangle $p'q'r'$ is magnified by a factor that is a function of \mathbf{a} and $\boldsymbol{\omega}$ and is rotated from triangle PQR by an angle that is also a function of \mathbf{a} and $\boldsymbol{\omega}$.

To prove the acceleration image theorem, we will use [Figure 4.15](#). Then

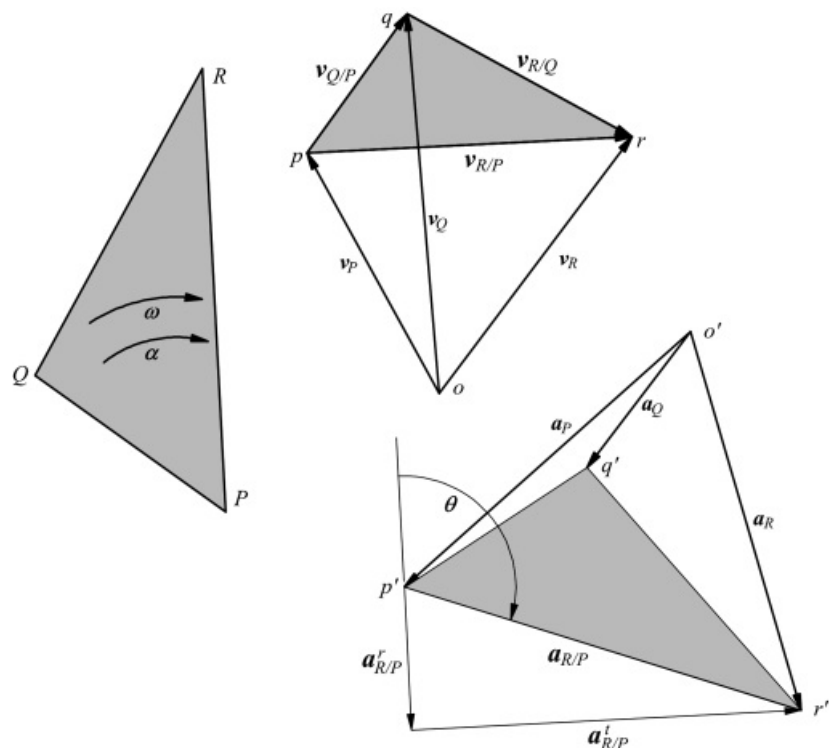


[Figure 4.15](#) The acceleration image theorem. The example used is the same as for the velocity image in [Figure 4.13](#). Triangle $p'q'r'$ is similar to triangle PQR in the original link. Hence it is also similar to triangle pqr , which is the velocity image of PQR . If a_P is plotted together with the radial and tangential components of the acceleration of R relative to P ($a_{R/P}$) to locate points p' and r' , point q' can be located from the image to give a_Q .

$$\alpha_{Q/P} = \ddot{y}'q' = -\omega^2 r_{Q/P} - \dot{\omega} r_{Q/P} n'$$

where n' is perpendicular to $r_{Q/P}$. Therefore the magnitude of the relative acceleration vector is given by

$$|p'q'| = PQ \sqrt{\omega^4 + \dot{\omega}^2}$$

Similarly

$$|q'r'| = QR \sqrt{\omega^4 + \alpha^2}$$

and

$$|p'q'| = RP \sqrt{\omega^4 + \alpha^2}$$

Hence, triangle $p'q'r'$ is similar to triangle PQR . The magnification factor is

$|p'q'|/PQ = |q'r'|/QR = |p'q'|/RP = \sqrt{\omega^4 + \alpha^2}$. Referring to [Figure 4.15](#), the angle of rotation is

$$\theta = \pi - \tan^{-1} \left(\frac{a_{R/P}^t}{\sigma_{R/P}^r} \right)$$

or

$$\theta = \pi - \tan^{-1} \left(\frac{\alpha}{\omega^2} \right)$$

Once again, this result can be extended to cover members of any shape by noting that any polygon may be broken down into triangles, and any area bounded by a plane curve may be approximated by a polygon as closely as desired.

Because the angle of rotation in the acceleration image is not usually 90° , similar triangles must be constructed by making corresponding angles equal.



Example 4.4

Graphical Acceleration Analysis of a Six-Bar Linkage

Given the dimensions of the linkage shown in Figure 4.16, find a_C and a_6 if $\omega_2 = 60 \text{ rpm CW}$ and $a_2 = 0$.

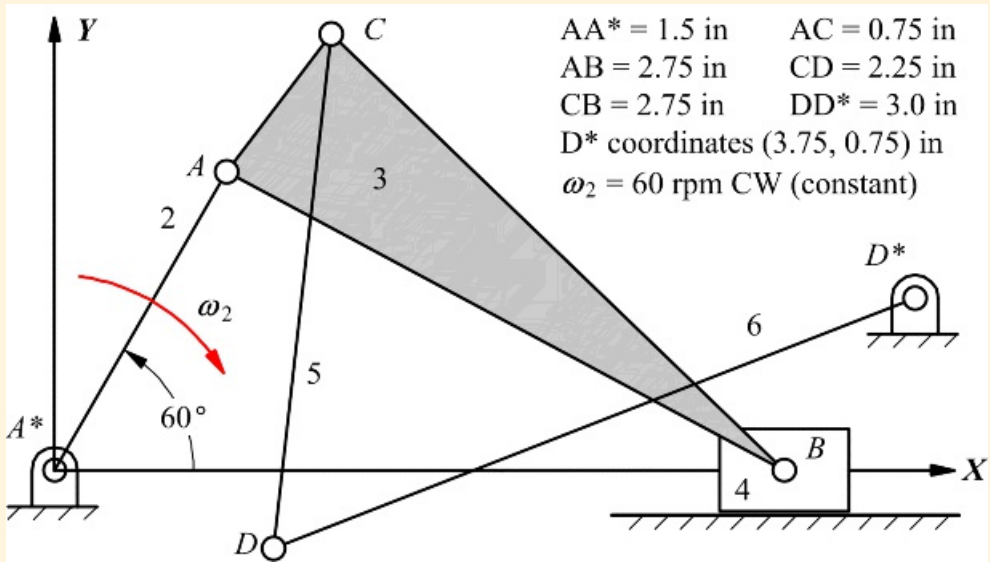


Figure 4.16 Problem statement for Example 4.4.

Solution

The results for the analysis are shown in Figure 4.17. The driving link and the input velocity and acceleration are shown in red. The scales for position, velocity, and acceleration are shown with the polygons. The velocity analysis follows the procedure developed in Example 4.3. The initial equations to be solved are for the slider-crank mechanism. That is

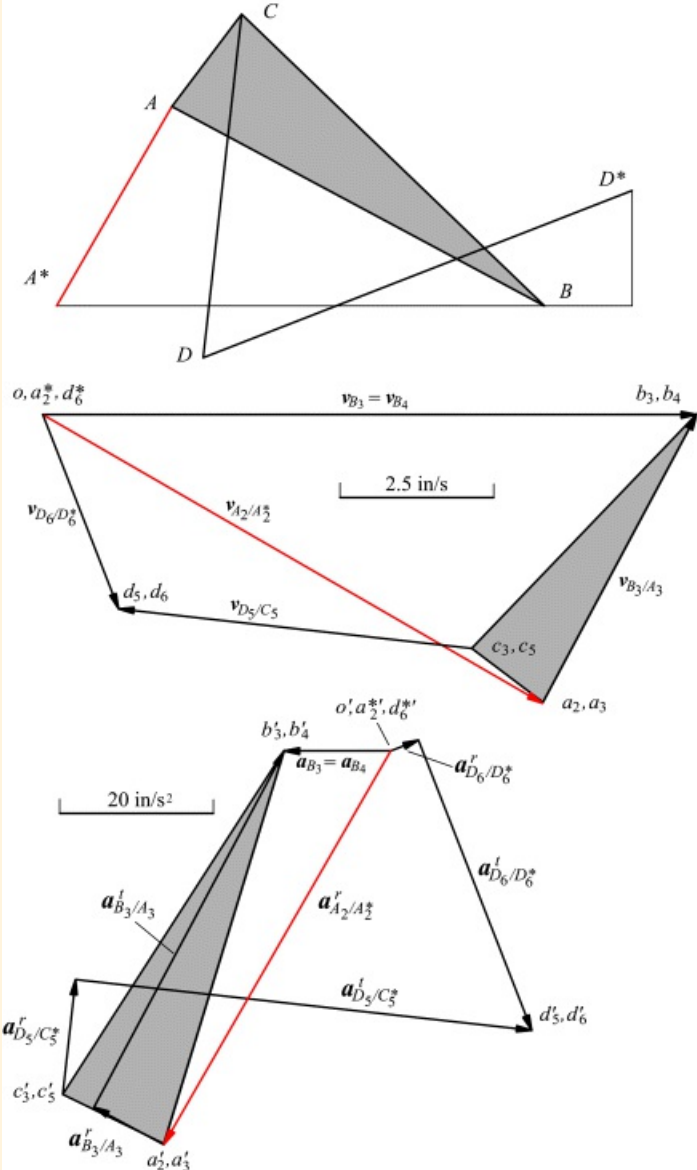


Figure 4.17 Position, velocity, and acceleration polygons for Example 4.4.

$$\dot{v}_{A_3} = \dot{v}_{B_2} = \dot{v}_{A_2/A_2^*} = \omega_2 \times \ddot{r}_{A/A_2}$$

and

$$\dot{v}_{B_2} = \dot{v}_{B_4} = \dot{v}_{A_3} + \dot{v}_{B_3/A_3}$$

Next we will find the velocity of point C_3 by image. Then the dyad (links 5 and 6) can be analyzed using

$$\begin{aligned}\dot{v}_{D_3} &= \dot{v}_{D_6} \\ \dot{v}_{D_5} &= \dot{v}_{C_3} + \dot{v}_{D_5/C_5} = \dot{v}_{C_3} + \omega_5 \times \dot{r}_{D/C} \\ \dot{v}_{D_6} &= \dot{v}_{D_6} + \dot{v}_{D_6/D_6^*} = \omega_6 \times \dot{r}_{D/D_6^*}\end{aligned}$$

Steps

1. Draw the linkage to scale.
2. Compute the magnitude of $v_{A_2} = v_{A_2/A_1^*}$ and identify its direction. Plot it as the vector $\overrightarrow{AA_2}$.

$$\omega_2 = \theta(2\pi/60) = 6.283 \text{ rad/s}$$

$$v_{A_2} = \omega_2 \times r_{A_2/A_1^*} = 6.283(1.5) = 9.42 \text{ in/s normal to } AA_2$$

3. Draw a line from point A_2 perpendicular to line AB .
4. Draw a line from O parallel to A^*B . The intersection of this line with that plotted in step 3 gives point b_3 (and b_4).
5. Construct triangle $a_3b_3c_3$ similar to triangle ABC , thereby locating point c_3 (and c_5). This step is a use of the velocity image theorem.
6. Draw a line from point c_5 perpendicular to line CD .
7. Draw a line from point O perpendicular to DD^* . The intersection of this line with that drawn in step 6 gives point d_5 (and d_6).
8. Measure the magnitudes of $v_{B_3/A_3} = a_3b_3$, $v_{C_3/D_3} = c_3d_3$, and $v_{D_6} = d_6d_5$.

$$v_{B_3/A_3} = 5.34 \text{ in/s}, v_{C_3/D_3} = 5.82 \text{ in/s}, v_{D_6} = 3.41 \text{ in/s}$$

9. Compute $\omega_2 = |v_{B_3/A_3}| / |r_{B/A}|$, $\omega_3 = |v_{C_3/D_3}| / |r_{C/D}|$, and $\omega_6 = |v_{D_6}| / |r_{D/D^*}|$.

$$|\omega_2| = |v_{B_3/A_3}| / |r_{B/A}| = 5.34 / 2.75 = 1.94 \text{ rad/s CCW}$$

$$|\omega_3| = |v_{C_3/D_3}| / |r_{C/D}| = 5.82 / 2.25 = 2.59 \text{ rad/s CW}$$

$$|\omega_6| = |v_{D_6}| / |r_{D/D^*}| = 3.41 / 3.0 = 1.14 \text{ rad/s CCW}$$

This completes the velocity analysis of the linkage.

10. For the acceleration analysis, use the same points in the same order as was done in the velocity analysis. Start with the equations

$$\ddot{\alpha}_{A_2} = \ddot{\alpha}_{A_2} = \ddot{\alpha}_{A_2/A_1^*} + \ddot{\alpha}_{A_2/A_1^*}$$

and

$$\ddot{\alpha}_{S_1} = \ddot{\alpha}_{A_2} + \ddot{\alpha}_{B_3/A_3} - \ddot{\alpha}_{A_2/A_1^*} - \ddot{\alpha}_{A_2/A_1^*} + \ddot{\alpha}_{B_3/A_3} + \ddot{\alpha}_{B_3/A_3}$$

Next we will find the acceleration of point C_3 (and C_5) by image. Then the dyad can be analyzed using

$$\ddot{\alpha}_{D_3} = \ddot{\alpha}_{C_3} + \ddot{\alpha}_{D_3/C_3} + \ddot{\alpha}_{D_3/C_3} = \ddot{\alpha}_{D_6} = \ddot{\alpha}_{D_6/D_6^*} + \ddot{\alpha}_{D_6/D_6^*}$$

First compute $\ddot{\alpha}_{A_2} = \ddot{\alpha}_{A_2/A_1^*}$ and plot as the vector $\overrightarrow{AA_2}$

$$\omega_{A_2} = \omega_2 \times (\omega_2 \times r_{A/A_2}) = 6.263^2(1.5) = 59.2 \text{ m/s}^2 \text{ in the } AA^* \text{ direction}$$

11. Compute the magnitudes of vectors ω'_{B_3/A_2} , ω'_{D_6/C_5} , ω'_{D_6/D_6^*} and identify their directions.

$$\omega'_{B_3/A_2} = \omega_3 \times (\omega_3 \times r_{B/A}) = 1.94^2(2.75) = 10.4 \text{ m/s}^2 \text{ in the } BA \text{ direction}$$

$$\omega'_{D_6/C_5} = \omega_6 \times (\omega_6 \times r_{D/C_5}) = 2.59^2(2.25) = 15.1 \text{ m/s}^2 \text{ in the } DC \text{ direction}$$

$$\omega'_{D_6/D_6^*} = \omega_6 \times (\omega_6 \times r_{D/D_6^*}) = 1.14^2(3.0) = 3.90 \text{ m/s}^2 \text{ in the } DD^* \text{ direction}$$

12. Plot vector ω'_{B_3/A_2} in the BA direction with its tail at A_2 .

13. Draw a line perpendicular to line BA from the tip of vector ω'_{B_3/A_2} .

14. Draw a line from o' parallel to line A^*B . The intersection of this line with that drawn in step 13 gives point B_3' .

15. Construct triangle $A_2 B_3' C_5$ similar to triangle ABC to locate point C_5' (and C_5). This step is a use of the acceleration image theorem.

16. Plot ω'_{D_6/C_5} in the DC direction with its tail at point C_5' .

17. Draw a line perpendicular to DC from the tip of vector ω'_{D_6/C_5} .

18. Plot ω'_{D_6/D_6^*} in the DD^* direction with its tail at o' .

19. Draw a line perpendicular to DD^* from the tip of vector ω'_{D_6/D_6^*} . The intersection of this line with that drawn in step 17 gives the point D_6' (and D_6).

20. Measure the magnitudes of $\omega_{B_3} = \omega_{B_3}$ and ω'_{D_6/D_6^*} and convert them to accelerations using the scaling factor.

$$|\omega_{B_3}| = 13.9 \text{ m/s}^2, |\omega'_{D_6/D_6^*}| = 40 \text{ m/s}^2$$

21. Compute $|\omega_3| = |\omega'_{D_6/D_6^*}| / |\omega_{D/C^*}|$:

$$\omega_3 = 40/13.9 = 13.3 \text{ rad/s}^2$$

22. The sense of α_6 is obtained by visualizing D rotating about D^* so as to move in the ω'_{D_6/D_6^*} direction.



Example 4.5

Using Velocity and Acceleration Image

The mechanism in [Figure 4.18](#) is drawn to scale. Also given is the velocity polygon for the slider-crank part of the linkage, and the acceleration of point B on the round link is shown on the acceleration polygon. Use the image technique to determine the velocity and acceleration of point C_4 . Then determine the velocity and acceleration images of link 4.

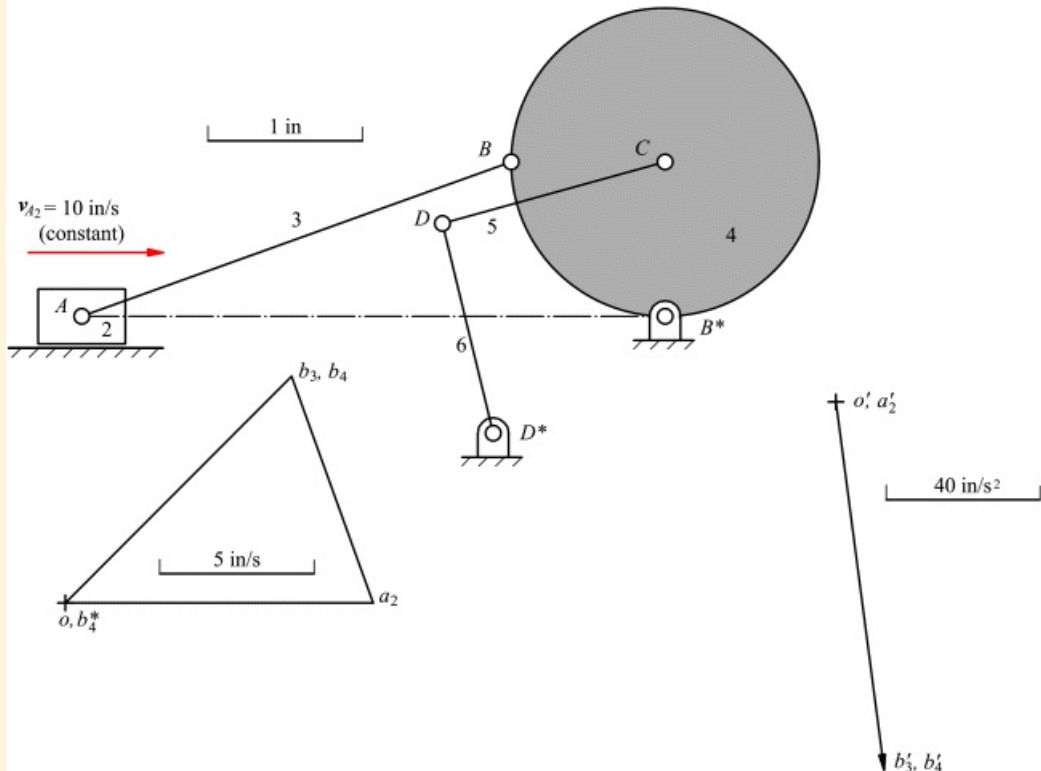


[Figure 4.18](#) Figure for Example 4.5.

Solution

To solve the problem, we only need to find the image of point C_4 on both the velocity and acceleration diagrams. The images of link 4 will both be circles with centers at c_4 and c'_4 , respectively, and with radii of $\dot{b}_4 c_4$ and $\ddot{b}_4 c'_4$, respectively. We find the velocity image of c_4 by constructing triangle $\dot{b}_4 c_4 \dot{b}'_4$ similar to BCB^* to locate c_4 and then drawing the circle centered at c_4 and with radius $\dot{b}_4 c_4$. Similarly, the acceleration image is found by constructing the triangle $\ddot{b}_4 c'_4 \dot{b}'_4$ similar to BCB^* and drawing the circle centered at c'_4 and with radius $\ddot{b}_4 c'_4$. The solution is shown in [Figure 4.19](#).

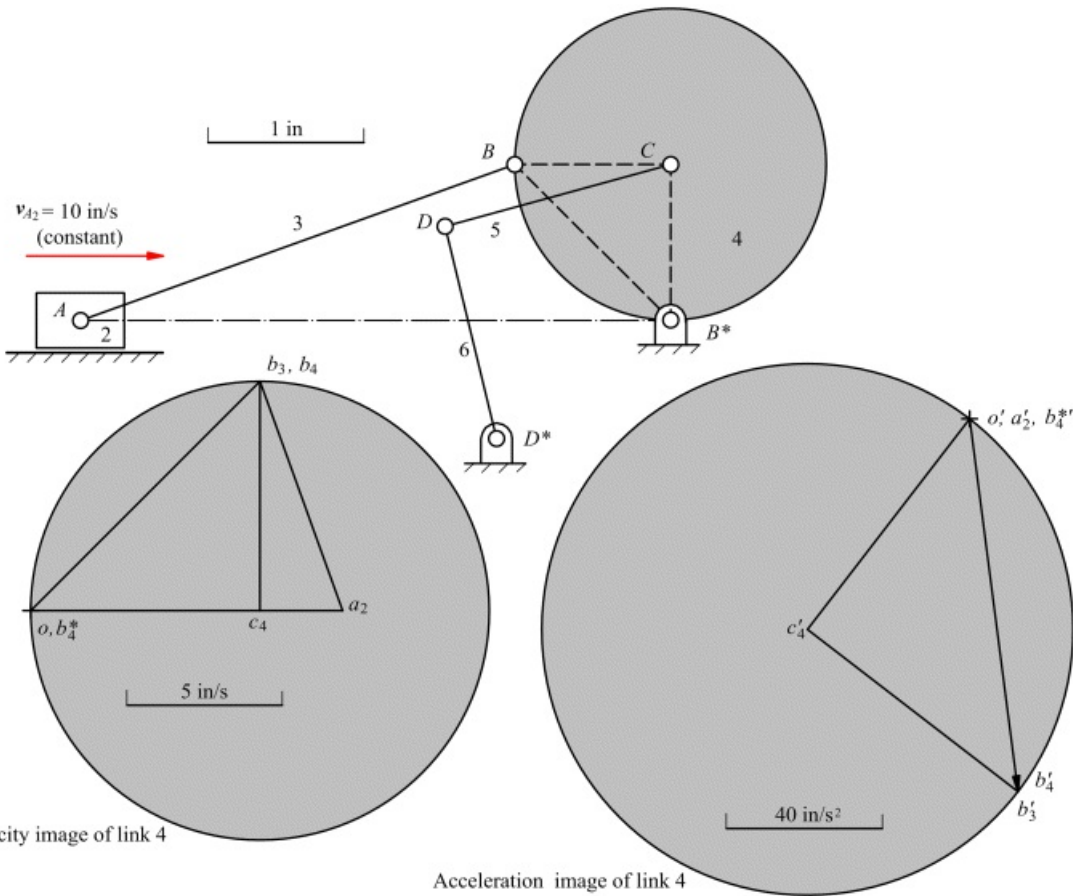


Figure 4.19 Solution to Example 4.5.



4.9 Solution by Geometric Constraint Programming

4.9.1 Introduction

Geometric Constraint Programming (GCP) can be used to solve with high accuracy any of the linkage analyses that can be approached by the traditional graphical approach, and it is especially useful for velocity analyses. Once one problem for a given mechanism is solved, additional problems of the same type can be solved with very little effort for linear quantities by simply changing dimensions. However, any information associated with angular velocities needs to be computed externally for output information. Once the velocity polygon is constructed for one position of a linkage, it can be solved for other positions by simply specifying a new position for the input link. GCP is also useful for acceleration analyses although it requires more user interaction than in the case of velocity analyses if the parametric program being used will not allow equations. Fortunately, most parametric-design programs will allow equations although it may be necessary to use the sketch mode to access this feature.

Even if some external calculations must be made, GCP still offers a significant time savings over traditional graphical analyses because the constraints allow perpendicular and parallel lines to be drawn easily. Also, the locations for the intersections of lines are precisely computed so that line lengths can be determined with very high accuracy.

Unlike the case with most of the design problems discussed in [Chapter 3](#), the user must have a basic knowledge of kinematics before GCP can be used successfully for velocity and acceleration analyses. In particular, GCP is simply another method to solve the vector equations developed for the velocity and acceleration analyses that the user develops. Therefore, the user must set up the equations properly before the solution process can be conducted. Also, parametric programs are not vector based in the sense that a direction is not associated with individual lines. It may not even be possible to automatically specify an arrowhead at the end of a given line. Therefore, the user must be able to identify the directions associated with the lines in the velocity and acceleration polygons to be able to interpret the lines as vectors. This is usually not an issue when GCP is used to solve the problem for one position since the points on the vector polygons can then be labeled. However, labels cannot be fixed to lines so that as the linkage is moved, the lines in the polygons will change in both length and position but the labels will not. In extreme cases, the lines associated with the input vectors may even switch directions. Therefore, the directions for the lines representing any input velocities and accelerations should be carefully checked at the end of each analysis.

4.9.2 Scaling Property of Velocity Polygons

GCP takes advantage of the fact that the shape of the velocity polygon is defined by the position information in the linkage. The size of the polygon is defined by the magnitude and scale used for the input velocity, but the choice of input link is immaterial. If the link lengths are constant as is the case with the problems in this chapter, the lengths of all vectors in the velocity polygon scale with the input velocity. Therefore, we can construct the initial polygon by assuming a linear velocity value for *any* point in the linkage. If we know the actual velocity of *some* point in the mechanism, we can use that velocity value and the value we obtained from the initial polygon to define a scale factor for the polygon. Based on that scaling factor, we can then compute the correct length of any vector in the velocity polygon.



Example 4.6

GCP Program for Six-Bar Mechanism

Develop a GCP program for solving the velocities in a six-bar linkage of the type shown in [Figure 4.14](#). Demonstrate the use of the program for analyzing the linkage for Example 4.4.

Solution

The six-bar linkage of the type shown in [Figure 4.14](#) can be assembled in four different configurations for a given set of link lengths. However, in GCP, the multiple configurations are not an issue until we actually add dimensions to the link lengths. Prior to dimensioning, we can drag the pivot points around to develop the appropriate configuration. We will construct the drawing of the linkage without adding dimensions to accommodate any configuration. We will also construct the velocity polygon without any dimensions. We can do this because the shape of the velocity polygon is dependent on the shape of the position drawing only. Ultimately, we will dimension the position diagram and one of the velocity vectors, and this will define the length of all of the other vectors in the velocity polygon.

To be general, we need to construct two velocity polygons, one for a CW rotation of the input crank and one for a CCW rotation. This is necessary because GCP does not recognize vector directions, and there is no way to automatically indicate the end of a line containing the arrowhead. Also, if the actual linkage analyzed is vastly different from the generic linkage developed before dimensions are added, the directions of the lines in the velocity polygons can flip. Therefore, the polygon that initially was established for a CW rotation of the input crank can correspond to the CCW rotation and vice versa. However, if the generic drawing is close to the final drawing, this is unlikely to be an issue. In any case, the proper polygon to use will be obvious from the alignment of the input velocity relative to the starting point or pole of each velocity polygon. For this reason and if the line color feature is available, it is usually convenient to use a special color such as red for the lines representing the input link and input velocity.

To begin the analysis, set up the following four layers:

1. *Linkage*: Contains the final linkage that can be animated
2. *Dimensions*: Contains the dimensions for the link lengths and other variables
3. *Vel Polygon*: Contains the constructions for the velocity polygon
4. *Pivot Dimensions*: Contains the dimensions associated with the ground pivots, slider block, slider line, and any other dimensions that are not of interest in the final drawing

Make the *Linkage* layer active, and begin by drawing a generic six-link mechanism as shown in [Figure 4.20](#). For convenience, we have identified the points with letters; however, we recognize that the letters will remain stationary as the linkage moves or the link lengths change. We have designated link 2 to be the driver by the color red. Notice that link 4 (the sliding block) is not shown in [Figure 4.20](#) because the function of the slider can be represented by a horizontal constraint at point *B*. For appearance, we will add the block later but it is not necessary from the standpoint of the analysis.

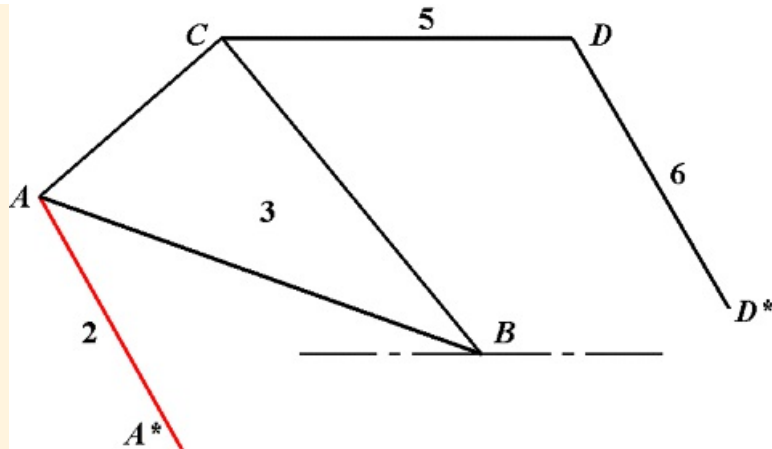


[Figure 4.20](#) Initial model for the graphics program for the velocity analysis of a six-link mechanism.

To solve a particular problem, begin initially constraining the linkage by fixing point A^* and constraining point B to move on a horizontal line. To improve the appearance of the linkage, we can add bushings, ground pivots, a slider block (link 4), and a slider line. However, hide the dimensions for these features in the *Pivot Dimensions* layer to avoid cluttering up the drawing. The procedure for adding the pivots, and so on, was discussed in [Chapter 3](#). The centers of the ground pivots are merged with points A^* and D^* , and the center of the block is merged with point B . The circles at A , C , and D are constrained to be equal to the circles at the ground pivots, and the centers of the circles are merged with the corresponding points. Initially, these are the only constraints. As the model now exists, all of the points except for A^* can be moved, and all of the link lengths can be changed by moving the corresponding points. The model is shown in [Figure 4.21](#).

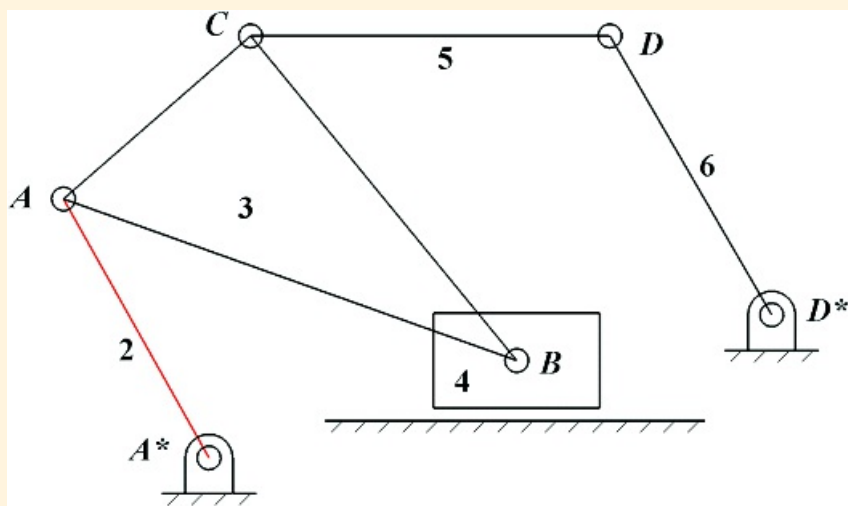


[Figure 4.21](#) Model with bushings, ground pivots, and block added.

For the velocity polygon, we will solve the following equations from Examples 4.4 and 4.5:

$$\begin{aligned}
 v_{A_3} &= v_{A_3} = v_{A_2}/A_2 \\
 v_{B_3} &= v_{B_3} = v_{A_3} + v_{B_3}/A_3 \\
 v_{C_3} &= v_{A_3} + v_{C_3}/A_3 \\
 v_{C_3} &= v_{B_3} + v_{C_3}/S_3 \\
 v_{C_5} &= v_{C_3} \\
 v_{D_5} &= v_{D_5} = v_{C_5} + v_{D_5}/C_5 \\
 v_{D_6} &= v_{D_6} + v_{D_6}/S_6
 \end{aligned}$$

The GCP procedure will follow the solution procedures used in Examples 4.4 and 4.5. We will label each velocity polygon with lowercase letters as we proceed; however, we again need to recognize again that the labels will remain in their original positions when the linkage crank is moved. We will have to move the labels once the linkage is located in its final position. As discussed above, it is convenient to draw two vector polygons, one corresponding to a positive (CCW) value for ω_2 and one corresponding to a negative value (CW). We will describe drawing the polygon for a CW value for ω_2 and then simply show the polygon for the CCW value. The two polygons will be similar in that the corresponding lines will all be parallel but in opposite directions. Start by making the *Vel Polygon* layer active. Begin construction of the CW polygon by drawing a line corresponding to $\dot{\theta}_2/A_2$ at some convenient location. Constrain the line to be perpendicular to the line AA^* . Fix the left end of the line and label the point there as o . Label the other end as a . Initially, the length of the line is arbitrary. Draw a line from o to represent the velocity $\dot{\theta}_2$. Constrain this line to be horizontal. Draw a second line from a , and constrain that line to be perpendicular to AB . This second line corresponds to $\dot{\theta}_3/A_3$. Trim the lines at the intersection, and label the intersection of the two lines as b .

To locate point c (c_3 and c_5) draw a line starting from b and a second line starting from a . These lines correspond to $\dot{\theta}_3/B_3$ and $\dot{\theta}_5/B_5$. Constrain the line starting from b to be perpendicular to BC and the line starting from a to be perpendicular to AC . Label the intersection of the two lines as c . Note that when the perpendicular constraint is set, either the line on the position diagram or the line on the velocity diagram can change. To keep the position diagram from moving, the lines on the position diagram can be *temporarily* fixed if desired. However, if this is done, it is necessary to delete the fixed constraint after the perpendicular constraint is applied.

To determine the velocity of D_5 and D_6 , draw a line starting from o and a second line starting from c . The first line corresponds to $\dot{\theta}_6/D_6$ and the second line corresponds to $\dot{\theta}_5/D_5$. Constrain the line starting from o to be perpendicular to line DD^* and the line starting from c to be perpendicular to DC . Merge the end points of the two lines and label the intersection as d . This completes the velocity polygon for a CW rotation of link 2. To check the program, drag any point other than A^* on the position diagram with the mouse. If the point will not move, check for unwanted constraints. Especially check that no line or point (other than A^* and o) has been fixed. All unwanted constraints need to be deleted before the drawing can function as a graphical program.

Draw the second polygon for a CCW rotation of link 2. Follow the same steps and set the same constraints. If possible, use a color such as red for the line corresponding to $\dot{\theta}_2/A_2$ in each polygon. Also, select the two lines corresponding to $\dot{\theta}_2/A_2$ and constrain them to be equal. This will eliminate the need to dimension both lines when solving a specific problem. The results for both polygons are shown in [Figure 4.22](#). Note that every line in the CCW polygon is in the opposite direction from the corresponding line in the CW polygon. For any given problem, only one of the diagrams will be used. The appropriate diagram will be the one where the line corresponding to the input velocity vector “points” in the proper direction. The direction is determined by treating the tail to be at the pole (point o) and the head to be at the opposite end. For each diagram, the label o will be at a fixed point so it will not move as the linkage is dimensioned.

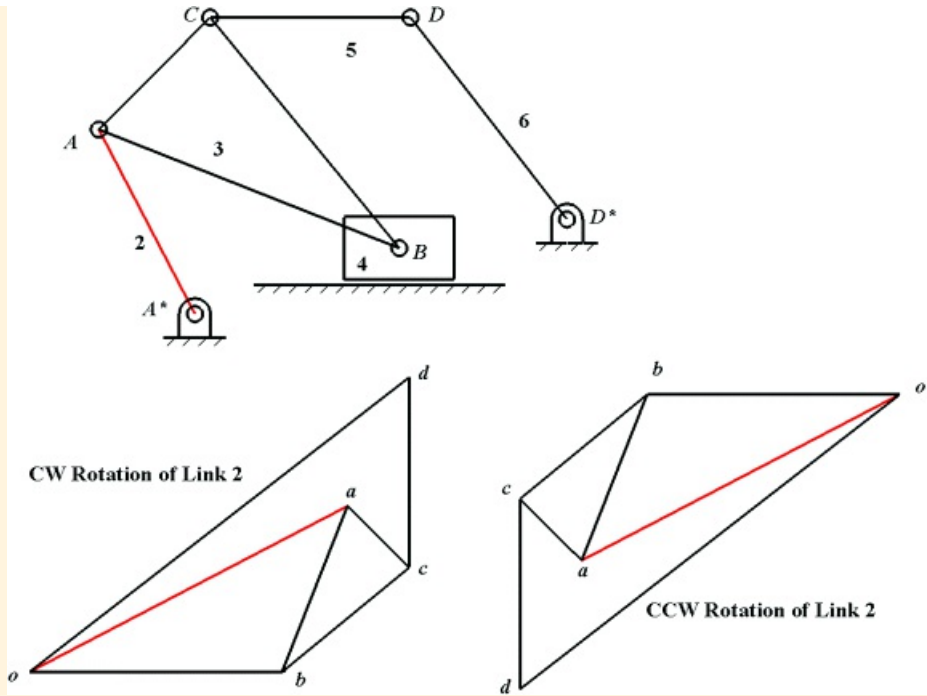


[Figure 4.22](#) Velocity polygons for CW and CCW rotations of the input crank (shown in red).

To solve Example 4.4, we need to drag point D to represent the configuration shown in [Figure 4.16](#). We can then use the dimension tool to assign the dimensions including the orientation of link 2. The shape of the velocity diagram will be determined by the orientation of the lines in the position diagram; however, to determine the size of the polygon, we need to specify the length of one line in the polygon. To do this, we can compute the value for the velocity of A_2 and use that value to determine the scale for the polygon. From Example 4.4, we know that the velocity of A_2 is 9.42 in/s. Therefore, a scale making 2 in on the velocity polygon correspond to 4 in/s is a reasonable value to use initially. If this value turns out to be too small or too large, it can easily be changed later. We do not need to make the velocity polygon especially large for accuracy because the parametric-design program will compute the lengths of the lines in the velocity polygon very accurately regardless of the scale used. Using this scale, the length of the line oa_3 should be $9.42/4 = 2.36$ in. We can set this dimension using the dimension tool. The final polygons are shown in [Figure 4.23](#). Based on the direction of line oa , the polygon on the left is appropriate for this problem.

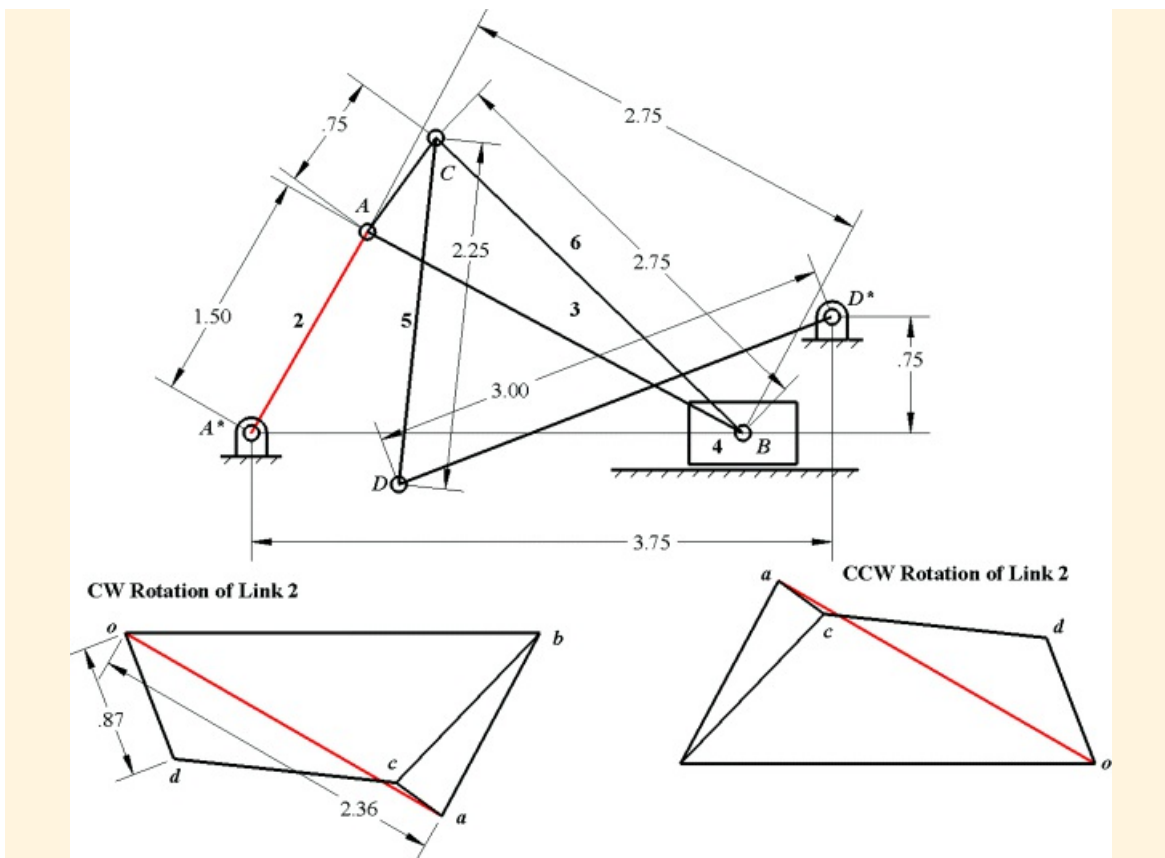


Figure 4.23 Velocity polygons for linkage in Example 4.4.

We can use the dimension tool to identify any of the lines of interest. If we wish to investigate other positions of the linkage, we should make the dimensions for all lines other than oa_3 as *driven* dimensions. To compare with the results from the traditional graphical analysis in Example 4.4, we can compute v_{D_6} . The line corresponding to v_{D_6} is od , and the length of this line is 0.87 in. The corresponding velocity value is $(4)(0.87) = 3.48$ in/s. This corresponds to the value of 3.41 in/s from the traditional graphical approach. The results compare well although the value determined using GCP will be more accurate.

4.9.3 Using GCP to Analyze Linkages That Cannot Be Analyzed by Classical Means for Velocities

In general, if we have a linkage where the driver link is not part of a four-bar loop that contains the frame as one of the members, it is not possible to analyze the linkage directly using the vector polygon approach. The Stephenson six-bar linkage shown in [Figure 4.24](#) can be solved using the techniques in the previous sections *provided* the driving crank is 5 or 6. However, if the linkage is driven by crank 2, the linkage cannot be analyzed directly using the traditional vector polygon techniques. This is because link 2 does not form a part of any four-bar loop in the linkage. Consequently, plotting the velocity of point A does not provide enough information to close a velocity polygon. In fact, we cannot even draw the linkage directly if the input angle is θ_2 when traditional drawing procedures are used. However, the problem can be solved easily using GCP.

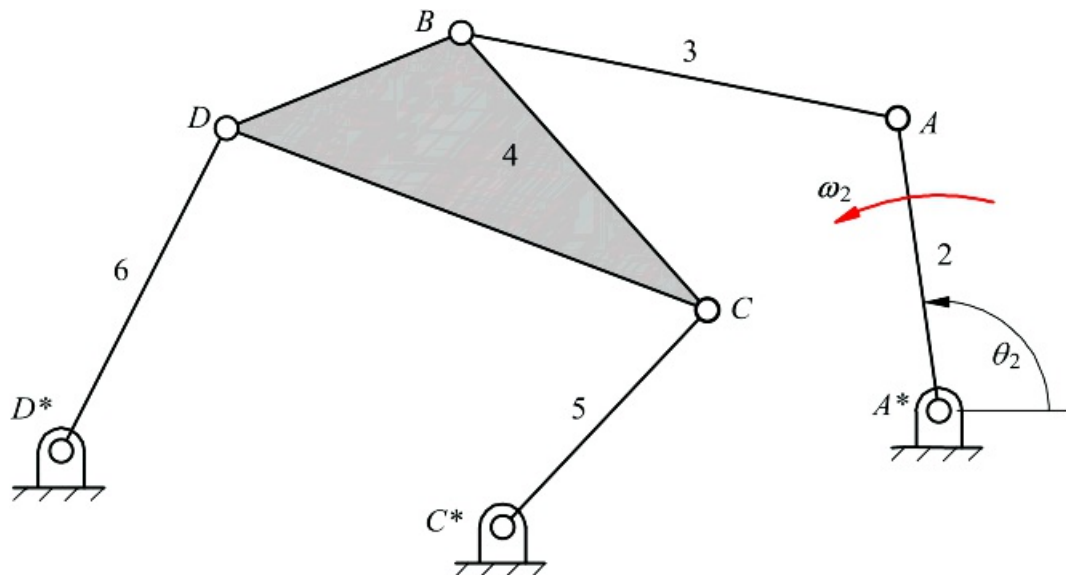


Figure 4.24 A simple linkage that can be analyzed using the techniques of the preceding sections only if it is driven by cranks 5 or 6, but not by crank 2. However, the linkage can be analyzed easily using GCP regardless of the driver link.

If the position of the linkage is known, a velocity solution can be achieved by recognizing that all of the velocities in the linkage are linearly related to the velocity of the input member. Therefore, we can analyze this linkage directly using GCP. We simply need to draw the linkage and develop a generic velocity polygon with either link 5 or 6 as the input link as was done in the previous example. We can then dimension the linkage and use the velocity of link 2 and a scale for the velocity polygon to determine the length of the line corresponding to the velocity of point *A*. We can then use the same scale and the length of any other line in the velocity polygon to determine the corresponding velocity.

As described, the procedure is limited to velocity analyses, and the linkage must contain a four-bar loop that involves the frame. If the linkage contains a four bar loop but it does not involve the frame, or an acceleration analysis is required, GCP can still be used to analyze the linkage. However, the procedure is much more involved and beyond the scope of this book. The procedure was developed by Goodman [4] and is based on inversion.



Example 4.7

Velocity Analysis of Stephenson Linkage Using GCP

The linkage shown in [Figure 4.24](#) is driven by crank 2. Find the angular velocities for all members of the linkage for the position in which θ_2 is 135° . The angular velocity of link 2 is 10 rad/s CCW . The other dimensions are:

$AA^* = 2.75 \text{ in}$	$AB = 2.5 \text{ in}$	$BC = 2.0 \text{ in}$
$DC = 3.5 \text{ in}$	$CC^* = 3.25 \text{ in}$	$DD^* = 2.0 \text{ in}$
$BD = 2.0 \text{ in}$	Coordinates of $A^*(4.5, -0.5)$	
Coordinates of $C^*(3.0, 0)$	Coordinates of $D^*(0,0)$	

Solution

We will begin the analysis by drawing the linkage in the position specified by the input data. First open a blank worksheet and set up the following four layers:

1. *Linkage*: Contains the final linkage which can be animated
2. *Dimensions*: Contains the dimensions for the link lengths and other variables
3. *Vel Polygon*: Contains the constructions for the velocity polygon
4. *Pivot Dimensions*: Contains the dimensions associated with the ground pivots, slider block, slider line, and any other dimensions that are not of interest in the final drawing

Make the *Linkage* layer active, and sketch the linkage in [Figure 4.24](#). Next use a combination of constraints and the dimension tool to constrain the link lengths according to the dimensions in the problem statement. The parametric-design program solves the position equations iteratively as the dimensions are added. However, the solution process is so fast that it is transparent to the user. After the linkage is fully constrained, add ground pivots and bushings as was done in the previous example to improve the appearance of the drawing. The final linkage model is shown in [Figure 4.25](#). The input link and input velocity vector are shown in red.

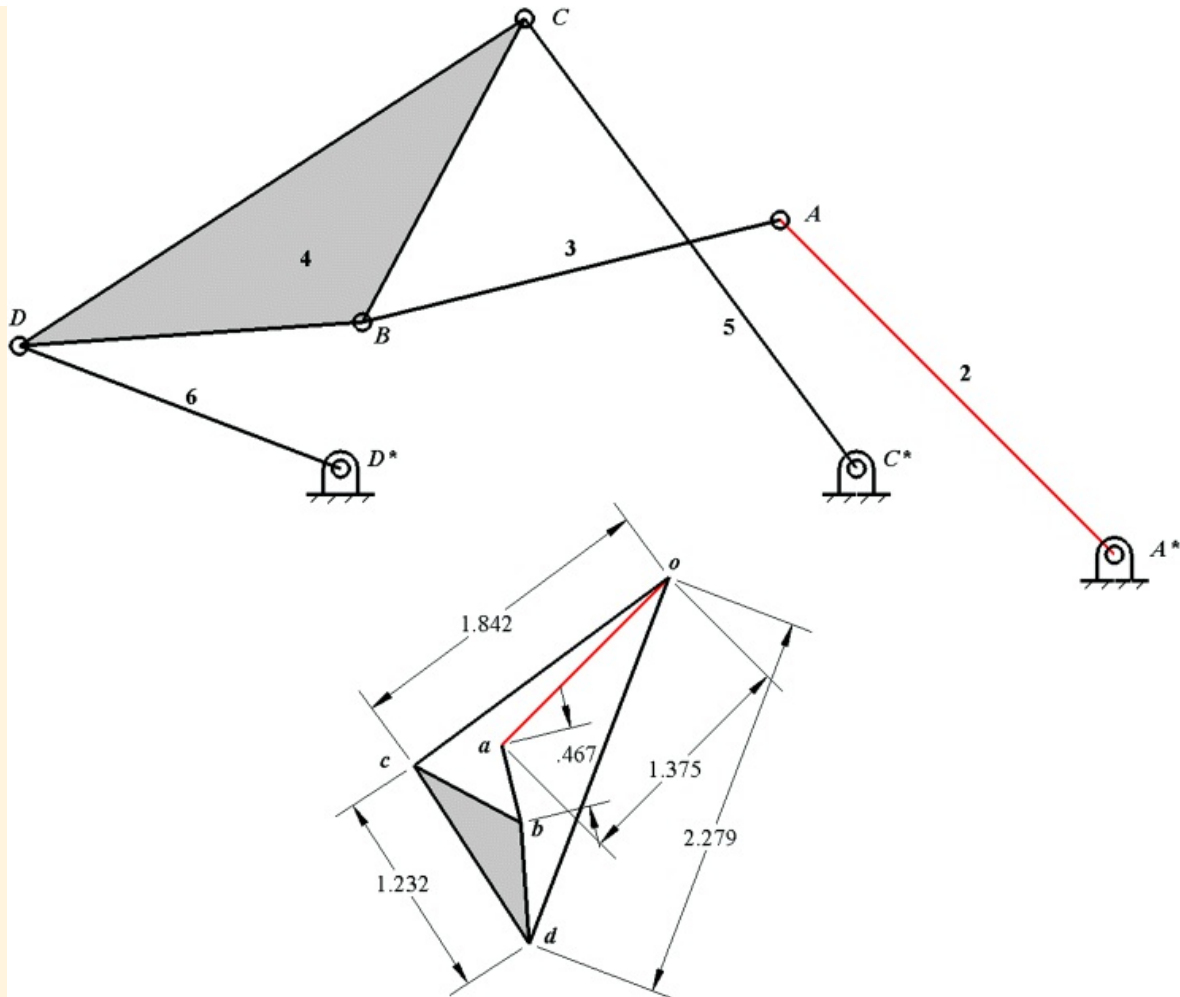


Figure 4.25 Position and velocity solution for Example 4.7.

The procedure for solving for the velocities is to draw the velocity polygon with an arbitrary linear velocity for point D_6 . We could construct two velocity polygons, one for a CCW rotation for link 6 and one for a CW rotational direction. However, as will be shown in the following, the velocity polygon can be drawn so quickly that we can simply redraw it if the direction turns out to be incorrect. We will know if we have assumed the correct direction if the direction of the angular velocity of link 2 is the input direction (CCW) for the assumed velocity of link 6.

For the velocity analysis, the basic equations that we will solve in order are

$$\begin{aligned}
 v_{B_6} &= v_{B_6} = v_{B_6} + v_{D_6}/\omega_6 \\
 v_{C_6} &= v_{C_6} = v_{D_6} - v_{C_6}/\omega_6 \\
 v_{C_6^*} &= v_{C_6^*} = v_{C_6}/\omega_6 \\
 v_{B_6} &= v_{B_6} = v_{B_6} - v_{B_6}/\omega_6 \\
 v_{B_6} &= v_{B_6} = v_{C_6} + v_{B_6}/\omega_6 \\
 v_{A_6} &= v_{A_6} = v_{A_6} + v_{A_6}/\omega_6 \\
 v_{A_6^*} &= v_{A_6^*} = v_{A_6^*}/\omega_6
 \end{aligned}$$

Steps

1. Make the *Vel Polygon* layer active. Draw an arbitrary line and constrain the line to be perpendicular to line DD^* . This line corresponds to the velocity of D_6 and D_4 . Use the dimension tool and temporarily

dimension the line to be 2 in long. This will stabilize the size of the velocity diagram, and we will later delete this dimension. Select the top end of the line and fix it. Label it with the letter o . Label the lower end as d .

2. Starting from point d , draw a line perpendicular to line CD . This new line corresponds to v_{C_4/D_4} . Draw a second line starting from point o and perpendicular to line CC^* . This new line corresponds to v_{C_5/C_5^*} . Merge the ends of the two new lines. The intersection of the two lines gives point c corresponding to the velocity of points C_4 and C_5 .
3. Starting from point d , draw a line perpendicular to line BD . This new line corresponds to v_{B_4/D_4} . Draw a second line starting from c and perpendicular to line BC . This new line corresponds to v_{B_5/C_5} . Merge the ends of the two new lines. The intersection of the two lines gives point b corresponding to the velocities of points B_4 and B_3 .
4. Starting from point b , draw a line perpendicular to line BA . This new line corresponds to v_{A_3/B_3} . Draw a second line starting from o and perpendicular to line AA^* . This second line corresponds to v_{A_2/A_2^*} . Merge the ends of the two new lines. The merged point for these two lines corresponds to the velocity of points A_3 and A_2 . The actual velocity of A_2 corresponds to the line from o to a .
5. Check that the direction for the computed velocity of A_2 corresponds to a CCW direction for the angular velocity of Link 2. The direction is indicated by knowing that the tail of vector is located at o . In this case, we assumed the correct direction for the direction of the velocity of point D so we do not need to redraw the diagram. If the direction had been incorrect, we would have redrawn the velocity polygon with line od drawn in the opposite direction. All other constructions and constraints would be the same.
6. Delete the original dimension used for line od . Change the color of oa to red to designate it as the input velocity. The linear velocity of point A is given by

$$v_{A_2} = v_{A_2/A_2^*} = \omega_2 \times v_{A_2/A_2^*}$$

Therefore the magnitude of the velocity of point A is given by

$$|v_{A_2}| = [\omega_2] |v_{A_2/A_2^*}| = (10)(2.73) = 27.3 \text{ in/s}$$

Based on this value, a reasonable scale for the velocity polygon is 1 in corresponds to 20 in/s. Using this scale factor, the length of oa should be $27.3/20 = 1.375$ in long. Again, there is no need to make the polygon unusually large because the parametric-design program will calculate the lengths of the lines extremely accurately if the constraints are set properly. Using the dimension tool, constrain line oa to be 1.375 in long.

7. Use the dimension tool to measure the lengths of the lines od , oc , ab , and cd . Also, notice the orientation of the lines. Make all of the dimensions *driven* to avoid overconstraining the linkage. The final polygon and linkage are shown in [Figure 4.25](#).
8. The measured distances are: $od = 2.279$ in, $oc = 1.842$ in, $cd = 1.232$ in, and $ab = 0.467$ in. Using the scaling factor (20), the magnitudes of the corresponding linear velocities are

$$\begin{aligned} |v_{D_6/D_6^*}| &= 20(2.279) = 45.58 \text{ in/s} \\ |v_{C_5/C_5^*}| &= 20(1.842) = 36.84 \text{ in/s} \\ |v_{C_4/D_4}| &= 20(1.232) = 24.64 \text{ in/s} \\ |v_{A_3/B_3}| &= 20(0.467) = 9.34 \text{ in/s} \end{aligned}$$

9. Compute the corresponding angular velocities ω_6 , ω_5 , ω_4 , and ω_3 . To obtain the directions, we need to observe the sense of the lines in the velocity diagram. As before, we identify the vectors corresponding to the lines in the position and velocity diagrams by treating the tail of the vector as the second subscript and the head of the vector as the first subscript. We need to remember also that the velocity of all fixed pivots (A^* , C^* , and D^*) are located at point o in the velocity polygon. For example, the direction of the vector v_{B_6/B_5} points from o to d in the velocity polygon and the position vector r_{B/D^*} points from D^* to D in the position diagram. The four angular velocities are then given by

$$\begin{aligned}\omega_6 &= \left(\frac{|v_{B_6/B_5}|}{|r_{B_6/B_5}|} = \frac{45.58}{2.0} = 22.8 \text{ rad/s} \right) \text{CCW} \\ \omega_5 &= \left(\frac{|v_{C_5/C_4}|}{|r_{C_5/C_4}|} = \frac{36.84}{3.25} = 11.3 \text{ rad/s} \right) \text{CCW} \\ \omega_4 &= \left(\frac{|v_{C_4/B_4}|}{|r_{C_4/B_4}|} = \frac{24.64}{3.5} = 7.04 \text{ rad/s} \right) \text{CCW} \\ \omega_3 &= \left(\frac{|v_{A_3/B_2}|}{|r_{A_3/B_2}|} = \frac{9.34}{2.5} = 3.74 \text{ rad/s} \right) \text{CCW}\end{aligned}$$

This completes the velocity analysis.



Example 4.8

Acceleration Analysis of Slider-Crank Linkage Using GCP

To illustrate the use of GCP for accelerations, we will resolve Example 4.2 and compare results. The objective is to find v_B , a_B , α_2 , and α_3 for the slider-crank linkage in the position shown in [Figure 4.10](#). The crank AA^* (link 2) is driven at a constant angular velocity of 10 rad/s CCW. Point B is the axis of the revolute joint connecting the connecting rod, link 3, to the slider, link 4. In the position shown, AA^* is at 45° to A^*B , and the link lengths are shown on the drawing. The angular velocity of link 2 is a constant 10 rad/s (CCW).

Solution

When GCP is used to generate a graphical program for accelerations, it is necessary to use equation constraints. However, if we do not need to develop a graphical program that will work for a variety of positions or dimensions, we can calculate the radial components of acceleration externally and simply apply the results as fixed dimensions. This lets us solve individual problems more accurately and more quickly than can be done with traditional graphical techniques, and this is the approach that will be applied here.

We will begin the analysis by drawing the linkage in the position specified by the input data. First open a blank worksheet and set up the following five layers

1. *Linkage*: Contains the final linkage, which can be animated
2. *Dimensions*: Contains the dimensions for the link lengths and other variables
3. *Vel Polygon*: Contains the constructions for the velocity polygon
4. *Acc Polygon*: Contains the constructions for the acceleration polygon
5. *Pivot Dimensions*: Contains the dimensions associated with the ground pivots, slider block, slider line, and any other dimensions that are not of interest in the final drawing

Make the *Linkage* layer active and sketch the linkage in [Figure 4.10](#). Next use a combination of constraints and the dimension tool to constrain the link lengths according to the dimensions given. We have drawn the linkage half scale so that all of the original link lengths need to be divided by 2. After the linkage is fully constrained, a ground pivot, bushings, slider block, and slider line have been added to improve the appearance of the drawing. The final linkage model is shown in [Figure 4.26](#).

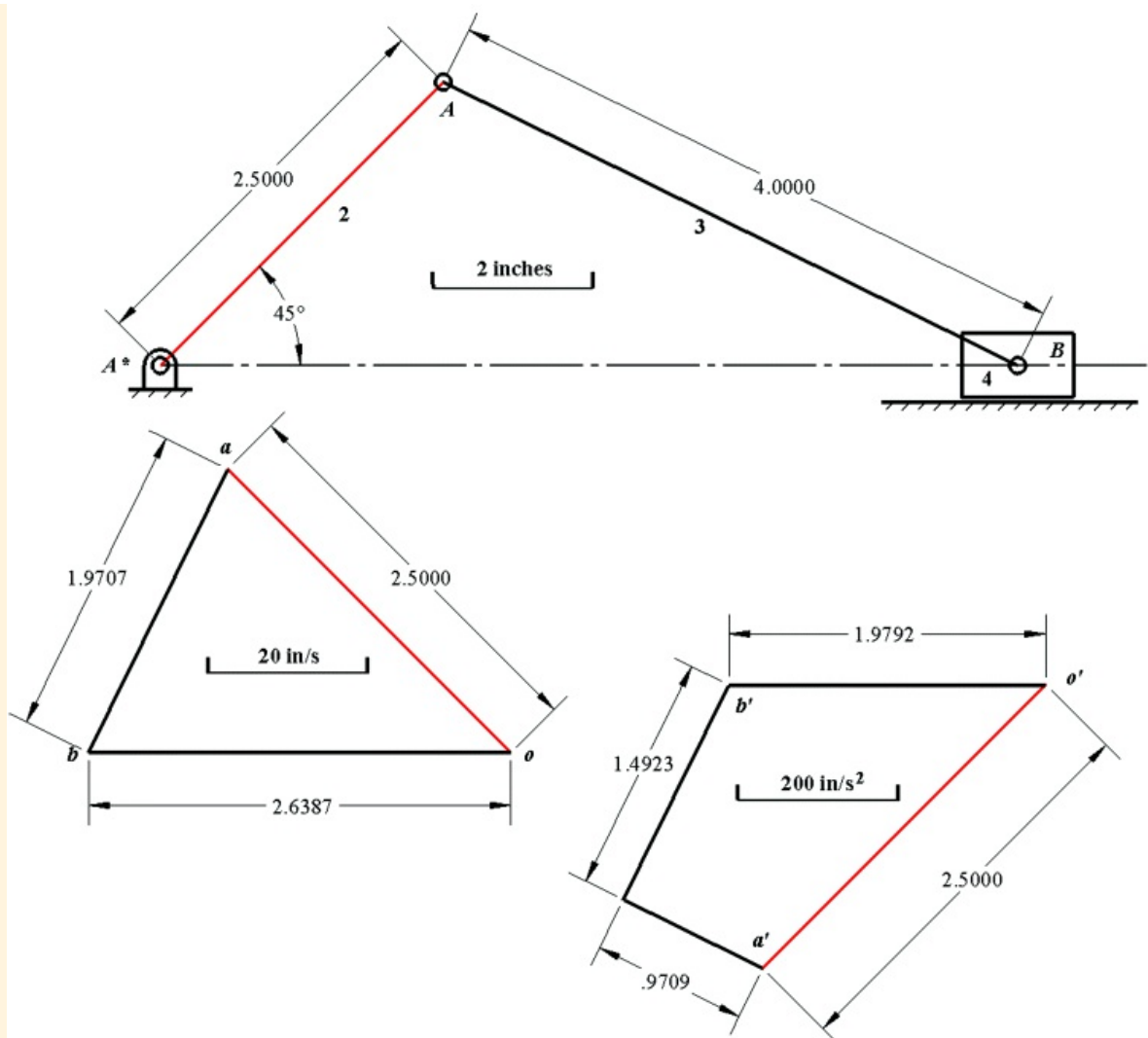


Figure 4.26 Velocity and acceleration polygons for Example 4.2 solved using GCP.

(a) Velocity Analysis

To begin the velocity analysis, we must write the equations for the linkage. These are given in the following

$$\begin{aligned} \dot{\theta}_{A_2} &= \dot{\theta}_{A_3} = \dot{\theta}_{A_2}/r_{A_2}^* = \dot{\theta}_{A_3}/r_{A_2}^* = \omega_2 \times r_{A_2}/r_{A_2} \\ \dot{\theta}_{B_3} &= \dot{\theta}_{A_3} + \dot{\theta}_{B_3}/r_{A_3} \end{aligned}$$

Because the angular velocity of link 2 is given, we can compute the velocity of A_2 and A_3 directly. Then

$$|\dot{\theta}_{A_2}/r_{A_2}^*| = |\dot{\theta}_2| r_{A_2}/r_{A_2}^* = (10 \text{ rad/s})(5 \text{ in}) = 50 \text{ in/s (normal to } \dot{\theta}_{A_2}/r_{A_2}^*)$$

The direction for $\dot{\theta}_{A_2}/r_{A_2}^*$ is perpendicular to $\dot{\theta}_{A/A^*}$ and the direction is defined by rotating $\dot{\theta}_{A/A^*}$ in the CCW direction.

To begin the GCP procedure, make the *Vel Polygon* layer active and choose a starting point (o) for the velocity polygon. Using o as the tail of the vector, draw a line upward and to the left and constrain it to be perpendicular to A^*A . Label the end of the line as a . Next draw a second line from o and constrain the line to be horizontal. Starting from a , draw a third line and constrain it to be perpendicular to AB . Merge the

ends of the last two lines drawn. The merged point will correspond to the unscaled position of b . Use a scale where 1 inch on the polygon corresponds to 20 in/s. Next use the dimension tool and constrain the line oa to be 2.5 corresponding to the scaled length of the vector \vec{v}_{A_3/A_2} . Also use the dimension tool to determine the lengths of ob (corresponding to \vec{v}_{B_3}) and ab (corresponding to \vec{v}_{B_3/A_3}). The results are shown in [Figure 4.26](#).

Based on the scaled dimensions in [Figure 4.26](#)

$$v_{B_3/A_3} = (20) \times 1.9707 = 39.414 \text{ in/sec}$$

and

$$v_{B_3} = (20) \times 2.6587 = 52.774 \text{ in/sec}$$

Therefore

$$\omega_3 = \left(\frac{|v_{B_3/A_3}|}{|v_{B/A}|} = \frac{39.414}{8} = 4.925 \text{ rad/s} \right) \text{CCW}$$

These values are more accurate than those computed in Example 4.2 although the numbers from both approaches are quite close.

(b) Acceleration Analysis

The equations for the acceleration analysis are

$$\begin{aligned} \ddot{\theta}_{A_2} &= \ddot{\theta}_{A_3} = \ddot{\theta}_{A_2^*} = \ddot{\theta}_{A_2/A_3^*} = \ddot{\theta}_{A_2/A_2^*} + \ddot{\theta}_{B_2/A_2^*} \\ \ddot{\theta}_{B_2} &= \ddot{\theta}_{A_3} + \ddot{\theta}_{B_2/A_2} = \ddot{\theta}_{A_2/A_2^*} + \ddot{\theta}_{B_2/A_2^*} = \ddot{\theta}_{B_2/A_3} + \ddot{\theta}_{B_2/A_2} \end{aligned}$$

We could use the equation feature in the parametric-design program to compute the radial components of acceleration based on the position and velocity information; however, it is equally convenient to compute the required values externally when only one position is required. Therefore

$$\begin{aligned} |\ddot{\theta}_{A_2/A_2^*}| &= |\omega_2|^2 |r_{A/A*}| = 10^2(5) = 500 \text{ in/s}^2 \\ |\ddot{\theta}_{A_2/A_2^*}| &= |\omega_2| |r_{A/A*}| = 0(5) = 0 \text{ in/s}^2 \end{aligned}$$

From the velocity analysis

$$|\ddot{\theta}_{B_2/A_3}| = |\omega_3|^2 |r_{B/A}| = \frac{|v_{B_3/A_3}|^2}{|r_{B/A}|} = \frac{39.414^2}{8} = 194.18 \text{ in/s}^2$$

The direction for the acceleration of B_3 must be horizontal. To begin the acceleration analysis, make the *Acc Polygon* layer active, choose a location for the acceleration pole, o' , and select the scale for the acceleration polygon as 200 in/s². Draw a line from o' in the direction of AA^* and constrain the line to be parallel to AA^* . Label the lower end of the line as a' . This corresponds to the vector \vec{r}_{A_2/A_2^*} . Using the dimension tool,

constrain the line to be 2.5 in long. Draw a line starting at o' and to the left of o' and constrain the line to be horizontal. This corresponds to the direction of \vec{v}_{B_3/A_3} . Starting at a' , draw a line in the direction of BA and constrain the line to be parallel to BA . Using the dimension tool, constrain the line to be $194.18/200 = 0.9709$ in long. This line corresponds to \vec{v}_{B_3/A_3} . Draw a line from the end of \vec{v}_{B_3/A_3} in the orthogonal direction and constrain the line to be perpendicular to AB . Merge the orthogonal line and the horizontal line through o' . Label the intersection as b' . The orthogonal line corresponds to \vec{a}_{B_3/A_3} . Use the dimension tool to measure the lengths of the last two vectors. This is shown in [Figure 4.26](#). From the acceleration polygon, the acceleration of B_3 is

$$a_{B_3} = 1.9792 \times 200 = 395.84 \text{ in/s}^2 \text{ to the left}$$

And the angular acceleration of link 3 is

$$\alpha_3 = \left(\frac{|\vec{a}_{B_3/A_3}|}{|\vec{v}_{B/A}|} = \frac{1.4523 \times 200}{8} = 37.307 \text{ rad/s}^2 \right) \text{ CW}$$

Again, these values are more accurate than those computed in Example 4.2 although the numbers from both approaches are quite close.



References

1. Hirschorn, J. (1962). *Kinematics and Dynamics of Plane Mechanisms*. New York, NY: McGraw-Hill.
2. Hall, A. (1966). *Kinematics and Linkage Design*. West Lafayette, IN: Balt Publishers.
3. Holowenko, A. R. (1955). *Dynamics of Machinery*. New York, NY: John Wiley & Sons.
4. Goodman, T. P. (1958). "An Indirect Method for Determining Accelerations in Complex Mechanisms." *Trans. ASME*, Nov. pp. 1676–1682.

Problems

Velocity and Acceleration Analysis of Single-Loop Mechanisms

4.1 In [Figure P4.1](#), link 2 is rotating CCW at the rate of 2 rad/s (constant). In the position shown, link 2 is horizontal and link 4 is vertical. Write the appropriate vector equations, solve them using vector polygons, and

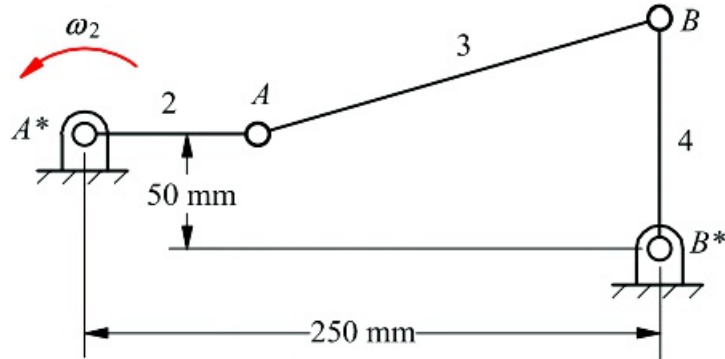


[Figure P4.1](#) Linkage for Problem 4.1.

- Determine v_{B4} , ω_3 , and ω_4
- Determine a_{B4} , α_3 , and α_4

Link lengths: $A^*A = 75 \text{ mm}$, $B^*B = 100 \text{ mm}$

4.2 In [Figure P4.2](#), A^* and B^* are on the same horizontal line. Link 2 is rotating CCW at the constant rate of 500 rad/s. In the position shown, link 2 is vertical. Write the appropriate vector equations, solve them using vector polygons, and

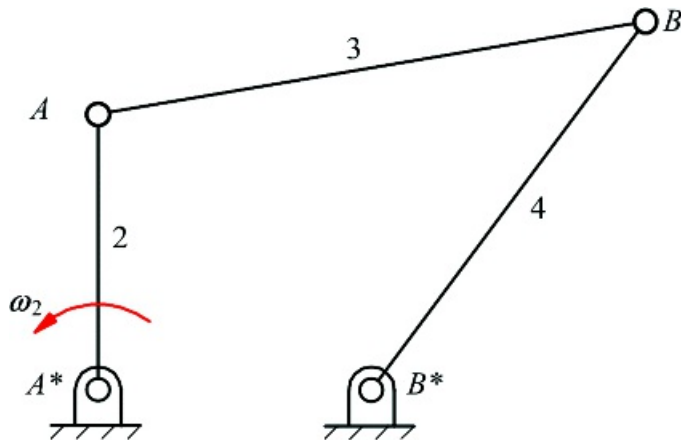


[Figure P4.2](#) Linkage for Problem 4.2.

- Determine v_{B4} , ω_3 , and ω_4
- Determine a_{B4} , α_3 , and α_4

Link lengths: $A^*A = A^*B^* = 1.2 \text{ in}$, $AB = 2.42 \text{ in}$, $B^*B = 2 \text{ in}$

4.3 In [Figure P4.3](#), A^* and B^* are on the same horizontal line. Link 2 is rotating CW at the constant rate of 10 rad/s. In the position shown, links 2 and 4 are vertical. Write the appropriate vector equations, solve them using vector polygons, and

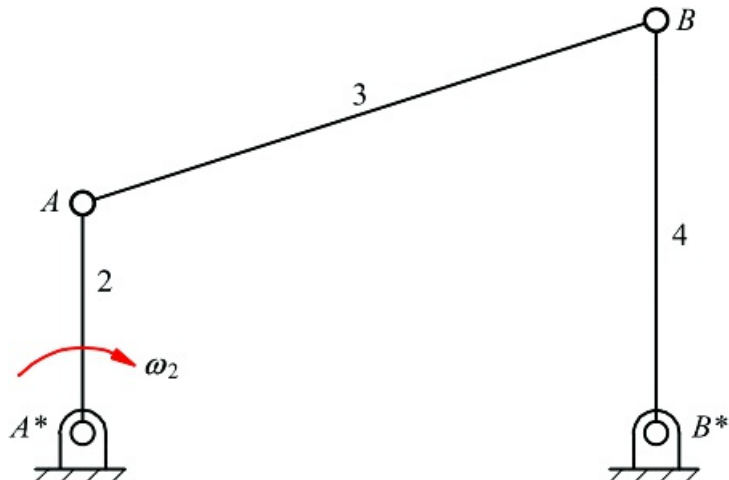


Figure P4.3 Linkage for Problem 4.3.

- Determine v_{B4} , ω_3 , and ω_4
- Determine a_{B4} , α_3 , and α_4

Link lengths: $A^*A = 100 \text{ mm}$, $AB = 250 \text{ mm}$, $B^*B = 180 \text{ mm}$

4.4 In [Figure P4.4](#), link 2 is rotating CW at the constant rate of 4 rad/s. In the position shown, Link 3 is horizontal. Write the appropriate vector equations, solve them using vector polygons, and

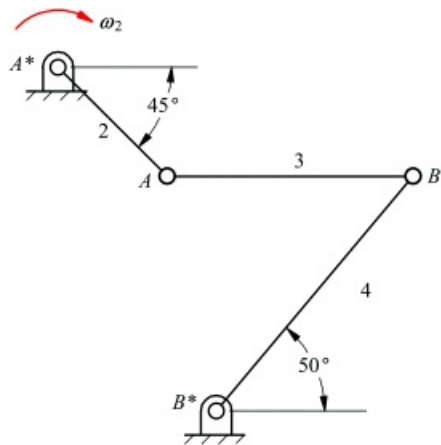


Figure P4.4 Linkage for Problem 4.4.

- Determine v_{B4} , ω_3 , and ω_4
- Determine a_{B4} , α_3 , and α_4

Link lengths: $A^*A = 100 \text{ mm}$, $AB = 160 \text{ mm}$, $B^*B = 200 \text{ mm}$

4.5 In [Figure P4.5](#), link 2 is rotating CCW at the constant rate of 4 rad/s. In the position shown, link 2 is horizontal and link 4 is vertical. Write the appropriate vector equations, solve them using vector polygons, and

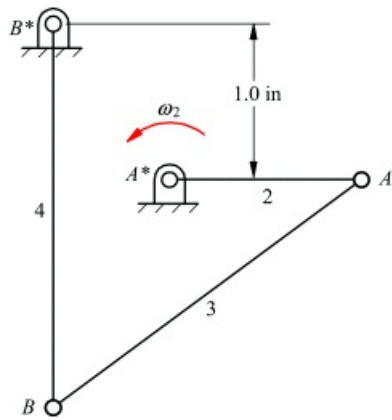


Figure P4.5 Linkage for Problem 4.5.

- Determine v_{B4} , ω_3 , and ω_4
- Determine a_{B4} , a_3 , and a_4

Link lengths: $A^*A = 1.25$ in, $AB = 2.5$ in, $B^*B = 2.5$ in

4.6 In [Figure P4.6](#), link 2 is rotating CW at the rate of 100 rad/s (constant). In the position shown, link 2 is horizontal. Write the appropriate vector equations, solve them using vector polygons, and

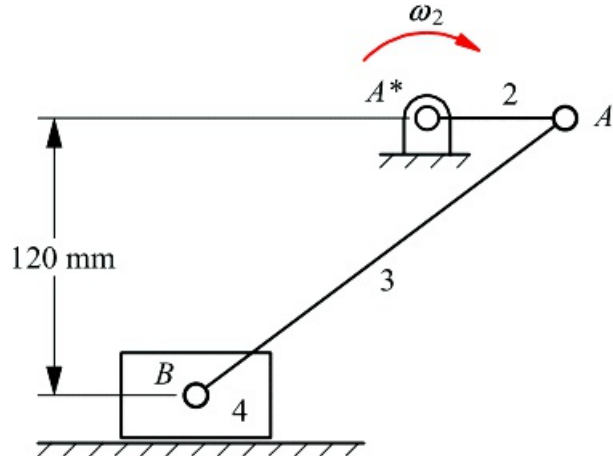
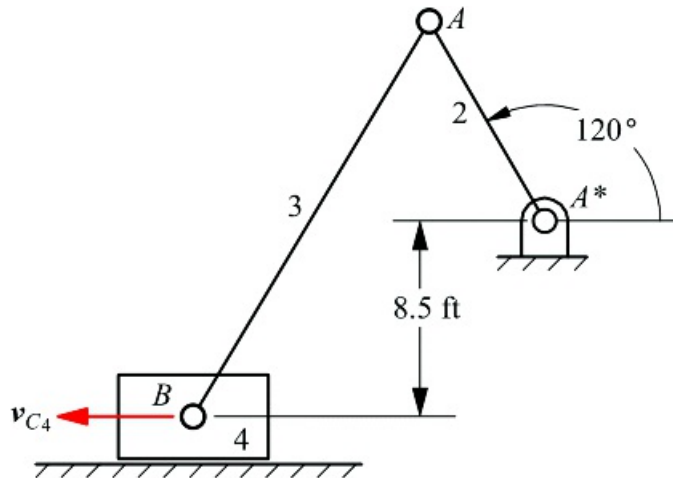


Figure P4.6 Linkage for Problem 4.6.

- Determine v_{B4} and ω_3
- Determine a_{B4} and a_3

Link lengths: $A^*A = 60$ mm, $AB = 200$ mm

4.7 In [Figure P4.7](#), link 4 is moving to the left at the constant rate of 4 ft/s. Write the appropriate vector equations, solve them using vector polygons, and



[Figure P4.7](#) Linkage for Problem 4.7.

- Determine ω_2 and ω_3
- Determine a_2 and a_3

Link lengths: $A^*A = 10 \text{ ft}$, $AB = 20 \text{ ft}$

4.8 In [Figure P4.8](#), link 4 is moving to the right at the constant rate of 20 in/s. Write the appropriate vector equations, solve them using vector polygons, and

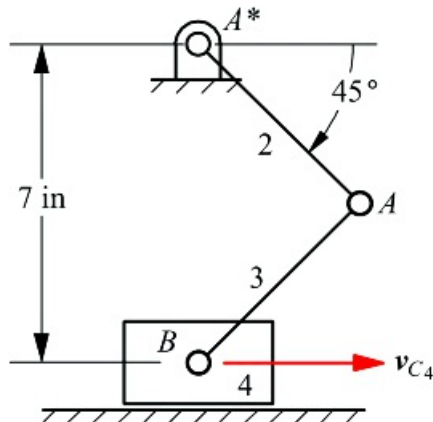


[Figure P4.8](#) Linkage for Problem 4.8

- Determine ω_2 and ω_3
- Determine a_2 and a_3

Link lengths: $A^*A = AB = 5 \text{ in}$

4.9 In [Figure P4.9](#), link 4 is moving to the left at the constant rate of 0.6 ft/s. Write the appropriate vector equations, solve them using vector polygons, and determine the velocity and acceleration of point A_3 .

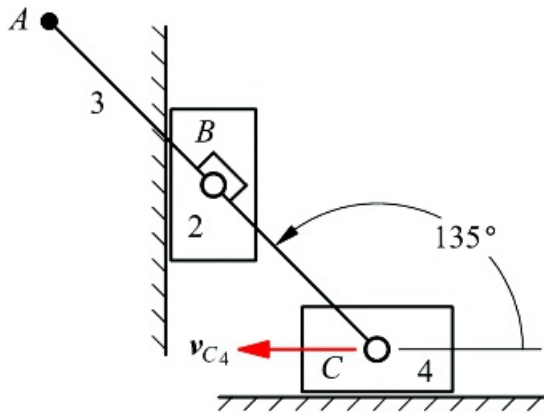


[Figure P4.9](#) Linkage for Problem 4.9.

Link lengths: $AB = BC = 5$ in

4.10 In [Figure P4.10](#), link 4 moves to the right with a constant velocity of 75 ft/s. Write the appropriate vector equations, solve them using vector polygons, and

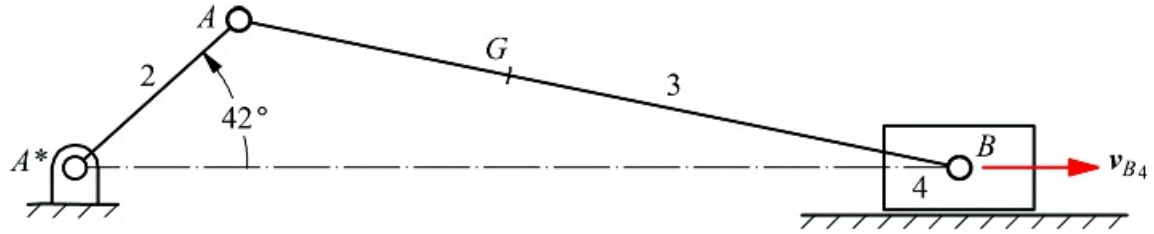


[Figure P4.10](#) Linkage for Problem 4.10.

- Determine v_{A2} , v_{G3} , ω_2 , and ω_3
- Determine a_{A2} , a_{G3} , α_2 , and α_3

Link lengths: $A^*A = 4.8$ in, $AB = 16$ in, $AG = 6.0$ in

4.11 For the four-bar linkage shown [Figure P4.11](#), assume that $\omega_2 = 50$ rad/s CW and $\alpha_2 = 1600$ rad/s² CW. Write the appropriate vector equations, solve them using vector polygons, and

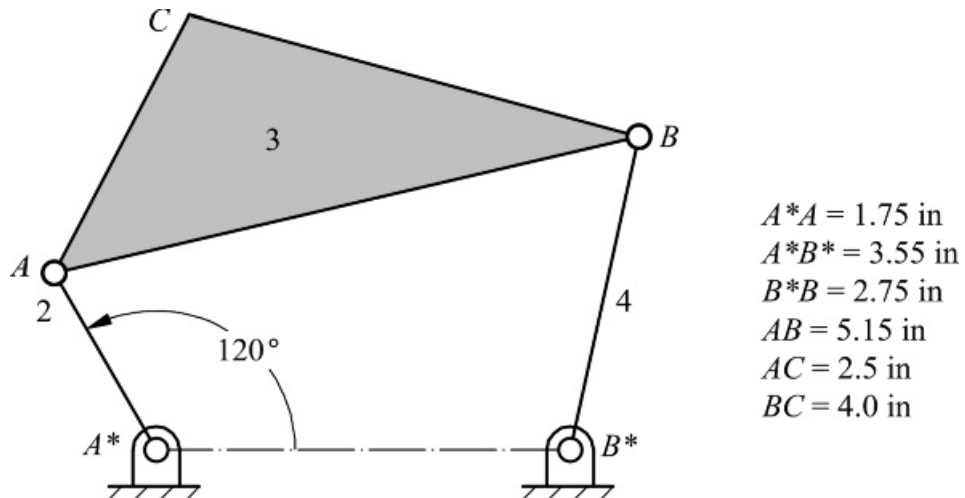


[Figure P4.11](#) Linkage for Problem 4.11.

- Determine v_{A2} , v_{B3} , v_{C3} , ω_3 , and ω_4
- Determine a_{A2} , a_{B3} , a_{C3} , α_3 , and α_4

4.12 Solve Problem 4.11 again if $\omega_2 = 50 \text{ rad/s}$ CCW and $a_2 = 0$.

4.13 In [Figure P4.13](#), link 2 is rotating CW at the constant rate of 180 rad/s. Write the appropriate vector equations, solve them using vector polygons, and

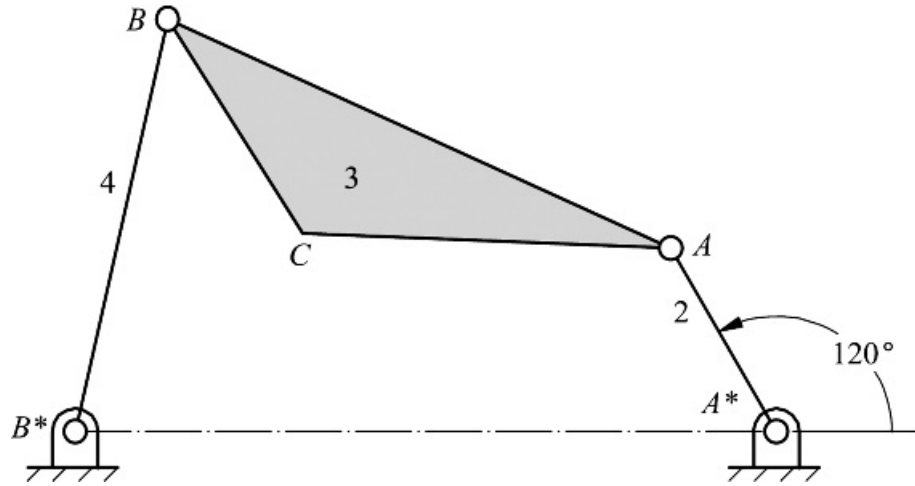


[Figure P4.13](#) Linkage for Problem 4.13.

- Determine v_{A2} , v_{B3} , v_{C3} , ω_3 , and ω_4
- Determine a_{A2} , a_{B3} , a_{C3} , a_3 , and a_4

Link lengths: $A^*A = 4.6 \text{ in}$, $AB = 12.0 \text{ in}$, $A^*B^* = 15.2 \text{ in}$, $B^*B = 9.2 \text{ in}$, $AC = 8.0 \text{ in}$, $BC = 5.48 \text{ in}$

4.14 The accelerations of points A and B in the coupler in [Figure P4.14](#) are as given. Determine the acceleration of the center of mass G and the angular acceleration of the body. Draw the vector representing a_G from G .

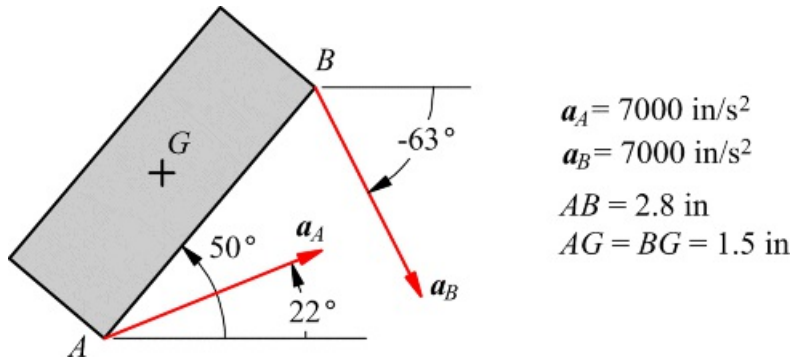


[Figure P4.14](#) Linkage for Problem 4.14.

4.15 Crank 2 of the push-link mechanism shown in [Figure P4.15](#) is driven at a constant angular velocity $\omega_2 = 60 \text{ rad/s}$ (CW). Find the velocity and acceleration of point D and the angular velocity and acceleration of links 3 and 4.

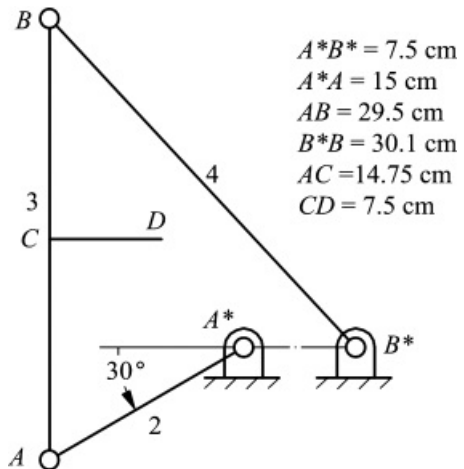


[Figure P4.15](#) Linkage for Problem 4.15.

4.16 For the straight-line mechanism shown in [Figure P4.16](#), $\omega_2 = 20 \text{ rad/s}$ (CW) and $\alpha_2 = 140 \text{ rad/s}^2$ (CW). Determine the velocity and acceleration of point C and the angular acceleration of link 3.

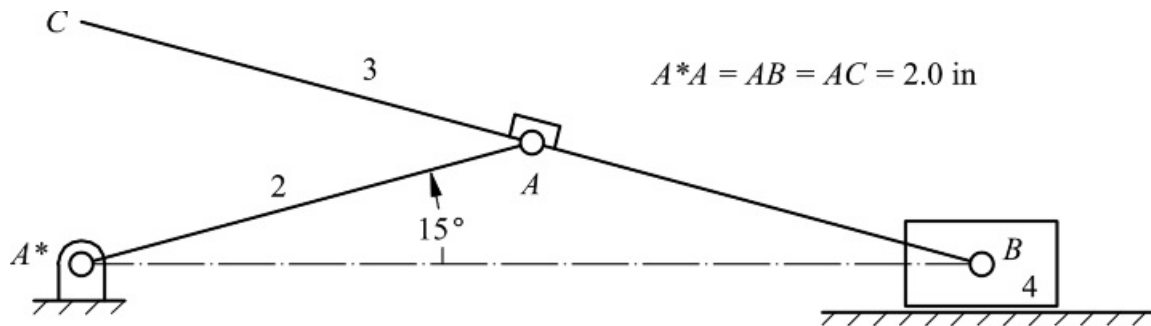


[Figure P4.16](#) Linkage for Problem 4.16.

4.17 For the data given in [Figure P4.17](#), find the velocity and acceleration of points B and C. Assume $v_A = 20 \text{ ft/s}$, $a_A = 400 \text{ ft/s}^2$, $\omega_2 = 24 \text{ rad/s}$ (CW), and $\alpha_2 = 160 \text{ rad/s}^2$ (CCW).

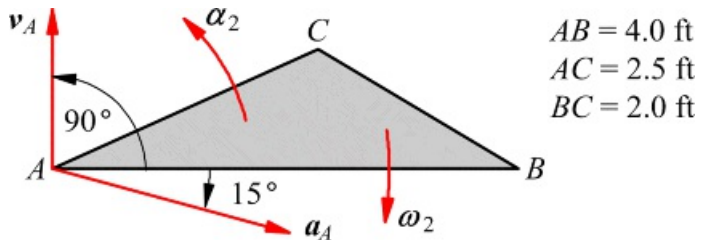


[Figure P4.17](#) Linkage for Problem 4.17.

4.18 In [Figure P4.18](#), link 2 is turning CCW at the constant rate of 10 rad/s. Draw the velocity and acceleration polygons for the mechanism, and determine α_{C3} and α_4 .

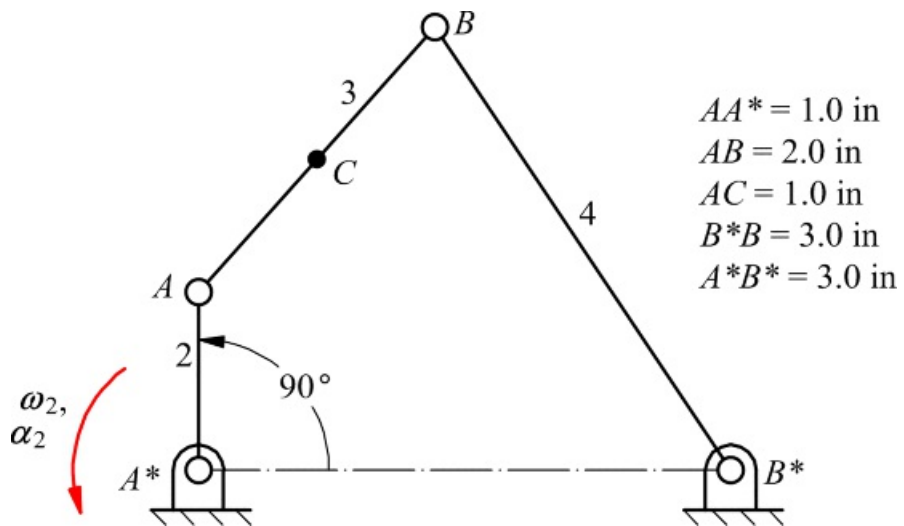


[Figure P4.18](#) Linkage for Problem 4.18.

4.19 If $\omega_2 = 100 \text{ rad/s CCW}$ (constant), find the velocity and acceleration of point C_4 in [Figure P4.19](#).

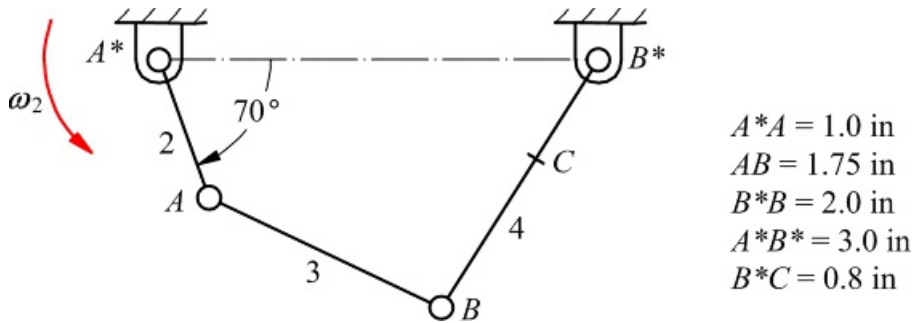


[Figure P4.19](#) Linkage for Problem 4.19.

Velocity and Acceleration Analysis of Multi-Loop Mechanisms

4.20 Draw the velocity polygon to determine the velocity of link 6 in [Figure P4.20](#). Points A^* , B , and D are on the same horizontal line. The angular velocity of link 2 is 6 rad/s CW.

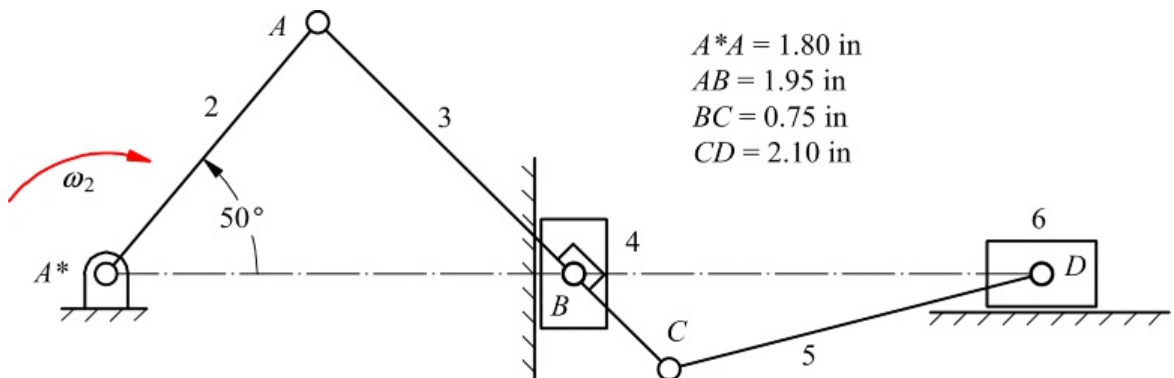


[Figure P4.20](#) Linkage for Problem 4.20.

4.21 Link 2 of the linkage shown in [Figure P4.21](#) has an angular velocity of 10 rad/s CCW. Find the angular velocity of link 6 and the velocities of points B , C , and D .

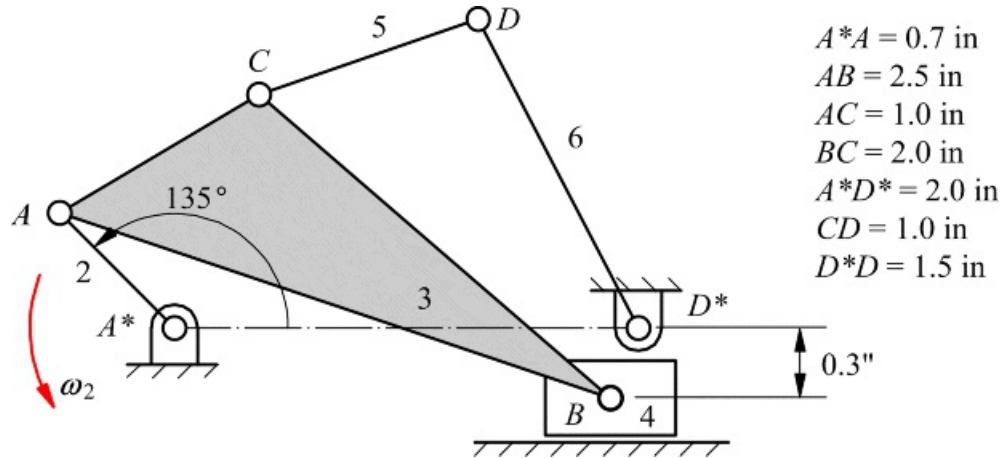


Figure P4.21 Linkage for Problem 4.21.

4.22 The linkage shown in Figure P4.22 is used to raise the fabric roof on convertible automobiles. The dimensions are given as shown. Link 2 is driven by a DC motor through a gear reduction. If the angular velocity $\omega_2 = 2 \text{ rad/s}$, CCW, determine the linear velocity of point H, which is the point where the linkage connects to the automobile near the windshield.

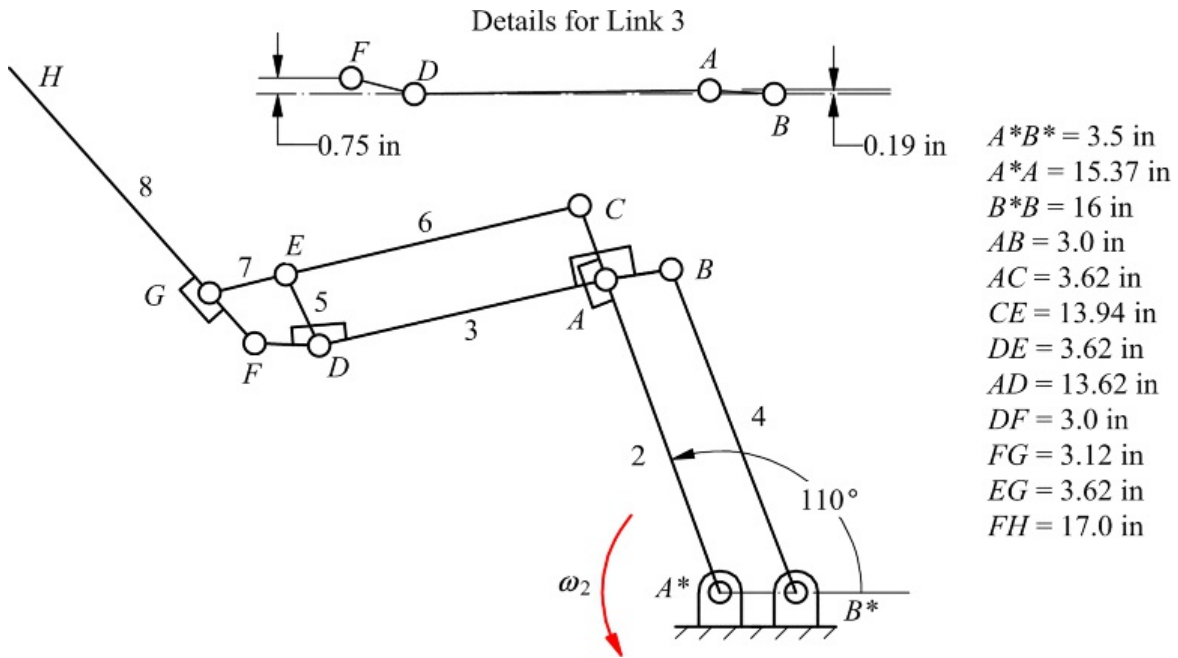
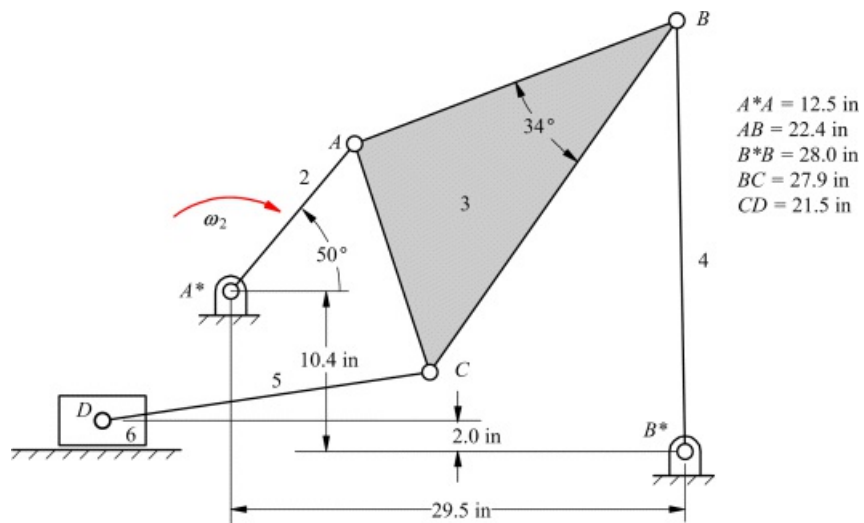


Figure P4.22 Linkage for Problem 4.22.

4.23 In Figure P4.23, the angular velocity of link 2 is 3 rad/s CW. Determine the sliding velocity of link 6 and the angular velocities of links 3 and 5.



[Figure P4.23](#) Linkage for Problem 4.23.

4.24 In [Figure P4.24](#), $v_{A2} = 15$ m/s (constant). Draw the velocity polygon, and determine the velocity of point D on link 6 and the angular velocity of link 5.

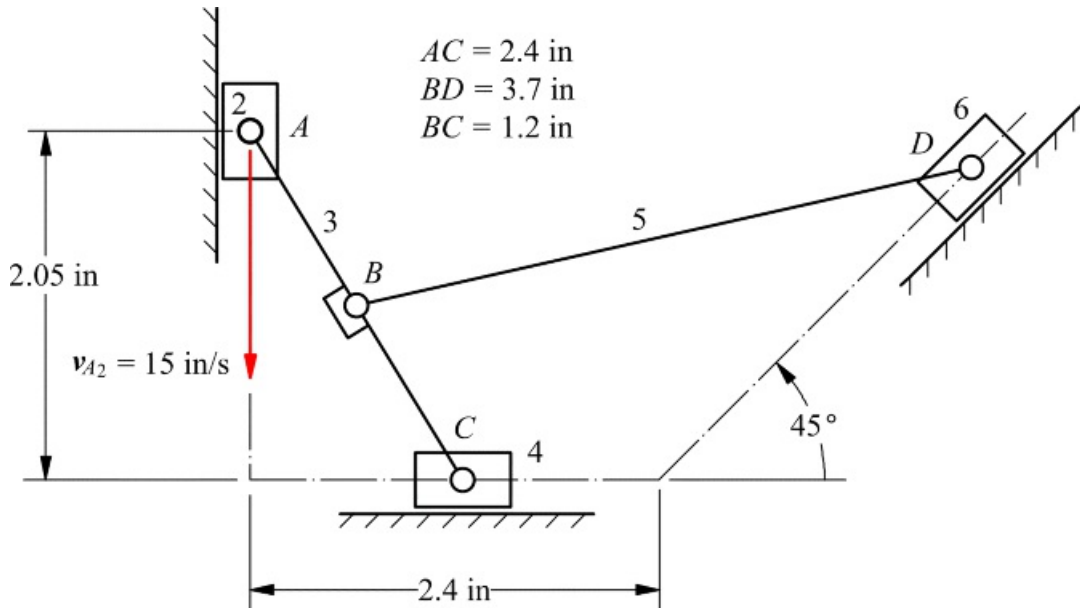


[Figure P4.24](#) Linkage for Problem 4.24.

4.25 In [Figure P4.25](#), points A^* and B are on the same horizontal line. Find the velocities of points B , C , and D of the double-slider mechanism shown in the figure if crank 2 rotates at 42 rad/s CCW.

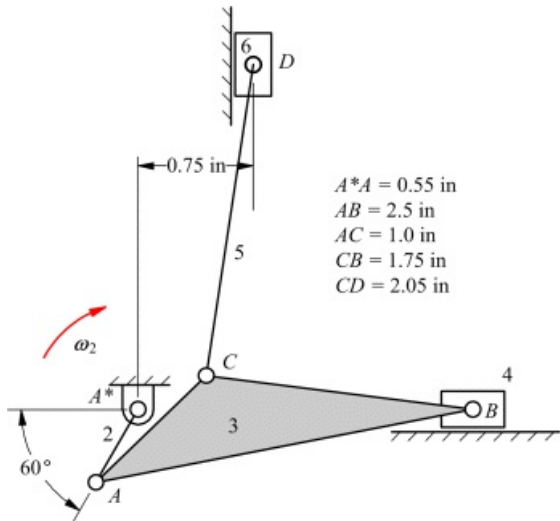


[Figure P4.25](#) Linkage for Problem 4.25.

4.26 Given $v_{B4} = 1.0 \text{ ft/s}$ to the left, find v_{D6} , as shown in [Figure P4.26](#).

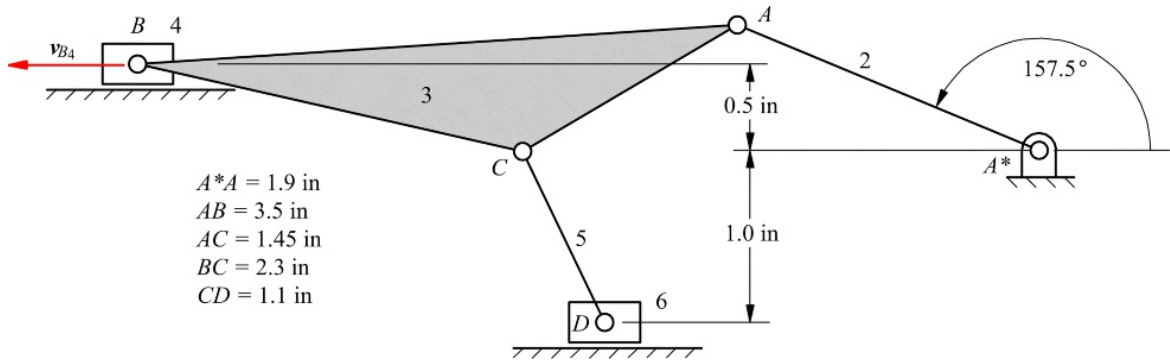


[Figure P4.26](#) Linkage for Problem 4.26.

4.27 If $v_{A2} = 10 \text{ in/s}$ as shown in [Figure P4.27](#), find v_{D5} .

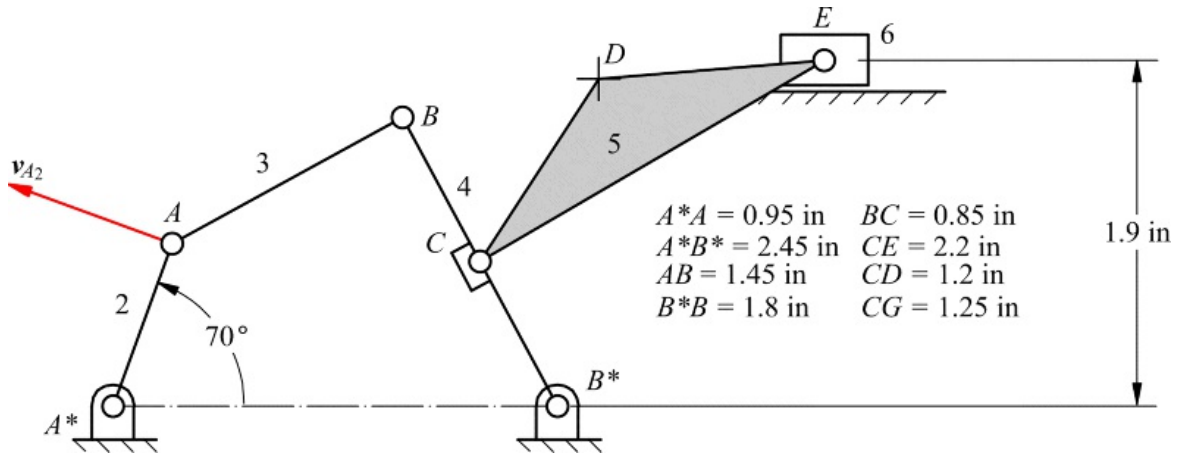


[Figure P4.27](#) Linkage for Problem 4.27.

4.28 If $v_{A2} = 10 \text{ in/s}$ as shown in [Figure P4.28](#), find the angular velocity of link 6.

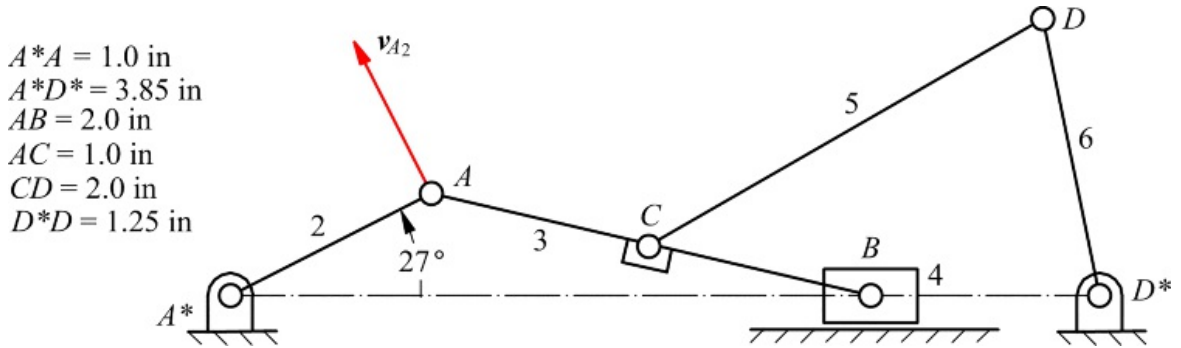


Figure P4.28 Linkage for Problem 4.28.

4.29 The angular velocity of link 2 of the mechanism shown in Figure P4.29 is 20 rad/s (CW) and its angular acceleration is 100 rad/s² (CW) at the instant being considered. Determine the linear velocity and acceleration of point D.

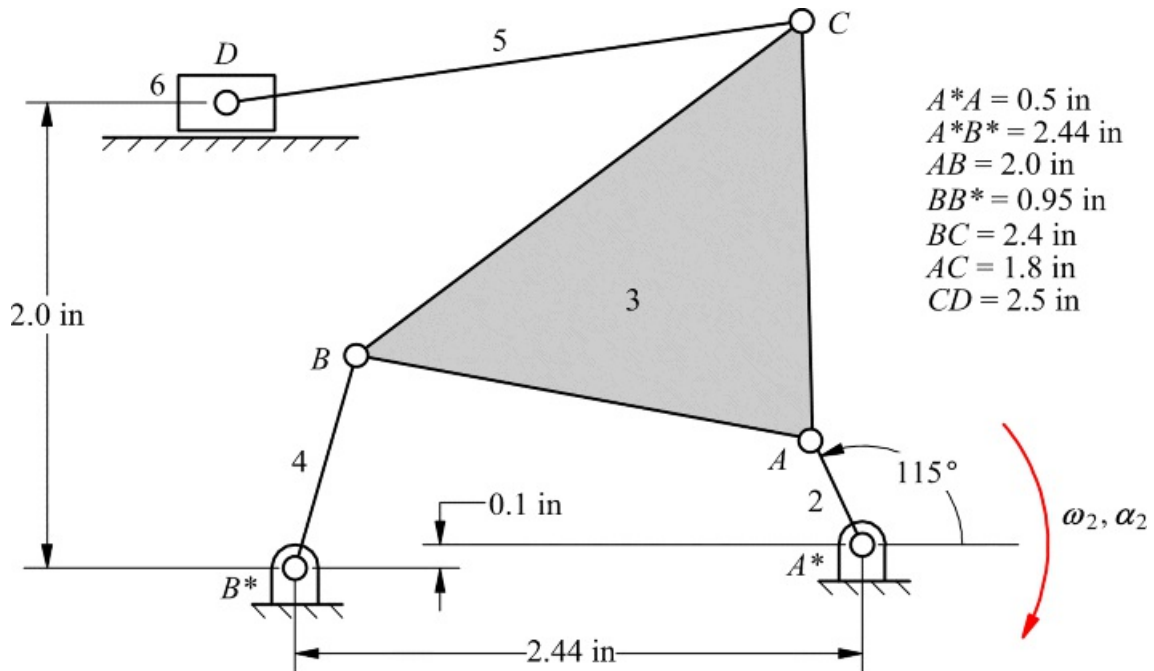
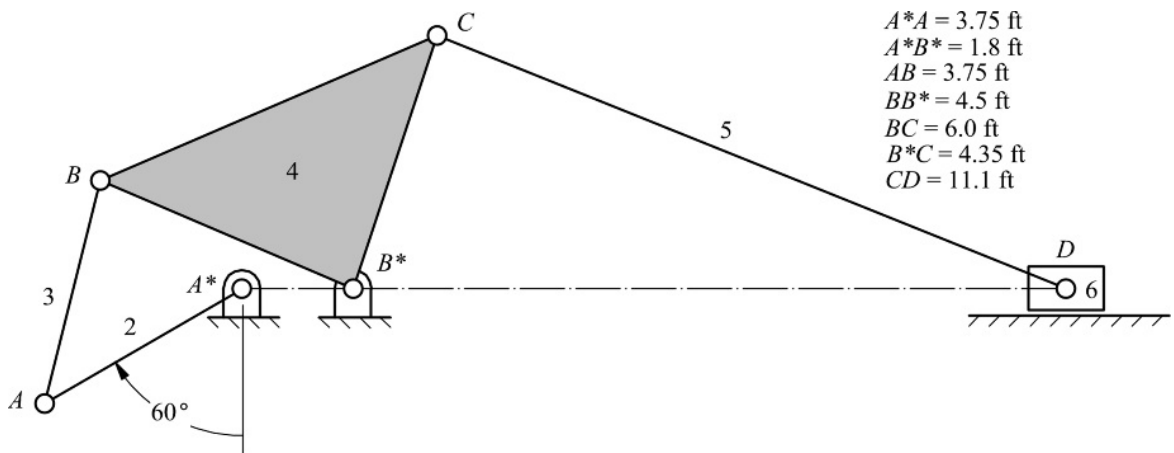


Figure P4.29 Linkage for Problem 4.29.

4.30 In the drag-link in Figure P4.30, link 2 is turning CW at the constant rate of 130 rpm. Construct the velocity and acceleration polygons and compute the following: ω_5 , ω_6 , and the angular acceleration of link 5.



[Figure P4.30](#) Linkage for Problem 4.30.

4.31 [Figure P4.31](#) shows the mechanism used in a two-cylinder 60° V-engine consisting, in part, of an articulated connecting rod. Link 2 rotates at 2000 rpm CW. Find the velocities and acceleration of points *B*, *C*, and *D* and the angular acceleration of links 3 and 5 when link 2 is vertical.

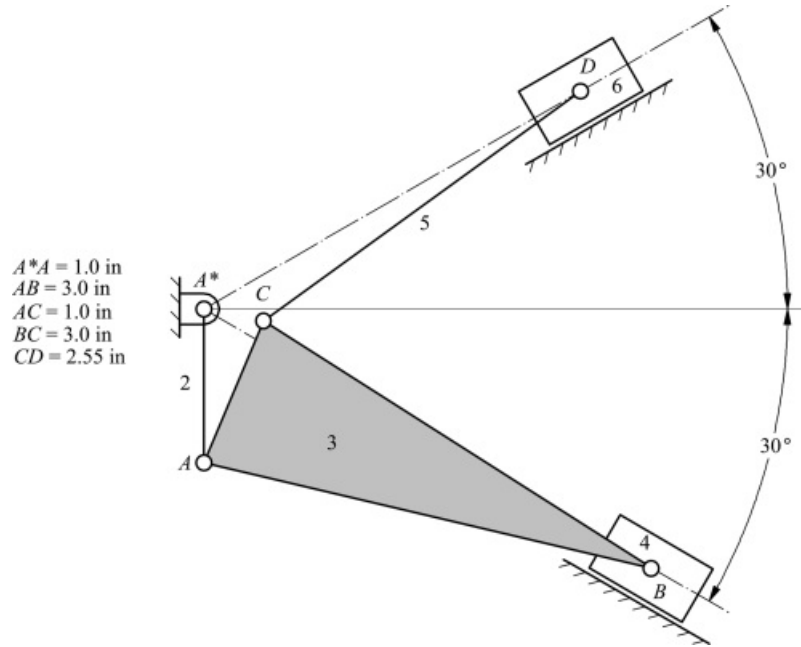


[Figure P4.31](#) Linkage for Problem 4.31.

4.32 In [Figure P4.32](#), $\omega_2 = 12 \text{ rad/s}$ CW (constant), links 2, 4, and 5 are horizontal, and link 3 is vertical. Write the appropriate vector equations, solve them using vector polygons, and

- Determine v_{B3} , v_{D6} , ω_3 , ω_4 , ω_5
- Determine a_{B3} , a_{D6} , α_3 , α_4 , α_5

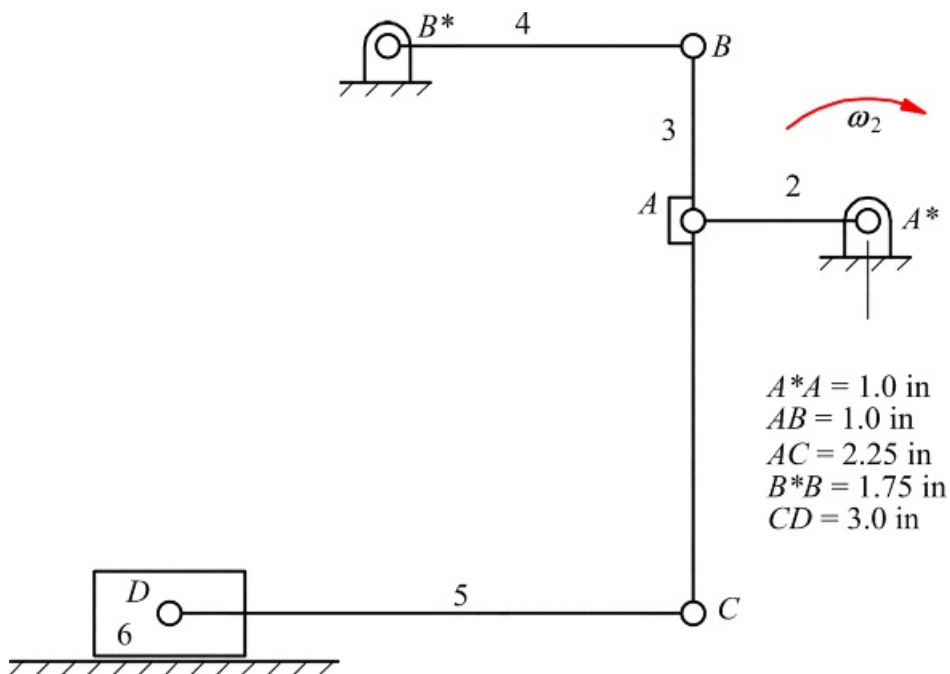


[Figure P4.32](#) Linkage for Problem 4.32.

4.33 In [Figure P4.33](#), $\omega_2 = 20 \text{ rad/s}$ CW, and $\alpha_2 = 60 \text{ rad/s}^2$ CW. Write the appropriate vector equations,

solve them using vector polygons, and

- a. Determine v_{B4} , v_{D6} , ω_3 , ω_5
 - b. Determine a_{B4} , a_{D6} , a_3 , a_5

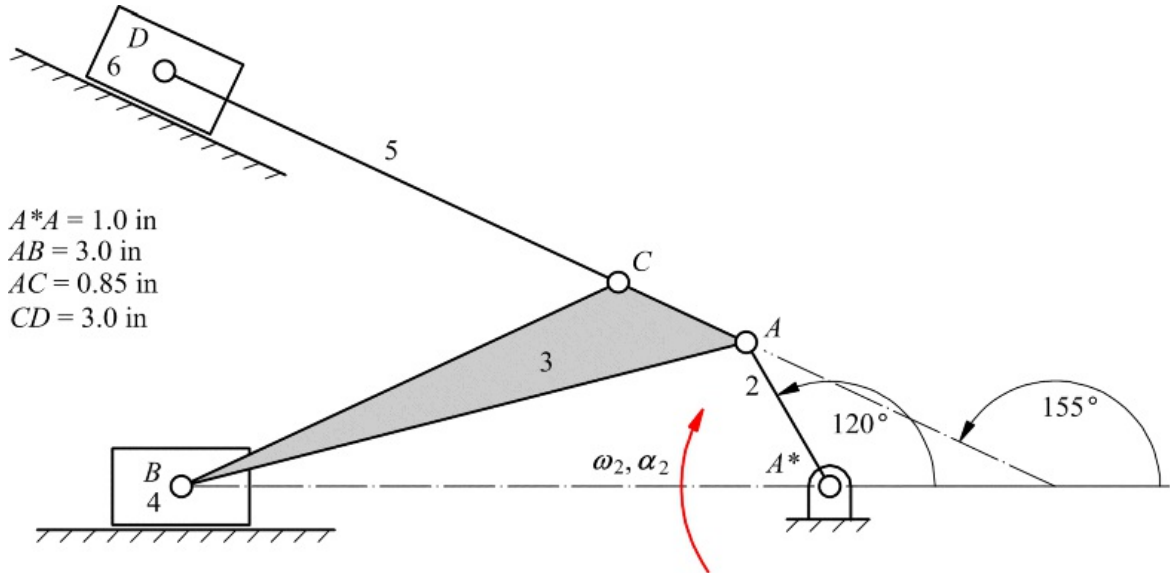


Figure P4.33 Linkage for Problem 4.33.

- 4.34** In Figure P4.34, $\omega_2 = 10 \text{ rad/s}$ CW (constant). D moves on the line B^*D , which is horizontal. Write the appropriate vector equations, solve them using vector polygons, and

- a. Determine v_{D6} , ω_4 , ω_5
 - b. Determine a_{D6} , a_4 , a_5

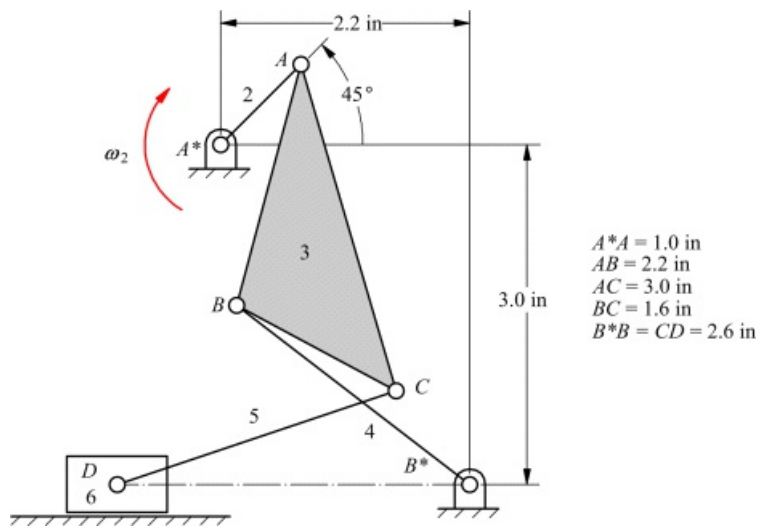


Figure P4.34 Linkage for Problem 4.34.

Velocity and Acceleration Images

- 4.35 In Figure P4.35, $\omega_2 = 4 \text{ rad/s CCW (constant)}$. Write the appropriate vector equations, solve them using vector polygons, and

- a. Determine v_{C3} , v_{B4} , and ω_3
 - b. Determine a_{C3} , a_{B4} , and α_3

Also find the point in link 3 that has zero acceleration for the position given.

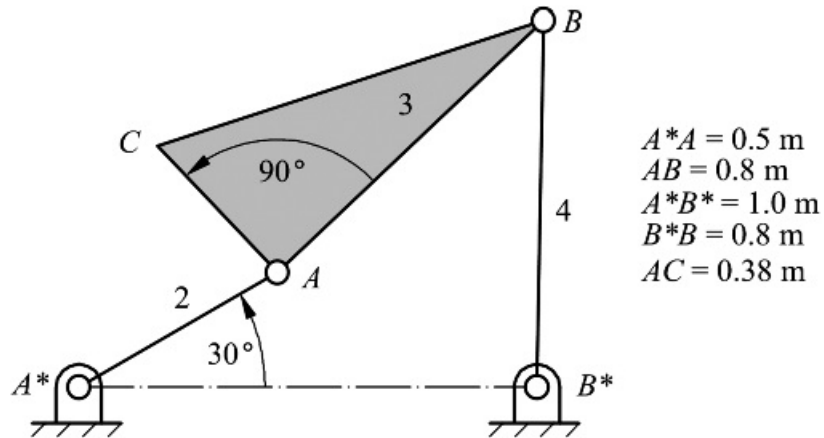


[Figure P4.35](#) Linkage for Problem 4.35.

4.36 A Watt straight-line linkage [see [Figure 8.2\(d\)](#)] is used to constrain the midpoint, C , of a live axle in a truck suspension to move along an approximate vertical straight line relative to the body, as shown in [Figure P4.36](#). A live axle (not shown in the figure) is a single member on which the wheels on opposite sides of the vehicle both turn. If the dimensions in the figure are $A^*A = B^*B = 2.5 \text{ ft}$, and $AB = 0.75 \text{ ft}$, find ω_2 , ω_3 , and ω_4 if $v_C = 5 \text{ ft/s}$ vertically upward.

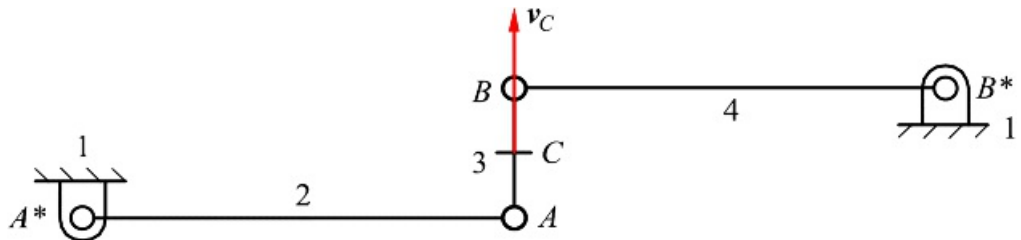


[Figure P4.36](#) Linkage for Problem 4.36.

4.37 Find the angular accelerations of links 2, 3 and 4 of the mechanism of Problem 4.36 if point C is accelerated upward at 8 ft/s^2 .

4.38 The Hoeken approximate straight-line mechanism shown in [Figure P4.38](#) is to be used to build a level luffing crane (see [Figure 8.1](#)). If $A^*B^* = 20 \text{ ft}$, $A^*A = 10 \text{ ft}$, $AB = B^*B = 25 \text{ ft}$, and $AC = 50 \text{ ft}$, find ω_2 if v_C is to be 4 ft/s horizontally as shown.

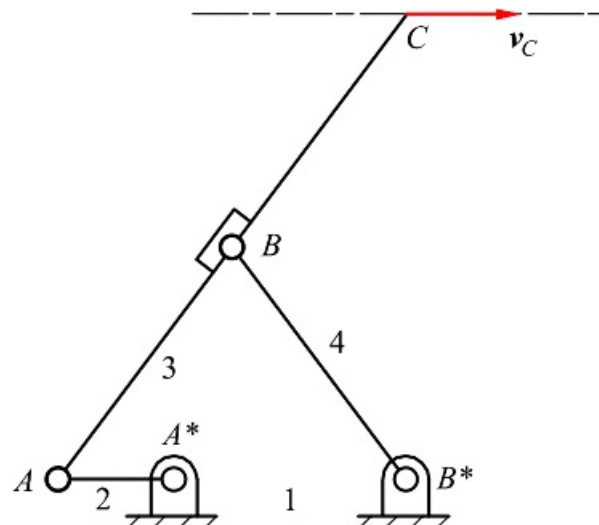


[Figure P4.38](#) Linkage for Problem 4.38.

4.39 In [Figure P4.39](#), the constant velocity of A is 10 in/s to the right. Draw the velocity and acceleration polygons and use the image technique to determine the velocity and acceleration of point C_4 . Then determine the velocity and acceleration images of link 4. Draw the images on the velocity and acceleration polygons.

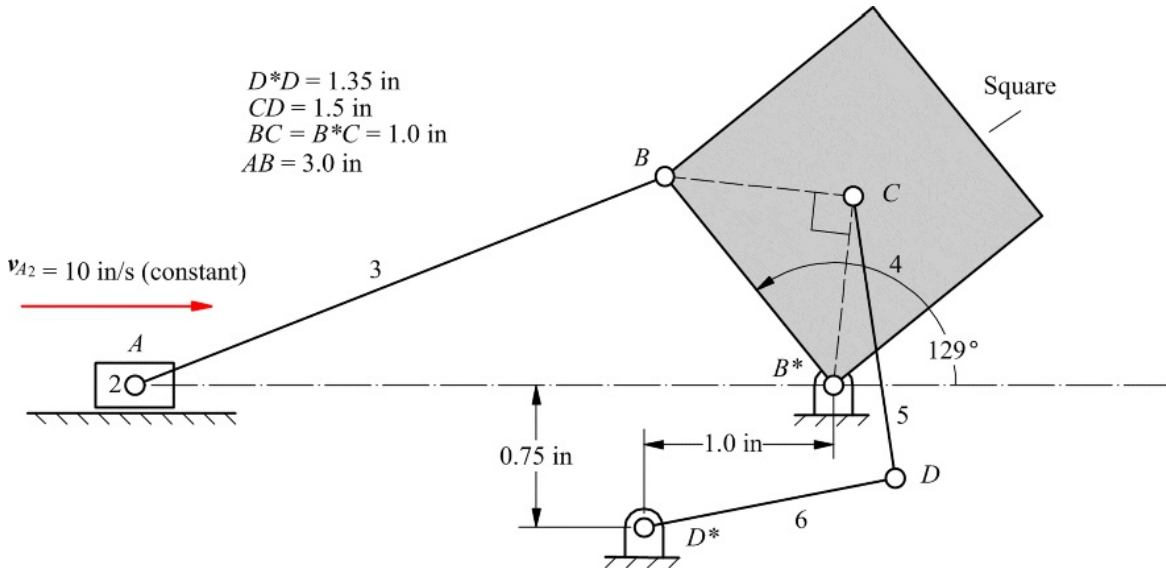


[Figure P4.39](#) Linkage for Problem 4.39.

4.40 In [Figure P4.40](#), the velocity of A_2 is 10 in/s to the right and is constant. Draw the velocity and acceleration polygons for the mechanism, and record values for angular velocity and acceleration of link 6 and D_6 . Use the image technique to determine the velocity of point C_4 , and locate the point in link 3 that has zero velocity.

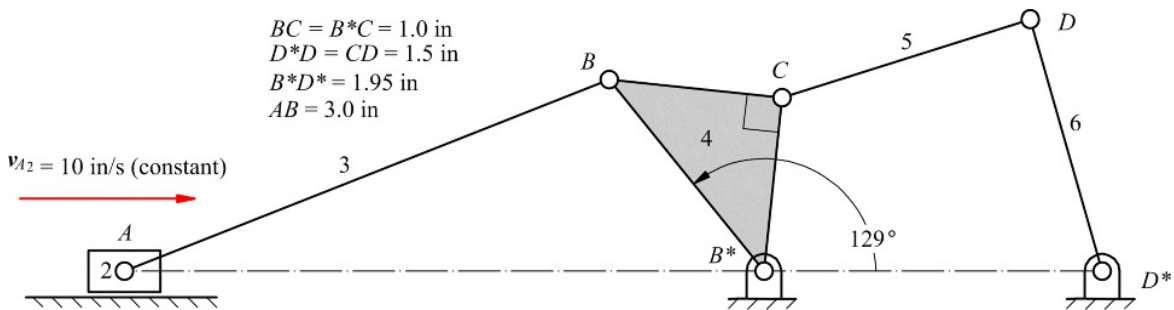


[Figure P4.40](#) Linkage for Problem 4.40.

4.41 The instant center of acceleration of a link can be defined as that point in the link that has zero acceleration at a given instant. If the accelerations of points A and B are as given in the rigid body shown in [Figure P4.41](#), find the point C in that link at which the acceleration is zero.

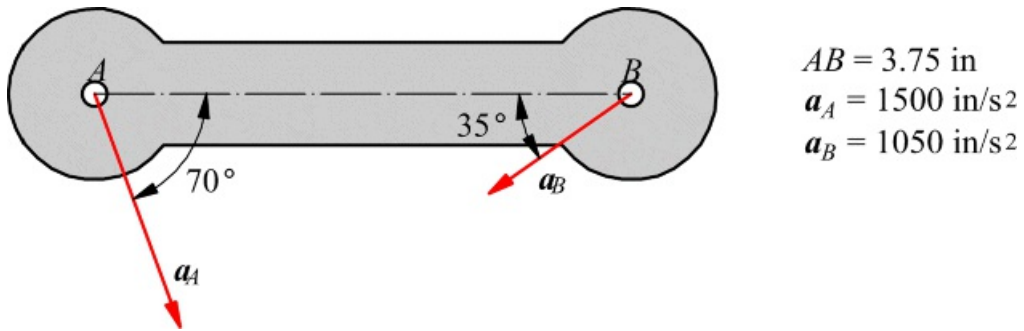


[Figure P4.41](#) Linkage for Problem 4.41.

4.42 For the mechanism shown in [Figure P4.42](#), $\omega_2 = 6.5 \text{ rad/s}$ (CCW), and $\alpha_2 = 40 \text{ rad/s}^2$ (CCW). Draw the

velocity polygon, and locate the velocity of point C using the image technique.

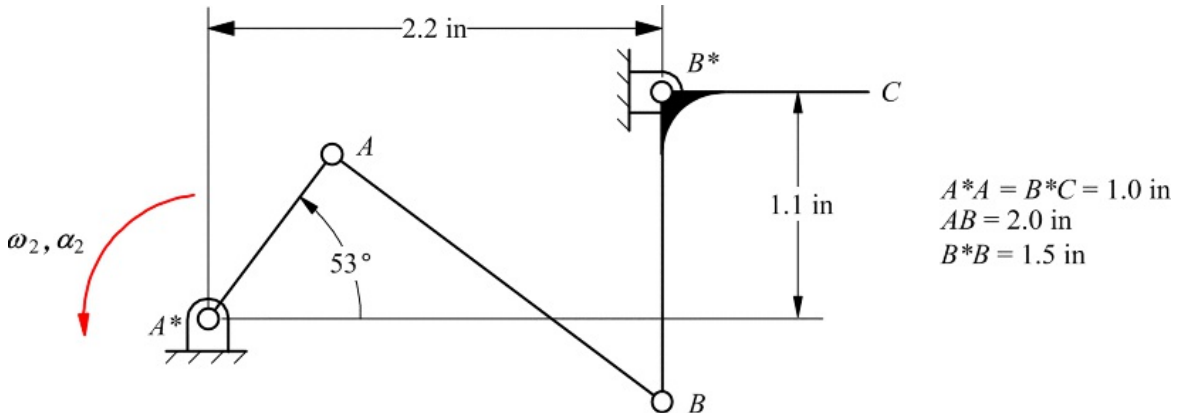


Figure P4.42 Linkage for Problem 4.42.

4.43 In the mechanism shown in Figure P4.43, find ω_6 and a_3 . Also, determine the acceleration of C_3 by image. Note that C_3 is a point on link 3.

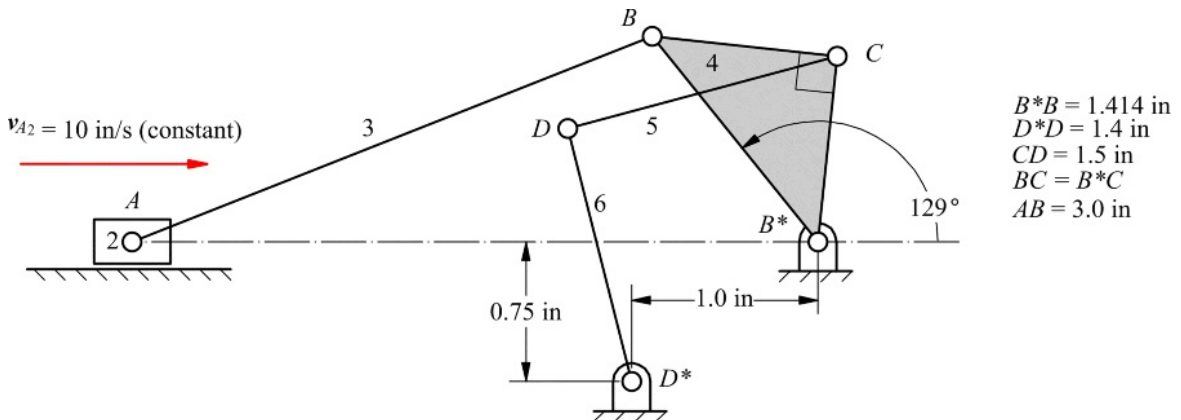


Figure P4.43 Linkage for Problem 4.43.

4.44 In the mechanism shown in Figure P4.44, $\omega_2 = 1 \text{ rad/s}$ (CCW) and $a_2 = 0 \text{ rad/s}^2$. Find ω_5 , a_5 , v_{E6} , and a_{E6} for the position given. Also find the point in link 5 that has zero acceleration for the position given.

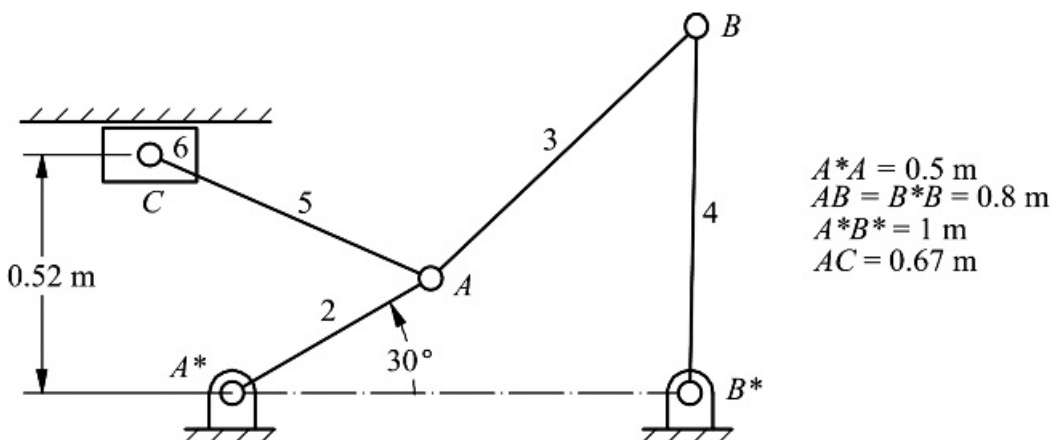
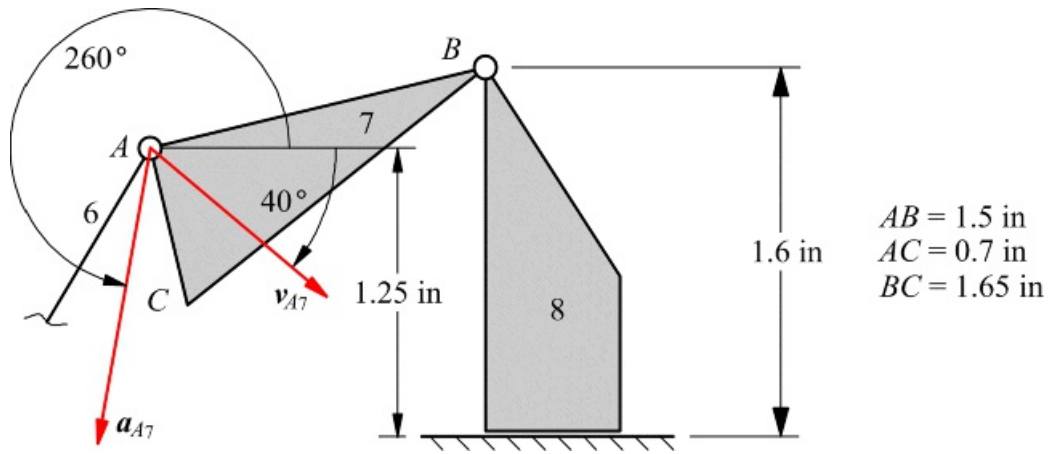


Figure P4.44 Linkage for Problem 4.44.

4.45 Part of an eight-link mechanism is shown in Figure P4.45. Links 7 and 8 are drawn to scale, and the velocity of point A_7 is 5.0 in/s in the direction shown. Link 8 slides on the frame. The acceleration of A_7 is 40.0 in/ s^2 in the direction shown. Find ω_7 and a_7 for the position given. Also find the velocity of C_7 by

image.



[Figure P4.45](#) Linkage for Problem 4.45.

4.46 In [Figure P4.46](#), link 2 is rotating CW at the rate of 3 rad/s (constant). In the position shown, link 2 is horizontal. Write the appropriate vector equations, solve them using vector polygons, and

- Determine v_{B4} , v_{C3} , ω_3 , and ω_4
- Determine a_{B4} , a_{C3} , α_3 , and α_4

Link lengths: $A^*A = B^*B = 3 \text{ in}$, $AB = BC = AC = 5.0 \text{ in}$

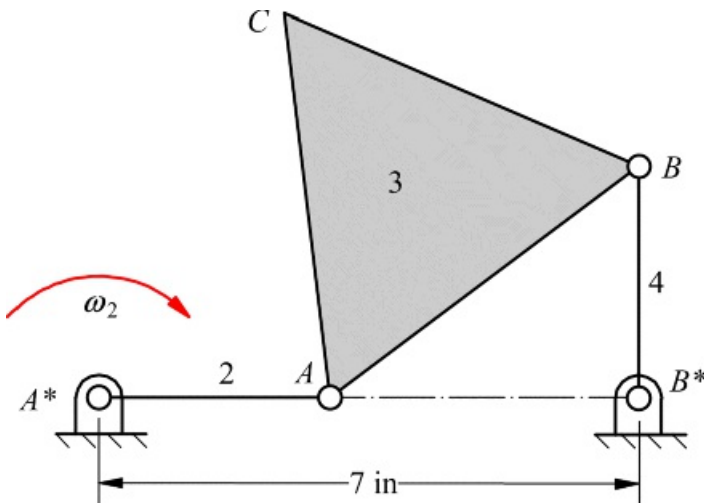


[Figure P4.46](#) Linkage for Problem 4.4.

4.47 Part of a 10-link mechanism is shown in [Figure P4.47](#). Links 7 and 8 are drawn to scale, and the velocity and acceleration vectors for points A_7 and D_8 are given. The magnitudes of the velocities are: $v_{A_7} = 6.0 \text{ in/s}$, $\alpha_{A_7} = 40 \text{ in/s}^2$, $v_{D_8} = 7.5 \text{ in/s}$, and $\alpha_{D_8} = 30 \text{ in/s}^2$.

Find ω_8 and α_7 for the position given. Also find the velocity of C_7 by image.

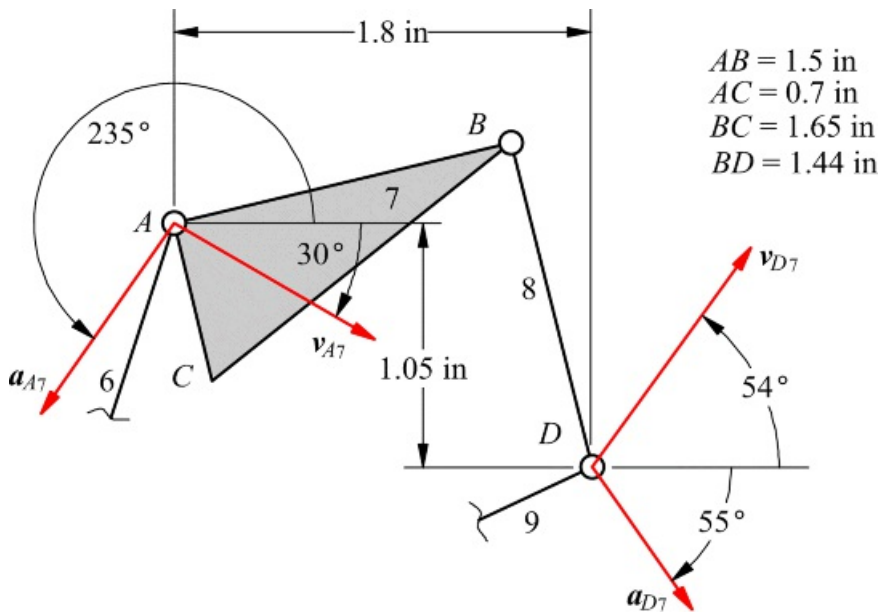


[Figure P4.47](#) Linkage for Problem 4.47.

Graphical Constraint Programming (GCP)

4.48 Solve Problem 4.1 using GCP. Identify the constraints that you apply. Note that the radial components of acceleration need to be computed externally to analyze the linkage for accelerations. However, because of the precision with which the constraints are applied, the problem can be solved more quickly and more accurately than when using conventional CAD programs or manual drawing.

4.49 Solve Problem 4.7 using GCP. Identify the constraints that you apply. Note that the radial components of acceleration must be computed externally to analyze the linkage for accelerations. However, because of the precision with which the constraints are applied, the problem can be solved more quickly and more accurately than when using conventional CAD programs or manual drawing.

4.50 Solve Problem 4.21 using GCP. Identify the constraints that you apply.

4.51 Solve Problem 4.25 using GCP. Identify the constraints that you apply.

4.52 Solve Problem 4.26 using GCP. Identify the constraints that you apply.

4.53 Solve Problem 4.28 using GCP. Identify the constraints that you apply.

4.54 Develop a graphical program to solve Problem 4.29. Note that the radial components of acceleration must be computed externally to the program.

4.55 Develop a graphical program to solve Problem 4.30. Note that the radial components of acceleration must be computed externally to the program.

4.56 Develop a graphical program to solve Problem 4.32. Note that the radial components of acceleration must be computed externally to the program.

4.57 Develop a graphical program to solve Problem 4.34. Note that the radial components of acceleration must be computed externally to the program.

5

LINKAGES WITH ROLLING AND SLIDING CONTACTS, AND JOINTS
ON MOVING SLIDERS



Prerequisite Knowledge Needed for Chapter 5

Knowledge of linkage structure from [Chapter 1](#) and relative velocities and accelerations from [Chapter 4](#). A familiarity with general dynamics and vector mechanics from basic mechanics courses. A knowledge of Geometric Constraint Programming (GCP) from [Chapters 2](#) and [4](#).



5.1 Introduction

The methods introduced in [Chapter 4](#) are straightforward and are perfectly adequate for the analysis of linkages that have only revolute joints or sliding joints on fixed slides. However, to analyze linkages with other types of joints, including those with moving sliding joints, it is necessary to base the analysis on a more complex theory. These types of joints are very common in industry. The complication here arises from differentiation of vector quantities that refer to moving reference frames.

As was discussed in [Chapter 1](#), a kinematic joint is formed by any contact between two bodies. The methods discussed in [Chapter 4](#) apply only to linkages in which all the joints have the very specialized surface of revolution geometry of revolute joints, or the equally special generalized cylindrical surface geometry of prismatic joints. There are many other possible types of kinematic joints, a number of which are of great practical importance. In this chapter, we provide the basic analysis tools needed to deal with linkages that include these more general joint types.

Many mechanisms include rolling contacts, and contacts with irregularly shaped bodies. A cam mechanism will often include a cylindrical follower rolling on the irregularly shaped cam. Any wheeled vehicle makes use of rolling contact with the terrain over which it travels. When two bodies are in rolling contact, the point in one body that contacts the other body is instantaneously at rest relative to that body. That is, its velocity relative to that body is zero. However, after an infinitesimally small time interval, that point becomes separated from the second body and is no longer at rest relative to it. Thus, although the velocity of the contacting point relative to the body contacted is zero, its acceleration is not zero and is, in fact, directed along the contact normal away from the contacted body.

Other commonly used mechanisms have sliding joints that are not fixed relative to the base, but rotate. The Coriolis component of acceleration that governs the direction of rotation of cyclonic weather systems can also lead to significant internal loads in mechanisms. This is particularly relevant to mechanisms that have rotating sliding joints.

To address problems involving linkages of these types, it is necessary first to think about what we mean by a reference frame and the implications of the relative motion of two reference frames for velocity and acceleration analysis.



5.2 Reference Frames

If a linkage involves only revolute joints or sliders on fixed lines, the equations developed in Sections 4.3 and 4.4 are sufficient for conducting the kinematic analysis. However, for other types of joints, the equations become more complex, and it is necessary to use more than one reference frame for the velocities and accelerations. In general, each link must be assumed to have a reference frame attached to it. In fact, when each link is manufactured, the machine tool that is used to form the link geometry will be guided relative to the local coordinate system or reference frame fixed to the link.

As shown in [Figure 5.1](#), the position of a given point (Q) can be quite different when it is measured relative to different reference frames. Furthermore, as will be demonstrated in the following, the velocity of a point relative to the fixed frame R depends not only on its velocity relative to the moving reference frame M , but also on the velocity and angular velocity of frame M relative to R . A similar situation applies to the accelerations.

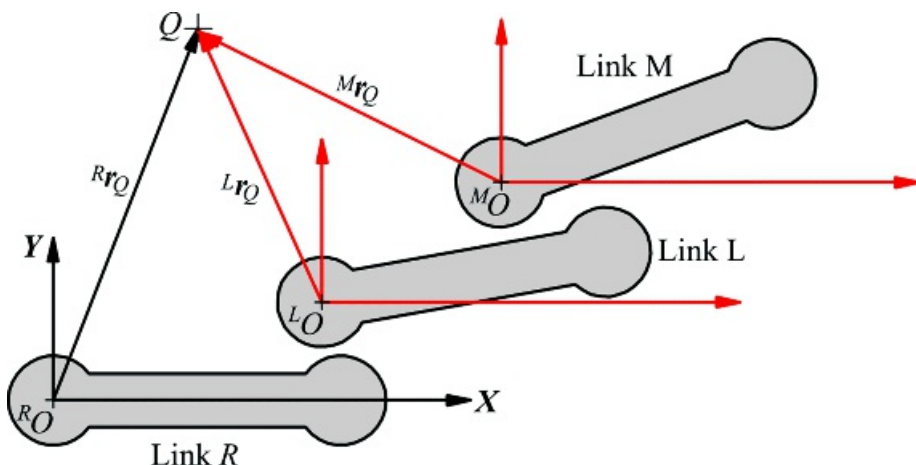


[Figure 5.1](#) Position of a point (Q) relative to three different coordinate systems. The position of point Q relative to reference frame M is $\overset{M}{r}_Q$. This vector is quite different from that of the position of Q relative to the reference frame fixed to link L ($\overset{L}{r}_Q$) or of the position of Q relative to the reference frame fixed to R ($\overset{R}{r}_Q$).

In general, we need to use multiple reference systems because we will know certain information about the motion only if we observe the motion from a moving coordinate system. In these instances, we will not be able to specify the same information if we restrict our observations from a single coordinate system fixed to the frame.

When it is important to distinguish the reference frames to which positions, velocities, and accelerations refer, we will use a superscript before the vector symbol to identify the relevant reference frame. Typically, we will use the link number or letter as the reference frame for that link. As an example, if B is a general link that is moving relative to another link R , $\overset{R}{\omega}_B$ is the angular velocity of the moving body, B , relative to frame R . The absolute velocity of point Q relative to frame R is $\overset{R}{v}_Q$, and the absolute position of point Q relative to the reference frame fixed to body B is $\overset{B}{r}_Q$. The angular acceleration of member 3 relative to the reference frame fixed in member 2 is $\overset{2}{\alpha}_3$.

This nomenclature is consistent with that used in robotics where it is essential to deal with multiple coordinate systems. It also gives a precise and unambiguous definition of the vectors that arise through the differentiation of the position and velocity equations. Vectors such as the Coriolis component of acceleration arise naturally from the terms generated because of the rotation of the moving coordinate systems used as the reference system for some points.

The vector $\overset{R}{v}_{B/A}$ is usually called the velocity of B relative to A in reference frame R . However, as discussed earlier, this definition is technically incorrect. Vectors must be measured relative to reference frames. Therefore, $\overset{R}{v}_{B/A}$ would be the velocity of point B relative to a reference frame R that has its origin at point A and moves so as

always to be parallel to the fixed frame. Similarly, one would call $\mathbb{r}_{Q/P}$ the position of Q relative to a reference frame, with origin at P , that remains, at all times, parallel to the frame R . The complexity of this statement explains the widespread use of the term “position of Q relative to P ” for $\mathbb{r}_{Q/P}$.

Often, when all vectors refer to the same reference frame R , we will drop the superscript R to simplify the notation. That is $\mathbb{r}_P = \mathbb{r}_{P/R}$. This was the case in [Chapter 4](#) when the fixed frame (link 1) was understood to be the reference frame for all vectors.

The basis of the velocity analysis of planar linkages is the relationship between the velocities of two different points when something about the motion of the two points is known relative to a moving coordinate system. To derive this relationship in a form suitable for the formulation of a velocity polygon, let us consider the points P and Q shown in [Figure 5.2](#). If $\mathbb{r}_{P/R}$ is the absolute position of point P relative to reference frame R , $\mathbb{r}_{Q/R}$ is the absolute position of Q relative to reference frame R , and $\mathbb{r}_{Q/P}$ is the vector from point P to point Q defined relative to the moving reference system B , then we can write

$$\mathbb{r}_{P/Q} = \mathbb{r}_{Q/R} - \mathbb{r}_{P/R} \quad (5.1)$$

Note that [Equation 5.1](#) is similar to [Equation 4.1](#) with the superscripts added to aid in keeping track of the reference frames. As indicated before, the vector $\mathbb{r}_{Q/P}$ is called the position of Q relative to P when the observer is fixed relative to reference system B .

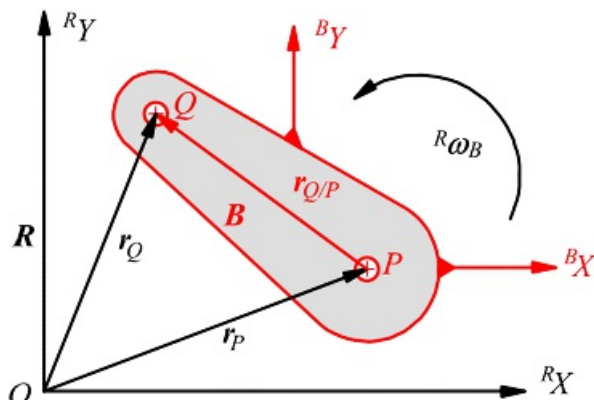


[Figure 5.2](#) Positions of two points in the moving link, B . The positions of points P and Q relative to the fixed reference frame, R , are given by r_P and r_Q , respectively. The angular velocity of B relative to R is $R\omega_B$. The quantities defined in the moving system, B , are shown in red.

Although P and Q may be fixed to body B , [Equation 5.1](#) is valid regardless of the link to which points P and Q are fixed (i.e., P and Q may be fixed to link B or any other link). However, to obtain the velocities, we must differentiate [Equation 5.1](#) when the observer is in reference frame R .

Note that, in the position considered, the coordinate axes for systems B and R must be parallel. Otherwise, we cannot add vector components as implied in [Equation 5.1](#). If the nominal coordinate systems attached to the two links are not parallel, we must use another set of coordinate systems that are momentarily parallel. The two coordinate systems fixed to a given link would be related by a simple coordinate transformation.



5.3 General Velocity and Acceleration Equations

5.3.1 Velocity Equations

When we differentiate [Equation 5.1](#) with the observer in the reference system R , we get

$$\frac{d}{dt}(\dot{r}_Q) = \frac{d}{dt}(r_P) + \frac{d}{dt}(r_{Q/P}) \quad (5.2)$$

The derivatives of the position vectors defined relative to reference system R can be represented in a straightforward manner as velocities relative to reference system R because the reference axes relative to which the vectors are defined are fixed to R and do not move with time. Therefore, [Equation 5.2](#) becomes

$$\dot{r}_Q = \dot{r}_P + \frac{d}{dt}(r_{Q/P}) \quad (5.3)$$

However, note that $r_{Q/P}$ is a vector defined relative to the coordinate system fixed to body B and the reference axes of body B rotate relative to those of reference system R with an angular velocity ω_B . Therefore the derivative $\frac{d}{dt}(r_{Q/P})$ must account for this rotation. In particular, the derivative involves two terms, one associated with the change in magnitude of the vector and one associated with the change in direction. This is apparent if we represent the vector $r_{Q/P}$ as a general three-dimensional vector in terms of its components and unit vectors. Then

$$\frac{d}{dt}(r_{Q/P}) = \frac{d}{dt}(x^B i + y^B j + z^B k)$$

and

$$\begin{aligned} \frac{d}{dt}(r_{Q/P}) &= \frac{d}{dt}(x^B i + y^B j + z^B k) \\ &= \left(\frac{dx}{dt} \hat{i} + \frac{dy}{dt} \hat{j} + \frac{dz}{dt} \hat{k} \right) + \left(x \frac{d\hat{i}}{dt} + y \frac{d\hat{j}}{dt} + z \frac{d\hat{k}}{dt} \right) \end{aligned} \quad (5.4)$$

The derivatives of the components in the first vector correspond to the change in the length of the vector, and this is defined relative to the coordinate system fixed to body B . Therefore, this is just the velocity defined relative to body B . The second term accounts for the rotation of the coordinate axes of B relative to the reference frame R .

Because \hat{i} , \hat{j} , and \hat{k} are unit vectors, only their directions can change with time. We can determine how to evaluate the derivatives if we look at an infinitesimal angular displacement $\delta\theta$ of body B relative to R during an infinitesimal time increment δt .

Because infinitesimal angular rotations are involved, we can treat $\delta\theta$ as a vector with x , y , z components (i.e., $\delta\theta = \delta\theta_x \hat{i} + \delta\theta_y \hat{j} + \delta\theta_z \hat{k}$) and determine how each component changes the directions of the unit vectors. The angular velocity will be the change in the angular position as the infinitesimal time increment δt approaches dt . That is

$$\omega_x = \frac{d\theta_x}{dt}; \quad \omega_y = \frac{d\theta_y}{dt}; \quad \omega_z = \frac{d\theta_z}{dt}$$

and

$${}^R\omega_B = \omega_x {}^B\dot{i} + \omega_y {}^B\dot{j} + \omega_z {}^B\dot{k} \quad (5.5)$$

To identify the trend in [Equation 5.4](#), consider the effect of the angular components about the X axis. For the X direction (unit vector ${}^B\dot{i}$), the change in the unit vector is represented in [Figure 5.3](#) as

$${}^R\delta({}^B\dot{i}) = 1^B\dot{j}\delta\phi_z - 1^B\dot{k}\delta\phi_y \quad (5.6)$$

The change takes place during the time increment δt . Therefore, dividing [Equation 5.6](#) by δt we get

$$\frac{{}^R\delta}{\delta t}({}^B\dot{i}) = {}^B\dot{j}\phi_z - {}^B\dot{k}\phi_y = {}^R\omega_B \times {}^B\dot{i} = \begin{bmatrix} {}^B\dot{i} & {}^B\dot{j} & {}^B\dot{k} \\ \omega_x & \omega_y & \omega_z \\ 1 & 0 & 0 \end{bmatrix}$$

Similarly

$$\begin{aligned} \frac{{}^R\delta}{\delta t}({}^B\dot{j}) &= {}^R\omega_B \times {}^B\dot{j} \\ \frac{{}^R\delta}{\delta t}({}^B\dot{k}) &= {}^R\omega_B \times {}^B\dot{k} \end{aligned}$$

Therefore,

$$\begin{aligned} x \frac{{}^R\delta S_i}{\delta t} + y \frac{{}^R\delta S_j}{\delta t} + z \frac{{}^R\delta S_k}{\delta t} &= {}^R\omega_B \times {}^B\dot{i} + {}^R\omega_B \times {}^B\dot{j} + {}^R\omega_B \times {}^B\dot{k} \\ &= {}^R\omega_B \times (x {}^B\dot{i} + y {}^B\dot{j} + z {}^B\dot{k}) = {}^R\omega_B \times {}^Bv_{G/B} \end{aligned}$$

Then

$$\begin{aligned} \frac{{}^R\delta}{\delta t}({}^Bv_{G/B}) &= \left(\frac{{}^R\delta x}{\delta t} {}^B\dot{i} + \frac{{}^R\delta y}{\delta t} {}^B\dot{j} + \frac{{}^R\delta z}{\delta t} {}^B\dot{k} \right) + \left(x \frac{{}^R\delta S_i}{\delta t} + y \frac{{}^R\delta S_j}{\delta t} + z \frac{{}^R\delta S_k}{\delta t} \right) \\ &= {}^Bv_{G/B} + {}^R\omega_B \times {}^Bv_{G/B} \end{aligned} \quad (5.7)$$

Now, [Equation 5.3](#) can be written as

$${}^Bv_G = {}^Bv_F + {}^Bv_{Q/F} + {}^R\omega_B \times {}^Bv_{G/F} \quad (5.8)$$

Before proceeding to the development of the acceleration equations, it is interesting to note that [Equation 5.7](#) is quite general. We could have derived a similar expression for the derivative of *any* vector that is defined relative to a moving coordinate system. For example, if s is any vector (e.g., position, velocity, acceleration) and if U and W are any two different coordinate systems

$$\frac{d}{dt}(\vec{v}_B) = \frac{d}{dt}(\vec{v}_S) + \vec{\omega}_W \times \vec{v}_S \quad (5.9)$$

Note that angular velocity is a property of a body and linear velocity is a property of a point. In both cases, it is necessary to specify, or at least understand, which reference frame is used to define the quantity. Also note that if the vector is defined in the coordinate system in which the observer stands, the term involving the angular velocity will be zero. That is

$$\vec{\omega}_U = 0$$

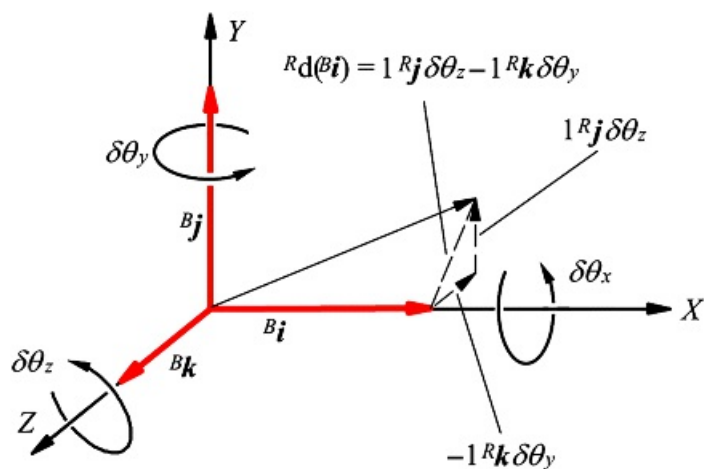


[Figure 5.3](#) Change in B_i due to a rotation about the X , Y , and Z axes of R .

5.3.2 Acceleration Equations

In general, angular acceleration can be written as

$${}^R \ddot{\omega}_B = \frac{d}{dt}({}^R \omega_B)$$

where again B is the moving body and R is the reference. As in the case of the angular velocity, the angular acceleration is a property of the entire body, and there is only one angular acceleration associated with the entire body. Angular acceleration is a vector and has a magnitude and direction.

If a velocity vector is defined in the coordinate system in which the observer is located, the corresponding acceleration can be expressed simply. For example, if the velocity vector is given by ${}^R v_Q$, then the acceleration is given by

$${}^R \ddot{v}_Q = \frac{d}{dt}({}^R v_Q)$$

To obtain the linear acceleration relationship for the points P and Q in [Figure 5.2](#), we can differentiate [Equation 5.8](#). Differentiating term by term with the observer in reference system R gives

$${}^R \ddot{v}_Q = \frac{d}{dt}({}^R v_Q) = \frac{d}{dt}({}^R v_P) + \frac{d}{dt}({}^P v_Q/P) + \frac{d}{dt}({}^R \omega_B \times {}^P r_{Q/P})$$

Considering each term and recognizing that vectors $\dot{\gamma}_{Q/P}$ and $\ddot{\gamma}_{Q/P}$ are both defined relative to the moving coordinate system (B), we get after differentiation

$$\ddot{\gamma}_{Q/B} = \ddot{\gamma}_{B/P} + \frac{\partial}{\partial t} (\dot{\gamma}_{Q/P}) - \ddot{\omega}_B \times \dot{\gamma}_{Q/P} + \ddot{\omega}_S \times \ddot{\gamma}_{Q/P} - \ddot{\omega}_B \times (\ddot{\gamma}_{Q/P} - \ddot{\omega}_B \times \dot{\gamma}_{Q/P})$$

Expanding and collecting terms gives

$$\ddot{\gamma}_{Q/B} = \ddot{\gamma}_{B/P} + \ddot{\gamma}_{Q/B} + 2\ddot{\omega}_B \times \dot{\gamma}_{Q/P} + \ddot{\omega}_B \times \ddot{\gamma}_{Q/P} + \ddot{\omega}_B \times (\ddot{\omega}_S \times \ddot{\gamma}_{Q/P}) \quad (5.10)$$

Note that in the last term, the operation $(\ddot{\omega}_B \times \ddot{\gamma}_{Q/P})$, must be carried out before the operation $\ddot{\omega}_B \times (\dot{\omega}_B \times \dot{\gamma}_{Q/P})$. Obviously, $(\omega \times \omega) \times r \neq \omega \times (\omega \times r)$.

The term $\ddot{\gamma}_{Q/P}$ is the acceleration of Q relative to P when the observer is in the moving body B . The term $2\ddot{\omega}_B \times \dot{\gamma}_{Q/P}$ is called the Coriolis acceleration and is a function of velocities only. It can be computed as soon as the velocity analysis is completed. The term $\ddot{\omega}_B \times \ddot{\gamma}_{Q/P}$ is the transverse or tangential component of acceleration identified before. This component of acceleration is perpendicular to the radius vector. The term $\ddot{\omega}_B \times (\dot{\omega}_B \times \dot{\gamma}_{Q/P})$ is the radial component of acceleration, and it points in the direction *opposite* to the radius vector.

5.3.3 Chain Rule for Positions, Velocities, and Accelerations

When dealing with mechanisms with a relatively large number of members, it is helpful to have relationships between the relative velocities and accelerations of several points and between the relative angular velocities and angular accelerations of several members. These relationships are particularly relevant to the spatial chain mechanisms discussed in [Chapter 9](#).

Positions, Velocities, and Accelerations of Points

Let A , B , C , D , and E be any arbitrary points moving with respect to the reference frame R as shown in [Figure 5.4](#). Then a position equation can be written as

$$\ddot{\gamma}_{E/A} = \ddot{\gamma}_{S/B} + \ddot{\gamma}_{B/C} + \ddot{\gamma}_{C/D} + \ddot{\gamma}_{D/A} \quad (5.11)$$

This type of equation is just a simple expression of vector addition, and it applies regardless of the number of points involved. For velocities, we can differentiate [Equation 5.11](#) with the observer in system R . Then

$$\dot{\gamma}_{E/A} = \dot{\gamma}_{S/B} + \dot{\gamma}_{B/C} + \dot{\gamma}_{C/D} + \dot{\gamma}_{D/A} \quad (5.12)$$

and the acceleration equation becomes

$$\ddot{\gamma}_{E/A} = \ddot{\gamma}_{S/B} + \ddot{\gamma}_{B/C} + \ddot{\gamma}_{C/D} + \ddot{\gamma}_{D/A} \quad (5.13)$$

[Equations 5.11](#) through [5.13](#) are applicable to any set of points, and they are especially useful when determining the kinematic information for points on mechanisms after the basic kinematic information associated with each link is known. They are also useful when analyzing manipulators and robots.

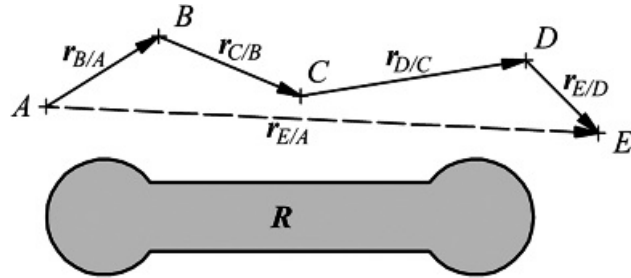


[Figure 5.4](#) Relationship among the positions of a series of points.

The relationship among three *arbitrary* points (A, B, C) is

$${}^3r_{C/A} = {}^Rr_{C/A} + {}^Rr_{S/A}$$

then

$${}^3r_{C/B} = {}^Rr_{C/A} - {}^Rr_{S/A} \quad (5.14)$$

Because A is arbitrary, [Equation 5.14](#) indicates that we can find the relative position between two points by subtracting the relative position vectors between the two points and the same third point. Similarly, for velocities and accelerations

$${}^3v_{C/B} = {}^Rv_{C/A} - {}^Rv_{S/A} \quad (5.15)$$

and

$${}^3a_{C/S} = {}^Ra_{C/A} - {}^Ra_{S/A} \quad (5.16)$$

Note the position of A, B , and C in each of the expressions.

Relative Angular Velocities

A chain rule for angular velocities works the same way as for linear velocities except that now reference systems are involved instead of points as shown in [Figure 5.5](#). Consider three coordinate systems (1, 2, and 3) that are *momentarily parallel*. Then

$${}^3\omega_3 = {}^1\omega_2 + {}^2\omega_2 \quad (5.17)$$

and

$${}^2\omega_3 = {}^1\omega_3 - {}^1\omega_2 \quad (5.18)$$

This means we can find the relative angular velocity between any two bodies by computing the angular velocity difference between each of the bodies and the same third body (in this case body 1).

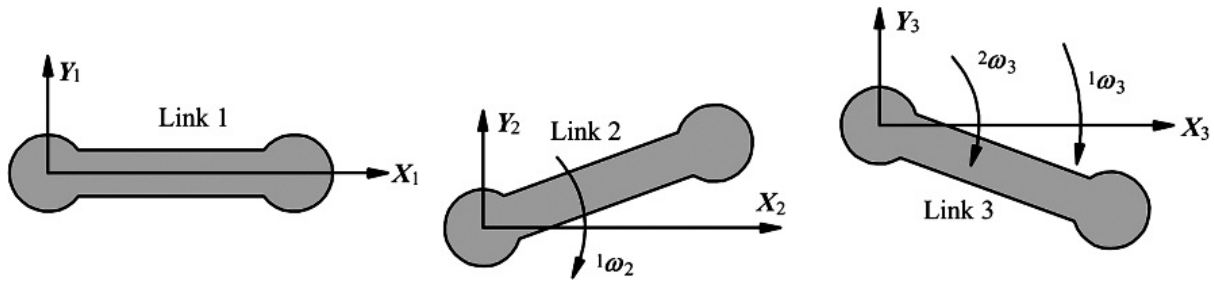


Figure 5.5 Relationship among the angular velocities for three links.

For n bodies, the relative angular velocities are related by

$${}^n\omega_n = {}^1\omega_2 + {}^2\omega_3 + {}^3\omega_4 + \dots + {}^{n-2}\omega_{n-1} + {}^{n-1}\omega_n$$

Relative Angular Accelerations

For relative accelerations, we can differentiate the relative velocity equation, [Equation 5.17](#). Then

$$\frac{d}{dt}({}^1\omega_3) = \frac{d}{dt}({}^1\omega_2) + \frac{d}{dt}({}^2\omega_3) \quad (5.19)$$

The first two terms are straightforward because the derivatives are both taken with respect to the reference system in which each vector is defined. That is

$$\frac{d}{dt}({}^1\omega_3) = {}^1\alpha_3 \quad \text{and} \quad \frac{d}{dt}({}^1\omega_2) = {}^1\alpha_2$$

The third term in [Equation 5.19](#) is a vector described in the second coordinate system (superscript 2). Therefore using [Equation 5.9](#), this term can be written as

$$\frac{d}{dt}({}^2\omega_3) = \frac{d}{dt}({}^2\omega_3) + {}^1\omega_2 \times {}^2\omega_3 = {}^2\omega_3 + {}^1\omega_2 \times {}^2\omega_3$$

The relative angular acceleration expression in [Equation 5.19](#) can then be written as

$${}^1\alpha_3 = {}^1\alpha_2 + {}^2\alpha_3 + {}^1\omega_2 \times {}^2\omega_3$$

This expression can be extended to n bodies using

$${}^1\alpha_n = {}^1\alpha_{n-1} + {}^{n-1}\alpha_n + {}^1\omega_{n-1} \times {}^{n-1}\omega_n$$

Then

$$\begin{aligned} {}^1\alpha_n &= {}^1\alpha_2 + {}^2\alpha_3 + {}^3\alpha_4 + \dots + {}^{n-2}\alpha_{n-1} + {}^{n-1}\alpha_n + {}^1\omega_2 \times {}^2\omega_3 + {}^1\omega_3 \times {}^2\omega_4 \\ &\quad + {}^1\omega_4 \times {}^3\omega_5 + \dots + {}^1\omega_{n-2} \times {}^{n-1}\omega_{n-1} + {}^1\omega_{n-1} \times {}^{n-1}\omega_n \end{aligned}$$

Note that in the plane, all of the ω 's will be parallel, making the cross products all zero. Thus in *planar* problems, the chain rule for angular accelerations reduces to a scalar equation in the magnitudes of the angular accelerations with signs according to the right hand screw rule (+ for CCW and - for CW).

$$\alpha_n = {}^1\alpha_2 + {}^2\alpha_3 + {}^3\alpha_4 + \cdots + {}^{n-2}\alpha_{n-1} + {}^{n-1}\alpha_n \quad (\text{planar problems only})$$



5.4 Special Cases for the Velocity and Acceleration Equations

[Equations 5.8](#) and [5.10](#) are the most general forms for the relative velocity and acceleration equations for points that we will encounter in the kinematic analysis of linkages. In most practical problems, some of the terms in the expressions are zero. Three special cases occur, and these will be discussed separately in the following sections.

5.4.1 Two Points Fixed in a Moving Body

This is the most common situation that exists in the analysis of mechanisms and is the case discussed in [Chapter 4](#). If P and Q are both fixed to B , as shown in [Figure 5.6](#), we have

$$\dot{r}_{Q/B/P} = \ddot{r}_{Q/B/P} = 0 \quad (5.20)$$

because P and Q do not have any motion relative to an observer in the moving body B . When [Equation 5.20](#) is used to simplify [Equations 5.8](#) and [5.10](#), the results are

$$\dot{r}_Q = \dot{r}_{P/B} + \dot{r}_{Q/P} = \dot{r}_{P/B} - \ddot{r}_{B/B} \times r_{Q/B} \quad (5.21)$$

which can be recognized as being the same form as [Equation 4.4](#), and

$$\ddot{r}_Q = \ddot{r}_{P/B} + \ddot{r}_{Q/P} = \ddot{r}_{P/B} - \ddot{r}_{B/B} \times r_{Q/B} + \ddot{r}_{B/B} \times (\ddot{r}_{B/B} \times r_{Q/B}) \quad (5.22)$$

which is the same form as [Equation 4.8](#).

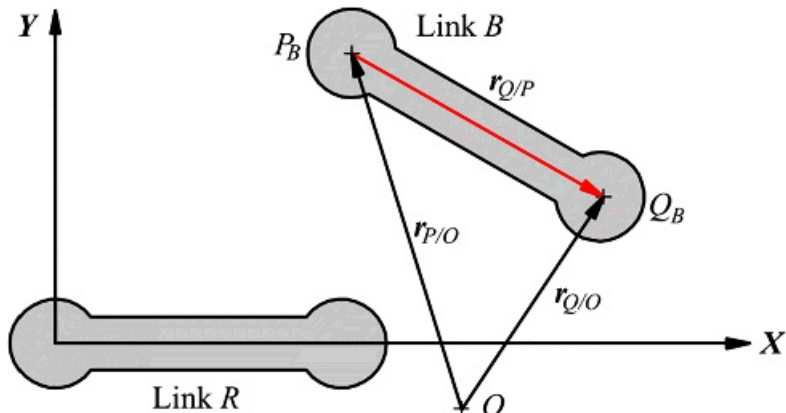


[Figure 5.6](#) Two points fixed to the same link.

Here we have dropped the superscript on $\dot{r}_{Q/P}$ because we do not need to differentiate the vector again, and all coordinate systems are assumed to be parallel. Because the coordinate systems are parallel, $\dot{r}_{Q/P}$ will have the same components in all systems. Note also that we could have rewritten [Equations 5.8](#) and [5.10](#) relative to any link; however, only the choice of the link (B) to which Q and P are attached simplifies the equation. Using the radial and tangential notation, we can also rewrite [Equation 5.22](#) as

$$\dot{r}_Q = \dot{r}_{P/B} + \dot{r}_{Q/P}^r + \dot{r}_{Q/P}^t$$

where

$$\dot{\omega}_{Q/P}^r = \dot{\omega}_S \times (\dot{\omega}_S \times r_{Q/P}) \quad (5.23)$$

and

$$\ddot{r}_{Q/P}^r = \ddot{\omega}_S \times r_{Q/P} \quad (5.24)$$

We will use the radial and tangential notation extensively in mechanism analyses. For planar mechanisms, $\dot{\omega}_{Q/P}^r$ and $\ddot{r}_{Q/P}^r$ will be orthogonal to each other because $\dot{\omega}_S$ and $\ddot{\omega}_S$ are both orthogonal to $r_{Q/P}$. In spatial mechanisms, however, this will not always be the case.

5.4.2 Two Points Are Instantaneously Coincident

A second special case in kinematics is that in which P and Q belong to different bodies but are momentarily coincident. This case is shown in [Figure 5.7](#). Then, $r_{Q/P}$ is momentarily zero, and [Equation 5.8](#) reduces to

$$\dot{r}_{Q/P} = \dot{r}_{Y_P} + \dot{\omega}_{Q/P} r_{Q/P} \quad (5.25)$$

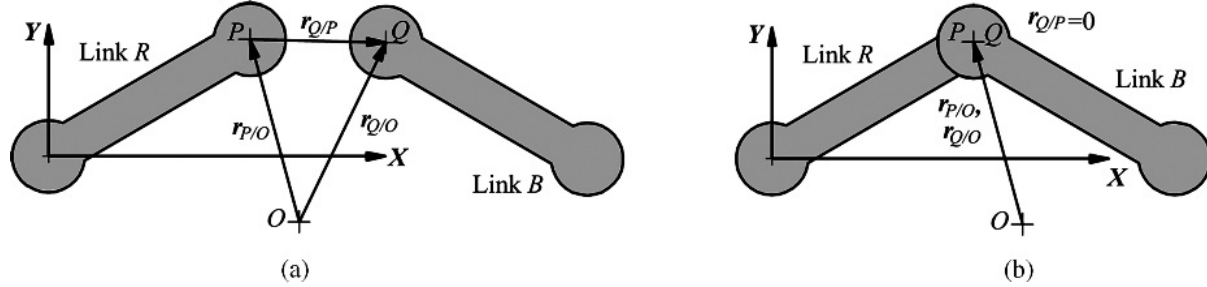


[Figure 5.7](#) Condition when two separate points (a) become momentarily coincident (b).

Because $\dot{\omega}_S \times r_{Q/P} = 0$ regardless of which link B is, the equation for the relative velocity remains the same regardless of the link chosen as the moving body. This means that the relative velocity term $\dot{\omega}_{Q/P}$ is independent of the coordinate system chosen for the “moving” body. Therefore

$$\dot{r}_{Q/P} = \dot{r}_{Y_P} + \dot{\omega}_{Q/P} r_{Q/P} = \dot{r}_{Y_B} + \dot{\omega}_{Q/B} r_{Q/B}$$

where M and B are *any* systems.

With $r_{Q/P} = 0$, the acceleration equation, [Equation 5.10](#), simplifies to

$$\ddot{r}_{Q/P} = \ddot{r}_{Y_P} + \ddot{\omega}_{Q/P} r_{Q/P} + 2\dot{\omega}_B \times \dot{r}_{Q/B} \quad (5.26)$$

Here, the Coriolis term is a function of velocities, so it can be computed as soon as the velocity analysis is completed. Only $\ddot{\omega}_{Q/P}$ involves new information not available from the velocity analysis.

5.4.3 Two Points Are Instantaneously Coincident and in Rolling Contact

If points P and Q are not only momentarily coincident, but are also in rolling contact, [Equations 5.25](#) and [5.26](#) can be simplified still further. This condition is shown in [Figure 5.8](#). If two points are in rolling contact, they have the same velocity so that their relative velocity must be zero. This means that

$$\begin{aligned}\mathcal{R}_{Q/P} &= \mathcal{R}_{Q/B} \cdot \mathcal{R}_{B/P} = \mathcal{Q} \\ \mathcal{R}_{Q/B} &\equiv \mathcal{R}_{P/B}\end{aligned}$$

and

$$\mathcal{R}_{Q/B} = \mathcal{R}_{Q/P} + \mathcal{R}_{P/B}$$

Using logic similar to that used with [Equation 5.26](#), it is apparent that while the relative acceleration $\mathcal{R}_{Q/P}$ is not usually zero, it is independent of whatever coordinate system is used for reference. This means that the relative acceleration will be the same when observed from any of the links in the mechanism.

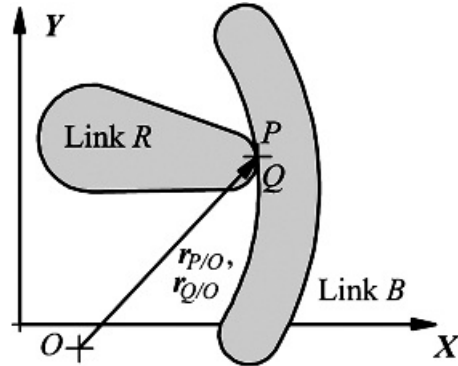


[Figure 5.8](#) Condition for rolling contact.



5.5 Linkages with Rotating Sliding Joints

Mechanisms in this class can have either a slider that slides on a line that is rotating or a pin-in-a-slot joint where the slot is straight and rotating. These cases are shown in [Figure 5.9](#) where the link numbers have been chosen arbitrarily.

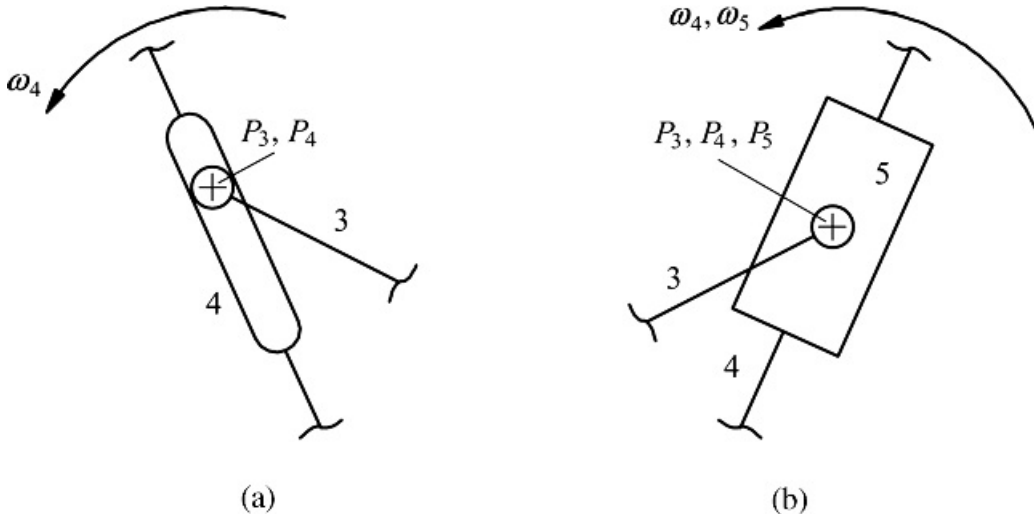


[Figure 5.9](#) Joints that can be analyzed as rotating sliding joints: (a) Pin in straight slot and (b) rotating slider. The link numbers have been chosen arbitrarily.

Mechanisms with sliders that rotate are common in practice. Typical examples are door closers, the hydraulic cylinders on power shovels, and the power cylinders on some robots. The pin-in-slot joints, often with a free-spinning roller centered on the pin, are typically used as inexpensive substitutes for slider joints. They function where the transmitted loads are low. Examples where they appear are electric toothbrush mechanisms and walking-toy mechanisms.

The analysis of these mechanisms can be approached using the special case in Section 5.4.2 for relative velocities and accelerations of coincident points. The resulting velocity and acceleration equations for two coincident points P and Q are given by [Equations 5.25](#) and [5.26](#). Dropping the superscript R for the frame, we get

$$v_Q = v_P + {}^B v_{Q/P}$$

and

$$\alpha_Q = \alpha_P + {}^B \alpha_{Q/P} + 2\omega_B \times {}^B v_{Q/P}$$

When the points are coincident, P and Q will share the same coordinates, and they will usually be designated by the same letter with a subscript identifying the link to which they are attached. For example, if 3 and 4 are the links to which the coincident points are attached, if body B corresponds to link 5, and if the frame is 1, the velocity and acceleration equations can be written as

$$v_{P_3} = v_{P_4} - {}^3 v_{P_3/P_4} \quad (5.27)$$

and

$$\ddot{\alpha}_{P_3} = \ddot{\alpha}_{P_4} - {}^3\ddot{\alpha}_{P_3/P_4} + 2\omega_3 \times {}^3\dot{\alpha}_{P_3/P_4} \quad (5.28)$$

Once again, ${}^3\dot{\alpha}_{P_3/P_4}$ is called the acceleration of P_3 relative to P_4 when the observer is in system 5. The term $2\omega_3 \times {}^3\dot{\alpha}_{P_3/P_4}$ is the Coriolis component of acceleration, and it can be written as $\ddot{\alpha}_{P_3/P_4}^C$. Equation 5.28 can then be written as

$$\ddot{\alpha}_{P_3} = \ddot{\alpha}_{P_4} + {}^3\ddot{\alpha}_{P_3/P_4} + \ddot{\alpha}_{P_3/P_4}^C$$

In planar motion, the Coriolis component is normal to ${}^3\dot{\alpha}_{P_3/P_4}$ and has the magnitude $2|\omega_3| |{}^3\dot{\alpha}_{P_3/P_4}|$. Its sense is obtained by imagining ${}^3\dot{\alpha}_{P_3/P_4}$ to be rotating about its tail in the $\ddot{\alpha}_S$ direction. The direction of movement of the head of ${}^3\dot{\alpha}_{P_3/P_4}$ gives the sense. To illustrate the manner in which Equations 5.27 and 5.28 are used in graphical linkage analyses, consider Example 5.1.



Example 5.1

Velocity and Acceleration Analysis of a Quick-Return Mechanism

Find the sliding velocities of the two slides, the angular accelerations of links 3 and 4, and the acceleration of slide 5 for the quick-return mechanism of [Figure 5.10](#). The dimensions are as shown. Link 2 is driven with a constant angular velocity of 10 rpm CCW.

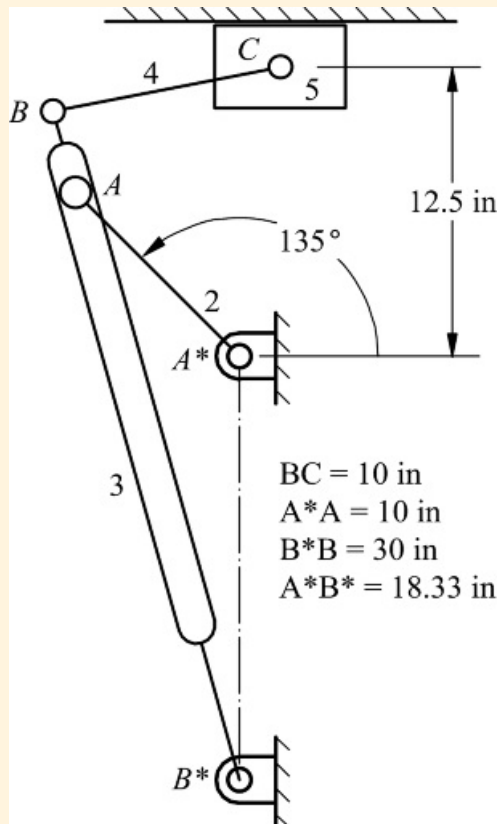


[Figure 5.10](#) The quick-return linkage analyzed in Example 5.1.

Solution

Link 2 is the driver, so we will begin the analysis with point A_2 . We will conduct the velocity analysis first. If that analysis is done carefully, we can proceed with the same points in the same order for the acceleration analysis. As in the examples in [Chapter 4](#), we will develop the basic equations first and then use the graphical procedure for solving them. The velocity of point A_2 is given by

$$\dot{v}_{A_2} = v_{A_2/A^*} = \omega_2 \times r_{A_2/A^*}$$

In the analysis of mechanisms of this type, it is important to identify the link in which the observer is located. Therefore, the left superscripts will be maintained when the coordinate system is different from system 1. We must now use the coincident point A_3 to be able to develop an equation relating a point on link 2 to a point on link 3. We can write the relative velocity equation in one of two ways

$$\dot{v}_{A_3} = v_{A_3} + v_{A_2/A_3} = v_{A_3} + {}^3\dot{v}_{A_2/A_3} \quad (5.29)$$

or

$$\dot{v}_{A_3} = \dot{v}_{A_2} + \ddot{v}_{A_2/A_3} = \dot{v}_{A_2} + {}^2\dot{v}_{A_3/A_2} \quad (5.30)$$

To solve the problem, we must be able to recognize the direction of the relative velocity defined in the moving coordinate system. Referring to the mechanism in [Figure 5.10](#), if the observer is fixed to link 2, it is not possible to identify directly the direction of the velocity ${}^2\dot{v}_{A_3/A_2}$ because the path that A_3 traces on link 2 is rotating; however, if the observer is in link 3, it is possible to identify the direction of the velocity ${}^3\dot{v}_{A_2/A_3}$ because the pin at A is constrained to move along the straight slot in link 3. Therefore, the direction of the velocity ${}^3\dot{v}_{A_2/A_3}$ must be along the slot. Because we can determine the direction of ${}^3\dot{v}_{A_2/A_3}$ by inspection, [Equation 5.29](#) is more useful than [Equation 5.30](#).

In problems such as this, it is important to identify clearly the links relative to which the velocity directions can be identified. The same points and links can be used for the subsequent acceleration analysis, and it is usually much easier to visualize velocities than it is to visualize accelerations.

After [Equation 5.29](#) is solved for the unknowns, \dot{v}_{A_3} will be known. Then \dot{v}_{B_3} can be found from the velocity image of link 3 using B^* , A_3 , and B_3 . Knowing \dot{v}_{B_3} , which is the same as \dot{v}_{B_1} , we can write the following equation for the velocity of C_4

$$\dot{v}_{C_4} = \dot{v}_{B_3} + \dot{v}_{C_4/B_3} \quad (5.31)$$

Because the directions of \dot{v}_{C_4} and \dot{v}_{C_4/B_3} are known, we can solve [Equation 5.31](#) for the unknowns. After [Equations 5.29](#) and [5.31](#) are solved, we can compute the angular velocities of links 3 and 4 from

$$\dot{\theta}_{B_3/B^*} = \omega_3 \times \dot{v}_{B_3/B^*}$$

and

$$\dot{\theta}_{C_4/B_3} = \omega_4 \times \dot{v}_{C_4/B_3}$$

For the acceleration analysis, we need only differentiate [Equations 5.29](#) and [5.31](#). The results are

$$\ddot{\theta}_{A_2} = \ddot{\theta}_{A_3} + \ddot{\theta}_{A_2/A_3}$$

$$\ddot{\theta}_{C_4} = \ddot{\theta}_{B_3} + \ddot{\theta}_{C_4/B_3} = \ddot{\theta}_{B_3} + \ddot{\theta}_{B_3/B^*} + {}^3\ddot{\theta}_{A_3/A_2} + 2(\omega_3 \times {}^2\dot{v}_{A_3/A_2})$$

Expanding the equations in terms of vectors relative to moving coordinate systems, we obtain

$$\ddot{\theta}_{A_2/A^*} + \ddot{\theta}_{A_3/A^*} = \ddot{\theta}_{A_3/B^*} + \ddot{\theta}_{A_3/B^*} + {}^3\ddot{\theta}_{A_3/A_2} + 2(\omega_3 \times {}^2\dot{v}_{A_3/A_2}) \quad (5.32)$$

After [Equation 5.32](#) is solved for the unknowns, $\ddot{\theta}_{A_3} = \ddot{\theta}_{A_3/B^*}$ will be known. Then $\ddot{\theta}_{B_3}$ can be found from the acceleration image of link 3 using B^* , A_3 , and B_3 . Knowing $\ddot{\theta}_{B_3}$, which is the same as $\ddot{\theta}_{B_1}$, we can expand the acceleration equation for C_4 as

$$\omega_{C_4} = \omega_{B_4} + \omega_{C_5/B_5} = \omega_{B_3/B^*} + \omega'_{C_4/B_4} + \omega'_{C_4/B_5} \quad (5.33)$$

where

$$\omega'_{B_2/A^*} = |\omega_2|^2 |r_{A/A^*}| \text{ from } A \text{ to } A^*$$

$$\omega'_{B_2/A^*} = \omega_2 \times r_{A/A^*} \text{ perpendicular to } AA^* \text{ (in this problem } \omega_2 = 0)$$

$$\omega'_{B_3/B^*} = |\omega_3|^2 |r_{A/B^*}| \text{ from } A \text{ to } B^*$$

$$\omega'_{B_3/B^*} = \omega_3 \times r_{A/B^*}, (\omega_3 \text{ is unknown but the result is perpendicular to } AB^*)$$

$${}^3\omega_{A_2/A_2} \text{ has a magnitude that is unknown but a direction that is along slot in link 3}$$

$$2(\omega_3 \times {}^3v_{A_2/A_2}) \text{ is the Coriolis acceleration perpendicular to } {}^3v_{A_2/A_2}$$

$$\omega_{C_5} \text{ is along the slider path of link 5}$$

$$\omega_{B_3/B^*} \text{ is found by acceleration image of link 3}$$

$$\omega'_{C_4/B_5} = |\omega_4|^2 |r_{C/B}| \text{ from } C \text{ to } B$$

$$\omega'_{C_4/B_5} = \omega_4 \times r_{C/B} \text{ (}\omega_4 \text{ is unknown but the result is perpendicular to } CB\text{)}$$

Based on the position and velocity analyses, there will be only two unknown magnitudes in [Equations 5.31](#) and [5.33](#). All of the directions will be known. Therefore, the equations can be solved.

Steps

1. Draw linkage to scale as shown in [Figure 5.11](#).

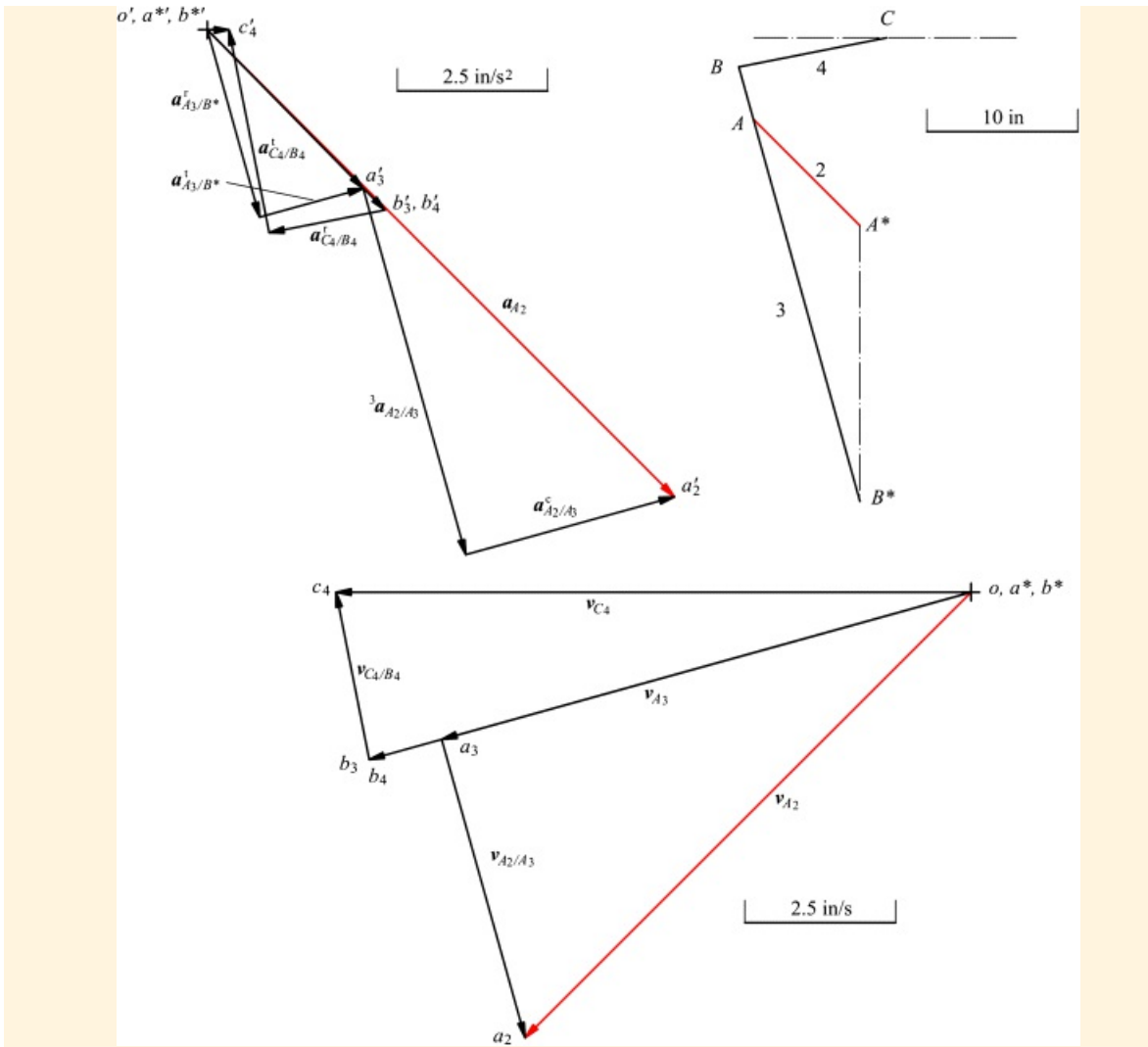


[Figure 5.11](#) Polygons for Example 5.1. Vectors based on the input values are shown in red.

2. Compute \mathbf{v}_{A_3} and plot \mathbf{v}_{A_3} normal to A^*A as a^*a_2 where

$$\omega_2 = 10 \times 2\pi/60 = 1.0472 \text{ rad/s}$$

$\mathbf{v}_{A_3} = \omega_2 \times \mathbf{r}_{A/A^*} = 10 \times 1.0472 = 10.472 \text{ in/s}$ perpendicular to AA^* in the direction shown in [Figure 5.11](#)

3. Draw a line through a_2 parallel to B^*B .
 4. Draw a line through o normal to B^*A . The intersection with the line from step 3 gives point a_3 .
 5. Locate b_3 using the velocity image $\frac{\dot{x}_3}{ca_3} = \frac{\dot{x}_3}{9.11} = \frac{8.3}{8.7} = \frac{20}{25.37}$ where

$$\dot{x}_3 = 9.11 \times (30/25.37) = 10.37 \text{ in/s}$$

6. Draw a line through b_3 normal to BC .
 7. Draw a line through o parallel to the slide. Its intersection with the line drawn in step 6 gives point c_4 .
 8. Measure $\mathbf{r}_{C_4} = \mathbf{r}_{c_4}$, $\mathbf{r}_{A_2/A_3} = \mathbf{a}_2\mathbf{a}_3$, $\mathbf{r}_{B_3/B^*} = \mathbf{r}_{b_3}$, and $\mathbf{r}_{C_4/S_4} = \mathbf{r}_{c_4}$ where

$$v_{C_6} = 10.54 \text{ in/s}, v_{B_3/B_2} = 5.15 \text{ in/s}, v_{S_3/P^*} = 10.37 \text{ in/s}, \text{ and } v_{C_4/B_3} = 2.84 \text{ in/s}$$

9. Compute $\omega_3 = |v_{B_3/B^*}| / |r_{B/B^*}|$ and $\omega_4 = |v_{C_4/B_3}| / |r_{C/S}|$ where

$$\omega_3 = 10.37 / 30 = 0.35 \text{ rad/s CW}$$

$$\omega_4 = 2.84 / 10 = 0.28 \text{ rad/s CCW}$$

10. Get the senses of ω_3 and ω_4 by looking at the directions of rotation of r_{B/B^*} and $r_{C/S}$ needed to determine the respective relative velocity directions.
11. Compute a_{A_2} and plot it as \vec{a}'_{A_2} . (Note that $\omega_2 = 0$ so $a_{A_2} = \vec{a}_{A_2/A^*}$)
 $a_{A_2} = \vec{a}_{A_2/A^*} = |\omega_2|^2 |r_{A/A^*}| = (1.0472)^2 (10) = 10.97 \text{ in/s}^2$ in the direction from A to A^*
12. Compute $a_{A_2/A_3}^C = 2|\omega_3| |v_{A_3/A_2}|$ and get the sense of \vec{a}_{A_2/A_3}^C by rotating v_{A_2/A_3} 90° in the ω_3 direction. Plot it with the tip at a'_{A_2} .

$$a_{A_2/A_3}^C = 2\omega_3 |v_{A_3/A_2}| = 2(0.35)(5.15) = 3.60 \text{ in/s}^2$$

13. Draw a line normal to \vec{a}_{A_2/A_3}^C (along the slot) and through the tail of \vec{a}_{A_2/A_3}^C . This line corresponds to \vec{s}_{A_2/A_3} .
14. Compute \vec{a}_{A_2/P^*} and plot it from o' in the AA^* direction.

$$a_{A_2/P^*} = |\omega_3|^2 |r_{A/P^*}| = (0.35)^2 (26.37) = 3.23 \text{ in/s}^2$$

15. Draw a line through the tip of \vec{a}_{A_2/A_3}^C normal to AB^* . This vector corresponds to \vec{a}_{A_2/P^*} . Its intersection with the line drawn in step 13 gives point a'_3 .
16. Measure $\vec{o}'\vec{a}_3$, and locate point b'_3 using the acceleration image $\frac{\vec{o}'\vec{b}_3}{\vec{o}'\vec{a}_3} = \frac{\vec{s}^*}{\vec{s}^* \vec{a}}$.

$$\frac{\vec{o}'\vec{b}_3}{\vec{o}'\vec{a}_3} = \frac{\vec{o}'\vec{b}_3}{3.60} = \frac{B^*B}{B^*A} = \frac{30}{26.37}$$

and

$$\vec{o}'\vec{b}_3 = 3.60(30/26.37) = 4.20 \text{ in/s}^2$$

17. Plot \vec{a}_{C_4/B_3} from point b'_3 parallel to CB .

$$a_{C_4/B_3} = |\omega_4|^2 |r_{C/S}| = (0.28)^2 (10) = 0.78 \text{ in/s}^2$$

18. Draw a line through the tip of \vec{a}_{C_4/B_3} normal to CB . This vector corresponds to \vec{a}_{C_4/B_3} .
19. Draw a line through o' parallel to the slide at C . Its intersection with the line generated in step 18 gives point c'_4 .

20. Measure \dot{s}_{A_3/B^*}^t and \dot{s}_{C_4/B_0}^t

$$\dot{s}_{A_3/B^*}^t = 1.79 \text{ in/s}^2 \text{ and } \dot{s}_{C_4/B_0}^t = 3.44 \text{ in/s}^2$$

21. Compute $\omega_3 = \frac{\left| \dot{s}_{A_3/B^*}^t \right|}{\left| r_{A/B^*} \right|}$ and $\omega_4 = \frac{\left| \dot{s}_{C_4/B_0}^t \right|}{\left| r_{C/B} \right|}$, and get the senses of these angular accelerations by considering the directions of rotation needed to rotate the position vectors in the directions of \dot{s}_{A_3/B^*}^t and \dot{s}_{C_4/B_0}^t respectively.

$$\begin{aligned}\omega_3 &= \frac{\left| \dot{s}_{A_3/B^*}^t \right|}{\left| r_{A/B^*} \right|} = \frac{1.79}{26.37} = 0.068 \text{ rad/s}^2 \text{ CW} \\ \omega_4 &= \frac{\left| \dot{s}_{C_4/B_0}^t \right|}{\left| r_{C/B} \right|} = \frac{3.44}{10} = 0.34 \text{ rad/s}^2 \text{ CCW}\end{aligned}$$

22. Measure ω_C . $\omega_C = 0.36 \text{ rad/s}^2$ directed to the right

One of the useful features of the quick-return linkage is a long range of motion with relatively uniform velocity on the forward stroke. The small value of ω_C is indicative of this property.



5.6 Rolling Contact

Rolling contact is quite often used in practical linkages. In addition to the obvious case of a wheel rolling on a surface or a rail, rolling contact between a cam and a roller follower is another common example. Also, the pitch cylinders of spur and helical gear pairs and the pitch cones of bevel gear pairs can be considered to be in pure rolling contact. In that case, although the actual physical contact between the gear teeth is a general combination of rolling and sliding, the gear pair can be modeled as a pair of simple elements in pure rolling contact from the point of view of investigating gross kinematic properties.

Rolling contact can be approached in two different ways depending on the level of detail desired. If the velocities and accelerations of the rolling elements themselves are immaterial, it is possible to solve for the velocities and accelerations of the other links in a rolling-contact problem by replacing the actual linkage with a virtual linkage that involves an extra binary link that is pinned to each of the rolling elements at their centers of curvature and with a length equal to the sum of the rolling elements' radii of curvature. If the velocities and accelerations of all the links are important, then detailed relative velocity relations are necessary to obtain the angular velocities of the rolling links. Both approaches will be discussed.

5.6.1 Basic Kinematic Relationships for Rolling Contact

[Figure 5.12](#) shows two rigid bodies in rolling contact. The bodies are arbitrarily taken as links 2 and 4. The instantaneous contact location is B , and the centers of curvature of the two bodies corresponding to B_2 and B_4 are O_2 and O_4 , respectively. At the point of contact for two bodies rolling on each other, there is no relative sliding between the two contacting points (B_2 and B_4) at the location of contact. Because B_2 and B_4 are not only momentarily coincident but also in rolling contact, they have the same velocity which means that their relative velocity must be zero. Thus

$$v_{S_2} = v_{S_4}$$

and

$$v_{S_2/S_4} = {}^4v_{B_2/B_4} = {}^4v_{B_2} = 0$$

Note that this is exactly the same velocity condition as that for a revolute joint. Therefore, for velocities *ONLY*, the point of rolling contact can be treated as a revolute joint. However, this is not true for accelerations.

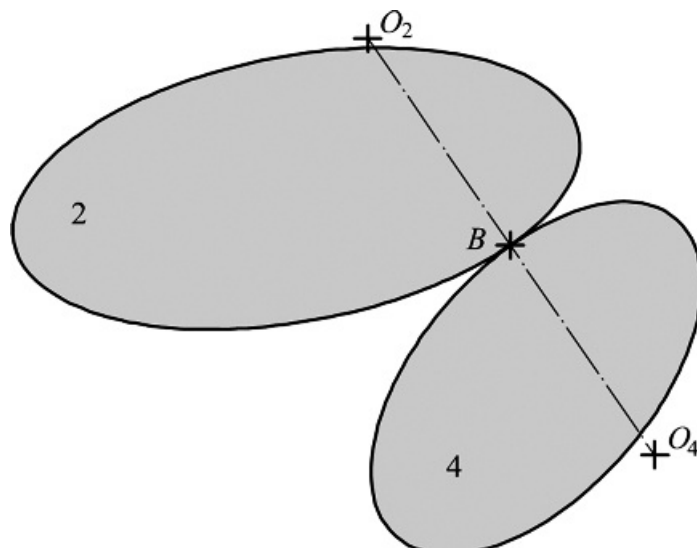


[Figure 5.12](#) Two links in rolling contact.

The relative acceleration $\ddot{\omega}_{B_2/B_4}$ is usually not zero, but it is independent of coordinate system. Therefore

$$\ddot{\omega}_{B_2/B_4} = {}^4\ddot{\omega}_{B_2/B_4} = {}^4\ddot{\omega}_{B_4} \quad (5.34)$$

From [Equation 5.34](#), it is apparent that the direction of $\ddot{\omega}_{B_2/B_4}$ is the same as the direction of ${}^4\ddot{\omega}_{B_4}$ which is the absolute acceleration of point B_2 observed from link 4. Therefore, it is useful to determine the path that B_2 traces on 4 (or B_4 traces on 2) to determine the direction of the acceleration of ${}^4\ddot{\omega}_{B_4}$. To do this, first imagine that link 2 is a circle and link 4 is a straight line.

From experience (for example, from looking at a bicycle tire reflector at night) we know that the path of B_2 will look as shown in [Figure 5.13](#). That is, the path forms a cusp at the contact location. The cusp will approach the contact point in a direction that is tangent to the common normal at the contact point, and the cusp will also leave the contact point in a direction that is tangent to the common normal. This means that the acceleration must be along the common normal at the point of contact. The same kind of relationship also applies for general bodies; that is, the direction of the relative acceleration will be along the common normal at the contact point.

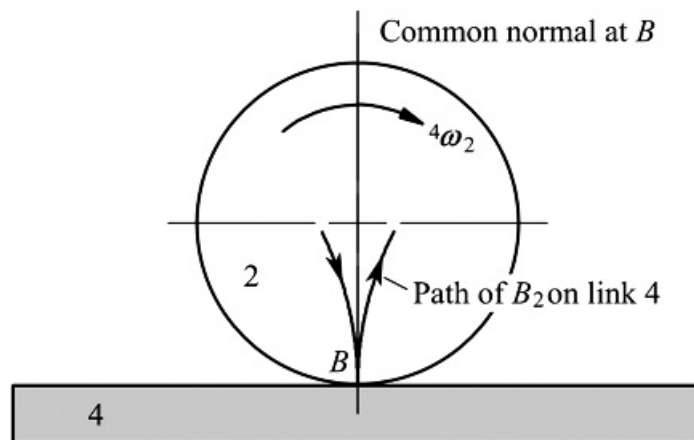


[Figure 5.13](#) Path of motion of B_2 relative to link 4.

To conduct an acceleration analysis of mechanisms involving rolling contact, it is necessary to determine both the magnitude and direction of the relative acceleration between the two contact points. Because we know that the direction of the relative accelerations will be along the common normal at the point of contact, we need only determine the magnitude.

To do this, first consider a general rigid body R as shown in [Figure 5.14](#). Because the contour of the rigid body must be known for a kinematic analysis, it will be possible to determine the center of curvature, O_R , corresponding to any point on the contour of that body. If a circle of radius $O_R B$ is drawn, that circle will be tangent to the contour at B , and it will share three points (separated by infinitesimal distances) with the contour of R . This circle is called the osculating circle to the curve at point B , and the circle is a unique property of the curve for the point considered. An example is shown in [Figure 5.14](#).

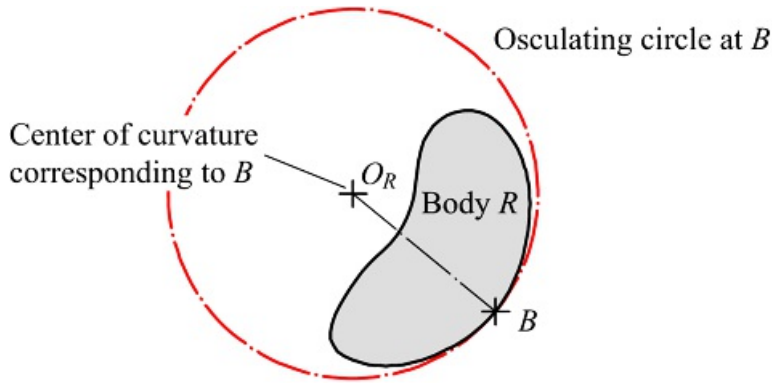


[Figure 5.14](#) Osculating circle.

If we consider two general links (2 and 4) in rolling contact, we can draw the osculating circle for each curve. As the two bodies roll together, the three points shared by the osculating circles will contact with each other. Therefore, for two differentially separated time periods, the curves could be replaced by their osculating circles. Because only two differentially separated time periods must be considered for accelerations, we can replace the original curves with their osculating circles, and the kinematic results for position, velocity, and acceleration will remain unchanged. If higher derivatives than accelerations are desired, however, we cannot replace the original surfaces with their osculating circles. Obviously, a different osculating circle may be required for each contact position if the surface of body R is totally general. However, if a kinematic analysis is to be conducted, the geometry of the surface must be known. The osculating circle corresponding to each point on the periphery can be identified from the location of the center of curvature of the curve at each point.

The replacement of a general surface with osculating circles is extremely useful in kinematics whenever higher pairs are involved. The special properties of circles make it relatively simple to analyze linkages with rolling and cam joints.

Because we can replace the two curves with their osculating circles, we can connect the two centers of curvature by a virtual link pinned to the two bodies at the centers of curvature, and the two bodies can still move relative to each other. This is precisely the condition existing when two gears in a standard transmission are meshed. For the sake of discussion, let the two bodies again be links 2 and 4 and the virtual link be designated as x as shown in [Figure 5.15](#). With this arrangement, we are now in a position to compute the relative acceleration $\dot{\theta}_{S_2/S_4}$. To do this, we will use [Equation 5.34](#) and compute $\ddot{\theta}_{S_2/S_4}$, which is equal to $\dot{\theta}_{S_2/S_4}$.

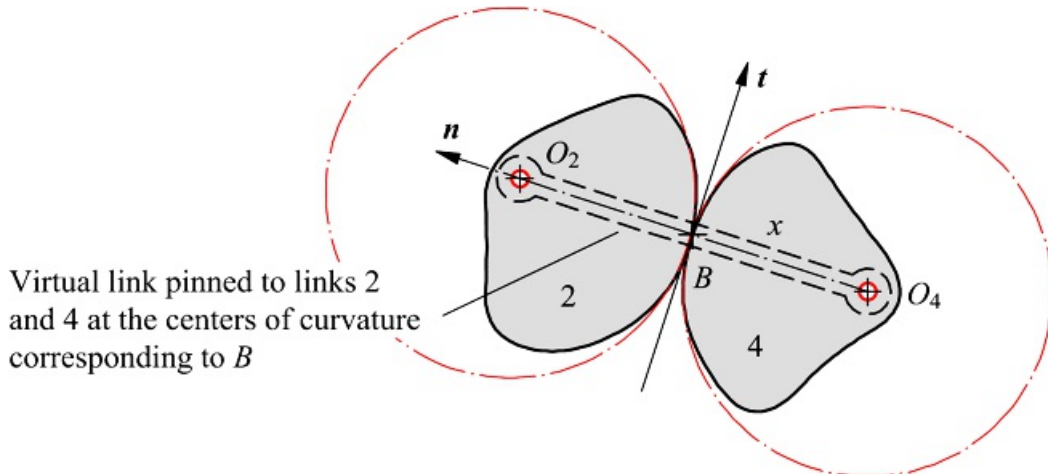


[Figure 5.15](#) Virtual link pinned at the centers of curvature of the two bodies in rolling contact.

As with any planar vector, the acceleration $\ddot{\theta}_{S_2/S_4}$ can be resolved into two orthogonal components. It is convenient to resolve the vector into one component along the common normal to the two curves at B and another along the common tangent. That is

$$\ddot{\alpha}_{B_2/B_4} = \ddot{\alpha}_{B_4/B_4} + \ddot{\alpha}_{B_4/B_2}$$

However, we know from our earlier discussion that the relative acceleration must lie along the common normal. Therefore, the tangential component must be zero, and the *total* relative acceleration between B_2 and B_4 can be represented as

$$\ddot{\alpha}_{B_2/B_4} = \ddot{\alpha}_{B_2/B_2}$$

We can compute the normal acceleration by writing the relative accelerations among the points B_2 , B_4 , O_2 , and O_4 in [Figure 5.15](#). That is

$$\ddot{\alpha}_{B_2/B_4} = \ddot{\alpha}_{B_4/B_4} = \ddot{\alpha}_{B_4/B_2} + \ddot{\alpha}_{(O_4)_z/(O_2)_z} + \ddot{\alpha}_{B_4/B_2}$$

Now consider individually each term on the right-hand side of the equation. Each term will be a function of velocities and can be computed in a variety of ways. For example

$$\ddot{\alpha}_{B_4/B_2} = \omega_4^2 |r_{B_2/O_4}| = |\omega_2 v_{B_2/O_4}| = \frac{(v_{B_2/O_4})^2}{|r_{B_2/O_4}|} \quad (\text{from } B_2 \text{ toward } O_4)$$

and

$$\ddot{\alpha}_{(O_4)_z/(O_2)_z} = \omega_4^2 |r_{O_4/B_2}| = |\omega_4 v_{O_4/B_2}| = \frac{(v_{O_4/B_2})^2}{|r_{O_4/B_2}|} \quad (\text{from } O_4 \text{ toward } B_2)$$

Similarly

$$\ddot{\alpha}_{(O_2)_z/(O_4)_z} = \omega_2^2 |r_{O_4/B_2}| = |\omega_2 v_{O_4/B_2}| = \frac{(v_{O_4/B_2})^2}{|r_{O_4/B_2}|} \quad (\text{from } O_2 \text{ toward } O_4) \quad (5.35)$$

To evaluate the first two expressions on the right-hand side of [Equation 5.35](#), we need to develop an expression for ω_2 . While this is relatively easy to do, it is unnecessary because the third expression involves only linear velocity and position information. If we have completed the velocity analysis, we will be able to determine v_{O_4/B_2} directly.

To summarize, in rolling contact problems, we know that the two contact points (e.g., B_2 and B_4) have the same velocity. Also, given the acceleration of one of the points, say B_4 , the acceleration of the other point can be computed from

$$\ddot{\alpha}_{B_2} = \ddot{\alpha}_{B_4} + \ddot{\alpha}_{B_4/B_2}$$

where $\ddot{\alpha}_{B_4/B_2}$ can be computed using

$$\ddot{\omega}_{B_2/O_4} = \frac{(v_{B_2/O_2})^2}{|r_{B_2/O_2}|} + \frac{(v_{O_2/O_4})^2}{|r_{O_2/O_4}|} + \frac{(v_{O_4/B_2})^2}{|r_{O_4/B_2}|}$$

(5.36)

In [Equation 5.36](#), the components will be parallel, but they may point in either direction. The direction is indicated under each component. The components are each along the common normal to the surfaces at the contact point so the components can be added algebraically, and only the final resultant needs to be plotted.

If one of the rolling surfaces is flat, the center of curvature will approach infinity, and the corresponding acceleration term will become zero. For example, if the rolling surface for link 2 is flat, then O_2 is at infinity, and the acceleration expressions reduces to

$$\ddot{\omega}_{B_2/O_4} = \frac{(v_{G_4/B_2})^2}{|r_{G_4/B_2}|} = |\omega_4 v_{O_4/B_2}| = \omega_4^2(r_{O_4/B_2}) \quad (\text{from } O_4 \text{ toward } B)$$



Example 5.2

Analysis of Linkage with a Rolling-Contact Joint

In the linkage shown in [Figure 5.16](#), link 4 is a gear rotating about B^* . Link 3 is a gear meshing with 4 and has an arm fixed to it which is hinged to link 2 at A . A fifth link (not shown) would be connected from C to B^* to maintain contact between links 3 and 4. Link 2 is driven at a constant angular velocity of 10 rad/s CCW. Find the angular acceleration of gear 4.

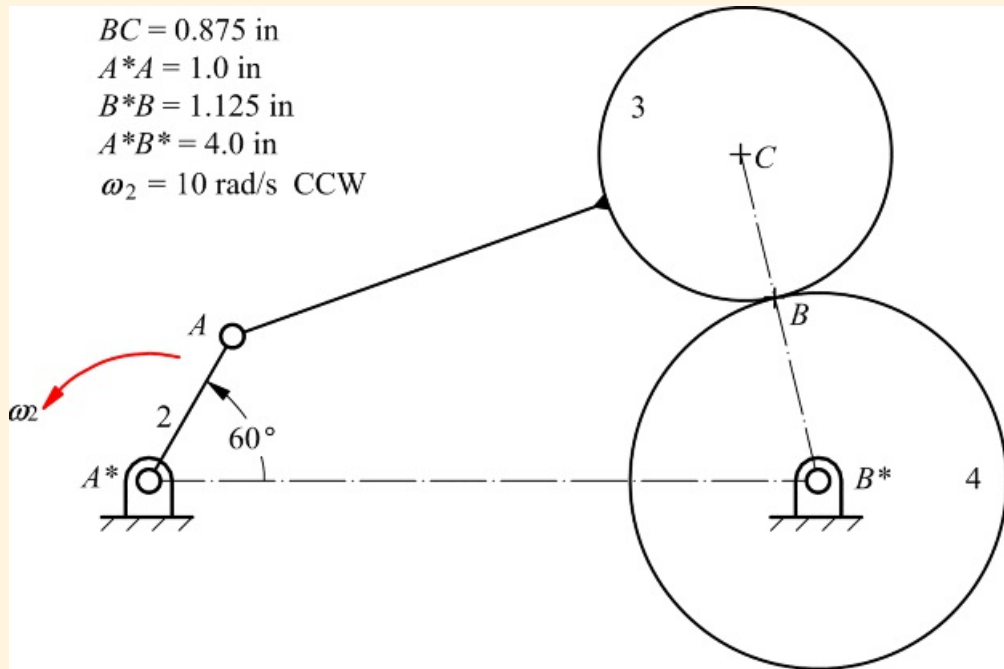


[Figure 5.16](#) The linkage of Example 5.2. This is an example of a geared five-bar linkage. Geared five-bar and six-bar linkages are used quite frequently as alternatives to four-bar linkages. They allow more flexibility in synthesis than four-bar linkages because there are more dimensions that can be varied.

Solution

In this instance, we cannot ignore the acceleration of either of the two contacting bodies. The angular acceleration of gear 3 is the same as that of arm AC to which it is rigidly affixed. The angular acceleration of gear 4 is the quantity to be found.

For the velocity analysis, the equations to be solved are

$$\begin{aligned} \dot{\varphi}_{A_2/A^*} &= v_{A_2} = \omega_2 \times r_{A/A^*} = v_{B_3} \\ v_{B_2} &= v_{A_3} + v_{B_3/A_3} \\ v_{B_4} &= v_{B_3} + v_{B_3/B_3} \\ v_{B_4} &= v_{B_6/B^*} \end{aligned}$$

For the acceleration analysis, the corresponding equations to be solved are

$$\ddot{\varphi}_{A_2/A^*} = \ddot{\varphi}_{A_3} = \ddot{v}_{B_6/B^*} + \ddot{v}_{A_4/A^*}$$

$$\begin{aligned}\omega_{S_3} &= \omega_{A_2} + \omega_{S_3/A_2} = \omega_{A_2} + \dot{\omega}_{S_3/A_2} + \ddot{\omega}_{S_3/A_2} \\ \omega_{S_4} &= \omega_{S_3} + \omega_{S_4/S_3} = \omega_{S_3} + \dot{\omega}_{S_4/S_3} \\ \omega_{S_4} &= \omega_{B_4/B^*} = \dot{\omega}_{S_4/B^*} + \ddot{\omega}_{B_4/B^*}\end{aligned}$$

The acceleration equations can be combined into a single equation that must be solved

$$\ddot{\omega}_{S_4/B^*} + \ddot{\omega}_{B_4/B^*} = \ddot{\omega}_{A_2/A^*} + \ddot{\omega}_{S_3/A_2} + \ddot{\omega}_{S_3/S_2} + \ddot{\omega}_{B_3/S_2}$$

Here the unknowns are the magnitudes of the two tangential components, $\ddot{\omega}_{S_3/A_2}$ and $\ddot{\omega}_{S_4/B^*}$. Solving for these will allow us to compute ω_3 and ω_4 .

Steps

1. Draw the linkage to scale as shown in [Figure 5.17](#). First locate A^* and B^* . Then draw link 2 and locate point A . Next find the center C , knowing that it is on a circle of radius AC centered at A and also on a circle of radius CB^* centered at B^* . After locating C , draw the line AC , and the circles corresponding to the pitch circles of the two gears.

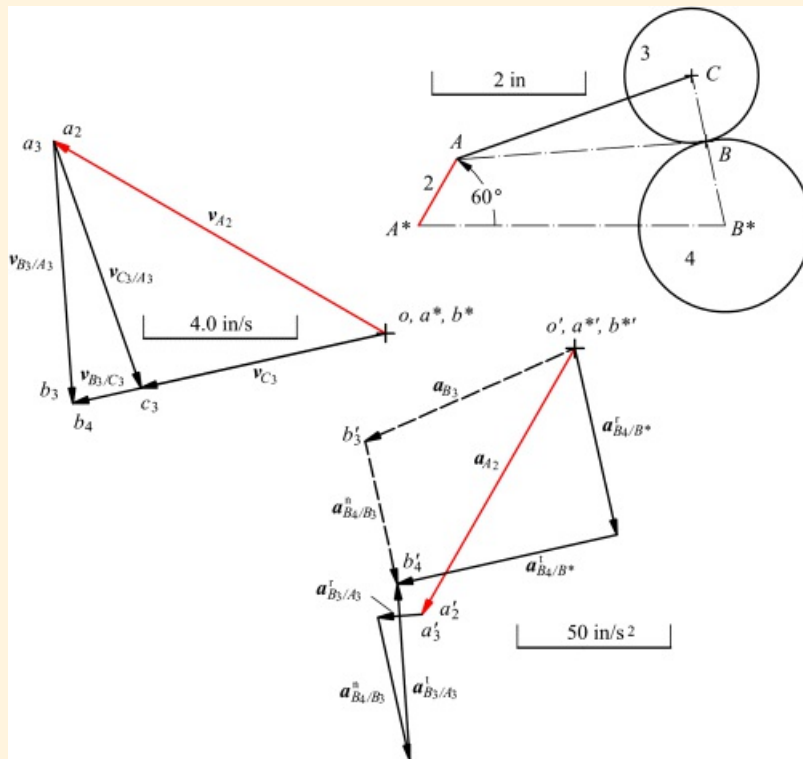


[Figure 5.17](#) The graphical solution of Example 5.2.

2. Pick a velocity scale and place the velocity pole o . Compute v_{A_2} and plot it as oa_2 . v_{A_2} is normal to AA^* .
3. Draw a line through o normal to B^*B (and B^*C).
4. Draw line AB .
5. Draw a line through a_2, a_3 normal to AB . The intersection of this line with the line generated in step 3 gives the velocity of the coincident points B_3 and B_4 . Notice that lines AC and AB are both fixed to link 3. Although at any instant, the point at B is fixed to member 3, a different B (and different point) is involved for each position of the linkage.

6. Draw a line through a_3 normal to AC . The intersection of this line with the line generated in step 3 gives the point c_3 . Point c_3 could also have been located from points a_3 and b_3 by using the velocity image theorem.
7. Measure v_{B_3/A_3} and v_{B_4/B^*} and compute $\omega_3 = |v_{B_3/A_3}| / |r_{B/A}|$, and $\omega_4 = |v_{B_4/B^*}| / |r_{B/B^*}|$. Find the senses needed to give the directions of v_{B_3/A_3} and v_{B_4/B^*} . Because of the pure rolling condition of the pitch circles of the gears, the velocity of point B is the same regardless of whether it is considered to be in member 3 or member 4.

$$\omega_3 = |v_{B_3/A_3}| / |r_{B/A}| = 6.84 / 3.26 = 2.10 \text{ rad/s CCW}$$

$$\omega_4 = |v_{B_4/B^*}| / |r_{B/B^*}| = 8.37 / 1.125 = 7.44 \text{ rad/s CCW}$$

For the acceleration analysis, also measure v_{B^*/C_2} and v_{C_3/S_3} . From the polygon

$$v_{B^*/C_2} = 6.54 \text{ in/s and } v_{C_3/S_3} = 1.83 \text{ in/s}$$

8. Compute $\alpha_{A_2/A^*} = \alpha_{A_2/A^*}^r = -|\omega_2|^2 r_{A/A^*} = \alpha_{A_2} = \alpha_{A_3}$ and plot as $\alpha' \alpha'_2$ (and $\alpha' \alpha'_3$).

$$\alpha_{A_2} = \alpha_{A_3} = (10)^2 (1) = 100 \text{ in/s}^2$$

9. Compute and plot $\alpha'_{S_3/A_3} = -|\omega_3|^2 r_{S/A}$ in the $-v_{B/A}$ direction from point a'_3 .

$$\alpha'_{S_3/A_3} = |\omega_3|^2 r_{S/A} = (2.10)^2 (3.26) = 14.4 \text{ in/s}^2$$

10. Compute α'_{B_4/S_3} using [Equation 5.36](#). Then

$$\alpha'_{B_4/S_3} = \frac{(v_{S_4/B^*})^2}{|r_{B/B^*}|} + \frac{(v_{B^*/C_2})^2}{|r_{B/C}|} + \frac{(v_{C_3/S_3})^2}{|r_{C/S}|} = \frac{8.37^2}{1.125} + \frac{6.54^2}{2.0} + \frac{1.83^2}{0.675} = 47.7 \text{ (B to B')}$$

The direction is from B to B^* because the first and last terms are larger than the middle term and we arbitrarily took the direction from B to B^* as positive.

Note also that $\alpha'_{S_4/B_3} = -\alpha'_{S_3/B_3}$ and has the direction from the center of gear 3 toward the center of gear 4. Plot α'_{B_4/S_3} from the tip of α'_{S_3/A_3} .

11. Draw a line through the tip of vector α'_{B_4/S_3} normal to AB .
12. Compute α'_{S_4/B^*} and plot α'_{S_4/B^*} from o' in the BB^* direction.

$$\alpha'_{S_4/B^*} = |\omega_4|^2 r_{B/B^*} = (7.44)^2 (1.125) = 62.3 \text{ in/s}^2$$

13. Draw a line through the tip of vector α'_{S_4/B^*} normal to BB^* . The intersection of this line with that drawn in step 11 gives b'_4 .

14. Compute $\omega_4 = \dot{\theta}_{B_4/B^*} / r_{B/B^*}$ and find the sense needed to rotate r_{B/B^*} to the direction of $\dot{\theta}_{B_4/B^*}$.

$$\omega_4 = \dot{\theta}_{B_4/B^*} / r_{B/B^*} = 73.4 / 1.125 = 65.2 \text{ rad/s}^2 \text{ CCW}$$

Note that this construction, with the vectors in the order shown, gives the correct position for b'_4 but not for b'_3 because $\omega_{B_4} = \omega_{B_3} + \omega_{B_3/B_4}$. However, if the correct position of b'_3 were required, either to get the absolute acceleration or if the acceleration image was to be constructed, it would be obtained by plotting \ddot{r}_{B_3/B_2} from b'_4 as shown in [Figure 5.17](#) by the dashed lines.

Although the acceleration of the contacting point in one body relative to that in the other has been worked out assuming circular contacting profiles, it can also be used if the profiles are not circular. The radius of the noncircular profile is simply replaced with the osculating circle of the profile at the point of contact.

5.6.2 Modeling Rolling Contact Using a Virtual Linkage

As a second example of rolling contact, we will consider the plate cam with roller follower shown in [Figure 5.18](#). In this mechanism, we are given the angular velocity and acceleration of link 2, and we wish only to know the angular velocity and acceleration of link 4. We are not interested in the velocity and acceleration of link 3. When this is the case, we can model the linkage with a virtual link between the centers of curvature of links 2 and 3 corresponding to the contact point P . The cam-follower mechanism can then be analyzed as the virtual four-bar linkage A^*ABB^* . Line A^*A is fixed to link 2, so the angular velocity and acceleration of A^*A will be the angular velocity and angular acceleration for link 2.

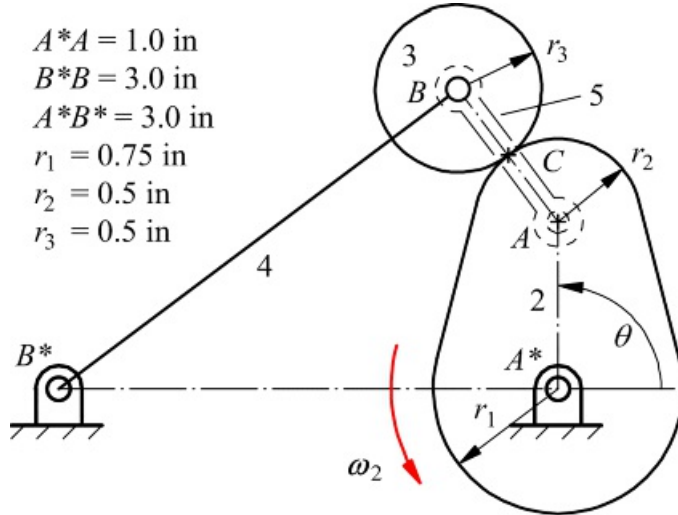


[Figure 5.18](#) A plate cam with roller follower. For given angular velocity and acceleration of the cam (link 2), the angular velocity and angular acceleration of the arm 4 can be found by replacing the linkage with the virtual four-bar A^*ABB^* . Here point A is the center of curvature of the cam profile at the contact point C .



Example 5.3

Analysis of a Geared-Linkage Rolling Contact

Find the angular velocity and angular acceleration of the link 4 of the linkage in [Figure 5.18](#) for $\theta = 90^\circ$ when the cam, link 2, is rotated CCW with a constant angular velocity of 1000 rpm.

Solution

The virtual mechanism in [Figure 5.18](#) is a four-bar linkage so the steps to analyzing this mechanism are the same as those required for the four-bar linkage in Example 4.1. The velocity equations that must be solved graphically are

$$\begin{aligned} v_{A_2/A^*} &= v_{A_3} = v_{A_3} = \omega_2 \times r_{A/A^*} \\ v_{S_2} &= v_{B_2} = v_{A_2} = v_{S_2/A_3} \\ v_{B_4} &= v_{A_4/S^*} \end{aligned}$$

where the virtual link is designated as link 5. The acceleration equations that must be solved are

$$\begin{aligned} \ddot{v}_{A_2/A^*} &= \ddot{v}_{A_3} = \ddot{v}_{A_3} = \ddot{v}_{A_3/A^*} + \ddot{\omega}_{A_3/A^*}^2 \\ \ddot{v}_{B_2} &= \ddot{v}_{B_4} = \ddot{v}_{A_2} = \ddot{v}_{A_3} + \ddot{\omega}_{S_2/A_3}^2 + \ddot{\omega}_{B_2/A_3}^2 \\ \ddot{v}_{B_4} &= \ddot{v}_{B_4/S^*} = \ddot{v}_{A_4/S^*} + \ddot{\omega}_{B_4/S^*}^2 \end{aligned}$$

Steps

1. Draw the mechanism to scale as shown in [Figure 5.19](#). Note that, for this analysis, we need draw only the virtual mechanism.

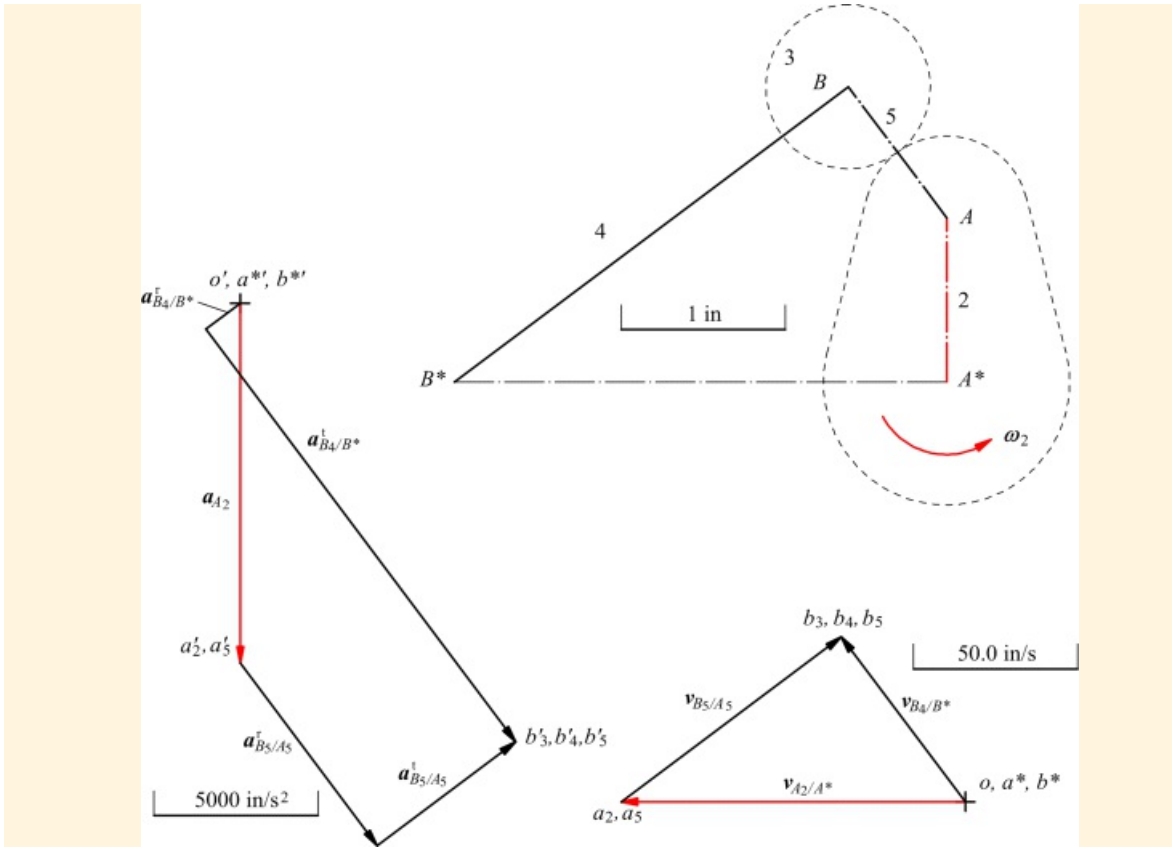


Figure 5.19 The velocity and acceleration polygons for Example 5.3.

2. Compute ω_2 in radians/s.

$$\omega_2 = 1000 \times 2\pi/60 = 104.7 \text{ rad/s}$$

3. Compute and plot $v_{A_2/A^*}, v_{A_2/B^*} = \omega_2 \times r_{A/A^*} = 1(104.7) = 104.7 \text{ in/s}$ normal to AA^*
4. Complete the velocity analysis graphically and measure v_{B_3/B^*} and v_{B_5/B^*} .

$$v_{B_3/B^*} = 62.8 \text{ in/s}; v_{B_5/B^*} = 83.5 \text{ in/s}$$

5. Compute ω_5 and ω_4 and determine their senses.

$$\begin{aligned}\omega_5 &= v_{B_5/A_5}/r_{B/A} = 83.5/1.0 = 83.5 \text{ rad/s CW} \\ \omega_4 &= v_{B_4/A_4}/r_{B/A} = 62.8/3.0 = 20.9 \text{ rad/s CCW}\end{aligned}$$

Notice that ω_5 is the angular velocity of the *virtual* link containing the line AB .

6. Compute and plot $a_{A_2/A^*} = a_{A_2/A^*}^r, a_{A_2/A^*}^t = (\omega_2)^2 r_{A/A^*} = (104.7)^2(1) = 11,000 \text{ in/s}^2$ in the AA^* direction
7. Compute and plot a'_{B_3/B^*} from point o' and a'_{B_5/A_5} from point a_5' .

$$a'_{B_3/B^*} = |\omega_4|^2 r_{B/B^*} = (20.9)^2(3.0) = 1,310 \text{ in/s}^2$$
 in the BB^* direction

$$a'_{B_5/A_5} = |\omega_5|^2 r_{B/A} = (83.5)^2(1.0) = 6,970 \text{ in/s}^2$$
 in the BA direction
8. Draw a line starting from the end of a'_{B_5/A_5} and perpendicular to BA . This line corresponds to a'_{B_5/A_5} .
Draw a second line from the end of a'_{B_3/B^*} and perpendicular to BB^* . This line corresponds to a'_{B_3/B^*} . The

intersection of the two lines will give \dot{x}_3' , \dot{y}_4' , \dot{y}_5 .

9. Measure $\dot{\theta}_{S_4/S^*}$.

$$\dot{\theta}_{S_4/S^*} = 15,700 \text{ rad/s}^2$$

Compute α_4 and determine its sense

$$\alpha_4 = \left| \dot{\theta}_{S_4/S^*} \right| / r_{S_4/S^*} = 15,700 / 3 = 5,230 \text{ rad/s}^2$$

Notice that the reason this relatively simple approach can be used is that we are not interested in the angular acceleration of the roller, link 3. α_3 is definitely not equal to α_5 , the angular acceleration of the line AB , which, for convenience, was called the virtual link 5.



5.7 Cam Contact

The analysis of mechanisms with cam joints can be conducted either directly or through the use of equivalent linkages. We will look at the direct approach first.

5.7.1 Direct Approach to the Analysis of Cam Contact

In the general case of cam contact, there will be both rolling and sliding at the contact point, and this is probably the most typical type of higher-pair contact between two bodies. If we look at two arbitrary bodies (e.g., 2 and 4 in [Figure 5.20](#)) at the contact location B_2 , we know B_2 and B_4 have the same coordinates

$$r_{B_2} = r_{B_4}$$

However

$$\dot{r}_{B_2} \neq \dot{r}_{B_4}$$

and

$$\dot{v}_{B_2/B_4} \neq 0$$

We can obtain some information on \dot{v}_{B_2/B_4} by recognizing that coincident points are involved and

$$\dot{v}_{S_2/S_4} = {}^4\dot{v}_{B_2/B_4} = {}^4\dot{v}_{B_2}$$

Therefore, to analyze the velocity of B_2 relative to B_4 or link 4, it is convenient to represent the velocity in terms of components in the tangential (t) and normal (n) directions relative to the tangent at the contact point as shown in [Figure 5.20](#). Then

$$\dot{v}_{B_2/B_4} = {}^4\dot{v}_{S_2/P_6} = {}^4\dot{v}_{B_2} - {}^4\dot{v}_{B_2}^n = {}^4\dot{v}_{B_2}^t$$

If the two bodies are rigid, there can be no component of velocity in the normal direction or the bodies would either penetrate each other or separate. Therefore, the normal component of the relative velocity must be zero, and the relative velocity direction must be along the common tangent to the two bodies at the point of contact. That is

$${}^4\dot{v}_{B_2}^n = 0$$

and

$$\dot{v}_{B_2/B_4} = {}^4\dot{v}_{S_2}^t = {}^4\dot{v}_{S_2/P_6}^t = \dot{v}_{B_2/P_6}^t$$

We cannot determine anything more about \dot{v}_{B_2/B_4}^t ; however, knowing the direction for the relative velocity usually provides sufficient information to conduct a velocity analysis.

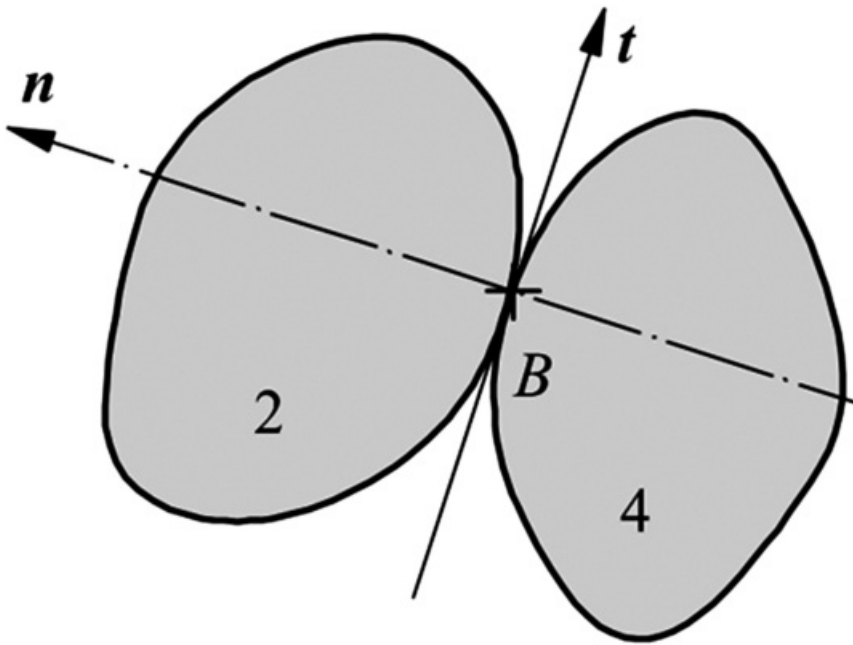


[Figure 5.20](#) Cam contact.

We also cannot determine anything about $\ddot{\omega}_{B_2/B_4}$ directly; however, if we expand $\ddot{\omega}_{B_2/B_4}$ into normal and tangential components, we can compute additional information about it. Then

$$\ddot{\omega}_{B_2/B_4} = \ddot{\omega}_{B_2/B_4}^n + \ddot{\omega}_{B_2/B_4}^t$$

Note that there is no Coriolis term because the acceleration is defined in link 1 and not link 4. This is directly analogous to the case of rolling contact except that now the tangential component is not zero. However, by definition, we know the direction of the tangential component.

Using the same nomenclature as in the case of rolling contact (see [Figure 5.15](#)), the normal component of relative acceleration is given by [Equation 5.36](#) or

$$\ddot{\omega}_{B_2/B_4}^n = \frac{(v_{B_2/O_2})^2}{|r_{B_2/O_2}|} + \frac{(v_{O_2/O_4})^2}{|r_{O_2/O_4}|} + \frac{(v_{O_4/B_4})^2}{|r_{O_4/B_4}|}$$

(2 to O₂) (O₂ to O₄) (O₄ to B)

If one of the cam surfaces is flat, the relative position vector corresponding to the center of curvature will approach infinity, and the corresponding acceleration term will become zero. For example, if the surface for link 2 is flat, then O_2 is at infinity, and the expression for the normal component of acceleration reduces to

$$\ddot{\omega}_{B_2/B_4}^n = \frac{(v_{O_4/B_4})^2}{|r_{O_4/B_4}|}$$

from O_4 to B



Example 5.4

Analysis of Mechanism with a Cam Joint

Find the velocity and acceleration of the cam follower (link 3) given in [Figure 5.21](#) if the cam is rotating at a constant angular velocity of 100 rad/s CCW.

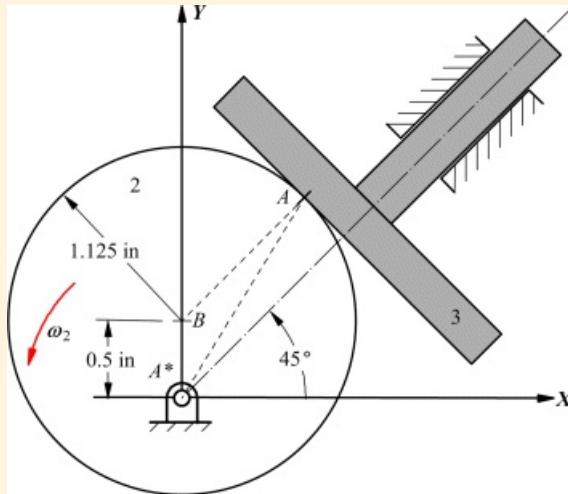


[Figure 5.21](#) Cam and flat-faced follower.

Solution

To analyze the problem, we can determine the velocity and acceleration of any point on link 3 because *all* points on link 3 have the same velocity and the same acceleration. The point to choose is the contact point A_3 . To solve for the velocity and acceleration of A_3 , first find the velocity of point A_2 . Then write the relative velocity expression between points A_2 and A_3 and solve for the velocity of A_3 . The relevant equations are

$$\dot{v}_{A_3} = \dot{v}_{A_2/A^*} = \omega_2 \times r_{A_2/A^*}$$

and

$$\ddot{v}_{A_2} = \ddot{v}_{A_2} - \ddot{v}_{A_2/A_3}$$

Next solve for the velocity of B_2 either directly or by image. This will be needed for the acceleration analysis. The acceleration equations that must be solved are

$$\begin{aligned}\ddot{v}_{A_2} &= \ddot{v}_{A_2/A^*} = \ddot{v}_{A_2/A^*}^r + \ddot{v}_{A_2/A^*}^t \\ \ddot{v}_{A_2} &= \ddot{v}_{A_2} + \ddot{v}_{A_3/A_2} = \ddot{v}_{A_2} + \ddot{v}_{A_3/A_2}^n + \ddot{v}_{A_3/A_2}^t\end{aligned}$$

and

$$\ddot{v}_{A_3/A_2}^n = \ddot{v}_{A_3/C_3}^n + \ddot{v}_{C_3/B_2}^n - \ddot{v}_{B_2/A_2}^n = \frac{(v_{A_3/C_3})^2}{[c_3]} - \frac{(v_{C_3/S_2})^2}{[s_2]} + \frac{(v_{B_2/S_2})^2}{[s_2]} - \frac{(v_{S_2/A_2})^2}{[s_2]}$$

where C_3 is the center of curvature of the cam follower surface and is located at infinity. The steps in solving the equations are given in the following.

Steps

1. Draw the mechanism to scale as shown in [Figure 5.22](#). To do this, draw the cam circle centered at B . Next locate point A^* at 0.5 in below B . Then construct a line through A^* at an angle of 45° . This locates the direction of travel of the flat-faced follower. Finally, draw a line perpendicular to the 45° line and tangent to the cam. This locates points A_2 and A_3 . Measure r_{A/A^*} and $r_{A/B}$

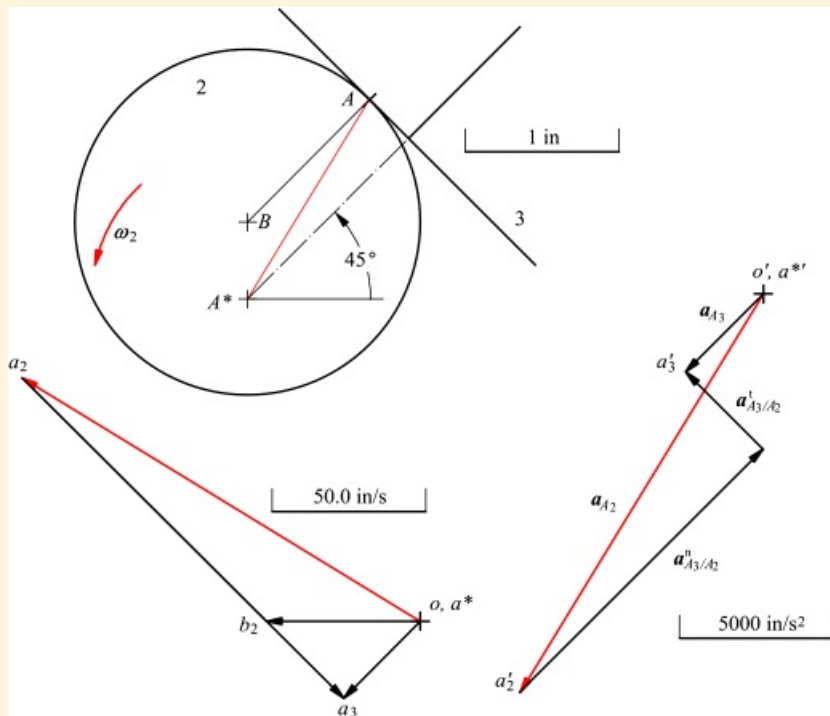


[Figure 5.22](#) Position, velocity, and acceleration polygons for Example 5.4.

$$\begin{aligned} \omega_{A/A^*} &= 1.52 \text{ rad/s} \\ \omega_B/A &= 1.12 \text{ rad/s} \end{aligned}$$

2. Compute $v_{A_2} = \omega_2 \times r_{A/A^*}$ where $v_{A_2} = 100(1.52) = 152 \text{ in/s}$ and it is perpendicular to A^*A in the direction shown in [Figure 5.22](#). Select a velocity scale and locate a_2 .
3. Draw a line from o at an angle of 45° with the horizontal. Point a_3 will be on this line.
4. Draw a line through the tip of a_2 and perpendicular to the line at 45° and also tangent to the cam and follower at the contact point. The intersection of this line with that drawn in step 3 locates a_3 where $v_{A_3} = 35 \text{ in/s}$ in the direction shown.
5. Locate b_2 by image and measure v_{B_2/A_2} where $v_{B_2/A_2} = 112 \text{ in/s}$.
6. Select an acceleration scale and compute and plot $\alpha_{A_2} = \omega_{A_2/A^*}^2$ where $\omega_{A_2/A^*}^2 = -[\omega_2]^2 r_{A/A^*} = (100)^2(1.52) = 15,200 \text{ in/s}^2$ in the AA^* direction.
7. Draw a line from o' at an angle of 45° with the horizontal. Point a'_3 will be on this line.
8. Compute $\alpha_{A_3/A_2}^{A_2}$, determine its direction, and plot the resulting vector through the tip of α_{A_2/A^*}^2 where $\alpha_{A_2/A_3}^{A_2} = \frac{(v_{B_2/A_2})^2}{[r_{B_2/A_2}]} = \frac{(112)^2}{112} = 11,200 \text{ in/s}^2$. The direction is from B to A .

9. Draw a line through the tip of and perpendicular to ω_{A_3/A_4}^* . The intersection of this line with the line drawn in step 7 will be the point a'_3 .

10. Measure ω_{A_3} where $\alpha_{A_3} = 3,580 \text{ in/s}^2$ in the direction shown.

5.7.2 Analysis of Cam Contact Using Equivalent Linkages

Another approach to determining the velocities and accelerations of cam linkages is to use the concept of equivalent linkages. For this we represent the two cam surfaces by their osculating circles and attach a binary link from one center of curvature to the other using revolute joints. As in the case of rolling contact, this technique can be used for velocities and accelerations, but it will not give correct results for higher derivatives. In [Figure 5.23](#), link 6 is a virtual link that usually changes length with each *finite* change in position. (It is constant for differential changes in position, however.)

Link 6 is a virtual link pinned to links 2 and 4 at the centers of curvature corresponding to B

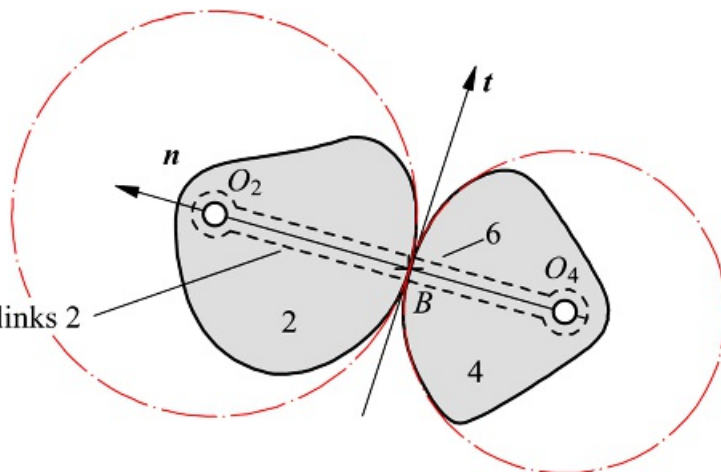


[Figure 5.23](#) Virtual link pinned at the centers of curvature of the two bodies in cam contact.

The use of equivalent linkages simplifies the velocity and acceleration analyses because the equivalent linkages are usually standard four-bar linkages or one of the inversions of the common slider-crank mechanism. For example, a simple three-link cam mechanism becomes a four-bar linkage when replaced by its equivalent linkage as shown in [Figure 5.24](#). In the example in [Figure 5.24](#), the kinematic information for link 4 (virtual link) can be computed; however, this is usually of no interest. It is important to remember that the equivalent linkage is valid for one position only. The length of the virtual link usually changes with each position of interest.

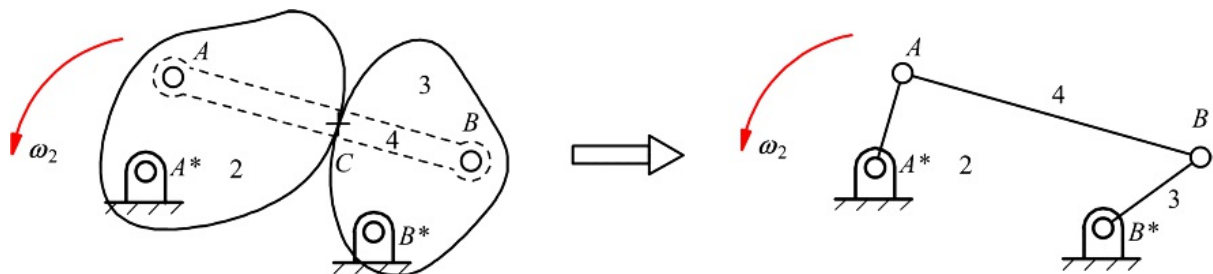


[Figure 5.24](#) Equivalent linkage for cam mechanism with curved cam surfaces and revolute joints between the cams and the frame.

If one of the surfaces is flat, the virtual link becomes infinitely long, and the movement of the virtual link can be represented by a slider. An example of this is shown in [Figure 5.25](#). The slider need not “slide” directly on the face of the flat cam surface through B. The only restriction is that it slide on a line that is parallel to the cam face.

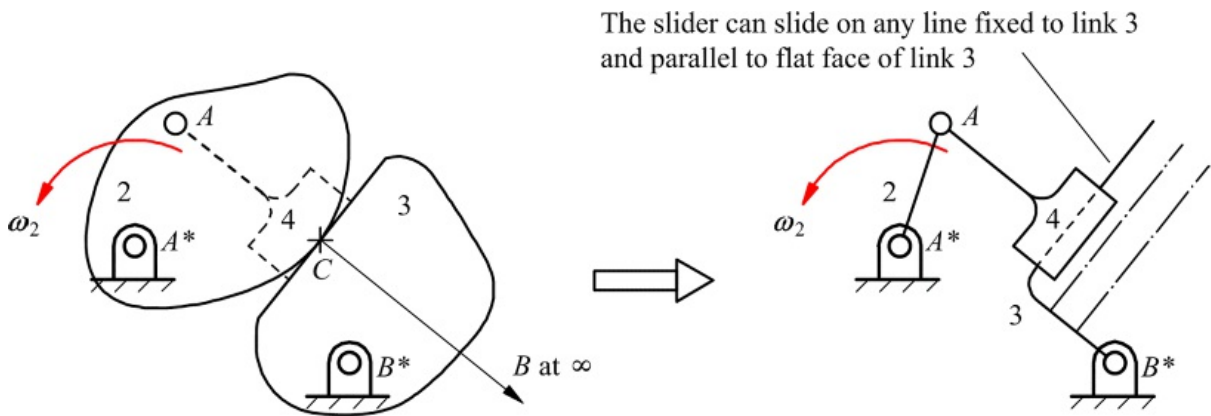


Figure 5.25 Equivalent linkage for cam mechanism with one flat-faced cam and revolute joints between the cams and the frame. The slider can slide on any line that is parallel to the cam face and fixed to link 3.

The equivalent linkage is analyzed as any other linkage with pin and slider joints would be. The kinematic properties computed for links 2 and 3 will be the same for both the equivalent linkage and the actual linkage. The equivalent linkages for the other two types of three-bar cam linkages are given in [Figure 5.26](#).

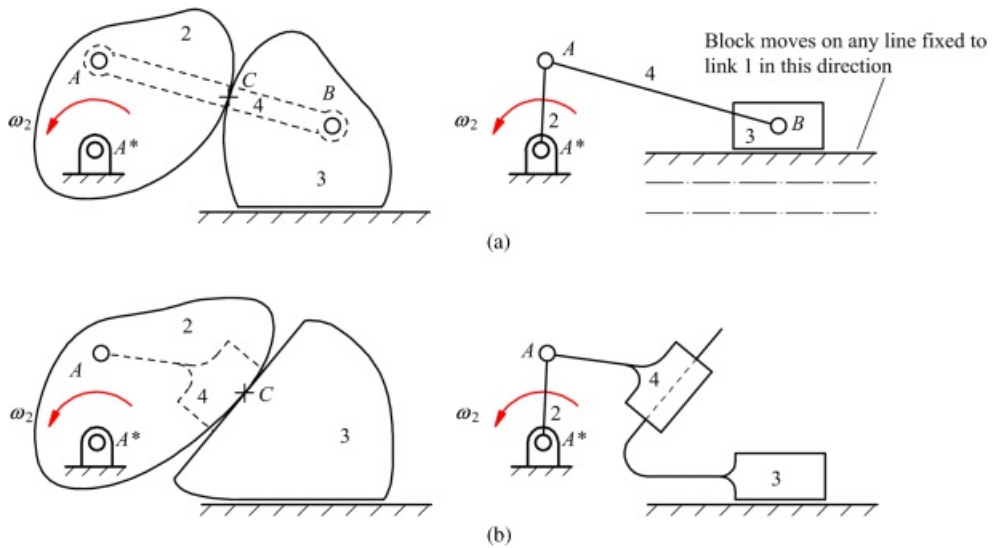


Figure 5.26 Equivalent linkage for cam mechanism. (a) Sliding joint between link 3 and frame. (b) Sliding between links 2 and 3 and between link 3 and frame.



Example 5.5

Mechanism Analysis Using an Equivalent Linkage

Use equivalent linkages to compute the velocity and acceleration of the cam follower (link 3) in [Figure 5.21](#) if the cam is rotating at a constant angular velocity of 100 rad/s CCW.

Solution

The mechanism in [Figure 5.21](#) is of the type represented in [Figure 5.26\(b\)](#). Therefore, link 3, the follower, will have a sliding joint with the frame and with the virtual link (link 4). The resulting equivalent linkage is shown in [Figure 5.27](#). Notice that the location of the line on which link 4 must slide relative to link 3 is arbitrary as long as the line is fixed to link 3 and is parallel to the face of link 3. Therefore, the line that passes through B is chosen for simplicity. Similarly, the location of the line on which link 3 slides relative to the frame is arbitrary as long as the line is inclined at an angle of 45° .

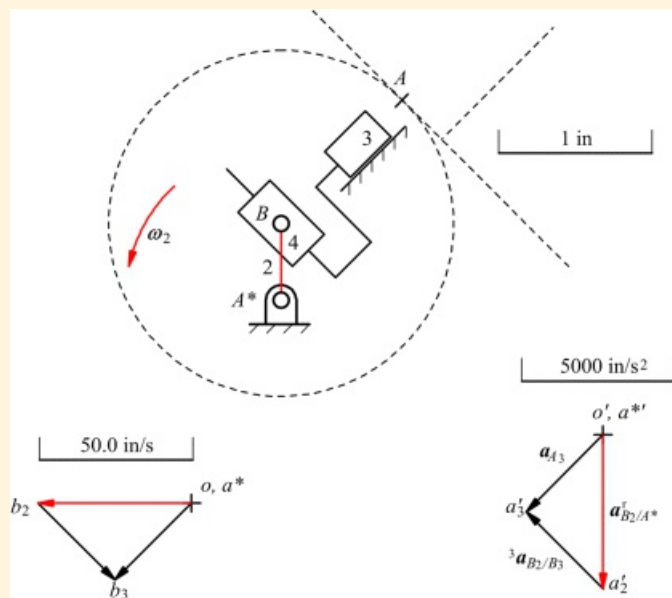


[Figure 5.27](#) Position, velocity, and acceleration polygons for Example 5.5.

For the equivalent linkage, we need only find the velocity and acceleration of point B_2 . The velocity and acceleration of B_3 can then be found using the procedure given in Section 5.5. The velocity equations that must be solved are

$$v_{B_3} = v_{B_2}/A^* = \omega_2 \times v_{B_3}/A^*$$

and

$$v_{B_2} = v_{B_3} + v_{B_3}/S_2 \quad (5.37)$$

Here we have written the velocity equation in terms of the velocity of B_2 relative to B_3 rather than vice versa because we can easily identify the direction of the velocity of B_2 relative to link 3. We also know the direction for the velocity and acceleration of B_3 . The acceleration equations that must be solved are

$$\begin{aligned}\omega_{B_2} &= \omega_{B_2/A^*} = \dot{\omega}_{B_2/A^*} + \omega_{B_2/A^*}^r \\ \alpha_{B_2} &= \alpha_{B_2} + \alpha_{B_2/B_3} = \alpha_{B_2} + \dot{\omega}_{B_2/B_3}^r + {}^3\alpha_{B_2/B_3}\end{aligned}$$

and

$$\omega_{B_2/B_3}^r = 2\omega_3 \times v_{B_2/B_3} = 0$$

The Coriolis term is a function of velocities only and can be computed as soon as the velocity analysis is completed; however, links 3 and 4 simply translate, making $\omega_{B_3} = 0$. Therefore, the acceleration expression becomes

$$\alpha_{B_2} = \alpha_{B_3} + {}^3\alpha_{B_2/B_3}$$

By geometry, ${}^3\alpha_{B_2/B_3}$ must move in the direction parallel to the face of the cam follower. Therefore, the equation has only two unknowns (once α_{B_3} is computed), and the equation can be solved for α_{B_3} and ${}^3\alpha_{B_2/B_3}$.

Steps

1. Draw the mechanism to scale using the procedure given in Example 5.4. Then draw the equivalent mechanism.
2. Pick a velocity scale and compute $v_{B_2} = \omega_2 \times r_{B_2/A^*}$ where $v_{B_2} = 100(0.5) = 50 \text{ in/s}$ and it is perpendicular to AB and points in the direction shown in [Figure 5.27](#). This will locate b_2 .
3. Draw a line from o at an angle of 45° with the horizontal. Point b_3 will be on this line.
4. Draw a line through the tip of b_2 and perpendicular to the line at 45° . This is the direction of v_{B_2/B_3} . The intersection of this line with that drawn in step 3 locates b_3 . $v_{B_2} = 35 \text{ in/s}$ in the direction shown
5. Choose an acceleration scale and compute and plot $\alpha_{B_2} = \alpha_{B_2/A^*}$
 $\alpha_{B_2/A^*} = -|\omega_2|^2 r_{B_2/A^*} = (100)^2(0.5) = 5000 \text{ in/s}^2$ in the BA^* direction
6. Draw a line from o' at an angle of 45° with the horizontal. This is the direction for α_{B_3} and point b'_3 will be on this line.
7. Draw a line through the tip of α_{B_2/A^*} and parallel to the face of the cam follower (link 3). This is the direction of ${}^3\alpha_{B_2/B_3}$. The intersection of this line with the line drawn in step 7 will be the point b'_3 .
8. Measure $\alpha_{B_3} = 3540 \text{ in/s}^2$ in the direction shown

This is the acceleration of link 3. Note that this is essentially the same value as obtained in Example 5.4. All points in link 3 have the same velocity and the same acceleration. Therefore, points B_3 and C_3 have the same velocity and the same acceleration. Also note that considerably less work is required to obtain the final result when equivalent linkages are used, and the final solution is likely to be more accurate because the constructions are simpler.

When equivalent linkages are used, no information is used about the relative motion at the contact points. If the relative motion between the coincident points at contact are of interest, these can be computed directly after the basic analysis is completed. This relative velocity would be of interest for lubrication considerations.



Example 5.6

Analysis of Sliding Velocity in a Cam Mechanism

Find the sliding velocity at the point of contact for the mechanism in Example 5.5.

Solution

The sliding velocity at the point of contact is the relative velocity between points A_2 and A_3 . This velocity can be computed from

$$v_{A_3/A_2} = v_{A_3} - v_{A_2} \quad (5.38)$$

Because $v_{A_3} = v_S$, we need only solve for v_{A_2} to determine v_{A_3/A_2} in [Equation 5.38](#). From Example 5.4, $v_{A_2} = \omega_2 \times r_{A/A^*}$ and it is perpendicular to AA^* as shown in [Figure 5.22](#). The velocity v_{A_2} is also shown in [Figure 5.22](#). The vector v_{A_3/A_2} is shown in [Figure 5.28](#). Measurement of the vector gives $v_{A_3/A_2} = 148 \text{ in/s}$, and the direction is shown in the figure.

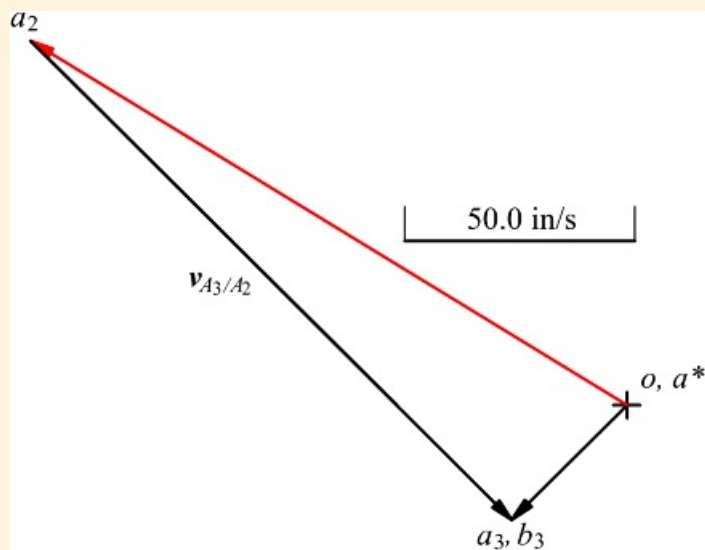


[Figure 5.28](#) Calculation of the relative velocity v_{A_3/A_2} .



5.8 General Coincident Points

In mechanisms, pin-in-slot joints are common, and occasionally the slots will be curved paths. Also, occasionally, sliders will be used on circular paths that rotate. Mechanisms employing these types of joints can be analyzed using general coincident points. Actually, we can use any coincident points to help in a kinematic analysis if we can recognize the path that one of the points traces on the other link, and the path does not even need to be a machined path. To recognize the path, we must usually pretend to “stand” in one link and watch the coincident point on the other link move.

For the analysis, we need the center of curvature of the path and the corresponding tangent to the path for the position of interest. The tangent is normal to the line from the coincident points to the center of curvature of the path. For illustration, assume that the two bodies in question are links 3 and 7, and the coincident points are located at P as shown in [Figure 5.29](#). Then for the arbitrary coincident points

$$\dot{v}_{P_3/P_7} = {}^7\dot{v}_{P_3/P_7} = -\dot{v}_{P_7/P_3} = -{}^3\dot{v}_{P_7/P_3}$$

Two paths will be traced, and these can be designated as path \bar{P}_3/\bar{P}_7 and path \bar{P}_7/\bar{P}_3 . The paths will share a common tangent vector at the coincident points, and the normal to the paths will contain the two coincident points and the two centers of curvature as shown in [Figure 5.29](#). The path that P_3 traces on link 7 (\bar{P}_3/\bar{P}_7) will be fixed to link 7, and the path \bar{P}_7/\bar{P}_3 that P_7 traces on link 3 will be fixed to link 3.

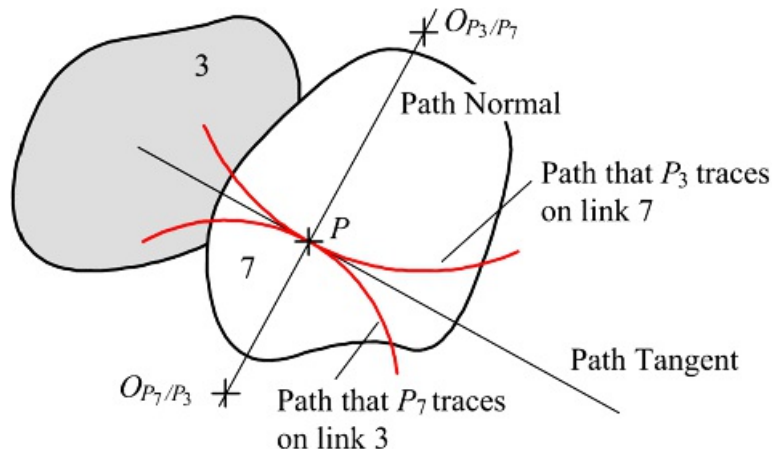


[Figure 5.29](#) Geometric properties of relative paths traced by coincident points.

To solve problems involving general coincident points, we must be able to recognize one of the relative paths by inspection. This means that we must be able to determine the center of curvature of the path. Sometimes, we can recognize one of the relative paths but not the other. This is still useful because of the relationships

$$\dot{v}_{P_7/P_3} = -{}^7\dot{v}_{P_3/P_7}$$

and

$$\dot{v}_{P_3/P_7} = -{}^3\dot{v}_{P_7/P_3}$$

This means that if we can recognize one of the paths, we can always rewrite the kinematic equations so that the information will appear in the correct form. Some examples of paths that are obvious are given in [Figure 5.30](#).

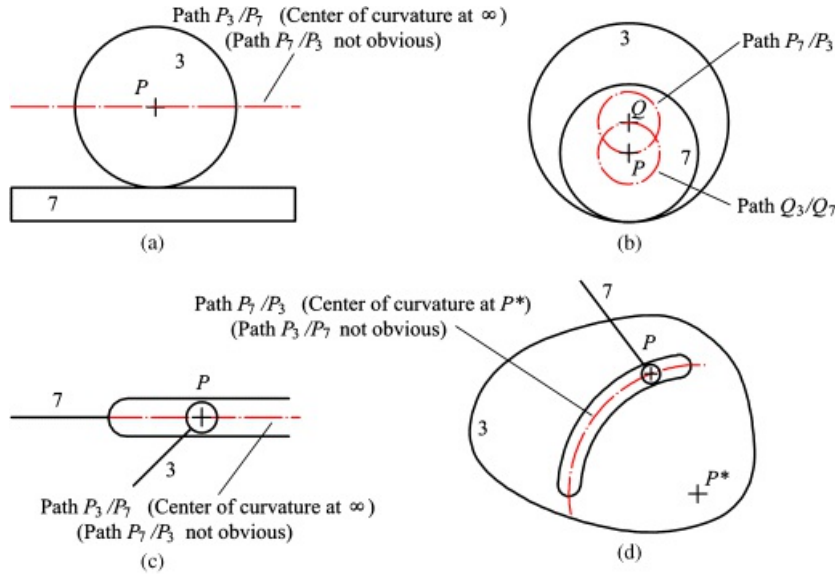


[Figure 5.30](#) Obvious relative paths of general coincident points.

5.8.1 Velocity Analyses Involving General Coincident Points

The velocity analysis of mechanisms that involve general coincident points require that the direction for the relative velocity vector (\dot{v}_{P_3/P_7} or \dot{v}_{P_7/P_3}) be known. This direction can be determined by using the same technique as was used in the analyses for cam pairs. For this, we replace the path P_3/P_7 by its osculating circle at P . Recall that we can do this without compromising the accuracy of the solution as long as we are interested in only velocities and accelerations. Next connect P_3 to the center of curvature O of the path P_3/P_7 by a virtual link x and revolute joints. The geometry is represented schematically in [Figure 5.31](#).

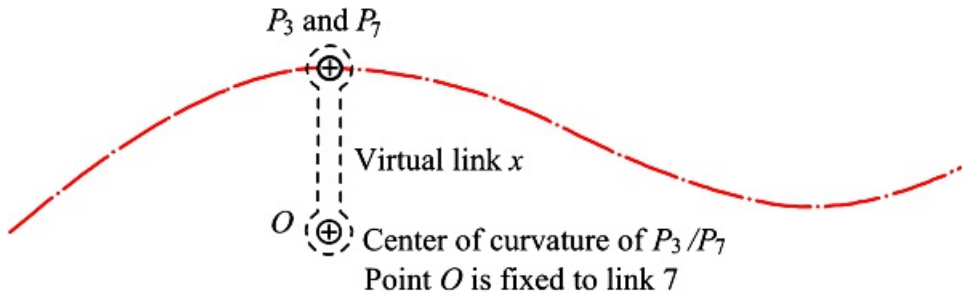


[Figure 5.31](#) Connecting virtual link from point P_3 to center of curvature of path that P_3 traces on link 7.

The motion of P_3 relative to link 7 will be the same as for P_x relative to link 7 if P_3 and P_x are considered to be pinned together. The relative velocity between P_3 and P_7 can then be written as

$$\dot{v}_{P_3/P_7} = \dot{v}_{P_3/P_7} = \dot{v}_{P_3/P_x} + \dot{v}_{P_x/C_x} + \dot{v}_{C_x/C_7} + \dot{v}_{C_7/P_7} \quad (5.39)$$

Because points P_3 and P_x and O_x and O_7 are considered to be pinned together, and the last term involves the motion of two points in system 7 as observed from system 7

$$\dot{v}_{P_3/P_7} = \dot{v}_{P_3/P_7} = \dot{v}_{P_x/C_x} \quad (5.40)$$

Because two points on the same rigid link are involved, the term on the right-hand side of [Equation 5.40](#) can be written as

$$\vec{v}_{P_3/P_7} = \vec{v}_{P_3/P_x} = \vec{v}_{P_3/O_x} = \vec{\omega}_x \times \vec{r}_{P/O} \quad (5.41)$$

This vector is perpendicular to the line from the point P to the center of curvature of the path P_3/P_7 , and it is therefore along the direction of the tangent to the path. Thus, when the direction for the relative velocity is required, we need only determine the center of curvature of the path P_3/P_7 and draw a line perpendicular to it.

Based on [Equation 5.41](#), the magnitude of the angular velocity term can be written as

$$|\vec{\omega}_x| = \frac{|\vec{v}_{P_3/P_7}|}{|\vec{r}_{P/O}|} \quad (5.42)$$

We are not interested in $\vec{\omega}_x$ directly, but we will use [Equation 5.42](#) in the acceleration analysis.

5.8.2 Acceleration Analyses Involving General Coincident Points

The acceleration analysis is slightly more complex than the velocity analysis when general coincident points are involved. For the relative acceleration, again assume that the path that P_3 traces on link 7 is known. This means that the center of curvature of the path is also known. The development of the relative acceleration expression is similar to that used for the case of a rotating slider and can be written as

$$\vec{a}_{P_3/P_7} = \vec{a}_{P_3/P_7} + 2\vec{\omega}_7 \times \vec{v}_{P_3/P_7} + \vec{\omega}_7 \times (\vec{\omega}_7 \times \vec{r}_{P_3/P_7}) + \vec{\omega}_7 \times \vec{r}_{P_3/P_7}$$

Because $\vec{r}_{P_3/P_7} = \vec{0}$ at the moment considered

$$\vec{a}_{P_3/P_7} = \vec{a}_{P_3/P_7} + 2\vec{\omega}_7 \times \vec{v}_{P_3/P_7} \quad (5.43)$$

The second term in the expression is the Coriolis term and is a function of position and velocity only. Therefore, it can be computed as soon as the velocity analysis is completed. The direction of the Coriolis term is given by the cross-product. Graphically, we can get the direction by rotating \vec{v}_{P_3/P_7} (which equals \vec{v}_{P_3/P_x}) 90° in the direction of $\vec{\omega}_7$.

The first term in [Equation 5.43](#) is simply the acceleration of P_3 as observed from system 7. This term can be written as

$$\vec{a}_{P_3/P_7} = \vec{a}_{P_3/\text{any point in system 7}} = \vec{a}_{P_3} \quad (5.44)$$

Unlike the case of the rotating slider, the direction for this acceleration component is not immediately obvious. However, by using the technique begun in the velocity analysis, we can determine a vector expression for this component that involves only one unknown.

To begin, replace the path P_3/P_7 by its osculating circle at P and rewrite the acceleration expression in [Equation 5.44](#) in terms of the virtual link x and the center of curvature of the path of P_3/P_7 . This is similar to what was done with velocities in [Equation 5.39](#). The relative acceleration between P_3 and P_7 can then be written as

$$\vec{a}_{P_3} = \vec{a}_{P_3/P_7} = \vec{a}_{P_3/P_x} + \vec{a}_{P_x/O_x} + \vec{a}_{O_x/O_7} + \vec{a}_{O_7/P_7}$$

Because points P_3 and P_x and O_x and O_7 are pinned together, and the last term involves the motion of two points

in system 7 as observed from system 7,

$${}^7\omega_{P_3} = {}^7\omega_{P_3/P_7} = {}^7\omega_{P_3/G_z} \quad (5.45)$$

Because two points on the same rigid link are involved, the term on the right-hand side of [Equation 5.45](#) can be written as

$${}^7\omega_{P_3/G_z} = {}^7\omega_{P_3/O_z} + {}^7\omega_{P_3/G_z}^n$$

The radial component is a function of velocities and position only and can be written with the aid of [Equations 5.40](#) and [5.42](#) as

$${}^7\omega_{P_3/G_z}^r = {}^7\omega_{G_z} \times {}^7v_{P/G} = \frac{|{}^7v_{P_3/G_z}|^2}{|r_{P/G}|} = \frac{|{}^7v_{P_3/P_7}|^2}{|r_{P/G}|} \text{ (from } P \text{ to } O\text{)}$$

The magnitude of the vector ${}^7\omega_{P_3/G_z}^t$ cannot be computed directly; however, we know that the direction is perpendicular to the line from the point P to the center of curvature of the path P_3/P_7 , and it is therefore along the direction of the tangent to the path. The total acceleration can now be represented as

$$a_{P_3/P_7} = {}^7\omega_{P_3/G_z}^r + {}^7\omega_{P_3/G_z}^t + 2\omega_7 \times {}^7v_{P_3/P_7}$$

or, in terms of the original subscripts

$$a_{P_3/P_7} = {}^7\omega_{P_3/P_7}^n + {}^7\omega_{P_3/P_7}^t + 2\omega_7 \times {}^7v_{P_3/P_7}$$

Here, we have rewritten ${}^7\omega_{P_3/P_7}^t$ as ${}^7\omega_{P_3/P_7}^n$ to emphasize that it is *normal* to the path P_3/P_7 . Of the three vectors on the right-hand side of the equation, only the magnitude of ${}^7\omega_{P_3/P_7}^t$ will be unknown after the velocity analysis. The directions for the individual terms are summarized in [Figure 5.32](#). Note that the normal and Coriolis terms are both perpendicular to the tangent of the path of P_3/P_7 ; however, only the normal component always points from P to the center of curvature of the path of P_3/P_7 . The direction of the Coriolis term will depend on the directions of both ω_7 and ${}^7v_{P_3/P_7}$.

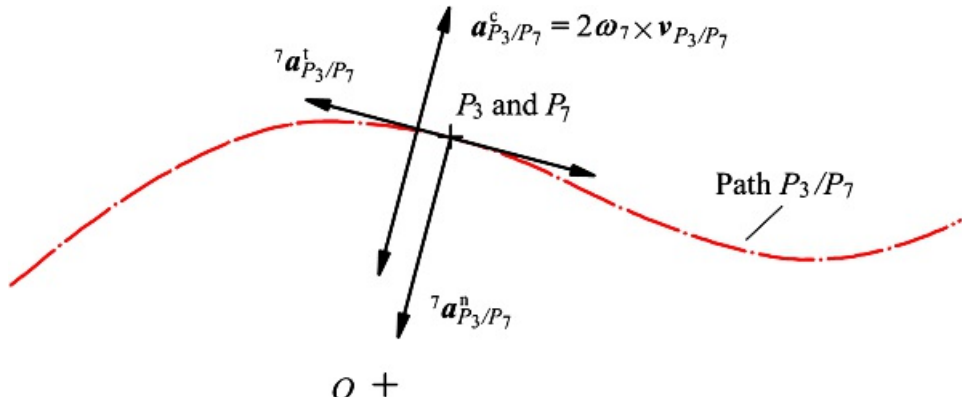


[Figure 5.32](#) Acceleration components associated with the relative acceleration between P_3 and P_7 .



Example 5.7

Analysis of Mechanism with Pin-in-Slot Joint

In the mechanism shown in the [Figure 5.33](#), point A_2 moves on a curved slot in link 3. The radius of the slot is 3 m. Points B^* , A , and C are collinear, and the other distances between points are as given in [Figure 5.33](#). Link 2 rotates with an angular velocity of 2 rad/s CCW and an angular acceleration of 3 rad/s² CCW. For the position shown, find:

1. ω_3 , a_3 , v_{C_3} , α_{C_3}
2. The center of curvature of the path that A_3 traces on link 2

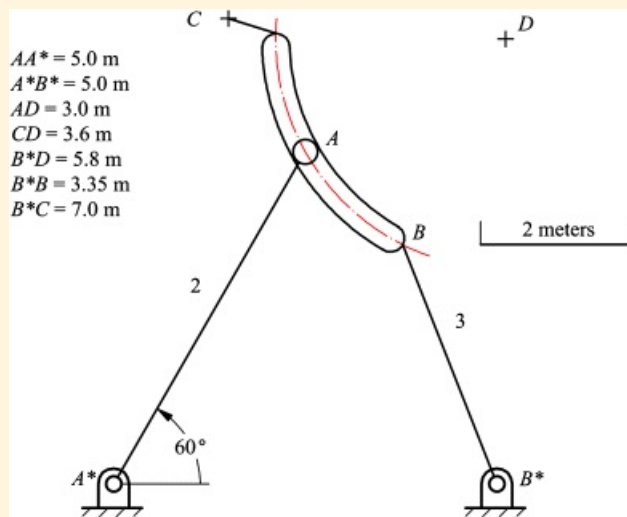


[Figure 5.33](#) Mechanism for Example 5.7.

Solution

For the velocity analysis, we first compute the velocity of point A_2 . That is

$$v_{A_2} = v_{A_2/A^*} = \omega_2 \times r_{A_2/A^*}$$

Next go to point A_3 on link 3

$$v_{A_2} = v_{A_2/B^*} = \omega_3 \times r_{A_2/B^*} + \dot{r}_{A_2/B^*}$$

Because ω_3 is unknown, this term cannot be computed without another equation. Consider the two coincident points A_2 and A_3 . Then

$$v_{A_2} = v_{A_2} = v_{A_2/A_3} \quad (5.46)$$

This equation is technically correct; however, we cannot recognize directly the path that A_3 traces on link 2, and the equation cannot be differentiated to help us in the acceleration analysis. Therefore, write the equation in terms of v_{A_2} . Then

$$\vec{v}_{A_3} = \vec{v}_{A_3} + \vec{v}_{A_2/A_3}$$

This equation is useful because we can recognize the path that A_2 traces on link 3 by inspection. This equation can be solved, although there are two unknown directions on the right hand side of the equation. This is handled by beginning one vector at the velocity pole and ending the other vector at the end of \vec{v}_{A_2} .

After the velocity polygon is drawn, we can measure \vec{v}_{A_3} and determine \vec{v}_{C_3} by image. We can also measure \vec{v}_{A_2/A_3} , which will be required for the acceleration analysis.

The velocity analysis uses two basic equations

$$\vec{v}_{A_2} = \vec{v}_{A_3/A^*}$$

and

$$\vec{v}_{A_3} = \vec{v}_{A_3/A^*} + \vec{v}_{A_2/A_3}$$

and these two equations show the solution path for the accelerations. Again start at A_2 . Then

$$\ddot{\omega}_{A_2} = \ddot{\omega}_{A_2/A^*} = \ddot{\omega}_{A_2/A^*} + \ddot{\omega}_{A_2/A_3}^t = \ddot{\omega}_3 \times \vec{v}_{A_2/A^*} + \ddot{\omega}_3 \times \vec{v}_{A_2/A_3}$$

Now differentiate the velocity expression involving A_3 .

$$\begin{aligned} \ddot{\omega}_{A_2} &= \ddot{\omega}_{A_2/S^*} + \ddot{\omega}_{A_2/A_3} = \ddot{\omega}_{A_3/S^*} - \ddot{\omega}_{A_2/S^*} + {}^3\ddot{\omega}_{A_2/A_3}^n - {}^3\ddot{\omega}_{A_2/A_3}^t - 2\ddot{\omega}_3 \times \vec{v}_{A_2/A_3} \\ &= \ddot{\omega}_3 \times \vec{v}_{A_3/S^*} + \ddot{\omega}_3 \times \vec{v}_{A/S^*} + {}^3\ddot{\omega}_{A_2/A_3}^n + {}^3\ddot{\omega}_{A_2/A_3}^t + 2\ddot{\omega}_3 \times \vec{v}_{A_2/A_3} \end{aligned} \quad (5.47)$$

This equation has only two unknowns and can be solved. We can compute the acceleration of C_3 using the acceleration image.

To find the center of curvature of the path that A_3 traces on link 2, we must find an expression that involves the radius of curvature of the path. This term is ${}^3\ddot{\omega}_{A_3/A_2}^n$ and it can be evaluated from the following

$$\ddot{\omega}_{A_2/A_3} = -\ddot{\omega}_{A_3/A_2}$$

therefore

$$\ddot{\omega}_{A_2/A_3}^n = -\ddot{\omega}_{A_3/A_2}^t$$

and

$$\ddot{\omega}_{A_2/A_3}^n = -\ddot{\omega}_{A_3/A_2}^t$$

Based on the terms normal to the path tangent

$${}^3\omega_{A_3/A_2}^n + 2\omega_3 \times v_{A_2/A_3} = -{}^2\omega_{A_3/A_2}^n - 2\omega_2 \times v_{A_3/A_2}$$

and

$${}^2\omega_{A_3/A_2}^n = \frac{|v_{A_3/A_2}|^2}{|r_{A/E}|}$$

or

$$|r_{A/E}| = \frac{|v_{A_3/A_2}|^2}{|{}^2\omega_{A_3/A_2}^n|}$$

where E gives the location of the center of curvature of the path that A_3 traces on link 2. The location of E on the proper side of A is found by the direction of ${}^2\omega_{A_3/A_2}^n$ because it points from A to the center of curvature of the path.

Steps

1. Select a scale and draw link 2 corresponding to a scaled distance of 5 m at an angle of 60° to the horizontal. This will locate point A as shown in [Figure 5.34](#). Draw an arc of radius AD centered at A . Then draw a second arc centered at B^* of length B^*D . The intersection of this arc with the first will locate point D . Next draw an arc centered at D and of radius AD . Draw a line of length B^*C from point B^* through point A . Also draw an arc centered at B^* and of radius B^*B . The intersection of this arc with that centered at D will locate B .

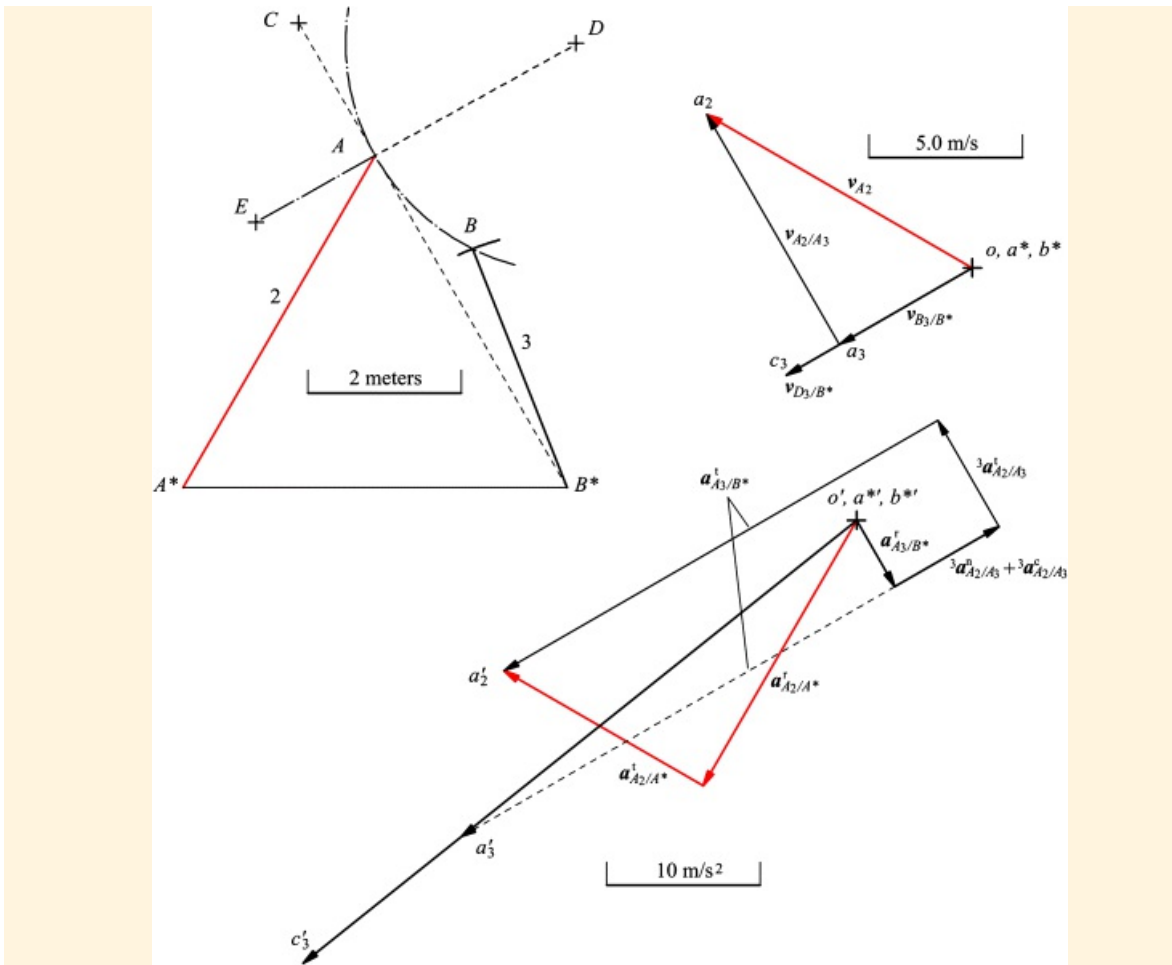


Figure 5.34 Solution to Example 5.7.

2. Select a velocity scale, compute $v_{A_3} = v_{A_2/A^*} = \omega_2 \times r_{A_2/A^*}$, and draw the vector from o in the direction $\overrightarrow{AA^*}$. The sense of v_{A_2} is determined by the rotation of r_{A_2/A^*} 90° in the direction of ω_2 . This will locate a_2 .

$$v_{A_2/A^*} = \omega_2 \times r_{A_2/A^*} = (2)(5) = 10 \text{ m/s}$$

3. Draw a line through o in the direction perpendicular to AB^* .
4. Draw a line through a_2 in the direction tangent to the path that A_2 traces on link 3 (perpendicular to the radius AD). The intersection of this line with that drawn in step 3 will locate point a_3 . Locate the arrowheads on the velocity polygon to conform with [Equation 5.46](#).
5. Locate point c_3 by image $dc_3 = \frac{r_{C_3}}{r_{A_2}} da_3 = 7.0 \text{ m/s}$ at an angle of 210° to the horizontal.
6. Measure $v_{A_3/B^*} = 8.7 \text{ m/s}$ at an angle of 120° to the horizontal.
7. Measure $v_{A_3/B^*} = 5.0 \text{ m/s}$ at an angle of 210° to the horizontal and compute ω_3 . Get the sense of ω_3 by rotating r_{A_3/B^*} 90° in the direction of v_{A_3/B^*} .

$$\omega_3 = \frac{|v_{A_3/B^*}|}{|r_{A_3/B^*}|} = \frac{5}{\frac{3}{5}} = 1 \text{ rad/s CCW}$$

8. Select the acceleration scale, and solve [Equation 5.47](#). First compute α_{A_2/A^*}^t and α_{A_2/A^*}^c . Starting from o' ,

draw the resulting vectors after scaling.

$$\ddot{v}_{A_2/A^*} = \omega_2 \times v_{A_2/A^*} = (2)(10) = 20 \text{ m/s}^2 \text{ opposite } r_{A/A^*}$$

$\ddot{v}_{A_2/A^*} = \omega_2 \times v_{A_2/A^*} = (3)(5) = 15 \text{ m/s}^2$ perpendicular to r_{A_2/A^*} in the direction given by rotating v_{A/A^*} through 90° in the direction of ω_2 . This vector is added to \ddot{v}_{A_2/A^*} as shown in [Figure 5.34](#). This locates \ddot{v}_{A_2/A_3} .

- Compute \ddot{v}_{A_3/B^*} , $\ddot{\omega}_{A_2/A_3}^N$ and \ddot{a}_{A_2/A_3}^C . All of these accelerations are functions of the velocity and position data.

$$\ddot{v}_{A_3/B^*} = \omega_3 \times v_{A_3/B^*} = 1(5) = 5 \text{ m/s}^2 \text{ opposite } r_{A_3/B^*}$$

$$\ddot{\omega}_{A_2/A_3}^N = \frac{|v_{A_2/A_3}|^2}{r_{A_2/B}} = \frac{(8.7)^2}{3} = 23.2 \text{ m/s}^2 \text{ opposite } r_{A_2/B}$$

$$\ddot{v}_{A_2/A_3}^N = 2\omega_3 \times v_{A_2/A_3} = 2(1)(8.7) = 17.4 \text{ m/s}^2 \text{ from D to A}$$

- Note that $\ddot{\omega}_{A_2/A_3}^N$ and \ddot{a}_{A_2/A_3}^C have opposite directions. Therefore, determine the resultant before plotting.

$$\ddot{\omega}_{A_2/A_3}^N + \ddot{a}_{A_2/A_3}^C = 23.2 - 17.4 = 7.83 \text{ m/s}^2 \text{ from A to B}$$

- Starting from o', add the vectors \ddot{v}_{A_3/B^*} and $\ddot{\omega}_{A_2/A_3}^N + \ddot{a}_{A_2/A_3}^C$ as shown in [Figure 5.34](#).
- Draw a line through the tip of $\ddot{\omega}_{A_2/A_3}^N + \ddot{a}_{A_2/A_3}^C$ in the direction perpendicular to $\ddot{\omega}_{A_2/A_3}^N + \ddot{a}_{A_2/A_3}^C$ and to DA (i.e. tangent to the path that A_2 traces on link 3).
- Draw a line through the tip of \ddot{v}_{A_2/A_3}^N in the direction perpendicular to AB^* . The intersection of this line with that from step 12 will give $\ddot{\omega}_{A_2/A_3}^A$ and \ddot{v}_{A_2/A_3}^A . The locations of the arrowheads (directions) are given by [Equation 5.47](#).
- Measure \ddot{v}_{A_2/A_3}^A and compute the magnitude of the angular acceleration, $\ddot{\omega}_3$.

$$\ddot{\omega}_3 = \frac{|\ddot{v}_{A_2/A_3}^A|}{r_{A_2/B}} = \frac{23.2}{5} = 11.2 \text{ rad/s}^2$$
. The sense is given by \ddot{v}_{A_2/A_3}^A and $v_{A_2/B}$. Namely, we rotate $v_{A_2/B}$ 90° in the direction of $\ddot{\omega}_3$ to get the direction of \ddot{v}_{A_2/A_3}^A . The direction is CCW.
- Locate the acceleration of C_3 by acceleration image. To do this, determine the absolute acceleration of A_3 . This is done by adding \ddot{v}_{A_2/A_3}^A to \ddot{v}_{A_2/A_3}^N to locate \ddot{a}'_3 as shown in [Figure 5.34](#). Then find a'_3 using $a'_3 = \ddot{v}_{A_2/A_3}^A \cdot \ddot{a}'_3 = 46.2 \text{ m/s}^2$ in the direction shown in [Figure 5.34](#)
- Compute $\ddot{\omega}_{A_3/B^*} = -(3\ddot{\omega}_{A_2/A_3}^A + 2\omega_3 \times v_{A_2/A_3} + 2\omega_3 \times v_{A_3/A_2})$. Arbitrarily select the direction AD as positive. Then,

$$\ddot{\omega}_{A_3/B^*} = -(23.2 - 17.4 + 34.3) = -42.6 \text{ m/s}^2$$

The minus sign means that the direction of the center of curvature of the path is opposite AD or in the

DA direction.

17. Compute the radius of curvature by locating E_2 using

$$r_{A/E} = \left| \frac{y_{A_3/A_2}}{\gamma_{\phi_{A_3/A_2}}^n} \right|^2 = \frac{(3.7)^2}{42.6} = 1.78 \text{ m}$$

The center of curvature is shown in [Figure 5.34](#).



5.9 Solution by Geometric Constraint Programming

As introduced in [Chapter 4](#), Geometric Constraint Programming (GCP) can be used to solve any of the linkage analyses in this chapter with high accuracy. If only one position is of interest, GCP can be used to analyze the mechanism with similar accuracy to that achieved by a digital computer program. In addition, a graphical program can be developed for velocities in a straightforward manner if the magnitude of the input vector is constant. Then, once the constructions for one problem for a given mechanism are developed, additional problems for the same type of mechanism can be solved with very little effort by simply changing dimensions.

The development of a simple graphical program for velocities is dependent on having the input velocity be constant in magnitude. The direction can change as long as the direction is directly dependent on the position of the linkage. There are two situations that complicate the use of GCP for developing a graphical program for velocity analyses. The first is when the input link is accelerating. In this case, the input velocity will change with both time and position. Most parametric-design programs do not have equation constraints that easily accommodate variations in time. Therefore, when the input link is accelerating, the use of GCP is generally restricted to analyzing individual positions where the magnitude of the input velocity is computed externally to the program. The second situation that complicates the development of a graphical program is when the *magnitude* of the input velocity vector varies with position. This typically occurs when ω is constant in the expression $v = \omega \times r$ for the input velocity, but r is not. In such cases, it is possible to use the graphical construction in Section 2B.3 of Appendix 2B of [Chapter 2](#) to determine v , but it is tedious and will involve scaling that must be factored into the scale factor for the final velocity polygon. Therefore, if the magnitude of the input velocity varies for either reason, it is generally preferable to use GCP to analyze the linkage for each single position rather than to develop a graphical program for all positions.

For a given position, both the position diagrams and velocity polygons will be drawn to scale, and the relative dimensions will be maintained when the scales are changed. Therefore, for velocities, the actual dimensions are not important until numerical answers are desired. The proper velocity magnitudes can then be determined by using the lengths of the line segments in the polygons and the scaling factors. For a given position, the same polygon can be used for any velocity value for the input link simply by changing the scaling factor.

For an acceleration analysis, both the radial and Coriolis components of acceleration will be nonlinear functions of the velocities and link positions. While the graphical constructions in Appendix 2B of [Chapter 2](#) can be used to construct lines corresponding to the proper values, they can result in figures that are much larger than the position and velocity polygons, and they can affect the scaling of the final acceleration polygon. Therefore, when an acceleration analysis is required, GCP is usually used for only a single position, and the nonlinear components of acceleration are computed externally. However, even in such cases, GCP still offers a significant time saving over traditional graphical analyses because the constraints allow perpendicular and parallel lines to be drawn easily and the line lengths are determined with high accuracy.

As was mentioned in [Chapter 4](#), GCP is simply another method to solve the vector equations that the user develops for the velocity and acceleration analyses. The user must set up the equations properly before the solution process can be conducted. Also, the user must be able to identify the directions associated with the lines in the velocity and acceleration polygons to be able to interpret the lines as vectors. GCP does not provide arrowheads. Therefore, the directions for the lines representing the vectors for velocities and accelerations should be carefully checked at the end of each analysis.



Example 5.8

Kinematic Analysis Using GCP for a Linkage with a Rotating Slider

The linkage shown in [Figure 5.35](#) is driven by crank 2. Find the angular velocity and acceleration for link 4 and the linear velocity and acceleration for D_4 for the position in which θ_4 is 95° . The angular velocity of link 2 is a constant 4 rad/s CCW .

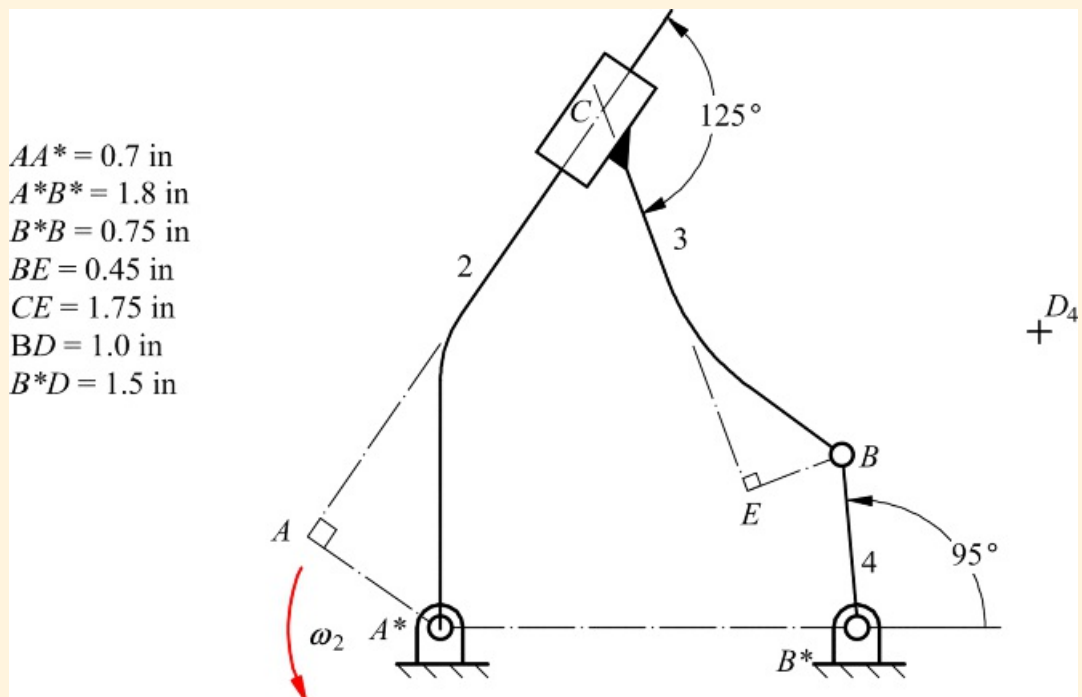


[Figure 5.35](#) Linkage for Example 5.8.

Solution

While this problem is simple to solve, the drawing shown is difficult to create using traditional graphical techniques because the angle between links 2 and 3 is given rather than the angle between link 2 and the frame. However, using GCP to develop the drawing is straightforward. To draw the linkage, first open a blank worksheet and set up the following five layers:

1. *Linkage*: Contains the final linkage that can be animated
2. *Dimensions*: Contains the dimensions for the link lengths and other variables
3. *Vel Polygon*: Contains the constructions for the velocity polygon
4. *Acc Polygon*: Contains the constructions for the acceleration polygon
5. *Pivot Dimensions*: Contains the dimensions associated with the ground pivots, slider block, and slider line

The use of the different layers is similar to that in previous examples so not all of the layers will be discussed here. Make the *Linkage* layer active, and sketch the linkage in [Figure 5.35](#). Next use a combination of constraints and the dimension tool to constrain the link lengths according to the dimensions in the problem statement. The parametric-design program solves the position equations iteratively as the dimensions are added so no trial-and-error process is required on the part of the user. After the linkage is fully constrained, add ground pivots and bushings as was done in the examples in [Chapter 4](#) to improve the appearance of the drawing. The final linkage model is shown in [Figure 5.36](#).

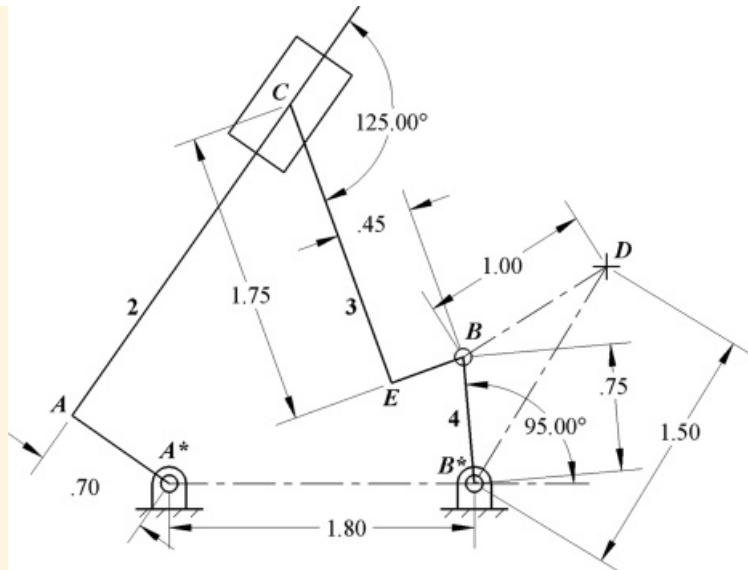


[Figure 5.36](#) Initial model for linkage in [Figure 5.35](#).

Before beginning with the velocity analysis, identify a strategy for analyzing the mechanism. A slider block is shown at C ; however, *all* of link 3 slides on link 2 in the direction indicated by the line AC . The block is pinned to link 4 at B . From a kinematic standpoint, we can place the block anywhere on link 3 as long as we maintain the constraint that it slides on link 2 in the direction indicated by the line AC . The simplest location for the block is to place it at B and to make the slide pass through B . This is shown in [Figure 5.37](#). The original links are shown as dashed lines, and FB is parallel to AC . Another advantage of GCP is that the mechanism can be moved to verify that link 4 in the new model moves exactly the same as it did in the original model.

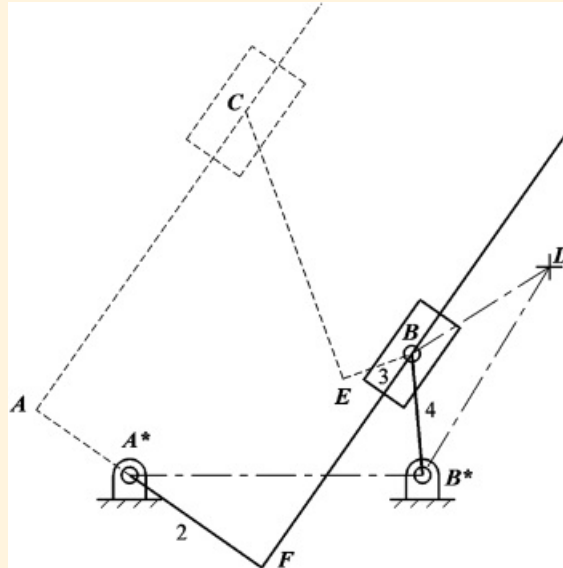


[Figure 5.37](#) Simplified model for linkage in [Figure 5.35](#).

For the velocity analysis, the basic equations that we will solve in order are

$$v_{B_2} = v_{B_2/A_2^*} = \omega_2 \times r_{S/A_2^*} \quad (5.48)$$

$$\begin{aligned} v_{B_2} &= v_{B_4} + v_{S_2/A_2} \\ v_{B_3} &= v_{B_4} - v_{S_3/S_2^*} = \omega_2 \times r_{S_3/S_2^*} \end{aligned} \quad (5.49)$$

In the expression for v_{B_3} , r_{S_3/A_2^*} varies with position because the slider slides on the line on link 2. Therefore, if we want to write a graphical program, we need to represent r_{S_3/A_2^*} as a variable in the analysis. While we could develop a graphical construction to do this, it is not worth the extra effort if the information for only one position is of interest. Therefore, we will measure r_{S_3/A_2^*} directly using the dimension tool and compute the magnitude of v_{B_3/A_2^*} externally to the program using [Equation 5.48](#).

After [Equations 5.49](#) are solved, we can find the velocity of point D_4 by solving the following equations simultaneously

$$\begin{aligned} v_{D_4} &= v_{B_4} + v_{D_4/B_4} \\ v_{D_4} &= v_{B_3^*} + v_{D_4/B_3^*} \end{aligned} \quad (5.50)$$

For the acceleration analysis, we can use the same set of points in the same order as was done in the velocity analysis. The first set of equations involves the coincident points at B . Then

$$\alpha_{S_2} = \alpha_{B_3/A_2^*} = \alpha_{B_3/A_2^*}^r + \alpha_{B_3/A_2^*}^t = \omega_2 \times (\omega_2 \times r_{S_2/A_2^*}) + \omega_2 \times r_{S_2/A_2^*}$$

and because $\omega_2 = 0$

$$\alpha_{S_2} = \alpha_{B_3/A_2^*} = \omega_2 \times (\omega_2 \times r_{S_2/A_2^*}) \quad (5.51)$$

also

$$\begin{aligned} \alpha_{S_2} &= \alpha_{B_3} + \alpha_{B_3/B_2} = \alpha_{B_2/A_2^*}^r + \alpha_{B_3/B_2}^t + 2\omega_2 \times v_{B_3/B_2} \\ \alpha_{S_3} &= \alpha_{B_4} = \alpha_{B_4/E}^r + \alpha_{B_4/E}^t = \omega_4 \times (\omega_4 \times r_{B_4/E^*}) + \omega_4 \times r_{B_4/E^*} \end{aligned} \quad (5.52)$$

After [Equations 5.52](#) are solved, we can determine the acceleration of D_4 by image.

Steps

1. Make the *Linkage* layer active, and draw the simplified model of the linkage in [Figure 5.37](#) full scale. Set the appropriate constraints so that the linkage can be animated by dragging the joint at B . After verifying that the linkage will move properly, use the dimension tool to constrain the angle between link 4 and the frame to be 95° , and measure the distance A^*B . The model is shown in [Figure 5.38](#).

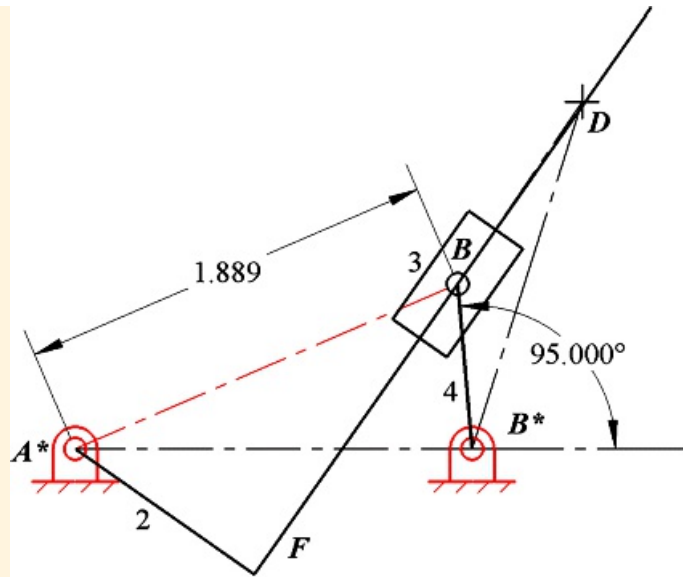


[Figure 5.38](#) Final model of linkage to be analyzed for Example 5.8.

2. Make the *Vel Polygon* layer active and select a velocity scale (1 in = 10 in/s). Use [Equation 5.48](#) to compute the velocity v_{B^*} .

$v_{B^*} = \omega_2 \times r_{B/A^*} = 4(1.889) = 7.55 \text{ in/s}$ perpendicular to A^*B in the direction obtained by rotating $\overline{v_{B/A^*}}$ by 90° CCW. Select a location for the velocity pole (o), and draw the line corresponding to v_{B^*} from o . Label the end as b_2 as shown in [Figure 5.39](#).

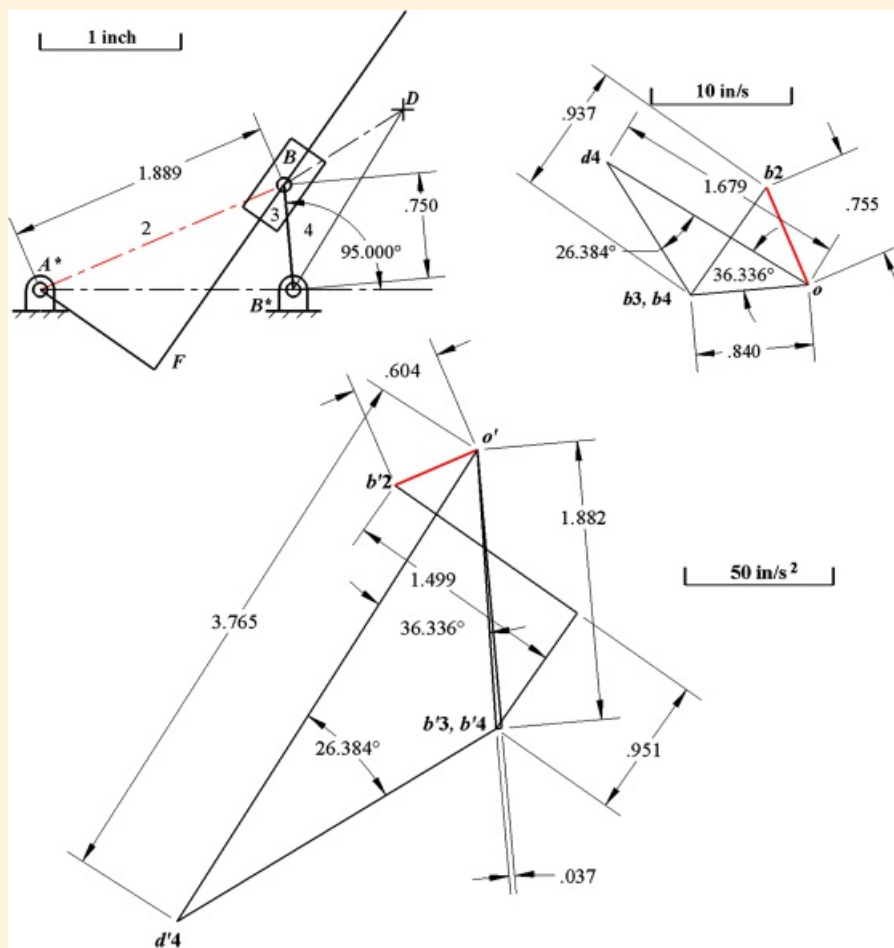


[Figure 5.39](#) Velocity and acceleration polygons for Example 5.8 generated by GCP.

- Next solve [Equation 5.49](#). Starting from point b_2 , draw a line parallel to line FB . This new line corresponds to \dot{v}_{B_3/B_2} . Draw a second line starting from point o and perpendicular to line BB^* . This line corresponds to \ddot{v}_{B_4/B_2} . Merge the ends of the two new lines. The intersection gives points b_3 and b_4 corresponding to the velocity of points B_3 and B_4 .
- Use [Equation 5.50](#) to solve for the velocity of D_4 . Starting from point o , draw a line perpendicular to line B^*D . This new line corresponds to \dot{v}_{D_4/B_2^*} . Draw a second line starting from b_4 and perpendicular to line BD . This new line corresponds to \dot{v}_{D_4/B_2} . Merge the ends of the two new lines. The intersection gives point d_4 corresponding to the velocity of point D_4 . This completes the constructions for the velocities.
- Use the dimension tool to measure the length of the ob_4 which corresponds to \dot{v}_{B_4/B_2^*} . The length of ob_4 is 0.84 in so based on a scale factor of 10 in/s = 1 in

$$\dot{v}_{B_4/B_2^*} = 10(0.84) = 8.40 \text{ in/s}$$

Based on [Equation 5.49](#), compute the magnitude of ω_d from

$$\omega_d = \frac{|\dot{v}_{B_4/B_2^*}|}{|r_{B_2/B_2^*}|} = \frac{8.40}{0.75} = 11.20 \text{ rad/s CCW}$$

Measure the distance b_3b_2 . This corresponds to \dot{v}_{B_3/B_2} which is required for the acceleration analysis. Then

$$\dot{v}_{B_3/B_2} = 10(0.937) = 9.37 \text{ and points from } b_2 \text{ toward } b_3 \text{ on the velocity diagram}$$

- Use the dimension tool to measure the length of the line od_4 . Also, notice the orientation of the line. The measured distance is $od_4 = 1.679$ in. Using the scaling factor (10), the magnitude of the corresponding linear velocity is

$$|\dot{v}_{B_2/B_2^*}| = 10(1.679) = 16.79 \text{ in/s}$$

The direction is indicated in the polygon by the line segment from o to d_4 . This completes the velocity analysis.

- Make the *Acc Polygon* layer active and select an acceleration scale (1 in = 50 in/s²). Use [Equation 5.51](#) to compute the acceleration of B_2 . Because ω_2 is constant

$$\ddot{v}_{B_2} = \ddot{v}_{B_2/B_2^*} = \omega_2 \times (\omega_2 \times r_{B_2/A^*}) = -|\omega_2|^2 r_{B_2/A^*} = (4)^2(1.889) = 30.22 \text{ in/s}^2 \text{ pointed from } B \text{ toward } A^*$$

Select a location for the acceleration pole (o') and draw the line 0.604 in long corresponding to \ddot{v}_{B_2} . Label the end of the line as b'_2 .

- Use [Equation 5.52](#) to compute the acceleration of B_3 and B_4 . Compute the radial component of acceleration and the Coriolis term

$$\ddot{v}_{B_4/B_2^*} = \omega_d \times (\omega_d \times r_{B_4/B_2^*}) = -|\omega_d|^2 r_{B_4/B_2^*} = (11.2)^2(0.75) = 94.08 \text{ in/s}^2 \text{ pointed from } B \text{ toward } B^*$$

$$\ddot{v}_{B_3/B_2}^C = 2\omega_2 \times v_{B_3/B_2} = 2(4)(9.37) = 74.96 \text{ in/s}^2 \text{ perpendicular to } FB \text{ and pointed down and to the right}$$

Starting from point o' , draw a line in the direction from B to B^* that is 1.882 in long. This corresponds to \ddot{v}_{B_4/B_2^*} . At the end of \ddot{v}_{B_4/B_2^*} , draw a perpendicular line. This corresponds to \ddot{v}_{B_4/B_2} . Next draw a line from b'_2 in the direction perpendicular to FB and 1.499 in long. This corresponds to \ddot{v}_{B_3/B_2}^C . At the end of \ddot{v}_{B_3/B_2}^C draw a line in the FB direction. This corresponds to \ddot{v}_{B_3/B_2} . The solution is where \ddot{v}_{B_3/B_2}

intersects $\alpha_{B_4/S}^i$. Label this intersection as points b_3' and b_4' . Note that $\alpha_{B_4/S}^i$ is very small.

9. Locate the acceleration of D_4 by image. In the velocity diagram, use the dimension tool to measure the angle od_4b_4 (26.384°) and the angle d_4ob_4 (36.336°). Draw a triangle on the acceleration polygon with $o'b'_4$ as a base and oriented to be approximately similar to $B^*B_4D_4$ and ob_4d_4 . Use the dimension tool to set the angle $d'_4o'b'_4$ to be 26.384° and the angle $o'd'_4b'_4$ to be 36.336° . This will locate d'_4 .
10. Use the dimension tool to measure the length corresponding to $\alpha_{B_4/S}^i$. The length is 0.037 in so based on a scale factor of $50 \text{ in/s}^2 = 1 \text{ in}$,

$$\alpha_{B_4/S}^i = 50(0.037) = 1.85 \text{ in/s}^2$$

Based on [Equation 5.52](#), compute the magnitude of α_4 from

$$\alpha_4 = \frac{\alpha_{B_4/S}^i}{\left| v_{B/S} \right|} = \frac{1.85}{0.75} = 2.47 \text{ rad/s}^2 \text{ CCW}$$

Note that α_4 is small but not zero. The value would have been very difficult to determine accurately by traditional graphical methods, but using GCP, determining an accurate value is very straightforward.

11. Use the dimension tool to measure the length of the lines $o'd'_4$. The measured distance is $o'd'_4 = 3.765$ in. Using the scaling factor (50), the magnitude of the corresponding linear acceleration of D_4 is

$$a_{D_4/S}^i = 50(3.765) = 188.3 \text{ in/s}^2$$

The direction is from o' to d'_4 .

Problems

Rotating Sliders

5.1 In [Figure P5.1](#), points A and B^* have the same horizontal coordinate, and $\omega_3 = 20 \text{ rad/s}$. Draw and dimension the velocity polygon. Identify the sliding velocity between the block and the slide, and find the angular velocity of link 2.

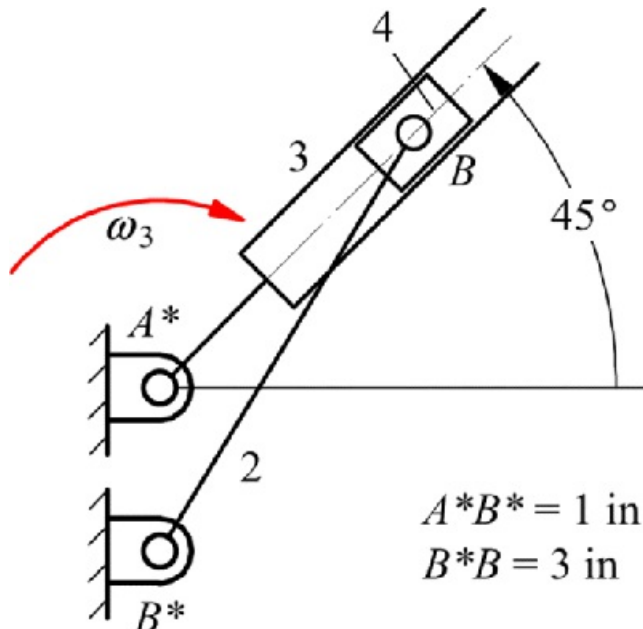


[Figure P5.1](#) Linkage for Problem 5.2.

5.2 If $\omega_2 = 20 \text{ rad/s CCW}$, as shown in [Figure P5.2](#), find the velocity of point C_3 .

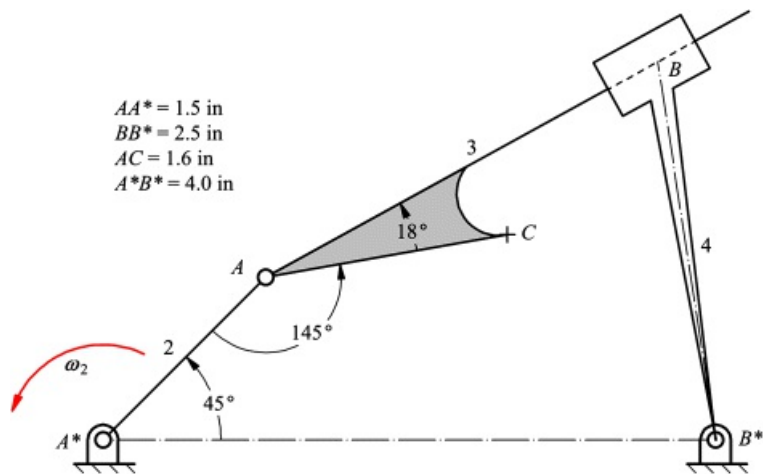


[Figure P5.2](#) Linkage for Problem 5.2.

5.3 If $\omega_2 = 500 \text{ rad/s CCW}$, find v_{D_4} , as shown in [Figure P5.3](#).

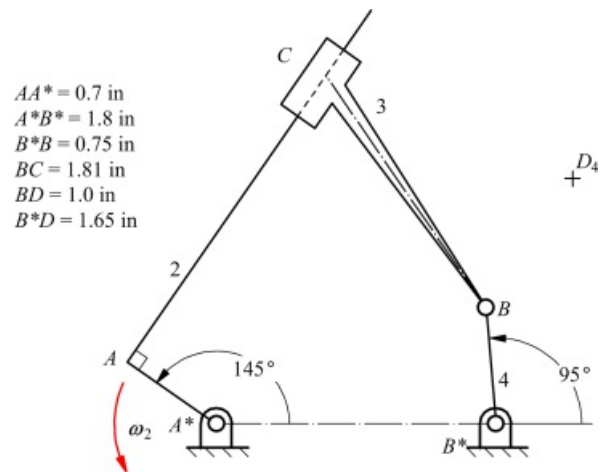


Figure P5.3 Linkage for Problem 5.3.

5.4 If $\omega_2 = 50 \text{ rad/s CCW}$, find v_{B4} , as shown in Figure P5.4.

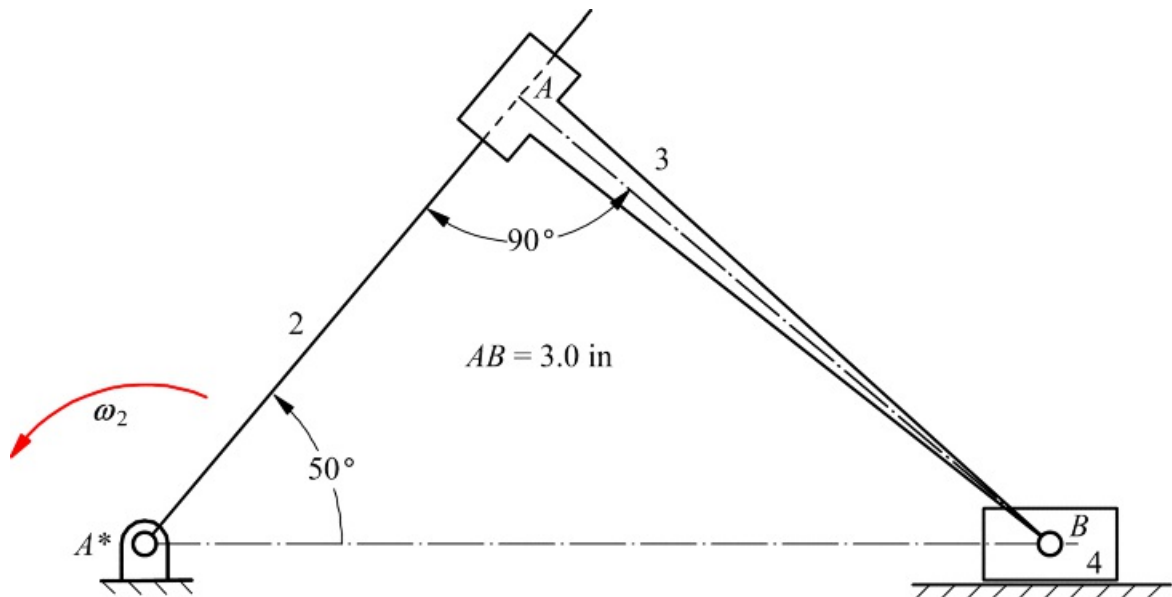


Figure P5.4 Linkage for Problem 5.4.

5.5 Determine the velocity and acceleration of point A on link 2 in Figure P5.5, if $\omega_4 = 20 \text{ rad/s}$ (constant).

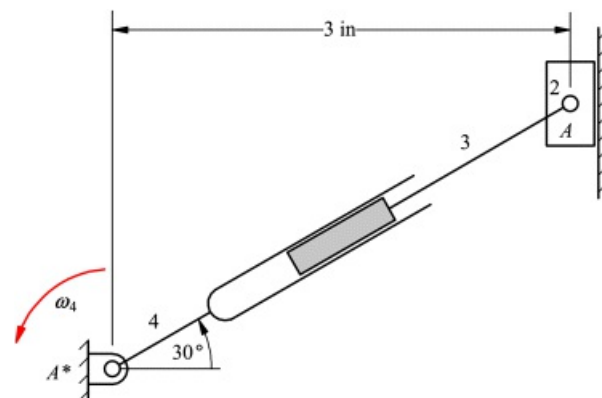


Figure P5.5 Linkage for Problem 5.5.

5.6 If $\omega_2 = 500 \text{ rad/s CCW}$, find ω_6 , as shown in Figure P5.6.

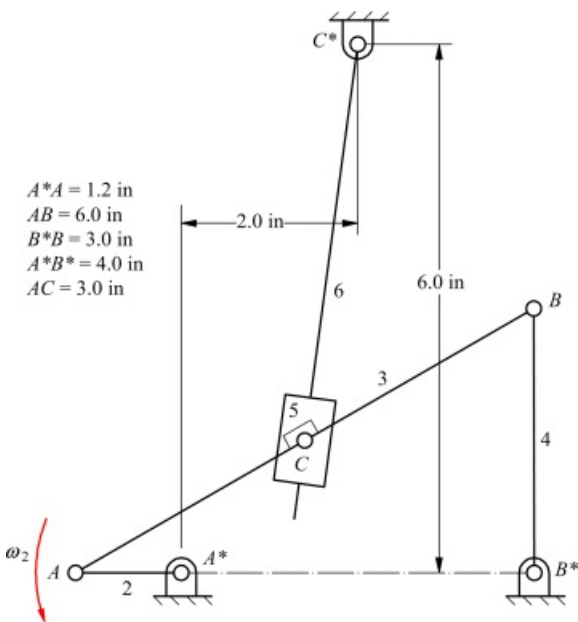


Figure P5.6 Linkage for Problem 5.6.

5.7 If $\omega_2 = 100 \text{ rad/s CCW}$, find the velocity of point D_5 in Figure P1.7.

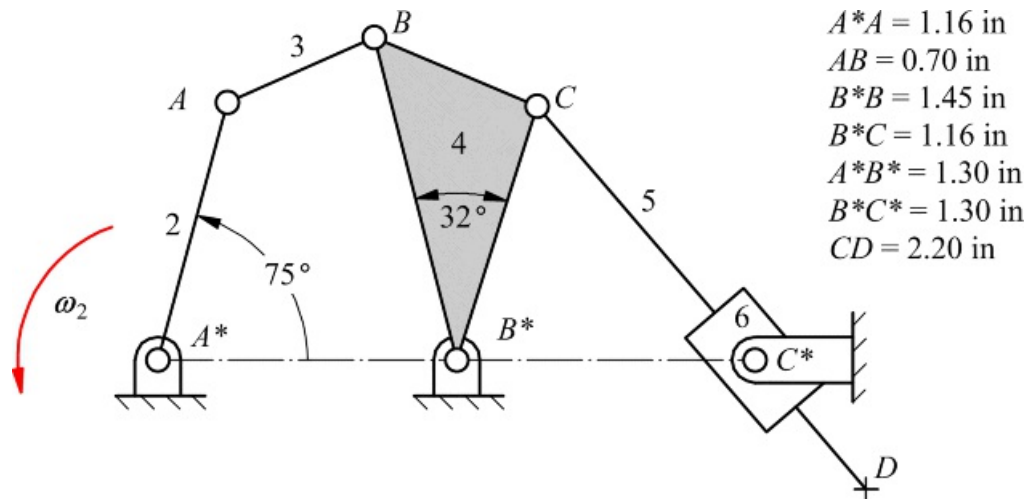
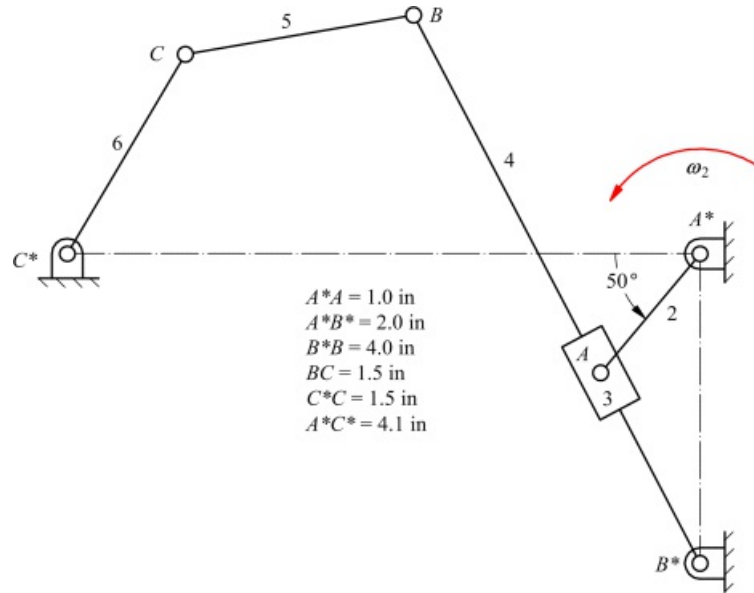


Figure P5.7 Linkage for Problem 5.7.

5.8 In Figure P1.8, if $\omega_2 = 10 \text{ rad/s CCW}$, find ω_6 .



[Figure P5.8](#) Linkage for Problem 5.8.

5.9 In [Figure P5.9](#), $\omega_2 = 20 \text{ rad/s CCW}$. Write the velocity equations and determine the following: v_{B4} , ω_4 , v_{D6} , ω_6 .

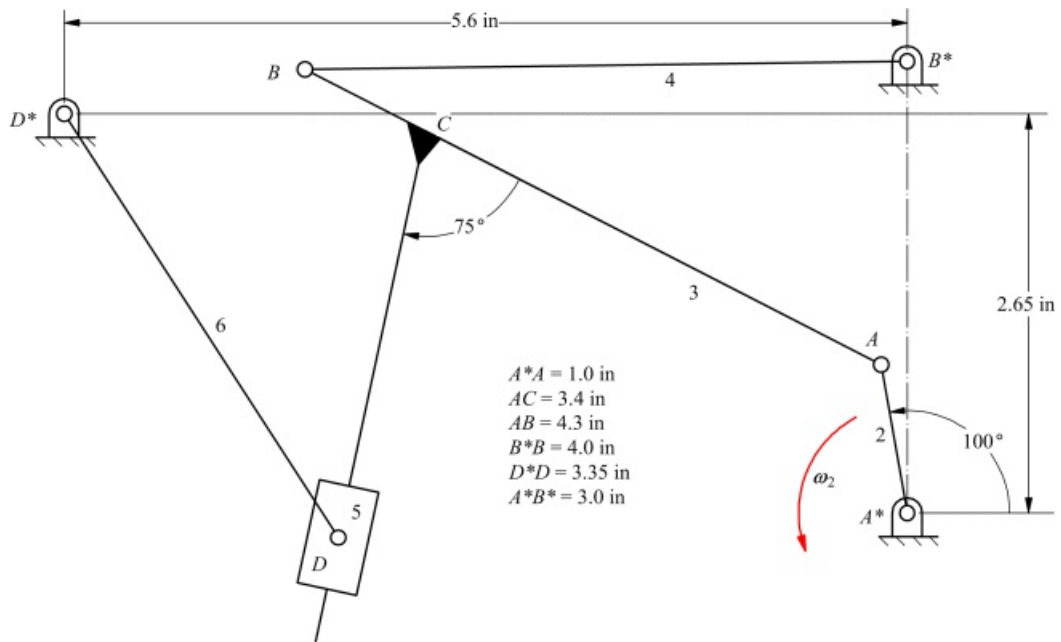


[Figure P5.9](#) Linkage for Problem 5.9.

5.10 If the velocity of point A on link 2 is 20 in/s, as shown in [Figure P5.10](#), find the velocity of point D on link 5. The slider (link 5) is 0.45 in long and 0.25 in wide, and point C is in the center of the slider.

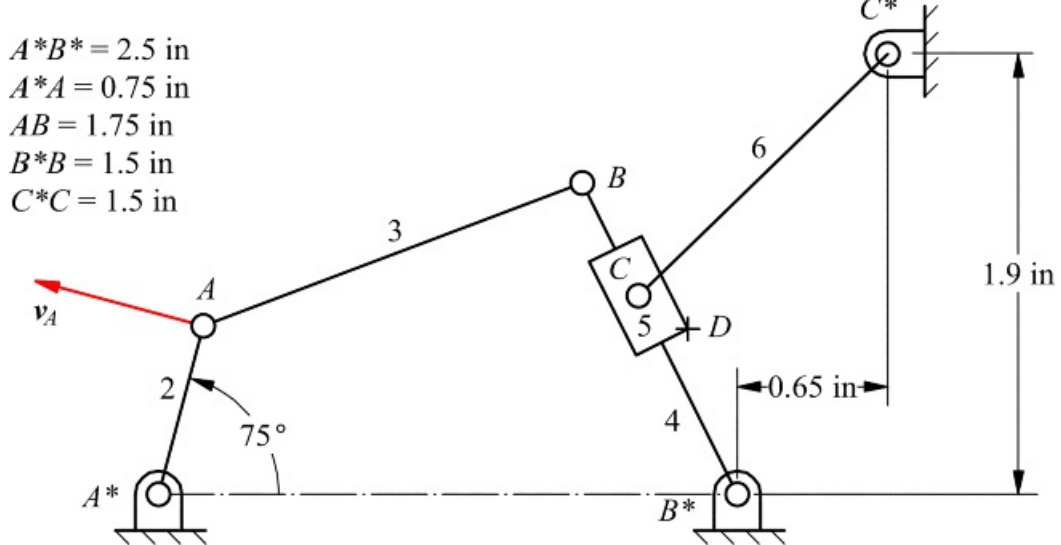


Figure P5.10 Linkage for Problem 5.10.

5.11 In the clamping device shown in [Figure P5.11](#), links 3 and 4 are an air cylinder. If the opening rate of the air cylinder is 5 cm/s and the opening acceleration of the cylinder is 10 cm/s², find the angular velocity and acceleration of link 2, and the linear velocity and acceleration of point C on link 2 when AA^* is perpendicular to A^*B^* .

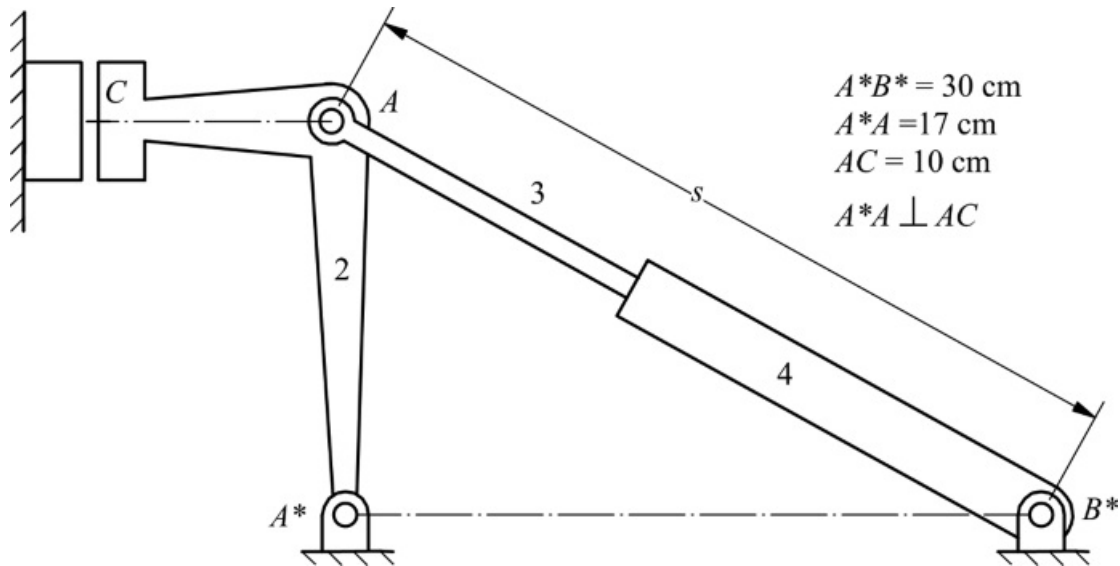
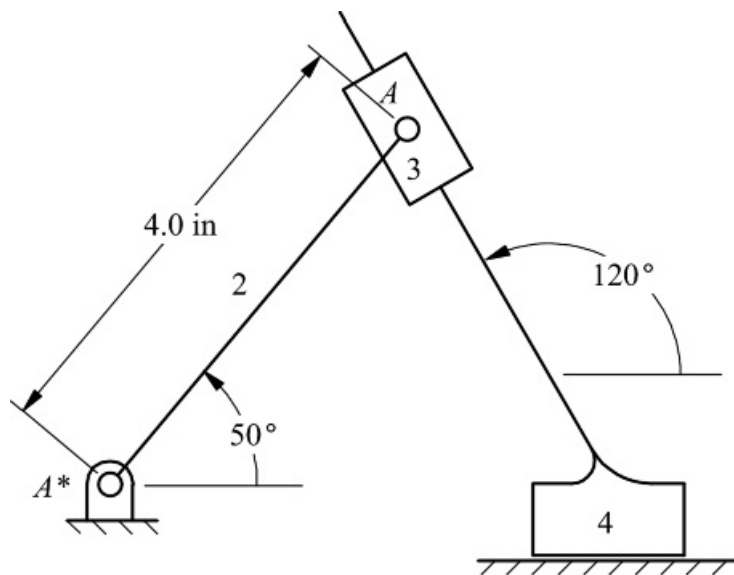


Figure P5.11 Linkage for Problem 5.11.

5.12 In [Figure P5.12](#), link 4 moves to the left with a velocity of 10 in/s and the acceleration is 100 in/s² to the left. Draw the velocity and acceleration polygons and solve for the angular velocity and acceleration of link 2.



[Figure P5.12](#) Linkage for Problem 5.12.

5.13 In [Figure P5.13](#), the angular velocity of link 2 is 10 rad/s CCW and the angular acceleration is 100 rad/s² CW. Determine the following: ω_{A_1} , v_{S_2} , α_{A_1} , α_{A_2} , v_{S_2} , α_d .

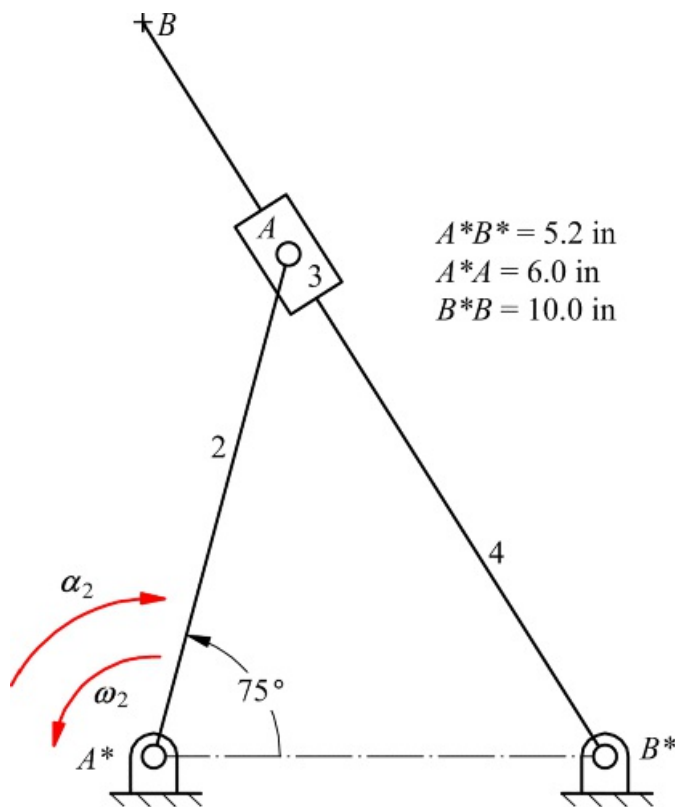


[Figure P5.13](#) Linkage for Problem 5.13.

5.14 Resolve Problem 5.13 if $\omega_2 = 2 \text{ rad/sec}$ (constant).

5.15 In [Figure P5.15](#), the angular velocity of link 2 is 10 rad/s CCW and the angular acceleration is 80 rad/s² CW. Determine the angular velocity and acceleration of links 3 and 4. On the velocity and acceleration diagrams, locate the velocity and acceleration of point D on link 3.

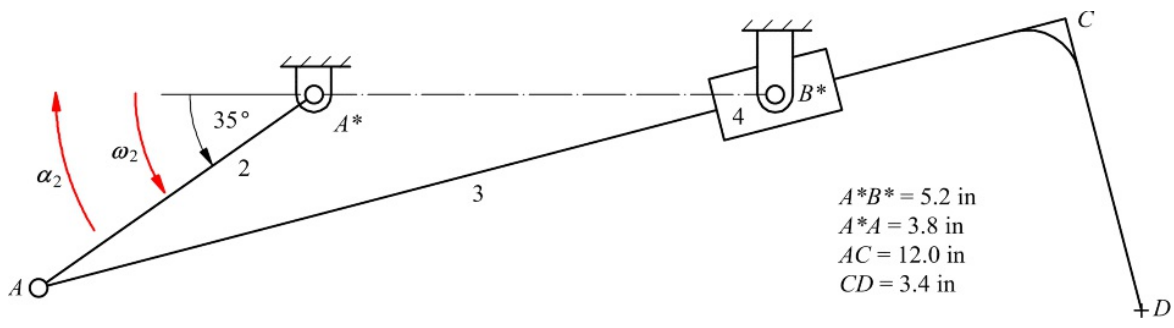


[Figure P5.15](#) Linkage for Problem 5.15.

5.16 In [Figure P5.16](#), $\omega_2 = 100 \text{ rad/s CCW (constant)}$. Find ω_4 , $^2\omega_4$, ω_3 , $^6\omega_5$, $^3\omega_5$, v_C , a_4 , 2a_4 , a_3 , 6a_5 , and a_C .

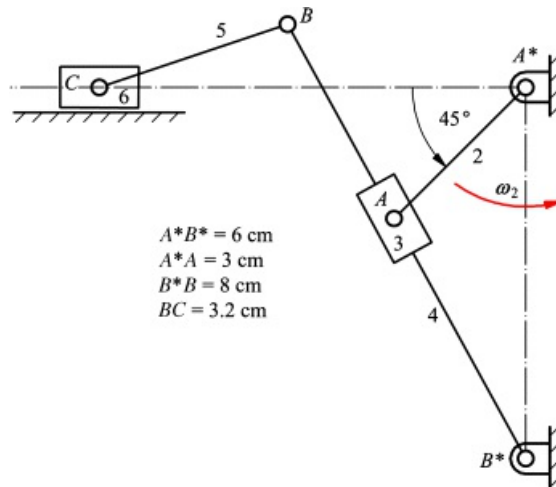


[Figure P5.16](#) Linkage for Problem 5.16.

5.17 In [Figure P5.17](#), the angular velocity of link 2 is 50 rpm CCW (constant). Determine the acceleration of point B_6 and the angular velocity of link 6.

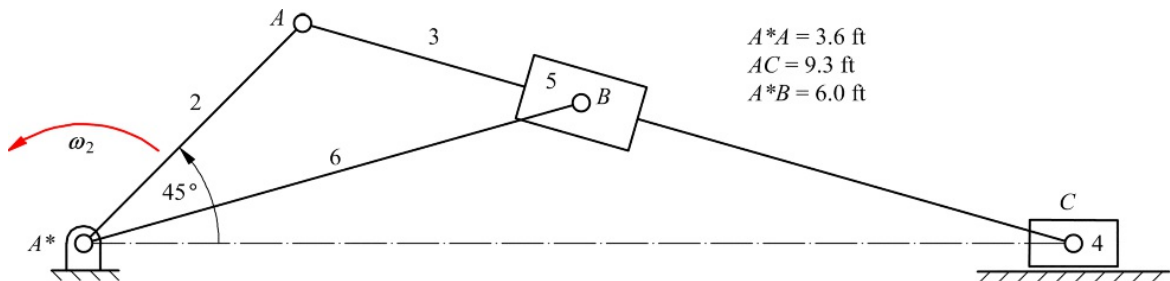


[Figure P5.17](#) Linkage for Problem 5.17.

5.18 In the position shown in [Figure P5.18](#), A^*A is horizontal. The angular velocity of link 2 is 10 rad/s CCW (constant). Draw the velocity diagram to determine the sliding velocity and acceleration of link 6.

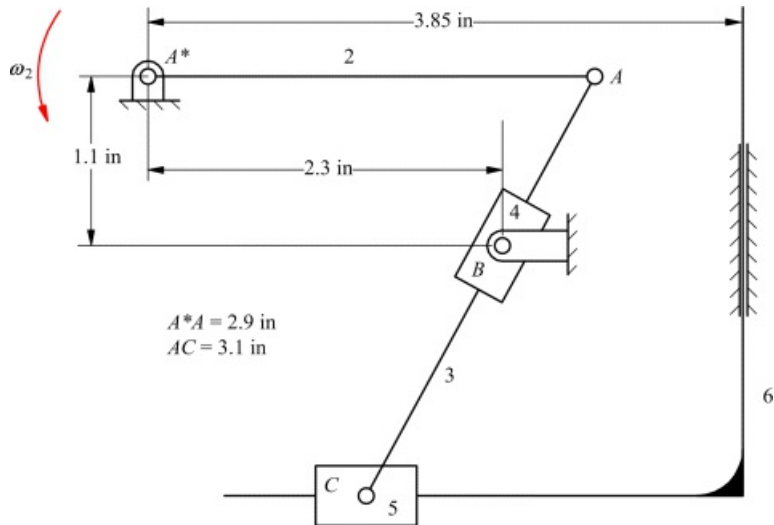


Figure P5.18 Linkage for Problem 5.18.

5.19 In the position shown in Figure P5.19, A^*A is horizontal. The angular velocity of link 2 is 50 rad/s CCW. Draw the velocity diagram to determine the sliding velocity of link 6. Determine a new position for point B (between A and C) so that the velocity of link 6 would be equal and opposite to the one calculated for the original position of point B.

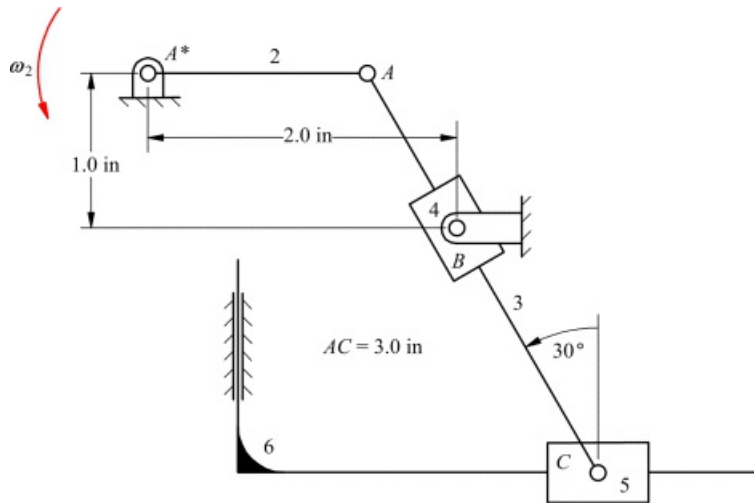
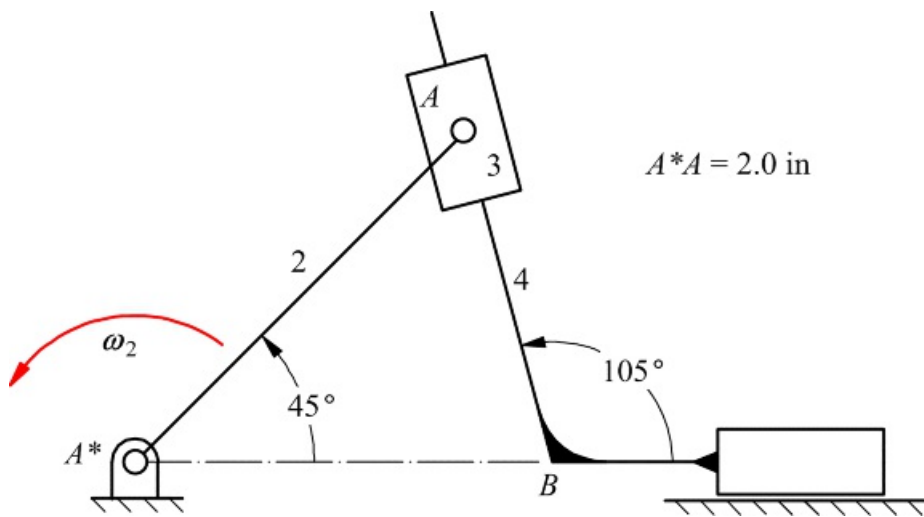


Figure P5.19 Linkage for Problem 5.19.

5.20 The scotch-yoke mechanism in Figure P1.20 is driven by crank 2 at $\omega_2 = 50 \text{ rad/s}$ (CCW). Link 4 slides horizontally. Find the velocity of point B on link 4.



[Figure P5.20](#) Linkage for Problem 5.20.

Rolling Contact

5.21 The circular cam shown in [Figure P5.21](#) is driven at an angular velocity $\omega_2 = 20 \text{ rad/s}$ (CW) and $\alpha_2 = 200 \text{ rad/s}^2$ (CW). There is rolling contact between the cam and the roller, link 3. Find the angular velocity and angular acceleration of the oscillating follower, link 4.

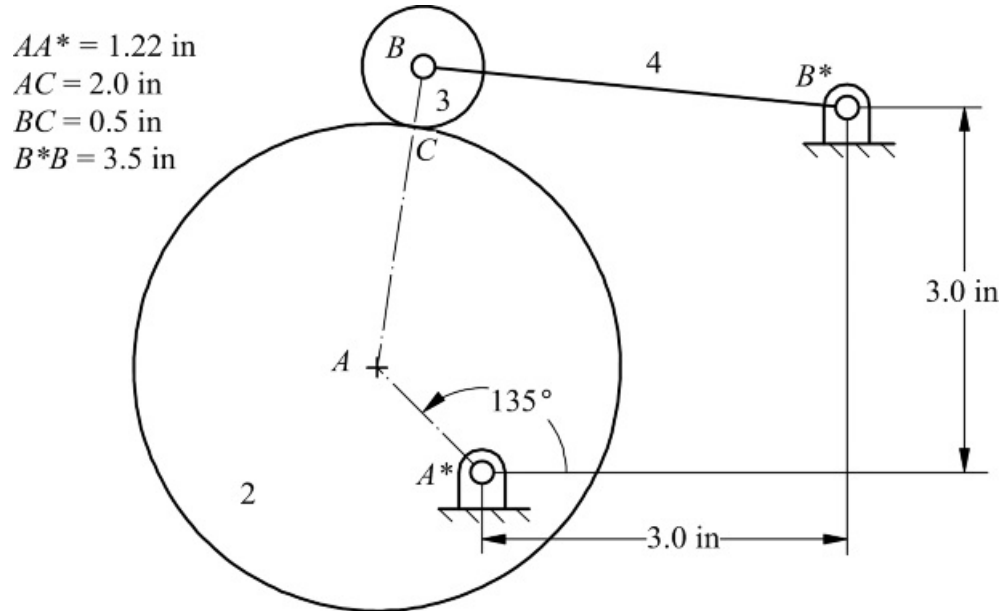


[Figure P5.21](#) Linkage for Problem 5.21.

5.22 For the mechanism shown in [Figure P5.22](#), assume that link 2 rolls on the frame (link 1) and link 4 rolls on link 3. Assume that link 2 is rotating CW with a constant angular velocity of 100 rad/s. Determine the angular acceleration of link 3 and link 4.

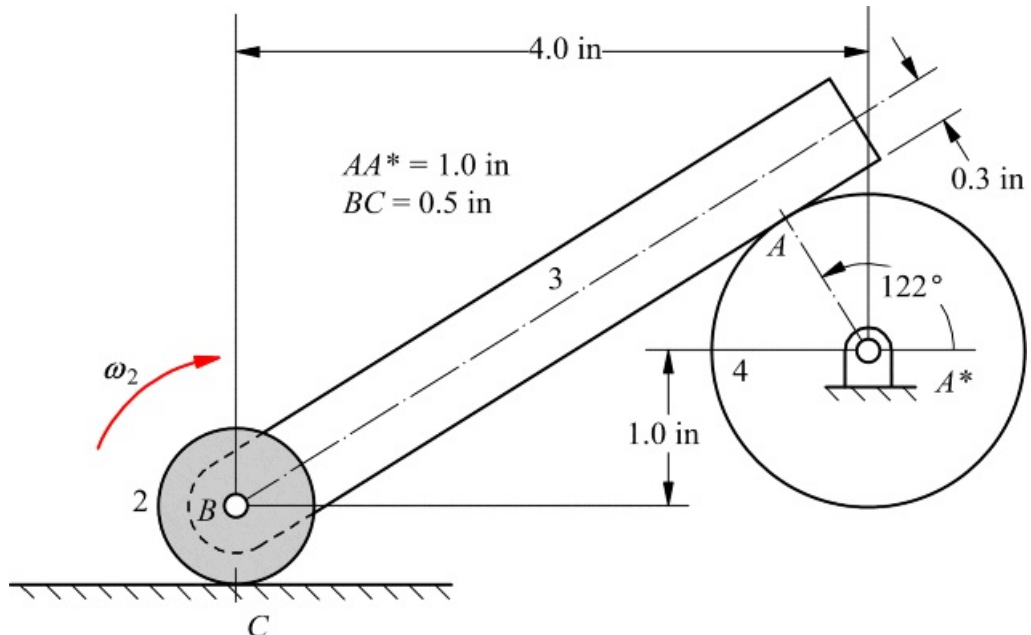


Figure P5.22 Linkage for Problem 5.22.

5.23 For the mechanism shown in Figure P5.23, assume that link 4 rolls on the frame (link 1). If link 2 is rotating CW with a constant angular velocity of 20 rad/s, determine the angular accelerations of links 3 and 4 and the acceleration of point C on link 3.

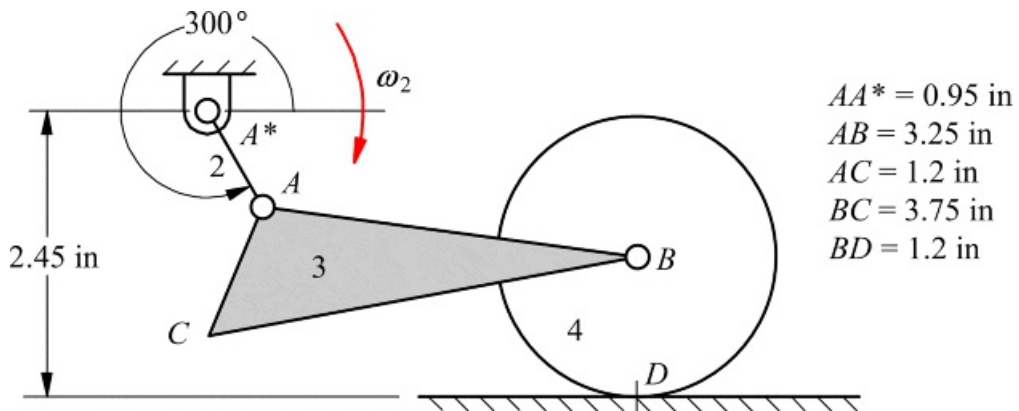


Figure P5.23 Linkage for Problem 5.23.

5.24 If $v_{A2} = 20 \text{ in/s}$ (constant) downward in Figure P5.24, find ω_3 , a_3 , v_{F3} , and a_{F3} .

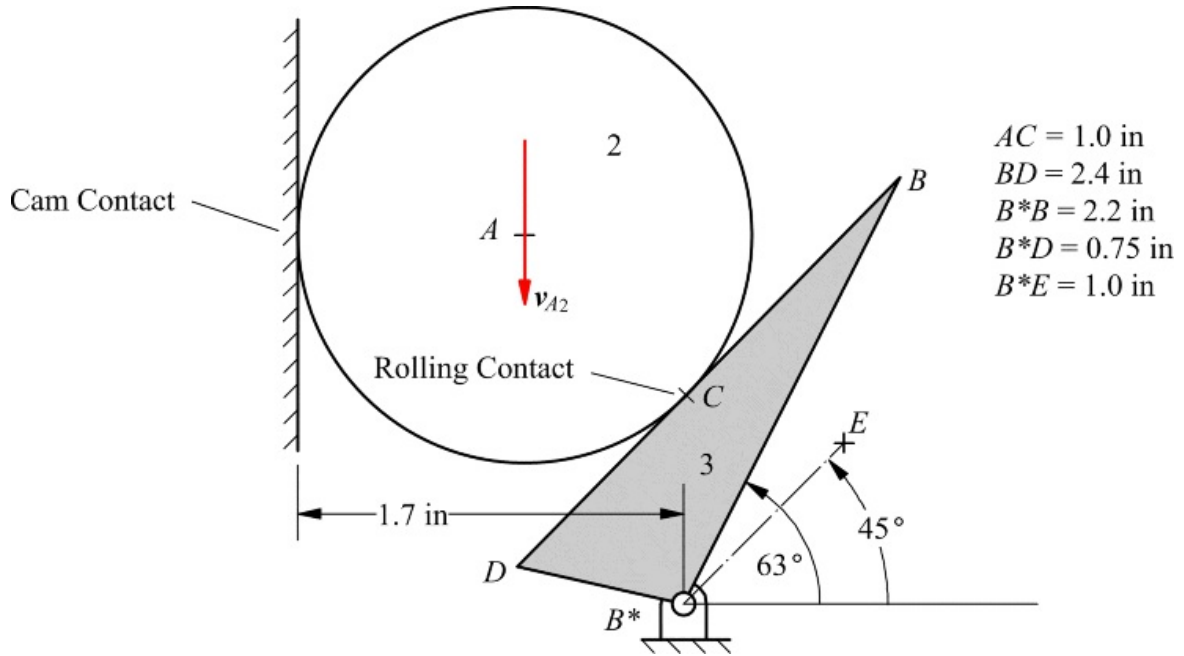


Figure P5.24 Linkage for Problem 5.24.

5.25 In Figure P5.25, points A , B , and C are collinear. If $v_{A2} = 20 \text{ in/s}$ (constant) downward, find v_{C3} , and a_{C3} .

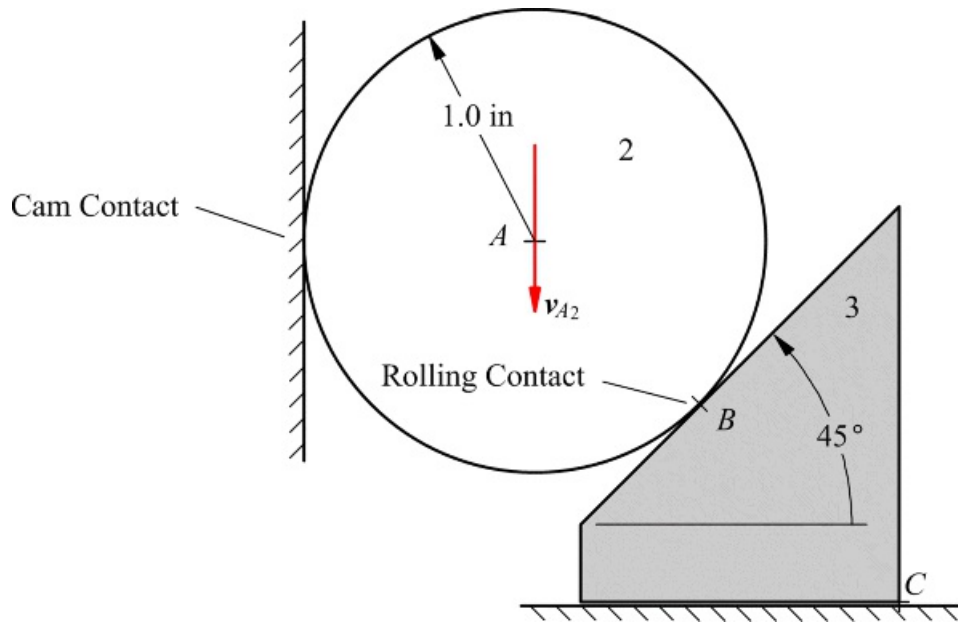


Figure P5.25 Linkage for Problem 5.25.

5.26 Part of an eight-link mechanism is shown in Figure P5.26. Points A , B , and C are collinear as are D , B , and E . Also, BC is perpendicular to BE . There is rolling contact at location B and the velocity and acceleration of points D_6 and C_5 are as shown. Find ω_8 and a_7 for the position given. Also find the velocity of E_8 by image.

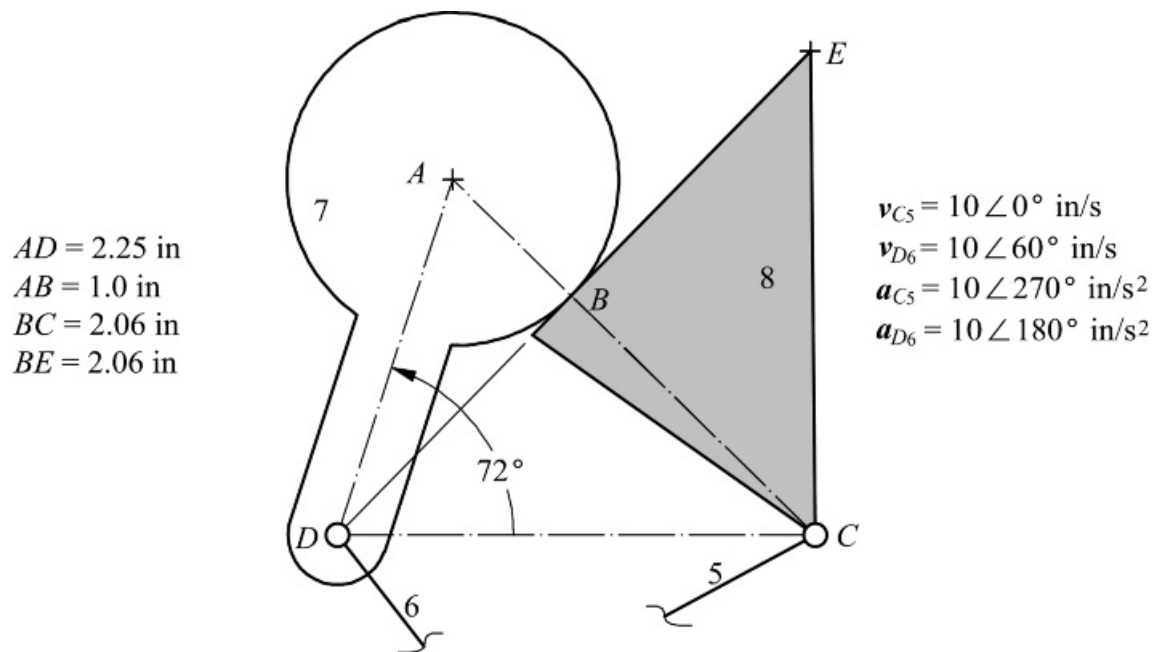


Figure P5.26 Linkage for Problem 5.26.

5.27 In the mechanism shown in Figure P5.27, link 2 is turning CW at the constant rate of 100 rad/s, and link 3 rolls on link 2. Draw the velocity and acceleration polygons for the mechanism, and determine α_{B_3} and \mathbf{a}_3 .

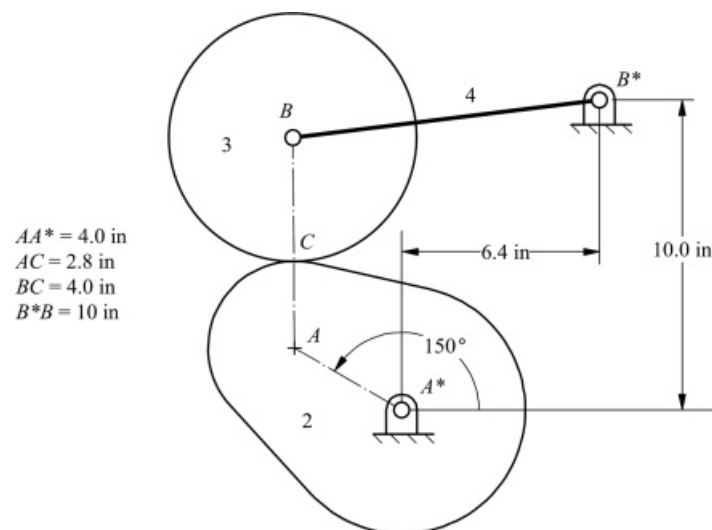


Figure P5.27 Linkage for Problem 5.27.

5.28 In the mechanism shown in Figure P5.28, link 2 is turning CW at the rate of 100 rpm, and link 3 rolls on link 2. Draw the velocity polygon for the mechanism, and determine v_{B_3} and ω_3 .

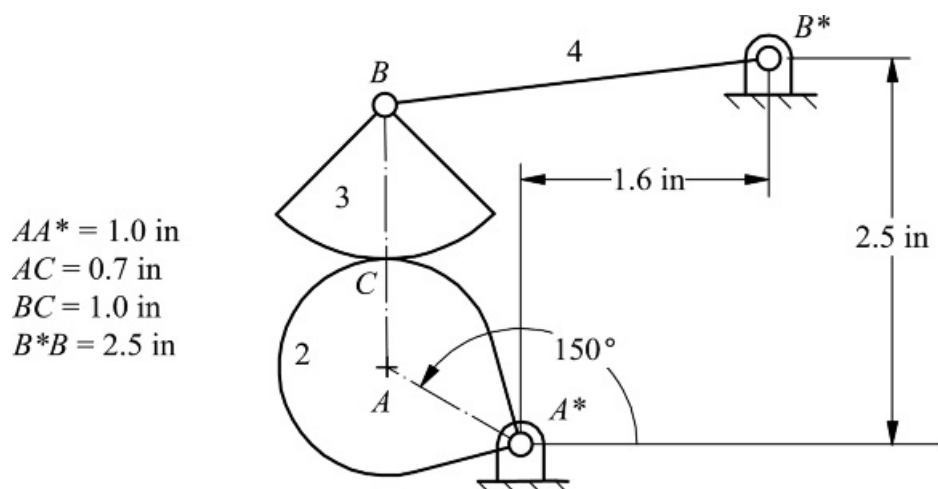


Figure P5.28 Linkage for Problem 5.28.

5.29 Assume that the angular velocity of link 2 in Figure P5.29 is 10 rad/s CW and link 3 rolls on link 7 without slipping, Find ω_7 .

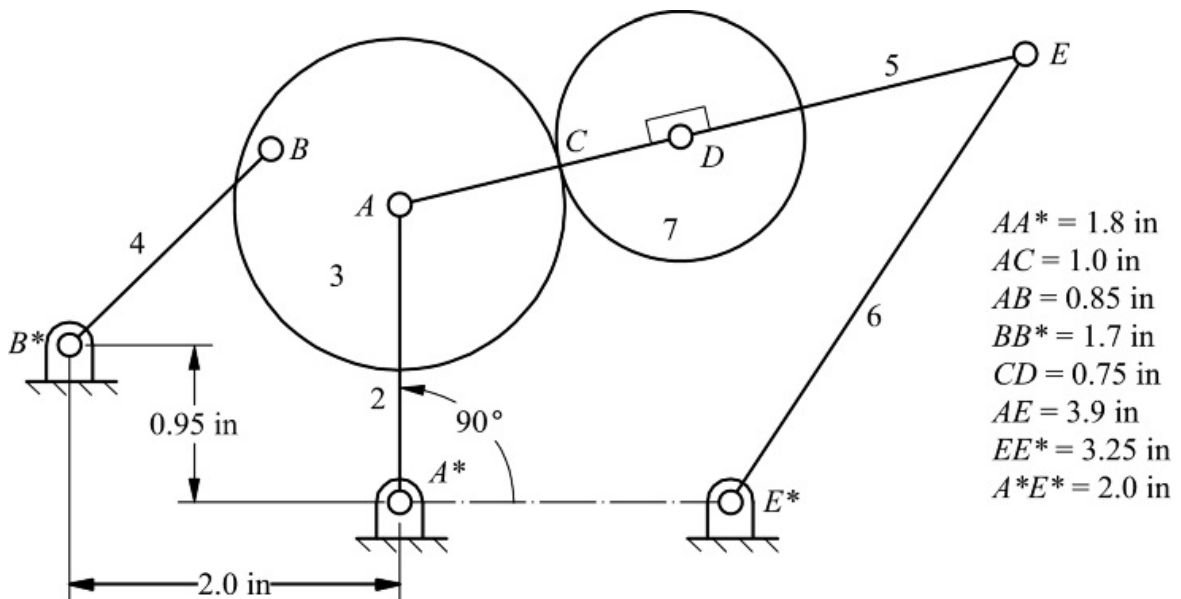
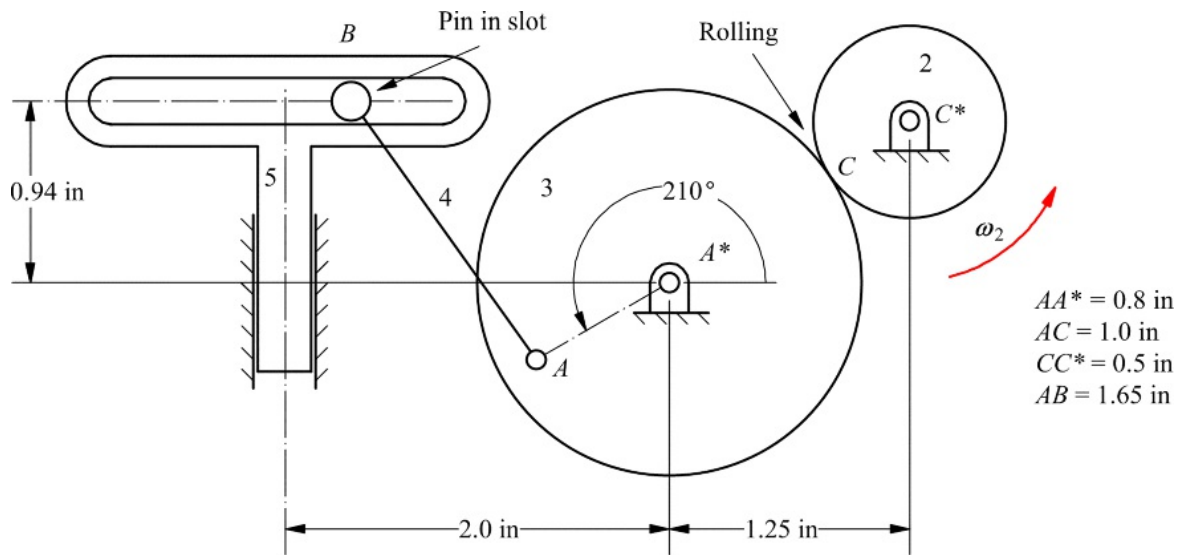


Figure P5.29 Linkage for Problem 5.29.

5.30 In the two-degree-of-freedom mechanism shown in Figure P5.30, ω_2 is given as 20 rad/s CCW. What should the linear velocity of 5 be so that $\omega_4 = 5$ rad/s CCW.



[Figure P5.30](#) Linkage for Problem 5.30.

Cam Contact

[5.31](#) In the mechanism shown in [Figure P5.31](#), $\omega_2 = 100 \text{ rad/s}$ CW. Determine v_{B_3}/B_2 and v_{B_3} using two approaches: (1) equivalent linkages and (2) coincident points at B .

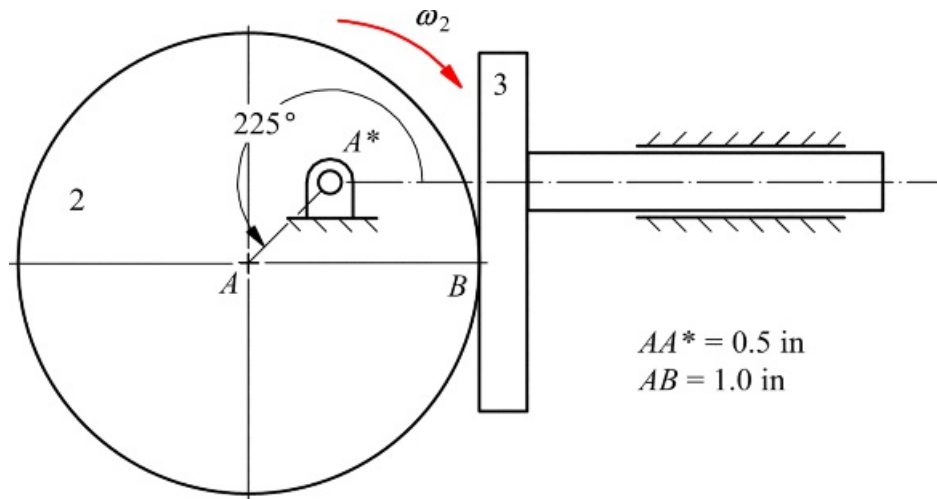


[Figure P5.31](#) Linkage for Problem 5.31.

[5.32](#) In the mechanism shown in [Figure P5.32](#), $\omega_2 = 100 \text{ rad/s}$ CCW. At the instant shown, point C , the center of curvature of link 3, lies directly above point B^* , and point A lies directly above point A^* . Determine v_{B_3}/B_2 and ω_2 using: (1) equivalent linkages and (2) coincident points at B .

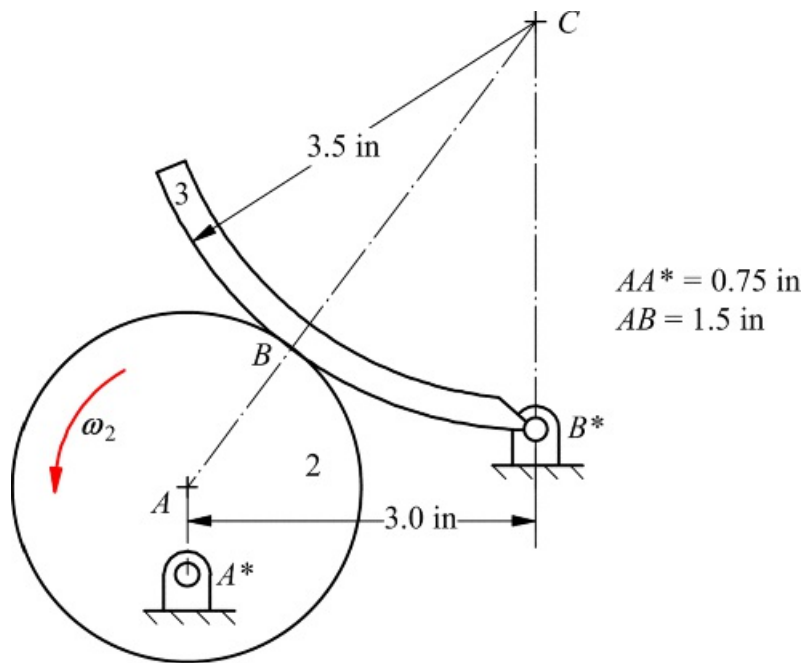


[Figure P5.32](#) Linkage for Problem 5.32.

5.33 In the position shown in [Figure P5.33](#), $\omega_2 = 100 \text{ rad/s}$ CCW and $\alpha_2 = 2,000 \text{ rad/s}^2$ CCW. Find the velocity and acceleration of link 3 using: (1) equivalent linkages and (2) coincident points at B.

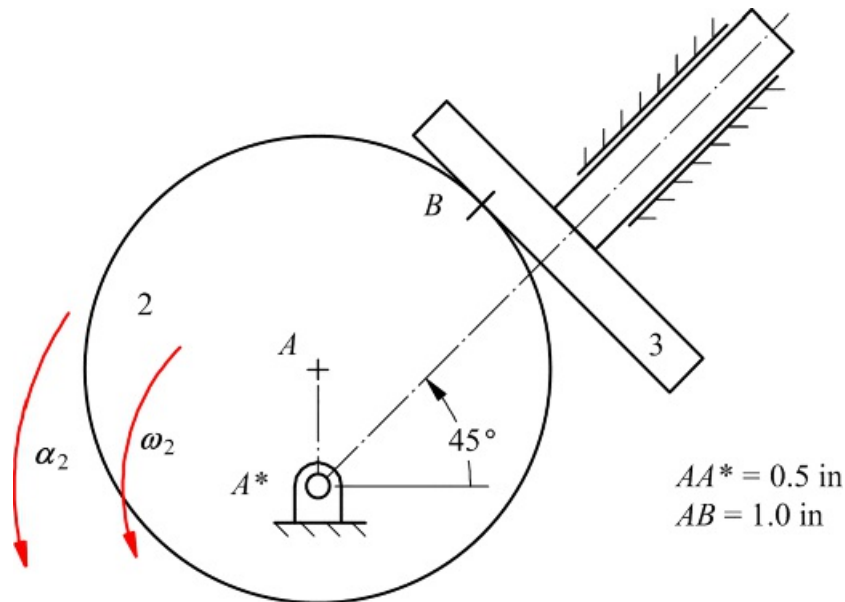


[Figure P5.33](#) Linkage for Problem 5.33.

5.34 If the cam (link 2) in [Figure P1.34](#) is turning CW with an angular velocity of 1000 rpm (constant), determine the linear velocity and acceleration of the follower. The cam profile at B is a circular arc centered at A.

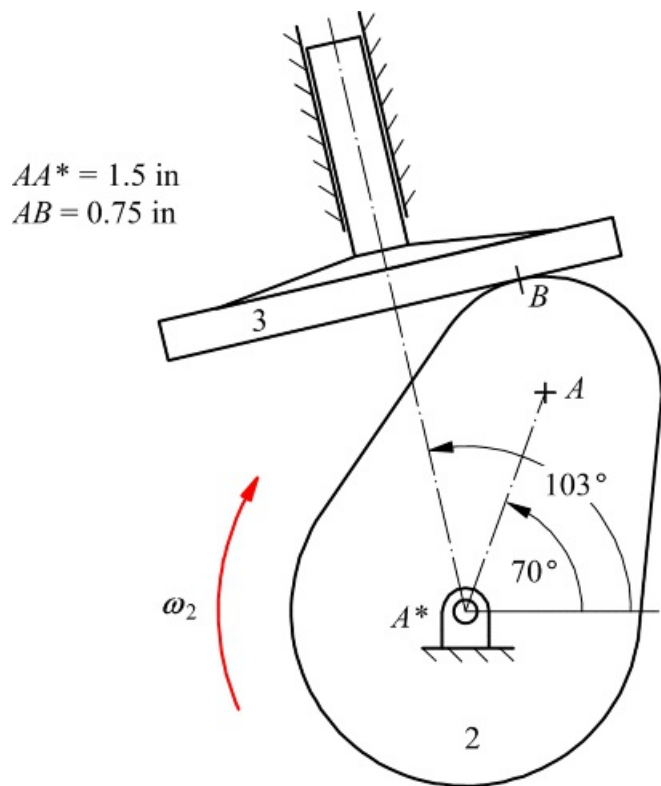


Figure P5.34 Linkage for Problem 5.34.

5.35 In [Figure P5.35](#), $v_{A2} = 500 \text{ in/s}$. Find ω_5 and ${}^3\omega_4$. Indicate on link 4 the point that has zero velocity. In the drawing, G and E are the centers of curvature of links 4 and 5, respectively, corresponding to location F. D is the center of curvature of link 3 corresponding to C. Also, point E lies exactly above point E^* .

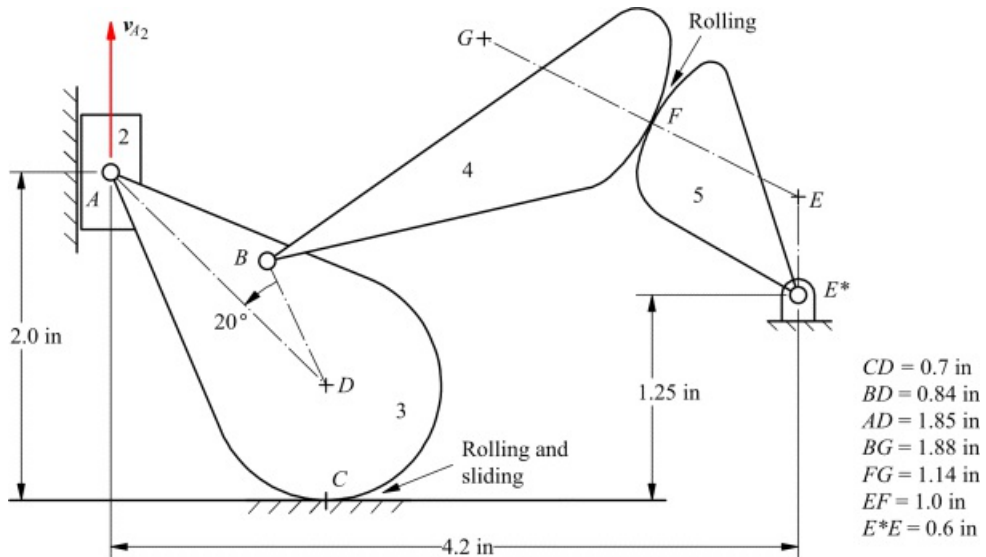
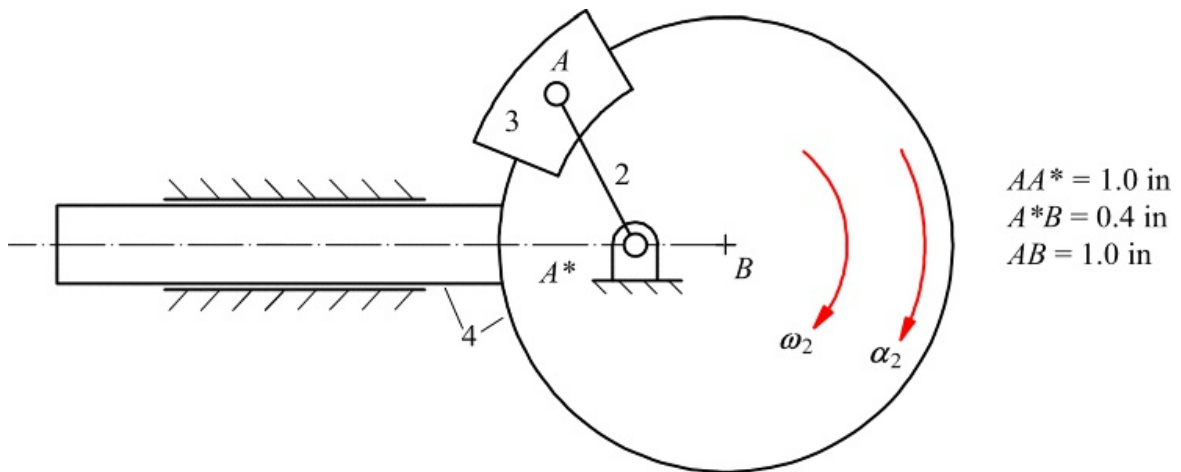


Figure P5.35 Linkage for Problem 5.35.

General Coincident Points

5.36 On the mechanism shown in [Figure P5.36](#), link 4 slides on link 1, and link 3 slides on link 4 around the circle arc. Link 2 is pinned to links 1 and 3 as shown. Determine the location of the center of curvature of the path that point A_4 traces on link 2. Assume that $\omega_2 = 10 \text{ rad/s}$ CW and $\alpha_2 = 100 \text{ rad/s}^2$ CW.



[Figure P5.36](#) Linkage for Problem 5.36.

5.37 For the mechanism shown in [Figure P5.37](#), find ω_2 , α_2 , v_{A2} , a_{A2} , v_{B3} , a_{B3} , and the location of the center of curvature of the path that point A_3 traces on link 2. Assume that $\omega_2 = 10 \text{ rad/s CCW}$ and $\alpha_2 = 100 \text{ rad/s}^2 \text{ CW}$.

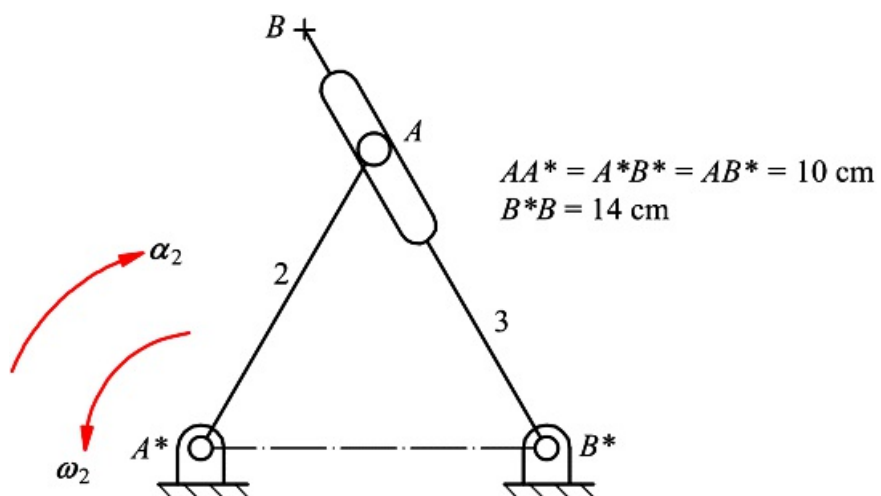


[Figure P5.37](#) Linkage for Problem 5.37.

5.38 If $\omega_2 = 10 \text{ rad/s CCW}$ (constant) in [Figure P5.38](#), find v_{A2} , v_{A3} , a_{A3} , and a_{B4} . The portion of link 2 on which member 3 slides forms the arc of a circle with radius 2 and centered at C.

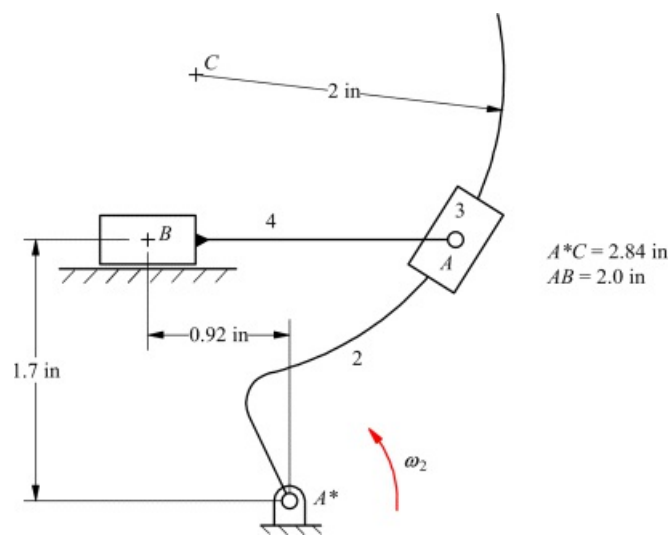


[Figure P5.38](#) Linkage for Problem 5.38.

5.39 In [Figure P5.39](#), $\omega_2 = 10 \text{ rad/s}$ CW (constant). Determine the angular acceleration of link 3 and the linear acceleration of point C on link 4.

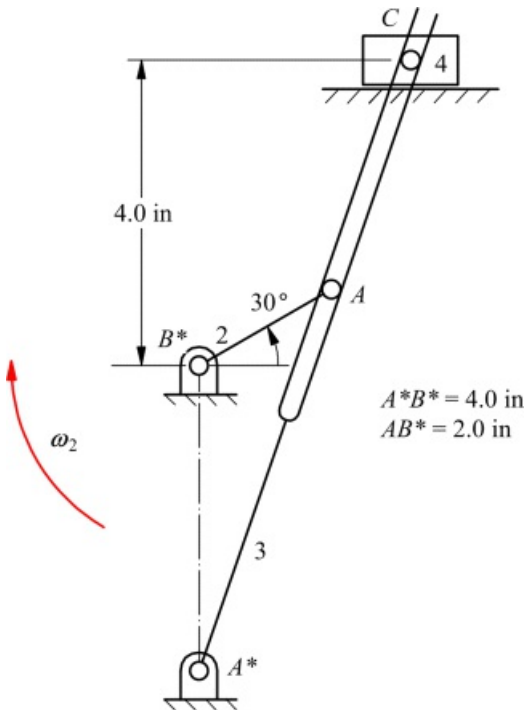


[Figure P5.39](#) Linkage for Problem 5.39.

5.40 In [Figure P5.40](#), slotted links 2 and 3 are independently driven at constant angular velocities of 10 and 20 rad/s CW and have angular accelerations of 100 and 400 rad/s² CW, respectively. Determine the acceleration of point A, the center of the pin carried at the intersection of the two slots.

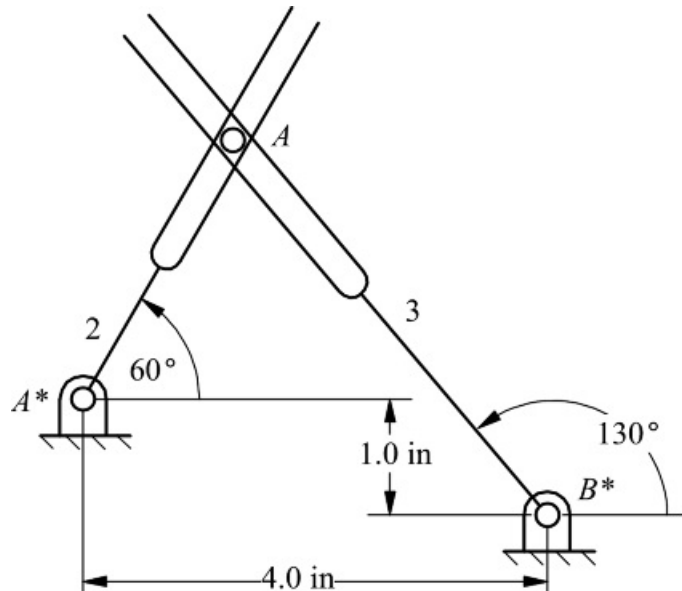


[Figure P5.40](#) Linkage for Problem 5.40.

5.41 For the mechanism shown in [Figure P5.41](#), the path of A on link 3 is a circular arc centered at C . Find ω_3 , a_3 , a_{A3} , and the location of the center of curvature of the path that point A_3 traces on link 2. Assume that $\omega_2 = 100 \text{ rad/s}$ CW (constant).

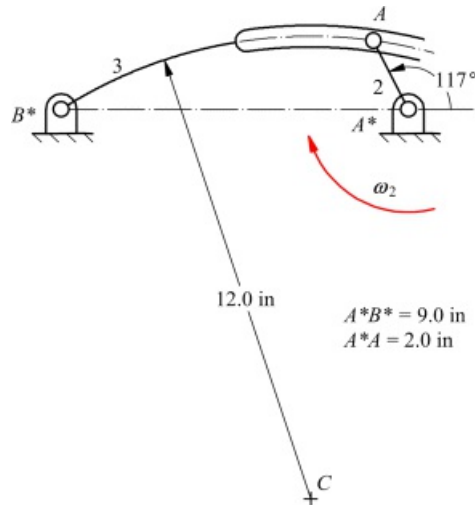


[Figure P5.41](#) Linkage for Problem 5.41.

5.42 For the mechanism shown in [Figure P5.42](#), points B^* , A , and D are collinear. Point A_2 moves in a curved slot on link 3 with center of curvature at C . For the position given, find ω_3 , a_3 , v_{A_3} , a_{A_3} , v_{D_3} , a_{D_3} , and the location of the center of curvature of the path that point A_3 traces on Link 2. Assume that $\omega_2 = 10 \text{ rad/s}$ CCW and $\alpha_2 = 30 \text{ rad/s}^2$ CCW.

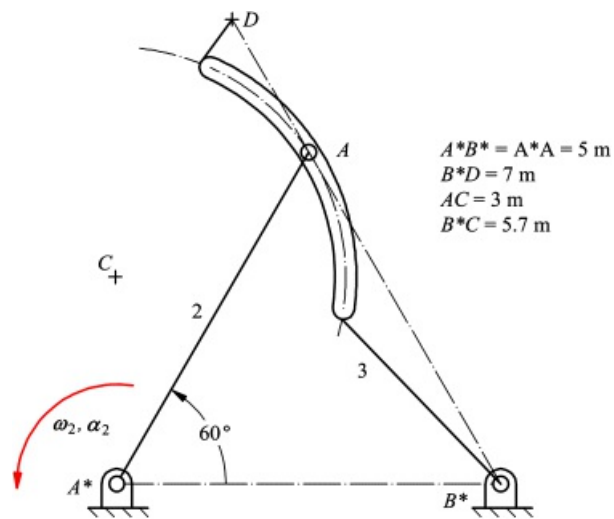


[Figure P5.42](#) Linkage for Problem 5.42.

5.43 For the mechanism shown in [Figure P5.43](#), find ω , a_3 , and the location of the center of curvature of the path that point A_3 traces on link 2. Assume that $\omega_2 = 100 \text{ rad/s}$ CW (constant).

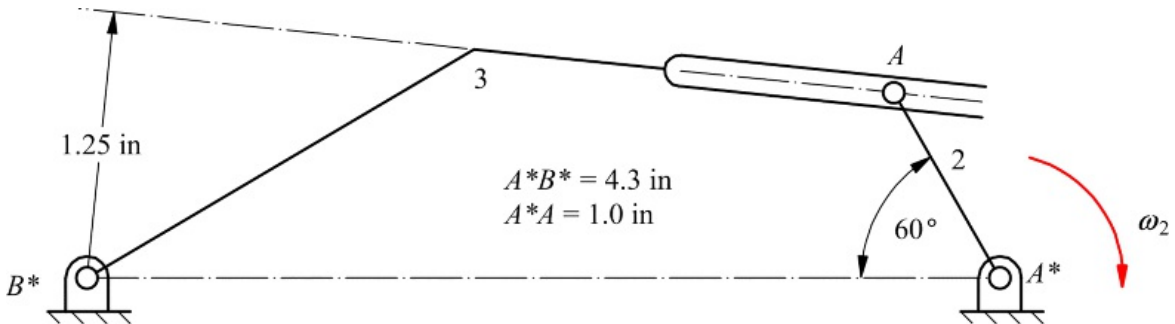


[Figure P5.43](#) Linkage for Problem 5.43.

5.44 If $\omega_2 = 10 \text{ rad/s}$ CCW (constant) in [Figure P5.44](#), find ω_3 , a_3 , and the center of curvature of the path

that A_3 traces on link 2. The slot on link 3 is a circular arc centered at B .

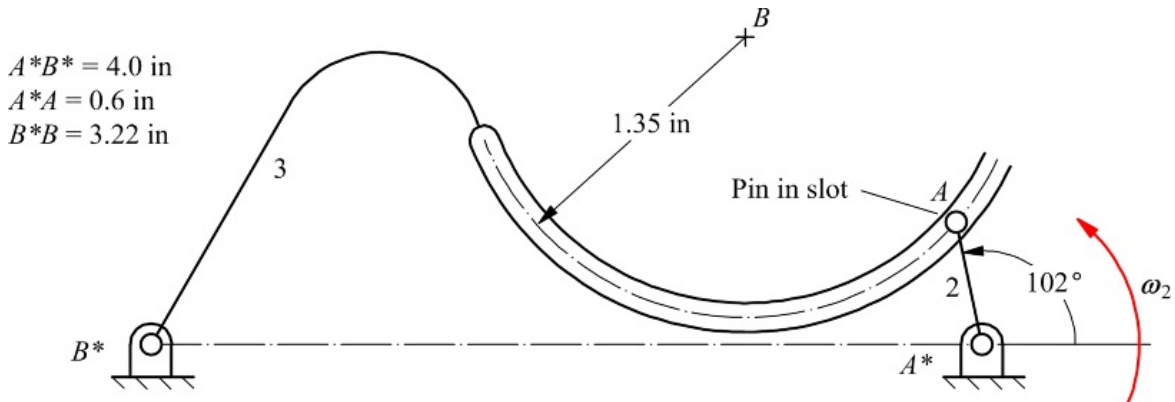


Figure P5.44 Linkage for Problem 5.44.

5.45 In Figure P5.45, if $\omega_2 = 10$ rad/s CW (constant), find α_3 .

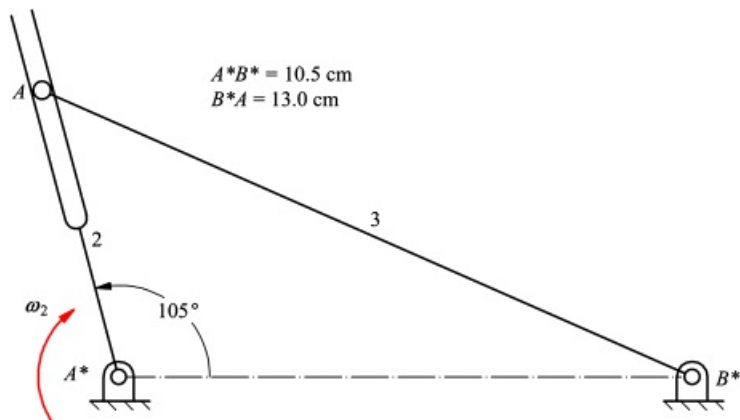


Figure P5.45 Linkage for Problem 5.45.

5.46 For the linkage shown in Figure P5.46, $\omega_2 = 20$ rad/s CCW and $\alpha_2 = 400$ rad/s² CCW. Determine ω_3 , and α_3 . The slot on link 3 that constrains pin A follows a circular arc centered at B .

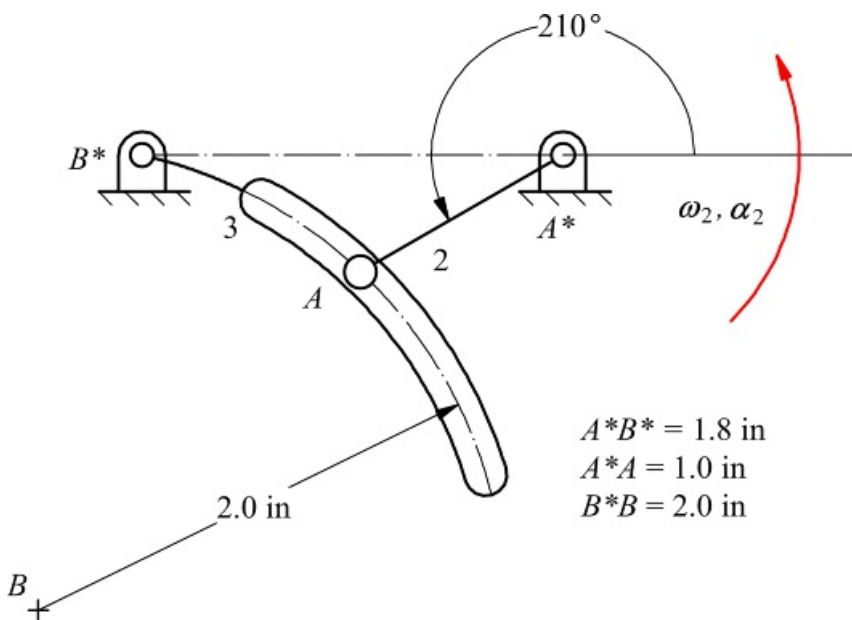


Figure P5.46 Linkage for Problem 5.46.

5.47 If $\omega_2 = 100$ rad/s CW (constant), find

- ω_3
- The center of curvature of the path that A_2 traces on link 3 (show on drawing).
- The center of curvature of the path that A_3 traces on link 2 (show on drawing).

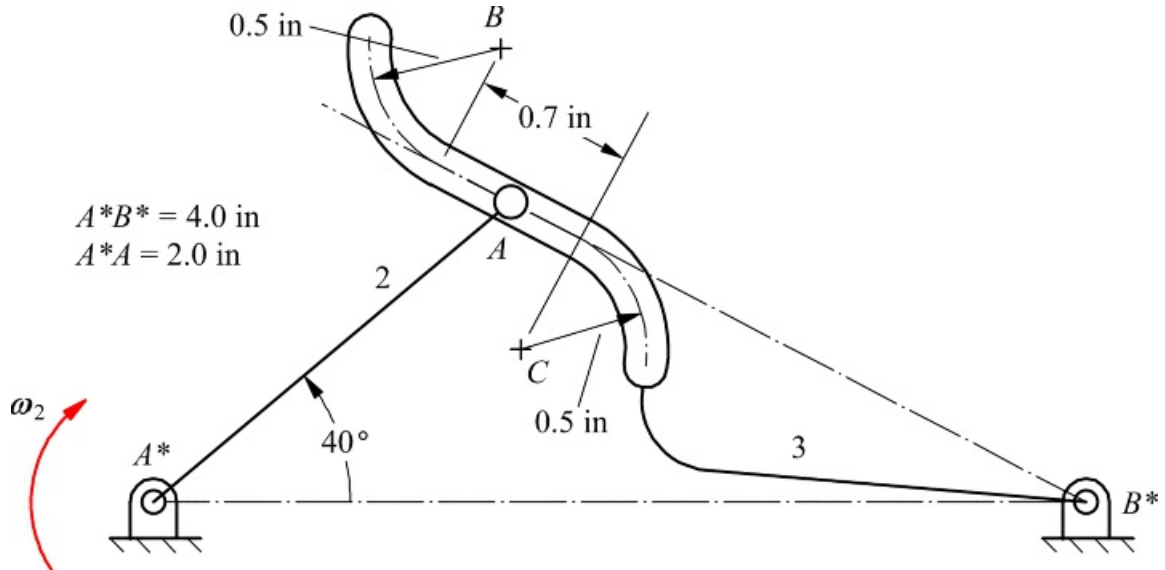


Figure P5.47 Linkage for Problem 5.47.

6

INSTANT CENTERS OF VELOCITY

Prerequisite Knowledge Needed for Chapter 6

A familiarity with the relative velocity equations from [Chapters 4](#) and [5](#), a familiarity with rolling contact from [Chapter 5](#), and a knowledge of Geometric Constraint Programming (GCP) from [Chapter 2](#).



6.1 Introduction

At every instant during the motion of a rigid body in a plane, there exists a point that is instantaneously at rest. This point is called the instant center with respect to the ground link. The concept of an instant center of velocity for two bodies with planar motion was first discovered by Johann Bernoulli in 1742 [2]. This concept was later extended by Chasles in 1830 [3] to include general spatial motion using the instantaneous screw axis concept.

The instant center technique for velocity analysis is particularly useful when only two or three velocities, or angular velocities, are of interest. It can be a very efficient technique, for example, for finding input-output velocity relationships of very complex mechanisms. When combined with virtual work, or conservation of energy ([Chapter 14](#)), it provides an efficient way to obtain input-output force or torque relationships and mechanical advantage. Instant centers are also very helpful when analyzing mechanisms with higher pairs, such as cam mechanisms, or gear trains. In principle, the instant center and velocity polygon techniques are *alternative* methods for solving the same set of problems. However, they are quite different techniques, and each is better suited to some situations than to others. Some experience is necessary to identify easily the most applicable technique for a particular problem.

It should be emphasized that instant centers of velocity are applicable to velocities *only* and are usually of no help if accelerations are ultimately of interest. If an acceleration analysis must be performed, then the velocity analysis should be conducted using one of the previously discussed traditional procedures based on vector methods.

There is also an instant center of acceleration for each link of a mechanism. However, instant centers of acceleration are of little use during the initial kinematic analysis. This is because, in general, more calculations are required to find the instant center of acceleration than would be required to find the accelerations of interest using methods previously outlined. Therefore, only instant centers of velocity will be considered here.



6.2 Definition

Given two bodies B and C moving with planar motion relative to each other and with the motion defined in a reference frame R , there is, in general, one and only one location P in the plane of motion where the coincident points at a given instant have the same velocity with respect to the reference frame R . One coincident point is fixed to body B and the other is fixed to body C . This location is called the instant center of velocity for bodies B and C and is represented by I_{BC} or I_{CB} . If P is the instant center location, then

$${}^B\omega_{P_B} = {}^C\omega_{P_C}$$

or

$${}^B\omega_{P_B/P_C} = {}^R\omega_{P_C/P_B} = \dot{\theta}$$

If the points are permanently attached to each other, they are called permanent instant centers. If the points are only momentarily coincident, they are called instantaneous instant centers.



6.3 Existence Proof

The existence of an instant center between arbitrary links B and R may be inferred, and its location found, by the use of the relationship between the velocities of two points in body B . In the following, all velocities are defined relative to system R , so the left superscript designating the coordinate system (R) will be omitted for simplicity.

$$\dot{v}_{P_B} = \dot{v}_{Q_B} + \omega_B \times r_{P/B}$$

Now, assume that Q is the instant center I_{BR} . Then, $\dot{v}_{Q_B} = 0 = \dot{v}_{I_{BR}}$ and

$$\dot{v}_{P_B} = \omega_B \times r_{P/Q} \quad (6.1)$$

From Section 4.4, we know that the radial component of the relative acceleration between two points P and Q on the same rigid link B is

$$\omega_B \times (\omega_B \times r_{P/Q}) = -\alpha_B^2 r_{P/Q}$$

Therefore, cross multiplication of both sides of [Equation 6.1](#) by ω_B gives

$$\omega_B \times \dot{v}_{P_B} = \omega_B \times (\omega_B \times r_{P/Q}) = -\alpha_B^2 r_{P/Q}$$

or

$$r_{P/Q} = -\frac{\dot{v}_{P_B}}{\alpha_B^2}$$

In planar motion $\omega_B \times \dot{v}_{P_B}$ is normal to \dot{v}_{P_B} and may be written as $(\omega_B)(\dot{v}_{P_B})n$, where n is a unit vector normal to \dot{v}_{P_B} with the sense given by visualizing \dot{v}_{P_B} rotating about its tail in the ω_B direction. Hence

$$r_{P/Q} = -\frac{\omega_B \times \dot{v}_{P_B}}{\alpha_B^2}$$

Thus, the distance, $r_{P/Q}$, in [Figure 6.1](#) from the instant center, I_{BR} , to point P is v_{P_B}/ω_B and the line IP is normal to \dot{v}_{P_B} . Its sense is such that rotation of $r_{P/Q}$ about I_{BR} in the ω_B direction produces \dot{v}_{P_B} .

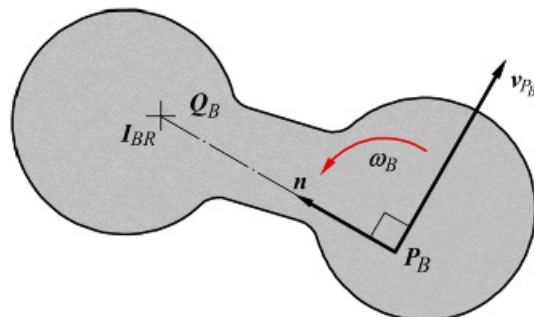


[Figure 6.1](#) Proof of the existence of an instant center of velocity in planar motion.

If more than one location in the plane of motion is found to be an instant center for two bodies, then those two bodies, for velocity analysis purposes, can be considered to be instantaneously fixed to each other. That is, if more than one location is an instant center, then all locations are instant centers. On the other hand, if no finite location can be found that qualifies as an instant center of relative motion of two bodies, then the two bodies are translating with planar motion with respect to each other. In this case, the instant center can be considered to be located at infinity and reached by a line drawn perpendicular to the relative velocity vector between two arbitrary, coincident points in the two bodies considered.

Instant centers are useful because they permit velocities to be computed easily. For example, if Q is the instant center location I_{BR} and we know the velocity of point \mathcal{Q}_1 by analysis, we know the velocity of \mathcal{Q}_2 directly.



6.4 Location of an Instant Center from the Directions of Two Velocities

Assume that we know the velocities of two points (P and Q) in body C where the velocities are defined relative to the coordinate system in a second body B . This condition is shown in [Figure 6.2](#). We can then search for some point in C that has zero velocity relative to body B . The location of this point is the instant center designated by I_{BC} or, in the development here, it can be represented simply as I . To find the instant center location, let I_B be the point in body B and I_C be the coincident point in body C . We can write relative velocity expressions for points P and Q as follows

$$\mathcal{B}v_{P_C} = \mathcal{B}\gamma_{P_C/I_B} = \mathcal{B}v_{P_C/I_C} + \mathcal{B}\gamma_{I_C/I_B}$$

and

$$\mathcal{B}v_{Q_C} = \mathcal{B}v_{Q_C/I_B} = \mathcal{B}\gamma_{Q_C/I_C} + \mathcal{B}v_{I_C/I_B}$$

However, by definition of the instant center

$$\mathcal{B}v_{I_C/I_B} = \mathcal{B}v_{I_C} = 0$$

so that

$$\mathcal{B}v_{P_C/I_B} = \mathcal{B}v_{P_C/I_C} = \mathcal{B}\omega_C \times \mathcal{B}r_{P_C/I_C}$$

and

$$\mathcal{B}v_{Q_C/I_B} = \mathcal{B}v_{Q_C/I_C} = \mathcal{B}\omega_C \times \mathcal{B}r_{Q_C/I_C}$$

By definition of the cross product, $\mathcal{B}v_{P_C/I_C}$ must be perpendicular to $\mathcal{B}r_{P_C/I_C}$ and $\mathcal{B}v_{Q_C/I_C}$ must be perpendicular to $\mathcal{B}r_{Q_C/I_C}$. The location of the instant center (I_{BC}) is given by the intersection of the two perpendicular lines as shown in [Figure 6.2](#).

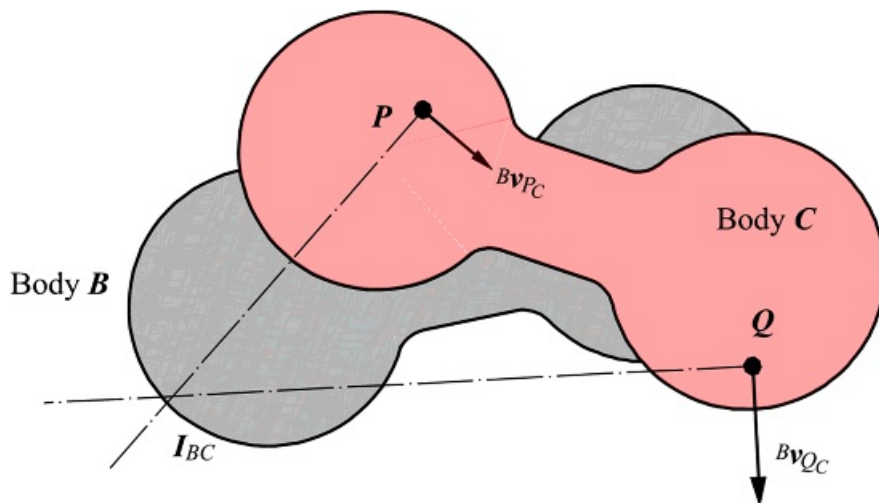


[Figure 6.2](#) Location of the instant center given the directions of the velocities of two points.



6.5 Instant Center at a Revolute Joint

The center of rotation at a revolute joint, I_{BC} , has the same velocity whether it is considered to be part of link B or link C . Therefore, it qualifies as a permanent instant center. This is indicated in [Figure 6.3](#).

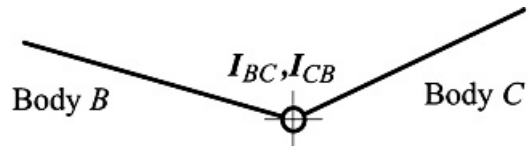


[Figure 6.3](#) Permanent instant center at the center of a revolute joint.



6.6 Instant Center of a Curved Slider

If body B is a block moving on a circular arc on body C as shown in [Figure 6.4](#), then the center of the arc is a stationary location common to both bodies. Therefore, this location qualifies as a permanent instant center. If the curve is not circular at the location of interest, it can be replaced by its osculating circle (for velocities and accelerations) and the center of the osculating circle or center of curvature of the path at the given point is the instant center. Actually, a circular slider is kinematically equivalent to a revolute joint. The center of the equivalent revolute is the center of curvature. That is, it is the instant center. A noncircular slide is realizable only as a higher pair.

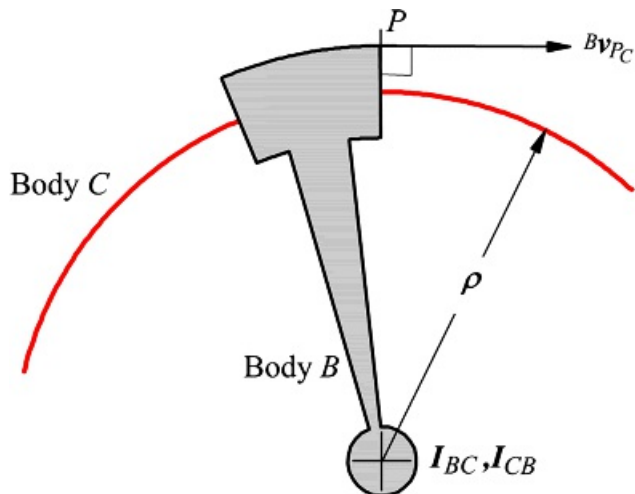


[Figure 6.4](#) Instant center of a curved slide.



6.7 Instant Center of a Prismatic Joint

If the radius of curvature, ρ , in the case of the curved slider is allowed to become very large, the arc will approach a straight line. Also, the location of the instant center will tend toward infinity. However, the velocity of P relative to system B will still remain perpendicular to the line from P to the instant center. Therefore, if we know the direction of the velocity of *any* point P relative to system B , we can find one locator for the instant center; that is, it must lie on a line perpendicular to the velocity vector as shown in [Figure 6.5](#).

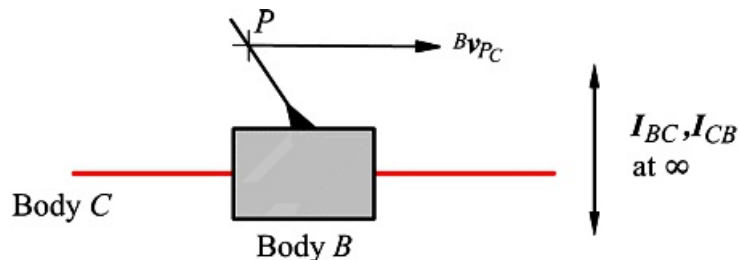


[Figure 6.5](#) Instant center of a prismatic joint.

Note that the location of the line to infinity is unimportant; only the direction is defined by the velocity direction. This can be thought of as being the parallax phenomenon in which the direction to a distant object appears to remain the same, regardless of the location of the observer.



6.8 Instant Center of a Rolling Contact Pair

The instant center of pure rolling contact between two rigid bodies B and C is located at the point of contact of the two bodies as shown in [Figure 6.6](#). This is a direct consequence of the rolling condition that the two points in contact be at rest relative to one another. The instant center for the relative motion of involute spur gears is at the pitch point: the point of rolling contact between their pitch circles.

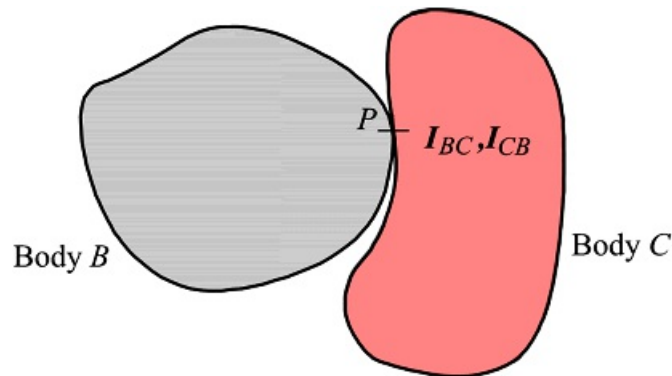


[Figure 6.6](#) Instant center of a rolling contact.



6.9 Instant Center of a General Cam-Pair Contact

When two planar bodies (B and C in [Figure 6.7](#)) are held in general cam contact, it is assumed that the bodies will neither penetrate each other nor separate. In general, the bodies both roll and slide on each other. If sliding is involved, the direction of relative sliding must be along the common tangent of the profiles of the two bodies as shown in [Figure 6.7](#). If P is the contact point location, then the velocity of point P_C relative to body B as well as the velocity of point P_B relative to body C will lie along the common tangent. Therefore, the instant center must be located on a line through P and perpendicular to the common tangent at the contact point P . This means that the instant center and the two centers of curvature (O_B and O_C) corresponding to P must be colinear.

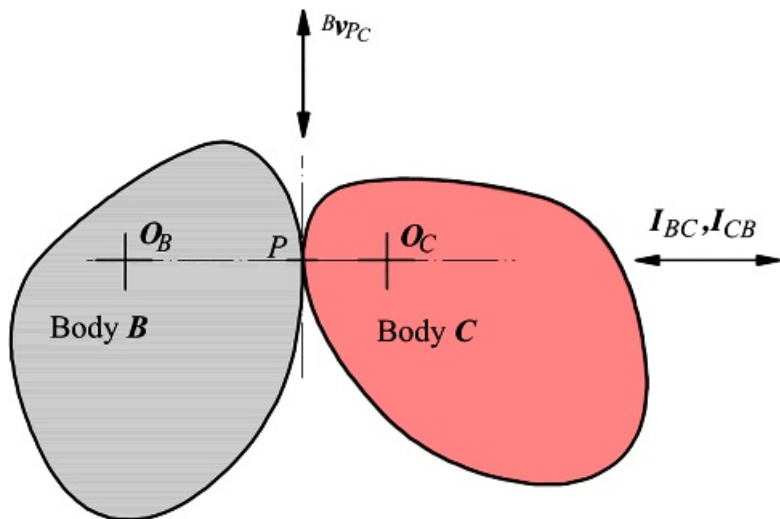


[Figure 6.7](#) Relationship between instant centers and sliding velocity in cam contact.

To locate precisely the position of I_{BC} , some further information about the relative motion of bodies B and C is required. For example assume that body B is link 2 and body C is link 3 and that links 2 and 3 are both connected to the frame by revolute joints as shown in [Figure 6.8](#). If we arbitrarily pick the point A as a candidate for the instant center, we see that the velocities v_{A2} and v_{A3} cannot be equal because they are not in the same direction. The only location where they can be equal in direction is at the point Q on a line through the two pivots. Note that the two fixed pivots are the instant centers I_{12} and I_{13} .

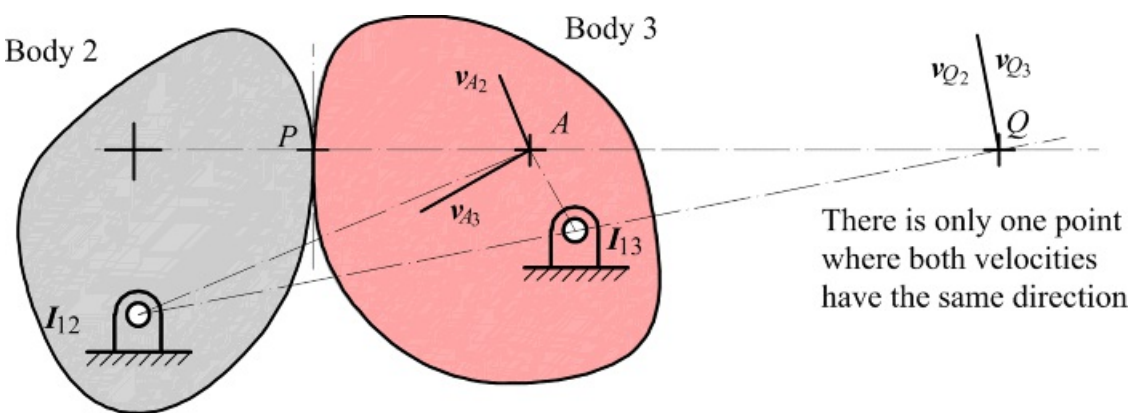


[Figure 6.8](#) The instant center location between two frame-mounted cams.



6.10 Centrodes

As two bodies, B and C , move relative to each other, I_{BC} traces a path on each of the bodies (path BC_B on body B and BC_C on body C). These paths are called the centrodes for the two bodies [4]. At any instant, the two paths will be in contact with each other at the instant center where there is zero relative velocity between the two bodies and therefore between the two centrodes. That is, the instant center acts as a point of rolling contact between the two centrodes. This means that as the two bodies move, the two centrodes will roll on each other. Conversely, the relative motion of the two bodies can be faithfully reproduced by rolling one centrode on the other no matter how the original motion was produced. Therefore, the analysis of the relative motion of two bodies moving with planar motion can always be transformed to the study of the centrodes for the two bodies rolling on each other.

These concepts can be extended into spatial motion in which the instant center becomes an instantaneous screw axis (ISA), and the loci of the ISAs in the two bodies are ruled surfaces called axodes [5]. These axodes roll on each other in a direction perpendicular to their generating instantaneous screw axes as well as sliding relative to each other along their instantaneous screw axes.

An example of the fixed and moving centrodes associated with the coupler of a four-bar linkage is shown in [Figure 6.9](#). This shows the centrodes generated by instant center I_{13} . The centrodes in [Figure 6.9](#) are very simple, but this is not the typical case. For crank-rocker mechanisms, the centrodes will extend to infinity (when the crank and rocker are parallel) in two directions, and for drag-link mechanisms, the centrodes can form multiple loops. Typical examples are shown in [Figures 6.10](#) and [6.11](#). These centrodes were generated with the MATLAB program *centrodes.m* included in the supplementary material for this book.

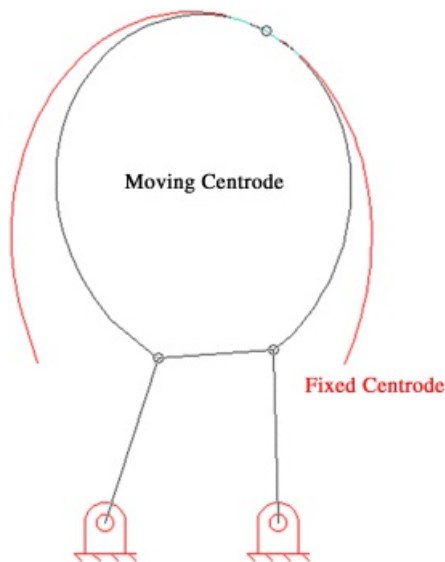


[Figure 6.9](#) Centrodes associated with instant center I_{13} for a double-rocker four-bar linkage.

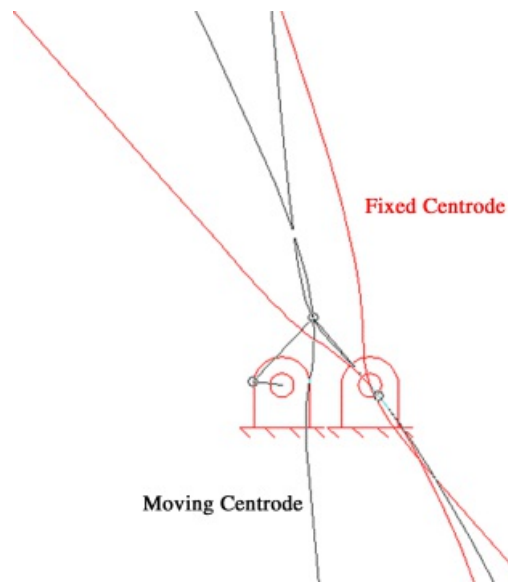


[Figure 6.10](#) Centrodes associated with instant center I_{13} for a crank-rocker four-bar linkage.

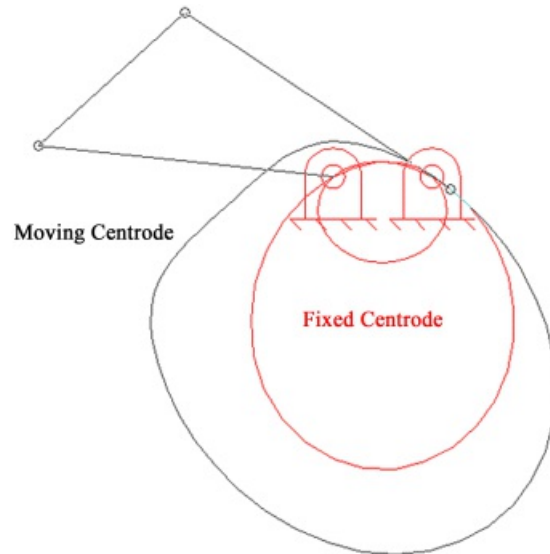


[Figure 6.11](#) Centrodes associated with instant center I_{13} for a drag-link four-bar linkage.

Another example of centrodes is shown in the model in [Figure 6.12](#). The mechanism model is a six-bar linkage, and the noncircular gears attached to the two frame-mounted links correspond to the centrodes of relative motion of those links. The motion of the two links attached to the gears is the same relative to the frame and to each other if the linkage is present without the gears and with the gears present but without the linkage.



[Figure 6.12](#) Six-bar linkage model with centrododes represented by noncircular gears. The gears roll on each other at the pitch points, and the pitch point is the instant center between the two frame-mounted cranks.



6.11 The Kennedy-Aronhold Theorem

If we have n bodies and we take them two at a time such that $I_{AB} = I_{BA}$, then the total number of instant centers is given by

$$M_{IC} = \frac{n(n-1)}{2} \quad (6.2)$$

Because of the large number of instant centers (ICs) occurring in a mechanism with a large number of links, it is desirable to develop a procedure that helps to identify the locations of the instant centers in a systematic manner. This can be done using the results of the Kennedy-Aronhold theorem.

In the late nineteenth century, Kennedy [6] from England and Aronhold [1] from Germany greatly extended the usefulness of instant centers by independently discovering the theorem of three centers. The theorem is stated as follows:

If three bodies are in relative planar motion (or two bodies moving relative to each other and to the fixed reference frame), there are three instant centers pertaining to the relative motion of pairs of those bodies. Those three instant centers are collinear.

Thus given three bodies A , B , and C moving with planar motion in reference frame R , the three instant centers I_{AB} , I_{AC} , and I_{BC} all lie on the same straight line in the plane as illustrated in [Figure 6.13](#). To prove the theorem, it is necessary to recognize that the instant center is really the location of two coincident points. One of these two points is embedded in each of the two laminae for which the instant center describes the relative motion. Hence, in [Figure 6.13](#)

I_{AB} corresponds to two points common to A and B

I_{AC} corresponds to two points common to A and C

I_{BC} corresponds to two points common to B and C

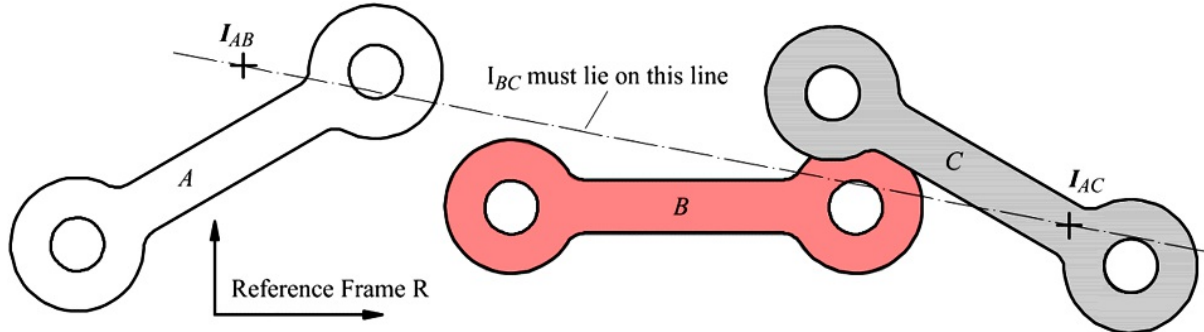


[Figure 6.13](#) Graphical representation of the Kennedy-Aronhold theorem.

Also,

$${}^R\varphi_{(I_{AB})_A} = {}^R\varphi_{(I_{AB})_B}$$

$${}^R\varphi_{(I_{AC})_A} = {}^R\varphi_{(I_{AC})_C}$$

$${}^A\gamma_{(I_{BC})_B} = {}^A\gamma_{(I_{BC})_C}$$

Assume that we know the locations of I_{AB} and I_{AC} and we want to find I_{BC} . We can first write

$${}^A\gamma_{(I_{BC})_B} = {}^A\gamma_{(I_{BC})_C}$$

Or because

$${}^A\gamma_{(I_{BC})_A} = {}^A\gamma_{(I_{BC})_B} = 0$$

$${}^A\gamma_{(I_{BC})_B} = {}^A\gamma_{(I_{BC})_B/(I_{AB})_A} = {}^A\gamma_{(I_{BC})_B/(I_{AC})_A} = {}^A\omega_B \times r_{I_{BC}/I_{AB}}$$

Also

$${}^A\gamma_{(I_{BC})_C} = {}^A\gamma_{(I_{BC})_C/(I_{AC})_A} = {}^A\gamma_{(I_{BC})_C/(I_{AB})_B} = {}^A\omega_C \times r_{I_{BC}/I_{AC}}$$

or equating the two relationships

$${}^A\omega_C \times r_{I_{BC}/I_{AC}} = {}^A\omega_B \times r_{I_{BC}/I_{AB}}$$

Since ${}^A\omega_C$ is parallel to ${}^A\omega_B$, then the r 's must also be parallel to make the cross products equal. Because both of the r 's pass through I_{BC} , they must be collinear. This can happen only if I_{AB} , I_{AC} , and I_{BC} all lie on the same line.

The Kennedy-Aronhold theorem can be used in the following way to find instant centers. Assume that we have two groups of three links such that two links are common to both groups. For example, as shown in [Figure 6.14](#), if we have I_{45} and I_{47} and I_{35} and I_{37} , links 5 and 7 are common to both groups. We know that I_{57} must lie on a line through I_{45} and I_{47} , and it must also lie on the line through I_{35} and I_{37} . The location is defined by the intersection of the two lines.

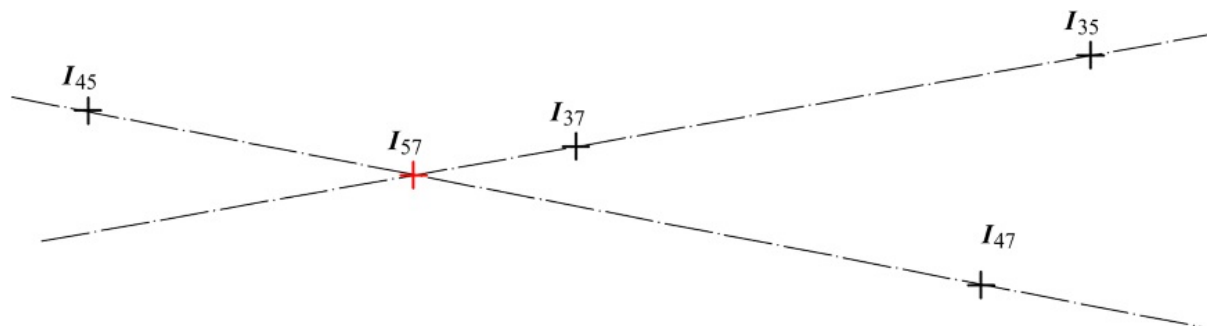


[Figure 6.14](#) Triplets of instant centers.

Therefore, by selecting two pairs of appropriate instant centers, we can locate the instant center that is common to the two groups of links. A way in which the Kennedy-Aronhold theorem can be used is illustrated by Example 6.1.



Example 6.1

Locating Instant Centers for a Four-Bar Linkage

Locate all instant centers of the four-bar linkage in the position shown in [Figure 6.15](#).

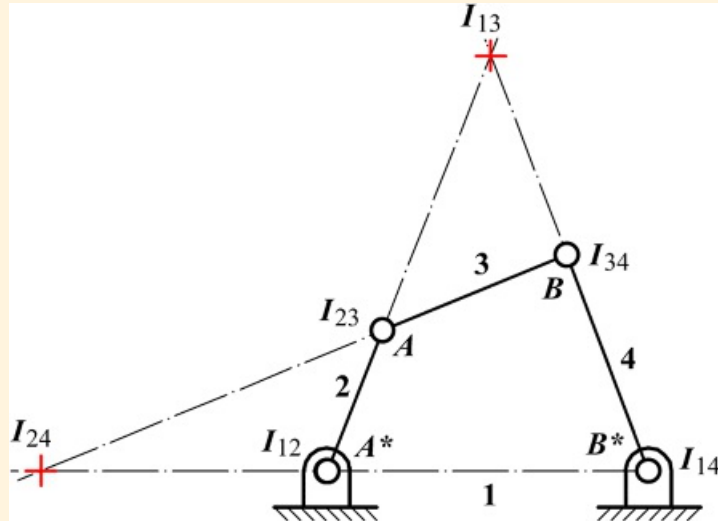


[Figure 6.15](#) Application of the Kennedy-Aronhold theorem to location of all instant centers of a four-bar linkage.

Solution

Based on [Equation 6.2](#), there are six instant centers. By inspection, I_{12} is at A^* , I_{23} is at A , I_{34} is at B , and I_{14} is at B^* . Thus, four of the six instant centers are already identified. To locate I_{13} , note that it is collinear with I_{12} and I_{23} and also with I_{14} and I_{34} . Thus it is at the intersection of AA^* and BB^* . Similarly, to locate I_{24} , note that it is collinear with the line through I_{12} and I_{14} and also with the line through I_{23} and I_{34} . Thus, it is at the intersection of A^*B^* and AB .

A set of three collinear instant centers always shares the same three subscripts, each subscript appearing on two of the instant centers. Given two instant centers with a common subscript, the third instant center, which completes the collinear set, has the two subscripts that are not common to the other two instant centers.



6.12 Circle Diagram as a Strategy for Finding Instant Centers

When the number of bodies is large, it is helpful to use some kind of bookkeeping method to help find all of the instant centers. One such method is the circle method that is based directly on the Kennedy-Aronhold theorem. The procedure is illustrated on the inverted slider-crank linkage in [Figure 6.16](#) as follows:

1. Draw the kinematic diagram for the mechanism to be analyzed.
2. Draw a circle of arbitrary radius and place tick marks representing each link number approximately equally spaced around the perimeter of the circle. Label the tick marks with the link numbers. An instant center will correspond to the *line* between two tick marks, and the instant center will be identified by the numbers at the tick marks.
3. By inspection, determine as many instant centers as possible, and draw a straight line between the corresponding tick marks at the numbers on the circle. For example, if I_{12} is known, then a line is drawn between the tick marks at 1 and 2. In [Figure 6.16](#), we know I_{12} , I_{23} , I_{14} , and I_{34} by inspection. Notice that I_{34} is located at infinity in the direction perpendicular to the relative velocity between links 3 and 4 because of the sliding action (see [Figure 6.5](#)).
4. If a line can be drawn between two tick marks on the circle such that the line is the only unknown side of *two* triangles, the instant center represented by that line can be found. The instant center lies at the intersection of the two lines drawn through the instant center pairs that are represented by the two known sides of each triangle. Once the instant center is located, the appropriate two points on the circle diagram are connected, and that line can be used to identify other instant centers.
5. Repeat the procedure in step 4 until all of the instant centers of interest are found. The originally unknown instant centers I_{13} and I_{24} are shown in red in [Figure 6.16](#).

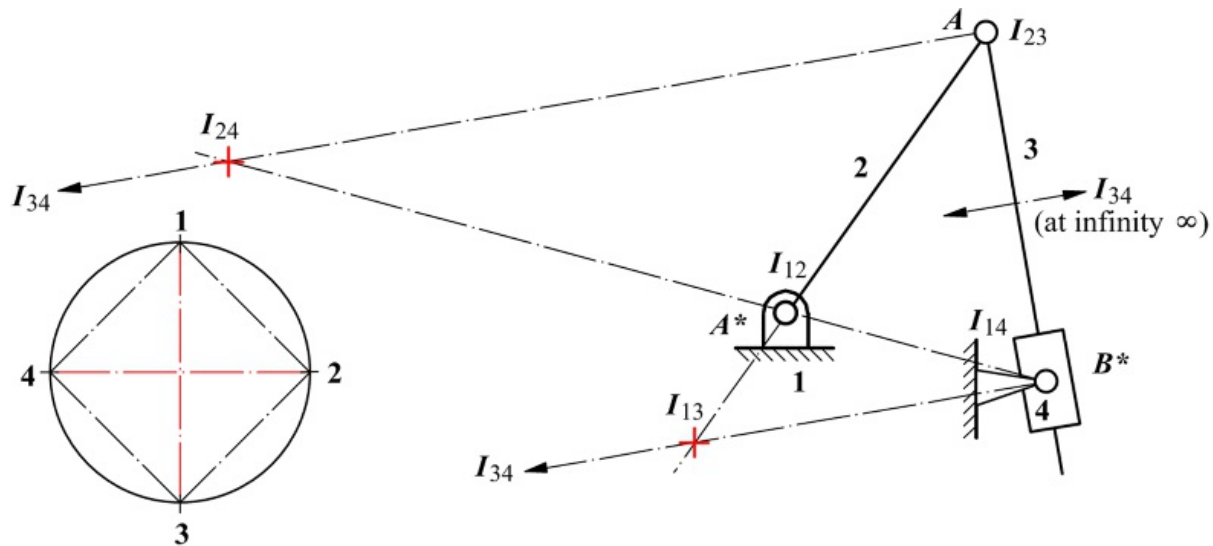


[Figure 6.16](#) Use of the circle diagram when locating instant centers.

As a second example, consider the slider-crank mechanism shown in [Figure 6.17](#). Again, the instant centers to be found are I_{24} and I_{13} . These can be found directly; however, it is again necessary to note that I_{14} is located at infinity along a line perpendicular to the slider velocity direction given.

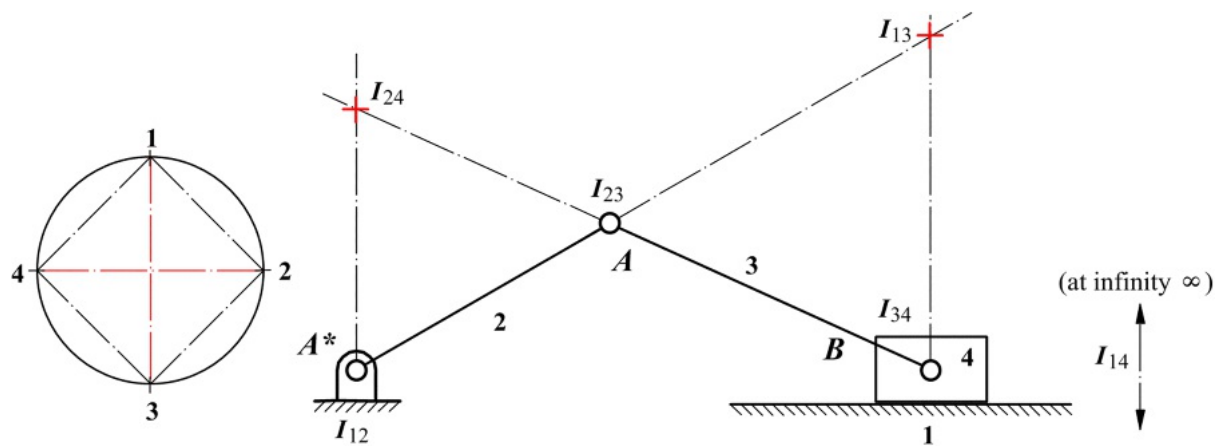


Figure 6.17 The instant centers of a slider-crank linkage.



6.13 Using Instant Centers to Find Velocities: The Rotating-Radius Method

Once the proper instant centers are found, they can be used to find the velocities of selected points in a rigid body. This can be done analytically; however, graphical methods are generally much faster to use. An especially useful method for finding velocities is the rotating radius method. To develop the method, assume we have an arbitrary link moving relative to the reference system. For the sake of illustration, assume that the link is 3 and the reference link is the frame (link 1). Let points P and Q be any points fixed to link 3 as shown in [Figure 6.18](#). Then, we can write

$$\dot{v}_{P_3/Q_3} = \omega_3 \times \dot{r}_{P_3/Q_3} = v_{P_3} - v_{Q_3}$$

and $v_{P_3} - v_{Q_3}$ is perpendicular to the line from P to Q . If point Q_3 has zero velocity relative to link 1, then

$$\dot{v}_{P_3/Q_3} = \dot{v}_{P_3}$$

However, the only point in link 3 that has zero velocity relative to the frame is I_{13} . Therefore

$$\dot{v}_{P_3} = \omega_3 \times \dot{r}_{P_3/I_{13}}$$

Because point P was *any* arbitrary point in link 3, this equation holds for *all* points in link 3. Therefore, if we know the angular velocity of the link and the instant center relative to the frame, we can compute the absolute velocity of any point in the body. Furthermore, the direction of the absolute velocity is perpendicular to the line from the point to the instant center.

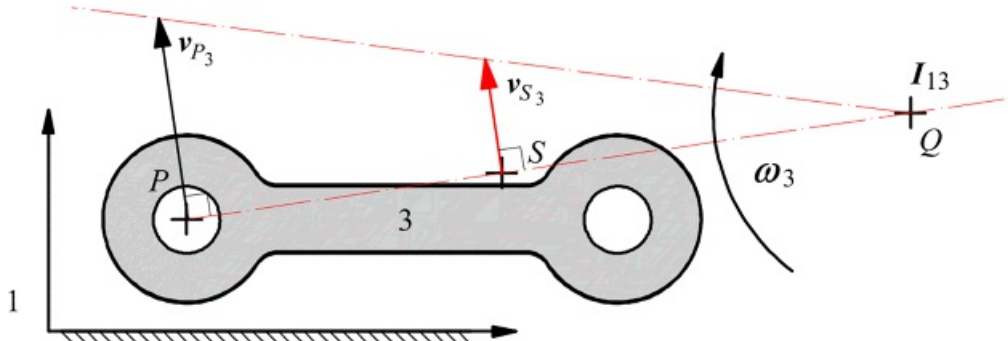


[Figure 6.18](#) The rotating radius method.

For other points, only the vector $\dot{r}_{P_3/I_{13}}$ will change as P changes. Considering the magnitude of the velocity

$$|v_{P_3}| = |\omega_3| |\dot{r}_{P_3/I_{13}}|$$

Because ω_3 is the same for all points in the link, the magnitude of the velocity for any other point S is given by

$$|v_{S_3}| = |\omega_3| |\dot{r}_{S_3/I_{13}}|$$

Therefore, dividing the two equations

$$\frac{|v_{P_3}|}{|v_{S_3}|} = \frac{|v_{P_3/I_{13}}|}{|v_{S_3/I_{13}}|}$$

or

$$|v_{S_3}| = |v_{P_3}| \frac{|v_{E_3/I_{13}}|}{|v_{P_3/I_{13}}|}$$

This magnitude applies to any point that is the same distance from the instant center. The magnitude of the velocity is directly proportional to its distance from the instant center. Hence if two points in the rigid body have the same radius magnitude $r_{S_3/I_{13}}$, they will have the same magnitude of velocity v_{S_3} ; however, the direction of their velocities will differ because the velocity is perpendicular to the line from the point to the instant center. This is illustrated by S and S' in [Figure 6.19](#). The actual direction of the velocity is obtained by recognizing that all points will appear to rotate about the instant center relative to the frame.

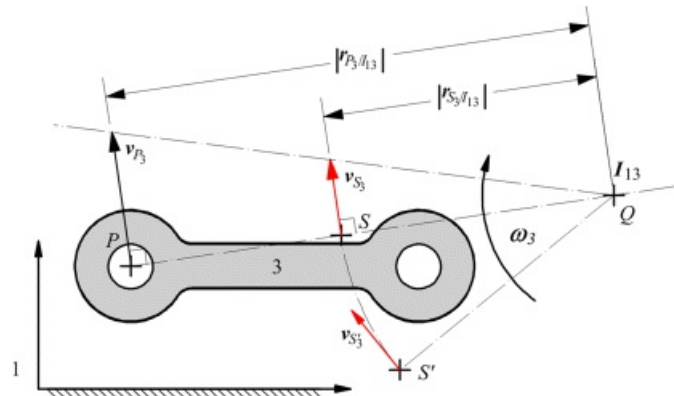


[Figure 6.19](#) The rotating radius method of obtaining the velocity of a point in a body relative to a reference frame (or another body) given the location of the instant center of the body and the velocity of some other point in the body relative to that frame.

This theory is the basis for the rotating radius method. The basic procedure is to find the magnitude of the velocity of one point in the rigid body and draw that velocity vector to scale on the link. The velocity of any other point on the body then can be found by recognizing that the magnitude of the velocity is proportional to the distance from the instant center. Proportional triangles can be drawn by using the line from the original point to the instant center as a base line. Alternately, the line from the new point to the instant center can be used as a baseline.



Example 6.2

Using the Rotating Radius Method to Find Velocities

Given the compound linkage shown in [Figure 6.20](#), the velocity of point A is given as shown. Find the velocity of the point B on link 5.

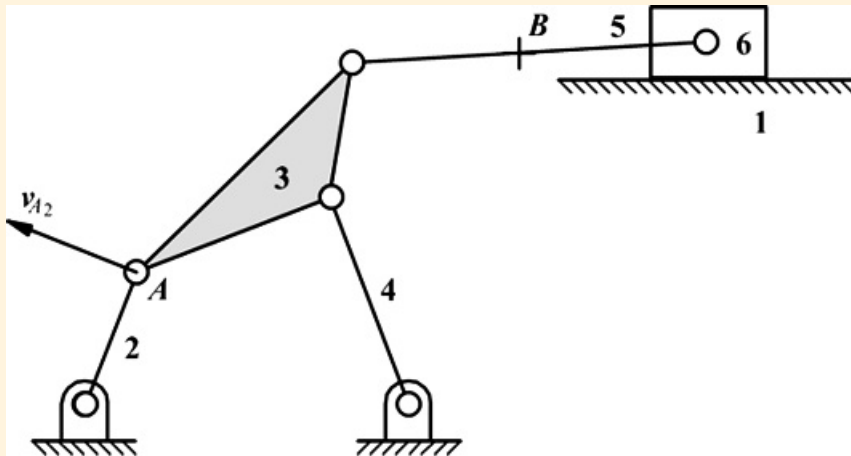


[Figure 6.20](#) Compound linkage for Example 6.2.

Solution

The first step is to determine the instant centers that are needed. This can be done by rewriting the given and desired information in terms of the link numbers and frame number. That is, we are given the velocity v_{A2} and we want to find v_{B5} relative to the frame (link 1). Here we see that the reference system is 1, and the two links involved are 2 and 5. In this problem and in general problems using instant centers, we will need to locate the three instant centers associated with these three links. The instant centers are:

1. I_{12} is the instant center between the reference frame and the link where the input information is given.
2. I_{15} is the instant center between the reference frame and the link where the velocity is to be found.
3. I_{25} is the instant center between the link where a velocity is specified and the link where the velocity is to be found.

When the linkage is analyzed, it is apparent that I_{12} can be found by inspection. Therefore, only I_{25} and I_{15} need to be constructed. This is done by first locating I_{13} using I_{12} and I_{23} and I_{14} and I_{34} . Next, I_{15} is found using I_{13} and I_{35} and I_{16} and I_{56} . Finally, I_{25} is found using I_{15} and I_{12} and I_{23} and I_{35} . The construction lines are shown in [Figure 6.21](#).

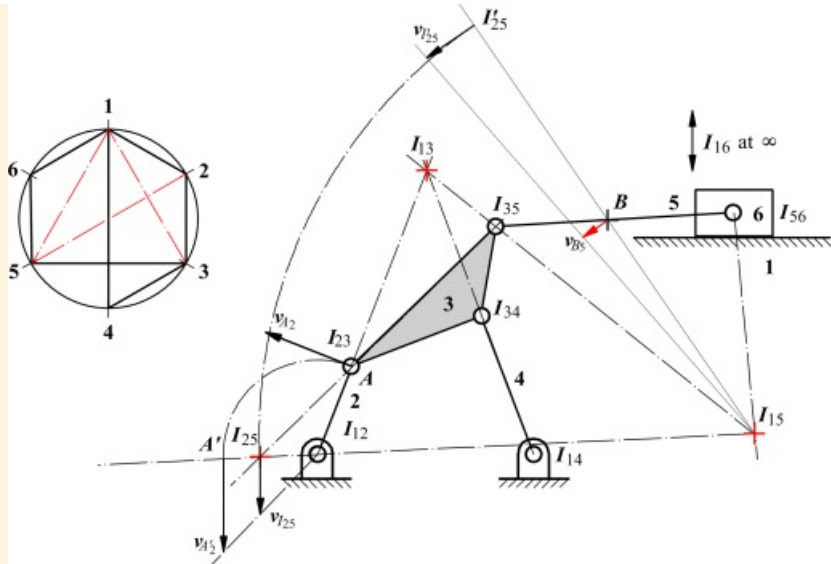


Figure 6.21 Use of the rotating radius method in a compound linkage.

After I_{25} is located, the velocity of I_{25} is found by rotating the triangle formed by the sides v_{A_2} and $I_{12}-A$ about I_{12} onto the baseline through I_{12} and I_{25} . The velocity of I_{25} is then found using proportional triangles. Next, the triangle defined by sides v_{125} and $I_{15}I_{25}$ is rotated about I_{15} onto the baseline through I_{15} and B . The velocity of B is then determined using proportional triangles. Note that when the velocity of I_{25} is found, the instant center is treated as a point in link 2, that is, $(I_{25})_2$. However, when the velocity of B_5 is to be found, the instant center is treated as a point in link 5. This illustrates the fact that the instant center location defines the location of two points, one in link 2 and the other in link 5; however, both points have the same velocity.



Example 6.3

Using Instant Centers to Analyze a Stephenson-II Six-Bar Linkage

Consider the Stephenson-II six-bar linkage in [Figure 6.22](#). Assume that ω_2 is given and we want to find ω_5 . This linkage has the characteristics of those described in Section 4.9; that is the driving link is not included in any four-link loop.

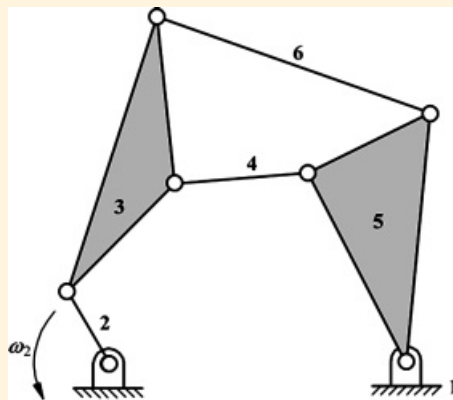


[Figure 6.22](#) Stephenson-II six-bar linkage for Example 6.3.

Solution

The use of instant centers to solve this problem is especially interesting because the linkage cannot be analyzed using the usual vector polygon approach described earlier.

Again, we need to determine which instant centers are required to solve the problem. Taking the frame link (1) as the reference, and looking at the information that is given and that is to be found, we see that three links (1, 2, 5) are identified. Therefore, we need to find I_{12} , I_{15} , and I_{25} . Of this set, only I_{25} cannot be determined by inspection. However, it can be found relatively easily from the instant centers that are available by inspection. First locate I_{35} using I_{36} and I_{56} and I_{34} and I_{45} . Then using I_{35} and I_{23} and I_{12} and I_{15} , locate I_{25} . The resulting instant centers are shown in [Figure 6.23](#). The velocity of the coincident points at I_{25} is given by

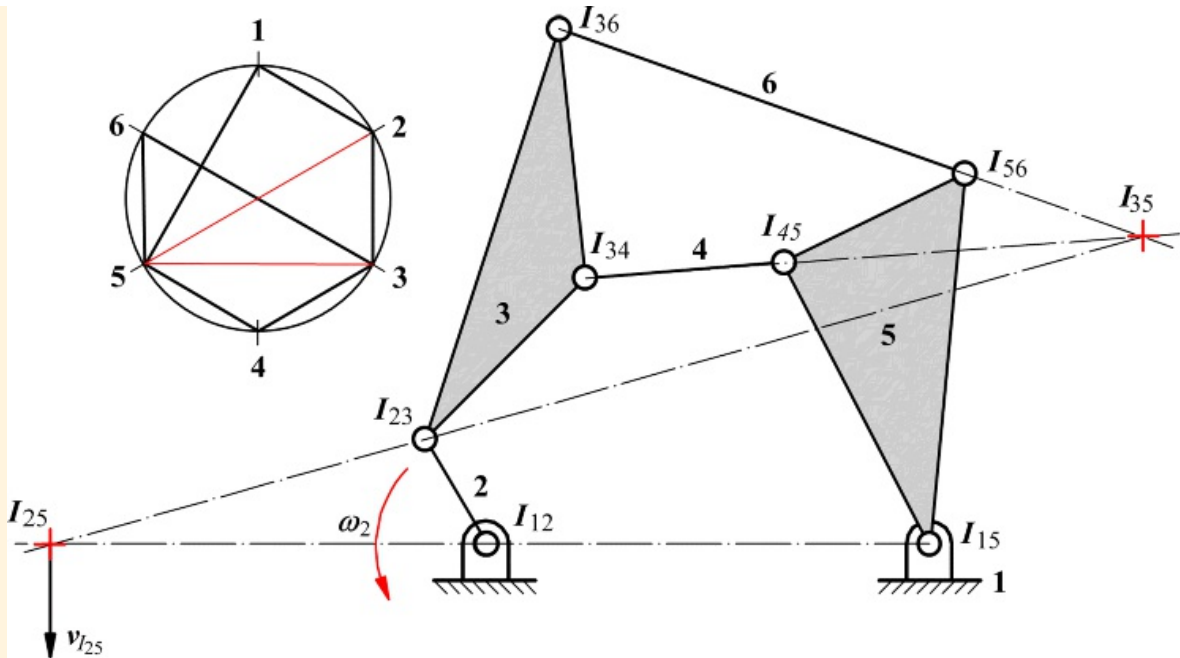


Figure 6.23 The instant-center method applied to a Stephenson-II six-bar linkage.

$$v_{(I_{25})_2} = \omega_2 \times r_{I_{25}/I_{12}} = v_{(I_{25})_5} = \omega_5 \times r_{I_{25}/I_{15}}$$

Therefore, the magnitudes of the vectors are related by

$$|v_{(I_{25})_2}| = |\omega_2| |r_{I_{25}/I_{12}}| = |v_{(I_{25})_5}| = |\omega_5| |r_{I_{25}/I_{15}}|$$

and

$$|\omega_5| = |\omega_2| \frac{|r_{I_{25}/I_{12}}|}{|r_{I_{25}/I_{15}}|} \quad (6.3)$$

This gives the magnitude of ω_5 . We can get the direction by determining the sense of the velocity of $v_{(I_{25})_5}$. Because the vector is generally downward, the angular velocity must be CCW to satisfy the cross product sign convention. In general, if I_{25} lies between I_{12} and I_{15} , then ω_2 and ω_5 will be in opposite directions. Otherwise, ω_2 and ω_5 will be in the same direction.



Example 6.4

Finding Instant Centers for a Quick-Return Mechanism

Find all the instant centers for the quick-return linkage shown in [Figure 6.24](#). The linkage is driven by link 2 rotating about the fixed revolute joint at point A^* . A pin fixed to link 2 at A slides in a slot in link 3. Link 3 rotates about a fixed revolute joint at point B^* . It is hinged at point B with the connecting link, 4. Link 4 connects to the horizontally sliding block, 5, via a revolute joint at point C . This type of linkage is used extensively in some machine tools (planers and shapers) because it generates a relatively slow and uniform forward, or cutting, stroke and a considerably quicker return stroke. The ratio of the durations of the two strokes can be determined by considering the angles through which the drive crank 2 rotates between the extreme positions of the rocker arm 3. The extreme positions are those in which A^*A is normal to B^*B .

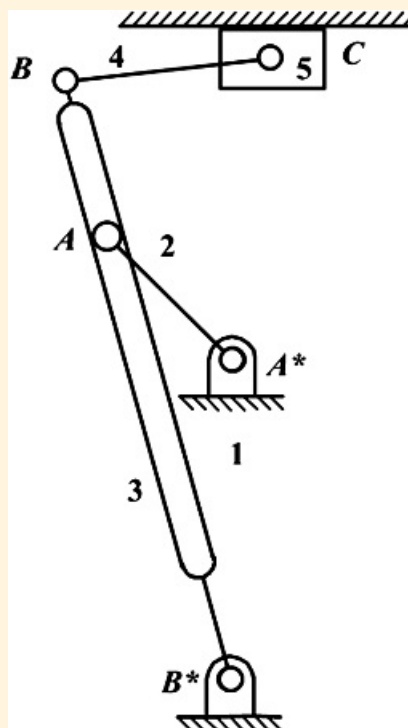


[Figure 6.24](#) The linkage for Example 6.4.

Solution

The instant centers are shown in [Figure 6.25](#). In practice, it is seldom necessary to locate all instant centers. The great advantage of the instant center technique is its ease of use for complicated linkages, particularly when only the angular velocity of one member or the velocity of one point is to be found. For this problem, only three instant centers are needed, although others may be required in the process of locating the three needed ones. The three instant centers needed are the set for the input link, output link, and base link. Here, the input link is the link whose angular velocity is given, or which contains a point whose velocity is given. The output link is the link whose angular velocity is sought or which contains the point whose linear velocity is sought.

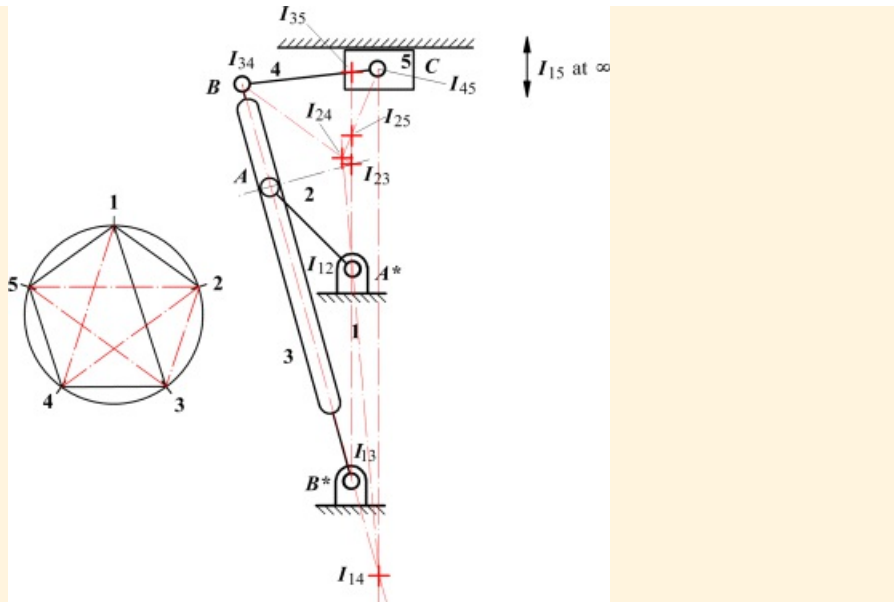


[Figure 6.25](#) Location of instant centers for Example 6.4.

When locating I_{25} , a problem comes up if we try to use I_{12} and I_{15} and I_{23} and I_{35} because the resulting lines are collinear. There is only one location for I_{25} , but it is not indicated by this set of points. When this happens, we need to look for an alternate set of points to use. If we use I_{12} and I_{15} and I_{24} and I_{45} , we get a unique intersection, which reveals the location of I_{25} . A more difficult case when we have non-intersecting lines is given in Example 6.5.



Example 6.5

Finding Instant Centers of a Quick-Return Mechanism in a Singular Position

Find all the instant centers of the quick-return linkage in Example 6.4 when point C is collinear with A^* and B^* . This is shown in [Figure 6.26](#).

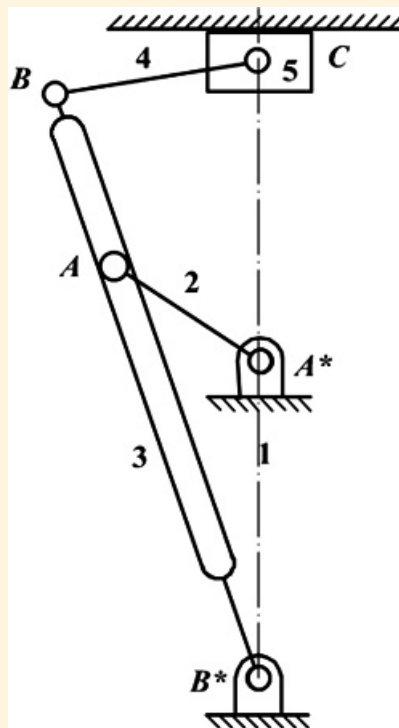


[Figure 6.26](#) The linkage for Example 6.5.

Solution

If an attempt is made to find the instant centers with the procedure used in Example 6.4, it will be possible to find I_{23} and I_{35} directly as shown in [Figure 6.27](#). However, it is not possible to find the locations of the remaining instant centers by simple construction because all of the remaining instant centers are located on the line defined by I_{12} and I_{13} . To determine the location of the remaining instant centers, let point C be moved slightly off of the line defined by I_{12} and I_{13} and locate the instant centers. The location of the instant centers in the true position can then be determined by visualizing their movement as C approaches its actual position. This is shown in [Figures 6.28](#) and [6.29](#). Note that as C moves toward the vertical position, I_{35} becomes coincident with I_{45} , I_{14} becomes coincident with I_{13} , and I_{25} and I_{24} become coincident with I_{23} .

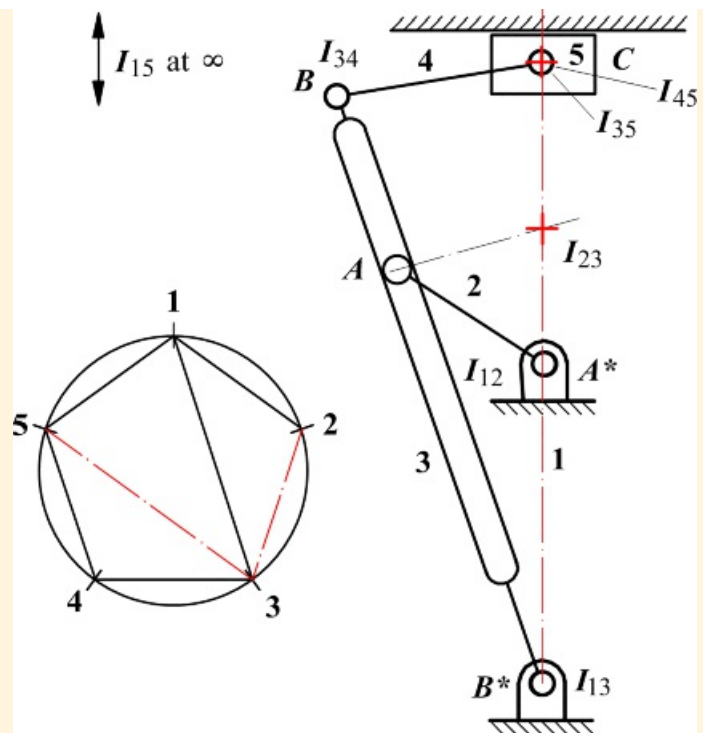


[Figure 6.27](#) Location of I_{23} and I_{35} in Example 6.5.

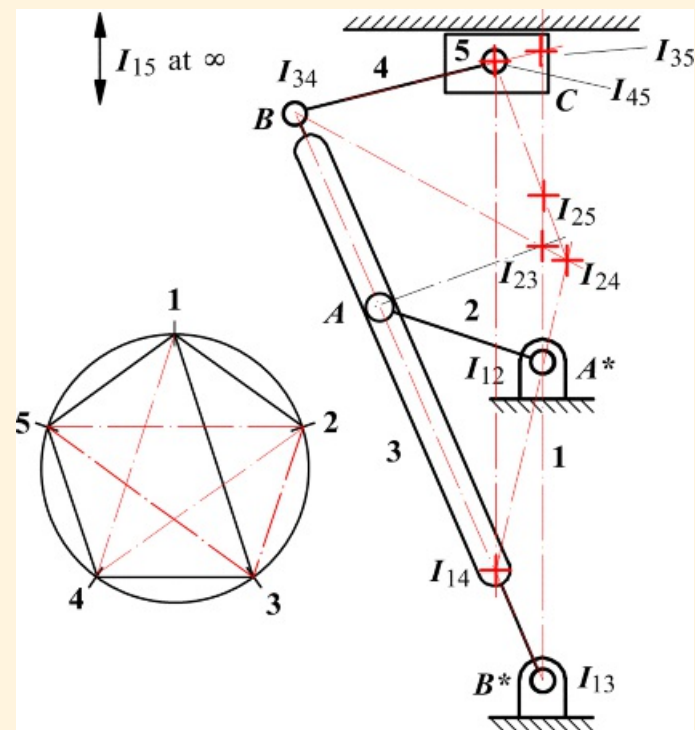


[Figure 6.28](#) Instant centers when C is not in line with A^* and B^* in Example 6.5.

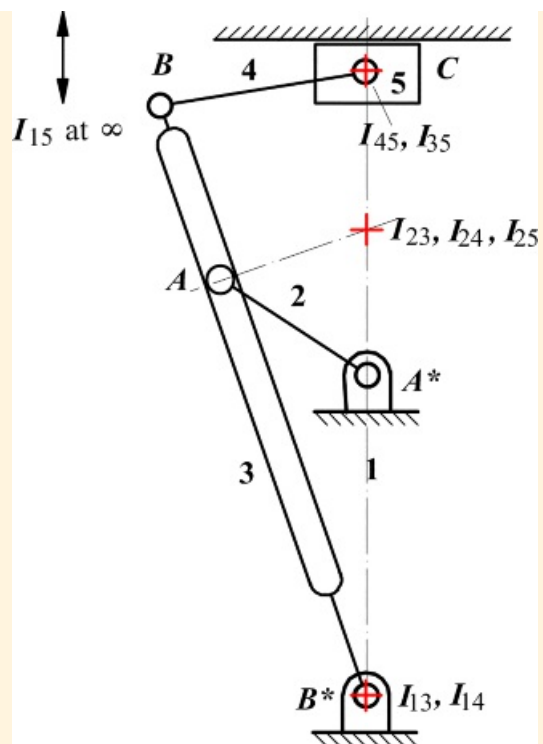


[Figure 6.29](#) Actual location of I_{24} , I_{25} , I_{35} , and I_{14} in Example 6.5.



Example 6.6

Using Instant Centers to Analyze a Gear Mechanism

Find the velocity of point *C* in Figure 6.30 given that the angular velocity of gear 2 is 10 rad/s CW. Point *B* is a hinge connecting links 4 and 5 and does not connect to gear 3. Point *A* is a pin in link 3 that engages a slot in link 4.

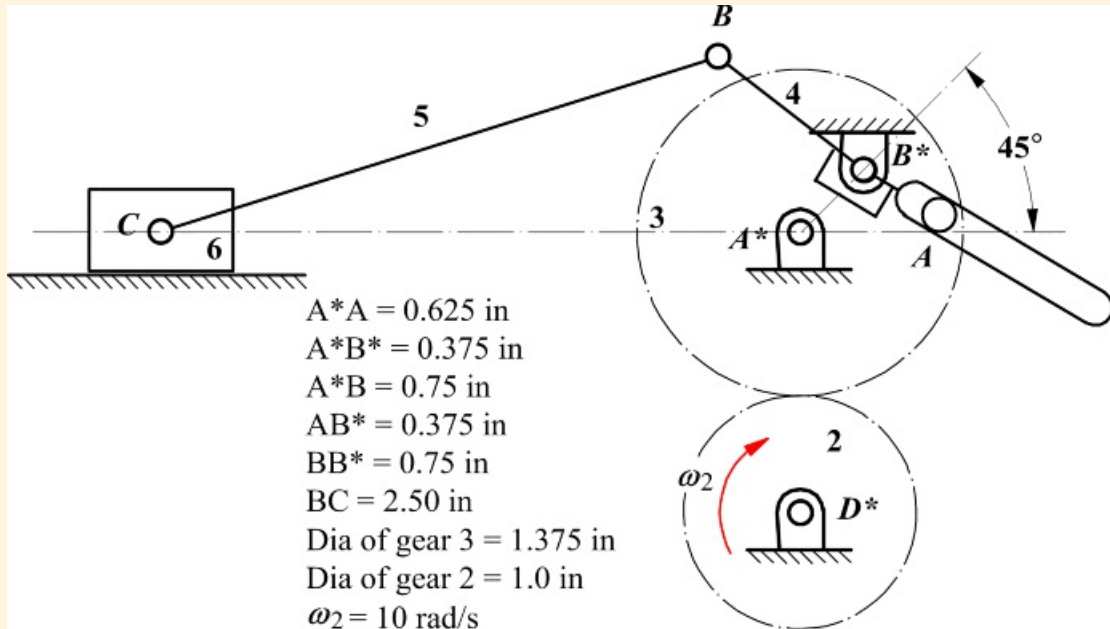
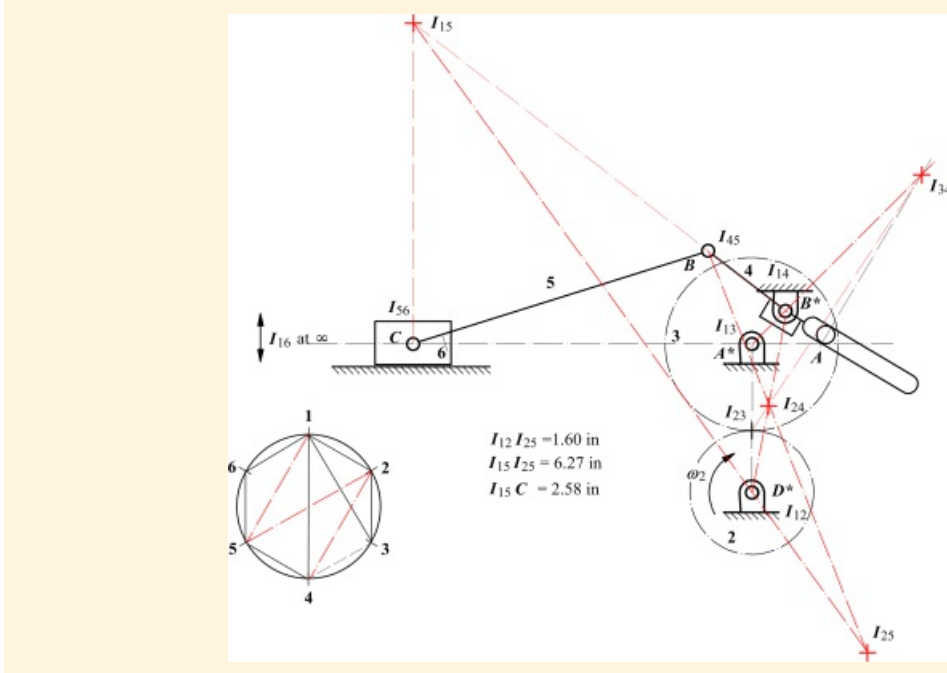


Figure 6.30 The linkage of Example 6.6.

Solution

To find the velocity of point C considered as a point in link 5 from the angular velocity of link 2 relative to link 1, the instant centers I_{12} , I_{15} , and I_{25} are needed. These may be located as shown in Figure 6.31.



[Figure 6.31](#) Location of instant centers for Example 6.6.

Then

$$\omega_5 = \omega_2 \frac{l_{12} s_{25}}{l_{15} s_{25}} = 10(1.60)/(6.27) = 2.55 \text{ rad/s CW}$$

$$v_C = \omega_5 \times (s_{15} C) = 2.55(2.58) = 6.58 \text{ in/s to the left}$$

Notice that the instant-center method is extremely efficient for simple input-output problems, such as this one, in which the velocities of only two links are of interest.



6.14 Finding Instant Centers Using Geometric Constraint Programming

In this chapter, we have implied that the instant-center approach to velocity analysis is to be accomplished using traditional drawing techniques. However, GCP offers a much better way to solve instant center problems. If only linear velocities are involved, the problems can be solved entirely within a 2D parametric CAD program. If angular velocities are involved, some external hand calculations will be required; however, the vast majority of the effort can be accomplished within the GCP environment. A major advantage in solving the problems using GCP is that the resulting figure not only solves the specific problem considered, but also provides a graphical program for solving similar problems using the same mechanism. All that is required to solve a separate problem is to change the dimensions. All of the constructions adjust based on the established constraints. It is also possible to move the given mechanism into different positions to determine how the instant centers and velocities change with position. From the examples in this chapter, it is apparent that small changes in geometry can cause large changes in velocities. These changes can be easily investigated using GCP.

When developing a graphical program using GCP, we still follow the same graphical procedures developed in this chapter. Namely, we will use the circle method to find the instant centers, although we will include the circle diagram on a layer that can be hidden. Also, as we construct the lines required to locate the instant centers, we will apply the necessary constraints and relations to ensure that the construction lines are accurate for any changes in the mechanism geometry.

The rotating radius method can also be applied, and it can be used to give the magnitudes of the velocities as the mechanism moves. However, it must be remembered that the lines in the GCP constructions are not vectors. Therefore, while the magnitudes, lines of action, and directions will be correct in the initial positions, the implied directions may not be correct for different positions as the mechanism is animated. Therefore, the user must verify the directions for any velocities determined in other than the initial position.

The following two examples illustrate the use of GCP for finding and using instant centers. The details on how to set constraints will not be given since these were covered in [Chapter 2](#).



Example 6.7

Use GCP to Solve Example 6.2

Given the compound linkage shown in [Figure 6.20](#), the velocity of point A is given as shown. Find the velocity of point B on link 5 using GCP.

Solution

The steps in solving the problem using GCP are similar to those used in Example 6.2 using manual construction techniques. In particular, we need to find I_{12} , I_{15} , and I_{25} and then use the rotating radius method to find v_B . The steps are as:

1. Open a blank drawing sheet and set up eight layers: *OrigDwg*, *OrigDim*, *IC-Const*, *IC-Locat*, *Dimensions*, *CircleDiag*, *FinalDwg*, and *RotRadius*. The purpose of each layer is:
 - a. *OrigDwg*: Contains original drawing with annotations but without dimensions
 - b. *OrigDim*: Contains driving dimensions for drawing. These are inputs to the graphical program.
 - c. *IC-Const*: Contains the construction lines to determine where the ICs are located
 - d. *IC-Locat*: Contains small crosses indicating the locations of the ICs
 - e. *Dimensions*: Contains miscellaneous dimensions such as those for the crosses in *IC-Locat* and those for the slider lines and ground pivots.
 - f. *CircleDiag*: Contains the circle diagram used to determine the lines that locate the ICs
 - g. *Final Dwg*: Contains the final linkage with cosmetic details such as slider blocks, ground pivots, and slider lines
 - h. *RotRadius*: Contains the construction using an adaptation of the rotating radius method to determine v_B .

The selection of these layers is arbitrary, but they represent a reasonable way to present the information and to selectively hide different types of information during the solution process.

2. Make *OrigDwg* the active layer and sketch the mechanism. Dimensions are unimportant at this stage of the process, but it will be helpful if the sketch can approximate the drawing in [Figure 6.20](#). The result is shown in [Figure 6.32](#). Cosmetic additions such as the slider line, slider, and ground pivots are unnecessary at this point. However, we have added small circles at the pin joints and have drawn an arrowhead on the end of the velocity vector at point A . The parametric design programs generally do not have a provision for optionally adding an arrowhead to a line. We have also annotated each joint with a letter to facilitate the later descriptions of the solution process. Otherwise, it would not be necessary to label the joints. The relevant constraints are:
 - a. A^* is fixed.
 - b. The points at the ends of lines that are connected are merged.
 - c. v_A is perpendicular to A^*A and the tail of the line is fixed to A .
 - d. A^* and C^* are constrained to lie on a horizontal line.
 - e. The slider line is constrained to be horizontal.
 - f. Point E is constrained to be coincident with the slider line.
3. Make *OrigDim* the active layer and use the dimension tool to dimension all of the lines in the model in [Figure 6.32](#). The results are shown in [Figure 6.33](#). Red has been used to designate driving dimensions. These dimensions can be changed to investigate the effect of geometry on the instant center locations.

After applying the dimensions, drag point A around A^* with the mouse. If the linkage can move and the linkage does not distort, the dimensions and constraints have been applied correctly. If the linkage will not move, check for unwanted constraints. If the linkage distorts when A is moved, some line or point is not dimensioned or constrained correctly.

4. Hide the layer *OrigDim* and make *CircleDia* the active layer. Draw a circle with six tick marks as was done in Example 6.2. Identify the obvious instant centers and draw the appropriate chord lines. Annotate the drawing with the obvious instant centers identified. The results are shown in [Figure 6.34](#).
5. Make the layer *IC-Const* active. We will find the instant centers I_{13} , I_{15} , and I_{25} in the same order as was used in Example 6.2. To locate I_{13} , first draw a construction line from I_{12} in the general direction of I_{23} but not through I_{23} . Use the coincident constraint to constrain the point at I_{23} to lie on the construction line. Similarly, draw a construction line from I_{14} and constrain I_{34} to lie on the line. Select the ends of the $I_{12}I_{23}$ and $I_{14}I_{34}$ lines and merge them. The merged point is I_{13} . For I_{15} , draw a construction line from I_{56} , select the line and the line for the slider pin, and constrain them to be perpendicular. Then draw a construction line from I_{13} and constrain I_{35} to lie on the line. Normally, the line will be reoriented so that it passes through I_{35} . Select the lower ends of the two construction lines and merge them. The merged point is I_{15} . Finally, draw a construction line from I_{35} and constrain I_{23} to lie on the line. Next draw a construction line from I_{15} and constrain I_{12} to lie on the line. Select the left ends of the two construction lines and merge them. The resulting merged point is I_{25} . Move the lines constructed on the circle diagram to the *CircleDiag* layer. Make *IC-Locat* the active layer and draw a cross at the location of the three instant centers that were located. It will be necessary to dimension the arms of each cross and to constrain both arms to be perpendicular. Also, use different colors or line types to distinguish among the instant center locations if the linkage is moved by dragging point A with the mouse.
6. Before determining the velocity of B_5 , hide the layers *IC-Const* and *Circle Diagram*. The only items that should be visible are the original annotated linkage and the locations of instant centers I_{13} , I_{15} , and I_{25} . The results are shown in [Figure 6.35](#). Make the layer *RotRadius* active. Draw a line from I_{12} and constrain it to be coincident with I_{25} , but the line should not terminate on I_{25} . Select the construction line and the line A^*A and make them equal. Label the endpoint of the construction line as A' . Draw a line from A' downward and constrain the line to be perpendicular to A^*A' . This line will represent the velocity of A' , and it is drawn downward to be consistent with the apparent direct of $\omega_{A'}$. We infer the direction of $\omega_{A'}$ based on the direction of ω_A . Select the perpendicular line and the line representing $\omega_{A'}$ and constrain them to be equal. Label the end of the perpendicular line as $v_{A'}$. Now draw a construction line from I_{12} , and constrain the line to be coincident with the point $v_{A'}$. Draw a line starting from I_{25} and constrain it to be perpendicular to the line through I_{12} and I_{25} . Also, constrain the end of the line to be coincident with the construction line. This line will give the velocity of I_{25} .

Draw a construction line from I_{15} and merge the other end with I_{25} . Next draw a construction line from I_{15} and constrain the line to pass through B_5 . However, make sure that the line does not terminate on B_5 . Select this construction line and the one from I_{15} to I_{25} and constrain them to be equal. Label the highest point of the line to be v_{B_5} . Draw a line from v_{B_5} and constrain the line to be perpendicular to $I_{15}v_{B_5}$. This line corresponds to the velocity of B_5 . Determine the sense of the velocity by determining the direction of the angular velocity ω_B , which we can infer to be CCW from the direction of the velocity of I_{25} . Select the lines corresponding to $v_{I_{25}}$ and v_{B_5} and constrain the lines to be equal. Label the end of the line corresponding to $v_{I_{25}}$ as v_{B_5} . Draw a construction line from I_{15} and constrain it to be coincident with the point defined by the tip of v_{B_5} . This is the proportionality line for defining the magnitude of the velocity of B_5 . The last step is to draw a line from B and constrain the end of the line to be coincident with the proportionality line. Finally constrain the line to be perpendicular to the line $I_{15}B$. The resulting line represents the velocity of B_5 . We can use the dimension tool to measure the line and determine the actual velocity magnitude based on the scale used to draw v_{B_5} . The results of the

construction are shown in [Figure 6.35](#). If we wish to show the velocity of B_5 as the mechanism is animated, we can move the line corresponding to v_{B_5} to the layer *OrigDwg*. It is important to actually set the constraints specified in the procedure. If the constraints are not actually set, they will not be maintained when the dimensions are changed or the linkage is moved.

7. While it is not necessary from the standpoint of determining v_{B_5} , cosmetic improvements can be made in the diagram of [Figure 6.35](#) by adding a slider line and ground pivots at A^* and C^* as shown in [Figure 6.36](#).

The graphical program for the problem is now complete. The linkage can be moved by dragging point A with the mouse, and any of the dimensions in the *OrigDim* layer can be changed to explore other mechanism shapes. [Figure 6.36](#) shows the final linkage in a different orientation and with different dimensions. As discussed earlier, the annotations do not move with the links so these were moved manually for [Figure 6.36](#).

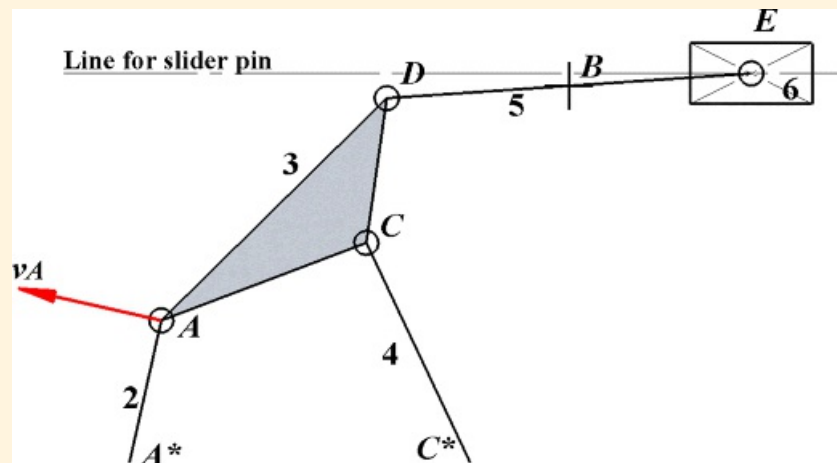


[Figure 6.32](#) Drawing corresponding to [Figure 6.20](#) generated in SolidWorks.

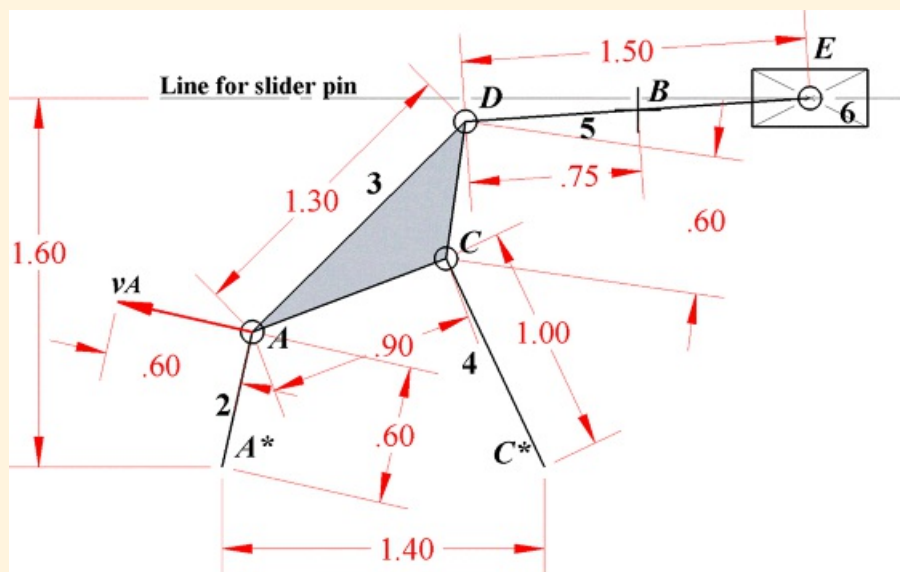


[Figure 6.33](#) Drawing with dimension constraints.

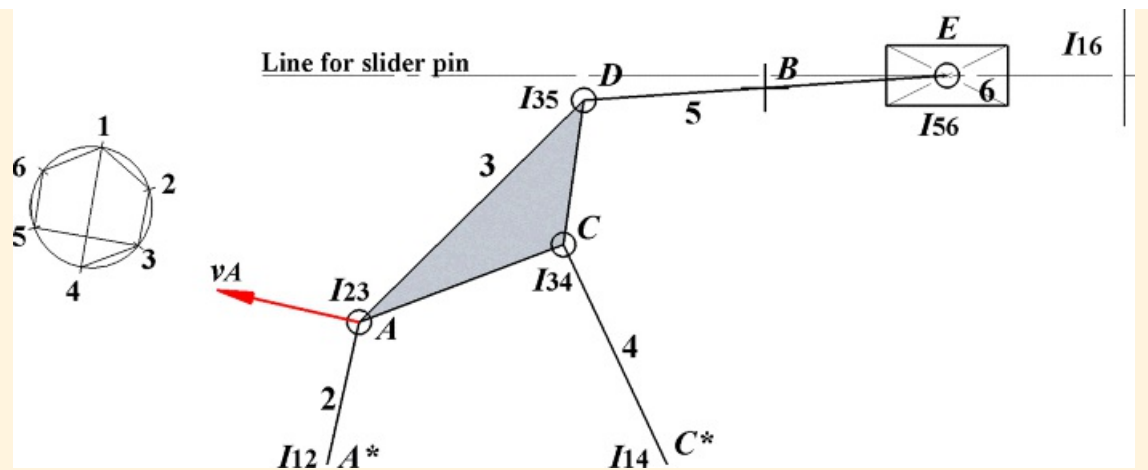


Figure 6.34 Drawing with obvious instant center locations identified.

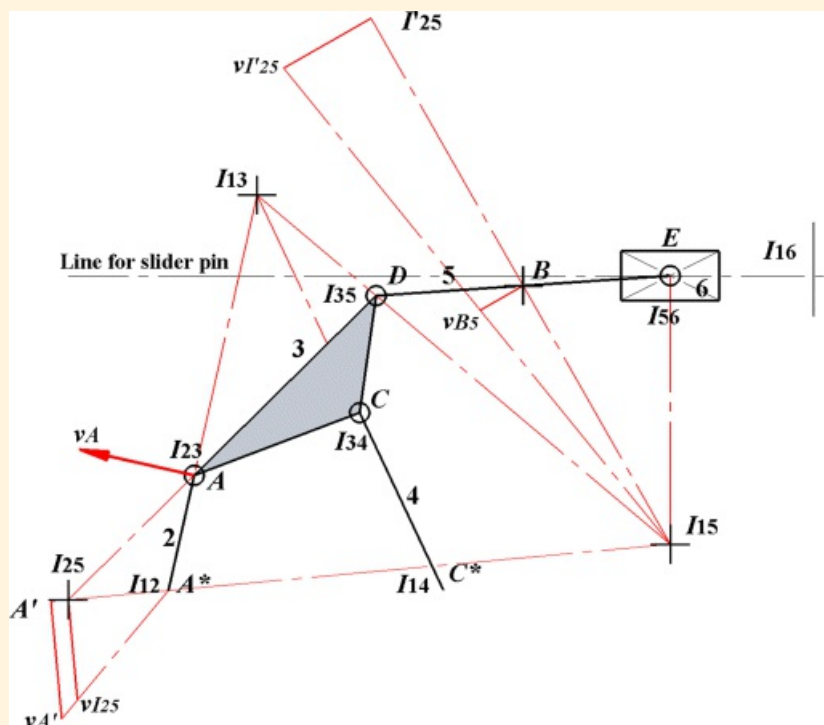
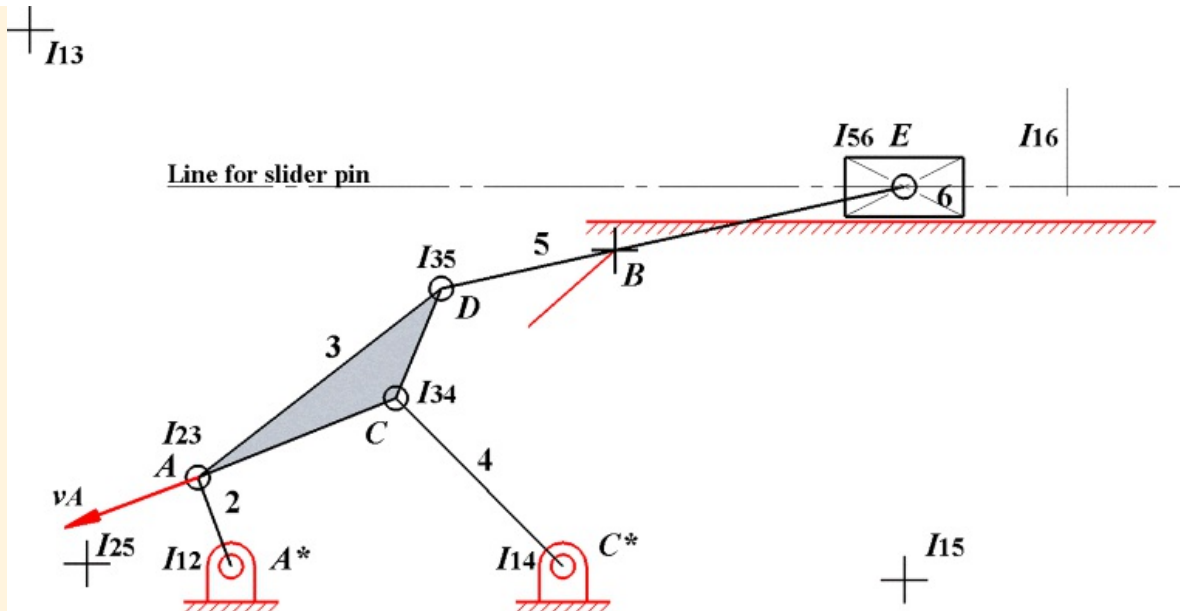


Figure 6.35 Using rotating radius method to determine the velocity of B_5 .



[Figure 6.36](#) Using GCP to analyze the linkage in [Figure 6.20](#) with different dimensions and orientation of link 2.



Example 6.8

Using GCP to Analyze a Stephenson-II Six-Bar Linkage

Consider the Stephenson-II six-bar linkage in [Figure 6.22](#). Assume that ω_2 is given and we want to find ω_5 . Use GCP to help find ω_5 and to develop a graphics program for the Stephenson-II linkage.

Solution

We will use GCP to solve the problem using instant centers. We will follow the same approach as in Example 6.3 except we will do the constructions in the parametric-design program and will dimension the linkage so that the dimensions can be used as inputs to the graphical program. Typically, the final calculation for ω_5 is done manually using [Equation 6.3](#).

As was the case in Example 6.7, the steps in solving the problem using GCP are similar to those used in Example 6.3 using manual construction techniques. Again, we need first to find I_{12} , I_{15} , and I_{25} . Begin the procedure by opening a blank drawing sheet and set up seven layers: *OrigDwg*, *OrigDim*, *IC-Const*, *IC-Locat*, *Dimensions*, *CircleDiag*, and *FinalDwg*. The purpose of each layer is the same as in Example 6.7. The solution process is almost identical to that used in Example 6.7 so only an overview will be given here.

Begin the process by sketching the mechanism and dimensioning it so that it corresponds to the shape shown in [Figure 6.22](#). The result is shown in [Figure 6.37](#) where we have also added pin bushings and ground pivots. The dimensions become the inputs to the graphical program to be developed. After the dimensions are set, move the mechanism by dragging point A with the computer mouse. If the mechanism will not move, check for unwanted constraints and delete them. If the mechanism distorts when it is moved, identify which entities are not dimensioned adequately and make the necessary adjustments.

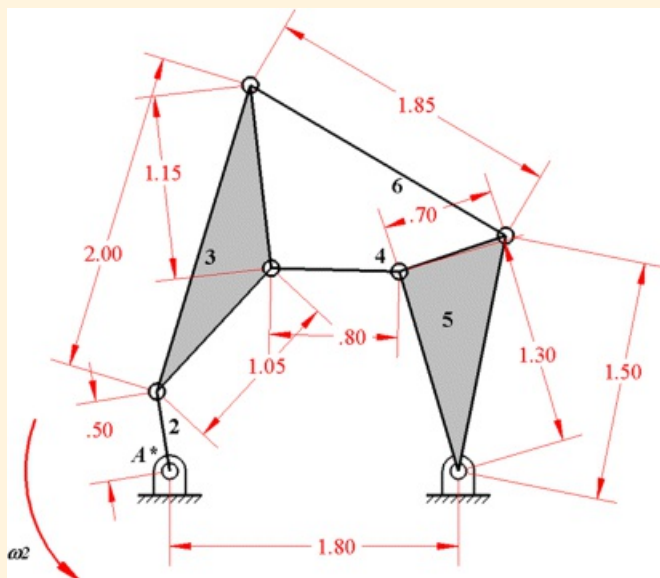


[Figure 6.37](#) Using GCP to draw and dimension the Stephenson-II mechanism.

Next draw a circle with six tick marks and locate the instant centers I_{12} , I_{15} , and I_{25} on the drawing. In particular locate I_{12} and I_{15} by inspection and locate I_{25} by first locating I_{35} using I_{36} and I_{56} and I_{34} and I_{45} . Then using I_{35} and I_{23} and I_{12} and I_{15} , locate I_{25} . When drawing the construction lines, be sure to explicitly set the necessary constraints. If the constraints are not properly set, the procedure can still be used to solve the specific problem, but it will not result in a graphical program that can be used to solve a class of problems. The locations of the instant centers are indicated in [Figure 6.38](#). In [Figure 6.38](#), we have also used the dimension tool to measure the distances $I_{15}I_{25}$ and $I_{12}I_{25}$. These can be used in [Equation 6.3](#) to

compute the magnitude of ω_5 . We can get the direction of ω_5 by determining the sense of the velocity $v_{(I_{35})_3} = v_{(I_{25})_3} = v_{(I_{25})_2}$. As in the case of Example 6.3, the direction is CCW.

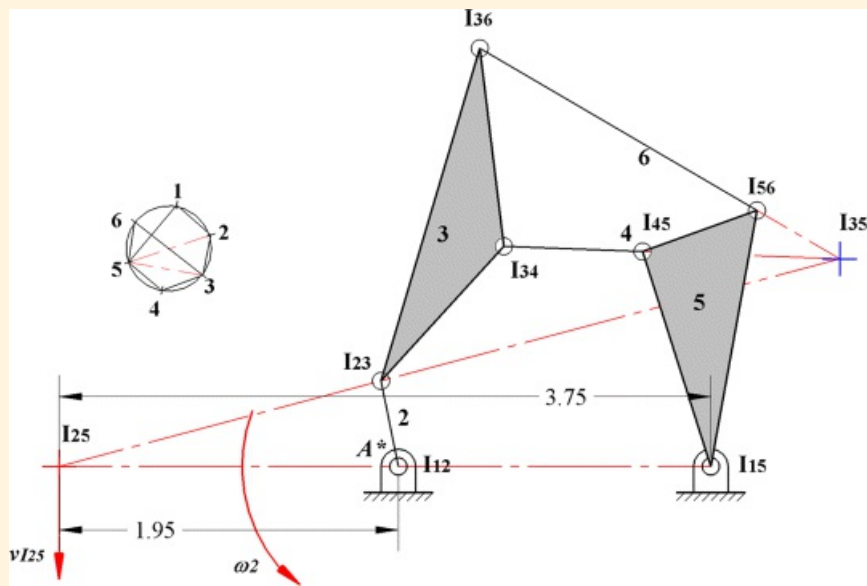


Figure 6.38 Using GCP to find the instant centers.



References

1. Aronhold, Siegfried H. (1872). "Outline of Kinematic Geometry." *Verein zur Beförderung des Gewerbelehrunterrichts in Preussen*, Vol. 51, pp. 129–155.
2. Bernoulli, Johann. (1742). "De Centro Spontaneo Rotationis," in *Johannis Bernoulli Opera Omnia*, Vol. 4. Geneva, CH: University of Lausanne.
3. Chasles, Michel. (1830). "Note sur les Propriétés Générales du Système de Deux Corps Semblables entr'eux." *Bulletin de Science Mathématiques, Astronomiques Physiques et Chimiques, Baron de Ferussac*, Paris, pp. 321–326.
4. Hartenberg, Richard S., and Denavit, Jacques. (1964). *Kinematic Synthesis of Linkages*. New York, NY: McGraw Hill, pp. 113–114.
5. Hunt, Kenneth H. (1978). *Kinematic Geometry of Mechanisms*. Oxford, UK: Oxford University Press, pp. 88–89.
6. Kennedy, Alexander B.W. (1886). *Mechanics of Machinery*. London, UK: Macmillan.



Problems

Note: All of the exercise problems can be solved using either traditional graphical methods or GCP. Also, when units are not given, readers are free to select whatever units they prefer.

- 6.1 Locate all of the instant centers in the mechanism shown in [Figure P6.1](#).

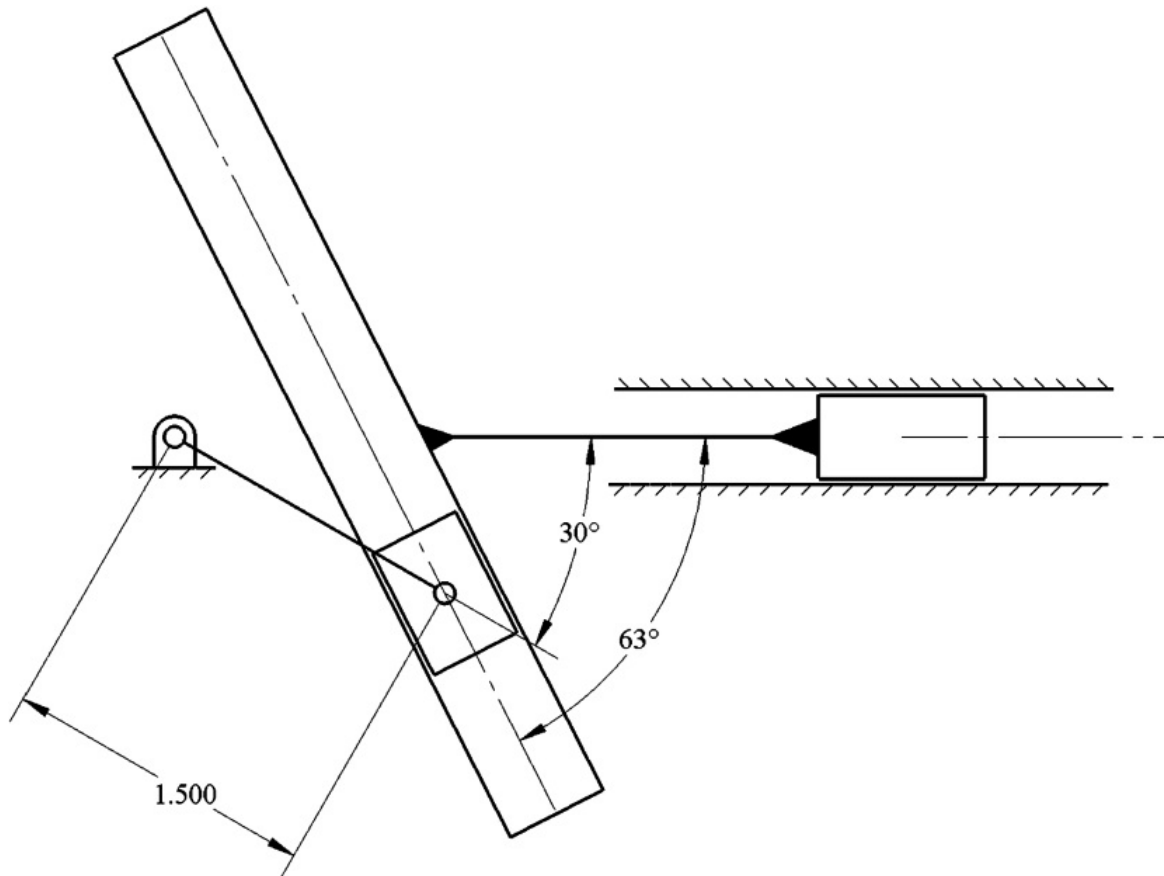


[Figure P6.1](#) Linkage for Problem 6.1.

- 6.2 Find all of the instant centers of velocity for the mechanism shown in [Figure P6.2](#).

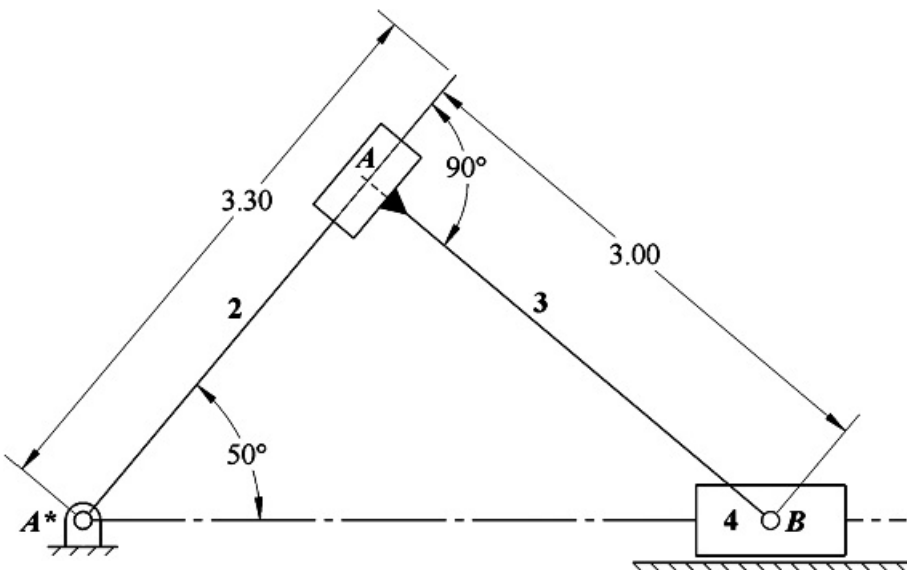


[Figure P6.2](#) Linkage for Problem 6.2.

6.3 In the linkage shown in [Figure P6.3](#), locate all of the instant centers.

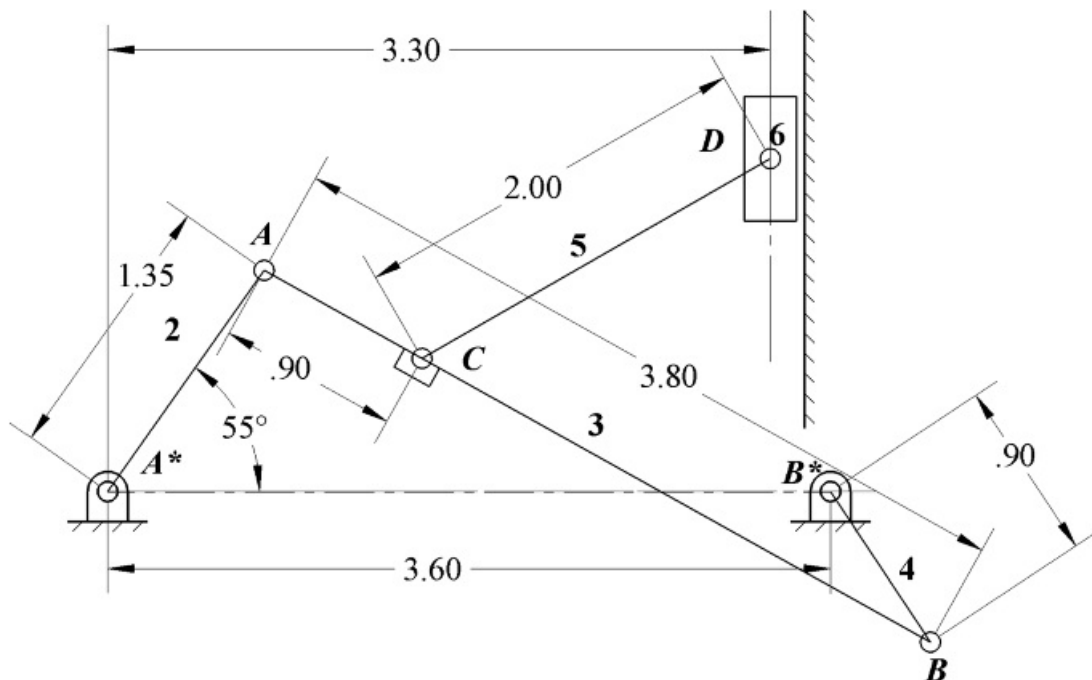


[Figure P6.3](#) Linkage for Problem 6.3.

6.4 Find all of the instant centers of velocity for the mechanism shown in [Figure P6.4](#). The dimensions are in centimeters.

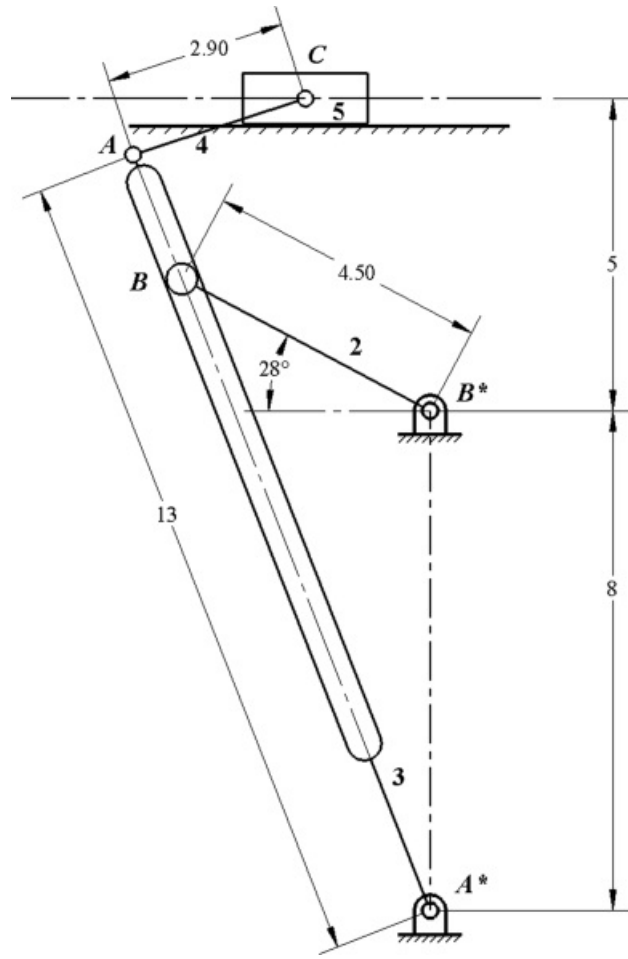


[Figure P6.4](#) Linkage for Problem 6.4.

6.5 Locate all of the instant centers in the mechanism in [Figure P6.5](#). If link 2 is turning CW at the rate of 60 rad/s, determine the linear velocity of points C and E using instant centers. The dimensions are in inches.

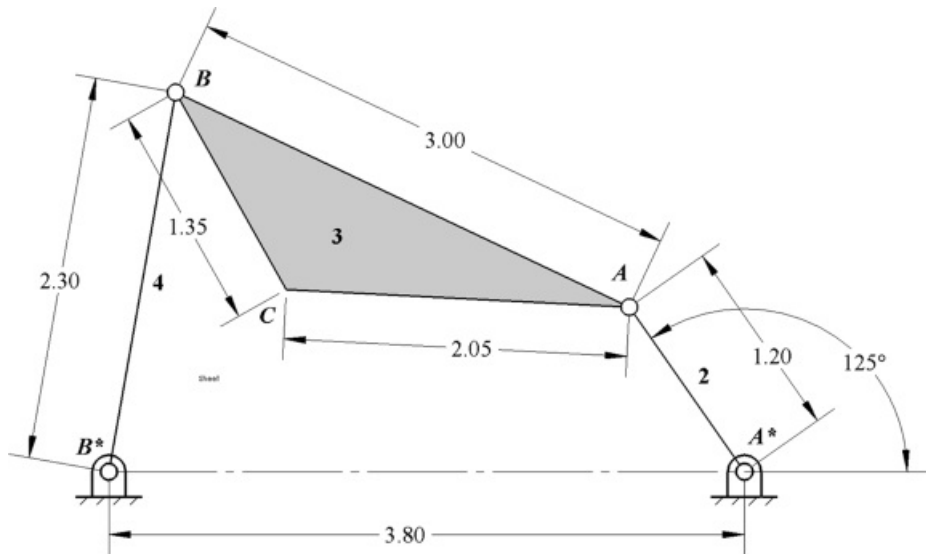


[Figure P6.5](#) Linkage for Problem 6.5.

6.6 Locate all of the instant centers in the mechanism shown in [Figure P6.6](#). If the cam (link 2) is turning CW at the rate of 900 rpm, determine the linear velocity of the follower using instant centers. The dimensions are in inches.

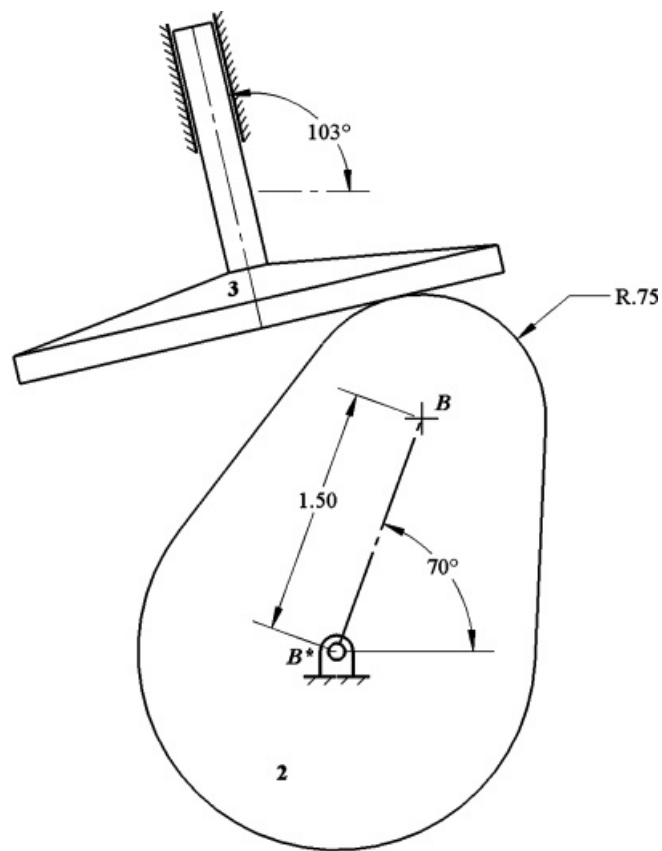


[Figure P6.6](#) Linkage for Problem 6.6.

6.7 Locate all of the instant centers in the mechanism in [Figure P6.7](#). If link 2 is turning CW at the rate of 36 rad/s, determine the linear velocity of point B_4 by use of instant centers. Determine the angular velocity of link 4 in rad/s and indicate the direction. Points B^* and C have the same vertical coordinate, and points A^* and B^* have the same horizontal coordinate. The dimensions are in centimeters.

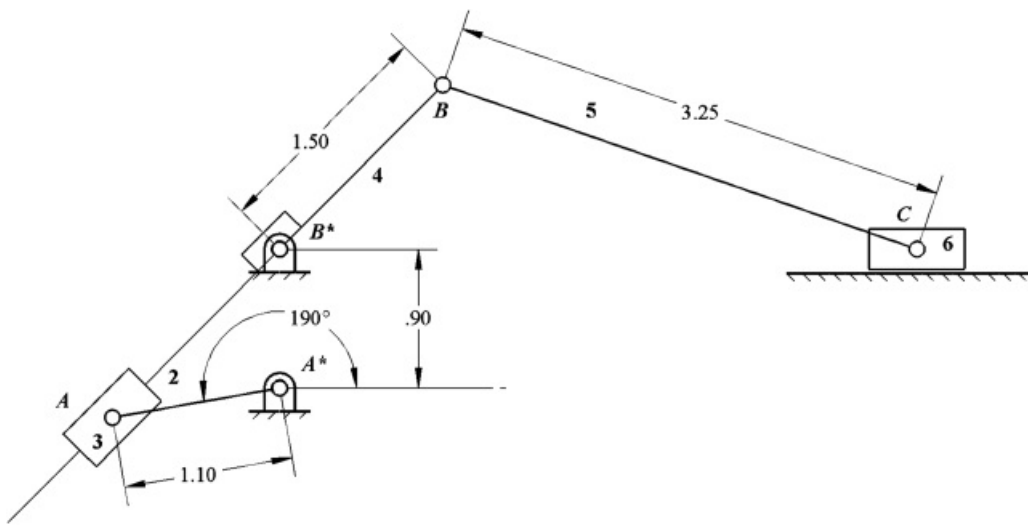


[Figure P6.7](#) Linkage for Problem 6.7.

6.8 Using the instant-center method, find angular velocity of link 6 in [Figure P6.8](#) if link 2 is rotating at 50 rpm CCW.

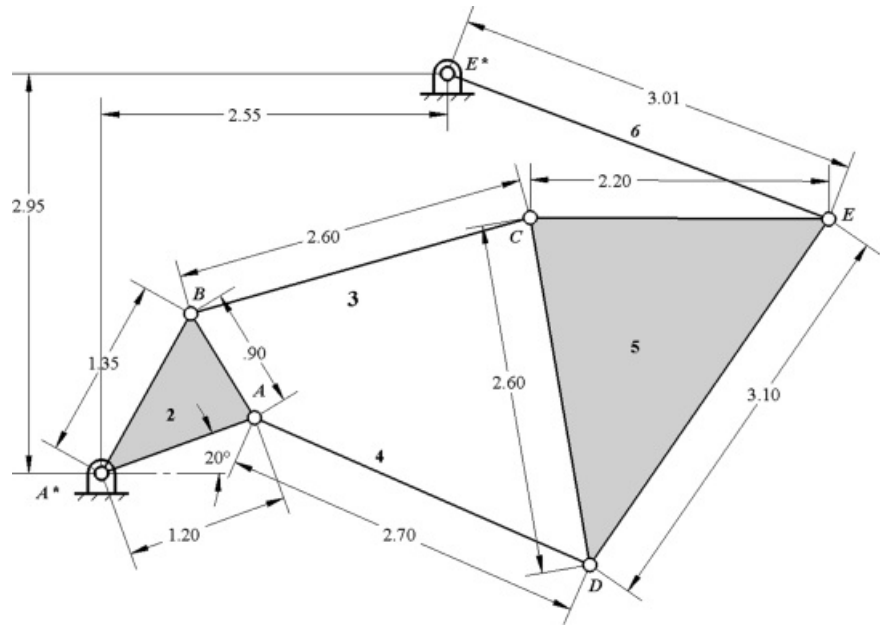


[Figure P6.8](#) Linkage for Problem 6.8.

6.9 In the operation of the mechanism in [Figure P6.9](#), link 3 strikes and trips link 5, which is initially at rest. High wear has been observed at the point of contact between links 3 and 5. As an engineer, you are asked to correct this situation. Therefore, you decide to do the following:

1. Determine the direction of the velocity of point C on link 3 at the moment of contact.
2. Relocate the ground pivot of link 4 to make the direction of the velocity of point C perpendicular to link 5 (hence less rubbing at the point of contact) when contact occurs. The dimensions are in inches.

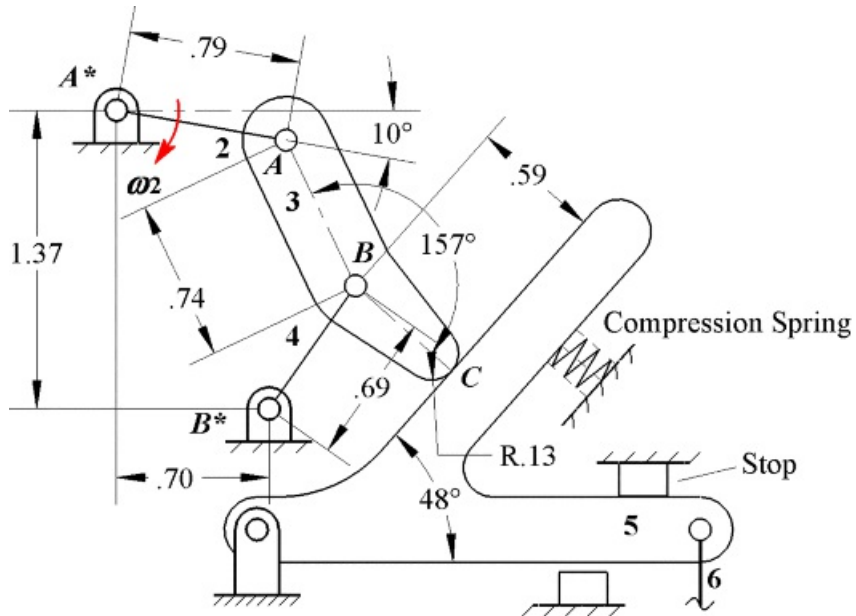


[Figure P6.9](#) Linkage for Problem 6.9.

6.10 For the linkage given in [Figure P6.10](#), $\omega_2 = 1 \text{ rad/s CCW}$. Find I_{26} using the circle-diagram method. Using v_{A2} and I_{26} , determine the magnitude and direction of v_{B6} using the rotating radius method. The dimensions are in inches.

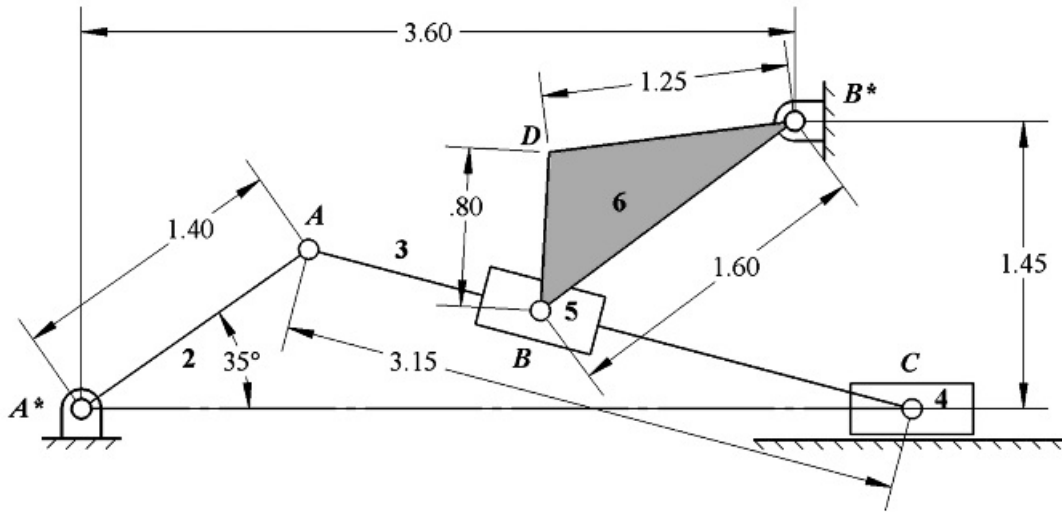


[Figure P6.10](#) Linkage for Problem 6.10.

6.11 Find the velocity of point *C* in [Figure P6.11](#) given that the angular velocity of gear 2 is 10 rad/s CW. *B* is a pin joint connecting links 4 and 5. Point *A* is a pin in link 3 that engages a slot in link 4. The units are in inches.

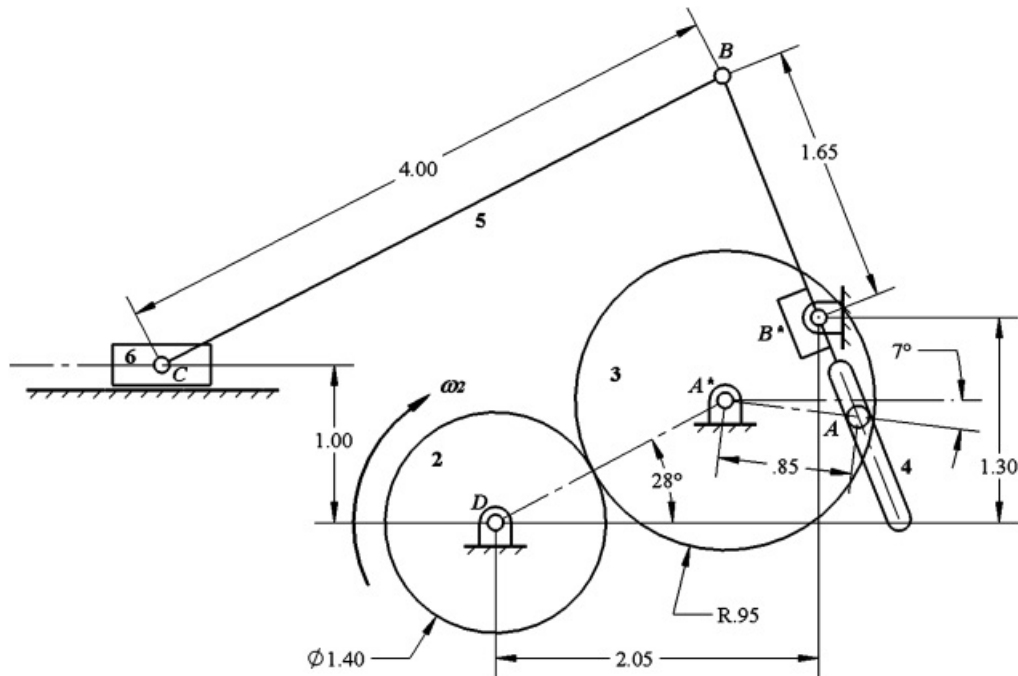


[Figure P6.11](#) Linkage for Problem 6.11.

4.12 If $\omega_2 = 5$ rad/s CCW in [Figure P6.12](#), find ω_5 using instant centers.

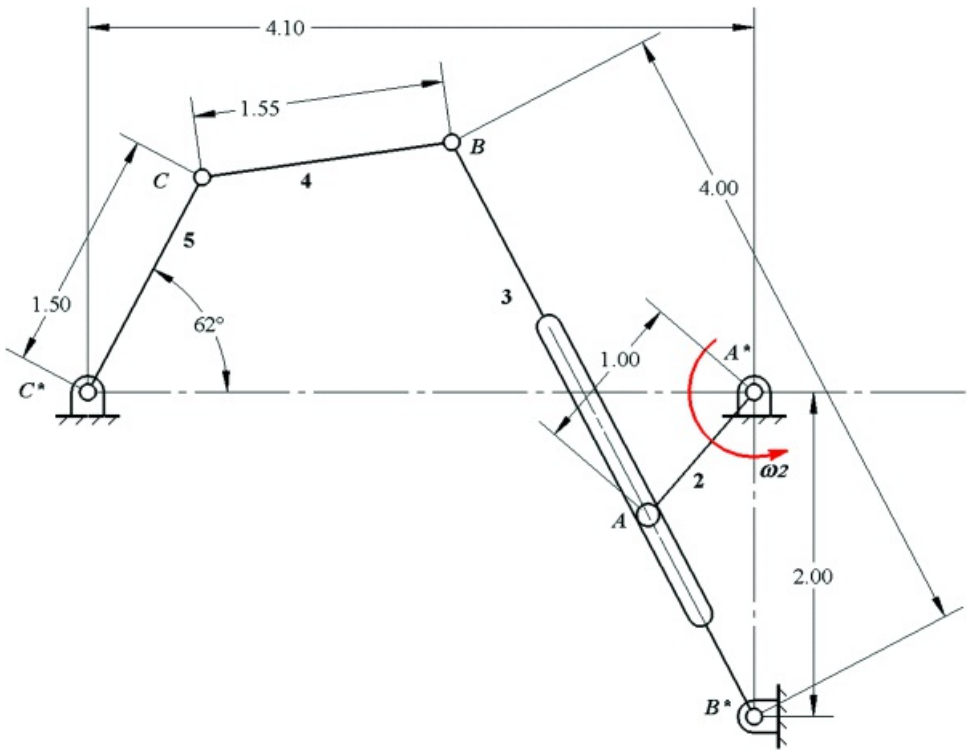


[Figure P6.12](#) Linkage for Problem 6.12.

6.13 If $\omega_2 = 1 \text{ rad/s CCW}$ in [Figure P6.13](#), find the velocity of point D on link 6 using the instant-center method. Show v_{D6} on the drawing. The dimensions are in inches.

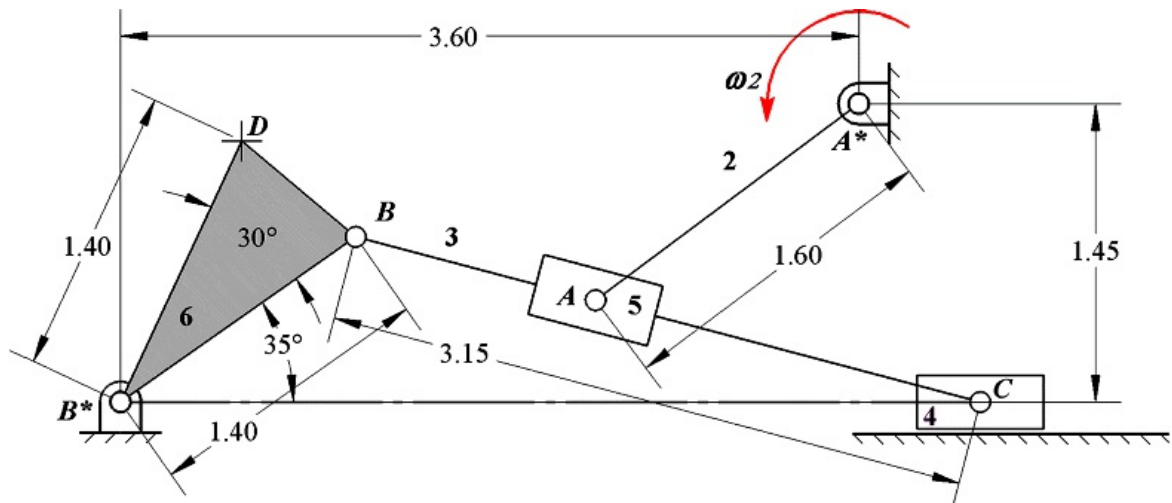


[Figure P6.13](#) Linkage for Problem 6.13.

6.14 If $v_{A2} = 10 \text{ in/s}$ as shown in [Figure P6.14](#), find v_{C4} using the instant-center method. The dimensions are in inches.

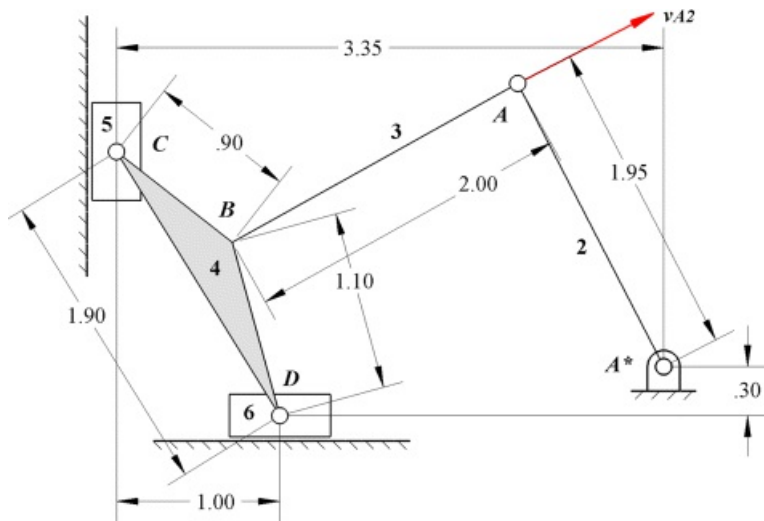


[Figure P6.14](#) Linkage for Problem 6.14.

6.15 If $v_{A2} = 10$ in/s as shown in [Figure P6.15](#), find v_{C4} using the instant-center method. The dimensions are in inches.

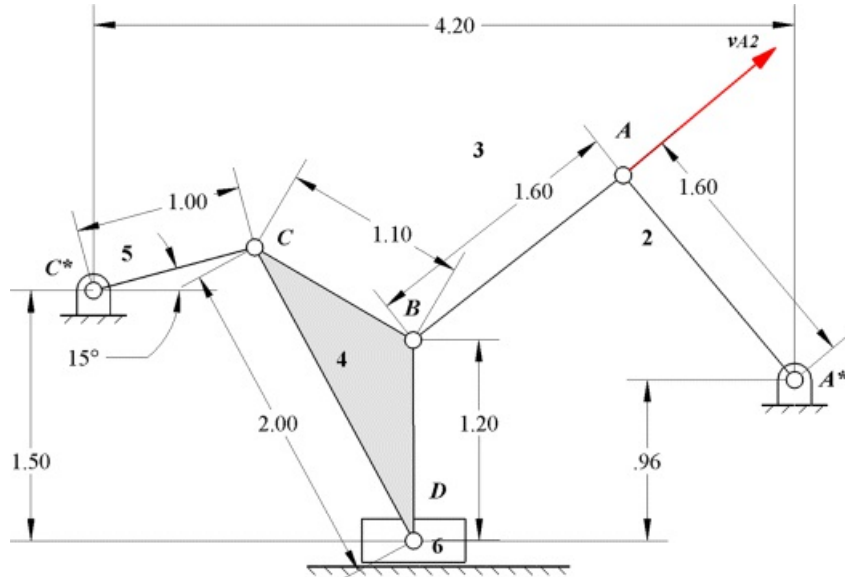


[Figure P6.15](#) Linkage for Problem 6.15.

6.16 If $v_{E2} = 10$ in/s as shown in [Figure P6.16](#), determine the velocity vector (direction and magnitude) for point F on link 5 using the instant-center method. The dimensions are in inches.

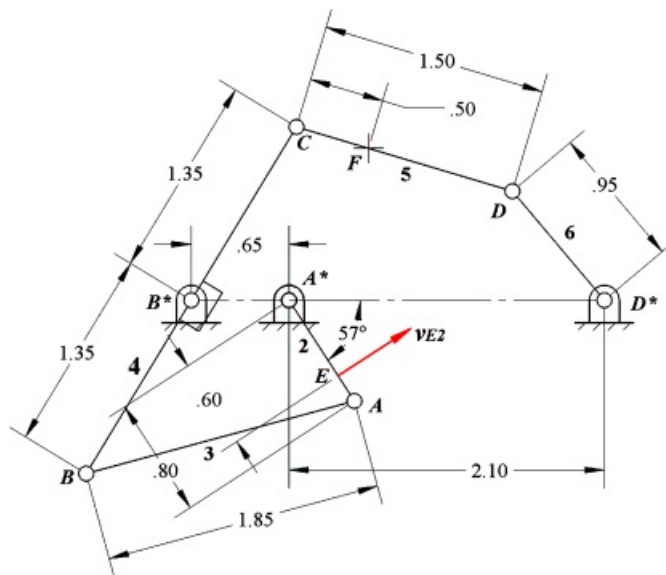


[Figure P6.16](#) Linkage for Problem 6.16.

[6.17](#) In the mechanism in [Figure P6.17](#), ω_2 is 20 rad/s CCW. Find I_{26} and use it to find the angular velocity of link 6.

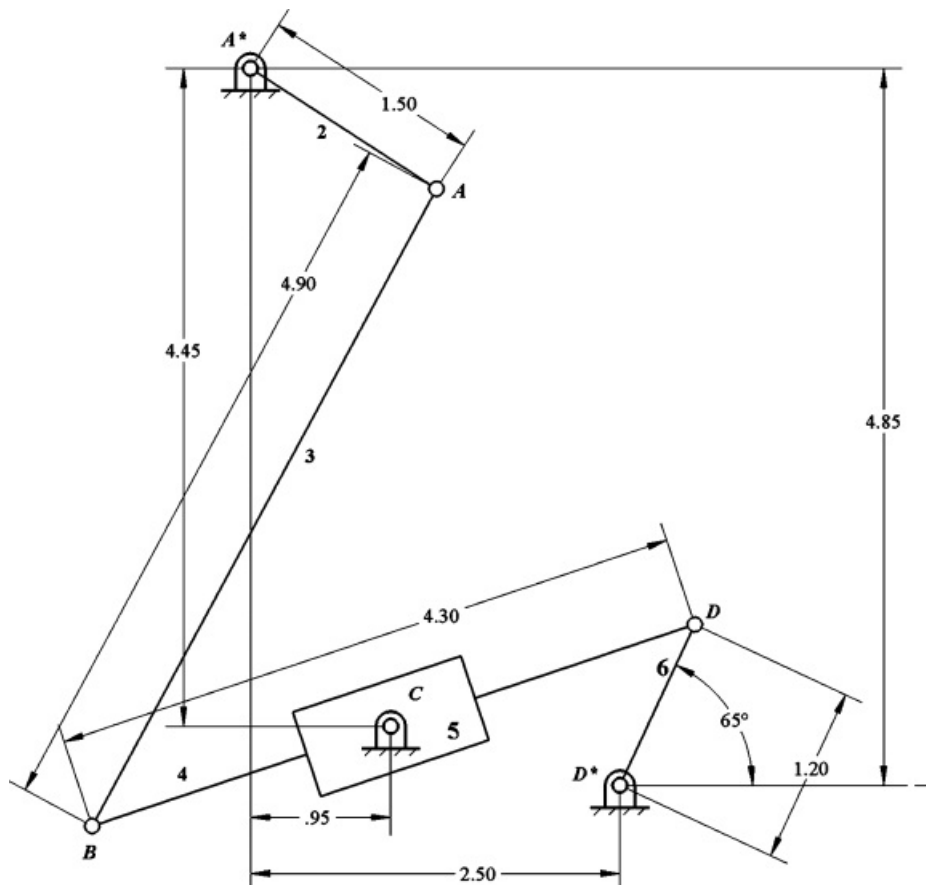


[Figure P6.17](#) Linkage for Problem 6.17.

[6.18](#) If $v_{A2} = 10$ in/s as shown in [Figure P6.18](#), determine the velocity vector (direction and magnitude) of point B_4 using the instant-center method. The dimensions are in inches.

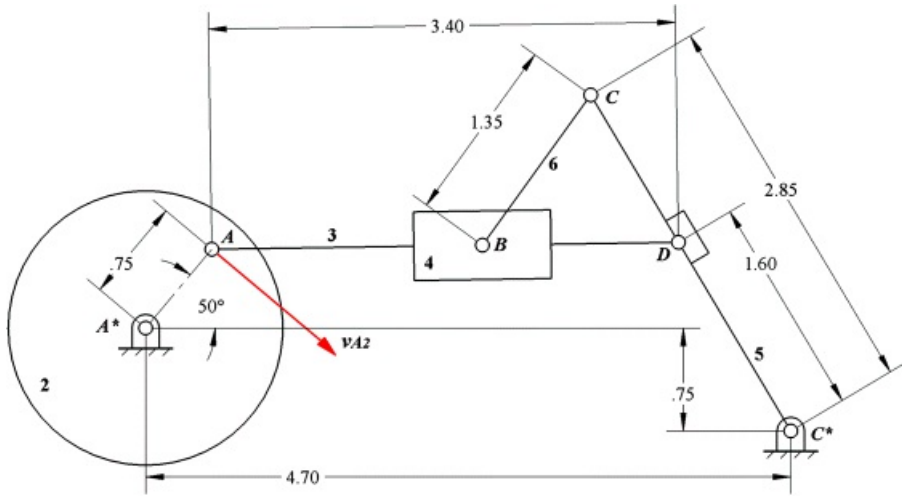


[Figure P6.18](#) Linkage for Problem 6.18.

6.19 If the velocity of A_2 is 10 in/s to the right in [Figure P6.19](#), find ω_6 using instant centers. The dimensions are in inches.

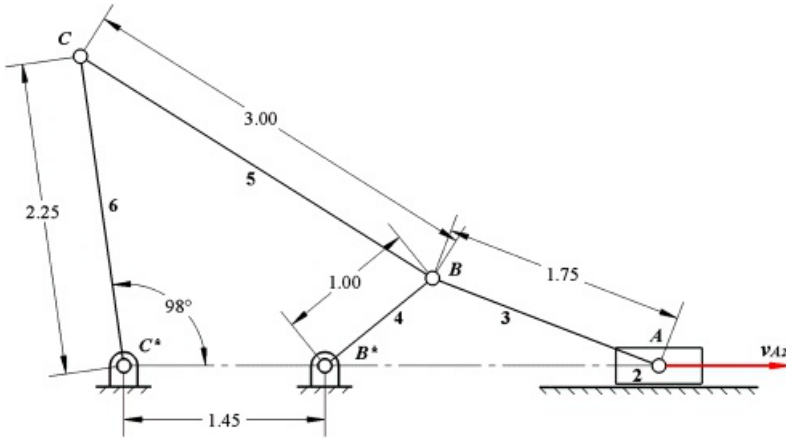


[Figure P6.19](#) Linkage for Problem 6.19.

6.20 Crank 2 of the push-link mechanism shown in [Figure P6.20](#) is driven at $\omega_2 = 60 \text{ rad/s}$ (CW). Find the velocity of points B and C and the angular velocity of links 3 and 4 using the instant-center method. The dimensions are in inches.

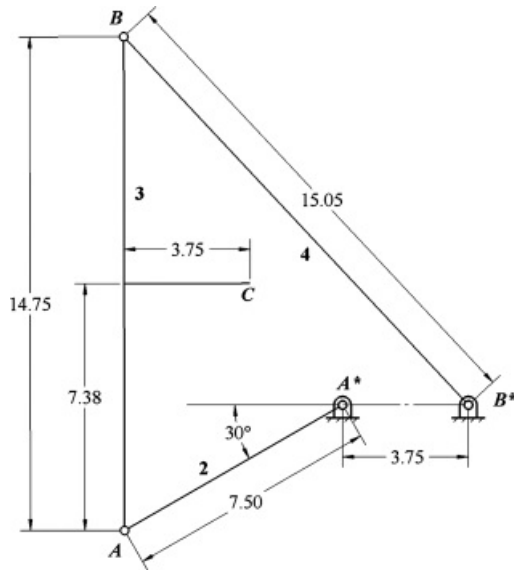


[Figure P6.20](#) Linkage for Problem 6.20.

6.21 If $\omega_3 = 1 \text{ rad/s CCW}$, find the velocity of points C and D using the instant-center method. Show the velocity vectors v_{C3} and v_{D4} on [Figure P6.21](#). The dimensions are in inches.

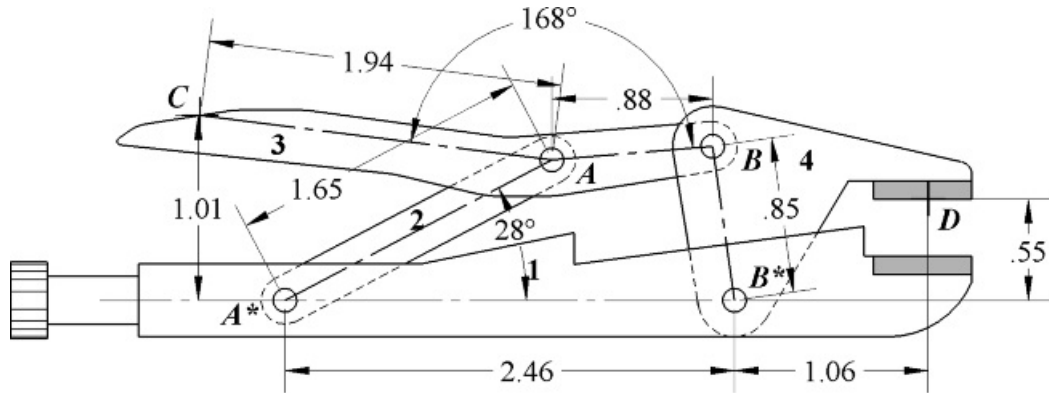


[Figure P6.21](#) Linkage for Problem 6.21.

6.22 The circular cam shown in [Figure P6.22](#) is driven at an angular velocity $\omega_2 = 15 \text{ rad/s (CW)}$. There is rolling contact between the cam and roller, link 3. Using the instant-center method, find the angular velocity of link 4.

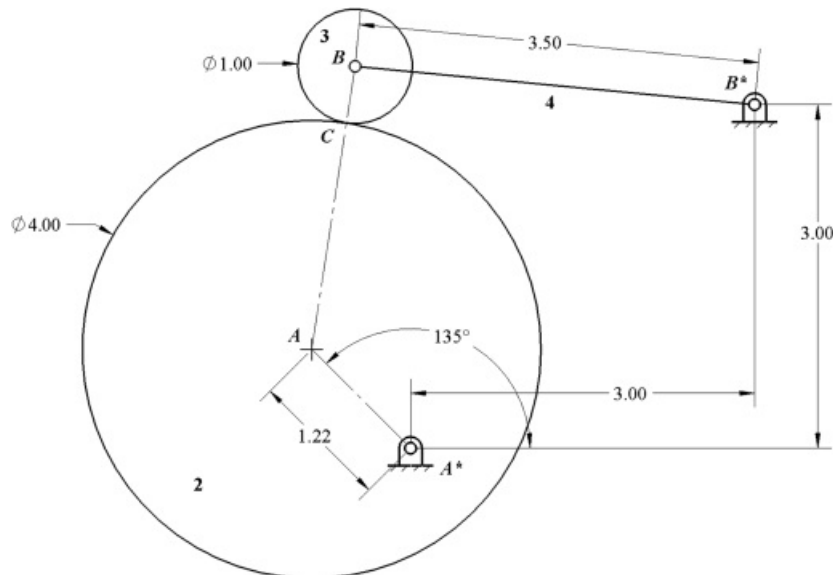


[Figure P6.22](#) Linkage for Problem 6.22.

6.23 In the eight-link mechanism in [Figure P6.23](#), most of the linkage is contained in the black box and some of the instant centers are located as shown. The velocity of point A is 100 in/s in the direction shown. Compute the velocity of point C_8 and determine the angular velocity of link 8. The dimensions are in inches.

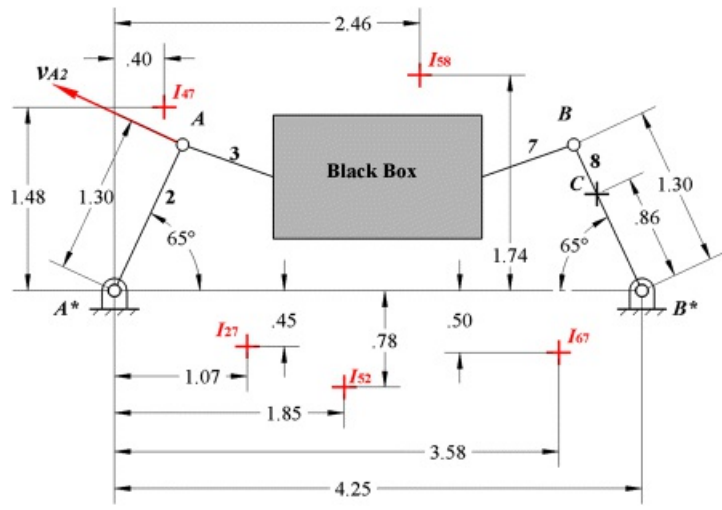


[Figure P6.23](#) Linkage for Problem 6.23.

6.24 If the velocity of point *A* on link 2 is 10 in/s as shown in [Figure P6.24](#), use the instant-center method to find the velocity of point *D* on link 5. The dimensions are in inches.

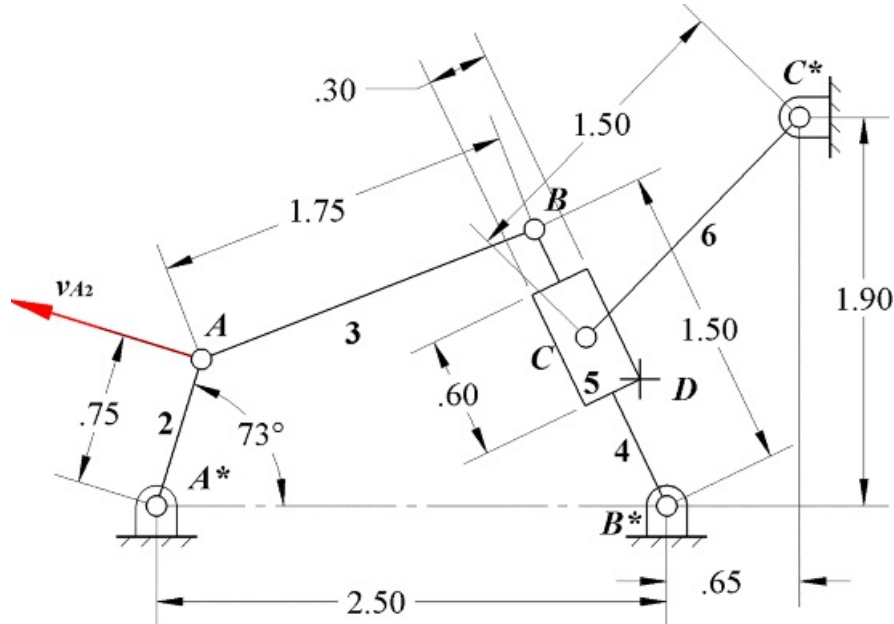


[Figure P6.24](#) Linkage for Problem 6.24.

6.25 Assume that link 7 rolls on link 3 without slipping, and find the following instant centers: I_{13} , I_{15} , and I_{27} . For the given value for ω_2 , find ω_7 using instant centers.

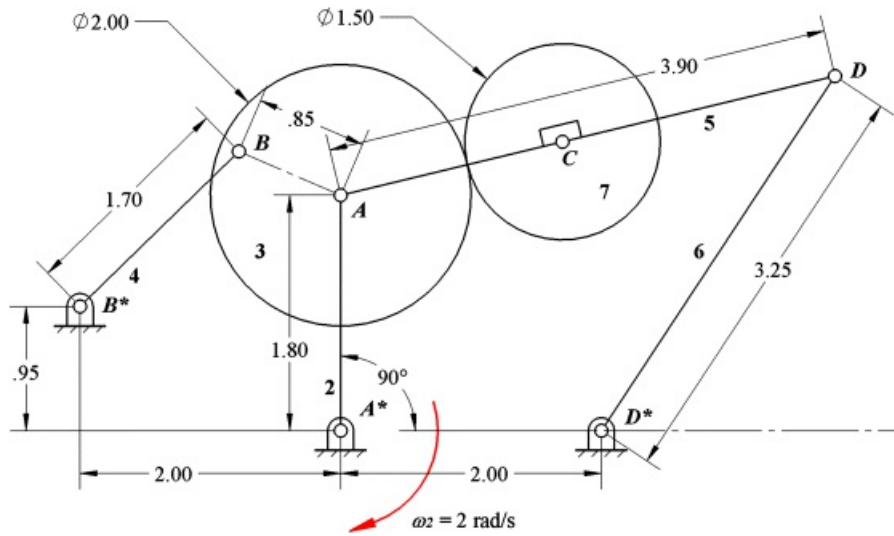


Figure P6.25 Linkage for Problem 6.25.

6.26 If $v_{A2} = 10 \text{ in/s}$ as shown in Figure P6.26, find v_{E5} using the instant-center method.

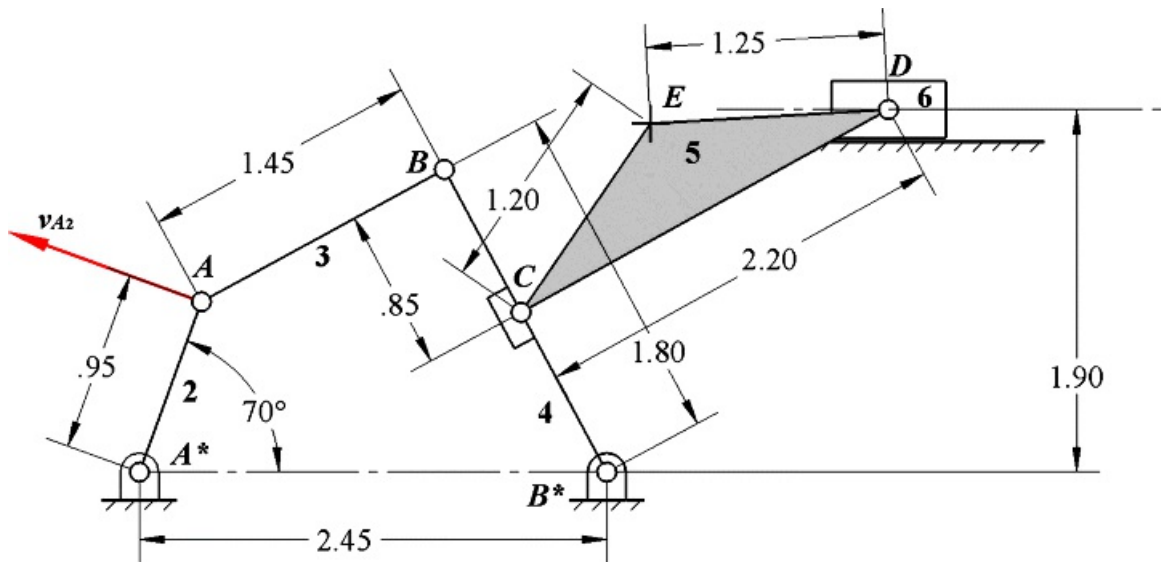
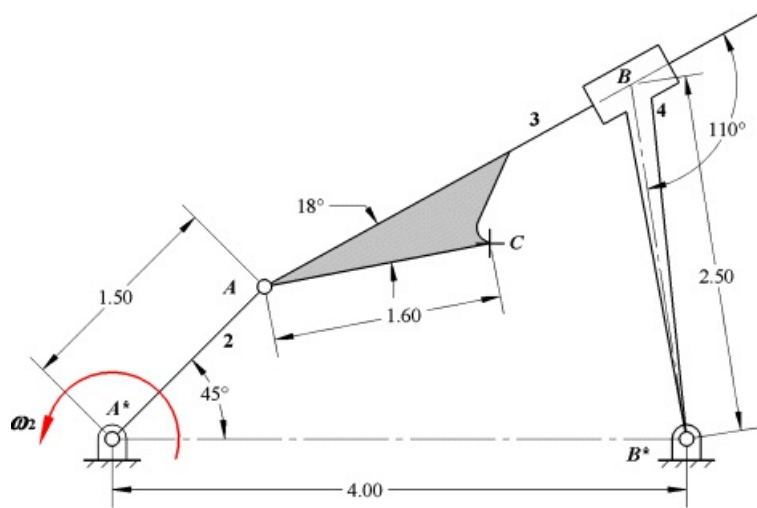


Figure P6.26 Linkage for Problem 6.26.

6.27 If $\omega_2 = 10 \text{ rad/s CCW}$, find the velocity of point C using the instant-center method. Show the velocity vector v_{C3} on Figure P6.27. The dimensions are in inches.



[Figure P6.27](#) Linkage for Problem 6.27.

6.28 If $\omega_2 = 100 \text{ rad/s CCW}$, find the velocity of point C using the instant-center method. Show the velocity vector v_{C4} on [Figure P6.28](#). The dimensions are in inches.

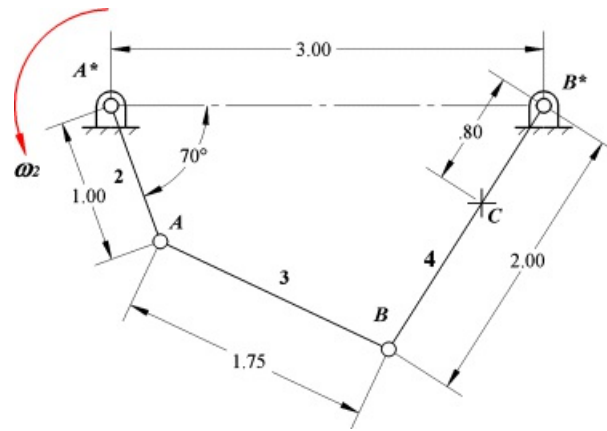


[Figure P6.28](#) Linkage for Problem 6.28.

6.29 In [Figure P6.29](#), if $\omega_2 = 5 \text{ rad/s CCW}$, find ω_6 using instant centers.

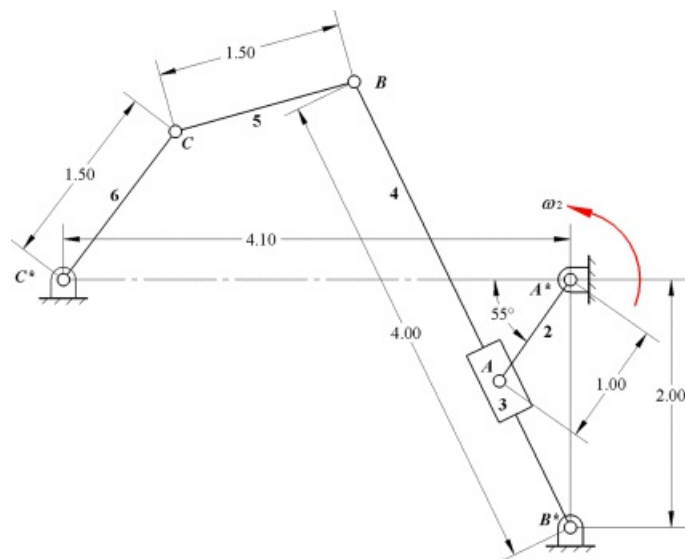


[Figure P6.29](#) Linkage for Problem 6.29.

6.30 If $\omega_2 = 100 \text{ rad/s CCW}$ in [Figure P6.30](#), find v_{C4} using instant centers and the rotating radius method. The dimensions are in inches.

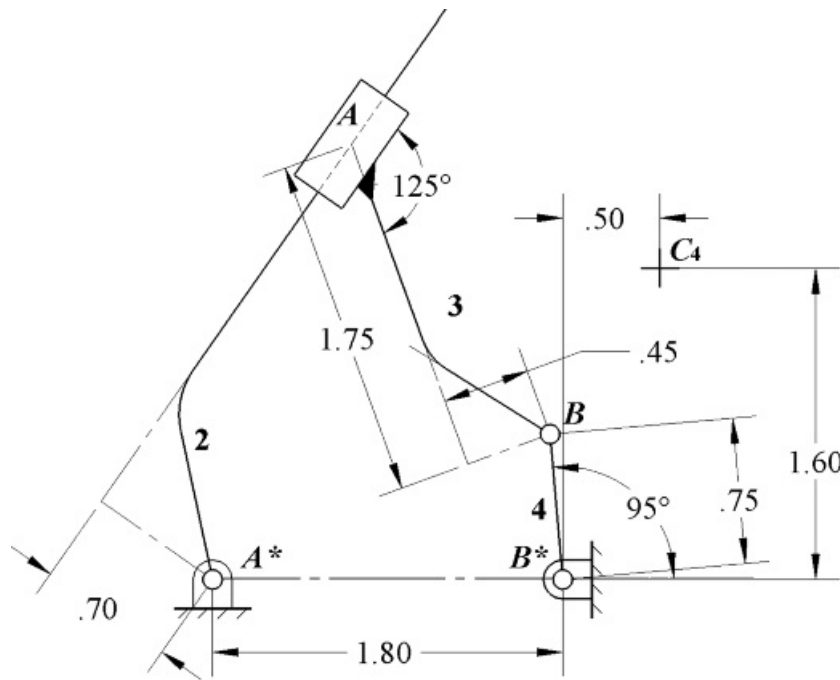


[Figure P6.30](#) Linkage for Problem 6.30.

6.31 If $v_{A2} = 10 \text{ in/s}$ as shown in [Figure P6.31](#), find the angular velocity (ω_6) of link 6 using the instant-center method. The dimensions are in inches.

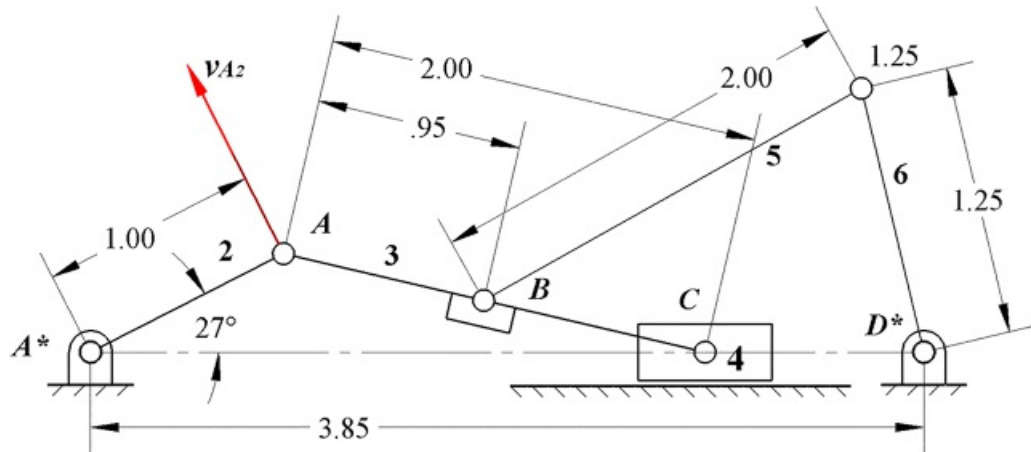


[Figure P6.31](#) Linkage for Problem 6.31.

6.32 If $\omega_2 = 50 \text{ rad/s CCW}$, find the velocity of point E using the instant-center method. Show the velocity vector v_{E5} on [Figure P6.32](#).

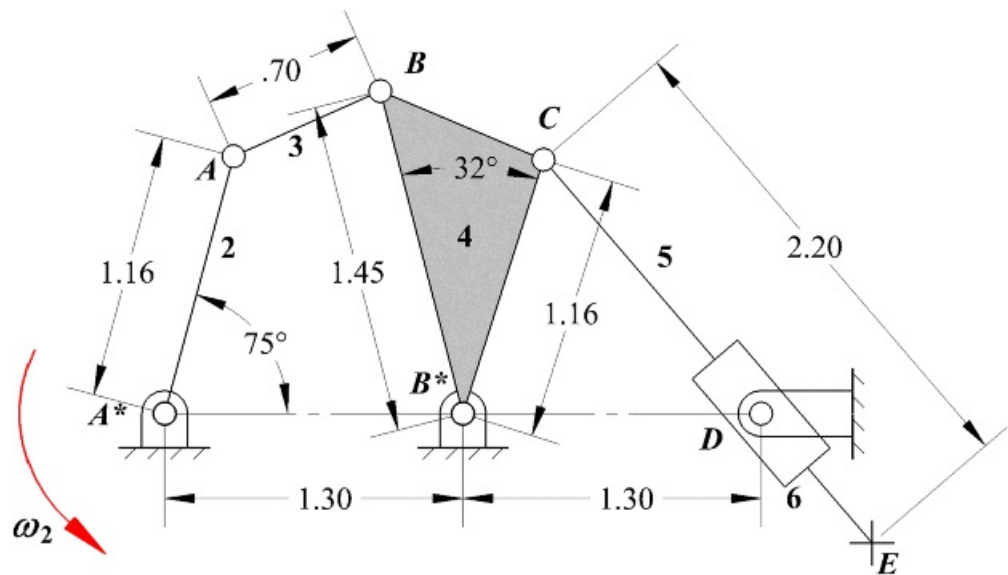


[Figure P6.32](#) Linkage for Problem 6.32.

6.33 In [Figure P6.33](#), if $\omega_2 = 100 \text{ rad/s CCW}$, find ω_6 . Link 2 is horizontal in the position shown.

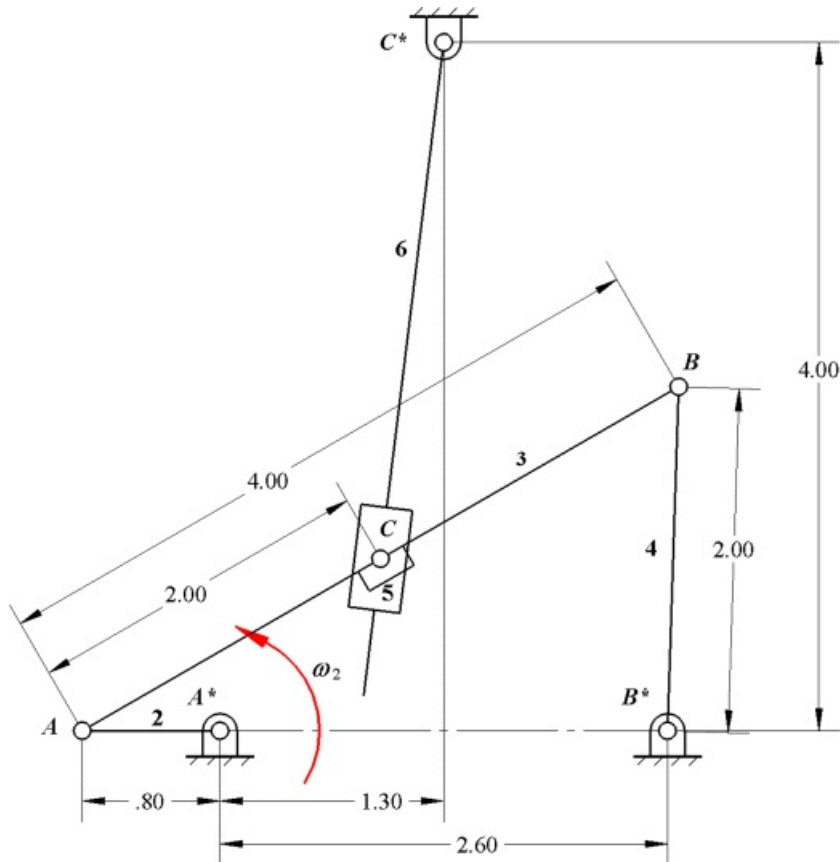


[Figure P6.33](#) Linkage for Problem 6.33.

Prerequisite Knowledge Needed for Chapter 7

A knowledge of the material on four-bar mechanisms from [Chapters 2, 3, and 4](#) and familiarity with analytical solution of a system of equations.



7.1 Introduction

In [Chapters 4](#) and [5](#), graphical techniques for position, velocity, and acceleration analysis of linkages were presented. However, as was pointed out, there are circumstances in which it is preferable to use analytical solution techniques that can be conveniently programmed on a digital computer. In situations where repetitive or extensive analyses are required, the use of computer software is highly desirable. In the present chapter, the equations used to construct analysis software are developed in detail.

The geometric constraints associated with mechanisms can be formulated using vector displacement, velocity, and acceleration closure equations. The displacement closure equations are based on the observation that there are two different, but equivalent, distinct paths connecting points on the same vector loop. For example, in the four-bar linkage shown in [Figure 7.1](#), one can reach point B from point A^* either by way of point A or point B^* .

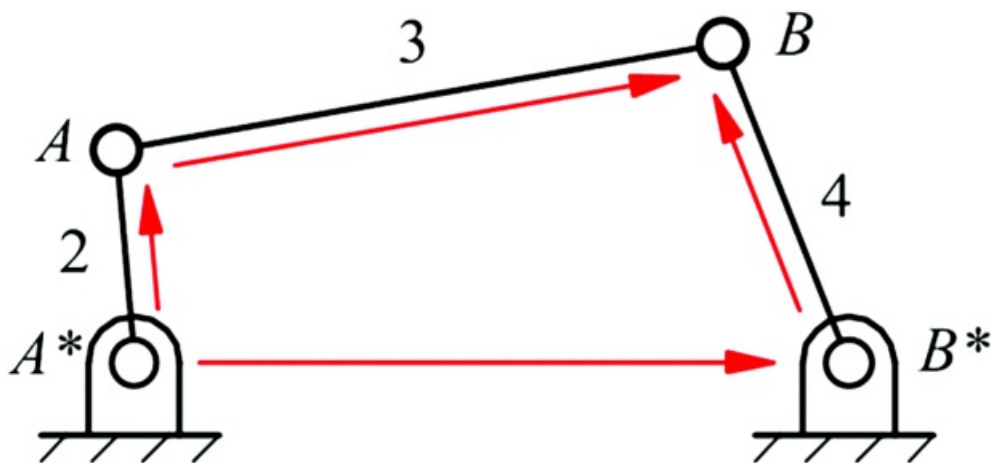


[Figure 7.1](#) Position loop closure of a four-bar linkage.

It is convenient to represent the terms in the closure equations by vectors and the procedures developed in this section work especially well for planar problems. It is also possible to apply the same general approach to spatial linkages. Another popular method for planar mechanisms, that involves slightly more computational work, is the complex number approach, in which the Cartesian vector components are expressed in terms of the real and imaginary parts of a complex number. The use of complex numbers is advantageous in some types of problems; however, the direct vector approach is preferred here. The complex number approach is outlined briefly at the end of this chapter.

There are also specialized techniques for forming closure equations for spatial mechanisms. The general trend is to work with coordinate transformation operators. For this, a set of body-fixed coordinates is established at each joint, and the product of a series of joint-to-joint coordinate transformation operators is taken. When this product is continued around the entire mechanism loop, it must be equal to the identity operator. The resulting operator equation can then be manipulated, if required, and corresponding elements are equated. Types of operators that have been used include dual complex number 2×2 matrices, dual quaternions, real number 4×4 matrices, and dual number 3×3 matrices. A discussion of the mathematics of these operators is beyond the scope of this text. The description of spatial linkages using matrix transformations is discussed in [Chapter 9](#).



7.2 Position, Velocity, and Acceleration Representations

7.2.1 Position Representation

For the purpose of developing an analytical model, we can define the relative locations of a series of points by a chain of vectors. The points will be associated with the links of a mechanism in some manner, but they do not have to be attached to specific links. An example is given in [Figure 7.2](#).

The position of point Q in the fixed reference frame is

$$\mathbf{r}_Q = \mathbf{r}_1 + \mathbf{r}_2 + \mathbf{r}_3 \quad (7.1)$$

Here, we will represent each vector by a length r_k and an angle θ_k , as shown in [Figure 7.3](#). All angles are measured counterclockwise from a line that remains parallel to the fixed horizontal axis attached to the reference frame.

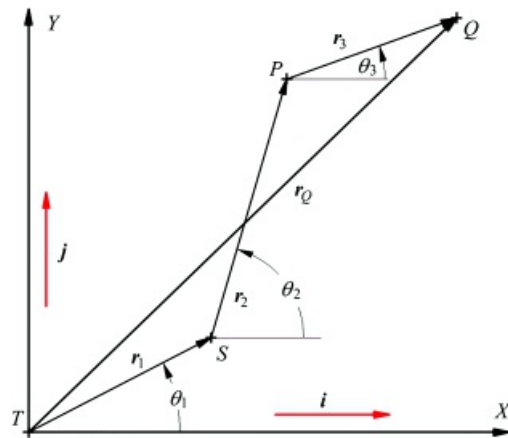


[Figure 7.2](#) Representation of a chain of points by a set of vectors.

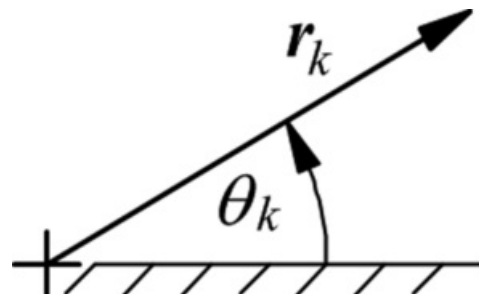


[Figure 7.3](#) Notation used for vectors.

With this notation, we can resolve each of the vectors in [Equation 7.1](#) into x and y components making use of the unit vectors i and j as follows

$$\begin{aligned} r_1 &= r_1(\cos \theta_1 i + \sin \theta_1 j) \\ r_2 &= r_2(\cos \theta_2 i + \sin \theta_2 j) \\ r_3 &= r_3(\cos \theta_3 i + \sin \theta_3 j) \end{aligned} \quad (7.2)$$

or

$$r_k = r_k(\cos \theta_k i + \sin \theta_k j) \quad (7.3)$$

7.2.2 Velocity Representation

To determine the velocity of point Q , r_Q in [Equation 7.1](#) can be differentiated. Then

$$v_Q = \dot{r}_Q = \dot{r}_1 + \dot{r}_2 + \dot{r}_3 \quad (7.4)$$

where

$$\dot{r}_k = \frac{d r_k}{dt} \quad (7.5)$$

Note that, in general, both the magnitude and direction of r_k can change. When we differentiate [Equation 7.3](#) using the chain rule of calculus, we obtain

$$\dot{r}_k = \dot{r}_k(\cos \theta_k i + \sin \theta_k j) + r_k(-\dot{\theta}_k \sin \theta_k i + \dot{\theta}_k \cos \theta_k j) \quad (7.6)$$

or

$$\dot{r}_k = (\dot{r}_k \cos \theta_k - r_k \dot{\theta}_k \sin \theta_k) i + (\dot{r}_k \sin \theta_k - r_k \dot{\theta}_k \cos \theta_k) j \quad (7.7)$$

If we compare the vector components indicated in [Equation 7.6](#) with the equations developed in Section 5.3, we will notice a similarity between corresponding terms. In particular, if $r_{Q/P}$ is the vector defining the relative position between two points P and Q , and body B is moving relative to the reference frame R as shown in [Figure 7.4](#), then

$$\dot{r}_k(\cos \theta_k i - \sin \theta_k j) = {}^B v_{Q/P} \quad (7.8)$$

and

$$r_k(-\dot{\theta}_k \sin \theta_k i + \dot{\theta}_k \cos \theta_k j) = \omega_B \times r_{Q/P} \quad (7.9)$$

[Equation 7.8](#) can be verified by recognizing that it gives the component of the velocity associated with changing the magnitude of the vector between the two points. This component is clearly in the direction of the vector r_k . The second term can be verified by computing the cross-product. Recognizing that

$$\omega_B = \dot{\theta}_k \vec{e}$$

and

$$r_{Q/P} = r_k = r_k(\cos \theta_k i + \sin \theta_k j),$$

We then have

$$\omega \times r_Q/p = \dot{\theta}_k k \times r_k (\cos \theta_k i + \sin \theta_k j) = \dot{\theta}_k r_k (\cos \theta_k i + \sin \theta_k j) \\ = r_k \dot{\theta}_k (-\sin \theta_k i + \cos \theta_k j)$$

[Equation 7.4](#) can also be expressed as

$$r_Q = \sum_{k=1}^3 r_k (\cos \theta_k i + \sin \theta_k j) + r_k (-\dot{\theta}_k \sin \theta_k i + \dot{\theta}_k \cos \theta_k j) \quad (7.10)$$

or

$$r_Q = \sum_{k=1}^3 (\dot{r}_k \cos \theta_k - r_k \dot{\theta}_k \sin \theta_k) i + (\dot{r}_k \sin \theta_k + r_k \dot{\theta}_k \cos \theta_k) j \quad (7.11)$$

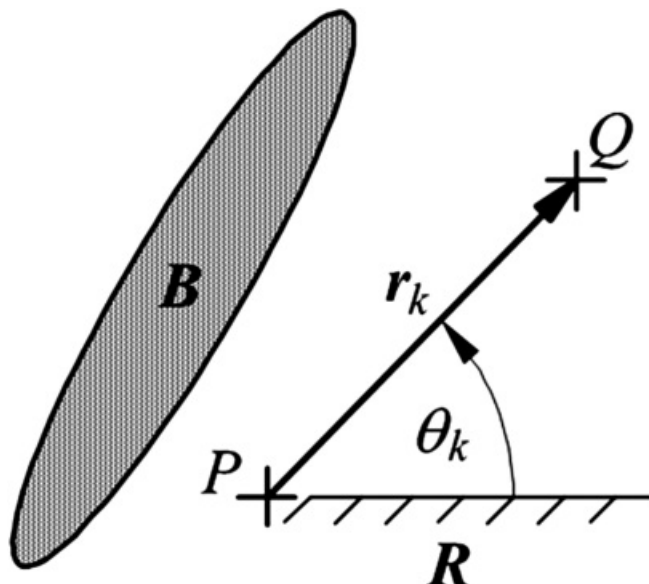


[Figure 7.4](#) Position vector between two points.

7.2.3 Acceleration Representation

To obtain the acceleration expression, we need only to differentiate the velocity expression ([Equation 7.4](#)). Symbolically, this is

$$\ddot{r}_Q = \ddot{r}_G = \ddot{r}_1 + \ddot{r}_2 + \ddot{r}_3 \quad (7.12)$$

where

$$\ddot{r}_k = \frac{d^2 r_k}{dt^2}$$

Because the vectors have been defined in a consistent manner ([Figure 7.3](#)), the form for the derivatives for all of the vectors will be the same. Therefore, we can develop the expression with a general vector r_k .

Note again that, in general, both the magnitude and direction of r_k can change. When we differentiate [Equation](#)

7.6 using the chain rule of calculus, we obtain

$$\ddot{r}_k = \ddot{r}_k(\cos \theta_k i + \sin \theta_k j) + r_k \dot{\theta}_k^2 (-\sin \theta_k i + \cos \theta_k j) - r_k \dot{\theta}_k^2 (\cos \theta_k i + \sin \theta_k j) + 2\dot{r}_k \dot{\theta}_k (-\sin \theta_k i + \cos \theta_k j) \quad (7.13)$$

or

$$\ddot{r}_k = [(r_k - r_k \dot{\theta}_k^2) \cos \theta_k - (r_k \dot{\theta}_k + 2\dot{r}_k \dot{\theta}_k) \sin \theta_k] i + [(r_k - r_k \dot{\theta}_k^2) \sin \theta_k + (r_k \dot{\theta}_k + 2\dot{r}_k \dot{\theta}_k) \cos \theta_k] j \quad (7.14)$$

As in the case of the velocity equations, we can compare the vector components indicated in [Equation 7.13](#) with the acceleration equations developed in Section 5.4. Using the same nomenclature as before ([Figure 7.4](#))

$$r_k(\cos \theta_k i + \sin \theta_k j) = {}^B \omega_B / \rho \quad (7.15)$$

$$r_k \dot{\theta}_k (-\sin \theta_k i + \cos \theta_k j) = \omega_B \times {}^B r_B / \rho \quad (7.16)$$

$$-r_k \dot{\theta}_k^2 (\cos \theta_k i + \sin \theta_k j) = \omega_B \times (\omega_B \times {}^B r_B / \rho) \quad (7.17)$$

and

$$2\dot{r}_k \dot{\theta}_k (-\sin \theta_k i + \cos \theta_k j) = 2\omega_B \times {}^B v_B / \rho \quad (7.18)$$

These can be verified by direct calculation.

If we add the individual components, we can obtain the acceleration of point Q . Then [Equation 7.12](#) can be expressed as

$$a_Q = \sum_{k=1}^3 [{}^B r_k (\cos \theta_k i + \sin \theta_k j) + r_k \dot{\theta}_k^2 (-\sin \theta_k i + \cos \theta_k j) - r_k \dot{\theta}_k^2 (\cos \theta_k i + \sin \theta_k j) + 2\dot{r}_k \dot{\theta}_k (-\sin \theta_k i + \cos \theta_k j)] \quad (7.19)$$

or

$$a_Q = \sum_{k=1}^3 [(r_k - r_k \dot{\theta}_k^2) \cos \theta_k - (r_k \dot{\theta}_k + 2\dot{r}_k \dot{\theta}_k) \sin \theta_k] i + [(r_k - r_k \dot{\theta}_k^2) \sin \theta_k + (r_k \dot{\theta}_k + 2\dot{r}_k \dot{\theta}_k) \cos \theta_k] j \quad (7.20)$$

7.2.4 Special Cases

[Equations 7.6](#) and [7.13](#) or [7.7](#) and [7.14](#) are the most general forms of the velocity and acceleration equations. However, in most mechanisms, usually some of the terms will be zero because of the special conditions associated with the way in which the vectors are defined. It is possible for any of the terms involved in the velocity and acceleration equations to be zero. However, a common case is to have the magnitude of a given position vector to

be constant. This is the case when the vector defines the relative positions of two points on a rigid link. When this happens, $\dot{\gamma}$ and $\ddot{\gamma}$ are zero. Then, the velocity and acceleration expressions become

$$\dot{r}_k = r_k \dot{\theta}_k (-\sin \theta_k i + \cos \theta_k j) \quad (7.21)$$

$$\ddot{r}_k = r_k \ddot{\theta}_k (-\sin \theta_k i + \cos \theta_k j) - r_k \dot{\theta}_k^2 (\cos \theta_k i + \sin \theta_k j) \quad (7.22)$$

or

$$\ddot{r}_k = [-r_k \dot{\theta}_k^2 \cos \theta_k - r_k \dot{\theta}_k \sin \theta_k] i + [-r_k \dot{\theta}_k^2 \sin \theta_k + r_k \dot{\theta}_k \cos \theta_k] j \quad (7.23)$$

7.2.5 Mechanisms to Be Considered

There are six commonly used single-loop chains with revolute and slider joints. We will look at two of these in detail to illustrate how the equations can be developed in each case. Then, we will describe the remaining four cases, as the equations for these can be developed similarly to the first two. We will then discuss more complex mechanisms that require several vector loops and mechanisms that contain higher pairs.



7.3 Analytical Closure Equations for Four-Bar Linkages

We will first give an overview of the development of the equations for the four-bar linkage using the general nomenclature discussed above. The procedures used to solve the equations for the four-bar linkage are similar to the procedures required for solving the equations associated with most other simple mechanisms.

The closure condition simply expresses the condition that a loop of a linkage closes on itself. For the four-bar linkage shown in [Figure 7.5](#), the closure equations would be

$$r_3 = r_2 + r_3 = r_1 + r_4 \quad (7.24)$$

or

$$r_2(\cos \theta_2 i + \sin \theta_2 j) + r_3(\cos \theta_3 i + \sin \theta_3 j) = r_1(\cos \theta_1 i + \sin \theta_1 j) + r_4(\cos \theta_4 i + \sin \theta_4 j) \quad (7.25)$$

Rewriting [Equation 7.25](#) in its component equations, one gets

$$r_2 \cos \theta_2 - r_3 \cos \theta_3 = r_1 \cos \theta_1 - r_4 \cos \theta_4 \quad (7.26)$$

$$r_2 \sin \theta_2 - r_3 \sin \theta_3 = r_1 \sin \theta_1 - r_4 \sin \theta_4 \quad (7.27)$$

[Equations 7.26](#) and [7.27](#) are the closure equations, and they must be satisfied throughout the motion of the linkage. The base vector will be constant, so r_1 and θ_1 are constants. If θ_2 is given, that is, if crank A^*A is a driving crank, it is necessary to solve [Equations 7.26](#) and [7.27](#) for θ_3 and θ_4 in terms of θ_2 . Once these expressions are obtained, $\dot{\theta}_3$, $\ddot{\theta}_3$, $\dot{\theta}_4$, and $\ddot{\theta}_4$ can be obtained in terms of $\dot{\theta}_2$, $\ddot{\theta}_2$, and $\dot{\theta}_2$ by differentiation. Velocities and accelerations of points in the mechanism can then be obtained from equations of the type of [Equations 7.11](#) and [7.19](#) recognizing that all of the vector magnitudes are constant ($\dot{r} = \ddot{r} = 0$).

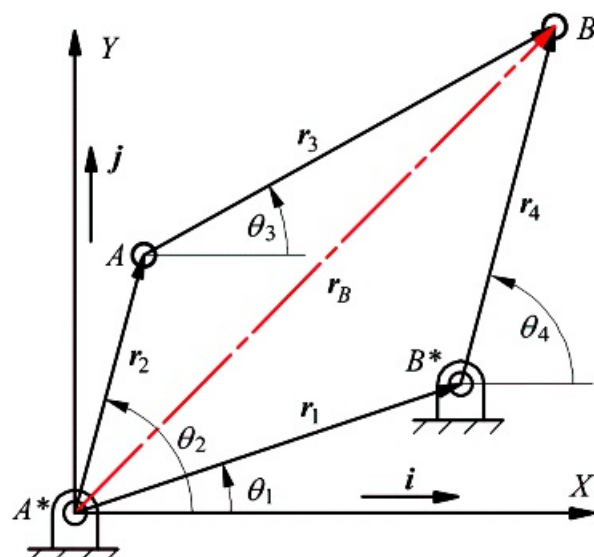


[Figure 7.5](#) Vector closure condition for a four-bar loop. The position of point B obtained by adding the vectors r_2 and r_3 must always be the same as that obtained by adding vectors r_1 and r_4 . Note that r_1 is a

constant vector that describes the base member of the linkage. Correspondingly, θ_1 is a constant angle.

When θ_3 is given, the coupler is the driver, and we must solve Equations 7.26 and 7.27 for θ_2 and θ_4 in terms of θ_3 . The procedure for doing this is very similar to that used when θ_2 is the input. Therefore, we will first reconsider briefly the case in which θ_2 is the input.

7.3.1 Solution of Closure Equations for Four-Bar Linkages When Link 2 Is the Driver

The analytical solution procedure follows the same major steps as in the graphical solution. That is, a position analysis must first be performed, then a velocity analysis, and finally the acceleration analysis. The position analysis, for a closed-loop linkage, comprises the solution of the closure equations for the joint angles or link orientations. Once this solution is obtained, the velocity and acceleration states are quickly obtainable using the differentiated equations. It will be seen, however, that the position analysis that is so easily performed graphically by construction of a drawing to scale, is a complex matter when performed analytically.

For all of the simple mechanisms that we will consider initially, the first step in solving the position equations is to identify the variable to be determined first. When the position equations involve two angles as unknowns, the solution procedure is to isolate the trigonometric function involving the angle to be eliminated on the left-hand side of the equation. To eliminate θ_3 in the linkage shown in Figure 7.5, first isolate it on one side of Equations 7.26 and 7.27 as follows

$$r_3 \cos \theta_3 = r_1 \cos \theta_1 + r_4 \cos \theta_4 - r_2 \cos \theta_2 \quad (7.28)$$

$$r_3 \sin \theta_3 = r_1 \sin \theta_1 + r_4 \sin \theta_4 - r_2 \sin \theta_2 \quad (7.29)$$

Notice that the angle θ_1 is a known constant. Now square both sides of both equations, add, and simplify the result using the trigonometric identity, $\sin^2 \theta + \cos^2 \theta = 1$. This gives

$$\begin{aligned} r_3^2 &= r_1^2 + r_2^2 + r_4^2 + 2r_1r_4(\cos \theta_1 \cos \theta_4 + \sin \theta_1 \sin \theta_4) \\ &\quad - 2r_1r_2(\cos \theta_1 \cos \theta_2 - \sin \theta_1 \sin \theta_2) - 2r_2r_4(\cos \theta_2 \cos \theta_4 + \sin \theta_2 \sin \theta_4) \end{aligned} \quad (7.30)$$

Equation 7.30 gives θ_4 in terms of the given angle θ_2 (and the constant angle θ_1) but not explicitly. To obtain an explicit expression, simplify Equation 7.30 by combining the coefficients of $\cos \theta_4$ and $\sin \theta_4$ as follows

$$A \cos \theta_4 + B \sin \theta_4 + C = 0 \quad (7.31)$$

where:

$$\begin{aligned} A &= 2r_1r_4 \cos \theta_1 + 2r_2r_4 \cos \theta_2 \\ B &= 2r_1r_4 \sin \theta_1 - 2r_2r_4 \sin \theta_2 \\ C &= r_1^2 + r_2^2 + r_4^2 - r_3^2 - 2r_1r_2(\cos \theta_1 \cos \theta_2 + \sin \theta_1 \sin \theta_2) \end{aligned} \quad (7.32)$$

To solve Equation 7.31, use the standard trigonometric identities for half angles given in the following

$$\sin \theta_4 = \frac{2 \tan \frac{\theta_4}{2}}{1 + \tan^2 \frac{\theta_4}{2}} \quad (7.33)$$

$$\tan \theta_4 = \frac{1 - \tan^2 \frac{\theta_4}{2}}{1 + \tan^2 \frac{\theta_4}{2}} \quad (7.34)$$

After substitution and simplification, we get

$$(C - A)t^2 + 2Bt + (A + C) = 0$$

where

$$t = \tan \frac{\theta_4}{2}$$

Solving for t gives

$$t = \frac{-2B + \sigma \sqrt{4B^2 - 4(C-A)(C+A)}}{2(C-A)} = \frac{-B + \sigma \sqrt{B^2 - C^2 + A^2}}{C-A} \quad (7.35)$$

and

$$\theta_4 = 2\arctan^{-1} t \quad (7.36)$$

where $\sigma = \pm 1$ is a sign variable identifying the assembly mode. Note that $\arctan^{-1} t$ has a valid range of $-\pi/2 \leq \arctan^{-1} t \leq \pi/2$. Therefore, θ_4 will have the range $-\pi \leq \theta_4 \leq \pi$. Unless the linkage is in one of the extreme positions of its motion range, there are two solutions for θ_4 corresponding to the two values of σ , and they are both valid. These correspond to two assembly modes or branches for the linkage. Once we pick the value for σ corresponding to the desired mode, the sign in an actual linkage stays the same for any value of θ_4 .

Because of the square root in [Equation 7.35](#), the variable t can be complex ($A^2 + B^2 < C^2$). If this happens, the mechanism cannot be assembled in the position specified. The assembly configurations would then appear as shown in [Figure 7.6](#).

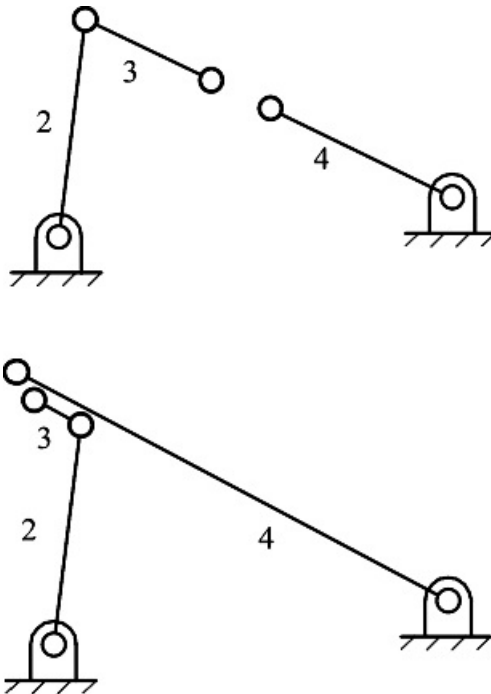


Figure 7.6 Double-rocker linkages cannot be placed in positions that are transitions between solution branches. The variable t would be complex in these cases.

After θ_4 is known, Equations 7.28 and 7.29 can now be solved for θ_3 . Dividing Equation 7.29 by Equation 7.28 and solving for θ_3 gives

$$\theta_3 = \tan^{-1} \left[\frac{r_1 \sin \theta_1 + r_4 \sin \theta_4 - r_2 \sin \theta_2}{r_1 \cos \theta_1 + r_4 \cos \theta_4 - r_2 \cos \theta_2} \right] \quad (7.37)$$

Note that in Equation 7.37, it is essential that the sign of the numerator and denominator be maintained to determine the quadrant in which the angle θ_3 lies. This results in a single solution for θ_3 that can be determined directly in MATLAB by using the ATAN2 function. The form of this function is

$$\text{ATAN2}(\sin \theta_3, \cos \theta_3) = \tan^{-1} \left[\frac{\sin \theta_3}{\cos \theta_3} \right]. \quad (7.38)$$

Equations 7.35 through 7.37 give a complete and consistent solution to the position problem. As indicated before, for any value of θ_3 , there are typically two values of θ_2 and θ_4 , given by substituting $\sigma = +1$ and -1 , respectively, in Equation 7.35. These two different solutions are shown in Figure 7.7. The two solutions correspond to an assembly ambiguity that also appears in the graphical construction.

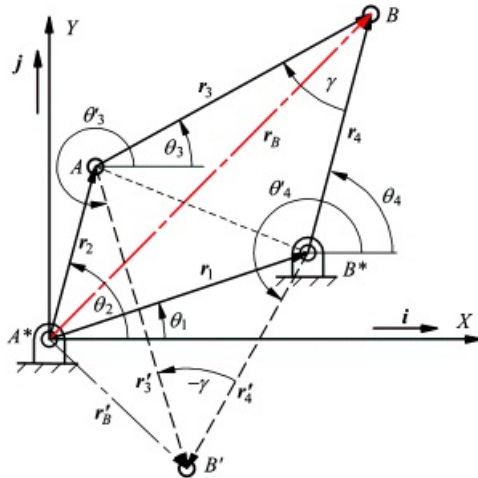


Figure 7.7 The two possible positions (B and B') of the point B for a given value of θ_3 . Note that $AB'B^*$ is the mirror image of ABB^* about the line AB^* . Notice that there are two different possible values of θ_4 and two different values of γ , corresponding to the two possible positions of point B . The sign of the angle ABB^* (γ) is reversed in the second solution, although the magnitude of $AB'B^*$ is the same. The sign of γ is a useful graphical indicator of which solution is being examined (see Section 3.4).

Note that the positions of r_3 and r_4 are symmetric about the line AB^* . Therefore, the angle $\gamma = \theta_4 - \theta_3$ has the same magnitude, but opposite sign, in each of the two positions. The sign of γ provides a useful indicator of which of the solution branches has been drawn, from the graphical point of view.

Once all of the angular quantities are known, it is relatively straightforward to compute the coordinates on any point on the vector loops used in the closure equations. In particular, the coordinates of A , B , and B^* are given by

$$r_A = r_2 = r_2(\cos \theta_2 i + \sin \theta_2 j) \quad (7.39)$$

$$\begin{aligned} r_B &= r_2 + r_3 = r_2(\cos \theta_2 i + \sin \theta_2 j) + r_3(\cos \theta_3 i + \sin \theta_3 j) \\ &= r_1 + r_4 = r_1(\cos \theta_1 i + \sin \theta_1 j) + r_4(\cos \theta_4 i + \sin \theta_4 j) \end{aligned} \quad (7.40)$$

and

$$r_{B^*} = r_1 = r_1(\cos \theta_1 i + \sin \theta_1 j) \quad (7.41)$$

7.3.2 Analysis When the Coupler (Link 3) Is the Driving Link

The analytical procedure given above when one of the frame-mounted links (link 2) in [Figure 7.5](#) is the driver is very similar to the graphical procedure. However, if the coupler is the driver, it is difficult to analyze the linkage graphically. The analytical procedure, on the other hand, is very straightforward and no more difficult to conduct than when one of the frame-mounted links is the driver. The details follow exactly the same procedure as that given in Section 7.3.1. Therefore, we will simply outline the procedure and tabulate the results.

In the procedure, we can assume that in [Figure 7.5](#) that $\theta_1, \theta_3, \theta_2$, and θ_3 are known, and $\theta_2, \theta_3, \theta_2, \theta_4, \theta_4$, and θ_4 are to be found. All of the link lengths and θ_1 are constants. For the position analysis, again begin with [Equations 7.26](#) and [7.27](#) and isolate the terms with either θ_2 or θ_4 . It is advantageous to select θ_2 for reasons that will become apparent. The resulting equations are

$$r_2 \cos \theta_2 = r_1 \cos \theta_1 + r_4 \cos \theta_4 - r_3 \cos \theta_3 \quad (7.42)$$

$$r_2 \sin \theta_2 = r_1 \sin \theta_1 + r_4 \sin \theta_4 - r_3 \sin \theta_3 \quad (7.43)$$

A comparison of [Equations 7.42](#) and [7.43](#) with [Equations 7.28](#) and [7.29](#) indicates that they are of exactly the same form except that the indices 2 and 3 are interchanged. Therefore, we can use directly the position solution derived in Section 7.3.1 if we interchange the indices 2 and 3.

When the coupler is the driver, there is an assembly-mode ambiguity similar to that when link 2 is the driver. This is illustrated in [Figure 7.8](#). It is necessary to know the appropriate mode before the analysis is begun; however, once the assembly mode is selected, it is the same for any position of the input link.

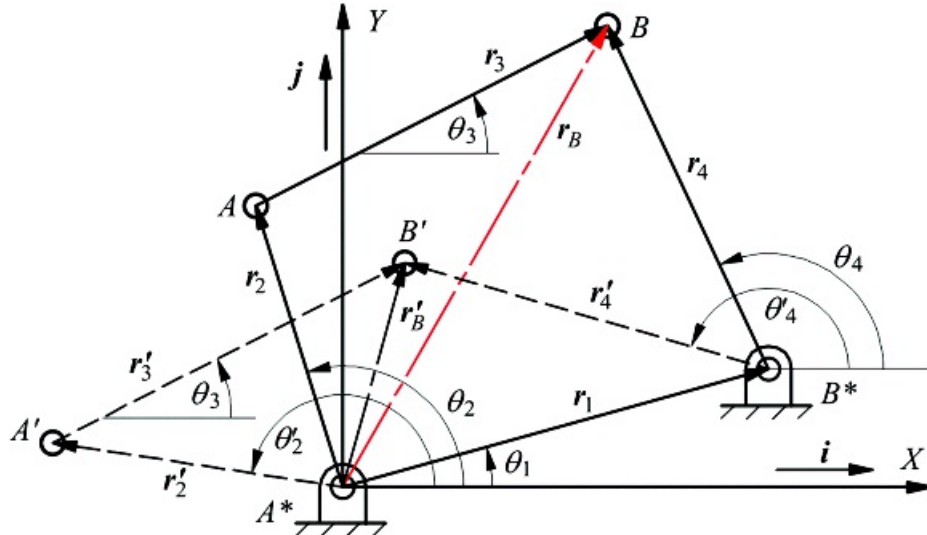


[Figure 7.8](#) The two possible positions (B and B') of the point B for a given value of θ_3 . There are two different possible values of θ_2 , and two different values of θ_4 corresponding to the two possible positions of point B .

The motion of the coupler in a coupler-driven four-bar linkage will be less than 360° unless the four-bar is a type I linkage with the coupler or base as the shortest link. When the linkage reaches its motion limits, links 2 and 4 will be parallel.

7.3.3 Velocity Equations for Four-Bar Linkages

The analytical form of the velocity equations can be developed by differentiating [Equation 7.24](#). The result is

$$\dot{\theta}_3 = \dot{\theta}_2 - \dot{\theta}_3 = \dot{\theta}_1 + \dot{\theta}_4 \quad (7.44)$$

When this equation is written in component form, the result is the same as that of differentiating [Equations 7.26](#) and [7.27](#). Recognizing that all of the link lengths are constant as is θ_1 , the resulting component equations are

$$r_2 \dot{\theta}_2 \sin \theta_2 + r_3 \dot{\theta}_3 \sin \theta_3 = r_4 \dot{\theta}_4 \sin \theta_4 \quad (7.45)$$

$$r_2 \dot{\theta}_2 \cos \theta_2 + r_3 \dot{\theta}_3 \cos \theta_3 = r_4 \dot{\theta}_4 \cos \theta_4 \quad (7.46)$$

If $\dot{\theta}_2$ is known, the only new unknowns are $\dot{\theta}_3$ and $\dot{\theta}_4$, and if $\dot{\theta}_3$ is known, the only new unknowns are $\dot{\theta}_2$ and $\dot{\theta}_4$. In either case, the equations can be solved most easily using a linear equation solver. In matrix form, [Equations 7.45](#) and [7.46](#) can be rearranged and rewritten as

$$\begin{bmatrix} -r_2 \sin \theta_2 & r_4 \sin \theta_4 \\ -r_2 \cos \theta_2 & r_4 \cos \theta_4 \end{bmatrix} \begin{Bmatrix} \dot{\theta}_3 \\ \dot{\theta}_4 \end{Bmatrix} = \begin{Bmatrix} r_M \dot{\theta}_M \sin \theta_M \\ r_M \dot{\theta}_M \cos \theta_M \end{Bmatrix} \quad (7.47)$$

where $M = 2$ and $J = 3$ for $\dot{\theta}_2$ as the input, and $M = 3$ and $J = 2$ for $\dot{\theta}_3$ as the input. The terms in the matrix and vector on the right-hand side of the equation will be known. The equation can therefore be solved manually, on a programmable calculator, or with the matrix solvers in programs such as MATLAB.

Once the angular velocities are known, it is a simple matter to compute the linear velocities of any of the points on the vector loop. The velocities of points A and B are given by

$$\dot{r}_A = \dot{r}_2 = r_2 \dot{\theta}_2 (-\sin \theta_2) \mathbf{i} + (\cos \theta_2) \mathbf{j} \quad (7.48)$$

and

$$\begin{aligned} \dot{r}_3 &= \dot{r}_2 + \dot{r}_3 = (-r_2 \dot{\theta}_2 \sin \theta_2 - r_3 \dot{\theta}_3 \sin \theta_3) \mathbf{i} + (r_2 \dot{\theta}_2 \cos \theta_2 + r_3 \dot{\theta}_3 \cos \theta_3) \mathbf{j} \\ &= \dot{r}_1 + \dot{r}_4 = (-r_4 \dot{\theta}_4 \sin \theta_4) \mathbf{i} + (r_4 \dot{\theta}_4 \cos \theta_4) \mathbf{j} \end{aligned} \quad (7.49)$$

7.3.4 Acceleration Equations for Four-Bar Linkages

The analytical form of the acceleration equations can be developed by differentiating [Equation 7.44](#). The result is

$$\ddot{r}_3 = \ddot{r}_2 + \ddot{r}_3 = \ddot{r}_1 + \ddot{r}_4 \quad (7.50)$$

When this equation is written in component form, the result is the same as differentiating [Equations 7.45](#) and [7.46](#). The resulting component equations are

$$r_2 \ddot{\theta}_2 \sin \theta_2 - r_2 \dot{\theta}_2^2 \cos \theta_2 + r_3 \ddot{\theta}_3 \sin \theta_3 - r_3 \dot{\theta}_3^2 \cos \theta_3 = r_4 \ddot{\theta}_4 \sin \theta_4 - r_4 \dot{\theta}_4^2 \cos \theta_4 \quad (7.51)$$

$$r_2 \ddot{\theta}_2 \cos \theta_2 - r_2 \dot{\theta}_2^2 \sin \theta_2 + r_3 \ddot{\theta}_3 \cos \theta_3 - r_3 \dot{\theta}_3^2 \sin \theta_3 = r_4 \ddot{\theta}_4 \cos \theta_4 - r_4 \dot{\theta}_4^2 \sin \theta_4 \quad (7.52)$$

When $\dot{\theta}_2$ is known along with all of the position and velocity terms, the only new unknowns are $\dot{\theta}_3$ and $\dot{\theta}_4$, and when $\dot{\theta}_3$ is known along with all of the position and velocity terms, the only new unknowns are $\dot{\theta}_2$ and $\dot{\theta}_4$. Again, because a linear problem is involved, these can be solved for most easily using a linear equation solver. In matrix form, [Equations 7.51](#) and [7.52](#) can be rearranged and rewritten as

$$\begin{bmatrix} -r_2 \sin \theta_2 & r_4 \sin \theta_4 \\ -r_2 \cos \theta_2 & r_4 \cos \theta_4 \end{bmatrix} \begin{Bmatrix} \ddot{\theta}_3 \\ \ddot{\theta}_4 \end{Bmatrix} = \begin{Bmatrix} r_M \ddot{\theta}_M \sin \theta_M + r_2 \dot{\theta}_2^2 \cos \theta_M + r_3 \dot{\theta}_3^2 \cos \theta_M - r_4 \dot{\theta}_4^2 \cos \theta_M \\ r_M \ddot{\theta}_M \cos \theta_M - r_2 \dot{\theta}_2^2 \sin \theta_M - r_3 \dot{\theta}_3^2 \sin \theta_M + r_4 \dot{\theta}_4^2 \sin \theta_M \end{Bmatrix} \quad (7.53)$$

where $M = 2$ and $J = 3$ for $\dot{\theta}_2$ as the input, and $M = 3$ and $J = 2$ for $\dot{\theta}_3$ as the input. The terms in the matrix and vector on the right-hand side of the equation will be known. The equation can therefore be solved manually, on a

programmable calculator, or with the matrix solvers in programs such as MATLAB. Notice that the coefficient matrix is the same for both the velocities (Equation 7.47) and the accelerations (Equation 7.53).

Once the angular accelerations are known, it is a simple matter to compute the linear accelerations of any of the points in the linkage. The accelerations of points A and B are given by

$$\ddot{r}_A = \ddot{r}_B = (-r_2\dot{\theta}_2 \sin \theta_2 - r_2\dot{\theta}_2^2 \cos \theta_2)i + (r_2\dot{\theta}_2 \cos \theta_2 - r_2\dot{\theta}_2^2 \sin \theta_2)j \quad (7.54)$$

and

$$\begin{aligned} \ddot{r}_S &= \ddot{r}_2 + \ddot{r}_3 = -(r_2\dot{\theta}_2 \sin \theta_2 + r_2\dot{\theta}_2^2 \cos \theta_2 + r_3\dot{\theta}_3 \sin \theta_3 + r_3\dot{\theta}_3^2 \cos \theta_3)i \\ &\quad + (r_2\dot{\theta}_2 \cos \theta_2 - r_2\dot{\theta}_2^2 \sin \theta_2 + r_3\dot{\theta}_3 \cos \theta_3 - r_3\dot{\theta}_3^2 \sin \theta_3)j \\ &= \ddot{r}_1 + \ddot{r}_4 = -(r_4\dot{\theta}_4 \sin \theta_4 + r_4\dot{\theta}_4^2 \cos \theta_4)i + (r_4\dot{\theta}_4 \cos \theta_4 - r_4\dot{\theta}_4^2 \sin \theta_4)j \end{aligned} \quad (7.55)$$

Now that the equations have been developed, it is relatively simple to write a computer program for the analysis of a four-bar linkage. To aid in this, the equations required are summarized in Table 7.1. The authors have found that MATLAB is a very convenient language for solving simple kinematic equations, and this program runs on a variety of platforms. MATLAB routines for analyzing four-bar linkages are contained in the supplementary material provided with this book.

Table 7.1 Summary of Position, Velocity, and Acceleration Equations for a Four-Bar Linkage. (Link 2 is the input link when $M = 2$ and $J = 3$. Link 3 is the input link when $M = 3$ and $J = 2$. Link 1 is assumed to be the frame. The link numbers and points are defined in Figure 7.5.)

Position
$A = 2r_1r_4 \cos \theta_1 - 2r_Mr_4 \cos \theta_M$
$B = 2r_1r_4 \sin \theta_1 - 2r_Mr_4 \sin \theta_M$
$C = r_1^2 + r_M^2 + r_4^2 - r_2^2 - 2r_1r_M(\cos \theta_1 \cos \theta_M + \sin \theta_1 \sin \theta_M)$
$\theta_4 = 2 \tan^{-1} \left \frac{-s + \sqrt{s^2 - C^2 + A^2}}{C - A} \right ; s = \pm 1$
$\theta_3 = \tan^{-1} \left \frac{r_1 \sin \theta_1 + r_4 \sin \theta_4 - r_2 \sin \theta_2}{r_1 \cos \theta_1 + r_4 \cos \theta_4 - r_2 \cos \theta_2} \right $
$r_A = r_2 = r_2(\cos \theta_2 i + \sin \theta_2 j)$
$r_B = r_2 + r_3 = r_2(\cos \theta_2 i + \sin \theta_2 j) + r_3(\cos \theta_3 i + \sin \theta_3 j)$
$= r_1 + r_4 = r_1(\cos \theta_1 i + \sin \theta_1 j) + r_4(\cos \theta_4 i + \sin \theta_4 j)$
$r_{S*} = r_1 = r_1(\cos \theta_1 i + \sin \theta_1 j)$
Velocity
$\begin{bmatrix} -r_2 \sin \theta_2 & r_2 \sin \theta_2 \end{bmatrix} \begin{Bmatrix} \dot{\theta}_2 \\ \dot{\theta}_4 \end{Bmatrix} = \begin{Bmatrix} r_2\dot{\theta}_2 \sin \theta_2 \\ r_4\dot{\theta}_4 \cos \theta_4 \end{Bmatrix}$
$\dot{r}_A = \dot{r}_2 = r_2\dot{\theta}_2(-\sin \theta_2 i + \cos \theta_2 j)$
$\dot{r}_B = (-r_2\dot{\theta}_2 \sin \theta_2)i + (r_2\dot{\theta}_2 \cos \theta_2)j$
Acceleration
$\begin{bmatrix} -r_2 \sin \theta_2 & r_2 \sin \theta_2 \end{bmatrix} \begin{Bmatrix} \ddot{\theta}_2 \\ \ddot{\theta}_4 \end{Bmatrix} = \begin{Bmatrix} r_2\dot{\theta}_2^2 \sin \theta_2 + r_4\dot{\theta}_4^2 \cos \theta_4 & r_2\dot{\theta}_2^2 \cos \theta_2 + r_4\dot{\theta}_4^2 \sin \theta_4 \\ r_2\dot{\theta}_2^2 \cos \theta_2 + r_4\dot{\theta}_4^2 \sin \theta_4 & r_2\dot{\theta}_2^2 \sin \theta_2 + r_4\dot{\theta}_4^2 \cos \theta_4 \end{Bmatrix}$
$\ddot{r}_A = \ddot{r}_B = (-r_2\dot{\theta}_2 \sin \theta_2 - r_2\dot{\theta}_2^2 \cos \theta_2)i + (r_2\dot{\theta}_2 \cos \theta_2 - r_2\dot{\theta}_2^2 \sin \theta_2)j$
$\ddot{r}_S = -(r_4\dot{\theta}_4 \sin \theta_4 + r_4\dot{\theta}_4^2 \cos \theta_4)i + (r_4\dot{\theta}_4 \cos \theta_4 - r_4\dot{\theta}_4^2 \sin \theta_4)j$



Example 7.1

Position Analysis of a Four-Bar Linkage

For a linkage with $r_1 = 1$, $r_2 = 2$, $r_3 = 3.5$, $r_4 = 4$, and $\theta_1 = 0$ shown in [Figure 7.9](#), compute the corresponding values of θ_3 and θ_4 for each of the solution branches when the driving crank is in the positions $\theta_2 = 0, \pi/2, \pi, -\pi/2$. Units for the lengths are not explicitly given in this example because the angular results are independent of the units for the lengths.

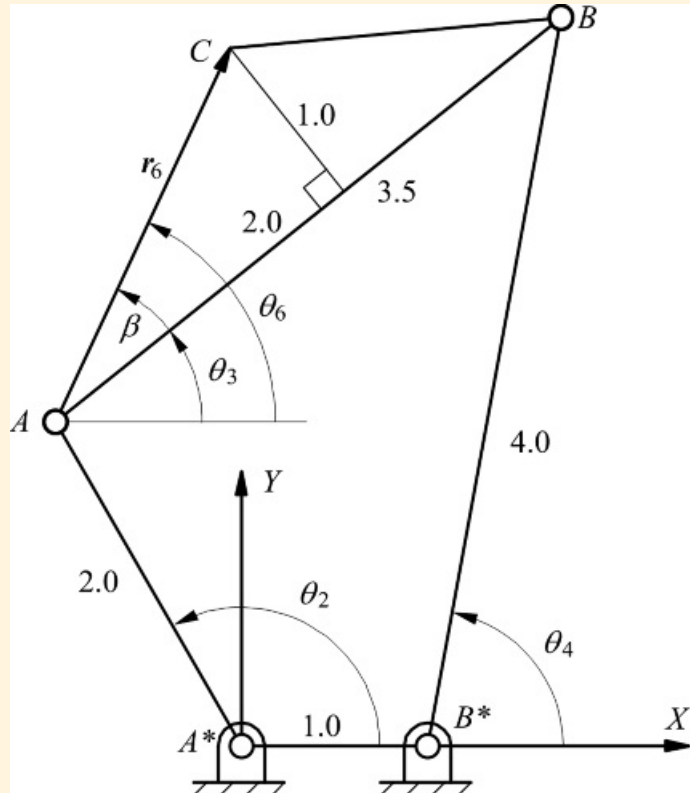


[Figure 7.9](#) The linkage for Example 7.1, 7.2, and 7.3.

Solution

The solution procedure is to use the equations in [Table 7.1](#). First compute A , B , and C in [Table 7.1](#) for each value of θ_2 and then select π . Next compute θ_4 and then θ_3 . The calculations for $\theta_2 = 0$ are as follows

$$\begin{aligned} A &= 2r_1r_4 \cos \theta_1 - 2r_2r_4 \cos \theta_2 = 2(1)(4) - 2(2)(4) \\ &= -8 \\ B &= 2r_1r_4 \sin \theta_1 - 2r_2r_4 \sin \theta_2 = 0 \\ C &= r_1^2 + r_2^2 + r_4^2 - r_3^2 - 2r_1r_2(\cos \theta_1 \cos \theta_2 + \sin \theta_1 \sin \theta_2) \\ &= 1^2 + 2^2 + 4^2 - 3.5^2 - 2(1)(2) = 4.75 \end{aligned}$$

$$\theta_4 = 2\pi n^{-1} \left[\frac{-B + \sigma \sqrt{B^2 - C^2 + A^2}}{C - A} \right]$$

$$= 2\pi n^{-1} \left[\frac{-8 + \sqrt{8^2 - 4.75^2 + (-8)^2}}{4.75 - 8} \right] = 2\pi n^{-1}(0.5049) = 53.58^\circ$$

$$\theta_3 = \tan^{-1} \left[\frac{r_1 \sin \theta_1 + r_4 \sin \theta_4 - r_2 \sin \theta_2}{r_1 \cos \theta_1 + r_4 \cos \theta_4 - r_2 \cos \theta_2} \right]$$

$$= \tan^{-1} \left[\frac{4 \sin(53.58^\circ)}{1 + 4 \cos(53.58^\circ) - 2} \right] = \tan^{-1} \left[\frac{3.2137}{1.3748} \right] = \tan^{-1}(2.3412) = 66.87^\circ$$

The remainder of the solution is summarized in [Table 7.2](#).

[Table 7.2](#) Summary of Results for Example 7.1

θ_2	σ	A	B	C	θ_4	θ_3
0	1	-8	0	4.75	53.58°	66.87°
	-1				-53.58°	-66.87°
$\pi/2$	1	8	-16	8.75	177.28°	-143.85°
	-1				55.85°	21.98°
π	1	24	0	12.75	-122.09°	-75.52°
	-1				122.09°	75.52°
$-\pi/2$	1	8	16	8.75	-55.85°	-21.98°
	-1				-177.28°	148.85°

The arithmetic may also be checked by comparing $\gamma = \theta_4 - \theta_3$ for $\sigma = \pm 1$. One value should be minus the other if both values are in the range $-\pi < \gamma \leq \pi$. It may be necessary to add or subtract 2π to either value to bring γ into the range $-\pi < \gamma \leq \pi$.



Example 7.2

Velocity and Acceleration Analysis of a Four-Bar Linkage with Crank Input

If, for the linkage in Example 7.1, $\dot{\theta}_2 = 10 \text{ rad/s}$ and $\ddot{\theta}_2 = 0$, compute $\dot{\theta}_3$, $\dot{\theta}_4$, $\ddot{\theta}_3$, and $\ddot{\theta}_4$ in the first of the four positions ($\theta_2 = 0$).

Solution

Using the equations in [Table 7.1](#), the velocity expression is

$$\begin{bmatrix} -r_3 \sin \theta_3 & r_4 \sin \theta_4 \\ r_3 \cos \theta_3 & r_4 \cos \theta_4 \end{bmatrix} \begin{Bmatrix} \dot{\theta}_3 \\ \dot{\theta}_4 \end{Bmatrix} = \begin{Bmatrix} r_2 \dot{\theta}_2 \sin \theta_2 \\ r_2 \dot{\theta}_2 \cos \theta_2 \end{Bmatrix}$$

$$\begin{bmatrix} -3.5 \sin(66.87^\circ) & 4 \sin(53.58^\circ) \\ 3.5 \cos(66.87^\circ) & 4 \cos(53.58^\circ) \end{bmatrix} \begin{Bmatrix} \dot{\theta}_3 \\ \dot{\theta}_4 \end{Bmatrix} = \begin{Bmatrix} 2(10)\sin(0^\circ) \\ 2(10)\cos(0^\circ) \end{Bmatrix} = \begin{bmatrix} -3.2187 & 3.2187 \\ -1.3749 & 2.3748 \end{bmatrix} \begin{Bmatrix} \dot{\theta}_3 \\ \dot{\theta}_4 \end{Bmatrix} = \begin{Bmatrix} 0 \\ 20 \end{Bmatrix}$$

Solving the linear set of equations gives $\dot{\theta}_3 = 20 \text{ rad/s}$ and $\dot{\theta}_4 = 20.0 \text{ rad/s}$. Both values are positive, so the corresponding angular velocities are counterclockwise. The acceleration expression is

$$\begin{bmatrix} -r_3 \sin \theta_3 & r_4 \sin \theta_4 \\ r_3 \cos \theta_3 & r_4 \cos \theta_4 \end{bmatrix} \begin{Bmatrix} \ddot{\theta}_3 \\ \ddot{\theta}_4 \end{Bmatrix} = \begin{Bmatrix} r_2 \ddot{\theta}_2 \sin \theta_2 + r_2 \dot{\theta}_2^2 \cos \theta_2 + r_3 \dot{\theta}_3^2 \cos \theta_3 - r_4 \dot{\theta}_4^2 \cos \theta_4 \\ r_2 \ddot{\theta}_2 \cos \theta_2 - r_2 \dot{\theta}_2^2 \sin \theta_2 - r_3 \dot{\theta}_3^2 \sin \theta_3 - r_4 \dot{\theta}_4^2 \sin \theta_4 \end{Bmatrix}$$

$$\begin{bmatrix} -3.2187 & 3.2187 \\ -1.3749 & 2.3748 \end{bmatrix} \begin{Bmatrix} \ddot{\theta}_3 \\ \ddot{\theta}_4 \end{Bmatrix} = \begin{Bmatrix} 0 + 2(10)^2 + 3.5(20)^2 \cos(66.87^\circ) - 4(20)^2 \cos(53.58^\circ) \\ 0 - 0 - 3.5(20)^2 \sin(66.87^\circ) - 4(20)^2 \sin(53.58^\circ) \end{Bmatrix} = \begin{Bmatrix} -200.0265 \\ -0.0363 \end{Bmatrix}$$

Solving the linear set of equations gives $\ddot{\theta}_3 = 147.5634 \text{ rad/s}^2$ and $\ddot{\theta}_4 = 86.4150 \text{ rad/s}^2$. Again, both values are positive, so the corresponding angular accelerations are counterclockwise.



7.4 Analytical Equations for a Rigid Body After the Kinematic Properties of Two Points are Known

The equations presented so far will permit the kinematic properties of the points on the vector loop to be computed directly. However, often we need to compute the position, velocity, and acceleration of points that are not directly on the vector loops. In general, given the kinematic properties of *one* point on a rigid body and the angular position, angular velocity, and angular acceleration of the body, we can compute the position, velocity, and acceleration of *any* defined point on the rigid body.

Consider the rigid body represented in [Figure 7.10](#). Assume that A and B are two points attached to an arbitrary link, say link 5, and a third point is defined relative to the line between points A and B by the angle β and the distance $r_{C/A}$, that is represented in [Figure 7.10](#) as r_6 . Then the linear position, velocity, and acceleration of point C can be computed directly if the following are known: $r_A, \dot{r}_A, \ddot{r}_A, \theta_5, \dot{\theta}_5, \ddot{\theta}_5$. The position of point C is given as

$$\vec{r}_C = \vec{r}_A + \vec{r}_6$$

or

$$r_C = r_A + r_6(\cos \theta_5 i + \sin \theta_5 j) \quad (7.56)$$

where

$$\theta_5 = \beta + \theta_3 \quad (7.57)$$

Recognizing that β is a constant, the velocity of point C is given by

$$\dot{r}_C = \dot{r}_A + r_6 \dot{\theta}_5 (-\sin \theta_5 i + \cos \theta_5 j) \quad (7.58)$$

and the acceleration is given by

$$\ddot{r}_C = \ddot{r}_A + r_6 \ddot{\theta}_5 (-\sin \theta_5 i + \cos \theta_5 j) - r_6 \dot{\theta}_5^2 (\cos \theta_5 i + \sin \theta_5 j) \quad (7.59)$$

Note that we have assumed here that $\theta_3, \dot{\theta}_3, \ddot{\theta}_3$ are known. Often, we will know the kinematic information for two points on a rigid link instead of these angular quantities. If we know the position, velocity, and acceleration of two points (say A and B), we can compute $\theta_3, \dot{\theta}_3, \ddot{\theta}_3$ and proceed as before. The angle can be computed from the x and y components of the position vectors for A and B using

$$\theta_3 = \tan^{-1} \left[\frac{r_{B_y} - r_{A_y}}{r_{B_x} - r_{A_x}} \right]$$

The angular velocity can be computed by rewriting [Equation 7.58](#) in terms of points A and B . That is

$$\dot{r}_3 = \dot{r}_A + r_3 \dot{\theta}_3 (-\sin \theta_3 i + \cos \theta_3 j)$$

Therefore

$$\dot{\theta}_3 = -\frac{\dot{r}_{B_x} - \dot{r}_{A_x}}{r_3 \sin \theta_3} = \frac{\dot{r}_{B_y} - \dot{r}_{A_y}}{r_3 \cos \theta_3}$$

Similarly, the angular acceleration can be computed by rewriting [Equation 7.59](#) in terms of A and B . That is

$$\ddot{r}_g = \ddot{r}_A + r_3 \dot{\theta}_3 (-\sin \theta_3 i + \cos \theta_3 j) - r_3 \dot{\theta}_3^2 (\cos \theta_3 i + \sin \theta_3 j)$$

Therefore

$$\ddot{\theta}_3 = -\frac{(\ddot{r}_{B_x} - \ddot{r}_{A_x}) + r_3 \dot{\theta}_3^2 \cos \theta_3}{r_3 \sin \theta_3} = \frac{(\ddot{r}_{B_y} - \ddot{r}_{A_y}) + r_3 \dot{\theta}_3^2 \sin \theta_3}{r_3 \cos \theta_3}$$

These equations are summarized in [Table 7.3](#), and a MATLAB function routine for the calculations is included with the supplementary material for this book.

[Table 7.3](#) Summary of Position, Velocity, and Acceleration Equations for an Arbitrary Point on a Rigid Body. The Vectors and Points Are Defined in [Figure 7.10](#).

If r_A and r_B are given instead of $\theta_3, \dot{\theta}_3, \ddot{\theta}_3$, first compute $\theta_3, \dot{\theta}_3, \ddot{\theta}_3$ using the following

$$\theta_3 = \tan^{-1} \left(\frac{r_{B_y} - r_{A_y}}{r_{B_x} - r_{A_x}} \right)$$

$$\dot{\theta}_3 = -\frac{r_{B_x} - r_{A_x}}{r_3 \sin \theta_3} = \frac{r_{B_y} - r_{A_y}}{r_3 \cos \theta_3}$$

$$\ddot{\theta}_3 = -\frac{(\ddot{r}_{B_x} - \ddot{r}_{A_x}) + r_3 \dot{\theta}_3^2 \cos \theta_3}{r_3 \sin \theta_3} = \frac{(\ddot{r}_{B_y} - \ddot{r}_{A_y}) + r_3 \dot{\theta}_3^2 \sin \theta_3}{r_3 \cos \theta_3}$$

Position

$$r_C = r_A + r_3 (\cos \theta_3 i + \sin \theta_3 j)$$

$$\theta_3 = \beta + \theta_3$$

Velocity

$$\dot{r}_C = \dot{r}_A + r_3 \dot{\theta}_3 (-\sin \theta_3 i + \cos \theta_3 j)$$

Acceleration

$$\ddot{r}_C = \ddot{r}_A + r_3 \dot{\theta}_3 (-\sin \theta_3 i + \cos \theta_3 j) - r_3 \dot{\theta}_3^2 (\cos \theta_3 i + \sin \theta_3 j)$$



Example 7.3

Velocity and Acceleration Analysis of Coupler Point

For the linkage in Examples 7.1 and 7.2 that are shown in [Figure 7.9](#), compute the velocity and acceleration of point C when $\theta_2 = 0$, $\dot{\theta}_2 = 10 \text{ rad/s}$, $\ddot{\theta}_2 = 0$, and $\sigma = 1$. Assume that the lengths are given in centimeters.

Solution

First compute the angle β between the line AB and the line AC . The angle is given by

$$\beta = \tan^{-1} \left[\frac{1}{2} \right] = 26.56^\circ$$

and the length AC is given by

$$r_3 = AC = 2.0 / \cos(26.56^\circ) = 2.236 \text{ cm}$$

Then the velocity of C_3 is given by

$$\dot{r}_C = r_2 \dot{\theta}_2 (-\sin \theta_2 i + \cos \theta_2 j) + r_3 \dot{\theta}_3 (-\sin \theta_3 i + \cos \theta_3 j)$$

Substitution of $\theta_2 = 0$, $\theta_3 = 66.87^\circ$, $\dot{\theta}_2 = 10 \text{ rad/s}$ and $\dot{\theta}_3 = 20 \text{ rad/s}$ from Example 7.2 gives

$$\theta_5 = \theta_3 + \beta = 66.87^\circ + 26.56^\circ = 93.43^\circ$$

and

$$\begin{aligned} \dot{r}_C &= 2(10)(0i + j) + 2.236(20.0)(-\sin 93.43^\circ i + \cos 93.43^\circ j) \\ &= 20j - 44.64i - 2.579j = (-44.64i + 17.32j) \text{ cm/s} \end{aligned}$$

The acceleration of C is given by

$$\begin{aligned} \ddot{r}_C &= r_2 \ddot{\theta}_2 (-\sin \theta_2 i + \cos \theta_2 j) - r_2 \dot{\theta}_2^2 (\cos \theta_2 i + \sin \theta_2 j) \\ &\quad + r_3 \ddot{\theta}_3 (-\sin \theta_3 i + \cos \theta_3 j) - r_3 \dot{\theta}_3^2 (\cos \theta_3 i + \sin \theta_3 j) \end{aligned}$$

Substitution of $\theta_2 = 0$, $\theta_3 = 66.87^\circ$, $\dot{\theta}_2 = 10 \text{ rad/s}$, $\dot{\theta}_3 = 20 \text{ rad/s}$, and $\ddot{\theta}_3 = 20 \text{ rad/s}^2$ gives

$$\begin{aligned} \ddot{r}_C &= 0 - 2(10)^2(i + 0j) + 2.236(147.56)(-\sin 93.43^\circ i + \cos 93.43^\circ j) \\ &\quad - 2.236(20.0)^2(\cos 93.43^\circ i + \sin 93.43^\circ j) = (-473.76i - 912.56j) \text{ cm/s}^2 \end{aligned}$$

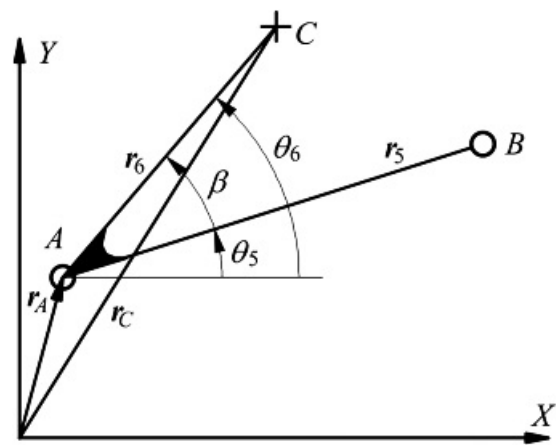


Figure 7.10 Calculation of the kinematic properties of a point on a link after the kinematic properties of one point and the angular velocity and acceleration of the link are known.



7.5 Analytical Equations for Slider-Crank Mechanisms

Next to the four-bar linkage, the slider-crank is probably the most commonly used mechanism. It appears in all internal combustion engines ([Figure 7.11](#)) and in numerous shop ([Figure 7.12](#)) and household devices ([Figure 7.13](#)). A general slider-crank mechanism is represented in [Figure 7.14](#). To develop the closure equations, locate vectors r_2 and r_3 as was done in the regular four-bar linkage. To form the other part of the closure equation, draw two vectors, one in the direction of the slider velocity and one perpendicular to the velocity direction. The variables associated with the problem are then located as shown in [Fig. 7.14](#). The loop closure equation is the same as that for the regular four-bar linkage

$$r_3 - r_2 + r_3 = r_1 + r_4 \quad (7.60)$$

or

$$r_2(\cos \theta_2 i + \sin \theta_2 j) + r_3(\cos \theta_3 i + \sin \theta_3 j) = r_1(\cos \theta_1 i + \sin \theta_1 j) + r_4(\cos \theta_4 i + \sin \theta_4 j) \quad (7.61)$$

where

$$\theta_4 = \theta_1 + \pi/2 \quad (7.62)$$

Rewriting [Equation 7.61](#) into its component equations gives

$$r_2 \cos \theta_2 - r_3 \cos \theta_3 = r_1 \cos \theta_1 + r_4 \cos \theta_4 \quad (7.63)$$

$$r_2 \sin \theta_2 - r_3 \sin \theta_3 = r_1 \sin \theta_1 + r_4 \sin \theta_4 \quad (7.64)$$

[Equations 7.62–7.64](#) must be satisfied throughout the motion of the linkage. The base vector, r_1 , will vary in magnitude but be constant in direction. The vector r_4 will be constant. Therefore, r_2 , r_3 , r_4 , θ_1 , and θ_4 are constants. If θ_2 is given, it is necessary to solve [Equations 7.63](#) and [7.64](#) for θ_3 and r_1 in terms of θ_2 . If r_1 is given, it is necessary to solve the same equations for θ_2 and θ_3 . And finally, if θ_3 is given, it is necessary to solve the equations for θ_2 and r_1 . Once these expressions are obtained, the unknown velocities and accelerations can be computed in terms of the knowns by differentiation.



[Figure 7.11](#) Internal combustion engine. An example of a slider-crank mechanism where the crank is the output link. Courtesy of Ford Motor Co., Detroit, Michigan



[Figure 7.12](#) Hydraulic jack. An example of a slider-crank mechanism where the coupler is the driver and the slider is the output link.

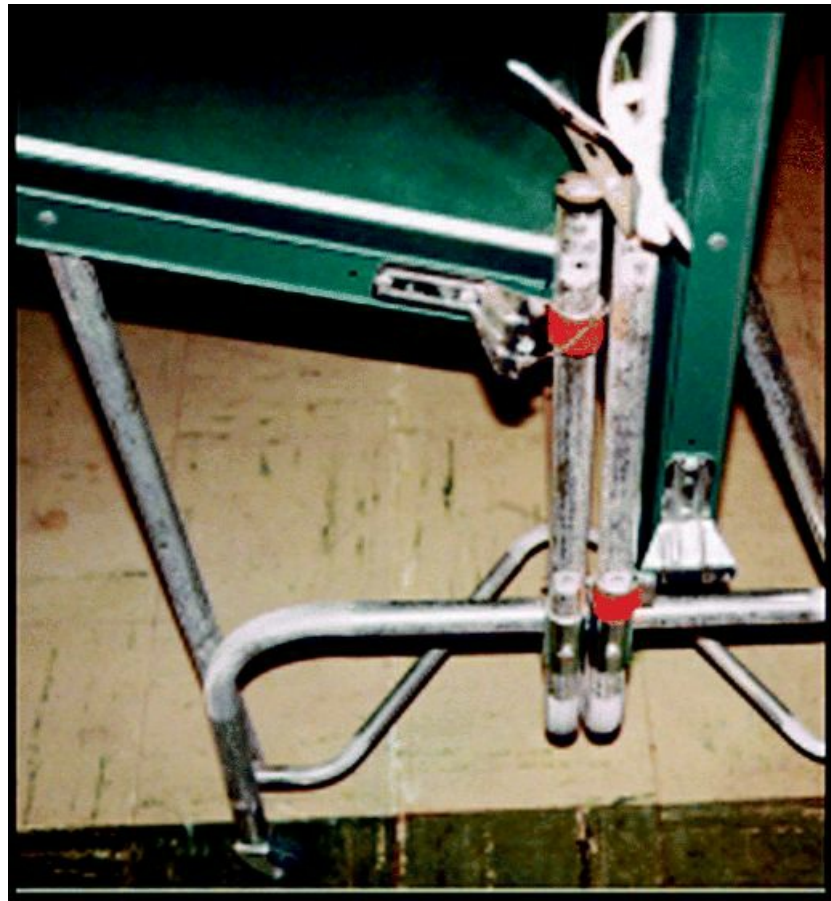


[Figure 7.13](#) Ping-pong table linkage. An example of a slider-crank mechanism where the coupler is the input link.

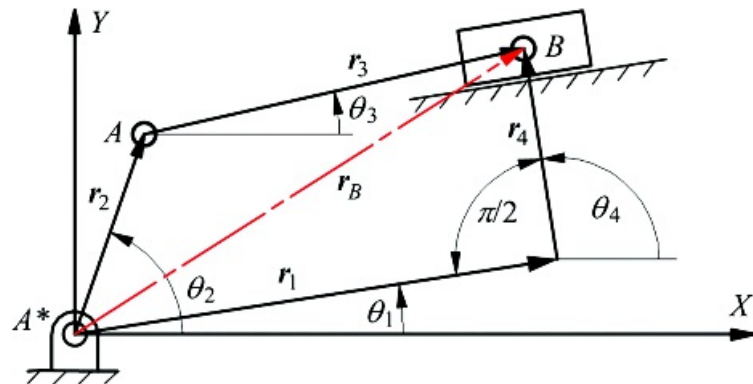


[Figure 7.14](#) Vector closure condition for a slider-crank mechanism. The position of point B obtained by adding the vectors r_3 and r_4 is the same as that obtained by adding vectors r_1 and r_2 .

7.5.1 Solution to Position Equations When θ_2 Is Input

The analytical solution procedure follows the same major steps as in the four-bar linkage case. To eliminate θ_3 , first isolate it using [Equation 7.63](#) and [7.64](#) as follows

$$r_3 \cos \theta_3 = r_1 \cos \theta_1 + r_4 \cos \theta_4 - r_2 \cos \theta_2 \quad (7.65)$$

$$r_3 \sin \theta_3 = r_1 \sin \theta_1 + r_4 \sin \theta_4 - r_2 \sin \theta_2 \quad (7.66)$$

Notice that in [Figure 7.14](#), the angles θ_1 and θ_4 are known constants, but r_1 varies and is unknown. Now square both sides of both equations and add. This gives

$$r_3^2(\cos^2 \theta_3 + \sin^2 \theta_3) = (r_1 \cos \theta_1 - r_4 \cos \theta_4 - r_2 \cos \theta_2)^2 + (r_1 \sin \theta_1 + r_4 \sin \theta_4 - r_2 \sin \theta_2)^2$$

Expansion and simplification using the trigonometric identity $\cos^2 \theta - \sin^2 \theta = 1$ gives

$$\begin{aligned} r_3^2 &= r_1^2 + r_2^2 + r_4^2 + 2r_1r_4(\cos \theta_1 \cos \theta_4 + \sin \theta_1 \sin \theta_4) \\ &\quad - 2r_1r_2(\cos \theta_1 \cos \theta_2 - \sin \theta_1 \sin \theta_2) - 2r_2r_4(\cos \theta_2 \cos \theta_4 + \sin \theta_2 \sin \theta_4) \end{aligned} \quad (7.67)$$

[Equation 7.67](#) gives r_1 in a quadratic expression involving θ_2 and the other known variables. To obtain a solution, collect together the coefficients of the different powers of r_1 as follows

$$r_1^2 + Ar_1 + B = 0 \quad (7.68)$$

where

$$\begin{aligned} A &= 2r_4(\cos \theta_1 \cos \theta_4 + \sin \theta_1 \sin \theta_4) - 2r_2(\cos \theta_1 \cos \theta_2 + \sin \theta_1 \sin \theta_2) \\ C &= r_2^2 + r_4^2 - r_3^2 - 2r_2r_4(\cos \theta_2 \cos \theta_4 + \sin \theta_2 \sin \theta_4) \end{aligned} \quad (7.69)$$

Solving for r_1 gives

$$r_1 = \frac{-A + \sigma\sqrt{A^2 - 4B}}{2} \quad (7.70)$$

where $\sigma = \pm 1$ is a sign variable identifying the assembly mode. There are two assembly modes corresponding to the two configurations shown in [Figure 7.15](#).

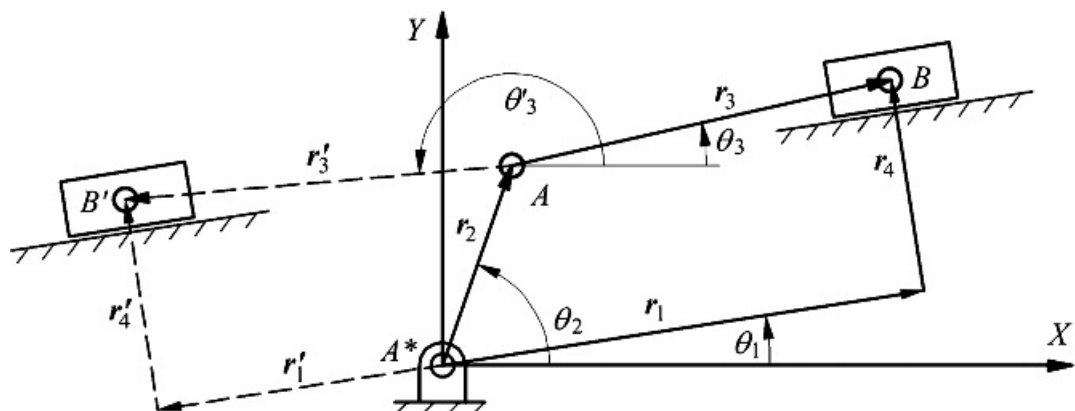


[Figure 7.15](#) The two possible positions (B and B') of the point B for a given value of θ_2 in a slider-crank mechanism.

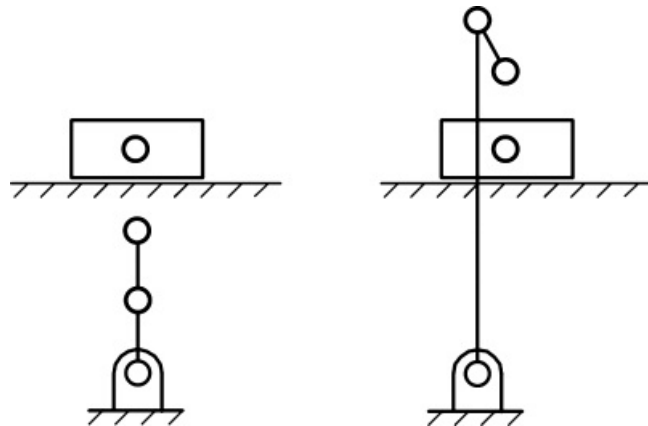


Figure 7.16 Configurations giving complex solutions for slider-crank position problem.

As in the case of the four-bar linkage, once we pick the value for σ corresponding to the desired mode, the sign in an actual linkage stays the same for any value of θ_2 .

Because of the square root in [Equation 7.70](#), the variable r_1 can be complex ($A^2 < 4B$). If this happens, the mechanism cannot be assembled in the position specified. The assembly would then appear as one of the configurations shown in [Figure 7.16](#).

Once a value for r_1 is determined, [Equations 7.65](#) and [7.66](#) can be solved for θ_3 . Dividing [Equation 7.66](#) by [Equation 7.65](#) and solving for θ_3 gives

$$\theta_3 = \tan^{-1} \left[\frac{r_1 \sin \theta_1 + r_4 \sin \theta_4 - r_2 \sin \theta_2}{r_1 \cos \theta_1 + r_4 \cos \theta_4 - r_2 \cos \theta_2} \right] \quad (7.71)$$

As in the case of the four-bar linkage, it is essential that the sign of the numerator and denominator in [Equation 7.71](#) be maintained to determine the quadrant in which the angle θ_3 lies.

Once all of the angular quantities are known, it is relatively straightforward to compute the coordinates of any point on the vector loops used in the closure equations. In particular, the coordinates of A and B are given by

$$r_A = r_2 = r_2(\cos \theta_2 i + \sin \theta_2 j) \quad (7.72)$$

and

$$r_B = r_2 + r_3 = r_2(\cos \theta_2 i + \sin \theta_2 j) + r_3(\cos \theta_3 i + \sin \theta_3 j) \quad (7.73)$$

7.5.2 Solution to Position Equations When θ_2 Is Input

The analytical solution procedure follows the same major steps as in the previous case. Referring to [Figure 7.14](#), we again start by eliminating θ_3 from [Equations 7.63](#) and [7.64](#) to get [Equation 7.67](#). Then we simplify [Equation 7.67](#) as follows

$$A \cos \theta_2 + B \sin \theta_2 + C = 0 \quad (7.74)$$

where

$$\left. \begin{aligned} A &= -2r_1 r_2 \cos \theta_1 - 2r_2 r_4 \cos \theta_4 \\ B &= -2r_1 r_2 \sin \theta_1 - 2r_2 r_4 \sin \theta_4 \\ C &= r_1^2 + r_2^2 + r_4^2 - r_3^2 - 2r_1 r_4 (\cos \theta_1 \cos \theta_4 + \sin \theta_1 \sin \theta_4) \end{aligned} \right\} \quad (7.75)$$

To solve [Equation 7.74](#), the trigonometric half-angle identities given in [Equations 7.33–7.34](#) can be used. Using these identities in [Equation 7.74](#) and simplifying gives

$$A(1-t^2) + B(2t) + C(1+t^2) = 0$$

where

$$t = \tan\left(\frac{\theta_2}{2}\right)$$

Further simplification gives

$$(C-A)t^2 + 2Bt + (A+C) = 0$$

Solving for t gives

$$t = \frac{-2B + \sigma\sqrt{4B^2 - 4(C-A)(C+A)}}{2(C-A)} = \frac{-B + \sigma\sqrt{B^2 - C^2 + A^2}}{C-A} \quad (7.76)$$

and

$$\theta_2 = 2\tan^{-1} t \quad (7.77)$$

where $\sigma = \pm 1$ is a sign variable identifying the assembly mode. Once again, because $\tan^{-1} t$ has a valid range of values $-\pi/2 \leq \tan^{-1} t \leq \pi/2$, θ_2 will have the range $-\pi \leq \theta_2 \leq \pi$. Typically, there are two solutions for θ_2 corresponding to the two values of σ , and they are both valid. These correspond to the two assembly modes shown in [Figure 7.17](#). Once we pick the value for σ corresponding to the desired mode, the sign in an actual linkage stays the same for any value of r_1 .

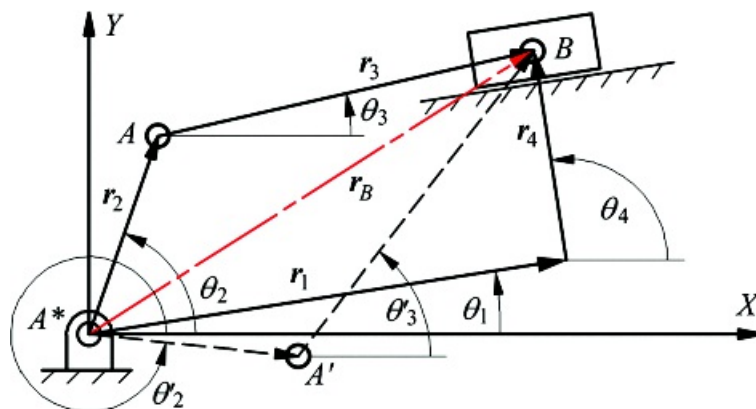


[Figure 7.17](#) Two possible assembly modes when the position, r_1 , of the slider is given as an input.

Because of the square root in [Equation 7.76](#), the variable t can be complex ($A^2 + B^2 < C^2$). If this happens, the mechanism cannot be assembled for the specified value of r_1 . The assembly configurations would then appear as shown in [Figure 7.18](#).

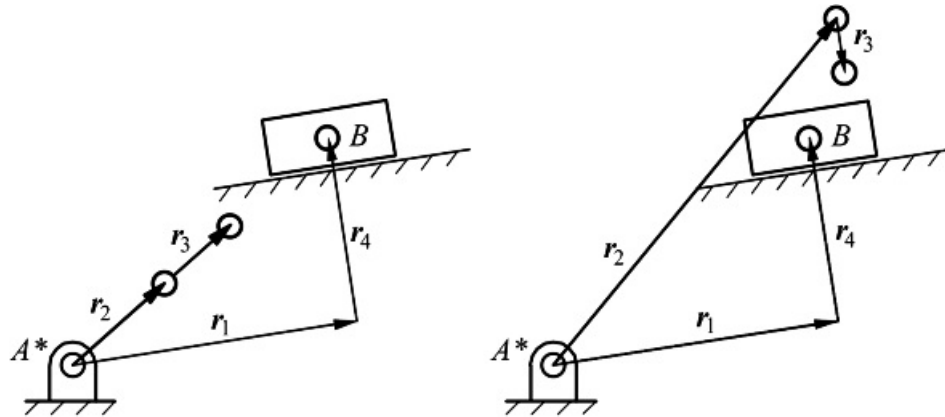


[Figure 7.18](#) Slider-crank mechanisms that cannot be assembled in the position chosen for r_1 . The variable t would be complex in these cases.

Knowing r_1 , [Equations 7.65](#) and [7.66](#) can now be solved for θ_2 . The resulting equation is [Equation 7.71](#). As in the previous cases, it is essential that the sign of the numerator and denominator in [Equation 7.71](#) be maintained to determine the quadrant in which the angle θ_2 lies. Note that the positions of r_2 and r_3 are symmetric about the line A^*B .

Once all of the angular quantities are known, it is relatively straightforward to compute the coordinates of any point on the vector loops used in the closure equations. The coordinates of points A and B are again given by [Equations 7.72](#) and [7.73](#).

7.5.3 Solution to Position Equations When θ_3 Is Input

When the coupler is the input link, values for θ_3 and its derivatives will be known. The analytical procedure for solving the position equations follows the same major steps as when θ_2 is the input. Therefore, we will simply outline the procedure and tabulate the results.

In the procedure, we can assume that θ_1 , θ_2 , θ_4 , $\dot{\theta}_1$, and $\ddot{\theta}_1$ are known, and θ_2 , $\dot{\theta}_2$, $\ddot{\theta}_2$, r_1 , \dot{r}_1 , and \ddot{r}_1 are to be found. The link lengths r_2 and r_3 and θ_1 and θ_4 are constants. For the position analysis, again begin with [Equations 7.63](#) and [7.64](#) and isolate the terms with either θ_2 or $\dot{\theta}_2$. It is advantageous to select θ_2 for the reasons given below. The resulting equations are

$$r_2 \cos \theta_2 = r_1 \cos \theta_1 + r_4 \cos \theta_4 - r_3 \cos \theta_3 \quad (7.78)$$

$$r_2 \sin \theta_2 = r_1 \sin \theta_1 + r_4 \sin \theta_4 - r_3 \sin \theta_3 \quad (7.79)$$

A comparison of [Equations 7.78](#) and [7.79](#) with [Equations 7.65](#) and [7.66](#) indicates that they are of the same form except that the indices 2 and 3 are interchanged. Therefore, we can use directly the position solution derived in Section 7.5.1 if we interchange the indices 2 and 3.

When the coupler is the driver, there is an assembly-mode ambiguity similar to that observed when link 2 is the driver. This is illustrated in [Figure 7.19](#). It is necessary to know the appropriate mode before the analysis can be completed; however, once the assembly mode is selected, it is the same for all positions of the input.

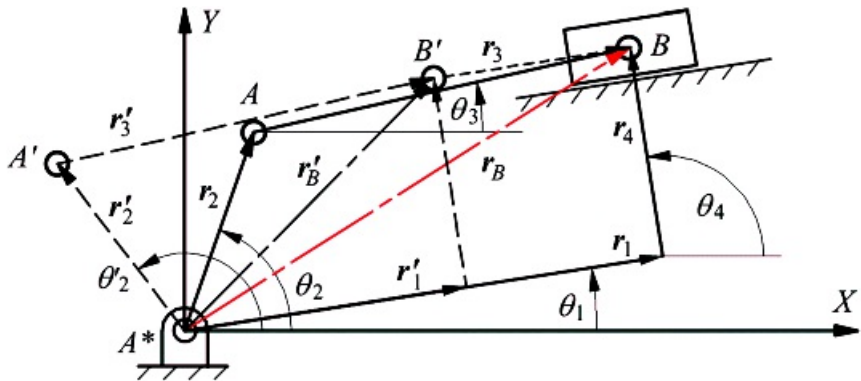


Figure 7.19 Two possible assembly modes when the coupler is the input link.

7.5.4 Velocity Equations for Slider-Crank Mechanism

The analytical form of the velocity equations can be developed by differentiating [Equation 7.60](#). The result is

$$\dot{r}_3 = \dot{r}_2 + \dot{r}_3 = \dot{r}_1 + \dot{r}_4 \quad (7.80)$$

When this equation is written in component form, the result is the same as differentiating [Equations 7.63](#) and [7.64](#). Recognizing that r_2 , r_3 , r_4 , θ_1 , and θ_4 are constants, the resulting component equations are

$$-r_2\dot{\theta}_2 \sin \theta_2 - r_3\dot{\theta}_3 \sin \theta_3 = \dot{r}_1 \cos \theta_1 \quad (7.81)$$

$$r_2\dot{\theta}_2 \cos \theta_2 + r_3\dot{\theta}_3 \cos \theta_3 = \dot{r}_1 \sin \theta_1 \quad (7.82)$$

The solution procedure depends on whether \dot{r}_1 , $\dot{\theta}_2$, or $\dot{\theta}_3$ is known. If $\dot{\theta}_2$ (or $\dot{\theta}_3$) is input, then \dot{r}_1 and $\dot{\theta}_3$ (or $\dot{\theta}_2$) will be unknown. Therefore, the matrix equation to be solved is

$$\begin{bmatrix} \cos \theta_1 & r_2 \sin \theta_2 \\ \sin \theta_1 & -r_2 \cos \theta_2 \end{bmatrix} \begin{Bmatrix} \dot{r}_1 \\ \dot{\theta}_3 \end{Bmatrix} = \begin{Bmatrix} -r_M \dot{\theta}_M \sin \theta_M \\ r_4 \dot{\theta}_M \cos \theta_M \end{Bmatrix} \quad (7.83)$$

where $M = 2$ and $J = 3$ for link 2 as the input, and $M = 3$ and $J = 2$ for link 3 as the input. If \dot{r}_1 is input, then $\dot{\theta}_2$ and $\dot{\theta}_3$ will be unknown. The matrix equation to be solved then is

$$\begin{bmatrix} -r_2 \sin \theta_2 & -r_3 \sin \theta_3 \\ r_2 \cos \theta_2 & r_3 \cos \theta_3 \end{bmatrix} \begin{Bmatrix} \dot{\theta}_2 \\ \dot{\theta}_3 \end{Bmatrix} = \begin{Bmatrix} \dot{r}_1 \cos \theta_1 \\ \dot{r}_1 \sin \theta_1 \end{Bmatrix} \quad (7.84)$$

The terms in the matrix and in the vector on the right-hand sides of [Equations 7.83](#) and [7.84](#) will be known. The equation can therefore be solved manually, on a programmable calculator, or with the matrix solvers in programs such as MATLAB.

Once the angular velocities are known, it is a simple matter to compute the linear velocities of any of the points on the vector loop. The velocities of points A and B are given by

$$\dot{r}_A = \dot{r}_2 = r_2\dot{\theta}_2(-\sin \theta_2 i + \cos \theta_2 j) \quad (7.85)$$

and

$$\ddot{r}_2 = \ddot{r}_2 + \ddot{r}_3 = (-r_2\dot{\theta}_2 \sin \theta_2 - r_3\dot{\theta}_3 \sin \theta_3)\hat{i} + (r_2\dot{\theta}_2 \cos \theta_2 + r_3\dot{\theta}_3 \cos \theta_3)\hat{j} \quad (7.86)$$

7.5.5 Acceleration Equations for Slider-Crank Mechanism

The analytical form of the acceleration equations can be developed by differentiating [Equation 7.80](#). The result is

$$\ddot{r}_3 = \ddot{r}_2 + \ddot{r}_3 = \ddot{r}_1 + \ddot{r}_2$$

When this equation is written in component form, the result is the same as differentiating [Equations 7.81](#) and [7.82](#). The resulting component equations are

$$-r_2\ddot{\theta}_1 \sin \theta_2 - r_2\dot{\theta}_1^2 \cos \theta_2 - r_2\ddot{\theta}_3 \sin \theta_3 - r_3\dot{\theta}_3^2 \cos \theta_3 = \ddot{r}_1 \cos \theta_1 \quad (7.87)$$

$$r_2\ddot{\theta}_1 \cos \theta_2 - r_2\dot{\theta}_1^2 \sin \theta_2 + r_3\ddot{\theta}_3 \cos \theta_3 - r_3\dot{\theta}_3^2 \sin \theta_3 = \ddot{r}_1 \sin \theta_1 \quad (7.88)$$

As was the case for velocities, the solution procedure depends on whether $\ddot{\theta}_1$, $\ddot{\theta}_2$, or $\ddot{\theta}_3$ is known. If $\ddot{\theta}_1$ (or $\ddot{\theta}_2$) is input, then \ddot{r}_1 and $\ddot{\theta}_3$ (or $\ddot{\theta}_1$) will be unknown, and the matrix equation to be solved is

$$\begin{bmatrix} \cos \theta_1 & -r_2 \sin \theta_2 \\ \sin \theta_1 & -r_2 \cos \theta_2 \end{bmatrix} \begin{Bmatrix} \ddot{r}_1 \\ \ddot{\theta}_3 \end{Bmatrix} = \begin{Bmatrix} -r_M\ddot{\theta}_M \sin \theta_M - r_M\dot{\theta}_M^2 \cos \theta_M - r_3\dot{\theta}_3^2 \cos \theta_3 \\ r_M\ddot{\theta}_M \cos \theta_M - r_M\dot{\theta}_M^2 \sin \theta_M - r_3\dot{\theta}_3^2 \sin \theta_3 \end{Bmatrix} \quad (7.89)$$

If \ddot{r}_1 is input, then $\ddot{\theta}_1$ and $\ddot{\theta}_2$ will be unknown, and the matrix equation to be solved then is

$$\begin{bmatrix} -r_2 \sin \theta_2 & -r_3 \sin \theta_3 \\ r_2 \cos \theta_2 & r_3 \cos \theta_3 \end{bmatrix} \begin{Bmatrix} \ddot{\theta}_2 \\ \ddot{\theta}_3 \end{Bmatrix} = \begin{Bmatrix} r_2\dot{\theta}_2^2 \cos \theta_2 + r_3\dot{\theta}_3^2 \cos \theta_3 + \ddot{r}_1 \cos \theta_1 \\ r_2\dot{\theta}_2^2 \sin \theta_2 + r_3\dot{\theta}_3^2 \sin \theta_3 + \ddot{r}_1 \sin \theta_1 \end{Bmatrix} \quad (7.90)$$

The terms in the matrix and in the vector on the right-hand sides of [Equations 7.89](#) and [7.90](#) will be known. The equation can therefore be solved manually, on a programmable calculator, or with the matrix solvers in programs such as MATLAB. Notice again that the coefficient matrix is the same for both the velocities ([Equations 7.83](#) and [7.84](#)) and the accelerations ([Equations 7.89](#) and [7.90](#)).

Once the angular accelerations are known, it is a simple matter to compute the linear acceleration of any point on the vector loop. The accelerations of points *A* and *B* are given by

$$\ddot{r}_A = \ddot{r}_2 = (-r_2\dot{\theta}_2 \sin \theta_2 - r_2\dot{\theta}_2^2 \cos \theta_2)\hat{i} + (r_2\dot{\theta}_2 \cos \theta_2 - r_2\dot{\theta}_2^2 \sin \theta_2)\hat{j} \quad (7.91)$$

and

$$\begin{aligned} \ddot{r}_B = \ddot{r}_2 + \ddot{r}_3 = & -(r_2\dot{\theta}_2 \sin \theta_2 + r_2\dot{\theta}_2^2 \cos \theta_2 + r_3\dot{\theta}_3 \sin \theta_3 + r_3\dot{\theta}_3^2 \cos \theta_3)\hat{i} \\ & +(r_2\dot{\theta}_2 \cos \theta_2 - r_2\dot{\theta}_2^2 \sin \theta_2 + r_3\dot{\theta}_3 \cos \theta_3 - r_3\dot{\theta}_3^2 \sin \theta_3)\hat{j} \end{aligned} \quad (7.92)$$

Now that the equations have been developed, it is relatively simple to write a computer program for the analysis of a slider-crank linkage. To aid in this, the equations required are summarized in [Tables 7.4](#) and [7.5](#). MATLAB programs for analyzing slider-crank linkages are included with the supplementary material for this book.



Example 7.4

Kinematic Analysis of Slider-Crank Mechanism with Crank Input

In the slider-crank mechanism shown in [Figure 7.20](#), $\theta_1 = 45^\circ$, $\dot{\theta}_2 = 10 \text{ rad/s}$, and $\ddot{\theta}_2 = 0$. The link lengths, r_2 and r_3 , are as shown, and the line of motion of point B_4 is along the line A^*B . Find the position, velocity, and acceleration of B_4 and the angular velocity and acceleration of link 3.

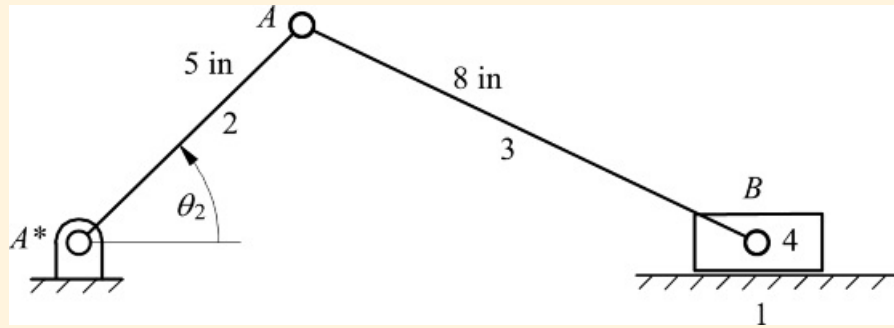


[Figure 7.20](#) The slider-crank linkage to be analyzed in Example 7.4.

Solution

For this problem, the crank is the input, and the analysis can be conducted using the equations in [Table 7.4](#) with $M = 2$ and $J = 3$. The known input information is

[Table 7.4](#) Summary of Position, Velocity, and Acceleration Equations for a Slider-Crank Mechanism When Either the Crank or the Coupler Is the Input (Link 2 is the input link when $M = 2$ and $J = 3$. Link 3 is the input link when $M = 3$ and $J = 2$. The link numbers and points are defined in [Figure 7.14](#).)

Position
$A = 2r_4(\cos \theta_1 \cos \theta_2 + \sin \theta_1 \sin \theta_2) - 2r_{45}(\cos \theta_1 \cos \theta_M + \sin \theta_1 \sin \theta_M)$
$B = r_{15}^2 + r_2^2 - 2r_{15}r_2(\cos \theta_M \cos \theta_4 + \sin \theta_{15} \sin \theta_4)$
$r_1 = \frac{A \pm \sigma\sqrt{A^2 - 4B}}{2}, \sigma = \pm 1$
$\theta_J = \tan^{-1} \left[\frac{r_1 \sin \theta_1 + r_4 \sin \theta_2 - r_{15} \sin \theta_M}{r_1 \cos \theta_1 + r_4 \cos \theta_2 - r_{15} \cos \theta_M} \right]$
$r_A = r_2(\cos \theta_2 i + \sin \theta_2 j)$
$r_B = r_2 + r_3 = r_2(\cos \theta_2 i + \sin \theta_2 j) + r_3(\cos \theta_3 i + \sin \theta_3 j)$
Velocity
$\begin{bmatrix} \cos \theta_1 & -r_2 \sin \theta_2 \\ \sin \theta_1 & -r_2 \cos \theta_2 \end{bmatrix} \begin{bmatrix} \dot{\theta}_1 \\ \dot{\theta}_2 \end{bmatrix} = \begin{bmatrix} -r_{45}\dot{\theta}_M \sin \theta_M \\ r_{45}\dot{\theta}_M \cos \theta_M \end{bmatrix}$
$\dot{r}_A = \dot{r}_2 = r_2 \dot{\theta}_2 (-\sin \theta_2 i + \cos \theta_2 j)$
$\dot{r}_B = \dot{r}_2 + \dot{r}_3 = (-r_2 \dot{\theta}_2 \sin \theta_2 - r_2 \dot{\theta}_3 \sin \theta_3)i + (r_2 \dot{\theta}_2 \cos \theta_2 + r_2 \dot{\theta}_3 \cos \theta_3)j$
Acceleration
$\begin{bmatrix} \cos \theta_1 & -r_2 \sin \theta_2 \\ \sin \theta_1 & -r_2 \cos \theta_2 \end{bmatrix} \begin{bmatrix} \ddot{\theta}_1 \\ \ddot{\theta}_2 \end{bmatrix} = \begin{bmatrix} -r_{45}\ddot{\theta}_M \sin \theta_M - r_{45}\dot{\theta}_M^2 \cos \theta_M - r_3\dot{\theta}_3^2 \cos \theta_3 \\ r_{45}\dot{\theta}_M^2 \cos \theta_M - r_{45}\ddot{\theta}_M \sin \theta_M - r_3\dot{\theta}_3^2 \sin \theta_3 \end{bmatrix}$
$\ddot{r}_A = \ddot{r}_2 = (-r_2 \dot{\theta}_2 \sin \theta_2 - r_2 \dot{\theta}_3 \cos \theta_3)i + (r_2 \dot{\theta}_2 \cos \theta_2 - r_2 \dot{\theta}_3 \sin \theta_3)j$
$\ddot{r}_B = -(r_2 \dot{\theta}_2 \sin \theta_2 + r_2 \dot{\theta}_3 \cos \theta_2 + r_3 \dot{\theta}_3 \sin \theta_3 + r_3 \dot{\theta}_3^2 \sin \theta_3)i + (r_2 \dot{\theta}_2 \cos \theta_2 - r_2 \dot{\theta}_3 \sin \theta_2 + r_3 \dot{\theta}_3 \cos \theta_3 - r_3 \dot{\theta}_3^2 \sin \theta_3)j$

$$\theta_1 = 0^\circ, \theta_2 = 45^\circ, \dot{\theta}_2 = 10 \text{ rad/s}, \ddot{\theta}_2 = 0$$

$$r_2 = 5 \text{ in}, r_3 = 8 \text{ in}, r_4 = 0 \text{ in}$$

Start with the position analysis, and first compute the constants A and B from [Equation 7.69](#)

$$\begin{aligned} A &= 2r_4(\cos \theta_1 \cos \theta_4 + \sin \theta_1 \sin \theta_4) - 2r_2(\cos \theta_1 \cos \theta_2 + \sin \theta_1 \sin \theta_2) \\ &= -2(5)(\cos 0^\circ \cos 45^\circ - \sin 0^\circ \sin 45^\circ) = -7.707 \\ B &= r_2^2 + r_4^2 - r_3^2 - 2r_2r_4(\cos \theta_2 \cos \theta_4 + \sin \theta_2 \sin \theta_4) \\ &= 5^2 - 8^2 = -39 \end{aligned}$$

The desired configuration of the linkage corresponds to the position of the slider with the larger x coordinate. Therefore, $\sigma = +1$. Then

$$r_1 = \frac{-A + \sigma\sqrt{A^2 - 4B}}{2} = \frac{-(7.707) + \sqrt{7.707^2 - 4(-39)}}{2} = 10.712 \text{ in}$$

Then θ_3 is given by

$$\theta_3 = \tan^{-1} \left[\frac{r_1 \sin \theta_1 - r_4 \sin \theta_4 - r_2 \sin \theta_2}{r_1 \cos \theta_1 + r_4 \cos \theta_4 - r_2 \cos \theta_2} \right] = \tan^{-1} \left[\frac{-(5) \sin 45^\circ}{10.712 - (5) \cos 45^\circ} \right] = -26.228^\circ$$

For the velocities, solve the linear set of velocity equations

$$\begin{aligned} \begin{bmatrix} \cos \theta_1 & -r_3 \sin \theta_3 \\ \sin \theta_1 & -r_3 \cos \theta_3 \end{bmatrix} \begin{Bmatrix} \dot{\theta}_1 \\ \dot{\theta}_3 \end{Bmatrix} &= \begin{Bmatrix} -r_2 \dot{\theta}_2 \sin \theta_2 \\ r_2 \dot{\theta}_2 \cos \theta_2 \end{Bmatrix} \\ \text{or} \quad \begin{bmatrix} 1 & 8\sin(-26.228^\circ) \\ 0 & -8\cos(-26.228^\circ) \end{bmatrix} \begin{Bmatrix} \dot{\theta}_1 \\ \dot{\theta}_3 \end{Bmatrix} &= \begin{Bmatrix} -5(10)\sin 45^\circ \\ 5(10)\cos 45^\circ \end{Bmatrix} \end{aligned}$$

then

$$\begin{bmatrix} 1 & -3.535 \\ 0 & -7.176 \end{bmatrix} \begin{Bmatrix} \dot{\theta}_1 \\ \dot{\theta}_3 \end{Bmatrix} = \begin{Bmatrix} -35.35 \\ 35.35 \end{Bmatrix} \text{ or } \begin{Bmatrix} \dot{\theta}_1 \\ \dot{\theta}_3 \end{Bmatrix} = \begin{Bmatrix} -52.77 \\ -4.927 \end{Bmatrix}$$

Therefore, $\dot{\theta}_1 = 52.774 \text{ in/sec}$ and $\dot{\theta}_3 = -4.927 \text{ rad/sec CCW}$ or 4.927 rad/sec CW .

For the accelerations, solve the linear set of acceleration equations,

$$\begin{bmatrix} \cos \theta_1 & -r_3 \sin \theta_3 \\ \sin \theta_1 & -r_3 \cos \theta_3 \end{bmatrix} \begin{Bmatrix} \ddot{\theta}_1 \\ \ddot{\theta}_3 \end{Bmatrix} = \begin{Bmatrix} -r_2 \ddot{\theta}_2 \sin \theta_2 - r_2 \dot{\theta}_2^2 \cos \theta_2 - r_3 \ddot{\theta}_3' \cos \theta_3 \\ r_2 \ddot{\theta}_2 \cos \theta_2 - r_2 \dot{\theta}_2^2 \sin \theta_2 - r_3 \ddot{\theta}_3' \sin \theta_3 \end{Bmatrix}$$

or

$$\begin{bmatrix} 1 & -3.333 \\ 0 & -7.176 \end{bmatrix} \begin{Bmatrix} \ddot{r}_1 \\ \ddot{\theta}_3 \end{Bmatrix} = \begin{Bmatrix} -5(10)^2 \cos 45^\circ - 3(-4.926)^2 \cos(-26.228^\circ) \\ -5(10)^2 \sin 45^\circ - 3(-4.926)^2 \sin(-26.228^\circ) \end{Bmatrix} = \begin{Bmatrix} -527.736 \\ -257.735 \end{Bmatrix}$$

then

$$\begin{Bmatrix} \ddot{r}_1 \\ \ddot{\theta}_3 \end{Bmatrix} = \begin{Bmatrix} -395.83 \\ 37.309 \end{Bmatrix}$$

Therefore, $\ddot{r}_1 = -395.83 \text{ in/s}^2$ and $\ddot{\theta}_3 = 37.30 \text{ rad/sec}^2$ CCW. The results can be checked with the graphical analysis in Example 4.2.



Example 7.5

Kinematic Analysis of a Slider-Crank Mechanism with a Slider Input

Reanalyze the slider-crank mechanism shown in [Figure 7.20](#) when $r_1 = 10.75$ in, $\dot{\theta}_1 = 50$ in/s, and $\ddot{\theta}_1 = 400$ in/s². The link lengths, r_2 and r_3 , are the same as in Example 7.4, and again the line of action of point B_4 is along the line A^*B . Find the position, angular velocity, and angular acceleration of link 2 and of link 3.

Solution

This is essentially the same problem as in Example 7.4 except that now the slider is the input link, and link 2 is the output. The analysis can be conducted using the equations in [Table 7.5](#). The known input information is

Table 7.5 Summary of Position, Velocity, and Acceleration Equations for a Slider-Crank Mechanism When the Slider (Link 4) Is the Input Link. (The link numbers and points are defined in [Figure 7.14](#).)

Position
$A = -2r_1 r_2 \cos \theta_1 - 2r_2 r_4 \cos \theta_4$
$B = -2r_1 r_2 \sin \theta_1 - 2r_2 r_4 \sin \theta_4$
$C = r_1^2 + r_2^2 + r_4^2 - r_3^2 + 2r_1 r_4 (\cos \theta_1 \cos \theta_4 + \sin \theta_1 \sin \theta_4)$
$\theta_2 = 2 \tan^{-1} \left \frac{-\sigma + c/\beta^2 - C^2 - A^2}{C - A} \right ; \sigma = \pm 1$
$\theta_3 = \tan^{-1} \left \frac{r_1 \sin \theta_1 + r_4 \sin \theta_4 - r_2 \sin \theta_2}{r_1 \cos \theta_1 + r_4 \cos \theta_4 - r_2 \cos \theta_2} \right $
$r_A = r_2 = r_2 (\cos \theta_2 \hat{i} + \sin \theta_2 \hat{j})$
$r_B = r_2 + r_3 = r_2 (\cos \theta_2 \hat{i} + \sin \theta_2 \hat{j}) + r_3 (\cos \theta_3 \hat{i} + \sin \theta_3 \hat{j})$
Velocity
$\begin{bmatrix} -r_2 \sin \theta_2 & -r_3 \sin \theta_3 \\ r_2 \cos \theta_2 & r_3 \cos \theta_3 \end{bmatrix} \begin{bmatrix} \dot{\theta}_2 \\ \dot{\theta}_3 \end{bmatrix} = \begin{bmatrix} \dot{r}_1 \cos \theta_1 \\ \dot{r}_1 \sin \theta_1 \end{bmatrix}$
$\dot{r}_A = \dot{r}_2 = r_2 \dot{\theta}_2 (-\sin \theta_2 \hat{i} + \cos \theta_2 \hat{j})$
$\dot{r}_B = \dot{r}_2 + \dot{r}_3 = (-r_2 \dot{\theta}_2 \sin \theta_2 - r_3 \dot{\theta}_3 \sin \theta_3) \hat{i} + (r_2 \dot{\theta}_2 \cos \theta_2 + r_3 \dot{\theta}_3 \cos \theta_3) \hat{j}$
Acceleration
$\begin{bmatrix} -r_2 \sin \theta_2 & -r_3 \sin \theta_3 \\ r_2 \cos \theta_2 & r_3 \cos \theta_3 \end{bmatrix} \begin{bmatrix} \ddot{\theta}_2 \\ \ddot{\theta}_3 \end{bmatrix} = \begin{bmatrix} r_2 \dot{\theta}_2^2 \cos \theta_2 + r_3 \dot{\theta}_3^2 \cos \theta_3 + \ddot{r}_1 \cos \theta_1 \\ r_2 \dot{\theta}_2^2 \sin \theta_2 + r_3 \dot{\theta}_3^2 \sin \theta_3 + \ddot{r}_1 \sin \theta_1 \end{bmatrix}$
$\ddot{r}_A = \ddot{r}_2 = (-r_2 \ddot{\theta}_2 \sin \theta_2 - r_2 \dot{\theta}_2^2 \cos \theta_2) \hat{i} + (r_2 \ddot{\theta}_2 \cos \theta_2 - r_2 \dot{\theta}_2^2 \sin \theta_2) \hat{j}$
$\ddot{r}_B = -(r_2 \ddot{\theta}_2 \sin \theta_2 + r_2 \dot{\theta}_2^2 \cos \theta_2 + r_3 \dot{\theta}_3 \sin \theta_3 + r_3 \dot{\theta}_3^2 \cos \theta_3) \hat{i} + (r_2 \dot{\theta}_2 \cos \theta_2 - r_2 \dot{\theta}_2^2 \sin \theta_2 + r_3 \dot{\theta}_3 \cos \theta_3 - r_3 \dot{\theta}_3^2 \sin \theta_3) \hat{j}$

$$\theta_1 = 0^\circ, r_1 = 10.75 \text{ in}, \dot{\theta}_1 = 50 \text{ in/s}, \ddot{\theta}_1 = 400 \text{ in/s}^2$$

$$r_2 = 5 \text{ in}, r_3 = 8 \text{ in}, r_4 = 0 \text{ in}$$

Start with the position analysis, and first compute constants A , B , and C

$$\begin{aligned}
A &= -2r_1r_2\cos\theta_1 - 2r_3r_4\cos\theta_4 = -2(10.75)(3) = -107.5 \\
B &= -2r_1r_2\sin\theta_1 - 2r_3r_4\sin\theta_4 = 0 \\
C &= r_1^2 + r_2^2 + r_3^2 + r_4^2 - 2r_1r_4(\cos\theta_1\cos\theta_4 + \sin\theta_1\sin\theta_4) = 10.75^2 + 5^2 - 3^2 = 76.56
\end{aligned}$$

For the configuration in Fig. 7.20, $\sigma = 1$. Then

$$\theta_2 = 2 \tan^{-1} \left[\frac{-B + \sigma \sqrt{B^2 - C^2 + A^2}}{C - A} \right] = 2 \tan^{-1} \left[\frac{+1 \cdot \sqrt{(-76.56)^2 + (-107.5)^2}}{76.56 - (-107.5)} \right] = 44.58^\circ$$

and

$$\theta_3 = \tan^{-1} \left[\frac{r_1 \sin\theta_1 - r_4 \sin\theta_4 - r_2 \sin\theta_2}{r_1 \cos\theta_1 + r_4 \cos\theta_4 - r_2 \cos\theta_2} \right] = \tan^{-1} \left[\frac{-5 \sin 44.58^\circ}{10.75 - 5 \cos 44.58^\circ} \right] = -26.02^\circ$$

For the velocities, solve the linear set of velocity equations

$$\begin{bmatrix} -r_2 \sin\theta_2 & -r_3 \sin\theta_3 \\ r_2 \cos\theta_2 & r_3 \cos\theta_3 \end{bmatrix} \begin{Bmatrix} \dot{\theta}_2 \\ \dot{\theta}_3 \end{Bmatrix} = \begin{Bmatrix} \dot{r}_1 \cos\theta_1 \\ \dot{r}_1 \sin\theta_1 \end{Bmatrix} \text{ or } \begin{bmatrix} -3 \sin 44.58^\circ & -3 \sin(-26.02^\circ) \\ 5 \cos 44.58^\circ & 8 \cos(-26.02^\circ) \end{bmatrix} \begin{Bmatrix} \dot{\theta}_2 \\ \dot{\theta}_3 \end{Bmatrix} = \begin{Bmatrix} 30 \\ 0 \end{Bmatrix}$$

then

$$\begin{bmatrix} -3.509 & 3.509 \\ 3.561 & 7.189 \end{bmatrix} \begin{Bmatrix} \dot{\theta}_2 \\ \dot{\theta}_3 \end{Bmatrix} = \begin{Bmatrix} 30 \\ 0 \end{Bmatrix} \text{ or } \begin{Bmatrix} \dot{\theta}_2 \\ \dot{\theta}_3 \end{Bmatrix} = \begin{Bmatrix} -9.527 \\ 4.719 \end{Bmatrix}$$

Therefore, $\dot{\theta}_2 = -9.527 \text{ rad/s CCW}$ and $\dot{\theta}_3 = 4.719 \text{ rad/s CW}$. For the accelerations, solve the linear set of acceleration equations

$$\begin{bmatrix} -r_2 \sin\theta_2 & -r_3 \sin\theta_3 \\ r_2 \cos\theta_2 & r_3 \cos\theta_3 \end{bmatrix} \begin{Bmatrix} \ddot{\theta}_2 \\ \ddot{\theta}_3 \end{Bmatrix} = \begin{Bmatrix} r_2 \dot{\theta}_2^2 \sin\theta_2 + r_3 \dot{\theta}_3^2 \cos\theta_3 + \ddot{r}_1 \cos\theta_1 \\ r_2 \dot{\theta}_2^2 \sin\theta_2 + r_3 \dot{\theta}_3^2 \sin\theta_3 + \ddot{r}_1 \sin\theta_1 \end{Bmatrix}$$

or

$$\begin{bmatrix} -3.509 & 3.509 \\ 3.561 & 7.189 \end{bmatrix} \begin{Bmatrix} \ddot{\theta}_2 \\ \ddot{\theta}_3 \end{Bmatrix} = \begin{Bmatrix} 5(9.527)^2 \cos 44.58^\circ + 8(4.719)^2 \cos(-26.02^\circ) + 400 \\ 5(9.527)^2 \sin 44.58^\circ + 8(4.719)^2 \sin(-26.02^\circ) \end{Bmatrix} = \begin{Bmatrix} 883.309 \\ 240.381 \end{Bmatrix}$$

Then

$$\begin{Bmatrix} \ddot{\theta}_2 \\ \ddot{\theta}_3 \end{Bmatrix} = \begin{Bmatrix} -145.933 \\ 105.726 \end{Bmatrix}$$

Therefore, $\ddot{\theta}_2 = -145.933 \text{ rad/s}^2 \text{ CCW}$ or $145.93 \text{ rad/s}^2 \text{ CW}$, and $\ddot{\theta}_3 = 105.726 \text{ rad/s}^2 \text{ CW}$.



7.6 Other Four-Bar Mechanisms with Revolute and Prismatic Joints

While Sections 7.3 and 7.5 provided detailed analytical equations for position, velocity, and acceleration of classical four-bar (RRRR) and slider-crank (RRRP) mechanisms, other mechanisms can be designed either (a) by changing the placement of the R and P joints within the mechanism, often called the “inversion” of the mechanism structure, or (b) by changing the number of R and P joints within the four-bar mechanism. For example, an inversion of the slider crank RRRP mechanism is RRPR. In the classical RRRP mechanism, the P-joint is connected between the ground and a moving link. In its RRPR inversion, the P-joint is moved to the middle of the chain. Note that this is the only inversion possible for this classical slider crank mechanism since RRPR and RPRR chains are topologically similar to each other. Similarly, one can design a four-bar mechanism with two P-joints. This will lead to three distinct structures of the mechanism: RRP chain, RRPP chain, RPPR chain.

The procedures described in Sections 7.3 and 7.5 illustrate how to perform position, velocity, and acceleration analysis of mechanisms made up with four rigid bodies with R and P joints moving in the plane. This same procedure can be extended for analysis of these other mechanisms.

7.6.1 Slider-Crank Inversion

The slider-crank inversion is a common mechanism when linear actuators are involved (e.g., [Figures 1.37](#) and [7.21](#)). It is also used in various pump mechanisms. As discussed in [Chapter 1](#), for low-load conditions, the slider is often replaced by a pin-in-a-slot joint. The resulting mechanisms can be analyzed using their governing equations by modeling the pin-in-a-slot joint as a revolute joint and slider joint connected by a link. A device that could be analyzed using this procedure is the walking toy shown in [Figure 7.22](#). A schematic of such a RRPR chain is shown in [Figure 7.23](#).



[Figure 7.21](#) Backhoe. Each joint is actuated by an inversion of the slider-crank mechanism.

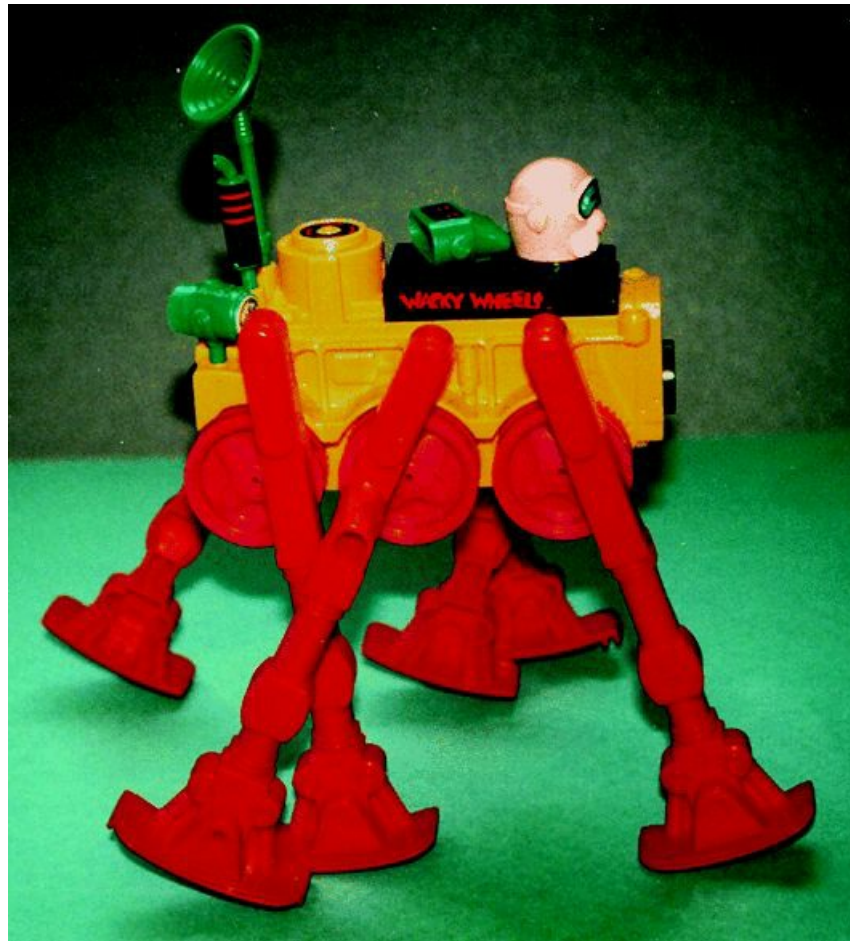


Figure 7.22 Walking toy. The pin-in-a-slot joints can be modeled as a separate revolute and slider joint connected by a link.

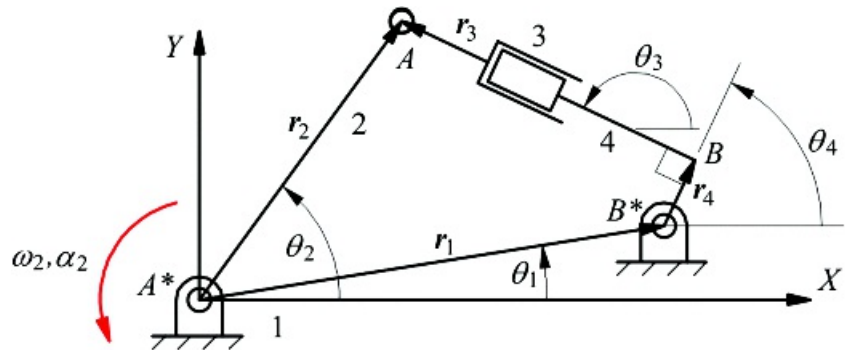
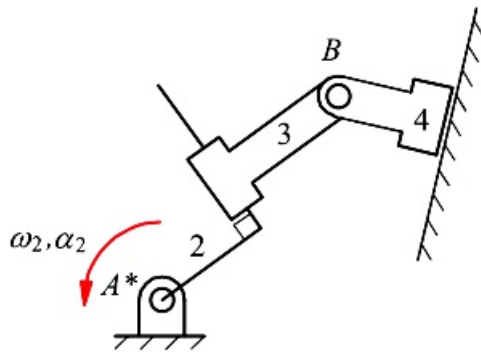


Figure 7.23 Vector closure condition for the slider-crank inversion. The position of point A indicated by \vec{r}_A is the same as that obtained by adding vectors $\vec{r}_1 + \vec{r}_2 + \vec{r}_3$.

7.6.2 A RPRP Mechanism

A schematic drawing of an RPRP mechanism is shown in [Figure 7.24](#). In the mechanism shown, link 2 is connected to the frame by a revolute joint and to the coupler by a prismatic joint. Link 4 is connected to the frame through a prismatic joint and to the coupler by a revolute joint. This is a less common mechanism than the various four-bar linkages and slider cranks; however, it does occur in industrial machinery. For example, one variation of it, the Rapson slide is used in marine steering gear.



[Figure 7.24](#) Schematic diagram of RPRP mechanism.

When there is a slider joint between two links, the actual location of the slider does not matter from a kinematic standpoint. Therefore, for simplicity, we can analyze the mechanism as if both sliders were at point *B*. The resulting mechanism then appears as shown in [Figure 7.25](#). In [Figure 7.25](#), the angles are not indicated for simplicity. The angles are again always measured counterclockwise from the horizontal as shown in [Figure 7.3](#). To develop the closure equations, locate vectors r_1 through r_4 as shown in [Figure 7.25](#). By locating point *B* using two different sets of vectors, the loop closure equation is then seen to be the same as that for the regular four-bar linkage.

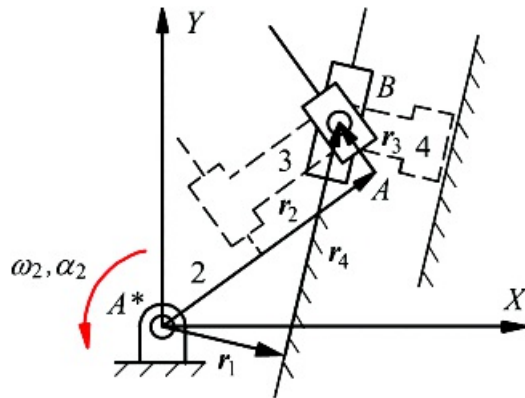


[Figure 7.25](#) Vector closure condition for RPRP mechanism. The position of point *P* obtained by the vectors r_2 and r_3 is the same as that obtained by adding vectors r_1 and r_4 .

7.6.3 A RRPP Mechanism

A schematic drawing of the RRPP mechanism is shown in [Figure 7.26](#). In the mechanism shown, link 2 is connected to the frame and to the coupler (link 3) by revolute joints. The coupler is connected to link 4 by a prismatic joint, and link 4 is connected to the frame through a prismatic joint. This mechanism occurs frequently in industrial machinery and household appliances. A common version of it is the scotch-yoke that is a compact mechanism for converting rotary motion to reciprocating motion.

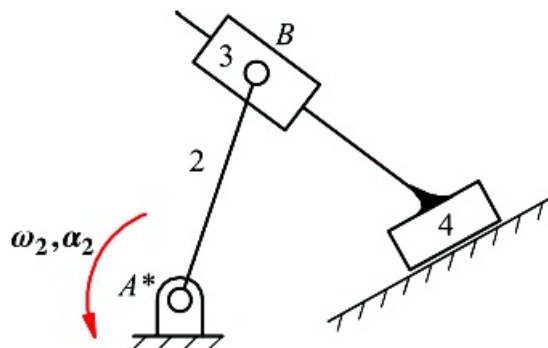


[Figure 7.26](#) Schematic diagram of RRPP mechanism.

To analyze the mechanism using vector closure equations, we must align vectors in the directions of the slider motions as shown in [Figure 7.27](#). Only three vectors are required to model the motion. Vector r_1 is fixed at an angle θ_1 and of variable length. This vector begins at point A^* and ends at point A , where A is the intersection of a line through A^* and in the direction of the velocity of link 4 relative to link 1 and a second line through B in the direction of the velocity of link 3 relative to link 4. The two lines intersect at an angle β . Vector r_2 is the crank and of fixed length but variable orientation. Vector r_3 is measured from point A and gives the displacement of slider 3 relative to link 4. To develop the closure equations, locate point B with vector r_2 and with vectors $r_1 + r_3$ as shown in [Figure 7.27](#).

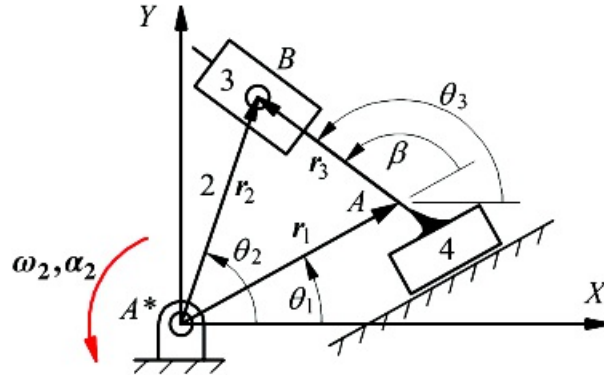


[Figure 7.27](#) Vector closure diagram of RRPP mechanism.

7.6.4 Elliptic-Trammel Mechanism

The elliptic-trammel is an inversion of the RRPP mechanism, and a schematic drawing of this mechanism is shown in [Figure 7.28](#). In the mechanism, links 2 and 4 are connected to the frame by prismatic joints and to the coupler by revolute joints. A significant feature of this mechanism is that coupler points trace ellipses on the frame, and it is used in machine tools for this purpose.

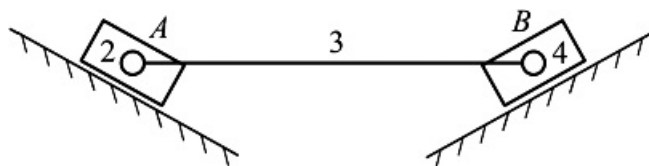


[Figure 7.28](#) Schematic diagram of an elliptic trammel mechanism.

To analyze the mechanism using vector closure equations, we must again align vectors in the directions of the slider motions as shown in [Figure 7.29](#). As in the case of the RRPP mechanism, only three vectors are required to model the motion. Vector r_1 is fixed at an angle θ_1 and of variable length. This vector begins at point O and ends at point A , where O is the intersection of a line through A and in the direction of the velocity of link 2 relative to link 1 and a second line through B in the direction of the velocity of link 4 relative to link 1. Point O is the origin of the frame coordinate system. The two lines intersect at an angle β , measured from r_2 to r_1 . Vector r_2 is fixed at an angle θ_2 and of variable length. Vector r_3 is measured from point A to point B . As shown in [Figure 7.29](#), to develop the closure equations, locate point A with vector r_1 and with vectors $r_2 + r_3$.

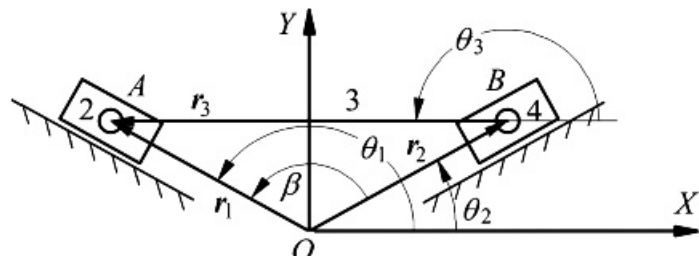


[Figure 7.29](#) Vector closure diagram for an elliptic-trammel mechanism.

7.6.5 Oldham Mechanism

The Oldham (RPPR) mechanism is another inversion of the RRPP mechanism, and a schematic drawing of this mechanism is shown in [Figure 7.30](#). In this mechanism, links 2 and 4 are connected to the frame by revolute joints and to the coupler by prismatic joints. Therefore, the angle, β , between links 2 and 4 is fixed.

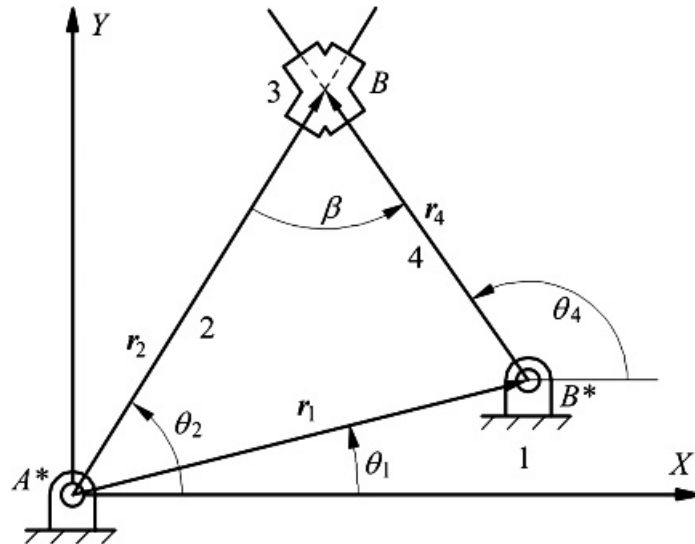


[Figure 7.30](#) Schematic diagram of Oldham mechanism.

To analyze the mechanism using vector closure equations, we must again align vectors in the directions of the slider motions as shown in [Figure 7.30](#). As in the case of the elliptic-trammel, only three vectors are required to model the motion. Vector r_1 is fixed at an angle θ_1 and is of constant length. Point A^* is the origin of the frame coordinate system. Links 2 and 4 intersect at an angle β , where β is measured from r_2 to r_4 . Vector r_2 is at an angle θ_2 with respect to a horizontal line and of variable length. Vector r_4 is at an angle θ_4 with respect to a horizontal line and of variable length. As shown in [Figure 7.30](#), to develop the closure equations, locate point B with vector r_3 and with vectors $r_1 + r_4$.



7.7 Closure or Loop Equation Approach for Compound Mechanisms

As in the case of simple, single-loop mechanisms, each vector is represented by a length r_i and an angle θ_i . All angles are measured counterclockwise from a fixed line parallel to the x axis attached to the frame as shown in [Figure 7.31](#).

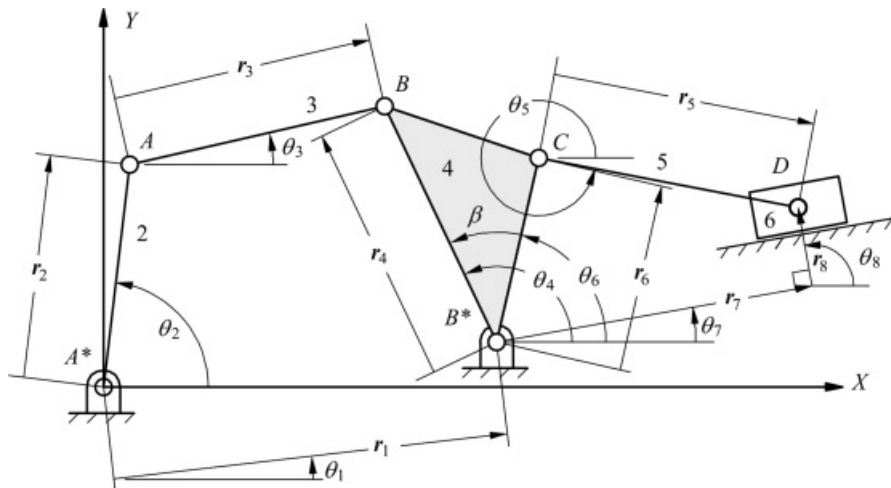


[Figure 7.31](#) Example of formulation of solution procedure using vector loops.

To illustrate the method for compound mechanisms, consider the kinematic diagram of the mechanism given in [Figure 7.31](#). Each member is represented by a directed length and an angle. The formulation of the analytical procedure based on vector loops for compound mechanisms is straightforward, but it requires a system if results are to be meaningful. A procedure will be outlined in the following that is illustrated on the mechanism in [Figure 7.31](#). It will be noted that the procedure presented is a generalization of that used for the single-loop mechanisms. In the mechanism shown, assume that θ_2 , θ_3 , and θ_5 are known values.

Procedure

1. Draw a kinematic sketch of the mechanism. The sketch need not be to scale; however, it must be accurate enough that the assembly mode(s) can be determined by inspection.
2. Establish a global coordinate system for the mechanism. This will establish the horizontal axis from which all angles will be measured and identify the system from which all global coordinates will be determined.
3. Represent the link between adjacent joints by a vector r_i defined by a directed line and an angle measured positive CCW from the x axis (or a line parallel to the x axis)

$$r_i = r_i \angle \theta_i$$

4. If sliders are involved, locate the slider by two vectors, one in the direction of the relative velocity between the slider and the slide and the second in a direction perpendicular to the direction of the velocity (see r_{α} and r_{β} in [Figure 7.31](#)).
5. Note which lengths and angles are fixed and which are variable. In the mechanism above, r_8 is the only *variable* length and θ_1 , θ_7 , θ_8 , and β are the only *fixed* angles.

If the vectors are properly defined, they will all be expressible as

$$r_i = r_i (\cos \theta_i \hat{i} + \sin \theta_i \hat{v})$$

The cosine term will always go with i and the sine term will go with j . Some angles may be functions of others. For example, $\theta_5 = \theta_4 - \beta$.

6. Identify all of the joints on the linkage, and be sure that each one is located at the end of one of the vectors. Then identify all of the independent vector loops in the linkage, and write a vector equation for each loop. For the mechanism in [Figure 7.31](#), there are two obvious vector loops represented by the following equations

$$r_1 + r_4 = r_2 + r_3 \quad (7.93)$$

$$r_3 + r_6 = r_4 + r_5 \quad (7.94)$$

7. Write the x, y scalar equations for each vector equation. Notice that the form of the equations is consistent, and once the basic vector equations are given (e.g., [Equations 7.93](#) and [7.94](#)), it is not even necessary to look at the mechanism to be able to write the component equations.

$$x \Rightarrow r_1 \cos \theta_1 + r_4 \cos \theta_4 = r_2 \cos \theta_2 + r_3 \cos \theta_3 \quad (7.95)$$

$$y \Rightarrow r_1 \sin \theta_1 + r_4 \sin \theta_4 = r_2 \sin \theta_2 + r_3 \sin \theta_3 \quad (7.96)$$

$$x \Rightarrow r_5 \cos \theta_5 + r_6 \cos \theta_6 = r_7 \cos \theta_7 + r_8 \cos \theta_8 \quad (7.97)$$

$$y \Rightarrow r_5 \sin \theta_5 + r_6 \sin \theta_6 = r_7 \sin \theta_7 + r_8 \sin \theta_8 \quad (7.98)$$

8. Identify any constraints among the lengths or angles that are not identified by the vector loops. In the mechanism in [Figure 7.31](#), θ_7 is related to θ_8 by $\pi/2$, and θ_6 is related to θ_4 through β . Therefore, the extra constraint equations are

$$\theta_8 = \theta_7 + \pi/2 \quad (7.99)$$

and

$$\theta_5 = \theta_4 - \beta \quad (7.100)$$

9. Count the total number of variables in the component equations and the extra constraint equations. If n is the total number of equations and f is the number of degrees of freedom for the mechanism, the total number of unknowns should be $n + f$. If the number of unknowns is larger than this, it is necessary to identify additional constraints or to reformulate the loop closure equations. In the mechanism in [Figure 7.31](#), the total number of unknowns is seven ($\theta_1, \theta_2, \theta_4, \theta_5, \theta_6, \theta_7$, and r_7), and the mechanism has only one degree of freedom. Therefore, $n + f = 7$, which indicates that the problem should be solvable. Note that the number of unknowns and the number of variables are not necessarily the same. In this mechanism, θ_8 is a constant but initially unknown. It must be computed using [Equation 7.98](#). [Equations 7.95–7.98](#) are nonlinear in the unknowns ($\theta_2, \theta_3, \theta_4, \theta_5, \theta_6, \theta_7$, and r_7), and most of the analysis difficulties are concentrated here.
10. For velocities, differentiate the position equations (x and y components) term by term. In the example case,

the velocity equations are

$$\dot{r}_1 + \dot{r}_4 = \dot{r}_2 + \dot{r}_3 \quad (7.101)$$

$$\dot{r}_3 + \dot{r}_6 = \dot{r}_1 + \dot{r}_4 \quad (7.102)$$

and recognizing which terms are constants and which are variables

$$x \Rightarrow -r_4\dot{\theta}_4 \sin \theta_4 = -r_2\dot{\theta}_2 \sin \theta_2 - r_3\dot{\theta}_3 \sin \theta_3 \quad (7.103)$$

$$y \Rightarrow r_4\dot{\theta}_4 \cos \theta_4 = r_2\dot{\theta}_2 \cos \theta_2 + r_3\dot{\theta}_3 \cos \theta_3 \quad (7.104)$$

$$\dot{\theta}_5 = \dot{\theta}_4 \quad (7.105)$$

$$x \Rightarrow -r_5\dot{\theta}_5 \sin \theta_5 - r_5\dot{\theta}_5 \sin \theta_5 = \dot{r}_7 \cos \theta_7 \quad (7.106)$$

$$y \Rightarrow r_5\dot{\theta}_5 \cos \theta_5 + r_6\dot{\theta}_6 \cos \theta_6 = \dot{r}_7 \sin \theta_7 \quad (7.107)$$

Note that once we have solved the position equations, only the angle and length derivatives will be unknown. Hence the equations are linear in the unknowns and can be easily solved. There are five linear equations in five unknowns ($\dot{\theta}_4$, $\dot{\theta}_5$, $\dot{\theta}_6$, $\dot{\theta}_7$, and \dot{r}_7). These can be solved directly by Gaussian elimination, by using a programmable calculator, or by using a matrix solver such as MATLAB.

- For accelerations, differentiate the velocity equations (x and y components) term by term. In the example case, the acceleration equations are

$$\ddot{r}_1 + \ddot{r}_4 = \ddot{r}_2 + \ddot{r}_3 \quad (7.108)$$

$$\ddot{r}_3 + \ddot{r}_6 = \ddot{r}_1 + \ddot{r}_4 \quad (7.109)$$

and in terms of components

$$x \Rightarrow -r_4\ddot{\theta}_4 \sin \theta_4 - r_4\dot{\theta}_4^2 \cos \theta_4 = -r_2\ddot{\theta}_2 \sin \theta_2 - r_2\dot{\theta}_2^2 \cos \theta_2 - r_3\ddot{\theta}_3 \sin \theta_3 - r_3\dot{\theta}_3^2 \cos \theta_3 \quad (7.110)$$

$$y \Rightarrow r_4\ddot{\theta}_4 \cos \theta_4 - r_4\dot{\theta}_4^2 \sin \theta_4 = r_2\ddot{\theta}_2 \cos \theta_2 - r_2\dot{\theta}_2^2 \sin \theta_2 + r_3\ddot{\theta}_3 \cos \theta_3 - r_3\dot{\theta}_3^2 \sin \theta_3 \quad (7.111)$$

$$\ddot{\theta}_5 = \ddot{\theta}_4 \quad (7.112)$$

$$x \rightarrow -r_3\ddot{\theta}_3 \sin \theta_3 - r_3\dot{\theta}_3^2 \cos \theta_3 - r_6\ddot{\theta}_6 \sin \theta_6 - r_6\dot{\theta}_6^2 \cos \theta_6 = \ddot{r}_1 \cos \theta_1 \quad (7.113)$$

$$y \rightarrow r_3\ddot{\theta}_3 \cos \theta_3 - r_3\dot{\theta}_3^2 \sin \theta_3 + r_6\ddot{\theta}_6 \cos \theta_6 - r_6\dot{\theta}_6^2 \sin \theta_6 = \ddot{r}_1 \sin \theta_1 \quad (7.114)$$

Note that once we have solved the position and velocity equations, only the derivatives of velocity will be unknown. Hence, the equations are linear in the unknowns and can be easily solved. There are five linear equations in five unknowns ($\dot{\theta}_3$, $\dot{\theta}_4$, $\dot{\theta}_5$, $\dot{\theta}_6$, and \ddot{r}_1). Once again, these can be solved directly by Gaussian elimination, by using a programmable calculator, or by using a matrix solver such as MATLAB.

7.7.1 Handling Points Not on the Vector Loops

The solution procedure outlined above will give the position, velocity, and acceleration of each point at a vertex of a vector loop in addition to the angular velocity and acceleration of each link. The angular velocities and accelerations are the $\dot{\theta}_i$ and $\ddot{\theta}_i$ terms, respectively. In general

$$\omega_i = \dot{\theta}_i \hat{k}$$

and

$$\alpha_i = \ddot{\theta}_i \hat{k}$$

Once the basic analysis is completed by solving the vector loop equations, we will be able to locate at least one point on each rigid body (link) as a function of time. We will also be able to determine the orientation of each rigid body as a function of time, that is, $\dot{\theta}_i$, ω_i , and α_i will be known or can be determined for each link.

Points that are not vertices of the vector loops must be associated with one of the rigid bodies in the mechanism. To determine the kinematic properties of a given point, we simply identify the point by a vector in terms of the known quantities, determine the x , y components of the vector, and differentiate. For example, assume that we want to know the kinematic properties of a point C on link 3 as shown in [Figure 7.32](#). Then,

$$\mathbf{r}_{C_3/A_2^*} = \mathbf{r}_2 + \mathbf{r}_3$$

or

$$\begin{aligned} \mathbf{r}_{C_3/A_2^*} &= r_2(\cos \theta_2 i + \sin \theta_2 j) + r_3[\cos(\beta + \theta_3)i + \sin(\beta + \theta_3)j] \\ &= [r_2 \cos \theta_2 + r_3 \cos(\beta + \theta_3)]i + [r_2 \sin \theta_2 + r_3 \sin(\beta + \theta_3)]j \end{aligned} \quad (7.115)$$

All terms on the right-hand side of [Equation 7.115](#) will be known. Therefore, the position vector can be computed directly. The velocity is given by

$$\mathbf{v}_{C_3/A_2^*} = \dot{\mathbf{r}}_2 + \dot{\mathbf{r}}_3$$

and

$$\begin{aligned} v_{C_3/A_2^*} &= r_2 \dot{\theta}_2 (-\sin \theta_2 i + \cos \theta_2 j) + r_9 \dot{\theta}_3 [-\sin(\beta + \theta_3) i + \cos(\beta + \theta_3) j] \\ &= [r_2 \dot{\theta}_2 \sin \theta_2 + r_9 \dot{\theta}_3 \sin(\beta + \theta_3)] i + [r_2 \dot{\theta}_2 \cos \theta_2 + r_9 \dot{\theta}_3 \cos(\beta + \theta_3)] j \end{aligned} \quad (7.116)$$

Again, all quantities on the right-hand side of [Equation 7.116](#) are known, and so the velocity of point *C* can be computed without difficulty. For the acceleration, differentiate the velocity expression. Then

$$a_{C_3/A_2^*} = \ddot{r}_2 + \ddot{r}_3$$

and

$$\begin{aligned} a_{C_3/A_2^*} &= r_2 \ddot{\theta}_2 (-\sin \theta_2 i + \cos \theta_2 j) - r_2 \dot{\theta}_2^2 (\cos \theta_2 i + \sin \theta_2 j) \\ &\quad + r_9 \ddot{\theta}_3 [-\sin(\beta + \theta_3) i + \cos(\beta + \theta_3) j] - r_9 \dot{\theta}_3^2 [\cos(\beta + \theta_3) i + \sin(\beta + \theta_3) j] \\ &= [-r_2 \ddot{\theta}_2 \sin \theta_2 - r_9 \ddot{\theta}_3 \sin(\beta + \theta_3) - r_2 \dot{\theta}_2^2 \cos \theta_2 - r_9 \dot{\theta}_3^2 \cos(\beta + \theta_3)] i \\ &\quad + [r_2 \ddot{\theta}_2 \cos \theta_2 + r_9 \ddot{\theta}_3 \cos(\beta + \theta_3) - r_2 \dot{\theta}_2^2 \sin \theta_2 - r_9 \dot{\theta}_3^2 \sin(\beta + \theta_3)] j \end{aligned} \quad (7.117)$$

Again, all quantities on the right-hand side of [Equation 7.117](#) are known and so the acceleration of point *C* can be computed without difficulty. Note that this procedure is simply a variation on the rigid body analysis given in [Section 7.4](#).

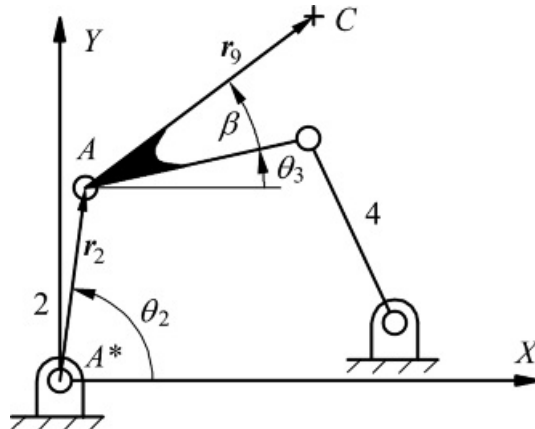


[Figure 7.32](#) Determination of velocity and acceleration of point *C* that is not a vertex of a vector loop.

7.7.2 Solving the Position Equations

A review of the analysis just developed shows that only the position equations are nonlinear in the unknowns. Therefore, specialized techniques are required to solve them. If a numerical solution is chosen, then an initial guess for the variables is required. This is best obtained by sketching the mechanism to scale. A numerical iteration method such as the Newton-Raphson method can be used to obtain refined values. If a series of input angles is to be investigated, then the final variable values for the previous input value can be used as the initial estimates of the variables for the next input value provided that the input angle increments are relatively small (i.e., within about 10° of each other).

Another numerical approach that is computationally more efficient than using Newton's method, but sometimes has convergence problems at end-of-travel positions, is to numerically integrate the velocity equations after a precise set of values for the variables is obtained by Newton's method. The input step size for this integration

should not exceed 2 degrees. This method is very convenient if a numerical integration is already needed for dynamic problems in which the equations of motion are required.

When it is possible, it is preferable to solve the displacement equations analytically. This method eliminates numerical instability problems present in both Newton's method and numerical integration. In general, it is always possible to solve the equations analytically if the mechanism can be analyzed by hand using traditional graphical methods with vector polygons as presented in [Chapters 4](#) and [5](#). When it is possible to do this, the position equations can be solved in sets of two equations in two unknowns as was done in Sections 7.3–7.5. If it is not possible to reduce the equations to a series of two equations in two unknowns, the equations must be solved iteratively using a numerical procedure such as Newton's method.

When it is possible to solve the position equations algebraically, one of two situations will usually occur. In the first situation, the compound mechanism can be treated as a series of simple mechanisms. In the second case, the compound mechanism cannot be represented as a series of simple mechanisms; however, the equations can be partitioned into a sequential set of two equations in two unknowns. These two situations will be presented separately.

[Compound Linkage as a Series of Simple Mechanisms](#)

When the compound linkage is a series of simple mechanisms, we can analyze each mechanism in sequence. The output for one mechanism is the input to the next mechanism. If we have computer routines to analyze the single-loop mechanisms, the routines can be concatenated to analyze the entire linkage. This is the case that exists in the mechanism of [Figure 7.31](#). When we examine the mechanism, we find that the first linkage is a four-bar linkage defined by vectors r_1 , r_2 , r_3 , and r_4 . This mechanism can be analyzed using the equations developed in Section 7.3. The four-bar loop drives link 4. Therefore, once the position, velocity, and acceleration for r_4 are known, the corresponding values for r_6 can be found using rigid body conditions (Section 7.4). Link 4 is the input for the slider-crank mechanism defined by r_5 , r_6 , r_7 , and r_8 . This mechanism can be analyzed using the equations in Section 7.5 to determine the kinematic properties of the slider.



Example 7.6

Kinematic Analysis of Compound Linkage

Determine the angular position, velocity, and acceleration of link 6 in the mechanism in [Figure 7.33](#) if the slider is moving at 10 cm/s (constant) to the right. The following dimensions are known

$$AB = 22.7 \text{ cm} \quad A^*C = 7.5 \text{ cm} \quad D^*D = 10.6 \text{ cm}$$

$$A^*A = 10.6 \text{ cm} \quad A^*D^* = 14.6 \text{ cm}$$

$$A^*B = 28 \text{ cm} \quad CD = 11.4 \text{ cm}$$

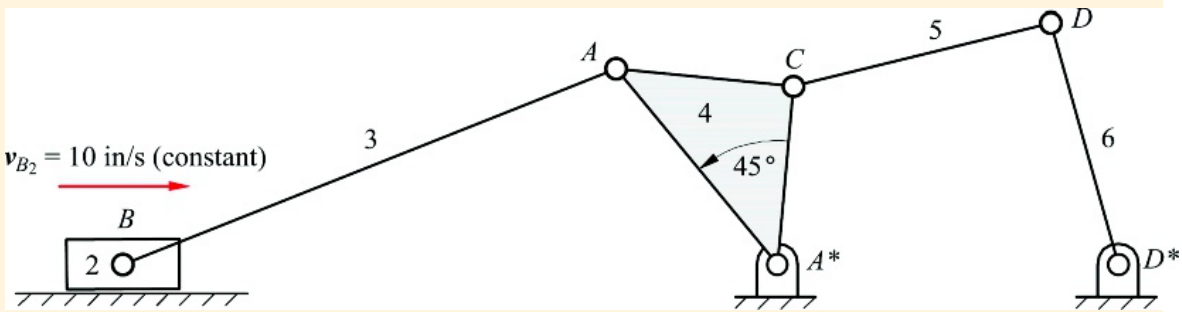


[Figure 7.33](#) Mechanism for Example 7.6.

Solution

We will analyze the mechanism as three linkage systems in series. First we will analyze the slider-crank mechanism using the equations in [Table 7.5](#). Next we will compute the position of A^*C from rigid body conditions ([Table 7.3](#)). Last, the four-bar linkage (A^*CDD^*) can be analyzed using [Table 7.1](#). The actual numerical calculations can be made using the MATLAB routines included in the supplementary material with this book.

To facilitate the analysis, the mechanism in [Figure 7.33](#) is represented by the vectors indicated in [Figure 7.34](#).

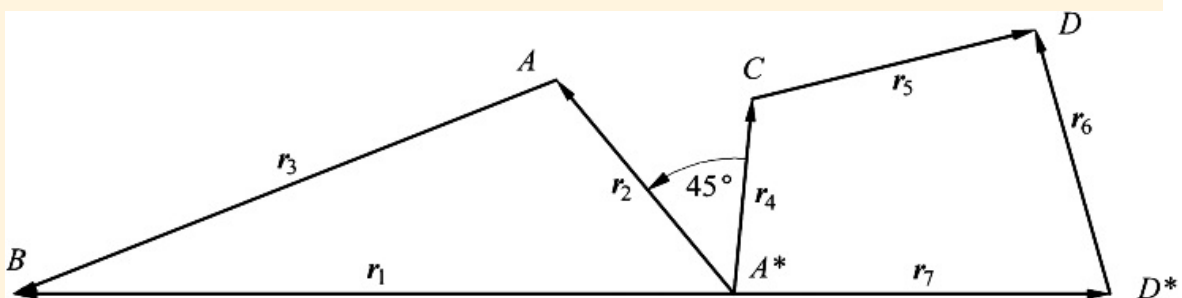


[Figure 7.34](#) Vectors representing mechanism in [Figure 7.33](#).

For the slider-crank part of the mechanism, the following magnitudes and directions are known

$$r_2 = 28, \theta_1 = 180^\circ, \dot{r}_1 = 10, \ddot{r}_1 = 0$$

$$r_2 = 10.6, r_3 = 22.7$$

The unknowns are θ_2 , $\dot{\theta}_2$, $\ddot{\theta}_2$, θ_3 , $\dot{\theta}_3$, and $\ddot{\theta}_3$. For this set of values, the equations in [Table 7.5](#) can be used. The value of σ is -1 for the geometry given, and the results are

$$\theta_1 = 180^\circ, \dot{\theta}_1 = 0 \text{ rad/s}, \ddot{\theta}_1 = 0 \text{ rad/s}^2$$

$$\theta_2 = 129.94^\circ, \dot{\theta}_2 = -0.9314 \text{ rad/s}, \ddot{\theta}_2 = 0.50 \text{ rad/s}^2$$

$$\theta_3 = -159.02^\circ, \dot{\theta}_3 = 0.299 \text{ rad/s}, \ddot{\theta}_3 = -0.455 \text{ rad/s}^2$$

The orientation of the vector r_4 will be related to that of the vector r_2 through the equation

$$\theta_4 = \theta_2 - 45^\circ$$

Therefore, the magnitudes and directions for the vectors defining the four-bar linkage are

$$r_4 = 7.5, \theta_4 = 84.94^\circ, \dot{\theta}_4 = -0.931 \text{ rad/s}, \ddot{\theta}_4 = 0.50 \text{ rad/s}^2$$

$$r_5 = 11.4, r_6 = 10.6, r_7 = 14.6, \theta_7 = 0^\circ$$

The unknowns are θ_5 , $\dot{\theta}_5$, $\ddot{\theta}_5$, θ_6 , $\dot{\theta}_6$, and $\ddot{\theta}_6$. For this set of values, the equations in [Table 7.1](#) can be used. The value of σ is -1 for the geometry given, and the results are

$$\theta_5 = 84.94^\circ, \dot{\theta}_5 = -0.931 \text{ rad/s}, \ddot{\theta}_5 = 0.50 \text{ rad/s}^2$$

$$\theta_6 = 13.87^\circ, \dot{\theta}_6 = 0.2175 \text{ rad/s}, \ddot{\theta}_6 = 0.0536 \text{ rad/s}^2$$

$$\theta_7 = 105.714^\circ, \dot{\theta}_7 = -0.023 \text{ rad/s}, \ddot{\theta}_7 = 0.5978 \text{ rad/s}^2$$

$$\theta_7 = 0^\circ, \dot{\theta}_7 = 0 \text{ rad/s}, \ddot{\theta}_7 = 0 \text{ rad/s}^2$$

General Cases in Which Two Equations in Two Unknowns Result

For simple lower-pair mechanisms with one loop equation, the position analysis will reduce to two scalar equations in two unknowns, and it is relatively easy to develop closed-form equations for the unknown variables. However, when analyzing more complex lower-pair mechanisms with n loop equations, the number of equations and the number of variable unknowns are both $2n$, and the solution can become much more complicated. However, not all the pair variables appear in each of the equations. Fortunately, it is often possible to group the

equations into smaller sets that can be solved independently in a serial fashion.

If a given lower-pair mechanism can be analyzed using the traditional vector-polygon approach, it is always possible to group the position equations in such a way that no more than two equations in two unknowns must be solved at any one time. For such mechanisms, the position equations can always be solved in closed form, and these types of mechanisms form the vast majority of the linkages that an engineer might design. For complex mechanisms that cannot be analyzed entirely using closed-form equations, it is often possible to analyze a part of the mechanism with closed-form equations after other parts are analyzed numerically.



7.8 Closure Equations for Mechanisms with Higher Pairs

The closure equation approach can also be used for mechanisms with higher pairs if we use the centers of curvature of the contact surfaces corresponding to the contact points. This is exactly the approach employed when equivalent mechanisms are used, and, in fact, we could represent the higher-pair mechanisms by their equivalent lower-pair mechanism and determine the kinematic properties by analyzing the corresponding lower-pair mechanism. By using the centers of curvature, however, we can also approach the problem without using equivalent mechanisms directly.

The approach using centers of curvature can be applied directly to mechanisms with cam joints and to mechanisms with rolling joints if the contact points (and the corresponding centers of curvature) are known. With rolling contact, locating the contact point as a function of the input motion requires that we know the initial contact point when the mechanism begins to move. Subsequent contact points are then located by enforcing the constraint that there is no slipping at the contacting surfaces. If circle arcs are involved, the resulting constraint equations are simple; however, if general surfaces are involved, the constraint equations require that the arc length on each contacting surface be determined by integration. For simplicity, we will limit the discussions here to cases in which the contact point either is known or can be determined simply.

For higher-pair mechanisms, the vector closure diagrams are set up using the same procedure as would be used when the mechanism is drawn. In general, the same points and vectors will be used. The procedure will be illustrated with three examples.



Example 7.7

Kinematic Analysis of Mechanism with Cam Contact

In the mechanism shown in [Figure 7.35](#), $\omega_2 = 10 \text{ rad/s}$ and is constant. Determine v_{B3}/B_2 , v_{B3} , a_{B3}/B_2 , and a_{B3} using vector closure equations.

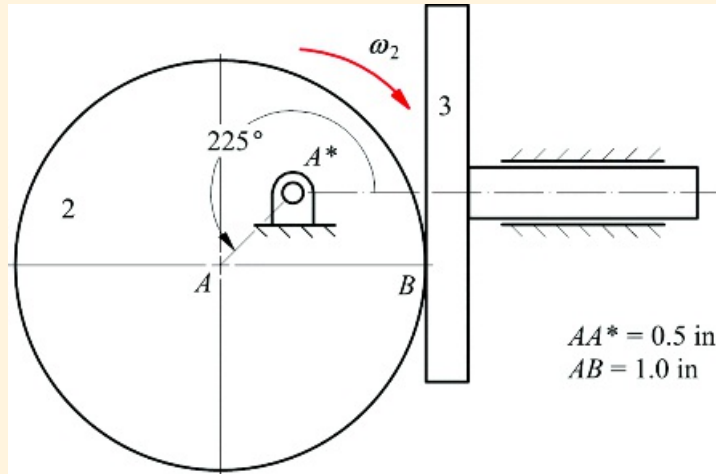


[Figure 7.35](#) Figure for Example 7.7.

Solution

To solve the problem, set up four vectors as shown in [Figure 7.36](#). The vector r_2 is from point A^* to point A , the center of curvature of link 2 corresponding to the contact point at B . Vector r_1 is from point A to point B , the contact location. The vector r_3 is constant in both direction and magnitude. Vector r_4 is from point A^* to the face of the cam follower. The direction of r_3 is constant, but the magnitude varies. Because r_3 is measured from a fixed point on the frame (point A^*) to the face of the cam follower, the first and second derivatives of r_3 correspond to the velocity and acceleration, respectively, of the cam follower. Vector r_4 is measured from the contact point to a line through A^* and in the direction of travel of the cam.

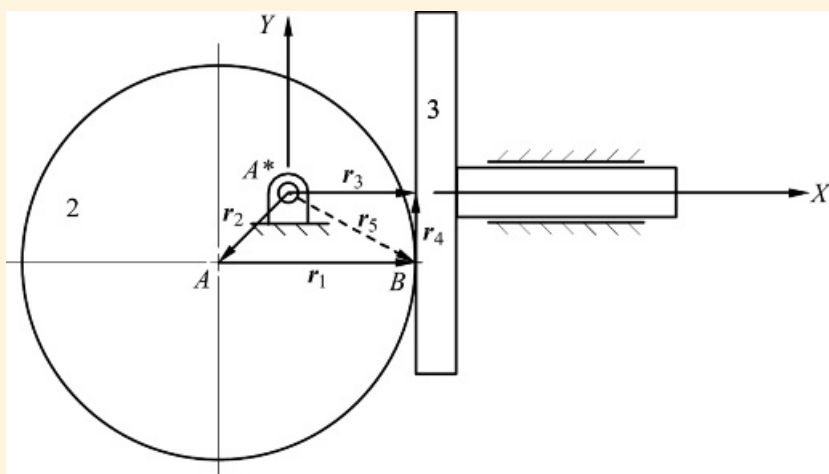


[Figure 7.36](#) Vector closure for Example 7.7.

The vector closure equation for the mechanism is

$$\ddot{r}_3 = \ddot{r}_2 - \dot{r}_1 + \ddot{r}_4 \quad (7.118)$$

and the corresponding velocity and acceleration expressions are given by

$$\dot{r}_3 = \dot{r}_2 - \dot{r}_1 + \ddot{r}_4 \quad (7.119)$$

and

$$\ddot{r}_3 = \ddot{r}_2 - \ddot{r}_1 + \ddot{r}_4 \quad (7.120)$$

Before actually solving the equations, we can summarize the variables that are known and unknown. These are

$$r_1 = 1.0 \text{ in}, \theta_1 = 0^\circ, \dot{\theta}_1 = 0 \text{ rad/s}, \ddot{\theta}_1 = 0$$

$$r_2 = 0.5 \text{ in}, \theta_2 = 225^\circ, \dot{\theta}_2 = -10 \text{ rad/s}, \ddot{\theta}_2 = 0$$

$$r_3 = ?, \dot{r}_3 = ?, \ddot{r}_3 = ?, \theta_3 = 0^\circ, \dot{\theta}_3 = 0 \text{ rad/s}, \ddot{\theta}_3 = 0$$

$$r_4 = ?, \dot{r}_4 = ?, \ddot{r}_4 = ?, \theta_4 = 90^\circ, \dot{\theta}_4 = 0 \text{ rad/s}, \ddot{\theta}_4 = 0$$

As in the cases of lower-pair mechanisms, the position equation must be solved first. The resulting linear velocity and acceleration equations can then be solved easily. Rewriting the position closure equation in component form gives

$$r_3 \cos \theta_3 = r_2 \cos \theta_2 + r_1 \cos \theta_1 + r_4 \cos \theta_4$$

$$r_3 \sin \theta_3 = r_2 \sin \theta_2 + r_1 \sin \theta_1 + r_4 \sin \theta_4$$

Simplifying based on the input values

$$r_3 = r_2 \cos \theta_2 + r_1$$

$$0 = r_2 \sin \theta_2 + r_4 \quad (7.121)$$

[Equations 7.121](#) are linear in the unknowns (r_3 and r_4) and can easily be solved. The results are

$$r_3 = r_2 \cos \theta_2 + r_1 = 0.5 \cos(225^\circ) + 1.0 = 0.646 \text{ in}$$

and

$$r_4 = -r_2 \sin \theta_2 = 0.354 \text{ in}$$

To conduct the velocity analysis, rewrite [Equation 7.119](#) in component form and simplify or differentiate [Equation 7.121](#) and simplify. In either case, the results are

$$\begin{aligned} \dot{r}_3 &= -r_2 \dot{\theta}_2 \sin \theta_2 \\ \dot{r}_4 &= -r_2 \dot{\theta}_2 \cos \theta_2 \end{aligned} \quad (7.122)$$

Substituting in the known values

$$\dot{r}_3 = -r_2 \dot{\theta}_2 \sin \theta_2 = -0.5(-10)\sin(225^\circ) = -3.535 \text{ in/sec}$$

$$\dot{r}_4 = -r_2 \dot{\theta}_2 \cos \theta_2 = -0.5(-10)\cos(225^\circ) = -3.535 \text{ in/sec}$$

The location of both B_2 and B_3 is given by $r_3 = r_1 + r_2$ in [Figure 7.36](#). Both points momentarily have the same coordinates. However, the velocities of the corresponding points are different. To determine the velocities, we must carefully interpret the vectors. The velocity of all points on the follower is the same. Therefore, the velocity of B_3 is given by \dot{r}_3 if r_3 remains horizontal. The velocity of B_2 is given by the derivative of a vector fixed to link 2 and directed from point A^* to B . This is \dot{r}_2 if we assume r_5 is fixed to link 2. Then the velocity of B_2 is given by $\dot{r}_2 = \dot{r}_1 + \dot{r}_2$ if we assume that both r_1 and r_2 are fixed to (i.e., rotate with) link 2. Then the components of the velocity of B_2 will be given by

$$v_{B_2} = \dot{r}_2 = \dot{r}_1 + \dot{r}_2 = (-r_1 \dot{\theta}_2 \sin \theta_1 - r_2 \dot{\theta}_2 \sin \theta_2) \hat{i} + (r_1 \dot{\theta}_2 \cos \theta_1 + r_2 \dot{\theta}_2 \cos \theta_2) \hat{j}$$

The relative velocity is given by

$$v_{B_3/B_2} = v_{B_3} - v_{B_2} = (\dot{r}_3 + r_1 \dot{\theta}_2 \sin \theta_1 + r_2 \dot{\theta}_2 \sin \theta_2) \hat{i} - (r_1 \dot{\theta}_2 \cos \theta_1 + r_2 \dot{\theta}_2 \cos \theta_2) \hat{j}$$

Substituting values for the variables

$$v_{B_3/B_2} = v_{B_3} - v_{B_2} = 0\hat{i} - (1.0(-10)\cos 0^\circ + 0.5(-10)\cos 225^\circ) \hat{j} = 6.404 \hat{j}$$

For the acceleration analysis, differentiate [Equation 7.122](#) and simplify. Then

$$\begin{aligned} \ddot{r}_3 &= -r_2 \ddot{\theta}_2 \sin \theta_2 - r_2 \dot{\theta}_2^2 \cos \theta_2 \\ \ddot{r}_4 &= -r_2 \ddot{\theta}_2 \cos \theta_2 + r_2 \dot{\theta}_2^2 \sin \theta_2 \end{aligned} \quad (7.123)$$

Substituting in the known values

$$\ddot{r}_3 = -r_2 \dot{\theta}_2 \sin \theta_2 + r_2 \dot{\theta}_2^2 \cos \theta_2 = 0 = 0.5(-10)^2 \cos 225^\circ = 35.35 \text{ in/sec}^2$$

$$\ddot{r}_4 = -r_2 \dot{\theta}_2 \cos \theta_2 + r_2 \dot{\theta}_2^2 \sin \theta_2 = 0 + 0.5(-10)^2 \sin 225^\circ = -35.35 \text{ in/sec}^2$$

Finally

$$\begin{aligned}\ddot{r}_{B_2} &= \ddot{r}_3 + \ddot{r}_2 = (-r_1 \dot{\theta}_2 \sin \theta_1 - r_1 \dot{\theta}_2 \cos \theta_2 - r_1 \dot{\theta}_2^2 \cos \theta_1 - r_1 \dot{\theta}_2^2 \cos \theta_2) \\ &\quad + (r_1 \dot{\theta}_2 \cos \theta_1 + r_2 \dot{\theta}_2 \cos \theta_2 - r_1 \dot{\theta}_2^2 \sin \theta_1 - r_2 \dot{\theta}_2^2 \sin \theta_2) \\ &= [0 - 0 - 1(-10)^2 - 0.5(-10)^2 \cos 225^\circ] i + [0 + 0 - 0 - 0.5(-10)^2 \sin 225^\circ] j \\ &= [-100 + 35.35] i + [35.35] j = -64.65 i + 35.35 j \text{ in/sec}^2\end{aligned}$$

and

$$\ddot{\theta}_{B_2/B_3} = \ddot{\theta}_{B_2} = \ddot{\theta}_{B_3} = [35.35 + 64.65] i - 35.35 j = 100i - 35.35j \text{ in/sec}^2$$



Example 7.8

Kinematic Analysis of a Mechanism with a Pin-in-Slot Joint

For the mechanism shown in [Figure 7.37](#), find ω_3 and a_3 if $\theta_2 = 100^\circ$ and $\omega_2 = 50 \text{ rad/s}$ CCW and is constant.

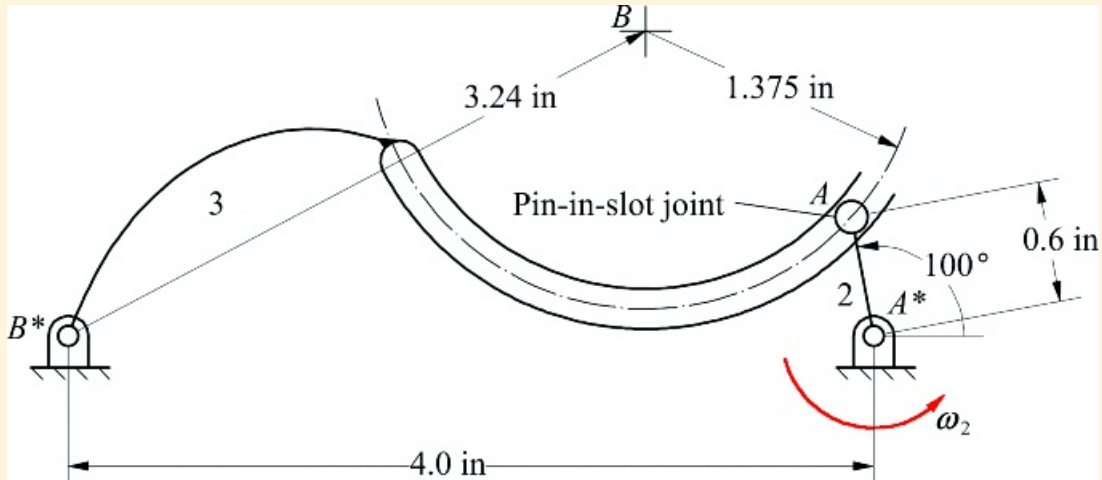


[Figure 7.37](#) Mechanism for Example 7.8.

Solution

To solve the problem, set up four vectors as shown in [Figure 7.38](#). The vector r_1 is from point A^* to B^* , and r_2 is from point A^* to A . The other two vectors involve the center of curvature, C , of the path that point B_2 traces on link 3. Vector r_3 is from point A to B , and r_4 is from point B^* to B . Both points B^* and B are fixed to link 3; therefore, r_4 is fixed to link 3. All of the vectors have constant lengths. The unknown angles are θ_3 and θ_4 because θ_1 is fixed and θ_2 is the known input angle. The known and unknown information can be summarized as follows

$$\begin{aligned} r_1 &= 4.0 \text{ in}, \theta_1 = 180^\circ, \dot{\theta}_1 = 0 \text{ rad/s}, \ddot{\theta}_1 = 0 \\ r_2 &= 0.6 \text{ in}, \theta_2 = 100^\circ, \dot{\theta}_2 = 50 \text{ rad/s}, \ddot{\theta}_2 = 0 \text{ rad/s}^2 \\ r_3 &= 1.375 \text{ in}, \theta_3 = ?, \dot{\theta}_3 = ? \text{ rad/s}, \ddot{\theta}_3 = ? \text{ rad/s}^2 \\ r_4 &= 3.24 \text{ in}, \theta_4 = ?, \dot{\theta}_4 = ? \text{ rad/s}, \ddot{\theta}_4 = ? \text{ rad/s}^2 \end{aligned}$$

Based on [Figure 7.38](#), the vector closure equation for this mechanism is

$$r_2 - r_3 = r_1 + r_4 \quad (7.124)$$

This equation is exactly the same as that for a four-bar linkage ([Equation 7.24](#)). Therefore, the equations developed for a four-bar linkage and summarized in [Table 7.1](#) can be applied directly to this example. The results are

$$\begin{aligned} \theta_3 &= 138.31^\circ, \dot{\theta}_3 = -22.21 \text{ rad/s}, \ddot{\theta}_3 = 73.77 \text{ rad/s}^2 \\ \theta_4 &= 27.69^\circ, \dot{\theta}_4 = 6.133 \text{ rad/s}, \ddot{\theta}_4 = -625.98 \text{ rad/s}^2 \end{aligned}$$

In the mechanism, vector r_4 is fixed to link 3. Therefore, $\omega_3 = 6.133 \text{ rad/s}$ (CCW) and $a_3 = -625.98 \text{ rad/s}^2$ (CW).

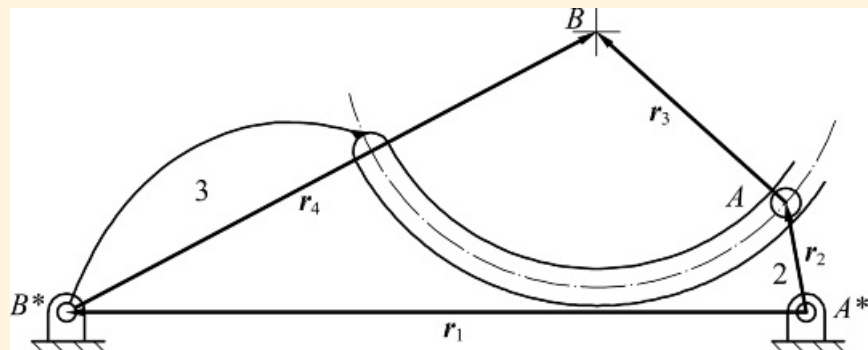


Figure 7.38 Vector loop for Example 7.8.



Example 7.9

Kinematic Analysis of Mechanism with Rolling Contact

In the mechanism shown in [Figure 7.39](#), link 2 is turning with a constant angular velocity of 200 rpm CCW. Determine the angular velocity and acceleration of link 4.

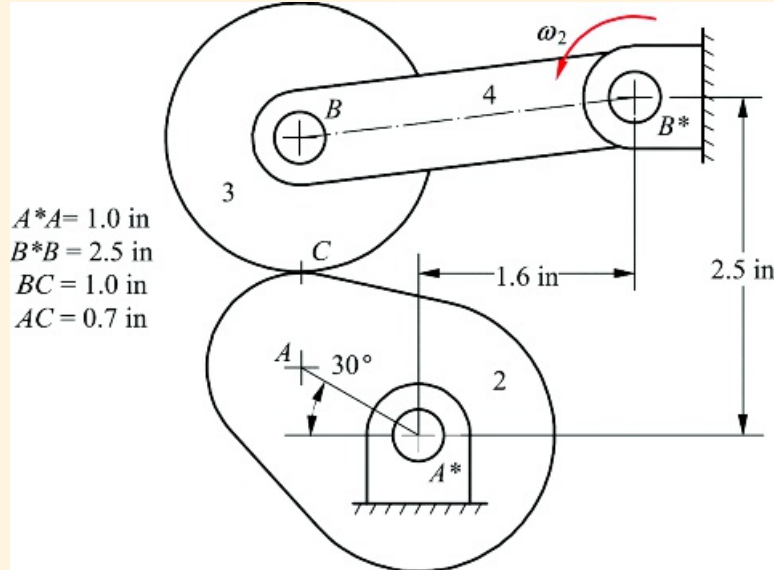


[Figure 7.39](#) Mechanism for Example 7.9.

Solution

This mechanism involves rolling contact at point *C*. It is relatively straightforward to determine the angular quantities associated with link 4 if we locate the vectors for the closure equations using the centers of curvature of links 2 and 3 corresponding to the contact location *C*. This approach will not yield any angular information for link 3, however. In fact, the velocity and acceleration of link 4 are the same whether there is rolling or slipping at *C*.

The vector closure diagram is given in [Figure 7.40](#). The vector r_1 is from point A^* to B^* , and r_2 is from point A^* to A . The other two vectors involve the center of curvature, B , of the path that point A_2 traces on link 3. Vector r_3 is from point A to B , the centers of curvature corresponding to C_2 and C_3 , respectively, and r_4 is from point B^* to B . Note that the points B^* and B of interest are those fixed to link 4. Therefore, r_4 can be treated as a vector fixed to link 4.

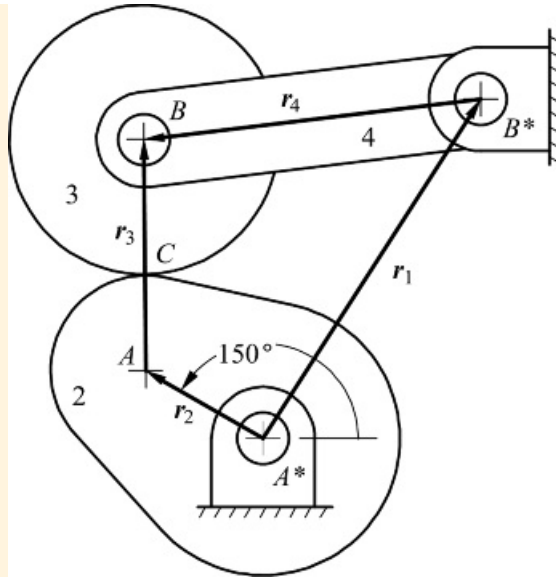


Figure 7.40 Vector loop for Example 7.9.

All of the vectors have constant lengths. The unknown angles are θ_3 and θ_4 because θ_1 is fixed and θ_2 is the known input angle. The angle θ_1 can be computed from

$$\theta_1 = \tan^{-1} \left[\frac{2.5}{1.0} \right] = 57.38^\circ$$

The known and unknown information can be summarized as follows

$$\begin{aligned} r_1 &= \sqrt{2.5^2 + 1.0^2} = 2.686 \text{ in}, \dot{\theta}_1 = 57.38^\circ, \ddot{\theta}_1 = 0 \text{ rad/s}, \ddot{\theta}_1 = 0 \\ r_2 &= 1.0 \text{ in}, \theta_2 = 150^\circ, \dot{\theta}_2 = 200 \left(\frac{2\pi}{60} \right) = 20.94 \text{ rad/s}, \ddot{\theta}_2 = 0 \text{ rad/s}^2 \\ r_3 &= (0.7 + 1.0) = 1.7 \text{ in}, \theta_3 = ?, \dot{\theta}_3 = ? \text{ rad/s}, \ddot{\theta}_3 = ? \text{ rad/s}^2 \\ r_4 &= 2.5 \text{ in}, \theta_4 = ?, \dot{\theta}_4 = ? \text{ rad/s}, \ddot{\theta}_4 = ? \text{ rad/s}^2 \end{aligned}$$

Based on [Figure 7.40](#), the vector closure equation for this mechanism is

$$r_2 - r_3 = r_1 + r_4$$

This equation is again exactly the same as for a four-bar linkage ([Equation 7.24](#)). Therefore, the equations developed for a four-bar linkage and summarized in [Table 7.1](#) can again be applied directly to this example. The results are

$$\begin{aligned} \theta_3 &= 90.54^\circ, \dot{\theta}_3 = -7.44 \text{ rad/s}, \ddot{\theta}_3 = 123.44 \text{ rad/s}^2 \\ \theta_4 &= -173.11^\circ, \dot{\theta}_4 = 7.26 \text{ rad/s}, \ddot{\theta}_4 = 133.41 \text{ rad/s}^2 \end{aligned}$$

In the mechanism, vector r_4 is fixed to link 3. Therefore, $\omega_4 = 7.26 \text{ rad/s}$ (CCW) and $\alpha_4 = 625.98 \text{ rad/s}^2$ (CCW).



7.9 Notational Differences: Vectors and Complex Numbers

Several different notations are in widespread use for analytical solution of planar kinematic problems. The two principal notations are based on vectors and complex numbers. It is the purpose of this section to compare these two notations. In principle, they are completely equivalent to one another, with every relationship written in one notation directly translatable to the other. Nevertheless, some relationships are more easily discerned when using one in preference to the other. Broadly speaking, the complex number notation tends to be most compatible with relationships that are most naturally expressed in polar coordinates. This includes most relationships describing the instantaneous motion state of a rigid body. These relationships are usually most compactly expressed in complex notation. Vector notation is, again broadly speaking, most compatible with relationships that are most naturally expressed in Cartesian coordinates. This is usually true whenever there is no single point that dominates the geometry of the system. In the opinion of the authors of this book, this includes the majority of situations to be studied. Also, planar vector notation is fully compatible with the corresponding techniques used for three-dimensional representation. Therefore, if only one notation is to be used, it should be the vector notation. For this reason, this text is based on the use of vector notation. Advanced students of the subject should seek proficiency in both types of notation.

In complex number notation, planar vector quantities are represented by identifying the real and imaginary parts with orthogonal components. Normally, the x component is represented by the real part and the y component by the imaginary part. That is, the complex number $z = x + iy$ represents the vector (x, y) . An important alternative form for z is

$$z = re^{i\theta} = r(\cos \theta + i \sin \theta) \quad (7.125)$$

where r is the length of the vector and θ is its direction relative to the x axis. That is

$$r = \sqrt{x^2 + y^2}$$

and

$$\theta = \tan^{-1}(y/x)$$

It is this form that is effective in expressing polar relationships.

Referring to [Figure 7.41](#), we can write the basic closure equation for the four-bar linkage with the vectors a, b, c , and d interpreted as complex numbers. Then

$$b + c = a + d \quad (7.126)$$

Using the form of [Equation 7.125](#), this can be written

$$be^{i\beta} + ce^{i\gamma} - a - de^{i\delta}$$

Decomposition of this expression into its real and imaginary parts, respectively, gives

$$\begin{aligned} b \cos \theta + c \cos \psi &= a + d \cos \phi \\ b \sin \theta + c \sin \psi &= d \sin \phi \end{aligned}$$

which are identical to the component equations developed using the vector formulation. The development of a position solution and of the velocity and acceleration solutions of this chapter is then identical to that given earlier.

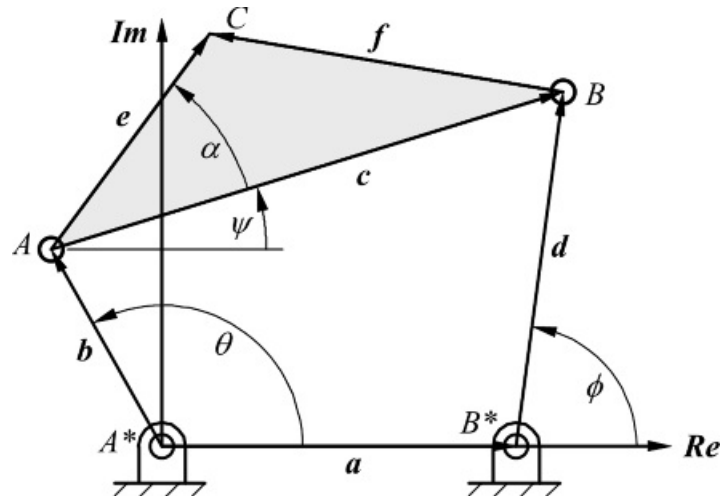


Figure 7.41 The real and imaginary axes used in setting up a complex number solution of the four-bar loop.

Alternatively, the elimination of one of the variables may be pursued in the complex variable form. [Equation 7.126](#) may be written in the form

$$b + c - a = d \quad (7.127)$$

Now, the conjugates of b , c , and d are, respectively,

$$\tilde{b} = b e^{-i\theta}, \tilde{c} = c e^{-i\theta}, \tilde{d} = d e^{-i\phi}$$

Also, the conjugate of a is \bar{a} since a is a real number. The conjugate of [Equation 7.127](#)

$$\tilde{b} + \tilde{c} - \bar{a} = \tilde{d}$$

is also true since the process of forming the conjugate simply changes the signs on all imaginary parts.

Multiplication of each side of [Equation 7.126](#) by its conjugate gives

$$(b + c - a)(\tilde{b} + \tilde{c} - \bar{a}) = d \tilde{d}$$

Now, referring to [Equation 7.125](#)

$$ac = r e^{i\theta}, c \bar{a} = r e^{-i\theta}$$

Also

$$\ddot{z} - \ddot{\bar{z}} = re^{i\theta} + re^{-i\theta} = r(\cos \theta + i \sin \theta) + r(\cos \theta - i \sin \theta) = 2r \cos \theta$$

Hence

$$\dot{b}\dot{\phi} = b^2 - c\dot{\phi} = c^2 \quad \dot{d}\dot{\psi} = d^2$$

Thus, expansion of the foregoing expression gives

$$b\ddot{\phi} + c\ddot{\phi} - c\ddot{\phi} + b\ddot{\phi} + \ddot{b}c = b\ddot{\phi} - \ddot{b}c - c\ddot{\phi} - \ddot{c}b = \ddot{a}\ddot{\phi}$$

By using the above properties and collecting the terms, the above equation can be simplified to the following form $b^2 + c^2 + a^2 + 2bc \cos(\phi - \psi) - 2ab \cos \theta - 2ac \cos \psi = \ddot{a}^2$, which does not have ϕ explicitly in the equation.

[Equation 7.126](#) lends itself to development of velocity and acceleration expressions. Differentiation with respect to time gives

$$b\dot{\phi}e^{i\theta} + c\dot{\phi}e^{i\psi} = id\dot{\phi}e^{i\phi}$$

or, removing the common factor i

$$b\dot{\phi}e^{i\theta} + c\dot{\phi}e^{i\psi} = d\dot{\phi}e^{i\phi} \quad (7.128)$$

Separation into the real and imaginary parts gives, respectively,

$$b\dot{\phi} \cos \theta + c\dot{\phi} \cos \psi = d\dot{\phi} \cos \phi$$

and

$$b\dot{\phi} \sin \theta + c\dot{\phi} \sin \psi = d\dot{\phi} \sin \phi$$

which may be recognized as the same form as those given in [Table 7.1](#).

Differentiation of [Equation 7.128](#) with respect to time gives

$$b\ddot{\phi}e^{i\theta} + ib\dot{\phi}^2e^{i\theta} + c\ddot{\phi}e^{i\psi} + ic\dot{\phi}^2e^{i\psi} = d\ddot{\phi}e^{i\phi} + id\dot{\phi}^2e^{i\phi}$$

Expansion of the $e^{i\theta}$ terms gives

$$\begin{aligned} & b\ddot{\phi}(\cos \theta + i \sin \theta) + ib\dot{\phi}^2(i \cos \theta - \sin \theta) + c\ddot{\phi}(\cos \psi + i \sin \psi) + ic\dot{\phi}^2(i \cos \psi - \sin \psi) \\ &= d\ddot{\phi}(\cos \phi + i \sin \phi) + id\dot{\phi}^2(i \cos \phi - \sin \phi) \end{aligned}$$

Hence, separation into the real and imaginary parts gives

$$b\ddot{\theta} \cos \phi - b\dot{\theta}^2 \sin \phi + c\ddot{\psi} \cos \varphi - c\dot{\psi}^2 \sin \varphi = d\ddot{\phi} \cos \phi - d\dot{\phi}^2 \sin \phi$$

and

$$b\ddot{\theta} \sin \phi + b\dot{\theta}^2 \cos \phi + c\ddot{\psi} \sin \varphi + c\dot{\psi}^2 \cos \varphi = d\ddot{\phi} \sin \phi + d\dot{\phi}^2 \cos \phi$$

which can be recognized as the same form as those given in [Table 7.1](#).

The foregoing illustrates the equivalence of the vector and complex number representations for simple planar mechanisms.

Problems

7.1 For the mechanism shown in [Figure P7.1](#), do the following:

- Write the vector equation for the linkage shown.
- Write the x and y displacement equations.
- Find the velocity component equations.
- Find the acceleration component equations.

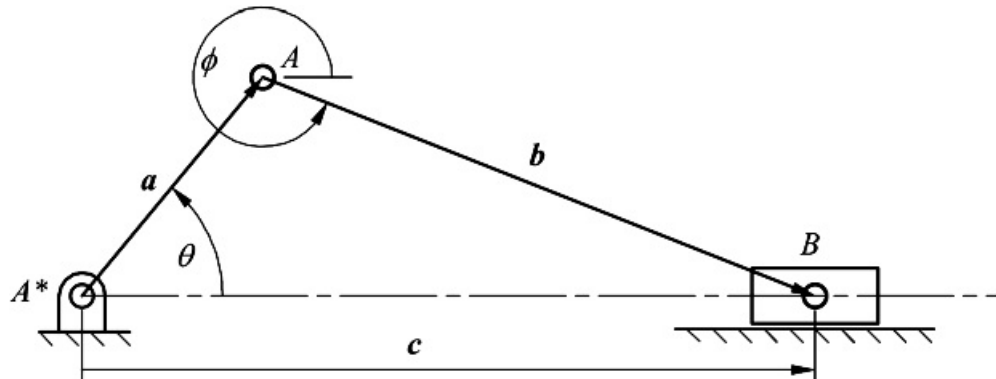


[Figure P7.1](#) Linkage for Problem 7.1.

7.2 In the mechanism in Problem 7.1, determine $\dot{\phi}$ analytically for the following values

$$a = 1 \text{ cm}, b = 4 \text{ cm}, \theta = 60^\circ, \dot{\theta} = 10^\circ \text{ rad/s}$$

7.3 In the mechanism shown in [Figure P7.3](#), $s = -10 \text{ in/s}$ and $\ddot{s} = 0$ for the position corresponding to $\phi = 60^\circ$. Find $\dot{\phi}$ and $\ddot{\phi}$ for that position using the loop equation approach.

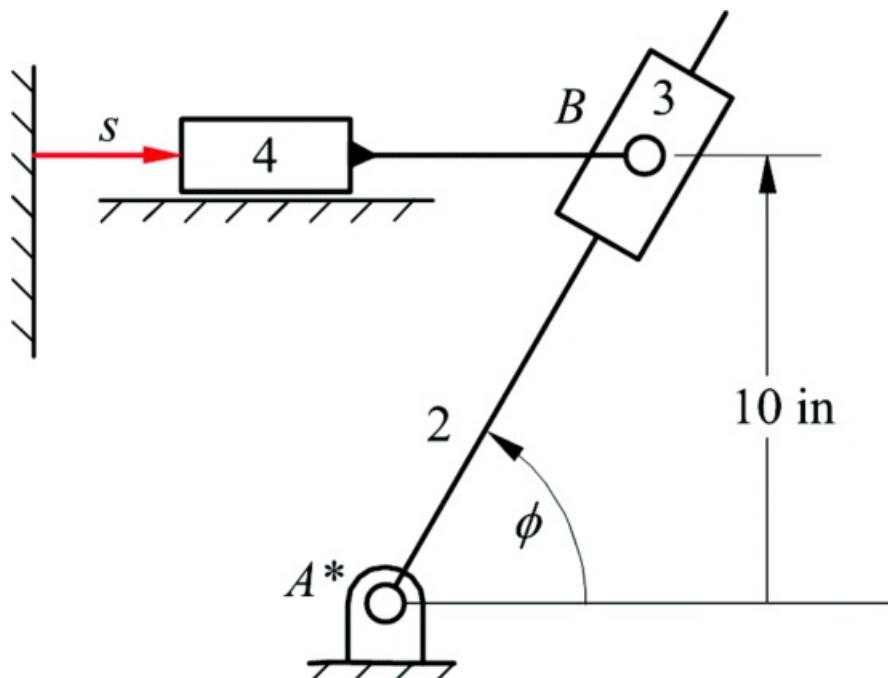


[Figure P7.3](#) Linkage for Problem 7.3.

7.4 In the mechanism in [Figure P7.3](#), assume that $\dot{\phi}$ is 10 rad/s CCW. Use the loop equation approach to

determine the velocity of point B_4 for the position defined by $\phi = 60^\circ$.

7.5 In the mechanism in [Figure P7.5](#), point A is moving to the right with a velocity of 10 cm/s. Use the loop equation approach to determine the angular velocity of link 3. Link 3 is 10 cm long, and ϕ is 120° in the position shown.

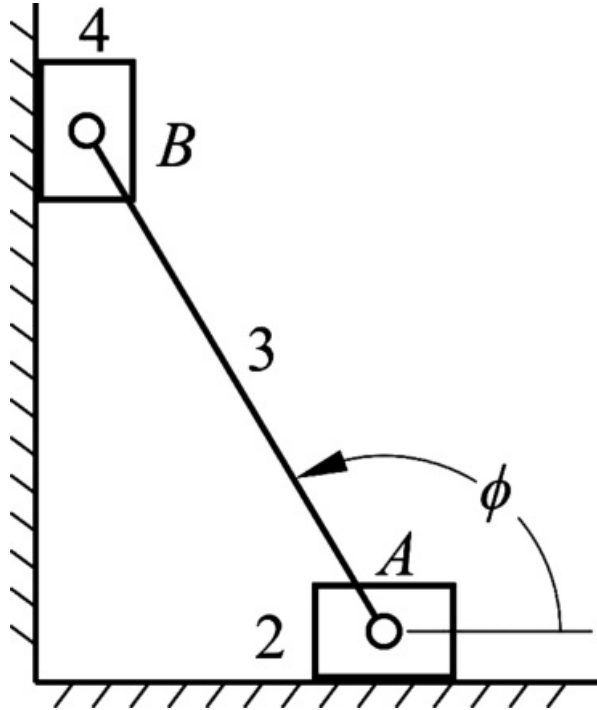


[Figure P7.5](#) Linkage for Problem 7.5.

7.6 Solve Problem 7.5 if $\phi = 150^\circ$.

7.7 The mechanism shown in [Figure P7.7](#) is a marine steering gear called Raphson's slide. A^*A is the tiller, and BC is the actuating rod. If the velocity of rod BC is a constant 10 inches per minute to the right, and $\theta = 300^\circ$, use the loop-equation approach to determine the angular acceleration of the tiller.

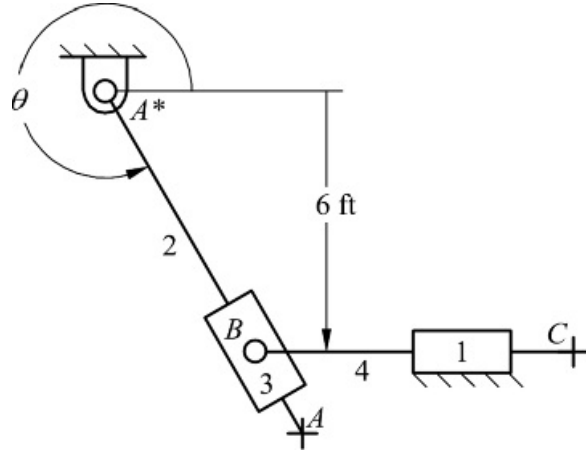


[Figure P7.7](#) Linkage for Problem 7.7.

7.8 Use loop equations to determine the velocity and acceleration of point B on link 2 in [Figure P7.8](#) when $\theta = 30^\circ$, $\dot{\theta} = 1 \text{ rad/s}$ CCW, and $\ddot{\theta} = 0$. Make point A the origin of your reference coordinate system.

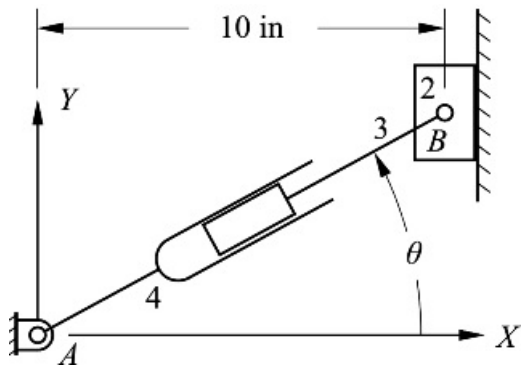


[Figure P7.8](#) Linkage for Problem 7.8.

7.9 In the mechanism shown in [Figure P7.9](#), $\theta = 30^\circ$, $\dot{\theta} = 1 \text{ rad/s CCW}$, and $\ddot{\theta} = 0$. Use loop equations to determine the velocity and acceleration of point B on link 4.

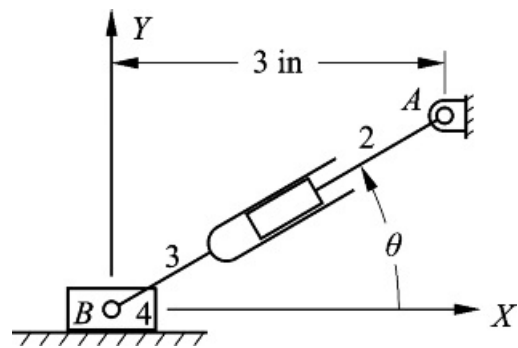


[Figure P7.9](#) Linkage for Problem 7.9.

7.10 In the mechanism for Problem 7.9, assume that v_{A*} is a constant 10 in/s to the left and θ is 45° . Use loop equations to determine the angular velocity and acceleration of link 3.

7.11 For the mechanism in the position shown in [Figure P7.11](#), link 2 is the driver and rotates with a constant angular velocity of 100 rad/s CCW. Write vector loop equations for position, velocity, and acceleration, and solve for the velocity and acceleration of point B on link 4.

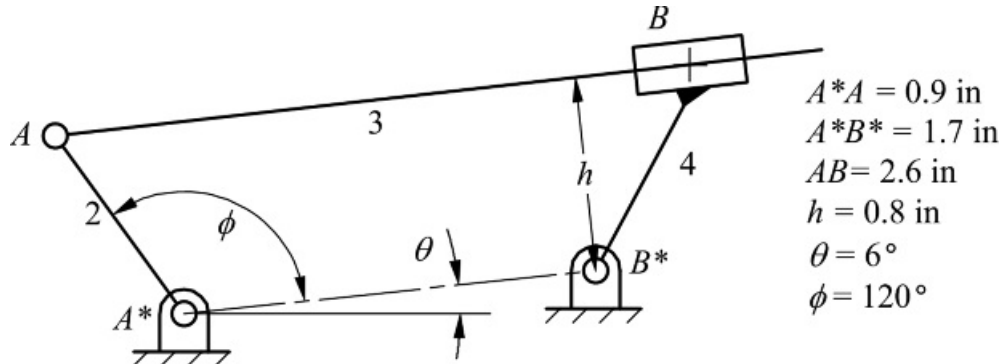


[Figure P7.11](#) Linkage for Problem 7.11.

7.12 For the mechanism in the position shown in [Figure P7.12](#), link 2 is the driver and rotates with a constant angular velocity of 50 rad/s CCW. Write vector loop equations for position, velocity, and acceleration and solve for the velocity and acceleration of point B on link 3.

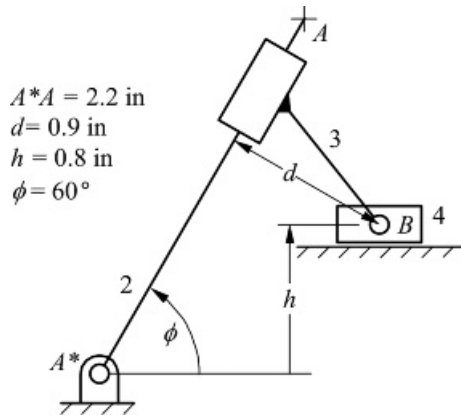


[Figure P7.12](#) Linkage for Problem 7.12.

7.13 In [Figure P7.13](#), link 3 slides on link 2, and link 4 is pinned to link 3 and slides on the frame. If $\omega_2 = 10$ rad/s CCW (constant), use loop equations to find the acceleration of link 4 for the position defined by $\phi = 90^\circ$.

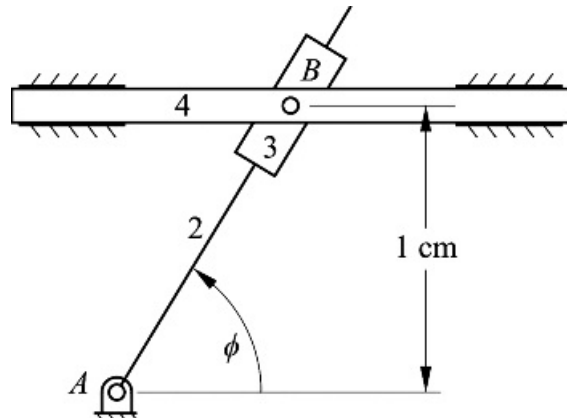


[Figure P7.13](#) Linkage for Problem 7.13.

7.14 For the mechanism in the position shown in [Figure P7.14](#), the cam (link 2) rotates with an angular velocity of 200 rad/s. Write the vector loop equations for position, velocity, and acceleration and determine the angular velocity and acceleration of the follower (link 3). Use $\phi = 60^\circ$ and neglect the follower thickness (i.e., assume that it is zero).

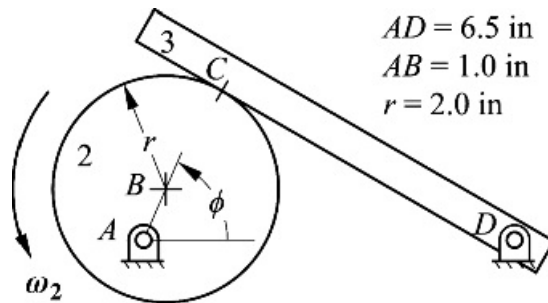


[Figure P7.14](#) Cam linkage for Problem 7.14.

7.15 In the mechanism shown in [Figure P7.15](#), link 3 is perpendicular to link 2. Write the vector loop equations for position and velocity. If the angular velocity of link 2 is 100 rad/s CCW, use the vector loop equations to solve for the velocity of point B_4 for the position corresponding to $\phi = 60^\circ$.

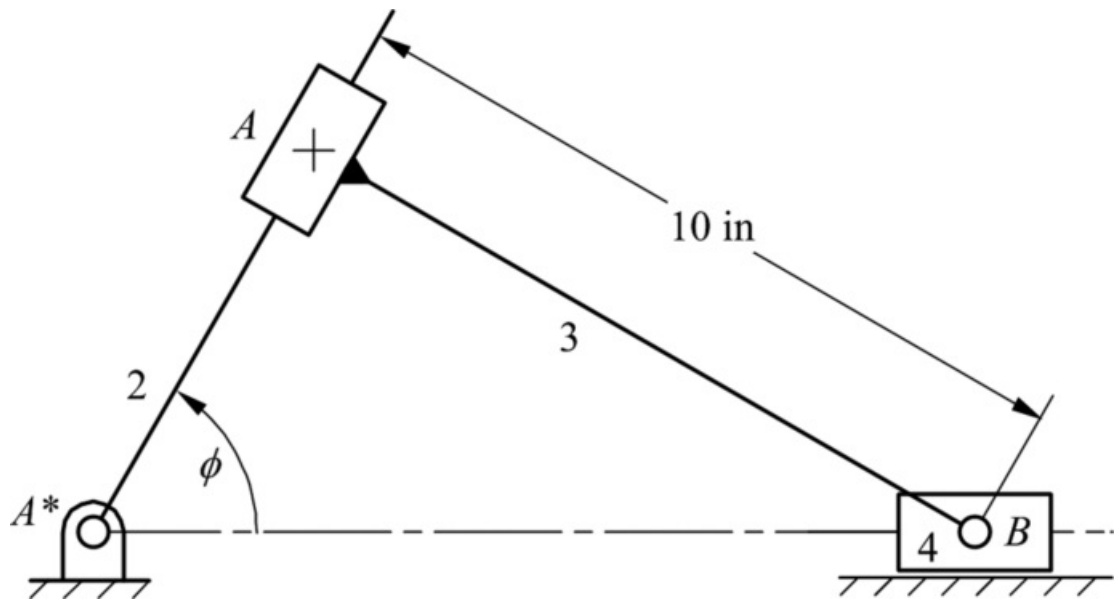


[Figure P7.15](#) Linkage for Problem 7.15.

7.16 In the simple, two-link mechanism in [Figure P7.16](#), v_{B_2} is 10 in/s to the right. Use the loop equation approach to determine v_{A_2} and ω_2 .

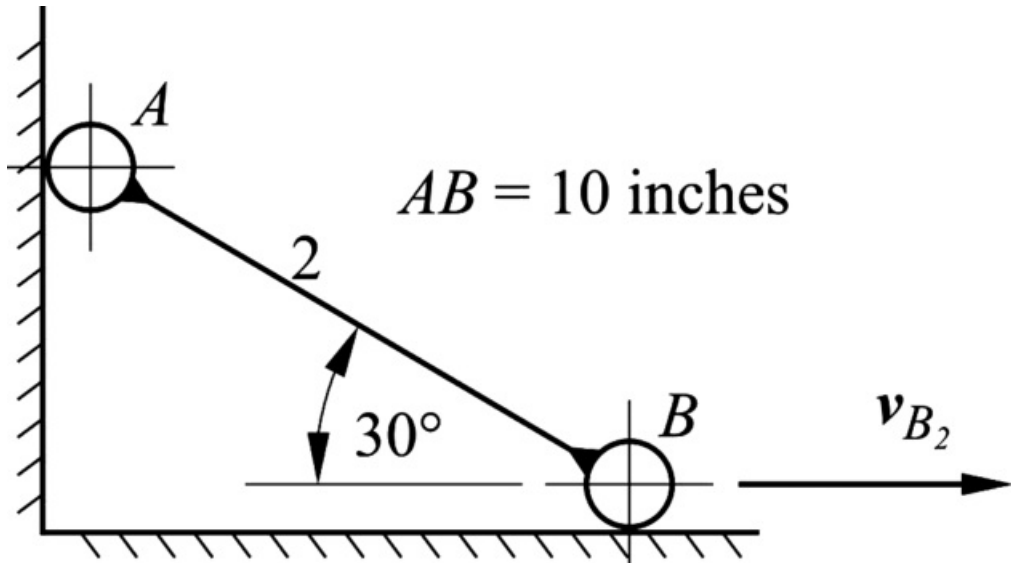


[Figure P7.16](#) Linkage for Problem 7.16.

7.17 In [Figure P7.17](#), the angular velocity of link 2 is 100 rad/s CCW and the dimensions of various links are given. Use loop equations to find the position and velocity of point C on link 3 when θ_2 is 90°.

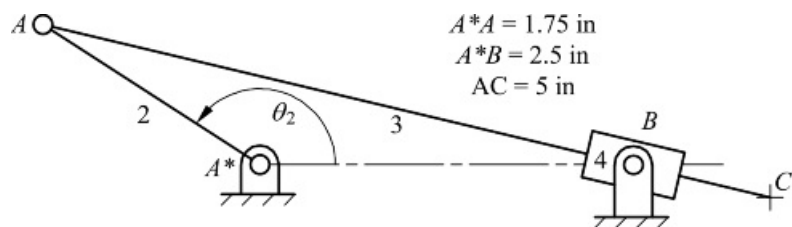


[Figure P7.17](#) Linkage for Problem 7.17.

7.18 In the scotch-yoke mechanism shown in [Figure P7.18](#), $\omega_2 = 10 \text{ rad/s}$, $a_2 = 100 \text{ rad/s}^2$, and $\theta_2 = 60^\circ$. Also, length $A*A = 20 \text{ in}$. Determine v_{A_4} and a_{A_4} using loop equations.

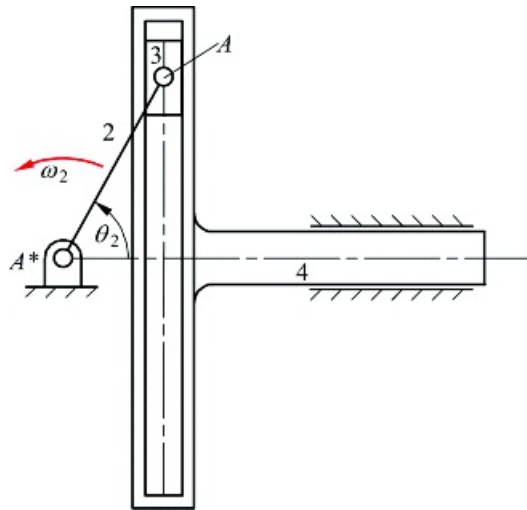


[Figure P7.18](#) Scotch-yoke linkage for Problem 7.18.

7.19 Use loop equations to determine the velocity and acceleration of point A on link 4. The angular velocity of link 2 is constant at 10 rad/s counterclockwise. Assume that $A^*B^* = 10$ in, $\theta_2 = 60^\circ$, and $\theta_3 = 90^\circ$.

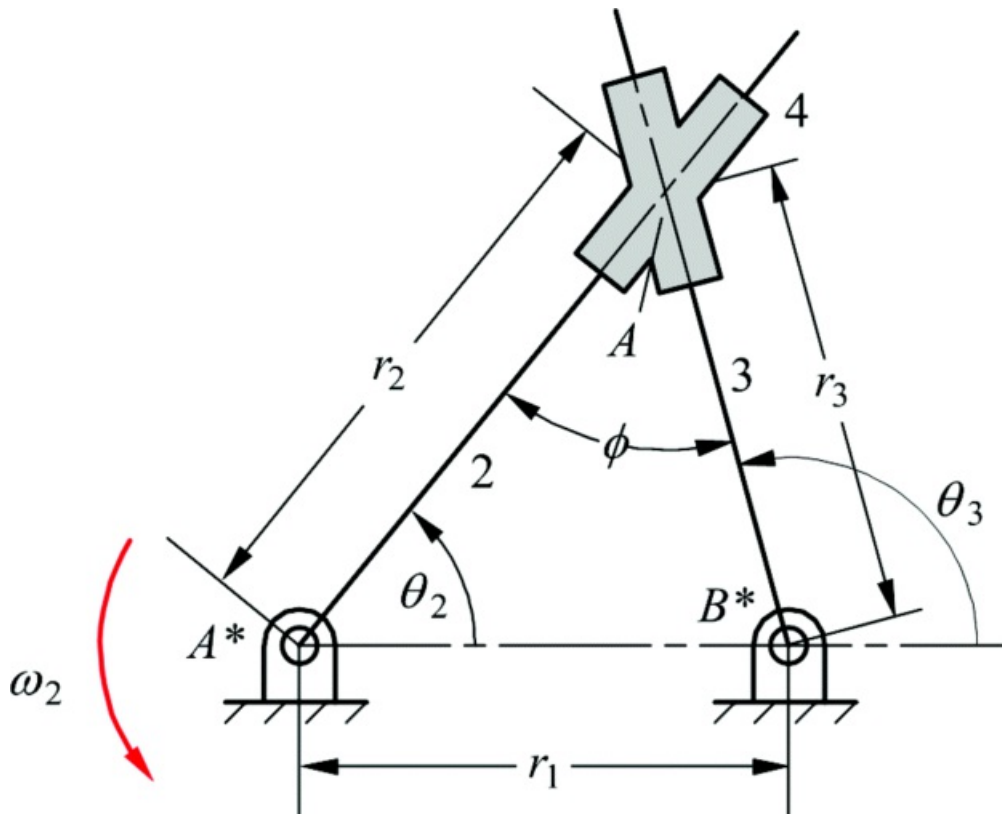


[Figure P7.19](#) Linkage for Problem 7.19.

7.20 The oscillating fan shown in [Figure P7.20](#) is to be analyzed as a double rocker. The fan housing is link 2, the motor shaft is connected to link 3, and link 4 is connected from the coupler to the frame. The actual input of the mechanism is the coupler, and ω_3 is a constant 956 (rad/s) in the counterclockwise direction. Compute the angular velocity and angular acceleration of link 2 if $\theta = 120^\circ$, $A^*B^* = 0.75$ in, $A^*A = B^*B = 3.0$ in, $AB = 0.50$ in.

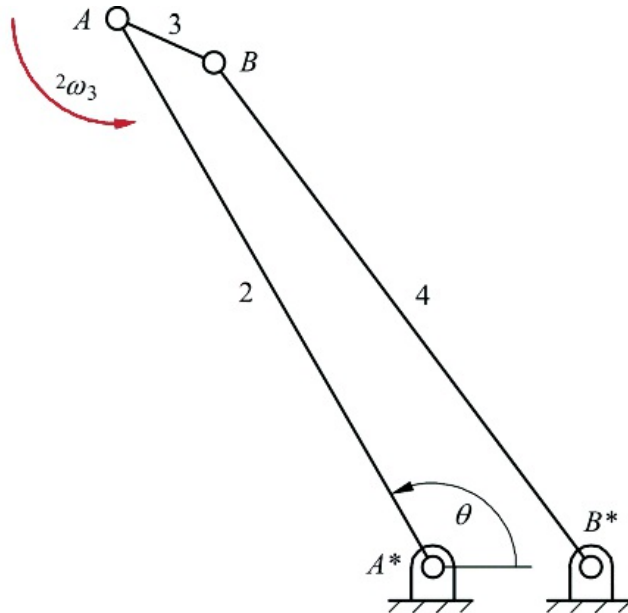
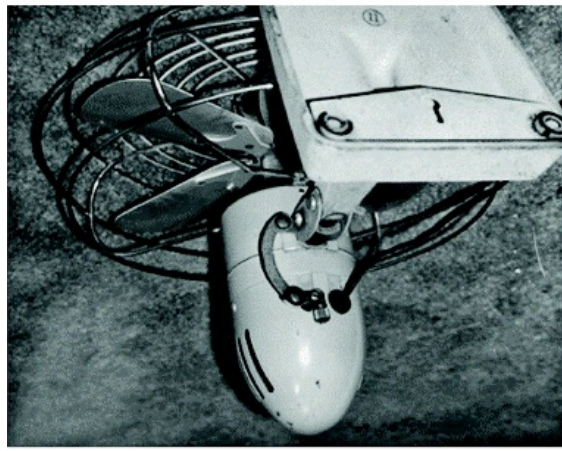


[Figure P7.20](#) Fan linkage for Problem 7.20.

7.21 The rear motorcycle suspension can be analyzed as an inverted slider-crank mechanism. The frame of the motorcycle is link 1 and the tire assembly is attached to link 2 at point C. The shock absorber is made up of links 3 and 4. As the bicycle goes over a bump in the position shown, the angular velocity of link 2 relative to the frame, ω_2 , is 5 rad/s CW, and the angular acceleration, α_2 , is 45 rad/s² CW. Compute the angular velocity and angular acceleration of link 3 for the position defined by $\theta = 187^\circ$.

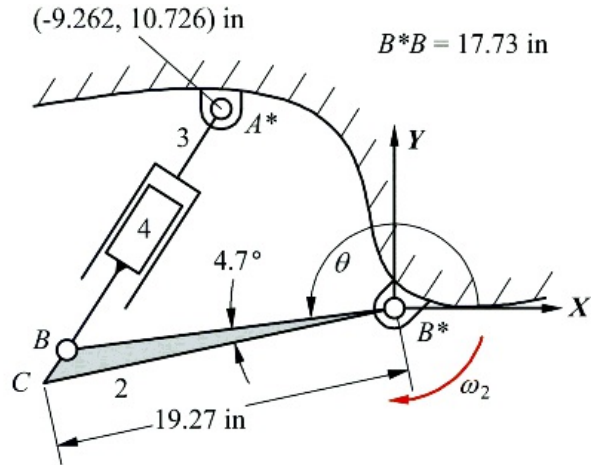


[Figure P7.21](#) Motorcycle linkage for Problem 7.21.

7.22 The door-closing linkage shown in [Figure P7.22](#) is to be analyzed as an inverted slider-crank linkage. Link 2 is the door, and links 3 and 4 are the two links of the door closer. Assume that the angular velocity of the door (link 2) is a constant 3.71 radians per second CW. Compute the angular velocity and angular acceleration of link 4 if the coordinates of B^* are (4.0, -3.5) in.

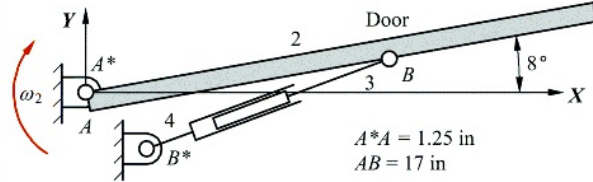


[Figure P7.22](#) Door closer linkage for Problem 7.22.

7.23 The general action of a person who is doing pushups can be modeled as a four-bar linkage as shown in [Figure P7.23](#). The floor is the base link and link 4 is the back and legs. Link 2 is the forearm and link 3 is the upper arm. For the purposes of analysis, the motion that is controlled is the motion of link 3 relative to link 2 (elbow joint). Assume that $2\omega_3$ is a constant 3.0 rad/s CCW. Compute the angular velocity and angular acceleration of link 4 if link 2 is oriented at 45° to the horizontal.

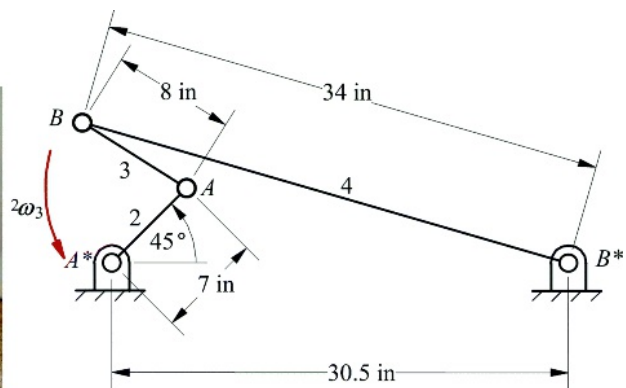
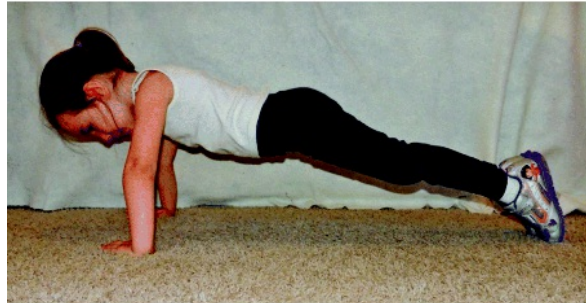


[Figure P7.23](#) Linkage representation of push-ups for Problem 7.23.

7.24 A carousel mechanism can be modeled as an inverted slider-crank mechanism as shown in [Figure P7.24](#). Point B is the location of the saddle on the horse. Assume that the angular velocity of the driver (link 2) is a constant 2 rad/s counterclockwise. Compute the velocity and acceleration of B_3 in the position shown if $A^*A = 8.0$ in, $A^*B^* = 101$ in, and $AB = 54$ in.

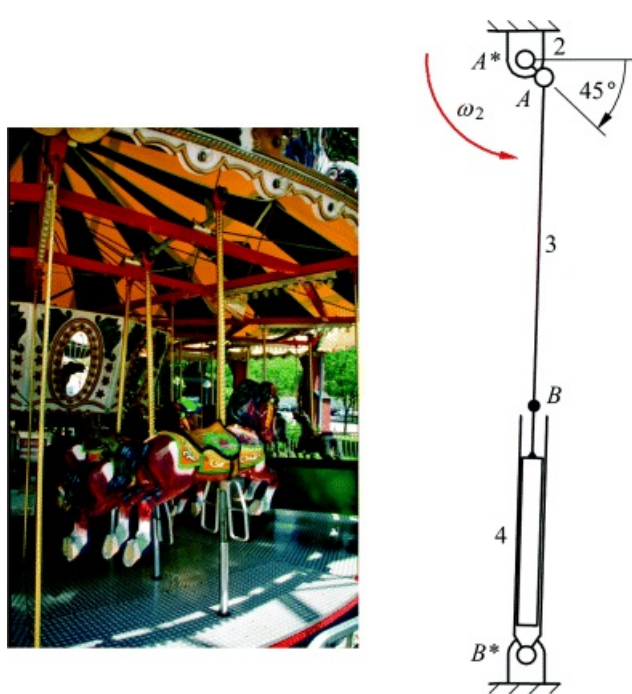


[Figure P7.24](#) Carousel linkage for Problem 7.24.

7.25 The shock absorber mechanism on a mountain bicycle is often based on a four-bar linkage as shown in [Figure P7.25](#). When a bump is hit, a resisting torque is applied to link 2 through a shock absorber. The frame of the bike is link 1, the wheel assembly comprises link 3, and the connecting linkage comprises links 2 and 4. As the bicycle goes over a bump in the position shown, the angular velocity, ω_2 , of link 2 relative to the frame is 205 rad/s CW, and the angular acceleration, α_2 , is 60 rad/s² CW. Compute the angular velocity and angular acceleration of link 3 for the position shown in [Figure P7.25](#).

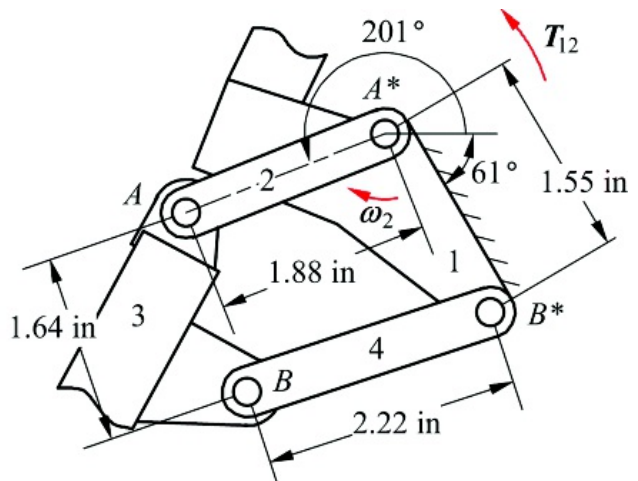


[Figure P7.25](#) Shock absorber linkage for Problem 7.25.

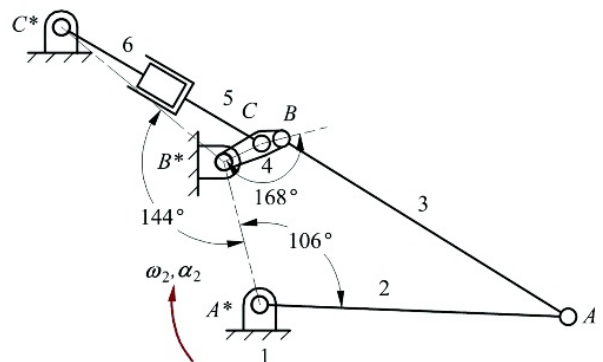
7.26 The rear suspension of many mountain bikes uses a Watt's type six-bar linkage where the main support unit containing the rear wheel is a four-bar linkage as shown in [Figure P7.26](#). The frame of the bike is link 1, the wheel assembly is link 3, and the connecting links are links 2 and 4. As the bicycle goes over a bump in the position shown, the angular velocity, ω_2 , of link 2 relative to the frame is 100 rad/s CW, and the angular acceleration, α_2 , is 100 rad/s² CW. Compute the angular velocity and angular acceleration of link 4 for the position shown.

$$AB = 15.29 \text{ in} \quad AA^* = 14.00 \text{ in} \quad BC = 0.91 \text{ in} \quad B^*C = 1.92 \text{ in}$$

$$B^*C^* = 9.56 \text{ in} \quad A^*B^* = 6.63 \text{ in} \quad BB^* = 2.82 \text{ in}$$



Figure P7.26 Bike linkage for Problem 7.26.



8

SPECIAL MECHANISMS

Prerequisite Knowledge Needed for Chapter 8

A knowledge of coupler curves from [Chapter 3](#) and velocity and acceleration analyses from [Chapter 5](#).



8.1 Special Planar Mechanisms

8.1.1 Introduction

Although much of this book is concerned with the design of planar mechanisms, there are some that for one reason or another require special attention.

The classes of mechanisms discussed here meet a variety of common needs in mechanical engineering practice. For this reason, they are important, but none requires such extensive treatment as to justify a chapter to themselves, as was the case with cam or gear mechanisms.

Generation of a straight line or circle by a simple linkage mechanism is a recurring theme. Slides or roller ways are not always acceptable for implementation in real mechanism designs, and there continues to be a place for simple, four-bar linkages that can approximate a straight-line or circular coupler point path with a high degree of accuracy. Likewise, linkages that can reproduce a path traced by one point at another tracing point with a change in scale find many uses ranging from machine tools for milling nonrotationally symmetric surfaces to remote actuation of robotic mechanisms.

Another recurring theme in mechanical engineering practice is the transfer of torque and motion between shafts that are not coaxial, particularly when the relative alignment of the shafts must change. Very common examples occur in the drive shafts of automobiles that must accommodate movements resulting in changes of shaft alignment due to suspension movements and/or steering movements. There are also numerous examples of this situation in construction and manufacturing machinery.

Automotive steering and suspension mechanisms are among the most common linkage mechanisms in practical use. They are usually designed as decoupled, fundamentally planar linkages. However, misalignments are deliberately introduced to produce desirable effects such as a tendency for the steering to center itself. Thus, they become spatial linkages with complex interactions.

Yet another recurring need in practical linkage design is for indexing: intermittent, timed advancement of a drive in a constant direction. This technology had very numerous and visible applications in the days of mechanical punched-card readers and similar business machines. The problem is of continuing practical importance with many applications in manufacturing and packaging machinery.

8.1.2 Straight-Line and Circle Mechanisms

One of the oldest and most common applications of coupler curves is to generate a straight line. Slides or roller ways are not always acceptable for implementation in real mechanism designs, and there continues to be a place for simple, four-bar linkages that can approximate a straight-line coupler point path with a high degree of accuracy. More complex mechanisms with more than four links have been developed to generate exact straight lines. A less used but equally interesting use of coupler points is to trace an approximate or perfect circle. This is used in machinery where it is necessary to duplicate the motion of a crank but where it is not possible to mount the bearings for a rotating shaft. Straight-line and circle mechanisms are especially useful when designing dwell mechanisms since these depend on a circular-arc or straight-line section of a coupler curve. Therefore, if the special mechanisms meet the requirements for space, function, and transmission angle, the classical straight-line and circle mechanisms can be used to design dwell mechanisms that can rival cams for accuracy.

Approximate Straight-Line Mechanisms

Approximate straight-line mechanisms occupy a very special place in the history of kinematics. These have been used in many practical devices from steam engines to modern ship cranes [2] (e.g., [Figure 8.1](#)). The coupler curves of a four-bar linkage are sixth order and cannot generate a straight line exactly; however, for a short distance, coupler curves can approximate a straight line very accurately. Historically, a large number of four-bar linkage configurations have been used to approximate a straight line, and Artobolevsky [1] describes 35 such mechanisms although he attributes all of them to five inventors (Chebyshev, Watt, Roberts, Evans, De Jong). Six of the most common approximate straight-line mechanisms are shown in [Figure 8.2](#). The linkages can be made any size

desired as long as the proportionality among the dimensions is maintained. Three of the linkages in [Figure 8.2](#) are discussed in the following.



[Figure 8.1](#) A level-luffing crane. The jib of the crane is configured as the coupler of a four-bar mechanism that generates an approximate horizontal straight line at the axis of the sheave (coupler point) over which the cable passes at the end of the jib.

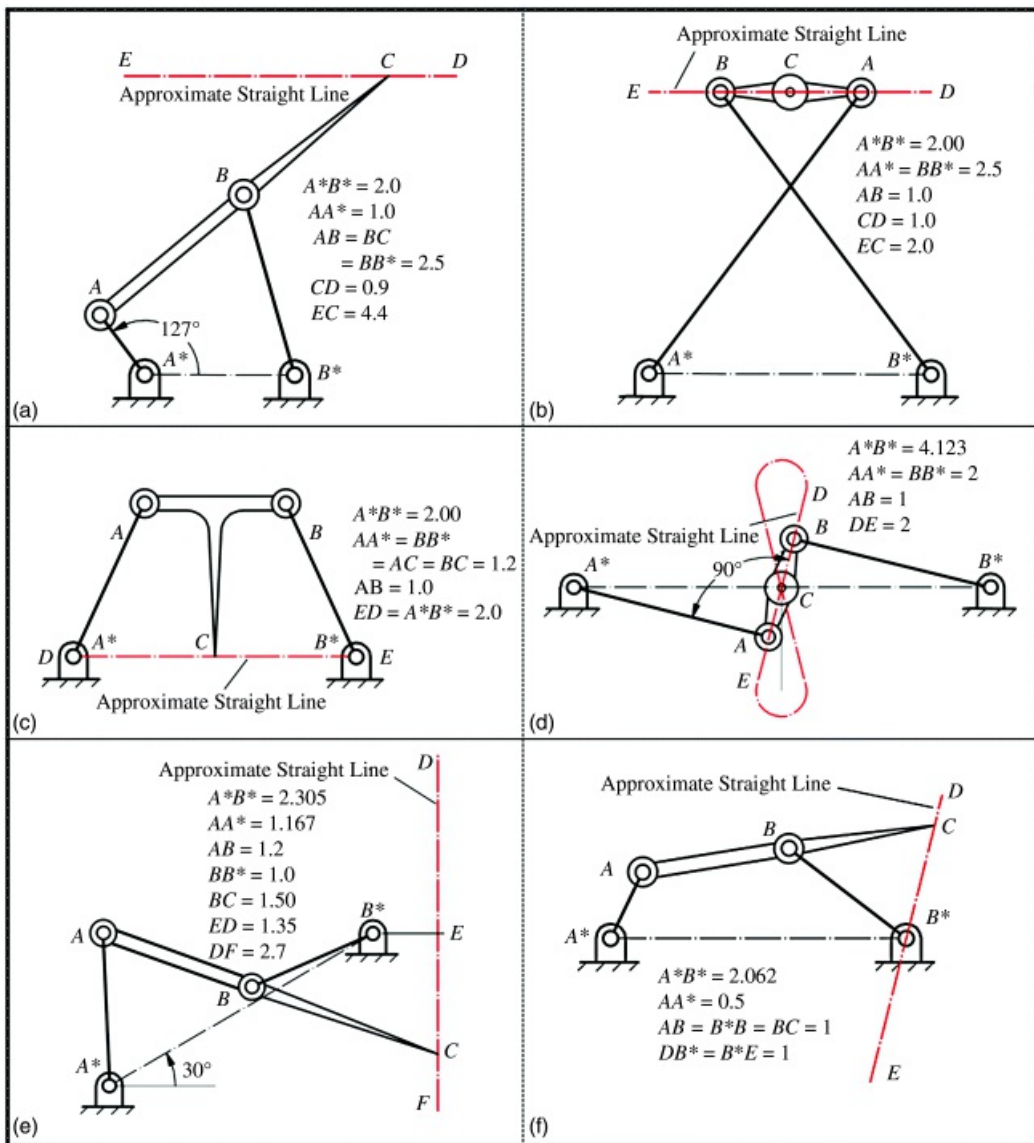


[Figure 8.2](#) Approximate straight-line mechanisms: (a) Hoeken linkage; (b) Chebyshev linkage; (c) Robert's linkage; (d) Watt linkage; (e) Evan's linkage #1; and (f) Evan's linkage #2.

Chebyshev's Straight-Line Mechanism

The Chebyshev approximate straight-line mechanism is also a linkage that is both of historical importance and of continuing practical importance. It is simple, and its advantages are that it provides a very long segment of the path of the coupler midpoint that is approximately linear and that both fixed pivots are on the same side of the linear path. However, the dimensions are somewhat critical. Referring to [Figure 8.2\(b\)](#), the required proportions are $AB = 1$, $AA^* = BB^* = 2.5$, and $A^*B^* = 2$. The tracing point is the midpoint of the coupler. As can be seen, it approximates a straight line for a considerable distance. It might be noted that these proportions require that the linkage be a type I double-rocker. Since it is normally used for linear guidance of the tracing point, it is usually used in a coupler-driven mode.

Robert's Straight-Line Mechanism

Robert's approximate straight-line mechanism is also a symmetrical four-bar linkage as shown in [Figure 8.2\(c\)](#). The coupler point indicated generates an approximate straight line for the motion between the fixed pivots. The proportions in [Figure 8.2\(c\)](#) are $AB = 1$, $AA^* = BB^* = AC = BC = 1.2$, and $AA^* = 2$; however, the dimension for AA^* , BB^* , AC and BC is not critical as long as it is larger than 1. The length of the straight-line region is increased as this dimension is increased. The dimensions shown in [Figure 8.2\(c\)](#) make the mechanism a type II double-

rocker; however, if a value larger than 1.5 is used, the mechanism becomes a type I double-rocker. The Robert's linkage is normally used for linear guidance of the tracing point so that it is normally used in the coupler-driven mode.

Watt's Straight-Line Mechanism

Toward the end of the eighteenth century when James Watt and his contemporaries were developing the practical steam engines that powered the industrial revolution, there was no available means of machining long ways to a high degree of straightness or of achieving low-friction linear motion. This was needed both to guide the crosshead of the piston rod and for the valve gear that opened the valves in coordination with the piston motion. The solution used by Watt and his contemporaries [[Figure 8.2\(d\)](#)] was to devise a four-bar mechanism with a relatively long coupler-point trajectory that approximated a straight line to an acceptable degree of accuracy.

Watt's straight-line mechanism continues to be of considerable practical importance. The linkage is simple, and the configuration is very flexible, allowing great freedom to the designer. For example, the ratio of the lengths of the cranks and coupler is not very critical. The linkage will produce reasonably straight motion over a wide range of dimensional ratios AB/AA^* . It is not even essential that the two cranks have the same length. The essential feature is that the dimensions be such that the linkage is capable of assuming a position like that shown in [Figure 8.2\(d\)](#) with the two cranks being parallel and opposed, and with the coupler normal to both. If the cranks are of equal length the tracing point is the midpoint of the coupler, and the line of the coupler in the position shown is the straight line that is approximated. Unlike the Chebyshev mechanism, the straight-line section of the Watt mechanism intersects the line of centers (A^*B^*). Depending on the application, this may or may not be desirable.

Because of its simplicity and ability to provide low friction, approximately linear guidance, Watt's straight-line mechanism is useful anywhere exact conformance to linear motion is not essential. For example, it has been used in rear automotive suspensions of the live axle type to restrain lateral motion of the axle by constraining the center point of the axle to move along an approximate vertical straight line relative to the body.

The tracing point for the coupler curve shown in [Figure 8.2\(d\)](#) is the midpoint of the coupler. The proportions of AA^* and AB are variable. In the case drawn, $AB = 1$ and $AA^* = 2$. The form of the coupler-curve is known as a lemniscate. As can be seen, the central limbs of the lemniscate are good approximations to straight lines over a considerable length.

There are many other four-bar linkage configurations that yield reasonable approximations to linear motion of a tracing point as indicated by Artobolevsky [1]. Those used in level-luffing cranes and similar devices need to have the tracing point outside the interval between the coupler pivots. Examples of candidate linkages are the Hoeken linkage and Evan's linkages in [Figure 8.2](#). In the level-luffing crane shown in [Figure 8.1](#) it is desirable that the path of the crane hook that carries the load be a horizontal straight line. This means that the load moves approximately in a horizontal plane when only turret and jib movements are used. Vertical motion is accomplished by the crane's winch hauling or lowering the cable. Horizontal motion of the load has two very significant advantages. First, little energy is used for turret or jib motions if the cranks are counterweighted to eliminate work done against gravity in moving the mechanism itself. The drives for those motions do not need to have a large capacity. Second, it is relatively easy for the crane operator to visualize a horizontal trajectory of the load and determine whether that trajectory will interfere with fixed obstacles such as the side of the ship.

Exact Straight-Line Mechanisms

It is also possible to generate a perfectly straight line with a linkage mechanism, but generally only at the cost of a relatively complex mechanism if large motions are desired. The first such mechanism to be invented was that of Peaucellier [1,3]. Hart[1,3] developed a simpler mechanism that also generates an exact straight line. Artobolevsky [1] identifies eleven different mechanisms with revolute joints, but all are much more complex than the four-bar approximate straight-line generators discussed above.

Several mechanisms based on the slider-crank mechanism will generate a straight line for limited motion [3]. These are of interest when a straight line in a direction other than the slider direction is required.

Four exact straight-line mechanisms are illustrated in [Figures 8.3–8.6](#). A Peaucellier linkage is shown in [Figure 8.3](#). This was the first and most famous exact straight-line mechanism to be discovered. The linkage has a rhombic

loop, $ABDC$, which forms a kite shape with the equal-length links A^*A and A^*D . The link B^*B is also equal in length to the base A^*B^* . Point C generates a true straight line normal to the base A^*B^* .

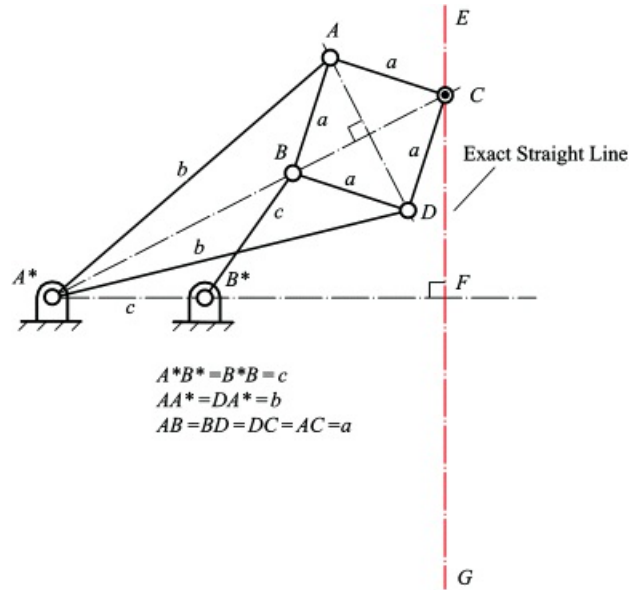


Figure 8.3 Peaucellier's exact straight-line mechanism. The path of point C is a true straight line normal to A^*B^* . For $a = 0.8$, $b = 2.4$, and $c = 1.0$, the straight-line length is given by $EG = FG = 1.9$.

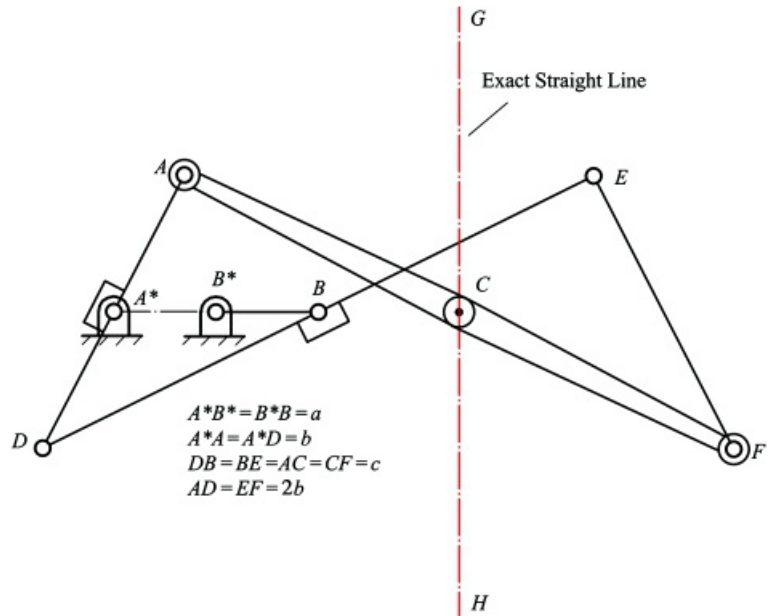
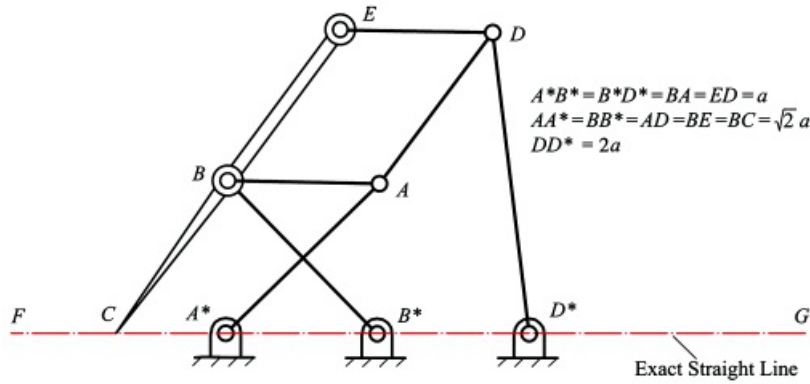
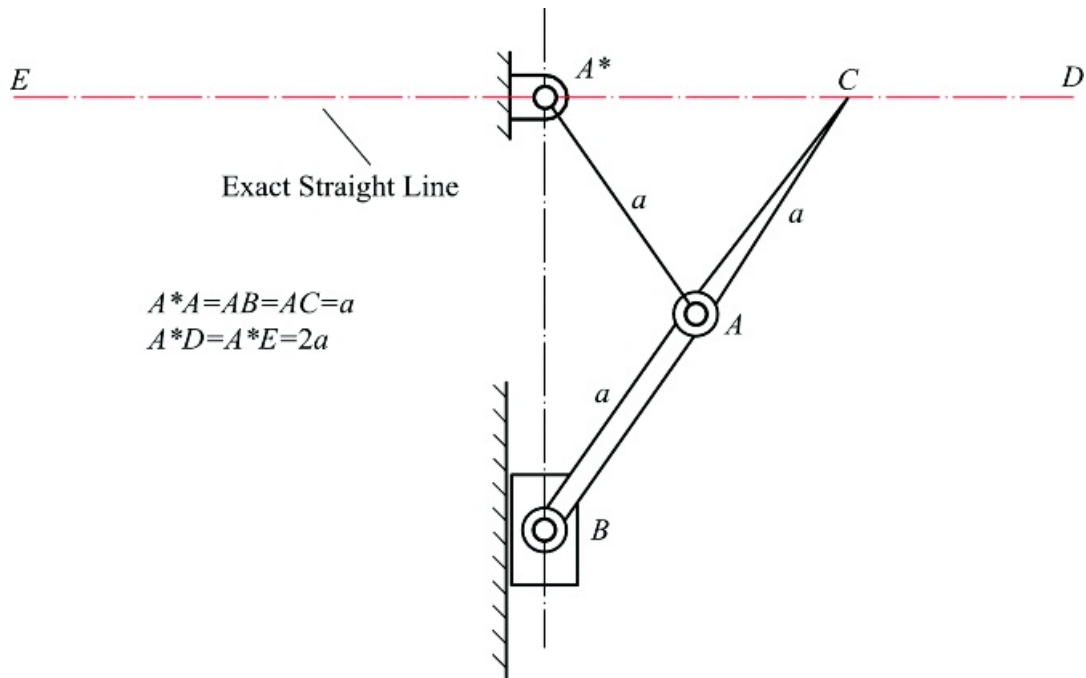


Figure 8.4 Hart's exact straight-line mechanism. The path of point C is a true straight line normal to A^*B^* . For $a = 1.0$, $b = 1.5$, and $c = 3.0$, the straight-line length is given by $CG = CH = 3.0$.



[Figure 8.5](#) Bricard's exact straight-line mechanism. The path of point C is a true straight line coincident with A^*B^* . For $a = 1.0$, the straight-line length is given by $FB^* = 2.42$, and $FG = 5.24$. To reach the entire range of the straight line, the linkage must be driven at C .



[Figure 8.6](#) Straight-line mechanism based on isosceles slider-crank mechanism. The entire range of the straight line can be reached if the mechanism is driven by the coupler.

As may be seen, this is a much more complex linkage than the four-bar loops used above to generate approximate straight lines. It has eight members and six joints, four of which are ternary joints. Linkages invented by Hart [3] and Bricard [1] are also shown in [Figures 8.4](#) and [8.5](#). These mechanisms require only six-link mechanisms, but they are still considerably more complex than the four-bar approximate straight-line generators in [Figure 8.2](#).

If a slider is introduced, it is possible to generate an exact straight line using the slider-crank mechanism in [Figure 8.6](#). The range of motion is limited and a slider is required, but the basic mechanism is quite simple. Based on the geometry of the linkage, the output motion will be a simple sine function of the drive link (simple harmonic motion). As indicated in [Figure 8.6](#), the mechanism is made up of isosceles triangles.

Circle Mechanisms

Linkage coupler points can be used to generate circular motion that will mimic the motion of a crank. This is useful when it is not possible to mount the bearings that would be necessary for an actual crank. Artobolevsky [1] identifies ten mechanisms that will generate circles or circle arcs to varying degrees of accuracy. Curves generated

by general four-bar linkages will be approximate except at the circle points, and the accuracy is usually less than for the approximate straight-line mechanisms. One example by Chebyshev is shown in [Figure 8.7](#). Exact circle mechanisms can be designed if a parallelogram is incorporated in the linkage. A very simple circle mechanism can be developed from a four-bar parallelogram linkage as shown in [Figure 8.8](#). In [Figure 8.8](#), the angular velocity of the virtual crank will be the same as that of the other two cranks. If a different velocity ratio or phase angle between the actual crank and virtual crank is required, six or eight links must be used. [Figure 8.9](#) shows a six-link mechanism attributed to Delong [1]. In this linkage, the virtual link moves in the same direction as the input crank; however, the virtual crank is out of phase with the input crank by 180°. The centerlines of the input crank (AA^*) and the virtual crank (CC^*) remain parallel at every point of the motion cycle. The Delong linkage is more complex than the parallelogram linkage in [Figure 8.9](#); however, the Delong linkage has better force transmission characteristics and can be used for a full rotation of the crank. At two points in the motion cycle, all of the links of the parallelogram linkage become collinear. Therefore, unless an external force or torque is applied (such as through a flywheel) at these transitions points, the parallelogram linkage cannot be used for a full rotation of the crank.

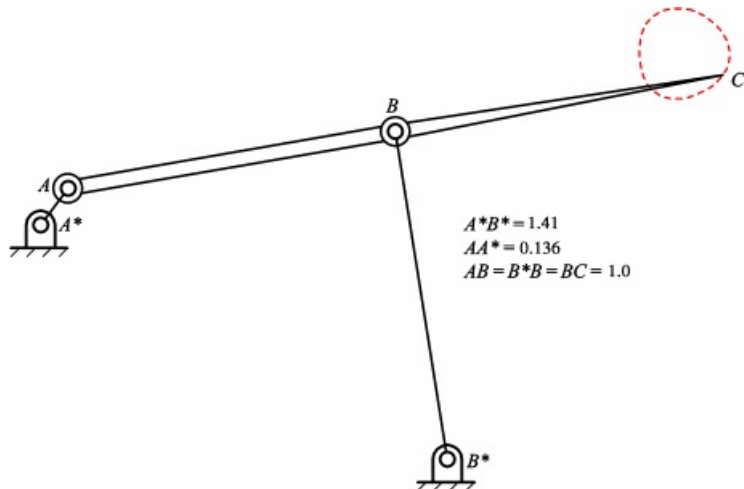


[Figure 8.7](#) Chebyshev's circle mechanism. The path of point C is an approximate circle. The radial deviation from a true circle is about 8 percent.

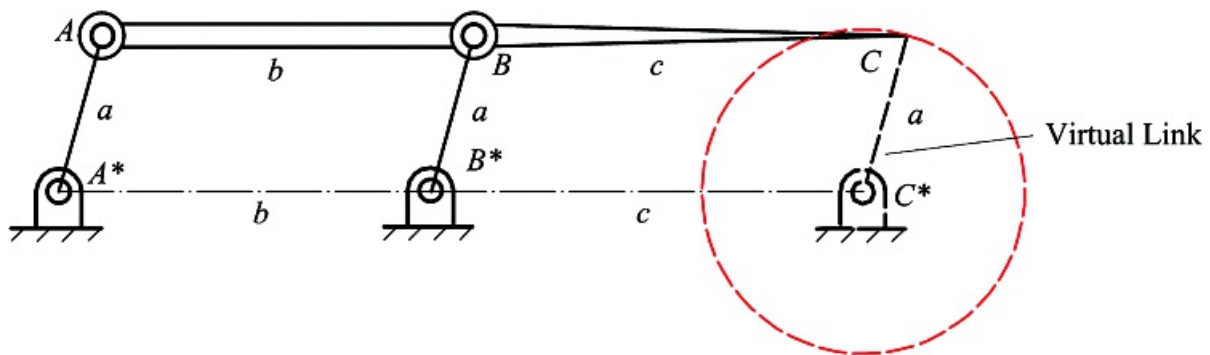


[Figure 8.8](#) Parallelogram circle mechanism. The path of point C traces an exact circle equal in radius to that of the other cranks; however, when A^*A is horizontal, the links become collinear. The torque/force transmission capabilities become zero at these points unless an external force or torque is applied.

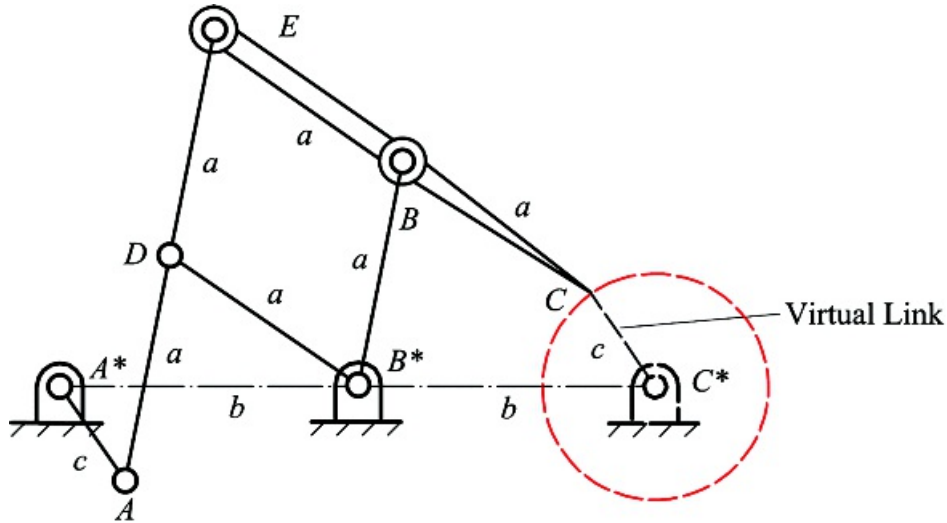


[Figure 8.9](#) Delong's circle mechanism. The path of point C traces an exact circle equal in radius to A^*A .

In the Delong linkage, the three critical lengths are a , b , and c as shown in [Figure 8.9](#). The values are arbitrary except that for the crank (AA^*) to be fully rotational

$$\dot{\psi} = \omega < 2\omega$$

Exact Straight-line Spatial Mechanisms

The previously discussed mechanisms are all planar. They are typically not used when an out-of-plane force must be supported. Out-of-plane forces can be accommodated by a relatively simple spatial mechanism invented by Pierre F. Sarrus in 1853. The linkage is represented in [Figure 8.10](#). The linkage consists of six links and six revolute joints. Based on [Equation 1.3](#), the nominal mobility for this number of links and joints is

$$M = 6(n - j - 1) + \sum_{i=1}^j f_i = 6(6 - 6 - 1) + 6 = 0$$

However, the mechanism clearly will move in the vertical direction. Therefore, this linkage is an example of the overconstrained linkages discussed in Section 1.10. The linkage not only moves all points in the platform (link 6 in [Figure 8.10](#)) along exact parallel straight lines, the overconstraint feature allows the linkage to resist out-of-plane forces efficiently.

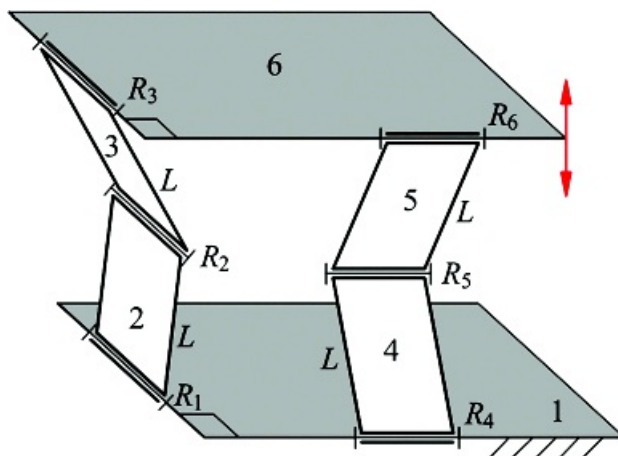


[Figure 8.10](#) Sarrus' exact straight-line mechanism.

The kinematic design of the Sarrus linkage is relatively simple. There are two sets of three joints. The joints in each set are parallel and therefore perpendicular to a given plane. The two planes perpendicular to the two sets of parallel joints are also perpendicular to each other. In addition, the guiding links are all of equal length, L , so the overall travel is $2L$ minus whatever distance is required to accommodate the thickness of the base support and the moving platform.

An example of the use of the Sarrus linkage is the translating miter saw shown in [Figure 8.11](#). The competing saws use guide rails that are bulky and require a significantly larger footprint than does the saw based on the Sarrus linkage. Because of the overconstrained nature of the linkage, the saw based on the Sarrus linkage is essentially as stiff and accurate as the saws based on linear rails.



[Figure 8.11](#) Gliding miter saw based on Sarrus' exact straight-line mechanism.

8.1.3 Pantographs

A plagiograph is a mechanism that exactly reproduces the path of a tracing point at a second tracer point, usually with a change of scale. The most common class of plagiographs is the family of pantograph mechanisms.

Pantographs have found many applications beyond that of plagiographs. These range from carrying contacts to overhead cables on electric trains and streetcars to legs of walking machines. As will be seen, pantographs are also of theoretical importance in that they lead to the theory of *cognate* linkages (see Section 3.5.3), which are different mechanisms capable of generating the same coupler point path. Cognate mechanisms, in turn, are of great usefulness in practical machine design as was indicated in [Chapter 3](#).

The Planar Collinear Pantograph

The special properties of the pantograph linkage have been used in a variety of applications. They also have important theoretical implications leading to the theory of cognate linkages, which will be introduced briefly later in this chapter.

A simple form of planar pantograph linkage is shown in [Figure 8.12](#) where length AB is equal to CD . Likewise, length AD is equal to BC . Consequently, $ABCD$ is a parallelogram, regardless of the position of the linkage. Further, the lengths OB and OC are in the ratio 1:4, as are the lengths CD and CE . It follows that triangle OBA is similar to triangle OCE , because OB/OC is equal to BA/CE and angle OBA is equal to angle OCE . Consequently,

the ratio of the lengths OA and OE is always 1:4. If point A traces any path in the plane of the linkage, point E will trace a geometrically similar path that is magnified by a factor of 4 compared with the path of point A . This is best understood by considering the path of point A to be a curve described in polar coordinates with origin at O . The position of the corresponding point on the path of point E is also described in polar coordinates centered on O . The angular coordinate of that point is the same as that of the corresponding point on the path of point A . Its radial coordinate is four times that of the corresponding point on the path of point A . Hence, the curve is the same. It is simply scaled up by a factor of 4.

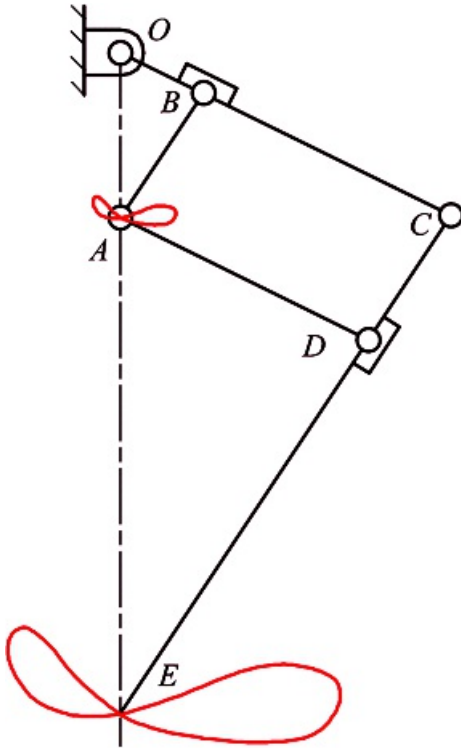


[Figure 8.12](#) A simple form of planar pantograph linkage. Any path traced by point A is reproduced by point E at a magnification of 4 : 1. $ABCD$ is a parallelogram. The ratios of lengths CD to CE and OB to OC are both 1 : 4. Link OC is connected to the base by a fixed revolute joint at O .

In consequence of the property described above, pantograph mechanisms have been used a great deal to copy and rescale text and other geometric figures. The magnification factor can be set to any desired value by varying the proportions of the links. In the form of the linkage that is shown in [Figure 8.12](#), it is always equal to the ratio of length OC to OB , which must also be equal to the ratio of CE to CD .

An example of the use of the pantograph mechanism to copy plane curves is a copying mill used to produce plate cams. The reader will find an in-depth discussion of cam geometry in [Chapter 10](#). Most plate cams are bounded by mathematically complicated curves. In order to produce cams using a copy mill, a master cam is produced at an enlarged scale by hand. The profile of the master is traced by a roller with its central axis located at point E of [Figure 8.12](#). The axis of the milling cutter is at point A . The ratio of the roller diameter to the cutter diameter is the pantograph ratio. Consequently, the mill produces a cam that is geometrically similar to the master but which is reduced in size by the pantograph ratio. The use of point E , rather than point A , to trace the master provides improved accuracy, because errors in the master profile are reduced by the pantograph ratio. The large size of the master also facilitates its accurate manufacture.

The application described above is an example of inversion of the linkage by interchanging the tracing points A and E . The pantograph can also be inverted by hinging it to the base with a fixed revolute coincident with A , rather than at point O . This is shown in [Figure 8.13](#). The path of point O is now copied by the geometrically similar path of point E . However, the magnification ratio is now 3 : 1 rather than 4 : 1. This is because, with these dimensions, the ratio of length AE to AO is 3 : 1.

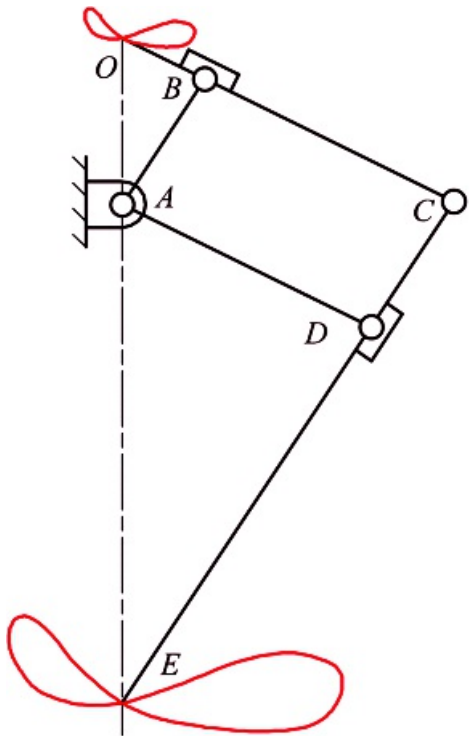


[Figure 8.13](#) The pantograph of [Figure 8.12](#) inverted by mounting with a fixed revolute at point A . The paths of points O and E are geometrically similar. The magnification factor is now $3 : 1$.

There are other variations on the same theme. [Figure 8.14](#) shows the pantograph linkage used in the legs of the Adaptive Suspension Vehicle (ASV) that was shown in [Figure 1.1](#). Here there is no fixed pivot. Rather, point O is on a vertical slide and point A is on a horizontal slide. The motion of point A alone, produced by a hydraulic cylinder, causes a horizontal rectilinear motion of the ankle point, E . The motion of point O alone, also produced by a hydraulic cylinder, causes a vertical rectilinear motion of point E . Simultaneous motion of points A and O results in motion of point E along a plane curve. This is what happens when the foot is picked up and the leg is swung back to its forward position. The magnification factor in this mechanism is $5 : 1$ for the drive motion (point A) and $4 : 1$ for the lift motion (point B).



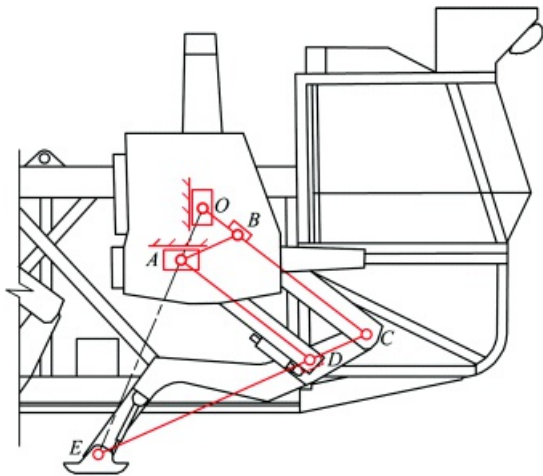


[Figure 8.14](#) The leg mechanism of the Adaptive Suspension Vehicle. Point O moves on a slide that is vertical relative to the leg-mounting structure to produce a corresponding vertical motion of the ankle point E . Point A moves on a slide that is horizontal relative to the vehicle body to drive point E along a horizontal path.

Skew Pantographs

A more general form of pantograph is the skew pantograph shown in [Figure 8.15](#). $OLMN$ is a parallelogram, and triangle NMQ is similar to triangle LPM . As shown below, triangle OPQ is always similar to triangle LPM . Consequently, the path traced by point Q is similar to that traced by point P , is rotated through angle α from the path of P about O , and is magnified by the ratio LM/LP .

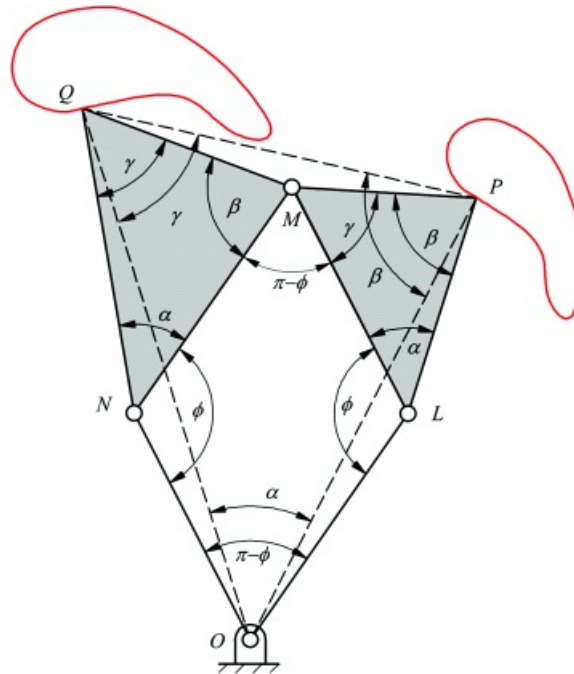


[Figure 8.15](#) A skew pantograph. $OLMN$ is a parallelogram and triangles LPM and NMQ are similar. The triangle OPQ is always similar to triangles LPM and NMQ . Consequently, the path traced by point Q is similar to that traced by point P . The path traced by Q is rotated relative to that traced by P through angle α and it is magnified by the ratio $OQ/OP = LM/LP$.

These properties are proved as follows. Note that since $OLMN$ is a parallelogram, $\angle MLO = \angle OLN = \phi$. Likewise, $\angle LON = \angle NML = \pi - \phi$.

Triangles PLO and ONQ are similar for the following reasons

$$\angle PLO = \angle ONQ = \phi + \alpha$$

also

$$\frac{NQ}{NM} = \frac{ML}{PL}$$

because triangles NMQ and LPM are similar and these are corresponding pairs of sides. Now $NM = OL$, and $ML = NO$ because $OLMN$ is a parallelogram. Making these substitutions, we get

$$\frac{NQ}{OL} = \frac{NO}{PL} \text{ or } \frac{NQ}{NO} = \frac{OL}{PL}$$

which establishes that triangles PLO and ONQ are similar since NQ and NO , and OL and PL , are corresponding side pairs and the equal angles $\angle PLO$ and $\angle ONQ$ are the included angles.

Also, triangle QMP is similar to PLO and ONQ for the following reasons

$$\angle QMP = 2\pi - \beta - \gamma = (\pi - \phi) = \pi + \phi - \beta - \gamma$$

Also, because α , β , and γ are the vertex angles of triangle LPM

$$\alpha + \beta + \gamma = \pi$$

so

$$\angle QMP = \pi + \phi - (\pi - \alpha) = \phi + \alpha = \angle ONQ$$

Because triangles NMQ and LPM are similar

$$\frac{MQ}{NQ} = \frac{PM}{LM}$$

or

$$\frac{PM}{MQ} = \frac{LM}{NQ} = \frac{ON}{NQ}$$

noting that $LM = ON$.

Therefore triangles QMP and ONQ are similar because the corresponding sides PM and MQ , and ON and NQ , are in the same ratio and the included angles QMP and ONQ are equal. Triangles QMP and PLO are similar because both are similar to ONQ .

It follows that

$$\angle NQO = \angle MQP$$

and so

$$\angle OQP = \angle NQM = \gamma$$

Likewise

$$\angle QPM = \angle OPL.$$

and so

$$\angle QPO = \angle MPL = \beta$$

Consequently,

$$\angle POQ = \alpha$$

and triangle OPQ is similar to triangles LPM and NMQ .

The geometric similarity of the paths of points P and Q can be inferred from an argument similar to that employed in the case of the collinear pantograph. If the path of point P is considered to be a curve described in polar coordinates centered on O , the radial coordinate is OP . The path of Q is also described in polar coordinates centered on O . The radial coordinate is LM/LP times that of point P , and the angle reference is rotated through angle α from that used for the path of point P .

Roberts' Theorem

If the path of point P of the skew pantograph of the preceding section is a circle, then that of point Q will also be a circle as shown in [Figure 8.16](#). Thus, if P is constrained to move on a circle by a crank rotating about fixed pivot, O_P , then a crank can also be connected to point Q from a fixed pivot at the center of its path: O_Q . Because the path of Q is similar to that of P and triangle OPQ is always similar to triangle LPM , it follows that triangle $OO_P O_Q$ is also similar to triangle LPM . This creates two planar four-bar linkages, $OLPO_P$ and $O_Q QNO$, for each of which M is a coupler point. Thus the path generated by point M as a coupler point of $OLPO_P$ is identical to the path traced by M as a coupler point of $O_Q QNO$. Thus, we have generated two completely different four-bar mechanisms that generate identical coupler curves. Linkages that have this property are called *cognates*.

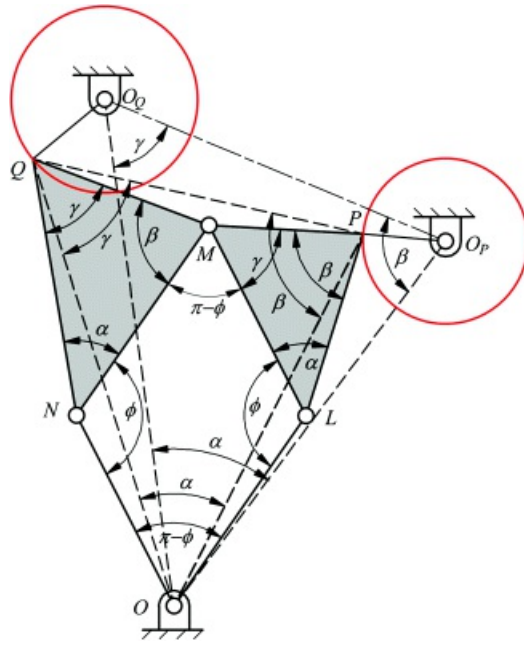


[Figure 8.16](#) A pair of cognate linkages. The path of point P in the skew pantograph of [Figure 8.15](#) is a circle centered on O_P . Therefore the path of point Q is also a circle, with center O_Q where triangle OO_PO_Q is similar to triangle LPM . Therefore cranks $O_P P$ and $O_Q Q$ can be added, and the assemblage will be mobile.

We can go further. If points R and S are located by constructing the parallelograms $O_P PMR$ and $O_Q QMS$, it can be shown that triangle MRS is similar to triangle LPM and hence that the four-bar linkage $O_P R S O_Q$ is also cognate to $OLPO_P$ and $O_Q QNO$, again with M as the tracing point. The assemblage shown in [Figure 8.17](#) is known as Roberts' mechanism.

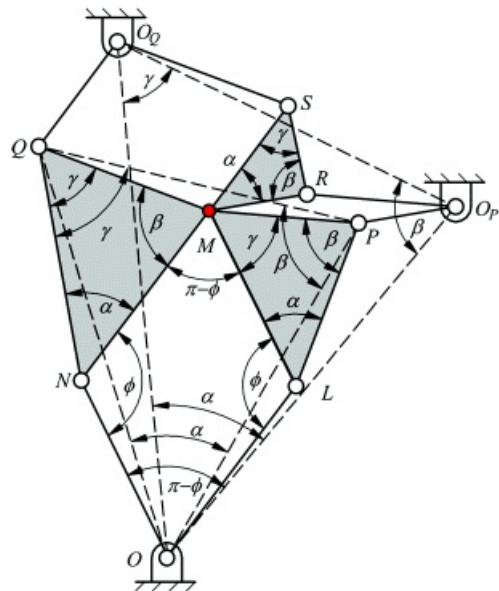


[Figure 8.17](#) A general Roberts' mechanism. The three four-bar linkages $OLPO_P$, $O_P R S O_Q$ and $O_Q QNO$ are all cognate with M as the coupler point for each.

Roberts' theorem states that if a planar four-bar mechanism is constructed, a coupler point is selected, and the corresponding coupler curve is traced, then there are two other four-bar linkages that will generate the identical coupler curve. That is, there are two four-bar linkages that are cognate to the original four-bar. They may be constructed by constructing the Roberts' mechanism based on the original four-bar. In the case of [Figure 8.17](#), if we view $OLPO_P$ as the original four-bar linkage, with M being the selected coupler point, then the cognates are

O_QQNO and O_PRSO_Q with M being the coupler point in both cases. Starting with points O , L , P , O_P , and M , the remainder of the figure may be constructed by first completing the parallelograms $OLMN$ and O_PRMP to locate points N and R . Triangles OO_PO_Q , NMQ , and MRS may then be constructed similar to triangle LPM to complete the figure.

If the original four-bar linkage is of Grashof type I, then the cognates will also be type I. Likewise, if the original four-bar is type II, then the cognates are also type II. Further, if the original four-bar is type I and is a crank-rocker linkage, then one of the cognates will also be a crank-rocker linkage. The other will be a type I double-rocker linkage. The cognates of a drag-link linkage are both also drag links. The cognates of a type I double-rocker linkage are both crank-rockers.

As indicated in [Chapter 3](#), cognate linkages can be very useful when a linkage has been found that generates a desired path but that solution linkage has undesirable properties such as interference with other components. Often one of the cognates will produce the desired path without the problems of the original linkage.



Example 8.1

Using Roberts' Theorem to Generate Cognates of the Chebyshev Mechanism

The Chebyshev linkage of [Figure 8.2](#) is a Type I double-rocker. As was discussed in Section 1.18, it is difficult to transfer motion from the tracing point of this linkage due to interference with the cranks since the coupler tumbles between the cranks. As discussed above, the cognates of a Type I double-rocker are both crank-rockers and should be free of this problem. Construct the cognates and, hence, produce a crank-rocker linkage with the same approximate straight-line coupler curve segment as the Chebyshev linkage.

Solution

Examination of [Figure 8.2](#) indicates that the coupler point is the midpoint of the line between the coupler pivots. That is, the triangle LPM of [Figure 8.17](#) has collapsed into a line. Therefore triangle $OO_P O_Q$ will also be collapsed to a line. Since O corresponds to L , O_P corresponds to P , and O_Q corresponds to M in these triangles (corresponding vertices have the same vertical angles), it follows that O_Q will be midway between O and O_P , as shown in [Figure 8.18](#). Similarly, triangles RMS and MNQ will collapse to line segments.

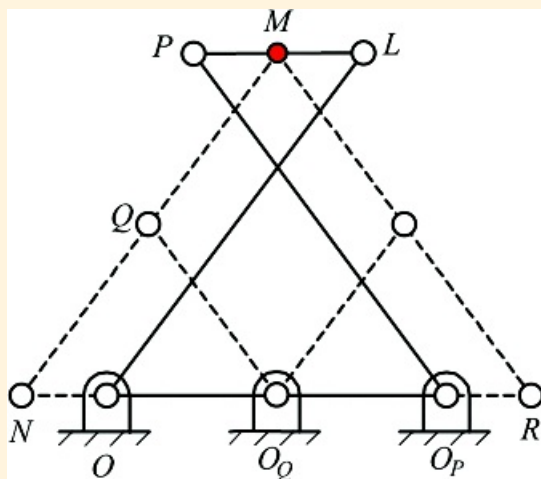


[Figure 8.18](#) Construction of the cognates of the Chebyshev linkage shown in [Figure 8.2](#). $OLPO_P$ is the original Chebyshev four-bar, and M is the coupler point. The cognates are $ONQO_Q$ and O_PRSO_Q . Their symmetry with one another is a result of the bilateral symmetry of the original linkage.

Parallelograms $OLMN$ and O_PPMR are constructed as shown in [Figure 8.18](#) to locate points N and R . The line MQN is drawn. Note that in [Figure 8.17](#), N corresponds to L , M corresponds to P , and Q corresponds to M in the two similar triangles LPM and NMQ . Therefore Q will be at the midpoint of NM in [Figure 8.18](#). Similarly, the line RSM is drawn to represent the coupler of the second cognate. The cranks $O_Q Q$ and $O_Q S$ are drawn in to complete the two cognates shown by the dashed lines in [Figure 8.18](#).

The cognate $ONQO_Q$ is drawn on its own in [Figure 8.19](#) with the path of point M plotted. Not only is it much easier to transfer motion from this linkage than from the original Chebyshev linkage, but the linkage can be driven by continuous rotation of the crank ON , if desired.

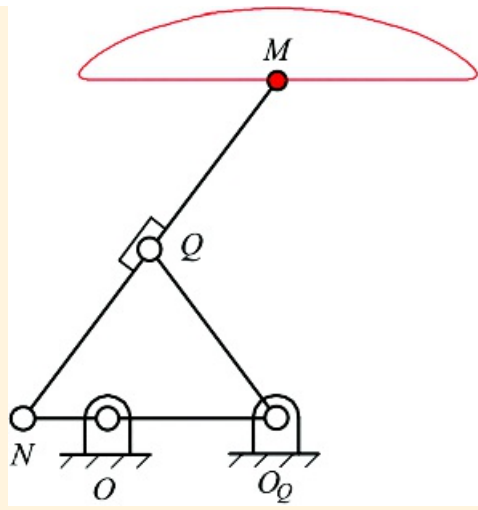


[Figure 8.19](#) The cognate $ONQO_Q$ from [Figure 8.18](#) with its coupler curve plotted.



8.2 Spherical Mechanisms

Although spatial mechanisms or linkages, in general, will be discussed in [Chapter 9](#), there are other classes of mechanisms that are not general spatial linkages in the sense of satisfying the spatial Kutzbach criterion ([Equation 1.3](#)) and are certainly not planar mechanisms. One of the most extensive and practically important such groups is the class of spherical mechanisms, that includes not only linkages but also spherical cam mechanisms and gears, namely bevel gears, and rolling contact bearings, namely tapered roller bearings.

Although it is beyond the scope of this book, spherical mechanism theory is an important component of spatial mechanism theory. This is because the rotational equations defined for spatial mechanisms in [Chapter 9](#) are identical for spherical mechanisms. However, the translation equations, also discussed in [Chapter 9](#), are absent in the case of spherical mechanisms. This allows inferences to be made on the basis of a spherical analog and applied to spatial mechanisms. There is also a way of generating valid translation equations directly from the rotational equations.

8.2.1 Introduction

Spherical linkages form a family much like planar linkages. However, whereas in a planar linkage all the revolute joint axes are parallel, in a spherical linkage they all intersect at a common point, called the concurrency point. Actually, planar linkages can be thought of as spherical linkages for which the concurrency point is at infinity.

There are many similarities in the properties of spherical and planar linkages. For example, spherical linkages obey the same form of the Kutzbach criterion that planar linkages do (Section 1.8)

$$M = 3(m - j - 1) + \sum_{i=1}^j f_i \quad (1.1)$$

Consequently, the simplest nontrivial spherical linkage is a four-bar linkage, just as in the planar case.

Also, there is a form of the Grashof inequality governing rotatability of joints that works for spherical linkages

$$\alpha_2 + \alpha_3 < \alpha_1 + \alpha_4$$

Here, instead of dealing with the lengths of the links, as in the case of a planar linkage, we work with the angles between successive joint axes. α_3 is the smallest angle between two successive joints, α_2 is the largest such angle, and α_1 and α_4 are the other two angles.

As in the planar case, the inequality governs the presence of joints in a four-bar linkage that can be completely rotated. If the inequality is satisfied, there are two completely rotatable joints. They are the joints whose axes bound the angle α_3 . Depending on which link is chosen as the base, the linkage will have characteristics similar to those of a crank-rocker planar four-bar, or a drag-link, or a type 1 double-rocker. If the inequality is not satisfied, there is no completely rotatable joint, and the linkage behaves like a type 2 planar linkage.

There is one variation from the planar analog. Whereas there is no limit on the length of a link in a planar linkage, beyond the fact that it must be less than the sum of the lengths of the other three links for it to be possible to assemble the loop, no side angle of a spherical linkage can be greater than 90° . This is because there are, in fact, always two angles between two lines that are supplements of one another. Either the angle, or its supplement can be viewed as the angle between two axes in a spherical four-bar linkage. If the angle is greater than 90° , its supplement is less than 90° so side angles in a spherical linkage can be said to have an upper limit of 90° .

The closure equations for a spherical four-bar linkage, such as that shown schematically in [Figure 8.20](#), may, in principle, be developed using a procedure analogous to that used to derive the closure equations for a planar four-bar linkage in [Chapter 7](#). However, this becomes very complex because the entities being dealt with are angles

rather than lengths. A more convenient procedure is to use the loop matrix transformations defined in [Chapter 9](#). Using either method, the relationship between the angle ϕ_1 , considered to be the input angle, and ϕ_2 , considered to be the output angle of the linkage of [Figure 8.20](#) can be expressed as follows

$$\begin{aligned} \sin \phi_1 \sin \phi_2 \sin \alpha_2 \sin \alpha_4 - \cos \phi_1 \cos \phi_2 \cos \alpha_1 \sin \alpha_2 \sin \alpha_4 + \cos \phi_1 \sin \alpha_1 \cos \alpha_2 \sin \alpha_4 \\ + \cos \phi_1 \sin \alpha_1 \sin \alpha_2 \cos \alpha_4 + \cos \alpha_1 \cos \alpha_2 \cos \alpha_4 = \cos \alpha_3 = 0 \end{aligned} \quad (8.1)$$

where ϕ_1 , ϕ_2 , ϕ_3 , and ϕ_4 are the joint angles and α_1 , α_2 , α_3 , and α_4 are the angles between the joint axes of the spherical four-bar loop as shown in [Figure 8.20](#).

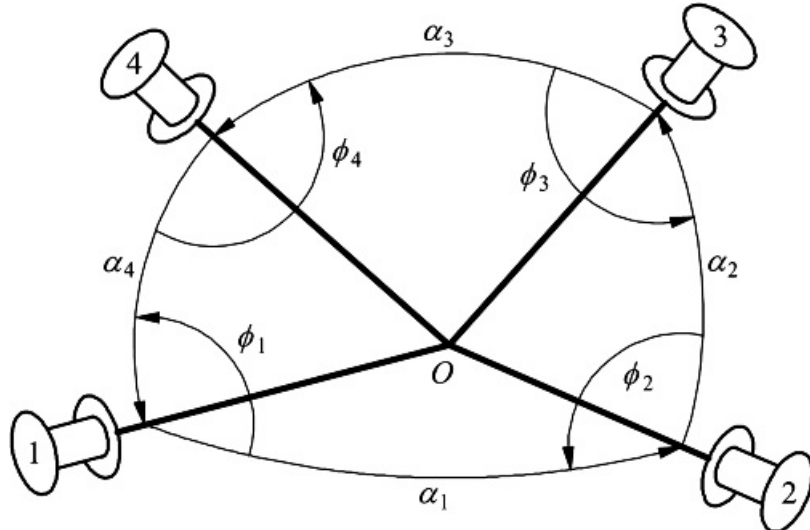


[Figure 8.20](#) A schematic representation of a spherical four-bar mechanism. The heavy lines represent the joint axes with concurrency point O . α_1 , α_2 , α_3 , and α_4 are the angles between the successive axes. ϕ_1 , ϕ_2 , ϕ_3 , and ϕ_4 are the joint angles.

If ϕ_1 is regarded as having a known value, this rather intimidating-looking equation has the form

$$P \cos \phi_2 + Q \sin \phi_2 + R = 0 \quad (8.2)$$

for which a solution was developed in [Chapter 7](#). Here

$$\begin{aligned} P &= -\cos \phi_1 \cos \alpha_1 \sin \alpha_2 \sin \alpha_4 + \sin \alpha_1 \sin \alpha_2 \cos \alpha_4 \\ Q &= \sin \phi_1 \sin \alpha_2 \sin \alpha_4 \\ R &= \cos \phi_1 \sin \alpha_1 \cos \alpha_2 \sin \alpha_4 + \cos \alpha_1 \cos \alpha_2 \cos \alpha_4 - \cos \alpha_3 \end{aligned} \quad (8.3)$$

Hence referring to [Table 7.1](#), we can obtain values for ϕ_2 given ϕ_1 from

$$\phi_2 = \frac{-Q + \sigma \sqrt{P^2 + Q^2 - R^2}}{R - P} \quad (8.4)$$

where $\sigma = \pm 1$ is a sign variable, and

$$\phi_2 = 2 \tan^{-1}(g) \quad (8.5)$$

We can also develop relationships between the angular velocities and accelerations about joints 1 and 2 by differentiation of [Equation 8.1](#). Differentiation of [Equation 8.1](#) with respect to time gives, after rearrangement

$$\dot{\phi}_2 = -\dot{\phi}_1 \frac{\sin \alpha_4 (\cos \phi_1 \sin \phi_2 \sin \alpha_2 + \sin \phi_1 \cos \phi_2 \cos \alpha_1 \sin \alpha_2 - \sin \phi_1 \cos \alpha_1 \cos \alpha_2)}{\sin \alpha_2 (\sin \phi_1 \cos \phi_2 \sin \alpha_4 + \cos \phi_1 \sin \phi_2 \cos \alpha_1 \sin \alpha_4 - \sin \phi_2 \sin \alpha_1 \sin \alpha_4)} \quad (8.6)$$

Further differentiation gives

$$\ddot{\phi}_2 = \frac{\ddot{\phi}_1 \dot{\phi}_2}{\dot{\phi}_1} + \frac{B}{A} \dot{\phi}_1 \dot{\phi}_2 + \frac{C}{A} \dot{\phi}_1^2 + \frac{D}{A} \dot{\phi}_2^2 \quad (8.7)$$

where

$$A = \sin \alpha_2 (\sin \phi_1 \cos \phi_2 \sin \alpha_4 + \cos \phi_1 \sin \phi_2 \cos \alpha_1 \sin \alpha_4 - \sin \phi_2 \sin \alpha_1 \cos \alpha_4) \quad (8.8)$$

$$B = 2 \sin \alpha_2 \sin \alpha_4 (\sin \phi_1 \sin \phi_2 \cos \alpha_1 - \cos \phi_1 \cos \phi_2)$$

$$C = \sin \alpha_4 (\sin \phi_1 \sin \phi_2 \sin \alpha_2 - \cos \phi_1 \cos \phi_2 \cos \alpha_1 \sin \alpha_2 + \cos \phi_1 \sin \alpha_1 \cos \alpha_2)$$

$$D = \sin \alpha_2 (\sin \phi_1 \sin \phi_2 \sin \alpha_4 - \cos \phi_1 \cos \phi_2 \cos \alpha_1 \sin \alpha_4 + \cos \phi_2 \sin \alpha_1 \cos \alpha_4)$$



Example 8.2

Analysis of Spherical Four-Bar Mechanism

A spherical four-bar linkage is constructed with the angle between the axes of joints 1 and 2 (α_1) being 120° , the angle between axes 2 and 3 (α_2) 90° , that between axes 3 and 4 (α_3) 75° , and that between axes 1 and 4 (α_4) 30° . Member 1 is the base and the mechanism is a spherical crank-rocker linkage. Find the output angle, ϕ_2 , when the driving joint angle, ψ_1 is 90° .

If the input crank is driven at a constant angular velocity of 10 rad/s , find the angular velocity, $\dot{\phi}_2$, of the driven crank, and its angular acceleration, $\ddot{\phi}_2$, in the same position.

Solution

Substitution of the values

$$\alpha_1 = 120^\circ, \alpha_2 = 90^\circ, \alpha_3 = 75^\circ, \alpha_4 = 30^\circ, \text{ and } \psi_1 = 90^\circ \text{ into Equation 8.3 gives}$$

$$P = 0.75, Q = 0.5, \text{ and } R = -0.2588$$

Substitution of these values into Equation 8.4 gives

$$s = -0.3803, \text{ or } s = 1.3515$$

Application of Equation 8.5 gives

$$\phi_2 = -39.63^\circ, \text{ or } \phi_2 = 107.00^\circ$$

The two solutions correspond to the two solutions obtained in the solution of the position problem of a planar four-bar, and have the same source in the reflection of the driven crank and coupler about the plane of the moving joint axis of the driving crank and the fixed joint axis of the driven crank.

Substitution of these values plus $\dot{\psi}_1 = 10 \text{ rad/s}$ into Equation 8.6 gives the values $\dot{\phi}_2 = 2.2302 \text{ rad/s}$ and $\dot{\phi}_2 = 0.8467 \text{ rad/s}$, respectively, corresponding to the two solutions for ϕ_2 given above. Further substitution into Equation 8.8 gives the following sets of values

For $\phi_2 = -39.63^\circ$:	$A = 0.8634, B = 0.3189, C = -0.3189, D = 0.2588$
For $\phi_2 = 107.00^\circ$:	$A = -0.8634, B = -0.4781, C = 0.4781, D = 0.2588$

When substituted into Equation 8.7 with $\dot{\psi}_1 = 0$ and the preceding values for $\dot{\phi}_1$ and $\dot{\phi}_2$, we get the following two values for the acceleration of the driven crank: $\ddot{\phi}_2 = -27.20 \text{ rad/s}^2$ and $\ddot{\phi}_2 = -50.90 \text{ rad/s}^2$, respectively. Once again, these correspond to the two possible solutions of the position problem.

8.2.2 Gimbals

A set of gimbals is a spherical serial chain that allows an axis through the concurrency point to be placed in any possible direction. Gimbals are often used in the mounts of directional instruments such as theodolites or telescopes. They are also used in gyroscopes to allow the rotor axis freedom to assume any direction relative to the base of the instrument.

8.2.3 Universal Joints

The simplest means of transferring motion between noncoaxial shafts is by means of one or two universal joints,

also known as Cardan joints in Europe and Hooke joints in Britain. For this reason, this very simple spherical mechanism appears in an enormous variety of applications. They may be found as components of the Stewart platform and 3-2-1 platform parallel mechanisms discussed in [Chapter 9](#) and in many other situations.

Properties of the Universal Joint

A common need in machinery is to transfer rotation between two shafts that are not parallel to one another and that may be free to move relative to one another. A universal joint is a simple spherical four-bar mechanism that transfers rotary motion between two shafts whose axes pass through the concurrency point. The joint itself consists of two revolute joints whose axes are orthogonal to one another. They are often configured in a cross-shaped member as shown in [Figure 8.21](#). One of these joints is arranged with its axis at 90° to that of the driving shaft, and the other has its axis at 90° to that of the driven shaft. In practice, the ends of the shafts are often configured as clevises to mate with the cruciform shafts of the intermediate member. Together with the bearings in which the two shafts turn, the universal joint forms a spherical four-bar linkage with three sides being at 90° angles. The fourth side is, in general, not 90° . This may be better seen in [Figure 8.22](#), in which only one side of each of the crossed intermediate shafts is shown.

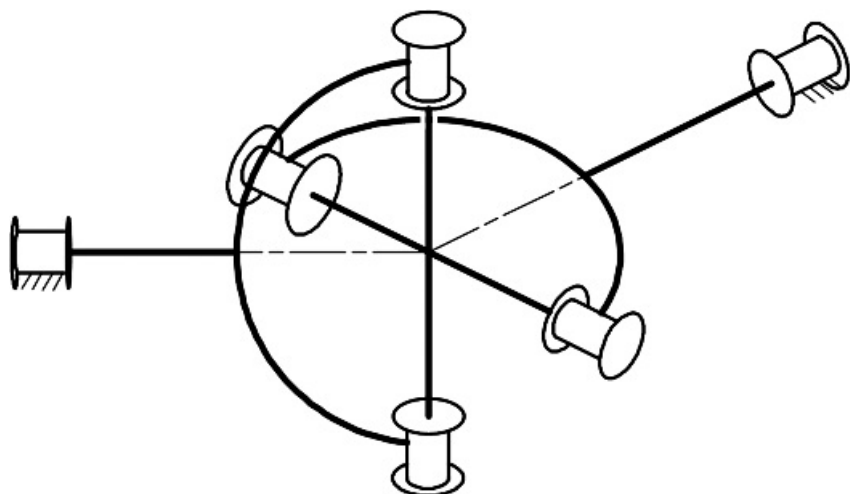


[Figure 8.21](#) Universal, Cardan, or Hooke joint.

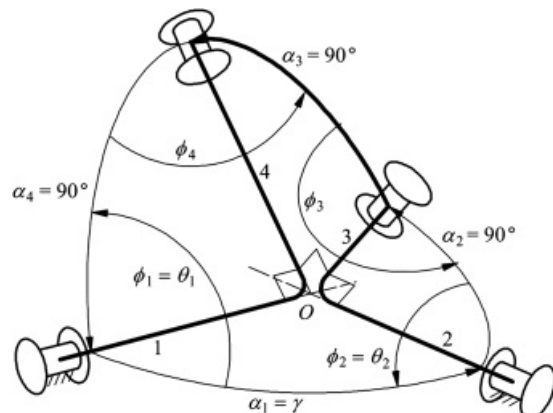


[Figure 8.22](#) Universal joint geometry: γ is the angular misalignment of the shafts; θ_1 is the angle of the input shaft; and θ_2 is the angle of the output shaft.

In general, the angular motion is not uniformly transferred from the driving shaft to the driven shaft. The relationship between the angles of the driving shaft, θ_1 , and the driven shaft, θ_2 , is

$$\cos \gamma = \tan \theta_1 \tan \theta_2 \quad (8.9)$$

where γ is the angular misalignment of the shafts. This relationship can be derived from [Equation 8.1](#). As is indicated in [Figure 8.22](#), $\alpha_2 = \alpha_3 = \alpha_4 = 90^\circ$. Also, $\alpha_1 = \gamma$ and $\phi_1 = \theta_1$, $\phi_2 = \theta_2$ where α_i and ϕ_i i = 1, 2, 3, 4, are consistent with [Equation 8.1](#). Substituting these values into [Equation 8.1](#) gives

$$\sin \theta_1 \sin \theta_2 - \cos \theta_1 \cos \theta_2 \cos \gamma = 0$$

which can be rearranged into [Equation 8.9](#).

If the driving shaft turns with a uniform angular velocity, the rotation of the driven shaft is not uniform but fluctuates. That is, a single universal joint is not a constant velocity coupling like those that will be discussed in the next section. However, if the angle between the shaft axes is small, the fluctuation will also be small and is acceptable in many applications.

The angular velocity relationship can be obtained by differentiating [Equation 8.9](#) rewritten in the form

$$\tan \theta_2 = \cos \gamma \cot \theta_1$$

Differentiation with respect to time gives

$$\dot{\theta}_2 \sec^2 \theta_2 = -\dot{\theta}_1 \csc^2 \theta_1 \cos \gamma$$

Hence the ratio of the magnitudes of the shaft velocities is

$$\frac{\omega_2}{\omega_1} = \frac{\dot{\theta}_2}{\dot{\theta}_1} = \frac{\cos^2 \theta_2 \cos \gamma}{\sin^2 \theta_1}$$

It is helpful to work in terms of the input angle, θ_1 , alone. Hence the angle equation is used to eliminate $\tan \theta_2$

$$\frac{\omega_2}{\omega_1} = \frac{\cos \gamma}{\sin^2 \theta_1 (1 + \tan^2 \theta_2)} = \frac{\cos \gamma}{\sin^2 \theta_1 (1 - \cos^2 \gamma \cos^2 \theta_1)} = \frac{\cos \gamma}{\sin^2 \theta_1 + \cos^2 \gamma \cos^2 \theta_1}$$

This expression can be further simplified by replacing $\cos^2 \theta$ by $1 - \sin^2 \theta$ as follows

$$\frac{\omega_2}{\omega_1} = \frac{\cos \gamma}{1 - \cos^2 \theta_1 + \cos^2 \gamma \cos^2 \theta_1} = \frac{\cos \gamma}{1 - \sin^2 \gamma \cos^2 \theta_1} \quad (8.10)$$

It may be seen that the velocity ratio is a function of θ_1 so that for constant input velocity the output velocity will fluctuate. The velocity ratio varies from

$$\frac{1}{\cos \gamma} \text{ to } \cos \gamma$$

during the motion cycle. This relationship is plotted in [Figure 8.23](#).



Example 8.3

Analysis of Universal Joint for Front-Wheel-Driven Car

A simple automotive vehicle is driven via the front wheels. Universal joints are used in the shafts connecting the differential to the front wheels, as a low-cost alternative to the constant-velocity joints that are normally used to allow rotation of the front wheels about vertical axes for steering. At full steering lock, the inside front wheel is rotated 30° from the straight-ahead position. Calculate the percentage fluctuation in wheel velocity in this position.

Solution

If shaft 1 in [Figure 8.22](#) is viewed as the shaft from the engine and shaft 2 is viewed as the half-shaft driving the wheel, in the full lock position, the angle between the axis of shaft 1 and the axis of shaft 2 will be 30°. That is, $\gamma = 180^\circ - 30^\circ = 150^\circ$. Applying [Equation 8.10](#)

$$\frac{\omega_2}{\omega_1} = \frac{\cos \gamma}{1 - \sin^2 \gamma \cos^2 \theta_1} = \frac{-0.8660}{1 - 0.25 \cos^2 \theta_1}$$

Thus, the maximum magnitude of the velocity ratio occurring when $\theta_1 = 0$ is $0.8660/0.75 = 1.155$, and the minimum magnitude occurring when $\theta_1 = 180^\circ$ is $0.8660/1.25 = 0.693$. Thus the maximum is 115 percent of the mean value of 1.0, and the minimum is 69 percent of the mean. The maximum percentage fluctuation is 31 percent of the mean.

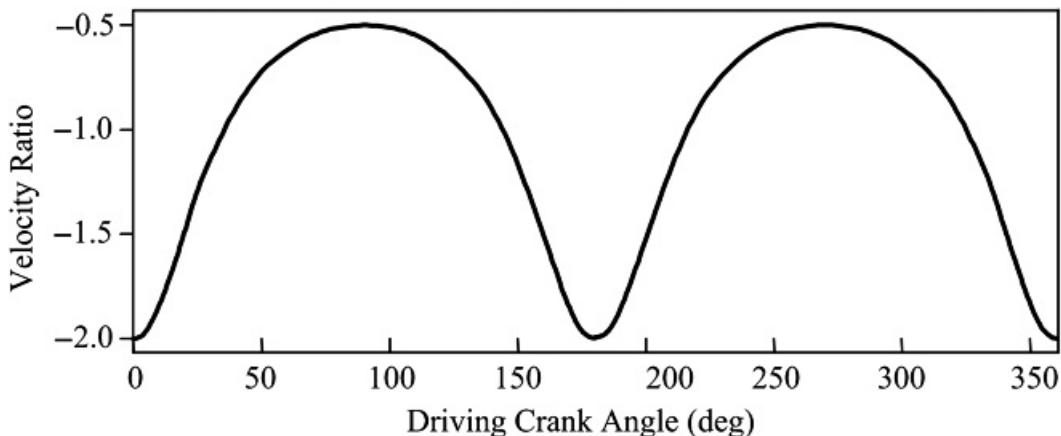


[Figure 8.23](#) Velocity ratio fluctuation for a universal joint with $\gamma = 120^\circ$. The negative values of the velocity ratio are an artifact of the way these angles are defined in [Figure 8.22](#). Examination of that figure indicates that θ_2 decreases when θ_1 increases. Looking from the driving shaft toward the driven shaft, this indicates that both shafts are rotating in the same direction.

Dual Universal Joints

By using two universal joints in a symmetric combination, it is possible to have the second joint cancel out the fluctuation generated by the first. This combination then produces a constant velocity action. If the joints are aligned so that axis 3 of the first coupling is parallel to axis 2 of the second, as shown in [Figure 8.24](#), then $\theta_1 = \theta_2$. Hence, using [Equation 8.9](#)

$$\begin{aligned}\cos \gamma &= \tan \theta_1 \tan \theta_2 \\ \cos \gamma &= \tan \theta'_1 \tan \theta'_2\end{aligned}\tag{8.11}$$

and

$$\tan \theta'_2 = \frac{\cos \gamma}{\tan \theta'_1} = \frac{\cos \gamma}{\tan \theta_2} = \frac{\cos \gamma \tan \theta_1}{\cos \gamma} = \tan \theta_1\tag{8.12}$$

Hence the output angle of the combined joint, θ'_2 , is always equal to the input angle θ_1 . The same relationship is true if the shafts are not angulated, as in [Figure 8.24](#), but are parallel and offset, as in [Figure 8.25](#). This is also a configuration of considerable practical importance. In fact, the drive shafts of almost all front-engine, rear-wheel-driven automobiles feature this arrangement.



Example 8.4

Analysis of Universal Joint of Rear-Wheel-Driven Car

A front engine, rear-wheel-driven automobile employs a drive shaft with two universal joints in the alignment of [Figure 8.25](#) to transmit torque from the output shaft of the gearbox to the differential. The differential is mounted on the rear axle, and the suspension is of the live axle type (solid rear axle). The universal joints accommodate movement of the rear axle permitted by the suspension. The differential shaft is nominally parallel to the gearbox shaft. However, the suspension setup maintains this relationship only to a good approximation. Also, some fore-aft rocking of the differential housing occurs because of elastic deflection and backlash in suspension components. The angle γ , as defined in [Figure 8.25](#), varies from 175° to 160° between the suspension stops. The error in γ at the rear universal joint is estimated to be $\pm 0.5^\circ$. Estimate the maximum percentage fluctuation in the velocity ratio between the gearbox shaft and the differential shaft.

Solution

Since the error in γ is small, we should be able to use a small-angle approximation with acceptable accuracy.

[Equation 8.11](#) becomes

$$\cos \gamma = \tan \theta_1 \tan \theta_2$$

and

$$\cos(\gamma + \delta\gamma) = \tan \theta'_1 \tan \theta'_2$$

or

$$\cos \gamma - \delta\gamma \sin \gamma = \tan \theta'_1 \tan \theta'_2$$

Noting that

$$\tan \theta'_1 = \tan \theta_2 = \frac{\cos \gamma}{\tan \theta_1}$$

$$\cos \gamma - \delta\gamma \sin \gamma = \frac{\cos \gamma \tan \theta'_2}{\tan \theta_1}$$

or

$$\tan \theta'_2 = \tan \theta_1 (1 - \delta\gamma \tan \gamma)$$

Differentiation of this expression with respect to time gives

$$\dot{\theta}_2 \sec^2 \theta_2 = \dot{\theta}_1 \sec^2 \theta_1 (1 - \delta y \tan \gamma)$$

Using

$$\sec^2 \theta_2 = 1 + \tan^2 \theta_2 = 1 + \tan^2 \theta_1 (1 - \delta y \tan \gamma)^2$$

the velocity ratio is given by

$$\frac{\dot{\theta}_2}{\dot{\theta}_1} = \frac{1 - \delta y \tan \gamma}{\cos^2 \theta_1 [1 + (\tan^2 \theta_1 (1 - \delta y \tan \gamma)^2)]} = \frac{1 - \delta y \tan \gamma}{1 - 2\delta y \tan \gamma \sin^2 \theta_1}$$

Here the small-angle approximation has been used by dropping the δy^2 term in the expansion of the denominator. This expression may be further simplified by multiplying top and bottom by the factor $1 + 2\delta y \tan \gamma \sin^2 \theta_1$ and again applying the small angle approximation. Then

$$\frac{\dot{\theta}_2}{\dot{\theta}_1} = (1 + 2\delta y \tan \gamma \sin^2 \theta_1)(1 - \delta y \tan \gamma) = 1 - \delta y \tan \gamma + 2\delta y \tan \gamma \sin^2 \theta_1$$

or

$$\frac{\dot{\theta}_2}{\dot{\theta}_1} = 1 - \delta y \tan \gamma \cos 2\theta_1$$

It is clear from this expression that the maximum magnitude of the velocity ratio, R , is $1 + \delta y \tan \gamma$, and the minimum value is $1 - \delta y \tan \gamma$. Applying the values given in this particular problem, $\tan \gamma$ will be at a maximum when $\gamma = 160^\circ$ and $\delta y = 15^\circ$. Then

$$\delta y = 0.5 \times \pi / 180 = 0.00873 \text{ rad.}$$

$$\tan \gamma = -0.364.$$

so

$$R_{\max} = 1.0032 \text{ and } R_{\min} = 0.9968$$

The maximum percentage fluctuation of the velocity ratio is 0.32 percent.

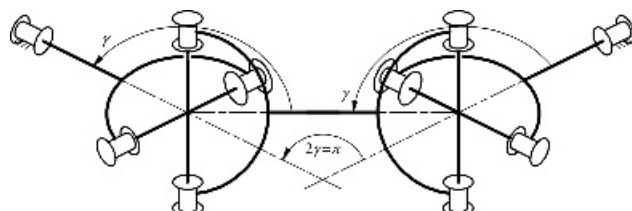


[Figure 8.24](#) Dual universal joints arranged symmetrically. The combination provides a true constant velocity coupling, as described in the text.

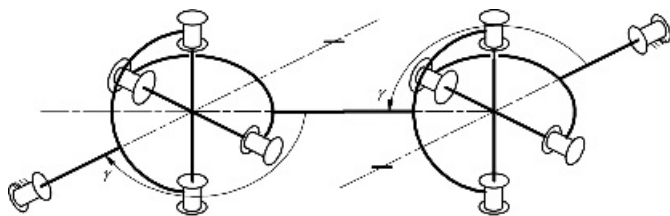


[Figure 8.25](#) Dual universal joints on parallel, offset shafts. This arrangement also gives motion transfer between the input and output shafts at a constant velocity ratio.



8.3 Constant-Velocity Couplings

As may be seen in the preceding subsections, universal joints are not constant velocity joints. Although paired universal joints can function as constant-velocity joints, the arrangement must satisfy special geometric conditions. There is a need for single joints that can provide true constant-velocity action and that can accommodate changes of alignment such as plunging (movement in the direction of the shaft axis) of one shaft relative to the other.

8.3.1 Geometric Requirements of Constant-Velocity Couplings

It has been shown that an essential requirement for constant-velocity transfer of rotation between nonaligned shafts is that the coupling mechanism be symmetric relative to the plane that bisects the spatial angle between the shaft axes [4]. Examination of [Figure 8.24](#) indicates that this condition is satisfied by the double universal joint. However, in many situations, such as the drive trains of front-wheel-driven automobiles, a more compact joint is needed.

8.3.2 Practical Constant-Velocity Couplings

A common commercial constant-velocity coupling uses bearing balls moving in shaped races between inner and outer journals to transmit torque. The races are shaped so that the centers of the balls are always in the plane of symmetry. The arrangement is shown in [Figure 8.26](#).

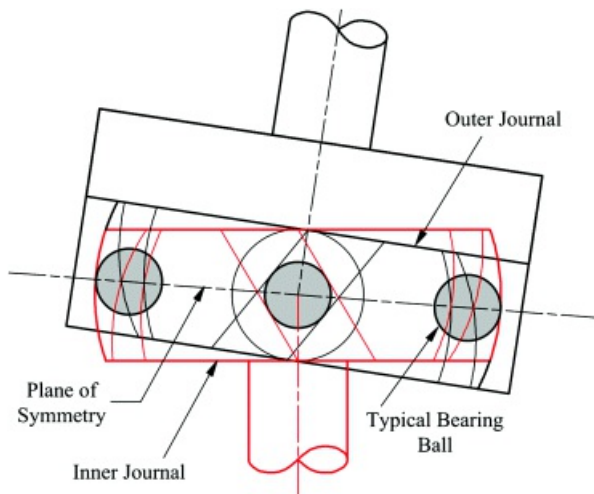


[Figure 8.26](#) Ball-type constant-velocity coupling. The balls, six in the configuration shown, roll in races cut in the inner and outer journals.

[Figure 8.26](#) shows a ball-type constant-velocity coupling with six balls, and [Figure 8.27](#) shows a photograph of the coupling. The inner journal has a spherical outer surface with six equally spaced races with semicircular cross sections cut into it. The centerline of each race is a great circle of a neutral sphere that is slightly larger than the surface of the journal. The planes of the great circles are inclined at equal angles to the journal axis, and alternate races are cut at opposing angles. The outer journal has a spherical inner surface slightly larger than the neutral sphere. Races are also cut into it with their centerlines being great circles in the neutral sphere. They are cut at the same angle to the journal axis as the races in the inner journal, and successive races are again cut at opposing angles. The joint is assembled with each ball rolling in inner and outer races that are at opposing angles.

Therefore, the ball center is always at the intersection of the race centerlines. This ensures that all ball centers lie in a common plane at all times. This plane bisects the angle between the two journal axes and is, therefore, a plane of symmetry. Since the ball centers all lie in a common plane of symmetry at all times, the symmetry condition is satisfied and the joint transmits motion with constant velocity.



[Figure 8.27](#) Ball-type constant-velocity coupling used in front-wheel-driven automobile.

This type of joint can be made relatively compact and is commonly used in automotive drive shafts to allow smooth torque transmission despite the movements of the wheels permitted by the suspension.



8.4 Automotive Steering and Suspension Mechanisms

8.4.1 Introduction

Automotive steering and suspension mechanisms are primarily designed as separate, planar mechanisms acting in different planes. However, they are interconnected because they have common links. Also, both have modifications that make them spatial linkages. For example, the axis about which the wheel turns in response to movements of the steering linkage is not vertical. The inclination of the axis, called camber, creates a tendency for the steering to center itself at low speed, since it results in the vehicle body being raised slightly whenever the wheels are turned away from the straight-ahead position. Camber is not effective in providing centering at high speed. However, another modification, called *caster*, provides this action. The wheel steering axis is moved forward relative to the wheel a little distance. The distance the wheel rotation axis trails the steering axis is the caster.

The interconnection, together with modifications such as camber that create a truly spatial character, can lead to undesirable dynamic interactions. It is very undesirable for suspension movements to be felt through the steering, or for the position of the steering linkage to influence suspension performance.

8.4.2 Steering Mechanisms

From a purely kinematic viewpoint, the essential geometry of an automotive steering linkage is that the axes of the front wheels should, at all times, be concurrent at the axis of the rear wheels. It is possible to synthesize a four-bar linkage that will constrain the front wheel axes to approximate this condition very closely. This is the basis of the Ackermann steering gear. As can be seen from [Figure 8.28](#), it is necessary that the front wheels be “toed out” to an increasing extent as the radius of curvature of the vehicle path is reduced.

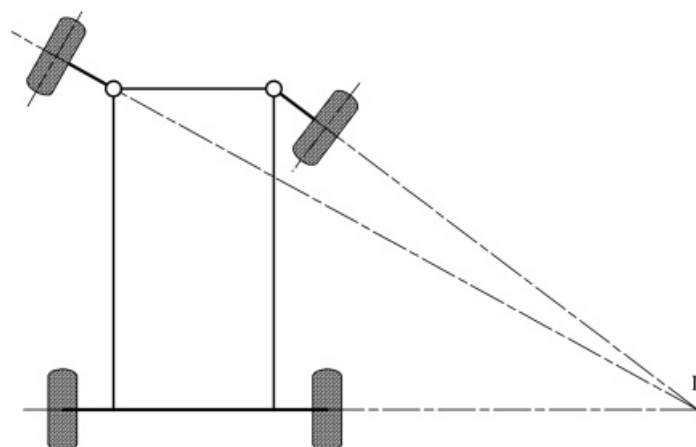


[Figure 8.28](#) The Ackermann steering condition. Since the axes of all four wheels meet at a common instantaneous center, the wheels can roll without any lateral scuffing action. This is the ideal steering geometry at low speeds.

However, a close approximation to Ackermann geometry is often not used on modern automobiles, particularly on high-performance vehicles and racecars. The reason is that steering at high speed is a dynamic problem. To change direction, it is necessary to develop lateral forces at the tire contacts with the road. The production of lateral force requires some slip between the wheel and the road. By using less toe-out than would be required by the Ackermann geometry, more lateral slip is generated at the outside front wheel, which also carries a greater share of the vehicle weight due to dynamic load transfer and is, therefore, able to generate more lateral force. Some racecar steering setups go so far as to reverse the kinematically ideal relationship by actually toeing the front wheels in by a small amount during turns. This very aggressive geometry produces very strong cornering action at the expense of tire wear, which is not such a concern in a race over a limited distance as it is in general automotive use.

Ackermann action, or any other desired relationship between the steering angles of the wheels, can be adequately approximated by an eight-bar steering linkage such as that shown in [Figure 8.29](#). Since the wheels move vertically

with suspension travel, it is necessary for the joints at the ends of the tie rods to be spherical joints. Thus, the linkage becomes spatial, although still approximating the designed planar behavior.

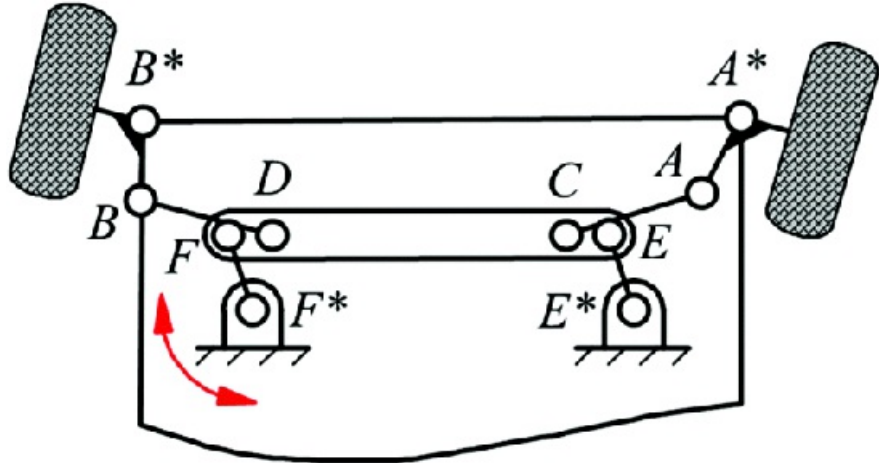


[Figure 8.29](#) A typical steering gear arrangement. The Pitman arm, F^*F , is turned by the steering column. The four-bar loop E^*EFF^* is a parallelogram. E^*E is the idler arm, and EF is the relay rod. AC and BD are the tie rods, and A^*A and B^*B , which are fixed to the structures that carry the stub axles, are called the steering arms. The steering arms turn about the steering knuckles A^* and B^* . Note that the linkage is bilaterally symmetric about the centerline of the vehicle.

In modern cars, it is more common to use a linear input to the steering linkage. This is typically produced by a rack-and-pinion type of steering box. This linear input is applied directly to the relay rod. This arrangement may be thought of as the limiting case of the mechanism in [Figure 8.29](#) as the arms O_EE and O_FF become infinitely long, producing the configuration of [Figure 8.30](#). It has the advantages of being simpler: six members versus eight, more compact, and potentially lighter.



Example 8.5

Analysis of Rack-and-Pinion Type Steering Linkage

A steering linkage for an automobile is shown in [Figure 8.30](#). The wheelbase of the automobile (distance between front and rear wheel axes) is $q = 100$ in. The distance between the steering knuckles is $p = 50$ in. The length of the steering arm is $a = 3$ in, and it is inclined at angle $\theta = 9^\circ$ to the plane of the wheel. The length of the tie rods is $b = 10$ in. When the wheels are in the straight-ahead position, the inner ends of the tie rods are distant $r = 10.08$ in from the steering knuckles in the lateral direction, and $s = 9.72$ in in the longitudinal direction.

Plot the x and y coordinates of the intersection of the front wheel axes for increments of 0.1 in of the rack displacement, u , in the range $0 < u \leq 1.5$ in, where the reference frame has its origin at the middle of the rear axle, as shown. The x coordinate can be interpreted as the radius of curvature of the path followed by the vehicle, and the y coordinate is the error from perfect Ackermann geometry. As indicated in [Figure 8.28](#), if the Ackermann condition were exactly met, y would be zero at all times. Also calculate the angles of the inner and outer front wheels relative to the straight-ahead position throughout this range.

Solution

The linkage can be analyzed as two slider-crank linkages acting in parallel with a common input, u , applied to the sliders. Resolving in the x and y directions respectively, we have for the right side

$$a \cos \theta + b \cos \mu = r - u \quad (8.13)$$

$$a \sin \theta + b \sin \mu = s \quad (8.14)$$

where μ is the tie rod angle as shown in [Figure 8.30](#).

Similarly, for the left side

$$a \cos \phi + b \cos \nu = r - u \quad (8.15)$$

$$a \sin \phi + b \sin \nu = s \quad (8.16)$$

μ may be eliminated from [Equations 8.13](#) and [8.14](#) by segregating the μ terms on one side of each equation, squaring both sides of both equations, and adding to give

$$b^2 = (r + u - a \cos \theta)^2 + (s - a \sin \theta)^2$$

or

$$b^2 = r^2 + s^2 + a^2 + u^2 + 2ru - 2au \cos \theta - 2ar \cos \theta - 2as \sin \theta \quad (8.17)$$

This equation has the form

$$P \cos \theta + Q \sin \theta + R = 0 \quad (8.18)$$

where

$$\begin{aligned} P &= 2as(u - r) \\ Q &= 2ass \\ R &= b^2 - a^2 - r^2 - s^2 - u^2 - 2ru \end{aligned} \quad (8.19)$$

Hence the standard solution of [Table 3.1](#) may be applied to obtain values of ϕ corresponding to given values of u . Two values of ϕ are obtained for each value of u , one positive and one negative. Only the negative value is consistent with the configuration shown in [Figure 8.30](#), so the positive value is discarded.

Similarly, elimination of V from [Equations 8.15](#) and [8.16](#) gives

$$b^2 - (r - u - a \cos \phi)^2 + (s - a \sin \phi)^2$$

or

$$b^2 = r^2 + s^2 + a^2 + u^2 - 2ru + 2au \cos \phi - 2ar \cos \phi - 2as \sin \phi \quad (8.20)$$

This equation has the form

$$P \cos \phi + Q \sin \phi + R = 0 \quad (8.21)$$

where

$$\begin{aligned} P' &= 2as(r - u) \\ Q &= 2ass \\ R &= b^2 - a^2 - r^2 - s^2 - u^2 - 2ru \end{aligned} \quad (8.22)$$

for which the solution is also given by [Table 3.1](#). Values of ϕ for incremental values of u throughout the specified range can be calculated. As was the case for ψ , two values of ϕ are obtained for each value of u , one positive and one negative. Only the negative solution is consistent with the configuration drawn in [Figure 8.30](#), so the positive solution is discarded.

Now $\gamma = \pi/2 - \theta - \alpha$, and $\delta = \phi + \alpha - \pi/2$, where γ and δ are the steering angles of the inner and outer front wheels, as shown in [Figure 8.30](#), and values of γ and δ may now be calculated. The resulting values of γ and δ throughout the range of values of u are listed in [Table 8.1](#). Also, γ and δ determine the location of the intersection, I , of the axes of the wheels

$$\tan \gamma = \frac{\delta - \gamma}{x - p/2} \quad \tan \delta = \frac{\delta - \gamma}{x + p/2} \quad (8.23)$$

Hence,

$$(x - p/2) \tan \gamma = (x + p/2) \tan \delta$$

which, when solved for x , gives

$$x = \frac{y}{2} \left(\frac{\tan y + (\tan \delta)}{\tan y - \tan \delta} \right) \quad (8.24)$$

Substitution for x into either of [Equation 8.23](#) allows solution for y to be

$$y = q - p \left(\frac{\tan y \tan \delta}{\tan y - \tan \delta} \right)$$

The results are tabulated in [Table 8.1](#) and are plotted in [Figure 8.31](#). It may be seen that the linkage gives a reasonable approximation to the Ackermann condition, except at very large wheel angles.

[Table 8.1](#) Numerical Values Obtained by Solution of Example 8.5

u	gamma	delta	x	y
0.2	4.13	3.99	1475.17	-4.65
0.3	6.25	5.94	973.19	-3.91
0.4	8.43	7.87	718.74	-2.86
0.5	10.67	9.79	563.51	-1.50
0.6	12.99	11.68	457.89	0.17
0.7	15.38	13.56	380.59	2.18
0.8	17.88	15.43	320.98	4.52
0.9	20.50	17.29	273.11	7.23
1.0	23.28	19.13	233.42	10.34
1.1	26.25	20.98	199.57	13.90
1.2	29.50	22.81	169.98	17.99
1.3	33.13	24.65	143.39	22.74
1.4	37.38	26.48	118.66	28.44
1.5	42.87	28.31	94.09	35.86

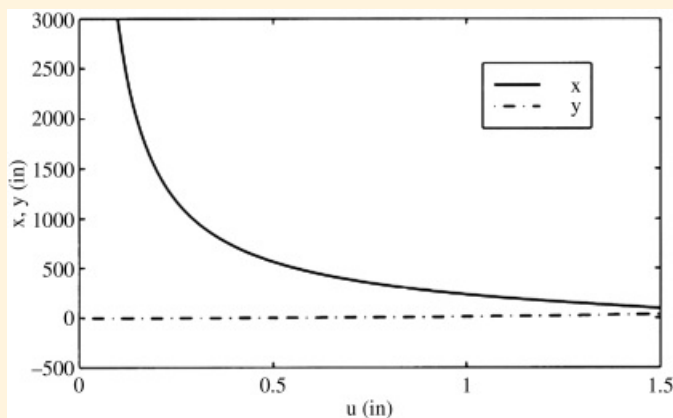


[Figure 8.31](#) The coordinates of the intersection of the front wheel axes, i , plotted against the rack displacement, u . x approximates the radius of curvature of the vehicle's path, and y is the error in

location of the intersection relative to the rear axle axis. That is, y is the deviation from the Ackermann condition. When $u = 0$, $x = \infty$ and $y = 0$. The values used in the plot are included in [Table 8.1](#).

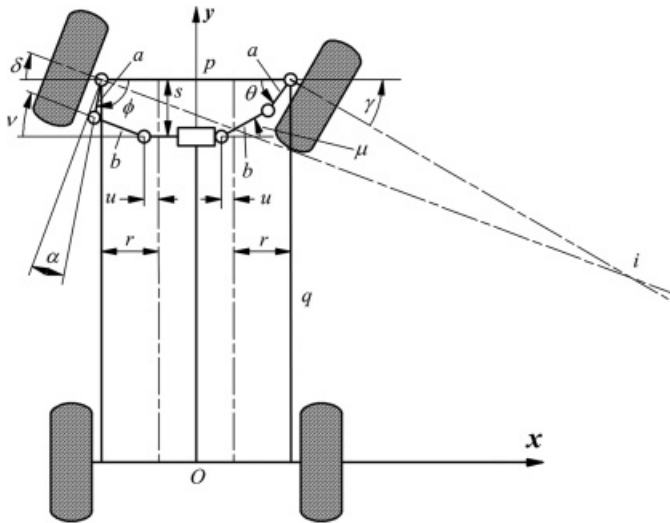


[Figure 8.30](#) The rack-and-pinion steering linkage geometry analyzed in Example 8.5. The position of the intersection of the front wheel axes as a function of the rack displacement, u , and the values of the wheel angles γ and δ are tabulated in [Table 8.1](#). The coordinates of i are plotted as a function of u in [Figure 8.31](#).

8.4.3 Suspension Mechanisms

An automotive suspension performs the function of a vibration filter, reducing the amplitudes of vibrations excited by geometric variations in the road surface. This is the function of the spring damper arrangements that are integral components of the suspension. Analysis of this vibration filtering action is normally covered in texts on mechanical vibrations and is beyond the scope of this book. Here we confine ourselves to the kinematic requirements of suspension mechanisms.

Automotive suspension mechanisms must allow controlled, single-degree-of-freedom motion of the wheel axis relative to the body of the vehicle. The travel allowed needs to be as close as possible to normal to the plane of the ground at the wheel contact. Also, it is necessary for the suspension mechanism to maintain the plane of the wheel as perpendicular as possible to the ground at all times. This is because automobile tires are designed to develop maximum lateral force when they are in the upright position, as opposed to motorcycle tires, which must function in inclined positions during hard cornering. Since the center of mass of an automotive vehicle is almost always higher than the wheel axes, there is a tendency for the body to roll toward the outside of a turn. Another objective of suspension design is to attempt to control this tendency to roll.

Automotive steering and suspension mechanisms are truly spatial mechanisms. However, their initial design generally rests on planar principles.

When viewed from the front, the instantaneous center of motion of the body of the vehicle relative to the ground is called the roll center. The location of the roll center for a typical independent suspension geometry is shown in [Figure 8.32](#). The center is located by using the Kennedy-Aronhold theorem as described in [Chapter 6](#).

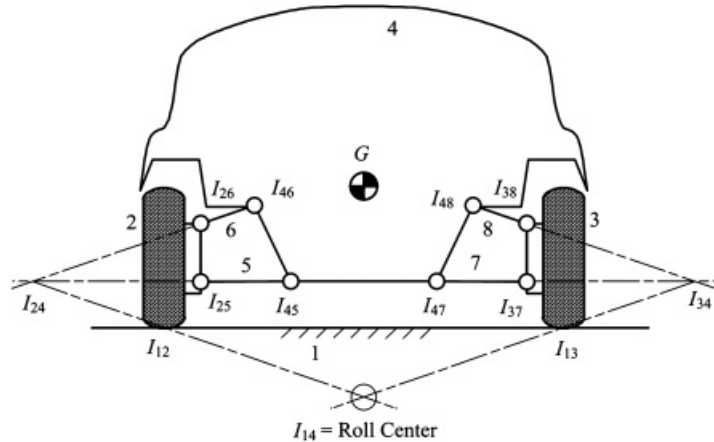


Figure 8.32 Roll-center geometry for an automotive independent suspension geometry. The roll center is the instantaneous center of relative motion of the vehicle body and the ground.

The roll center moves as the position of the vehicle body moves. Whereas the roll center will be on the vehicle centerline for a road vehicle at rest on a level surface, it will shift off that line in the asymmetric positions that result from cornering. There is also a roll center for the rear suspension, so one can think of a roll axis, which is the line that passes through both roll centers.

The location of the roll center relative to the center of mass of the vehicle governs the effect of inertial forces due to cornering on the system. If the vertical distance between the roll center and the center of mass is large, the moment produced by lateral acceleration will be large. A suspension geometry that brings the roll center progressively closer to the center of mass with increasing body roll might be attractive because, if the action of the suspension springs was linear, it would lead to increasing roll stiffness with increasing roll angle.

Suspension designers think of the roll center as the point of transfer of the inertial force between the sprung and unsprung masses of the vehicle. The unsprung mass is the wheels and suspension members attached to them whose position is directly determined by the road surface. The sprung mass is everything that moves when the springs are deflected.



8.5 Indexing Mechanisms

Indexing mechanisms are intermittent motion mechanisms that hold position alternately with a timed, unidirectional motion of the output member. This is distinct from other types of intermittent motion mechanisms such as dwell cams, which alternate forward and return motion with holding position. The output member of an indexing mechanism always advances in the same direction. Indexing mechanisms are practically important in such applications as weaving looms, in advancing work pieces in repetitive manufacturing operations, and in many instrument mechanisms.

8.5.1 Geneva Mechanisms

Geneva mechanisms are the most common type of indexing mechanism. Geneva mechanisms come in many varieties, both planar and spherical. When advancing, it is kinematically similar to an inverted slider-crank. When holding position, it functions as a simple journal bearing.

The name Geneva mechanism originated because these mechanisms were used in mechanical watch and clock movements in the days when mechanical movements were dominant, and Switzerland was the world center of the industry.

A simple example of a Geneva mechanism is shown in [Figure 8.33](#). The pin, P , on the driving wheel engages the slots in the star-shaped driven wheel to advance the driven wheel one-quarter turn for every rotation of the driving wheel. In between the advance movements, the eccentric cylindrical journal surfaces cut into the star wheel engage with the journal surface on the driving wheel to lock the star wheel in position, although the driving wheel continues to rotate. The centerline of the slot must be tangent to the circle, with radius r , described by the center of the pin at the position in which the pin enters or leaves the slot. If this condition is not satisfied, there will be infinite acceleration at the beginning of advancement and infinite deceleration at the end. This condition dictates that the center distance of the two wheels should be $\sqrt{2}r$. It also requires that the outer radius of the star wheel be r . The radius of the journal surfaces is flexible. The centers of the cylindrical cutouts on the star wheel lie on a circle with radius $\sqrt{2}r$.

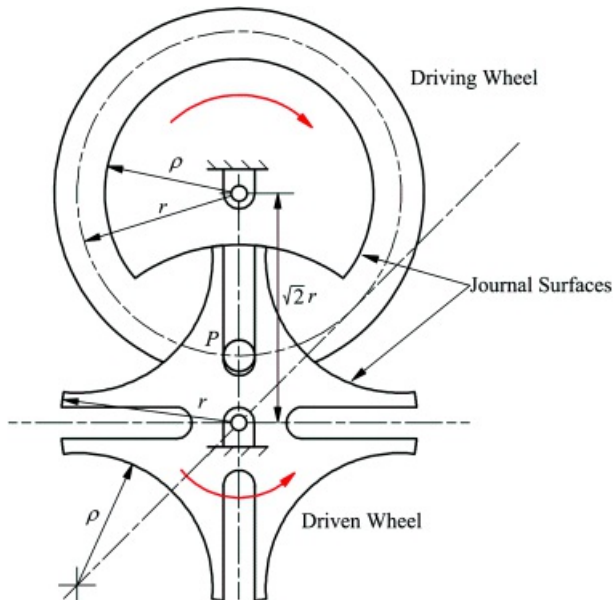


[Figure 8.33](#) A four-station Geneva mechanism. The output member is the star wheel. The star wheel is advanced by the pin in the input wheel. The star wheel is advanced one-quarter of a revolution counterclockwise for every revolution of the input wheel. The advance movement occurs during one-quarter of a cycle with the star wheel being locked by the journal surface on the input wheel for the other three-quarters of the cycle.

During the advancing phase of the cycle, the mechanism is kinematically equivalent to an inverted slider-crank.

One of its attractions is that it smoothly accelerates and then decelerates the star wheel.

The motion of the star wheel may be analyzed by reference to [Figure 8.34](#). Resolving the sides of the triangle whose vertices are the two shaft axes and the pin axis in the vertical and horizontal directions

$$\begin{aligned} r \sin \theta &= x \sin \phi \\ r \cos \theta + x \cos \phi &= \sqrt{2}r \end{aligned} \quad (8.25)$$

Elimination of x by substitution from the first of these equations into the second gives

$$\cos \phi + \frac{\sin \theta}{\tan \phi} = \sqrt{2}$$

after canceling the common factor r . Rearrangement of this expression gives

$$\tan \phi = \frac{\sin \theta}{\sqrt{2 - \cos \theta}} \quad (8.26)$$

or

$$\phi = \tan^{-1} \left(\frac{\sin \theta}{\sqrt{2 - \cos \theta}} \right) \quad (8.27)$$

Differentiation of [Equation 8.26](#) with respect to time followed by simplification gives

$$\dot{\phi}(1 + \tan^2 \phi) = \dot{\theta} \frac{(\sqrt{2 \cos \theta} - 1)}{(\sqrt{2 - \cos \theta})^2}$$

Substitution for $\tan \phi$ from [Equation 8.26](#) gives, after rearrangement and simplification

$$\dot{\phi} = \dot{\theta} \frac{(\sqrt{2 \cos \theta} - 1)}{(3 - 2\sqrt{2 \cos \theta})} \quad (8.28)$$

Differentiation again with respect to time gives, after simplification,

$$\ddot{\phi} = \ddot{\theta} \left(\frac{\sqrt{2 \cos \theta} - 1}{3 - 2\sqrt{2 \cos \theta}} \right) - \dot{\theta}^2 \frac{\sqrt{2 \sin \theta}}{(3 - 2\sqrt{2 \cos \theta})^2}$$

In the usual case in which the driving wheel is driven at constant angular velocity, the first term disappears and

$$\dot{\phi} = \frac{\theta^2}{\sqrt{2}\sin\theta} \cdot \frac{\sqrt{2}\sin\theta}{(3 - 2\sqrt{2}\cos\theta)^2} \quad (8.29)$$

[Equations 8.27](#), [8.28](#) and [8.29](#) are plotted versus θ (in degrees) in [Figure 8.35](#). $\dot{\phi}$ is plotted in radians. Of course, $\dot{\phi}$ varies from -45° to 45° during the advancement. The angular velocity curve is actually $\dot{\phi}/\dot{\theta}$, and the angular acceleration curve is $\ddot{\phi}/\dot{\theta}^2$.

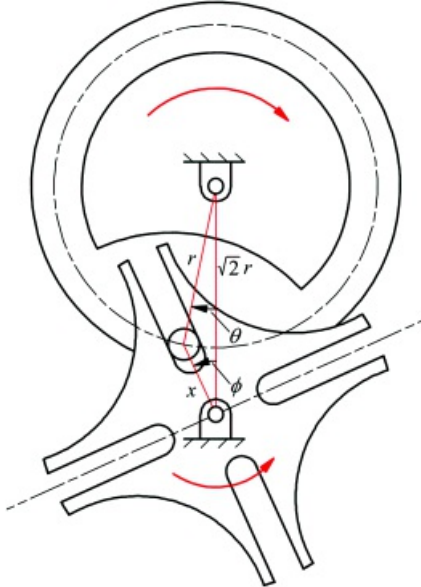


[Figure 8.34](#) Kinematic modeling of the Geneva mechanism of [Figure 8.33](#). Θ is the angle of rotation of the driving wheel, measured from the line of centers Φ is the angle of rotation of the star wheel.

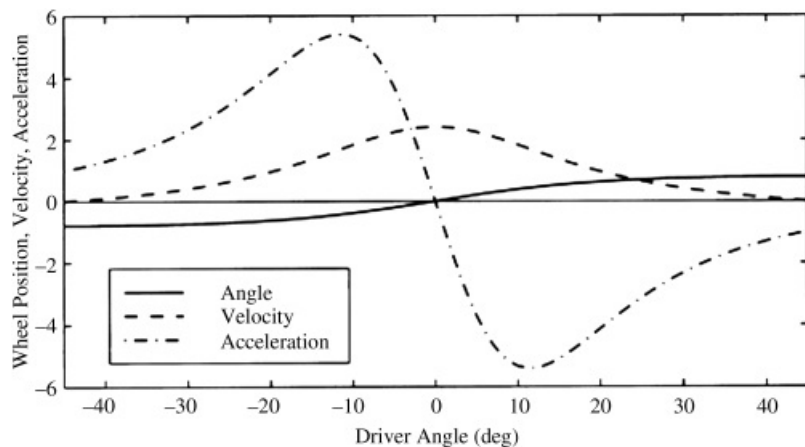


[Figure 8.35](#) Position, velocity, and acceleration of the driven wheel of the Geneva mechanism shown in [Figures 8.33](#) and [8.34](#) during the advancement phase of the motion cycle. The angular position of the star wheel is in radians. The angular velocity and acceleration curves are respectively normalized to the driver angular velocity and driver angular velocity squared.

As can be seen from [Figure 8.35](#), the velocity and acceleration curves are smooth and well behaved, but the derivative of the acceleration (jerk) is infinite at the beginning and end of the advancement. So far, we have considered only the simplest version of the Geneva mechanism: the four-station planar variety. The number of stations is the number of slots in the star wheel and may, in principle, be any number, although the geometric lower limit is three. There is also a practical upper limit at which the journal surfaces on the star wheel become too short to effectively lock the output between advancements. The number of pins on the driving wheel is usually one, but drivers with two or more are possible.

The essential geometry for relating the number of stations to the duration of the advancement is shown in [Figure 8.36](#). Here α is the angle between the slot centerline and the line of centers of the two wheels at the moment of engagement or disengagement of the pin. That is, α is half the angle between successive slots, or $360^\circ/(2N)$, where N is the number of stations. As already noted, the slot axis must be tangent to the circle traversed by the pin center at these positions in order to avoid infinite accelerations. This determines the relationship between N and the duration of the advancement, which is $\pi - 2\alpha$ by inspection of the figure. Consequently, the duration of the advancement increases with the number of stations, approaching a limit of 180° as the number of stations becomes very large. This has the advantage of making the advancement motion gentler but the possible disadvantage of decreasing the duration of the period for which the output is stationary. The trade-off between these effects and the desirability of avoiding gearing downstream of the indexing mechanism determine the choice of the number of stations. Gearing downstream of an indexing mechanism should be avoided due to the inaccuracy and uncertainty in position introduced by necessary backlash in the gear train. Gear backlash is not usually a problem if the gears are in uniform motion. However, the discontinuous motion output from an indexing mechanism and consequent reversals of acceleration result in slapping across the backlash interval. Hence, any speed reduction should be done upstream of the indexing mechanism.

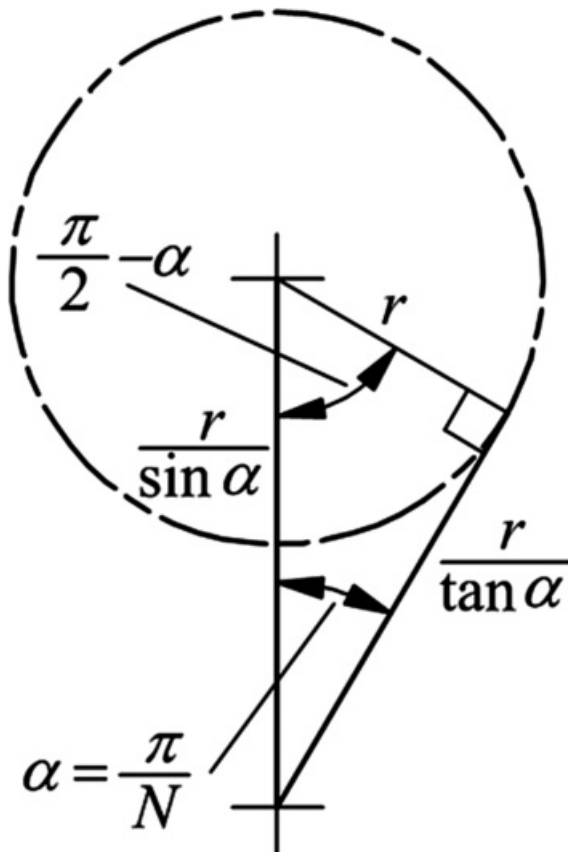


[Figure 8.36](#) Critical geometry for a Geneva mechanism with N stations. α is the angle between the slot centerline and the line of centers at the moment of engagement of the pin; α is half the angle between successive slots on the star wheel.

The number of stations also determines the ratio of the center distance of the wheel axes to the pin radius and the outside diameter of the star wheel. By inspection of [Figure 8.36](#), the former ratio is $1/\sin \alpha$ and the latter is $1/\tan \alpha$.

Noting that $\alpha = \pi/N$, [Equations 8.27–8.29](#), respectively, become for this more general case

$$\phi = \tan^{-1} \left(\frac{\sin \alpha \sin \theta}{1 - \sin \alpha \cos \theta} \right) \quad (8.30)$$

$$\dot{\phi} = \dot{\theta} \sin \alpha \left(\frac{\cos \theta - \sin \alpha}{1 + \sin^2 \alpha - 2 \sin \alpha \cos \theta} \right) \quad (8.31)$$

$$\ddot{\phi} = -\dot{\theta}^2 \cdot \frac{\sin \alpha \cos^2 \alpha \sin \theta}{(1 + \sin^2 \alpha - 2 \sin \alpha \cos \theta)^2} \quad (8.32)$$

Spherical Geneva mechanisms allow indexed motion transfer between angulated shafts. More important, a large number of stations can be accommodated without losing positive locking action between advances.



Example 8.6 Analysis of Geneva Wheel

An indexing drive is to be driven by a synchronous electric motor turning at 360 rpm (the speed of a synchronous motor is locked to the alternating-current cycle frequency and so is essentially constant). The single pin driver is to turn a six-station Geneva wheel. Compute the following

- The number of advances per second
- The angle through which the Geneva wheel advances during every revolution of the driving wheel
- The duration in seconds of the dwell in the output motion
- The peak angular velocity of the output shaft
- The peak angular acceleration of the output shaft

Solution

- The number of advances per second is the number of revolutions of the driver per second, which is $360/60 = 6$.
- The angle advanced is $2\alpha = 360^\circ/N = 60^\circ$, with N , the number of stations, being 6 in this case. Hence $\alpha = 30^\circ$.
- The fraction of the cycle during which the output is locked (dwelling) is

$$\lambda = \frac{180 - 2\alpha}{360}$$

with α in degrees giving $\lambda = 1/3$. The duration of the complete cycle is $T = 1/6$ s from part (a). Hence the duration of the dwell is

$$t_d = \lambda T = 1/18 = 0.0555 \text{ s}$$

- Referring to [Equation 8.32](#), $\dot{\theta}$ is at its maximum value when $\theta = 0$. Also, for $N = 6$

$$\sin \alpha = 0.5$$

so, substituting this value and $\theta = 0$ in [Equation 8.31](#)

$$\dot{\theta}_{max} = \dot{\theta}$$

$\dot{\theta}$ is the angular velocity of the drive wheel so

$$\dot{\theta} = 2\pi \times 6 = 37.70 \text{ rad/s}$$

Therefore

$$\dot{\phi}_{\text{max}} \approx 37.70 \text{ rad/s}$$

Note that ϕ is positive in the CCW direction and θ is positive in the CW direction (see [Figure 8.34](#)). Therefore the positive values for both ϕ and θ indicate that the star wheel rotates in the opposite direction to the driver.

- e. It is necessary to determine the value of θ that maximizes $\dot{\phi}$. A straightforward way to do this would be to plot [Equation 8.32](#) in the same way as in [Figure 8.35](#), but with $\alpha = 30^\circ$, and the angle θ at which it occurs could then be read directly from the plot.

Alternatively, we can differentiate [Equation 8.32](#) to identify the extrema of $\dot{\phi}$. Noting that $\ddot{\theta}$ is constant

$$\frac{d\dot{\phi}}{d\theta} = \frac{-\dot{\theta}^2 \sin \alpha \cos^2 \alpha}{(1 + \sin^2 \alpha - 2 \sin \alpha \cos \theta)^3} [(1 + \sin^2 \alpha - 2 \sin \alpha \cos \theta) \cos \theta - 4 \sin \alpha \sin^2 \theta]$$

and so

$$\frac{d\dot{\phi}}{d\theta} = 0$$

when

$$(1 + \sin^2 \alpha) \cos \theta - 2 \sin \alpha \cos^2 \theta - 4 \sin \alpha \sin^2 \theta = 0$$

Replacement of $\sin^2 \theta$ by $1 - \cos^2 \theta$ and rearrangement of the equation gives

$$\cos^2 \theta + \gamma \cos \theta - 2 = 0$$

where

$$\gamma = \frac{1 + \sin^2 \alpha}{2 \sin \alpha} \quad (8.33)$$

The preceding equation can be treated as a quadratic equation in the variable $\cos \theta$. Solving for $\cos \theta$

$$\cos \theta = \frac{-\gamma \pm \sqrt{\gamma^2 + 8}}{2}$$

It is possible to show that only the positive value of the square root gives a value of $\cos \theta$ with magnitude between 0 and 1 in the allowable range of π ($0 < \alpha < 60^\circ$), so only that solution is valid. Hence, $\dot{\phi}$ is at a maximum when

$$\theta = \pm \cos^{-1} \left(\frac{-\gamma + \sqrt{\gamma^2 + 8}}{2} \right) \quad (8.34)$$

where the \pm sign now comes from inversion of the cosine, not from the quadratic solution. Equations 8.33 and 8.34 are of general validity for locating the maximal values of $\dot{\phi}$. In the present case, substituting $\sin \alpha = 0.5$ in Equation 8.33 gives

$$y = 1.25$$

Hence Equation 8.34 gives

$$\theta = \pm 22.9^\circ$$

Substitution of these values into Equation 8.32 gives

$$\frac{\ddot{\phi}}{\dot{\phi}^2} = \pm 1.372$$

Hence, since $\dot{\phi} = 37.70$ rad/s, the peak angular acceleration is 1,950 rad/s².



References

1. Artobolevsky, Ivan I. (1975), *Mechanisms in Modern Engineering Design*, MIR Publishers, Moscow.
2. Sumitomo Heavy Industries Material Handling Systems Co., Ltd, (2014) <http://www.shi.co.jp/shi-mb/english/product/jibcrane.html>.
3. Hain, Kurt, (1967), *Applied Kinematics, 2nd Ed*, Translated by D. P. Adams et al., McGraw-Hill, New York, NY.
4. Hunt, K. H., (1978), *Kinematic Geometry of Mechanisms*, Clarendon Press, Oxford.



Problems

Cognate Linkages

8.1 A coupler curve has the approximate straight-line section shown in [Figure P8.1](#). Design a four-bar linkage that will generate the portion of the curve shown. Describe the linkage in sufficient detail that it can be manufactured.

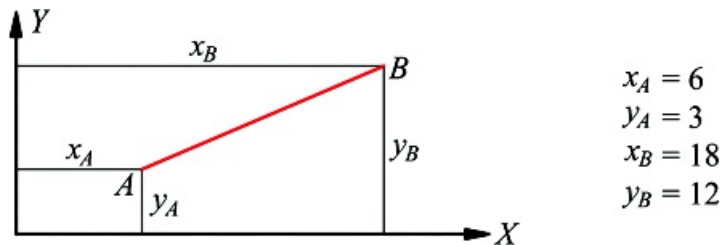


[Figure P8.1](#) Part of coupler curve for Problem 8.1.

8.2 Now solve Problem 8.1 if $x_A = 3$, $y_A = 3$, $x_B = 20$, and $y_B = 15$.

8.3 Determine the cognate linkages that will trace the same coupler curve as that traced by point C in [Figure P8.3](#).

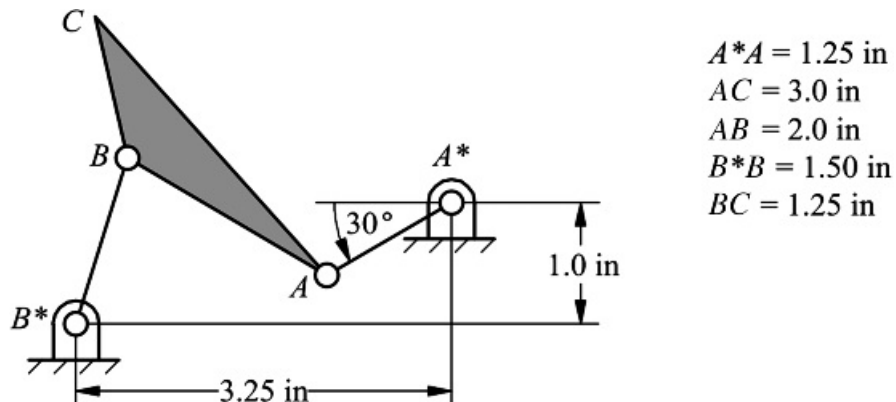


[Figure P8.3](#) Original linkage for Problem 8.3.

8.4 Determine the cognate linkages that will trace the same coupler curve as that traced by point C in [Figure P8.4](#).

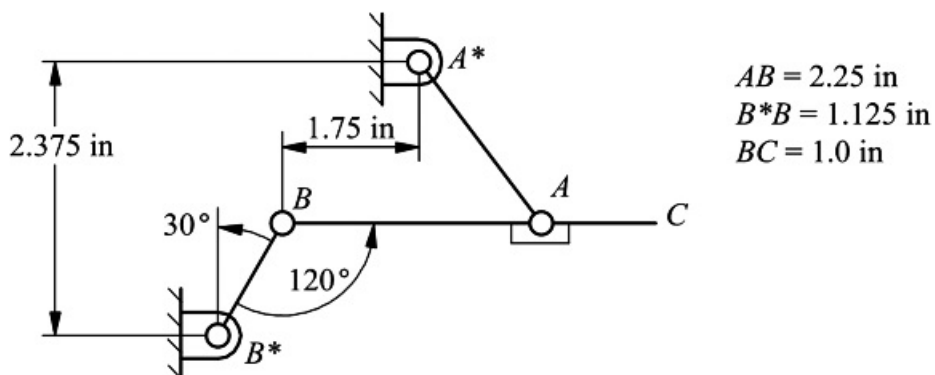


[Figure P8.4](#) Original linkage for Problem 8.4.

Spherical Four-Bar Linkages

8.5 A spherical four-bar linkage is shown in [Figure P8.5](#). If the angular velocity of link 2 is 100 rad/s (constant), find the angular velocity and angular acceleration of link 4 as a function of the rotation of link 2.

Plot the angular velocity and angular acceleration of link 4 for a full rotation of link 2. Make the calculations for the assembly mode shown in the figure.

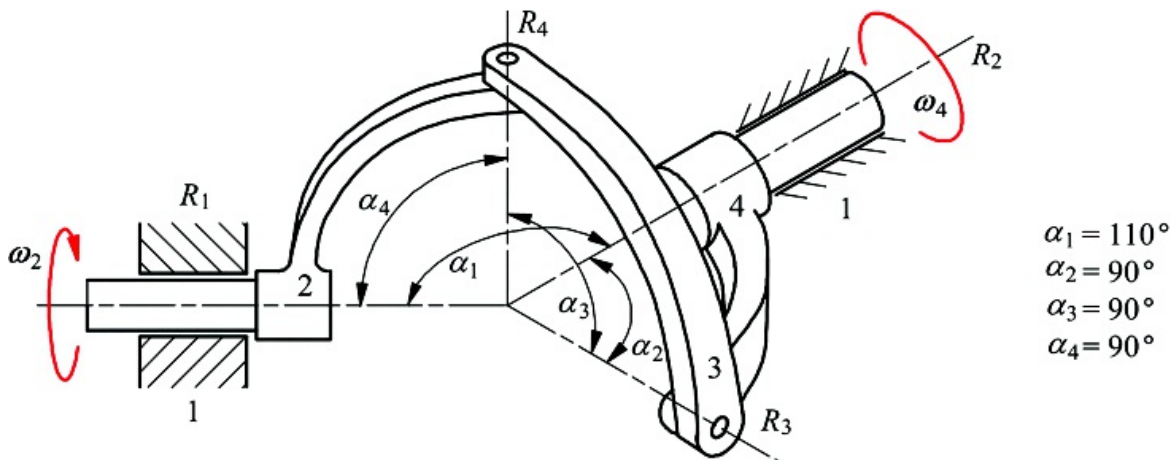


Figure P8.5 Spherical linkage for Problem 8.5.

8.6 Now solve Problem 8.5 if $\alpha_1 = 150^\circ$ but all other data remain the same.

Steering Linkages

8.7 The mechanism shown in [Figure P8.7](#) is used for a steering linkage for an automobile. The wheelbase is 110 in, and link F^*F is driven by the steering column. The toe-in angle (α) in [Figure 8.30](#) is 9°. If the link dimensions are given as shown, determine the y error in the Ackermann steering condition (see [Figures 8.28–8.31](#)) for a 10° CCW rotation of F^*F . Recall that the linkage E^*EFF^* is a parallelogram.

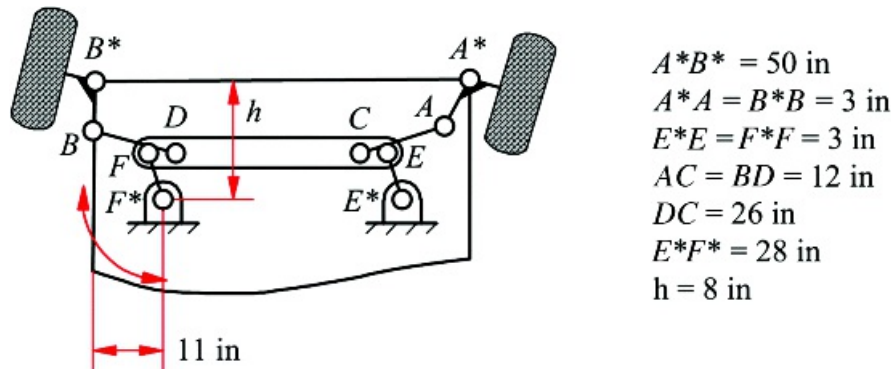


Figure P8.7 Steering linkage for Problem 8.7.

8.8 Write a computer program to analyze the steering linkage shown in Problem 8.7. If only h can change, determine the optimum value for h that will give the least error in y for the Ackermann steering condition for a $\pm 15^\circ$ rotation of $O_F F$.

8.9 In the rack-and-pinion mechanism shown in [Figure 8.30](#), the wheelbase is 125 in. If the link dimensions are as given below, plot the y error in the Ackermann steering condition as a function of the displacement u (see [Figure 8.28](#)) for a ± 1.5 -in displacement of u :

$$\begin{array}{ll} p = 55 \text{ in} & b = 12 \text{ in} \\ s = 3.5 \text{ in} & r = 11 \text{ in} \\ \angle C = 10^\circ & x = 6.0 \text{ in} \end{array}$$

8.10 A new subcompact automobile is being designed for rack-and-pinion steering. Assume that the wheelbase is 90 in. Determine the other dimensions such that the error in the Ackermann steering condition is as small as possible for a ± 1.5 -in displacement of the rack.

Geneva Mechanisms

8.11 The center distance between the driver and follower of a Geneva mechanism is to be 3 in. The driver is to rotate five revolutions for each rotation of the follower. The driving pin is to enter the slot tangentially so that there will be no impact load. Do the following

- a. Design the Geneva mechanism and draw it.
- b. Determine the angular velocity and acceleration of the Geneva wheel for one fifth of a revolution if the angular velocity of the driver is 100 rpm CCW. Plot the results.

8.12 Now solve Problem 8.11 if the input link rotates three revolutions for each rotation of the follower. Conduct the velocity and acceleration analysis for one third of a rotation.

Prerequisite Knowledge Needed for Chapter 9

A knowledge of the material on four-bar mechanisms from [Chapters 4](#) and [5](#), a knowledge of the material on special mechanisms from [Chapter 8](#), and a familiarity with linear algebra and solution of simultaneous nonlinear equations.



9.1 Spatial Mechanisms

9.1.1 Introduction

There are many mechanisms that do not conform to planar, spherical, or other relatively simple motion domains. The landing gear of many aircraft involves a complex sequence of unfolding and rotation movements. The examples of automotive suspension and steering linkages have already been discussed in [Chapter 8](#). Control linkages used on farm and construction machinery are additional examples. Many problems involving spatial mechanisms can be attacked using the vector analysis techniques of courses in statics and dynamics. This is true if the information to be elicited is in the velocity or acceleration domains. Unfortunately, if the position of the linkage must be determined, such methods are likely to fall short in any but the simplest mechanism configurations. In order to develop systematic methods for handling position problems in spatial mechanisms, it is necessary to develop new tools. This chapter provides a brief introduction to the most commonly used methods. More advanced texts specifically directed at kinematics and dynamics of spatial mechanisms or robots may be consulted for more extensive treatments of these topics.

In this chapter, we will develop methods for modeling simple spatial mechanisms. Among other applications, the material presented in this chapter is fundamental to the construction of coordination software for robotic mechanisms. It is appropriate to consider, first of all, the behavior of serial-chain mechanisms. A serial chain is simply a set of members connected in series. Each member has two joints connecting it to its neighbors, except for the end members, which have only one joint. This is actually a very important type of structure from a practical viewpoint because it is the configuration of most industrial robots. We will start by developing the methods necessary for systematic position, velocity, and acceleration analysis of serial chains in which all joints are actively controlled and then introduce cases involving closed-loop structures and passive joints later in the chapter.

The study of spatial mechanisms is a large and complex subject. Even a very basic treatment would be much more extensive than we can supply in this one chapter. Consequently, this presentation is limited to an introduction to some of the more important fundamental concepts and the provision of some tools that can be employed to solve relatively simple spatial linkage problems.

9.1.2 Velocity and Acceleration Relationships

The relationship between the velocities of two points embedded in the same moving body, which was derived for planar motion in [Chapter 4](#), is actually perfectly general for three-dimensional motion

$$v_B = v_A + \omega \times r \quad (4.4)$$

Similarly, the relationship between the accelerations of two points on a rigid body

$$\ddot{r}_B = \ddot{r}_A + \ddot{\omega} \times r_{B/A} + \omega \times (\omega \times r_{B/A}) \quad (4.8)$$

is also valid for three-dimensional motion. These expressions, for which three-dimensional proofs were developed in [Chapter 4](#), form the basis for velocity and acceleration analysis of simple spatial mechanisms.

In many cases, these relationships can be applied directly. Examples are developed in the next two subsections. The limitations of this approach become evident only when the mechanism position is not known a priori and the configuration is sufficiently complex that the position cannot be determined by inspection. As pointed out for planar mechanisms in [Chapters 4](#) and [5](#), analysis must proceed in the following order: position analysis, velocity analysis, then acceleration analysis. Spatial system geometry does not lend itself to graphical analysis because the essential geometry cannot be captured in a single, two-dimensional representation. Consequently, any systematic approach to spatial linkage analysis must be analytical and numerical. As was the case with planar mechanisms, the analytical position problem tends to be more complex than the velocity and acceleration problems. It is, therefore,

advantageous to develop effective means of dealing with the position solution of spatial mechanisms and then to develop velocity and acceleration formulations that are fully compatible with the technique used for position modeling. This will be done in Section 9.2 and subsequent sections of this chapter.

However, as noted above, simple vector analysis based on [Equations 4.4](#) and [4.8](#) does work if the position of the mechanism is not an issue. It is, therefore, worthwhile studying some examples using this approach before moving to a more systematic and powerful approach. Keeping track of the reference frame to which points in a given body are referred is even more important in spatial mechanism analysis than in planar mechanisms. Consequently, the notation used in [Chapter 5](#), in which the reference frame to which a vector is referred is indicated by a superscript placed before the symbol, will be used again here.



Example 9.1

Analysis of Simple Spatial Linkage

A disk shown in [Figure 9.1](#) is rotating about a horizontal axis at A with an angular velocity with magnitude Ω . The entire assembly rotates about the vertical axis with an angular velocity with magnitude ω . Determine the velocity of point q located on the perimeter of the disk at an angle of β from the y axis. The radius r of the disk is given. Determine the velocity at the instant when the x, y coordinate axes on the disk are parallel with the fixed X, Y axes, and the rotation axis at A is parallel to the fixed Z axis.

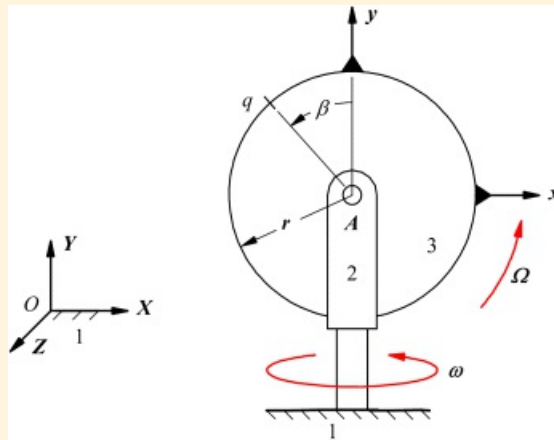


[Figure 9.1](#) The mechanism analyzed in Example 9.1.

Solution

The problem may be restated in the following form: Given ${}^1\omega_2 = \omega j$ and ${}^2\omega_3 = \Omega k$, where j and k are unit vectors respectively parallel to the y and z axes of the disk, together with the quantities r and β , find

$$\vec{v}_q = {}^1v_{q_3/O_1}$$

We can use the chain rule developed in Section 5.3.3, but it is first necessary to recognize that location A gives the points that are easiest to use as a basis for the analysis.

$${}^1v_{q_3/O_1} = {}^1v_{q_3/A_3} + {}^1v_{A_3/A_1} + {}^1v_{A_1/O_1}$$

A_3 and A_1 are permanently coincident and ${}^1v_{A_1} = 0$. As A_1 and O_1 are both fixed to link 1, then

$${}^1v_{A_3/A_1} = {}^1v_{A_1/O_1} = 0$$

and

$${}^1v_{q_3/O_1} = {}^1v_{q_3/A_3} + {}^2v_{q_3/A_3} - {}^2\omega_3 \times {}^2r_{q_3/A_3}$$

Now,

$${}^2v_{q_3/A_3} = 0$$

and

$${}^1\omega_3 = \omega j + \Omega k = {}^1\omega_2 + {}^2\omega_3$$

Also

$${}^3r_{G_3/R_3} = -r \sin \beta i + r \cos \beta j$$

At this instant, the coordinate frames are all parallel. Therefore the original cross-product can be written as

$${}^1\omega_3 \times {}^3r_{G_3/R_3} = \begin{vmatrix} i & j & k \\ 0 & \omega & \Omega \\ -r \sin \beta & r \cos \beta & 0 \end{vmatrix} = -(\Omega r \cos \beta)i - (\Omega r \sin \beta)j + (\omega r \sin \beta)k$$

And the solution is

$$r_G = {}^1r_{G_3/G_1} = -(\Omega r \cos \beta)i - (\Omega r \sin \beta)j + (\omega r \sin \beta)k$$



Example 9.2

Velocity Analysis of Spatial Manipulator

A simple three-degree-of-freedom spatial manipulator arm is shown in [Figure 9.2](#). In this arm, $AB = BC = CD = 2$ meters, and AB is perpendicular to the y axis, CB is perpendicular to AB , and CD is perpendicular to BC . The variables associated with the three revolute joints are the angles γ , θ , and ϕ defined as shown. At a given instant of time, rotary potentiometers and tachometers integral with each revolute joint servomotor (A , B , and C) indicate that $\gamma = 30^\circ$, $\theta = 30^\circ$, $\phi = 75^\circ$. The relative motion of the links in revolutions per minute is given as $\dot{\gamma} = 20$, $\dot{\theta} = -10$, and $\dot{\phi} = 15$. (Positive angles and angular velocities are in the same directions as the angles shown in [Figure 9.2](#).) At this instant, find the velocity of point D located on link 4 relative to the fixed reference frame.

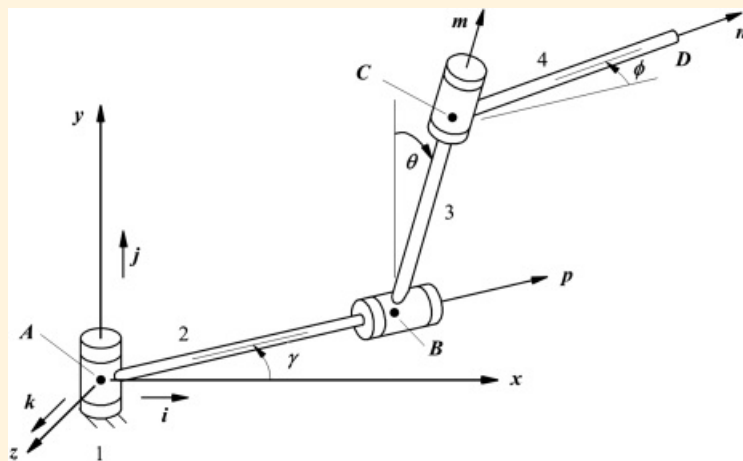


[Figure 9.2](#) The three-degree-of-freedom manipulator analyzed in Example 9.2.

Solution

In our nomenclature, we want to find

$$\dot{v}_{D_4} = {}^1\dot{v}_{D_4/C_4} + {}^1\dot{v}_{C_4/B_3} + {}^1\dot{v}_{B_3/A_2}$$

The velocity equation for point D is

$${}^1\dot{v}_{D_4/A_1} = {}^1\dot{v}_{D_4/C_4} + {}^1\dot{v}_{C_4/B_3} + {}^1\dot{v}_{B_3/A_2}$$

which can be expanded to give

$${}^1\dot{v}_{D_4/A_1} = {}^1\omega_4 \times {}^4r_{D_4/C_4} + {}^1\omega_3 \times {}^3r_{C_4/B_3} + {}^1\omega_2 \times {}^2r_{B_3/A_2}$$

Let p and m be unit vectors along lines AB and BC , respectively. The components of p and m resolved in the fixed frame are

$$p = \cos \gamma i - \sin \gamma k$$

and referring to [Figure 9.3](#)

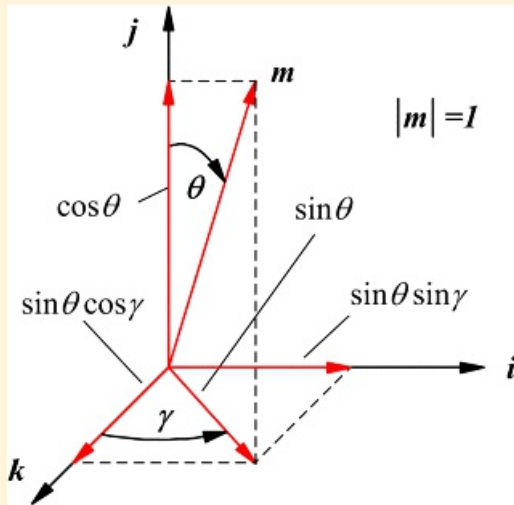


[Figure 9.3](#) Decomposition of the vector m into components parallel to the axes of the fixed reference frame.

$$m = \cos \theta j + \sin \theta (\cos \gamma k + \sin \gamma i) = \sin \theta \sin \gamma i + \cos \theta j + \sin \theta \cos \gamma k$$

To decompose n , think of it being initially parallel to p . Then imagine that n moves in a plane inclined at an angle of θ to the x - z plane, as shown in [Figure 9.4](#). Another way to interpret it is that the object CD is located by a sequence of three successive body-fixed rotations: Y axis by angle γ , X axis by θ , Y axis by ϕ . The direction n is the x axis of this new rotated frame

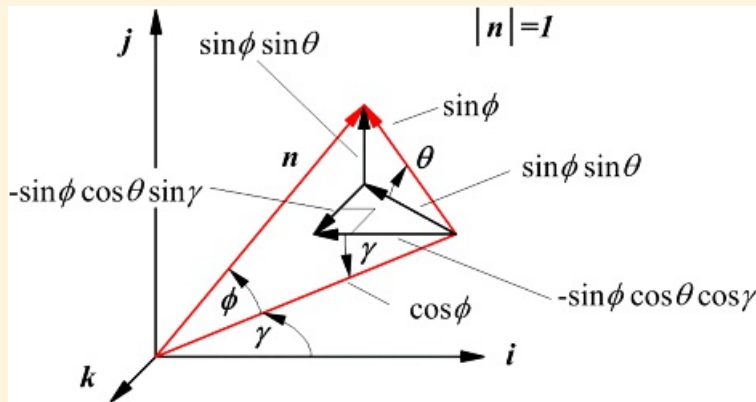


[Figure 9.4](#) Decomposition of the vector n into components parallel to the axes of the fixed reference frame.

$$\begin{aligned} n &= \cos \phi j + \sin \phi (\sin \theta j - \cos \theta (\cos \gamma k + \sin \gamma i)) \\ &= (\cos \phi \cos \gamma - \sin \phi \cos \theta \sin \gamma) j + (\sin \phi \sin \theta j - (\cos \phi \sin \gamma + \sin \phi \cos \theta \cos \gamma) k \end{aligned}$$

The relative angular velocity expressions that are given in the problem statement may now be expressed in the following forms

$$\begin{aligned} {}^1\omega_2 &= \dot{\gamma} j = 20(2\pi)/60j = 2.094j \text{ rad/s} \\ {}^2\omega_3 &= \dot{\theta} p = -10(2\pi)/60p = -1.047p \text{ rad/s} \\ &= -1.047(\cos \gamma i - \sin \gamma k) = (-0.9069i + 0.5236k) \text{ rad/s} \\ {}^3\omega_4 &= \dot{\phi} m = 15(2\pi)/60m = 1.571m \text{ rad/s} = 1.571(\sin \theta \sin \gamma i + \cos \theta j + \sin \theta \cos \gamma k) \\ &= (0.3927i + 1.360j + 0.6302k) \text{ rad/s} \end{aligned}$$

The angular velocities relative to the fixed reference frame necessary for evaluating the cross-products are then found using the chain rule (Section 5.3.3). That is

$${}^1\omega_3 = {}^1\omega_2 + {}^2\omega_3 = 2.094j - 0.9069i + 0.5236k = (-0.9069i + 2.094j + 0.5236k) \text{ rad/s}$$

and

$$\begin{aligned} {}^1\omega_4 &= {}^1\omega_3 + {}^3\omega_4 = -0.9069i - 2.094j + 0.5236k - 0.3927i + 1.360j + 0.6302k \\ &= (-0.514i - 3.454j + 1.204k) \text{ rad/s} \end{aligned}$$

The required displacement vectors are

$$\begin{aligned} {}^2r_{B_2/A_2} &= 2p = 2(\cos \gamma i - \sin \gamma k) = (1.732i - k) \text{ m} \\ {}^3r_{C_3/B_3} &= 2m = 2(\sin \theta \sin \gamma i + \cos \theta j + \sin \theta \cos \gamma k) = (0.5i + 1.732j + 0.866k) \text{ m} \\ {}^4r_{D_4/C_4} &= 2n = 2((\cos \phi \cos \gamma - \sin \phi \cos \theta \sin \gamma)i + (\sin \phi \sin \theta j - (\cos \phi \sin \gamma + \sin \phi \cos \theta \cos \gamma)k) \\ &= (-0.388i + 0.966j - 1.703k) \text{ m} \end{aligned}$$

The terms in the velocity equation can now be computed as follows

$$\begin{aligned} {}^1v_{B_2/A_2} &= {}^1\omega_2 \times {}^2r_{B_2/A_2} = 2.094j \times (1.732i - k) = (-2.094i - 3.527k) \text{ m/s} \\ {}^1v_{C_3/B_3} &= {}^1\omega_3 \times {}^3r_{C_3/B_3} = (-0.9069i + 2.094j + 0.5236k) \times (0.5i + 1.732j + 0.866k) \\ &= (0.906i + 1.047j - 2.613k) \text{ m/s} \\ {}^1v_{D_4/C_4} &= {}^1\omega_4 \times {}^4r_{D_4/C_4} = (-0.514i - 3.454j + 1.204k) \times (-0.388i + 0.966j - 1.703k) \\ &= (-7.062i - 1.345j + 0.844k) \text{ m/s} \end{aligned}$$

Therefore, the velocity of point D relative to the fixed reference frame is

$$\begin{aligned} {}^1r_{D_4/A_4} &= {}^1v_{B_2/A_2} + {}^1v_{C_3/B_3} + {}^1v_{D_4/C_4} \\ &= (-2.094i - 3.527k) + (0.906i + 1.047j - 2.613k) + (-7.062i - 1.345j + 0.844k) \\ &= (-8.251i - 0.298j - 5.401k) = 9.366(-0.830i - 0.130j - 0.547k) \text{ m/s} \end{aligned}$$

The final result has been expressed in the form of the magnitude of velocity multiplied by a unit vector having the direction of the velocity.

Note that the complexities of this example originated in the necessity of resolving position vectors into components in the axis directions of the fixed reference frame. This resolution can be difficult to visualize and is a potential source of error. Removing those difficulties is a primary motivation of the matrix

transformation approach to solving the position problem that is presented in Section 9.3.



Example 9.3

Acceleration Analysis of Spatial Manipulator

In the spatial manipulator arm shown in [Figure 9.2](#) and considered in Example 9.2, the acceleration readings at the instant examined are $\ddot{\gamma} = 3 \text{ rad/s}^2$, $\ddot{\theta} = 1 \text{ rad/s}^2$, and $\ddot{\phi} = -2 \text{ rad/s}^2$. As in the previous example, $AB = BC = CD = 2$ meters and AB is perpendicular to the y axis, CB is perpendicular to AB , and CD is perpendicular to BC . Also $\gamma = 30^\circ$, $\theta = 30^\circ$, $\phi = 75^\circ$, $\dot{\gamma} = 20 \text{ rpm}$, $\dot{\theta} = -10 \text{ rpm}$, and $\dot{\phi} = 15 \text{ rpm}$.

Find the acceleration of point D relative to the fixed reference frame.

Solution

We shall make use of the following results from Example 9.2

$$\begin{aligned}\ddot{x} &= \cos \gamma \ddot{\gamma} - \sin \gamma \ddot{\theta} \\ \ddot{y} &= \sin \theta \sin \gamma \ddot{\gamma} + \cos \theta \cos \gamma \ddot{\theta} \\ \ddot{z} &= (\cos \phi \cos \gamma - \sin \phi \cos \theta \sin \gamma) \ddot{\gamma} + (\sin \phi \sin \gamma - \cos \phi \cos \theta \cos \gamma) \ddot{\theta}\end{aligned}$$

$$\begin{aligned}{}^1\omega_2 &= 2.094i \text{ rad/s} \\ {}^1\omega_3 &= (-0.9069i + 2.094j + 0.5236k) \text{ rad/s} \\ {}^1\omega_4 &= (-0.514i + 3.434j + 1.204k) \text{ rad/s}\end{aligned}$$

$$\begin{aligned}{}^2r_{S_2/A_1} &= 2\ddot{x} = (1.732i - k) \text{ m} \\ {}^2r_{C_3/S_2} &= 2\ddot{y} = (0.54 + 1.732j + 0.866k) \text{ m} \\ {}^4r_{D_4/C_3} &= 2\ddot{z} = (-0.388i + 0.956j - 1.702k) \text{ m}\end{aligned}$$

$$\begin{aligned}{}^1\gamma_{S_2/A_1} &= {}^1\omega_2 \times {}^2r_{S_2/A_1} = (-2.094i - 3.627k) \text{ m} \\ {}^1v_{C_3/S_2} &= {}^1\omega_3 \times {}^2r_{C_3/S_2} = (0.906i + 1.047j - 2.618k) \text{ m/s} \\ {}^1v_{D_4/C_3} &= {}^1\omega_4 \times {}^4r_{D_4/C_3} = (-7.052i - 1.345j + 0.844k) \text{ m/s}\end{aligned}$$

The fundamental equation that must be solved to obtain ${}^1\alpha_{D_4/S_2}$ is

$${}^1\alpha_{S_2/A_1} = {}^1\alpha_{D_4/C_3} + {}^1\alpha_{C_3/S_2} + {}^1\alpha_{S_2/A_1}$$

The individual terms in this equation will be evaluated separately. However, it is first necessary to evaluate the angular accelerations relative to the fixed reference frame.

The relative angular acceleration expressions are

$$\begin{aligned} {}^1\omega_2 &= \dot{\theta} j = 3j \text{ rad/s}^2 \\ {}^2\omega_3 &= \dot{\theta} p = 1p = 1(\cos \gamma i - \sin \gamma k) = (0.866i - 0.300k) \text{ rad/s}^2 \\ {}^3\omega_4 &= \dot{\phi} m = -2m = -2(\sin \theta \sin \gamma i + \cos \theta j + \sin \theta \cos \gamma k) \\ &= (-0.300i - 1.732j - 0.866k) \text{ rad/s} \end{aligned}$$

so the angular accelerations relative to the fixed reference frame are

$$\begin{aligned} {}^1\omega_2 &= \ddot{\theta} j = 3j \text{ rad/s}^2 \\ {}^1\omega_3 &= {}^1\omega_2 \times {}^2\omega_3 + {}^1\omega_2 \times {}^2\omega_3 = 3j + 0.866i - 0.300k + 2.094j \times (-0.9069i + 0.3236k) \\ &= (1.962i + 3j + 1.399k) \text{ rad/s}^2 \\ {}^1\omega_4 &= {}^1\omega_3 + {}^3\omega_4 + {}^1\omega_3 \times {}^3\omega_4 = 1.962i + 3j + 1.399k - 0.300i - 1.732j - 0.866k \\ &\quad + (-0.907i + 2.094j + 0.524k) \times (0.3927i + 1.380j + 0.6802k) \\ &= (2.174i + 2.091j - 1.523k) \text{ rad/s}^2 \end{aligned}$$

Now the individual acceleration terms are

$$\begin{aligned} {}^1a_{B_2/A_2}^r &= {}^1\omega_2 \times {}^4v_{B_2/A_2} = 2.094j \times (-2.094i - 3.267k) = (-7.595i + 4.385k) \text{ m/s}^2 \\ {}^1a_{B_2/A_2}^t &= {}^1\omega_2 \times {}^4r_{B_2/A_2} = 3j \times (1.732i - k) = (-3i - 5.196k) \text{ m/s}^2 \end{aligned}$$

$$\begin{aligned} {}^1a_{C_3/B_3}^r &= {}^1\omega_3 \times {}^4v_{C_3/B_3} = (-0.907i - 2.094j + 0.524k) \times (0.9069i + 1.047j - 2.618k) \\ &= (-6.031i - 1.900j - 2.847k) \text{ m/s}^2 \\ {}^1a_{C_3/B_3}^t &= {}^1\omega_3 \times {}^4r_{C_3/B_3} = (1.962i + 3j + 1.399k) \times (0.3i + 1.732j + 0.866k) \\ &= (0.175i - 1.010j - 1.898k) \text{ m/s}^2 \end{aligned}$$

$$\begin{aligned} {}^1a_{D_4/C_4}^r &= {}^1\omega_4 \times {}^4v_{D_4/C_4} = (-0.514i + 3.454j + 1.204k) \times (-7.062i - 1.345j + 0.844k) \\ &= (4.535i - 8.069j + 25.083k) \text{ m/s}^2 \\ {}^1a_{D_4/C_4}^t &= {}^1\omega_4 \times {}^4r_{D_4/C_4} = (2.174i + 2.091j - 1.523k) \times (-0.383i + 0.965j - 1.704k) \\ &= (-2.100i + 4.304j + 2.911k) \text{ m/s}^2 \end{aligned}$$

The total acceleration of point *D* is now given by

$$\begin{aligned} {}^1a_{D_4/A_4} &= (-7.595i - 3.000j - 6.031i + 0.175i + 4.535i - 2.100i) \\ &\quad + (-1.900j - 1.000j - 8.069j + 4.304j) \\ &\quad + (4.385i - 5.196i - 2.847i + 1.898i + 25.083i + 2.911i)k \\ &= (-14.025i - 6.57j + 26.23k) \text{ m/s}^2 = 30.43(-0.460i - 0.219j + 0.861k) \text{ m/s}^2 \end{aligned}$$

The final form of the result is expressed as the magnitude of the acceleration times a unit vector in the direction of the acceleration. Problems of this type can be solved relatively quickly with the aid of a programmable hand calculator set up to solve three-dimensional cross-products. Less powerful calculators will require some repetitious mathematical manipulations by the user but still enable such problems to be solved in a reasonable time without resorting to the use of a computer.



9.2 Robotic Mechanisms

Robotic mechanisms form a very important class of spatial mechanisms. They are distinct from most of the mechanisms discussed elsewhere in this book in that they have a large number of actuated degrees of freedom. Whereas many mechanisms have only one degree of freedom, actuated by a single drive, robotic mechanisms have four, five, six, or more with independent actuation of each degree of freedom. This leads to the problem of coordination, which may be stated as: Given the desired motion of the robot “hand,” what should the commanded values of the joint actuator variables be to achieve that motion? In a complex one-degree-of-freedom mechanism, there may be a considerable number of output motions all driven by a single input. These motions are coordinated kinematically via the mechanism. In a robotic mechanism, on the other hand, the coordination is done electronically by a computer integrated into the machine. The need for a theory for robotic coordination has led to the formulation of the following important sub-problems: Two important types of problems in robotic coordination have come to be known as the *direct* and *inverse* kinematics problems. They may be stated as follows.

The *direct kinematics* problem for a serial chain, such as that shown in [Figure 9.5](#), is

Given the positions of all of the joints, find the position of the “hand” relative to the “base.”

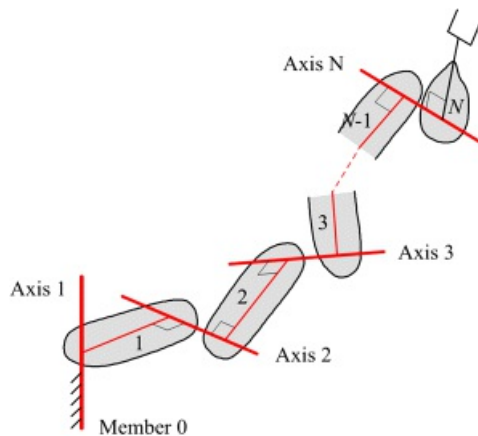


[Figure 9.5](#) A general serial chain with axial joints. The chain has N joint axes, labeled as 1 to N , and $N + 1$ members labeled as 0 to N . Member 0 is the fixed base member.

We will commonly refer to the free end member of a serial chain as the “hand,” following from the common application of this type of analysis to robotic systems. In robotics, the free end member is also often called the *end effector*. This term results from its function as being the tool with which a manipulator interacts with the work piece. We use hand for convenience, although the end member may not resemble a human hand and need not be a tool. Likewise, it is convenient to refer to the other end member as the “base,” even though in some situations it may not be fixed relative to the earth.

A more precise and general statement of the direct kinematics problem is

Given the values of the joint parameters, equal to the mobility (number of degrees of freedom) of the mechanism, find the relative position of any two designated members.

The *inverse kinematics* problem for the serial chain, shown in [Figure 9.5](#), is

Given the position of the hand relative to the base, find the positions of all of the joints.

Once again, this is a simplified statement applying only to the serial chain. A more general statement is

Given the relative positions of two members of a mechanism, find all of the joint parameters.

As will be seen later, it is necessary to qualify further the statements of the inverse kinematics problem. Those given above apply without qualification only to the case in which the mechanism has six degrees of freedom.

Analogs of the direct and inverse kinematics problems can be stated in terms of joint rates and member velocities. These are also very important problems in the development of robotic software. They can be stated for the serial

chain as follows.

The *direct rate kinematics* problem for the serial chain is

Given the positions of all members of the chain and the rates of motion about all joints, find the total velocity of the hand.

Here, the rate of motion about the joint is the angular velocity of rotation about a revolute joint or the translational velocity of sliding along a prismatic joint. The total velocity of a member is the velocity of the origin of the reference frame fixed to it combined with its angular velocity. That is, the total velocity has six independent components and, therefore, completely represents the velocity field of the member.

The *inverse rate kinematics* problem for a serial chain is

Given the positions of all members of the chain and the total velocity of the hand, find the rates of motion of all joints.

It is important to note that these definitions include an assumption that the position of the mechanism is completely known. In many situations, this means that either the direct or inverse position kinematics problem must be solved before the direct or inverse rate kinematics problem can be addressed.



9.3 Direct Position Kinematics of Serial Chains

9.3.1 Introduction

The problem to be addressed here is to find the hand position of a serial chain when the joint positions are known. This is a very important problem from the point of view of constructing manipulator coordination algorithms because the joint positions are directly measured by sensors mounted on the joints. It is necessary to compute the positions of the joint axes relative to the fixed reference frame. This is done by means of the solution presented below.

The first problem in developing a mathematical model of a spatial mechanism, such as a robot, is that of algebraically describing the position of a rigid body in space. There are many ways to do this. The approach we will use here is the most common one in which the position of a body is represented by the elements of a matrix coordinate transformation. This will be done by writing a position transformation between two Cartesian coordinate frames, one in the body and the other in the fixed frame. The parameters that describe this transformation can then be said to describe the position of the body relative to the fixed frame.

Let $[x, y, z]$ be a fixed reference frame and $[x', y', z']$ a reference frame fixed in the moving body (Figure 9.6). The coordinates of the point P in the fixed reference frame may be obtained from its coordinates in the moving reference frame by a transformation of the form

$$\mathbf{p} = Q\mathbf{p}' + \mathbf{q} \quad (9.1)$$

$$\mathbf{p} = \begin{bmatrix} x \\ y \\ z \end{bmatrix}, \quad \mathbf{p}' = \begin{bmatrix} x' \\ y' \\ z' \end{bmatrix}$$

Here Q is a 3×3 matrix, and \mathbf{q} is the position of the origin of the moving reference frame relative to the fixed reference frame.

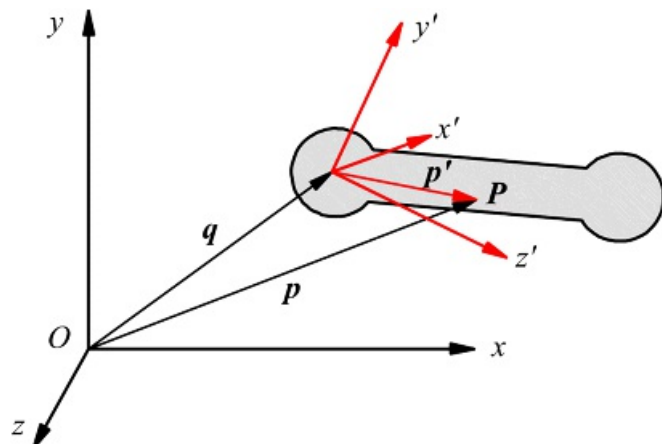


[Figure 9.6](#) Relationship between body reference frame $[x', y', z']$ and fixed reference frame $[x, y, z]$. P is an arbitrary point, p' is the position of P in the body fixed reference frame, and p is the position of that point in the fixed reference frame.

Now, if the geometry of the moving body is known in terms of the reference frame (x', y', z') fixed in it, the position of any point in that body with respect to the fixed frame is also known provided the matrix Q and the vector \mathbf{q} are known. The transformation can be regarded as describing the position of the moving body in space.

The matrix Q has a very special property: It is an orthogonal matrix. For an orthogonal matrix

$$Q^T Q = I \quad \text{or} \quad Q^T = Q^{-1} \quad (9.2)$$

The property of orthogonality follows from the assumption that the body is rigid.

An important feature of the description of the position of a body in space by coordinate transformation elements, that is, the elements of Q and q , is that there are 12 elements in these two entities, 9 in Q

$$Q = \begin{bmatrix} q_{11} & q_{12} & q_{13} \\ q_{21} & q_{22} & q_{23} \\ q_{31} & q_{32} & q_{33} \end{bmatrix}$$

and 3 in q

$$q = \begin{bmatrix} q_1 \\ q_2 \\ q_3 \end{bmatrix}$$

Since only six coordinates are needed to fix the position of a body in space, these 12 quantities cannot be independent. There must be at least six independent relationships among them. The orthogonality condition, $Q^T Q = I$, provides these relationships

$$Q^T Q = \begin{bmatrix} q_{11} & q_{21} & q_{31} \\ q_{12} & q_{22} & q_{32} \\ q_{13} & q_{23} & q_{33} \end{bmatrix} \begin{bmatrix} q_{11} & q_{12} & q_{13} \\ q_{21} & q_{22} & q_{23} \\ q_{31} & q_{32} & q_{33} \end{bmatrix} = \begin{bmatrix} 1 & 0 & 0 \\ 0 & 1 & 0 \\ 0 & 0 & 1 \end{bmatrix}$$

giving

$$\begin{aligned} q_{11}^2 + q_{21}^2 + q_{31}^2 &= 1 & (i) \\ q_{11}q_{12} + q_{21}q_{22} + q_{31}q_{32} &= 0 & (ii) \\ q_{11}q_{31} + q_{21}q_{23} + q_{31}q_{33} &= 0 & (iii) \\ q_{12}q_{31} + q_{22}q_{21} + q_{32}q_{31} &= 0 \\ q_{12}^2 + q_{22}^2 + q_{32}^2 &= 1 & (iv) \\ q_{12}q_{33} + q_{22}q_{23} + q_{32}q_{33} &= 0 & (v) \\ q_{13}q_{31} + q_{23}q_{21} + q_{33}q_{31} &= 0 \\ q_{13}q_{12} + q_{23}q_{22} + q_{33}q_{32} &= 0 \\ q_{13}^2 + q_{23}^2 + q_{33}^2 &= 1 & (vi) \end{aligned} \quad (9.3)$$

As can be seen, three of these equations are repeated, so only the six marked are distinct. Therefore, only three of the elements of Q are independent. The rest can be generated from these three by means of Equations (i) to (vi). It follows that six variables are needed to specify the transformation in [Equation 9.1](#): three elements of Q and the three elements of q . That is, as expected, six coordinates are needed to describe the position of the body.

9.3.2 Concatenation of Transformations

In Section 9.3.1, the concept of representing the position of a body in space by means of a coordinate transformation was introduced. A reference frame is fixed to the body and the transformation is written that converts the coordinates of points relative to that frame into their coordinates relative to the fixed frame. It has the form

$$\bar{p} = Q\bar{p}' + q$$

(9.1)

Here \bar{p}' is the position of a point relative to the reference frame fixed in the body, \bar{p} is the position of the same point referred to the fixed reference frame, Q is a 3×3 matrix that rotates the body reference frame until it is parallel to the fixed frame, and q is the position of the origin of the body reference frame relative to the fixed frame.

We will now consider the application of this model to a serial chain in which $N+1$ members are connected by N joints with each member having two joints formed in it except for the two end members, which have only one joint each. [Figure 9.5](#) shows a general serial chain.

The important feature here is to establish a convention that defines a consistent location for the reference frame in each member of the chain. The transformations representing the positions of the joints can then be applied successively to produce the transformation relating the end members of the chain.

[Figure 9.7](#) shows the important geometric features of a binary link on which are mounted two axial joints. The term *axial joint* is used to define any joint that has a fixed axis of motion. Among lower pairs, revolute, screw, and cylindrical joints are axial. A prismatic joint can also be regarded as axial with an axis in the direction of translation. The axis, in this case, is not unique and may be specified as lying along any convenient line parallel to the direction of translation. As will be seen, the restriction to axial joints allows simple expression of the transformation matrices. Because the overwhelming majority of kinematic joints in practical use are axial joints, this simplification is not unduly restrictive.

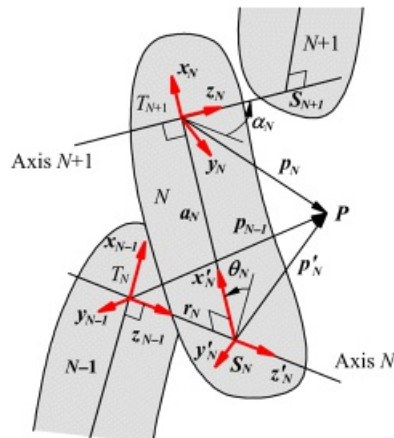


[Figure 9.7](#) The “skeleton” of a binary link. A binary link is one with two axial joints. The geometry of the link and the position of the joint on axis N are completely defined by the parameters a_N , the length of the common normal of the joint axes; r_N , the distance along axis N from the foot of the common normal of link $N - 1$ to that of link N ; α_N , the twist angle between axis N and axis $N + 1$; and θ_N , the angle between the normal of axis $N - 1$ and that of axis N .

The two joints mounted on member N are named joints N and $N + 1$. The common normal to the two joint axes, $S_N T_{N+1}$, has length a_N , and the distance $T_N S_N$ along axis N between the foot of the common normal to joints $N - 1$ and N and that of joints N and $N + 1$ is the offset, r_N . The angle between these two normals is the joint angle θ_N . The positive direction of each normal for the purpose of defining this angle is directed from the lower numbered axis to the higher. The angle between axes N and $N + 1$ is the twist angle α_N . The reference frame fixed to the N th member has its origin located at T_{N+1} : the foot of the common normal on axis $N + 1$. The x_N axis is aligned with the common normal, as shown, and the z_N axis lies along axis $N + 1$. Reference frame $N - 1$ is located in the corresponding position on member $N - 1$. An intermediate reference frame N' , $[x', y', z']$, is also fixed to body N . Its origin is at S_N , the foot of the common normal on axis N . The x'_N axis lies along that normal, and the z'_N axis lies along axis N .

The joint axes together with the common normal on the links can be thought of as defining the “skeleton” of the linkage. The parameters a_N , r_N , α_N , and θ_N together completely define link N and the position of joint N for the

purposes of kinematic geometry.

Let us consider the transformation from reference frame N to frame N' . For the position of an arbitrary point P we have

$$\mathbf{p} = [x_N, y_N, z_N]^T \text{ and } \mathbf{p}' = [x'_N, y'_N, z'_N]^T$$

where

$$\begin{aligned} x'_N &= x_N + \alpha_N \\ y'_N &= y_N \cos \alpha_N - z_N \sin \alpha_N \\ z'_N &= y_N \sin \alpha_N + z_N \cos \alpha_N \end{aligned}$$

The last two equations are readily derived with the aid of [Figure 9.8](#), which shows a view of the system directed along the $x_N x_{N'}$ axis. The preceding equations can be written in the form

$$\mathbf{p}'_N = \mathbf{V}_N \mathbf{p}_N + \mathbf{v}_N \quad (9.4)$$

where

$$\mathbf{V}_N = \begin{bmatrix} 1 & 0 & 0 \\ 0 & \cos \alpha_N & -\sin \alpha_N \\ 0 & \sin \alpha_N & \cos \alpha_N \end{bmatrix} \text{ and } \mathbf{v}_N = \begin{bmatrix} \alpha_N \\ 0 \\ 0 \end{bmatrix}$$

The transformation from the $N - 1$ frame to the N' frame is obtained from

$$\mathbf{p}_{N-1}' = [x_{N-1}', y_{N-1}', z_{N-1}]^T$$

where

$$\begin{aligned} x_{N-1}' &= x'_N \cos \theta_N - y'_N \sin \theta_N \\ y_{N-1}' &= x'_N \sin \theta_N + y'_N \cos \theta_N \\ z_{N-1}' &= z'_N + r_N \end{aligned}$$

[Figure 9.9](#) illustrates these relationships. It shows frames $N - 1$ and N' viewed along axis N . The equations can be written in the form

$$\mathbf{p}_{N-1}' = \mathbf{U}_N \mathbf{p}'_N + \mathbf{w}_N \quad (9.5)$$

where

$$\mathbf{U}_N = \begin{bmatrix} \cos \theta_N & -\sin \theta_N & 0 \\ \sin \theta_N & \cos \theta_N & 0 \\ 0 & 0 & 1 \end{bmatrix}, \quad \mathbf{w}_N = \begin{bmatrix} 0 \\ 0 \\ r_N \end{bmatrix}$$

Expanding [Equation 9.5](#) yields

$$\bar{p}_{N-1} = U_N(\bar{V}_N \bar{p}_N + \bar{v}_N) + \bar{w}_N$$

which can be further rearranged to

$$\bar{p}_{N-1} = U_N(\bar{V}_N \bar{p}_N + \bar{z}_N) \quad (9.6)$$

where

$$\bar{z}_N = \bar{v}_N + U_N^T \bar{w}_N = [v_N, \dot{\theta}_N, r_N]^T$$

[Equation 9.6](#) has the same form as [Equation 9.1](#) but is specialized for an axial joint.

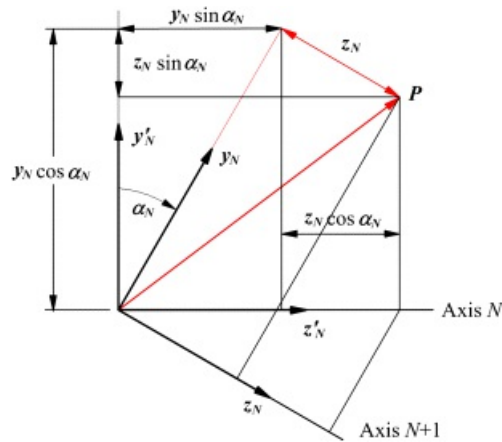


[Figure 9.8](#) View along the common normal of axes N and $N+1$. The coordinates of point P in the N and N' frames can be related by taking components as shown.

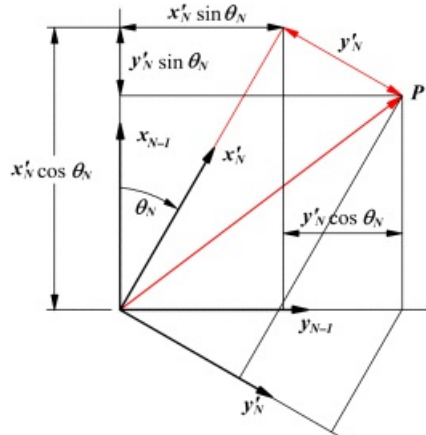


[Figure 9.9](#) View along axis N . The coordinates of point P in the $N-1$ and N' frames can be related by taking components as shown.

Depending on which of the parameters of the transformation in ([Equation 9.6](#)) are allowed to vary, it can represent different types of axial joints. A revolute is obtained by allowing $\dot{\theta}_N$ to vary while keeping all other dimensions constant. A prismatic joint is obtained by allowing r_N to vary while $\dot{\theta}_N$ and all other dimensions remain constant.

It is now possible to write a transformation expressing the position of member N of a chain such as that shown in [Figure 9.5](#). The transformation is expressed in terms of the joint variables. For a chain containing only axial joints

$$\tilde{p}_0 = U_1(V_1U_2(V_2U_3(\dots U_N(V_Np_N + \tilde{s}_N) + \dots) + \tilde{s}_2) + \tilde{s}_1) \quad (9.7)$$

This equation can be used to find the position in a fixed frame, p_0 , of any point given its position p_N , relative to the end member, and the position coordinates of the joints in the chain. Alternatively, it may be used to derive equations between the joint position coordinates given the position of one end member relative to the other. In this latter case, the position of member N relative to member 0 is given by a known transformation

$$p_0 = Q p_N + q \quad (9.1)$$

Since this transformation and [Equation 9.7](#) must be identical, we have

$$Q = U_1V_1U_2V_2U_3\dots U_NV_N \quad (9.8a)$$

The scalar component equations from [Equation 9.8a](#) are called the rotation equations. Also

$$q = U_1V_1U_2V_2U_3\dots V_{N-1}U_Ns_N + \dots + U_1V_1U_2s_2 + U_1s_1 \quad (9.8b)$$

The scalar component equations from [Equation 9.8b](#) are called the translation equations.

9.3.3 Homogeneous Transformations

The transformation

$$\tilde{p}_{N-1} = U_N(V_Np_N + \tilde{s}_N) \quad (9.6)$$

that converts from the coordinate frame on link N to that on link $N - 1$ can be written as a single, four-dimensional matrix-vector multiplication. Note that the notation of “prime” below should not be confused with the one in [Figure 9.7](#) to denote an intermediate frame.

$$\tilde{p}'_{N-1} = A_N\tilde{p}'_N \quad (9.9)$$

where

$$A_N = \begin{bmatrix} \cos \theta_N & -\sin \theta_N \cos \alpha_N & \sin \theta_N \sin \alpha_N & a_N \cos \theta_N \\ \sin \theta_N & \cos \theta_N \cos \alpha_N & -\cos \theta_N \sin \alpha_N & a_N \sin \theta_N \\ 0 & \sin \alpha_N & \cos \alpha_N & r_N \\ 0 & 0 & 0 & 1 \end{bmatrix} \quad (9.10)$$

and

$$\vec{r}_N = \begin{bmatrix} x_N \\ y_N \\ z_N \\ 1 \end{bmatrix} \quad (9.11)$$

The three-by-three sub-matrix in the top left-hand corner of A_N can be recognized as $U_N V_N$, while the fourth column is $U_N s_N$ with 1 added as the fourth element. The reader may verify that, when expanded, [Equations 9.6](#) and [9.9](#) give the same three component equations. The fourth equation given by the latter is $1 = 1$.

Using this formulation, [Equations 9.8a](#) and [9.8b](#), which relate hand position to the joint variables, assume the form (for $N = 6$)

$$\vec{r}' = A_1 A_2 A_3 A_4 A_5 A_6 \quad (9.12)$$

where

$$A' = \begin{bmatrix} q_{11} & q_{12} & q_{13} & q_1 \\ q_{21} & q_{22} & q_{23} & q_2 \\ q_{31} & q_{32} & q_{33} & q_3 \\ 0 & 0 & 0 & 1 \end{bmatrix} \quad (9.13)$$

This very compact formulation is attractive and variants of it have been extensively used in spatial mechanism theory, computer graphics, and robotics. It is particularly attractive when ease of programming is the most important consideration.

[Equation 9.9](#) is called a homogeneous transformation because it has the form of a transformation of the homogeneous coordinates used in projective geometry.



Example 9.4

Computation of Homogeneous Transformation

The geometric parameters for the manipulator shown in [Figure 9.10](#) are shown in [Table 9.1](#). If the joint variables have the values $\theta_1 = 60^\circ$, $\theta_2 = 120^\circ$, $\theta_3 = 135^\circ$, $r_4 = 4.0$, $\theta_5 = -60^\circ$, and $\theta_6 = 45^\circ$, find the homogeneous transformation Q' that specifies the position of the hand.

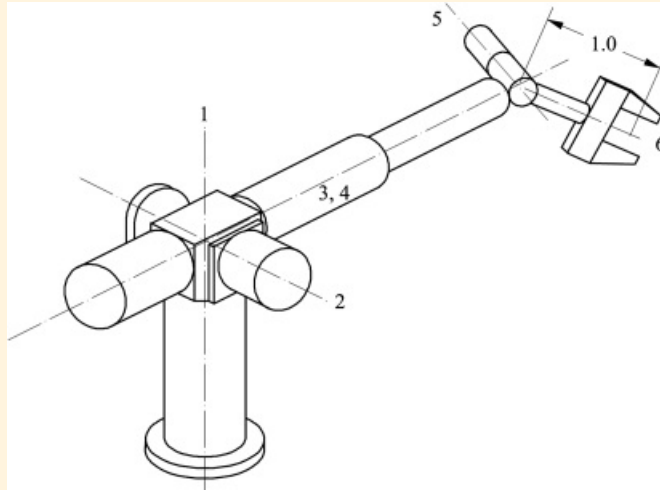


[Figure 9.10](#) The manipulator of Example 9.4. The geometric parameters are summarized in [Table 9.1](#).

[Table 9.1](#) Geometric Parameters for Example 9.4

i	a_i	r_i	α_i	θ_i
1	0	0	90°	60°
2	0	0	90°	120°
3	0	0	0	135°
4	0	4.0	90°	0
5	0	0	90°	-60°
6	0	1.0	0	45°

Notice that, because joint 4 is a prismatic joint, the joint variable is r_4 and θ_4 is a fixed geometric parameter. All of the other joints are revolute so that θ_i is the joint variable and a_i is a fixed geometric parameter for all i except 4.

Solution

Substitution of a_1 , α_1 , r_1 , and θ_1 from [Table 9.1](#) gives

$$A_1 = \begin{bmatrix} 0.5 & 0 & 0.8660 & 0 \\ 0.8660 & 0 & -0.5 & 0 \\ 0 & 1 & 0 & 0 \\ 0 & 0 & 0 & 1 \end{bmatrix}$$

Similarly

$$A_2 = \begin{bmatrix} -0.5 & 0 & 0.8660 & 0 \\ 0.8660 & 0 & 0.5 & 0 \\ 0 & 1 & 0 & 0 \\ 0 & 0 & 0 & 1 \end{bmatrix}, \quad A_3 = \begin{bmatrix} -0.7070 & -0.7070 & 0 & 0 \\ 0.7070 & -0.7070 & 0 & 0 \\ 0 & 0 & 1 & 0 \\ 0 & 0 & 0 & 1 \end{bmatrix}, \quad A_4 = \begin{bmatrix} 1 & 0 & 0 & 0 \\ 0 & 0 & -1 & 0 \\ 0 & 1 & 0 & 4 \\ 0 & 0 & 0 & 1 \end{bmatrix}$$

$$A_5 = \begin{bmatrix} 0.5 & 0 & -0.8660 & 0 \\ -0.8660 & 0 & -0.5 & 0 \\ 0 & 1 & 0 & 0 \\ 0 & 0 & 0 & 1 \end{bmatrix}, \quad A_6 = \begin{bmatrix} 0.7070 & -0.7070 & 0 & 0 \\ 0.7070 & 0.7070 & 0 & 0 \\ 0 & 0 & 1 & 1 \\ 0 & 0 & 0 & 1 \end{bmatrix}$$

Applying (Equation 9.12), we multiply these matrices together to get

$$Q' = A_1 A_2 A_3 A_4 A_5 A_6 = \begin{bmatrix} 0.3220 & 0.2945 & -0.8993 & 0.8323 \\ -0.9423 & 0.0096 & -0.3340 & 2.6660 \\ -0.0897 & 0.9555 & 0.2803 & 2.2816 \\ 0 & 0 & 0 & 1 \end{bmatrix}$$

Then Q' is the transformation matrix that describes the position of the hand.

An inconvenience of working with the A_N matrices, rather than the U_N and V_N matrices from which they are derived, is that, unlike U_N and V_N , A_N is not an orthogonal matrix. That is,

$$A_N^{-1} \neq A_N^T$$

To derive an expression for A_N^{-1} it is most efficient to return to Equation 9.6

$$\tilde{p}_{N-1} = U_N(V_N p_N + s_N) \quad (9.6)$$

Pre-multiplication of both sides by U_N^T gives

$$U_N^T \tilde{p}_{N-1} = V_N p_N + s_N$$

Moving s_N to the other side of the equation and then pre-multiplying by V_N^T gives

$$p_N = V_N^T (U_N^T \tilde{p}_{N-1} - s_N) \quad (9.14)$$

In the same manner as Equation 9.10, this expression can be written as a 4×4 matrix expression

$$p'_N = A_N^{-1} \tilde{p}'_{N-1} \quad (9.15)$$

where

$$A_N^{-1} = \begin{bmatrix} \cos \theta_N & \sin \theta_N & 0 & -\alpha_N \\ -\sin \theta_N \cos \alpha_N & \cos \theta_N \cos \alpha_N & \sin \alpha_N & -r_N \sin \alpha_N \\ \sin \theta_N \sin \alpha_N & -\cos \theta_N \sin \alpha_N & \cos \alpha_N & -r_N \cos \alpha_N \\ 0 & 0 & 0 & 1 \end{bmatrix} \quad (9.16)$$

and

$$\vec{x}_N^t = \begin{bmatrix} x_N \\ y_N \\ z_N \\ 1 \end{bmatrix} \quad (9.11)$$

as before.

The reader may verify that the expressions for A_N and A_N^{-1} given by Equations 9.10 and 9.16 satisfy the relationship

$$A_N^{-1} A_N = I$$



9.4 Inverse Position Kinematics

As stated earlier, the inverse kinematics problem for the serial chain shown in [Figure 9.5](#) is

Given the position of the hand relative to the base, find the positions of all of the joints.

This amounts to finding the joint parameters if the homogeneous matrix, Q' , of [Equation 9.12](#) is given. Solution requires expansion of [Equation 9.12](#) using the expression given by [Equation 9.10](#) for each of the matrices A_N . N of the resulting set of scalar equations are selected to be solved for the variables θ_i , $i = 1, \dots, N$, describing the positions of revolute joints, or v_i describing the positions of prismatic joints. The resulting equations are nonlinear and are sometimes very difficult to solve, although the simple geometries commonly used are tractable.

Nevertheless, the solution of the inverse position equations is beyond the scope of this book. Fortunately, this problem is of less practical importance than the direct position kinematics and inverse rate kinematics problems, which must be solved online many times per second in most manipulator coordination schemes.



9.5 Rate Kinematics

9.5.1 Introduction

As was stated above, the direct rate kinematics problem for the serial chain is

Given the positions of all members of the chain and the rates of motion about all joints, find the total velocity of the hand.

The rate of motion about the joint is the angular velocity of rotation about a revolute joint or the translational velocity of sliding along a prismatic joint. The total velocity of a member is the velocity of the origin of the reference frame fixed to it combined with its angular velocity. That is, the total velocity has six independent components and therefore completely represents the velocity field of the member.

The inverse rate kinematics problem for a serial chain is

Given the positions of all members of the chain and the total velocity of the hand, find the rates of motion of all joints.

Once again, it is important to notice that these definitions include an assumption that the position of the mechanism is completely known. In many situations, this means that either the direct or inverse position kinematics problem must be solved before the direct or inverse rate kinematics problem can be addressed.

When controlling a movement of an industrial robot that operates in the point-to-point mode, it is not only necessary to compute the final joint positions needed to assume the desired final hand position. It is also necessary to generate a smooth trajectory for motion between the initial and final positions. There are, of course, infinitely many possible trajectories for this purpose. However, the most straightforward and successful approach employs algorithms based on the solution of the inverse rate kinematics problem. This technique originated in the work of Whitney [1] and of Pieper and Roth [2].

9.5.2 Direct Rate Kinematics

According to the chain rule for angular velocities developed in Section 5.3.3, the angular velocity of the hand of a serial chain, such as that shown in [Figure 9.5](#), with $N = 6$ joints (seven members including the base) is

$$\dot{\omega}_H = \dot{\omega}_0 + \dot{\omega}_1 + \dot{\omega}_2 + \dot{\omega}_3 + \dot{\omega}_4 + \dot{\omega}_5 + \dot{\omega}_6 \quad (9.17)$$

Here the base member to which the fixed reference frame is attached is referred to as member 0. Each member has a reference frame attached to it, and so $\dot{\omega}_j$ is the angular velocity of member j relative to a reference frame fixed to member i . If i and j are consecutive members, $\dot{\omega}_j$ becomes the angular velocity of one member relative to the other about the joint that connects them. That is

$$\dot{\omega}_j = \dot{\theta}_j \hat{\omega}_j \quad (9.18)$$

where $\hat{\omega}_j$ is a unit vector having the direction of axis i .

Combining [Equation 9.18](#) with [Equation 9.17](#), the angular velocity $\dot{\omega}_H$ of the hand is related to the joint rates by

$$\dot{\omega}_H = \sum_{k=1}^N \dot{\theta}_k \hat{\omega}_k \quad (9.19)$$

where $\hat{\omega}_k$ is a unit vector having the direction of joint axis k .

The velocity of the origin, O_N , of the reference frame fixed to the hand (frame 6) relative to the fixed frame (frame 0) can be obtained by summing the components of that velocity due to motion about the respective joints. The velocity of point O_N relative to frame 0 produced by motion about joint i is

$${}^0v_{O_N} = {}^{i-1}\omega_i \times {}^3r_i \quad (9.20)$$

Where 3r_i is the vector from any point on axis i to point O_N . Following the convention of [Figure 9.7](#), the origin O_{i-1} of frame $i - 1$ is on axis i . Hence 3r_i can be interpreted as the vector from O_{i-1} to O_N referred to the fixed reference frame. That is, when $N = 6$,

$${}^0v_{O_6} = {}^0v_{O_{6,1}} + {}^0v_{O_{6,2}} + {}^0v_{O_{6,3}} + {}^0v_{O_{6,4}} + {}^0v_{O_{6,5}} + {}^0v_{O_{6,6}}$$

More generally

$${}^0v_{O_N} = \sum_{i=1}^N {}^{i-1}\omega_i \times {}^3r_i = \sum_{i=1}^N \dot{\theta}_i {}^3w_i \times {}^0r_i$$

Now, if 0p_i is the position, relative to the fixed reference frame, of the origin of reference frame $i - 1$ on joint axis i , then

$${}^0r_i = {}^0p_{H+1} - {}^0p_i$$

Here the position of O_6 is indicated by ${}^0p_{H+1}$. In general, reference frame 6 is not placed with its origin on a joint axis, since there is no axis $N + 1$. However, for consistency, it is convenient to use the same notation for the location of the origin of frame N as for the other reference frames.

Therefore

$$\begin{aligned} {}^0v_{O_N} &= \sum_{i=1}^N \dot{\theta}_i {}^3w_i \times \left({}^0p_{H+1} - {}^0p_i \right) \\ {}^0v_{O_N} &= {}^0\omega_H \times {}^0p_{H+1} - \sum_{i=1}^N \dot{\theta}_i {}^3w_i \times {}^0p_i \end{aligned} \quad (9.21)$$

To make use of [Equations 9.19](#) and [9.21](#), it is necessary to be able to calculate w_i and \mathbf{p}_i for each joint axis. This is actually a problem of direct position kinematics.

The notation used is that of [Figure 9.7](#). Joint axes k and $k + 1$ are fixed in member k . The reference frame on member k is placed with its z axis along joint axis $k + 1$ and with its x axis in the direction of the common normal from joint axis k to $k + 1$. The members and joints are numbered serially outward, the fixed frame being 0 and the hand 6.

In reference frame k , $w_{k+1} = k = [0, 0, 1, 0]^T$. A convenient point on axis $k+1$ to use is the origin of frame k . Hence, in frame k , $\mathbf{p}_{k+1} = 0 = [0, 0, 0, 1]^T$.

Notice that in the 4×4 representation, the fourth element of a unit vector, such as k , is zero. This is because a unit vector expresses only a direction, and hence the position information in the fourth column of the A_k matrix has no relevance. If the fourth element of the unit vector w were not zero, w would no longer be one, and would

change with the transformation by the A_k matrices. With zero as the fourth element, the magnitude of a unit vector is one and remains one when the vector is multiplied by A_k .

Using [Equation 9.9](#), position vectors of a point ${}^k p_k$ in frame k and the same point ${}^{k-1} p_k$ in frame $k - 1$ are related by

$${}^{k-1} p_k = A_k {}^k p_k \quad (9.22)$$

where

$$A_k = \begin{bmatrix} \cos \theta_k & -\sin \theta_k \cos \alpha_k & \sin \theta_k \sin \alpha_k & a_k \cos \theta_k \\ \sin \theta_k & \cos \theta_k \cos \alpha_k & -\cos \theta_k \sin \alpha_k & a_k \sin \theta_k \\ 0 & \sin \alpha_k & \cos \alpha_k & r_k \\ 0 & 0 & 0 & 1 \end{bmatrix} \quad (9.10)$$

As indicated in [Figure 9.7](#), α_k is the angle between axes k and $k + 1$, a_k is the length of the common normal between those axes, and r_k is the distance along axis k from the origin of frame $k - 1$ to the foot of that common normal. A unit vector ${}^k v_k$ in frame k is related to the same vector, ${}^{k-1} v_k$ in frame $k - 1$ by

$${}^{k-1} v_k = A_k {}^k v_k \quad (9.23)$$

[Equations 9.20](#) and [9.21](#) can now be used recursively to obtain the vectors \mathbf{p}_k and w_k referred to frame 0.



Example 9.5

Direct Rate Kinematics of a Three-Axis Manipulator

The inner three joint axes of a manipulator are shown in [Figure 9.11](#). The geometric parameters of the links, the joint positions, and the joint rates are tabulated in [Table 9.2](#). Calculate the angular velocity of member 3 and the velocity of the wrist concurrency point, P , relative to the fixed reference frame.

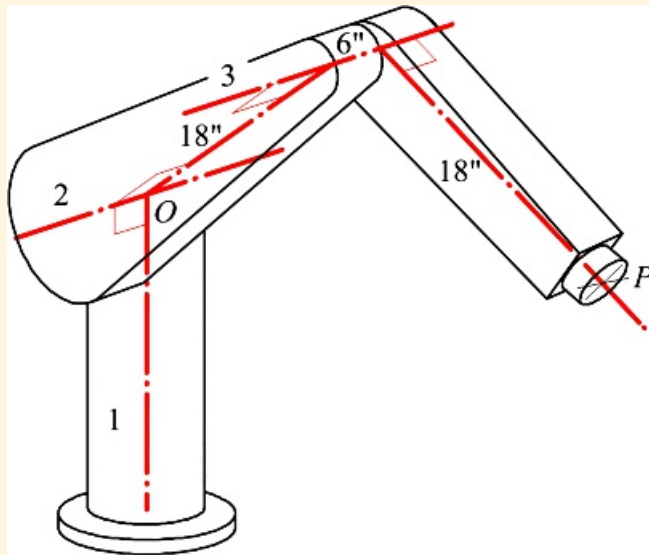


[Figure 9.11](#) The three-axis manipulator analyzed in Example 9.5.

[Table 9.2](#) Parameters for Robot in [Figure 9.11](#)

i	a_i (in)	r_i (in)	ω_i	Θ_i	$\dot{\theta}_i$ (rad/s)
1	0	0	90°	45°	1
2	18	0	0	30°	-0.75
3	18	6	0	-60°	0.5

Solution

Since there are only three joint axes, we substitute $N = 3$ in [Equations 9.19](#) and [9.21](#)

$${}^0\omega_3 = \sum_{k=1}^3 \dot{\theta}_k {}^0\omega_k \quad (a)$$

$${}^0\omega_3 = {}^0\omega_3 \times {}^0\omega_4 - \sum_{i=1}^3 \dot{\theta}_i {}^0\omega_i \times {}^0\omega_i \quad (b)$$

$$\begin{aligned} \rho_1 &= \emptyset \\ {}^0\omega_1 &= k \end{aligned}$$

So

$${}^0\omega_1 = \dot{\theta}_1 {}^0w_1 = 1\dot{\theta} = \dot{\theta} \text{ rad/s}$$

Applying [Equation 9.22](#)

$$\rho_2 = A_1\theta = \begin{bmatrix} \cos 45^\circ & 0 & \sin 45^\circ & 0 \\ \sin 45^\circ & 0 & -\cos 45^\circ & 0 \\ 0 & 1 & 0 & 0 \\ 0 & 0 & 0 & 1 \end{bmatrix} \begin{bmatrix} 0 \\ 0 \\ 0 \\ 1 \end{bmatrix} = \theta$$

and from [Equation 9.23](#)

$${}^0w_2 = A_1\dot{\theta} = \begin{bmatrix} \cos 45^\circ & 0 & \sin 45^\circ & 0 \\ \sin 45^\circ & 0 & -\cos 45^\circ & 0 \\ 0 & 1 & 0 & 0 \\ 0 & 0 & 0 & 1 \end{bmatrix} \begin{bmatrix} 0 \\ 0 \\ 0 \\ 1 \end{bmatrix} = \begin{bmatrix} \sin 45^\circ \\ -\cos 45^\circ \\ 0 \\ 0 \end{bmatrix} = \begin{bmatrix} 0.7071 \\ -0.7071 \\ 0 \\ 0 \end{bmatrix} = 0.7071(i-j)$$

Therefore

$${}^1\omega_2 = \dot{\theta}_2 {}^0w_2 = -0.75 \times 0.7071(i-j) = 0.5303(i-j) \text{ rad/s}$$

Similarly, applying [Equation 9.22](#) twice to transform from frame 2 to frame 0 we get

$$\begin{aligned} \rho_3 &= A_1A_2\theta = \begin{bmatrix} \cos 45^\circ & 0 & \sin 45^\circ & 0 \\ \sin 45^\circ & 0 & -\cos 45^\circ & 0 \\ 0 & 1 & 0 & 0 \\ 0 & 0 & 0 & 1 \end{bmatrix} \begin{bmatrix} \cos 30^\circ & -\sin 30^\circ & 0 & 18 \cos 30^\circ \\ \sin 30^\circ & \cos 30^\circ & 0 & 18 \sin 30^\circ \\ 0 & 0 & 1 & 0 \\ 0 & 0 & 0 & 1 \end{bmatrix} \begin{bmatrix} 0 \\ 0 \\ 0 \\ 1 \end{bmatrix} \\ &= \begin{bmatrix} 11.023 \\ 11.023 \\ 9.000 \\ 1 \end{bmatrix} = 11.023i + 11.023j + 9.000k \end{aligned}$$

and applying [Equation 9.23](#) twice

$$\begin{aligned} {}^0w_3 &= A_1A_2\dot{\theta} = \begin{bmatrix} \cos 45^\circ & 0 & \sin 45^\circ & 0 \\ \sin 45^\circ & 0 & -\cos 45^\circ & 0 \\ 0 & 1 & 0 & 0 \\ 0 & 0 & 0 & 1 \end{bmatrix} \begin{bmatrix} \cos 30^\circ & -\sin 30^\circ & 0 & 18 \cos 30^\circ \\ \sin 30^\circ & \cos 30^\circ & 0 & 18 \sin 30^\circ \\ 0 & 0 & 1 & 0 \\ 0 & 0 & 0 & 1 \end{bmatrix} \begin{bmatrix} 0 \\ 0 \\ 0 \\ 1 \end{bmatrix} \\ &= \begin{bmatrix} \sin 45^\circ \\ -\cos 45^\circ \\ 0 \\ 0 \end{bmatrix} = \begin{bmatrix} 0.7071 \\ -0.7071 \\ 0 \\ 0 \end{bmatrix} = 0.7071(i-j) = {}^0w_2 \end{aligned}$$

Since joint axes 2 and 3 are parallel, ${}^0\omega_3$ should be equal to ${}^0\omega_2$. Hence

$${}^2\omega_3 = \dot{\theta}_3 {}^0\omega_3 = 0.5 \times 0.7071(i-j) = 0.3536(i-j) \text{ rad/s}$$

Finally, we need the location of point P . Point P is the origin of reference frame 3. That is, point \mathbf{p}_4

$$\begin{aligned} \mathbf{p}_4 &= A_1 A_2 A_3 \mathbf{p}_{\text{tip}} \\ &= \begin{bmatrix} \cos 45^\circ & 0 & \sin 45^\circ & 0 \\ \sin 45^\circ & 0 & -\cos 45^\circ & 0 \\ 0 & 1 & 0 & 0 \\ 0 & 0 & 0 & 1 \end{bmatrix} \begin{bmatrix} \cos 30^\circ & -\sin 30^\circ & 0 & 18 \cos 30^\circ \\ \sin 30^\circ & \cos 30^\circ & 0 & 18 \sin 30^\circ \\ 0 & 0 & 1 & 0 \\ 0 & 0 & 0 & 1 \end{bmatrix} \\ &= \begin{bmatrix} \cos 60^\circ & \sin 60^\circ & 0 & 18 \cos 60^\circ \\ -\sin 60^\circ & \cos 60^\circ & 0 & -18 \sin 60^\circ \\ 0 & 0 & 1 & 6 \\ 0 & 0 & 0 & 1 \end{bmatrix} \begin{bmatrix} 0 \\ 0 \\ 0 \\ 1 \end{bmatrix} = \begin{bmatrix} 0.5000 & 0.8660 & 0 & 0 \\ 0.6123 & -0.3536 & -0.7071 & 17.803 \\ 0 & 0 & 0 & 1 \\ 0 & 0 & 0 & 1 \end{bmatrix} \begin{bmatrix} 0 \\ 0 \\ 0 \\ 1 \end{bmatrix} \\ &= \begin{bmatrix} 26.238 \\ 17.803 \\ 0 \\ 1 \end{bmatrix} = 26.238i + 17.803j \end{aligned}$$

Now, using Equation a gives

$$\begin{aligned} {}^0\omega_3 &= \dot{\theta}_1 {}^0\omega_1 + \dot{\theta}_2 {}^0\omega_2 + \dot{\theta}_3 {}^0\omega_3 = {}^0\omega_1 + {}^1\omega_2 + {}^2\omega_3 = k + 0.3536(j-i) + 0.3536(i-j) \\ &= -0.1767i + 0.1767j + k \text{ rad/s} \end{aligned}$$

and using Equation b

$${}^0v_{\mathbf{p}_3} = {}^0\omega_3 \times {}^0\mathbf{p}_4 - \sum_{i=1}^3 \dot{\theta}_i {}^0\omega_i \times {}^0\mathbf{p}_i = {}^0\omega_3 \times {}^0\mathbf{p}_4 - {}^0\omega_1 \times {}^1\mathbf{p}_1 - {}^1\omega_2 \times {}^2\mathbf{p}_2 - {}^2\omega_3 \times {}^3\mathbf{p}_3$$

or

$$\begin{aligned} {}^0v_{\mathbf{p}_3} &= (-0.1767i + 0.1767j + k) \times (26.238i + 17.803j) - 0 - 0 - 0.3536(i-j) \\ &\quad \times (11.023i + 11.023j + 9.000k) \\ &= -14.62i + 29.47j - 15.59k \end{aligned}$$

9.5.3 Inverse Rate Kinematics

As is well known, the position of the hand relative to the fixed frame can be described by means of a set of six independent algebraic equations containing the joint position variables $\theta_1, \dots, \theta_6$. There are numerous ways to formulate such a set of equations. Differentiation with respect to time of the direct position kinematics equations yields a set of equations of the form

$$\dot{\mathbf{r}} = \mathbf{F} \dot{\boldsymbol{\theta}} \quad (9.24)$$

where v is a six-component velocity vector, $\dot{\theta} = [\dot{\theta}_1, \dot{\theta}_2, \dots, \dot{\theta}_N]^T$ is an N dimensional vector composed of the joint rates, and \mathbf{J} is a $6 \times N$ matrix whose elements are, in general, nonlinear functions of $\theta_1, \dots, \theta_N$. \mathbf{J} is called the Jacobian matrix of this algebraic system. If the joint positions $\theta_1, \dots, \theta_N$ are known, [Equation 9.24](#) yields six linear algebraic equations in the joint rates $\dot{\theta}_1, \dots, \dot{\theta}_N$. If the joint rates are given, solution of [Equation 9.24](#) for v is a solution of the direct rate kinematics problem. Notice that \mathbf{J} can be regarded as a known matrix for this purpose provided all the joint positions are known.

Solution of [Equation 9.24](#) for the joint rates is possible if $N = 6$. In the remainder of this chapter discussion will be limited to this case. A mode of control for $N > 6$ compatible with the work presented here makes use of pseudo-inversion of the Jacobian to eliminate the ambiguity due to the additional degrees of freedom. This is beyond the scope of this book.

The ease of computation of the elements of the Jacobian matrix from the joint positions, and of inverse solution of [Equation 9.24](#), is very strongly dependent on the way in which this equation is formulated. Since these computations must be repeated at each time step in a real-time rate coordination algorithm, the formulation becomes critical to the efficiency of the software. A very elegant and efficient geometric relationship between the rates of motion about the joints of a linkage and the velocity states of the members is available in the form of screw system theory. Therefore, in order to make use of geometric information to give an efficient formulation of [Equation 9.24](#), an algebraic formulation based on [Equations 9.19](#) and [9.21](#) will be used.

The angular velocity ω of the hand of a six-axis serial manipulator is related to the joint rates by

$${}^0\omega_6 = \sum_{k=1}^6 \dot{\theta}_k {}^0w_k \quad (9.19)$$

where w_k is a unit vector having the direction of joint axis k .

Using [Equation 9.21](#)

$${}^0v_{G_6} = {}^0w_6 \times {}^0\phi_7 - \sum_{i=1}^6 \dot{\theta}_i {}^0w_i \times {}^0\phi_i$$

it is convenient in this case to combine ${}^0\omega_6 \times {}^0\phi_7$ with ${}^0v_{G_6}$ because, for inverse rate kinematics, we may assume that ${}^0\omega_6$ will be known, and ${}^0\phi_7$ may be calculated from the readings of the joint position sensors. Let

$${}^0\beta = {}^0v_{G_6} - {}^0\omega_6 \times {}^0\phi_7 \quad (9.25)$$

Then

$${}^0\beta = \sum_{i=1}^6 \dot{\theta}_i {}^0\phi_i \times {}^0w_i \quad (9.26)$$

the velocity ${}^0\beta$ can be thought of as the velocity of the point in the hand, possibly extended, which is instantaneously coincident with the origin of frame 0.

[Equation 9.26](#) can be written in the form

$${}^0\beta = \sum_{k=1}^6 \dot{\theta}_k {}^0\lambda_k \quad (9.27)$$

where $\dot{\theta}_k = \dot{\rho}_{\theta_k} \times \dot{\rho}_{w_k}$. If joint k is a slider, the k th term is replaced by $\dot{\rho}_{\theta_k} \dot{\theta}_k$. Note that the joint rates for sliders do not appear in [Equation 9.19](#).

[Equations 9.19](#) and [9.27](#) can now be combined to form a system of the form of [Equation 9.24](#)

$$\nu = \begin{bmatrix} \varphi \\ \psi \\ \theta \end{bmatrix}, \quad \Gamma = \begin{bmatrix} w_1 & \dots & w_6 \\ \lambda_1 & \dots & \lambda_6 \end{bmatrix} \quad (9.28)$$

Again, if the k th joint is a slider, the k th column of Γ is replaced by $[\emptyset \ w_k]^T$.

To compute the elements of Γ , it is necessary to have expressions for w_k and ρ_k in terms of the joint angles. These are easily obtained in a recursive form convenient for computation by means of a direct position kinematics solution in the same way as was done in Example 9.5.

As already noted, the direct rate kinematics problem is that of finding $\nu = [\varphi \ \psi \ \theta]^T$ given the joint rates $\dot{\theta}_1, \dots, \dot{\theta}_6$. It is solved by direct substitution of the joint rates in [Equation 9.24](#) to give ν directly. The direct rate kinematics problem is important when doing an acceleration analysis for the purpose of studying dynamics. The total velocities of the members are needed for the computation of Coriolis and centripetal acceleration components.

The important problem from the point of view of robotic coordination is the inverse rate kinematics problem. As will be outlined below, it is the basis of all robot software that generates prescribed trajectories relative to the world or fixed coordinate frame.

To solve the linear system of equations in the joint rates obtained by decomposing [Equation 9.24](#) into its component equations when ν is known, it is necessary to invert the Jacobian matrix Γ . The equation becomes

$$\dot{\theta} = \Gamma^{-1} \nu$$

Since Γ is a 6×6 matrix, numerical inversion is not very attractive in real-time software that must run at computation cycle rates of the order of 100 Hz or more. Worse, it is quite possible for Γ to become singular ($\Gamma \vdash 0$). The inverse does not then exist. Even when the Jacobian matrix does not become singular, and, in fact, singularity is a rare occurrence in practice, it may become ill conditioned, leading to degraded performance in significant portions of the manipulator's working envelope.

Most industrial robot geometries are simple enough that the Jacobian matrix can be inverted analytically, leading to a set of explicit equations for the joint rates. This greatly reduces the number of computation operations needed as compared with numerical inversion.



9.6 Closed-Loop Linkages

As was the case for planar linkages, closing a loop in the linkage results in the generation of a set of closure equations. In order to find the positions of all joints, given the position of one joint chosen as the input joint, it is necessary to solve the closure equations. The mobility criterion

$$M = 6(m - j - 1) + \sum_{i=1}^j f_i \quad (1.3)$$

can be used to determine the connectivity sum of the joints in a single closed loop spatial linkage that has mobility one. In a single closed loop, $m = j$, so [Equation 1.3](#) gives

$$1 = -6 + \sum_{i=1}^j f_i$$

or

$$\sum f_i = 7.$$

If all joints have connectivity one, this implies that the linkage has seven joints, and hence seven members.

The closure equations can be generated using the transformation [Equation 9.9](#)

$$\beta_{N-1} = A_N \beta_N \quad (9.9)$$

If this transformation is applied between successive pairs of members around the loop, one eventually returns to the original reference frame. Hence

$$\beta = A_1 A_2 A_3 A_4 A_5 A_6 \beta_I \quad (9.29)$$

Expansion of [Equation 9.29](#) produces a set of equations in the seven joint variables. By selecting six of these equations and solving them, it is possible to find all joint variables given the value of one input variable. The problem is actually very similar to the inverse position problem of the open-chain linkage and presents similar difficulties of solution.



Example 9.6

Derivation of Input-Output Relationship of Universal Joint

Develop an equation relating the input and output shaft angles of the universal joint discussed in Section 8.2.3.

Solution

The mechanism is shown in [Figure 9.12](#), which is similar to [Figure 8.22](#). Its geometric parameters and kinematic variables are listed in [Table 9.3](#). Here θ_1 and θ_2 are considered to be the input and output angles. The angle between shafts 1 and 2 is $\alpha_1 = \gamma$. All the other angles between successive joint angles: $\alpha_2 = \alpha_3 = \alpha_4 = 90^\circ$.

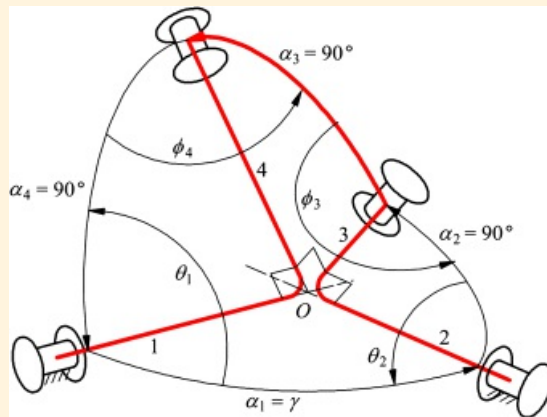


[Figure 9.12](#) The geometric parameters and kinematic variables of the universal joint analyzed in Example 9.7. Note that this figure is similar to [Figure 8.22](#).

[Table 9.3](#) Geometric Properties of Universal Joint in Example 9.6

i	a_i	r_i	α_i	Θ_i
1	0	0	γ	θ_1
2	0	0	90°	θ_2
3	0	0	90°	θ_3
4	0	0	90°	θ_4

Applying [Equation 9.29](#) to the four-bar loop

$$l = A_1 A_2 A_3 A_4 \quad (9.30)$$

There is great advantage in trying to simplify the equations as much as possible before expansion. In this case, we can separate the variables θ_1 and θ_2 from θ_3 and θ_4 by post-multiplying both sides of the equation first by A_4^{-1} and then by A_3^{-1} to get

$$A_1 A_2 = A_4^{-1} A_3^{-1} \quad (9.31)$$

It is now time to expand into component equations by substituting from [Equations 9.10](#) and [9.18](#)

$$\begin{aligned}
& \begin{bmatrix} \cos \theta_1 & -\sin \theta_1 \cos \gamma & \sin \theta_1 \sin \gamma & 0 \\ \sin \theta_1 & \cos \theta_1 \cos \gamma & -\cos \theta_1 \sin \gamma & 0 \\ 0 & \sin \gamma & \cos \gamma & 0 \\ 0 & 0 & 0 & 1 \end{bmatrix} \begin{bmatrix} \cos \theta_2 & 0 & \sin \theta_2 & 0 \\ \sin \theta_2 & 0 & -\cos \theta_2 & 0 \\ 0 & 1 & 0 & 0 \\ 0 & 0 & 0 & 1 \end{bmatrix} \\
& = \begin{bmatrix} \cos \theta_4 & \sin \theta_4 & 0 & 0 \\ 0 & 0 & 1 & 0 \\ \sin \theta_4 & -\cos \theta_4 & 0 & 0 \\ 0 & 0 & 0 & 1 \end{bmatrix} \begin{bmatrix} \cos \theta_3 & \sin \theta_3 & 0 & 0 \\ 0 & 0 & 1 & 0 \\ \sin \theta_3 & -\cos \theta_3 & 0 & 0 \\ 0 & 0 & 0 & 1 \end{bmatrix}
\end{aligned}$$

Performing the matrix multiplications and equating corresponding elements, we get the following system of scalar equations. Note that only the three-by-three sub-matrix in the top left-hand corner gives nontrivial equations. The remaining equations, which are $0 = 0$ or $1 = 1$, are not written out below.

$$\begin{aligned}
& \cos \theta_1 \cos \theta_2 - \sin \theta_1 \sin \theta_2 \cos \gamma = \cos \theta_3 \cos \theta_4 & (3, 1) \\
& \sin \theta_1 \sin \gamma = \sin \theta_3 \cos \theta_4 & (3, 2) \\
& \cos \theta_1 \sin \theta_2 + \sin \theta_1 \cos \theta_2 \cos \gamma = \sin \theta_4 & (3, 3) \\
& \sin \theta_1 \cos \theta_2 + \cos \theta_1 \sin \theta_2 \cos \gamma = \sin \theta_3 & (2, 1) \\
& -\cos \theta_1 \sin \gamma = -\cos \theta_3 & (2, 2) \\
& \sin \theta_1 \sin \theta_2 - \cos \theta_1 \cos \theta_2 \cos \gamma = 0 & (2, 3) \\
& \sin \theta_2 \sin \gamma = \cos \theta_3 \sin \theta_4 & (3, 1) \\
& \cos \gamma = \sin \theta_3 \sin \theta_4 & (3, 2) \\
& -\cos \theta_2 \sin \gamma = -\cos \theta_4 & (3, 3)
\end{aligned}$$

These are all valid relationships between the angle variables $\theta_1, \theta_2, \theta_3$, and θ_4 . They are not independent, since the corresponding elements on each side of the equation are related by [Equations 9.3](#). Inspection of these equations reveals that Equation (2, 3) contains only the two variables of interest, θ_1 and θ_2 . This equation can be readily manipulated into the form

$$\tan \theta_1 \tan \theta_2 = \cos \gamma \quad (8.9)$$

which was the result to be derived. As was shown in Section 8.2.3 of [Chapter 8](#), this equation gives the input-output relationship of the shaft angles of the universal joint.



9.7 Lower-Pair Joints

Linkages containing any combination of lower pair joints (see [Table 1.1](#)) can be analyzed by the methods presented in this chapter. For the *axial* joints, namely revolute, prismatic, screw, and cylindrical joints, a single transform is needed for each joint. Referring to [Equation 9.10](#)

$$A_N = \begin{bmatrix} \cos \theta_N & -\sin \theta_N \cos \alpha_N & \sin \theta_N \sin \alpha_N & \omega_N \cos \theta_N \\ \sin \theta_N & \cos \theta_N \cos \alpha_N & -\cos \theta_N \sin \alpha_N & \omega_N \sin \theta_N \\ 0 & \sin \alpha_N & \cos \alpha_N & r_N \\ 0 & 0 & 0 & 1 \end{bmatrix} \quad (9.10)$$

we see that this same transform works in all four cases. The only difference is in which of the parameters are regarded as being variable. In the case of a revolute, θ_N is the variable and r_N is a constant. For a prismatic joint, r_N is variable and θ_N is a constant. In the case of a screw joint, θ_N and r_N both vary, but they are not independent of one another, being related by the equation

$$r_N = R_N + h_N \theta_N \quad (9.32)$$

where R_N and h_N are constants. Here, h_N is the pitch of the screw and R_N is the constant value of the joint offset when θ_N is zero. Finally, in the case of a cylindrical joint, both r_N and θ_N are variables, and they may vary completely independently of one another.

The two remaining lower-pair joint types, spherical and planar joints, may each be modeled by means of kinematically equivalent chains of three revolute joints. In the case of the spherical joint, the three revolute axes are concurrent at the center of the spherical joint being modeled, and the joint axes are successively orthogonal. That is, the middle joint axis is orthogonal to each of the other two. Those other two joint axes are not, in general, orthogonal to each other. In fact, the angle between them varies with motion about the middle joint. In the case of a planar joint, the three revolute axes are parallel and orthogonal to the plane of motion of the plane joint being modeled. These two equivalent chains are shown in [Figures 9.13](#) and [9.14](#), respectively.

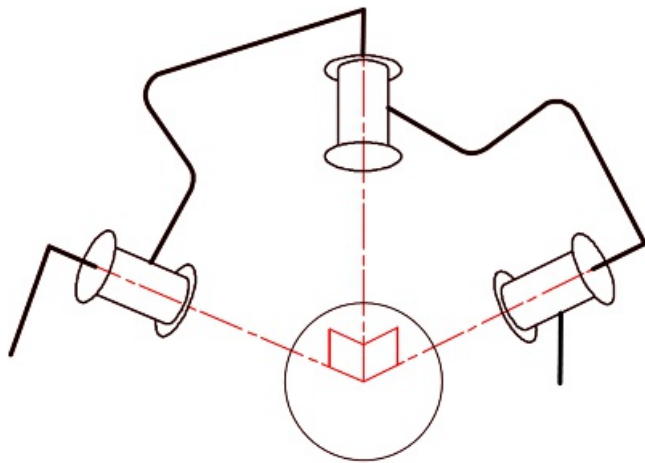


[Figure 9.13](#) Chain of three revolute joints that is kinematically equivalent to a spherical joint.

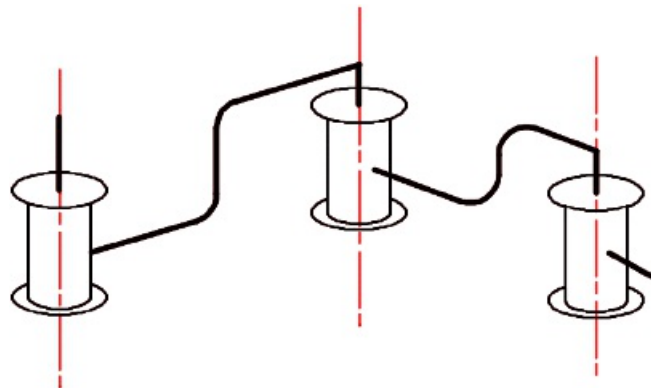


[Figure 9.14](#) Chain of three revolute joints that is kinematically equivalent to a planar joint.

The primary application of these equivalent mechanisms is in linkages that include closed loops. This is because spherical and plane joints are always passive joints that cannot be used in open-chain structures.



Example 9.7

Input-Output Relationship of a Simple Coupling

Two nonintersecting shafts turn in cylindrical joints, as shown in [Figure 9.15](#). The shaft axes are at angle μ to one another, and the length of their common normal is m . The two shafts are coupled by means of an offset spherical joint, as shown in the figure. The center of the spherical joint is distant p and q from the two shafts as shown. Develop equations relating the angle of shaft 2 to that of shaft 1 and the axial displacements of both shafts to the angular displacement of shaft 1.

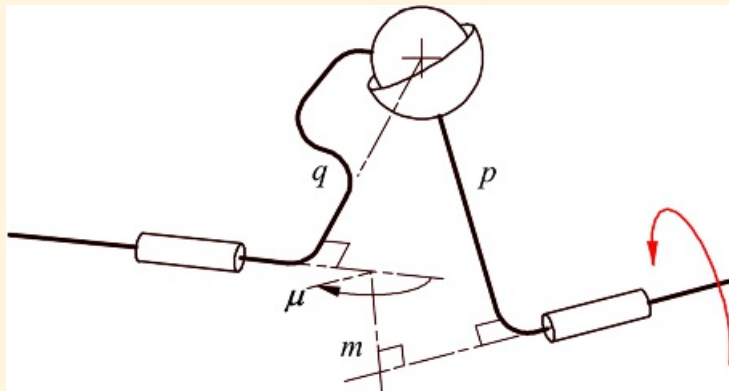


[Figure 9.15](#) The simple coupling between two skew shafts that is analyzed in Example 9.7. The linkage has only three members connected in a single loop via two cylindrical joints and a spherical joint.

Solution

As indicated above, the spherical joint can be replaced by the kinematically equivalent combination of three successively orthogonal revolute joints, with concurrency point at the center of the sphere. This substitution is shown in [Figure 9.16](#). We are at liberty to arrange the directions of the axes of joints 3 and 5 relative to 2 and 1, respectively, for convenience. Hence, we choose to make axis 3 parallel to 2 and axis 5 parallel to 1. The linkage geometric parameters and joint variables are then as shown in [Table 9.4](#).

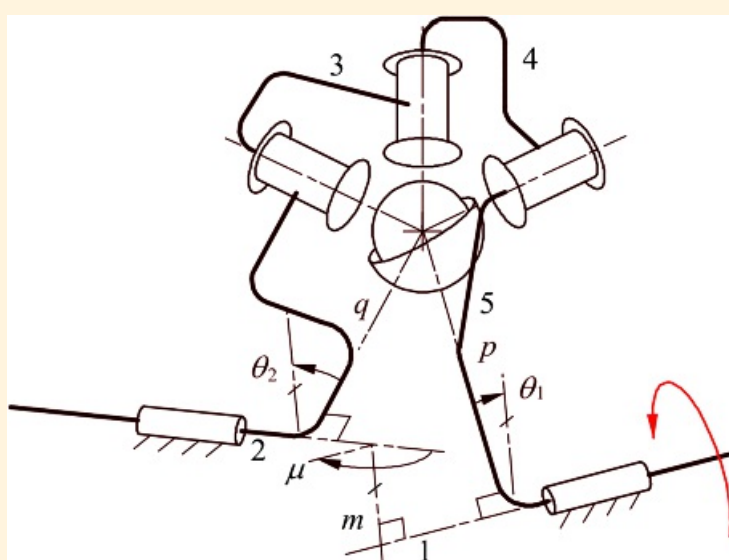


[Figure 9.16](#) The linkage of [Figure 9.15](#) with a chain of three successively orthogonal revolutes substituted for the spherical joint. The concurrency point of the revolute axes is at the center of the

spherical joint that is replaced.

Table 9.4 Parameters for the Linkage in Example 9.7

i	a_i	r_i	α_i	θ_i
1	m	r_1	μ	θ_1
2	q	r_2	0	θ_2
3	0	0	90°	θ_3
4	0	0	90°	θ_4
5	p	0	0	θ_5

In this case we have five joints, so the closure equation is

$$A_1 A_2 A_3 A_4 A_5 = I$$

As in the case of the previous example, it is advantageous to rearrange the equation to split up the variables before expanding. Post-multiplying in succession by A_5^{-1} , A_4^{-1} , A_3^{-1} gives the form

$$A_1 A_2 = A_5^{-1} A_4^{-1} A_3^{-1}$$

We now embark on expansion of this equation, again referring to [Equations 9.10](#) and [9.18](#)

$$A_1 A_2 = \begin{bmatrix} \cos \theta_1 & -\sin \theta_1 \cos \mu & \sin \theta_1 \sin \mu & m \cos \theta_1 \\ \sin \theta_1 & \cos \theta_1 \cos \mu & -\cos \theta_1 \sin \mu & m \sin \theta_1 \\ 0 & \sin \mu & \cos \mu & r_1 \\ 0 & 0 & 0 & 1 \end{bmatrix} \begin{bmatrix} \cos \theta_2 & -\sin \theta_2 & 0 & q \cos \theta_2 \\ \sin \theta_2 & \cos \theta_2 & 0 & q \sin \theta_2 \\ 0 & 0 & 1 & r_2 \\ 0 & 0 & 0 & 1 \end{bmatrix}$$

and

$$A_5^{-1} A_4^{-1} A_3^{-1} = \begin{bmatrix} \cos \theta_5 & \sin \theta_5 & 0 & -p \\ -\sin \theta_5 & \cos \theta_5 & 0 & 0 \\ 0 & 0 & 1 & 0 \\ 0 & 0 & 0 & 1 \end{bmatrix} \begin{bmatrix} \cos \theta_4 & \sin \theta_4 & 0 & 0 \\ 0 & 0 & 1 & 0 \\ \sin \theta_4 & -\cos \theta_4 & 0 & 0 \\ 0 & 0 & 0 & 1 \end{bmatrix} \begin{bmatrix} \cos \theta_3 & \sin \theta_3 & 0 & 0 \\ 0 & 0 & 1 & 0 \\ \sin \theta_3 & -\cos \theta_3 & 0 & 0 \\ 0 & 0 & 0 & 1 \end{bmatrix}$$

Combining these expressions, performing the matrix multiplication, and equating corresponding elements of the matrices on either side gives the following set of equations

$$\begin{aligned}
& \cos \theta_1 \cos \theta_2 - \sin \theta_1 \sin \theta_2 \cos \mu = \cos \theta_3 \cos \theta_4 \cos \theta_5 + \sin \theta_3 \sin \theta_5 & (1,1) \\
& -\cos \theta_1 \sin \theta_2 - \sin \theta_1 \cos \theta_2 \cos \mu = \sin \theta_3 \cos \theta_4 \cos \theta_5 - \cos \theta_3 \sin \theta_5 & (1,2) \\
& \sin \theta_1 \sin \mu = \sin \theta_4 \cos \theta_5 & (1,3) \\
& q(\cos \theta_1 \cos \theta_2 - \sin \theta_1 \sin \theta_2 \cos \mu) + r_2 \sin \theta_1 \sin \mu + m \cos \theta_1 = -p & (1,4) \\
& \sin \theta_1 \cos \theta_2 + \cos \theta_1 \sin \theta_2 \cos \mu = -\cos \theta_3 \cos \theta_4 \sin \theta_5 + \sin \theta_3 \cos \theta_5 & (2,1) \\
& -\sin \theta_1 \sin \theta_2 + \cos \theta_1 \cos \theta_2 \cos \mu = -\sin \theta_3 \cos \theta_4 \sin \theta_5 - \cos \theta_3 \cos \theta_5 & (2,2) \\
& \cos \theta_1 \sin \mu = \sin \theta_4 \sin \theta_5 & (2,3) \\
& q(\sin \theta_1 \cos \theta_2 + \cos \theta_1 \sin \theta_2 \cos \mu) - r_2 \cos \theta_1 \sin \mu + m \sin \theta_1 = 0 & (2,4) \\
& \sin \theta_2 \sin \mu = \cos \theta_3 \sin \theta_4 & (3,1) \\
& \cos \theta_2 \sin \mu = \sin \theta_3 \sin \theta_4 & (3,2) \\
& \cos \mu = -\cos \theta_4 & (3,3) \\
& q \sin \theta_2 \sin \mu + r_2 \cos \mu + r_1 = 0 & (3,4)
\end{aligned}$$

The equations corresponding to the fourth row of the matrices are trivial.

We have no interest in the angles of the “virtual” joints: θ_3 , θ_4 , and θ_5 . The variables of interest are the independent variable θ_1 and the dependent variables θ_2 , r_1 , and r_2 . Inspection of these equations reveals that the (1,4), (2,4), and (3,4) equations contain only these latter four variables. Therefore, it should be possible to solve these three equations to obtain expressions for θ_2 , r_1 , and r_2 in terms of θ_1 .

If the (1,4) equation is multiplied by $\cos \theta_1$ and added to the (2,4) equation multiplied by $\sin \theta_1$, the r_2 terms cancel, and using $\cos^2 \theta_1 + \sin^2 \theta_1 = 1$, the resulting equation reduces to

$$q \cos \theta_2 + m = -p \cos \theta_1$$

or

$$\theta_2 = \pm \cos^{-1} \left\{ \frac{m + p \cos \theta_1}{q} \right\}$$

Here the second solution corresponds to physically sliding the shaft out of cylindrical joint 2, turning member 2 through 180° and sliding the shaft back into the bushing in the opposite direction, and then sliding along the joint axis until the spherical joint returns to its original position. This would not be physically possible without encountering interference unless the bushing and shaft are duplicated, in which case member 2 would be symmetric and the two solutions would be indistinguishable from one another. Therefore, nothing is lost by ignoring the second solution. Hence

$$\theta_2 = \cos^{-1} \left\{ \frac{m + p \cos \theta_1}{q} \right\} \quad (a)$$

Multiplying the (1,4) equation by $\sin \theta_1$ and subtracting from it the (2,4) equation multiplied by $\cos \theta_1$ gives, after similar simplification

$$-q \sin \theta_2 \cos \mu + r_2 \sin \mu = -p \sin \theta_1$$

or

$$r_2 = \frac{q \sin \theta_2 \cos \mu - p \sin \theta_1}{\sin \mu} \quad (b)$$

Consequently, once θ_2 has been obtained from Equation (a), this expression can be used to compute r_2 .

Finally, after θ_2 and r_2 have been computed, the (3,4) equation can be used to solve for r_1

$$r_1 = \frac{p \sin \theta_1 \cos \mu - q \sin \theta_2}{\sin \mu} \quad (c)$$

Solution of Equations (a), (b), and (c) in sequence solves the problem of obtaining the values of θ_2 , r_1 , and r_2 for any given value of θ_1 .



9.8 Motion Platforms

9.8.1 Mechanisms Actuated in Parallel

The mechanisms discussed in this section are spatial mechanisms, and detailed analysis is complex and requires methods developed from those presented in earlier sections of this chapter. However, we will give a simple presentation here, since these are mechanisms that have considerable practical importance. The mechanisms in this class provide multiple actuated degrees of freedom, typically three or six, in the same way that the serial-chain mechanisms discussed earlier in this chapter do. As compared with those serial mechanisms, parallel mechanisms are stronger and stiffer but are usually more restricted in the range of motion they provide.

9.8.2 The Stewart-Gough Platform

Although it is far from the simplest parallel mechanism, we will discuss the Stewart-Gough platform first because of its practical and historic importance. The Stewart-Gough platform has six limbs acting in parallel to connect the “platform” member to the base. Each limb has a linear actuator, such as a hydraulic cylinder or a ball screw that provides the kinematic equivalent of an actuated prismatic joint. Each limb is connected to the base and the platform by a spherical joint at one end and a universal joint at the other. In [Figure 9.17](#), the spherical joints are indicated as being at the upper ends of the limbs and the universal joints at the lower ends, but they may be reversed.

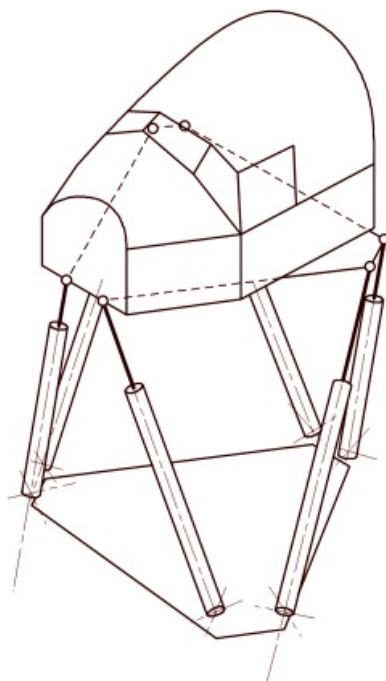


[Figure 9.17](#) A Stewart-Gough platform used as the motion base of a flight simulator.

Stewart-Gough platforms have been very widely used as motion bases for aircraft simulators and similar devices. The great strength and stiffness of the mechanism, together with its ability to produce universally controlled spatial motion, make it ideal for this application. Its relatively restricted motion range is not usually a serious limitation in this type of application.

Stewart-Gough platforms have mathematical properties that, in some respects, bear an inverse relationship to the corresponding properties of serial chains. The *inverse* position problem for a Stewart-Gough platform is very straightforward. Restating the problem: Given the transformation describing the position of the floating platform reference frame relative to the base reference frame, find the limb lengths.

Referring to [Figure 9.18](#), the problem may be restated as follows

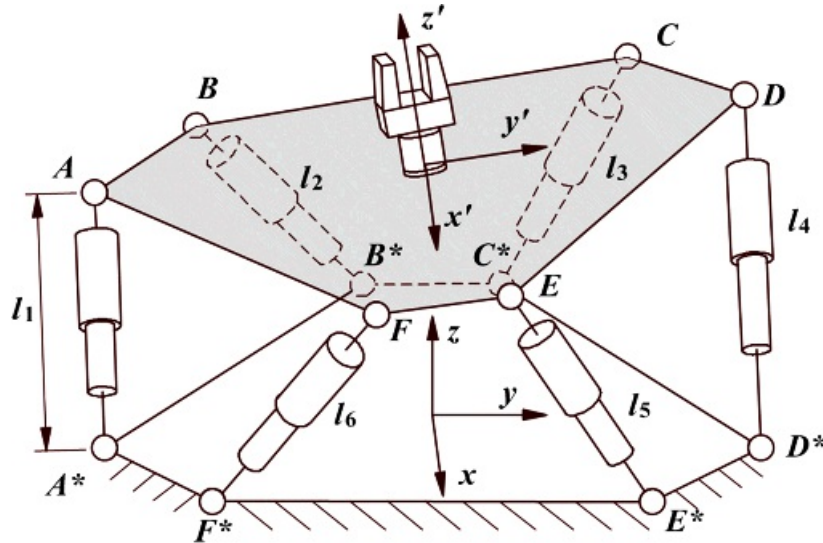


[Figure 9.18](#) The Stewart-Gough platform model used in describing its kinematic properties in the text.

Given the 4×4 transformation

$$p = Q p' \quad (9.33)$$

relating coordinates referred to the fixed and floating frames, respectively, find the lengths $l_i, i = 1, \dots, 6$.

Since the positions of the points A, B, C, D, E, F can be assumed to be known relative to the primed reference frame, [Equation 9.33](#) can be used to obtain their positions relative to the fixed frame. Similarly, the positions of the points A^*, B^*, C^*, D^*, E^* can be assumed to be known relative to the fixed frame. Then the Pythagorean theorem can be used to find

$$l_1 = \|p_A - p_{A^*}\| \quad (9.34)$$

where p_A is the position of A relative to the fixed frame and p_{A^*} is the position of A^* relative to that frame. Similarly, the lengths of the other limbs can be calculated.

In contrast, the *direct* position problem, namely, given $l_i, i = 1, \dots, 6$, find the transformation matrix Q in [Equation 9.33](#), is quite difficult and has multiple solutions: 16 for the configuration shown in [Figure 9.18](#). This is in contrast to the serial chain as described earlier. There the *direct* problem was straightforward and single valued, and the *inverse* problem was demanding and multivalued.

The inverse symmetry is even more marked in the velocity domain. The *inverse* rate kinematics may be solved directly. The *direct* rate problem requires inversion of a 6×6 matrix with structure closely related to the Jacobian matrix described in Section 9.5.3.

9.8.3 The 3-2-1 Platform

The 3-2-1 platform ([Figure 9.19](#)) is a special configuration that has some practical importance. It is arranged so that the motion and force equations decouple for small displacements. For this reason it has been used in three-dimensional vibration testing tables and for similar functions. The same configuration can be used as a six-component force sensor, with the actuators replaced by uniaxial load cells.

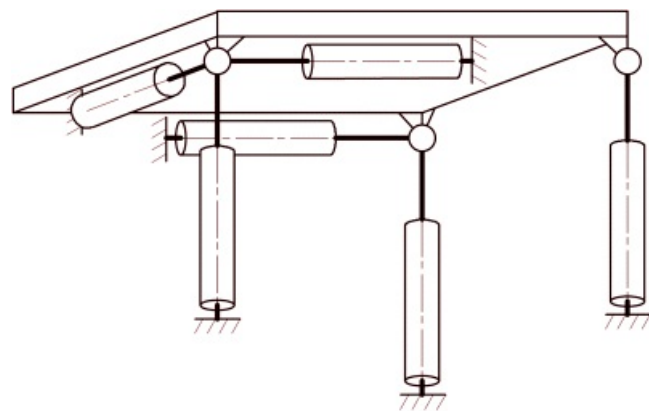


[Figure 9.19](#) A 3-2-1 motion platform. This is actually a variant of the Stewart-Gough platform. For small displacements, the motion components are decoupled.



References

1. Whitney, D. E. (1972). "The Mathematics of Coordinated Control of Prosthetic Arms and Manipulators." *J. Dyn. Syst. Meas. Control*, pp. 303–309.
2. Pieper, D. L., and Roth, B. (1969). "The Kinematics of Manipulators under Computer Control." *Proceedings of the Second International Conference on the Theory of Machines and Mechanisms*, Warsaw, September.



Problems

- 9.1 For the information given in [Figure P9.1](#), find the velocity of point *B*. Show all equations used with terms properly labeled.

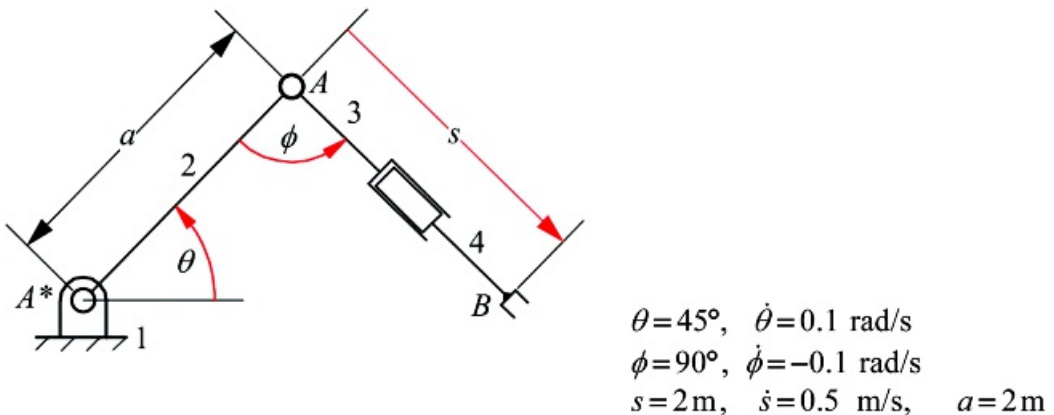


[Figure P9.1](#) Linkage for Problem 9.1.

- 9.2 In the manipulator shown in [Figure P9.2](#), the joint axes at A^* and A are oriented along the z and x axes, respectively, and link 3 is perpendicular to link 2. For the position shown, find the velocity of point *B*. Links 2 and 3 lie in the y - z plane.

$$\dot{\theta} = 100 \text{ rad/s}, \dot{\phi} = 10 \text{ rad/s}, A^*A = AB = 10 \text{ m}$$

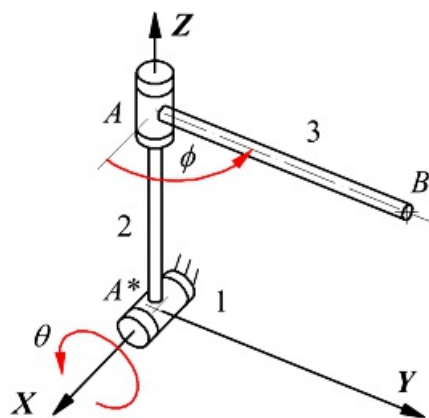


[Figure P9.2](#) Manipulator linkage for Problem 9.2.

- 9.3 For the information given in [Figure P9.3](#), find the velocity and acceleration of point *B*.

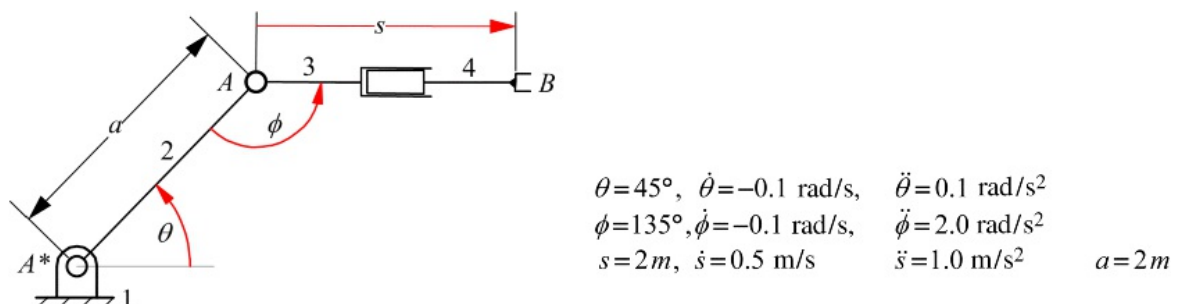


[Figure P9.3](#) Linkage for Problem 9.3.

9.4 For the information given in [Figure P9.4](#), find the velocity and acceleration of Point *B*.

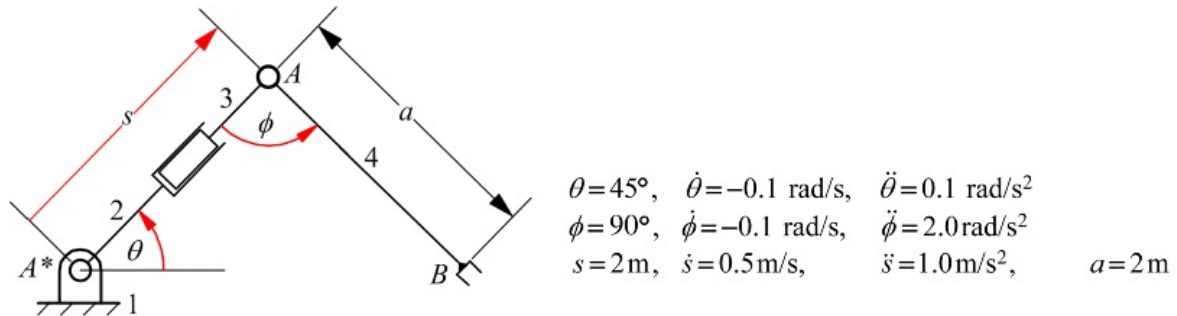


[Figure P9.4](#) Linkage for Problem 9.4.

9.5 The planar open chain linkage shown in [Figure P9.5](#) has link lengths $A^*A = AB = 1 \text{ ft}$. Joint A^* is driven with $\dot{\omega}_2 = 10 \text{ rad/s CCW}$. Joint A is also driven with $\dot{\omega}_3 = 3 \text{ rad/s CW}$. Write the relevant equations and sketch the velocity polygon. Then find $\dot{\omega}_2$ and $\dot{\omega}_3$.

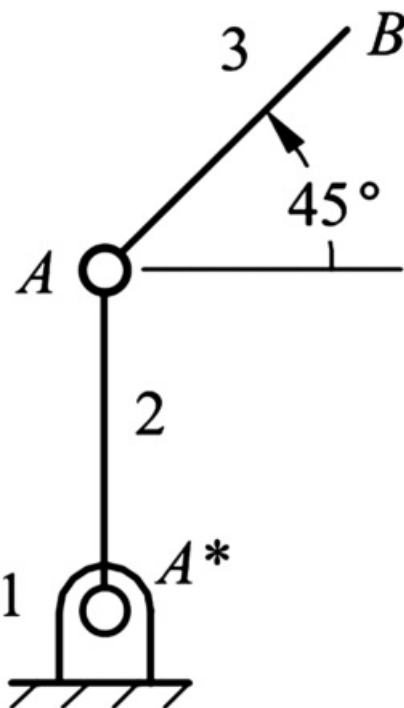


[Figure P9.5](#) Planar manipulator linkage for Problem 9.5.

9.6 The open-chain linkage shown in [Figure P9.6](#) has link lengths $A^*A = 1 \text{ ft}$, and $AB = AC = 1.5 \text{ ft}$. Joint A^* is driven with $\dot{\omega}_2 = 10 \text{ rad/s CCW}$. Joints A and B are driven with $\dot{\omega}_3 = 13 \text{ rad/s CCW}$ and $\dot{\omega}_4 = 8 \text{ rad/s CW}$. Write the relevant equations and sketch the velocity polygon. Then find $\dot{\omega}_2$, $\dot{\omega}_3$, and $\dot{\omega}_4$.

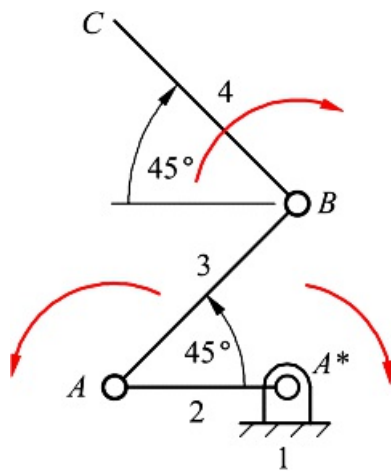


[Figure P9.6](#) Planar manipulator linkage for Problem 9.6.

9.7 The angular velocities at which the joints A^* , A , and B are driven in Problem 9.6 are constant. Write the appropriate equations, sketch the acceleration polygon, and solve for a_C .

9.8 The planar open-chain linkage shown in [Figure P9.8](#) has link lengths $A^*A = 0.75$ ft, $AB = 1.0$ ft, $BC = 1.5$ ft. Link 3 is horizontal and link 4 is vertical. Joint A^* is driven with $\omega_2 = 20 \text{ rad/s CCW}$. Joint A and B are also driven with $\omega_3 = 10 \text{ rad/s CCW}$ and $\omega_4 = 3 \text{ rad/s CCW}$. Write the relevant equations and sketch the velocity polygon. Then find ω_2 , ω_3 , and ω_4 .

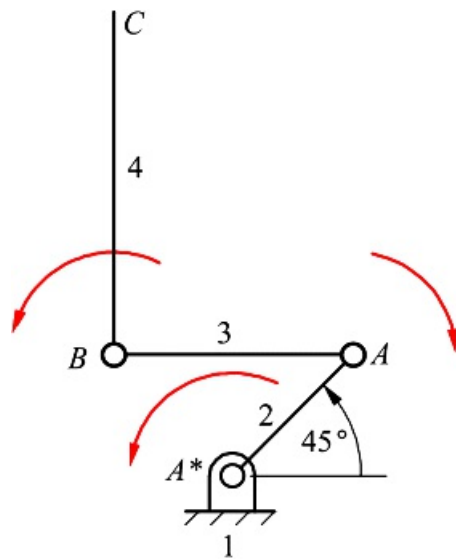


[Figure P9.8](#) Planar manipulator linkage for Problem 9.8.

9.9 The angular velocities at which the joints A^* , A , and B are driven in Problem 9.8 are constant. Write the appropriate acceleration equations, sketch the acceleration polygon, and solve for a_C .

9.10 The planar open-chain linkage shown in [Figure P9.10](#) has link lengths $A^*A = 1.0$ ft and $AB = BC = 2.0$ ft. Joint A^* is driven with $\omega_2 = 10 \text{ rad/s CCW}$. Write the relevant equations and sketch the velocity polygon. Then find ω_2 and ω_4 if $v_C = 0$.

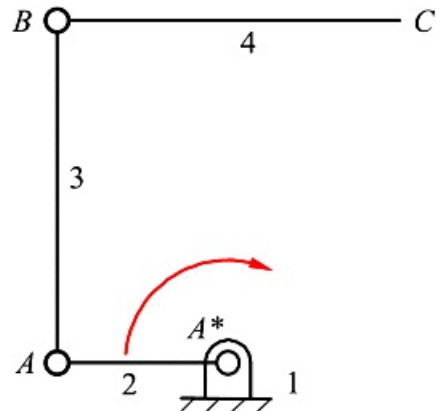


[Figure P9.10](#) Planar manipulator linkage for Problem 9.10.

9.11 The planar open-chain mechanism shown in [Figure P9.11](#) has link lengths $A^*A = AB = BC = 1.0$ ft. Joint A^* is driven with $\dot{\omega}_{A^*} = 5 \text{ rad/s}$. Write the relevant equations and sketch the velocity polygon. Then find $\dot{\omega}_3$ and $\dot{\omega}_4$ if $v_C = 0$.

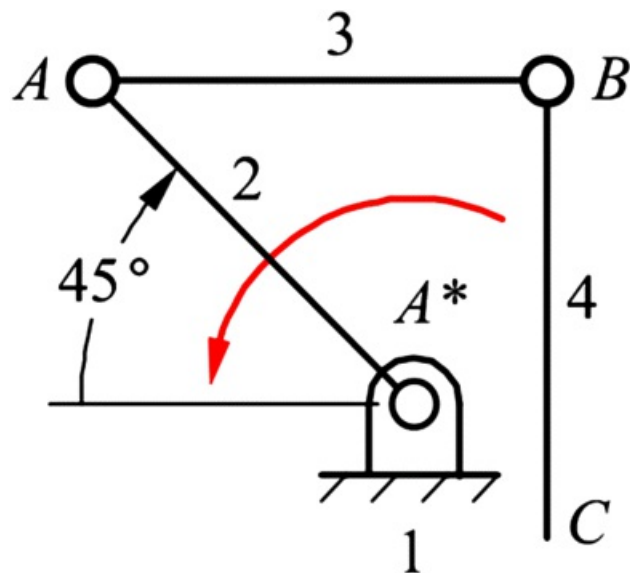


[Figure P9.11](#) Planar manipulator linkage for Problem 9.11.

9.12 The angular velocity of link 2 in Problem 9.10 is constant, and point C is at rest. Write the appropriate acceleration equations and sketch the acceleration polygon to find \mathbf{a}_3 and \mathbf{a}_4 .

9.13 The angular velocity of link 2 in Problem 9.11 is constant, and point C is at rest. Write the appropriate acceleration equations and sketch the acceleration polygon to find \mathbf{a}_3 and \mathbf{a}_4 .

9.14 For the planar manipulator given in [Figure P9.14](#), compute the following:

- $\dot{\omega}_{A_2}/\dot{\omega}_{A_1^*}, \ddot{\omega}_{B_1}/\ddot{\omega}_{A_1}, \ddot{\omega}_{C_4}/\ddot{\omega}_{A_1^*}, \ddot{\omega}_{C_6}/\ddot{\omega}_{A_1^*}$
- $\dot{\omega}_{A_2}, \ddot{\omega}_{A_3}, \ddot{\omega}_{A_4}, \ddot{\omega}_{A_5}/\ddot{\omega}_{A_1^*}, \ddot{\omega}_{B_3}/\ddot{\omega}_{A_1^*}, \ddot{\omega}_{C_4}/\ddot{\omega}_{A_1^*}$
- $\dot{\omega}_{A_2}, \dot{\omega}_{A_3}, \dot{\omega}_{A_4}, \ddot{\omega}_{A_5}/\ddot{\omega}_{A_1^*}, \ddot{\omega}_{B_3}/\ddot{\omega}_{A_1^*}, \ddot{\omega}_{C_4}/\ddot{\omega}_{A_1^*}$

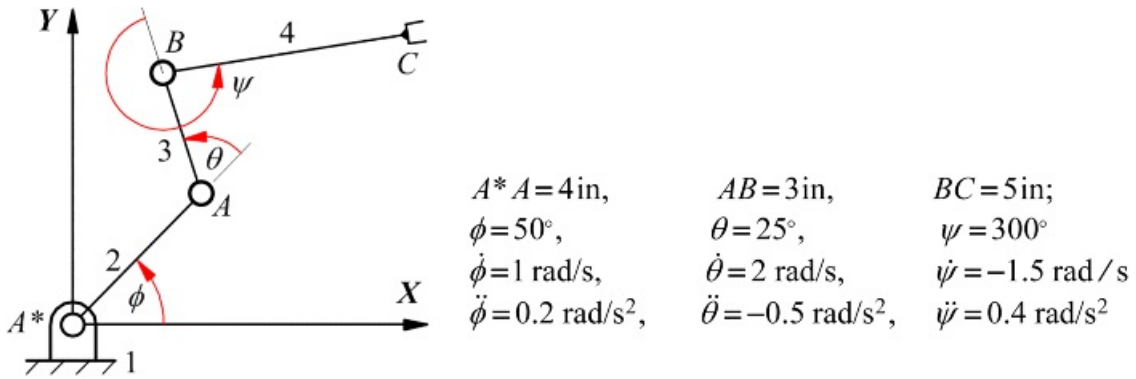


Figure P9.14 Planar manipulator linkage for Problem 9.14.

9.15 In the spatial manipulator in Figure P9.15, link 2, the unit vector l , and the unit vector m are all in the XZ plane. The vector m is perpendicular to l , and the unit vector n is perpendicular to m . The angle ϕ is measured positive CCW about the m axis. Compute the following:

- a. ${}^1\varphi_{A_2/A_1^*}, {}^1\varphi_{B_3/A_2}, {}^1\varphi_{B_3/A_1^*}$
- b. ${}^1\omega_{A_2}, {}^1\omega_{B_3}, \dot{\varphi}_{A_2/A_1^*}, \dot{\varphi}_{B_3/A_1^*}$
- c. ${}^1\tau_{A_2}, {}^1\tau_{B_3}, \ddot{\varphi}_{A_2/A_1^*}, \ddot{\varphi}_{B_3/A_1^*}$

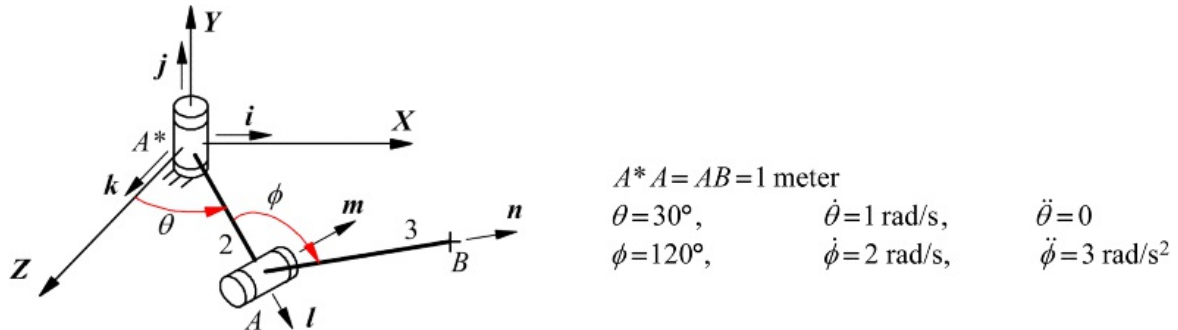


Figure P9.15 Manipulator linkage for Problem 9.15.

9.16 In the manipulator shown in Figure P9.16, the joint axes at A^* and A are oriented along the Z and m axes, respectively. Link 2 lies in the XY plane, and link 3 is perpendicular to link 2. For the position shown, link 3 is vertical (parallel to Z). Determine ${}^1\varphi_{B_3/A_1^*}, {}^1\varphi_{A_3/A_1^*}, {}^1\tau_{B_3}$.

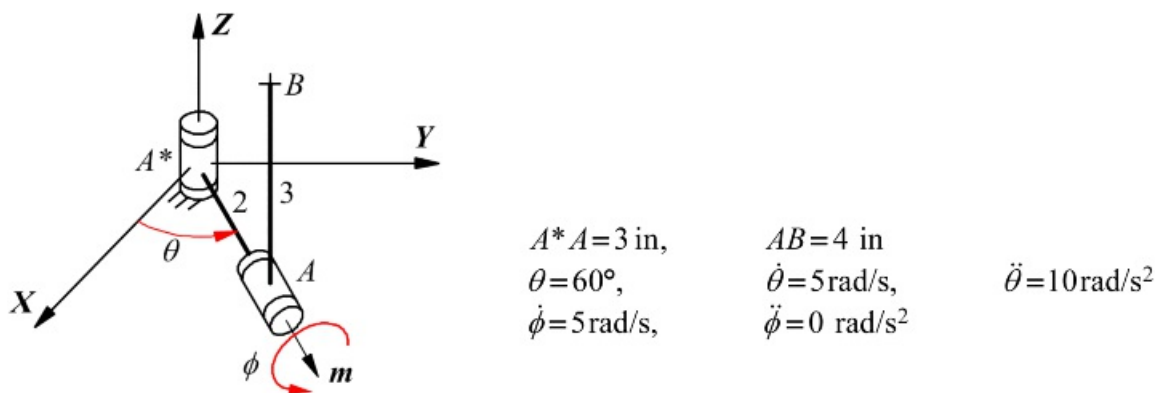
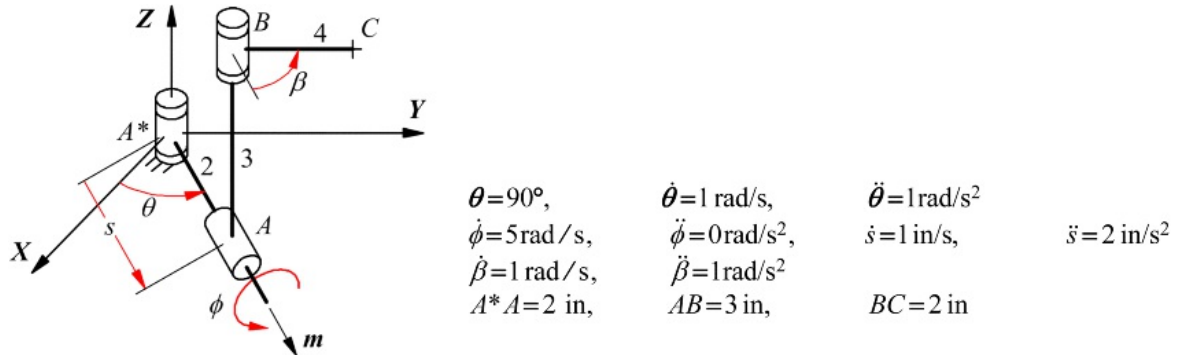


Figure P9.16 Manipulator linkage for Problem 9.16.

9.17 In the manipulator shown in Figure P9.17, the joint axis at A^* is oriented along the Z axis, and the axis at A is oriented along the m axis. In the position to be analyzed, link 2 lies in a plane parallel to the XY plane and points along a line parallel to the Y axis. Link 3 is perpendicular to link 2. Link 4 is perpendicular to link 3 and lies along a line parallel to the Y axis. For the position to be analyzed, link 3 is vertical (parallel to Z).

The joints between link 2 and the frame at A^* and between links 3 and 4 are revolute joints, and that at A is a cylindrical joint. From a previous analysis, we know that ${}^1\dot{\theta}_{B_3/A_1^*} = 1.33 - \beta$, ${}^1\ddot{\theta}_{A_3/A_1^*} = -4\beta$, and ${}^1\omega_{B_3} = \dot{s} - \beta\ddot{s}$. Using this information, determine ${}^1v_{C_4/A_1^*}$, ${}^1\dot{\theta}_{B_3/A_1^*}$, ${}^1\ddot{\theta}_{A_3/A_1^*}$.



[Figure P9.17](#) Manipulator linkage for Problem 9.17.

9.18 In the manipulator shown in [Figure P9.18](#), the joint axes at A^* and A are oriented along the Z and m axes, respectively. In the position to be analyzed, link 2 lies in a plane parallel to the XY plane and points along a line parallel to the Y axis, and link 3 is perpendicular to link 2. For the position to be analyzed, link 3 is vertical (parallel to Z). The joint between link 2 and the frame at A^* is a revolute joint, and that at A is a cylindrical joint. Determine ${}^1\dot{\theta}_{B_3/A_1^*}$, ${}^1\ddot{\theta}_{A_3/A_1^*}$, ${}^1\omega_{B_3}$.

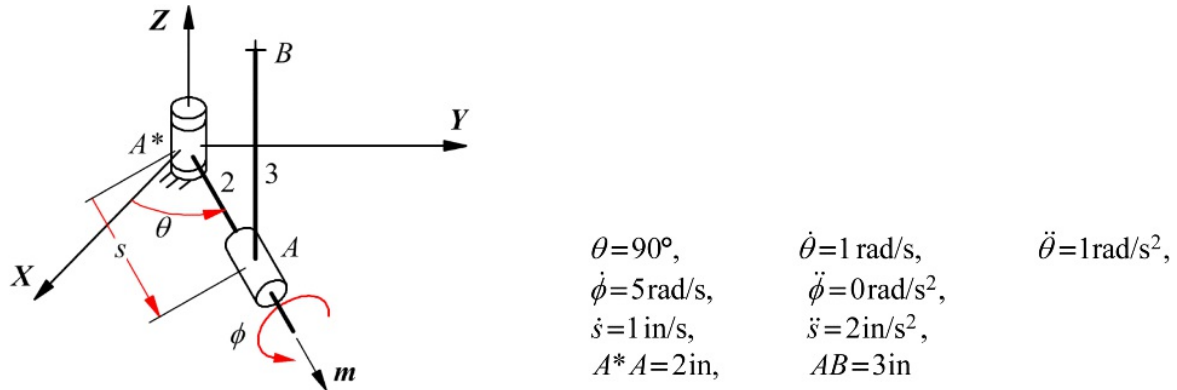


[Figure P9.18](#) Manipulator linkage for Problem 9.18.

9.19 In the manipulator in [Figure P9.19](#), the joint axis at A is oriented along the Z axis. In the position to be analyzed, link 2 lies in a plane parallel to the YZ plane and points along a line parallel to the Y axis. Link 3 is perpendicular to link 2 and lies parallel to the XY plane. The joint between link 2 and the frame is a cylindrical joint, and the joint between links 2 and 3 is a revolute joint. Using the information given, determine ${}^1v_{C_3/A_1^*}$, ${}^1\dot{\theta}_{B_3/A_1^*}$, ${}^1\ddot{\theta}_{A_3/A_1^*}$.

$$\begin{aligned}\theta &= 90^\circ, & \dot{\theta} &= 1 \frac{\text{rad}}{\text{sec}}, & \ddot{\theta} &= 0 \frac{\text{rad}}{\text{sec}^2}, \\ \dot{\phi} &= 1 \frac{\text{rad}}{\text{sec}}, & \ddot{\phi} &= 0 \frac{\text{rad}}{\text{sec}^2}, \\ s &= 1 \text{ in.}, & \dot{s} &= 0 \frac{\text{in}}{\text{sec}}, & \ddot{s} &= 1 \frac{\text{in}}{\text{sec}^2}, \\ AB &= 1 \text{ in.}, & BC &= 1 \text{ in.} \end{aligned}$$

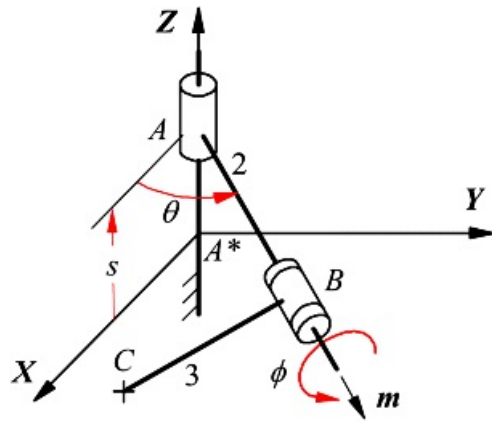
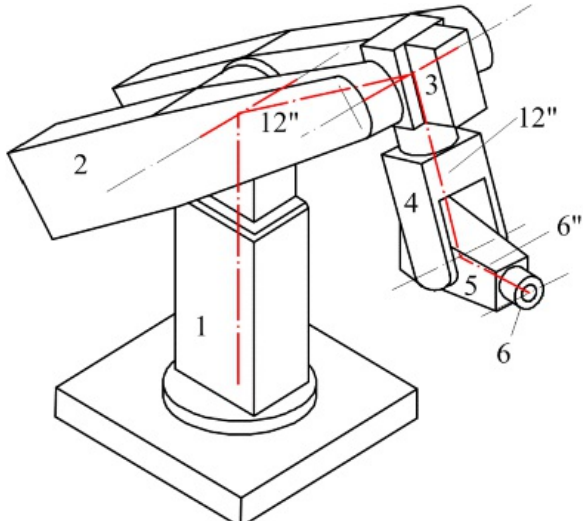


[Figure P9.19](#) Manipulator linkage for Problem 9.19.

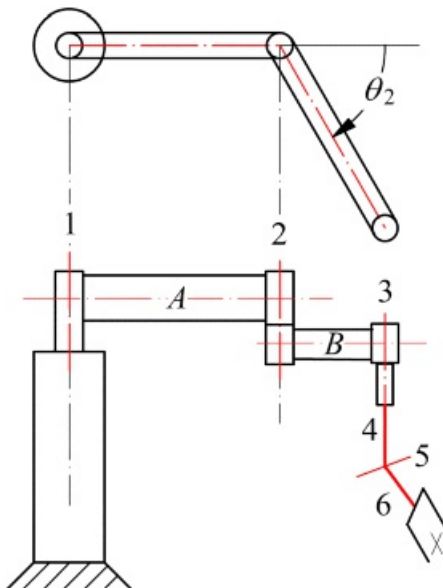
[9.20](#) In the manipulator shown in [Figure P9.20](#), all joints are revolutes. The link parameters and joint angles are as tabulated. Find the 4×4 matrix, Q' , that expresses the position of the mounting flange for the end effector in the position specified by the values of θ_i given in the table.



i	a_i	η_i	α_i	θ_i
1	0	0	90°	30°
2	12 in	0	0°	45°
3	0	0	90°	-50°
4	0	12 in	90°	-20°
5	0	0	90°	40°
6	0	6 in	0°	30°

[Figure P9.20](#) Manipulator linkage for Problem 9.20.

[9.21](#) The SCARA robot geometry shown in [Figure P9.21](#) is often used for assembly robots because it is suited to moving and placing parts vertically over a relatively large horizontal area. All of its joint axes, except axis 4, are revolutes. Axis 4 is a prismatic joint. Axes 1, 2, 3, and 4 are parallel, and axes 3 and 4 are coincident (note that this does not produce degeneracy because 3 is a revolute joint and 4 is a prismatic joint). For a given position of the manipulator, the linkage parameters are as tabulated. Find the matrix Q' that expresses the position of the end effector for the tabulated values of the joint variables.



i	a_i	r_i	α_i	θ_i
1	15 in	0	0°	60°
2	15 in	4 in	0°	45°
3	0	0	0°	-50°
4	0	9 in	90°	0°
5	0	0	90°	0°
6	0	6 in	0°	30°

Figure P9.21 SCARA robot for Problem 9.21.

9.22 For the manipulator in Example 9.4, Figure 9.10, and Table 9.1, find the 4×4 matrix, Q' , that expresses the position of the gripper when the joint positions are as follows: $\theta_1 = -30^\circ$, $\theta_2 = 150^\circ$, $\theta_3 = 10^\circ$, $r_4 = 2.5$, $\theta_4 = -45^\circ$, $\theta_5 = 0^\circ$.

9.23 For the three-axis manipulator of Example 9.5, Figure 9.11, and Table 9.2, find the angular velocity of member 3 and the velocity of the wrist concurrency point, P , relative to the fixed reference frame when the joint positions and rates are as follows: $\theta_1 = -60^\circ$, $\theta_2 = 45^\circ$, $\theta_3 = -30^\circ$, $\dot{\theta}_1 = -0.5 \text{ rad/s}$, $\dot{\theta}_2 = 0.3 \text{ rad/s}$, $\dot{\theta}_3 = 1.0 \text{ rad/s}$.

9.24 For a SCARA robot of basic geometry similar to that of Problem 9.21, the geometric parameters and joint variables in a general position are tabulated below. The Jacobian matrix that relates the velocity of the end effector to the joint velocities is also given.

- Find the angular velocity of the end effector when the joint positions and rates are $\theta_1 = 30^\circ$, $\theta_2 = 15^\circ$, $\theta_3 = -15^\circ$, $r_4 = 0.1$, $\theta_4 = 0^\circ$, $\theta_5 = 45^\circ$ and $\dot{\theta}_1 = -0.2 \text{ rad/s}$, $\dot{\theta}_2 = 0.3 \text{ rad/s}$, $\dot{\theta}_3 = -0.2 \text{ rad/s}$, $\dot{\theta}_4 = 0.03 \text{ in/s}$, $\dot{\theta}_5 = 0$, $\dot{\theta}_6 = 0.1 \text{ rad/s}$.
- Verify that the system is singular whenever either $\theta_2 = 0^\circ$ or $\theta_3 = 0^\circ$.

i	a_i (in)	r_i (in)	α_i	θ_i
1	0.5	0	0°	θ_1
2	0.4	0	0°	θ_2
3	0	0	0°	θ_3
4	0	r_4	90°	θ_4
5	0	0	90°	θ_5
6	0.1	0	0°	θ_6

$$J = \begin{bmatrix} 0 & 0 & 0 & 0 & 0 & \sin \theta_6 \\ 1 & 1 & 1 & 0 & 0 & -\cos \theta_6 \\ 0 & 0 & 0 & 0 & 1 & 0 \\ 0.4 \sin \theta_3 + 0.5 \sin(\theta_2 + \theta_3) & 0.4 \sin \theta_3 & 0 & 0 & 0 & 0 \\ 0 & 0 & 0 & 1 & 0 & 0 \\ -0.4 \cos \theta_3 - 0.5 \cos(\theta_2 + \theta_3) & -0.4 \cos \theta_3 & 0 & 0 & 0 & 0 \end{bmatrix}$$

10

PROFILE CAM DESIGN

Prerequisite Knowledge Needed for Chapter 10

A knowledge of how to compute the location of center points from [Chapter 3](#) and a familiarity with locating and using instant centers from [Chapter 6](#).



10.1 Introduction

Cams are used for essentially the same purpose as linkages, that is, generation of irregular motion. Cams have an advantage over linkages because cams can be designed for much tighter motion specifications. In fact, in principle, any desired motion program can be exactly reproduced by a cam. Cam design is also, at least in principle, simpler than linkage design, although in practice, because the dynamics of the total cam-follower system must usually be considered, it can be very laborious. The design of cams has been addressed in a number of CAD programs [2, 3], and most cam manufacturers have in-house programs for custom design. In addition, many books on kinematics, including this one, have available programs to facilitate cam design. However, before using these programs, it is important for the user to understand the issues involved, and presenting the design issues is one of the goals of this book.

The disadvantages of cams are manufacturing expense, poor wear resistance, and relatively poor high-speed capability. Although computer numerical control (CNC) machining does cut the cost of cam manufacture in small lots, cams are still quite expensive in comparison with linkages. In large lots, molding or casting techniques cut cam costs, but not to the extent that stamping and other techniques cut linkage costs for similar lot sizes. Also, high-speed cams generally require surface grinding that is inherently more expensive than milling or stamping.

Unless roller followers are used, cams can wear quickly. However, roller followers are bulky and sometimes require larger cams than do flat-faced followers, creating size and dynamic problems. In addition, the bearings in roller followers create their own reliability problems.

The worst problems with cams are, however, noise and follower bounce at high speeds. The result of this is a preoccupation with dynamic optimization in cam design.

Cam design usually requires two steps (from a geometric point of view):

1. Synthesis of the motion program for the follower
2. Generation of the cam profile

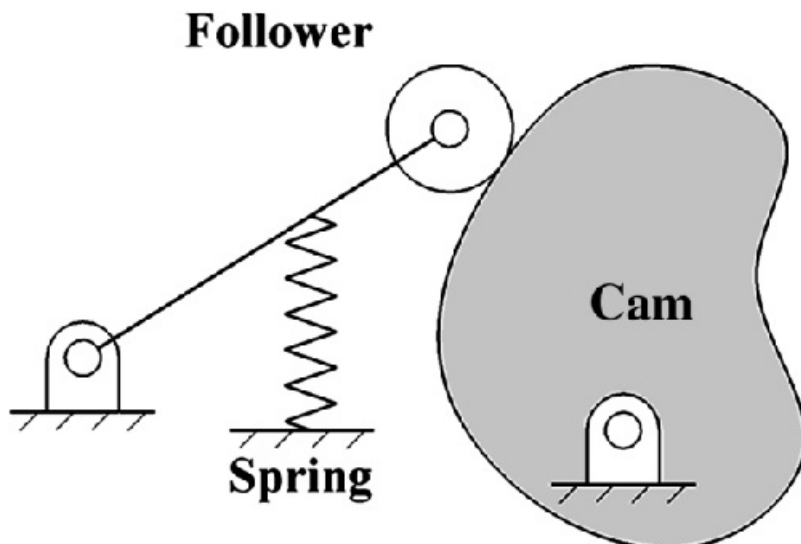
If the motion program is fully specified throughout the motion cycle by the problem statement, as is the case, for example, with the stitch pattern cams in sewing machines, the first step is not needed. More usually, the motion program is specified only for portions of the cycle, allowing the synthesis of the remaining portions for optimal dynamic performance. An example is the cam controlling the valve opening in an automotive engine. Here the specification is that the valve should be fully closed for a specified interval and more or less fully open for another specified interval. For the portions of the cycle between those specified, a suitable program must be synthesized. This can be done, with varying levels of sophistication, to make the operation of the cam as smooth as possible. In general, the higher the level of dynamic performance required, the more difficult the synthesis process.

The second stage of the process, profile generation, is achieved by kinematic inversion. The cam is taken as the fixed link and a number of positions of the follower relative to the cam are constructed. If done graphically, a curve tangent to the various follower positions is drawn and becomes the cam profile. If the process is performed analytically, discrete points on the cam profile are located directly as a function of the cam rotation angle, and, theoretically, any level of accuracy can be achieved by using small enough increments for the cam rotation angle.

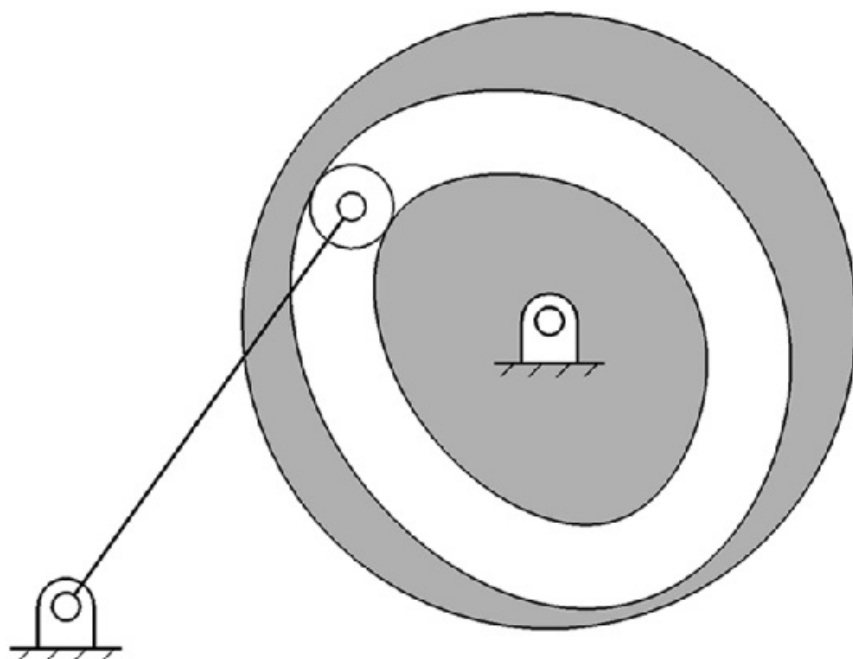


10.2 Cam-Follower Systems

A general cam-follower system consists of three elements as shown in [Figure 10.1](#). The first two are the cam and follower, and the third is some means of ensuring that the follower remains in contact with the cam. There are two general ways of ensuring that the follower contacts the cam. The first is to force the follower to remain against the cam. This is usually done with a spring as shown in [Figure 10.1](#) or in unusual cases by a weight on the follower. The second way to ensure contact is by constraining the follower motion by geometry. This is normally possible only with roller followers. The constraining is usually done by using a grooved cam or by using a conjugate cam. A grooved cam is depicted in [Figure 10.2](#) and a conjugate cam in [Figure 10.3](#). A grooved cam is essentially two cams, one internal and one external, such that the roller can contact either surface depending on the force direction [1, 2]. For this type of cam to be acceptable, the tolerances on both cam surfaces and the roller must be very tight.



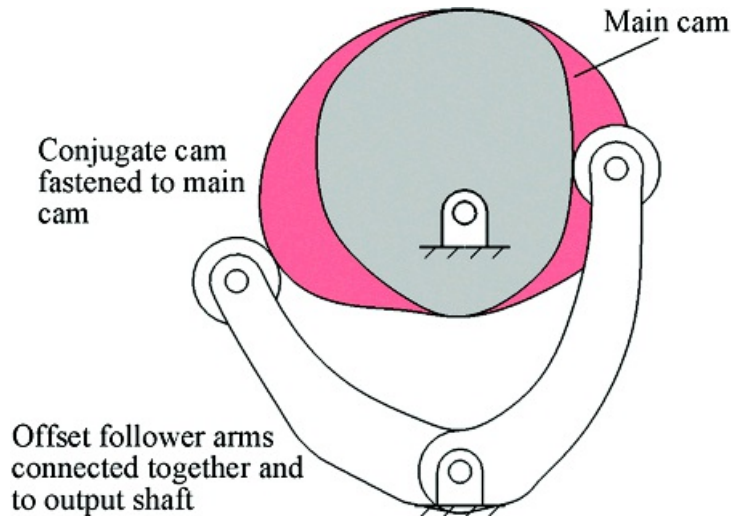
[Figure 10.1](#) Elements of a cam-follower system.



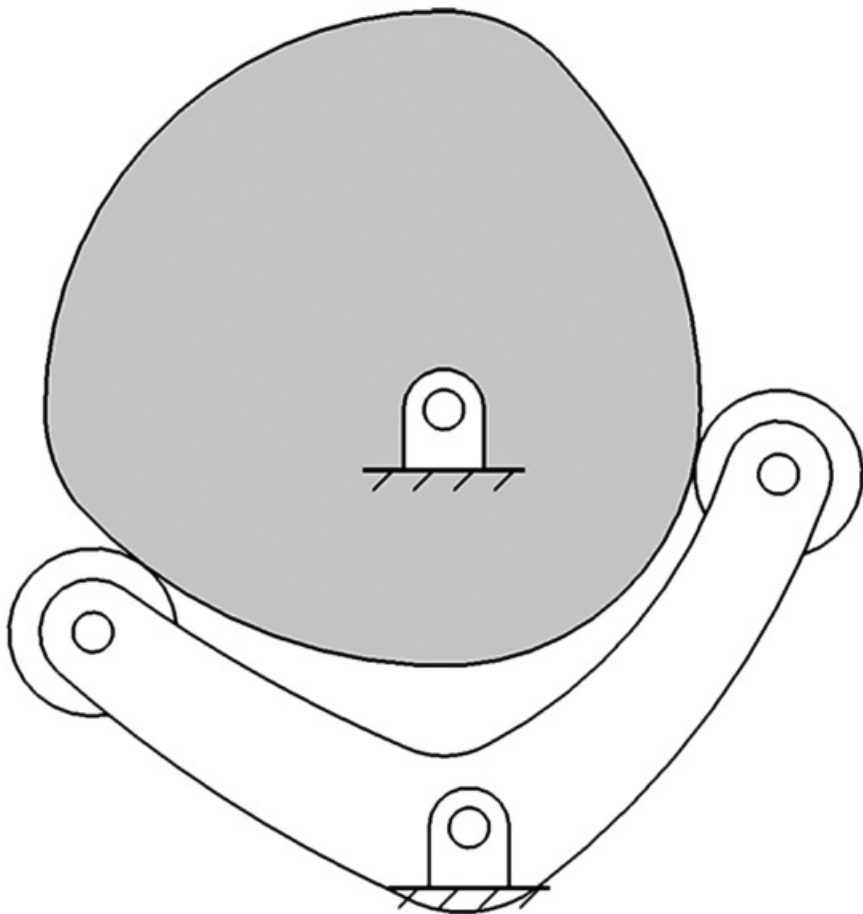
[Figure 10.2](#) Grooved cam and oscillating follower.

Conjugate cam design is slightly more involved than for a traditional cam. In the most general case, two cams are

fastened together and two followers are attached to the same output shaft but offset to accommodate the two cams as shown in [Figure 10.3](#). The cam design must be such that the two followers can maintain contact with the two cams at all times. In the design process, the main cam for which the design specification is required is designed first. Then the second cam is designed so that the second follower maintains constant contact with it. Since the position of the second follower will be known for every position of the first follower, the envelope for the second cam is defined as soon as the first cam is designed. In the conjugate cam, the two followers can be preloaded against the two cams to ensure high accuracy. Also, if there is no spring force on the followers, the contact stresses can be considerably lower than with a traditional spring-loaded cam. In the case of very special cam geometries when the conjugate cam is the same as the main cam, only a single cam is necessary. This is called a self-conjugate or constant-width cam and is represented in [Figure 10.4](#). Self-conjugate cams are symmetric about at least one axis through the center of rotation. Several example geometries appropriate for constant-width cams are given on the web [1]. Also, the design and analysis of self-conjugate cams are discussed by a number of authors, for example [4–7].



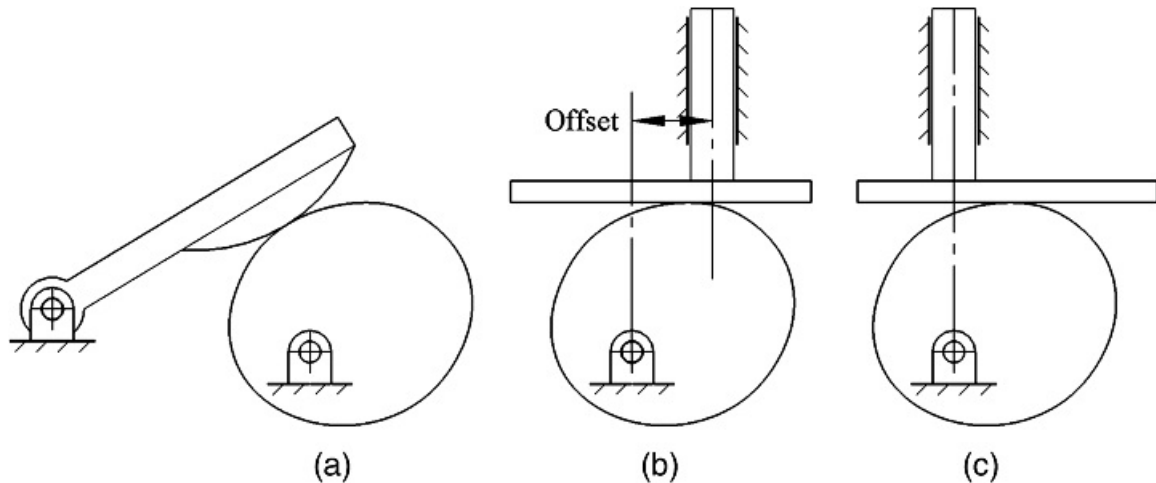
[Figure 10.3](#) Conjugate cam with oscillating roller follower.



[Figure 10.4](#) Self-conjugate or constant-width cam with oscillating roller follower.

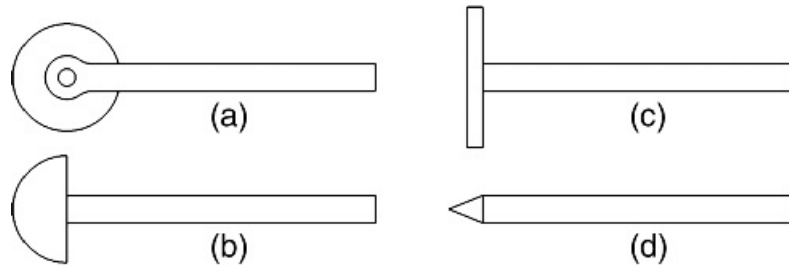
When a spring is used to force the follower against the cam, the spring force must be high enough to oppose any acceleration that the cam imparts to the follower. Otherwise, if the acceleration and resulting dynamic force is too large, the follower will lose contact with the cam. This results in follower “bounce.” For high-speed cams, the necessary force from the spring can be quite large, and the force from the spring can contribute significantly to the torque required on the cam shaft. The spring can also have a significant impact on the cam system dynamics because it stores energy during the rise part of the cycle and releases energy during the return cycle. If the spring force is large enough, it can even drive the cam during the return part of the cycle, and a negative torque (braking torque) might be required for that part of the cycle.

A follower is characterized by its motion relative to the ground link and by the geometry of its face that contacts the cam. The cam-follower motion may be either rotational or translational, and translating followers may be either radial or offset. Examples of these are shown in [Figure 10.5](#). A radial offset for a translating flat-faced follower does not affect the input-output relationship for the cam and follower. However, the machine-design aspects can be significantly affected because the stresses and effects of friction can increase significantly as the offset is increased.



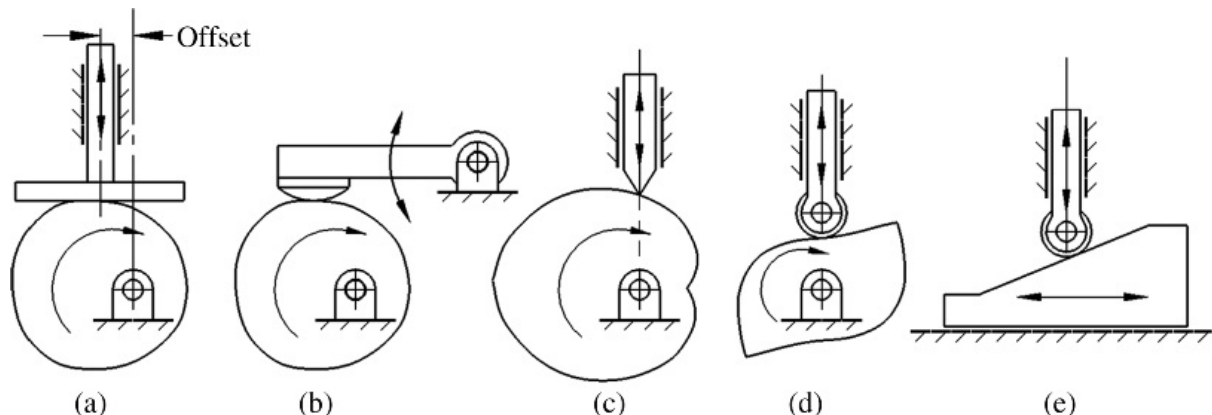
[Figure 10.5](#) (a) Cylindrical-faced oscillating follower; (b) offset flat-faced translating follower; and (c) radial flat-faced translating follower.

The follower surfaces may be either knife-edged, flat-face, spherical (or cylindrical), or roller as shown in [Figure 10.6](#). Actually, these geometries are all of the same class depending on the radius of curvature of the follower face. That is, the knife-edge has a radius of curvature that is zero, the flat-face has a radius of curvature that is infinite, and the general roller and cylindrical followers have a finite (but not zero) radius of curvature. In this discussion, only planar cams will be considered, so no distinction between spherical and cylindrical follower faces will be made. Also, if only geometric information is of interest, no distinction needs to be made between roller and rigid cylindrical-faced followers. There is a significant difference from an overall machine-design standpoint because lubrication and surface-wear issues will be quite different for the two cases. However, these issues will not be discussed here. Nonkinematic issues are discussed in most references on general cam design, for example [1,4].



[Figure 10.6](#) (a) Roller follower; (b) cylindrical-faced follower; (c) flat-faced follower; and (d) knife-edged follower.

Although here we will consider only planar, rotating cams, in practice a large number of different cam geometries are found. Some of the different types of cams and follower systems are shown in [Figure 10.7](#). The circular cam in [Figure 10.7\(h\)](#) is also a self-conjugate cam.



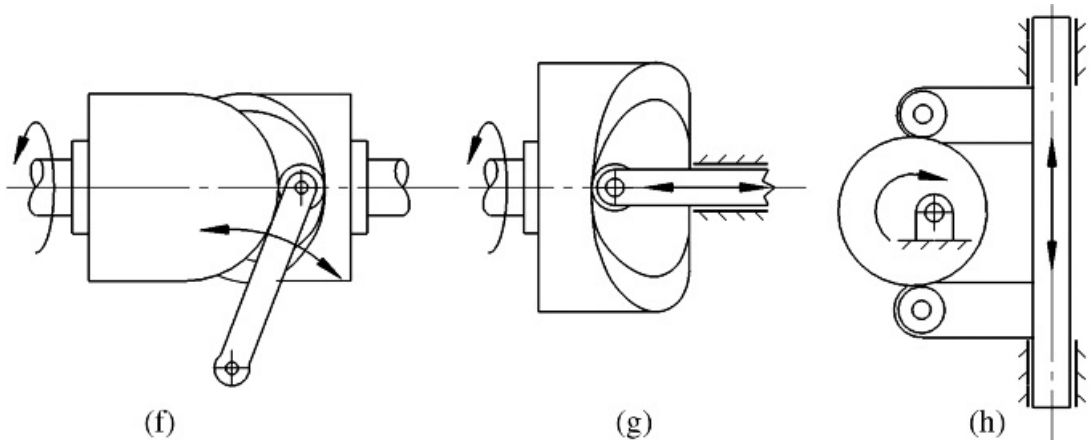
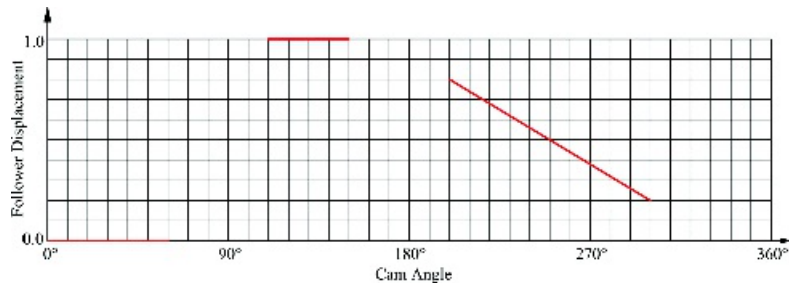


Figure 10.7 Some types of cams: (a) Offset flat-faced translating follower; (b) oscillating cylindrical-faced follower; (c) radial (heart) cam and translating knife-edged follower; (d) radial two-lobe frog cam and translating roller follower; (e) wedge cam and translating roller follower; (f) cylindrical cam and oscillating roller follower; (g) end or face cam and translating roller follower; (h) yoke cam and translating roller follower.



10.3 Synthesis of Motion Programs

As indicated earlier, in cam design, the problem specification usually defines only a portion of the motion of the follower. Therefore, the problem of motion-program synthesis is that of filling in, in an optimal way, the portions of the motion cycle that are not completely specified. The characteristics of the problem may be demonstrated by consideration of a cam that is required to drive a translating follower that dwells at 0° for a cam rotation of 60° , dwells at 1.0 in for a cam rotation of 110° to 150° , and is required to move with constant velocity from a displacement of 0.8 in to 0.2 in for 200° to 300° of cam rotation. The specified portions of the motion program are displayed in [Figure 10.8](#).



[Figure 10.8](#) The statement of the required displacements of a cam design problem in graphical form.

A simple solution to the problem of filling the gaps is to move the cam at constant velocity between the specified segments, giving a follower displacement diagram as shown in [Figure 10.9](#). Notice, however, that if this is done, the velocity is discontinuous at cam angles 60° , 110° , 150° , 200° , 300° , and 360° causing the acceleration to become infinite at these locations. Since the follower cannot be constrained to have an infinite acceleration, this leads to a loss of contact and/or excessive local stresses and resultant noise and wear problems.

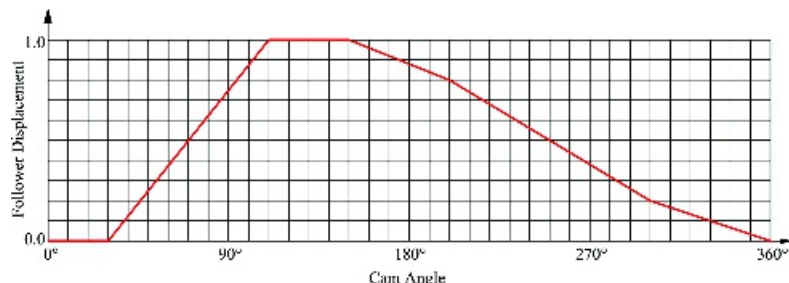


[Figure 10.9](#) A cam angle-follower displacement program that satisfies the displacement requirements specified in [Figure 10.8](#).

The preceding motion program matches only the *displacements* at the ends of the segments. The infinite acceleration problem can be removed by matching both displacement and velocity at the ends of segments of the program. One way to do this is to subdivide each synthesized segment into two parts with a constant acceleration on the first and constant deceleration on the second. On such a subsegment, if the acceleration is a , the velocity is given by

$$v = v_0 + at$$

where v_0 is the velocity at the beginning of the segment. The displacement is given by

$$s = s_0 + v_0 t + \frac{at^2}{2}$$

where s_0 is the displacement at the beginning of the segment. Now, if the cam is driven at constant velocity,

$$\theta = \theta_0 + \omega t$$

where θ is the cam angle, θ_0 is the cam angle at the beginning of the segment, and ω is the angular velocity. Hence

$$s = s_0 + \frac{(\theta - \theta_0)}{\omega}$$

$$v = v_0 + \omega \frac{(\theta - \theta_0)}{\omega}$$

and

$$s = s_0 + v_0 \frac{(\theta - \theta_0)}{\omega} + \omega \frac{(\theta - \theta_0)^2}{2\omega^2}$$

Therefore, the relationship between s and θ , as plotted on the follower displacement diagram, is parabolic (see [Figure 10.10](#)). Cam-follower displacement programs that use this type of transition are called parabolic. The cam profiles developed from them are also called “parabolic.” It is important to understand that a so-called parabolic cam *does not* have a parabolic curve in its profile. Rather, the parabolas are in the transition curves used in the follower displacement schedule.

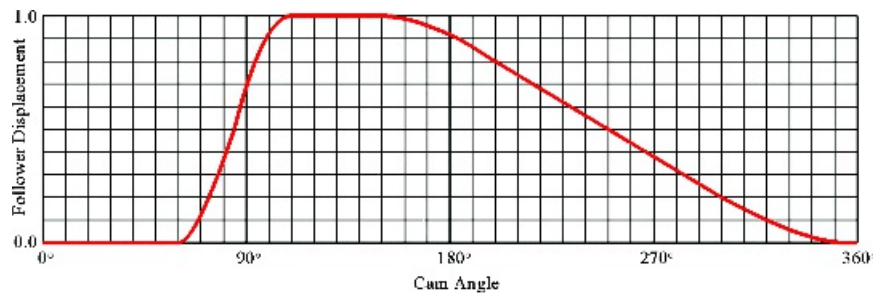


[Figure 10.10](#) A follower displacement program that satisfies the displacement requirements of [Figure 10.8](#) using parabolic transitions. This is called a *parabolic* follower-displacement program.



10.4 Analysis of Different Types of Follower-Displacement Functions

Several different standard functions can be used to connect the parts of the displacement diagram where a specific type of motion is required. These displacement profiles ultimately determine the shape of the cam. Many different types of motions have been used in practice, and some have been extensively studied. These include

1. Uniform motion
2. Parabolic motion
3. Harmonic motion
4. Cycloidal motion
5. General polynomial motion

The first two types of programs have already been introduced. The first four types of programs can be generated graphically as well as analytically, but the fifth type is generated only analytically. Both graphical and analytical development will be considered here, where possible. Both methods assume that the angular velocity, ω , of the cam is constant ($\alpha = 0$). If this is the case, then

$$y = y(\theta)$$

and

$$\theta = \theta_0 + \omega t$$

Here, y is used as a generic output variable. It may correspond to either a linear or angular displacement of the follower. Note that if the cam motion is given as a function of time, the motion can be easily represented as a function of the cam rotation in degrees using the preceding expressions.

The higher derivatives are given by

$$\dot{y} = \frac{dy(\theta)}{dt} = \frac{dy}{d\theta} \frac{d\theta}{dt} = y' \omega$$

and

$$\ddot{y} = \frac{d^2y(\theta)}{dt^2} = \frac{d}{dt} \left(\frac{dy}{d\theta} \frac{d\theta}{dt} \right) = \frac{d^2y}{d\theta^2} \left(\frac{d\theta}{dt} \right)^2 + \frac{dy}{d\theta} \frac{d^2\theta}{dt^2} = \frac{d^2y}{d\theta^2} \omega^2 + \frac{dy}{d\theta} \alpha - y'' \omega^2 + y' \alpha$$

But because ω is constant, $\alpha = 0$ and

$$\ddot{y} = y'' \omega^2$$

Therefore, \dot{y} is a simple constant times y' , and \ddot{y} is also a constant times y'' . Consequently, even though we ultimately want to know the response to the time derivatives (\dot{y} and \ddot{y}), we may work directly with the derivatives (y' and y'') with respect to the cam displacement. If the cam's angular velocity is not a constant, then the cam's profile can be designed for only one operating situation if higher derivatives are important. Therefore, cams are almost never designed for other than constant velocity. In the following, a constant-velocity cam is assumed, and y

is again used to represent either an angular or linear displacement of the follower.

The follower curves can be studied in terms of the simple diagram shown in [Figure 10.11](#). Note that the diagram shows the cam angle only up to 360° . After 360° , the curve simply repeats itself; that is, the displacement at 361° is the same as at 1° . A general displacement diagram will be made up of three or more parts

1. Rises (1 or more)
2. Returns (1 or more)
3. Dwells (0 or more)

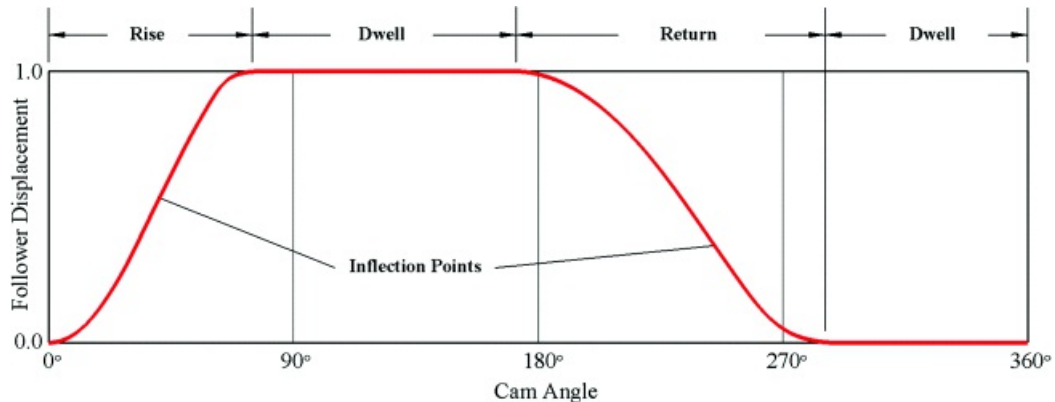


[Figure 10.11](#) Terminology used when discussing follower-displacement programs.

Both the rise and return parts will contain one or more inflection points. These are points where a maximum slope is reached, and they correspond to points on the cam surface with maximum steepness. These points are identified by the locations where the curvature of the diagram changes sign. At the inflection points, the radius of curvature of the curve is infinite.

In each of the standard curve cases, we will look mainly at the rise part of the follower profile. The return part can be determined using the mirror images of the curves considered.

10.4.1 Uniform Motion

Uniform motion is represented in [Figure 10.12](#). To derive the equations for the follower displacement, a general form for the mathematical expression corresponding to the type of motion is assumed. The general equation will have undetermined constants in it, and these constants can be found by matching boundary conditions at the two ends of the curve. For uniform motion, the general form of the curve used is

$$y = C\varphi$$

If L is the amount of the rise, and β is the cam rotation angle required for the rise, then the constant C must be L/β and y becomes

$$y = \frac{L}{\beta}\varphi$$

During the rise, the velocity and acceleration are

$$\dot{y} = \frac{L}{\beta^2}$$

and

$$\ddot{y} = 0$$

The displacement, velocity, and acceleration are all plotted in [Figure 10.12](#). As noted earlier, the acceleration is infinite at the points where the uniform motion meets the dwells. Therefore, even for low speeds and elastic members, the forces transmitted will be very large. For *very* low speeds, however, this type of displacement diagram might be acceptable.

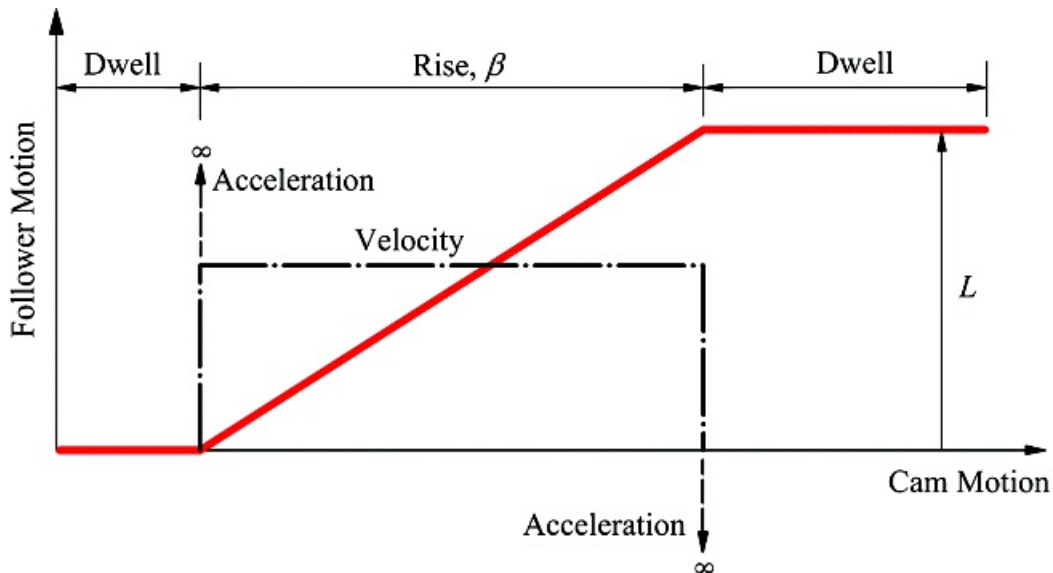


[Figure 10.12](#) Displacement, velocity, and acceleration relations for uniform motion.

10.4.2 Parabolic Motion

The equations for parabolic motion can be derived using the same procedure as described in Section 10.3. However, two parabolas must be used for each transition between two dwells. The two parabolas meet at the point midway between the ends of the two dwell regions. The general form for both parabolas is

$$y = C_0 + C_1\theta + C_2\theta^2 \quad (10.1)$$

and

$$\begin{aligned} y &= C_1 + 2C_2\theta \\ y'' &= 2C_2 \end{aligned} \quad (10.2)$$

The parabolic equation in [Equation 10.1](#) has three constants; therefore, we can match three conditions with the equation. If the cam displacement is taken as 0 at the beginning of the rise, then at $\theta = 0$, $y = y' = 0$. This gives, $C_0 = C_1 = 0$. Also, at $\theta = \beta/2$, $y = L/2$. Therefore, the displacement and first, second, and third derivatives with respect to θ are

$$\begin{aligned}
 y &= 2L \left(\frac{\theta}{\beta} \right)^2 \\
 y' &= 4 \frac{L}{\beta^2} \theta \\
 y'' &= 4 \frac{L}{\beta^2} \\
 y''' &= 0
 \end{aligned} \tag{10.3}$$

and the velocity, acceleration, and jerk are

$$\begin{aligned}
 \dot{y} &= 4 \frac{L\theta}{\beta^2} \\
 \ddot{y} &= 4 \frac{L\omega^2}{\beta^2} \\
 \dddot{y} &= 0
 \end{aligned}$$

Here we have included the third time derivative, which is called jerk. This derivative is proportional to the change in force and for high-speed cams is an important aspect of the motion. At the point at which the curve meets the first dwell, the velocity and acceleration are continuous, but the jerk is infinite. Although not so serious as having an infinite acceleration pulse, an infinite jerk pulse can excite undesirable vibratory behavior in the system.

For the second half of the rise, the conditions to match are at $\theta = \beta/2$, $y = L/2$, and at $\theta = \beta$, $y = L$, and $y' = 0$. Then from [Equations 10.1](#) and [10.2](#)

$$\begin{aligned}
 \frac{L}{2} &= C_0 + C_1 \frac{\theta}{2} + C_2 \left(\frac{\theta}{2} \right)^2 \\
 L &= C_0 + C_1 \theta + C_2 \theta^2 \\
 0 &= C_1 + 2C_2 \theta
 \end{aligned}$$

The solution to this linear set of equations yields

$$\begin{aligned}
 C_0 &= -L \\
 C_1 &= \frac{4L}{\beta} \\
 C_2 &= -\frac{2L}{\beta^2}
 \end{aligned}$$

so that

$$y = L \left[1 - 2 \left(1 - \frac{\theta}{\beta} \right)^2 \right] \tag{10.4}$$

and

$$y = \frac{4L}{\beta} \left(1 - \frac{\beta}{\beta} \right)$$

$$y' = -\frac{4L}{\beta^2}$$

$$y'' = 0$$

Finally, the velocity, acceleration, and jerk are given by

$$\dot{y} = \frac{4L\omega}{\beta} \left(1 - \frac{\beta}{\beta} \right)$$

$$\ddot{y} = -\frac{4L\omega^2}{\beta^2}$$

$$\dddot{y} = 0$$

These equations apply to the segment of the diagram to the right of the inflection point shown in [Figure 10.13](#).

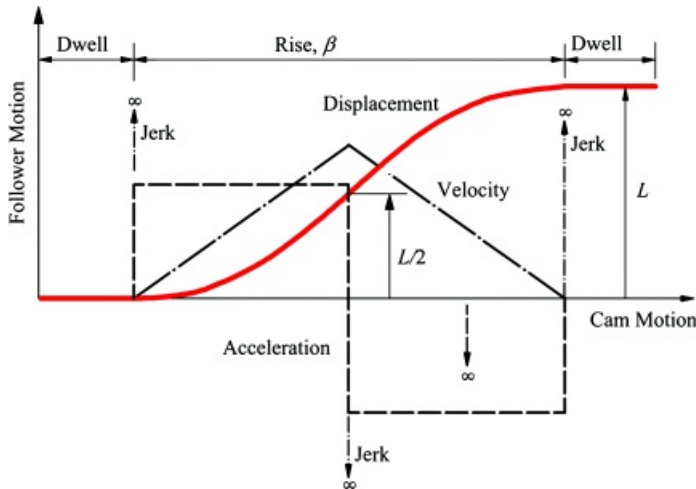


[Figure 10.13](#) Displacement, velocity, acceleration, and jerk relations for parabolic motion during rise.

A cam return using parabolic motion is shown in [Figure 10.14](#). To determine the equations for the return from $y = L$ to 0 during the angular displacement β , we can use [Equation 10.1](#) again but with different boundary conditions and recognizing that β does not start at 0.

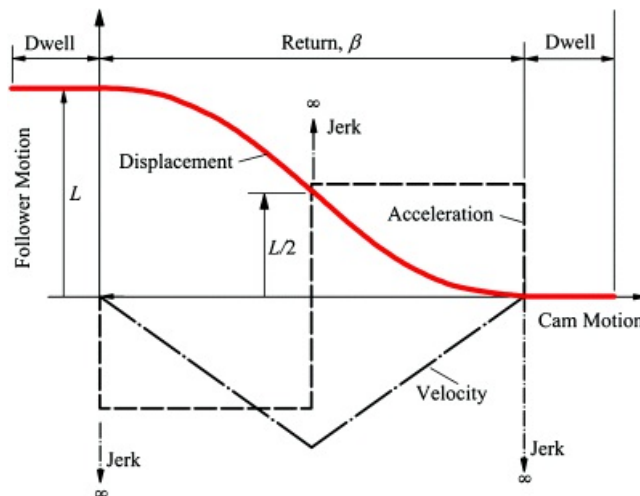


[Figure 10.14](#) Displacement, velocity, acceleration, and jerk relations for parabolic motion during return.

In general, the rise and return will not always start at $\phi = 0$. However, to simplify the equations, we can use a simple coordinate transformation and shift the origin of the coordinate system to start the equations at 0. If the rise or return actually starts at $\phi = \gamma$, we only need to substitute $\phi = (\phi - \gamma)$ wherever ϕ appears in the equations starting from [Equation 10.1](#).

Making the substitution of ϕ for ϕ and recognizing that for the first part of the return, $y = L$ and $y' = 0$ at $\phi = 0$ and $y = L/2$ at $\phi = \beta/2$, we get $C_0 = L$, $C_1 = 0$, and $C_2 = -\frac{2L}{\beta^2}$. For these conditions, the displacement equation is

$$y = L \left[1 - 2 \left(\frac{\phi}{\beta} \right)^2 \right] \quad (10.5)$$

For the second half of the return, the conditions to match are at $\phi = \beta/2$, $y = L/2$, and at $\phi = \beta$, $y = 0$ and $y' = 0$. For these conditions

$$y = 2L \left(1 - \left(\frac{\phi}{\beta} \right)^2 \right) \quad (10.6)$$

If we compare [Figures 10.13](#) and [10.14](#), we will notice that the rise and return sections are symmetric in shape. This will happen when the two segments have the same mathematical form and the same boundary conditions. When the two segments are symmetric, we can designate the return as y and the rise as y . Then

$$y = L - y$$

and $y' = -y'$; $y'' = -y''$; $y''' = -y'''$; and so forth. These conditions are evident when we compare [Equations 10.3](#) and [10.5](#) and [Equations 10.4](#) and [10.6](#). We can use this relationship to derive the return equations for any of the standard curves.



Example 10.1

Design for Parabolic Motion

Design a parabolic cam follower-displacement program to provide a dwell with zero lift for the first 120° of the motion cycle, and a dwell at 0.8 in lift for cam angles from 180° to 210°. The cam profile will be laid out using 10° plotting increments. Assume that the cam rotates with constant angular velocity and let the cam rotation angle be designated by θ .

Solution

The motion specification is as shown in [Figure 10.15](#). For the first part of the rise between $\phi = 120^\circ$ and $\phi = 150^\circ$, [Equation 10.3](#) applies if we use $\beta = (\theta - 120^\circ)$, $L = 0.8$, and $\beta = 60^\circ$. The resulting expression for the first part of the rise is

$$y = L \left[1 - 2 \left(1 - \frac{\theta}{\beta} \right)^2 \right] = 0.8 \left[1 - 2 \left(1 - \frac{(\theta - 120)}{60} \right)^2 \right] \quad (10.7)$$

For the second part of the rise between $\theta = 150^\circ$, $\theta = 180^\circ$, [Equation 10.4](#) applies if we again use $\beta = (\theta - 120^\circ)$, $L = 0.8$, and $\beta = 60^\circ$. The resulting expression is

$$y = L \left[1 - 2 \left(1 - \frac{\theta}{\beta} \right)^2 \right] = 0.8 \left[1 - 2 \left(1 - \frac{(\theta - 120)}{60} \right)^2 \right] \quad (10.8)$$

Using [Equations 10.7](#) and [10.8](#), the successive parts of the rise are given in [Table 10.1](#). For the first part of the return between $\theta = 210^\circ$ and $\theta = 285^\circ$, [Equation 10.5](#) applies if we use $\beta = (\theta - 210^\circ)$, $L = 0.8$ and $\beta = 150^\circ$. The resulting expression for the first part of the return is

$$y = L \left[1 - 2 \left(\frac{\theta}{\beta} \right)^2 \right] = 0.8 \left[1 - 2 \left(\frac{(\theta - 210)}{150} \right)^2 \right] \quad (10.9)$$

For the second part of the return between $\theta = 285^\circ$ and $\theta = 360^\circ$, [Equation 10.6](#) applies if we use $\beta = (\theta - 210^\circ)$, $L = 0.8$, and $\beta = 150^\circ$. The resulting expression is

$$y = 2L \left(1 - \frac{\theta}{\beta} \right)^2 = 1.6 \left(1 - \frac{(\theta - 210)}{150} \right)^2 \quad (10.10)$$

Using [Equations 10.9](#) and [10.10](#), points on the return curve are given in [Table 10.2](#). The resulting transition curves are plotted in [Figure 10.16](#). Notice that the lift values are tabulated to four decimal places. Cam and follower systems normally use very rigid components and even small profile variations are important. For this reason, we normally work with at least four decimal places when doing cam calculations. Gears are another type of profile mechanism in which the components are very rigid and, consequently, even tiny profile variations can be important. Four-decimal place accuracy cannot be displayed with typical graphical constructions. However, this accuracy can be achieved with CNC milling and precision grinding.

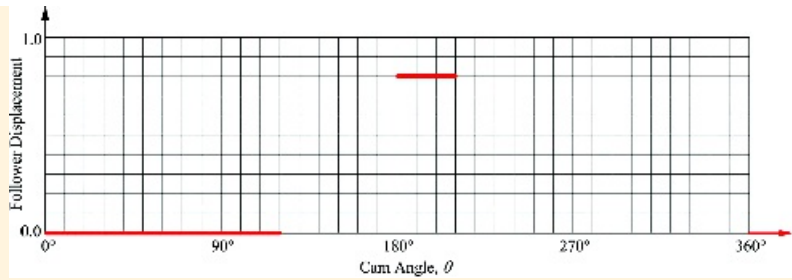


[Figure 10.15](#) The motion specification for Example 10.1.

[Table 10.1](#) Cam-Follower Data for Rise in Example 10.1

θ	120°	130°	140°	150°	160°	170°	180°
y	0.0000	0.0444	0.1778	0.4000	0.6222	0.7556	0.8000

[Table 10.2](#) Cam-Follower Data for Return in Example 10.1

θ	210°	220°	230°	240°	250°	260°	270°	280°
y	0.8000	0.7929	0.7716	0.7360	0.6862	0.6222	0.5440	0.4516
θ	290°	300°	310°	320°	330°	340°	350°	360°
y	0.3484	0.2560	0.1778	0.1138	0.0640	0.0284	0.0071	0.0000

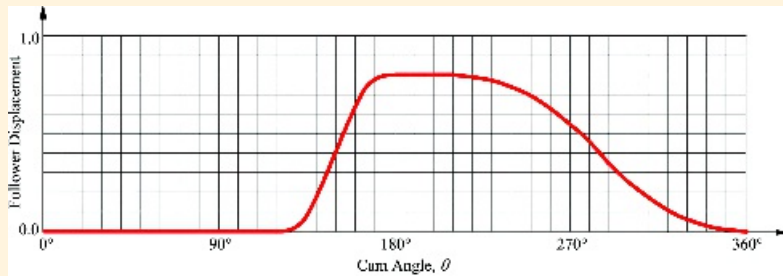


[Figure 10.16](#) The parabolic follower-displacement program generated in Example 10.1.

10.4.3 Harmonic Follower-Displacement Programs

Harmonic motion can be generated by an offset (eccentric) circular cam with a radial follower and is therefore a common form to use for a displacement diagram. Cams with this type of transition curve are commonly referred to as “harmonic cams.” The equations for harmonic motion are formed from the basic equation

$$y = C_0 + C_1 \cos C_2 \theta = C_0 \left(1 + \frac{C_1}{C_0} \cos C_2 \theta \right)$$

The displacement, velocity, acceleration, and jerk diagrams are shown in [Figure 10.17](#). Harmonic motion produces a sine velocity curve and a cosine acceleration curve. There is no discontinuity at the inflection point, so that y is defined by a single equation for all angles between zero and β . The equations for the rise starting from $\theta = 0$ and ending at $\theta = \beta$ and $y = L$ are

$$\begin{aligned}
y &= \frac{L}{2} \left(1 - \cos \frac{\pi \theta}{\beta} \right) \\
y' &= \frac{\pi L}{2\beta} \sin \frac{\pi \theta}{\beta}; \quad \dot{y} = \frac{\pi L \omega}{2\beta} \sin \frac{\pi \theta}{\beta} \\
y'' &= \frac{L}{2} \left(\frac{\pi}{\beta} \right)^2 \cos \frac{\pi \theta}{\beta}; \quad \ddot{y} = \frac{L}{2} \left(\frac{\pi \omega}{\beta} \right)^2 \cos \frac{\pi \theta}{\beta} \\
y''' &= -\frac{L}{2} \left(\frac{\pi}{\beta} \right)^3 \sin \frac{\pi \theta}{\beta}; \quad \dddot{y} = -\frac{L}{2} \left(\frac{\pi \omega}{\beta} \right)^3 \cos \frac{\pi \theta}{\beta}
\end{aligned} \tag{10.11}$$

If we use symmetric boundary conditions for both the rise and return, the equations for the return from $\theta = 0, y = L$ to $\theta = \beta, y = 0$ are

$$\begin{aligned}
y &= \frac{L}{2} \left(1 + \cos \frac{\pi \theta}{\beta} \right) \\
y' &= -\frac{\pi L}{2\beta} \sin \frac{\pi \theta}{\beta}; \quad \dot{y} = -\frac{\pi L \omega}{2\beta} \sin \frac{\pi \theta}{\beta} \\
y'' &= -\frac{L}{2} \left(\frac{\pi}{\beta} \right)^2 \cos \frac{\pi \theta}{\beta}; \quad \ddot{y} = -\frac{L}{2} \left(\frac{\pi \omega}{\beta} \right)^2 \cos \frac{\pi \theta}{\beta} \\
y''' &= \frac{L}{2} \left(\frac{\pi}{\beta} \right)^3 \sin \frac{\pi \theta}{\beta}; \quad \dddot{y} = \frac{L}{2} \left(\frac{\pi \omega}{\beta} \right)^3 \sin \frac{\pi \theta}{\beta}
\end{aligned} \tag{10.12}$$



Example 10.2

Design for Harmonic Motion

Design a harmonic cam to satisfy the same motion specifications as for Example 10.1. That is, the motion program is to provide a dwell at zero lift for the first 120° of the motion cycle and a dwell at 0.8 in lift for cam angles from 180° to 210°. The cam profile will be laid out using 10° plotting intervals.

Solution

The motion specification is as shown in [Figure 10.15](#) where θ is the cam rotation angle.

The rise in the interval 120° to 180° can be computed using [Equation 10.11](#) if we use $\vartheta = (\theta - 120)$, $L = 0.8$, and $\beta = 60^\circ$. The resulting expression for the rise is

$$y = \frac{L}{2} \left(1 - \cos \frac{\pi\vartheta}{\beta} \right) = 0.4 \left(1 - \cos \frac{\pi(\theta - 120)}{60} \right) \quad (10.13)$$

The results are given in [Table 10.3](#).

[Table 10.3](#) Cam-Follower Data for Rise Using Harmonic Motion in Example 10.2

θ	120°	130°	140°	150°	160°	170°	180°
y	0.0000	0.0536	0.2000	0.4000	0.6000	0.7464	0.8000

For the return in the interval 210° to 360°, [Equation 10.12](#) applies if we use $\vartheta = (\theta - 210)$, $L = 0.8$, and $\beta = 150^\circ$. The resulting expression for the return is

$$y = \frac{L}{2} \left(1 + \cos \frac{\pi\vartheta}{\beta} \right) = 0.4 \left(1 + \cos \frac{\pi(\theta - 210)}{150} \right) \quad (10.14)$$

Using this equation, the successive values for y are given in [Table 10.4](#). The tabulated rise values may be compared with those of Example 10.1 to observe the differences between comparable parabolic and harmonic transition curves. If plotted, the follower displacement program would be difficult to distinguish from [Figure 10.16](#). However, there will be important differences in the values for the derivatives. The generation of the cam profile for this example can be found in Example 10.3.

[Table 10.4](#) Cam-Follower Data for Return in Example 10.2

θ	210°	220°	230°	240°	250°	260°	270°	280°
y	0.8000	0.7913	0.7654	0.7236	0.6677	0.6000	0.5236	0.4418
θ	290°	300°	310°	320°	330°	340°	350°	360°
y	0.3582	0.2764	0.2000	0.1323	0.0764	0.0346	0.0087	0.0000

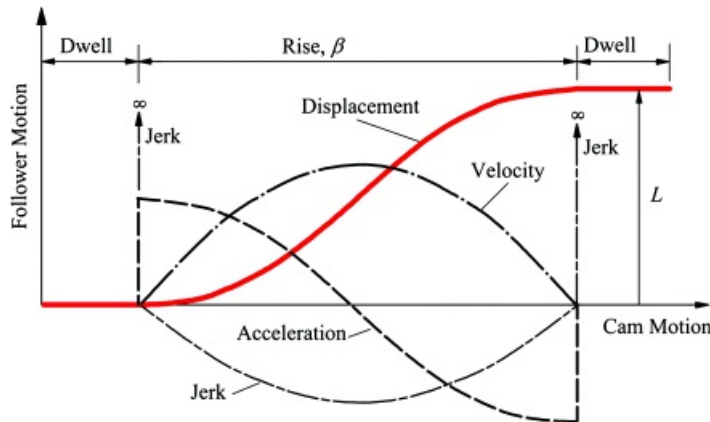


[Figure 10.17](#) Shapes of the displacement, velocity, acceleration, and jerk curves for harmonic motion.

10.4.4 Cycloidal Follower-Displacement Programs

All of the motions given above have nonzero values of acceleration (and therefore infinite jerk) at the beginning and end of the rise/dwell and therefore are limited to relatively low speeds. Cycloidal motion has zero acceleration at the beginning and end of the rise/dwell and so is useful for relatively high speeds.

A cycloidal transition produces a sinusoidal acceleration curve. The equations for the rise are

$$\begin{aligned}
 y &= L \left(\frac{\theta}{\beta} - \frac{1}{2\pi} \cos \frac{2\pi\theta}{\beta} \right) \\
 y' &= \frac{L}{\beta} \left(1 - \cos \frac{2\pi\theta}{\beta} \right); \quad \dot{y} = \frac{L\omega}{\beta} \left(1 - \cos \frac{2\pi\theta}{\beta} \right) \\
 y'' &= \frac{2\pi L}{\beta^2} \sin \frac{2\pi\theta}{\beta}; \quad \ddot{y} = 2\pi L \left(\frac{\omega}{\beta} \right)^2 \sin \frac{2\pi\theta}{\beta} \\
 y''' &= \frac{4\pi^2 L}{\beta^3} \cos \frac{2\pi\theta}{\beta}; \quad \dddot{y} = 4\pi^2 L \left(\frac{\omega}{\beta} \right)^3 \cos \frac{2\pi\theta}{\beta}
 \end{aligned}$$

These curves are plotted in [Figure 10.18](#). There is no discontinuity at the inflection point, and therefore the equations are valid for values of θ from zero to β . The rise and return curves are symmetric, and the return is given by $y = L - y$. Therefore, $y' = -y'$, $y'' = -y''$, and $y''' = -y'''$.

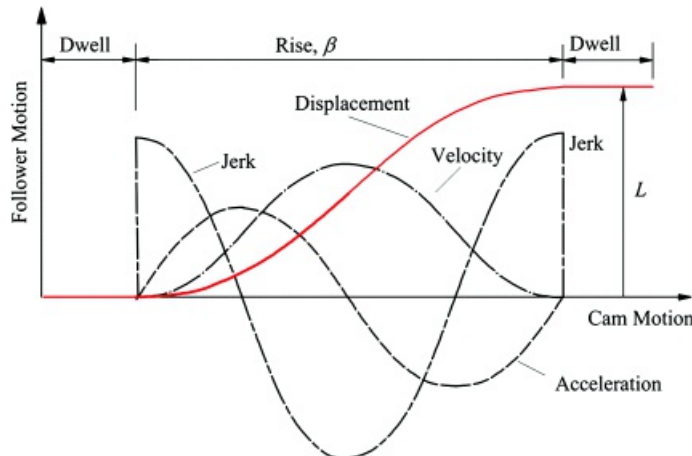


[Figure 10.18](#) Shapes of the displacement, velocity, acceleration, and jerk relations for cycloidal motion.

10.4.5 General Polynomial Follower-Displacement Programs

For high-speed machines, it is common to specify a general polynomial profile for a cam. Depending on the order of the polynomial chosen, it is theoretically possible to match almost any conditions posed by the designer. A polynomial curve can be fitted to the rise or return. Only odd-order polynomials are appropriate for rises or returns between dwells if the same conditions are to be matched at both ends of the polynomial. A first-order polynomial gives constant velocity and infinite acceleration at the beginning and end of the transition. This is the uniform motion profile discussed above. A third-order polynomial gives a parabolic velocity variation, linear acceleration, and infinite jerk at the beginning and end of the transition. A fifth-order polynomial gives finite acceleration and jerk within the interval, but the derivative of jerk is infinite at the ends of the transition. A fifth-order fit is the practical maximum unless great care is taken during manufacturing. Dynamic effects due to manufacturing errors tend to become more important than those due to curve fitting at this stage.

For a general polynomial follower displacement, the displacement function is given by

$$y = f(\theta) = \sum_{i=0}^n A_i \theta^i \quad (10.15)$$

where θ is the cam angle, and the A 's must be determined from the conditions to be matched. [Equation 10.15](#) permits us to match the same number of conditions as there are A 's, that is, $n + 1$ conditions.

When n is large and the angles are measured in degrees, the terms in the summation can vary greatly in size. For example, if θ is 100° and n is 10, the coefficients of θ^i in the equation can vary hugely, and round-off error may make it difficult to obtain an accurate solution. Therefore, it is convenient to rewrite the displacement equation in terms of the cam rotation angle β , which gives the range over which the equation is to be used. The resulting equation is

$$y = f(\theta) = \sum_{i=0}^n C_i \left(\frac{\theta}{\beta}\right)^i \quad (10.16)$$

Now the coefficients of the constants are always numbers between 0 and 1, and round-off error problems will be greatly reduced. In addition, the constants do not depend on the units used for θ as long as θ and β have consistent units. The constants in the two equations are related by the simple expression

$$A_i = \frac{C_i}{\beta^i}$$

The conditions to be matched will typically involve at least the velocity and acceleration of the follower, and the required equations for these conditions can be written as

$$y = f(\theta) = \frac{1}{\beta} \frac{d\theta}{d\beta} \sum_{i=1}^n i C_i \left(\frac{\theta}{\beta}\right)^{i-1}$$

and

$$\dot{y} = \ddot{f}(\theta) = \frac{1}{\beta} \frac{d^2\theta}{d\beta^2} \sum_{i=1}^n i C_i \left(\frac{\theta}{\beta}\right)^{i-1} + \frac{1}{\beta^2} \left(\frac{d\theta}{d\beta}\right)^2 \sum_{i=2}^n i(i-1) C_i \left(\frac{\theta}{\beta}\right)^{i-2}$$

Notice that the summation on the velocity term starts at 1 because C_0 does not appear in the equation, and the

summation on the second acceleration term starts at 2 because neither C_0 nor C_1 appears in the acceleration equation.

Now if a constant-velocity cam is used (the usual case)

$$\frac{d\theta}{dt} = \omega$$

and

$$\frac{d^2\theta}{dt^2} = 0$$

where ω is the angular velocity of the cam. The follower equations may then be written as

$$y = f(\theta) = \sum_{i=0}^n C_i \left(\frac{\theta}{\beta}\right)^i$$

$$\dot{y} = \dot{f}(\theta) = \frac{\omega}{\beta} \sum_{i=1}^n i C_i \left(\frac{\theta}{\beta}\right)^{i-1}$$

$$\ddot{y} = \ddot{f}(\theta) = \left(\frac{\omega}{\beta}\right)^2 \sum_{i=2}^n i(i-1) C_i \left(\frac{\theta}{\beta}\right)^{i-2}$$

$$\dddot{y} = \dddot{f}(\theta) = \left(\frac{\omega}{\beta}\right)^3 \sum_{i=3}^n i(i-1)(i-2) C_i \left(\frac{\theta}{\beta}\right)^{i-3}$$

As an example of the use of the polynomial profile, assume that we begin and end the follower displacement with a dwell as shown in [Figure 10.19](#) and assume that we want to match the position, velocity, and acceleration at both the beginning and end of the period being considered.

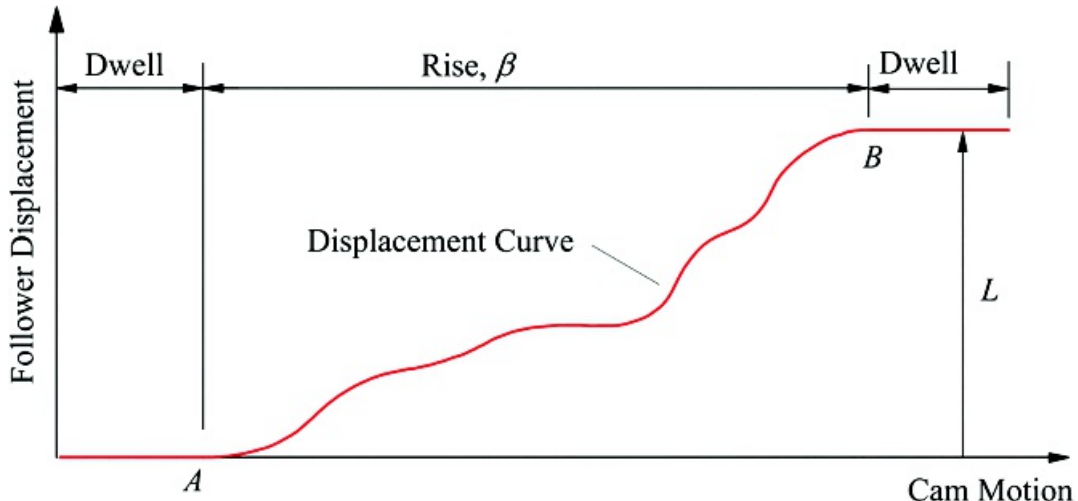


[Figure 10.19](#) Initial information for polynomial profile example.

For points A and B in [Figure 10.19](#), the following conditions apply

$$\begin{aligned} \text{At } \theta = 0, y &= \dot{y} = \ddot{y} = 0 \\ \text{At } \theta = \beta, y &= L \quad \text{and} \quad \dot{y} = \ddot{y} = 0 \end{aligned}$$

There are six conditions, so the position equation must have six constants. The resulting equations for position, velocity, and acceleration are

$$y = \sum_{i=0}^5 C_i \left(\frac{\theta}{\beta}\right)^i = C_0 + C_1 \left(\frac{\theta}{\beta}\right) + C_2 \left(\frac{\theta}{\beta}\right)^2 + C_3 \left(\frac{\theta}{\beta}\right)^3 + C_4 \left(\frac{\theta}{\beta}\right)^4 + C_5 \left(\frac{\theta}{\beta}\right)^5$$

$$\dot{y} = \frac{\omega}{\beta} \left[C_1 + 2C_2 \left(\frac{\theta}{\beta}\right) + 3C_3 \left(\frac{\theta}{\beta}\right)^2 + 4C_4 \left(\frac{\theta}{\beta}\right)^3 + 5C_5 \left(\frac{\theta}{\beta}\right)^4 \right]$$

$$\ddot{y} = \left(\frac{\omega}{\beta}\right)^2 \left[2C_2 + 6C_3 \left(\frac{\theta}{\beta}\right) + 12C_4 \left(\frac{\theta}{\beta}\right)^2 + 20C_5 \left(\frac{\theta}{\beta}\right)^3 \right]$$

Evaluation of these equations at the beginning and end of the rise period gives the following six equations that must be solved

$$0 = C_0$$

$$0 = \frac{\omega}{\beta} C_1$$

$$0 = \left(\frac{\omega}{\beta}\right)^2 2C_2$$

$$L = C_0 + C_1 + C_2 + C_3 + C_4 + C_5$$

$$0 = \frac{\omega}{\beta} [C_1 + 2C_2 + 3C_3 + 4C_4 + 5C_5]$$

$$0 = \left(\frac{\omega}{\beta}\right)^2 [2C_2 + 6C_3 + 12C_4 + 20C_5]$$

Solution for the unknown constants C_2 through C_5 gives

$$C_0 = C_1 = C_2 = 0$$

$$C_3 = 10L; \quad C_4 = -15L; \quad C_5 = 6L$$

The displacement equation can then be written in the form

$$y = 10L \left(\frac{\theta}{\beta}\right)^3 - 15L \left(\frac{\theta}{\beta}\right)^4 + 6L \left(\frac{\theta}{\beta}\right)^5$$

This is the so-called 3-4-5 polynomial transition because of the powers of the terms that remain in the expression. The first three derivatives and the velocity, acceleration, and jerk are given by

$$y = \frac{30L}{\beta} \left[\left(\frac{\theta}{\beta}\right)^2 - 2\left(\frac{\theta}{\beta}\right)^3 + \left(\frac{\theta}{\beta}\right)^4 \right]; \quad \dot{y} = \frac{30\omega L}{\beta} \left[\left(\frac{\theta}{\beta}\right)^2 - 2\left(\frac{\theta}{\beta}\right)^3 + \left(\frac{\theta}{\beta}\right)^4 \right]$$

$$\ddot{y} = \frac{60L}{\beta^2} \left[\left(\frac{\theta}{\beta}\right) - 3\left(\frac{\theta}{\beta}\right)^2 + 2\left(\frac{\theta}{\beta}\right)^3 \right]; \quad \ddot{y} = 60L \left(\frac{\omega}{\beta}\right)^2 \left[\left(\frac{\theta}{\beta}\right) - 3\left(\frac{\theta}{\beta}\right)^2 + 2\left(\frac{\theta}{\beta}\right)^3 \right]$$

$$\dddot{y} = \frac{60L}{\beta^3} \left[1 - 6\left(\frac{\theta}{\beta}\right) + 6\left(\frac{\theta}{\beta}\right)^2 \right]; \quad \dddot{y} = 60L \left(\frac{\omega}{\beta}\right)^3 \left[1 - 6\left(\frac{\theta}{\beta}\right) + 6\left(\frac{\theta}{\beta}\right)^2 \right]$$

These general relationships are plotted in [Figure 10.20](#). The displacement results are visually similar to the cycloidal curve, but the velocity, acceleration, and jerk are somewhat different. The rise and return curves are symmetric, and the return is given by $y = L - \bar{y}$. Therefore, $\dot{y} = -\dot{\bar{y}}$, $\ddot{y} = -\ddot{\bar{y}}$, and $\dddot{y} = -\dddot{\bar{y}}$.

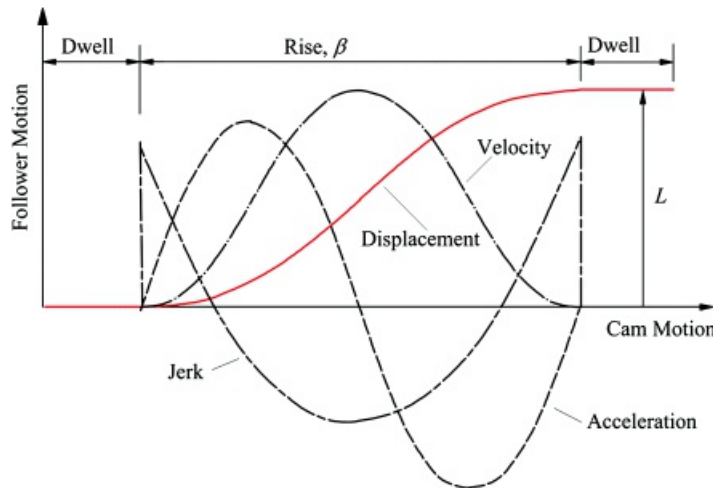


[Figure 10.20](#) Shapes of the displacement, velocity, acceleration, and jerk relations for the 3-4-5 polynomial motion.

In general, this type of cam will begin and end its motion more slowly than the other types, and in order to produce such a cam, extreme machining accuracy is required, especially at the beginning and end of the motion. The machining is usually done on a CNC milling machine followed by precision grinding.

To compare the profiles generated by the different follower-displacement programs, let $\beta = L = 1$ and vary θ from 0 to π . We can then compute y as a function of θ in increments of 0.05 radians. The results are shown in [Table 10.5](#). Notice that the variation among the different profiles is very small in most cases, and it is difficult to distinguish among the curves visually. However, the derivatives are very sensitive to small variations so that the velocity, acceleration, and jerk vary greatly from curve to curve. This emphasizes that extreme manufacturing accuracy must be achieved if the benefits of using the different follower-displacement programs are to be realized.

[Table 10.5](#) Comparison of the Different Types of Cam-Follower Motion for $\beta = L = 1$

θ	y (Linear)	y (Parabolic)	y (Harmonic)	y (Cycloidal)	y (Polynomial)
0.00	0.0000	0.0000	0.0000	0.0000	0.0000
0.05	0.0500	0.0050	0.0062	0.0008	0.0012
0.10	0.1000	0.0200	0.0245	0.0065	0.0086
0.15	0.1500	0.0450	0.0545	0.0212	0.0266
0.20	0.2000	0.0800	0.0955	0.0486	0.0579
0.25	0.2500	0.1250	0.1464	0.0908	0.1035
0.30	0.3000	0.1800	0.2061	0.1486	0.1631

0.35	0.3500	0.2450	0.2730	0.2212	0.2352
0.40	0.4000	0.3200	0.3455	0.3065	0.3174
0.45	0.4500	0.4050	0.4218	0.4008	0.4069
0.50	0.5000	0.5000	0.5000	0.5000	0.5000
0.55	0.5500	0.5950	0.5782	0.5992	0.5931
0.60	0.6000	0.6800	0.6545	0.6935	0.6826
0.65	0.6500	0.7550	0.7270	0.7788	0.7648
0.70	0.7000	0.8200	0.7939	0.8514	0.8369
0.75	0.7500	0.8750	0.8536	0.9092	0.8965
0.80	0.8000	0.9200	0.9045	0.9514	0.9421
0.85	0.8500	0.9550	0.9455	0.9788	0.9734
0.90	0.9000	0.9800	0.9755	0.9935	0.9914
0.95	0.9500	0.9950	0.9938	0.9992	0.9988
1.00	1.0000	1.0000	1.0000	1.0000	1.0000



10.5 Determining the Cam Profile

Once the follower motion is determined as a function of the cam displacement, the cam profile can be found either graphically or analytically. For extremely accurate cams, the geometry must be determined analytically and the machining done using CNC milling machines followed by precision grinding. For low-speed cams, however, a graphical layout and manual machining may be adequate.

If we restrict our discussions to planar, rotating cams, four general types of followers are possible. They are a translating cylindrical-faced follower, a translating flat-faced follower, an oscillating cylindrical-faced follower, and an oscillating flat-faced follower (Figure 10.21).

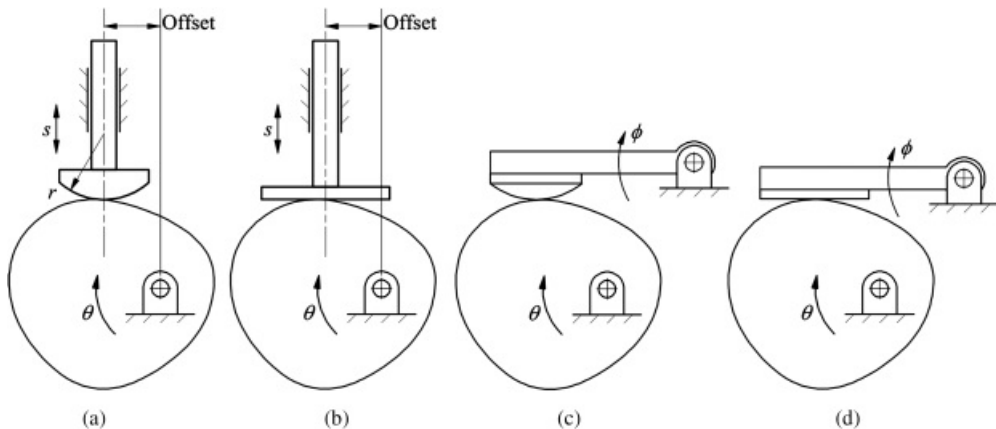


Figure 10.21 Common follower configurations for planar rotating cams: (a) Translating cylindrical-faced follower; (b) translating flat-faced follower; (c) oscillating cylindrical-faced follower; and (d) oscillating flat-faced follower.

Notice that the cam geometry is the same for a nonrotating cylindrical-faced follower and for a roller follower. Therefore, we can consider either when designing the cam as long as the radius of the follower is the same in both instances. We will consider both graphical and analytical approaches to the design of the cam for each type of follower shown in Figure 10.21. Even though the graphical approach is rarely used in industry, this approach visually illustrates the issues in cam generation, and some cam design-computer programs are based directly on the graphical generation process.

10.5.1 Graphical Cam Profile Layout

Cam profiles are laid out graphically using inversion. That is, the cam is viewed as stationary, and the successive positions of the follower are located relative to it. This results in a polar plot of successive follower positions. The cam profile is then filled in as the envelope curve of the follower positions.

The first step in laying out the cam profile is to select a base circle radius. The base circle represents the position of the follower at zero lift. The center of the base circle is at the center of rotation of the cam, and the base circle is the largest circle that is tangent to the cam and can be drawn entirely within the cam interior. Successive lift values are plotted radially outward from the base circle.

Choosing a large base circle radius results in a large cam. However, if the base circle is too small the cam profile may have hollows of smaller radius than the follower. Since the follower will bridge across such a hollow, it will not follow the desired lift program. Obviously, this situation must be avoided, and it is therefore necessary to have a means of computing the radius of curvature of the cam profile at different locations.

The pressure angle of a cam is the angle between the contact normal and the velocity vector of the point on the follower at the contact location. The pressure angle will vary as the cam rotates, except at a dwell where it is constant. Reducing the maximum pressure angle reduces the contact loads and the moment on the follower bearings. This promotes smoother operation with less wear. Depending on the friction values, if the pressure angle is high enough, the cam will lock up and cannot be moved regardless of the torque applied. It is normally

recommended that the pressure angle be kept to less than $\pm 30^\circ$ unless special design considerations are made [8]. Increasing the base circle radius decreases the maximum value of the pressure angle. Thus, it is good practice to use the largest base circle that the design space constraints will allow. As a general rule of thumb, the base circle radius should be two to three times the maximum lift value.



Example 10.3

Layout of Cam Profile for Radial Roller Follower

Lay out a cam profile using the harmonic follower-displacement profile of Example 10.2. That is, the follower is to dwell at zero lift for the first 120° of the motion cycle and to dwell at 0.8 in lift for cam angles from 180° to 210° and rise and return with harmonic motion. The cam is to have a translating roller follower with a 1 in roller diameter. The cam will rotate CW. Lay out the cam profile using 10° plotting increments.

Solution

The basic motion specification is as shown in [Figure 10.15](#). Using the results of Example 10.2, the lift values to be used are as given in [Table 10.6](#). Notice that the dwells correspond to locations on the cam where the radius is constant (i.e., the cam profile is a circle arc).

[Table 10.6](#) Follower Displacements for Example 10.3

θ	$0, 360^\circ$	10°	20°	30°	40°	50°	60°	70°	80°
y	0.0000	0.0000	0.0000	0.0000	0.0000	0.0000	0.0000	0.0000	0.0000
θ	90°	100°	110°	120°	130°	140°	150°	160°	170°
y	0.0000	0.0000	0.0000	0.0000	0.0536	0.2000	0.4000	0.6000	0.7464
θ	180°	190°	200°	210°	220°	230°	240°	250°	260°
y	0.8000	0.8000	0.8000	0.8000	0.7913	0.7654	0.7236	0.6677	0.6000
θ	270°	280°	290°	300°	310°	320°	330°	340°	350°
y	0.5236	0.4418	0.3582	0.2764	0.2000	0.1323	0.0764	0.0346	0.0087

The layout of the cam is accomplished by first drawing radial lines at 10 degree increments. Because the cam rotates CW, the radial lines are laid off and labeled in the CCW direction as shown in [Figure 10.22](#). Next, the base circle and the prime circle are drawn. The *base circle* is chosen to have a 1.5 in radius, and it is the largest circle that can be drawn inside the cam profile without intersecting the cam profile. The radius of the *prime circle* is equal to $r_b + r_0$ where r_b is the base circle radius, and r_0 is the radius of the roller follower.

Therefore, in this problem, the prime-circle radius is 2.0 in. The cam profile is initially laid off from the prime circle to give the pitch curve. The *pitch curve* is the curve traced by the center of the roller follower. Notice that the pitch curve would be the cam profile if r_0 were zero. This corresponds to the case of a knife-edged follower.

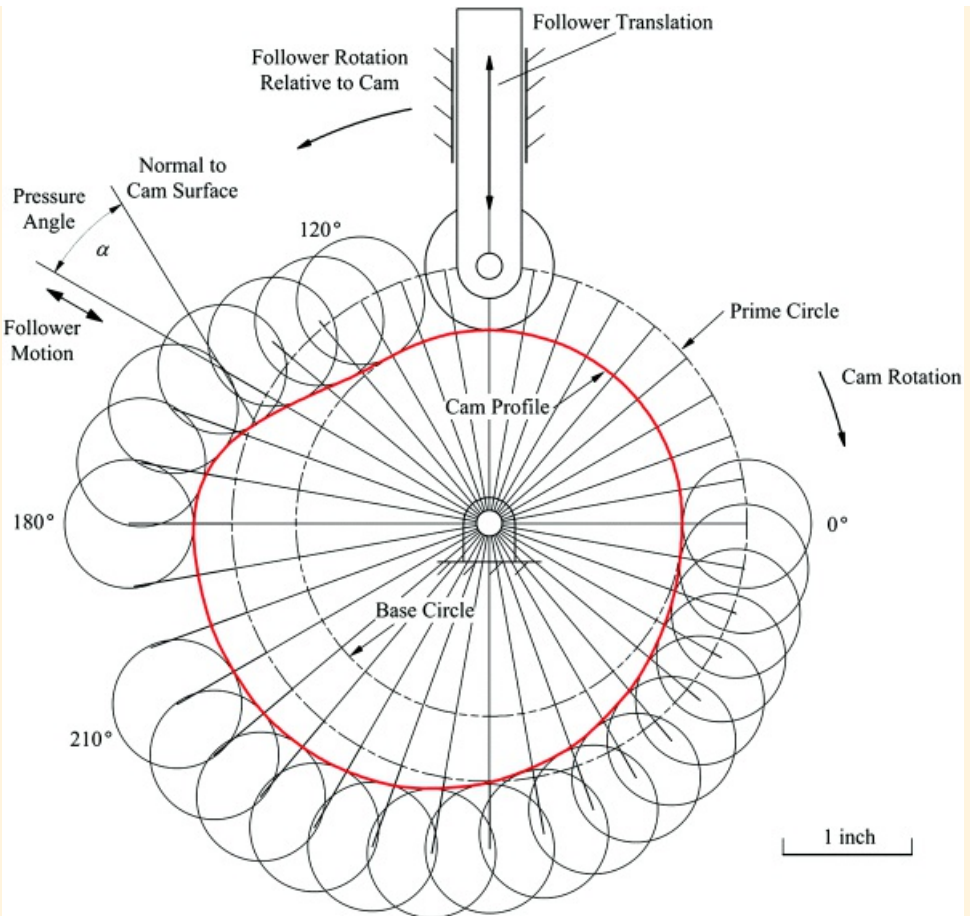


[Figure 10.22](#) Layout of the cam profile for Example 10.3. The process of laying out a cam profile is one of inversion. That is, the cam is viewed as being stationary and successive positions of the follower are plotted relative to it. In this case, a prime circle of 2.0 in radius was chosen. This represents the location of the follower center at zero lift. Positive lift values are plotted outward from the prime circle. The successive positions of the follower are then drawn using the plotted points as centers. Finally, the profile is plotted as an envelope curve of the successive follower positions. Because of the inversion, if the cam is to rotate CW, the positions of the follower must be plotted in the opposite direction, that is CCW.

Once the radial lines and prime circle are established, the displacements can be laid off from the prime circle as shown in [Figure 10.22](#). The radius of the follower is drawn with its center located on the pitch curve at each location. The cam can be defined by drawing a curve tangent to roller locations as shown in [Figure 10.22](#).

As indicated earlier, an important parameter for cam motion is the pressure angle. In the case of the translating roller follower, this is the angle between the follower travel and the normal to the curve at the point of contact. For a given force on the follower roller, the force in the direction of travel of the cam will be proportional to the cosine of the pressure angle. The force normal to the travel direction of the follower is proportional to the sine of the pressure angle. Wear on the follower stem will increase with the normal force; therefore, from design considerations, we want the pressure angle (α) to be as small as possible.

The maximum pressure angle will occur at the *pitch points*. These correspond to the inflection points on the follower displacement curves (see [Figure 10.11](#)). If the torque on the cam is more or less constant, the pressure angles at the pitch points will correspond to the parts of the cycle where the maximum normal force occurs and hence when the follower stem wear will be greatest. It will also correspond to the parts of the cycle where the follower will tend to bind in the stem bearing. As indicated above, because of problems with wear and binding, the pressure angle is usually limited to angles on the order of $\pm 30^\circ$. If the pressure angle becomes excessive, the base circle should be increased or the follower displacement profile changed.

The problem statement indicated that a roller follower was to be designed. However, the construction would be *exactly* the same if a solid, cylindrical-faced follower were involved. From the standpoint of the cam geometry, the important issues are the radius of the cylindrical face and the direction of translation relative to the cam. From a machine-design standpoint, however, the roller follower is preferred because the effect of friction at the cam follower interface is minimized due to rolling contact.



Example 10.4

Layout of Cam Profile for Translating Flat-Faced Follower

Again, lay out a cam profile using the harmonic-displacement profile of Examples 10.2 and 10.3; that is, the follower is to dwell at zero lift for the first 120° of the motion cycle and to dwell at 0.8 in lift for cam angles from 180° to 210° and rise and return with harmonic motion. The cam is to have a translating, flat-faced follower that is offset by 0.2 in. The cam will rotate CW. Lay out the cam profile using 10° plotting intervals.

Solution

The basic motion specification is the same as in Example 10.3 (Table 10.6). The layout of the cam is again accomplished by first drawing radial lines at 10° increments. Because the cam rotates CW, the radial lines are laid off and labeled in the CCW direction as is done in Figure 10.23. Next the base circle is drawn. Because a flat-faced follower is being designed, there is no prime circle. However, selection of the base circle requires careful consideration.

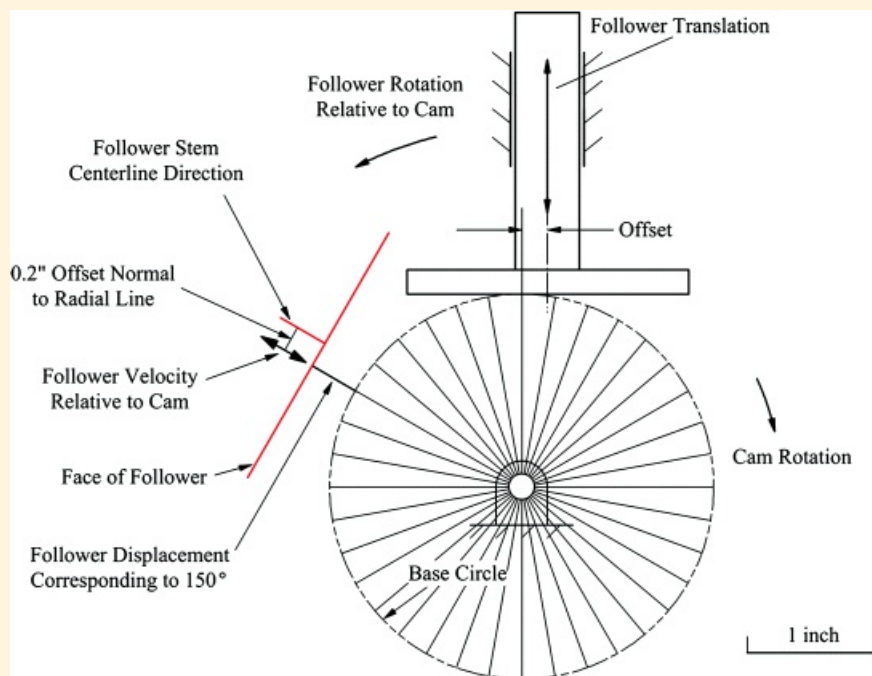


Figure 10.23 Basic construction lines for determining cam profile for flat-faced follower.

A major restriction on the cam profile driving a flat-faced follower is that the profile must form a convex surface. This means that the vectors from every point on the cam to the corresponding center of curvature must point toward the interior of the cam. An alternative way to approach the convexity problem is to imagine an arbitrary line drawn across the face of the cam. If it is possible to select an arbitrary line that intersects the cam at more than two points, the cam profile is not convex. If the cam is not convex, the flat-faced follower cannot contact the cam at all points, and the desired motion will not be generated. This condition will be illustrated mathematically when an analytical approach to cam synthesis is discussed. Clearly, the cam generated in Figure 10.22 does not satisfy the convexity condition; however, this is not necessarily an issue with roller followers. When the resulting cam is not convex for flat-faced followers, we must increase the size of the base circle or change the follower displacement function. The effect of changing the base circle can be easily investigated by running the cam design program in *KinDAP* supplied with the supplementary material with this book.

To begin the construction, we can select a base circle somewhat arbitrarily. However, if the radius of curvature at some location on the resulting cam is too small, the base circle diameter must be increased.

The follower is offset, but this does not affect the geometry of the cam. All points on the follower have the same velocity because its motion is pure translation. Therefore, from a kinematic standpoint, the actual location of the follower stem is not important, and in the constructions, it need not be drawn. From a machine design standpoint it is important, however, because the larger the offset, the higher the moment on the follower stem and the higher the bearing forces and resulting wear.

We can lay off the displacements in [Table 10.6](#) from the base circle and along the radial lines. Next, draw a line perpendicular to each radial line at the location on the radial line corresponding to the displacement location. These perpendicular lines correspond to the face of the follower. This is illustrated in [Figure 10.23](#). The lines for different positions of the follower will form an envelope that defines the geometry of the cam surface. We construct the outline of the cam by drawing a curve that is tangent to the lines corresponding to the different positions of the follower face.

As the lines corresponding to the different positions of the follower face are drawn, successive lines will intersect. For the geometry to be valid, the angle increment for successive intersections must be positive (move in the direction of the follower rotation relative to the cam). If an intersection of the face lines for two successive positions reverses in direction, it will not be possible to generate the cam, and a larger base circle must be used. This situation is illustrated in the current problem in [Figure 10.24](#) for the positions corresponding to rotation angles of 150°, 160°, 170°, and 180°. In [Figure 10.24](#), a base circle radius of 1.5 in was chosen. The intersections corresponding to 150° and 160° and to 160° and 170° move in the CCW direction, but the increment corresponding to 170° and 180° reverses in the CW direction. This situation makes the cam nonconvex and indicates that the base circle is too small and must be increased.

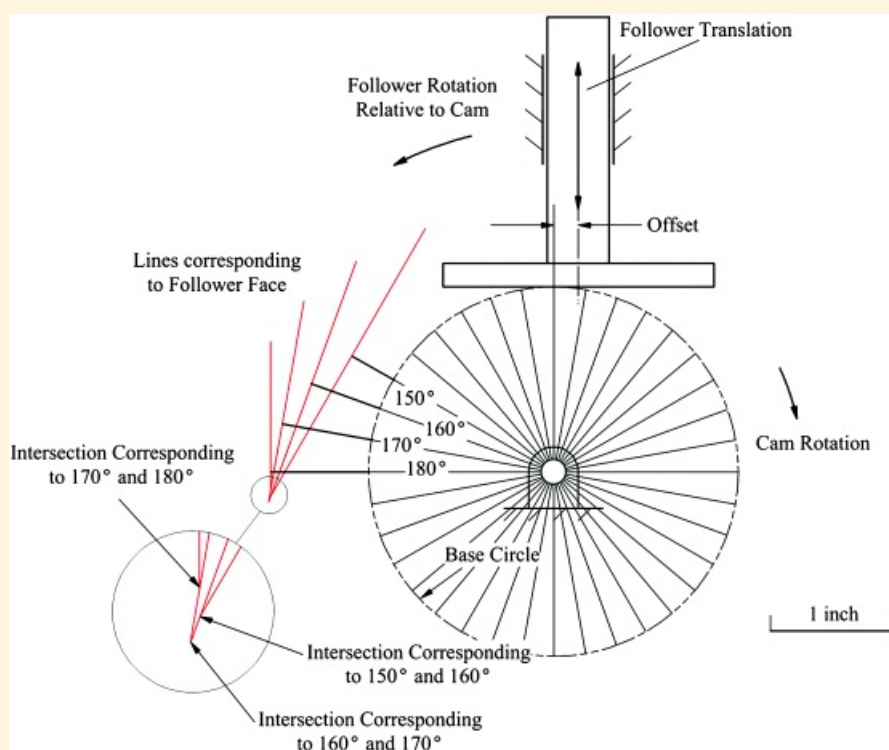


[Figure 10.24](#) Condition when the base circle is too small to generate an acceptable cam for a flat-faced follower.

The smallest base circle is the one for which the face line intersection corresponding to 170° and 180° is no longer in the CW direction. This occurs when the follower-face lines corresponding to 160°, 170°, and 180° intersect at a point that happens when the base circle radius is approximately 2.8 in. This value for the minimum base circle was determined using *KinDAP*. For this base circle, the cam will have a point or cusp corresponding to the location where the face lines intersect. The envelope of the face lines and the resulting

cam is shown in [Figure 10.25](#). The cam designed for the roller follower and for the same displacement profile is also shown in [Figure 10.25](#) for comparison. Based on the size of the cam required, a flat-faced follower would be a poorer choice for this type of displacement profile than would be the roller follower.

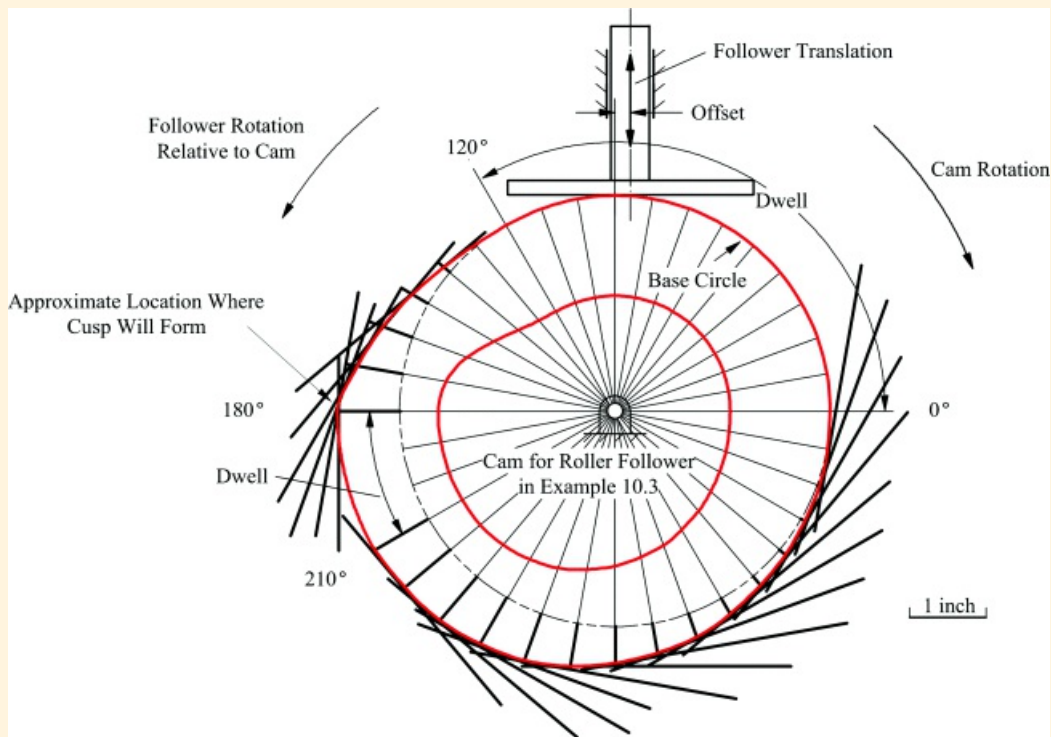


[Figure 10.25](#) Cam for Example 10.4. The base circle is approximately the minimum possible for the flat-faced follower to generate the profile indicated in [Table 10.6](#) without cusps. The cam generated for the roller follower in Example 10.3 is included for comparison.

As indicated before, an important parameter for cam motion is the pressure angle. When a flat-faced follower is used, the normal to the follower profile is always in the direction of the follower travel assuming that the follower stem is perpendicular to the follower face. This makes the pressure angle always zero; however, there can be significant lateral loads on the follower bearings caused by the frictional force at the cam-follower interface and by the moment generated by the normal force at the cam-follower interface and the offset line of action. The friction force can be reduced by lubrication but never completely eliminated, and the bearing couple that opposes the moment from the normal force must be addressed in the design of the bearings for the cam and follower system. Depending on the lubrication and design, the lateral forces can be as high as or higher than the corresponding lateral force with a roller follower. Also, the cam may become so large to avoid the convexity condition that the roller follower would be preferred from size considerations.

Another important parameter that must be determined for the design of a cam for a flat-faced follower is the size (length) of the follower face. It is essential that the face be long enough on both sides to maintain contact with the cam on a tangent line. The minimum length of the follower face can be established by direct measurement. The actual length would be equal to the minimum length plus a small margin.



Example 10.5

Layout of Cam Profile for Oscillating, Cylindrical Follower

Lay out a cam profile assuming that the follower starts from a dwell for 0° to 120° of cam rotation, and the cam rotates CW. The rise occurs during the cam rotation from 120° to 200° . The follower then dwells for 40° of cam rotation, and the return occurs for the cam rotation from 240° to 360° . The amplitude of the follower rotation is 30° , and the follower radius is 0.75 in. Lay out the cam profile using 20° plotting increments. (This plotting increment is too coarse for the development of an accurate cam; however, it will be used to simplify the resulting drawing).

Solution

The basic motion specification is visually similar to that shown in [Figure 10.15](#); however, the follower motion is a rotation instead of a translation. To begin the design, we must determine the follower rotation, ϕ , as a function of the cam rotation, θ . Assume parabolic motion for the follower. From Section 10.4.2, the equations for each part of the motion are

$$\begin{aligned} 0^\circ < \theta < 120^\circ & \quad \phi = 0^\circ \\ 120^\circ \leq \theta \leq 160^\circ & \quad \phi = 2L\left(\frac{\theta}{\beta}\right)^2 = 60\left(\frac{\theta - 120}{80}\right)^2 \\ 160^\circ \leq \theta \leq 200^\circ & \quad \phi = L\left[1 - 2\left(1 - \frac{\theta}{\beta}\right)^2\right] = 30\left[1 - 2\left(1 - \frac{\theta - 120}{80}\right)^2\right] \\ 200^\circ \leq \theta \leq 240^\circ & \quad \phi = 30^\circ \\ 240^\circ \leq \theta \leq 300^\circ & \quad \phi = L\left[1 - 2\left(\frac{\theta}{\beta}\right)^2\right] = 30\left[1 - 2\left(\frac{\theta - 240}{120}\right)^2\right] \\ 300^\circ \leq \theta \leq 360^\circ & \quad \phi = 2L\left(1 - \frac{\theta}{\beta}\right)^2 = 60\left(1 - \frac{\theta - 240}{120}\right)^2 \end{aligned}$$

Here, L is treated as the generic amplitude of the follower motion. In this case, L is given as 30° .

Using these equations, the lift values to be plotted are as given in [Table 10.7](#). Notice that the dwells correspond to locations on the cam where the radius is constant.

[Table 10.7](#) Follower Displacements for Example 10.5

θ	$0, 360^\circ$	20°	40°	60°	80°	100°	120°	140°	160°
ϕ	0.0000	0.0000	0.0000	0.0000	0.0000	0.0000	0.0000	3.7500°	15.0000°
θ	180°	200°	220°	240°	260°	280°	300°	320°	340°
ϕ	26.2500°	30.0000°	30.0000°	30.0000°	28.3333°	23.3333°	15.0000°	6.6666°	1.6666°

The cam-follower system is similar to that shown in [Figure 10.26](#), and the locations shown in [Figure 10.26](#) will be used to describe the layout of the cam. In particular, A is the location of the axis of rotation of the cam, B is the contact point, C is the center of curvature of the follower, and D is the rotation axis of the follower.

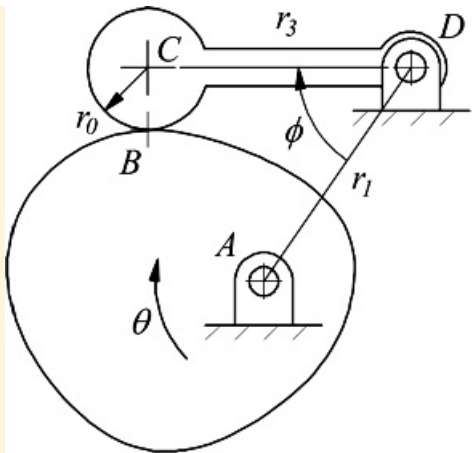


Figure 10.26 Cam-follower system to be designed in Example 10.5.

The first step in the cam layout is to draw the base circle and prime circle. The *base circle* is chosen to have a 1.25-in radius, and the radius of the *prime circle* is equal to $r_b + r_0 = 1.25 + 0.75 = 2.0$ in. The base circle radius is the radius of the cam during the dwell for the first 120° of cam rotation.

The second step is to select the distance from the cam rotation axis to the pivot of the follower (*AD*). The larger the value chosen, the smaller the pressure angle; however, this distance also directly affects the size of the cam-follower system. We will choose the distance between pivots to be 4 in. When we invert the motion, the follower pivot will appear to rotate around the cam. Therefore, we must draw a circle with a radius of 4 in about the cam center for the follower pivot circle. The pivot circle is shown in [Figure 10.27](#).

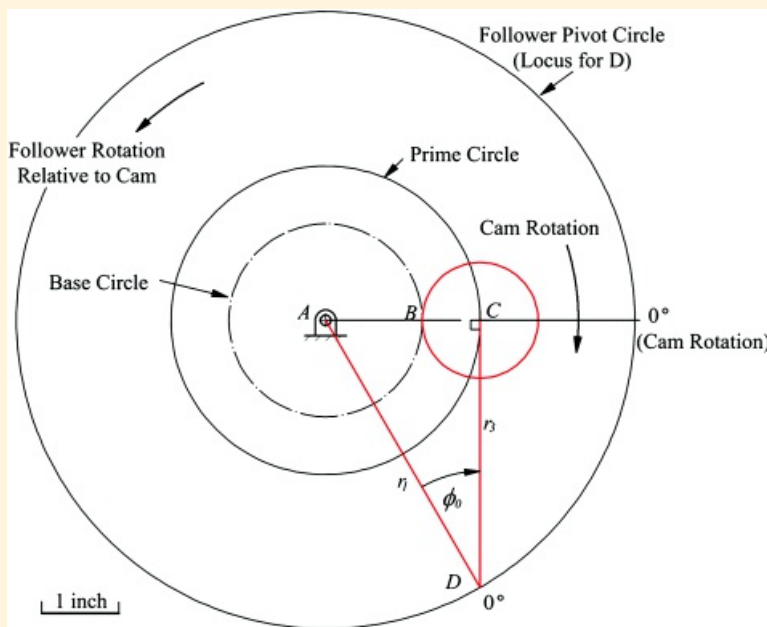


Figure 10.27 Location of the follower in the initial position. This determines the reference angle Φ_0 .

The third step is to determine the length of the follower ($CD = r_3$) and the reference angle ϕ_0 for ϕ . We will locate the follower in the initial dwell position in such a way that the pressure angle is zero. This is done by drawing a line tangent to the prime circle through the ray corresponding to $\theta = 0$. The intersection of this tangent line with the follower pivot circle will give the location of the follower pivot for the initial position of the cam. Two intersections are possible. One will correspond to a CW rotation of the cam, and the second will correspond to a CCW rotation. Based on the problem statement, we will choose the intersection corresponding to the CW rotation of the cam as shown in [Figure 10.27](#). Because a right triangle is involved, the follower length is given by

$$r_2 = \sqrt{r_1^2 - (r_3 + r_0)^2} = \sqrt{4^2 - 2^2} = 3.464$$

We also need to determine the base angle, ϕ_3 , because all subsequent angular displacements of the follower will be measured relative to this angle. The angle ϕ_3 is given directly by

$$\phi_3 = 180^\circ - \left(\frac{r_3 + r_0}{r_2} \right) = 180^\circ - \left(\frac{2}{3.464} \right) = 30.00^\circ$$

The location of pivot D for the follower when the cam angle is 0° gives the first position of the follower pivot. Subsequent positions of the pivot will be at angle increments of 20° . Therefore, the fourth step in the cam layout is to draw radial lines at 20° increments from the cam rotation axis to the follower pivot circle starting from the initial position of AD corresponding to the cam rotation angle of 0° . Label the radial lines corresponding to the beginning and end of dwells. The radial locations are shown in [Figure 10.28](#).

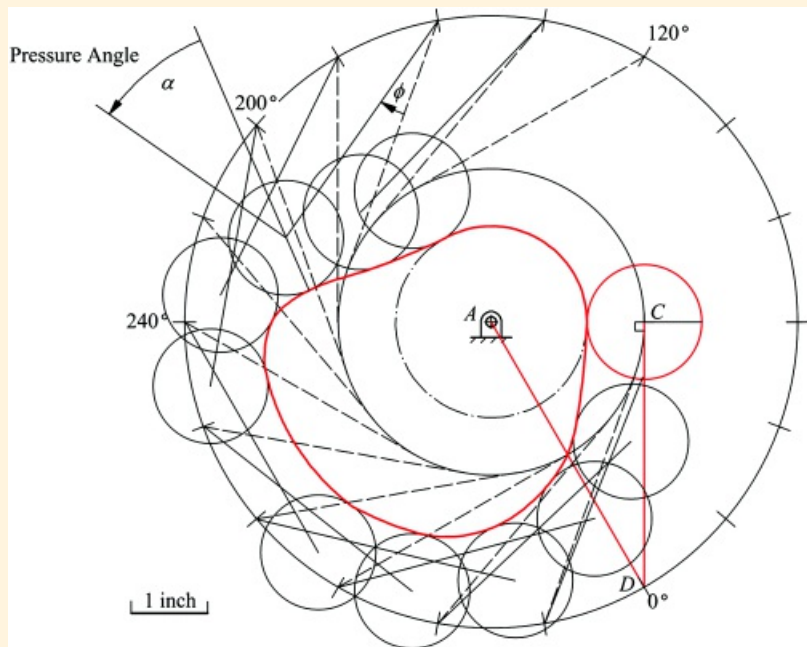


[Figure 10.28](#) Final layout of the cam profile for Example 10.5.

The fifth step is to draw a line tangent to the prime circle from the intersection of the radial lines and the follower pivot circle as shown in [Figure 10.28](#). These lines give the position of the follower relative to the cam, if the cam is a simple cylinder. These lines will give the base lines from which to measure the ϕ angles given in [Table 10.7](#). Next lay off lines 3.464-in in length at the angles indicated in [Table 10.7](#) from the corresponding base lines. The ends of these lines will be the centers of the cylindrical cam follower in the different positions. Draw circles corresponding to the follower, and construct the cam surface tangent to the follower positions. The final cam is shown in [Figure 10.28](#).

As in the case of a translating roller follower, an important parameter for cam motion is the pressure angle. For the oscillating cylindrical follower, this is the angle between the velocity of the contact point on the follower (vector normal to line from contact point and point D) and the normal to the cam at the contact point. To reduce wear on the follower pivot, we want the pressure angle, α , to be as small as possible. In the design shown in [Figure 10.28](#), the pressure angle will become fairly high (greater than 30°) in the rise region. To improve the design, the diameter of the base circle should be increased.

The problem statement indicated that a cylindrical follower was to be designed. However, the construction would be *exactly* the same if a roller follower were involved. From the standpoint of the cam geometry, the

important issues are the radius of the cylindrical face and the direction of motion relative to the cam.



Example 10.6

Layout of Cam Profile for Oscillating Flat-Faced Follower

Lay out the rise portion of the cam profile for the follower motion indicated in [Table 10.7](#). The cam will rotate *counterclockwise*. Assume that the follower offset is 0.54-in, and lay out the cam profile using 20° plotting intervals. Again, this plotting interval is too coarse for an accurate cam; however, it will be used to illustrate the procedure.

Solution

The cam-follower system is similar to that shown in [Figure 10.29](#), and the locations shown in that figure will be used to describe the layout of the cam. Point *A* is the location of the axis of rotation of the cam, *B* is the rotation axis of the follower, and *d* is the face offset from *B*. Point *D* is the location of the contact point on the follower. Point *C* give the intersection point for the face and a line that passes through point *B* and is perpendicular to the face.

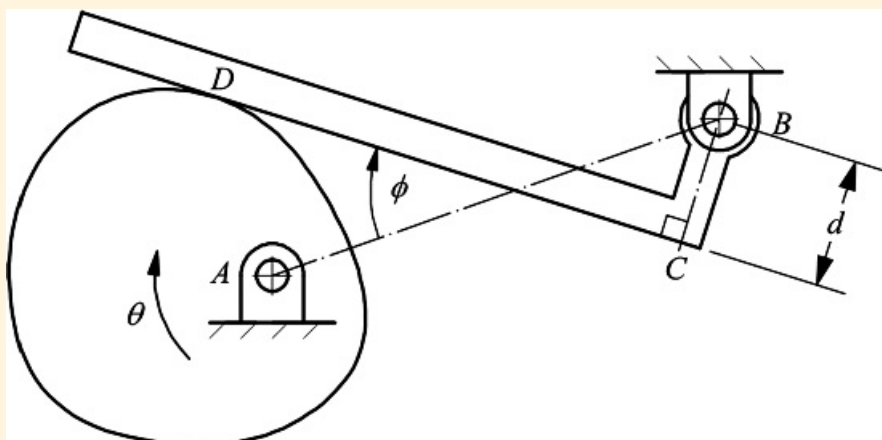


[Figure 10.29](#) Cam-follower system to be designed in Example 10.6.

The first step in the cam layout is to select and draw the base circle. The base circle is chosen to be 2.0 in.

The second step is to select the distance from the cam rotation axis to the pivot of the follower (*AB*). The value chosen will affect the size of the cam, and typically the smallest value possible is chosen. The pivot distance must be large enough that the cam does not contact the follower pivot. Also, the force between the cam and follower will increase as the distance decreases. Therefore, it may be necessary to increase the pivot distance from machine design considerations. We will choose the distance between pivots to be 4 in. When we invert the motion, the follower pivot will appear to rotate around the cam. Therefore, we must draw a circle with a radius of 4 in about the cam center for the follower pivot circle as shown in [Figure 10.30](#).

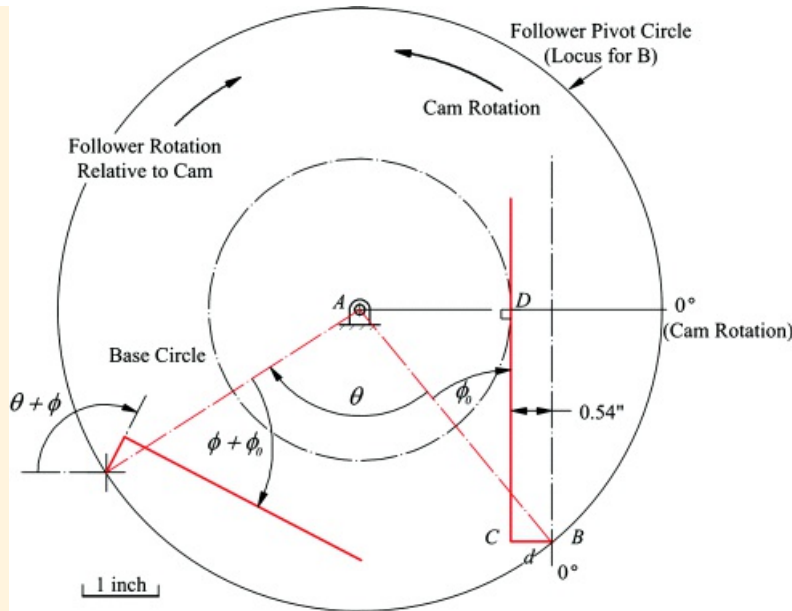
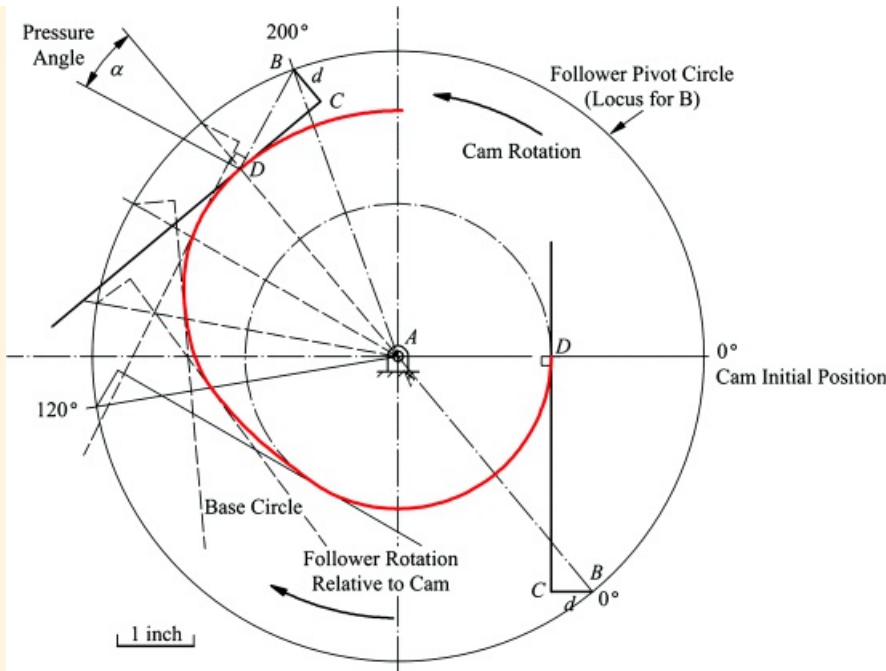


Figure 10.30 Determining the initial position of the follower and the general motion of the follower.

The third step is to determine the reference position for the follower. The initial location of the follower will affect the length of the follower and therefore the cost of the system. For simplicity, we will locate the follower in the initial dwell position (cam angle $\theta = 0^\circ$) to locate the point D . First draw a vertical line tangent to the base circle at D as shown in [Figure 10.30](#). Next draw a second, parallel line that is offset by 0.54-in to the right of the first line. The intersection of this line with the follower pivot circle will locate B in the initial position. This is shown in [Figure 10.30](#). The offset is represented by a line through B and perpendicular to the line representing the face of the follower. This locates point C . Note that line BC is horizontal in this position. As the follower rotates relative to the cam, the line BC and the rest of the follower will rotate through an angle of $\theta + \phi$. Therefore, to locate the follower in each position, we need only locate BC at a CW angle of $\theta + \phi$ relative to the horizontal as shown in [Figure 10.30](#).

The fourth step in the cam layout is to draw radial lines at 20° increments from the cam rotation axis to the follower pivot circle starting from the initial position of AB corresponding to the cam rotation angle of 0° . These will give the positions of B for each 20° rotation of the cam. Label the radial lines corresponding to the beginning and end of the first dwell and the second dwell. In the dwell regions, the cam will have a circular contour. These radial lines are shown in [Figure 10.31](#).



[Figure 10.31](#) Final layout of the rise portion of the cam profile for Example 10.6.

The fifth step is to draw the line BC at a CW angle of $\theta + \phi$ at each position of B . Next starting at C , draw a line perpendicular to BC on the CW side of BC for each position of B . This will locate the successive positions of the follower face. Construct the cam surface tangent to the follower positions. The rise portion of the final cam is shown in [Figure 10.31](#).

Because of the follower offset, the pressure angle will not be constant as was the case with the translating flat-faced follower. The pressure angle will depend on the contact point as shown in [Figure 10.31](#) and will be equal to $\tan^{-1}(d/CD)$. If the follower offset, d , is zero, the pressure angle will be a constant, that is, 0° . Because of this, the offset should be zero unless specific design conditions dictate otherwise.

10.5.2 Analytical Determination of Cam Profile

Although the graphical approach can work well for low-speed cams, for high speeds greater accuracy is required, making analytical techniques necessary. The analytical approach to determining the cam profiles also uses inversion. The general procedure is to establish a coordinate system on the cam and to locate the positions of the follower relative to that coordinate system. Successive positions of the follower will generate an envelope that will define the geometry of the cam profile. Consequently, envelope theory has been used traditionally for defining the cam profile [8, 9]. However, an alternative approach based on instant centers of velocity originally illustrated by Davidson [10] and exploited by Wu et al. [11] determines the cam profile points directly, and therefore, this is the approach considered here. The instant-center approach will be used here for each of the four different follower systems considered earlier.

Analytical Determination of Cam Profile for an Offset, Translating Cylindrical Follower

Prior to determining the geometry of the cam, it is assumed that the basic motion specification for the follower is known in the form $z = f(\theta)$, where z is the displacement of the follower and θ is the cam rotation angle. Here $f(\theta)$ is typically given by one of the follower displacement functions discussed in Sections 10.3–10.4. The base circle radius (r_b), the follower radius (r_0), and the offset d are also assumed to be known. The positive direction for d is defined by rotating the stem of the follower 90 degrees in the CCW direction. The procedure is essentially the same for both a roller follower and a cylindrical-faced follower, and for simplicity, the cylindrical-faced follower will be considered here.

Two positions of the follower relative to the cam are shown in [Figure 10.32](#). In the figure, it is assumed that the

cam rotates CW, which means that the follower moves relative to the cam in the CCW direction. Link 1 is the frame, link 2 is the cam, and link 3 is the translating follower.

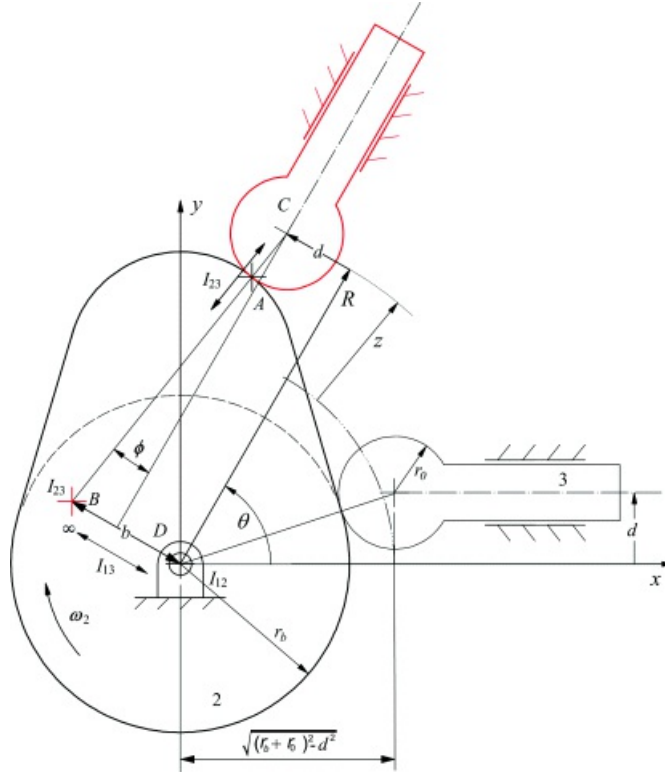


[Figure 10.32](#) Two positions of the roller follower relative to cam.

To start the procedure, locate the three instant centers (I_{12} , I_{13} , I_{23}) for the system in the displaced position corresponding to θ . Based on the Kennedy-Aronhold theorem, the three instant centers will be collinear, and I_{23} will be on a line through the contact point and the normal line to the tangent to both surfaces at the point of contact. The three instant centers for the three bodies are located in the figure relative to the frame, which is rotated by the angle θ relative to the cam in [Figure 10.32](#). The coordinate system attached to the cam is designated as (x, y) . The cam rotates about point D . Point C is the center of the cylindrical follower, point A is the contact point on the cam, and point B is the instant center location I_{23} . Point B is a distance b from the center of rotation of the cam.

The variable z gives the displacement along the translation axis of the follower. The radial distance measured parallel to the slider path from the center of the follower to the origin of the coordinate system located at the center of the cam is given by

$$R = \sqrt{(r_b + r_0)^2 - s^2} + z \quad (10.17)$$

By definition of the instant center, the velocity of B on link 2 is the same as the velocity of B on link 3. That is

$$v_{B_2} = v_{S_3}$$

For B on link 2

$$v_{S_3} = \omega_2 \dot{\theta}$$

Where ω_2 is the angular velocity of the cam (link 2). Because the motion of link 3 is a pure translation relative to the frame, all points in link 3 have the same linear velocity; therefore

$$v_{B_3} = \frac{dR}{dt} = \frac{dR}{d\theta} \frac{d\theta}{dt} = \omega_2 \frac{dR}{d\theta} = \omega_2 R'$$

Since the velocities for B_2 and B_3 are equal

$$\omega_2 b = \omega_2 R'$$

and

$$b = R' \quad (10.18)$$

From [Equation 10.17](#)

$$R' = z'$$

where

$$z' = \text{sgn} f'(\theta)$$

The variable sgn is used because of a sign ambiguity in $f'(\theta)$. We obtain $f'(\theta)$ from the follower motion diagram. However, the same diagram is used for both CW and CCW motions of the cam. In the displacement diagram, the rise section will have a positive value that corresponds to the CCW rotation of the follower relative to the cam. If the cam rotates CCW relative to the frame, the follower will rotate CW relative to the cam and the angular velocity of the follower relative to the cam will be negative. Therefore, the nominal sign for $f'(\theta)$ will be incorrect. The variable sgn accounts for the sign of ω_2 . When the cam rotates CW, $\text{sgn} = 1$, and when the cam rotates CCW, $\text{sgn} = -1$. With this modification, the value computed for b using [Equation 10.18](#) will be correct for both directions of rotation of the cam.

The pressure angle (ϕ) is the angle between the common normal line at the contact point and the velocity direction for the follower. This angle is indicated in [Figure 10.32](#). From the figure

$$\phi = \tan^{-1} \left(\frac{b - d}{R} \right) = \tan^{-1} \left[\frac{R' - d}{R} \right] \quad (10.19)$$

The coordinates of the point A on the cam surface are the components of the vector r and can be computed with the aid of [Figure 10.33](#). The direction of r is given by the angle ($\gamma + \theta$), and we need to determine expressions for both the magnitude and direction of r . From [Figure 10.33](#)

$$r = \tan^{-1} \left[\frac{d + r_0 \sin \phi}{R - r_0 \cos \phi} \right]$$

and

$$r = \sqrt{(d + r_0 \sin \phi)^2 + (R - r_0 \cos \phi)^2}$$

Therefore,

$$\begin{aligned} x_R &= r \cos(\gamma + \theta) \\ y_R &= r \sin(\gamma + \theta) \end{aligned} \quad (10.20)$$

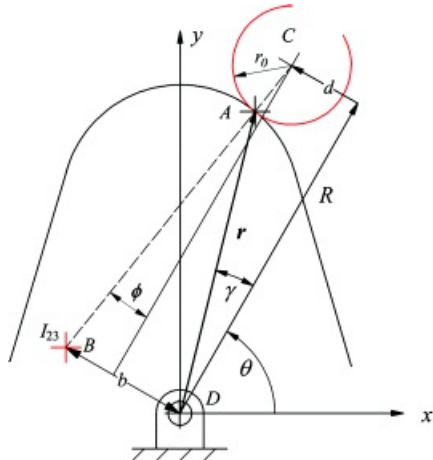


Figure 10.33 Geometry for computing the coordinates of point A.

Cam Radius of Curvature

The radius of curvature for a cam is important for several reasons. These include:

- If the cam is concave in a given area, the radius of curvature determines the minimum radius of the cutter that can be used to machine the cam and the minimum radius of the follower that can be used with the cam.
 - The contact stresses between the cam and the follower are a function of the cam radius of curvature. For a given cylindrical or roller follower, the contact stresses reduce as the cam radius of curvature approaches that of the follower.

If we have a parametric expression for the cam geometry in terms of $x(\theta)$ and $y(\theta)$, an expression for the radius of curvature, ρ , in the xy plane is given from calculus [10] as

$$\rho = \frac{\sqrt{[(dx/d\theta)^2 + (dy/d\theta)^2]}^3}{(dx/d\theta)(d^2y/d\theta^2) - (dy/d\theta)(d^2x/d\theta^2)} = \frac{\sqrt{[(x')^2 + (y')^2]^3}}{(x')(y'') - (y')(x'')} \quad (10.21)$$

To determine ρ , we need to differentiate the parametric expressions for $x(\theta)$ and $y(\theta)$ and substitute the derivatives into [Equation 10.21](#). [Equations 10.20](#) are in parametric form; however, the derivatives will be quite complex. Therefore, in this instance, it is preferable to determine the radius of curvature as a function of θ numerically.

If the points defining the cam profile are relatively close together, accurate results for the radius of curvature can be determined by fitting a series of circles through successive sets of three points along the cam profile. We will select the points such that the center point is at the location of interest, and the other two points are the adjacent ones on each side of the chosen point. Designate these positions as $p_{i-1} = (x_{i-1}, y_{i-1})$, $p_i = (x_i, y_i)$, and $p_{i+1} = (x_{i+1}, y_{i+1})$. Also, let the approximate location for the center of curvature be designated as $p_c = (x_c, y_c)$. We can now use [Figure 10.34](#) to derive an expression for finding the coordinates of p_c . If ρ is the radius of the circle through p_{i-1} , p_i and p_{i+1}

$$\begin{aligned} \rho^2 &= (x_{i+1} - x_c)^2 + (y_{i+1} - y_c)^2 \\ \rho^2 &= (x_i - x_c)^2 + (y_i - y_c)^2 \\ \rho^2 &= (x_{i-1} - x_c)^2 + (y_{i-1} - y_c)^2 \end{aligned}$$

Expanding

$$\begin{aligned} \rho^2 &= x_{i+1}^2 - 2x_{i+1}x_c + x_c^2 + y_{i+1}^2 - 2y_{i+1}y_c + y_c^2 \\ \rho^2 &= x_i^2 - 2x_i x_c + x_c^2 + y_i^2 - 2y_i y_c + y_c^2 \\ \rho^2 &= x_{i-1}^2 - 2x_{i-1}x_c + x_c^2 + y_{i-1}^2 - 2y_{i-1}y_c + y_c^2 \end{aligned}$$

Subtracting the second equation from the first and last equations and simplifying gives

$$\begin{aligned} (x_{i+1}^2 - x_i^2) + (y_{i+1}^2 - y_i^2) &= 2(x_{i+1} - x_i)x_c + 2(y_{i+1} - y_i)y_c \\ (x_{i-1}^2 - x_i^2) + (y_{i-1}^2 - y_i^2) &= 2(x_{i-1} - x_i)x_c + 2(y_{i-1} - y_i)y_c \end{aligned}$$

The result can be expressed in matrix form as

$$\begin{bmatrix} 2(x_{i+1} - x_i) & 2(y_{i+1} - y_i) \\ 2(x_{i-1} - x_i) & 2(y_{i-1} - y_i) \end{bmatrix} \begin{bmatrix} x_c \\ y_c \end{bmatrix} = \begin{bmatrix} (x_{i+1}^2 - x_i^2) + (y_{i+1}^2 - y_i^2) \\ (x_{i-1}^2 - x_i^2) + (y_{i-1}^2 - y_i^2) \end{bmatrix} \quad (10.22)$$

This linear matrix equation can be solved easily for (x_c, y_c) . The magnitude of the radius of curvature of the cam at the point of the curve is then given by

$$\rho = |r_{p_i/p_c}| = \sqrt{(x_i - x_c)^2 + (y_i - y_c)^2} \quad (10.23)$$

Once the center of curvature is known, the sign of the radius of curvature can be found by taking the cross-product of the vector $r_{p_i/p_{i-1}}$ with the vector r_{p_{i+1}/p_i} . The vectors are shown in [Figure 10.34](#), and the cross-product is given by

$$r_{p_i/p_{i-1}} \times r_{p_{i+1}/p_i} = [(x_i - x_{i-1})(y_{i+1} - y_i) - (x_{i+1} - x_i)(y_i - y_{i-1})] \hat{k} \quad (10.24)$$

A positive value for $r_{p_i/p_{i-1}} \times r_{p_{i+1}/p_i}$ will correspond to a positive radius of curvature and a negative value will correspond to a negative radius of curvature.

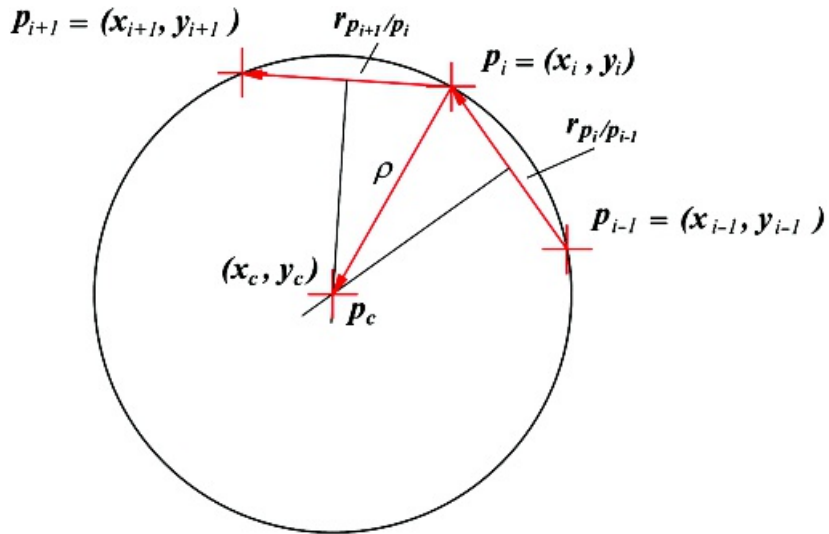


[Figure 10.34](#) Using three points to determine the magnitude and sign of ρ .

The procedure for determining the sign of ρ in [Figure 10.34](#) is based on a CW rotation of the cam. If the cam rotates in the CCW direction, the signs on the vectors will be reversed. This will result in the sign of ρ being reversed. Therefore, when the cam rotation is CCW, the computed value for the sign of ρ must be multiplied by -1 .

As indicated, the radius of curvature will have a magnitude and direction, and both are important. If the radius of curvature is positive, the cam is convex at (x_i, y_i) . If the radius of curvature is negative, the cam is concave. If the determinant of the coefficient matrix in [Equation 10.22](#) is zero, then (x_c, y_c) is at infinity, r_{p_i/p_c} is infinite, and an inflection point is indicated. If $(x_c, y_c) = (x_i, y_i)$, the radius of curvature is zero and a cusp is indicated.

Technically, a cusp can be concave or convex, and either situation is usually undesirable. The transition between concave and convex areas of the cam results in the radius of curvature becoming infinite. The physical interpretations of the various signs of ρ are shown in [Figure 10.35](#).

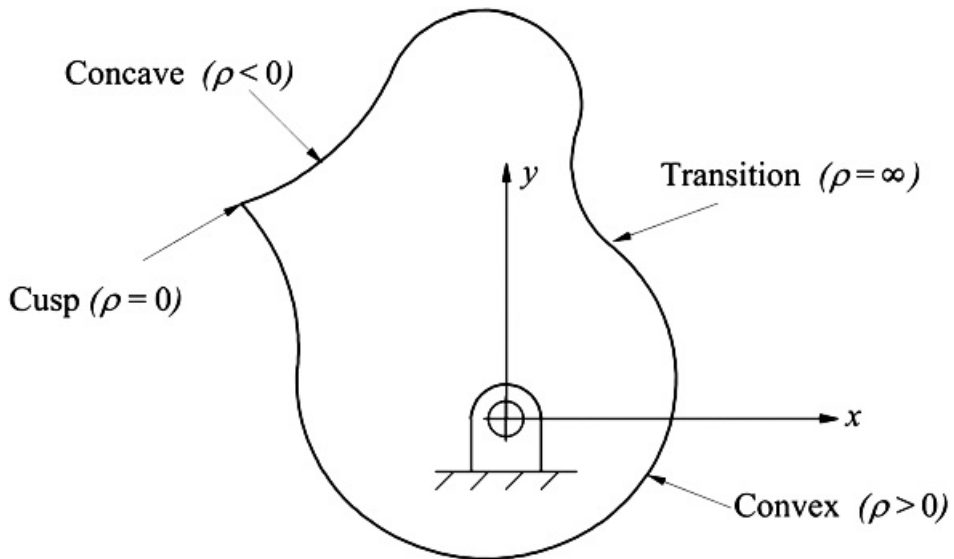


[Figure 10.35](#) Interpretation of the sign of ρ .

Given the displacement function for the follower, the cam contour can be determined as a function of θ using [Equations 10.20](#). Theoretically, any accuracy for the cam surface can be achieved by using smaller and smaller increments for θ . The equations for the cam and follower are summarized in [Table 10.8](#).

[Table 10.8](#) Summary of Equations for Determining the Cam Profile Coordinates, Pressure Angle, and Radius of Curvature for a Translating Cylindrical-Faced or Roller Follower. The follower displacement is given by $f(\theta)$, the

radius of the follower is r_0 , d is the offset, and the base circle radius is r_b .

Follower Displacement
$z = f(\theta)$
$R = \sqrt{(r_b + r_0)^2 - d^2} + z$
$\theta^* = z = \text{sgn } f'(\theta)$ (sgn = 1 for CW rotation of cam; sgn = -1 for CCW rotation of cam)
Pressure Angle
$\psi = \frac{dR(\theta)}{d\theta} = R'$
$\phi = \tan^{-1} \left(\frac{b-d}{R(\theta)} \right) = \tan^{-1} \left[\frac{R(\theta)-d}{R(\theta)} \right]$
Cam Coordinates
$y = \tan^{-1} \left(\frac{d+r_0 \sin \phi}{R-r_0 \cos \phi} \right)$
$r = \sqrt{(d+r_0 \sin \phi)^2 + (R-r_0 \cos \phi)^2}$
$x = x_c = r \cos(\phi + \theta)$
$y = y_c = r \sin(\phi + \theta)$
Radius of Curvature
Order cam profile points as $(x_i, y_i), i = 1, \dots, n$ where n is number of points around perimeter of cam profile
$\begin{bmatrix} 2(x_{i+1} - x_i) & 2(y_{i+1} - y_i) \\ 2(x_{i-1} - x_i) & 2(y_{i-1} - y_i) \end{bmatrix} \begin{Bmatrix} x_c \\ y_c \end{Bmatrix} = \begin{Bmatrix} (x_{i+1}^2 - x_i^2) + (y_{i+1}^2 - y_i^2) \\ (x_{i-1}^2 - x_i^2) + (y_{i-1}^2 - y_i^2) \end{Bmatrix}$
$\rho = r_{x_c/x_c} = \sqrt{(x_i - x_c)^2 + (y_i - y_c)^2}$
$r_{x_i/x_{i+1}} \times r_{x_{i+1}/x_i} = \text{sgn}[(x_i - x_{i-1})(y_{i+1} - y_i) - (x_{i+1} - x_i)(y_i - y_{i-1})] \rho$



Example 10.7

Cam Profile Coordinates for Translating Roller Follower

Determine the cam profile assuming that the follower starts with a dwell from 0° to 90° and rotates CW. The rise occurs with cycloidal motion during the cam rotation from 90° to 180° . The follower then dwells for 60° of cam rotation, and the return occurs with harmonic motion for the cam rotation from 240° to 360° . The amplitude of the follower translation is 2 cm, and the follower radius is 1 cm. The base circle radius is 4 cm, and the offset is 0.5 cm.

Solution

To solve the problem, we must identify the equations for the follower motion as a function of the cam rotation angle θ , and then select an increment for θ . When the follower equations are to be programmed, it is convenient to leave them in their basic form without simplifications. From Section 10.4, the equations (expressed in terms of radians) for each part of the motion are

$$0 \leq \theta \leq \pi/2; \quad f(\theta) = f' = f'' = f''' = 0$$

$$\begin{aligned} &\pi/2 \leq \theta \leq \pi; \quad \beta = \pi/2; \quad \dot{\theta} = \theta - \pi/2; \quad L = 2 \\ f(\theta) &= L \left(\frac{\theta}{\beta} - \frac{1}{2} \cos \frac{2\pi\theta}{\beta} \right); \quad f'(\theta) = \frac{L}{\beta} \left(1 - \cos \frac{2\pi\theta}{\beta} \right); \quad f''(\theta) = \frac{2\pi L}{\beta^2} \sin \frac{2\pi\theta}{\beta}; \quad f'''(\theta) = \frac{4\pi^2 L}{\beta^3} \cos \frac{2\pi\theta}{\beta} \end{aligned}$$

$$\pi \leq \theta \leq 4\pi/3; \quad f(\theta) = 2; \quad f' = f'' = f''' = 0$$

$$\begin{aligned} &4\pi/3 \leq \theta \leq 2\pi; \quad \beta = 2\pi/3; \quad \dot{\theta} = \theta - 4\pi/3; \quad L = 2 \\ f(\theta) &= \frac{L}{\beta} \left[1 + \cos \frac{\pi\theta}{\beta} \right]; \quad f'(\theta) = -\frac{L\pi}{\beta^2} \sin \frac{\pi\theta}{\beta}; \quad f''(\theta) = -\frac{L}{\beta} \left(\frac{\pi}{\beta} \right)^2 \cos \frac{\pi\theta}{\beta}; \quad f'''(\theta) = \frac{L}{\beta} \left(\frac{\pi}{\beta} \right)^3 \sin \frac{\pi\theta}{\beta} \end{aligned}$$

These equations correspond to $f(\theta)$ in [Table 10.8](#), and using the equations in [Table 10.8](#) we can compute the coordinates of the cam as accurately as we wish. For this problem, an angle increment of 0.1 in was used. The problem was solved using the cam program in *KinDAP* included with the supplementary material for this book. With this program, it is possible to evaluate quickly the cam profile for regions where the follower roller is too large. The cam, displacement diagram, radius of curvature, and pressure angle plots are shown in [Figure 10.36](#).

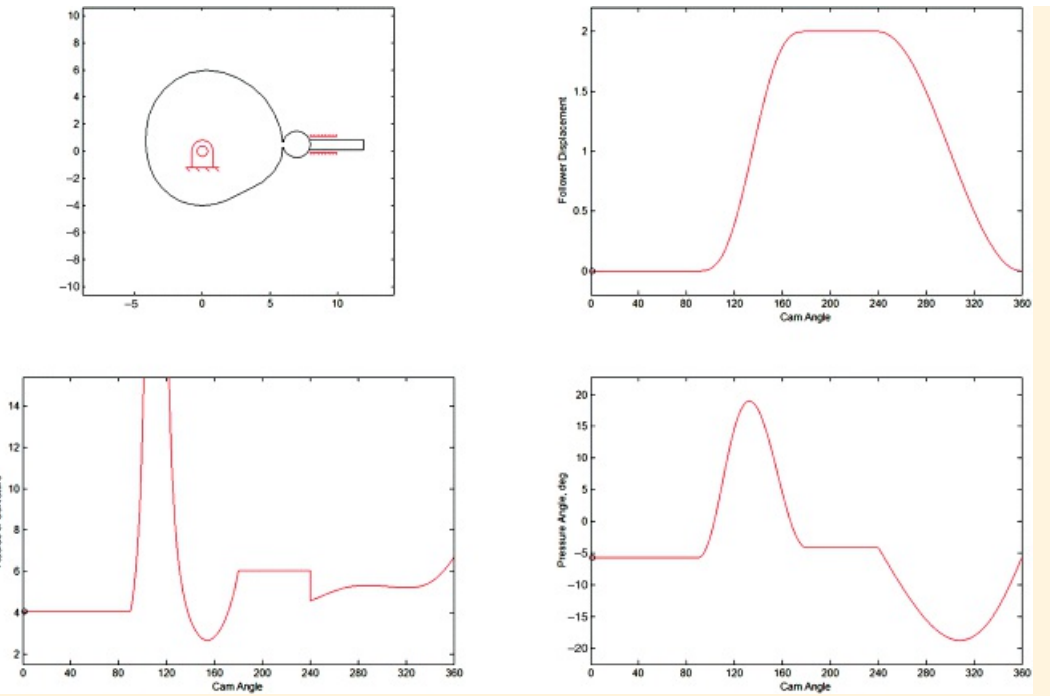


Figure 10.36 Cam profile, follower displacement, radius of curvature, and pressure angle for Example 10.7.

Analytical Determination of the Cam Profile for a Translating Flat-Faced Follower

Prior to determining the geometry of the cam, it is assumed that the basic motion specification for the follower is known in the form $z = f(\theta)$, where z is the displacement of the follower and θ is the cam rotation angle. Again $f(\theta)$ is typically given by one of the follower displacement functions discussed in Section 10.4. The base circle radius (r_b) is also assumed to be known.

Two positions of the follower relative to the cam are shown in [Figure 10.37](#). Again, it is assumed that the cam rotates CW such that the follower moves CCW relative to the cam. Link 1 is the frame, link 2 is the cam, and link 3 is the flat-faced translating follower. The three instant centers (I_{13} , I_{12} , I_{23}) for the three bodies are also located in the figure relative to the frame that is rotated by the angle θ relative to the cam in [Figure 10.37](#). The coordinate system attached to the cam is designated as (x, y) . The cam rotates about point C . Point A is the contact point on the cam, and point B is the instant center location I_{23} . Point B is a distance b from the center of rotation of the cam.

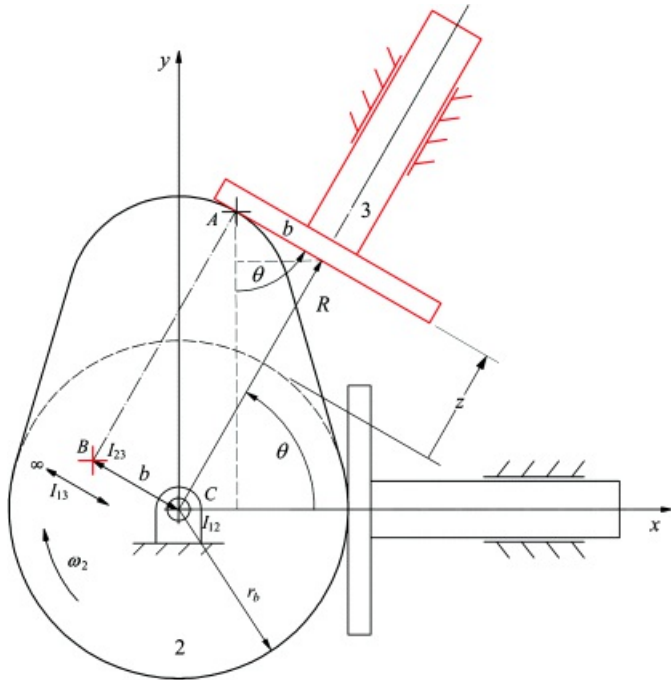


Figure 10.37 Geometry for translating flat-faced follower rotated relative to cam.

The variable z gives the displacement along the translation axis of the follower. The radial distance from C to the face of the follower is given by

$$R = r_b + z \quad (10.25)$$

By definition of the instant center, the velocity of B on link 2 is the same as the velocity of B on link 3. That is

$$v_{B_2} = v_{B_3}$$

For B on link 2

$$v_{B_2} = \omega_2 \dot{\theta}$$

where ω_2 is the angular velocity of the cam (link 2). Because the motion of link 3 is pure translation relative to the frame, all points in link 3 have the same linear velocity; therefore

$$v_{B_3} = \frac{dR}{dt} = \frac{dR}{d\theta} \frac{d\theta}{dt} = \omega_2 \frac{dR}{d\theta} = \omega_2 R'$$

Since the velocities for B_2 and B_3 are equal

$$\omega_2 \dot{\theta} = \omega_2 R'$$

or

$$\dot{\theta} = R'$$

And from [Equation 10.25](#)

$$z' = z' \quad (10.26)$$

where

$$z' = \operatorname{sgn} f'(\theta) \quad (10.27)$$

As discussed in the case for an oscillating cylindrical-faced follower in the previous section, $\operatorname{sgn} = +1$ for a CW rotation of the cam (represented in [Figure 10.37](#)), and $\operatorname{sgn} = -1$ for a CCW rotation of the cam.

Because b also gives the distance from the contact point to the radial center line of the follower stem, the maximum and minimum values for b for all rotation angles θ will give the limits for the length of the follower face. A positive value for b means that the contact point is above the centerline of the follower stem. A negative value means that the contact point is below the centerline. In general, b_{\max} and b_{\min} will not have the same magnitude. Therefore, we need to specify both the minimum distance above the center line of the follower stem and the minimum distance below the follower stem to ensure that the follower will always contact the cam correctly. If F_{\max} and F_{\min} are the distances above and below the centerline of the follower stem, then

$$\begin{aligned} F_{\max} &> |b_{\max}| \\ F_{\min} &> |b_{\min}| \end{aligned}$$

And the total face length, F , is given by

$$F = F_{\max} + F_{\min}$$

Once b is known, the coordinates of the point A on the cam surface can be determined directly in terms of b , R , and θ from the geometry in [Figure 10.37](#). Then

$$\begin{aligned} x &= R \cos \theta - b \sin \theta \\ y &= R \sin \theta + b \cos \theta \end{aligned}$$

and in terms of z

$$\begin{aligned} x &= [r_0 + z] \cos \theta - z' \sin \theta \\ y &= [r_0 + z] \sin \theta + z' \cos \theta \end{aligned} \quad (10.28)$$

In general, we want to use the smallest base circle that will satisfy the geometric constraints. Normally, the base circle is determined in part by the pressure angle; however, for a translating flat-faced follower with the follower face normal to the follower stem, the pressure angle is *always zero*. Therefore, we must select another criterion for determining the base circle radius. The minimum base circle radius will be the one that avoids cusps and concave areas in the cam profile.

For some displacement profiles, as the base circle radius reduces, areas of the cam can become concave, or convex areas can become sharper and sharper and eventually form a sharp point or cusp (see [Figure 10.35](#)). These conditions give the limiting radius for the base circle. A cusp is indicated when the radius of curvature of the cam in a given region becomes zero, and a concave region is indicated when the radius of curvature becomes negative.

When the base circle reduces, a cusp can form in a convex region with a very small radius of curvature that eventually becomes zero. When a concave region is formed, the originally convex region of the cam begins with a very large positive radius of curvature. As the base circle reduces, the radius of curvature eventually becomes infinite and then transforms to a very large negative radius of curvature. A flat-faced follower cannot become tangent to the cam in a concave region even if the region is almost flat. Fortunately, both conditions can be detected by computing the radius of curvature around the cam contour and ensuring that the radius of curvature is always positive.

To compute the radius of curvature of the cam, we can use [Equation 10.21](#) directly because the expression for the first and second derivatives for $x(\theta)$ and $y(\theta)$ are simple to obtain. The derivatives are given in the following

$$\frac{dx}{d\theta} = z' \cos \theta - [r_b + z] \sin \theta - z'' \sin \theta - z' \cos \theta = -[r_b + z + z''] \sin \theta$$

and

$$\frac{d^2x}{d\theta^2} = -[z' + z''] \sin \theta - [r_b + z + z''] \cos \theta$$

Also

$$\frac{dy}{d\theta} = z' \sin \theta + [r_b + z] \cos \theta + z'' \cos \theta - z' \sin \theta = [r_b + z + z''] \cos \theta$$

and

$$\frac{d^2y}{d\theta^2} = [z' + z''] \cos \theta - [r_b + z + z''] \sin \theta$$

Substituting these expressions into [Equation 10.21](#) and simplifying gives

$$\rho = \frac{\sqrt{[(x')^2 + (y')^2]^2}}{(x')(y'') - (y')(x'')} = [r_b + z + z'']$$

The radius of curvature can be written directly in terms of $f(\theta)$ as

$$\rho = [r_b + f(\theta) + f''(\theta)]$$

To avoid cusps and concave regions

$$\rho > 0$$

at all locations around the cam contour. Therefore

$$[r_b + f(\theta) + f''(\theta)] > 0 \quad (10.30)$$

for all θ . Both $f(\theta)$ and $f''(\theta)$ will be determined by the follower displacement schedule. Therefore, only r_b can be externally controlled in [Equation 10.30](#); that is,

$$r_b > -[f(\theta) + f''(\theta)]$$

If $[f(\theta) + f''(\theta)]$ is positive for all values of θ , then any positive or zero value of the base circle radius will be acceptable from a concavity and cusp standpoint.

The equations necessary to determine points on the cam profile and to determine the length of the follower face are summarized in [Table 10.9](#). These can easily be programmed to determine the (x, y) coordinates of points on the cam profile relative to the cam coordinate system, and a MATLAB program in *KinDAP* for doing this is included in the supplementary material for this book. Given the (x, y) coordinates, the cam can be machined on a CNC milling machine. The accuracy of the profile will be determined in part by the angle increment chosen for the cam rotation angle θ .

[Table 10.9](#) Summary of Equations for Determining the Cam Profile Coordinates, Minimum Face Length, and Minimum Base Circle Radius for a Translating Flat-Faced Follower. The follower displacement is given by $f(\theta)$, and the base circle radius is r_b .

Follower Displacement
$z = f(\theta)$
$R = r_b + z$
$R' = z' = \text{sgn} f'(\theta)$ (sgn = 1 for CW rotation of cam; sgn = -1 for CCW rotation of cam)
Cam Coordinates
$x = [r_b + z] \cos \theta - z' \sin \theta$
$y = [r_b + z] \sin \theta + z' \cos \theta$
Minimum Face Length
$b = R'$
$R > b_{\min} + b_{\max} $
Radius of Curvature
$\rho = [r_b + f(\theta) - f''(\theta)]$



Example 10.8

Cam Profile Coordinates for Translating Flat-Faced Follower

Determine the cam profile for the follower motion given in Example 10.7. First find the minimum base circle radius to avoid cusps, and use that base circle to design the cam.

Solution

To solve the problem, we must determine the derivatives of the functions for the follower displacement. Because derivatives are involved, the angles in the displacement functions will be converted to radians. For the different intervals, the functions and derivatives are summarized in the following

$$0 \leq \theta \leq \pi/2; \quad f(\theta) = f' = f'' = f''' = 0$$

$$\begin{aligned} & \pi/2 \leq \theta \leq \pi; \quad \beta = \pi/2; \quad \dot{\theta} = \theta - \pi/2; \quad L = 2 \\ f(\theta) &= L \left(\frac{\theta}{\beta} - \frac{1}{2\pi} \cos \frac{2\pi\theta}{\beta} \right); \quad f'(\theta) = \frac{L}{\beta} \left(1 - \cos \frac{2\pi\theta}{\beta} \right); \quad f''(\theta) = \frac{2\pi L}{\beta^2} \sin \frac{2\pi\theta}{\beta}; \quad f'''(\theta) = \frac{4\pi^2 L}{\beta^3} \cos \frac{2\pi\theta}{\beta} \end{aligned}$$

$$\pi \leq \theta \leq 4\pi/3; \quad f(\theta) = 2; \quad f' = f'' = f''' = 0$$

$$\begin{aligned} & 4\pi/3 \leq \theta \leq 2\pi; \quad \beta = 2\pi/3; \quad \dot{\theta} = \theta - 4\pi/3; \quad L = 2 \\ f(\theta) &= \frac{L}{2} \left[1 + \cos \frac{\pi\theta}{\beta} \right]; \quad f'(\theta) = -\frac{L\pi}{2\beta} \sin \frac{\pi\theta}{\beta}; \quad f''(\theta) = -\frac{L}{2} \left(\frac{\pi}{\beta} \right)^2 \cos \frac{\pi\theta}{\beta}; \quad f'''(\theta) = \frac{L}{2} \left(\frac{\pi}{\beta} \right)^3 \sin \frac{\pi\theta}{\beta} \end{aligned}$$

Given the equations for the follower displacement, we now need only to increment θ and to evaluate the expressions in [Table 10.9](#) to determine the minimum base circle radius and limiting values for the face length. We can then determine the cam coordinates. The values are computed for 10° increments of θ in [Table 10.10](#). From that table, it is clear that the base circle radius must be at least 3.147 cm and the follower face needs to be at least 2.47 cm above the centerline and 1.5 cm below it. Note that a negative value for b implies a distance below the stem centerline, and a positive value implies a distance above the centerline.

[Table 10.10](#) Values for $f(\theta)$ and Its Derivatives for Follower Displacement Specified for Example 10.8

θ	$f(\theta)$ (cm)	$f'(\theta)$ (cm)	$f''(\theta)$ (cm)	$r_{b\min}$ (cm)	b (cm)
0°	0.000	0.000	0.000	0.000	0.000
-dwell-					
90°	0.000	0.000	0.000	0.000	0.000
100°	0.018	0.298	3.274	-3.291	0.298
110°	0.131	1.052	5.016	-5.147	1.052
120°	0.391	1.910	4.411	-4.802	1.910
130°	0.780	2.470	1.742	-2.522	2.470
140°	1.220	2.470	-1.742	0.522	2.470

150°	1.609	1.910	-4.411	2.802	1.910
160°	1.869	1.052	-5.016	3.147	1.052
170°	1.982	0.298	-3.274	1.291	0.298
180°	2.000	0.000	0.000	-2.000	0.000
		-dwell-			
240°	2.000	-0.000	-2.250	0.250	-0.000
250°	1.966	-0.388	-2.173	0.207	-0.388
260°	1.866	-0.750	-1.949	0.083	-0.750
270°	1.707	-1.061	-1.591	-0.116	-1.061
280°	1.500	-1.299	-1.125	-0.375	-1.299
290°	1.259	-1.449	-0.582	-0.676	-1.449
300°	1.000	-1.500	0.000	-1.000	-1.500
310°	0.741	-1.449	0.582	-1.324	-1.449
320°	0.500	-1.299	1.125	-1.625	-1.299
330°	0.293	-1.061	1.591	-1.884	-1.061
340°	0.134	-0.750	1.949	-2.083	-0.750
350°	0.034	-0.388	2.173	-2.207	-0.388

The cam will be designed with a base circle radius of 3.2 cm, and the follower face will be 2.6 cm above the stem centerline and 1.5 cm below it. The results obtained from the MATLAB program in *KinDAP* included in the supplementary material with this book are shown in [Figure 10.38](#). To illustrate the effect of choosing a base circle radius less than the critical value, the program was rerun with the base circle radius of 1 cm. The results are shown in [Figure 10.39](#). The result is clearly a cam that cannot be manufactured.

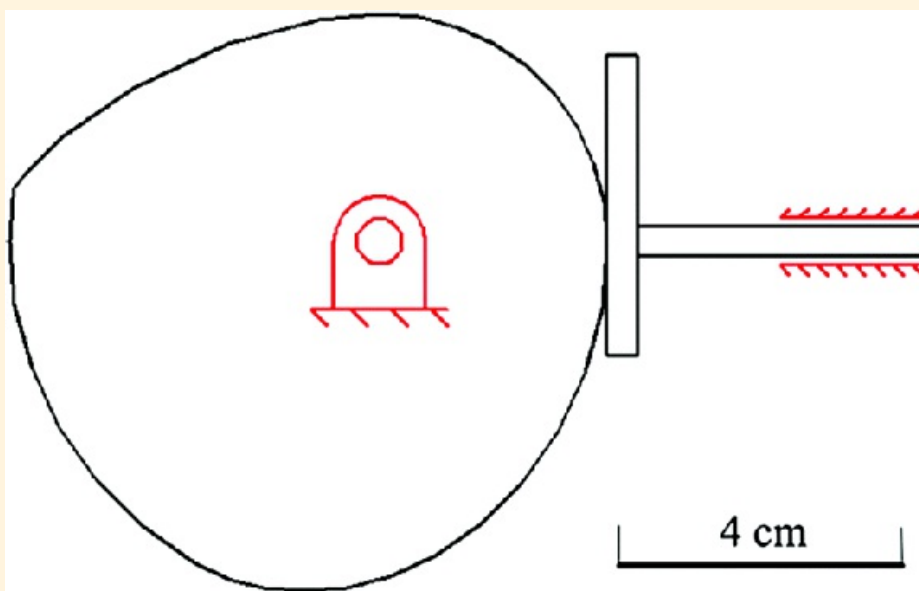


[Figure 10.38](#) Cam designed for Example 10.8 with a base circle radius of 3.2 cm.

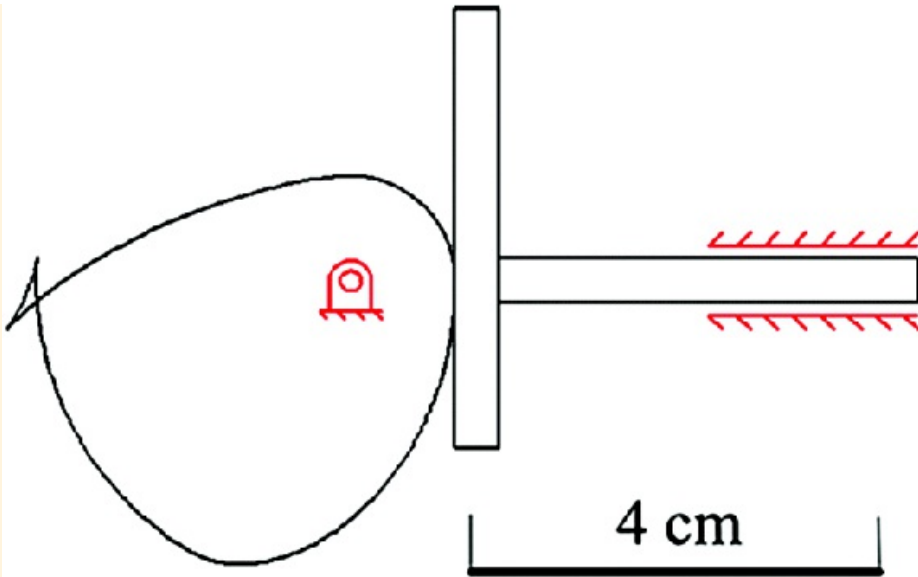


Figure 10.39 Results for Example 10.8 when a base circle radius of 1 cm is used. This cam cannot be manufactured. The smallest value for the base circle radius to avoid cusps is 3.147.

Analytical Determination of the Cam Profile for an Oscillating Cylindrical Follower

As in the case of the translating roller follower, the equations for an oscillating cylindrical follower can be derived with the use of instant centers. Again, we must invert the mechanism so that the follower appears to rotate about the cam. To begin the procedure, we will assume that the cam base circle radius is r_b , the radius of the cylindrical follower is r_3 , the pivot distance is r_1 , and the distance from the follower pivot to the center of the cylindrical contour is r_2 . Values for these variables must be selected before the cam contour design is begun. The follower rotates about the pivot at E with an angular displacement of ϕ where $\phi = f(\theta)$ is given by the displacement function for the follower.

In the procedure, the follower is assumed to begin in its lowest position when the follower contacts the base circle of the cam as shown in [Figure 10.40](#). For this position, we need to determine ϕ_0 which is the initial angle for the follower. The motion of the follower will be measured relative to ϕ_0 . From [Figure 10.40](#), ϕ_0 can be computed using the law of cosines. That is

$$\phi_0 = \cos^{-1} \left[\frac{r_1^2 + r_3^2 - (r_b - r_2)^2}{2r_1r_3} \right] \quad (10.31)$$

To start the procedure, locate the three instant centers (I_{12} , I_{13} , I_{23}) for the system in the displaced position corresponding to θ . The locations of the three instant centers are shown in [Figure 10.40](#). The instant center location, designated by both I_{23} and D in the figure, is at a distance b from the cam pivot at A . By the definition of the instant center, location D corresponds to two coincident points, one fixed to link 2 (D_2) and the second fixed to link 3 (D_3), and the two coincident points have the same velocity relative to the frame. The magnitude of the velocity of D_2 is given by

$$v_{D_2} = \omega_2 b$$

and the direction is perpendicular to the line through I_{12} and I_{13} . Also

$$\omega_2 = \frac{d\theta}{dt}$$

The velocity of D_3 is given by

$$v_{D_3} = \omega_3(r_1 + b)$$

where ω_3 is the angular velocity of link 3. The angular velocity of link 3 can be written in terms of the rotation angle as

$$\omega_3 = \frac{d(\phi - \phi_0)}{dt} = \frac{d\phi}{dt}$$

From the calculus chain rule

$$\frac{d\phi}{dt} = \frac{d\phi}{d\theta} \frac{d\theta}{dt} = \frac{d\phi}{d\theta} \omega_2 = \dot{\psi} \omega_2 \quad (10.32)$$

Therefore

$$v_{D_3} = \dot{\psi} \omega_2 (r_1 + b)$$

Equating the velocities of D_2 and D_3 gives

$$\omega_2 b = \dot{\psi} \omega_2 (r_1 + b)$$

or

$$\dot{\psi} = \frac{\omega_2 r_1}{1 - \psi} \quad (10.33)$$

where

$$\dot{\psi} = \text{sgn} f'(\theta) \quad (10.34)$$

As discussed in the case for a translating cylindrical-faced follower, $\text{sgn} = +1$ for a CW rotation of the cam (represented in [Figure 10.40](#)), and $\text{sgn} = -1$ for a CCW rotation of the cam.

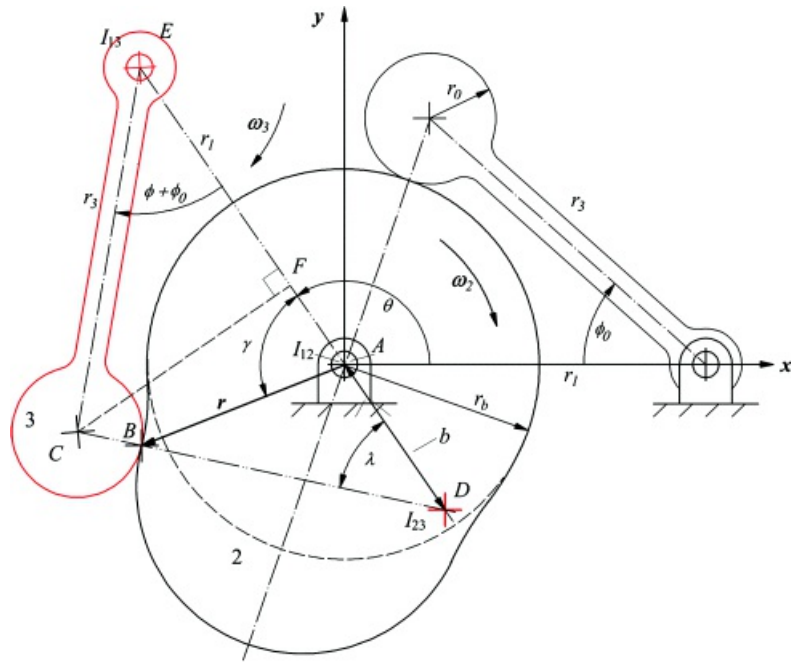


[Figure 10.40](#) Oscillating cylindrical-faced follower in initial and arbitrary positions.

The coordinates of points on the cam profile can be computed with the aid of the right triangle CFE and polygon $CFAB$ in [Figure 10.40](#). The angle λ is given by

$$\lambda = \tan^{-1} \left[\frac{r_3 \sin(\phi + \phi_0)}{r_1 + b - r_3 \cos(\phi + \phi_0)} \right] \quad (10.35)$$

The coordinates of points on the cam profile are given by the coordinates of the vector r in [Figure 10.40](#) if we know the magnitude and direction of r . From [Figure 10.40](#), the magnitude of r is given by

$$r = \sqrt{[r_1 - r_3 \cos(\phi + \phi_0) - r_0 \cos \lambda]^2 + [r_3 \sin(\phi + \phi_0) - r_0 \sin \lambda]^2} \quad (10.36)$$

The direction of r is given by $\gamma + \theta$ where

$$\gamma = \tan^{-1} \left[\frac{r_3 \sin(\phi + \phi_0) - r_0 \sin \lambda}{r_1 - r_3 \cos(\phi + \phi_0) - r_0 \cos \lambda} \right] \quad (10.37)$$

The coordinates of the point on the cam corresponding to θ are

$$\begin{aligned} x_B &= r \cos(\gamma + \theta) \\ y_B &= r \sin(\gamma + \theta) \end{aligned} \quad (10.38)$$

The pressure angle is indicated by ϵ in [Figure 10.41](#). It is the angle between the velocity of point B_3 and the normal line to the surface at the point of contact. The direction for the velocity of B_3 is perpendicular to the line BE . The normal to the surface is the line BD from the contact point to the instant center I_{23} . From the geometry in [Figure 10.41](#), an expression for the pressure angle is

$$\varepsilon = \phi + \phi_0 - \psi + \lambda - \frac{\zeta}{2} \quad (10.39)$$

We can compute ψ by using the law of cosines. We can compute ζ based on knowing two of the internal angles for triangle CDE . Knowing ζ , we can compute BE using the law of cosines. Finally, we can then use BE and the law of cosines again to obtain ψ . The expressions are

$$\zeta = \pi - (\phi + \phi_0) - A$$

$$BE = \sqrt{r_2^2 + r_3^2 - 2r_2r_3 \cos \zeta} \quad (10.40)$$

and

$$\psi = \cos^{-1} \left[\frac{r_3^2 + BE^2 - r_0^2}{2r_3BE} \right] \quad (10.41)$$

To compute the radius of curvature of the cam as a function of θ , we could again use [Equation 10.21](#) with the parametric equations given by [Equation 10.38](#). However, because of the complexity of the derivatives, it is again simpler to determine the radius of curvature numerically. The same procedure with [Equations 10.22–10.24](#) given for the oscillating roller follower can be used to compute the radius of curvature once a series of points around the cam contour is determined.

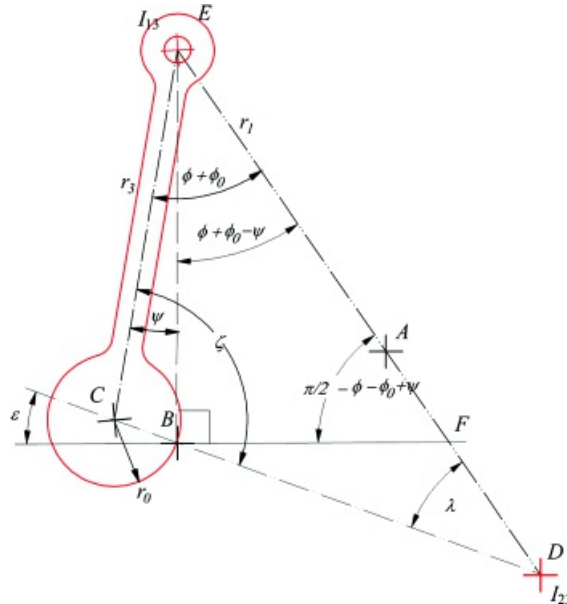


[Figure 10.41](#) Geometry for computing pressure angle.

The equations necessary to determine points on the cam profile are summarized in [Table 10.11](#). The equations for the radius of curvature for the cam are taken from [Table 10.8](#). The equations in [Table 10.11](#) can easily be programmed to determine the (x, y) coordinates of points on the cam profile relative to the cam coordinate system, and a MATLAB program in *KinDAP* for doing this is included with the supplementary material for this book. Given the (x, y) coordinates of points around the perimeter of the cam, the cam can be machined on a CNC milling machine. The accuracy of the profile will be determined in part by the size of the angle increment chosen for the cam rotation angle θ .

Table 10.11 Summary of Equations for Determining the Cam Profile Coordinates and Pressure Angle for an Oscillating Cylindrical-Faced or Roller Follower. The follower oscillation ϕ is given by $f(\theta)$, the radius of the follower is r_0 , the base circle radius is r_b , the distance between the cam and follower pivots is r_1 , and the length of the follower is r_3 .

Follower Displacement
$\text{Follower angle} = \phi + \dot{\phi}_3$
$\phi = f(\theta)$
$\psi' = \text{sgn } f'(\theta)$ (sgn = 1 for CW rotation of cam; sgn = -1 for CCW rotation of cam)
Cam Coordinates
$\dot{\phi}_3 = \cos^{-1} \left[\frac{r_1^2 + r_3^2 - (r_b + r_0)^2}{2r_1r_3} \right]$
$\lambda = \frac{\dot{\phi}_3}{\dot{\theta}}$
$\lambda = \tan^{-1} \left[\frac{r_3 \sin(\phi + \phi_0)}{r_1 + b - r_3 \cos(\phi + \phi_0)} \right]$
$r = \sqrt{[r_1 - r_3 \cos(\phi + \phi_0) - r_0 \cos \lambda]^2 + [r_3 \sin(\phi + \phi_0) - r_0 \sin \lambda]^2}$
$\gamma = \tan^{-1} \left[\frac{r_3 \sin(\phi + \phi_0) - r_0 \sin \lambda}{r_1 - r_3 \cos(\phi + \phi_0) - r_0 \cos \lambda} \right]$
$x = x_S = r \cos(\gamma - \phi)$
$y = y_S = r \sin(\gamma - \phi)$
Pressure Angle
$\zeta = \alpha - (\phi + \phi_0) - \lambda$
$SE = \sqrt{r_3^2 + r_0^2 - 2r_3r_0 \cos \zeta}$
$\psi = \cos^{-1} \left[\frac{\beta + SE^2 - \gamma^2}{2r_3r_0} \right]$
$\epsilon = \zeta - \phi - \dot{\phi}_3 + \psi - \lambda$
Radius of Curvature
$\frac{2(x_{i+1} - x_i) - 2(y_{i+1} - y_i)}{2(x_{i-1} - x_i) - 2(y_{i-1} - y_i)} \begin{Bmatrix} x_c \\ y_c \end{Bmatrix} = \begin{Bmatrix} (x_{i+1}^2 - x_i^2) - (y_{i+1}^2 - y_i^2) \\ (x_{i-1}^2 - x_i^2) - (y_{i-1}^2 - y_i^2) \end{Bmatrix}$
$r = r_{x_i/x_c} = \sqrt{(x_i - x_c)^2 + (y_i - y_c)^2}$
$r_{x_i/x_{i-1}} \times r_{x_{i+1}/x_i} = \text{sgn}[(x_i - x_{i-1})(y_{i+1} - y_i) - (x_{i+1} - x_i)(y_i - y_{i-1})] \cdot \epsilon$



Example 10.9

Cam Profile Coordinates for a Roller Follower That Oscillates

Determine the cam profile assuming that the follower dwells while the cam rotates *c*ounterclockwise from 0° to 90°. The rise occurs with 3-4-5 polynomial motion during the cam rotation from 90° to 180°. The follower then dwells for 90° of cam rotation, and the return occurs with harmonic motion for the cam rotation from 270° to 360°. The amplitude of the follower oscillation is 30°, and the follower radius is 1 in. The base circle radius is 2 in and the distance between pivots is 6 in. The length of the follower is to be determined such that the pressure angle starts out at zero.

Solution

To solve the problem, we must identify the equations for the follower motion as a function of the cam rotation angle θ and then select an increment for θ . Because the cam is rotating CCW, the variable sgn in [Equation 10.34](#) will be -1. For a given angular displacement, the rise will be the same if the cam is to be designed for CW or CCW rotation. Therefore, although we will use negative increments for the cam angle, we will use the magnitude of the cam angle to compute $f(\theta)$. In the equations, we will let β be the magnitude of θ . Then from Section 10.4, the equations (expressed in terms of radians) for each part of the motion become

$$0 \leq \theta \leq \pi/2$$

$$\dot{\theta} = 0$$

$$\begin{aligned} & \text{for } 0 \leq \theta \leq \pi/2, \quad (\beta = \pi/2; \quad L = \pi/6; \quad \hat{\theta} = \bar{\theta} - \pi/2) \\ & \phi = 1.0L \left(\frac{\theta}{\beta} \right)^3 - 1.5L \left(\frac{\theta}{\beta} \right)^4 + 6L \left(\frac{\theta}{\beta} \right)^5; \quad \phi' = \frac{30L}{\beta} \left[\left(\frac{\theta}{\beta} \right)^2 - 2 \left(\frac{\theta}{\beta} \right)^3 + \left(\frac{\theta}{\beta} \right)^4 \right]; \\ & \phi'' = \frac{60L}{\beta^2} \left[\left(\frac{\theta}{\beta} \right) - 3 \left(\frac{\theta}{\beta} \right)^2 + 2 \left(\frac{\theta}{\beta} \right)^3 \right]; \quad \phi''' = \frac{60L}{\beta^3} \left[1 - 6 \left(\frac{\theta}{\beta} \right) + 6 \left(\frac{\theta}{\beta} \right)^2 \right] \end{aligned}$$

$$\pi/2 \leq \bar{\theta} \leq 3\pi/2$$

$$\dot{\theta} = \left(\frac{\pi}{6} \right);$$

$$\begin{aligned} & \text{for } \pi/2 \leq \bar{\theta} \leq 2\pi, \quad (\beta = \pi/2; \quad L = \pi/6; \quad \hat{\theta} = \bar{\theta} - 3\pi/2) \\ & \phi = \frac{L}{2} \left[1 + \cos \frac{\pi \hat{\theta}}{\beta} \right]; \quad \phi' = -\frac{L\pi}{2\beta} \sin \frac{\pi \hat{\theta}}{\beta}; \quad \phi'' = -\frac{L}{2} \left(\frac{\pi}{\beta} \right)^2 \cos \frac{\pi \hat{\theta}}{\beta}; \quad \phi''' = \frac{L}{2} \left(\frac{\pi}{\beta} \right)^3 \sin \frac{\pi \hat{\theta}}{\beta} \end{aligned}$$

To determine the length, r_3 , of the follower that will give zero pressure angle in the initial position, refer to [Figure 10.40](#). From that figure, the angle between the $(r_0 + r_b)$ and r_3 must be 90° for the pressure angle to be zero during the initial dwell. Therefore

$$r_3 = \sqrt{r_1^2 + (r_2 + r_0)^2} = \sqrt{6^2 + (2+1)^2} = 5.196 \text{ in}$$

The equations for ϕ and r_3 can be used to determine ϕ_0 in [Table 10.11](#), and using the equations in [Table 10.11](#) we can compute the coordinates of the cam as accurately as we wish by using a small increment for the cam rotation angle θ .

For the calculations, the angle θ is incremented in the negative direction (the follower rotates CW relative to the cam). Therefore, the points corresponding to the cam contour will be generated and labeled initially in the CW direction. However, the equations in [Table 10.11](#) were derived assuming that the points are ordered in the CCW direction. Therefore, after all of the points are generated, they must be reordered in the CCW direction. After the points are reordered in this way, the cam profile can be plotted.

For plotting purposes, we have used the MATLAB cam program in *KinDAP* included in the supplementary material with this book with an angle increment of -1° , which is adequate for visual purposes. If we want to machine the cam with high accuracy, a finer increment for θ would be used. The cam, displacement diagram, radius of curvature, and pressure angle plots are shown in [Figure 10.42](#).

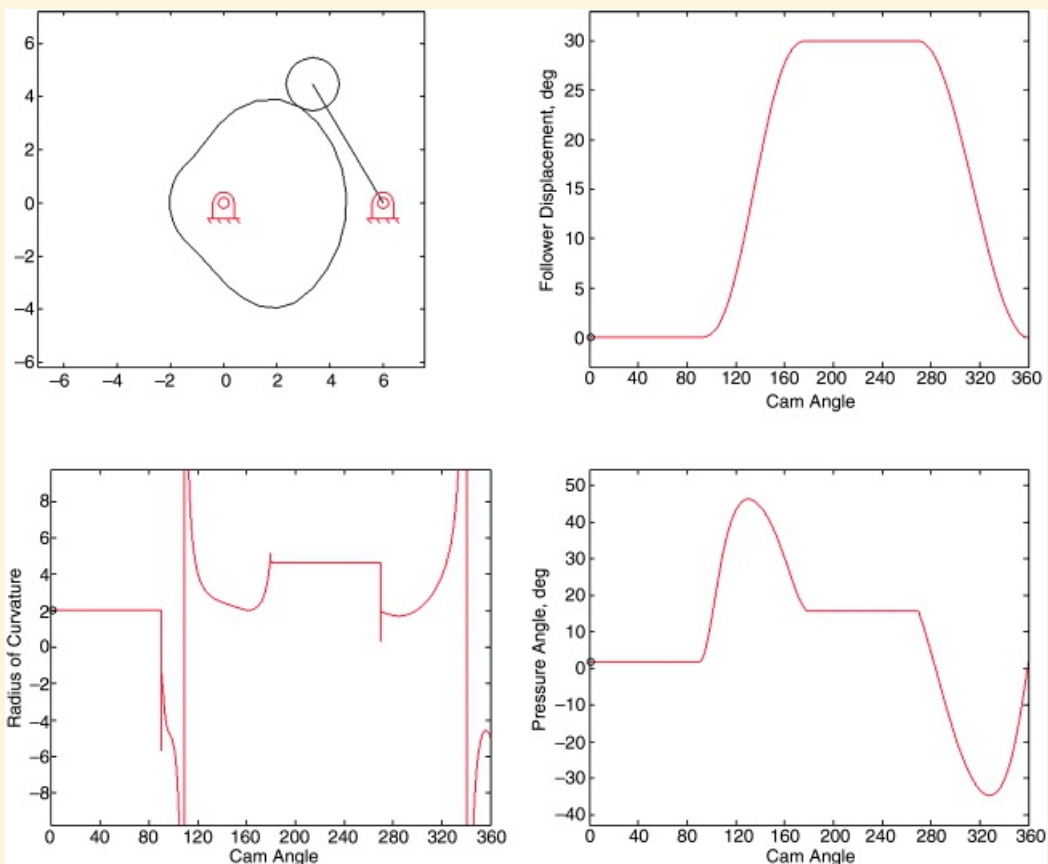


[Figure 10.42](#) Cam profile, follower displacement, radius of curvature, and pressure angle for Example 10.9.

Analytical Determination of the Cam Profile for a Flat-Faced Follower That Oscillates

The cam-follower system is shown in [Figure 10.43](#), and the locations shown in that figure will be used to describe the design of the cam for an oscillating flat-faced follower. Point *A* is the location of the axis of rotation of the cam, *B* is the axis of rotation of the follower, and d is the follower offset. Point *D* is the location of the tangent point between the face of the follower and the cam surface, and *C* is located at the intersection of the follower face and a line from *B* perpendicular to the follower face.

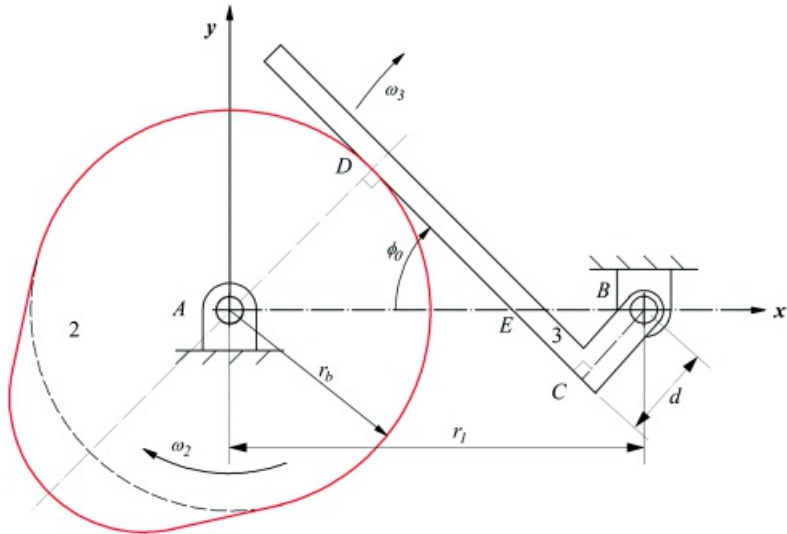


Figure 10.43 Geometry for oscillating flat-faced follower in initial position.

The development of the equations for an oscillating flat-faced follower is similar to that used for the oscillating roller follower. As in the other cases, we must invert the mechanism so that the follower appears to rotate about the cam. To begin the procedure, we will assume that the cam base radius r_b , the pivot distance r_1 , and the follower displacement angle ϕ are known. Again, ϕ will be equal to $f(\theta)$ from the follower displacement equations.

In the procedure, we will find the instant center I_{23} and use it to locate the coordinates of the contact points on the cam contour. The first step is to determine the reference angle ϕ_0 that gives the orientation of the follower in the initial position. From the geometry in [Figure 10.43](#), $AD = r_3$ and from the similar triangles ADE and BCE

$$\frac{AE}{r_3} = \frac{r_1 - r_b}{d}$$

or

$$AE = \frac{r_1 r_b}{r_b + d}$$

Then

$$DE = \sqrt{AE^2 - r_3^2}$$

and

$$\phi_0 = \tan^{-1} \frac{r_3}{DE} \quad (10.45)$$

For each position of the cam given by θ , we will know $\phi = f(\theta)$ from the follower displacement equations. The orientation of the follower face relative to the cam is then given by the angle $\phi + \phi_0$.

To locate the follower relative to the cam as the cam rotates, we can invert the motion relative to the cam. For simplicity, we will again assume that the cam rotates CW relative to the frame, which means that the frame rotates CCW relative to the cam. A typical position is shown in [Figure 10.44](#). To determine the coordinates of the cam

profile, we need to be able to compute the components of the vector r . For this, we need the magnitude of r and the angle γ , and the procedure for determining these is similar to the process used for the oscillating cylindrical-faced follower.

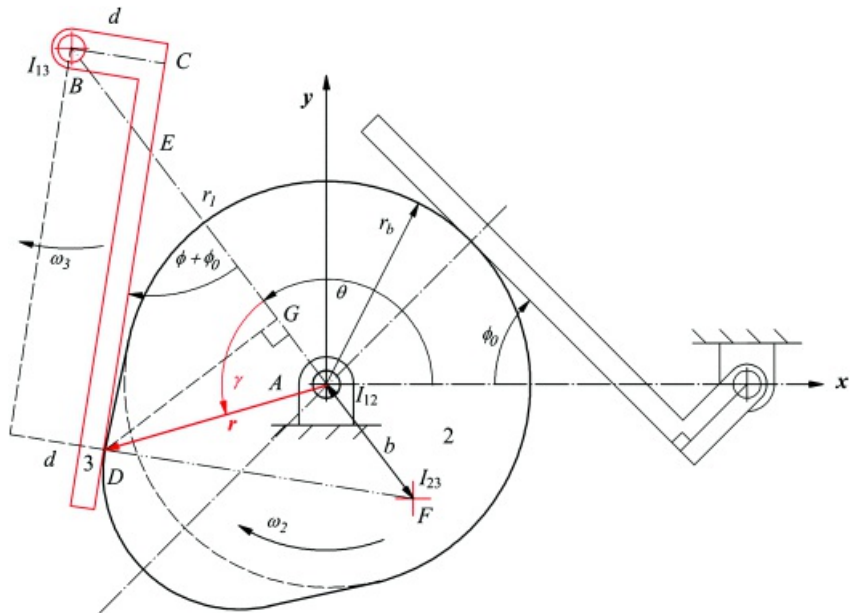


Figure 10.44 Motion of oscillating flat-faced follower relative to cam.

Again, begin the procedure by locating the three instant centers (I_{12} , I_{13} , I_{23}) for the system in the displaced position corresponding to θ . In particular, I_{23} will be on a line through the contact point and perpendicular to both surfaces at the point of contact. It will also be on a line through I_{12} and I_{13} . The location of I_{23} is shown in [Figure 10.44](#). The instant center location, designated by both I_{23} and F in the figure, is at a distance b from the cam pivot at A . By the definition of the instant center, location F corresponds to two coincident points, one fixed to link 2 (F_2) and the second fixed to link 3 (F_3), and the two coincident points have the same velocity relative to the frame. The magnitude of the velocity of F_2 is given by

$$v_{F_2} = \omega_2 b \quad (10.46)$$

where the direction is perpendicular to the line through I_{12} and I_{13} , and ω_2 is the angular velocity of link 2. Also

$$v_{F_2} = \frac{d\phi}{dt} \quad (10.47)$$

The velocity of F_3 is given by

$$v_{F_3} = \omega_3(r_1 + b) \quad (10.48)$$

where ω_3 is the angular velocity of link 3. The angular velocity of link 3 can be written in terms of the rotation angle as

$$\omega_3 = \frac{d(\phi - \phi_0)}{dt} = \frac{d\phi}{dt}$$

From the calculus chain rule

$$\frac{d\phi}{dt} = \frac{d\phi}{d\theta} \frac{d\theta}{dt} = \frac{d\phi}{d\theta} \omega_2 = \dot{\phi}' \omega_2$$

Therefore

$$v_{F_3} = \dot{\phi}' \omega_2 (r_1 + b)$$

Equating the velocities of F_2 and F_3 gives

$$\omega_2 b = \dot{\phi}' \omega_2 (r_1 + b)$$

or

$$b = \frac{\dot{\phi}' r_1}{1 - \dot{\phi}'} \quad (10.49)$$

where

$$\dot{\phi}' = \operatorname{sgn} f'(\phi) \quad (10.50)$$

As discussed in the case for an oscillating cylindrical-faced follower, $\operatorname{sgn} = +1$ for a CW rotation of the cam (represented in [Figure 10.44](#)), and $\operatorname{sgn} = -1$ for a CCW rotation of the cam.

We can find r using the triangle ADG in [Figure 10.44](#). From that figure, the distance CD is given by

$$CD = (r_1 + b) \cos(\phi + \phi_0)$$

and the distance AG is then given by

$$AG = r_1 - d \sin(\phi + \phi_0) = CD \cos(\phi + \phi_0)$$

The distance DG is given by

$$DG = CD \sin(\phi + \phi_0) - d \cos(\phi + \phi_0)$$

Then

$$r = \sqrt{AG^2 + DG^2} \quad (10.51)$$

and

$$\gamma = \tan^{-1} \left[\frac{DG}{AG} \right]$$

The coordinates of the point on the cam corresponding to θ are

$$\begin{aligned} x_D &= r \cos(\gamma + \phi) \\ y_D &= r \sin(\gamma + \phi) \end{aligned} \quad (10.52)$$

To compute the pressure angle at any given position, we must find the angle between a vector in the direction of the follower travel and a vector that is normal to the follower face at each location as shown in [Figure 10.45](#). The direction corresponding to the velocity of point D_3 is perpendicular to the line BD . The normal direction is perpendicular to the face CD , and this normal line is also the line from D to the instant center I_{23} at F . Therefore, the angle ψ between the lines DC and BD will be the pressure angle. This angle is given by

$$\psi = \tan^{-1} \left[\frac{d}{CD} \right] \quad (10.53)$$

The simplicity of the equation for computing the pressure angle is another benefit of using the instant center approach to computing the cam profile.

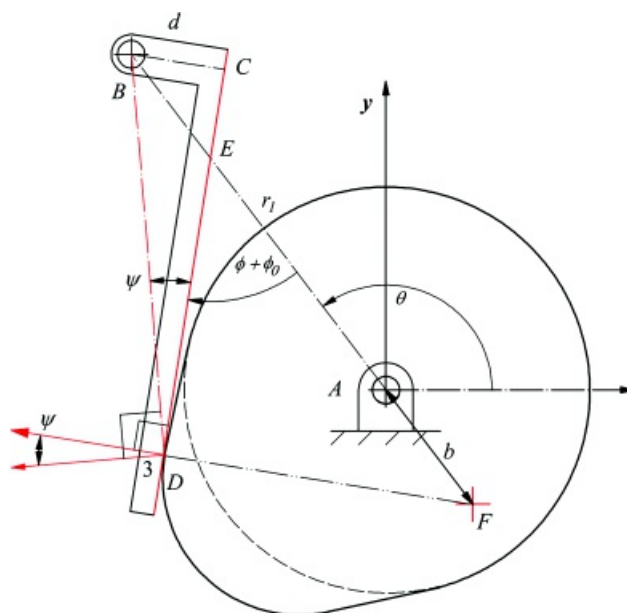


[Figure 10.45](#) Geometry for finding pressure angle.

To compute the radius of curvature of the cam as a function of θ , we could again use [Equation 10.21](#) with the parametric equations given by [Equation 10.52](#). However, because of the complexity of the derivatives, it is again simpler to determine the radius of curvature numerically. The same procedure given for the oscillating roller follower can be used to compute the radius of curvature once a series of points around the cam contour is determined.

The equations necessary to determine points on the cam profile are summarized in [Table 10.12](#). The equations for the radius of curvature are taken from [Table 10.8](#). The equations in [Table 10.12](#) can be easily programmed to determine the coordinates of points on the cam profile, and a MATLAB program in *KinDAP* for doing so is included with the supplementary material for this book. Given the coordinates of a set of sequential points on the profile, the cam can be machined on a CNC milling machine. The accuracy of the profile will be determined in

part by the size of the increment chosen for the cam rotation angle θ .

Table 10.12 Summary of Equations for Determining the Cam Profile Coordinates for an Oscillating Flat-Faced Follower. The follower oscillation ϕ is given by $f(\theta)$, the follower offset is d , the base circle radius is r_b , and the distance between the cam and follower pivots is r_1 .

Follower Displacement
Follower angle = $\phi + \delta_3$
$\delta = f(\theta)$
$\delta' = \text{sgn} f'(\theta)$ (sgn = 1 for CW rotation of cam; sgn = -1 for CCW rotation of cam)
Cam Coordinates
$AE = \frac{r_b r_1}{r_b + d}$ $DE = \sqrt{AE^2 - r_b^2}$
$\delta_3 = \tan^{-1} \frac{r_b}{DE}$
$\psi = \frac{\delta' \theta}{r_1}$
$CD = (r_1 + d) \cos(\psi + \delta_3)$ $AC = r_1 + d \sin(\psi + \delta_3) \cdot CD \cos(\psi + \delta_3)$ $DC = CD \sin(\psi + \delta_3) \cdot d \cos(\psi + \delta_3)$
$r = \sqrt{AC^2 + DC^2}$
$\gamma = \tan^{-1} \left \frac{DC}{AC} \right $
$x = x_D = r \cos(\gamma + \delta)$ $y = y_D = r \sin(\gamma + \delta)$
Pressure Angle
$\psi = \tan^{-1} \left \frac{d}{r_D} \right $
Radius of Curvature
$\left[\begin{array}{l} 2(x_{i+1} - x_i) - 2(y_{i+1} - y_i) \\ 2(x_{i-1} - x_i) - 2(y_{i-1} - y_i) \end{array} \right] \left\{ \begin{array}{l} x_c \\ y_c \end{array} \right\} = \left\{ \begin{array}{l} (x_{i+1}^2 - x_i^2) + (y_{i+1}^2 - y_i^2) \\ (x_{i-1}^2 - x_i^2) + (y_{i-1}^2 - y_i^2) \end{array} \right\}$
$\rho = r_{p_i/p_c} = \sqrt{(x_i - x_c)^2 + (y_i - y_c)^2}$
$r_{p_i/p_{i-1}} \times r_{p_{i+1}/p_i} = \text{sgn} [(x_i - x_{i-1})(y_{i+1} - y_i) - (x_{i+1} - x_i)(y_i - y_{i-1})]$



Example 10.10

Cam Profile Coordinates for Oscillating Flat-Faced Follower

Assume that the follower starts from a dwell from 0° to 45° and rotates CW. The rise occurs with harmonic motion during the cam rotation from 45° to 180° . The follower then dwells for 90° of cam rotation, and the return occurs with harmonic motion for the cam rotation from 270° to 360° . The amplitude of the follower oscillation is 20° , and the follower offset is 0.5 in. The base circle radius is 2 in, and the distance between pivots is 6 in.

Solution

To solve the problem, we must specify the length of the follower face, identify the equations for the follower motion as a function of the cam rotation angle θ , and then select an increment for θ . The length of the follower face is somewhat arbitrary as long as it is large enough to maintain contact with the cam. The minimum value can be calculated by computing the distance CD for each position of the follower relative to the cam. However, in this example, we will select the length to be 9 in, which is large enough to ensure that the follower will maintain contact with the cam.

The second part of the displacement schedule is similar to that used in Example 10.9, and the equation for the rise portion can be obtained from Section 10.7. The resulting equations (expressed in terms of radians) are

$$0 \leq \theta \leq \pi/4$$

$$\phi = 0$$

$$\pi/4 \leq \theta \leq \pi, \quad (\beta = \pi/2; \quad L = \pi/2; \quad \bar{\theta} = \theta - \pi/4)$$

$$\phi = \frac{L}{2} \left[1 - \cos \frac{\pi \bar{\theta}}{\beta} \right]; \quad \phi' = \frac{L\pi}{2\beta} \sin \frac{\pi \bar{\theta}}{\beta}; \quad \phi'' = \frac{L}{2} \left(\frac{\pi}{\beta} \right)^2 \cos \frac{\pi \bar{\theta}}{\beta}; \quad \phi''' = -\frac{L}{2} \left(\frac{\pi}{\beta} \right)^2 \sin \frac{\pi \bar{\theta}}{\beta}$$

$$\pi \leq \theta \leq 3\pi/2$$

$$\phi = \left(\begin{array}{c} \theta \\ 0 \end{array} \right);$$

$$3\pi/2 \leq \theta \leq 2\pi, \quad (\beta = \pi/2; \quad L = \pi/2; \quad \theta = \theta - 3\pi/2)$$

$$\phi = \frac{L}{2} \left[1 + \cos \frac{\pi \bar{\theta}}{\beta} \right]; \quad \phi' = -\frac{L\pi}{2\beta} \sin \frac{\pi \bar{\theta}}{\beta}; \quad \phi'' = -\frac{L}{2} \left(\frac{\pi}{\beta} \right)^2 \cos \frac{\pi \bar{\theta}}{\beta}; \quad \phi''' = \frac{L}{2} \left(\frac{\pi}{\beta} \right)^2 \sin \frac{\pi \bar{\theta}}{\beta}$$

Given the equations for the follower displacement, we now need only increment θ and evaluate the expressions in [Table 10.12](#) to determine the cam coordinates and pressure angle. The values are computed for 1° increments of θ in [Table 10.12](#). The results obtained from the MATLAB program in *KinDAP* included in the supplementary material with this book are shown in [Figure 10.46](#).

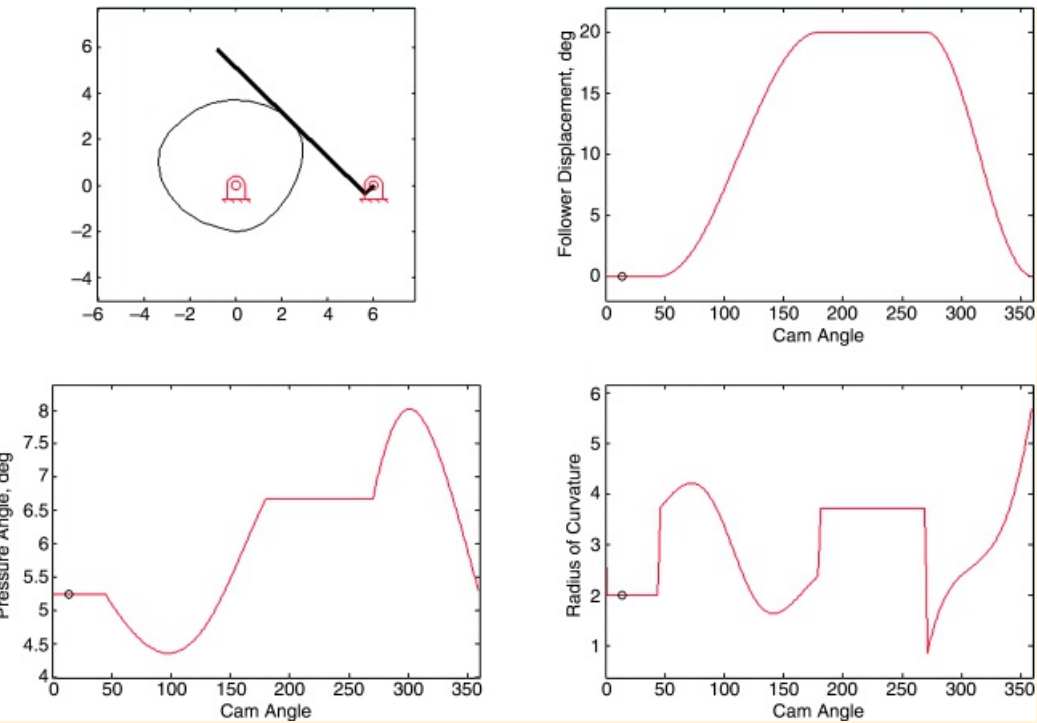


Figure 10.46 Cam profile, follower displacement, pressure angle, and radius of curvature for Example 10.10.

It is much more difficult to design a cam for an oscillating flat-faced follower than for the other types of followers. For example, if the amplitude of oscillation in Example 10.10 is changed to 30° , a cam will be developed that has a discontinuity and therefore cannot be manufactured. Changing the base circle radius may not always improve the situation, and the extent to which the base circle can be changed is limited by the distance between pivots. The problem can be improved by reducing the amplitude of oscillation, by changing the function chosen for the rise/return, or by increasing the range chosen for the rise/return. However, in some cases, it may be necessary to choose another type of follower.



References

1. Rothbart, Harold A. (2004). *Cam Design Handbook*. New York, NY: McGraw-Hill.
2. Interactive Cam Design. (2014). http://www.softintegration.com/chhtml/toolkit/mechanism/cam/cgi_osc.html.
3. Norton Associates Engineering. (2014). <http://www.designofmachinery.com/>.
4. Chen, Fan Y. (1982). *Mechanics and Design of Cam Mechanisms*. New York, NY: Pergamon Press.
5. Dhande, S. G. (1984). “Kinematic Analysis of Constant-Breadth Cam-Follower Mechanisms.” *Journal of Mechanisms, Transmission, and Automation in Design*, Vol. 106, pp. 214–221.
6. Zhonge, Y., and Smith, M. R. (2002). “Synthesis of Constant-Breadth Cam Mechanisms.” *Mechanism and Machine Theory*, Vol. 37, pp. 941–953.
7. Anonymous. (2014). “Curves of Constant Width.” http://en.wikipedia.org/wiki/Curve_of_constant_width.
8. Hanson, R. S., and Churchill, F. T. (1962). “Theory of Envelopes Provides New Cam Design Equations.” *Prod. Eng.*, Vol. 20, August, pp. 45–55.
9. Waldron, K. J., and Kinzel, G. L. (2003). *Kinematics, Dynamics, and Design of Machinery*, 2nd Ed. Hoboken, NJ: John Wiley & Sons, pp. 391–446.
10. Davidson, J. K. (1978). “Calculating Cam Profiles Quickly.” *Mach. Des.*, 7, pp. 151–155, December.
11. Wu, L. I., Liu, C. H., and Chen, T. W. (2009). “Disk Cam Mechanisms with Concave-Faced Followers.” *Proceedings of the Institution of Mechanical Engineers, Part C: Journal of Mechanical Engineering Science*, Vol. 223, pp. 1443–1448.



Problems

Follower Displacement Schedules

10.1 A cam that is designed for cycloidal motion drives a flat-faced follower. During the rise, the follower displaces 1 in for 180° of cam rotation. If the cam angular velocity is constant at 100 rpm, determine the displacement, velocity, and acceleration of the follower at a cam angle of 60° .

10.2 A constant-velocity cam is designed for harmonic motion. If the flat-faced follower displaces 2 in for 180° of cam rotation and the cam angular velocity is 100 rpm, determine the displacement, velocity, and acceleration when the cam angle is 45° .

10.3 A cam drives a radial, knife-edged follower through a 1.5 in rise in 180° of cycloidal motion. Give the displacement at 60° and 100° . If this cam is rotating at 200 rpm, what are the velocity (ds/dt) and the acceleration (d^2s/dt^2) at $\theta = 60^\circ$?

10.4 Draw the displacement schedule for a follower that rises through a total displacement of 1.5 in with constant acceleration for 1/4th revolution, constant velocity for 1/8th revolution, and constant deceleration for 1/4th revolution of the cam. The cam then dwells for 1/8th revolution, and returns with harmonic motion in 1/4th revolution of the cam.

10.5 Draw the displacement schedule for a follower that rises through a total displacement of 20 mm with constant acceleration for 1/8th revolution, constant velocity for 1/4th revolution, and constant deceleration for 1/8th revolution of the cam. The cam then dwells for 1/4th revolution, and returns with harmonic motion in 1/4th revolution of the cam.

10.6 Draw the displacement schedule for a follower that rises through a total displacement of 30 mm with constant acceleration for 90° of rotation and constant deceleration for 45° of cam rotation. The follower returns 15 mm with harmonic motion in 90° of cam rotation and dwells for 45° of cam rotation. It then returns the remaining 15 mm with harmonic motion during the remaining 90° of cam rotation.

10.7 Draw the displacement schedule for a follower that rises through a total displacement of 3 in with cycloidal motion in 120° of cam rotation. The follower then dwells for 90° and returns to zero with harmonic motion in 90° of cam rotation. The follower then dwells for 60° before repeating the cycle.

10.8 As shown in [Figure P10.8](#), a cam returns from a full lift of 1.2 in during its initial 60° rotation. The first 0.4 in of the return is half-cycloidal. This is followed by a half-harmonic return. Determine β_1 and β_2 so that the motion has continuous first and second derivatives. Draw a freehand sketch of y' , y'' , and y''' indicating any possible mismatch in the third derivative.

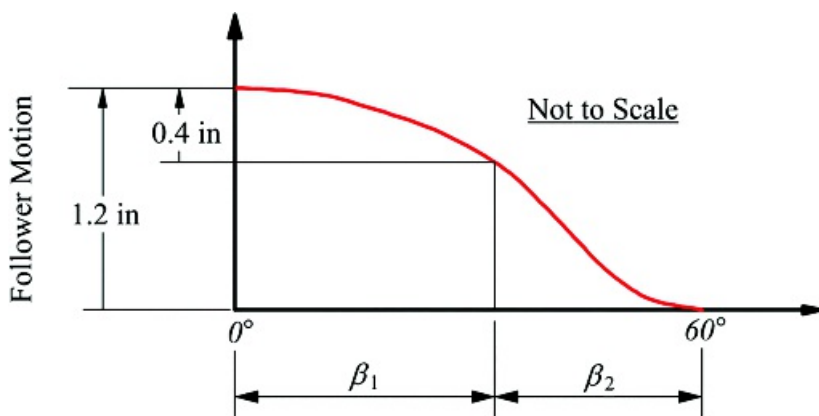


[Figure P10.8](#) Cam follower displacement diagram for Problem 10.8.

10.9 Assume that s is the cam-follower displacement and θ is the cam rotation, as shown in [Figure P10.9](#). The rise is 1.0 cm after 1.0 radian of rotation, and the rise begins and ends at a dwell. The displacement equation

for the follower during the rise period is

$$s = h \sum_{i=0}^n C_i \left(\frac{\theta}{\beta}\right)^i$$

If the position, velocity, and acceleration are continuous at $\theta = 0$, and the position and velocity are continuous at $\theta = 1.0$ rad, determine the value of n required in the equation, and find the coefficients C_i if $\beta = 2$ rad/s. Note: Use the minimum possible number of terms.

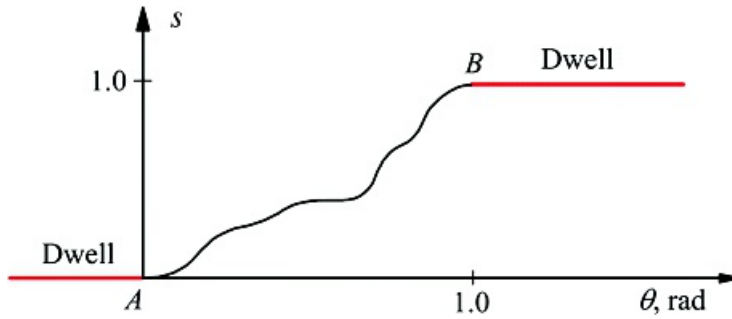


[Figure P10.9](#) Cam follower displacement diagram for Problem 10.9.

[10.10](#) Solve Problem 10.9 if $\theta = 0.8$ rad at the end of the rise, and $\dot{\theta} = 200$ rad/s.

[10.11](#) For the cam displacement schedule given in [Figure P10.11](#), h is the rise, β is the angle through which the rise takes place, and s is the displacement at any given angle θ . The displacement equation for the follower during the rise period is

$$s = h \sum_{i=0}^n a_i \left(\frac{\theta}{\beta}\right)^i$$

Determine the required expressions for $a_0 \dots a_5$ such that the displacement, velocity, and acceleration functions are continuous at the end points of the rise portion.

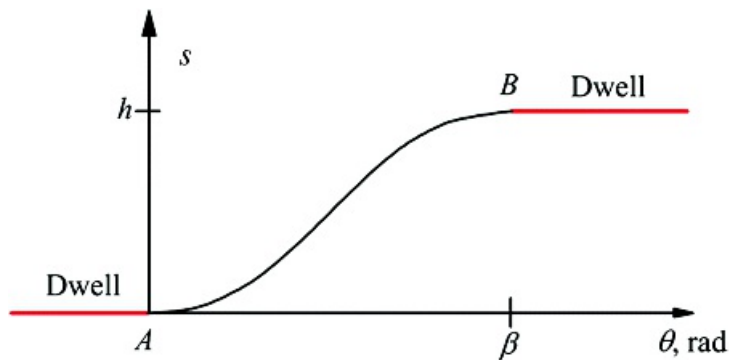


[Figure P10.11](#) Cam follower displacement diagram for Problem 10.11.

[10.12](#) Solve Problem 10.11 if $h = 20$ mm and $\beta = 120^\circ$.

[10.13](#) Solve Problem 10.11 if $h = 2$ in and $\beta = 90^\circ$.

[10.14](#) Assume that s is the cam-follower displacement and θ is the cam rotation, as shown in [Figure P10.14](#). The rise is h after β degrees of rotation, and the rise begins at a dwell and ends with a constant velocity segment. The displacement equation for the follower during the rise period is

$$s = h \sum_{i=0}^n C_i \left(\frac{\theta}{\beta}\right)^i$$

If the position, velocity, and acceleration are continuous at $\theta = 0$ and the position and velocity are continuous at $\theta = \beta$, determine the number n required in the equation, and find the coefficients C_i that will satisfy the requirements if $s = h = 1.0$.

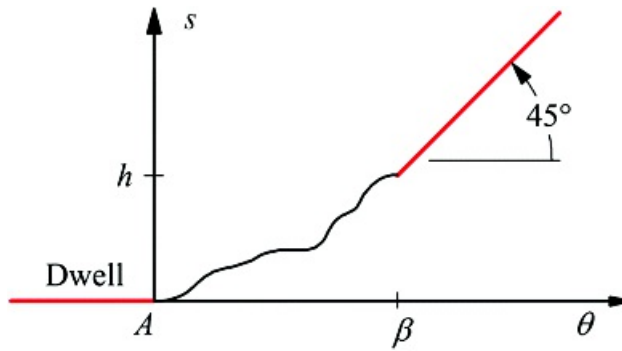


[Figure P10.14](#) Cam follower displacement diagram for Problem 10.14.

10.15 A follower moves with harmonic motion a distance of 20 mm in 45° of cam rotation. The follower then moves 20 mm more with cycloidal motion to complete its rise. The follower then dwells and returns 25 mm with cycloidal motion and then moves the remaining 15 mm with harmonic motion in 45° . Find the intervals of cam rotation for the cycloidal motions and dwell by matching velocities and accelerations, then determine the equations for the displacement (S) as a function of θ for the entire motion cycle.

Graphical Cam Design

10.16 Construct the part of the profile of a disk cam that follows the displacement diagram shown in [Figure P10.16](#). The cam has a 5 cm diameter prime circle and is rotating CCW. The follower is a knife-edged, radial, translating follower. Use 10° increments for the construction.

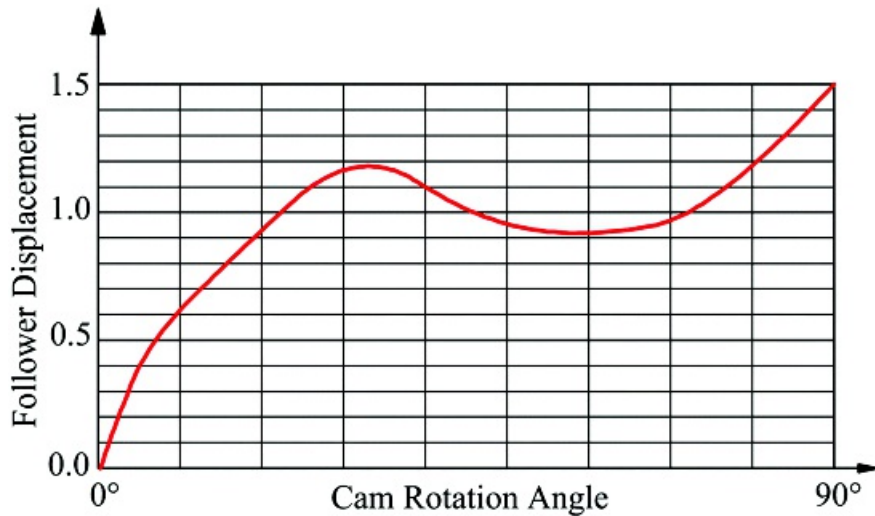


[Figure P10.16](#) Cam follower displacement diagram for Problem 10.16.

10.17 Construct the profile of a disk cam that follows the displacement diagram shown in [Figure P10.17](#). The follower is a radial roller and has a diameter of 10 mm. The base circle diameter of the cam is to be 40 mm and the cam rotates CW.

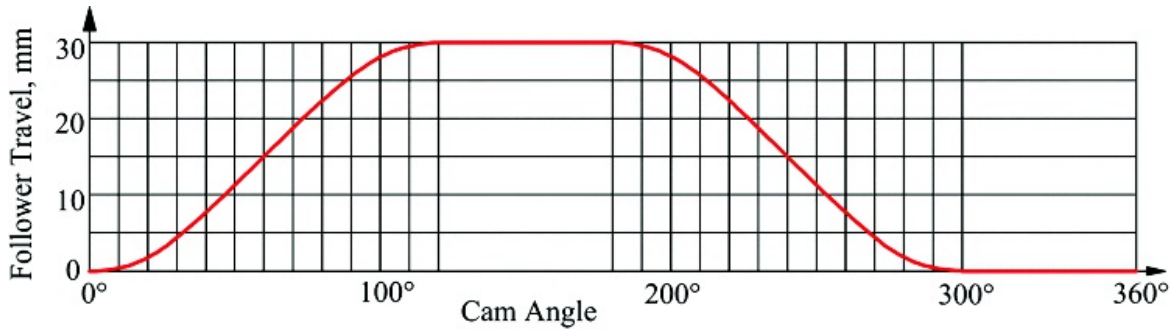


[Figure P10.17](#) Cam follower displacement diagram for Problem 10.17.

10.18 Accurately sketch one half of the cam profile (stations 0–6) for the cam follower, base circle, and displacement diagram given in [Figure P10.18](#). The base circle diameter is 1.2 in.

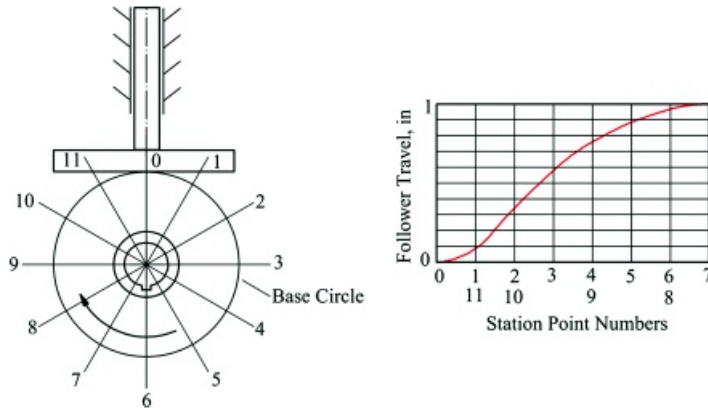


[Figure P10.18](#) Cam follower displacement diagram for Problem 10.18.

10.19 Lay out a cam profile using a harmonic follower displacement (both rise and return). Assume that the cam is to dwell at zero lift for the first 100° of the motion cycle and to dwell at a 1 in lift for cam angles from 160° to 210°. The cam is to have a translating, radial, roller follower with a 1 in roller diameter, and the base circle radius is to be 1.5 in. The cam will rotate CW. Lay out the cam profile using 20° plotting intervals.

10.20 Lay out a cam profile using a cycloidal follower displacement (both rise and return) if the cam is to dwell at zero lift for the first 80° of the motion cycle and to dwell at 2 in lift for cam angles from 120° to 190°. The cam is to have a translating, radial, roller follower with a roller diameter of 0.8 in. The cam will rotate CCW, and the base circle diameter is 2 in. Lay out the cam profile using 20° plotting intervals.

10.21 Lay out a cam profile assuming that an oscillating roller follower starts from a dwell for 0° to 140° of cam rotation, and the cam rotates CW. The rise occurs with parabolic motion during the cam rotation from 140° to 220°. The follower then dwells for 40° of cam rotation, and the return occurs with parabolic motion for the cam rotation from 260° to 360°. The amplitude of the follower rotation is 35°, and the follower radius is 1 in. The base circle radius is 2 in, and the distance between the cam axis and follower rotation axis is 4 in. Lay out the cam profile using 20° plotting intervals such that the pressure angle is 0 when the follower is in the bottom dwell position.

10.22 Lay out the rise portion of the cam profile if a flat-faced, translating, radial follower's motion is uniform. The total rise is 1.5 in, and the rise occurs over 100° of cam rotation. The follower dwells for 90° of cam rotation prior to the beginning of the rise, and dwells for 80° of cam rotation at the end of the rise. The cam will rotate CCW, and the base circle radius is 3 in.

Analytical Cam Design

10.23 In [Figure P10.23](#), the disk cam is used to position the radial flat-faced follower in a computing mechanism. The cam profile is to be designed to give a follower displacement S for a CCW cam rotation θ according to the function $S = k\theta^2$ starting from dwell. For 60° of cam rotation from the starting position, the

lift of the follower is 1.0 cm. By analytical methods, determine the distances R and L when the cam has been turned 45° from the starting position. Also calculate whether cusps in the cam profile would occur in the total rotation of 60° .

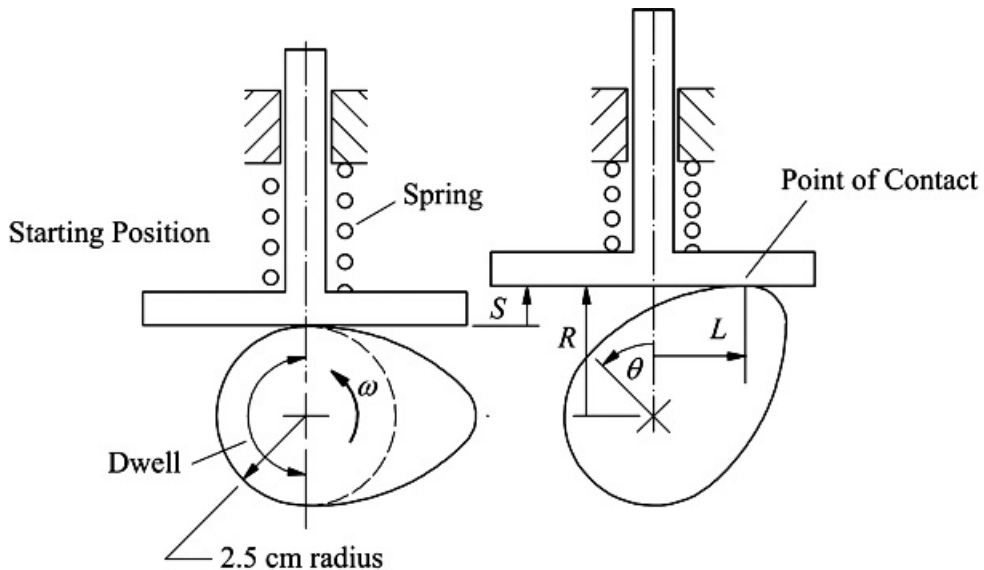


[Figure P10.23](#) Cam and follower geometry for Problem 10.23.

10.24 Determine the cam profile assuming that the translating cylindrical-faced follower starts from a dwell from 0° to 80° , and the cam rotates CW. The rise occurs with cycloidal motion during the cam rotation from 80° to 180° . The follower then dwells for 60° of cam rotation, and the return occurs with harmonic motion for the cam rotation from 240° to 360° . The amplitude of the follower translation is 3 cm, and the follower radius is 0.75 cm. The base circle radius is 5 cm, and the offset is 0.5 cm.

10.25 Solve Problem 10.24 if the amplitude of the follower translation is 4 cm, and the follower radius is 1 cm. The base circle radius is 5 cm, and the offset is 1 cm.

10.26 Solve Problem 10.24 if the cam rotates CCW.

10.27 Determine the cam profile assuming that the translating flat-faced follower starts from a dwell from 0° to 80° and rotates CW. The rise occurs with parabolic motion during the cam rotation from 80° to 180° . The follower then dwells for 60° of cam rotation, and the return occurs with harmonic motion for the cam rotation from 240° to 360° . The amplitude of the follower translation is 3 cm. First find the minimum base circle radius based on avoiding cusps, and use that base circle to design the cam.

10.28 Solve Problem 10.27 if the cam rotates CCW.

10.29 Determine the cam profile assuming that an oscillating cylindrical-faced follower dwells while the cam rotates CCW from 0° to 100° . The rise occurs with 3-4-5 polynomial motion during the cam rotation from 100° to 190° . The follower then dwells for 80° of cam rotation, and the return occurs with harmonic motion for the cam rotation from 270° to 360° . The amplitude of the follower oscillation is 25° , and the follower radius is 0.75 in. The base circle radius is 2 in, and the distance between pivots is 6 in. The length of the follower is to be determined such that the pressure angle starts out at zero.

10.30 Solve Problem 10.29 if the cam rotates CW.

10.31 Design a cam and oscillating roller follower assuming that the follower starts from a dwell for 0° to 80° of cam rotation and the cam rotates CW. The rise occurs with cycloidal motion during the cam rotation from 80° to 200° . The follower then dwells for 40° of cam rotation, and the return occurs with cycloidal motion for the cam rotation from 240° to 360° . The amplitude of the follower rotation is 45° . Determine the cam base circle radius, distance between cam and follower pivots, the length of the follower, and the radius of the follower for acceptable performance.

10.32 Determine the cam profile assuming that an oscillating, flat-faced follower starts from a dwell from 0°

to 45° and rotates CCW. The rise occurs with harmonic motion during the cam rotation from 45° to 180° . The follower then dwells for 90° of cam rotation, and the return occurs with harmonic motion for the cam rotation from 270° to 360° . The amplitude of the follower oscillation is 20° , and the follower offset is 0.5 in. The base circle radius is 5 in, and the distance between pivots is 8 in.

10.33 Solve Problem 10.32 if the cam rotates CW.

10.34 Design the cam system assuming that an oscillating, flat-faced follower starts from a dwell for 0° to 100° of cam rotation and the cam rotates CCW. The rise occurs with uniform motion during the cam rotation from 100° to 200° . The follower then dwells for 40° of cam rotation, and the return occurs with parabolic motion for the cam rotation from 240° to 360° . The oscillation angle is 20° .

10.35 Design the cam system assuming that an oscillating flat-faced follower starts from a dwell for 0° to 50° of cam rotation and the cam rotates CW. The rise occurs with cycloidal motion during the cam rotation from 50° to 200° . The follower then dwells for 90° of cam rotation, and the return occurs with harmonic motion for the cam rotation from 290° to 360° . The oscillation angle is 25° .

10.36 Determine the cam profile assuming that the translating knife-edged follower starts from a dwell from 0° to 80° and rotates CW. The rise occurs with cycloidal motion during the cam rotation from 80° to 180° . The follower then dwells for 60° of cam rotation, and the return occurs with harmonic motion for the cam rotation from 240° to 360° . The amplitude of the follower translation is 4 cm. The base circle radius is 5 cm, and the offset is 0.5 cm.

10.37 A translating flat-faced follower is to move through a total displacement of 20 mm with harmonic motion as the cam rotates through 30° . Find the minimum radius of the base circle that is necessary to avoid cusps.

10.38 A translating flat-faced follower is to move through a total displacement of 3 in with cycloidal motion as the cam rotates through 90° . Find the minimum radius of the base circle that is necessary to avoid cusps.

10.39 A radial roller follower is to move through a total displacement of $L = 19$ mm with harmonic motion while the cam rotates 60° . The roller radius is 5 mm. Use the program supplied with the book to find the minimum radius necessary to avoid cusps during the interval indicated.

10.40 A radial roller follower is to move through a total displacement of $L = 45$ mm with cycloidal motion. The roller radius is 5 mm, and the cam rotates 90 degrees during the rise. Use the program supplied with the book to find the minimum radius necessary to avoid cusps during the interval.

10.41 Assume that a flat-faced translating follower is used with the displacement schedule in Problem 10.10. Determine if a cusp is present at $\theta = 30^\circ$.

10.42 Assume that a flat-faced translating follower is used with the displacement schedule in Problem 10.12. Determine if a cusp is present at $\theta = 90^\circ$.

11

SPUR GEARS

Prerequisite Knowledge Needed for Chapter 11

A familiarity with vector mechanics and instant centers.



11.1 Introduction

The mechanisms discussed in previous chapters are used primarily as non-uniform-motion or force transformers. In the case in which uniform motion (constant-velocity ratio) or force transmission is required, circular gears, friction drives, belt drives, and chain drives are preferred. In such devices, if the input shaft turns at a constant speed, then the output shaft will turn at a constant angular speed. In practice, however, there may be a small but undesirable oscillatory motion superposed on the output motion because of imperfections in the system.

When low power is to be transmitted, constant-velocity transfer can be achieved by friction drives; a simplified version of such a drive is shown in [Figure 11.1](#). In the device shown, disk 2 is the driver and disk 3 is driven, and both disks are assumed to be perfect circular cylinders in contact at point P . Link 1 is fixed, and there is a spring that forces disk 3 against disk 2. The disks rotate about points A and B . Assuming that there is no slip at location P , the two disks will roll on each other, and the condition for rolling can be written as

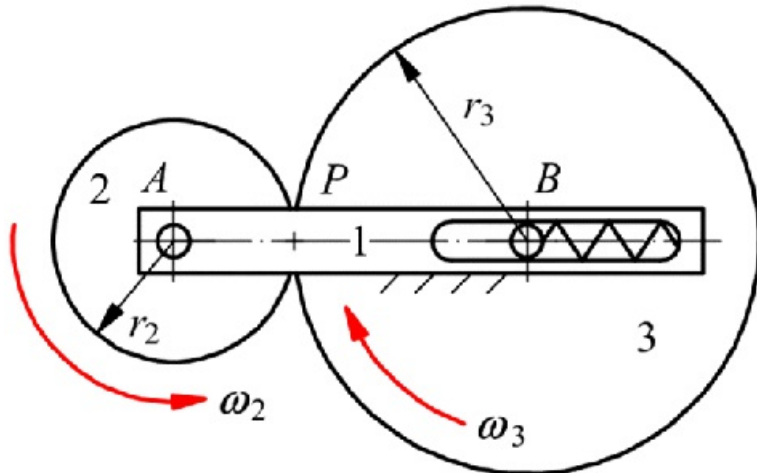


[Figure 11.1](#) Friction disks.

$$v_{P_2} = v_{P_3}$$

or

$$\omega_2 r_2 = \omega_3 r_3$$

The vector form is needlessly cumbersome for simple friction drives, and only the magnitudes need to be considered. The directions can be determined easily by inspection, that is, the two disks in [Figure 11.1](#) rotate in opposite directions. Then

$$\omega_2 r_2 = \omega_3 r_3$$

or

$$\frac{\omega_2}{\omega_3} = \frac{r_3}{r_2} \quad (11.1)$$

where $\omega_2 = [\omega_2]$, $\omega_3 = [\omega_3]$, r_2 is the radius of disk 2, and r_3 is the radius of disk 3. Thus, the friction drive velocity ratio (the input angular velocity divided by the output angular velocity) is constant and inversely proportional to

the ratio of the disk radii. Note that if a plus sign were assigned to one of the ω 's, the other ω would have a negative sign.

If an external disk drives an internal disk as shown in [Figure 11.2](#), the velocity ratio given by [Equation 11.1](#) would still apply; however, in that case, the two angular velocities would be in the same direction.

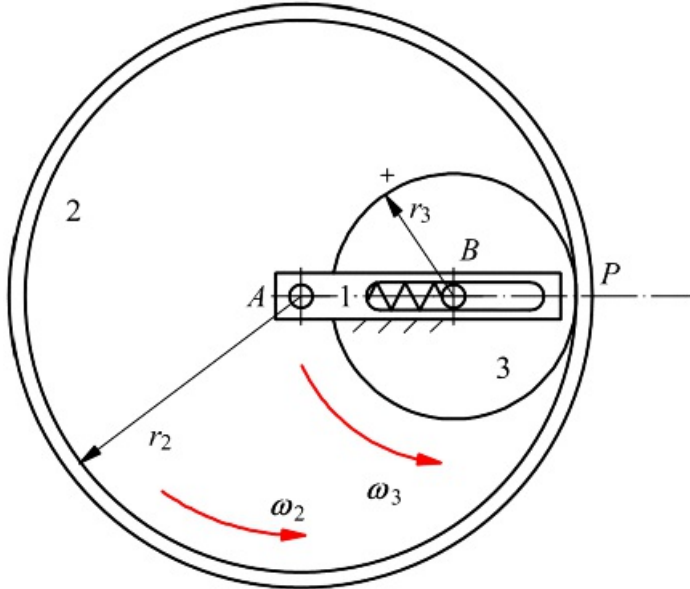


[Figure 11.2](#) Internal friction drive.

A friction drive can transmit torque only if the normal force at the contact point is sufficient to prevent slippage. If large torques are involved, large Hertzian contact stresses will be created at the contact point and subsequent pitting and galling of the contact surfaces are inevitable [1]. The wear can be lessened by using very hard contact surfaces. In addition, special lubricants have been developed that prevent actual molecular contact of the frictional surfaces but have a sufficiently high shear strength in very thin sections to provide a usable coefficient of friction.

Friction drives are used for their quietness and smoothness of operation relative to gear and chain drives. In addition, they are easily adaptable to situations in which a variable-speed transmission is required. One major disadvantage of friction drives is their relatively low power capacities. Another is that for maximum efficiency and life, they must be operated in extremely clean environments because particles can cause rapid wear rates and accelerated failure.

In the rugged environments in which most industrial machinery must operate, the use of friction drives is not practical. Instead, gear systems are often used. The gear teeth of mating gears prevent slip between disks. The gears contact each other like cam surfaces; however, for smooth, low-maintenance operation, the gear teeth have a special geometry that permits constant-velocity transfer. If designed properly, two meshing gears will behave very much the same as two friction disks, which is why gears are usually modeled grossly as two disks rolling on each other.



11.2 Spur Gears

Gears are used to transmit power from one shaft to another, and the power is usually transferred in such a way that the velocity ratio is constant. If the velocity ratio is not constant, the driven gear will be continuously accelerated and decelerated when the driving gear rotates at constant velocity. This results in cyclic stresses, vibration, noise, and other problems. Profiles of meshing gear teeth that give constant-velocity ratio are termed conjugate. As discussed later in this chapter, given the geometry of any gear tooth profile, it is possible to construct a conjugate profile using graphical and analytical techniques similar to those used for finding cam profiles. However, there are relatively few profile types that are useful for most applications.

Spur gears are the simplest type of gear commonly used in industry. The characteristic of spur gears is that the gear-rotation axes are all parallel and the gear teeth are parallel to the rotation axes. The gear may be equivalent to a rolling cylinder of any radius called the pitch cylinder. When the pitch cylinder radius becomes infinitely large, the teeth are located on a plane, and such a gear is called a rack. A simple pair of meshing gears is shown in [Figure 11.3](#). When two gears of unequal size are meshed, the smaller gear is referred to as the pinion and the larger gear as the “gear” or “wheel.” A pinion and rack are shown in [Figure 11.4](#).



[Figure 11.3](#) Meshing spur gears.

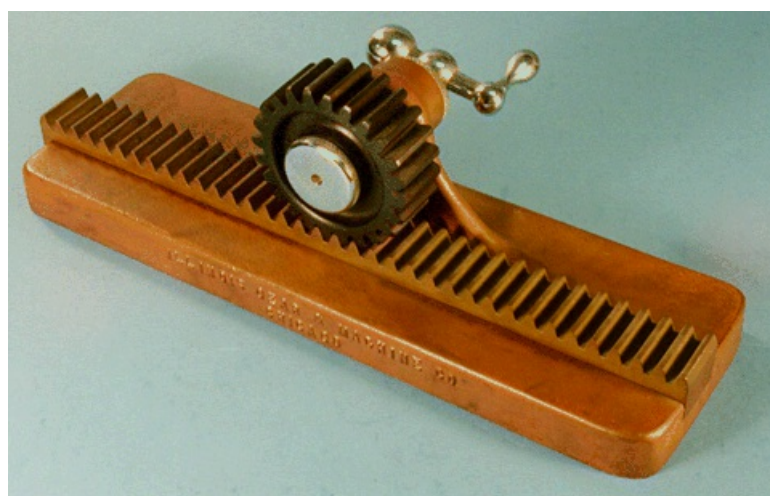


[Figure 11.4](#) Pinion and rack.



11.3 Condition for Constant-Velocity Ratio

[Figure 11.5](#) represents the teeth of two gears that rotate about A and B , respectively. The tooth profiles contact each other at point P . The instantaneous center for the motion of gear 3 relative to gear 2 lies on the normal to the profiles at the point of contact. By the Kennedy-Aronhold theorem, it also lies on the line joining the centers of rotation of gears 2 and 3 relative to the base. Thus, the instantaneous center of motion of gear 3 relative to gear 2 must be at point I_{23} , which is also known as the pitch point, P .

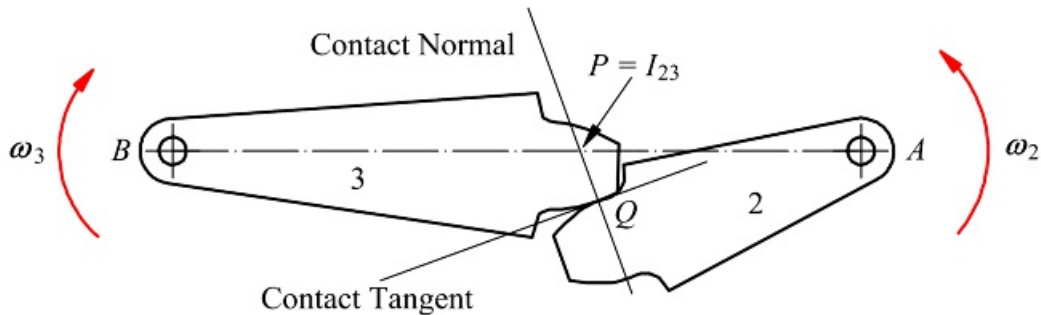


[Figure 11.5](#) The location of the instantaneous center of relative rotation of members 2 and 3 that respectively rotate relative to the base about A_2 and B_3 . The instantaneous center (pitch point) is P (I_{23}). The angular velocities of members 2 and 3 relative to the base are, respectively, ω_2 and ω_3 . For the external gears shown, the senses of ω_2 and ω_3 are opposite.

Hence

$$\omega_2 \dot{A}_2 P = \omega_2 \dot{A}_2 I_{23} = -\omega_3 \dot{B}_3 I_{23} = -\omega_3 \dot{B}_3 P$$

or considering magnitudes only

$$R = \frac{\omega_2}{\omega_3} = \frac{\dot{B}_3 P}{\dot{A}_2 P} \quad (11.2)$$

where R is the velocity ratio. Thus, a constant-velocity ratio implies that $\dot{B}_3 P / \dot{A}_2 P$ is constant. That is, P is a fixed point on the line of centers between the two gears.

Summarizing, for conjugate profiles, the normal to the profiles at the point of contact always intersects the line of centers at the same point. This is the fundamental law of gearing. This point (P) or pitch point is the instantaneous center of the relative motion of the gears.

The velocity, v_s , with which the gear teeth slide over one another is important because the rate of wear of the gear teeth depends on it. The sliding velocity at Q is the relative velocity between the coincident points at the contact location Q ; that is, it is the velocity v_{Q_2/Q_3} . From [Chapter 5](#), the magnitude of the relative velocity between two coincident points can be written as

$$v_s = {}^1 v_{Q_2/Q_3} = {}^3 v_{Q_2/Q_3} = {}^3 v_{Q_3/P_2} + {}^3 v_{P_2/P_3} + {}^3 v_{P_3/Q_3} = {}^3 v_{Q_3/P_2} = {}^3 \omega_2 (r_{Q_2/P})$$

where 1 is used to designate the ground link. The relative velocity can be written as

$${}^3 \omega_2 = {}^1 \omega_2 - {}^1 \omega_3$$

Dropping the superscripts that are associated with the ground link

$$v_3 = [r_{Q/P}] [\omega_2 - \omega_1]$$

or using the simpler nomenclature

$$v_2 = r_{Q/P} [\omega_2 - \omega_1] \quad (11.3)$$

The sliding velocity is proportional to the distance between the contact point Q and the pitch point P . When P and Q coincide, the sliding velocity becomes zero and the teeth are instantaneously rolling on one another.



11.4 Involutes

Of the many shapes that are possible for tooth geometries, the involute and cycloid are the most common. Of these two forms, the involute is used in almost all cases except in mechanical watches and clocks, in which the cycloidal form is still found. The involute form has several advantages, but two are most important. The first is that it is very easy to manufacture involute gears with simple tooling. The second is that the constant-velocity ratio is maintained even when the center distance between the two gears is changed. This is important in manufacturing, because it is never possible to mount the gears precisely at the designed center distance.

The involute profile is developed from a circle called a base circle. The involute of a given base circle is the curve traced by any fixed point on a taut string that is being unwound from the base circle as shown in [Figure 11.6](#). The involute curve has the following important properties

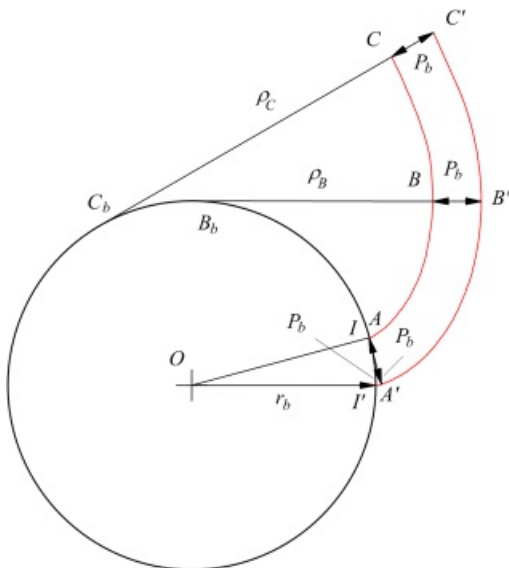


[Figure 11.6](#) Generation of an involute by a point on a stretched string unwound from a cylinder. $A'B'C'$ and $A''B''C''$ are two involutes generated off the same base circle that has radius r_b . The string is originally wrapped around the base circle with its end at I' . When it has been unwrapped until it is tangent to the base circle at A , its end is at A' . Therefore line AA' has the same length as the curvilinear distance II' . ($\overline{II'} \equiv \overline{AA'}$) When it has been unwrapped so that its end is at point B' , it is tangent to the base circle at B_b . Similarly, when the end is at C' , the string is tangent to the base circle at C_b . Similarly, the point on the string that is initially at A is at B when the end of the string is at B' , and it is at C when the end is at C' . Hence the normal distance between the two involutes is constant.

1. The normal to the involute at any point of the curve is tangent to the base circle.
2. The length of the normal is equal to the corresponding arc of the base circle, that is $B_bB = \text{arc } B_bI$, $C_bC = \text{arc } C_bI$. Consequently, the normal distance between two involutes of the same base circle is equal to their base pitch, that is, $AA' = BB' = CC' = \text{arc } II' = p_b$.
3. The length of the normal is equal to the local radius of curvature of the involute, that is, $B_bB' = \rho_B$, $C_bC' = \rho_C$.
4. Any two involute profiles are mutually conjugate regardless of the base circle diameters.
5. The path of contact between two involute profiles is rectilinear. Consequently, the pressure angle is constant.
6. A gear with involute tooth profiles can be generated by a straight-sided rack cutter.
7. Two involute profiles remain conjugate if their center distance is changed.

Proofs 1, 2, 3 are obtained by inspection of [Figure 11.6](#).

Proof 4: See [Figure 11.7](#). This figure shows two involute profiles in contact in an arbitrary position. The normal at the point of contact Q is tangent to both base circles. This normal remains the same regardless of the motion of the profiles. Hence, its intersection, P , with the line of centers is fixed and the velocity ratio is constant. The velocity ratio is

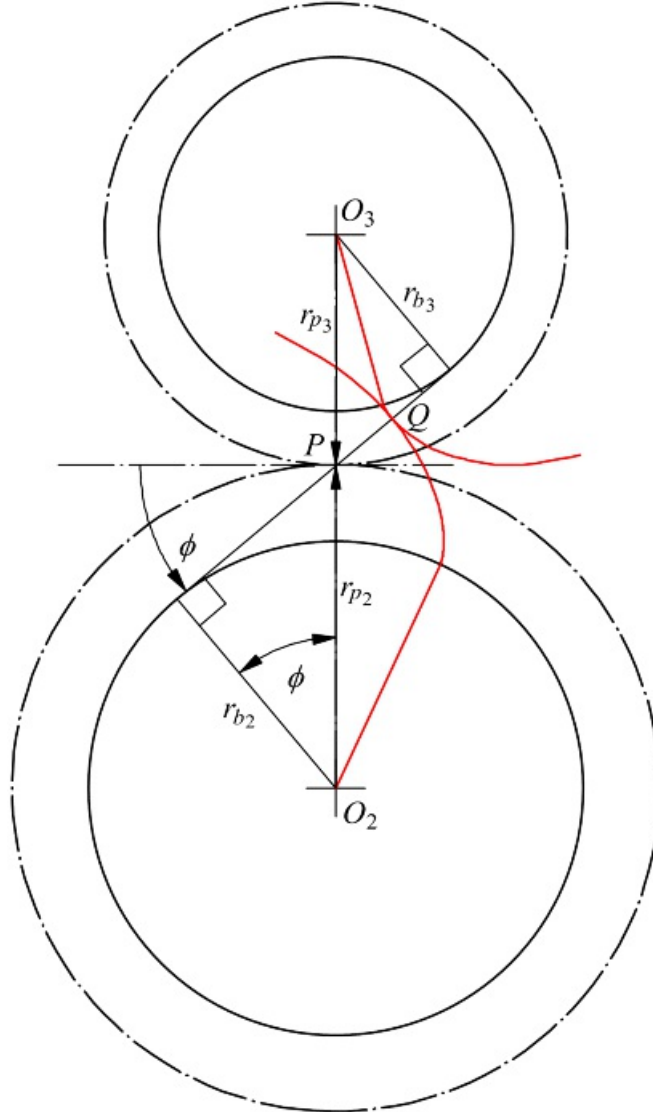


[Figure 11.7](#) Two involutes in contact. The normal to both curves at the point of contact, Q , is tangent to both base circles. Hence it always passes through the fixed point P . Therefore two involutes are always conjugate.

$$\frac{r_p}{r} = \frac{\mathcal{O}_3P}{\mathcal{O}_2P} = \frac{r_{p_3}}{r_{p_2}} \quad (11.4)$$

where $r_{p_2} = \mathcal{O}_2P$ is the radius of the pitch circle of gear 2 and $r_{p_3} = \mathcal{O}_3P$ is the radius of the pitch circle of gear 3. The pitch circles are the dashed circles shown in [Figure 11.7](#). The radii of the pitch circles are related to those of the corresponding base circles by the equations

$$r_{p_2} = \frac{r_{b_2}}{\cos \phi} \quad (11.5)$$

and

$$r_{D_3} = \frac{r_{D_2}}{\cos \phi}$$

These equations follow from the fact illustrated in [Figure 11.7](#) that r_{D_2} is the hypotenuse of a right-angled triangle. r_{D_3} is another side of that triangle, and ϕ is the angle included between them. The same condition holds for gear 3. Therefore

$$\beta = \frac{r_{P_3}}{r_{P_2}} = \frac{r_{D_3}}{r_{D_2}} \quad (11.6)$$

where r_{P_2} , r_{P_3} are the pitch circle radii. The constant angle ϕ made by the contact normal with the tangent to the pitch circles at point P is called the pressure angle.

Proofs 5, 6: Since the normal at the point of contact is always the same line, it follows that the point of contact simply moves backward and forward along this line. This profile is conjugate to a straight-sided rack. That is, if we have a linear profile inclined at angle ϕ to the line OP that simply slides back and forth without rotating, the involute profile is conjugate to it. The normal at the point of contact is always normal to the linear profile as indicated in [Figure 11.8](#). Because it is also always tangent to the base circle, it is always the line shown. The point P is fixed. This implies that a gear with involute teeth can be cut by a cutter in the shape of a straight-sided rack that reciprocates in a direction parallel to the axis of the gear blank.

Proof 7: The proof of item 7 follows from the proof of item 4, because the involute profiles are arbitrary and their center distance is arbitrary.

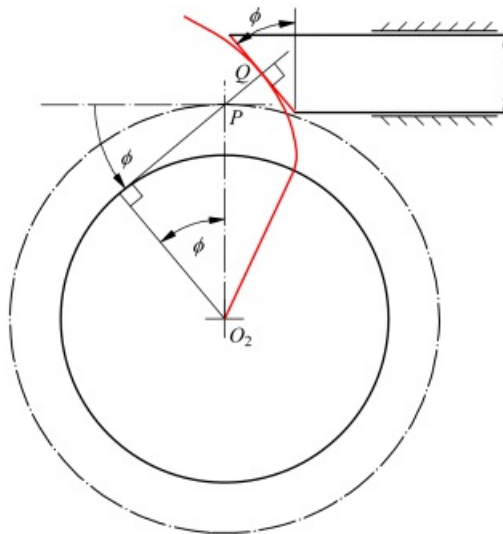


[Figure 11.8](#) Conjugacy of involute to a straight-sided rack.



11.5 Gear Terminology and Standards

11.5.1 Terminology

Several terms commonly used for describing gears can be defined with the aid of [Figure 11.9](#). The *pitch circle* is the circle centered on the gear axis passing through the point of contact. The pitch circles of meshing gears roll on one another, and the point of contact is the *pitch point*. The *pitch circle diameter* or *pitch diameter* will be designated as d_p .

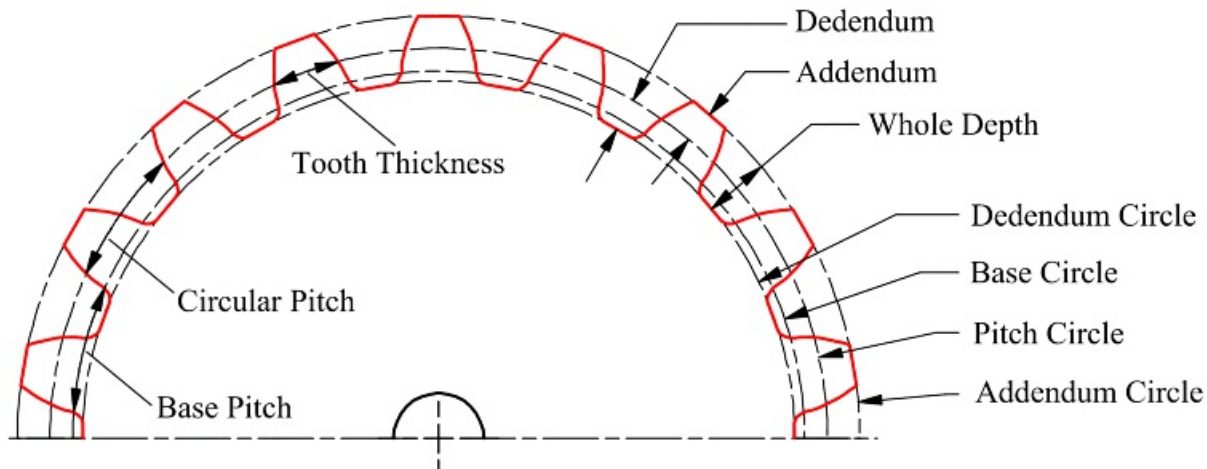


[Figure 11.9](#) Gear tooth in-plane geometry terminology.

Although a gear will be designed to have a particular pitch circle, the actual pitch circle will depend on the gear with which it meshes and the center distance.

The *circular pitch*, p_c , is the curvilinear distance measured on the pitch circle from a point on one tooth to the corresponding point on the next tooth.

The *base pitch*, p_b , is the curvilinear distance measured on the base circle from a point on one tooth to the corresponding point on the next tooth.

The *diametral pitch*, P_d , is the number of teeth on the gear per unit of pitch diameter. That is

$$P_d = N/d_p \quad (11.7)$$

where N is the number of teeth on the gear. Also, from the definition of circular pitch

$$p_c = \pi d_p/N \quad (11.8)$$

so

$$P_d = \pi/p_c \quad (11.9)$$

or

$$P_d p_c = \pi \quad (11.10)$$

The base pitch is given by

$$p_b = \pi d_b / N \quad (11.11)$$

From [Equation 11.5](#) the base circle diameter and the pitch circle diameter are related by

$$d_p = \frac{d_b}{\cos \phi}$$

Therefore, [Equation 11.8](#) can be rewritten as

$$p_c = \pi d_p / N = \frac{\pi d_b}{N \cos \phi} = \frac{p_b}{\cos \phi} \quad (11.12)$$

or

$$p_b = p_c \cos \phi \quad (11.13)$$

In the metric system, gears are specified by the ratio of the pitch diameter in mm to the number of teeth. This ratio is called the *module*, m , that is expressed as follows

$$m = \frac{d_p}{N} \quad (11.14)$$

From [Equation 11.8](#)

$$p_c = m N \quad (11.15)$$

[Equation 11.15](#) gives p_c in mm, so the units must be converted if p_c is to be expressed in inches. The *addendum circle* passes through the tips of the gear teeth, and the *dedendum circle* passes through the base of the gear teeth. The *addendum* is the radial distance from the pitch circle to the top land (see [Figure 11.10](#)) of the gear, and the *dedendum* is equal to the radial distance from the pitch circle to the bottom land of the tooth. The *whole depth* is the sum of addendum and dedendum.

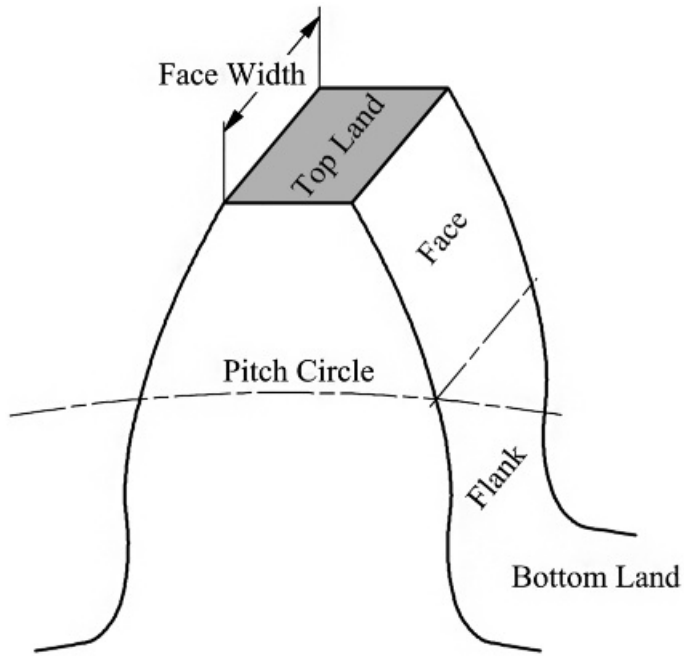


Figure 11.10 Gear tooth axial geometry terminology.

With involute gears, the contact between the two gears occurs on the pressure line. This line then is called the *line of action*.

11.5.2 Standards

If two gears are to mesh, it is necessary that their pitches be the same. Since the base pitch, circular pitch, diametral pitch, and module are uniquely related, if any one of these pitch measures is the same for both gears, all will be.

Gears cut to standard dimensions (see [Table 11.1](#)) are interchangeable in the sense that any two standard gears can be meshed together. For this to be possible, the following conditions are required:

1. The pressure angles must be the same.
2. The diametral pitches must be the same.
3. The gears must have the same addendum and same dedendum.
4. The tooth thicknesses must be equal to one-half the circular pitch.

Table 11.1 Standard AGMA^a and USASI^b Tooth Systems for Involute Spur Gears [2]

System ^c	Coarse Pitch ($1P$ to $19.99P$) Full Depth	Fine Pitch ($20P$ to $200P$) Full Depth	Stub Teeth	
Pressure angle, f	20°	25°	25°	20°
Addendum, a	$1/P_d$	$1/P_d$	$1/P_d$	$0.8/P_d$
Dedendum, b	$1.25/P_d$	$1.25/P_d$	$1.20/P_d + 0.002 \text{ in}$	$1/P_d$
Working depth, h_k	$2/P_d$	$2/P_d$	$2/P_d$	$1.6/P_d$
Whole depth, h_t (min.)	$2.25/P_d$	$2.25/P_d$	$2.25/P_d + 0.002 \text{ in}$	$1.8/P_d$
Circular tooth thickness, t	$\pi/2P_d$	$\pi/2P_d$	$\pi/2P_d$	$\pi/2P_d$
Fillet radius of basic rack, r_f	$0.3/P_d$	$0.3/P_d$	Not	

			standardized	
Basic clearance, c (min.)	$0.25/P_d$	$0.25/P_d$	$0.2/P_d + 0.002$ in	$0.2/P_d$
Clearance, c (shaved or ground teeth)	$0.35/P_d$	$0.35/P_d$	$0.35/P_d + 0.002$ in	
Minimum width of top land, t_o	$0.25/P_d$	$0.25/P_d$	Not standardized	
^a American Gear Manufacturers' Association				
^b United States of America Standards Institute				
^c The standard pitches in common use are: 1 to 2 varying by 1/4 pitch, 2 to 4 varying by 1/2 pitch, 4 to 10 varying by 1 pitch, 10 to 20 varying by 2 pitch, and 20 to 200 varying by 4 pitch.				

This is what permits vendors to offer off-the-shelf gears. It is also what makes possible applications such as the change gears used in a lathe to set up different cutting and feed rates. However, nonstandard gears are also used in many applications for a variety of reasons, some of which will be discussed later in this chapter. In general, nonstandard gears have to be designed as a meshing pair, and neither member of the pair will mesh satisfactorily with a standard gear.

[Table 11.1](#) shows the standard equations for the 20° and 25° pressure angles that are the most commonly used standard gears. A gear system that is now little used is the $14\frac{1}{2}^\circ$ pressure angle system. This system was used extensively in the past when gears were cast because the sine of $14\frac{1}{2}^\circ$ is approximately $\frac{1}{4}$, which facilitated pattern layout. As will be shown later, the $14\frac{1}{2}^\circ$ system is inferior to the systems with higher pressure angles because the gears must have a larger number of teeth to avoid interference than are required in the 20° and 25° systems. Therefore, for a relatively small number of teeth, gears in the $14\frac{1}{2}^\circ$ system will have a lower beam strength and a lower load rating than corresponding gears in the 20° and 25° systems.

While any diametral pitch is technically possible, the standard pitches in common use are 1 to 2 varying by 1/4 pitch, 2 to 4 varying by 1/2 pitch, 4 to 10 varying by 1 pitch, 10 to 20 varying by 2 pitch, and 20 to 200 varying by 4 pitch.

Based on the equations in [Table 11.1](#), the physical size of the gear teeth decreases as the diametral pitch, P_d , increases. This is also shown in [Figure 11.11](#). In general, for a given set of pitch diameters, the load transfer will be smoother and undesirable affects such as noise will be lower if a large number of small teeth is used rather than a small number of larger teeth. This is because more teeth share the load when smaller teeth are used.

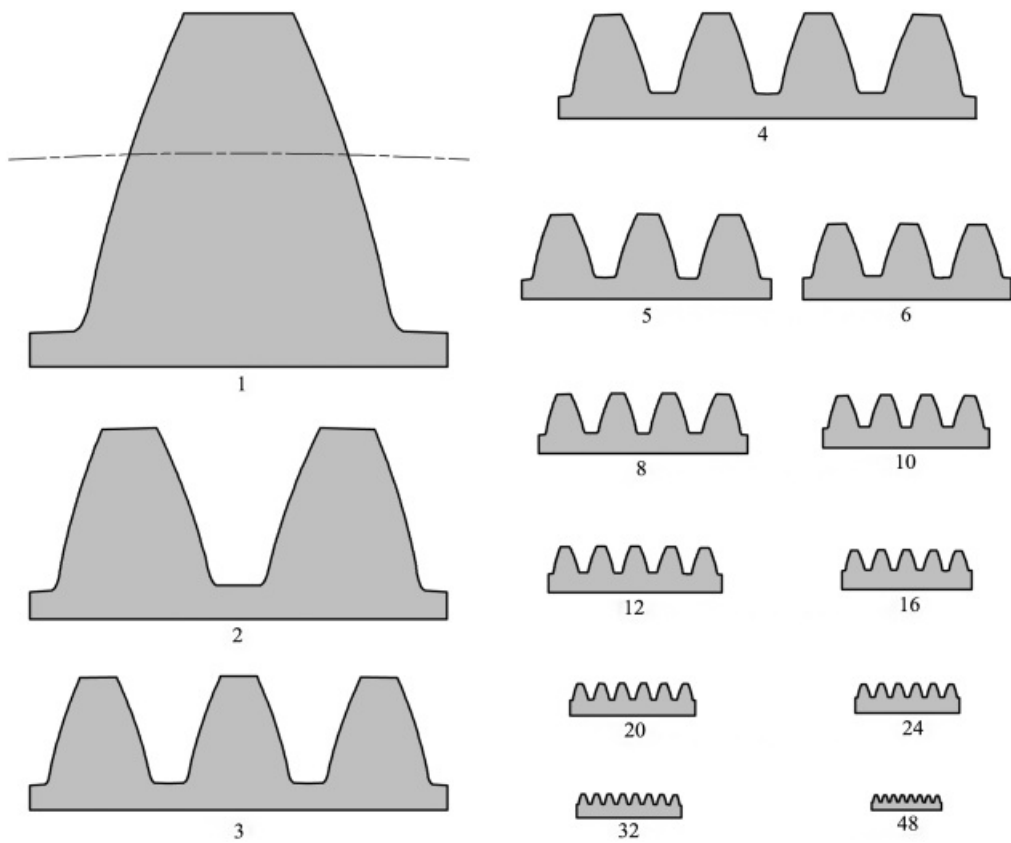


[Figure 11.11](#) Relative sizes of gear teeth with diametral pitches shown.



11.6 Contact Ratio

An important feature of gear action is the *contact ratio*, which can be thought of as the *average* number of tooth pairs that are in contact through the gear cycle. Thus, a contact ratio of 1.2 indicates that one tooth pair is contacting 80 percent of the time and two pairs 20 percent of the time, and this is generally considered to be the minimum contact ratio that should be used for typical designs. If the contact ratio is less than one, contact will be lost part of the time, and the gear pair cannot function properly. A larger contact ratio normally means smoother running gears and enhanced load-carrying capacity and stiffness, since the load is transferred in parallel between several tooth pairs. However, to take full advantage of a high contact ratio, very accurately cut tooth profiles are necessary.

[Figure 11.12](#) shows a pair of mating teeth in the two positions in which they first come in contact and are at the point of losing contact. Between these two positions, the point of contact moves along the line of contact through the pitch point as described in Section 11.4. As can be seen from the figure, the locations of first and last contact are determined by the addenda of the teeth. Contact is initiated at point *I*, which is the intersection of the pressure line with the addendum circle of gear 3. Contact is terminated at point *F*, which is the intersection of the pressure line with the addendum circle of gear 2.

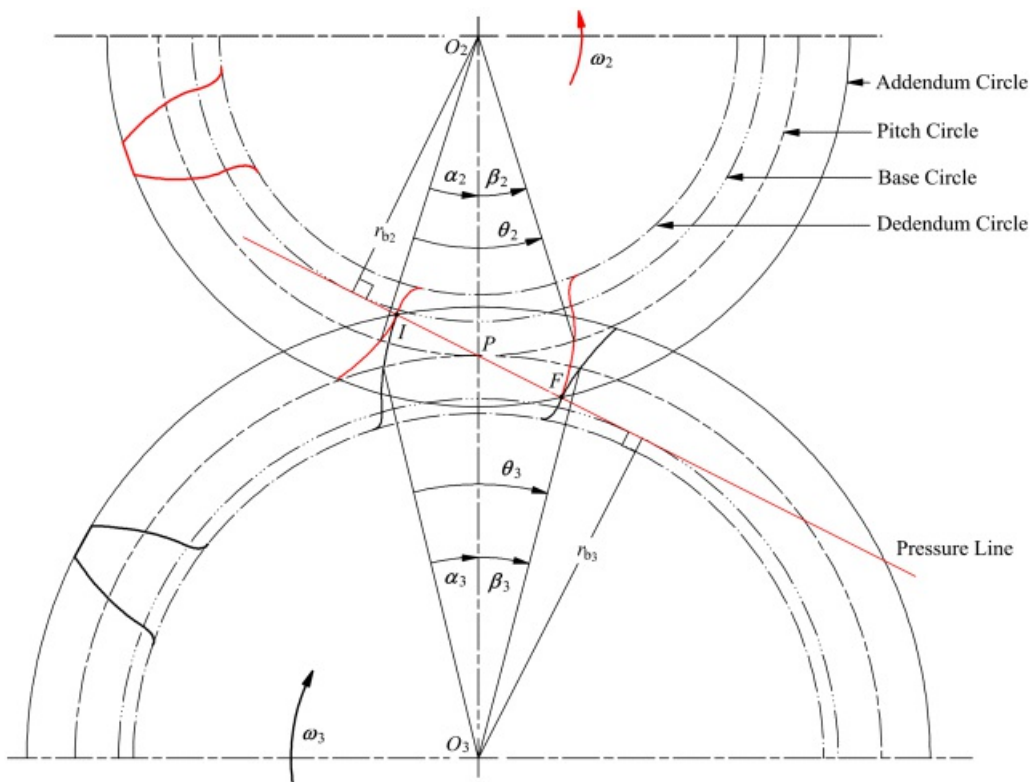


[Figure 11.12](#) Contact geometry: The contact angle of gear 2 is θ_2 and that of gear 3 is θ_3 .

For gear 2, the angle of approach, α_2 , is the angle through which the gear rotates from the time of first contact between a pair of teeth and the time at which the contact point reaches the pitch point. Correspondingly, the angle of recess, β_2 , is the angle through which the gear rotates from the time at which contact is at the pitch point to the time at which contact is lost. The angle $\theta_2 - \alpha_2 + \beta_2$ is the angle of contact of gear 2 when in mesh with gear 2. Meshing gear 2 with another gear will change both α_2 and β_2 if the size of the second gear changes.

Because the distance the contact point moves along the path of contact is equal to the curvilinear distance around the base circle, according to the relationship illustrated in [Figure 11.12](#)

$$\omega_2 = \frac{r\theta}{r_{b2}}$$

And

$$\beta_2 = PF/r_{b_2}$$

Hence

$$\beta_2 = IF/r_{b_2}$$

The distance IP from the point of initial contact to the pitch point can be computed from the geometry shown in [Figure 11.13](#), where r_{b_2} , r_{p_2} , and r_{a_2} are, respectively, the base circle radius, the pitch circle radius and the addendum (tip) circle radius of the driven gear (gear 3). Here, ϕ is the pressure angle, and u is the length IP . Application of the cosine rule to triangle IPO_3 gives

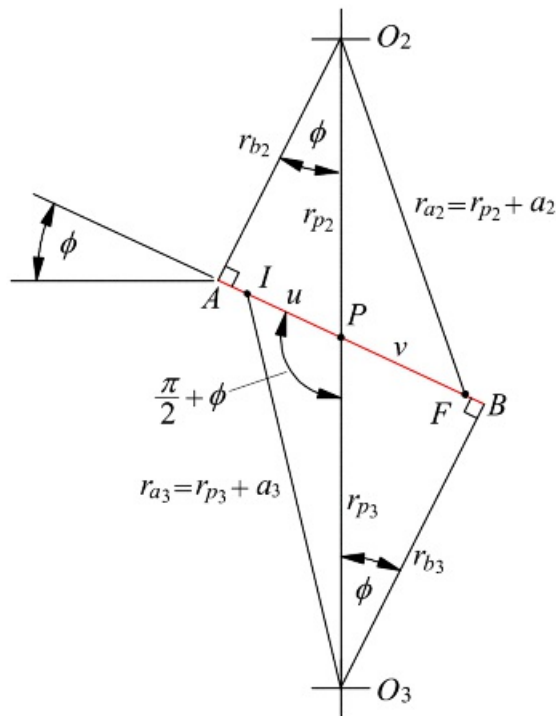


[Figure 11.13](#) The geometry used in computing the length of the path of contact, IF . The points O_2 , O_3 , P , I , and F are the same as those shown in [Figure 11.12](#).

$$r_{a_3}^2 = u^2 + r_{p_3}^2 - 2ur_{p_3} \cos(\phi + \pi/2) = u^2 + r_{p_3}^2 + 2ur_{p_3} \sin \phi$$

or

$$u^2 + [2r_{p_3} \sin \phi] u + (r_{p_3}^2 - r_{a_3}^2) = 0$$

Solving this quadratic equation for u and simplifying using $\sin^2 \phi + \cos^2 \phi = 1$ gives

$$u = -r_{p_3} \sin \phi \pm \sqrt{r_{a_3}^2 - r_{p_3}^2 \cos^2 \phi}$$

Now $r_{a_3} = r_{p_3} + a_3$, where a_3 is the addendum of gear 3. Therefore, this equation can also be written in the form

$$w = -r_{p_3} \sin \phi \pm \sqrt{(r_{p_3} + a_3)^2 - r_{p_3}^2 \cos^2 \phi}$$

It can be shown that the term under the square root is always positive, and only the positive root is consistent with the geometry presented. Therefore

$$w = \sqrt{(r_{p_3} + a_3)^2 - r_{p_3}^2 \cos^2 \phi} - r_{p_3} \sin \phi \quad (11.16)$$

Because of the similarity between the triangles in [Figure 11.13](#), [Equation 11.16](#) may also be used to compute $v = PF$ by replacing r_{p_3} with r_{p_2} and a_3 with a_2 . That is

$$v = \sqrt{(r_{p_2} + a_2)^2 - r_{p_2}^2 \cos^2 \phi} - r_{p_2} \sin \phi$$

As shown in [Figures 11.12](#) and [11.13](#), the distance along both respective base circles between the involutes in the initial and final positions is

$$\begin{aligned} \lambda &= IF - IP + PF = w + v \\ \lambda &= \sqrt{(r_{p_3} + a_3)^2 - r_{p_3}^2 \cos^2 \phi} - r_{p_3} \sin \phi + \sqrt{(r_{p_2} + a_2)^2 - r_{p_2}^2 \cos^2 \phi} - r_{p_2} \sin \phi \end{aligned} \quad (11.17)$$

Using [Equations 11.7–11.13](#) and [11.17](#), the contact ratio can now be computed as the ratio of the length of the path of contact to the base pitch. That is

$$\begin{aligned} m_c &= \frac{\lambda}{p_b} = \frac{\lambda}{p_c \cos \phi} = \frac{\lambda p_d}{\pi \cos \phi} \\ &= \frac{p_d \left\{ \sqrt{(r_{p_3} + a_3)^2 - r_{p_3}^2 \cos^2 \phi} - r_{p_3} \sin \phi + \sqrt{(r_{p_2} + a_2)^2 - r_{p_2}^2 \cos^2 \phi} - r_{p_2} \sin \phi \right\}}{\pi \cos \phi} \end{aligned} \quad (11.18)$$

As stated above, the significance of the contact ratio (m_c) is that it determines the load sharing among the teeth. If the contact ratio is less than 1, there will be periods in which contact is completely lost and the gears cannot function correctly. If the contact ratio is close to 1, variations caused by errors in mounting or wear may cause loss of contact. In practice, contact ratios less than 1.2 should be avoided.



Example 11.1

Contact Ratio for Two 20° Pressure-Angle Gears

Two gears are in mesh such that one gear (gear 2) has 20 teeth and the other (gear 3) has 30. The diametral pitch for each gear is 4, and the working pressure angle is 20°. Standard gears are involved in each case, and the addendum constant is 1. Determine the length of the contact line and the contact ratio.

Solution

To compute the contact ratio, we need to determine the base pitch and all of the terms in [Equation 11.17](#). From [Table 11.1](#), the addendum for both gears is given by

$$a = \frac{1}{P_d} = \frac{1}{4} = 0.25 \text{ in} = a_2 = a_3$$

Similarly, the circular pitch for both gears is given by

$$p_c = \frac{\pi}{P_d} = \frac{\pi}{4} = 0.785 \text{ in}$$

and from [Equation 11.13](#), the base pitch is related to the circular pitch by

$$p_b = p_c \cos \phi = 0.785 \cos 20^\circ = 0.738 \text{ in}$$

From [Equation 11.7](#), the two pitch radii are given by

$$r_{p_2} = \frac{N_2}{2P_d} = \frac{20}{2(4)} = 2.5 \text{ in}$$

and

$$r_{p_3} = \frac{N_3}{2P_d} = \frac{30}{2(4)} = 3.75 \text{ in}$$

The length of the line of contact is given by [Equation 11.17](#) as

$$\begin{aligned} l &= \sqrt{(r_{p_2} - a_2)^2 - (r_{p_2} \cos \phi)^2} + r_{p_2} \sin \phi + \sqrt{(r_{p_3} - a_3)^2 - (r_{p_3} \cos \phi)^2} + r_{p_3} \sin \phi \\ &= \sqrt{(2.5 + 0.25)^2 - (2.5 \cos 20^\circ)^2} + 2.5 \sin 20^\circ + \sqrt{(3.75 + 0.25)^2 - (3.75 \cos 20^\circ)^2} + 3.75 \sin 20^\circ \\ &\approx 1.185 \text{ in} \end{aligned}$$

From [Equation 11.18](#), the contact ratio is

$$m_c = \frac{\lambda}{p_3} = \frac{1.185}{0.7380} = 1.6052$$

Therefore, on average, approximately 1.6 teeth are in contact as the gears mesh.



11.7 Involutometry

It is important, for the purpose of analyzing stress and deflection of gear teeth, to be able to compute the thickness of a tooth at any radius. From [Figure 11.14](#), the arc distance AB is equal to the linear distance BT . Therefore

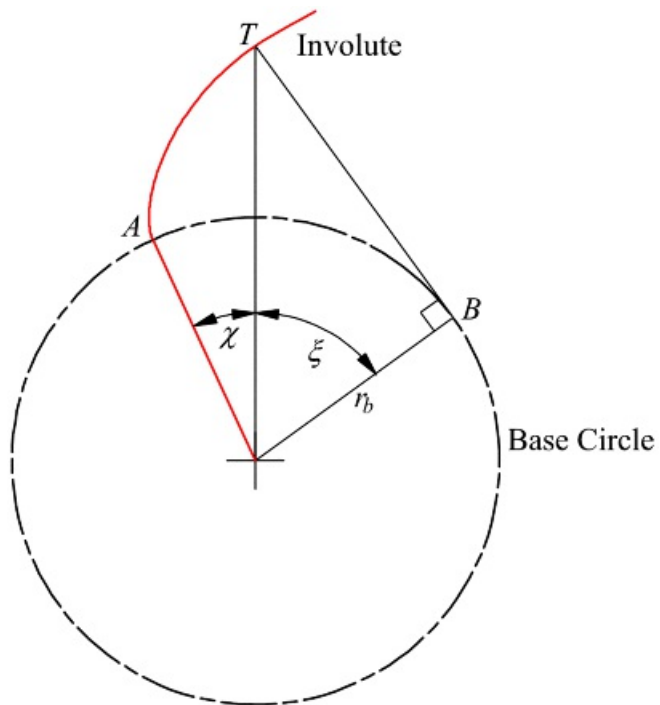


[Figure 11.14](#) The basic geometry for the definition of the involute function.

$$AB = BT = r_b \tan \xi$$

and

$$\xi = AB/r_b = \xi = \tan \xi = \xi$$

ξ is called the involute function of ξ , written $\text{inv}(\xi)$

$$\text{inv}(\xi) = \tan \xi = \xi \quad (11.19)$$

Involute functions can be easily computed using a computer or calculator. The thickness of the tooth at any radius r can be computed using involute functions.

Referring to [Figure 11.15](#)

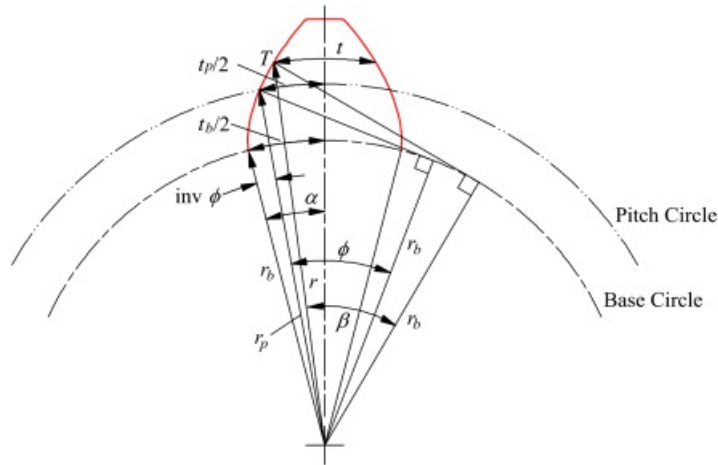


Figure 11.15 Computation of the tooth thickness, t , at any radius, r . Tooth thickness is computed as a *curvilinear* length along the circumference of the circle of radius r through point T .

$$\frac{t_p}{2r_p} = \alpha - \text{inv} \phi$$

or

$$\alpha - \frac{t_p}{2r_p} = \text{inv} \phi$$

Also, at any general location defined by r

$$\frac{t}{2r} = \alpha - \text{inv} \beta$$

Hence

$$\frac{t}{2r} = \frac{t_p}{2r_p} + \text{inv} \phi - \text{inv} \beta \quad (11.20)$$

where

$$\cos \beta = \frac{r_b}{r} = \frac{r_p \cos \phi}{r} \quad (11.21)$$



Example 11.2 Thickness of Gear Tooth

Find the thickness at the addendum and base circles of a tooth of diametral pitch 4 on a gear with 30 teeth cut with a 20° pressure angle, standard dimensions, and with the tooth thickness at the pitch circle equal to half the circular pitch.

Solution

First compute the radii at the three locations for which the tooth thickness is desired. The radius of the pitch circle is given by [Equation 11.7](#) as

$$r_p = \frac{N}{2P_d} = \frac{30}{2(4)} = 3.75 \text{ in}$$

Using [Table 11.1](#), the addendum radius is given by

$$r_a = r_p + a = r_p + \frac{1}{P_d} = 3.75 + \frac{1}{4} = 4.0 \text{ in}$$

The base circle radius is given by [Equation 11.5](#) as

$$r_b = r_p \cos \phi = 3.75 \cos 20^\circ = 3.524 \text{ in}$$

From [Table 11.1](#), the circular tooth thickness is

$$s_p = \frac{\pi}{2P_d} = \frac{\pi}{2(4)} = 0.393 \text{ in}$$

Next compute the angle β in [Figure 11.16](#) at the addendum circle. From [Equation 11.21](#), we have

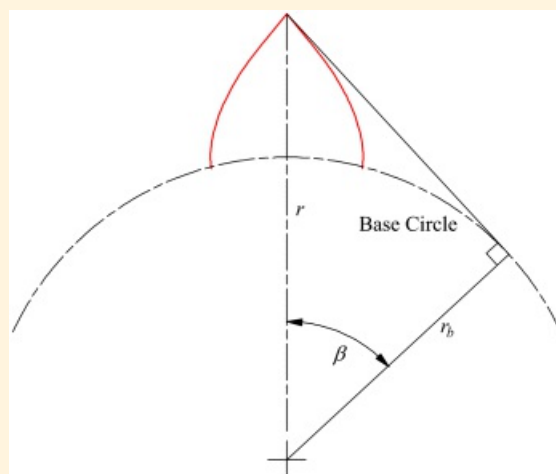


[Figure 11.16](#) Limiting case for r (tooth thickness = 0).

$$\beta_a = \cos^{-1} \left[\frac{r_p \cos \phi}{r_h} \right] = \cos^{-1} \left[\frac{3.75 \cos 20^\circ}{4.0} \right] = 28.241^\circ$$

The value of β at the base circle is zero.

From [Equation 11.20](#), the equation for the tooth thickness at the addendum is

$$s_a = 2r_a \left(\frac{s_p}{2r_p} + \operatorname{inv} \phi - \operatorname{inv} \beta_a \right) = 2(4.0) \left(\frac{0.393}{2(3.75)} + \operatorname{inv} 20^\circ - \operatorname{inv} 28.241^\circ \right) = 0.184 \text{ in}$$

The value of β at the base circle is zero. Therefore, the tooth thickness at the base circle is

$$s_b = 2r_b \left(\frac{s_p}{2r_p} + \operatorname{inv} \phi - \operatorname{inv} \beta_b \right) = 2(3.524) \left(\frac{0.393}{2(3.75)} + \operatorname{inv} 20^\circ - 0 \right) = 0.474 \text{ in}$$



Example 11.3

Minimum Thickness of Gear Tooth

From Example 11.2, it is clear that the gear tooth thickness becomes smaller as the radius increases from the base circle radius. In the limiting case, the tooth thickness is zero. For the gear in Example 11.2, determine the maximum radius that could be specified for the addendum circle if a nonstandard gear were used.

Solution

From [Equation 11.20](#) and [Figure 11.17](#), the gear tooth thickness becomes zero when

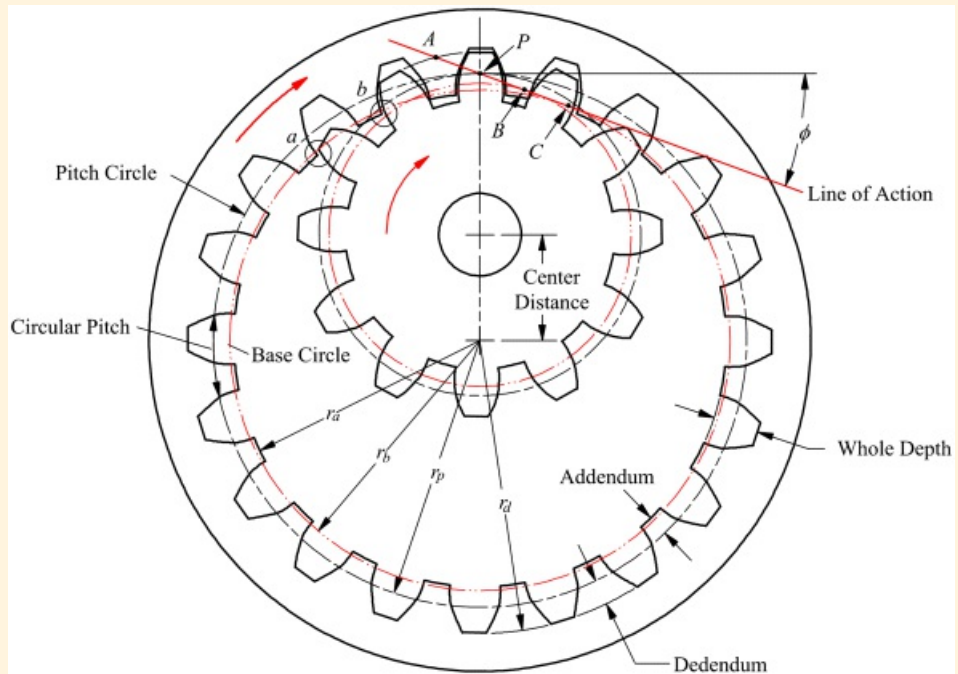


[Figure 11.17](#) Internal pinion and gear.

$$2r \left(\frac{\delta_p}{2r_p} + \operatorname{inv}\phi - \operatorname{inv}\beta \right) = 0 \quad (11.22)$$

[Equation 11.22](#) is satisfied when

$$\operatorname{inv}\beta = \frac{\delta_p}{2r_p} + \operatorname{inv}\phi = \frac{0.393}{2(3.75)} + \operatorname{inv}20^\circ = 0.0673$$

This equation can be solved for β by using a table of values for the involute function or by simply computing a series of values for $\operatorname{inv}\beta$ in a spreadsheet or with a program such as MATLAB. The solution is $\beta = 32.13^\circ$. From [Figure 11.16](#), it is clear that β and r are related by

$$r = r_t / \cos \beta \quad (11.23)$$

Therefore

$$r = r_b / \cos \beta = 3.524 / \cos 32.13^\circ = 4.161 \text{ m} \quad (11.24)$$



11.8 Internal Gears

An internal or annular gear is a gear that has its center on the same side of the pitch circle as the pinion meshing with it as shown in [Figure 11.17](#). The addendum circle for the internal gear is inside the pitch circle, and the teeth are concave rather than convex. Internal gears are commonly used in planetary gear systems and compact gear boxes. The primary advantage of an internal gear set is the compactness of the drive. Also, both the pinion and gear rotate in the same direction. Other advantages are the lower contact stresses because the surfaces conform better than do external gear sets. There are also lower relative sliding between teeth and a greater length of contact possible between mating teeth since there is no limit to the involute profile on the flank of the internal gear.

Because of the tooth shape, the bending strength of the internal teeth is much greater than the strength of the teeth on the pinion. Therefore, the pinion is always the weaker member unless different materials are used for the two gears.

As in the case of external gears, the contact occurs along the line of action that is tangent to both base circles and passes through the pitch point or point of tangency between the two pitch circles. Referring to [Figure 11.17](#), the line of action is tangent to the base circle of the internal gear at *C* and to the base circle of the pinion at *B*. If contact occurs between *B* and *C*, interference will result because the involute part of the pinion tooth does not cross the line of action until *B* is reached. Contact continues until point *A* is reached, where *A* is the intersection of the line of action with the addendum of the pinion. Therefore, the length of the line of action is *AB*, and the addendum of the gear should not extend beyond point *B*.

A different type of interference between the gear and pinion can also occur when the number of teeth on both gears varies only slightly. The interference is called fouling and it occurs at inactive profiles when the teeth of the pinion withdraw from the space of the gear. Potential sites for fouling are locations *a* and *b* in [Figure 11.18](#). To remove the potential for fouling, internal gears are usually cut with a shaper cutter that has two teeth fewer than the internal gear being cut. This automatically relieves the tips of the internal gear and eliminates the potential for fouling for any pinion with fewer teeth than the cutter [3].

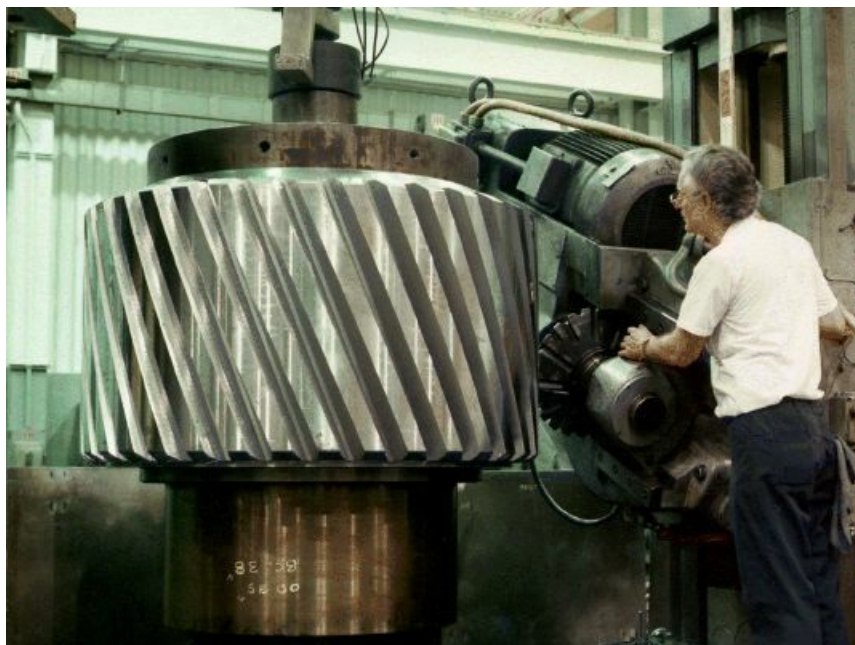


[Figure 11.18](#) Milling gear teeth using a formed cutter. For a given gear pitch, eight cutters are required to form gears with 12 or more teeth to a rack. Courtesy of Horsburgh & Scott Company, Cleveland, Ohio

Standard tooth proportions are not used for internal gears because the addendum of the gears must be shorter than those given in [Table 11.1](#) to avoid interference. However, the basic equations for circular and diametral pitch apply, and the contact ratio and angles of action can be determined in the same manner as for external gears.



11.9 Gear Manufacturing

Gear teeth can be formed in a large number of ways including various forms of casting: sand casting, investment casting, and die casting. They can be cut from flat stock using electron-discharge machining (EDM), CNC milling, and even precision sawing (and secondary machining or grinding). Gears made from polymers, aluminum, magnesium, and so on can be extruded and cut to width. Gears made from polymers can also be injection molded. Thin gears can be blanked from sheet stock.

Gears that must carry large loads relative to their overall size are usually made of high-strength materials such as steel. Some gears, such as bevel gears, can be forged; however, the vast majority of production gears are machined from blanks. Very small quantities can be machined using EDM, CNC milling, or horizontal milling with a formed cutter; however, when large volumes are involved, the machining is usually done with a generating cutter. In formed cutters, the tooth takes the exact shape of the cutter. Therefore, a separate cutter is technically required for each gear pitch and each number of teeth because the shape of the space between the teeth varies with both pitch and tooth number. In reality, the change in space is not significant in many cases. For a given pitch, only eight cutters are required to cut any gear in the range of 12 teeth to a rack with reasonable accuracy. However, such gears are usually not accurate enough for high speeds. A separate set of cutters is then required for each pitch [4]. [Figure 11.18](#) shows an example of milling using a formed cutter.

In a generating cutter, the tool has a shape different from the tooth profile, and the tool is moved relative to the gear blank to produce the desired gear shape.

When large volumes are involved, the fabrication of gears normally involves the following steps:

1. Blank fabrication
2. Forming of teeth
3. Refining of teeth
4. Heat treatment
5. Grinding, deburring, and cleaning
6. Finish coating

Blank fabrication involves all of the general and special features of the gear blank. This includes forming the hub and keyways. Tooth generation includes machining the gear teeth using one of the processes discussed below. The refining operations include shaving, grinding, burnishing, and lapping and are used to improve the accuracy of the gear teeth. These are necessary to remove machining marks and to improve the gear quality. The higher the gear quality, the greater the power rating and the lower the noise generated by meshing gear pairs. Heat treatment includes case hardening, which is necessary for high-performance gears to improve the resistance to surface pitting and tooth fracture. If heat treated, the gears must be reground if high accuracy is required. Deburring and cleaning are essential for all gears regardless of how they have been manufactured or the accuracy desired. Finish coatings include processes such as anodizing aluminum or depositing diamond films, but they may involve only grease or paint. The objective is to improve corrosion resistance, to reduce friction and wear, or simply to improve appearance.

Machining by shaping and hobbing are the most common methods of gear tooth generation. The objective is to slowly mesh a gear blank into a cutting tool that has teeth that will be conjugate with the teeth cut into the blank. The cutting action is always orthogonal to the side of the gear blank. In the shaping process, the cutter looks like a gear but is made of a much harder material (see [Figures 11.19](#) and [11.20](#)). When the gear is shaped, the reciprocating shaper cutter is moved radially into the blank until the pitch circle of the cutter and the gear blank are tangent. After each cutting stroke, the cutter is raised above the blank, and both the blank and the cutter roll a very small amount on their pitch circles. The process continues until all of the teeth are cut. Shaping is the main method used to produce internal gears and gears integral with a shaft that has a shoulder next to the gear.

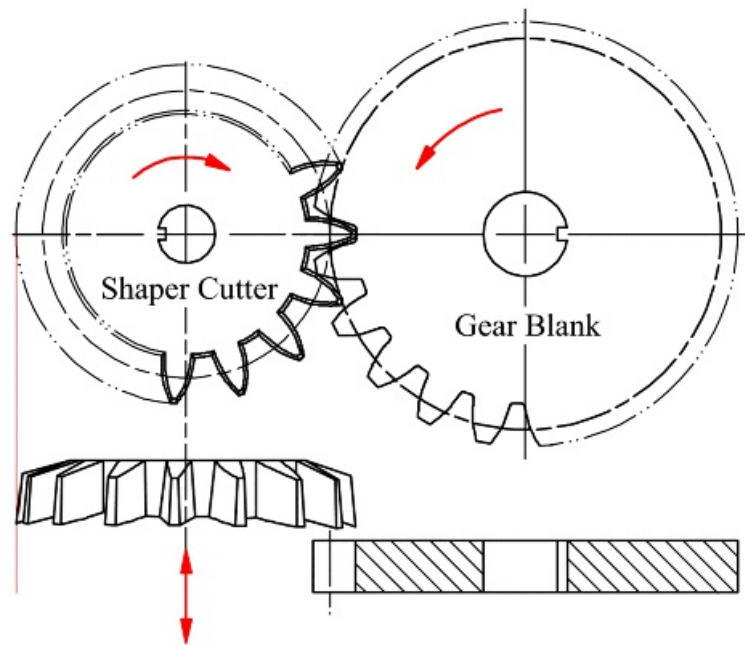


[Figure 11.19](#) Forming gear teeth with a shaper.

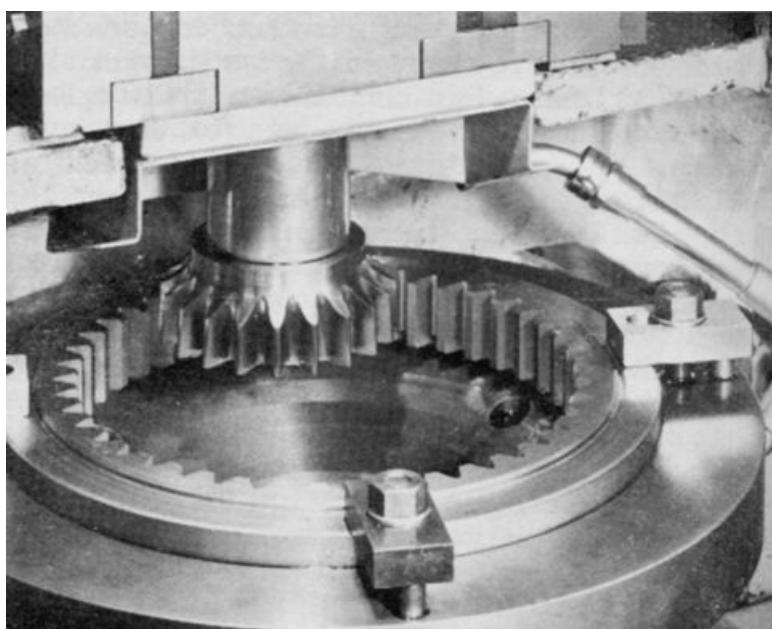


[Figure 11.20](#) Shaping an internal gear. Courtesy of Bourn & Koch, Rockford, Illinois

The shaping cutter can also be in the form of a rack. In this case, the pitch circle of the cutter is a straight line, and the cutter moves on a straight line tangent to the pitch circle of the gear. Relative to the gear, the pitch line of the rack appears to roll around the pitch circle of the gear. The gear teeth are formed by the envelope of the rack teeth as shown in [Figure 11.21](#).

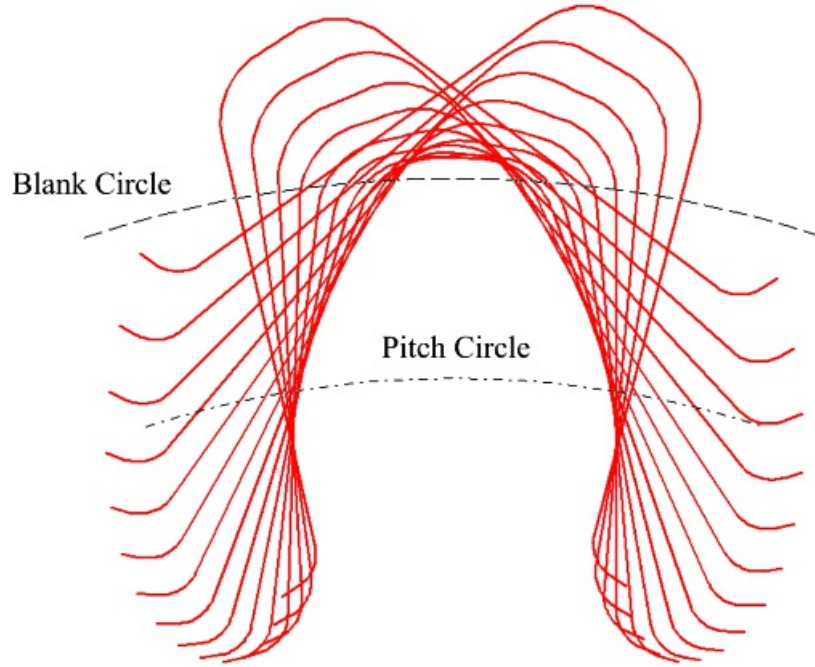


[Figure 11.21](#) Envelope of rack teeth relative to gear blank.

Hobbing is a method of generating gear teeth that is geometrically similar to generating the teeth with a rack cutter. The teeth of a hob are of the same shape as those on a rack cutter. However, the teeth are attached to a helical path on a cylindrical cutter. The hob looks like a worm gear with horizontal slices taken out of it. It is similar in appearance to a machine screw tap. The hob action is shown in [Figure 11.22](#), and a hobbing machine is shown in [Figure 11.23](#). In the hobbing machine, the hob teeth are aligned with the axis of the gear teeth. The hob and blank are rotated continuously at the proper angular velocity ratio, and the hob is fed slowly across the face of the width of the blank from one side to the other to form the teeth. The hobbing process is the most popular among the machining processes because it produces the most teeth in a given time and because the same tool can be used to cut helical as well as spur gear teeth. However, for internal gears, a gear shaper must be used.

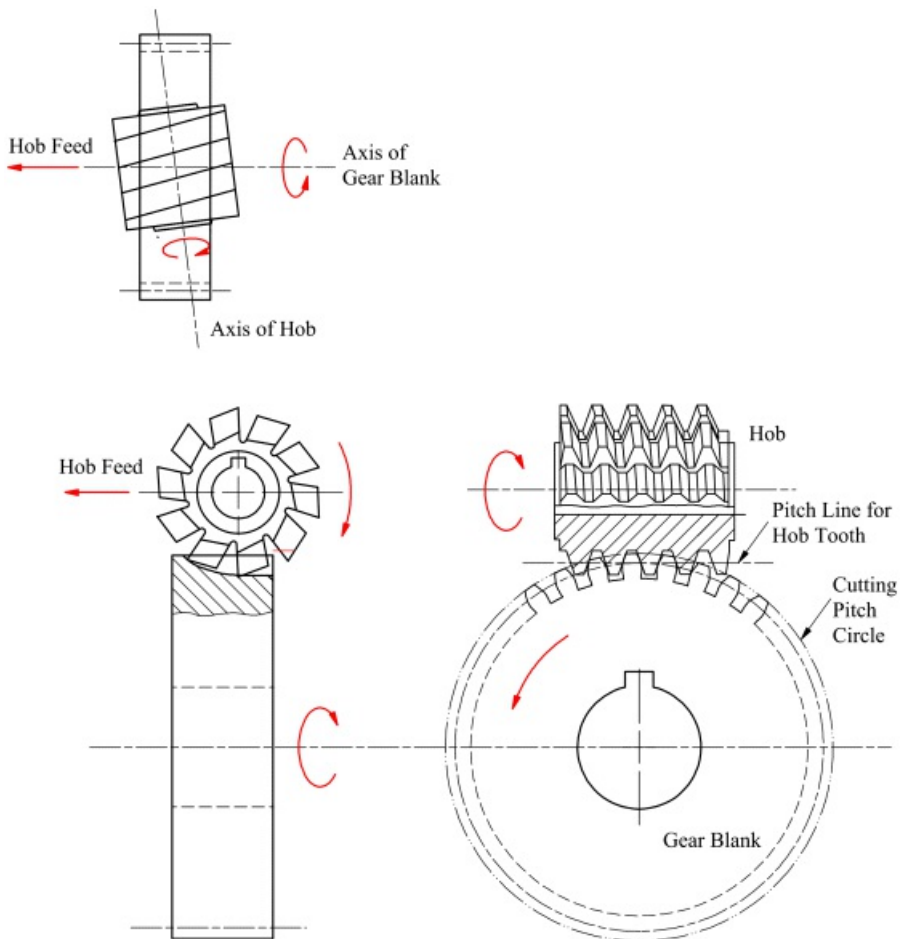
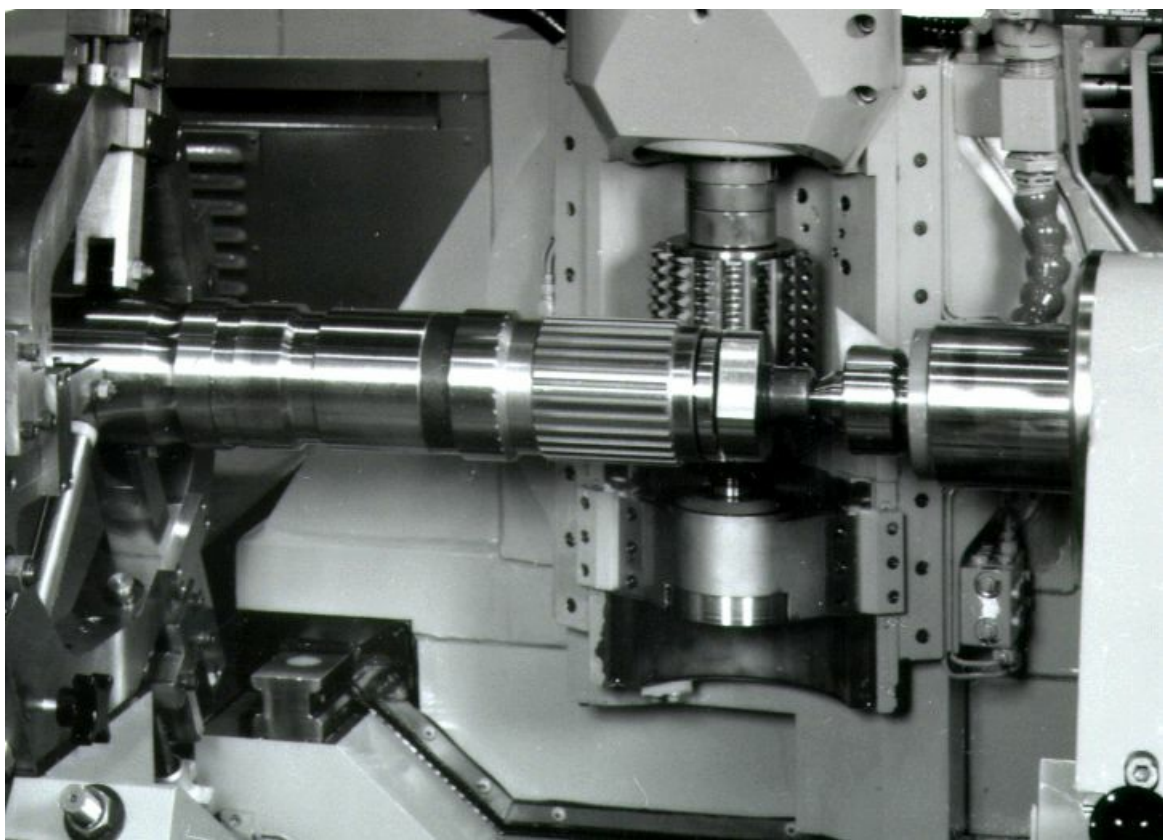


Figure 11.22 Tooth generation with hob.



[Figure 11.23](#) Hobbing spur gear teeth. Courtesy of Bourn & Koch, Rockford, Illinois



11.10 Interference and Undercutting

If the path of contact extends beyond the point of tangency with the base circle of the pinion, called the interference point, the tips of the teeth on the gear come into contact with portions of the pinion tooth profile inside the base circle. Because the involute is not defined inside the base circle, conjugate action is lost, and, in fact, the tips of the gear teeth will interfere with the lower portion of the pinion tooth flank if the tooth is machined with a formed cutter. If the pinion is generated with a rack-type cutter or hob, the cutter teeth will undercut the pinion teeth and weaken them. This situation is shown in [Figure 11.24](#). Thus, it is very undesirable to have the path of contact extend past the interference point.

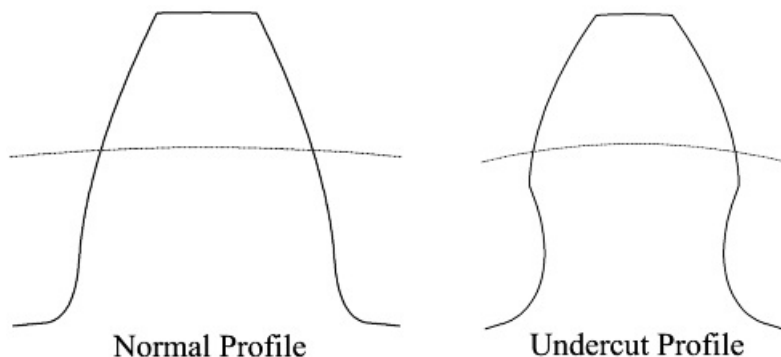


[Figure 11.24](#) Normal and undercut gears.

In [Figure 11.25](#), two gears are shown in mesh. The interference point on gear 2 is point *A* and that on gear 3 is point *D*. The addendum circle of gear 3 intersects the line of action at *B*, and the addendum circle of gear 2 intersects the line of action at *C*. If the addendum circle for gear 2 extends beyond point *D* or the addendum circle of gear 3 extends beyond point *A*, interference will occur. Actually, we need only investigate one of these conditions because, as indicated in [Figure 11.25](#), interference will always occur first on the smaller gear. Therefore, we need only check point *D*. In [Figure 11.25](#), if we visualize the pitch diameter of gear 2 becoming larger, point *C* will gradually move toward point *D*. Eventually, there will be a diameter that causes point *C* to move beyond point *D*, and interference will occur. If gear 2 is actually a shaper cutter, the material in the interference region will simply be removed. If, however, the teeth on gear 3 were formed by a smaller shaper cutter or cut directly, for example, by using a conforming milling cutter, then material might exist in the problem region. In that case, when gear 2 is meshed with gear 3, there will be volumetric interference, and the gear loads could be high enough to cause premature failure.

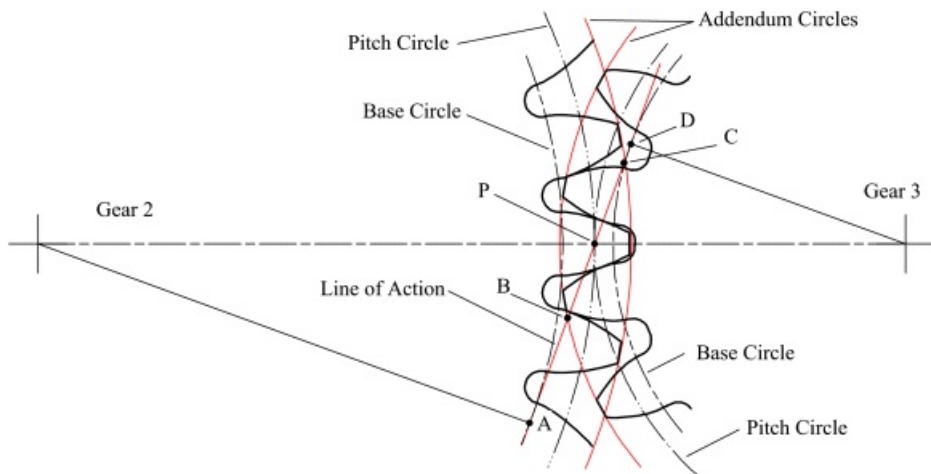


[Figure 11.25](#) Meshing conditions for two gears.

The worst case for interference or undercutting is when the pinion is meshed with a rack or generated with a rack cutter. This condition is shown in [Figure 11.26](#). Therefore, if we design the gear to avoid interference with a rack,

the gear will mesh with all other standard gears satisfying the criteria in Section 11.5.2. Undercutting becomes more severe as the number of teeth on the gear is reduced because for a given diametral pitch, the pitch diameter decreases when the number of teeth is reduced. As a result, there will be a critical number of teeth on the gear to just avoid undercutting. The minimum number of teeth to avoid undercutting can be determined by identifying when the addendum circle of the rack cutter extends beyond the interference point on the gear. This can be done using the simplified geometry in [Figure 11.27](#). Using that figure

$$v = \frac{r_p}{\sin \phi} = r_p \tan \phi$$

or

$$r_p = \frac{v}{\tan^2 \phi} \quad (11.25)$$

We may use k/P_d as the addendum for a standard gear, where k is a constant (1 for full-depth gears and 0.8 for stub tooth gears), and from [Equation 11.7](#)

$$2z_p = \frac{k}{P_d}$$

Substituting into [Equation 11.25](#) gives

$$N = \frac{2k}{\sin^2 \phi} \quad (11.26)$$

Results for some of the common pressure angles and systems are summarized in [Table 11.2](#). Note that the number of teeth must be a whole number for a continuously rotating gear. Also notice that the minimum number of teeth varies inversely with the pressure angle. Therefore, the minimum number of teeth for a $14\frac{1}{2}^\circ$ pressure angle is 32, while for a 20° pressure angle it is 18. This is one of the reasons why the $14\frac{1}{2}^\circ$ system is rarely used in modern machinery.

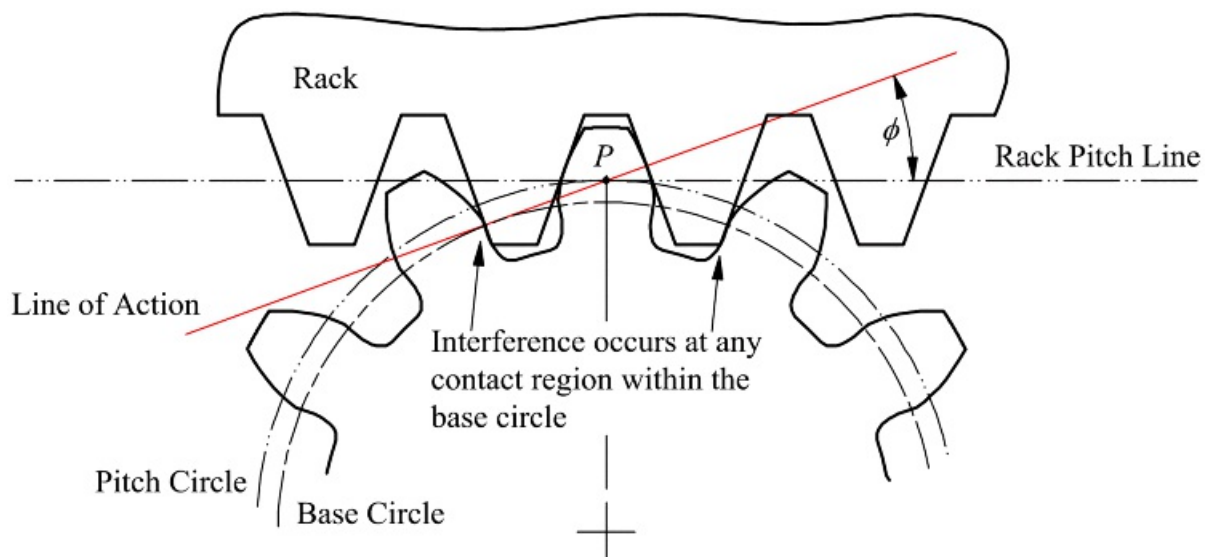


[Figure 11.26](#) Interference will occur at all contact locations within the base circle.

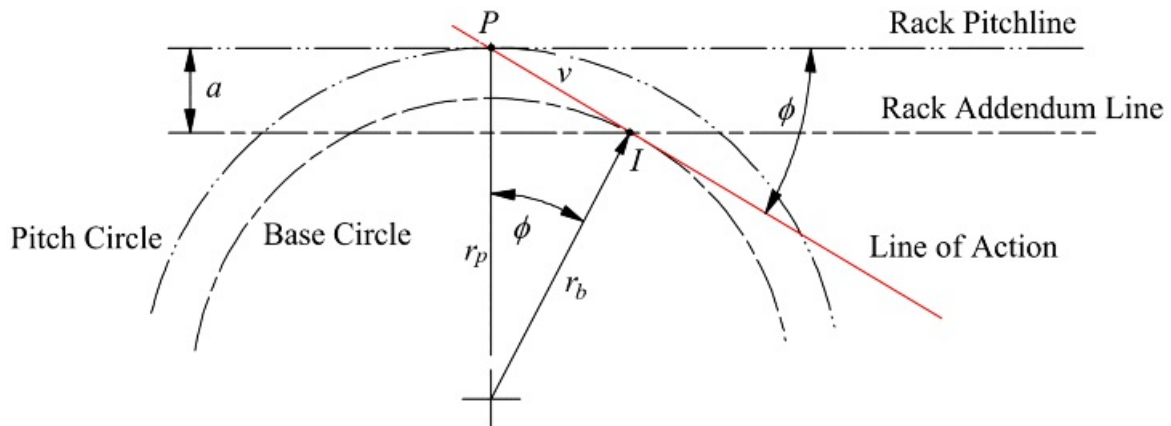


[Figure 11.27](#) Geometry for determining undercutting.

[Table 11.2](#) Minimum Number of Teeth to Avoid Undercutting for Standard Gears

System	Full Depth	Full Depth	Full Depth	Stub
ϕ	141°	20°	25°	20°
k	1	1	1	0.8
N	31.9	17.10	11.20	13.68
N_{\min}	32	18	12	14



11.11 Nonstandard Gearing

Sometimes, for reasons of saving space, the above minima are violated. Interference can still be avoided by offsetting the cutting rack so that the addendum line of the rack passes through the interference point or outside it. This requires a larger blank for the pinion. The net effect is to increase the addendum of the pinion and decrease its dedendum. The removal of undercutting is accompanied by other beneficial effects; the tooth shape is stronger and the contact ratio is improved. However, a nonstandard gear results.

Referring to [Figure 11.28](#), the cutter can be offset a distance e to bring the addendum line through the pitch point. This offset distance can be computed from

$$e = a + r_p \cos \phi - r_p \quad (11.27)$$

where ϕ is the cutting pressure angle and r_p is the cutting pitch radius. We can eliminate r_b from [Equation 11.27](#) using [Equation 11.5](#) and the expression $\sin^2 \phi + \cos^2 \phi = 1$. Then

$$e = a + r_p \cos^2 \phi - r_p = a - r_p \sin^2 \phi$$

The expression for the tooth thickness can be used to relate tooth thickness at any radius to the actual meshing pressure angle (ϕ_m)

$$\left. \begin{aligned} s_{m_2} &= 2r_{m_2} \left(\frac{t_2}{2r_2} + \operatorname{inv} \phi - \operatorname{inv} \phi_m \right) \\ s_{m_3} &= 2r_{m_3} \left(\frac{t_3}{2r_3} + \operatorname{inv} \phi - \operatorname{inv} \phi_m \right) \end{aligned} \right\}$$

where s_{m_2} and s_{m_3} are the thicknesses at the meshing pitch circle, and r_{m_2} and r_{m_3} are the meshing pitch radii.

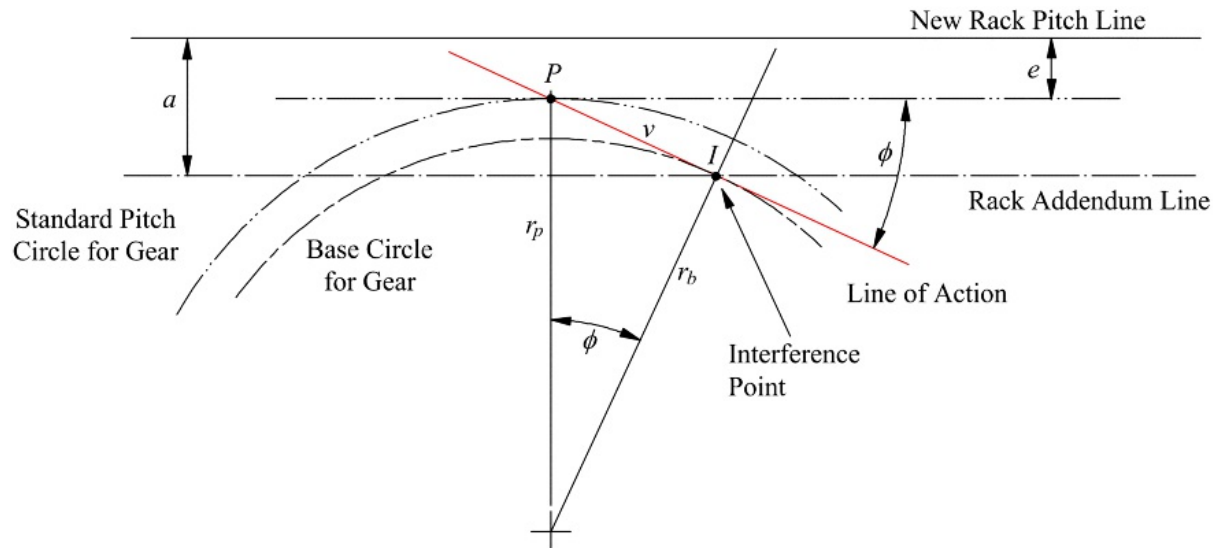


[Figure 11.28](#) Geometry for determining undercutting when the hob is withdrawn by an amount e .

Now

$$s_{m_2} + s_{m_3} = \frac{2\pi r_{m_2}}{N_2}$$

and

$$\frac{r_{m_2}}{r_{m_3}} = \frac{r_3}{r_2} = \frac{N_3}{N_2}$$

Therefore

$$s_{m_2} + s_{m_3} = 2r_{m_2} \left(\frac{s_2}{2r_2} + \text{inv } \phi - \text{inv } \phi_m \right) + 2r_{m_3} \left(\frac{s_3}{2r_3} + \text{inv } \phi - \text{inv } \phi_m \right)$$

gives

$$\frac{2\pi r_{m_2}}{N_2} = 2r_{m_2} \left(\frac{s_2}{2r_2} + \text{inv } \phi - \text{inv } \phi_m \right) + \frac{2N_3}{N_2} r_{m_3} \left(\frac{s_3}{2r_3} + \text{inv } \phi - \text{inv } \phi_m \right)$$

or

$$\frac{2\pi}{N_2} = \frac{s_2 + s_3}{r_2} + \frac{2(N_3 - N_2)}{N_2} (\text{inv } \phi - \text{inv } \phi_m)$$

giving

$$\text{inv } \phi_m = \text{inv } \phi - \frac{2\pi r_2 \cdot N_2 (s_2 + s_3)}{2r_2 (N_2 + N_3)}$$

(11.28)

This equation permits computation of ϕ_m given the cutting pitch radius, r_2 , of the gear, the cutting pressure angle, ϕ , the tooth numbers, N_2 and N_3 , the tooth thickness, s_2 , at the cutting pitch circle of the gear, and the tooth thickness, s_3 , of the pinion at the cutting pitch radius.

Table 11.3 Minimum Values of Addendum for Unequal Addendum and Dedendum Gears to Avoid Undercutting^a

Number of Pinion Teeth	AGMA 20-Degree Coarse-Pitch System		Minimum Number of Gear Teeth	AGMA 20-Degree Fine Pitch System		Minimum Number of Gear Teeth
	a_P	a_G		a_P	a_G	
7	1.4143 ^b	0.4094	42
8	1.43669 ^b	0.4679	39
9	1.4190 ^b	0.5264	36
10	1.468	0.532	25	1.4151	0.5849	33

11	1.409	0.591	24	1.3566	0.6434	30
12	1.351	0.649	23	1.2982	0.7019	27
13	1.292	0.708	22	1.2397	0.7604	25
14	1.234	0.766	21	1.1812	0.8189	23
15	1.117	0.825	20	1.1227	0.8774	21
16	1.117	0.883	19	1.0642	0.9358	19
17	1.058	0.942	18	1.0057	0.9943	18
18	1.000	1.000	18	1.0000	1.0000	

^aThe values in this table are for one diametral pitch; divide them by the desired diametral pitch to obtain the addendum.

^bNot proportional to the increase in tooth thickness; a reasonable top land must be provided.

Referring to [Figure 11.29](#)

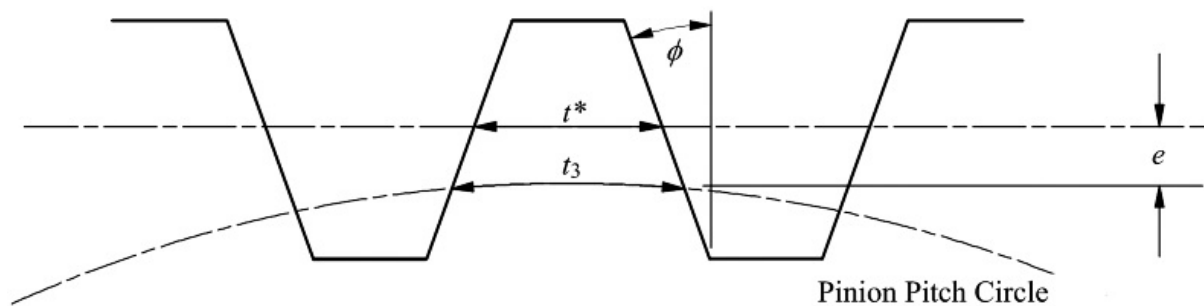


[Figure 11.29](#) Cutting nonstandard pinion.

$$t_3 = t^* + 2e \tan \phi$$

and

$$t^* = \frac{P_d}{2} = \frac{s}{2P_d}$$

Hence

$$t_3 = \frac{s}{2P_d} + 2e \tan \phi \quad (11.29)$$

but

$$s = e - r_3 \sin^2 \phi$$

or

$$s = \frac{1}{P_d} - \frac{N_3}{2P_d} \sin^2 \phi \quad (11.30)$$

The equations for spur tooth gearing are summarized in [Table 11.4](#).



Example 11.4 Computing Nonstandard Gear Geometry

A 13-tooth pinion with diametral pitch 6 and 20° cutting pressure angle is to mate with a 50-tooth gear. Find the center distance and meshing pressure angle if the pinion is cut with a standard cutter offset so that the addendum line passes through the interference point. (Compare the center distance with the corresponding value for a standard pinion.)

Solution

From [Equation 11.30](#)

$$e = \frac{1}{P_d} - \frac{N_2}{2P_d} \sin^2 \phi = \frac{1}{6} - \frac{13}{2 \times 6} \sin^2 20^\circ = 0.03994$$

From [Equation 11.29](#)

$$s_2 = \frac{\pi}{2P_d} + 2e \tan \phi = \frac{\pi}{2 \times 6} + 2 \times 0.03994 \tan 20^\circ = 0.25037$$

From [Equation 11.7](#)

$$r_2 = \frac{N_2}{2P_d} = \frac{50}{2 \times 6} = 4.1667$$

and from [Table 11.1](#)

$$s_2 = \frac{2\pi r_2}{2N_2} = 0.26180$$

From [Equation 11.28](#)

$$\text{inv } \phi_m = \text{inv } \phi - \frac{2\pi r_2 - N_2(s_2, s_3)}{2r_2(N_2 + N_3)} = \text{inv } 20^\circ - \frac{2\pi \times 4.1667 - 50(0.25037 + 0.26180)}{2 \times 4.1667(50 + 13)} = 0.017873$$

To find the value for ϕ_m , it is possible to use tables [4] or the value can be found using a simple program. A MATLAB function, *inverse_inv(y)*, is available with the supplementary material for this book for doing this. The result is

$$\phi_m = 21.127^\circ$$

Next use [Equation 11.5](#) to compute

$$r_{2e} = \frac{r_2}{\cos \phi_m} = \frac{r_2 \cos \phi}{\cos \phi_m} = 4.1975$$

and

$$r_{3e} = \frac{r_3}{\cos \phi_m} = \frac{r_3 \cos \phi}{\cos \phi_m} = \frac{N_3 \cos \phi}{2P_d \cos \phi_m} = \frac{13 \cos 20^\circ}{2 \times 5 \times \cos 21.127^\circ} = 1.0914 \text{ in}$$

The meshing center distance is

$$C_m = 4.1975 + 1.0914 = 5.2889 \text{ in}$$

The standard center distance

$$C_s = r_2 + r_3 + r_2 + \frac{N_2}{2P_d} = 4.1975 + \frac{13}{2 \times 6} = 5.2500 \text{ in}$$

Table 11.4 Summary of Spur Gear Formulas

Quantity	Formula
Diametral pitch	$P_d = \frac{d}{z_p} = \frac{d}{z_c} = \frac{s}{z_c}$
Circular pitch	$p_c = \frac{s}{z_c} = \frac{\pi d_p}{N} = \pi m = \frac{p_b}{\cos \phi} = \frac{\pi d_b}{N \cos \phi}$
Base pitch	$p_b = \frac{\pi d_b}{N} = p_c \cos \phi = \frac{\pi d_b \cos \phi}{N}$
Module	$m = \frac{d_p}{N} = \frac{1}{p_d} = \frac{s}{z_c}$
Tooth thickness at pitch circle	$t = \frac{s_c}{2} = \frac{s}{2P_d} = \frac{\pi d_p}{2N} = \frac{p_c}{2} = \frac{p_b}{2 \cos \phi} = \frac{\pi d_b}{2N \cos \phi}$
Pitch diameter	$d_p = \frac{d}{z_p} = \frac{\pi d_b}{\cos \phi} = Nm$
Outside diameter	$d_o = d_p + 2a$ (typically $a = k/P_d$ where $k = 1$ or 0.8)
Root diameter	$d_r = d_p - 2b$ (typically $b = q/P_d$ where $q = 1.25, 1.2$, or 1)
Base circle diameter	$d_b = d_p \cos \phi$
Center distance	$C = r_{p1} + r_{p3} = \frac{d_{p1} + d_{p3}}{2} = \frac{N_1 + N_3}{2} = \frac{z_c (M_2 + M_3)}{2\pi}$
Length of line of contact	$\lambda = \sqrt{(r_{p1} - a_2)^2 + r_{p1}^2 \cos^2 \phi} = r_{p1} \sin \phi$ $= \sqrt{(r_{p3} - a_2)^2 + r_{p3}^2 \cos^2 \phi} = r_{p3} \sin \phi$
Contact ratio	$\kappa_{bc} = \frac{\lambda}{p_b} = \frac{\lambda}{p_c \cos \phi} = \frac{\lambda s_d}{\pi \cos \phi}$
Velocity ratio	$R = \frac{\omega_1}{\omega_3} = \frac{r_{p1}}{r_{p3}} = \frac{d_{p1}}{d_{p3}} = \frac{N_1}{N_3}$
Tooth thickness at radius r	$t = 2r \frac{t_p}{2r_p} = 2r \sin \phi = 2r \sin \beta; \cos \beta = \frac{r_b}{r} = \frac{r_p \cos \phi}{r}$
Involute function	$\text{inv } \phi = \text{inv } \hat{\phi} - \hat{\phi}$
No. of teeth at undercutting	$N_u = \frac{2\pi s_d}{\text{inv } \phi}$
Hob withdrawal for no undercutting	$\varepsilon = \frac{1}{z_c} - \frac{N_3 \sin^2 \phi}{2r_p \cos \phi}$



11.12 Cartesian Coordinates of an Involute Tooth Generated with a Rack

It is often desirable to know the coordinates of the tooth profile for a given generating rack. This is of interest for drawing the gear or for machining the gear on a standard CNC milling machine without form cutters. If only the involute portion is required, it is relatively easy to compute the coordinates of points on the gear contact surface. However, if the entire profile is desired, the procedure is considerably more difficult. The problem can be approached directly if the geometry of the rack is known analytically [5,6]. However, an indirect approach developed by Vijayakar [7] is more general and applicable to a wide range of gear generators. This approach, which is relatively easy to program, is given here. The data required to generate the gear are a description of the rack, the number of teeth on the gear, and the outer diameter of the gear.

11.12.1 Coordinate Systems

[Figure 11.30](#) shows a coordinate system attached to the rack that is assumed to be fixed. The origin of the system is at the intersection of the centerline of a rack tooth and the pitch line of the rack. The coordinates of any point P on the surface of the rack can be defined by (x_r, y_r) relative to the coordinate system fixed to the rack. Also, the outer normal to the rack at this point can be represented by (n_x, n_y) . For any specified rack geometry, the coordinates and outer normal at any point on the rack profile are easily obtained.

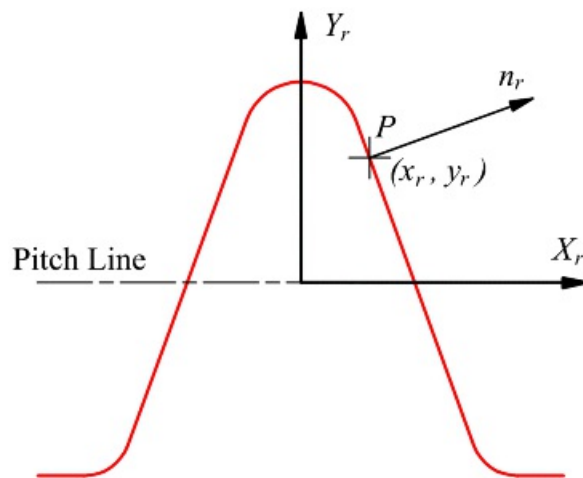


[Figure 11.30](#) Rack and its attached coordinate system.

[Figure 11.31](#) shows a gear tooth with an attached coordinate system with its origin at the center of the gear. Let point P' be a point on the gear profile that corresponds to point P on the rack. As the gear pitch circle rolls on the rack pitch line, the point P on the rack makes sliding (cam) contact with the point P' on the gear.

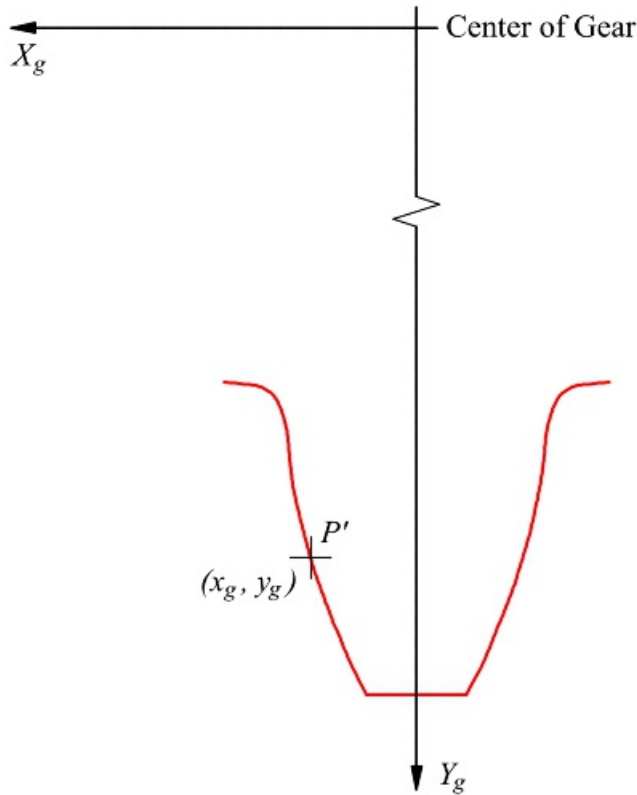


[Figure 11.31](#) Gear and its attached coordinate system.

[Figure 11.32](#) shows the relative position of the gear and rack after the gear has rolled through the angle ϕ . The pitch circle radius of the gear is r_p . For this arbitrary orientation of the gear, the transformation from the rack coordinate system to the gear coordinate system is defined by the matrix equation

$$\begin{Bmatrix} x_g \\ y_g \end{Bmatrix} = \begin{bmatrix} -\cos \phi & \sin \phi \\ -\sin \phi & -\cos \phi \end{bmatrix} \begin{Bmatrix} x_r - r_p \phi \\ y_r - r_p \end{Bmatrix} \quad (11.31)$$

As the gear rolls, the relative velocity of the point P' on the gear with respect to the rack (fixed system) is given by

$$\dot{v}_{P'} = \dot{v}_{B/C} + \dot{v}_{F'/R}$$

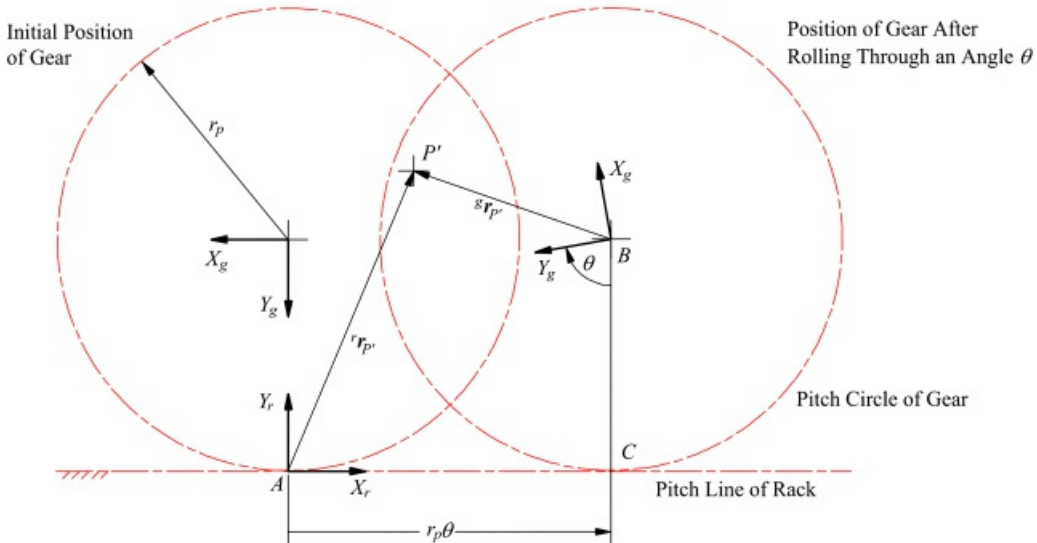


Figure 11.32 Relative orientation of gear and rack coordinate systems during generation.

Recognizing that C is the instant center between the gear and the rack and points P' , A , B , and C are all fixed to the gear

$$v_{P'} = \omega_g \times r_{B/C} + \omega_g \times r_{P'/B} = \omega_g \times (r_{B/C} + r_{P'/B}) = \omega_g \times r_{P'/C}$$

where ω_g is the angular velocity of the gear relative to the rack. In matrix form, this equation becomes

$$v_{P'} = -\omega_g \begin{Bmatrix} y_r \\ r_g \theta - x_r \end{Bmatrix}$$

Because cam contact is involved at the contact point (assumed to be P'), the relative velocity of the point on the gear should have no component normal to the rack. Hence the dot product between the normal and $v_{P'}$ must be zero. Then

$$v_{P'} \cdot \begin{Bmatrix} n_x \\ n_y \end{Bmatrix} = 0$$

or

$$-n_x y_r + (x_r - r_g \theta) n_y = 0$$

The roll angle for the gear at which the point P makes contact with a point on the gear is given by

$$\phi = \frac{x_y n_y - x_n y_s}{r_p n_y} \quad (11.32)$$

Given any point P on the rack, its coordinates, and its normal vector, the roll angle at which it makes contact with the gear can be computed using [Equation 11.32](#). The coordinates of the corresponding point P' on the gear can be obtained by substituting for ϕ in [Equation 11.31](#). Therefore, a sequence of points on the gear profile can be found that corresponds to a sequence of points on the rack profile.

The procedure is to begin with points at the tip of the rack tooth and to sequence through the points until the corresponding points on the gear are located beyond the addendum circle. If r_o is the outer radius of the gear, the extreme points are reached when the coordinates given in [Equation 11.31](#) satisfy the inequality

$$\sqrt{x_g^2 + y_g^2} \geq r_o$$

Before drawing the gear tooth profile, it is necessary to check for undercutting. If undercutting occurs, the tooth profile generated using the foregoing procedure will look like that shown in [Figure 11.33](#). The part $B-C-D-B$ must be detected, and the parts associated with this region eliminated from the sequence of points used to define the gear profile.

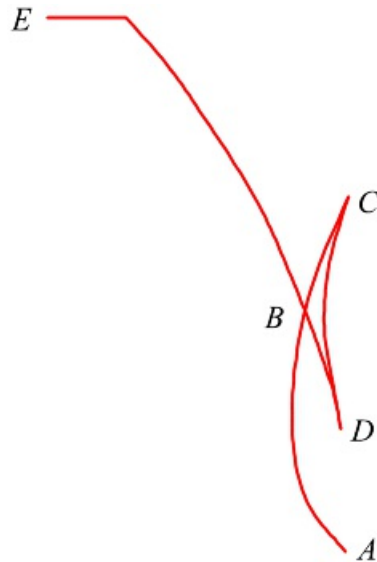


[Figure 11.33](#) Gear profile with undercutting.

Let $r_i; i = 1, 2, \dots, n$ be a sequence of vectors corresponding to the points on the gear tooth profile. To detect the cross-over point B shown in [Figure 11.33](#), we need to check whether there are integers i and j such that the line segment $(i, i+1)$ that joins r_i with r_{i+1} intersects the line segment $(j, j+1)$. [Figure 11.34](#) shows two line segments (a, b) and (c, d) . These line segments will intersect if and only if [6]

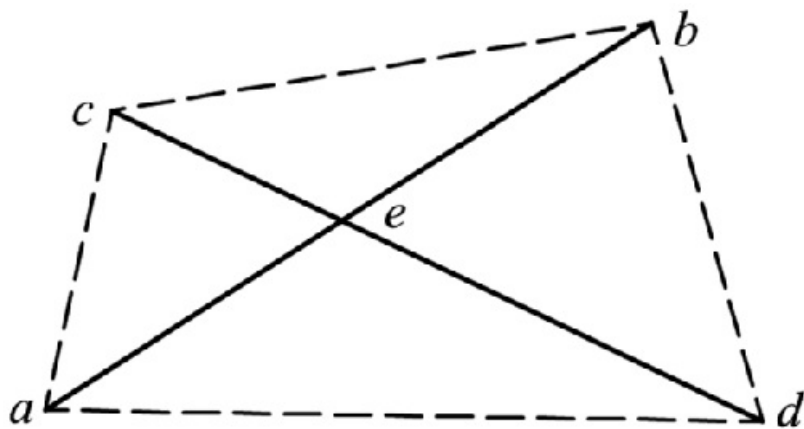


[Figure 11.34](#) Determination of the point of intersection of two line segments.

$$A(c, b, e) \cdot A(a, b, d) < 0$$

and

$$A(c, d, a) \cdot A(c, d, b) < 0$$

where

$$A(a, b, c) = (r_b - r_a) \times (r_c - r_a)$$

and

$$r_a = \begin{Bmatrix} x_a \\ y_a \\ 0 \end{Bmatrix}, r_b = \begin{Bmatrix} x_b \\ y_b \\ 0 \end{Bmatrix}, r_c = \begin{Bmatrix} x_c \\ y_c \\ 0 \end{Bmatrix}, \text{ and } r_d = \begin{Bmatrix} x_d \\ y_d \\ 0 \end{Bmatrix}$$

The location of the point of intersection will be given by r_e where

$$r_e = \alpha r_a + (1 - \alpha)r_b$$

where

$$\alpha = \frac{|A(c, d, b)|}{|A(c, d, a)| + |A(c, d, b)|}$$

Using this method, the whole profile can be searched for segments $(i, i+1)$, $i = 1, 2, \dots, n-2$ and $(j, j+1)$, $j = i+1, i+2, \dots, n-1$ that intersect. If such an i and j are found, then all points on the profile between $i+1$ and $j+1$ are discarded and replaced by the single point r_e at the point of intersection.

11.12.2 Gear Equations

Once the set of points is defined for the single tooth, this set of coordinates can be rotated in increments of $2\pi/N$ to form the other teeth. If θ is the rotation angle, the coordinates (X_i, Y_i) of successive teeth are related to the original coordinates (x_i, y_i) by

$$\begin{aligned} X_i &= x_i \cos \theta - y_i \sin \theta \\ Y_i &= x_i \sin \theta + y_i \cos \theta \end{aligned}$$

The rotation angle is incremented for each tooth to be drawn. For example, for the first tooth, $\theta = 0$; for the second tooth, $\theta = 2\pi/N$; for the third tooth, $\theta = 4(2\pi/N)$; and for the j th tooth, $\theta = (j-1)(2\pi/N)$. A MATLAB routine for drawing the rack, gear tooth, and gear is provided with the supplementary material with this book.



Example 11.5 Geometry of Simple Rack

Half of the tooth for a standard rack is represented in [Figure 11.35](#). Determine the equations for each region and the equations for the corresponding normal vectors.

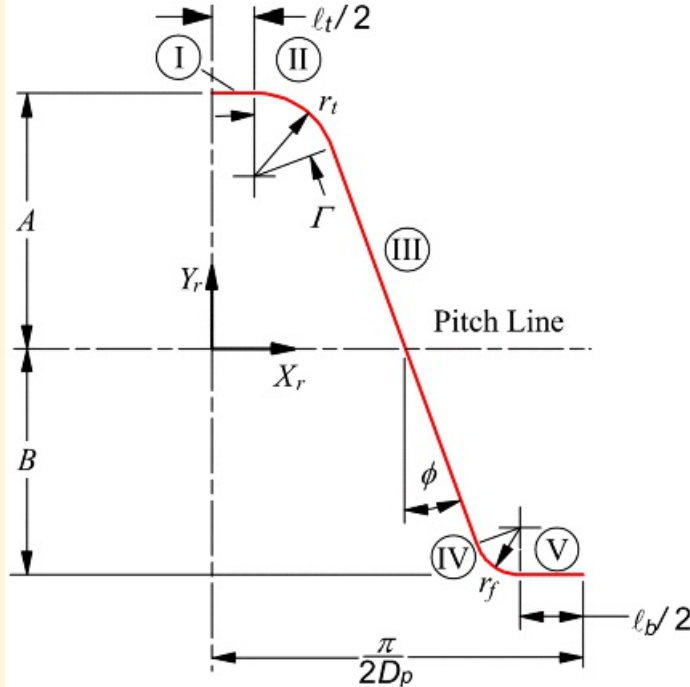


[Figure 11.35](#) Geometry of a basic rack.

Solution

Before developing the equations for the different regions, define the following terms

D_p	= diametral pitch
A	= addendum of rack
B	= dedendum of rack
ϕ	= pressure angle
r_t	= radius of tip of rack tooth
r_f	= radius of fillet of rack tooth

Miscellaneous terms can be computed based on geometry to be

$$\begin{aligned} \Gamma &= \frac{\pi}{2} - \phi \\ \ell_t &= \frac{\pi}{2D_p} - 2A \tan \phi - 2r_t \tan\left(\frac{\pi}{2}\right) \\ \ell_b &= \frac{\pi}{2D_p} - 2B \tan \phi - 2r_f \tan\left(\frac{\pi}{2}\right) \end{aligned}$$

It is assumed that the maximum radius, r_p , at the tip of the rack is a full radius that occurs when ℓ_t is zero.

Then, the maximum tip radius is

$$r_t = \frac{\frac{\kappa}{2D_p} - 2A \tan \phi}{2 \tan\left(\frac{\Gamma}{2}\right)}$$

Similarly, it is assumed that the maximum radius, r_b , at the fillet of the rack is a full radius that occurs when β_b is zero. Then, the maximum fillet radius is

$$r_f = \frac{\frac{\kappa}{2D_p} - 2B \tan \phi}{2 \tan\left(\frac{\Gamma}{2}\right)}$$

The coordinates of the points and normal vectors along the rack profile in each region are given by

Region I (top land)

$$\begin{Bmatrix} x_r \\ y_r \end{Bmatrix} = \begin{Bmatrix} \beta\zeta/2 \\ A \end{Bmatrix}; \quad \begin{Bmatrix} n_x \\ n_y \end{Bmatrix} = \begin{Bmatrix} 0 \\ 1 \end{Bmatrix} \quad 0 < \beta \leq 1$$

Region II (tip radius)

$$\begin{Bmatrix} x_r \\ y_r \end{Bmatrix} = \begin{Bmatrix} \ell_t/2 + r_t \sin(\beta \Gamma) \\ A - r_t [1 - \cos(\beta \Gamma)] \end{Bmatrix}; \quad \begin{Bmatrix} n_x \\ n_y \end{Bmatrix} = \begin{Bmatrix} \sin(\beta \Gamma) \\ \cos(\beta \Gamma) \end{Bmatrix} \quad 0 < \beta \leq 1$$

Region III (tooth flank)

$$\begin{Bmatrix} x_r \\ y_r \end{Bmatrix} = \begin{Bmatrix} ((1-\beta)[\ell_t/2 + r_t \sin(1)] + \beta[\kappa/(2D_p) - \ell_b/2 - r_f \sin(1)]) \\ (1-\beta)[A - r_t(1 - \cos(\Gamma))] + \beta[-B + r_f(1 - \cos(\Gamma))] \end{Bmatrix};$$

$$\begin{Bmatrix} n_x \\ n_y \end{Bmatrix} = \begin{Bmatrix} \cos \phi \\ \sin \phi \end{Bmatrix} \quad 0 < \beta \leq 1$$

Region IV (root fillet)

$$\begin{Bmatrix} x_r \\ y_r \end{Bmatrix} = \begin{Bmatrix} \kappa/(2D_p) - \ell_b/2 - r_f \sin[(1-\beta)\Gamma] \\ -B + r_f[1 - \cos[(1-\beta)\Gamma]] \end{Bmatrix}; \quad \begin{Bmatrix} n_x \\ n_y \end{Bmatrix} = \begin{Bmatrix} \sin[(1-\beta)\Gamma] \\ \cos[(1-\beta)\Gamma] \end{Bmatrix} \quad 0 < \beta \leq 1$$

Region V (bottom land)

$$\begin{Bmatrix} x_r \\ y_r \end{Bmatrix} = \begin{Bmatrix} \kappa/(2D_p) - \ell_b/2(1-\beta) \\ -B \end{Bmatrix}; \quad \begin{Bmatrix} n_x \\ n_y \end{Bmatrix} = \begin{Bmatrix} 0 \\ 1 \end{Bmatrix} \quad 0 < \beta \leq 1$$



Example 11.6 Generation of Gear

Assume that the rack in Example 11.5 is used to generate a gear. The pressure angle is 20° with a diametral pitch (D_p) of 10 teeth per inch. The tip and root radii are both 0.01 in. The addendum constant for the rack is 1.25, and the dedendum constant is 1.1. There are 15 teeth on the gear, and the addendum constant for the gear is 1.0. Determine the shape of the gear tooth.

Solution

Because of the number of calculations required to solve the problem, it is efficient to program the equations given in Example 11.5. This was done using the program *geardr.m* provided with the supplementary material with this book. The hob profile (half of a tooth) is shown in [Figure 11.36](#), and the tooth and gear profiles are shown in [Figures 11.37](#) and [11.38](#). Notice that the gear is undercut.

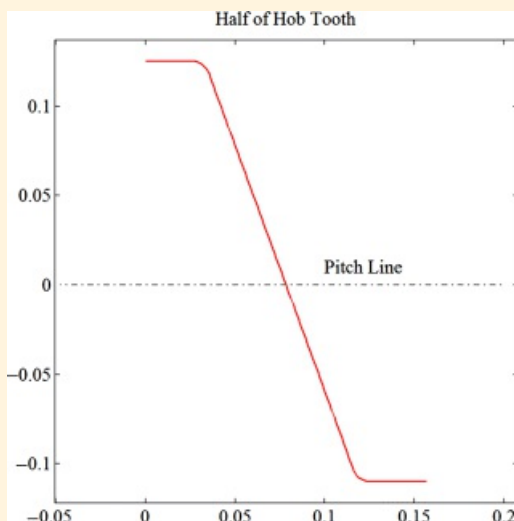


[Figure 11.36](#) Profile of half of a hob tooth.

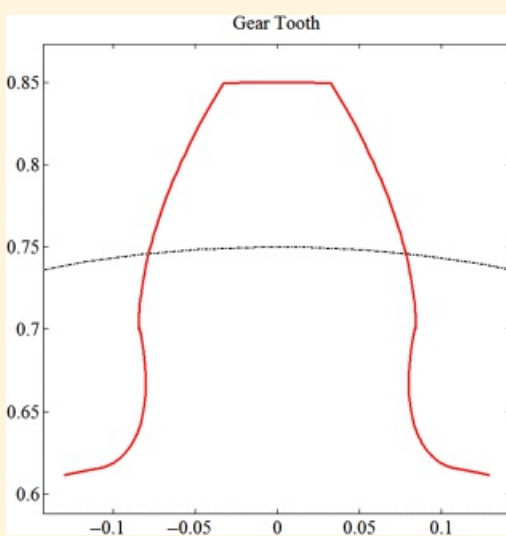


[Figure 11.37](#) Generated gear tooth.

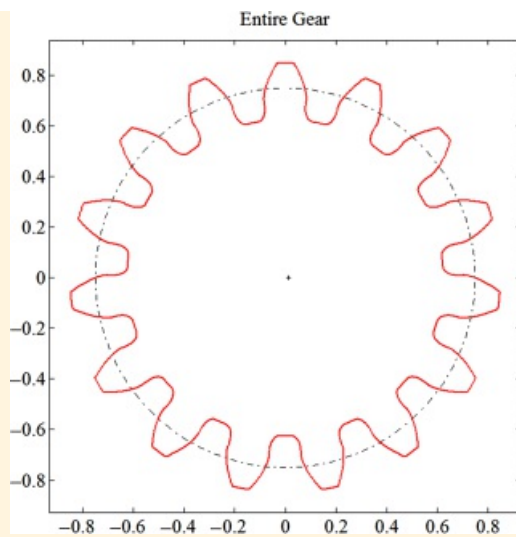


[Figure 11.38](#) Profile of generated gear.



References

1. Dudley, D.W. (1984). *Handbook of Practical Gear Design*. New York, NY: McGraw-Hill.
2. American Gear Manufacturers' Association (AGMA). (1968). "Tooth Proportions for Coarse Pitch Involute Spur Gears." AGMA Publication 201.02 and 201.02A.
3. Mabie, H. H., and Ocvirk, F. W. (1975). *Mechanisms and Dynamics of Machinery*, 3rd Ed. New York, NY: John Wiley & Sons.
4. Shigley, J. E. (1975). *Kinematic Analysis of Mechanisms*. New York, NY: McGraw-Hill.
5. Kinzel, G. L., and Farley, D. M. (1983). "A Computer Approach to the Generation of Conjugate Tooth Forms." *Proceedings of the Sixth IFToMM Congress on Theory of Machines and Mechanisms*, New Delhi, December 15–20, pp. 778–782.
6. Mitchiner, R. G., and Mabie, H. H. (1982). "The Determination of the Lewis Form Factor and the AGMA Geometry Factor J for External Spur Gear Teeth." *Transactions of ASME*, Vol. 104, January, pp. 148–158.
7. Vijayakar, S. (1987). *Finite Element Methods for Quasi-Prismatic Bodies with Application to Gears*. PhD dissertation, The Ohio State University.



Problems

11.1 Two spur gears have a diametral pitch of 6. Gear 2 has 24 teeth and gear 3 has 48. The working pressure angle is 20° , and both gears are standard involutes. Determine the length of the contact line and the contact ratio.

11.2 For the gear pairs given below and meshing at their correct center-to-center distance, determine whether any interference is present and determine the contact ratio for each case. Assume that the addendum is $1/P_d$ in each case, and if any interference is present, assume the interference is removed by cutting off the ends of the gear teeth before determining the contact ratio.

- a. $14\frac{1}{2}^\circ$ involute gears having 30 and 45 teeth
- b. 20° involute gears having 20 teeth and a rack
- c. 25° involute gears having 30 and 60 teeth

11.3 A 20° involute pinion having 30 teeth is meshing with a 60-tooth internal gear. The addendum of the pinion is $1.25/P_d$, and the addendum of the gear is $1/P_d$. Is there any interference? Determine the contact ratio. If there is interference, assume that the interfering portion is removed by cutting off the ends of the teeth.

11.4 What is the largest gear that will mesh with a 20° standard full-depth gear of 22 teeth with no interference?

11.5 What is the smallest gear that will mesh with a 20° standard full-depth gear of 22 teeth with no interference?

11.6 Assume a gear has a diametral pitch of 6. Determine the addendum, dedendum, and clearance if the pressure angle is 20° full depth, 25° full depth, 20° stub teeth.

11.7 Assume two meshing gears have a diametral pitch of 6 and a 20° pressure angle. The gear has 38 teeth, and the pinion has 24. Determine the design center distance. Now assume that the center distance is increased by 0.01 in. Determine the pressure angle for the new center distance.

11.8 Assume a standard full-depth rack has a diametral pitch of 2. Determine the smallest gear that will mesh with the rack without interference if the pressure angle is: (a) 20° , (b) 25° .

11.9 Assume two meshing gears have a diametral pitch of 8 and a 25° pressure angle. The gear has 60 teeth and the pinion has 30. Determine the design center distance. Now assume that the center distance is increased by 0.012 in. Determine the pressure angle for the new center distance.

11.10 Two standard gears have a diametral pitch of 2 and a pressure angle of $14\frac{1}{2}^\circ$. The tooth numbers are 14 and 16. Determine whether interference occurs. If it does, compute the amount that the addendum(s) must be shortened to remove the interference and the new contact ratio.

11.11 Two standard gears have 18 and 32 teeth, respectively. The diametral pitch is 10, and the pinion rotates at 1000 rpm. Determine the following: (a) center distance, (b) pitch diameters, (c) circular pitch, (d) pitch line velocity, (e) angular velocity of the gear.

11.12 Two standard gears have a diametral pitch of 10 and a velocity ratio of 2.5. The center distance is 3.5 in. Determine the number of teeth on each gear.

11.13 Is it possible to specify arbitrary values for the velocity ratio, center distance, and diametral pitch in a problem such as that given in Problem 11.12? Explain.

11.14 Two standard meshing gears are to have 9 and 36 teeth, respectively. They are to be cut with a 20° full-depth cutter with a diametral pitch of 3. (a) Determine the amount that the addendum of the gear is to be shortened to eliminate interference. (b) If the addendum of the pinion is increased the same amount, determine the new contact ratio.

11.15 Two standard meshing gears are to have 13 and 20 teeth, respectively. They are to be cut with a 20° full-depth cutter with a diametral pitch of 2. To reduce interference, the center distance is increased by 0.1 in. Determine the following:

- a. Whether the interference is completely eliminated
- b. The pitch diameters of both gears
- c. The new pressure angle
- d. The new contact ratio

11.16 Assume that you have a 13-tooth pinion and a 50-tooth gear. What is the smallest (nonstandard) pressure angle that can be used if interference is to be avoided? What is the smallest pressure angle that can be used if only standard pressure angles can be considered?

11.17 A standard, full-depth spur gear has a pressure angle of 25° and an outside diameter of 225 mm. If the gear has 48 teeth, find the module and circular pitch.

11.18 The pinion of a pair of spur gears has 16 teeth and a pressure angle of 20° . The velocity ratio is to be 3:2, and the module is 6.5 mm. Determine the initial center distance. If the center distance is increased by 3 mm, find the resulting pressure angle.

11.19 Two standard, full-depth spur gears are to have 10 teeth and 35 teeth, respectively. The cutter has a 20° pressure angle with a module of 10 mm. Determine the amount by which the addendum of the gear must be reduced to avoid interference. Then determine the length of the new path of contact and the contact ratio.

11.20 A standard, full-depth spur gear tooth has been cut with a 20° hob and has a diametral pitch of 6. The tooth thickness at a radius of 2.1 in is 0.1860 in. Determine the thickness of the gear tooth at the base circle.

11.21 A pair of standard, full-depth spur gears has been cut with a 25° hob. The pinion has 31 teeth and the gear 60 teeth. The diametral pitch is 4. Find the velocity ratio, the pitch circle radii, the outside diameters, the center distance, and the contact ratio.

11.22 A pair of standard, full-depth spur gears has been cut with a 25° hob. The pinion has 14 teeth and the gear 51 teeth. The diametral pitch is 5. Find the velocity ratio, the pitch circle radii, the outside diameters, the center distance, and the contact ratio.

11.23 A pair of standard, full-depth spur gears has been cut with a 20° hob. The pinion has 27 teeth and the gear 65 teeth. The diametral pitch is 2. Find the velocity ratio, the pitch circle radii, the outside diameters, the center distance, and the contact ratio.

12

HELICAL, BEVEL, AND WORM GEARS

Prerequisite Knowledge Needed for Chapter 12

A knowledge of the material on spur gears from [Chapter 11](#) and a familiarity with vector mechanics.



12.1 Helical Gears

Helical gears have the same involute tooth form as spur gears but are cut with the teeth inclined to the gear axes so that the intersections of tooth faces with cylindrical surfaces about the gear axis are helices. This produces a progressive contact action with contact beginning at a point at one end of the tooth, enlarging progressively to an inclined line across the tooth face, and then diminishing progressively to a point at the other end of the tooth. This progressive action carries important benefits in reductions of gear noise and vibration. Because of the gradual load transfer and longer teeth, helical gears will also have a higher load rating for a given size gear than spur gears. Another advantage of helical gears is that the gear axes do not need to be parallel. Because of these advantages, helical gears are almost always used in high-speed transmissions where noise and high power are issues. Examples of helical gears are shown in [Figures 12.1–12.4](#).



[Figure 12.1](#) Helical gears.



[Figure 12.2](#) Herringbone gears.



Figure 12.3 Helical rack and pinion.



Figure 12.4 Crossed helical gears.

The helical tooth geometry results in a reaction thrust component along the shaft axis, which therefore requires a thrust bearing. For this reason, gears are sometimes cut with two sets of helical teeth with opposite pitch. The resulting chevron-shaped teeth lead to the name “herringbone gears” for this type (see [Figure 12.2](#)). Herringbone gears do not have an axial reaction thrust component.

12.1.1 Helical Gear Terminology

As indicated in [Figure 12.5](#), the terminology for helical gears is defined in two planes, the transverse plane and the normal plane. The transverse plane is viewed along the axis of the gear shaft, and the normal plane is viewed along the tooth of the gear. The rotation of the gear is in the transverse plane; however, the gear is manufactured by a cutting action along the normal plane.

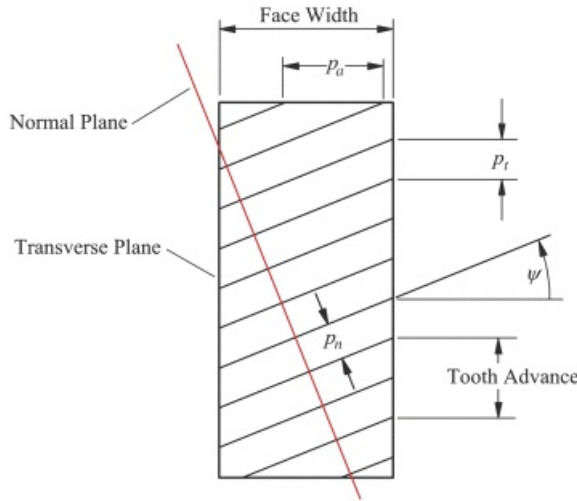


Figure 12.5 End view of helical gear showing normal and transverse planes. ψ is the helix angle, the angle at which the teeth are inclined to the axis of the gear; p_n is the circular pitch in a plane normal to the tooth; p_t is the transverse circular pitch in a plane normal to the gear axis.

Three pitches must be considered when evaluating the geometry of helical gears. These are the normal pitch, the transverse pitch, and the axial pitch.

When a helical gear is generated, the properties in the normal plane will correspond to those of the hob or shaper cutter. In particular, the normal pitch, p_n , is related to the normal diametral pitch, P_n , by

$$p_n = \frac{\pi}{P_n} \quad (12.1)$$

and both p_n and P_n are the same as those for the cutter if the gear is cut with a hob. The normal pitch is usually the one specified in gear catalogs.

Also, from [Figure 12.5](#)

$$p_t = p_n \cos \psi \quad (12.2)$$

where p_t is the transverse circular pitch and ψ is the helix angle. The transverse circular pitch is the distance from tooth to tooth on the pitch cylinder when observed from the transverse plane. The transverse circular pitch is related to the transverse diametral pitch through an equation similar to [Equation 12.1](#). That is,

$$p_t = \frac{\pi}{P_t} \quad (12.3)$$

and

$$P_t = \frac{\pi}{d_t} \quad (12.4)$$

where d_t is the diameter of the pitch cylinder. From [Equations 12.1–12.4](#)

$$\frac{s}{P_t} = \frac{\pi}{P_t} \cos \psi$$

or

$$P_t = P_n \cos \psi \quad (12.5)$$

The transverse diametral pitch has the traditional meaning of being the number of teeth per inch of pitch diameter in the transverse plane. However, the normal diametral pitch is less obvious. We can still think of P_n as the number of teeth per inch of pitch diameter if the gear were a spur gear with a pitch diameter equal to the transverse pitch diameter. Obviously, the helical gear appears as an ellipse when viewed from the normal plane; however, the circular approximation is useful when considering the local geometry in the vicinity of an individual tooth.

In the metric system, the module, m_p , is used, and

$$m_p = \frac{d_p}{P_t} = \frac{m_n}{\cos \psi}$$

where m_n is the module for the hob. Comparing [Equations 12.1–12.5](#), we see that the metric system and the conventional system used in the United States are related by

$$m_p = \frac{1}{P_t} \text{ and } m_n = \frac{1}{P_t}$$

and

$$P_t = \pi m_t \text{ and } P_n = \pi m_n$$

The third pitch is the axial pitch, p_a (see [Figure 12.5](#)). This is the distance from a point on one tooth to the corresponding point on an adjacent tooth measured at the pitch cylinder and in the direction of the rotation axis. The axial pitch is related to the other pitches by

$$p_a = \frac{P_t}{\tan \psi} = \frac{P_n}{\sin \psi} \quad (12.6)$$

There are two pressure angles for helical gears, one for each of the two principal planes, and the relationship among the pressure angles and the helix angle is shown in [Figure 12.6](#). The transverse pressure angle, ϕ_2 , is measured in the transverse plane, and the normal pressure angle, ϕ_1 , is measured in the normal plane.

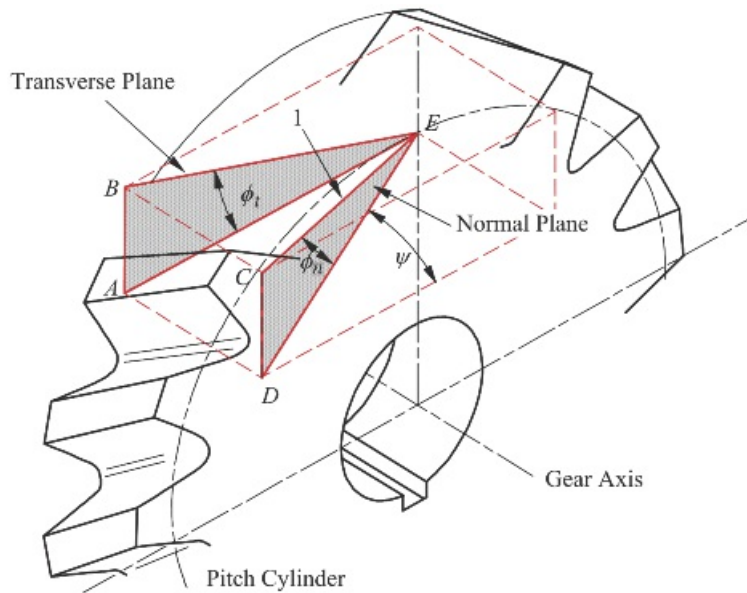


Figure 12.6 Relationship among normal and transverse pressure angles and helix angle.

Because helical gears are usually cut with the same hob cutters as spur gears, the normal diametral pitch and pressure angle usually have standard spur gear values, but the transverse diametral pitch and pressure angle do not. Since the transverse diametral pitch and pressure angle determine the kinematic characteristics of the gear pair, it is important to be able to obtain them from the corresponding normal values and the helix angle. Conversely, the tooth stiffness and strength are determined by the thickness in the normal plane. Thus, this is the plane used when analyzing tooth stresses.

The relationship among ϕ_n , ϕ_t , and ψ can be determined by looking at the lines AE , BE , CE , and DE in [Figure 12.6](#). Assume that line CE is 1 unit long and normal to the gear tooth at the pitch cylinder. Triangle CED is in the normal plane, BEA is in the transverse plane, AED is in the plane tangent to the pitch circle at point E , and $BADC$ is a rectangle.

Then DE is the projection of CE in the tangent plane, BE is the projection of CE in the transverse plane, and AE is the projection of BE in the tangent plane. From simple geometry

$$AB = CD$$

Because $CE = 1$

$$\begin{aligned} DE &= \cos \phi_n \\ CD &= \sin \phi_n \\ AE &= DE \cos \psi = \cos \phi_n \cos \psi \\ AB &= AE \tan \phi_t = \cos \phi_n \cos \psi \tan \phi_t \end{aligned}$$

And because $AB = CD$

$$\sin \phi_n = \cos \phi_n \cos \psi \tan \phi_t$$

or

$$\tan \phi_t = \frac{\tan \phi_n}{\cos \psi} \quad (12.7)$$

12.1.2 Helical Gear Manufacturing

As was the case for spur gears, the vast majority of helical gears are manufactured by hobbing ([Figure 12.7](#)) or shaping ([Figure 12.8](#)). When gears are hobbed, the hob axis is inclined at an angle equal to the gear helix angle relative to the gear rotation axis. The hob properties correspond to the gear properties in the normal plane. Therefore, the normal diametral pitch (P_n) of the gear is equal to the diametral pitch (P_d) of the hob. The same hob can be used to cut both spur and helical gears.



[Figure 12.7](#) Hobbing helical gear. Courtesy of Bourn & Koch, Rockford, Illinois



[Figure 12.8](#) Shaping a helical gear. Courtesy of Bourn & Koch, Rockford, Illinois

If the gear is an internal gear, if it has a shoulder, or if it is a herringbone gear ([Figure 12.2](#)), the gear cannot be hobbed. Such gears are normally fabricated by shaping. The shaper axis is parallel to the gear rotation axis. Therefore, the shaper properties correspond to the transverse plane. The transverse circular pitch of the gear is equal to the transverse circular pitch of the shaper cutter, so that [Equations 12.3](#) and [12.4](#) apply to both the cutter and gear. When the gear is shaped, the same cutter cannot be used for both helical and spur gears.

12.1.3 Minimum Tooth Number to Avoid Undercutting

One of the advantages of helical gears is that they can have fewer teeth on the pinion than can the corresponding spur gear and still avoid undercutting. The minimum number of teeth to avoid undercutting can be found by using [Figure 11.27](#) and [Equation 11.25](#) in [Chapter 11](#), where all quantities are for the transverse plane. Then

$$r_p = \frac{a}{\sin^2 \phi_i} \quad (12.8)$$

where a is the addendum for the cutter used to form the gear. The cutter properties are associated with the *normal* plane. Therefore

$$a = \frac{x}{x_n}$$

and [Equation 12.8](#) can be rewritten as

$$r_p = \frac{x}{x_n \sin^2 \phi_i}$$

The pitch radius (r_p) is related to the number of teeth (N) and transverse diametral pitch (P_t) by

$$r_p = \frac{N}{2P_t} \quad (12.9)$$

Therefore

$$\frac{N}{2P_t} = \frac{k}{P_n \sin^2 \phi_i}$$

Using [Equation 12.5](#) and simplifying, the minimum number of teeth to avoid undercutting is given by

$$N = \frac{2kP_t}{P_n \sin^2 \phi_i} = \frac{2k \cos \psi}{\sin^2 \phi_i} \quad (12.10)$$

Values for N as a function of helix angle and *normal* pressure angle are given in [Table 12.1](#) for standard full-depth ($k = 1$) gears cut with a hob. The values were computed by first solving [Equation 12.7](#) for ϕ_i for selected values of ψ and ϕ_n , and then substituting the results into [Equation 12.10](#). Notice that for very large helix angles, the number of teeth on the gear can be reduced to 1. This is the case that exists with worm gears, which will be discussed later in this chapter. The helix angle for helical gears is usually limited to 45°.

[Table 12.1](#) Minimum Tooth Numbers as a Function of the Helix Angle for Standard Values of the Normal Pitch

$\psi \downarrow$	ϕ_n (Deg.) \rightarrow	14 1/2°	20°	25°
0° (spur gear)		32	18	12
5°		32	17	12
10°		31	17	11
15°		29	16	11
20°		27	15	10
25°		25	14	9
30°		22	12	8
35°		19	10	7
40°		15	9	6
45°		12	7	5
50°		10	6	4
55°		7	4	3
60°		5	3	3
65°		4	2	2
70°		2	2	2
75°		2	1	1
80°		1	1	1

Unlike spur gears, two helical gears can be meshed with either parallel shafts or crossed shafts. The properties in [Equations 12.1–12.10](#) apply to individual helical gears regardless of the axis orientation of the meshing gear.

12.1.4 Helical Gears with Parallel Shafts

Two parallel-shaft gears will mesh if the following conditions are satisfied:

1. Both gears have equal pitches
2. Both gears have equal helix angles
3. The helix angles on the two gears are opposite hand. This means that one helix is left-handed and the other is right-handed (see [Figure 12.9](#)).

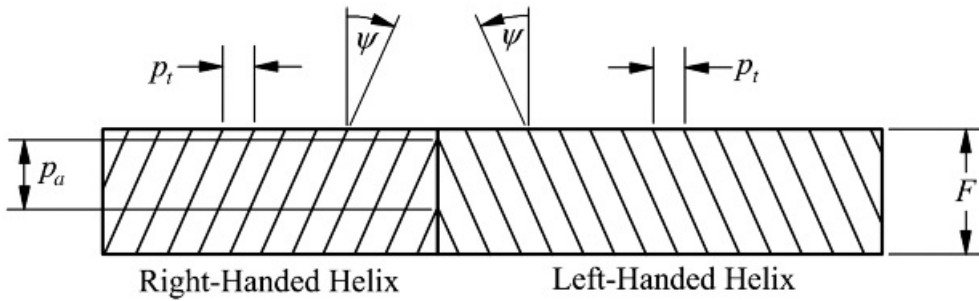


[Figure 12.9](#) Conditions for two helical gears to mesh.

Velocity Ratio and Center Distance

The expressions for the angular velocity ratio and the center distance for two parallel-shaft helical gears are the same as the corresponding expressions for spur gears. The velocity ratio is given by

$$\frac{\omega_2}{\omega_3} = \frac{r_{p_3}}{r_{p_2}} = \frac{d_{t_3}}{d_{t_2}} = \frac{N_3/P_t}{N_2/P_t} = \frac{N_3}{N_2} \quad (12.11)$$

where ω_2 , r_{p_2} , d_{t_2} , and N_2 are the angular velocity magnitude, pitch radius, pitch diameter, and number of teeth, respectively, on gear 2. The corresponding values are for gear 3. The center distance is given by

$$C = r_{p_2} + r_{p_3} = \frac{d_{t_2} + d_{t_3}}{2} \quad (12.12)$$

or in terms of the pitches

$$C = \frac{N_2 + N_3}{2P_t} = \frac{N_2 + N_3}{2P_t \cos \psi} \quad (12.13)$$

Minimum Face Width

The maximum face width of a pair of spur gears is limited by the accuracy of alignment; however, the minimum face width can be much smaller than the circular pitch. Helical gears are much more expensive to produce than spur gears, and therefore, from practical considerations, the face width must be large enough to achieve the stated benefits as compared with spur gears. In general, the face width (F) should be larger than the axial pitch (p_a), and the AGMA [1] recommends that the face width be at least 15 percent larger than the axial pitch. Typically, the face width is at least two times the axial pitch [2]. The axial pitch is given by [Equation 12.6](#). Therefore the limiting condition for the face width is

$$F \geq \frac{1.15p_t}{\tan \psi} \quad (12.14)$$

or

$$\bar{x} \geq \frac{1.15p_a}{\sin \psi} \quad (12.15)$$

Contact Ratio

Mating spur gears make contact on a line that is parallel to the axis of rotation as shown in [Figure 12.10](#). Helical gear teeth make contact on a line that is diagonal across the gear teeth as shown in [Figure 12.11](#). Contact between the two teeth begins at *A*, and as the gears mesh the contact moves diagonally across the gear tooth. When contact is being lost at *B* on one side of the tooth, it is just beginning at *C* on the other side. This gradual contact is one of the benefits of helical gears.

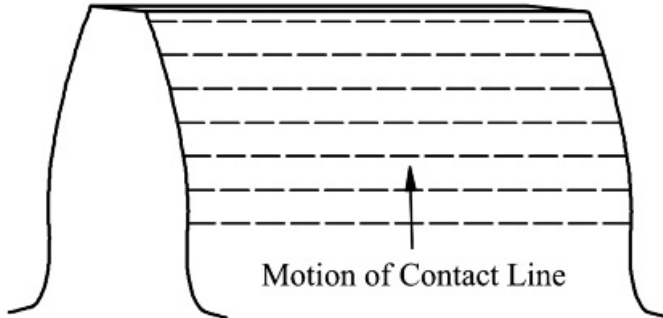


[Figure 12.10](#) Contact lines for spur gear.

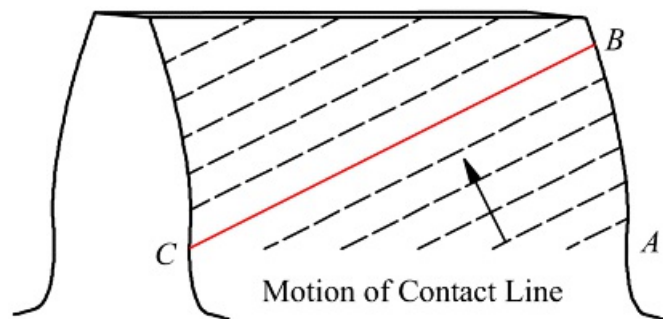


[Figure 12.11](#) Contact lines for helical gear.

The contact ratio of helical gears is increased over that of equivalent spur gears by the axial overlap of the teeth. Therefore, the contact ratio (m_c) is the sum of the transverse contact ratio (m_{ct}) and the axial or face contact ratio (m_{cf}). The transverse contact ratio is computed in the same manner as for spur gears. Therefore, the transverse contact ratio is given as

$$\text{m}_{ct} = \frac{p_t l}{s \cos \phi_i} \quad (12.16)$$

where

$$l = \sum_{i=1}^3 \left\{ -r_p \sin \phi_i + \sqrt{(r_{p_i} + c_i)^2 - r_{p_i}^2 \cos^2 \phi_i} \right\} = \sum_{i=1}^3 \left\{ -r_p \sin \phi_i + \sqrt{c_i^2 + 2c_i r_{p_i} + r_{p_i}^2 \sin^2 \phi_i} \right\}$$

The axial contact ratio is the ratio of the face width of the gear to the axial pitch. This is

$$m_{c_a} = \frac{F}{p_a} = \frac{F \tan \psi}{p_t} \quad (12.17)$$

Notice that the transverse contact ratio is not defined for a single gear; however, the axial contact ratio depends on the properties of a single gear. The normal and tangential pitches will be the same for both gears. If the face widths are different, the face width of the narrower gear is used in [Equation 12.17](#).

The total contact ratio is

$$m_c = m_{c_b} + m_{c_a} \quad (12.18)$$

As in the case of spur gears, m_c gives the average number of teeth in contact during the gear action. The contact ratio for helical gears is always higher than for comparable spur gears.



Example 12.1 Helical Gear Geometry

A pair of helical gears with 19 and 34 teeth, respectively, and a 30° helix angle are cut with a standard spur gear hob that has a diametral pitch of 4 and a pressure angle of 20° . Find the transverse diametral pitch, the pitch cylinder radii, and the axial, transverse, and total contact ratios. The face width is 12 in.

Solution

The properties of the gears in the normal direction will be the same as those of the hob. The transverse diametral pitch (P_t) for both gears is related to the normal diametral pitch by [Equation 12.5](#). Based on the diametral pitch of the hob

$$P_t = P_n \cos \psi = 4 \cos 30^\circ = 3.464.$$

The pitch cylinder diameters are related to the diametral pitch through [Equation 12.4](#). Therefore

$$\delta_i = \frac{N_i}{P_i}$$

and

$$r_{t_1} = \frac{N_1}{2P_t} = \frac{19}{2(3.464)} = 2.742 \text{ in}$$

and

$$r_{t_2} = \frac{N_2}{2P_t} = \frac{34}{2(3.464)} = 4.908 \text{ in}$$

The transverse contact ratio is given by [Equation 12.16](#) as

$$m_{c_t} = \frac{p_t \lambda}{s \cos \phi_t}$$

where

$$A = \sum_{i=1}^3 \left\{ -r_{g_i} \sin \phi_i + \sqrt{a_i^2 + 2a_i r_{g_i} + r_{g_i}^2 \sin^2 \phi_i} \right\}$$

The addenda are determined by the hob. Because a standard hob is used, both addenda are given by

$$s = \frac{1}{P_A} = \frac{1}{4} = 0.25 \text{ in}$$

The transverse circular pitch is given by [Equation 12.3](#) as

$$p_t = \frac{s}{P_t} = \frac{s}{3.484} = 0.907$$

and the transverse pressure angle is given by [Equation 12.7](#) as

$$\phi_t = \tan^{-1} \left(\frac{\tan \phi_p}{\cos \psi} \right) = \tan^{-1} \left(\frac{\tan 20^\circ}{\cos 30^\circ} \right) = 22.796^\circ$$

Now

$$\begin{aligned} \lambda &= -r_{p_2} \sin \phi_t + \sqrt{a_2^2 + 2a_2 r_{p_2} + r_{p_2}^2 \sin^2 \phi_t - r_{p_3} \sin \phi_t + \sqrt{a_3^2 + 2a_3 r_{p_3} + r_{p_3}^2 \sin^2 \phi_t}} \\ &= -2.742 \sin 22.796^\circ + \sqrt{(0.25)^2 + 2(0.25)(2.742) + [2.742 \sin 22.796^\circ]^2} \\ &\approx -4.908 \sin 22.796^\circ + \sqrt{(0.25)^2 + 2(0.25)(4.908) + [4.908 \sin 22.796^\circ]^2} = 1.1131 \end{aligned}$$

Therefore, the transverse contact ratio is

$$m_{c_t} = \frac{p_t \lambda}{s \cos \phi_t} = \frac{0.907(1.1131)}{s \cos 22.796^\circ} = 0.3486$$

The axial contact ratio is given by [Equation 12.17](#) as

$$m_{c_a} = \frac{F \tan \psi}{p_t} = \frac{12 \tan 30^\circ}{0.907} = 7.6394$$

The total contact ratio is

$$m_c = m_{c_t} + m_{c_a} = 0.3486 + 7.6394 = 7.98$$

Therefore, an average of approximately 8 teeth will be in contact as the gears mesh.



Example 12.2

Helical Gear Replacement of Spur Gears

Sometimes it is desirable to replace an existing set of spur gears to eliminate a noise problem or to increase the capacity of a gearbox. Assume the original spur gears are 14 pitch, 20° full-depth gears with 30 and 85 teeth. These are to be replaced by a set of helical gears without any major modifications to the gearbox. The size and angular velocity ratio are to remain the same. Determine the helix angle, outside diameters of the blanks, and the face width of the replacement gears. The new helical gears can be cut with the same hob as was used for the spur gears.

Solution

If there are to be no major modifications to the gearbox, the center distance must remain the same. The original pitch radii are given by

$$r_{p_2} = \frac{N_2}{2P_d} = \frac{30}{2(14)} = 1.071 \text{ in}$$

and

$$r_{p_1} = \frac{N_1}{2P_d} = \frac{85}{2(14)} = 3.036 \text{ in}$$

and the center distance is

$$C = r_{p_2} + r_{p_1} = \frac{N_2 + N_1}{2P_d} = \frac{30 + 85}{2(14)} = 4.107 \text{ in}$$

The velocity ratio is also to remain constant. The original velocity ratio was

$$\frac{\omega_2}{\omega_1} = \frac{N_3}{N_2} = \frac{85}{30} = \frac{17}{6} \quad (12.19)$$

For the helical gears, we need to determine the helix angle and the number of teeth on each gear. We will find the number of teeth and transverse diametral pitch first and then determine the helix angle. The velocity ratio is given by [Equation 12.11](#) as

$$\frac{\omega_2}{\omega_3} = \frac{r_{p_1}}{r_{p_2}} = \frac{\phi_{t_3}}{\phi_{t_2}} = \frac{N_3/P_t}{N_2/P_t} = \frac{N_3}{N_2}$$

and the center distance is given by [Equation 12.12](#)

$$C = r_{p_2} + r_{p_3} = \frac{\phi_{t_2} + \phi_{t_3}}{2}$$

From these two equations, it is clear that the pitch radii for the helical gears must be the same as the corresponding radii for the spur gears. However, the tooth numbers can and will be different. The transverse diametral pitch is related to the normal diametral pitch by

$$P_t = P_n \cos \psi \quad (12.5)$$

and to the teeth numbers by

$$P_t = \frac{N_2}{2r_{p_2}} = \frac{N_3}{2r_{p_3}} \quad (12.20)$$

From [Equation 12.5](#), it is clear that $P_t < P_n$. Therefore, based on [Equation 12.20](#), the tooth numbers on the helical gears must be less than those on the spur gears. As a result, when we investigate tooth numbers that satisfy [Equation 12.19](#), we need consider only values that are lower than the corresponding values for the spur gears. A set of values is

N_2	$N_3 = \frac{17N_2}{6}$
30	85 (spur gear)
29	82.167
28	79.333
27	76.500
26	73.667
25	70.833
24	68

From the table, the first set of teeth numbers that are integers are $N_2 = 24$ and $N_3 = 68$. For these numbers, the transverse pitch is given by [Equation 12.20](#) as

$$P_t = \frac{N_2}{2r_{p_2}} = \frac{N_3}{2r_{p_3}} = \frac{24}{2(1.071)} = \frac{68}{2(3.036)} = 11.199$$

From [Equation 12.5](#)

$$\psi = \cos^{-1} \left(\frac{P_t}{P_n} \right) = \cos^{-1} \left(\frac{11.199}{14} \right) = 36.877^\circ$$

Notice that this is the lowest helix angle possible (other than 0°) if the center distance and velocity ratio are to be maintained. The blank diameters of the two gears are given by

$$D_{p_2} = 2r_{p_2} + 2c_2 = 2r_{p_2} + 2 \frac{k}{P_n} = 2(1.071) + 2 \frac{1}{14} = 2.286 \text{ in}$$

and

$$D_{p_2} = 2r_{p_2} + 2a_3 = 2r_{p_2} + 2\frac{s}{p_a} = 2(3.036) + 2\frac{1}{14} = 6.214 \text{ in}$$

The minimum face width is given by [Equation 12.14](#)

$$F \geq \frac{1.15p_t}{\tan \psi} \text{ or } F \geq \frac{1.15s}{p_t \tan \psi}$$

Therefore,

$$F \geq \frac{1.15s}{11.199 \tan 36.877^\circ} \text{ or } F > 0.430$$

$$\text{Use } F = \frac{7}{16} \text{ in}$$

Designing for Axial Force

When spur gears transmit power, the force between the gears lies entirely in the transverse plane. However, when helical gears mesh, there will be an axial force component because of the helix angle. This axial load must be considered when designing the shaft bearings. If the load is too large to be carried by the bearings, two helical gears of opposite hand can be used instead of a single gear. Alternatively, and more commonly, a herringbone gear ([Figure 12.2](#)) can be used. A herringbone gear is in essence two helical gears of opposite hand cut on the same gear blank.

A summary of the equations specific to parallel-shaft helical gears is given in [Table 12.2](#). Most of the equations in [Table 11.4](#) apply to helical gears if the transverse plane is used. Therefore, most of the equations in [Table 11.4](#) have not been repeated in [Table 12.2](#).

[Table 12.2](#) Summary of Helical Gear Formulas (Parallel Shafts)

Quantity	Formula
Transverse diametral pitch	$P_t = \frac{N}{d_t} = \frac{N}{2r_p} = \frac{\pi}{p_t} = p_n \cos \psi = \frac{1}{m_t} = \frac{\cos \psi}{m_z}$
Transverse circular pitch	$p_t = \frac{\pi}{P_t} = \frac{\pi d_t}{N} = \pi m_t = \frac{p_n}{\cos \psi} = p_a \tan \psi$
Normal diametral pitch	$P_n = \frac{p_t}{\cos \psi} = \frac{N}{2r_p \cos \psi} = \frac{\pi}{p_n} = \frac{1}{m_n} = \frac{1}{m_t \cos \psi}$
Normal circular pitch	$p_n = \frac{\pi}{P_n} = \pi m_n = p_t \cos \psi = p_a \sin \psi$
Axial pitch	$p_a = \frac{p_n}{\tan \psi} = \frac{p_n}{\sin \phi}$
Pitch cylinder diameter	$d_t = \frac{p_t}{P_t} = \frac{N}{p_n \cos \psi} = \frac{N p_t}{\pi} = \frac{N p_n}{\pi \cos \psi} = \frac{N m_n}{\cos \psi}$
Center distance	$C = r_{p_1} + r_{p_2} - \frac{d_2 \cos \phi_2 - d_1 \cos \phi_1}{2} = \frac{p_1 (M_2 + M_1)}{2z} - \frac{p_2 (M_2 + M_1)}{2z \cos \psi}$
Velocity ratio	$\beta = \frac{r_{p_1}}{r_{p_2}} = \frac{r_{p_1}}{r_{p_2}} = \frac{d_1}{d_2} = \frac{M_1}{M_2}$
Minimum face width	$F \geq \frac{1.15s}{\tan \psi} \text{ or } F \geq \frac{1.15s}{p_t \tan \psi}$
No. of teeth at undercutting	$N = \frac{2aP_t}{\sin^2 \phi_t} = \frac{2tP_t}{p_n \sin^2 \phi_t} = \frac{2k \cos \psi}{\sin^2 \phi_t} (k = 1 \text{ for HD or } 0.8 \text{ for SD})$
Length of line of contact	$A = \sqrt{(r_{p_1} + a_2)^2 - r_{p_2}^2 \cos^2 \phi} = r_{p_2} \sin \phi$ $= \sqrt{(r_{p_1} + a_2)^2 - r_{p_2}^2 \cos^2 \phi} = r_{p_2} \sin \phi$
Transverse contact ratio	$m_{c_t} = \frac{A}{p_t \cos \phi_t} = \frac{A P_t}{\pi \cos \phi_t}$
Axial contact ratio	$m_{c_a} = \frac{E}{p_a} = \frac{F \tan \psi}{p_t}$

Total contact ratio	$\text{m}_{\text{c}} = \text{m}_{\text{c}_i} + \text{m}_{\text{c}_a}$
Transverse pressure angle	$\tan \phi_t = \frac{\text{m}_{\text{c}}}{\cos \psi}$

12.1.5 Crossed Helical Gears

Helical gears need not be used on parallel shafts but can be used to transfer power between nonparallel, nonintersecting shafts (Figure 12.4). When the shafts are not parallel, the gears are called crossed helical gears.

The only requirement for crossed helical gears to mesh properly is that they have the same normal pitch. The transverse pitches need not be the same, and the helix angles need not be the same. The helix angles can be of the same or opposite hand.

The velocity ratio for crossed helical gears can be developed from [Equation 12.11](#) as

$$\frac{R}{R} = \frac{\omega_2}{\omega_3} = \frac{N_3}{N_2} = \frac{d_{2z}P_{2z}}{d_{3z}P_{3z}} = \frac{d_{2z}P_n \cos \psi_2}{d_{3z}P_n \cos \psi_3} = \frac{d_{2z} \cos \psi_2}{d_{3z} \cos \psi_3} \quad (12.21)$$

If the angle between the shafts of the meshing crossed helical gears is Σ and the helix angles are ψ_2 and ψ_3 , the relationship among the three angles is

$$\Sigma = \psi_2 \pm \psi_3 \quad (12.22)$$

where the plus sign applies if the gears are of the same hand, and the minus sign applies if the gears are of the opposite hand. This is shown in [Figure 12.12](#).

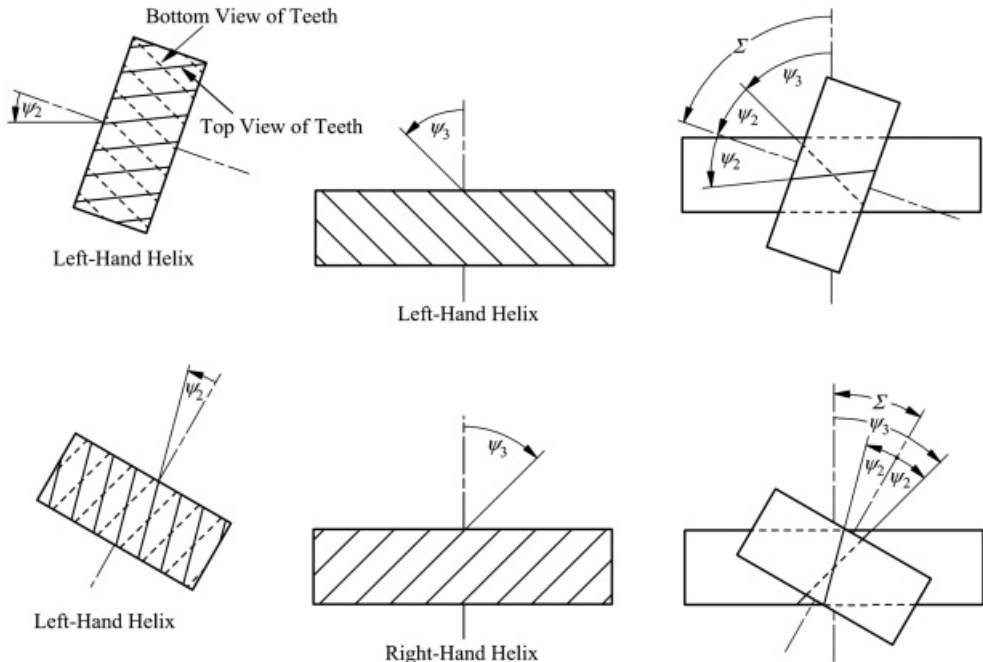


[Figure 12.12](#) Relationship among shaft angle and helix angles for crossed helical gears.

The center distance in the U.S. system between crossed helical gears is given by

$$C = r_{p_2} + r_{p_3} = \frac{N_2}{2P_{3z}} + \frac{N_3}{2P_{2z}} = \frac{N_2}{2P_n \cos \psi_2} + \frac{N_3}{2P_n \cos \psi_3} = \frac{1}{2P_n} \left[\frac{N_2}{\cos \psi_2} + \frac{N_3}{\cos \psi_3} \right] \quad (12.23)$$

and recalling that

$$\cos \psi = \frac{1}{m}$$

the center distance in the metric system is

$$C = r_{\nu_2} + r_{\nu_3} = \frac{N_2}{2P_{t_2}} + \frac{N_3}{2P_{t_3}} = \frac{N_2 m_n}{2 \cos \psi_2} + \frac{N_3 m_n}{2 \cos \psi_3} = \frac{m_n}{2} \left[\frac{N_2}{\cos \psi_2} + \frac{N_3}{\cos \psi_3} \right] \quad (12.24)$$

This equation applies regardless of the hand of the gears.

Crossed helical gears are not used to transmit large amounts of power because the gears theoretically have only point contact where the teeth mesh. This is in contrast to parallel-shaft helical gears, which have line contact. For large power transfers between nonparallel shafts, bevel or hypoid gear sets are preferred. Worm gear sets can also be used when high velocity ratios are required.

A summary of the equations specific to crossed helical gears is given in [Table 12.3](#).

[Table 12.3](#) Summary of Crossed Helical Gear Formulas

Quantity	Formula
Shaft angle	$\Sigma = \psi_2 \pm \psi_3$
Pitch cylinder diameter	$d_t = \frac{p_t}{P_n} = \frac{N}{P_n \cos \psi} = \frac{N p_n}{\pi} = \frac{N p_n}{\pi \cos \psi} = N m_n$
Center distance	$C = \frac{\nu_2 + \nu_3}{2} = \frac{187 + 183}{2P_{t_2}} = \frac{11}{2P_{t_2}} = \frac{11}{2P_n} \left[\frac{187 + 183}{\cos \psi_2 + \cos \psi_3} \right] = \frac{m_n}{2} \left[\frac{N_2 + N_3}{\cos \psi_2 + \cos \psi_3} \right]$
Velocity ratio	$\bar{R} = \frac{\omega_2}{\omega_3} = \frac{N_3}{N_2} = \frac{d_{t_2} P_{t_3}}{d_{t_3} P_{t_2}} = \frac{d_{t_2} P_n \cos \psi_3}{d_{t_3} P_n \cos \psi_2} = \frac{d_{t_2} \cos \psi_3}{d_{t_3} \cos \psi_2}$



Example 12.3 Crossed Helical Gear Geometry

Assume that two crossed helical gears have a shaft angle of 65 degrees and a velocity ratio of 2:1. The pinion (gear 2) has a normal diametral pitch of 10, a helix angle of 30°, and 70 teeth. Determine the helix angle, pitch diameter, and number of teeth on the meshing gears. Also find the center distance. Both gears are right-handed, and both are cut with the same hob.

Solution

First find the pitch diameter for gear 2 using

$$d_{p_2} = \frac{N_2}{P_n} = \frac{N_2}{P_n \cos \psi_2} = \frac{70}{10 \cos 30^\circ} = 8.063 \text{ in}$$

From the expression for the velocity ratio, the number of teeth on gear 3 is

$$N_3 = N_2 \frac{\omega_2}{\omega_3} = 70 \frac{2}{1} = 140$$

Next find the helix angle of the second gear, using [Equation 12.22](#) with a plus sign. Then

$$\Sigma = \psi_2 + \psi_3$$

where $\Sigma = 65^\circ$ and $\psi_2 = 30^\circ$. Solving gives $\psi_3 = 35^\circ$.

The pitch diameter for gear 3 is then given by

$$d_{p_3} = \frac{N_3}{P_n \cos \psi_3} = \frac{140}{10 \cos 35^\circ} = 17.091 \text{ in}$$

The center distance is given by

$$C = \frac{d_{p_2} + d_{p_3}}{2} = \frac{8.063 + 17.091}{2} = 12.587 \text{ in}$$



12.2 Worm Gears

If the tooth of a helical gear makes a complete revolution on the pitch cylinder, the resulting gear is called a worm. This occurs when the helix angle and the gear face width are relatively large. In worms, the helix angle can exceed 80° . The mating gear is called a worm gear or worm wheel. Worm gear sets are used to connect nonintersecting shafts (usually at 90°) when the desired velocity reduction is large. A worm gear set is shown in [Figure 12.13](#).

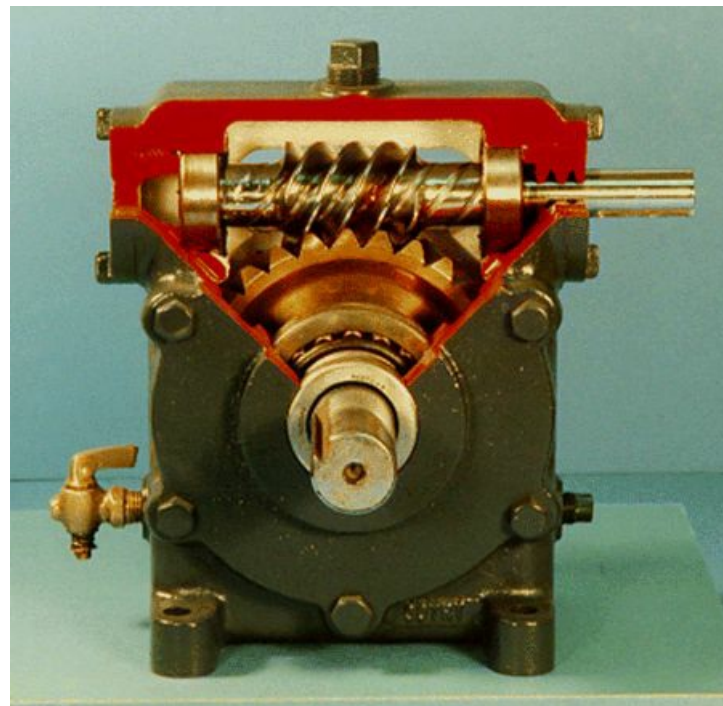
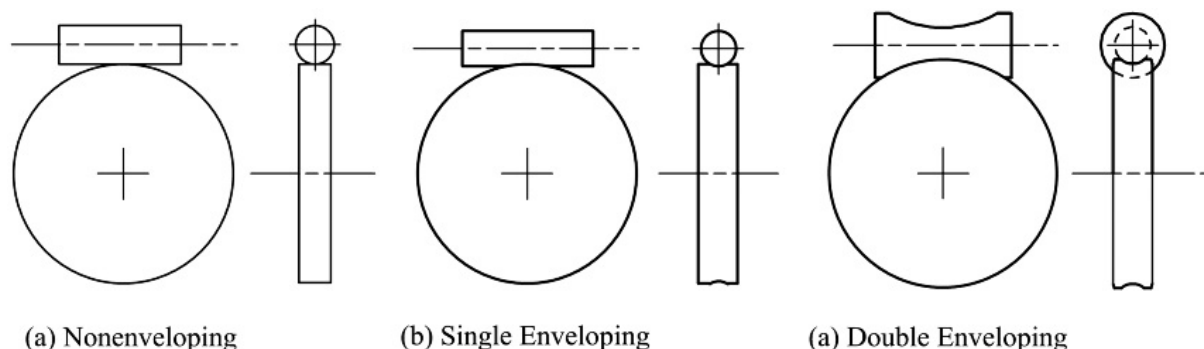


[Figure 12.13](#) Example of worm gear set.

Involute worms can be meshed with either spur or helical gears; however, point contact occurs and relatively small forces can be transmitted. Usually, the worm gear set is cut so that the gear partially envelops the worm. The design is either nonenveloping, single enveloping, or double enveloping. The three cases are illustrated schematically in [Figure 12.14](#). The worm and gear are nonenveloping ([Figures 12.14a](#)) when the worm is meshed with a simple helical gear and point contact occurs. The worm and gear are single enveloping when the gear is cut to partially envelop the worm ([Figures 12.13](#) and [12.14b](#)), and they are double enveloping when the pitch surface of the worm is cut in the shape of an hour glass and meshed with a gear that also envelops the worm partially ([Figure 12.14c](#)). The single and double enveloping worm gear sets will have line contact and can transmit considerably more power than can nonenveloping worm gear sets.



(a) Nonenveloping

(b) Single Enveloping

(c) Double Enveloping

[Figure 12.14](#) Types of worm gear sets.

Note that in the cases of nonenveloping and single enveloping worm gear sets, the worm can drive the gear either

by a rotation of the worm or by a translation of the worm along the axis tangent to the worm axis. Therefore, the alignment of the worm in the tangential direction is not critical. However, in double enveloping worm gear sets, the tangential alignment is critical. Both single and double enveloping worm gear sets must be accurately aligned in the axial and radial directions. Nonenveloping worm gears need to be accurately aligned in only the radial direction. The shaft angles of all worm gear sets must be accurately aligned.

12.2.1 Worm Gear Nomenclature

A schematic drawing of a single enveloping worm gear set is shown in [Figure 12.15](#). The two gears have the same hand. The helix angle is defined in the same manner as was done for helical gears; however, as indicated in [Figure 12.15](#), the helix angle is usually quite large. The lead angle, λ , is the complement of the helix angle, ψ , that is

$$\lambda + \psi = \frac{\pi}{2} \quad (12.25)$$

The lead, L , is the amount that the worm will advance with one revolution of the worm gear. If there is only one tooth, the lead is equal to the axial pitch, p_a . In general, if N_2 is the number of teeth on the worm,

$$L = N_2 p_a \quad (12.26)$$

If one tooth of the worm is unwrapped from the pitch cylinder, the lead of the worm is related to the lead angle, λ , as shown in [Figure 12.16](#). The relationship is

$$\tan \lambda = \frac{L}{\pi d_{t_2}} \quad (12.27)$$

The pitch diameter of the worm gear is the same as that for helical gears, that is

$$d_{t_3} = \frac{\pi d_{t_2} \cos \psi_2}{\cos \lambda}$$

where N_3 is the number of teeth on the gear. The velocity ratio is given by [Equation 12.21](#) as

$$\frac{\omega_2}{\omega_3} = \frac{N_3}{N_2} = \frac{d_{t_3} \cos \psi_3}{d_{t_2} \cos \psi_2} \quad (12.28)$$

For a worm and worm gear to mesh properly with shafts at right angles, the following must be satisfied:

1. The helix angle of the gear must equal the lead angle of the worm.
2. The transverse circular pitch of the gear must equal the axial pitch of the worm.

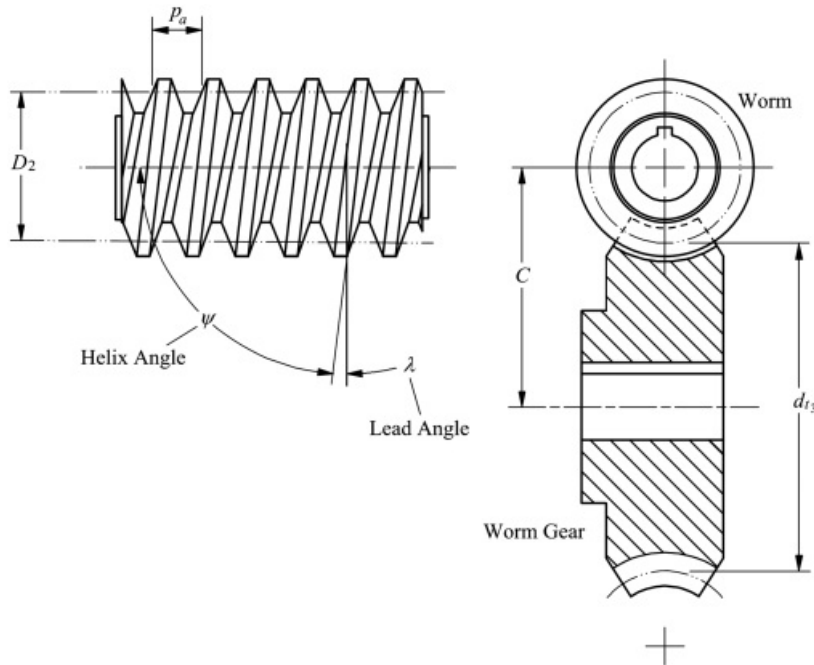


[Figure 12.15](#) Worm gear nomenclature.

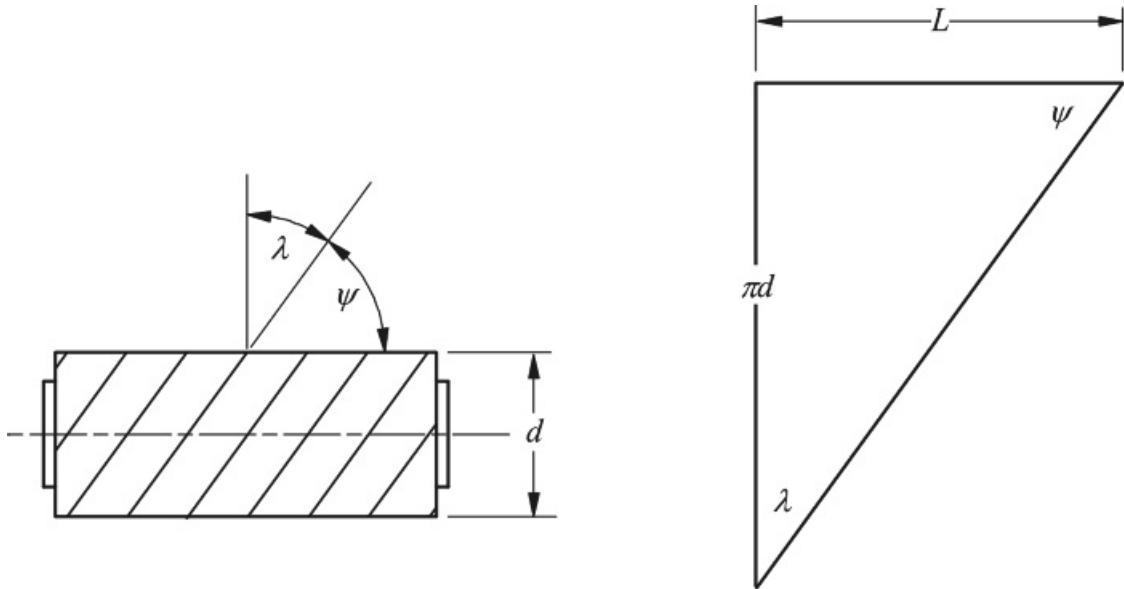


[Figure 12.16](#) Representation of worm gear lead.

If the shafts of the worm and gear are at 90° to each other, then

$$\psi_2 + \psi_3 = \frac{\pi}{2} \quad (12.29)$$

and $\psi_3 = \lambda$. [Equation 12.28](#) can then be written as

$$\frac{\omega_2}{\omega_3} = \frac{d_{t3} \cos \psi_3}{d_{t2} \cos \psi_2} = \frac{d_{t3} \cos \psi_3}{d_{t2} \cos(\pi/2 - \psi_3)} = \frac{d_{t3} \cos \psi_3}{d_{t2} \sin \psi_3} = \frac{d_{t3}}{d_{t2} \tan \psi_3} = \frac{d_{t3}}{d_{t2} \tan \lambda}$$

Therefore, from [Equation 12.27](#)

$$\frac{\omega_2}{\omega_3} = \frac{d_{t_3}}{d_{t_2}} \frac{\pi d_{t_2}}{L} = \frac{\pi d_{t_3}}{L} \quad (12.30)$$

Worm gear sets may or may not be driven from both the worm and gear. In some applications, it is necessary for the drive to be self-locking. In such cases, only the worm can be the driver. In other cases, it must be possible to drive the worm gear set from either the worm or gear. Worms usually have relatively few teeth (one to eight), and when the number of teeth is small, the worm must be the driver. If the lead angle of the worm is greater than the friction angle of the surfaces in contact, the drive will be reversible. The coefficient of friction, μ , is related to the friction angle, δ , by $\mu = \tan \delta$. Therefore $\lambda > \tan^{-1} \mu$, so the worm gear set will be self-locking if the lead angle satisfies

$$\lambda < \tan^{-1} \mu \quad (12.31)$$

In general, a worm gear set cannot be back driven if the lead angle is less than 5° (helix angle $> 85^\circ$).

A summary of the equations for worm gears is given in [Table 12.4](#). A more complete list of equations is given by Townsend [6].

[Table 12.4](#) Summary of Worm Gear Formulas (Gear 2 Is the Worm and 3 Is the Gear)

Quantity	Formula
Axial pitch	$p_a = \frac{p_t}{\tan \psi} = \frac{p_z}{\sin \varphi}$
Lead	$L = N_2 p_a = \pi d_{t_2} \tan \lambda$
Lead angle	$\tan \lambda = \frac{L}{N_2 d_{t_2}} = \frac{N_2 p_a}{\pi d_{t_2}}$
Minimum length of worm [6]	$f = 2 \sqrt{\left(\frac{d_{t_2} \cdot 2\pi}{2}\right)^2 + \left(\frac{d_{t_2} \cdot 2\pi}{2}\right)^2}$
Normal circular pitch	$p_n = \frac{p}{z} = \pi m_n = p_t \cos \psi = p_z \sin \psi = p_a \cos \lambda$
Shaft angle	$\Sigma = \psi_2 \pm \psi_3$
Pitch cylinder diameter	$d_t = \frac{p}{p_t} = \frac{N}{p_n \cos \psi} = \frac{N p_t}{\pi} = \frac{N p_a}{\pi \cos \psi} = N \sec \psi$
Effective face width of gear [6]	$F_e = \sqrt{(d_{t_2} + s + b)^2 - (d_{t_2})^2}$
Center distance	$C = \frac{\omega_2 + \omega_3}{2} = \frac{\pi \psi_2 + \pi \psi_3}{2 p_{t_2}} = \frac{\pi}{2 p_{t_2}} \left[\frac{\psi_2}{\cos \psi_2} + \frac{\psi_3}{\cos \psi_3} \right] = \frac{\pi m_2}{2} \left[\frac{N_2}{\cos \psi_2} + \frac{N_3}{\cos \psi_3} \right]$
Velocity ratio	$R = \frac{\omega_2}{\omega_3} = \frac{N_3}{N_2} = \frac{d_{t_2} p_{t_3}}{d_{t_2} p_{t_2}} = \frac{d_{t_2} p_n \cos \psi_3}{d_{t_2} p_n \cos \psi_2} = \frac{d_{t_2} \cos \psi_3}{d_{t_2} \cos \psi_2}$



Example 12.4 Worm and Gear Geometry

Assume that a worm has three teeth and is driving a gear with 60 teeth. The shaft angle is 90° , the gear transverse circular pitch is 1.25 in, and the pitch diameter of the worm is 3.8 in. Find the helix angle of the gear, the center distance, and the lead angle of the worm. If the coefficient of friction between the worm and gear is 0.1, estimate whether or not the worm gear set can be back driven.

Solution

The worm lead is given by [Equation 12.26](#) as

$$L = N_2 p_g = 3(1.25) = 3.75 \text{ in}$$

And from [Equation 12.30](#) the pitch diameter of the gear is

$$d_{t_2} = \frac{\alpha_2 L}{\alpha_3 \pi} = \frac{60 \cdot 3.75}{3 \cdot \pi} = 23.87 \text{ in}$$

The lead angle, λ , of the worm can be computed from [Equation 12.27](#) as

$$\lambda = \tan^{-1} \left(\frac{L}{\pi d_{t_2}} \right) = \tan^{-1} \left(\frac{3.75}{\pi \cdot 3.8} \right) = 17.44^\circ$$

Therefore, the helix angle of the gear is

$$\psi_2 = \lambda = 17.44^\circ$$

and the helix angle of the worm is given by [Equation 12.29](#) as

$$\psi_1 = 90^\circ - \psi_2 = 90^\circ - 17.44^\circ = 72.56^\circ$$

The center distance is given by

$$C = r_{p_2} + r_{p_1} = \frac{d_{t_2} + d_{t_1}}{2} = \frac{3.75 + 23.87}{2} = 13.81 \text{ in}$$

If the worm gear set is to be reversible, $\lambda > \tan^{-1}\mu$. For the conditions given

$$\tan^{-1}\mu = \tan^{-1}(0.1) = 5.71^\circ$$

Therefore, the worm gear set is reversible.



12.3 Involute Bevel Gears

When power must be transferred between nonparallel intersecting shafts, bevel gears are usually used. In bevel gears, the pitch surfaces are cones. The shafts must have intersecting centerlines, but the intersection can be at any angle, although 90° ([Figure 12.17](#)) is the most common angle.



[Figure 12.17](#) Bevel gears with 90° shaft angle.

The shafts have to be mounted so that the apexes of the pitch cones of the mating gears are coincident ([Figure 12.18](#)). The cones roll on each other without slipping and have spherical motion. Each point on each gear remains at a constant distance from the common apex.

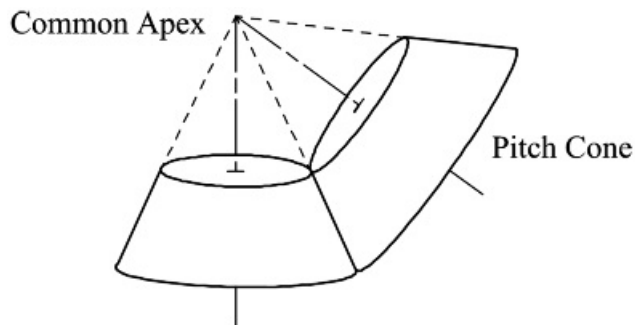


[Figure 12.18](#) Pitch cones for bevel gears.

The pitch diameter for bevel gears is the pitch cone diameter at the larger end ([Figure 12.19](#)). The meshing bevel gears are contained within a sphere of radius r_0 , as shown in [Figure 12.19](#), where the bases of the cones are contained on the surface of the sphere. The pitch cone angles, γ_b , determine the shaft angle, Ξ , as shown in [Figure 12.19](#). These angles are related by

$$\Xi = \gamma_2 + \gamma_3 \quad (12.32)$$

The velocity ratio for bevel gears is similar to that for spur and helical gears, that is

$$\frac{N_2}{N_3} = \frac{d_3}{d_2} = \frac{r_3}{r_2} \quad (12.33)$$

where N_2 and N_3 are the numbers of teeth on gears 2 and 3, respectively, and d_2 and d_3 are the diameters at the large end of the pitch cones of gears 2 and 3, respectively (see [Figure 12.19](#)). r_2 and r_3 are the corresponding pitch

radii.

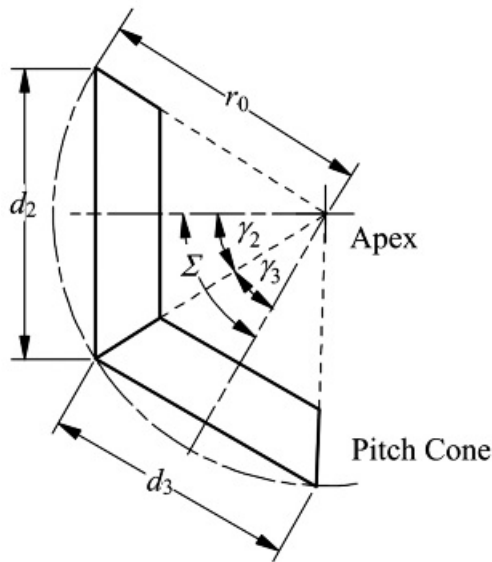


[Figure 12.19](#) Relationship among pitch-cone angles.

The pitch diameters can be related to the cone angles by considering the geometry represented in [Figure 12.19](#). In particular

$$\sin \gamma_2 = \frac{d_2}{2r_c} = \sin(\Sigma - \gamma_3) = \sin \Sigma \cos \gamma_3 - \cos \Sigma \sin \gamma_3$$

Dividing by $\sin \Sigma \sin \gamma_3$ gives

$$\frac{\sin \gamma_2}{\sin \Sigma \sin \gamma_3} = \frac{\cos \gamma_3}{\sin \gamma_3} - \frac{\cos \Sigma}{\sin \Sigma}$$

or

$$\frac{1}{\sin \Sigma} \left[\frac{\sin \gamma_2}{\sin \gamma_3} + \cos \Sigma \right] = \frac{1}{\tan \gamma_3} \quad (12.34)$$

From the geometry

$$\frac{\sin \gamma_2}{\sin \gamma_3} = \frac{d_2}{d_3} \quad (12.35)$$

From [Equations 12.34](#) and [12.35](#)

$$\tan \gamma_2 = \frac{\sin \Sigma}{[d_2/d_3 + \cos \Sigma]} = \frac{\sin \Sigma}{[N_2/N_3 + \cos \Sigma]} \quad (12.36)$$

Similarly

$$\tan \gamma_2 = \frac{\sin \Sigma}{[d_3/d_2 + \cos \Sigma]} = \frac{\sin \Sigma}{[N_3/N_2 + \cos \Sigma]} \quad (12.37)$$

When the shaft angle is 90° , which is the most common case, Equations 12.36 and 12.37 reduce to

$$\tan \gamma_2 = \frac{d_3}{d_2} = \frac{N_3}{N_2} \quad (12.38)$$

and

$$\tan \gamma_2 = \frac{d_2}{d_3} = \frac{N_2}{N_3} \quad (12.39)$$

12.3.1 Tredgold's Approximation for Bevel Gears

Because of the spherical geometry of bevel gears, it is difficult to draw and evaluate bevel gear properties such as contact ratio. Tredgold's approximation lets us approximate the bevel gears as equivalent spur gears. This approximation is used extensively, and the terminology of bevel-gear teeth has evolved around it [2]. The approximation is accurate enough for most practical purposes as long as the gear has eight or more teeth.

Tredgold's approximation involves the concept of a back cone for both meshing gears as shown in Figure 12.20. The approximation recognizes that the action of the gear teeth in the vicinity of the contact location at the large end of the gear teeth is very similar to the action between two spur gears that have pitch radii r_{p2} and r_{p3} equal to the back cone radii r_{e2} and r_{e3} .

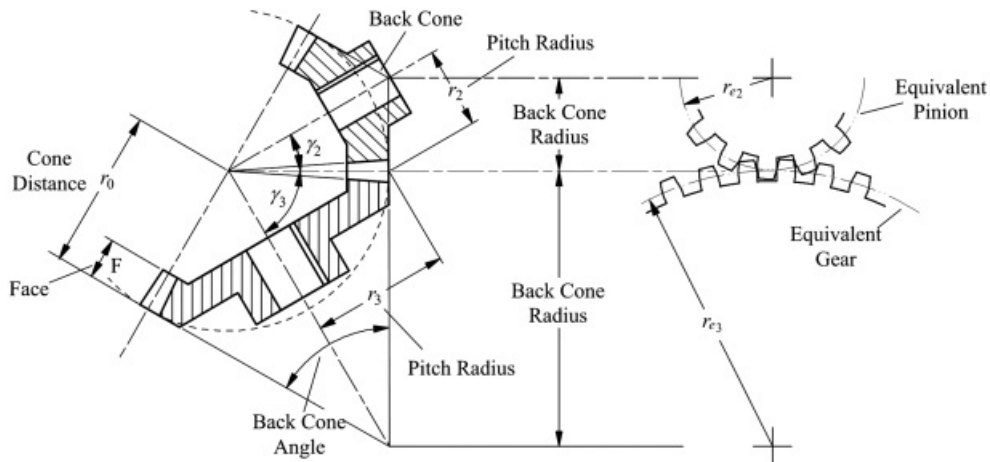


Figure 12.20 Approximation of bevel gears as equivalent spur gears (Tredgold's approximation).

Based on the geometry in Figure 12.20, the pitch radii for the equivalent spur gears are given by

$$r_{e2} = \frac{r_2}{\cos \gamma_2} \quad (12.40)$$

and

$$r_{e3} = \frac{r_3}{\cos \gamma_3} \quad (12.41)$$

If p_c is the circular pitch at the large end of the bevel gears, the numbers of teeth on the equivalent spur gears are given by

$$N_{e1} = \frac{2\pi r_{e1}}{p_c} \quad (12.42)$$

and

$$N_{e2} = \frac{2\pi r_{e2}}{p_c} \quad (12.43)$$

Note that N_{e1} and N_{e2} need not be integers in Equations 12.42 and 12.43.

12.3.2 Additional Nomenclature for Bevel Gears

Figure 12.21 shows some of the additional terms used with bevel gears. Notice that most of the information characteristic of teeth sizes is defined for the large end of the gear teeth. Also notice that the apex of the pitch cone is not coincident with the apex of the face cone. This is to ensure that there is a constant clearance between the addendum of the given gear and the dedendum of the meshing gear. This also allows a larger fillet at the small end of the tooth than would otherwise be possible.

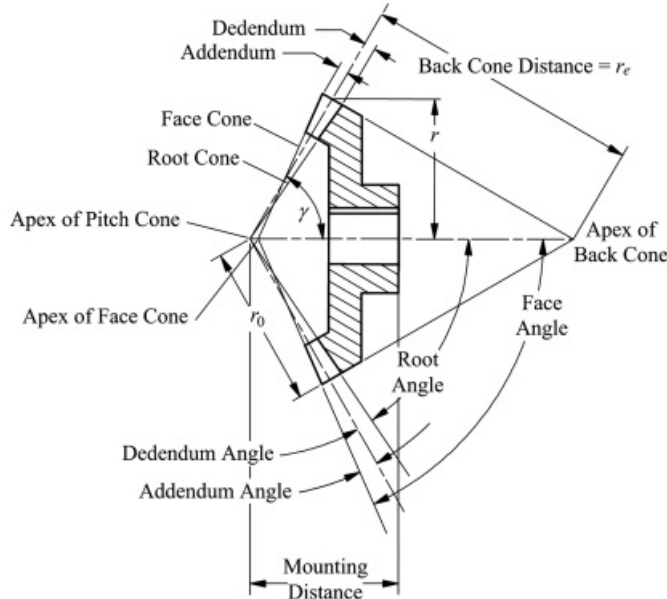


Figure 12.21 Nomenclature for bevel gears.

The AGMA [4] recommends a 20° pressure angle for bevel gears with 14 or more teeth and 25° for gears with 13 or fewer teeth. The minimum pressure angle is determined by undercutting on the pinion.

Bevel gears are usually mounted in a cantilever fashion. Because of this, the meshing gears will deflect away from each other, and the smaller end of the gears will carry even less load than they would without deflections. Because the large end of the gear tooth will carry most of the load, the face width of the teeth will be relatively small.

Typical design practices are to limit the face width to

$$F < 0.3r_e \text{ or } \frac{10.0}{p_d} \text{ (or } 10.0 \text{ mm)} \quad (12.44)$$

whichever is smaller [3]. This guideline is beneficial from a manufacturing standpoint because simpler tooling can be used with a narrower face width.

In addition to the general type shown in [Figure 12.18](#), there are three special types of bevel gears

1. Crown bevel gears
2. Miter gears
3. Angular bevel gears

Each of these is discussed briefly in the following.

12.3.3 Crown Bevel Gears and Face Gears

Crown bevel gears are the bevel-gear equivalent of a rack. A crown gear has a 90° pitch angle, and its teeth profiles are theoretically parts of great circles (the spherical equivalent of a straight line in the plane). The pitch cone of a crown gear is a cylinder of infinite radius, and the resulting involute teeth have straight sides. The pitch surface is a plane. Crown gears are shown in [Figures 12.22](#) and [12.23](#).

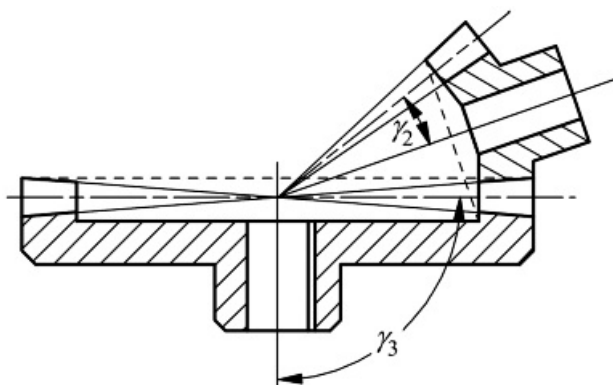


[Figure 12.22](#) Crown gear geometry.



[Figure 12.23](#) Crown gear model.

Face gears consist of a spur or helical pinion in combination with a conjugate gear of disk form. The face gear has the appearance of a crown gear except that the addendum and dedendum angles are zero. The gear is generated with a reciprocating pinion-shaped cutter that has the same diametral pitch and pressure angle as the mating pinion and is substantially the same size [5]. Face gears are shown in [Figures 12.24](#) and [12.25](#).

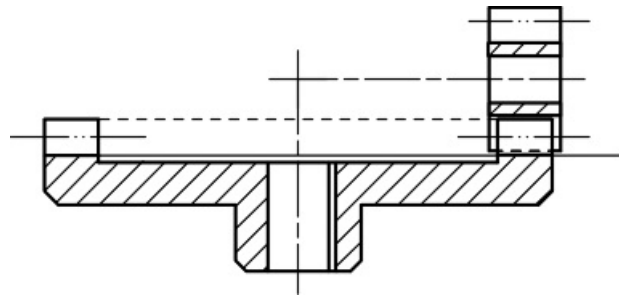


[Figure 12.24](#) Face gear geometry.



[Figure 12.25](#) Face gear and pinion [5].

12.3.4 Miter Gears

Miter gears are mating bevel gears with equal numbers of teeth and with axes at right angles. These gears are used to transmit power around a 90° corner. Miter gears are shown in [Figures 12.26](#) and [12.27](#).

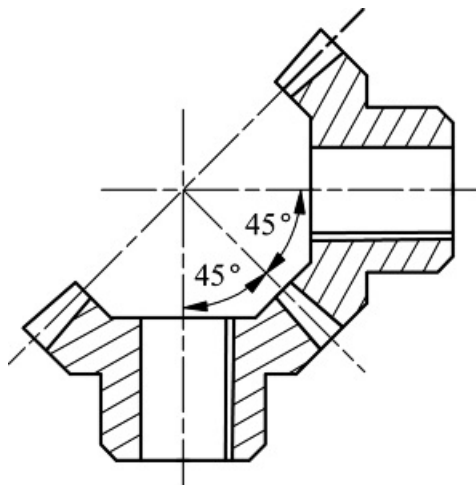


[Figure 12.26](#) Miter gear geometry.



[Figure 12.27](#) Miter gear model.

12.3.5 Angular Bevel Gears

Angular bevel gears have a shaft angle different from 90° . This is the most general type of bevel gear. Examples of angular bevel gears without a 90° shaft angle are shown in [Figures 12.28](#) and [12.29](#).

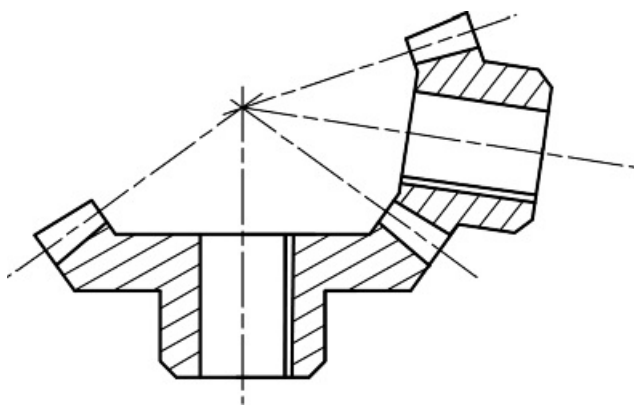


[Figure 12.28](#) Angular bevel gear geometry.



Figure 12.29 Angular bevel gear model.

The AGMA [4] gives a standardized approach to determine bevel gear tooth proportions. Bevel gears in this system have unequal addendums for mating teeth. Tables are provided for 20° pressure angle gears with a 45° pitch angle. For angular bevel gears with a shaft angle different from 90°, a calculation procedure is given.

A summary of the equations for bevel gears is given in [Table 12.5](#). A more complete list of equations is given by Townsend [6].

Table 12.5 Summary of Straight Bevel Gear Formulas (Pitch Information Is for the Large End of Gear)

Quantity	Formula
Pitch diameter	$d = \frac{N}{\beta} = \frac{N_2}{\beta} = N_3$
Pitch angle of gear	$\text{CLL } \gamma_2 = \frac{\sin \Sigma}{[d_3/d_2 + \cos \Sigma]} = \frac{\sin \Sigma}{[N_3/N_2 + \cos \Sigma]}$
Pitch angle of pinion	$\text{CLL } \gamma_3 = \frac{\sin \Sigma}{[d_2/d_3 + \cos \Sigma]} = \frac{\sin \Sigma}{[N_2/N_3 + \cos \Sigma]}$
Circular Pitch	$p = \frac{p}{\beta} = \bar{p} N_3$
Shaft angle	$\Sigma' = \gamma_2 + \gamma_3$
Equivalent spur gear radius	$r_{e_i} = \frac{r_i}{\cos \gamma_i}, i = 2, 3$
No. teeth on equiv. spur gear	$N_{e_i} = \frac{2\pi r_{e_i}}{p}, i = 2, 3$
Outer cone distance	$r_o = \frac{d_2}{2 \tan \gamma_2} = \frac{d_3}{2 \tan \gamma_3}$
Minimum face width	$F < 0.37, \text{ or } \frac{10.0}{\beta} (\text{or } 10.0 \text{ mm})$
Velocity ratio	$\frac{\omega_2}{\omega_3} = \frac{N_3}{N_2} = \frac{d_3}{d_2} = \frac{r_3}{r_2}$

12.3.6 Zerol Bevel Gears

The previous examples of bevel gears have straight teeth. In addition to these gears, there are two types of bevel gears that have curved teeth. Zerol gears are patented bevel gears that have curved teeth but zero spiral angle at the middle of the teeth. Zerol gears have the same general tooth actions as straight bevel gears, and they can be used to

replace straight-toothed bevel gears. The primary advantage over straight-toothed bevel gears is that they can be cut in the same machines used for spiral bevel gears, and the teeth can be easily ground.

Most modern straight-toothed bevel gears are also slightly convex, so the contact occurs in the central section of the teeth. This avoids contact on the narrower (and weaker) part of the teeth and allows a slight amount of adjustment when the gears are installed.

12.3.7 Spiral Bevel Gears

An example of spiral bevel miter gears is shown in [Figure 12.30](#). Spiral bevel gears have obliquely curved teeth. As in the case of straight-toothed bevel gears, the pitch cones of spiral bevel gears intersect and have a common apex. Spiral bevel gears are analogous to helical gears and are used for the same purpose. Spiral bevel gears have a gradual load transfer as the teeth engage, and they are much quieter and stronger than straight toothed bevel gears.

Therefore, spiral bevel gears are used for essentially all high-speed applications. The spiral angle ([Figure 12.31](#)) is such that the tooth face advances due to the spiral exceeding the circular pitch. This provides a smooth transition of load from tooth to tooth and minimizes much of the tooth vibration that creates gear whine. This is in contrast to straight and Zerol bevel gears, with which the load is transferred from tooth to tooth immediately across the entire contact area. The geometries of Zerol and spiral bevel gears are compared in [Figure 12.32](#). The AGMA [5] gives standardized equations and graphs for determining spiral bevel tooth profiles.



[Figure 12.30](#) Spiral bevel miter gears.

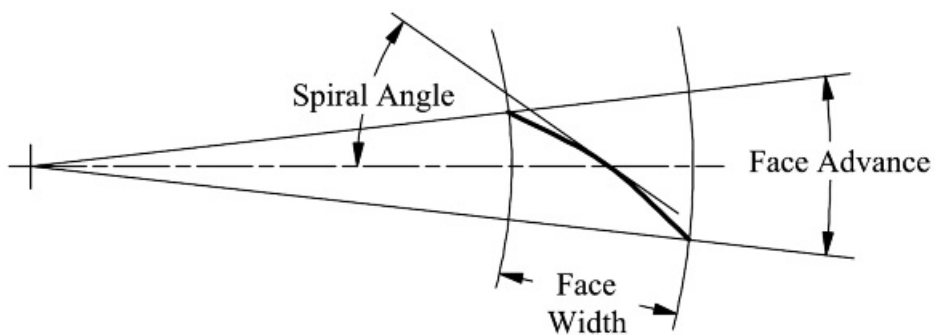


[Figure 12.31](#) Geometry of one spiral gear tooth.

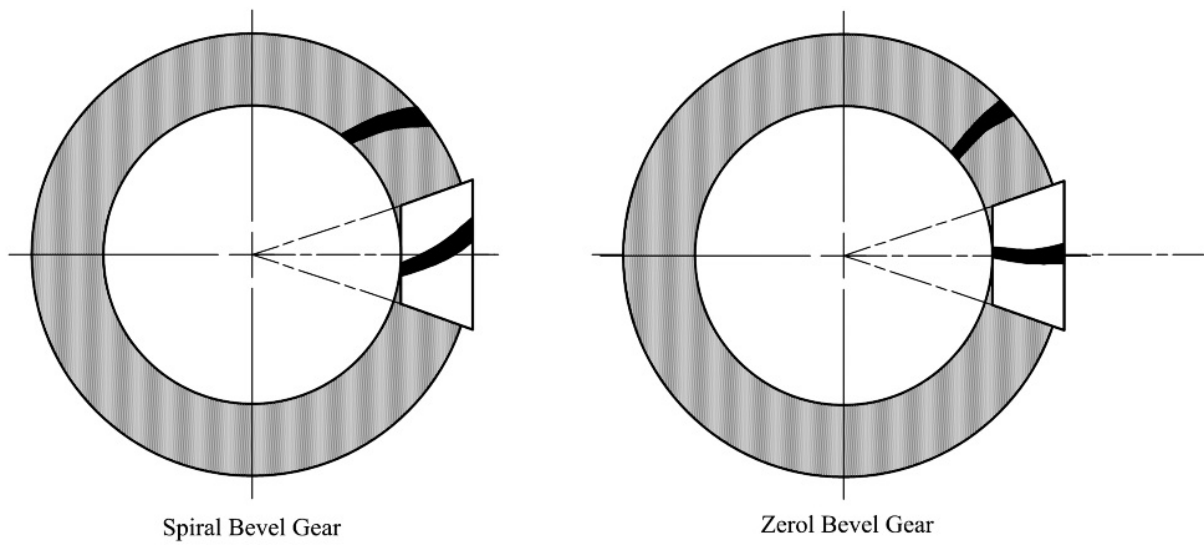


[Figure 12.32](#) Comparison of spiral bevel gear and Zerol bevel gear.

12.3.8 Hypoid Gears

Hypoid gears are similar in appearance to spiral bevel gears; however, the shaft axes do not intersect (see [Figure 12.33](#)). The pitch surfaces of hypoid gears are not cones, as in the case of spiral bevel gears, but are hyperboloids of revolution (see [Figure 12.34](#)). This permits the teeth to maintain line contact.

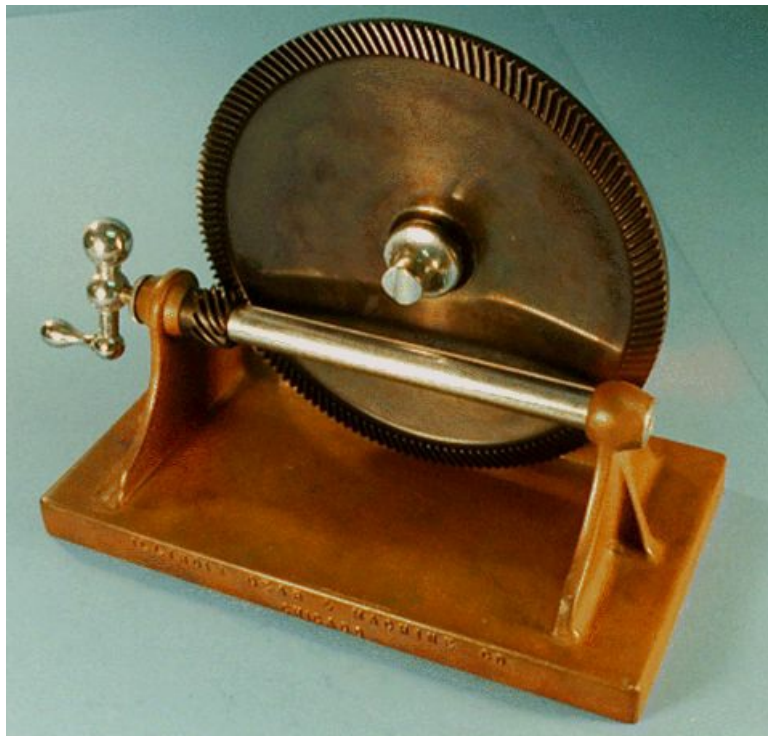


[Figure 12.33](#) Hypoid gear set.

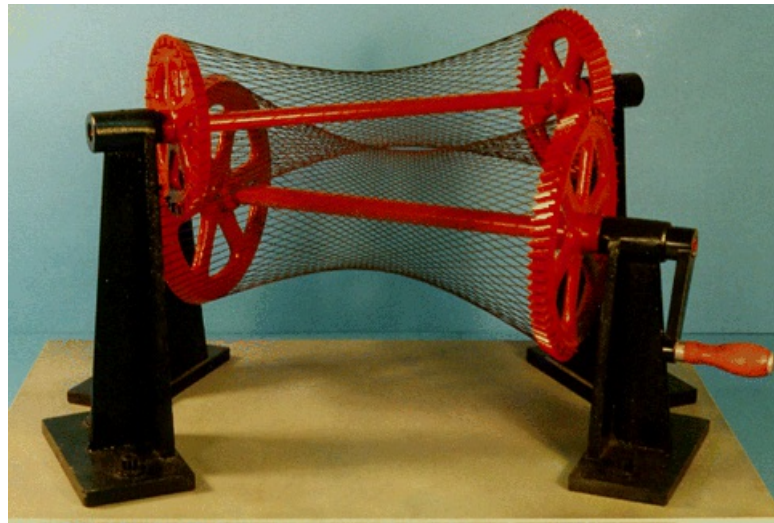


[Figure 12.34](#) The pitch surfaces of hypoid gears are hyperboloids of revolution.

Hypoid gears are used in the differentials of rear wheel-driven automobiles because the geometry lowers the level of the drive shaft. This permits a lower body. Another advantage of hypoid gears over spiral bevel gears is that the hypoid pinion teeth are stronger. This is because the hypoid pinion can be designed so that the spiral angle of the pinion is larger than that of the gear. This results in a larger and stronger pinion tooth than that of a spiral bevel pinion. Because of the length of contact on each gear tooth, hypoid gears are quieter than spiral bevel gears. They can also be used with higher reduction ratios.



References

1. American Gear Manufacturers' Association (AGMA). (1968). "Tooth Proportions for Coarse Pitch Involute Spur Gears." AGMA Publication 201.02 and 201.02A.
2. Shigley, J. E. (1975). *Kinematic Analysis of Mechanisms*. New York, NY: McGraw-Hill.
3. Mabie, H. H., and Reinholtz, C. F. (1987). *Mechanisms and Dynamics of Machinery*, 4th Ed. New York, NY: John Wiley & Sons.
4. American Gear Manufacturers' Association (AGMA). (1988). "Design Manual for Bevel Gears." AGMA Publication 2005-B88, May.
5. American Gear Manufacturers' Association (AGMA). (1973). "Fine-Pitch On-Cutter Face Gears for 20-Degree Involute Spur Pinions." AGMA Publication 203.03, May.
6. Townsend, D. P. (1992). *Dudley's Gear Handbook*. New York, NY: McGraw-Hill.



Problems

- 12.1** Two helical gears are cut with a spur gear hob that has a diametral pitch of 4 and a pressure angle of 20° . The pinion has 15 teeth, the gear has 35 teeth, and the helix angle is 30° . Determine the minimum recommended face width. Using the minimum face width, find the transverse diametral pitch, the pitch cylinder radii, and the axial, transverse, and total contact ratios.
- 12.2** Two helical gears are cut with the same tooth numbers and with the same cutter as given in Problem 12.1. The helix angle is 30° . Find the transverse pressure angle, the transverse diametral pitch, and the axial pitch.
- 12.3** Two parallel helical gears are cut with a 20° normal pressure angle and a 45° helix angle. They have a diametral pitch of 12 in the normal plane and have 10 and 41 teeth, respectively. Find the transverse pressure angle, transverse circular pitch, and transverse diametral pitch. Also determine the minimum face width, and using that face width, determine the total contact ratio.
- 12.4** A helical gear has 18 teeth and a transverse diametral pitch of 6. The face width is 1.5, and the helix angle is 25° . Determine the axial pitch, normal pitch, lead, transverse pitch diameter, and minimum face width.
- 12.5** Two helical gears have 20 and 34 teeth and a normal diametral pitch of 8. The left-handed pinion has a helix angle of 40° and a rotational speed of 1000 rpm. The gear is also left-handed and has a helix angle of 40° . Determine the angular velocity of the gear, transverse diametral pitch of each gear, and pitch diameters.
- 12.6** Two standard spur gears have a diametral pitch of 10, a pressure angle of 20° , and a velocity ratio equal to 3.5:1. The center distance is 8.55 in. Two helical gears are to be used to replace the two spur gears such that the center distance and angular velocity ratio remain unchanged. The helical gears are also to be cut with the same hob as that used to cut the spur gears. Determine the helix angle, tooth numbers, and minimum face width for the new gears if the helix angle is kept to a minimum.
- 12.7** Two standard spur gears have a diametral pitch of 16 and a pressure angle of 20° . The tooth numbers are 36 and 100, and the gears were meshed at a standard center distance. After the gear reducer was designed and tested, the noise of the drive was found to be excessive. Therefore, the decision was made to replace the spur gears with helical gears. The helix angle chosen was 22° , and the tooth numbers were to remain unchanged. Determine the change in center distance required.
- 12.8** A spur gear transmission consists of a pinion that drives two gears. The pinion has 24 teeth and a diametral pitch of 12. The velocity ratio for the pinion and one gear is 3:2 and for the pinion and the other gear is 5:2. To reduce the noise level, all three gears are to be replaced by helical gears such that the center distances and velocity ratios remain the same. The helical gears will be cut with a 16 pitch, 20° hob. If the helix angle is kept as low as possible, determine the number of teeth, face width, hand, helix angle, and outside diameter for each of the gears.
- 12.9** A pair of helical gears have a module in the normal plane of 3 mm, a normal pressure angle of 20° , and a helix angle of 45° . The gears mesh with parallel shafts and have 30 and 48 teeth. Determine the transverse module, the pitch diameters, the center distance, and the minimum face width.
- 12.10** Two 20° spur gears have 36 and 90 teeth and a module of 1.5. The spur gears are to be replaced by helical gears such that the center distance and velocity ratio are not changed. The maximum allowed face width is 12.7 mm, and the hob module is 1.5 mm. Design the helical gear pair that has the smallest helix angle possible. Determine the numbers of teeth, the face width, the helix angle, and the outside diameters of the gears.
- 12.11** Two helical gears are cut with a 20° hob with a module of 2. One gear is right-handed, has a 30° helix angle, and has 36 teeth. The second gear is left-handed, has a 40° helix angle, and has 72 teeth. Determine the shaft angle, the angular velocity ratio, and the center distance.
- 12.12** Two crossed shafts are connected by helical gears such that the velocity ratio is 3:1 and the shaft angle is

60° . The center distance is 10 in, and the normal diametral pitch is 8. The pinion has 35 teeth. Assume that the gears are the same hand and determine the helix angles, pitch diameters, and recommended face widths.

12.13 Two crossed shafts are connected by helical gears such that the velocity ratio is 3:2 and the shaft angle is 90° . The center distance is 5 in. Select a pair of gears that will satisfy the design constraints. What other information might be considered to reduce the number of arbitrary choices for the design?

12.14 A helical gear with a normal diametral pitch of 8 is to be used to drive a spur gear at a shaft angle of 45° . The helical gear has 21 teeth, and the velocity ratio is 2:1. Determine the helix angle for the helical gear and the pitch diameter of both gears.

12.15 Two crossed helical gears connect shafts making an angle of 45° . The pinion is right-handed, has a helix angle of 20° , and contains 30 teeth. The gear is also right-handed and contains 45 teeth. The transverse diametral pitch of the gear is 5. Determine the pitch diameter, the normal pitch, and the lead for each gear.

12.16 The worm of a worm gear set has 2 teeth, and the gear has 58 teeth. The worm axial pitch is 1.25 in, and the pitch diameter is 3 in. The shaft angle is 90° . Determine the center distance for the two gears, the helix angle, and the lead for the worm.

12.17 The shaft angle between two shafts is 90° , and the shafts are to be connected through a worm gear set. The center distance is 3 in, and the velocity ratio is 30:1. Determine a worm and gear that will satisfy the design requirements. Specify the number of teeth, lead angle, and pitch diameter for each gear. Also, determine the face width for the gear.

12.18 A worm with two teeth drives a gear with 50 teeth. The gear has a pitch diameter of 8 in and a helix angle of 20° . The shaft angle between the two shafts is 80° . Determine the lead and pitch diameter of the worm.

12.19 Two straight-toothed bevel gears mesh with a shaft angle of 90° and a diametral pitch of 5. The pinion has 20 teeth, and the gear ratio is 2:1. The addendum and dedendum are the same as for 20° stub teeth. For the gear, determine the pitch radius, cone angle, outside diameter, cone distance, and face width.

12.20 A pair of straight-toothed bevel gears mesh with a shaft angle of 90° and a diametral pitch of 6. The pinion has 18 teeth, and the gear ratio is 2:1. The addendum and dedendum are the same as for 20° full-depth spur-gear teeth. Determine the number of teeth on the gear and the pitch diameters of both the pinion and gear. Also, for the gear, determine the pitch-cone angle, outside diameter, cone distance, and face width.

12.21 A pair of straight-toothed bevel gears mesh with a shaft angle of 80° and a diametral pitch of 7. The pinion has 20 teeth and a pitch cone angle of 40° . The gear ratio is 3:2. Determine the number of teeth on the gear and the pitch diameters of both the pinion and gear. Also, determine the equivalent spur gear radii for both the pinion and the gear.

12.22 A pair of straight-toothed bevel gears mesh with a shaft angle of 45° and a module of 5.08. The pinion has 16 teeth and a pitch cone angle of 20° . The gear ratio is 3:2. Determine the number of teeth on the gear and the pitch diameters of both the pinion and gear. Also determine the back-cone distance and the back-cone angle for the gear.

13

GEAR TRAINS

Prerequisite Knowledge Needed for Chapter 13

A knowledge of the material on general gears from [Chapters 11](#) and [12](#) and a familiarity with vector mechanics.



13.1 General Gear Trains

In [Chapters 11](#) and [12](#), the characteristics of individual gears were discussed. However, in general, gears are of interest to designers only when they are used in pairs as motion and/or force transducers. These gear pairs can be combined in many ways to achieve desired input/output relationships. A combination of one or more gear pairs that are interrelated is called a gear train. All complex gear trains are combinations of the simple, compound, and planetary gear trains discussed in this chapter.



13.2 Direction of Rotation

As discussed in [Chapters 11](#) and [12](#), the velocity ratio for two meshing gears (2 and 3) is

$$R = \pm \frac{\omega_2}{\omega_3} = \pm \frac{r_3}{r_2} = \pm \frac{N_3}{N_2} \quad (13.1)$$

where r_i and N_i are the pitch radii and number of teeth on gear i ($i = 2, 3$), the plus sign goes with an external gear meshing with an internal gear, and the minus sign goes with two external gears meshing.

When planar gears are involved, [Equation 13.1](#) can be used directly because all of the vectors are parallel. However, when bevel and crossed helical gears are involved, the angular velocities must be treated as vectors. For bevel gears, a relatively simple way to do this is to recognize that at the pitch point (the end of the tangent line to the pitch surfaces), rolling occurs, and the velocity at the pitch point on both gears is the same. From this, the direction of rotation can be inferred from the simple velocity relationship

$$v_{P_2} = v_{P_3} = \omega_2 \times r_2 = \omega_3 \times r_3 \quad (13.2)$$

where the pitch radius vectors (r_2 and r_3) for gears 2 and 3, respectively, are directed from the rotation axis to the pitch point. For bevel gears, the large end of the gear is used for the measurement of the pitch radii. This is shown in [Figure 13.1](#).

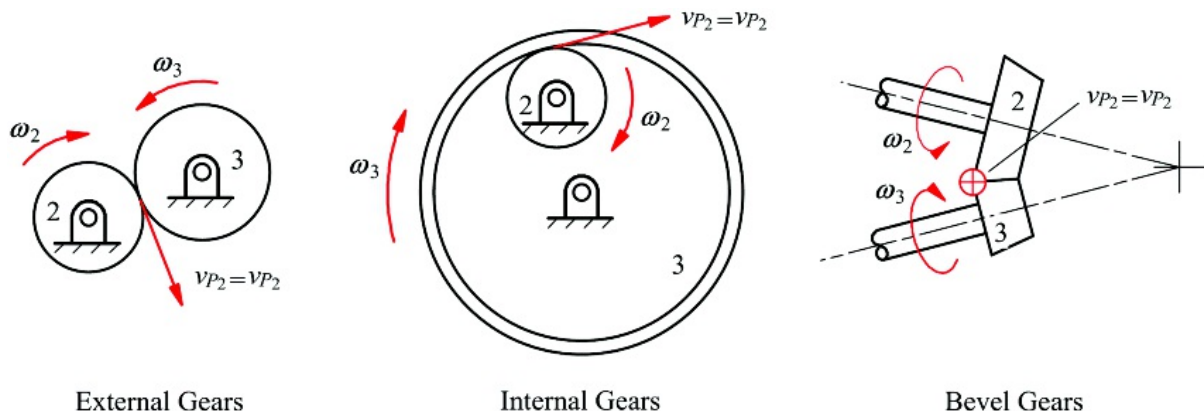


[Figure 13.1](#) The direction of the angular velocities of two meshing gears can be determined from the direction of the velocity of the pitch point.

When crossed helical gears are involved, the process becomes a little more complicated because the hand of the gears, that is, the direction of twist of the helical teeth, affects the direction of rotation of the driven gear as shown in [Figure 13.2](#). To determine the direction of rotation of the pinion relative to the gear, treat the pinion as a screw and the gear as fixed. Observe the motion of the pinion relative to the gear as the pinion is rotated and the gear is viewed along the gear axis. If the pinion appears to advance toward the gear when the pinion is rotated, in reality the gear would rotate counterclockwise. If the pinion appears to withdraw from the gear when the pinion is rotated, the gear would rotate clockwise.

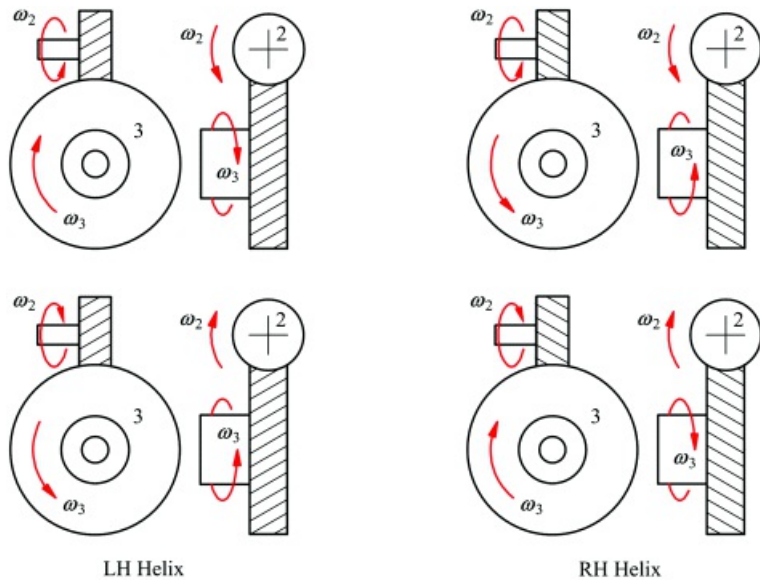
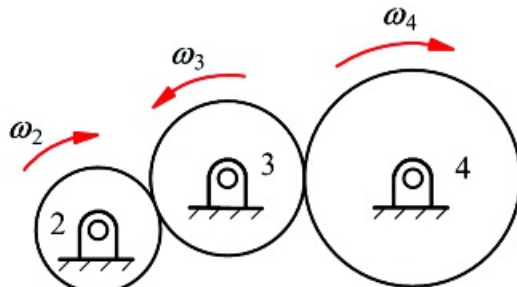


Figure 13.2 The direction of the angular velocities for crossed helical gears.



13.3 Simple Gear Trains

Simple gear trains can be divided into two types depending on whether idler gears are involved or not. Simple gear trains have only one gear on each shaft. These shafts rotate on bearings that are attached to the same frame. The gears may be of any type, for example, spur, bevel, hypoid, and worm. [Figures 13.3–13.5](#) show various simple gear trains.



[Figure 13.3](#) A simple gear train with all external gears and one idler (gear 3).

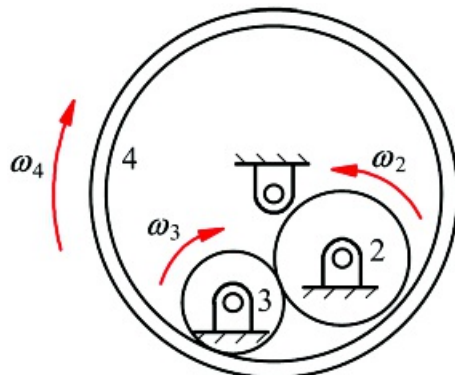


[Figure 13.4](#) A simple gear train with external gear and one idler (gear 3).

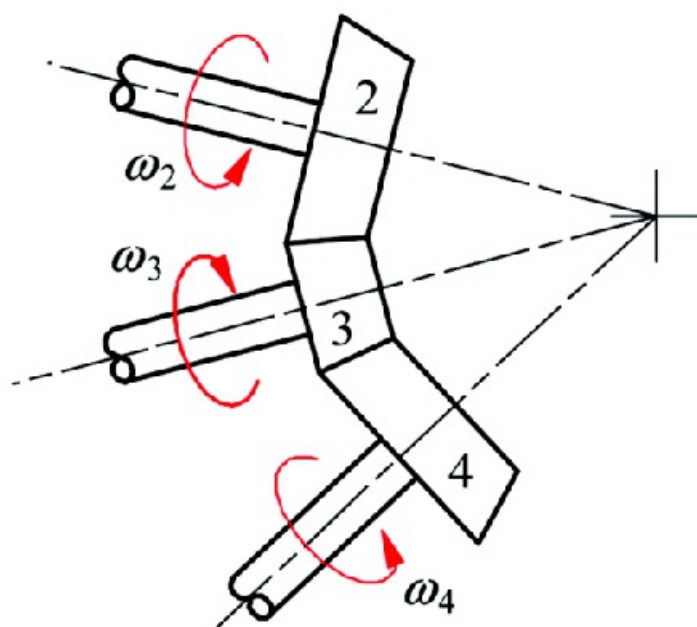


[Figure 13.5](#) A simple gear train with external bevel gears and one idler (gear 3).

The idler gears in simple gear trains can serve two purposes in design. One is to change the direction of motion of

the output gear, and the second is to provide a spacer when two gears cannot be directly meshed because of the shaft locations. This occurs when there is a limit to the sizes that two gears can be, but the shaft location is specified for reasons other than kinematics.

In gear trains, the overall gear reduction ratio for the gearbox is usually of interest. This can be determined by writing the velocity ratio in terms of the tooth numbers at each mesh. For example, in [Figure 13.3](#)

$$\frac{\omega_2}{\omega_3} = -\frac{N_3}{N_2} \quad (13.3)$$

and

$$\frac{\omega_3}{\omega_4} = -\frac{N_4}{N_3} \quad (13.4)$$

Multiplying [Equation 13.4](#) by [Equation 13.3](#) gives

$$\frac{\omega_2 \omega_3}{\omega_3 \omega_4} = \left(-\frac{N_3}{N_2}\right) \left(-\frac{N_4}{N_3}\right)$$

or

$$\frac{\omega_2}{\omega_4} = (-1)^2 \left(\frac{N_4}{N_2}\right) = \frac{N_4}{N_2} \quad (13.5)$$

If we analyze the gear train in [Figure 13.4](#), we will get

$$\frac{\omega_2 \omega_3}{\omega_3 \omega_4} = \frac{\omega_2}{\omega_4} = \left(-\frac{N_3}{N_2}\right) \left(\frac{N_4}{N_3}\right) = (-1)^1 \left(\frac{N_4}{N_2}\right) = -\left(\frac{N_4}{N_2}\right) \quad (13.6)$$

The analysis of the gear train in [Figure 13.5](#) is more difficult because we must treat the angular velocities as vectors to determine the directions mathematically. However, if we trace the angular-velocity directions using the procedure indicated in [Figure 13.1](#), we can determine the direction and compute the magnitude of the angular velocities separately. If we do this, we will find that the magnitude of the overall velocity ratio is given by

$$\frac{\omega_2}{\omega_4} = \frac{N_4}{N_2}$$

If we add more idler gears, the effect will be the same. Namely, the magnitude of the velocity ratio between the input and output shafts is a function of the numbers of teeth on the input and output gears only. The magnitude of the velocity ratio is independent of the size and number of idler gears. The sign of the train ratio for parallel-shaft gears, however, does depend on the number of idler gears. In particular, at each mesh between external gears, the velocity ratio changes sign. For internal gears, the velocity ratio remains the same sign. Therefore, if n is the number of meshes between *external* gears, the sign of the velocity ratio is given by $(-1)^n$. Note that each idler gear will have at least two mesh points.

A simple gear train can involve any number and types of gears. However, each gear in the gear train must be able to mesh with any other gear. Therefore, each gear must have the same normal pitch if the gears are to mesh

properly.

13.3.1 Simple Reversing Mechanism

An idler gear can be used in a simple reversing mechanism shown in [Figure 13.6](#). This is a procedure commonly used to reverse the direction of rotation of the lead screw on small metal lathes. The procedure adds an extra idler to the simple gear train when the direction of rotation is to be reversed. The mechanism works well only when the gears are slowly moving or at rest, since there is no provision for ensuring that the gears will mesh easily when the direction change is made.

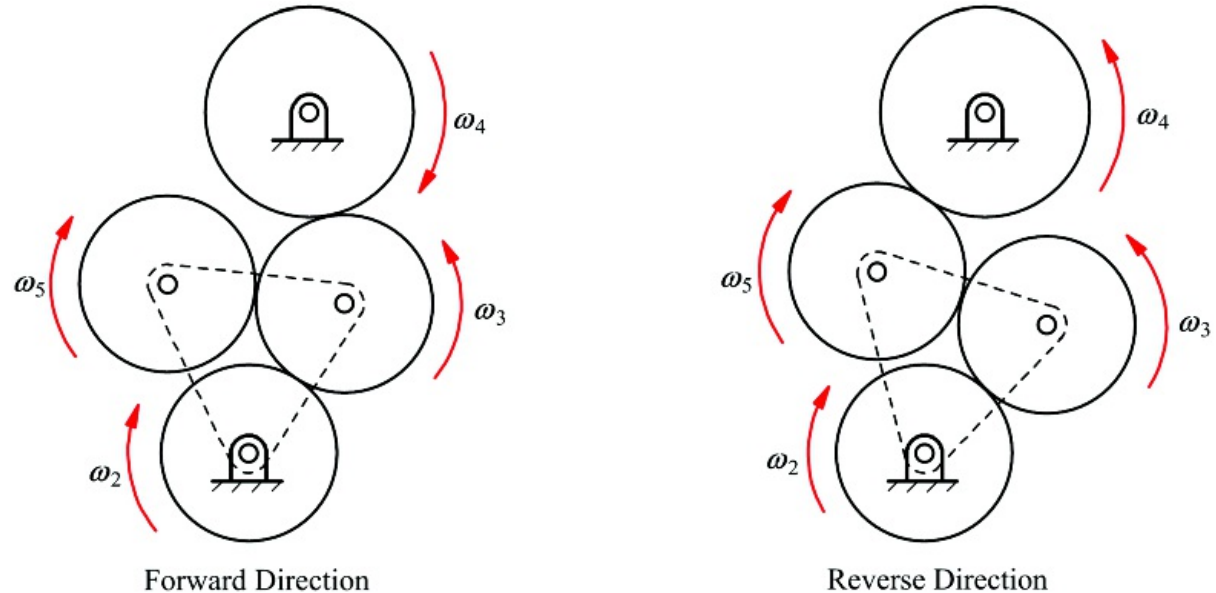


[Figure 13.6](#) A simple reversing mechanism using an extra idler gear.



13.4 Compound Gear Trains

For all types of gears, the velocity ratio is limited for each mesh by practical size and undercutting considerations. For example, in spur gears, the velocity ratio at any mesh should not exceed 1:5. For larger reductions, compound gear trains should be used. Compound gear trains are characterized by the presence of two or more gears attached to the same shaft. The shafts, however, still rotate on bearings that are fixed to the frame. Unlike simple gear trains, the gears in a compound gear train need not and generally will not be of the same type. This is evident in [Figure 13.7](#), which shows an example of a commercial gear reducer.

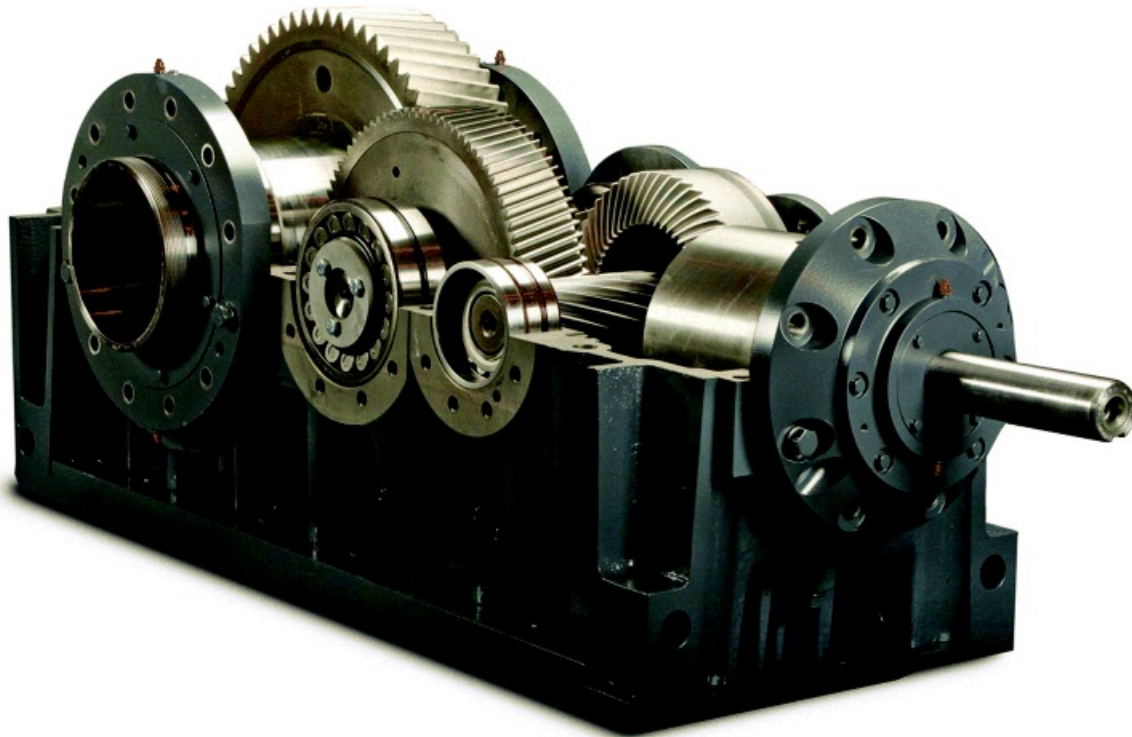


[Figure 13.7](#) A compound gear train. (Courtesy of Rexnord, West Milwaukee, Wisconsin)

The velocity ratios attainable in a compound gear train can be any size, with ratios in the thousands being possible. There is no theoretical limit to the number of passes (gear meshes) that can be made; however, practical issues such as friction and the functional need restrict the number in most applications.

A compound gear train is shown in [Figure 13.8](#). The symbolism often used for gear trains is also illustrated in the figure. The velocity ratio for the gear mesh can be written as

$$\frac{\omega_2}{\omega_3} = -\frac{N_3}{N_2} \quad (13.7)$$

and

$$\frac{\omega_4}{\omega_3} = -\frac{N_5}{N_4} \quad (13.8)$$

Because gears 3 and 4 are rigidly attached to the same shaft, we know that $\omega_3 = \omega_4$. The overall gear train velocity ratio is given by ω_2/ω_5 .

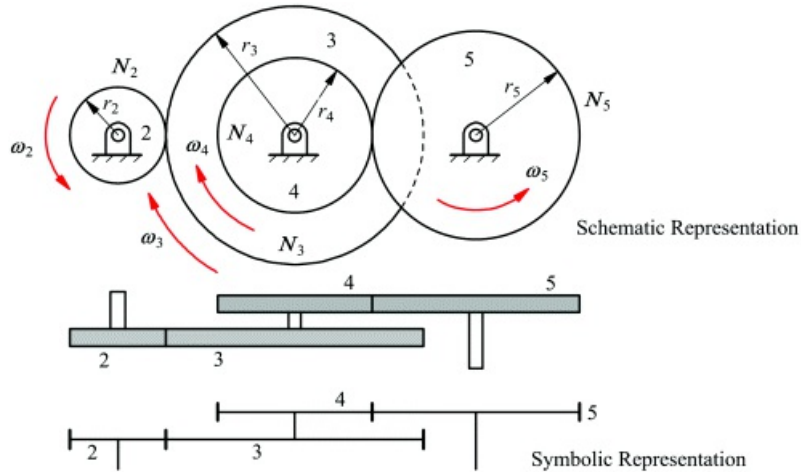


[Figure 13.8](#) A compound gear train.

If we solve [Equation 13.7](#) for ω_2 and [Equation 13.8](#) for ω_5 and use $\omega_3 = \omega_4$, the overall velocity ratio can be written as

$$\frac{\omega_2}{\omega_5} = \frac{-\omega_3 \frac{N_3}{N_2}}{-\omega_4 \frac{N_4}{N_5}} = \frac{\frac{N_3}{N_2}}{\frac{N_4}{N_5}} = \frac{N_3 N_5}{N_2 N_4} \quad (13.9)$$

or

$$\frac{\omega_2}{\omega_5} = \frac{\omega_2 \omega_4}{\omega_3 \omega_5} = \frac{N_3 N_5}{N_2 N_4} \quad (13.10)$$

From [Equation 13.10](#), it is clear that we can compute the overall velocity ratio from the product of the velocity ratios at each mesh. We can do this either in terms of the velocities directly, or more beneficially, in terms of the tooth numbers. Notice that when parallel-shaft gearing is involved, we can also use the ratios of the pitch circle radii (or diameters), since these will be directly proportional to the tooth numbers. [Equation 13.10](#) can then be extended to

$$\frac{\omega_2}{\omega_5} = \frac{\omega_2 \omega_4}{\omega_3 \omega_5} = \frac{N_3 N_5}{N_2 N_4} = \frac{r_3 r_5}{r_2 r_4} \quad (13.11)$$

However, the most convenient parameter to use when computing velocity ratios is the tooth number on each gear. This is because the velocity ratios can be directly equated to the tooth ratios for all types of gearing, whereas the ratios of the pitch cylinder radii alone are not valid for gears with nonparallel shafts.

If we start with gear 2 as the input gear, we can treat each mesh of the gear train as having an input side and an output side. For example, in [Figure 13.8](#), at the mesh between gears 2 and 3, gear 2 would be the driver and gear 3 would be the driven gear. At the mesh between gears 4 and 5, gear 4 would be the driver and gear 5 would be the driven gear. Therefore, N_3 and N_5 would be associated with driven gears, and N_2 and N_4 would be associated with driver gears. In [Equation 13.11](#), the velocity ratio can be represented as the product of the driven gear numbers divided by the product of the driver gear numbers. This situation holds in general for compound gear trains. Mathematically, if n is the number of gear meshes (including idlers that each have two meshes), a general expression for the magnitude of the velocity ratio can be written as

$$\frac{\omega_{\text{output}}}{\omega_{\text{input}}} = \frac{\prod_{i=1}^n N_i}{\prod_{j=2}^m N_j} = \frac{\text{product of drive}_1^M \text{ tooth numbers}}{\text{product of drive}_2^M \text{ tooth numbers}} \quad (13.12)$$

Assuming that the gears are numbered sequentially, in [Equation 13.12](#), i includes only the tooth numbers for the odd gear numbers and j includes only the tooth numbers for the even gear numbers. The sign of the gear ratio depends on the type of gears. If all parallel-shaft gears are involved, we can use an extension of [Equation 13.4](#). Then

$$\frac{\omega_{\text{output}}}{\omega_{\text{input}}} = (-1)^m \frac{\prod_{i=1}^n N_i}{\prod_{j=2}^m N_j} = (-1)^m \frac{\text{product of drive}_1^M \text{ tooth numbers}}{\text{product of drive}_2^M \text{ tooth numbers}}$$

where m is the number of meshes involving external gears.



Example 13.1

Analysis of Compound Gear Train

Assume that the compound gear train in [Figure 13.9](#) has the tooth numbers given in parentheses. The angular velocity of gear 2 is 200 rpm in the direction shown. Find the magnitude and direction of the angular velocity of gear 10 and the velocity (magnitude and direction) of the rack that is gear 11.

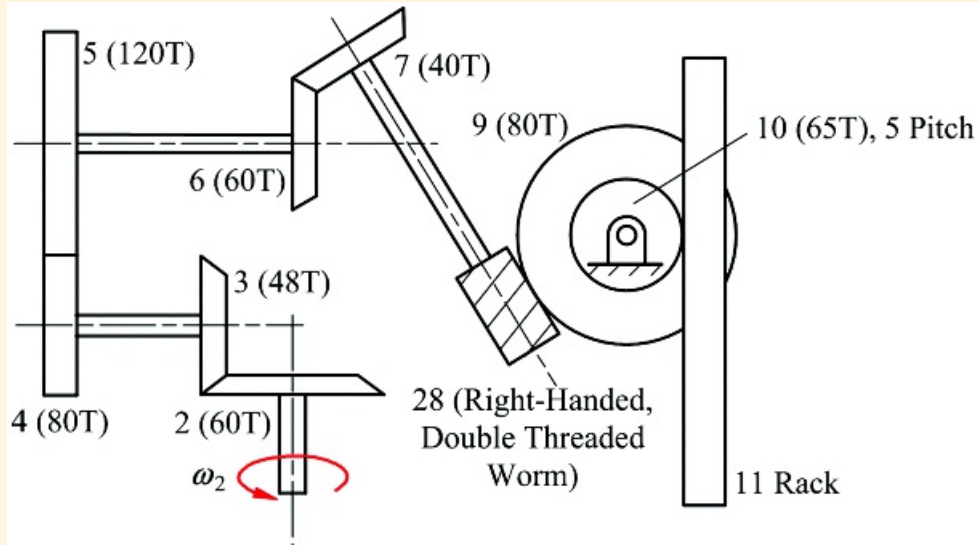


[Figure 13.9](#) The gear train for Example 13.1.

Solution

The velocity ratio for the gear drive between gears 2 and 9 is given by

$$\frac{\omega_9}{\omega_2} = \frac{N_2 N_4 N_5 N_3}{N_3 N_5 N_7 N_2}$$

Therefore

$$\omega_9 = \omega_2 \frac{N_2 N_4 N_6 N_8}{N_3 N_5 N_7 N_2}$$

and

$$\omega_9 = 200 \frac{60 \cdot 80 \cdot 60 \cdot 2}{48 \cdot 120 \cdot 40 \cdot 80} = 6.25 \text{ rpm}$$

The velocity of the rack will be equal to the linear velocity of the pitch point on gear 10. The angular velocity of gear 10 is equal to the angular velocity of gear 9. The pitch diameter of gear 10 is given by

$$\delta_{10} = \frac{N_{10}}{P_{10}} = \frac{65}{5} = 13 \text{ in}$$

Therefore, the pitch velocity is given by

$$v = \frac{\pi D_1 \omega_1}{2} = (0.25)(12)(2\pi/60) = 4.255 \text{ m/s}$$

However, we must now determine in which direction the rack moves (up or down). To do this, trace the pitch point velocities at each mesh. This is shown in [Figure 13.10](#). Gear 8 is a right-handed worm gear. Therefore, it will advance relative to gear 9 for a clockwise rotation. Consequently, gear 9 will rotate clockwise relative to the frame (link 1). If gear 9 and 10 rotate clockwise, then the rack will move down as shown.

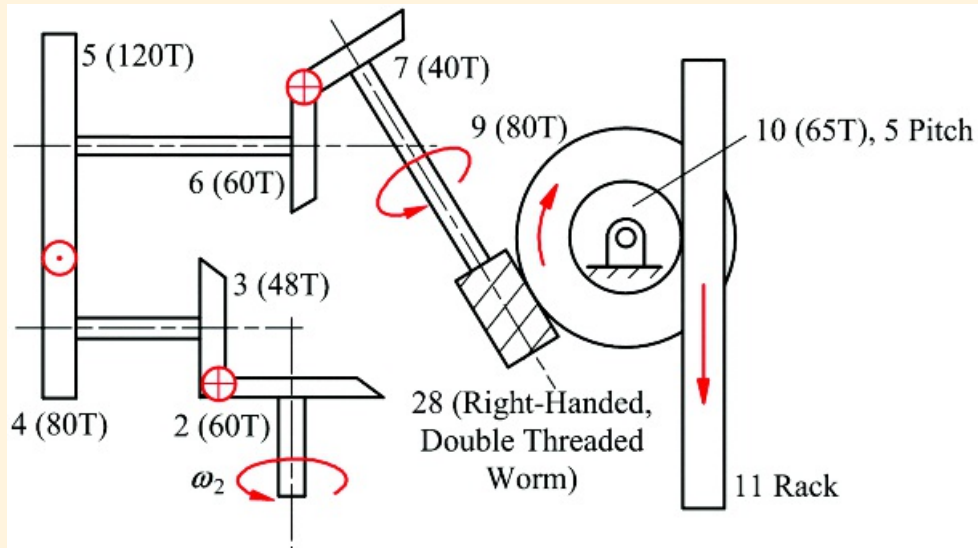


[Figure 13.10](#) The directions of gear motion for Example 13.1.

13.4.1 Concentric Gear Trains

In a concentric gear train, the input and output shafts are collinear. An example of a concentric gear train is shown in [Figure 13.11](#). These gear trains are analyzed in much the same way as any compound gear train; however, the design is somewhat more complex. In the following, we will restrict the discussion to parallel-shaft gearing with a double reduction to illustrate a possible design procedure.

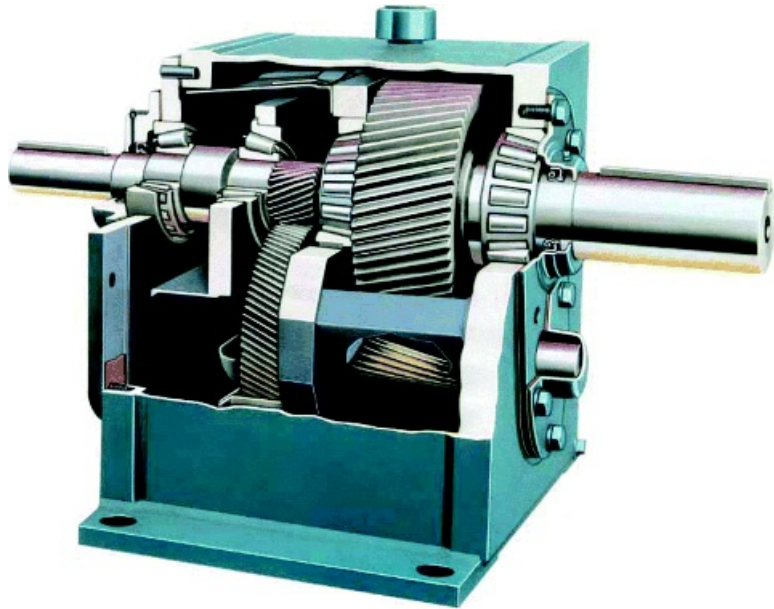


Figure 13.11 Falk UltraMax Concentric Gear Drive. (Courtesy of Rexnord, West Milwaukee, Wisconsin)

A concentric gear train with a two-stage reduction is shown in [Figure 13.12](#). A principal requirement for a concentric gear reducer is that

$$r_2 + r_3 = r_4 + r_5 \quad (13.13)$$

In addition, there may be a precise requirement for the overall reduction ratio. From before, the reduction ratio is given by

$$R = \frac{\omega_2}{\omega_5} = \frac{r_3 r_5}{r_1 r_4} = \frac{N_3 N_5}{N_1 N_4} \quad (13.14)$$

To mesh properly, gears 2 and 3 must have the same normal pitch, and gears 4 and 5 must have the same normal pitch. If helical gears are involved, we must select the helix angles, and this will give us some latitude in the design. Then

$$\frac{N_2}{2r_2} = P_{n2} \cos \psi_2 \quad (13.15)$$

$$\frac{N_3}{2r_3} = P_{n2} \cos \psi_2$$

and

$$\frac{N_4}{2r_4} = P_{n4} \cos \psi_4 \quad (13.16)$$

$$\frac{N_5}{2r_5} = P_{n4} \cos \psi_4$$

In [Equations 13.13–13.16](#) there are 12 unknowns and six equations. In addition, there is the constraint that the tooth numbers must be integers. Therefore, we can select six of the variables to solve the equations subject to the constraint that the tooth numbers are integers.

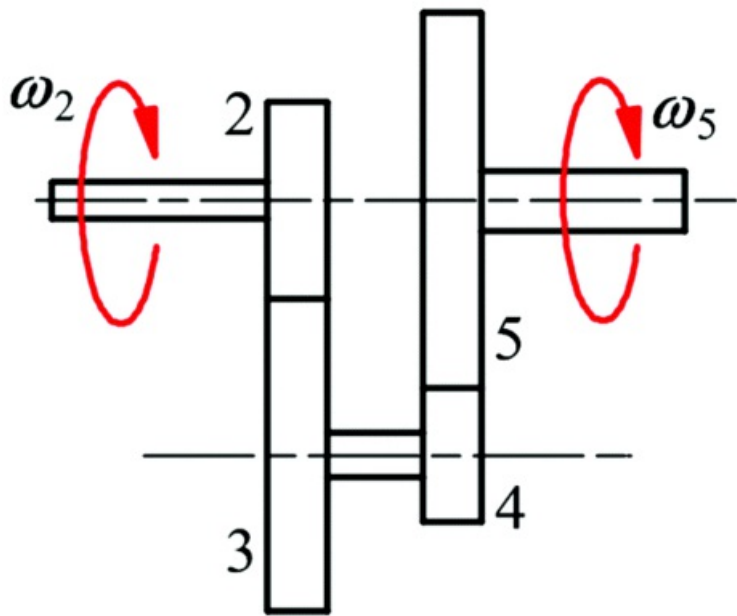


[Figure 13.12](#) A concentric gear reducer with a two-stage reduction.

One design approach is to select first the tooth numbers to satisfy [Equation 13.14](#), which is typically the most difficult equation to satisfy. This is equivalent to selecting three of the variables. It may not always be easy or even possible to select tooth numbers in a practical range to solve [Equation 13.14](#) exactly. If the values of R are formed by ratios of small whole numbers, for example $1/2$, $7/4$, $4/9$, many choices of whole numbers will satisfy the problem. In such cases, the best choice can be selected on the basis of criteria other than kinematics. However, other values of R are impossible to generate with simple gears. Examples are the square root of 2 and the ratio of two prime numbers (e.g., $503/2003$). In such cases, it may only be possible to approximate the value for R .

When the machine function does not require an exact ratio, it is usual to select tooth numbers for a meshing gear pair that do not have common factors. This improves wear performance, because a defect on a gear tooth of one gear will make contact with all of the teeth on the mating gear equally rather than selectively making contact with a small number of teeth.

A number of elegant procedures are available for selecting the tooth numbers given R [1], especially when R is given as a fraction where the numerator and denominator are whole numbers. Such procedures may be aided by tables of factors. For example, if $R = p/q$, we would look for values of N_3 and N_5 such that $N_3N_5 = p$ and values of N_2 and N_4 such that $N_2N_4 = q$. Alternatively, if the ranges for the tooth numbers are limited, we might conduct an exhaustive search for all possible combinations of tooth numbers that satisfy the condition for R . On modern computers, such a search is easy to program and takes very little time to conduct. A simple MATLAB program, *factor.m*, for finding factors of any integer, is included in the supplementary material with this book.

After the tooth numbers are established, we can select one of the normal diametral pitches, for example, P_{n2} , and the corresponding helix angle (ψ_2). Then solve for r_2 and r_3 . Given r_2 and r_3 , [Equations 13.13](#) and [13.16](#) can be solved for r_4 , r_5 , and P_{n4} cos ψ_4 . Pick a standard value for P_{n4} , and solve for the helix angle, ψ_4 .

This discussion deals with kinematics alone. Other very important aspects of gear design are stress and wear considerations. The topic is properly treated in almost any book on machine design. Therefore, we will limit our discussion to kinematics with the assumption that sizing the teeth to carry the loading will be addressed elsewhere.



Example 13.2 Concentric Gearbox Design

Assume that a concentric gearbox is to be designed for a velocity ratio of $R = 20:1$. The first stage reduction is to have a helix angle of 30° and normal diametral pitch of 8. Both sets of gears will have a normal pressure angle of 20° . Find values for the tooth numbers, pitch cylinder radii for all of the gears, and the diametral pitch and helix angle for gears 4 and 5.

Solution

To avoid undercutting, we will limit the tooth numbers for N_2 and N_3 to 12 teeth (see [Table 12.1](#)). For the smallest possible gearbox, assume that N_2 is 12. Initially, select N_4 to be 12 also. If the minimum helix angle for gears 4 and 5 is found to be less than 30° , we can specify it to be 30° , which will make 12 an acceptable tooth number. If the helix angle must be larger than 30° , the minimum value for N_4 could be smaller than 12. The velocity ratio can be written as

$$R = \frac{2N_3}{n}$$

where n is any integer. From [Equation 13.14](#), $n = N_2 N_4$. Therefore, $n = 144$, and $20n$ is 2880.

To determine the factors for 2880, the MATLAB factor program was used. There are 42 factors for 2880. These are 1, 2, 3, 4, 5, 6, 8, 9, 10, 12, 15, 16, 18, 20, 24, 30, 32, 36, 40, 45, 48, 60, 64, 72, 80, 90, 96, 120, 144, 160, 180, 192, 240, 288, 320, 360, 480, 576, 720, 960, 1440, 2880. To determine the gear numbers for N_3 and N_5 , pick one of the factors for N_3 and divide 2880 by that factor to determine N_5 . When designing the two-stage gear reducer, it is generally desirable to make the two gear reductions about the same. This avoids making one gear significantly larger than the others. Of the factors, 48 and 60 will give gear reductions of 4 and 5 for the two stages. Therefore, let us select 60 for the first stage (N_3). Then $2880/60 = 48$ for the second stage (N_5). This will permit larger teeth (lower P_n) on the low-speed end of the gear reducer without making the gear diameters significantly larger than those for the high-end gears.

From [Equations 13.15](#)

$$r_2 = \frac{N_2}{2P_{n2} \cos \psi_2} = \frac{12}{2(8) \cos 30^\circ} = 0.866 \text{ m}$$

and

$$r_3 = \frac{N_3}{2P_{n3} \cos \psi_3} = \frac{N_3}{2P_{n2} \cos \psi_2} = \frac{60}{2(8) \cos 30^\circ} = 4.334 \text{ m}$$

From [Equations 13.16](#)

$$\frac{N_4}{N_3} = \frac{r_4}{r_3} = \frac{12}{48} = \frac{1}{4}$$

Therefore

$$r_3 = 4r_4$$

Substituting this expression into [Equation 13.13](#),

$$r_4 + r_3 = 5r_4 = r_2 + r_3 = 0.366 + 4.330 = 5.196 \text{ in}$$

Therefore

$$r_4 = \frac{5.196}{5} = 1.039 \text{ in}$$

and

$$r_5 = 4r_4 = 4(1.039) = 4.156 \text{ in}$$

The only remaining unknowns are P_{44} and ψ_4 . From [Equations 13.16](#)

$$P_{44} \cos \psi_4 = \frac{N_4}{2r_4} = \frac{12}{2(1.039)} = 5.775$$

To illustrate the procedure, select a normal diametral pitch of 7. Then

$$\psi_4 = \cos^{-1}\left(\frac{5.775}{7}\right) = \cos^{-1}(0.825) = 34.4^\circ$$

Note that in this example we have arbitrarily selected the diametral pitches. In an actual problem, these, along with the face widths, would be selected in part to accommodate the torque and speed requirements.



13.5 Planetary Gear Trains

Both simple and compound gear trains have the restriction that their gear shafts must rotate in bearings fixed to the frame. However, this is a requirement that limits the versatility of the gear train. If one or more shafts rotate around another shaft as well as spinning about their own axes, the gear train is called a planetary or epicyclic gear train. Planetary gear trains are used extensively for compact gear reducers ([Figure 13.13](#)). Also, because they are basically devices with multiple degrees of freedom, they are used in automatic transmissions for automobiles and trucks ([Figure 13.14](#)).



[Figure 13.13](#) A planetary gear reducer in winch transmission. Courtesy of Warn Industries, Inc., Clackamas, Oregon



[Figure 13.14](#) Planetary gears in automatic transmission. Courtesy of Ford Motor Co., Dearborn, Michigan

Determining the velocity ratio for planetary gear trains is more difficult than for plain simple and compound gear trains. The motion of the gears involves the motion of the moving shaft or carrier along with the motion of the gears with respect to the carrier.

13.5.1 Planetary Gear Nomenclature

A simple planetary drive is shown schematically in [Figure 13.15](#). Planetary gear trains are typically made up of the following:

1. Sun gear (may or may not be fixed)
2. Planet gears (one or more)

3. Planet carrier
4. Internal ring gear (not used in all planetary gear trains)

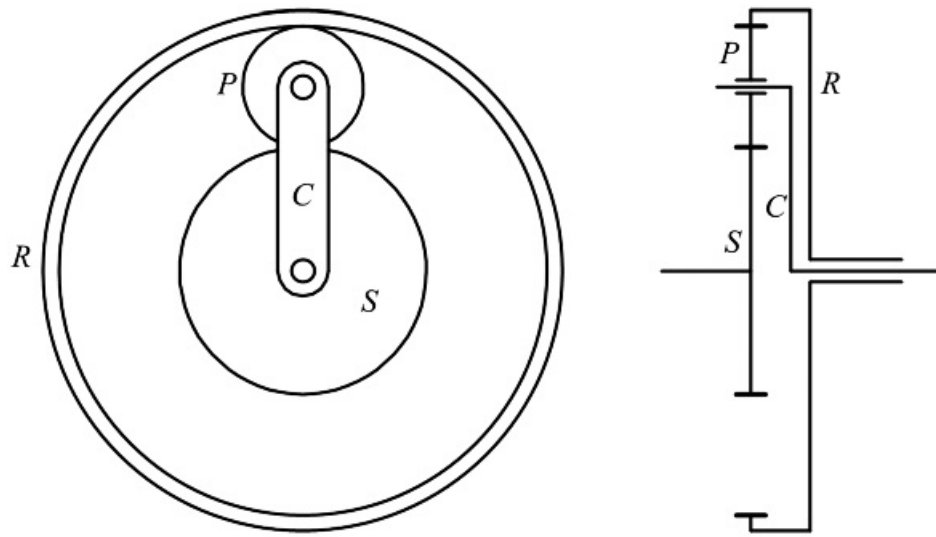


Figure 13.15 A simple planetary gear train.

The symbolism used to represent planetary drives is also shown in [Figure 13.15](#). This symbolism allows the designer to represent the structure of the planetary drive simply.

In [Figure 13.15](#), note that the carrier, ring gear, and sun gear all rotate about concentric axes. Also, three axes are evident from the simple figure. As shown below, the planetary gear train has two degrees of freedom, and the angular motion of two of the axes must be specified before the angular motion of the third can be determined.

Very high velocity reductions can be achieved with compound planetary gear trains. These systems involve compound planetary gears as shown in [Figure 13.16\(a\)](#). This also permits the ring gear in [Figure 13.15](#) to be replaced by another sun gear. The carrier can involve several shafts containing four or more planetary gears as shown in [Figure 13.16\(b\)](#) for still greater reductions. And finally, it is possible to connect planetary gears in series as shown in [Figure 13.16\(c\)](#). In [Figure 13.16](#), the bearings associated with the frame link are not shown. It is understood that frame bearings will be required for all of the shafts rotating with fixed axes.

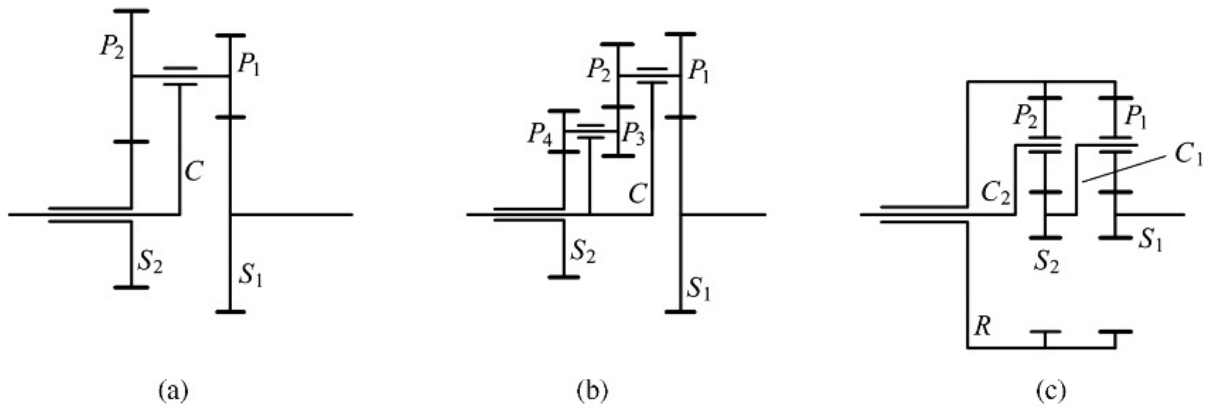
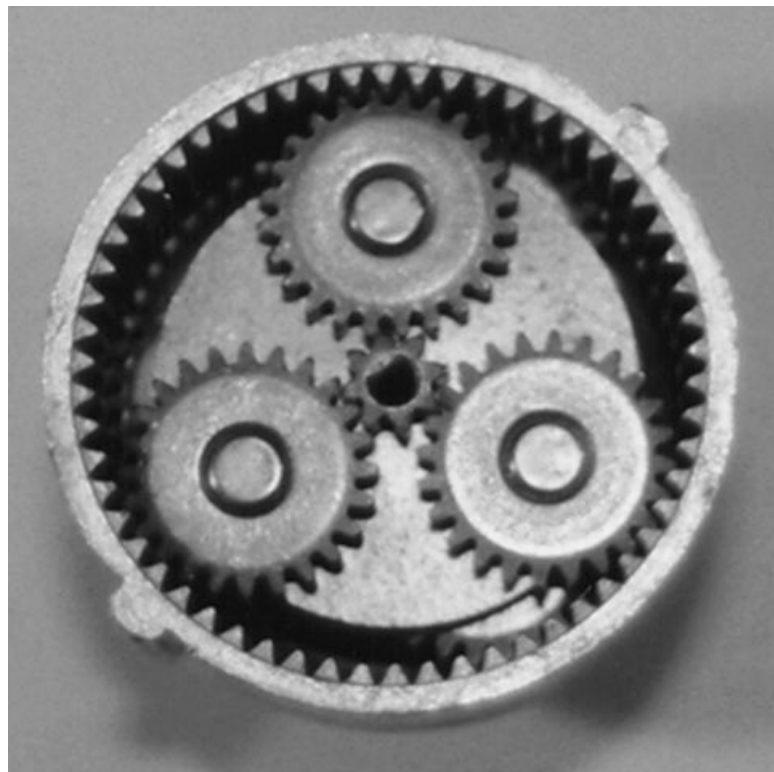


Figure 13.16 Complex planetary gear trains

When planetary gear trains are connected in series, very high gear reductions are possible. Such gear reducers are common in small power tools. [Figure 13.17](#) shows a small planetary gear reducer made up of two planetary systems in series used in a power screwdriver.



[Figure 13.17](#) Planetary gear train used in a power screwdriver.

In the planetary gear trains indicated in [Figure 13.16](#), two of the shafts are inputs and one is the output. Typically, the angular velocity of one of the bodies is zero, but this is not required.

In [Figures 13.13–13.17](#), all of the gears in the planetary drives are parallel-shaft gears. However, this is not necessary. Perhaps the most common planetary drive is the differential ([Figure 13.18](#)) in rear-wheel driven vehicles. This is a right-angle drive that involves a hypoid ring gear and pinion and bevel gear planets.

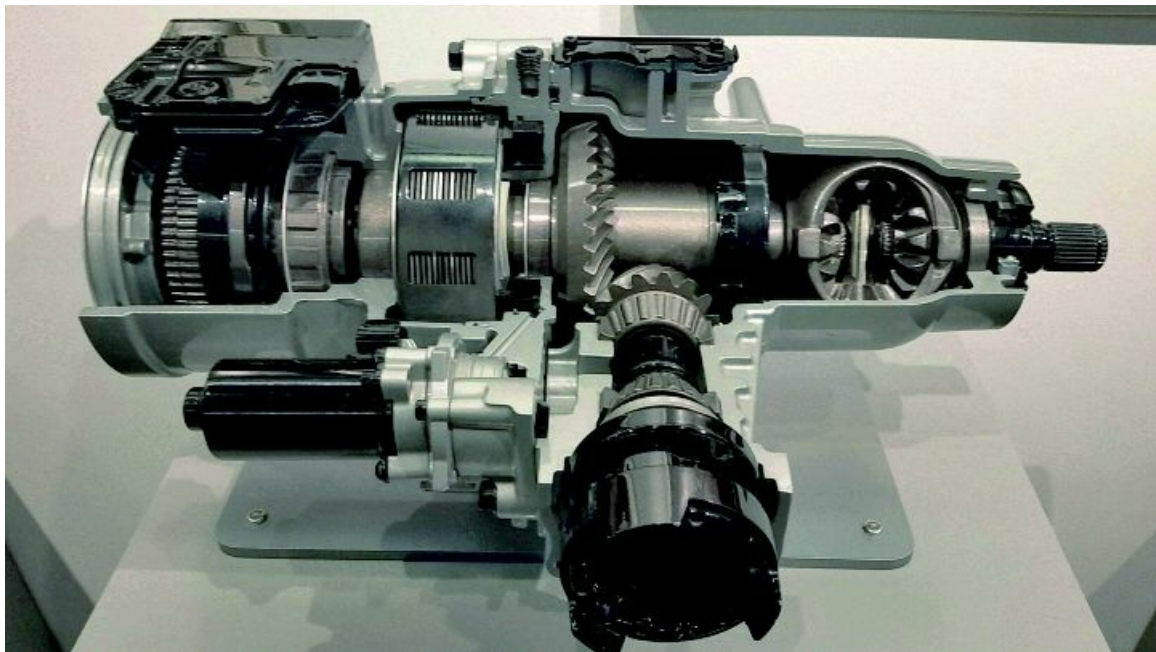


[Figure 13.18](#) A hypoid gear set and differential bevel gears used in a two-speed rear drive module as part of an all-wheel drive powertrain for a 2015 SUV. (Courtesy of American Axle & Manufacturing, Inc., Detroit, MI)

Planetary gear trains are commonly analyzed using either the equation method or the tabular method. We will look at each procedure separately by analyzing example gear trains.

13.5.2 Analysis of Planetary Gear Trains Using Equations

In the equation method, the procedure is to write relative angular velocity equations (relative to the frame) for each of the gears with fixed rotation axes. Also, write relative velocity equations for the same gears relative to the carrier. If the angular velocities of two of the shafts are given, this procedure will always yield enough equations to solve for the angular velocities of all of the members in the system.



Example 13.3

Basic Procedure Using Equation Method

Assume that the gear train in [Figure 13.15](#) has the frame as member 1, the sun gear as member 2, the planet as member 3, and the ring gear as member 4. Gear 2 is the input and rotates clockwise with an angular velocity of ω_2 . Find an equation that involves the angular velocity of the carrier, ω_C , and the tooth numbers for the individual gears.

Solution

There are two gears (2 and 4) that rotate about fixed axes in the system, and we can write the following angular velocity relationships for these gears using the chain rule for angular velocities

$$\omega_2 = \dot{\omega}_2 + \omega_C \quad (13.17)$$

and

$$\omega_4 = \dot{\omega}_4 + \omega_C \quad (13.18)$$

If we make the carrier the reference link, the gears will move as an ordinary gear train in which the planet gear acts as an idler. Therefore, we can compute the velocity ratio relative to the carrier as

$$\frac{\dot{\omega}_2}{\dot{\omega}_4} = -\frac{N_4}{N_2} \quad (13.19)$$

Next solve [Equations 13.17](#) and [13.18](#) for $\dot{\omega}_2$ and $\dot{\omega}_4$, respectively. Then

$$\dot{\omega}_2 = \omega_2 - \omega_C \quad (13.20)$$

and

$$\dot{\omega}_4 = \omega_4 - \omega_C \quad (13.21)$$

Now divide [Equation 13.20](#) by [13.21](#) and equate the result to [Equation 13.19](#). The result is

$$\frac{\omega_2 - \omega_C}{\omega_4 - \omega_C} = -\frac{N_4}{N_2} \quad (13.22)$$

[Equation 13.22](#) gives the relationship for the velocities of the shafts coming from the gear train. Given any two of the angular velocities, the third can be determined. Note that it is important to identify the direction of the angular velocities with a plus or minus sign. Typically, we could select counterclockwise (CCW) as plus and clockwise (CW) as minus.



Example 13.4

Analysis of Planetary Gear Train Using Equation Method

Assume that the carrier in [Figure 13.19](#) is member 6 and that it and gear 5 are driven clockwise at 150 and 50 rpm, respectively, when viewed from the right end. Find the magnitude and direction of the angular velocity of gear 2.

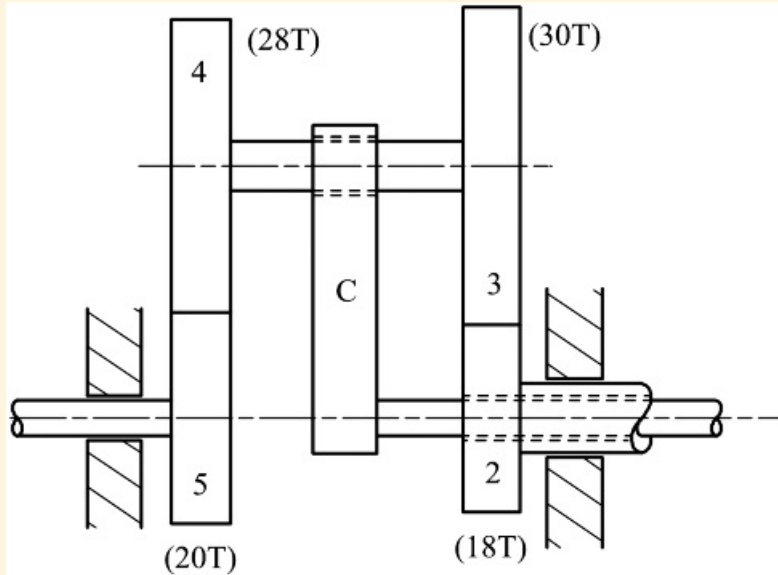


[Figure 13.19](#) The planetary gear train for Example 13.4.

Solution

There are two gears (2 and 5) that rotate about fixed axes in the system. As in the case of the previous example, we can write the angular velocity relationships for these gears using the chain rule for angular velocities. The equations are

$$\omega_2 = \epsilon_{\omega_2} + \omega_C \quad (13.23)$$

and

$$\omega_5 = \epsilon_{\omega_5} + \omega_C \quad (13.24)$$

The angular velocity ratio of gears 2 and 5 relative to the carrier is

$$\frac{\epsilon_{\omega_2}}{\epsilon_{\omega_5}} = \frac{N_5 N_3}{N_4 N_2} \quad (13.25)$$

Notice that the velocity ratio is positive because both gears rotate in the same direction relative to the arm. Next solve [Equations 13.23](#) and [13.24](#) for ϵ_{ω_2} and ϵ_{ω_5} , respectively. Then

$$\epsilon_{\omega_2} = \omega_2 - \omega_C$$

(13.26)

and

$$C\omega_3 = \omega_3 - \omega_C \quad (13.27)$$

Now divide [Equation 13.26](#) by [13.27](#) and equate the result to [Equation 13.25](#). This gives

$$\frac{\omega_2 - \omega_C}{\omega_3 - \omega_C} = \frac{C\omega_2}{C\omega_3} = \frac{N_5 N_3}{N_4 N_2} \quad (13.28)$$

Assuming CCW as positive, from the problem statement, $\omega_C = -150 \text{ rpm}$ and $\omega_5 = -50 \text{ rpm}$. The tooth numbers are given in [Figure 13.19](#). Substituting the known values into [Equation 13.28](#) gives

$$\frac{\omega_2 + 150}{-50 + 150} = \frac{20}{28} \left(\frac{30}{18} \right)$$

or

$$\omega_2 + 150 = 119.04$$

or

$$\omega_2 = -30.95 \text{ rpm}$$

Therefore, the velocity of gear 2 is 30.95 rpm in the clockwise direction.



Example 13.5

Analysis of Second Planetary Gear Train Using Equation Method

Assume that gear 2 in [Figure 13.20](#) is driven at a speed of 60 rpm in the counterclockwise direction viewed from the right end. Gear 4 meshes with a fixed ring gear and with gear 5 as shown. Find the magnitude and direction of the angular velocity of gear 5.

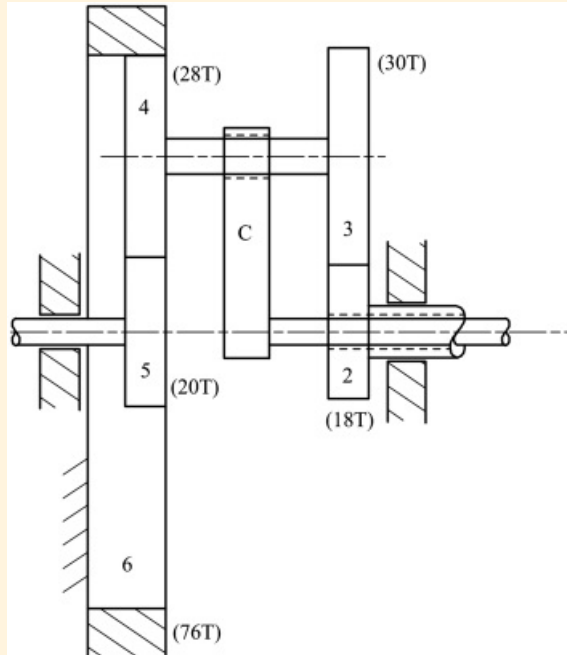


[Figure 13.20](#) The planetary gear train for Example 13.5.

Solution

There are three gears (2, 5, and 6) that can rotate about fixed axes in the system. We have included gear 6 in this list but ultimately will use the fact that its velocity is zero. As in Examples 13.3 and 13.4, we will solve the problem by writing relative velocity equations for all of the gears that have shafts that can rotate in fixed bearings. After rearranging, the resulting equations are

$$\omega_2 = \omega_2 - \omega_C \quad (13.29)$$

$$\omega_3 = \omega_3 - \omega_C \quad (13.30)$$

and

$$\omega_6 = \omega_6 - \omega_C \quad (13.31)$$

The angular velocity ratio of gears 2 and 5 relative to the carrier is

$$\frac{\omega_2}{\omega_5} = \frac{N_3 N_3}{N_4 N_2} \quad (13.32)$$

and that of gears 2 and 6 relative to the carrier is

$$\frac{\omega_2}{\omega_6} = -\frac{N_6 N_3}{N_4 N_2} \quad (13.33)$$

Now, divide [Equation 13.2](#) by [Equation 13.30](#) and equate the result with [Equation 13.32](#). This gives

$$\frac{\omega_2 - \omega_C}{\omega_5 - \omega_C} = \frac{N_3 N_3}{N_4 N_2} \quad (13.34)$$

Similarly, divide [Equation 13.29](#) by [13.31](#) and equate the result with [Equation 13.33](#) to get

$$\frac{\omega_2 - \omega_C}{\omega_6 - \omega_C} = -\frac{N_6 N_3}{N_4 N_2} \quad (13.35)$$

[Equations 13.34](#) and [13.35](#) are the equations necessary for analyzing the planetary gear train. From the problem statement, we know that $\omega_2 = 60$ rpm and $\omega_5 = 0$. With these known values, only ω_C is unknown in [Equation 13.35](#). Substituting the known values into [Equation 13.35](#) gives

$$\frac{60 - \omega_C}{0 - \omega_C} = -\frac{70}{28} \left(\frac{30}{18} \right) = -4.5238$$

Solving gives

$$\omega_C(1 + 4.5238) = 60 \Rightarrow \omega_C = 10.86 \text{ rpm}$$

Given ω_C and ω_2 , we can solve [Equation 13.34](#) for ω_3 . Substituting the known values into [Equation 13.34](#) gives

$$\frac{60 - 10.86}{\omega_3 - 10.86} = \frac{20}{28} \left(\frac{30}{18} \right) = 1.19$$

Solving for ω_3

$$\omega_3 - 10.86 = \frac{60 - 10.86}{1.19} = 14.28 \Rightarrow \omega_3 = 25.14 \text{ rpm}$$

The value is positive, so ω_3 is rotating counterclockwise when viewed from the right.



Example 13.6

Analysis of Planetary Gear Trains in Series

A two-stage planetary gear drive is represented in [Figure 13.21](#). Gear 2 is the input member and carrier 7 is the output member. Gear 4 is a ring gear and is fixed. The carrier of the first stage is part of member 6, and it is rigidly connected to the gear (member 6) that drives the second stage. Determine the velocity ratio of the gear drive.

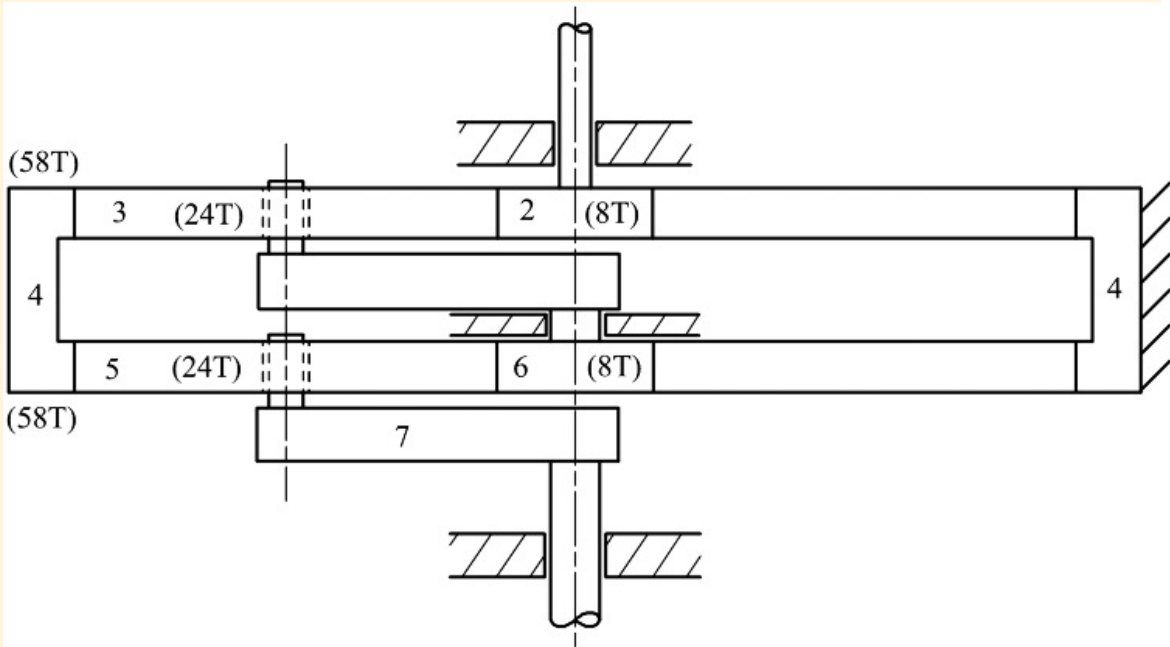


[Figure 13.21](#) The planetary gear train for Example 13.6.

Solution

There are three gears (2, 4, and 6) that can rotate about fixed axes in the system. Again, we will include the fixed ring gear in the equations and will set the velocity to zero once the equations are developed. As in the previous examples, we will solve the problem by writing relative velocity equations for all of the gears that have shafts that can rotate in fixed bearings. However, we must separate the two stages of the planetary drives when we write the equations. The first stage includes gears 2, 3, and 4 and the carrier is member 6. The second stage includes gears 6, 5, and 4 and carrier 7. The first stage can be analyzed independently of the second stage to determine the velocity of gear 6 in terms of the velocity of gear 2. The second stage can then be analyzed to determine the velocity of the second carrier (7) in terms of the velocity of gear 6. By combining the results of both stages, the velocity of link 7 can be determined as a function of the velocity of gear 2 to determine the overall velocity ratio for the gear train.

After rearranging, the first-stage relative velocity equations are

$${}^6\omega_2 = \omega_2 - \omega_3 \quad (13.36)$$

$${}^6\omega_6 = \omega_6 - \omega_5 \quad (13.37)$$

The angular velocity ratio of gears 2 and 4 relative to the carrier (member 6) is

$$\frac{\dot{\omega}_{26}}{\dot{\omega}_{46}} = -\frac{N_4}{N_2} \quad (13.38)$$

Now, divide [Equation 13.36](#) by [Equation 13.37](#) and equate the result with [Equation 13.38](#). This gives

$$\frac{\omega_2 - \omega_5}{\omega_4 - \omega_5} = \frac{\dot{\omega}_{26}}{\dot{\omega}_{46}} = -\frac{N_4}{N_2} \quad (13.39)$$

Because $\omega_5 = 0$, this equation can be rewritten for ω_2 as a function of ω_4 . The result is

$$\omega_2 = \omega_6(1 + N_4/N_2) \quad (13.40)$$

We can now analyze the second stage in exactly the same manner as the first stage except that now the gears are 6, 5, and 4, and the carrier is 7. After rearranging, the second-stage relative velocity equations are

$$\dot{\omega}_{65} = \omega_5 - \omega_6 \quad (13.41)$$

$$\dot{\omega}_{64} = \omega_4 - \omega_6 \quad (13.42)$$

The angular velocity ratio of gears 4 and 6 relative to the carrier (member 7) is

$$\frac{\dot{\omega}_{64}}{\dot{\omega}_{65}} = -\frac{N_6}{N_4} \quad (13.43)$$

Now, divide [Equation 13.41](#) by [Equation 13.42](#) and equate the result with [Equation 13.43](#). This gives

$$\frac{\omega_6 - \omega_7}{\omega_6 - \omega_5} = \frac{\dot{\omega}_{64}}{\dot{\omega}_{65}} = -\frac{N_6}{N_4} \quad (13.44)$$

Because $\omega_5 = 0$, this equation can be rewritten for ω_7 as a function of ω_4 . The result is

$$\omega_7 = \frac{\omega_6}{1 + N_4/N_6} \quad (13.45)$$

Combining [Equations 13.45](#) and [13.40](#) and substituting the known tooth numbers gives

$$\frac{\omega_7}{\omega_2} = \left(1 + \frac{N_4}{N_2}\right) \left(1 + \frac{N_4}{N_6}\right) = \left(1 + \frac{53}{3}\right) \left(1 + \frac{53}{3}\right) = 68.06$$

Notice that in this example, the size of the planet gears does not affect the velocity ratio. They will have an impact on the size of the gearbox, however. Also notice that members 2 and 7 both rotate in the same

direction.



Example 13.7

Analysis of Planetary Gear Train with Bevel Gears

All of the planetary gear trains considered in the previous examples involved only parallel-shaft gears. In this example, we will analyze an example with bevel gears. The gear train is shown in [Figure 13.22](#). The input to the gear train is gear 2 and the output is gear 6. The carrier is member 3 that rotates freely about the shaft on gear 6. Also the compound planet gears (4 and 5) rotate about the axis of the carrier. Gear 7 is fixed to the frame. Assume that gear 2 rotates with an angular velocity of 100 rpm in the counterclockwise direction viewed from the right end. Find the angular velocity of gear 6.

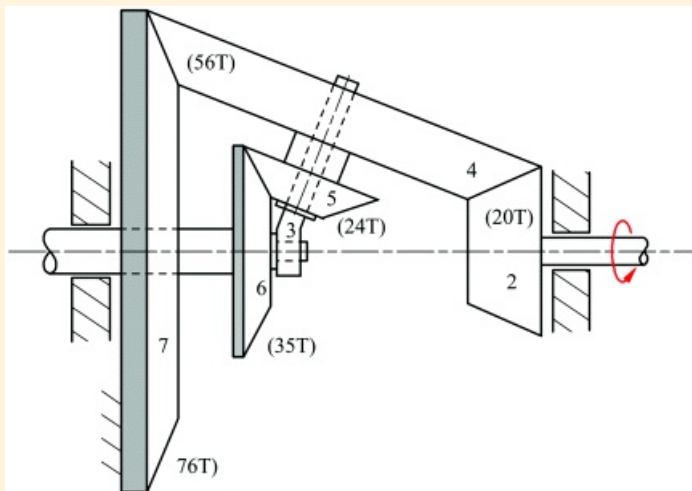


[Figure 13.22](#) The planetary gear train for Example 13.7.

Solution

Even though bevel gears are involved, we can approach the analysis in exactly the same way that was used for the parallel-shaft gears. There are three gears (2, 6, and 7) that can rotate about fixed axes in the system. Again, we will include gear 7 in this list but ultimately will use the fact that its velocity is zero. As in the previous examples, we will solve the problem by writing relative velocity equations for all of the gears that have shafts that can rotate in fixed bearings. After rearranging, the resulting equations are

$$\dot{\omega}_2 = \omega_2 - \omega_3 \quad (13.46)$$

$$\dot{\omega}_5 = \omega_5 - \omega_3 \quad (13.47)$$

and

$$\dot{\omega}_7 = \omega_7 - \omega_3 \quad (13.48)$$

The angular velocity ratio of gears 2 and 6 relative to the carrier (3) is

$$\frac{\dot{\omega}_2}{\dot{\omega}_3} = -\frac{N_4 N_6}{N_2 N_5} \quad (13.49)$$

In [Equation 13.49](#) we must determine the direction by inspection. This will show that if the carrier is fixed and the motion is inverted so that all of the other links and gears (including 4) can move relative to the carrier, gears 2 and 6 will move in opposite directions. Similarly, the motion of gears 2 and 7 relative to the carrier is

$$\frac{\dot{\omega}_2}{\dot{\omega}_7} = -\frac{N_7}{N_2} \quad (13.50)$$

Again, relative to the carrier, gears 2 and 7 are seen to move in opposite directions. Now, divide [Equation 13.46](#) by [Equation 13.48](#) and equate the result with [Equation 13.50](#). This gives

$$\frac{\omega_2 - \omega_3}{\omega_7 - \omega_3} = -\frac{N_7}{N_2} \quad (13.51)$$

Also divide [Equation 13.46](#) by [Equation 13.47](#) and equate the result to [Equation 13.49](#). This gives

$$\frac{\omega_2 - \omega_3}{\omega_5 - \omega_3} = -\frac{N_4 N_6}{N_2 N_5} \quad (13.52)$$

[Equations 13.51](#) and [13.52](#) are the equations necessary for analyzing the planetary gear train. From the problem statement, we know that $\omega_2 = 100$ and $\omega_7 = 0$. With these known values, only ω_3 is unknown in [Equation 13.51](#). Substituting the known values into [Equation 13.51](#) gives

$$\frac{100 - \omega_3}{0 - \omega_3} = -\frac{70}{20} = -3.8$$

Solving gives

$$\omega_3(1 + 3.8) = 100 \Rightarrow \omega_3 = 20.83 \text{ rpm}$$

Given ω_3 and ω_2 , we can solve [Equation 13.52](#) for ω_5 . Substituting the known values into [Equation 13.52](#) gives

$$\frac{100 - 20.83}{\omega_5 - 20.83} = -\frac{56}{20} \left(\frac{35}{24}\right) = -4.083$$

Solving for ω_5

$$\omega_5 = \frac{100 - 20.83}{-4.083} + 20.833 = 1.444 \text{ rpm}$$

The value is positive, so ω_6 is rotating in the same direction as ω_2 . Therefore, ω_6 is rotating

counterclockwise when viewed from the right. The overall velocity ratio for the gearbox is

$$\frac{\omega_2}{\omega_5} = \frac{100}{1.444} = 69.2$$

13.5.3 Analysis of Planetary Gear Trains Using Tabular Method

Overview

The tabulation method is based on the knowledge that a planetary gear train is a linear system. The absolute angular velocity of any gear x that rotates about an axis fixed to the frame can be written as

$$\omega_x = \epsilon_{\omega_x} + \omega_C \quad (13.53)$$

where ω_C is the absolute angular velocity of the carrier, and ϵ_{ω_x} is the angular velocity of the gear relative to the carrier. Also, because [Equation 13.53](#) is linear, we can multiply the input values by a constant, and the output value will be multiplied by the same constant. The tabular method is based on the idea of the linear relationship shown in [Equation 13.53](#) and superposition.

A simple planetary gear train is fundamentally a two-degree-of-freedom device. Therefore, we must specify two input velocities or displacements to compute the unknown displacement. For discussion, consider the planetary gear train shown in [Figure 13.23](#). There is a compound gear for the planets and two sun gears, and the members are each assigned a number. Assume that the carrier is one of the input members, gear 2 is the other input member, and the known velocities are ω_2 and ω_5 , respectively.

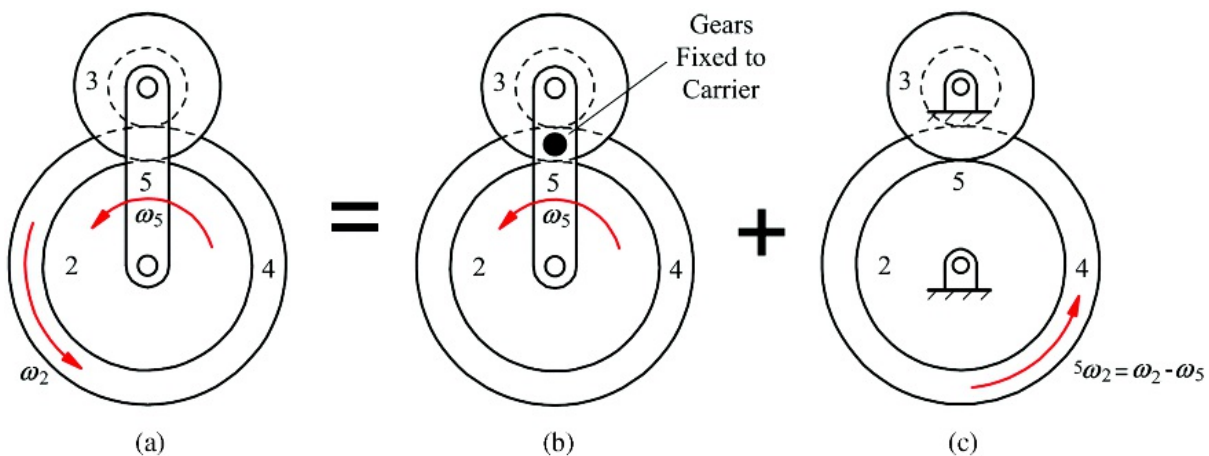


[Figure 13.23](#) Analysis of a planetary drive using superposition.

Now let us fix all of the gears to the carrier and rotate all of the gears by the velocity ω_5 . Then all of the gears, including gear 2, will have an initial angular velocity of ω_5 . To correct the angular velocity of gear 2 without changing the angular velocity of the carrier, let us fix the angular velocity of the carrier and move all of the gears relative to the carrier such that angular velocity of gear 2 ends up with the correct value when added to the velocity (ω_5) from step 1. This will also change all of the angular velocities in the gear train. The vector sum of the angular velocities from steps 1 and 2 for each gear will give the correct values. The vector sum is simply an algebraic sum because all of the gears have parallel shafts. The procedure, shown schematically in [Figure 13.23](#), is formalized in the tabular method of analysis as follows.

Procedure

The tabulation method begins with a table in which there is one column for each member in the gear train and a row for each of the following three steps:

1. Assume that all of the gears are locked to the carrier and rotate the assembly with an angular velocity equal to the angular velocity of the carrier member. Tabulate this velocity under each member in the train.
2. Fix the arm, and rotate the second input member such that it ends up with the proper input velocity when steps 1 and 2 are added together. Tabulate the resulting velocity for each member in the train.
3. Add the results from steps 1 and 2 for each member in the train.

We will illustrate the procedure with three examples.



Example 13.8

Tabulation Method for Simple Planetary Gear Train

Assume that the planetary gear train in [Figure 13.24](#) has the frame as member 1, the sun gear as member 2, the planet gear as member 3, the ring gear as member 4, and the carrier as member 5. Gear 2 is the input and rotates counterclockwise with an angular velocity of 100 rpm and the carrier rotates counterclockwise with an angular velocity of 200 rpm. Find the angular velocities of gears 3 and 4.

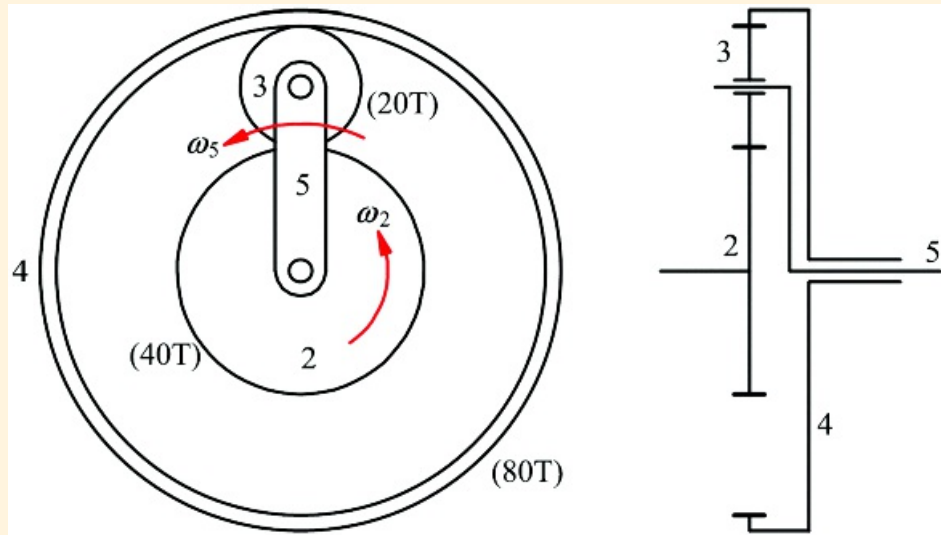


[Figure 13.24](#) The planetary gear train for Example 13.8.

Solution

Following the procedure given above, the solution table is shown in [Table 13.1](#). The four members of the system are associated with the columns, and the steps are associated with the rows. Step 1 of the procedure is to rotate the entire assembly by +200 rpm, which is the velocity of the carrier. Next, we will fix the carrier and rotate gear 2 by the velocity required to make its total angular velocity 100 rpm. To do this, we need to rotate gear 2 by $\omega_2 - \omega_5 = \omega_2 = 100 - 200 = -100$ rpm.

[Table 13.1](#) Results for Example 13.8 (rpm)

Step	Carrier 5	Gear 2	Gear 3	Gear 4
1. Gears locked	200	200	200	200
2. Carrier fixed	0	-100	200	50
3. Total	200	100	400	250

When gear 2 rotates -100 rpm relative to the carrier, gears 3 and 4 will also rotate relative to the carrier. The angular velocity of gear 3 relative to the carrier will be

$$\omega_3 = -\frac{\dot{\theta}_2}{\dot{\theta}_3} \omega_2 = -\frac{40}{20} (-100) = 200$$

and

$$\dot{\omega}_4 = -\frac{N_2}{N_4} \dot{\omega}_2 = -\frac{40}{80}(-100) = +50$$

These values are entered into [Table 13.1](#). The final results are obtained by adding the results from the first two steps. From this, it is apparent that gear 3 rotates 400 rpm and gear 4 rotates 250 rpm, both in the counterclockwise (+) direction.



Example 13.9

Solution to Example 13.7 Using Tabulation Method

Analyze the planetary gear train in Example 13.7 using the tabulation method.

Solution

The problem is to determine the velocity ratio for the gear train, where the velocity ratio is defined by ω_2/ω_6 . If we set $\omega_5 = 1$ and solve for the velocity of ω_2 , the velocity ratio will be given directly by the value for ω_2 . From the problem statement, we also know that $\omega_7 = 0$.

In the table, we will include only gears that rotate about axes that have bearings fixed to the frame. The planet gears rotate about the arm axis, which is skewed relative to the axis of the other gears. Therefore, the angular velocity of the planets is not obtained by a simple algebraic addition of the values from steps 1 and 2.

In the tabulation procedure, we assume that the velocity of the carrier is known. However, in this problem, the velocities of gears 6 and 7 are known. Therefore, we must treat the velocity of the carrier as unknown and solve for it. For step 1, assume that the gears are locked to the carrier and the assembly is turned by $+x$ rpm. This is shown in [Table 13.2](#). In step 2, we must rotate gear 7 relative to the carrier such that when the results of the first two steps are added, the final velocity for gear 7 will be zero. Clearly, then, gear 7 must be rotated by $-x$ rpm relative to the carrier. The remaining values in the second row of the table are determined by analyzing the gear train relative to the carrier.

[Table 13.2](#) Results for Example 13.9 (in rpm)

Step	Carrier 3	Gear 2	Gear 6	Gear 7
1. Gears locked	x	x	x	x
2. Carrier fixed	0	$x \frac{N_1}{N_2} = x \frac{16}{20}$	$-x \frac{\dot{N}_1 \dot{N}_2}{\dot{N}_6 \dot{N}_5} = -x \frac{16}{35} \left(\frac{24}{20} \right)$	$-x$
3. Total	x	$-x \left[1 + \frac{16}{20} \right] = x(4.8)$	$x \left[1 - \frac{16}{35} \left(\frac{24}{20} \right) \right] = x(0.0694)$	0

Next sum the results from steps 1 and 2. From the problem statement, we know that $\omega_5 = 1$, and in the table, we can see that the velocity of gear 6 is also given by

$$\omega_6 = x(0.0694) = 1$$

Therefore

$$x = 14.41$$

and

$$\omega_2 = x(4.8) = 14.412(4.8) = 69.2$$

Therefore the velocity ratio for the planetary gear train is

$$\omega_2/\omega_6 = 69.2$$

which is the same as was computed in Example 13.7.



Example 13.10

Solution to Ferguson's Paradox Using Tabulation Method

This is an interesting application of planetary gearing, and the planetary gear system employed is called Ferguson's paradox [3]. The mechanism is shown in [Figure 13.25](#). Gear 2 is fixed to the frame, and gear 5 is a planet that rotates relative to the carrier, which is member 6. Gears 2, 3, and 4 have tooth numbers 100, 101, and 99, respectively. All of the gears are cut from the same blank so that they will all mesh with gear 5, which has 20 teeth. If the carrier makes 100 revolutions CCW, determine the number of revolutions made by gears 3, 4, and 5.

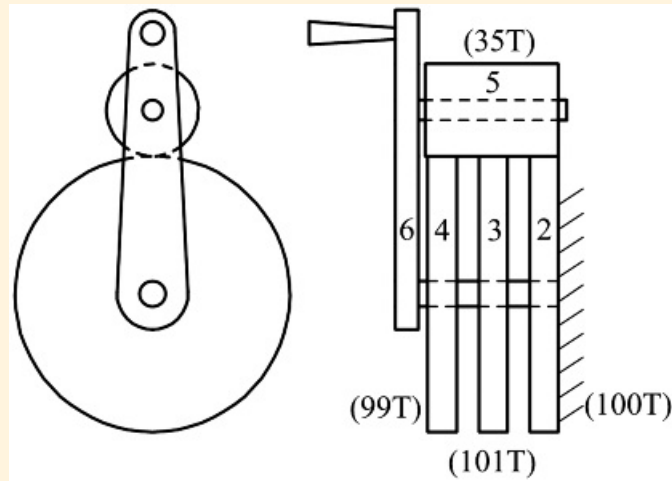


[Figure 13.25](#) The planetary gear train for Example 13.10.

Solution

Based on the problem statement, we know that the carrier moves 100 revolutions and gear 2 is fixed. As in the previous examples, the first step is to fix all of the gears to the carrier and rotate the assembly by 100 turns. This is shown in [Table 13.3](#). In step 2, we must rotate gear 2 relative to the carrier such that when the results of the first two steps are added, the final number of revolutions for gear 2 is zero. Therefore, gear 2 must be rotated by -100 revolutions relative to the carrier. The remaining values in the second row of the table are determined by analyzing the gear train relative to the carrier.

[Table 13.3](#) Results for Example 13.10 (in revolutions)

Step	Carrier 6	Gear 2	Gear 3	Gear 4	Gear 5
1. Gears locked	100	100	100	100	100
2. Carrier fixed	0	-100	-100/1.01	-100/0.99	100/35
3. Total	100	0	1	-1	102.86

Next sum the results from steps 1 and 2. The number of turns made by each gear in the mechanism is shown in the third row of [Table 13.3](#). Notice that gear 3 makes 1 revolution in the direction of the motion of the carrier while gear 4 makes 1 revolution in the opposite direction. Gear 2 is fixed by design. Therefore, as the carrier is turned, gear 3 will rotate very slowly in the direction of the carrier and gear 4 will rotate very slowly in the opposite direction.



13.6 Harmonic Drive Speed Reducers

Very high speed reductions can be achieved by connecting several planetary drives in series. However, the resulting system will require a relatively large number of gears and will be relatively heavy. The harmonic drive is a simple solution for mechanical systems requiring a large speed reduction in a light-weight space. Speed reduction from 30 to 130 is available in a single stage. All of the gear devices discussed up to this point have been based on rigid-body assumptions. This means that elastic deformations are assumed to be negligible. The function of the harmonic drive is based on the principle of strain-wave gearing which requires a flexible element. The harmonic drive consists of three main components as shown in [Figures 13.26](#) and [13.27](#). The input shaft is connected to an ellipse-shaped wave generator. The output shaft is connected to a flexible sleeve with machined spline teeth around one end (flexspline). The wave generator distorts the splined end of the flexspline so that it engages with a rigid circular splined member.

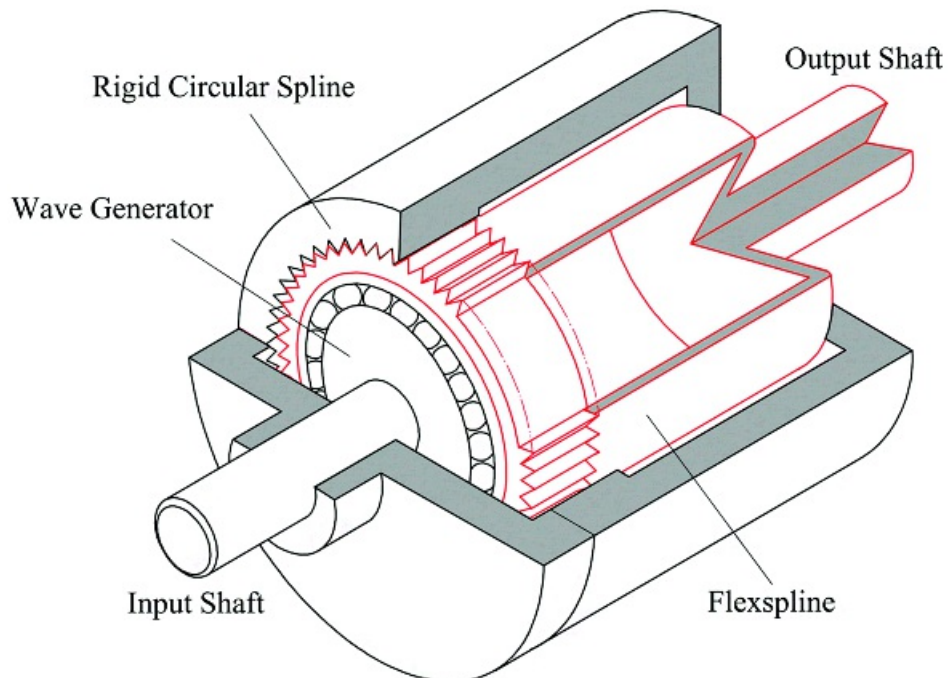


[Figure 13.26](#) Basic components of typical harmonic drive.

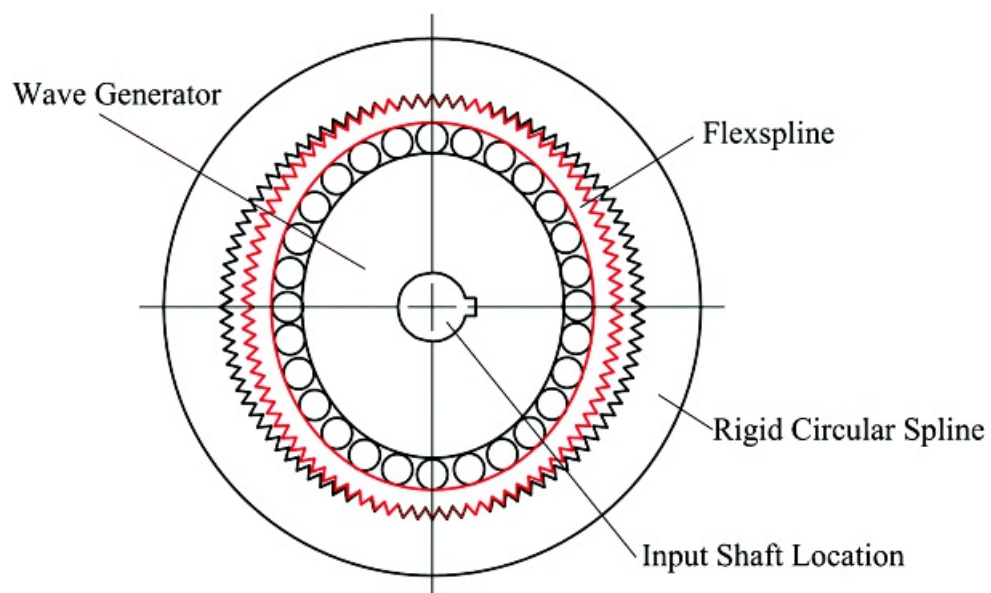


[Figure 13.27](#) Schematic drawing of a typical harmonic drive showing components.

The reduction ratio for a harmonic drive is given by [4]

$$R = \frac{N_f}{N_C - N_f} \quad (13.54)$$

Where

N_f	= number of teeth on the flexible flex spine
N_C	= number of teeth on the rigid circular spline ($N_C > N_f$)

For the largest reduction ratio, we want the difference between N_C and N_f to be as small as possible. Also, we want the difference to be as small as possible to minimize the distortion and the stresses in the flexspline. However, the difference needs to be large enough that the two splines touch at only the ends of the major axis of the ellipse. Typically, the minimum difference required is 2. As implied by [Equation 13.54](#), the input shaft and output shaft rotate in opposite directions.

In addition to a very high-speed reduction ratio in a single stage, harmonic drives tend to have a number of other advantages over rigid gear drives. They have very low backlash and very precise positioning accuracy, making them suitable for precision applications with high inertial loads, although elastic distortions (windup) in the flexspline can degrade the positioning accuracy slightly [5]. Because they can achieve very high speed reduction ratios in a single stage, harmonic drives tend to be very small and lightweight compared to conventional gear reducers for given torque and power requirements. In addition, their high efficiency allows the drives to have a high torque to weight ratio.

Because harmonic drives have concentric input and output shafts, they share the same centerline. In addition, the input and output shafts can be hollow to allow cables, supply lines, laser beams, and the like to easily pass through the center of the gearbox.

Harmonic drives tend to be high performance devices. The flexspline has been optimized to reduce cyclic stresses and stress concentrations so harmonic drives tend to have a mean time before failure at least comparable to conventional gear reducers. In addition, because of the nature of the hollow flexspline, the torsional stiffness tends to be high.

The main disadvantage of harmonic drives is relatively high cost. Therefore, harmonic drives tend to be used in high performance applications where the advantages of the drives are essential. Typical applications include speed reducers at robotic joints, solar array drives in space, satellite and space vehicles, aircraft positioning devices, and machine tools.

Harmonic drive reductions are a specialty item that is manufactured by a limited number of companies, mainly in Japan and Germany. Therefore, the typical engineer will identify the speed reduction, torque, and speed requirements, and select the appropriate design from standard sizes available on either the web or in vendor catalogs.



References

1. Merritt, H. E. (1971). *Gear Engineering*. New York, NY: John Wiley & Sons.
2. Mabie, H. H., and Reinholtz, C. F. (1987). *Mechanisms and Dynamics of Machinery*, 4th Ed. New York, NY: John Wiley & Sons.
3. Shigley, J. E. (1975). *Kinematic Analysis of Mechanisms*. New York, NY: McGraw-Hill.
4. Chironis, N. P., and Slater, N. (1996). *Mechanisms and Mechanical Devices Sourcebook*, 2nd Ed. New York, NY: McGraw-Hill.
5. Dudley, D. W., Ed. (1962). *Gear Handbook: The Design, Manufacture, and Application of Gears*. New York, NY: McGraw-Hill.

Problems

Compound Gear Trains

13.1 Find the angular velocity of gear 8 if the angular velocity of gear 2 is 800 rpm in the direction shown in [Figure P13.1](#).

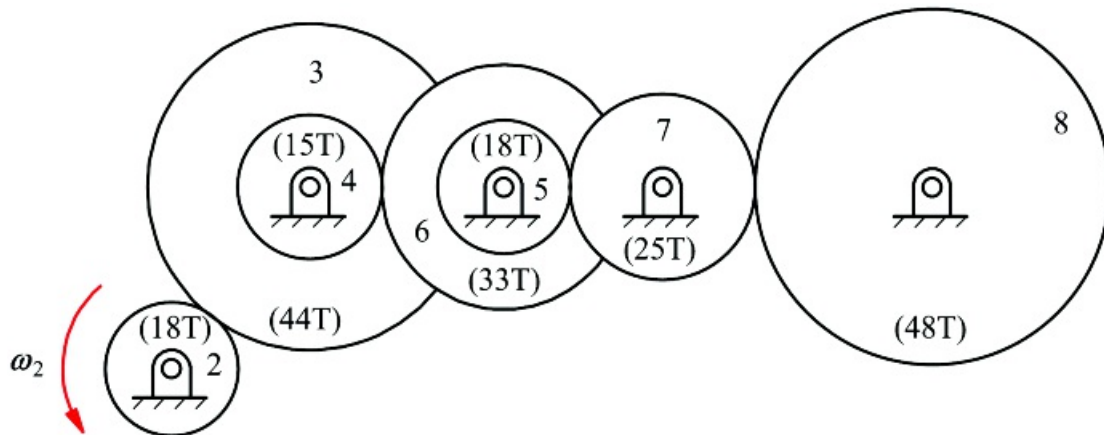


[Figure P13.1](#) Gear train for Problem 13.1.

13.2 Find the velocity of gear 8 in Problem 13.1 if the angular velocity of the driver (gear 2) is 300 rpm in the clockwise direction.

13.3 The gear train given in [Figure P13.3](#) is for a machine tool. Power is input to the gearbox through the pulley indicated, and the output power to the machine table is through gear 13. Gears 2 and 3, 4 and 5, and 11 and 12 are compound gears that can move axially on splined shafts to mesh with various different gears so that various combinations of overall gear ratios ($\frac{\omega_1}{\omega_2}$) can be produced. Determine the number of ratios possible and the overall gear ratio for each possibility.

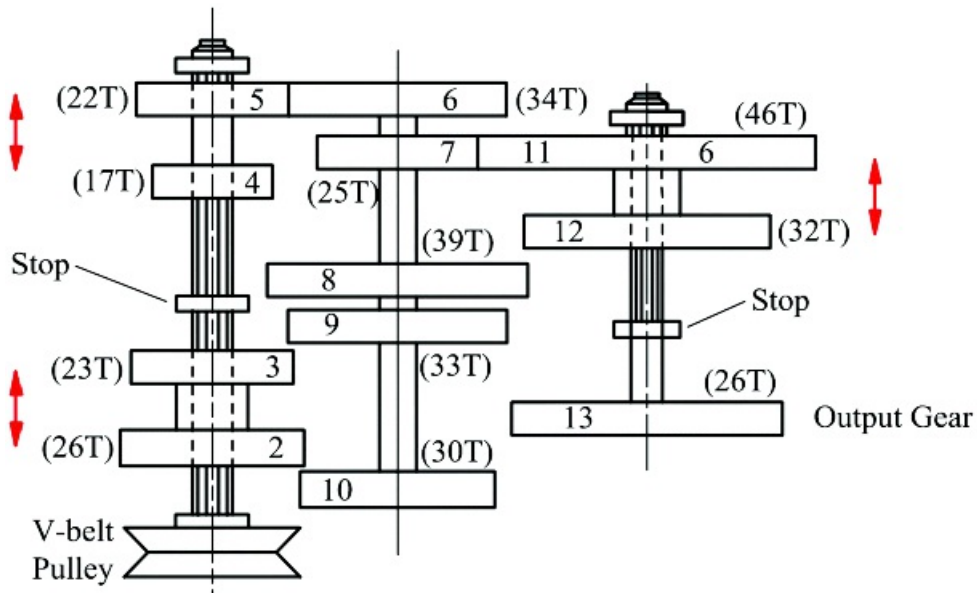


[Figure P13.3](#) Gear train for Problem 13.3.

13.4 A simple three-speed transmission is shown in [Figure P13.4](#). The power flow is as follows: (a) first gear: gear 4 is shifted to mesh with gear 7; power flows through gears 2, 5, 7, 4; (b) second gear: gear 3 is shifted to mesh with gear 6; power flows through gears 2, 5, 6, 3; (c) third gear: gear 3 is shifted so that the clutch teeth on gear 3 mesh with those on gear 2; a direct drive results; (d) reverse gear: gear 4 is shifted to mesh with gear

9; power flows through gears 2, 5, 8, 9, 4. An automobile with this transmission has a differential ratio of 3:1 and a tire outside diameter of 24 in. Determine the engine speed for the car under the following conditions: (i) first gear and the automobile is traveling at 15 mph; (ii) third gear and the automobile is traveling at 55 mph; and (iii) reverse gear and the automobile is traveling at 3.5 mph.

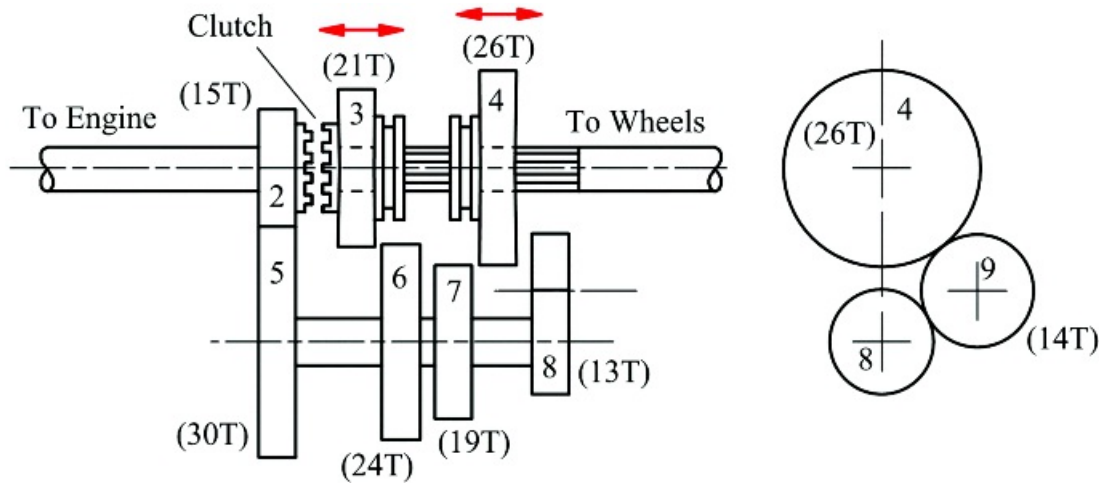


[Figure P13.4](#) Gear train for Problem 13.4.

13.5 Part of the gear train for a machine tool is shown in [Figure P13.5](#). Compound gears 2 and 3 slide on a splined shaft so that gear 3 can mesh with gear 4 or gear 2 can mesh with gear 6. Also, compound gears 14 and 15 slide on a splined shaft so that gear 14 can mesh with gear 16 or gear 15 can mesh with gear 17. (a) If gear 3 meshes with gear 4, what are the two possible spindle speeds for a motor speed of 1800 rpm? (b) Now assume that gear 14 meshes with gear 16, and gear 2 meshes with gear 6. Gears 2, 3, 4, and 6 are standard and have the same diametral pitch. What are the tooth numbers on gears 2 and 6 if the spindle speed is 130 ± 3 rpm?

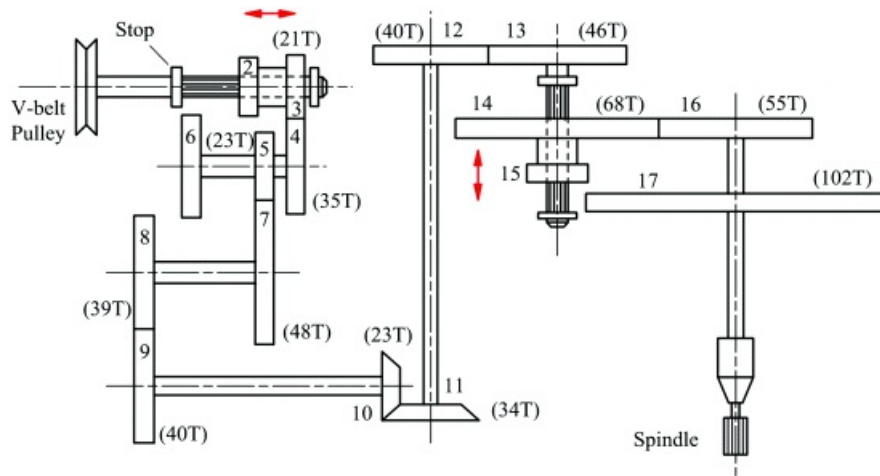


[Figure P13.5](#) Gear train for Problem 13.5.

13.6 An internal gear having 160 teeth and rotating counterclockwise at 30 rpm is connected through a gear train to an external gear, which rotates at 120 rpm in the counterclockwise direction. Using the minimum number of gears, select gears from the following list that will satisfy the design requirements. Tooth numbers for the available gears are 20, 22, 25, 30, 32, 34, 35, 40, 50, 55, 60, and 64. There is only one gear with each tooth number, and each gear has the same diametral pitch.

13.7 Solve Problem 13.6 if the external gear is concentric with the internal gear (the rotation axis is the same for both gears) and the external gear rotates clockwise.

13.8 Solve Problem 13.6 if the external gear is concentric with the internal gear and the external gear rotates counterclockwise.

13.9 Solve Problem 13.6 if the external gear rotates at 50 rpm.

13.10 In Figure P13.10, determine the diametral pitch and number of teeth on gears 4 and 5 if the speed of gear 2 (ω_2) is to be 10 times the speed of gear 5 (ω_5). The pitches of the two gears should be as nearly equal as possible, and no gear should have fewer than 15 teeth.

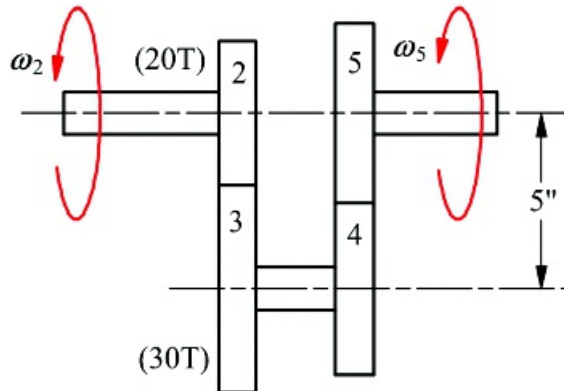


Figure P13.10 Concentric gear train for Problem 13.10.

13.11 Solve Problem 13.10 if ω_2 is to be 8 times the speed of gear 5 (ω_5).

13.12 Solve Problem 13.10 if ω_2 is to be 6.5 times the speed of gear 5 (ω_5).

13.13 The gear train shown in Figure P13.13 is a candidate for the spindle drive of a gear-hobbing machine. The gear blank and the worm gear (gear 10) are mounted on the same shaft and rotate together. If the gear blank is to be driven clockwise, determine the hand of the hob. Also determine the velocity ratio (ω_8/ω_5) to cut 72 teeth on the gear blank.

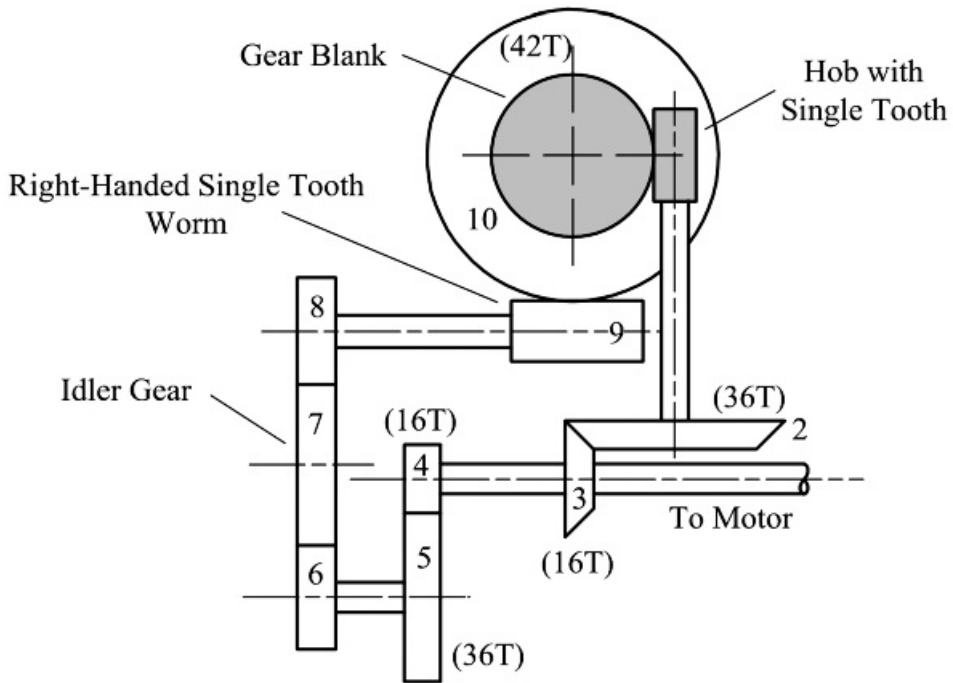


Figure P13.13 Gear train for Problem 13.13.

13.14 Assume that the input shaft of a transmission rotates clockwise at 1800 rpm. The output shaft is driven at 160 rpm in the counterclockwise direction. None of the gears in the transmission is to be an idler, and the gear ratio at any given mesh is not to exceed 3:1. Gears are available that have all tooth numbers between 13 and 85; however, only one gear is available with each tooth number. Select the appropriate gears for the transmission, and sketch the configuration designed. Label the gears and tooth numbers.

13.15 Solve Problem 13.14 if the output shaft rotates at 210 rpm in the counterclockwise direction.

13.16 Solve Problem 13.14 if the output shaft rotates at 200 rpm in the clockwise direction.

13.17 A simple gear reduction is to be used to generate a gear ratio equal to π . Make up a table of possible gear ratios where the maximum number of teeth on either gear is 100. This can be conveniently done using a simple computer program. Identify the gear set that most closely approximates the desired ratio. What is the error?

13.18 A simple gear reduction is to be used to generate the gear ratio 0.467927. Make up a table of possible gear ratios where the maximum number of teeth on either gear is 100. Identify the gear set that most closely approximates the desired ratio. What is the error?

13.19 A simple gear reduction is to be used to generate a gear ratio equal to $\sqrt[3]{2}$. Make up a table of possible gear ratios where the maximum number of teeth on either gear is 100. Identify the gear set that most closely approximates the desired ratio. What is the error?

13.20 An alternative gear train is shown in [Figure P13.20](#) as a candidate for the spindle drive of a gear hobbing machine. The gear blank and the worm gear (gear 9) are mounted on the same shaft and rotate together. If the gear blank is to be driven clockwise, determine the hand of the hob. Next determine the velocity ratio (ω_3/ω_5) to cut 75 teeth on the gear blank. Finally, select gears 3 and 5 that will satisfy the ratio. Gears are available which have all of the tooth numbers from 15 to 40.

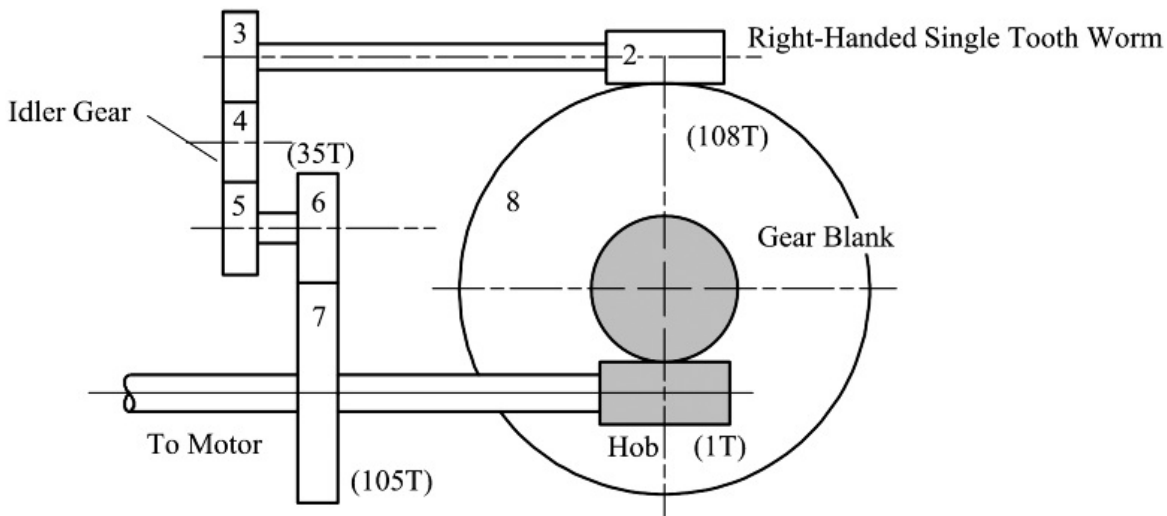


[Figure P13.20](#) Gear train for Problem 13.20.

13.21 A simple gear reduction unit is to be used to generate the gear ratio 2.105399. Make up a table of possible gear ratios where the maximum number of teeth on all gears is 100. Identify the gear set that most closely approximates the desired ratio. Note that this can be done most easily with a computer program. What is the error?

Planetary Gear Trains

13.22 In the gear train shown in [Figure P13.22](#), gears 3 and 4 are integral. Gear 3 meshes with gear 2, and gear 4 meshes with gear 5. If gear 2 is fixed and $\omega_5 = 100 \text{ rpm}$ counterclockwise, determine the angular velocity of the carrier.

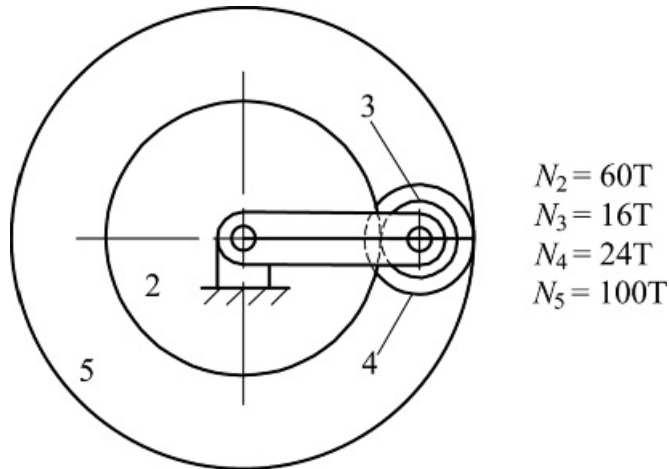


[Figure P13.22](#) Planetary gear train for Problem 13.22.

13.23 Solve Problem 13.22 if gear 5 is fixed and $\omega_2 = 100 \text{ rpm}$ counterclockwise.

13.24 Solve Problem 13.22 when $N_2 = 70 \text{ T}$, $N_3 = 35 \text{ T}$, $N_4 = 15 \text{ T}$ and $N_5 = 120$.

13.25 In [Figure P13.25](#), axis $y-y$ is fixed while axes $x-x$ and $z-z$ move with the arm. Gear 7 is fixed to the carrier. Gears 3 and 4, 5 and 6, and 8 and 9 are fixed together, respectively. Gears 3 and 4 move with planetary motion. If the tooth numbers are $N_2 = 16\text{T}$, $N_3 = 20\text{T}$, $N_4 = 22\text{T}$, $N_5 = 14\text{T}$, $N_6 = 15\text{T}$, $N_7 = 36\text{T}$, $N_8 = 20\text{T}$, $N_9 = 41\text{T}$, and $N_{10} = 97\text{T}$, determine the speed and direction of the output shaft.

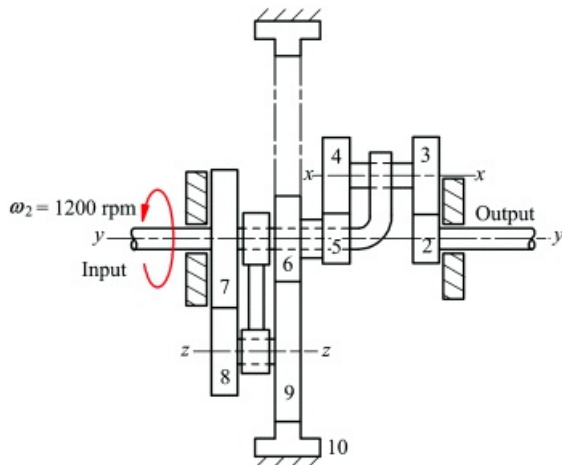


[Figure P13.25](#) Planetary gear train for Problem 13.25.

13.26 Solve Problem 13.25 when $N_2 = 16\text{T}$, $N_3 = 20\text{T}$, $N_4 = 16\text{T}$, $N_5 = 20\text{T}$, $N_6 = 15\text{T}$, $N_7 = 40\text{T}$, $N_8 = 15\text{T}$, $N_9 = 40\text{T}$, and $N_{10} = 95\text{T}$.

13.27 Solve Problem 13.25 when $N_2 = 14\text{T}$, $N_3 = 30\text{T}$, $N_4 = 14\text{T}$, $N_5 = 30\text{T}$, $N_6 = 15\text{T}$, $N_7 = 60\text{T}$, $N_8 = 15\text{T}$, $N_9 = 60\text{T}$, and $N_{10} = 135\text{T}$.

13.28 In the gear train shown in [Figure P13.28](#), gears 2 and 4, 6 and 7, and 3 and 9 are fixed together. If the angular velocity of the carrier is given, determine the angular velocity of gear 9.

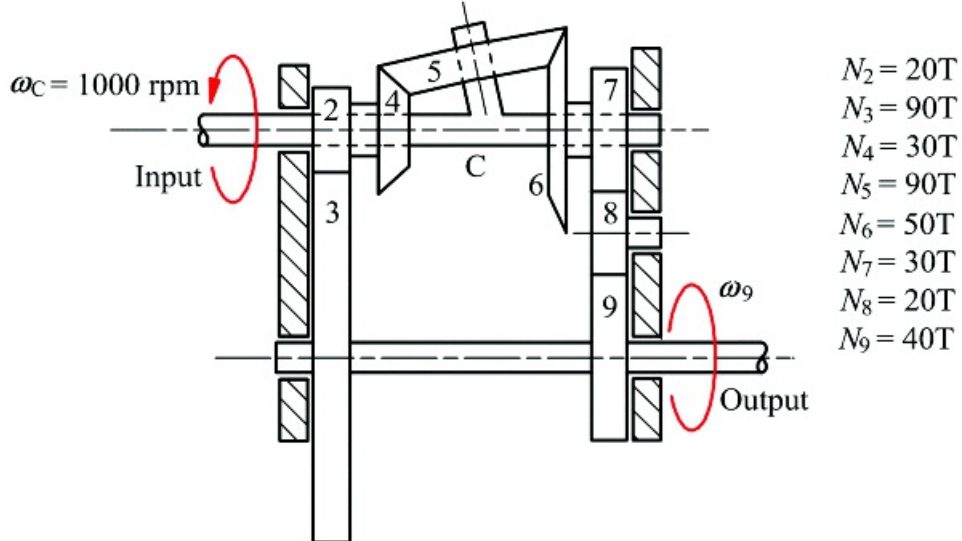


Figure P13.28 Planetary gear train for Problem 13.28.

13.29 Solve Problem 13.28 if $N_2 = 10T$, $N_3 = 100T$, $N_7 = 20T$, $N_8 = 10T$, and $N_9 = 70T$.

13.30 Solve Problem 13.28 but assume that the shaft connecting gears 3 and 9 is the input shaft and the shaft of the carrier is the output shaft. Assume $\omega_S = 500 \text{ rpm}$ counterclockwise and compute ω_C .

13.31 The differential for a rear-wheel driven vehicle is shown schematically in Figure P13.31. If the drive shaft turns at 900 rpm, what is the speed of the vehicle if neither tire slips and the outside diameter of the tires is 24 in?

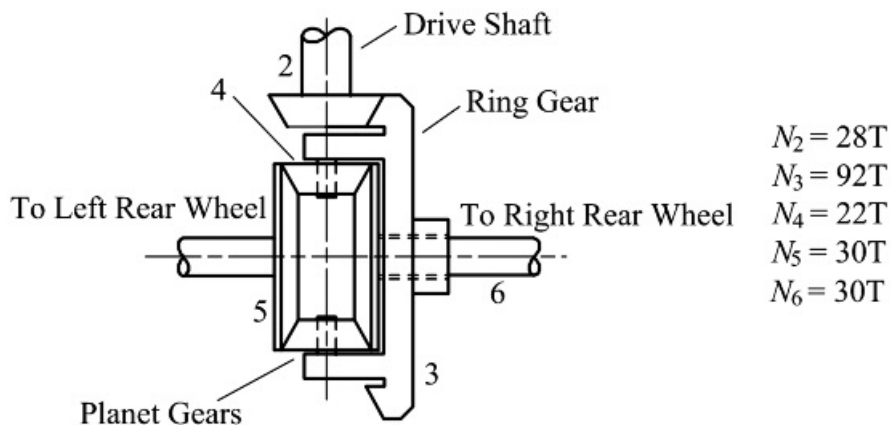


Figure P13.31 Planetary gear train for Problem 13.31.

13.32 Assume that the vehicle in Problem 13.31 is stopped so that the right wheel sits on a small icy patch and can spin freely while the left wheel does not spin. Determine the angular velocity of the right wheel if the angular speed of the drive shaft is 500 rpm.

13.33 Assume that the vehicle in Problem 13.31 is traveling at 35 mph and turns around a curve with a radius of 50 ft from the centerline of the vehicle. The center-to-center distance between the treads of the right and left wheels is 60 in. Compute the rotational speed of each rear wheel, the rotational speed of the ring gear, and the rotational speed of the drive shaft.

13.34 In the mechanism shown in Figure P13.34, derive an expression for the angular velocity of gear 7 (ω_7) in terms of ω_2 and ω_8 and the tooth numbers N_2 , N_3 , N_4 , N_5 , N_6 , and N_7 . Take counterclockwise viewing from the left as positive for the rotation of gears 2, 3, 4, 5, and 6. Viewed from the front of the page, take counterclockwise as the positive direction for gear 7.

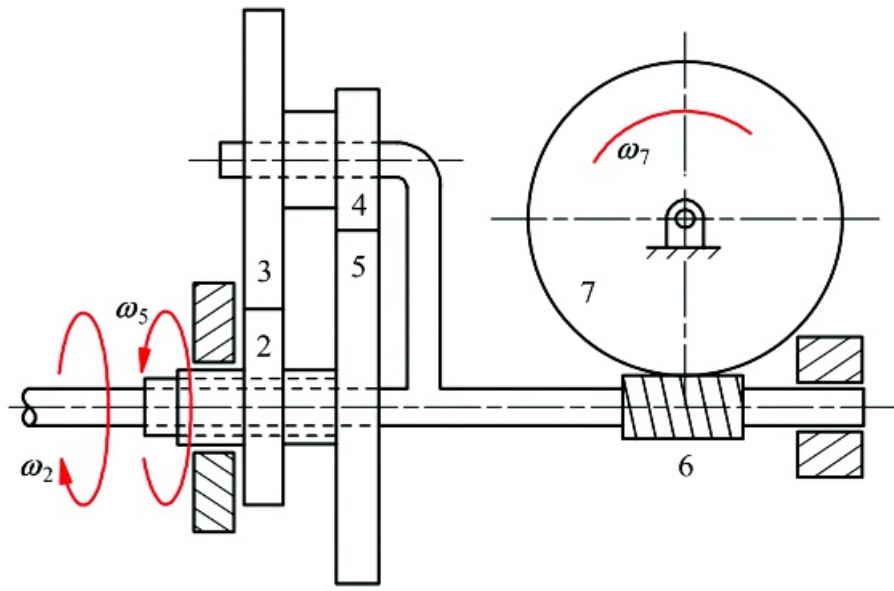


Figure P13.34 Planetary gear train for Problem 13.34.

13.35 In Problem 13.34, assume that $\omega_2 = 100 \text{ rpm}$, $\omega_5 = -50 \text{ rpm}$, $N_2 = 40T$, $N_3 = 60T$, $N_4 = 30T$, $N_5 = 70T$, $N_6 = 8T$, and $N_7 = 50T$. Determine the angular velocity of both gears 6 and 7.

13.36¹ Figure P13.36 shows a schematic diagram of a semiautomatic transmission from the Model-T automobile. This was the forerunner of today's automatic transmission. A plate clutch, two banded clutches, and a system of pedals and levers (used to engage and disengage these plate and band clutches) operated in the proper sequence are shown in the table in Figure P13.36. Determine the output/input speed ratio for each condition.

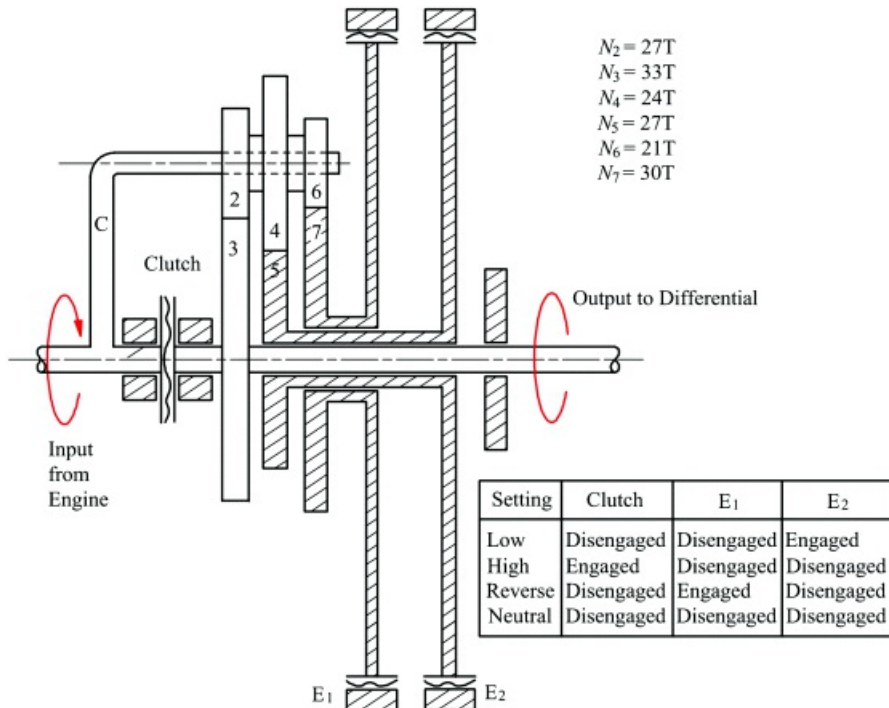
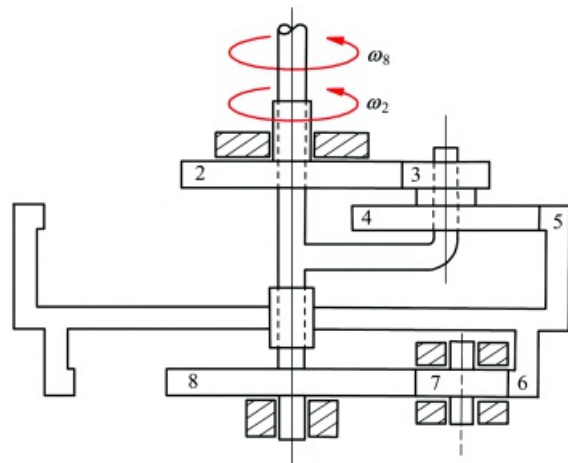


Figure P13.36 Planetary gear train for Problem 13.36

13.37 In problem 13.36, if the engine rotates at 400 rpm determine the angular velocity of gear 5 when the transmission is in low gear.

13.38 In the mechanism shown in Figure P13.38, let the input be gear 2 and assume that all of the gear tooth

numbers (N_2 , N_3 , N_4 , N_5 , N_6 , N_7 , and N_8) are known. Derive an expression for the angular velocity of gear 8.



[Figure P13.38](#) Planetary gear train for Problem 13.38.

Note

1. Problem courtesy of Dr. Michael Stanisic, Notre Dame University

Prerequisite Knowledge Needed for Chapter 14

The prior knowledge needed for this chapter includes an undergraduate course in statics. For Sections 14.10 and 14.11, knowledge is needed of the instantaneous center method of mechanism velocity analysis that can be found in [Chapter 6](#).



14.1 Introduction

Machines are used to apply mechanical force, energy, or power for useful purposes. So far, in this book, we have been concerned mainly with motion. However, mechanisms are used to transmit and apply force, as well as to generate desired motions. In many applications, the motion is unimportant, usually because it is slow. What is important is the application of force. The simplest and original “machines” transmitted force from an input location to an output location while magnifying or diminishing it. Examples are the first- and second-order levers, wedges, and pulley mechanisms. These are usually regarded as static machines. Many other forms of machines can be analyzed by the methods of statics because they function without motion, or because the velocities of their motions are small enough that dynamic effects can be neglected. Examples are many types of clamps, pliers, and cutter jacks, winches, and other heavy lifting devices and many kinds of latches and toggles. Further, many machines require structural supports such as brackets, beams, frames, and trusses.

The design analysis of these mechanisms and their associated structures depends on static force analysis. In many other cases, mechanisms must deliver forces of controlled magnitude while generating a specified motion. If the motion is sufficiently slow for inertial forces to be neglected in comparison with the applied loads, the techniques of static force analysis can be applied. Further, even when inertial forces must be included, in the common case in which the motion can be considered to be known, D'Alembert's principle can be used to convert dynamic force analysis problems into the forms of static force analysis problems. This will be discussed in detail in [Chapter 15](#).

The primary techniques used are fundamentally similar to the static equilibrium techniques taught in introductory engineering mechanics courses. Mechanisms and machines commonly have a relatively large number of members, some of which may have relatively complex geometries, which make manual solution of statics problems laborious. We will augment these methods with a powerful technique that leads to especially efficient solutions for some kinds of static machine problems. This is the method of virtual work treated in Section 14.11. This approach requires a knowledge of the velocity analysis methods discussed in earlier chapters, and particularly the method of instantaneous centers treated in [Chapter 6](#).

The basis of all static analysis is Newton's third law, as embodied in the concept of static equilibrium. The material in this chapter is composed of systematic ways of applying static equilibrium so that correct solutions to relatively complex problems can be reliably generated.

A further powerful motivation for pursuing static or dynamic force analysis is that conversion of a kinematic design into a real, physical mechanism design requires consideration of the loads on components, and the stresses and deflections of those components. The loads on each member of a machine are usually of great interest to the machine designer because it is the engineer's responsibility to select the material to be used and to size the component so that it can safely resist those loads. That is, computation of the complete set of loads acting on a member in any critical situation provides essential initial data for a stress or deflection analysis of that member. Up to now in this book, we have usually indicated members by lines or simple polygons. It must always be remembered that this is a geometric convenience and that the lines and polygons represent physical objects with additional dimensions made of real engineering materials. Analysis of the worst-case stresses or deflections and application of a relevant failure theory allow selection of materials and dimensions with the assurance that the part will withstand that loading condition without failing. The output of the static force analysis typically yields the forces and moments to be applied to models of the individual components for subsequent finite element analysis to identify failure situations either involving sufficient dimensional change to cause malfunction, or by permanent deformation or fracture.

As indicated above, there is nothing intrinsically different in the methods we use to do static force analysis of mechanisms for analysis of the relatively simple systems used as examples in introductory courses on statics. It is not so long ago that force analysis of a mechanism consisted of writing out and solving a set of static equilibrium equations. This step has been mostly been automated by modern mechanism-simulation packages. However, it is still necessary to ensure that the system is correctly modeled, and that all forces are applied to the system on the correct lines of action. For this reason, it is still essential for the user of modeling software to understand how it works. This process is described in the remainder of this chapter.



14.2 Forces, Moments, and Couples

A force is a vector that has a definite line of action on a given link of the mechanism but not necessarily a definite point of application. If $\hat{i}, \hat{j}, \hat{k}$ are unit vectors respectively parallel to the x, y , and z axes of a Cartesian reference frame, the components of \mathbf{F} in the directions of those axes are given by the dot products

$$F_x = \mathbf{F} \cdot \hat{i}, F_y = \mathbf{F} \cdot \hat{j}, F_z = \mathbf{F} \cdot \hat{k} \quad (14.1)$$

and

$$\mathbf{F} = F_x \hat{i} + F_y \hat{j} + F_z \hat{k}$$

Forces may be internally applied forces such as a force due to a gas acting on a piston or body forces such as a weight or a magnetic force.

Two forces that have intersecting lines of action can be summed into a single, equivalent force as shown in [Figure 14.1](#). The resultant force will act along a line that passes through the point of intersection and lies in the plane defined by the two force vectors.

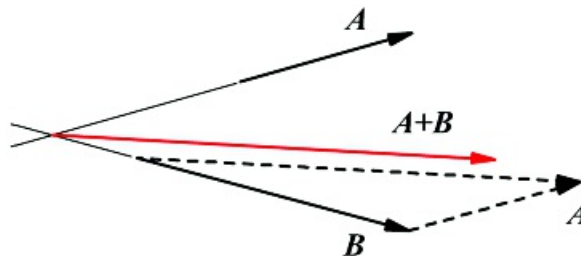


[Figure 14.1](#) The resultant ($A + B$) is equivalent to the forces A and B acting simultaneously.

If two forces are equal and opposite but not collinear, the two forces cannot be resolved into a single force, but they still have an effect on the body to which they are applied. The vector sum of the two equal and opposite forces will be zero. The forces constitute a couple as shown in [Figure 14.2](#). The moment of the couple is defined by

$$M = \mathbf{r} \times \mathbf{F} = \begin{vmatrix} \hat{i} & \hat{j} & \hat{k} \\ r_x & r_y & r_z \\ F_x & F_y & F_z \end{vmatrix} = (r_y F_z - r_z F_y) \hat{i} + (r_z F_x - r_x F_z) \hat{j} + (r_x F_y - r_y F_x) \hat{k} \quad (14.2)$$

where

$$\mathbf{r} = r_x \hat{i} + r_y \hat{j} + r_z \hat{k}$$

The moment of a couple is independent of the point of application. It is a free vector that can be assumed to be applied anywhere on the body of interest. Also, the magnitude and direction are independent of how \mathbf{r} is chosen. Two couples are equal if their moments (M in [Equation 14.2](#)) are equal.

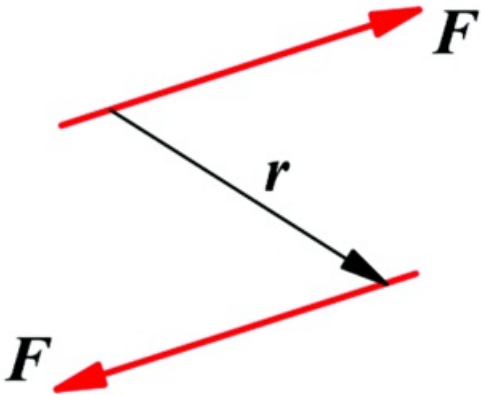


[Figure 14.2](#) Two equal and opposite but noncollinear forces form a couple.

The moment generated about a point by a single force, as shown in [Figure 14.3](#) is also given by [Equation 14.2](#). It is sometimes convenient to represent the moment in terms of the normal vector, r_n , from the point to the force. Then

$$M = r_n \times F \quad (14.3)$$

When this is done, we can compute the moment magnitude directly from the magnitudes of r_n and F . That is, $M = r_n(F)$. When this procedure is used, we must determine the direction of the moment by inspection.

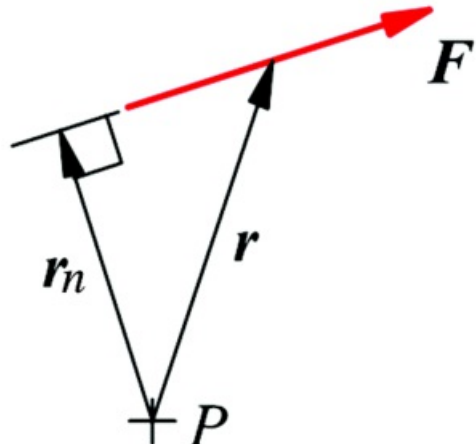


[Figure 14.3](#) The moment of a force about a point.

The moment will be perpendicular to both F and r or r_n . In planar problems, the moment will be normal to the plane containing F and r . In this chapter, we will emphasize planar problems. Notice that the moment of a force about a point is very much dependent on the location of the point.

If a force and a couple (F and M) are applied to a rigid body, the system can be replaced by a single force such that the force will have the same effect on the system as the original force and couple. The new force vector will be equal to the original force vector but offset relative to the line of action of the original force vector by the normal distance b . Here b is computed in such a way that $M = b \times F$. Therefore

$$b = |b| = \frac{|M|}{|F|} = \frac{M}{F} \quad (14.4)$$

In principle, the vector b can be drawn from either side of the line of action of F . However, the proper side of the line of action is the one that will make the sign of $b \times F$ the same as the sign of M . An example is shown in [Figure](#)

14.4.

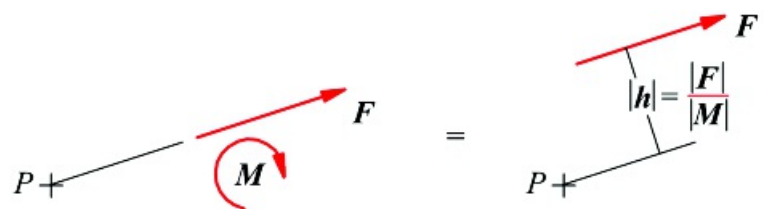


Figure 14.4 Replacing a force-moment system by a single force that is offset by the distance h .



14.3 Static Equilibrium

A direct consequence of Newton's first two laws of motion is that, if a body is at rest, the sum of all forces acting on the body must be zero. Further, the sum of the moments of those forces about any point must also be zero. Thus, for any member of a structure

$$\sum \mathbf{F} = \mathbf{0} \quad (14.5)$$

$$\sum M_O = 0 \quad (14.6)$$

where $\sum \mathbf{F}$ is the vector sum of all forces acting on the body, and $\sum M_O$ is the vector sum of the moments of those forces about any chosen point, O . Equations 14.5 and 14.6 are called the equations of *static equilibrium*.

The basis of the static force analysis of any structure is the algebraic solution of the static equilibrium equations written for every member in the system. Equations 14.5 and 14.6 are typically associated with free-body diagrams. When the equations are written, they include all of the forces and moments associated with a given free body.



14.4 Free-Body Diagrams

The first step in any static analysis of a mechanism is the construction or, more usually, sketching of a free-body diagram of each member of the mechanism. This needs to be done even when a digital simulation package is used for solution. All forces acting on each member, including the forces of action and reaction between the members, as well as externally applied loads, must be indicated on the free-body diagram.

A free-body diagram is a bookkeeping device to ensure that all relevant force components are included in the static equilibrium equations. The omission of *any* force component will lead to totally incorrect results. Experience has shown that disregard of the step of drawing free-body diagrams almost always results in incorrect equations and results. As a consequence, experienced machine designers never skip this step, although students often do!

The forces that can be transmitted across an ideal (frictionless) kinematic joint are related to the motions permitted by that joint. Basically, the work done by the transmitted forces in the directions of permitted motion must be zero. For example, a revolute joint permits rotation about its axis. Any force that is normal to that axis and whose line of action intersects it does no rotational work. Therefore, any force component in the plane of motion passing through the joint axis is transmitted. It is usually convenient to represent this set of possible forces by two components parallel to the x and y axis directions of the fixed reference frame, as shown in [Figure 14.5\(a\)](#). In accordance with Newton's third law, the force components transmitted to one of the bodies joined from the other are equal and opposite to the force components received by the second body from the first. Therefore, when the free bodies are drawn these force components appear in equal and opposite pairs.

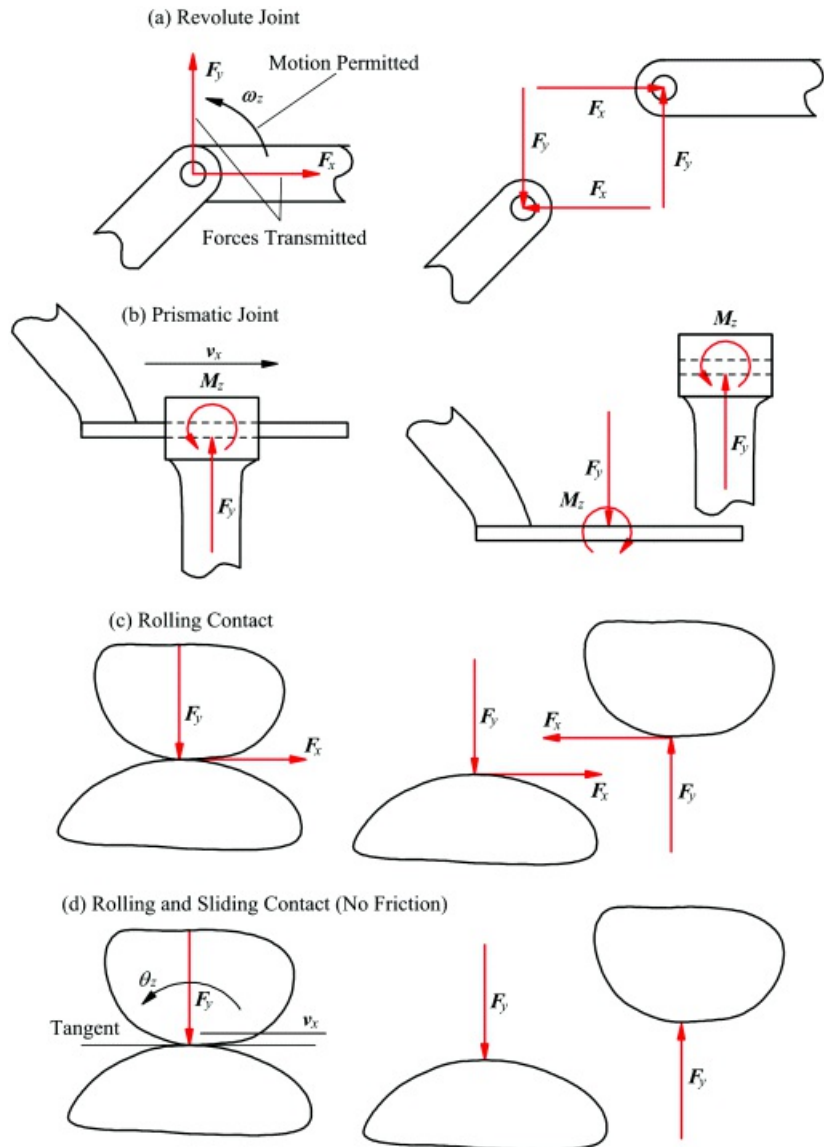


[Figure 14.5](#) Force components transmitted by different types of kinematic joints in planar linkages.

Similarly, a prismatic joint permits linear motion in one direction. A force normal to that direction does no work in the direction of motion. Also, a torque in the direction normal to the plane of motion will do no work in the direction of permitted motion. Therefore, these components will be transmitted by the prismatic joint, as indicated in [Figure 14.5\(b\)](#). Once again, the transmitted force and torque components will appear as equal and opposite pairs when the free bodies are drawn.

A rolling contact joint is similar to a revolute joint in permitting only pure rotation about the point of contact. The difference is that the axis of a revolute joint is fixed relative to each of the bodies that it joins, whereas the point of rolling contact migrates along the profiles of both bodies. The transmitted force system is also similar to that of a revolute joint, as indicated in [Figure 14.5\(c\)](#). A rolling and sliding contact permits both rotation in the direction normal to the plane of motion and sliding in the direction of the tangent at the point of contact. When friction is neglected, the only force component at the joint is a force along the normal at the point of contact. Consequently, this is the only force component that can be transmitted by such a joint, as indicated in [Figure 14.5\(d\)](#).

As has been indicated, the forces transmitted by kinematic joints appear in equal and opposite pairs acting on the two members joined in the free-body diagrams. These are seldom the only forces acting in the system. Usually there will also be loads imposed on the system by external agencies. These external loads do not usually appear as equal and opposite pairs.

In addition to indicating all active force components on a set of free-body diagrams, it is good practice to include the dimensional information needed to locate the lines of action of the forces. This information will be needed when writing the static equilibrium equations.



Example 14.1 Drawing Free-Body Diagrams

Draw free-body diagrams of all members of the vice-grip pliers in the position shown in [Figure 14.6](#). The objective of analysis will be to relate the magnitude of the force, F_H , exerted by the user's hand to the gripping forces, F_G , exerted on the workpiece. The plane of action of the pliers mechanism can be regarded as being parallel to the horizontal plane, so there are no gravity loads in the plane of action.

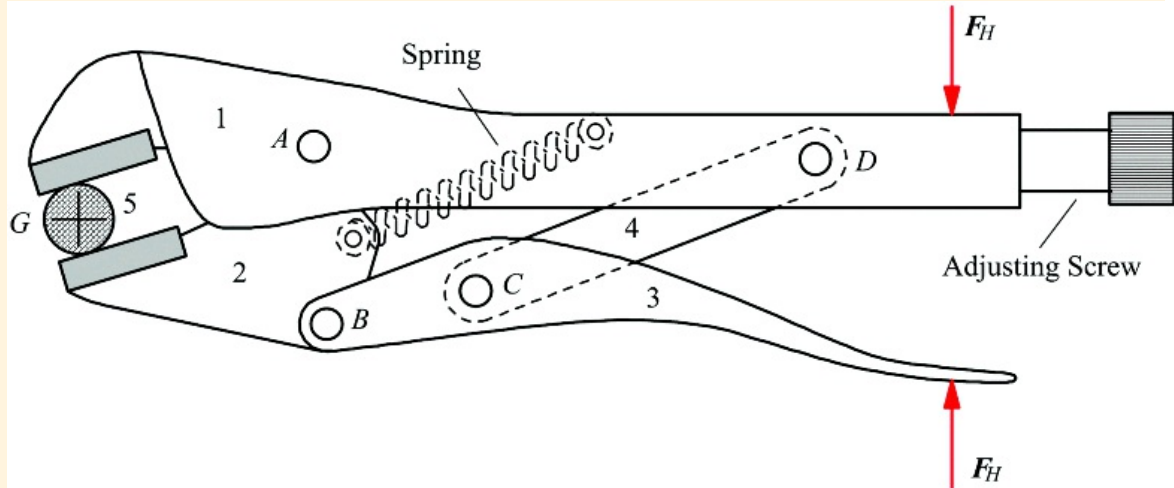


[Figure 14.6](#) The vice-grip pliers of Example 14.1.

Solution

Free-body diagrams of the individual components in the pliers are shown in [Figure 14.7](#). The only external loads on the system are the equal and opposite forces F_H exerted on the handles by the user's hand. The system as a whole can be regarded as a single free body ([Figure 14.6](#)) expressing the requirement that the system as a whole be in static equilibrium. Since it is a planar system, if there are only two external forces acting on the system, those forces must be equal and opposite and must act along the same line of action.

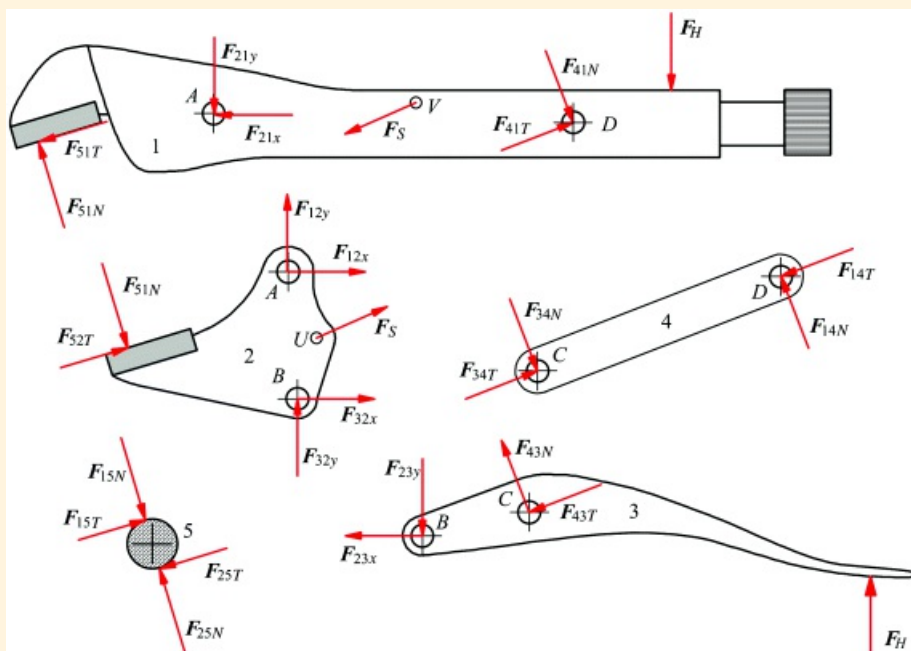


[Figure 14.7](#) The free-body diagrams of Example 14.1.

In [Figure 14.7](#), the force between two links is represented by the letter F with a subscript including the numbers for the two links. The force F_{23} is interpreted as the force that link 2 exerts on link 3. Similarly, F_{32} is the force that link 3 exerts on link 2. Clearly, $F_{23} = -F_{32}$. If a force is an external force, the subscript will correspond to the location where the force is applied or to the type of force (e.g., F_S or F_H).

The forces, F_S , exerted on the system by the spring can also be treated as external forces for the purposes of the present analysis. Once again, these two forces are equal and opposite and act along the spring axis. The magnitude of F_S would be computed based on the current length of the spring, the free length, and the spring constant.

The two contacts between the workpiece and the jaws of the vice grip are modeled as rolling contacts. That is, they transmit only forces whose lines of action pass through the contact points. These contact forces are, in principle, unknown in both magnitude and direction. Therefore they are represented by two orthogonal force components F_{25N} and F_{25T} (or by F_{15N} and F_{15T}). In fact, since there are only two forces acting on the workpiece, those two forces must be equal, opposite, and collinear. That is, $F_{25T} = F_{15T} = 0$.

The joints connecting the members of the mechanism are all revolutes. That is, each of them transmits a force whose line of action passes through the revolute axis. These forces are initially unknown in both magnitude and direction. It is convenient to represent them by means of two components with specified directions but unknown magnitudes. In many cases those directions are arbitrarily assigned to be parallel to the x and y axes of the fixed reference frame, but it is not necessary that they have those directions. In the case of joints C and D the force components are taken to be along the line CD and normal to that line. This is helpful in this case because the link CD actually has only two forces acting on it, one at C and one at D , so equilibrium of that link requires that those forces be equal, opposite, and collinear. Therefore, in link 4, $F_{14N} = F_{34N} = 0$, and $F_{14L} = -F_{34L}$. Note, however, that F_{14L} and F_{34L} may be either compressive or tensile.

Notice that every internal force component appears in two of the free-body diagrams and that the senses of the two equal components are opposed. It is convenient to label the two components of each pair identically rather than putting a negative sign on one of them. This is consistent if we regard the labels as representing their magnitudes and the vectors drawn as representing their directions, but it can be confusing because it seems different from the conventions used earlier in this book. It is always necessary to use positive and negative signs on the components when writing equilibrium equations.



14.5 Solution of Static Equilibrium Problems

A body is in static equilibrium when the resultant (sum) of all the forces acting on it is zero and the resultant of all their moments about any point is zero.

If a system of rigid bodies, such as a mechanism, is in static equilibrium, then each individual body is in equilibrium under the action of all the forces acting on it, including those exerted on it by other members. A free-body diagram should be drawn for each member, and the appropriate force and moment equilibrium equations should then be written for each free body and solved for the unknown forces or moments.

For an analytical force analysis, we must know the coordinates of all points involved in the analysis. Therefore, before the force analysis is conducted, a position analysis must be conducted. As indicated in [Chapters 4 through 7](#), the position equations will be nonlinear. After the position analysis is conducted, however, the force equations will be linear (unless friction is involved), and therefore they can be easily solved. We will illustrate the procedure with three examples.



Example 14.2

Force Analysis of Four-Bar Linkage

Analyze the linkage in [Figure 14.8](#) to find the torque T_{12} required if $P = 120 and the driver link 2 is at an angle of 135° with the horizontal axis.$

$AA^* = 6 \text{ in}$	$BB^* = 12 \text{ in}$	$A^*B^* = 8 \text{ in}$
$AB = 18 \text{ in}$	$CB^* = 5 \text{ in}$	

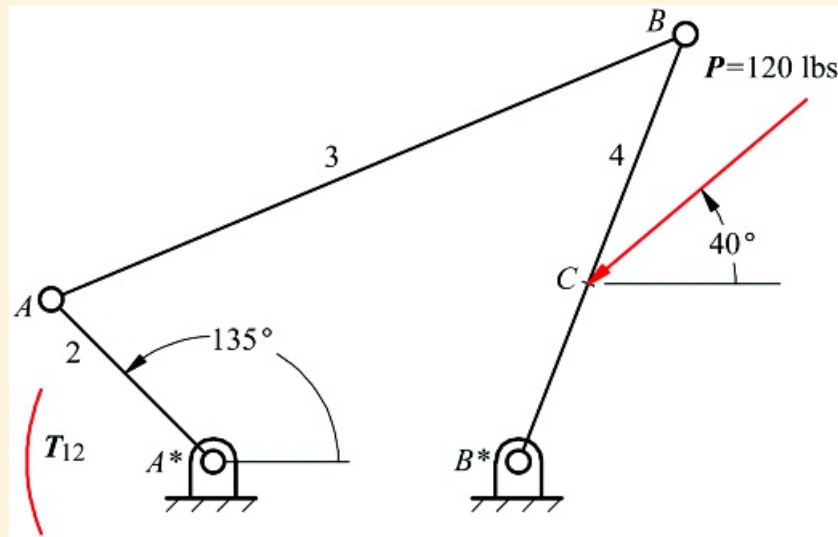


[Figure 14.8](#) Mechanism for Example 14.2.

Solution

Before the force analysis can be conducted, we must determine the coordinates of the points relative to the coordinate system shown in [Figure 14.9](#). This can be done using the procedures discussed in [Chapter 7](#), and all vectors will be defined using the sign convention and nomenclature given in [Chapter 7](#) (see [Figure 7.3](#)). This will let us determine the angular orientation of each link and each force. After the position analysis, we can summarize the known position and force information as follows

$$P = 120 \angle 22.55^\circ = -91.96 - 77.1j$$

$$F_{34} = F_{34} \angle 22.55^\circ = F_{34}(0.9228i + 0.3851j)$$

$$r_{A/A^*} = r_{A/A^*} \angle 135^\circ = 6.0 \angle 135^\circ = -4.243i + 4.243j$$

$$r_{B/B^*} = r_{B/B^*} \angle 22.55^\circ = 18 \angle 22.55^\circ = 16.61i + 6.93j$$

$$r_{B/S^*} = r_{B/S^*} / \cos 68.65^\circ = 12 / \cos 68.65^\circ = 4.3684 + 11.18j$$

and

$$r_{C/S^*} = r_{C/S^*} / \cos 68.65^\circ = 5 / \cos 68.65^\circ = 1.8203 - 4.657j$$

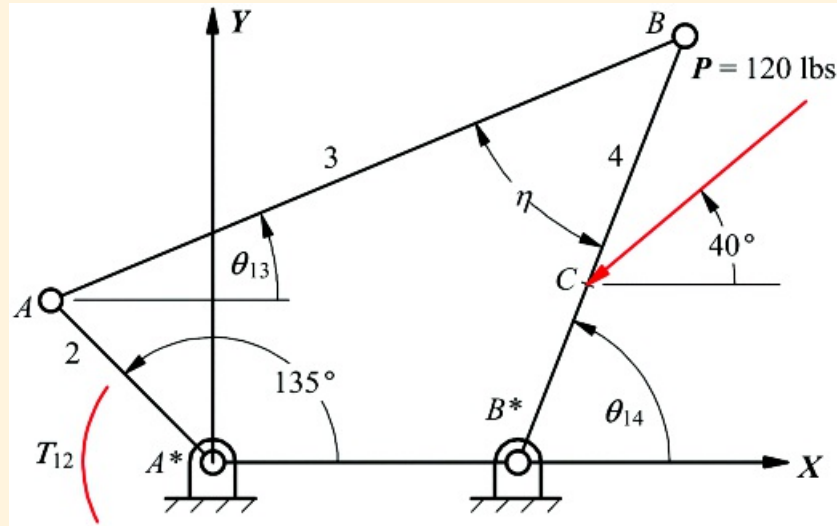


Figure 14.9 Coordinate axes for mechanism in Example 14.2.

To begin the analysis, draw the general free-body diagrams for each link as shown in [Figure 14.10](#). Again, we can simplify the free-body diagram for link 3 by noting that it is a two-force member with no applied moments. We will represent F_{14} by its x and y components. For the analysis, begin with link 4, because this is the only location where a force magnitude is known. There are only three unknowns associated with this link. These are the magnitude of F_{34} and the magnitude of the two components of F_{14} . We do not need to determine F_{14} to solve the problem. To compute F_{34} , sum moments about point B^* in the free-body diagram for link 4. Then

$$M_{B^*} = r_{B/S^*} \times M_{34} + r_{C/S^*} \times R = 0 \quad (14.7)$$

where

$$r_{B/S^*} \times M_{34} = \begin{vmatrix} i & j & k \\ 4.360 & 11.18 & 0 \\ 0.9228F_{34} & 0.3851F_{34} & 0 \end{vmatrix} = -8.635F_{34}k$$

and

$$r_{C/S^*} \times R = \begin{vmatrix} i & j & k \\ 1.820 & 4.657 & 0 \\ -91.9 & -77.1 & 0 \end{vmatrix} = 287.6k$$

Therefore

$$F_{34} = 287.6 / 8.635 = 33.31 \text{ lb}$$

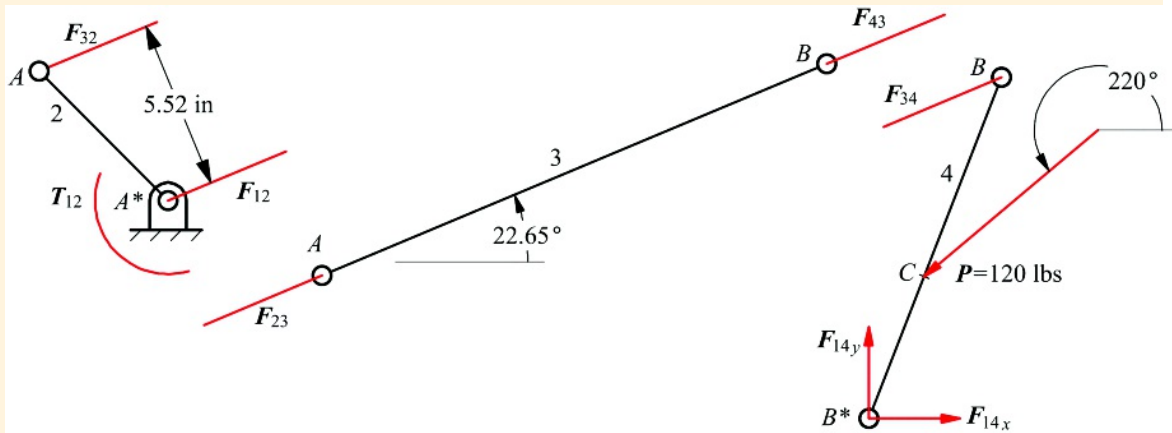


Figure 14.10 Free-body diagrams for analytical force analysis for Example 14.2.

Because the force is positive

$$F_{34} = 33.31 \angle 22.65^\circ \text{ lb}$$

From the free-body diagrams

$$F_{32} = -F_{23} = F_{43} = -F_{34}$$

Therefore

$$F_{32} = -33.31 \angle 22.65^\circ = -30.74i - 12.83j \text{ lb}$$

Now considering the free-body diagram for link 2, we can sum moments about point A^* . The result of this is

$$\sum M_{A^*} = r_{A/A^*} \times F_{32} + T_{12} = 0 \quad (14.8)$$

Here we are using the convention that a positive value for T_{12} corresponds to a counterclockwise torque. From [Equation 14.7](#)

$$T_{12} = -r_{A/A^*} \times F_{32} = -\begin{vmatrix} i & j & k \\ -4.243 & 4.243 & 0 \\ -30.74 & -12.83 & 0 \end{vmatrix} = -184.8 \text{ in-lb CW}$$

or

$$T_{12} = 184.8 \text{ in-lb CW}$$



14.6 Transmission Angle in a Four-Bar Linkage

In [Chapter 3](#), the transmission angle in a four-bar linkage was mentioned in conjunction with the design of optimal linkages for crank-rocker mechanisms. Transmission angle is the angle η in [Figure 14.9](#). If we reexamine [Equation 14.8](#), we find that

$$[F_{12}] = [r_{A/B} \times F_{32}] \quad (14.9)$$

For a given position of the linkage, the magnitude and orientation of $r_{B/A}$ and F_{32} will be fixed, and the magnitude of the torque required for equilibrium will be directly proportional to the magnitude of F_{32} . Therefore, the torque required to maintain equilibrium will increase with the magnitude of F_{32} . Now examining [Equation 14.9](#) and using an alternative expression for the cross-product gives

$$[r_{B/B^*} \times F_{34}] = |r_{B/B^*}| |F_{34}| \sin \eta = [r_{C/B^*} \times F]$$

or

$$|F_{34}| = \frac{|r_{C/B^*} \times F|}{|r_{B/B^*}| \sin \eta} = |F_{32}| \quad (14.10)$$

From [Equation 14.10](#) it is clear that the magnitude of the force F_{32} increases rapidly in a nonlinear fashion as the transmission angle η approaches 0 or π , and F_{32} reaches a minimum value for $\pi/2$. To reduce the torque required for equilibrium, we need to reduce the magnitude of F_{32} , which means we want to make the transmission angle as close to $\pi/2$ as possible. This is consistent with the optimization procedure discussed in [Chapter 3](#), where the objective was to minimize $\pi/2 - \eta$.

In general the transmission angle should be held between 30° and 150° . If the transmission angle approaches 0 or 180° , high-bearing loads, excessive wear, and binding in the joints can be expected.



Example 14.3

Force Analysis of an Oil-Drilling Mud Pump

A pump used for pumping drilling mud in oil well drilling has two double-acting cylinders. The linkage of the piston to the crankshaft for each cylinder is arranged as shown in [Figure 14.11](#).

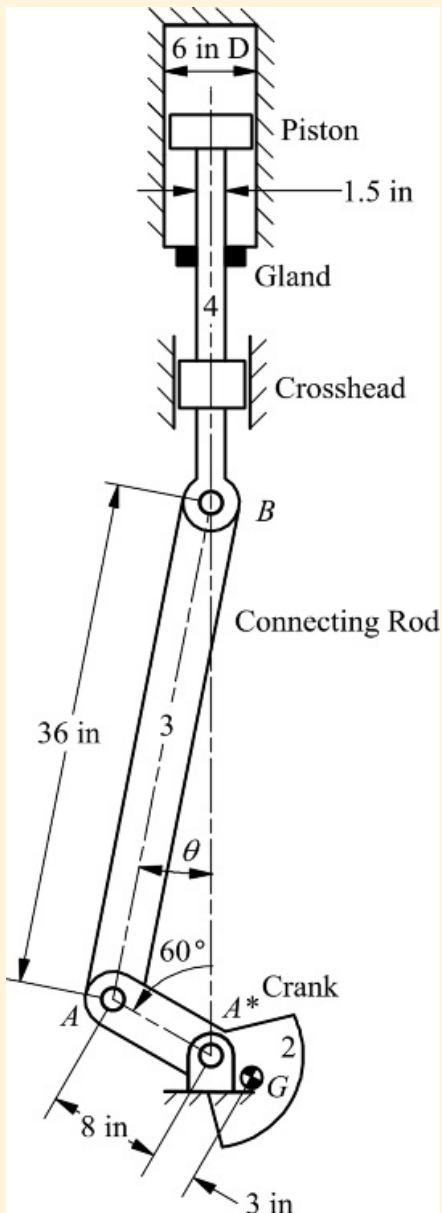


[Figure 14.11](#) The mechanism of an oil-drilling mud pump analyzed in Example 14.3.

On the upstroke, the gauge pressure in the cylinder above the piston is 750 psi above atmospheric, and on the bottom side of the piston the pressure is 5 psi *below* atmospheric. The bore of the cylinder has a diameter of 6 in, and the piston rod diameter is 1.5 in. The weight of the connecting rod, which can be regarded as a uniform rod, is 50 lb. The weight of the piston, piston rod, and crosshead assembly is 30 lb. The crank weighs 45 lb. and has its center of mass 3 in from the crankshaft axis as shown. The frictional resistance from the piston and gland seals and the crosshead is estimated to total 12 lb. In the position shown, find the torque that must be applied to the crank by the motor, the axial loads in the connecting rod and piston rod,

the loads on all three bearings, and the side thrust resisted by the crosshead.

Solution

Before the force analysis can be conducted, we need to determine the orientation of the connecting rod and the force on the piston. The angle ABA^* can be calculated using the sine rule

$$\frac{\sin \theta}{3} = \frac{\sin 60^\circ}{36}$$

or

$$\theta = 11.095^\circ$$

The area of the top face of the piston is

$$A_T = \pi \times 3^2 = 28.27 \text{ in}^2$$

Therefore the downward force on the top of the piston is

$$750 \times A_T = 21,210 \text{ lb}$$

The net area of the bottom face of the piston is

$$A_B = A_T - \pi \times 0.75^2 = 26.51 \text{ in}^2$$

Therefore the force on the bottom of the piston is

$$5 \times A_B = 130 \text{ lb}$$

This is also downward because the pressure is lower than atmospheric below the piston. The free-body diagrams for the pump members are shown in [Figure 14.12](#). Note that we have assumed the directions for the force components. If an assumed direction is wrong, the calculated force component will be negative. Also notice that in the free-body diagram for the piston, we have shown the moment M_{14} . This moment will be removed by the bearings that are not shown in the drawing. Therefore, we will not consider M_{14} in this analysis; however, it would need to be computed when the bearings are designed.

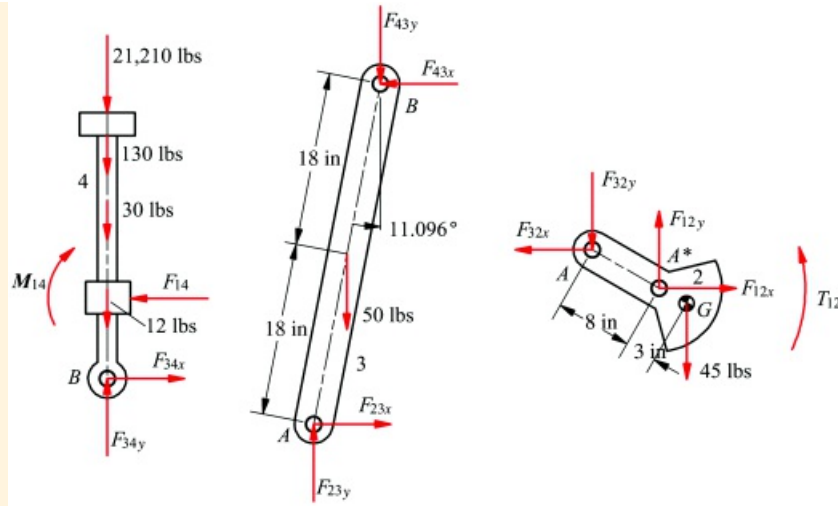


Figure 14.12 The free-body diagrams for the mechanism of [Figure 14.11](#) and Example 14.3.

Applying static equilibrium to the piston (link 4)

$$\sum F_x = 0 = F_{M4} - F_{14}, \quad \text{so} \quad F_{M4} = F_{14}$$

$$\sum F_y = 0 = F_{M4y} - 21,210 - 30 - 12 - 130 \quad \text{so} \quad F_{M4y} = 21,380$$

Here we have rounded the result to four significant figures. Hence the piston rod axial load is 21,380 lb.

Applying static equilibrium to the connecting rod

$$\sum F_x = 0 = F_{23x} - F_{43x} \quad \text{so} \quad F_{23x} = F_{43x} = F_{M4} = F_{14}$$

Again note that we have assumed the direction for the force components and are dealing only with magnitudes.

$$\sum F_y = 0 = F_{23y} - 21,380 - 50 \quad \text{so} \quad F_{23y} = 21,430$$

For the moment summation, we will use the forces and the normal distances from their lines of action to the point about which the summation of moments is made. For link 3, we will sum moments about point A

$$\sum M_A = \sum r_i F_i = F_{43x}(36) \cos 11.096^\circ - 21,380(36) \sin 11.096^\circ - 50(18) \sin 11.096^\circ$$

giving

$$F_{43x} = 4,200 \text{ lb}$$

Hence the connecting rod load at B is $\sqrt{21,430^2 + 4,200^2} = 21,840 \text{ lb}$. This is also the load on the bearing at B.

Applying static equilibrium to the crank and noting that $F_{23x} = F_{32x}$ and $F_{23y} = F_{32y}$

$$\sum F_x = 0 = F_{12x} - 4200 \rightarrow F_{12x} = 4200 \text{ lbs}$$

$$\sum F_y = 0 = F_{12y} - 21,430 - 45 \rightarrow F_{12y} = 21,480 \text{ lbs}$$

$$\sum M_A = 0 = F_{12} - 21,430(8) \sin 60^\circ + 4,200(8) \cos 60^\circ - 45(3) \sin 60^\circ$$

So

$$F_{12} = -165,200 \text{ lb-lb}$$

or

$$F_{12} = 13,800 \text{ ft-lb CW}$$

The bearing load at A is

$$F_{12} = \sqrt{21,480^2 + 4,200^2} = 21,900 \text{ lb}$$

This completes the analysis.



14.7 Friction Considerations

In the previous examples, we have considered friction briefly. In this section, we will investigate the effect of friction more formally for various types of joints. Friction can be extremely important in the design of mechanisms. If not properly handled, friction can greatly reduce the efficiency of a mechanism and increase power requirements. Because of friction, mechanical work is converted to heat, and the resulting heat buildup can degrade the materials in the mechanism, especially when polymers are used. Friction also contributes to wear, and in extreme cases friction can cause a mechanism to seize up.

The friction force is perpendicular to the contact force at a joint, and assuming Coulomb friction, the friction force will be proportional to the normal contact force. The direction of the friction force is determined by the direction of the relative motion or impending relative motion. Therefore, before a friction force analysis is conducted, it is important to conduct a velocity analysis in enough detail to determine the direction of the relative motion between different links. The magnitudes of the relative velocities are not required if Coulomb friction is assumed. The relative velocity magnitudes will be needed, however, if viscous friction is assumed. In the discussions here, only Coulomb friction will be considered. In the following, we will consider friction in cam joints, sliding or prismatic joints, and revolute joints.

14.7.1 Friction in Cam Contact

Two links (2 and 3) in cam contact are shown in [Figure 14.13](#). If we treat the problem as planar, the two links will have point contact at the cam joint, and the contact force can be resolved into two components, one normal to the common tangent and one along the common tangent. The component in the direction of the common tangent will be the friction force, and it can be related to the normal force by

$$F_{32f} = \mu F_{32n}$$

where μ is the coefficient of friction. Note that when Coulomb friction is assumed. This means that the friction force depends on μ and F_{32n} only; that is, F_{32f} is independent of the contact area. If the bodies have relative motion, μ will be equal to the kinetic coefficient of friction. If the bodies are at rest but the motion is impending, then the value of μ can range from 0 to μ_s , the static coefficient of friction. The actual coefficient of friction is equal to μ_s only when motion is impending.

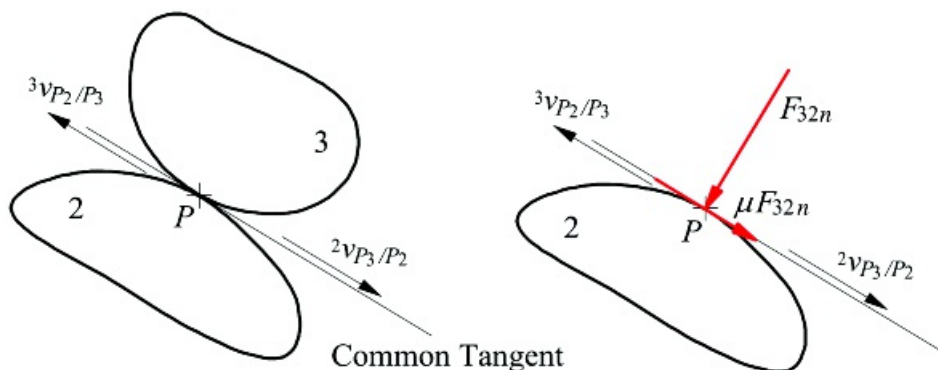


[Figure 14.13](#) Friction forces in a cam joint.

To determine the direction of the friction force on link 2, we must determine the direction for the velocity $3v_{P_2/P_3} = 3\gamma_{P_3}$. This is the relative velocity of the contact point on link 2 relative to link 3. The direction of the friction force will be opposite to this relative velocity vector. Alternatively, we can determine the velocity of P_3 relative to link 2 or $2v_{P_3/P_2} = 2\gamma_{P_3}$. This is the point on link 3 that is causing the force on link 2. The friction force on link 2 will be in the same direction as the velocity $2v_{P_3/P_2} = 2\gamma_{P_3}$. Simplistically, we can think of P_3 dragging against link 2 to cause the friction force. In this case, the friction force will be in the direction of the dragging

motion, that is, in the direction of ${}^2v_{P_3}$.

14.7.2 Friction in Slider Joints

Two links (3 and 5) in sliding contact are shown in [Figure 14.14\(a\)](#). The slider (link 3) is assumed to have two loads P and W applied to it from links other than link 5. If we resolve the force from link 5 on link 3 into two components, the normal force will be perpendicular to the contact surface and the friction force will be tangent to it as shown in [Figure 14.14\(b\)](#). The direction of the friction force will be opposite to the velocity of any point on the slider relative to link 5. In [Figure 14.14\(b\)](#), point A_3 is chosen as a typical point.

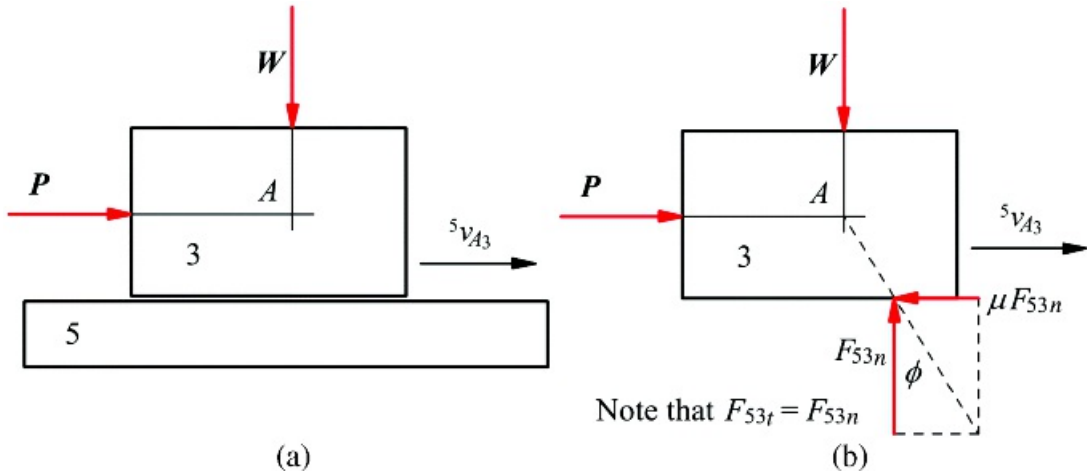


[Figure 14.14](#) Friction forces in a slider joint.

The two components of the force F_{53} can be resolved into a single force if the friction angle ϕ is known. This angle is given by

$$\phi = \tan^{-1} \left(\frac{\mu F_{53n}}{F_{53n}} \right) = \tan^{-1}(\mu) \quad (14.11)$$

Note that, from force equilibrium on link 3, $W = F_{53n}$ and $P = \mu F_{53n}$. If both P and W are given and the block is in static equilibrium, then μ cannot be specified. It will assume whatever value is required for equilibrium. However, μ cannot be larger than the static coefficient of friction if the mechanism is not moving, or the kinetic coefficient of friction if the mechanism is moving. If μ is given, then P can be computed if F_{53n} is known.

If the normal force and friction force are resolved into a single force oriented at an angle of ϕ relative to the normal direction, link 3 becomes a three-force member. Therefore, the forces must intersect at a point as shown in [Figure 14.14\(b\)](#). This will indicate the location where the total force F_{53} is applied to link 3. It is possible that the point of application of the force must be beyond the physical limits of the block. When this occurs, the block will tend to rotate, and if the block is not supported on both top and bottom, static equilibrium cannot be maintained. This condition is indicated in [Figure 14.15\(a\)](#). When designing a mechanism, we must provide for a support on both sides of the slider whenever there is a possibility that the friction force will become large enough to cause tipping.

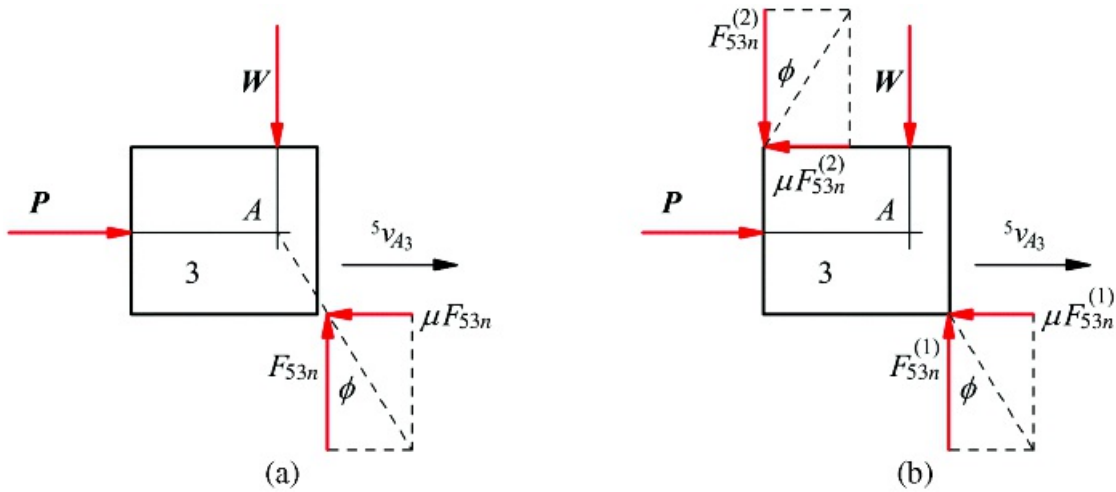


[Figure 14.15](#) Condition indicating that the block must contact the slide at two locations.

If the location for contact from one side of the block is beyond the physical boundary of the block, the block will tip slightly and bring the opposite side into contact. There will then be a normal and friction force on both sides of the block. When this occurs, we must treat the force F_{53} as two components ($F_{53}^{(1)}$ and $F_{53}^{(2)}$) as shown in [Figure 14.15\(b\)](#). The two components will be oriented at an angle $\pm\phi$ with respect to the normal direction; however, one component will be oriented at an angle of $+\phi$, and the other component will be oriented at an angle of $-\phi$ as shown in [Figure 14.15\(b\)](#).

When the condition indicated in [Figure 14.15](#) is satisfied, we can analyze the problem directly by summing forces and moments.

The problem can be simplified by resolving $F_{53}^{(1)}$ and $F_{53}^{(2)}$ into a single force that acts through the intersection of the lines of action of the two components. This is shown in [Figure 14.16\(a\)](#). Initially, we will not know the direction for the resultant; however, we now have a three-force member, and the lines of action of all of the forces must intersect at a point. The directions of P and W are already known, and their lines of action intersect at A . Therefore, the line of action of the resultant F_{53} must be along the line AB as shown in [Figure 14.16\(b\)](#). The individual components can then be determined by summing forces.

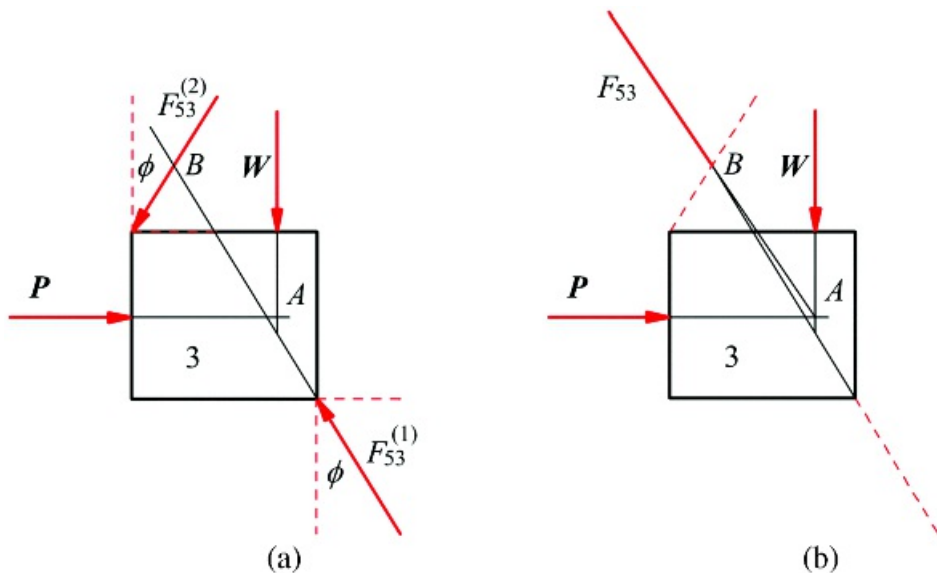


[Figure 14.16](#) Resolving the two components of the slider force into a single component.

The procedure indicated here can be used regardless of how the block is actually constrained; for example, it can be mounted over a rod or captured within a cylinder.

14.7.3 Friction in Revolute Joints

Although slider friction is probably the most significant problem area in mechanisms when friction is addressed, pin friction is also important, especially when transmission angles are poor.

Pin friction occurs in a revolute joint at the contact point between the pin and bearing. The effect is to create a torque called a friction torque in the joint. The magnitude of the torque can be determined by considering in detail how the forces are transmitted through the joint. A revolute joint between two arbitrary links (2 and 4) is represented in [Figure 14.17](#). In the figure, the clearance in the joint is greatly exaggerated. The nominal radius of the pin in the joint is R , and the friction coefficient is again taken as μ .

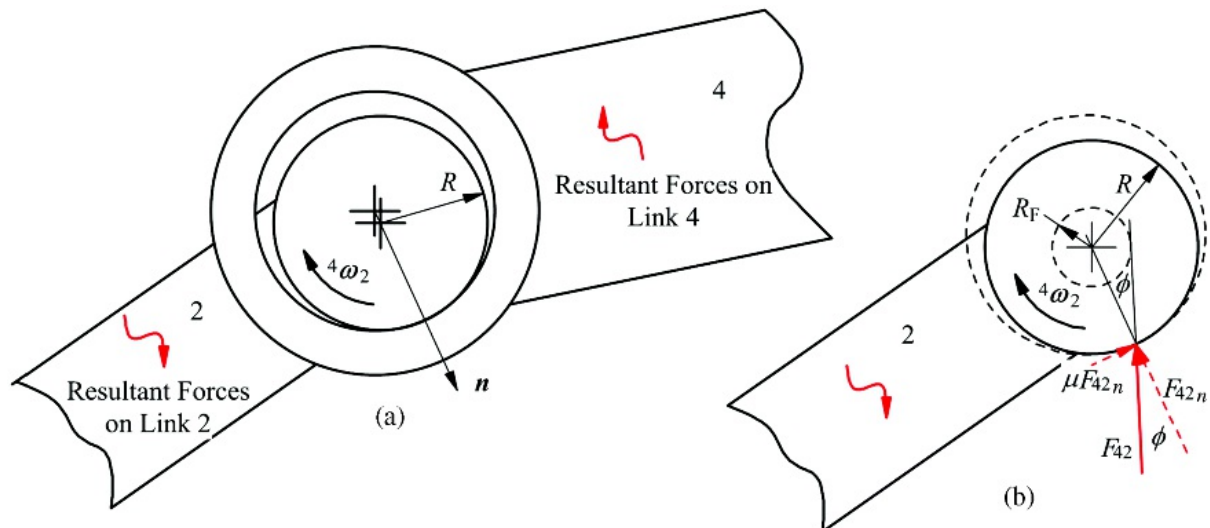


[Figure 14.17](#) A revolute joint with friction.

[Figure 14.17\(b\)](#) shows the forces that act on the pin part of the joint. The friction force is again equal to μ times the normal force, and the friction angle ϕ is computed as was done in [Equation 14.11](#). That is, $\phi = \tan^{-1}(\mu)$. Because of the friction force, a torque must be applied to link 2 for static equilibrium. This torque caused by the friction force is called the friction torque, and its magnitude is equal to

$$T_F = \mu F_{42n} R \quad (14.12)$$

The friction force opposes the motion of link 2 relative to link 4, and therefore the torque resulting from the friction force also opposes the relative motion. The total contact force is the resultant of the friction force and the normal force. As shown in [Figure 14.17\(b\)](#), the line of action of the resultant force F_{42} will be tangent to a circle called the friction circle, and the radius of the friction circle is given by

$$R_F = R \sin \phi \quad (14.13)$$

There will be a friction circle associated with each revolute joint, and in each case, the joint force will be tangent to the friction circle. The joint force must be located on the proper side of the friction circle to oppose the relative motion. The effect of the friction circles is to alter slightly the line of action of the joint forces. A binary link with a revolute joint at both ends will still be a two-force member, but the line of action of the forces will not pass through the rotation axes. As shown in [Figure 14.18](#), there are four possible lines of action for the joint forces, depending on which side of the friction circles the joint forces are located.

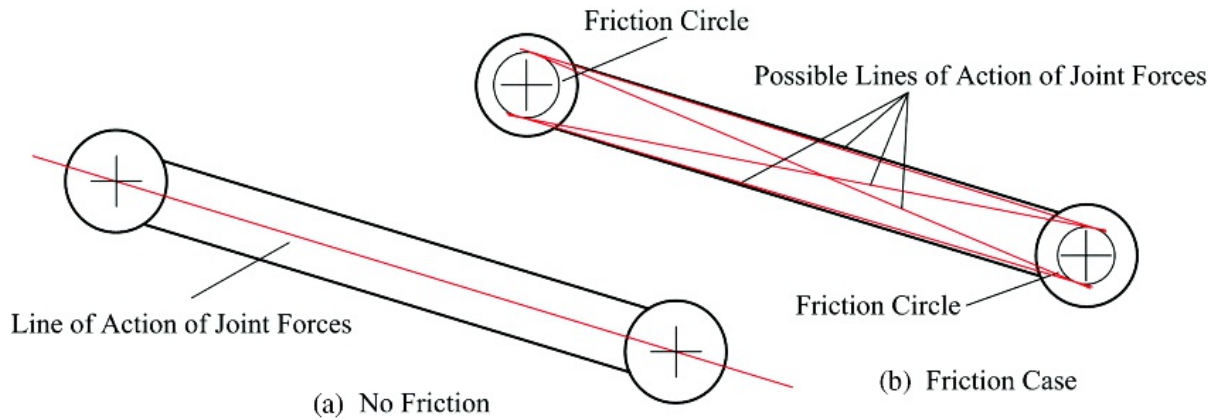


[Figure 14.18](#) Possible lines of action of joint forces when pin friction is involved.

To determine the proper side of the friction circles for the joint forces, it is necessary to know the general direction of the forces and the relative motion at the joints before the analysis is begun. This is usually done by conducting a frictionless analysis first and by conducting a velocity analysis. If the direction is chosen incorrectly, the wrong side of the friction circle will be indicated to oppose the relative motion in the joint. This in turn will slightly alter the exact direction of the joint force. Therefore, if any of the joint forces are negative (wrong direction assumed), the analysis must be redone using the proper directions.



Example 14.4

Analysis of Slider-Crank Mechanism with Friction

A slider-crank mechanism has a piston load of 200 lbs in the direction shown in [Figure 14.19](#), and the crank angle (θ_2) is 120° . The coefficient of friction in each pin and between the slider and frame is 0.2, and the diameter of the pin at each revolute joint is 2 in. Find the torque T_{12} required for static equilibrium with and without friction.

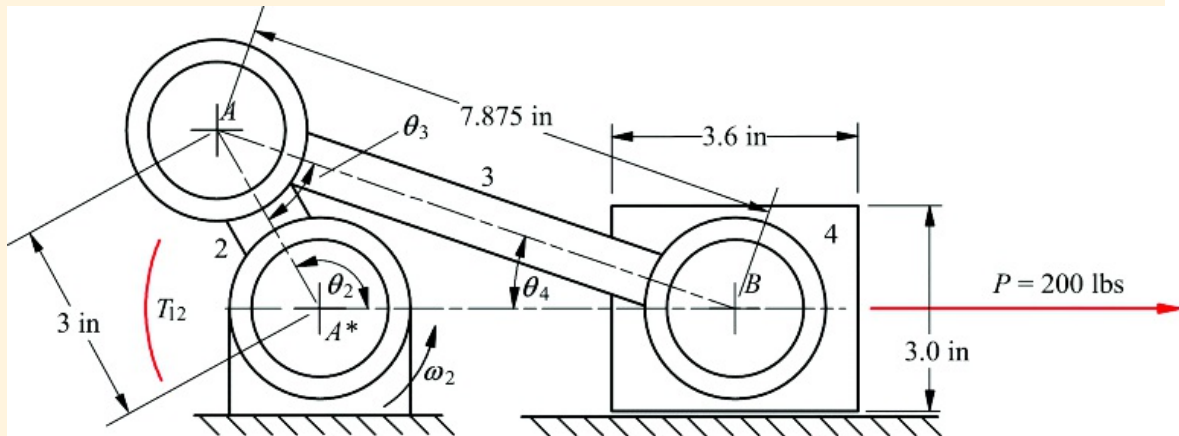


[Figure 14.19](#) The mechanism for Example 14.4.

Solution

We will perform the analysis graphically. Before the friction analysis is conducted, we need to determine the relative motion at each joint and the general direction of the forces at each joint. We can determine the relative motion by inspection because we need only to identify whether individual angles are increasing or decreasing. For the direction of the crank rotation given:

$\dot{\theta}_2$ is increasing

$\dot{\theta}_3$ is decreasing

$\dot{\theta}_4$ is decreasing

To determine the general directions of the joint forces, a zero-friction analysis can be conducted. For this analysis, the free-body diagrams and force polygons are shown in [Figure 14.20](#). To begin this analysis, we recognize that link 3 is a two-force member. Therefore, the line of action of the joint forces is along the line AB . Link 4 is then a three-force member, and the lines of action of the three forces intersect at point B . By summing forces vectorially on link 4, the magnitudes of all of the forces can be determined. The force summation equation is

$$\sum F = 0 = F_{1A} - F_{23} - F_{43} - F_{34} \quad (14.14)$$

The force polygon gives the magnitude and direction for each of the vectors. From equilibrium considerations at each joint, we know

$$F_{32} = -F_{23} = F_{43} = -F_{34} \quad (14.15)$$

and

$$M_{12} = -M_{32}$$

(14.16)

This gives us the general direction of all forces at the joints. To determine the torque T_{12} for equilibrium in the nonfriction case, sum moments about point A of the free-body diagram for link 2. From this we get

$$T_{12} = \frac{M_{12}}{r} = \frac{212}{1.27} = 166 \text{ in-lb}$$

By inspection, the torque must be counterclockwise. Therefore

$$T_{12} = 166 \text{ in-lb CCW (no friction case)}$$

To analyze the system with friction, we need to compute the friction angle and friction circle radius for each joint. The friction angle is

$$\phi = \tan^{-1}(u) = \tan^{-1}(0.2) = 11.31^\circ$$

From [Equation 14.14](#), the friction circle radius at each joint is

$$R_f = R \sin \phi = 1 \times \sin(11.31^\circ) = 0.20 \text{ in}$$

The friction circles are shown in [Figure 14.21](#). We must now determine at which side of the friction circles the forces are located. Considering joint B on link 3 first, the force F_{43} is tensile and link 3 is rotating counterclockwise relative to link 4 ($\dot{\theta}_4$ is getting smaller). We must locate F_{43} tangent to the friction circle such that it opposes this counterclockwise rotation. This means that F_{43} must be located on the upper side of the friction circle. Then, F_{34} will be located on the upper side of the corresponding friction circle on link 4.

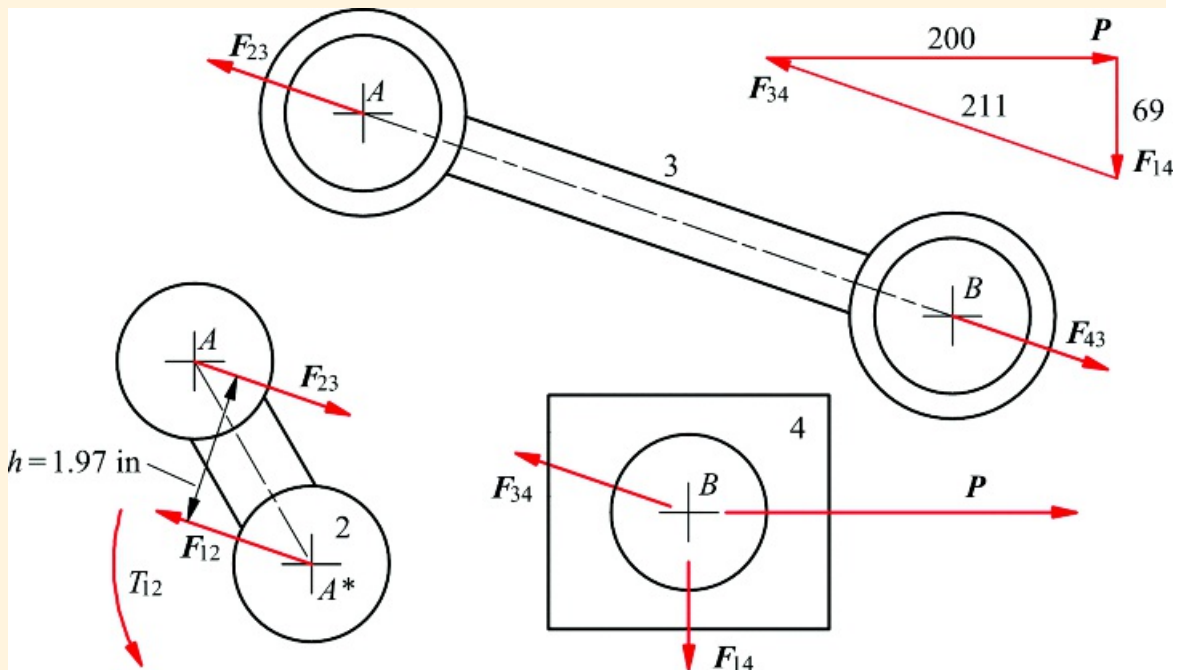


[Figure 14.20](#) Free-body diagrams and force polygon for zero-friction case in Example 14.4.

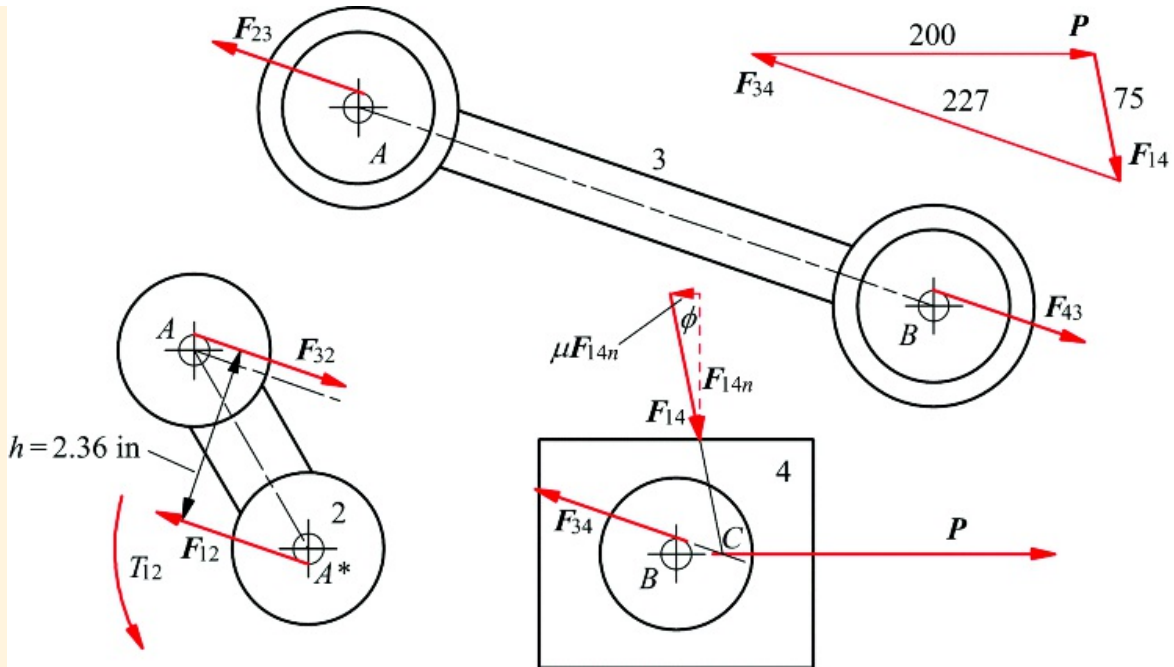


[Figure 14.21](#) Free-body diagrams and force polygon for friction case in Example 14.4.

Next consider joint *B* on link 3. Force F_{43} is tensile, and link 3 rotates clockwise relative to link 2 (θ_3 is decreasing). We must locate F_{23} tangent to the friction circle such that it opposes this clockwise rotation. This means that F_{23} must be located on the upper side of the friction circle. Similarly, F_{32} will be located on the upper side of the corresponding friction circle on link 2.

Moving to joint *A* on link 2, the force F_{12} is oriented approximately as shown in [Figure 14.20](#). Also, link 2 is rotating counterclockwise relative to link 1. If F_{12} is to provide a torque that opposes this motion, it must be located on the lower part of the friction circle as shown in [Figure 14.21](#).

On link 4, we must orient the force F_{14} relative to the block. Because link 4 is a three-force member, all of the forces must intersect at a point. Because we know the lines of action of P and F_{34} , we know the location of the point of intersection (*C* in [Figure 14.21](#)). We also know that the block is moving to the left relative to the frame so that the friction force must be directed toward the right. Therefore, F_{14} must be inclined as shown in [Figure 14.21](#), and its line of action must intersect the other two forces on link 4 at *C*. Note that F_{14} makes contact within the physical limits of the block, and therefore the block does not tip. If contact were indicated beyond the physical limits of the block, we would have to use the procedure indicated in [Figure 14.15](#).

Now the directions of the forces on link 4 are known. We can sum forces using [Equation 15.14](#) and solve for the unknowns. The force polygon is shown in [Figure 14.21](#). From the force polygon and [Equations 14.15](#) and [14.16](#), we can determine the forces on link 2. The torque T_{12} can then be computed. The magnitude of T_{12} is given by

$$T_{12} = hF_{22} = 2.36(227) = 540 \text{ in-lb}$$

By inspection, the torque must be counterclockwise. Therefore

$$T_{12} = 540 \text{ in-lb CCW}$$

Because of friction, the torque needed for equilibrium has increased by almost 30 percent. The friction

coefficients used in this example are high in order to illustrate the procedure. However, the torque requirements to drive a mechanism can increase significantly when friction is involved. Therefore, the designer should reduce the effects of friction either by careful bearing design and lubrication or by altering the linkage geometry (when possible) to reduce the sensitivity of the mechanism to friction.



14.8 In-Plane and Out-of-Plane Force Systems

It is important to remember, when analyzing planar mechanisms, that although motion occurs only parallel to a single plane, it is possible to apply fully three-dimensional force systems to the mechanism. Only the components of force and moment that act in the plane of motion affect the action of the mechanism. These *in-plane* force components are the two components of force parallel to the plane of motion and the moment vector normal to that plane. If the force system is resolved into Cartesian components, the remaining three components—the force normal to the plane of motion and the two components of moment parallel to the plane of motion—do not affect the action of the mechanism. However, they may contribute to the jamming of prismatic joints, and they apply loads to the members and contribute to the stresses in those members. These *out-of-plane* force components act on the mechanism as a structure.

Deflections due to out-of-plane forces are particularly important in planar mechanisms since an excessive deflection may result in significant deviations from parallelism of the joint axes, which can result in binding of the mechanism or generation of excessive internal stresses. For this reason, the deflection of members is often a concern even when strength is more than adequate.

Since in-plane and out-of-plane force systems affect a mechanism in quite different ways, it is convenient to decompose the force analysis of a planar mechanism into separate analyses of the in-plane and out-of-plane force systems. However, this must be done with some care, since an in-plane force may contribute to an out-of-plane moment and vice versa.



Example 14.5 Analysis of Out-of-Plane Forces

The SCARA robot shown in [Figure 14.22](#) has vertical revolute axes 1, 2, and 3. It carries a payload of 50 lb with center of mass on the axis of joint 3. In addition, the members 2 and 3 can be regarded as uniform beams with respective weights 60 lb and 40 lb. Characterize all the loads on members 2 and 3 in the position shown.

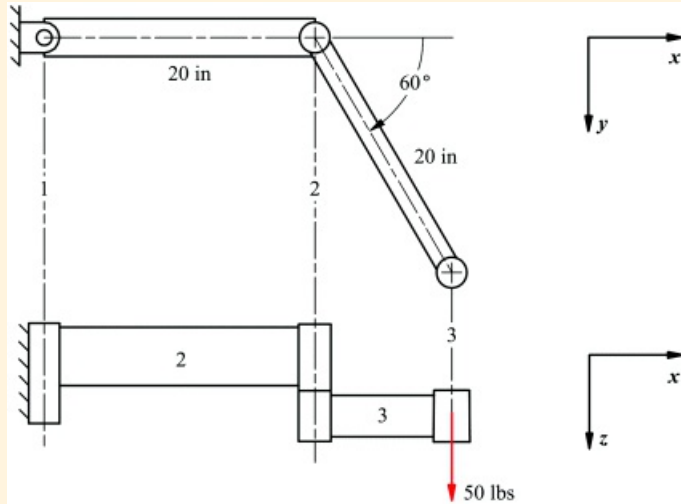


[Figure 14.22](#) The SCARA robot considered in Example 14.5.

Solution

Here all the forces are out-of-plane forces. As far as a force analysis is concerned, the manipulator behaves as a cranked cantilever beam. To find the loads on the links 2 and 3, it is first necessary to draw free-body diagrams of each of them. A free-body diagram of link 3 in the x - z plane is shown in [Figure 14.23](#).

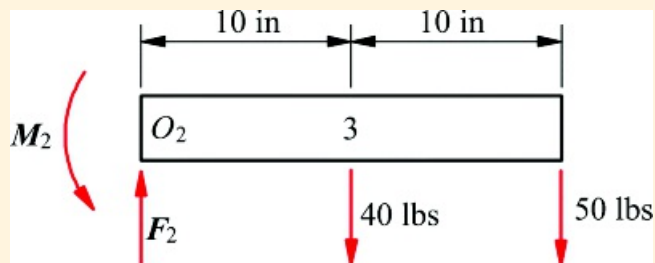


[Figure 14.23](#) The free-body diagram of link 3.

As may be seen, link 3 is a simple cantilever beam considered to be embedded at joint 2. The shear force F_2 and bending moment M_2 at joint 2 can be found by writing the vertical force equilibrium equation and the moment equation about O_2

$$\sum F_y = 0 : \quad F_2 = 40 + 50 = 90 \text{ lb}$$

$$\sum M_{O_2} = 0 : \quad M_2 = 40 \times 10 + 50 \times 20 = 1,400 \text{ in-lb}$$

The free-body diagram for link 2 is shown in [Figure 14.24](#).

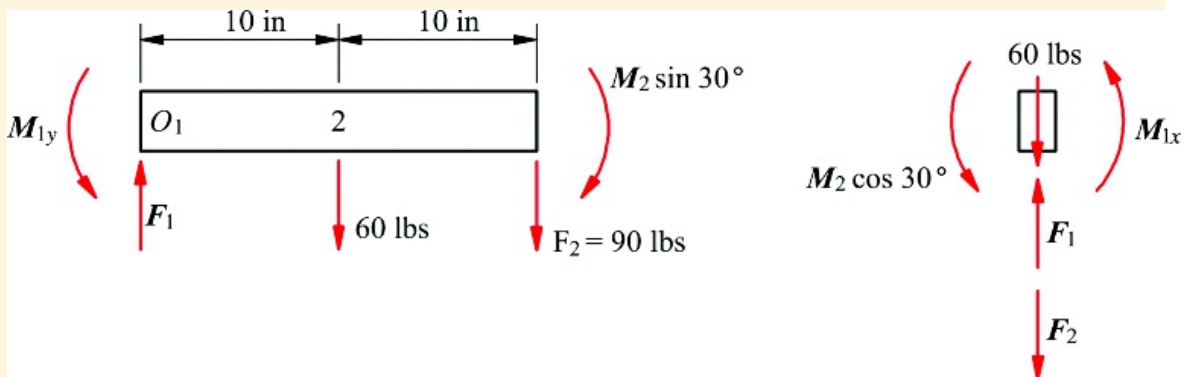


[Figure 14.24](#) The free-body diagram of link 2. This figure shows the view of the member in its x - y plane together with an end view showing the torsional components. The bending moment M_2 at joint 2 is applied, along with the shear force to link 2. However, because of the 60° angle between the longitudinal axes of Links 2 and 3, it is necessary to resolve M_2 into a component $M_2 \sin 30^\circ$ in the plane of link 2, along with a component $M_2 \cos 30^\circ$, which is a torsional moment about its longitudinal axis.

The reaction force F_1 and moments M_{1y} and M_{1x} at joint axis 1 can now be computed using vertical force equilibrium together with moment balances about the y and x directions.

In the plane of the beam

$$\sum F_y = 0, \quad F_1 = 60 + 90 = 150 \text{ lbs}$$

$$\sum M_y = 0 : \quad M_{1y} = 1400 \sin 30^\circ - 60 \times 20 - 60 \times 10 = 3100 \text{ in-lbs}$$

About the longitudinal axis of the beam

$$\sum M_x = 0 : \quad M_{1x} = -1400 \cos 30^\circ = -1212 \text{ in-lbs}$$

Notice that, although there are no forces in the plane of motion and no motion of the system, there are still significant forces acting on the members. It is always necessary to consider out-of-plane forces, as well as in-plane forces.



Example 14.6

Three-Dimensional Force Analysis of Robot

The SCARA robot of [Figure 14.22](#) and Example 14.5 is required to exert a 20 lb horizontal tool force on the line of action shown in [Figure 14.25](#). Find the torques that must be exerted by the actuators at joints 1 and 2 and the reaction forces and moments at the joints. The weights of the members and end effector remain the same as in Example 14.5.

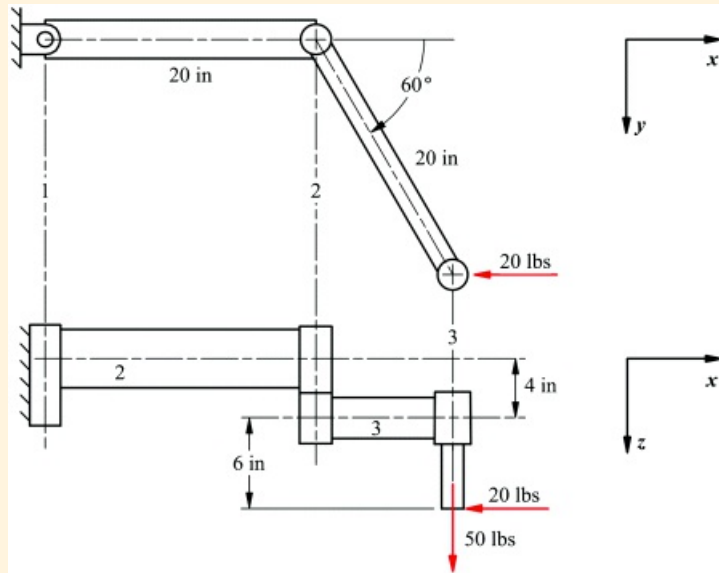


[Figure 14.25](#) A 20 lb horizontal tool load has been added to the weight load in Example 14.5. In this example, we have both in-plane and out-of-plane force systems.

Solution

There are many different possible approaches to this problem. However, when dealing with fully three-dimensional systems like this, it is usually best to decide on three orthogonal coordinate axis directions and resolve all force and moment components into those directions. This may yield more equations than other choices of directions in which to resolve, but it has the advantage of being a very systematic procedure that reduces the chance of error.

It is first necessary to draw free-body diagrams of each of the two bodies in the system. Since the force system is three-dimensional, in [Figure 14.26](#) we have resorted to three orthogonal views of each member to ensure that every force component is visible. In fact, each component should appear on at least two of these views.

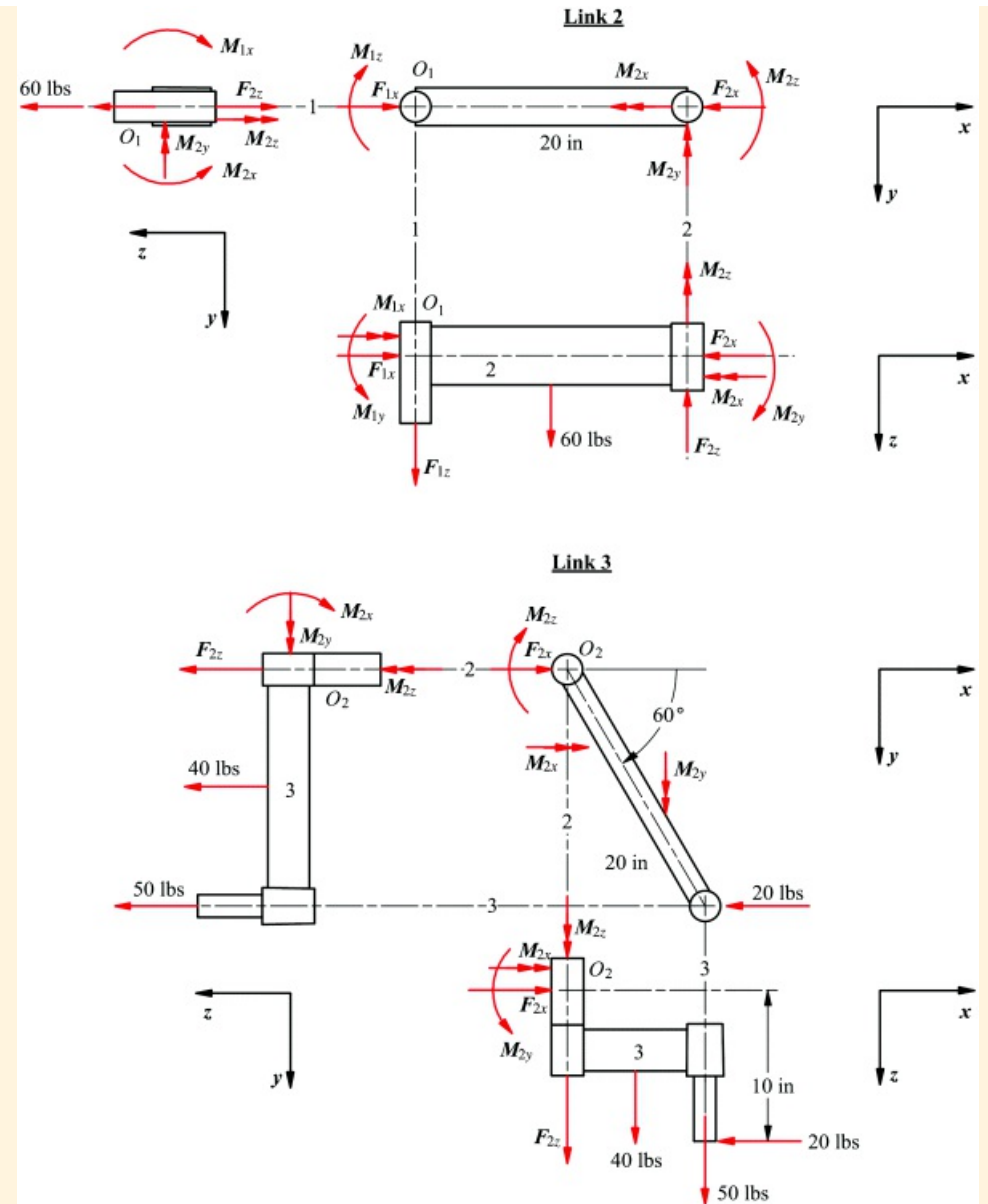


Figure 14.26 Free-body diagrams for Example 14.5. Each free body is shown in three orthogonal views: projected on the x-y plane, the x-z plane, and the y-z plane, respectively.

We can now proceed to write the six static equilibrium equations for each member by referring to the free-body diagrams in [Figure 14.26](#)

Link 3

$$\sum F_x = 0 : \quad F_{2x} = 20$$

$$\sum F_y = 0 : \quad 0 = 0$$

$$\sum F_z = 0 : \quad F_{2z} + 40 + 50 = 0$$

Taking moments about point O_2

$$\sum M_z = 0 : \quad M_{2x} + 50 \times 20 \sin 60^\circ + 40 \times 10 \sin 60^\circ = 0$$

$$\sum M_y = 0 : \quad M_{2y} = 10 \times 20 + 50 \times 20 \cos 60^\circ + 40 \times 10 \cos 60^\circ$$

$$\sum M_z = 0 : \quad M_{2z} + 20 \times 20 \sin 60^\circ = 0$$

Solution gives

$$F_{2x} = 20 \text{ lb}$$

$$F_{2z} = -90 \text{ lb}$$

$$M_{2x} = -1212 \text{ in-lb}$$

$$M_{2y} = 500 \text{ in-lb}$$

$$M_{2z} = -346 \text{ in-lb}$$

Link 2

$$\sum F_x = 0 : \quad F_{1x} = F_{2x}$$

$$\sum F_y = 0 : \quad 0 = 0$$

$$\sum F_z = 0 : \quad F_{1z} + 60 = F_{2z}$$

Taking moments about point O₁

$$\sum M_z = 0 : \quad M_{1x} = M_{2x}$$

$$\sum M_y = 0 : \quad M_{1y} = M_{2y} + 60 \times 10 - F_{2z} \times 20$$

$$\sum M_z = 0 : \quad M_{1z} = M_{2z}$$

Substitution of the previously calculated values for F_{2x} , F_{2z} , M_{2x} , M_{2y} , and M_{2z} gives

$$F_{1x} = 20 \text{ lb}$$

$$F_{1z} = -150 \text{ lb}$$

$$M_{1x} = -1212 \text{ in-lb}$$

$$M_{1y} = 900 + 600 - (-90) \times 20 = 3300 \text{ in-lb}$$

$$M_{1z} = -346 \text{ in-lb}$$

This completes the solution. The torques M_{1z} and M_{2z} that must be produced by the actuators at joints 1 and 2, respectively, are both 346 in-lb in magnitude. The reaction forces and moments F_{1x} , F_{1z} , M_{1x} , M_{1y} , F_{2x} , F_{2z} , M_{2x} , M_{2y} may be compared with the results of Example 14.5. As may be seen, the vertical forces F_{1z} and F_{2z} remain the same, as does M_{1x} . The other forces and moments are changed by the presence of the horizontal tool load.



14.9 Conservation of Energy and Power

When a linkage is subjected to significant loads only on the input and output links and the system can be regarded as static, a quick and easy method of computing the ratio of input force/torque to output force/torque is available. This is particularly useful if a velocity analysis has already been performed for other reasons, because a velocity analysis is needed as part of the solution.

For a given mechanism, the input power equals the output power if the following are satisfied:

1. There are no energy losses in the mechanism. This means that there is no friction in the joints or no other form of energy dissipation.
2. There is no energy stored in the mechanism as it moves. This means that there are no springs in the system and that the energy associated with potential energy because of the weight of the links and the change in the centers of gravity of the links is negligible.
3. The velocities are small enough or the masses are small enough that changes in kinetic energy are negligible.

Thus, if the input and output loads are torques T_i and T_o , respectively, and the angular velocities of the input and output links are ω_i and ω_o respectively

$$T_i \cdot \omega_i + T_o \cdot \omega_o = 0$$

The + sign in the equation implies that if T_i is in the same direction as ω_i , as is often, but not necessarily, the case, then T_o will be in the opposite direction to ω_o .

Similarly, if the input and output are forces F_i and F_o , and v_{pi} and v_{po} are the respective velocities of their points of application, then

$$F_i \cdot v_{pi} - F_o \cdot v_{po} = 0$$

Similarly, for a force input and torque output

$$F_i \cdot v_{pi} - T_o \cdot \omega_o = 0$$

and for a torque input and force output

$$T_i \cdot \omega_i - F_o \cdot v_{po} = 0$$

or, in general

$$\sum_{k=1}^m T_k \cdot \omega_k + \sum_{j=1}^n F_j \cdot v_{pj} = 0 \quad (14.17)$$

where T_k , $k = 1, 2, \dots, m$ are all torques acting on members of the system and ω_k , $k = 1, 2, \dots, m$, are the angular velocities of the links to which they are respectively applied. F_j , $j = 1, 2, \dots, n$ are all forces acting on the system, and v_{pj} , $j = 1, 2, \dots, n$ are the respective velocities of their points of applications. Thus, more generally, if the necessary velocity information for the system is available, a static force analysis can be performed using energy conservation as an alternative to static equilibrium. Depending on the system characteristics, this may or may not

be more efficient than performing a force analysis using free-body diagrams and the equations for static equilibrium.

When computing the power, the dot product for the force-velocity expression is given by

$$F_j \cdot v_{pj} = F_j v_{pj} \cos \theta_j = F_x v_x + F_y v_y + F_z v_z$$

where the magnitudes of the force and torque can be both positive and negative, and θ_j is the angle between F_j and v_{pj} . The dot product of the torque and angular velocity can be computed by multiplying the magnitudes of the two vectors, again realizing that the signs can be either positive or negative depending on whether the torque and angular velocity are in the same direction or opposite directions. Situations of positive and negative power are illustrated schematically in [Figure 14.27](#).

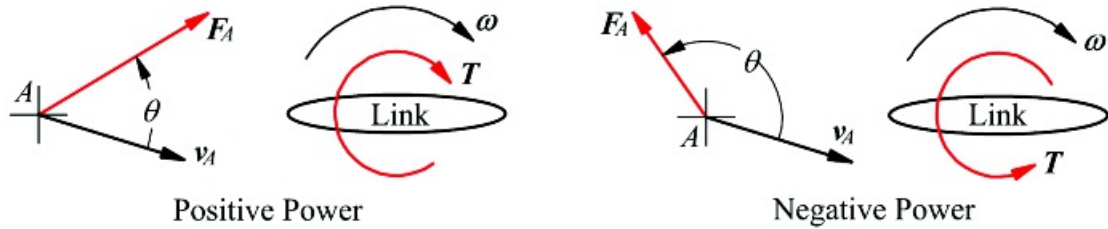


[Figure 14.27](#) Situations for positive and negative power.

The velocity analysis can be conducted using any procedure that is convenient. Note, however, that only the velocities for the points and links associated with the application of external forces and torques are needed. Because only selected velocities are usually required in [Equation 14.17](#), force analyses using the conservation of energy are often done in conjunction with the use of instant centers for the velocity analysis. Of course, if the velocities are already known from some other type of analysis, these can be used directly.

Note that even though [Equation 14.17](#) involves the magnitudes of the velocities, the results will not depend on the value chosen for the input velocity. This must be the case because we could also conduct the force analysis using free-body diagrams and the equations for force equilibrium, and these equations are a function of position and the applied forces only. Recall that the velocity problem is a linear problem. Therefore, if the input velocity is multiplied by a constant, then all of the velocities including the angular velocities will be multiplied by the same constant. Therefore, if we divide [Equation 14.17](#) by the magnitude of the input velocity, the force/torque results will be unchanged. Because of this, we need not know the actual value for the input velocity before conducting the force analysis. In fact, the mechanism need not be moving at all. Because of this, a common value to choose for the input velocity is 1.



Example 14.7

Analysis of Slider-Crank Mechanism Using Conservation of Power

Estimate the necessary driving torque for the mud pump of Example 14.3 using conservation of power.

Solution

To obtain a quick estimate of the forces, we will neglect the effect of the weight of the components. This is justifiable because those weights are much smaller than the piston load of $P = 21,340$ lb (Example 14.3).

We will conduct the velocity analysis using instant centers because only two velocities are required. Because the piston load can be considered to act at point B on member 4 and the driving torque acts on member 2, we need I_{12} , I_{14} , and I_{24} to develop the necessary relationship between the input and output velocity using the instantaneous center method. I_{24} is located as shown in [Figure 14.28](#). The distance $I_{24}I_{12}$ can be scaled from the drawing or calculated. To calculate it, use angle A^*BA (11.096° from 14.3) and first find

$$\phi = \angle A I_{24} A^* = 90^\circ - 11.096^\circ = 78.904^\circ$$

$$\beta = \angle A A^* I_{24} = 90^\circ - 60^\circ = 30^\circ$$

and

$$\gamma = \angle A^* A I_{24} = 180^\circ - \phi - \beta = 180^\circ - 78.904^\circ - 30^\circ = 71.096^\circ$$

Now use the sine rule to find the length $r = A^* I_{24}$

$$r = \sin \gamma \frac{A A^*}{\sin \phi} = \frac{3 \sin 71.096^\circ}{\sin 78.904^\circ} = 7.713 \text{ in}$$

The velocity of I_{24} is equal to the velocity of B_4 where the force of 21,340 lb is applied. Also, if we consider I_{24} to be a point on link 2,

$$v_{I_{24}} = \omega_2 \times r_{I_{24}/A^*}$$

and the magnitude is the velocity of I_{24}

$$v_{I_{24}} = \omega_2 (r_{I_{24}/A^*})$$

From conservation of power

$$T \cdot \omega_2 + P \cdot v_{B_4} = 0 \quad (14.18)$$

Let us assume that link 2 is rotating clockwise. Then P and ω_{B4} are in opposite directions. Therefore, power is being taken out at the piston and put into the system at the crank. Consequently, the torque, T , must be in the same direction as the angular velocity of link 2 or clockwise. We need only to use [Equation 14.18](#) to find the magnitude of T . This gives

$$T = P \frac{\dot{v}_{B4}}{\omega_3} = P \frac{\dot{v}_{B4}}{\omega_3} = P \frac{\dot{\theta} I_{34} (r_{B4}/R^*)}{\omega_3} = P (\ddot{s}_{34}/R^*)$$

Therefore

$$T = 21,340(7.713) = 164,600 \text{ in-lb} \quad \text{or} \quad 13,700 \text{ ft-lb CW}$$

This may be compared with the value of $T = 13,800$ ft-lb obtained from the full static equilibrium analysis. The difference between the values is accounted for by the fact that the weights of the linkage members were included in the former analysis.

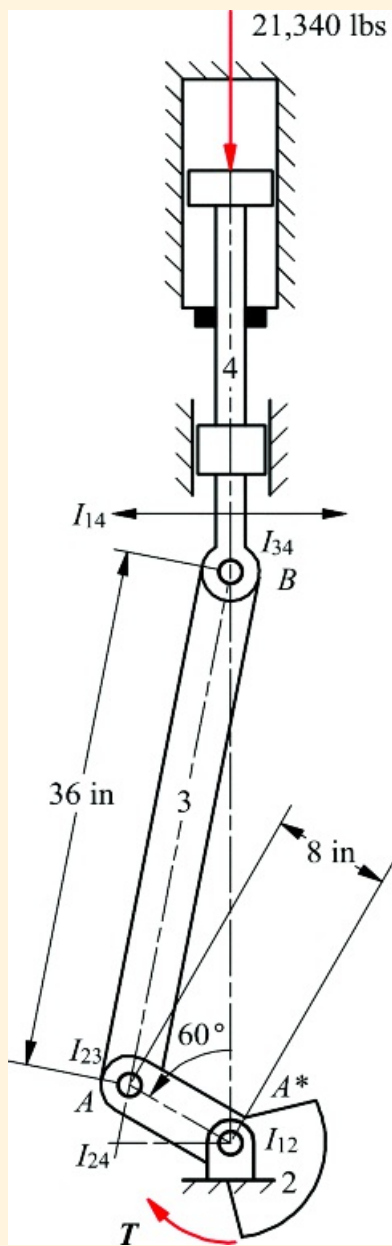


[Figure 14.28](#) Location of instant centers for mud pump.



Example 14.8

Analysis of Four-Bar Linkage Using Conservation of Power

In the four-bar linkage represented in [Figure 14.29](#), a torque T_{12} is applied to link 2, and it is resisted by a torque T_{14} applied to link 4. Find a relationship for the mechanical advantage of the mechanism in terms of the mechanism geometry.

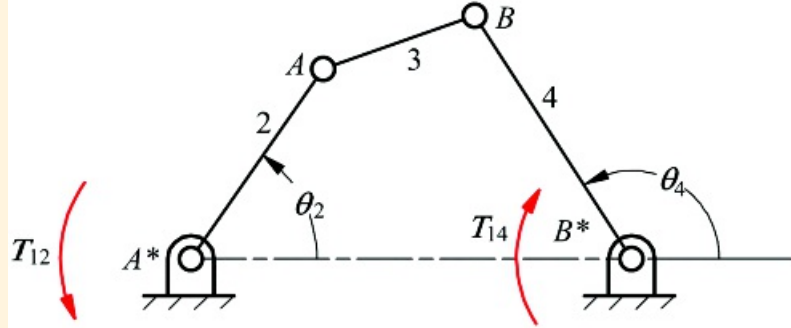


[Figure 14.29](#) The linkage for Example 14.8.

Solution

The mechanical advantage (MA) for the linkage is a function of position and is given by

$$MA = \frac{\text{Output torque}}{\text{Input torque}} = \frac{T_{14}}{T_{12}} \quad (14.19)$$

Therefore, we must find a geometric relationship equal to the ratio of the output torque divided by the input torque. We will use conservation of power for the analysis and conduct the velocity analysis using instant centers of velocity. To begin, the power expression is

$$T_{12} \cdot \omega_2 - T_{14} \cdot \omega_4 = 0 \quad (14.20)$$

From this expression, if T_{12} and ω_2 are in the same direction, then T_{14} and ω_4 must be in opposite directions. Therefore, if we know the signs of T_{12} , ω_2 , and ω_4 , we can determine the sign of T_{14} by inspection after a kinematic analysis is conducted. Consequently, we can concentrate on the magnitude of T_{14} , which we can compute directly from [Equation 14.20](#). That is

$$T_{14} = -T_{12} \frac{\omega_2}{\omega_4}$$

Therefore, considering only magnitudes,

$$\frac{T_{14}}{T_{12}} = \frac{\omega_2}{\omega_4} \quad (14.21)$$

Based on our knowledge of instant centers, the ratio ω_2/ω_4 will be a function of geometry only. To find the

ratio of angular velocities, we need first to find the instant centers I_{12} , I_{14} , and I_{24} . These are shown in [Figure 14.30](#). The velocity of the two points located at I_{24} is given by

$$v_{I_{24}} = \omega_2 \times r_{I_{24}/I_{12}} = \omega_4 \times r_{I_{24}/I_{14}}$$

and

$$|\omega_2 r_{I_{24}/I_{12}}| = |\omega_4 r_{I_{24}/I_{14}}|$$

Therefore

$$\frac{\omega_2}{\omega_4} = \frac{r_{I_{24}/I_{14}}}{r_{I_{24}/I_{12}}} \quad (14.22)$$

[Equation 14.22](#) shows that the ratio of the angular velocities is clearly a function of position, that is, of the location of the instant centers.

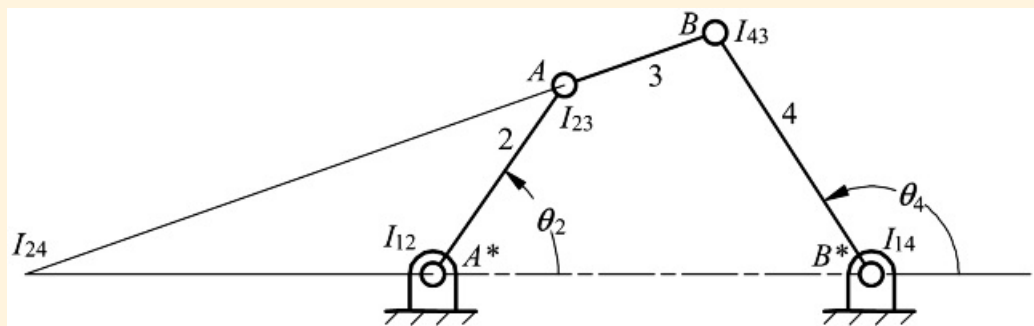


[Figure 14.30](#) Instant center locations for the linkage in [Figure 14.29](#).

Now combining [Equations 14.19](#), [14.21](#) and [14.22](#) gives

$$MA = \frac{T_{14}}{T_{12}} = \frac{\omega_2}{\omega_4} = \frac{r_{I_{24}/I_{14}}}{r_{I_{24}/I_{12}}}$$

Note that the sign of either ω_2 or ω_4 can be negative. Therefore, mechanical advantage may be positive or negative, although in many instances only the magnitude is of interest. When MA is positive, the torques are in the same direction, and when it is negative they are in opposite directions. In this particular example, $r_{I_{24}/I_{12}}$ and $r_{I_{24}/I_{14}}$ (and therefore ω_2 and ω_4) will be in the same direction when I_{24} is located outside of I_{12} and I_{14} . They will be in opposite directions when I_{24} is between I_{12} and I_{14} .



14.10 Virtual Work

It is possible to apply the conservation of energy method to obtain force relationships in truly static systems in which no actual movement occurs. The technique is to imagine a small displacement of the point of application of the input force and compute the corresponding displacement of the point or points of application of the output force or forces. The sum of the work done by all external forces must be zero. This is the principle of *virtual work*. It is identical to conservation of energy except that the displacements are virtual or imaginary. The advantage is that, if only the input–output force relationship is of interest, this method avoids the labor of finding all the forces internal to the mechanism. It should also be noted that, in contrast to the methods discussed so far in this chapter, this method depends on the methods of kinematic analysis discussed in [Chapters 4](#) through [6](#).

The problem of deriving a consistent set of displacements of the points of application of the external forces, which is the key to this technique, can be converted to a velocity analysis. If the velocity of each application point is multiplied by the same small time interval, the result is a set of consistent, small displacements. The time interval, being the same in all cases, will cancel from the energy equation so that it becomes, in fact, identical to [Equation 14.17](#). The way in which the method is used will be illustrated by the following example.



Example 14.9

Analysis of Vice Grip Using Virtual Work

Find the grip force, F_G , when the force applied to the handles of the vice-grip pliers of [Figure 14.6](#) is 25 lb. The lines of action of the grip forces and hand forces are located as indicated in [Figure 14.7](#).

Solution

Although the system depicted in [Figure 14.6](#) is truly static, we can still imagine a small displacement such as might occur if the workpiece were compliant and deflected a little. When using virtual work, we must account for all of the work done during the virtual displacement. In [Figure 14.31](#), work will be done by the forces at G and H and by the spring force. However, the spring force is so much less than the other forces that the energy stored in the spring can be ignored.

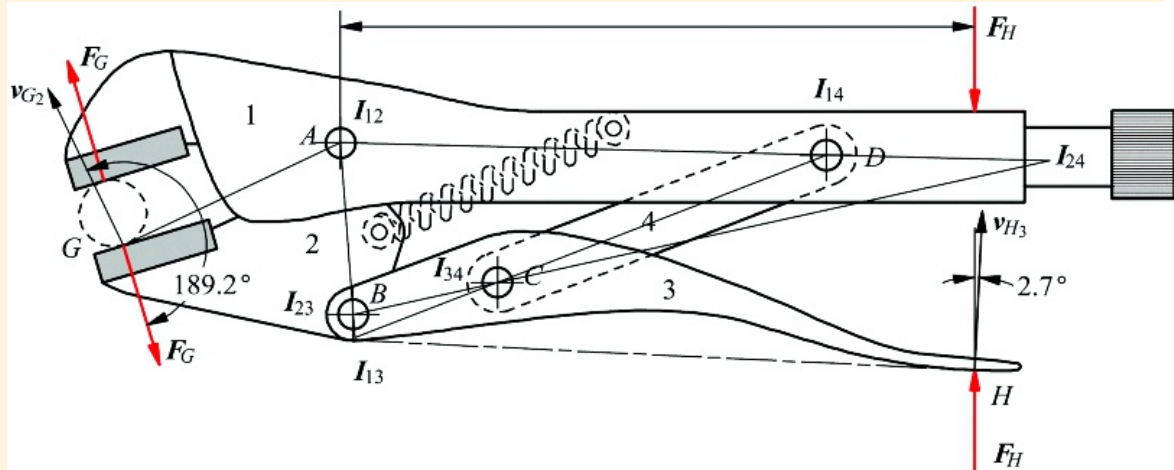


[Figure 14.31](#) Locations of the instantaneous centers for the vice-grip pliers of Example 14.9.

To obtain consistent displacements efficiently, we can again use the instantaneous center method. The six instantaneous centers of the mechanism are located as shown in [Figure 14.31](#). If member 1 is treated as the base and the point of application of F_H on the lower handle is displaced, there will also be a displacement of the point of application of F_G on the lower jaw. Since the former is on member 3 and the latter is on member 2, we need I_{13} , I_{12} , and I_{23} to obtain the necessary consistent pair of velocities (or displacements).

Scaling from the drawing shown in [Figure 14.31](#)

$$I_{12}I_{23} = 1.43 \text{ in} \text{ and } I_{13}I_{23} = 0.195 \text{ in}$$

Hence

$$\omega_2/\omega_3 = 0.195/1.43$$

Also

$$MM_{13} = 5.15 \text{ in} \text{ and } GH_{12} = 2.00 \text{ in}$$

Now

$$v_G/v_H = (\dot{\theta}_{12} \times \omega_2)/(\dot{\theta}_{13} \times \omega_3) = (2.00 \times 0.195)/(5.15 \times 1.43)$$

or

$$v_G = 0.053 v_H$$

Also, the angle between v_H and F_H is 2.7° , while that between v_G and F_G is 189.2° . Hence

$$F_G v_G \cos 2.7^\circ - F_G v_G \cos 189.2^\circ = 0$$

or

$$v_G \times 25 \times \cos 2.7^\circ + F_G \times v_G \times 0.153 \times \cos 189.2^\circ = 0$$

Notice that the equation may be divided by v_H , indicating that the results are independent of the value chosen for v_H . The final result for F_G is

$$F_G = 477 \text{ lb}$$

In the present instance we chose not to include the spring force because it was assumed to be negligible. It could have been included, however, by finding the virtual velocity of its point of application on link 2 and including the scalar product of that velocity with the spring force in the conservation of energy equation: [Equation 14.17](#). Including the spring would reduce F_G only slightly.



14.11 Gear Loads

14.11.1 Spur Gears

In the following analysis, we will assume that the spur gears have an involute profile. If friction is neglected, the force exerted by one of a pair of meshing gears on the other acts along the line normal to the teeth at the point of contact. That is, it acts along the line of action or pressure line shown in [Figure 14.32](#).

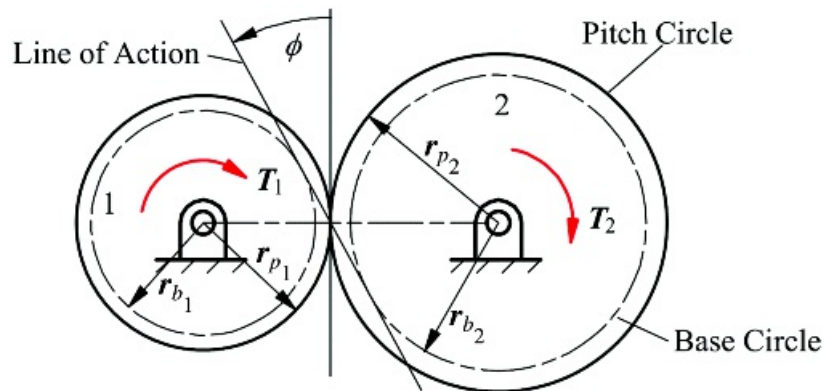


[Figure 14.32](#) Torque transmitted through spur gears.

Free-body diagrams of the gear and pinion are as shown in [Figure 14.33](#). The normal force W is tangent to the base circles of both the pinion and gear, and the torque on the pinion is

$$T_1 = W r_{b_1} = W r_{p_1} \cos \phi \quad (14.23)$$

The torque on the gear is

$$T_2 = W r_{b_2} = W r_{p_2} \cos \phi \quad (14.24)$$

Therefore

$$\frac{T_2}{T_1} = -\frac{r_{p_2}}{r_{p_1}} = -\frac{N_2}{N_1}$$

where N_1 and N_2 are the numbers of teeth on the pinion and gear, respectively. The minus signs are a reminder that T_2 is actually in the opposite direction to T_1 .

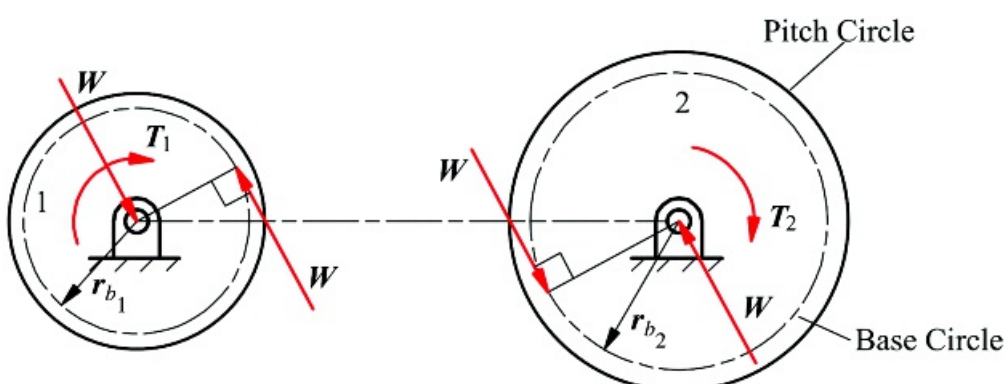


[Figure 14.33](#) Free-body diagrams of spur gears.

Also, from [Equations 14.23](#) and [14.24](#)

$$W = \frac{T_1}{r_{p_1} \cos \phi} = \frac{T_2}{r_{p_2} \cos \phi} \quad (14.25)$$

It may be seen that W is also the load on the bearings supporting the shafts of both the gear and the pinion.

If friction is considered, an additional force component of μW , where μ is the coefficient of friction, appears tangent to the teeth at the point of contact. This is shown in [Figure 14.34](#). Because W is constant, the friction force is constant in magnitude, and the bearing reactions (F_B) are also constant in magnitude and given by

$$F_B = \sqrt{W^2 + (\mu W)^2} = W\sqrt{1 + \mu^2}$$

However, the torques are

$$T_1 = W r_{b1} - \mu W y \quad (14.26)$$

$$T_2 = W r_{b2} - \mu W y \quad (14.27)$$

The distances x and y vary as the point of contact moves along the path of contact. However

$$x + y = r_{b1} \tan \psi + r_{b2} \tan \psi = (r_{p1} + r_{p2}) \sin \psi = \frac{N_1 + N_2}{2P} \sin \psi \quad (14.28)$$

where P is the diametrical pitch. From [Equations 14.26–14.28](#)

$$\frac{T_2}{T_1} = \frac{\frac{N_2}{2P} \cos \psi - \mu \left(\frac{N_1 + N_2}{2P} \sin \psi - x \right)}{\frac{N_1}{2P} \cos \psi - \mu x}$$

or

$$\frac{T_2}{T_1} = \frac{\frac{N_2}{2P} \cos \psi - \mu(N_1 + N_2) \sin \psi + 2\mu P x}{N_1 \cos \psi - 2\mu P x}$$

Thus, T_2/T_1 is no longer constant but is a function of the position, x , of the point of contact. This is a source of torsional vibration. The amount of variation is a function of the length of the path of contact. Strictly speaking what we have calculated here is the magnitude of T_2/T_1 . Once again, these torques are actually in opposite directions. Note that T_2/T_1 is always less than N_2/N_1 when averaged over the contact cycle. The sharing of loads among two or more pairs of teeth in contact does not change the bearing loads, but it does affect the torque fluctuations and tends to diminish them. Since the load sharing depends on the tooth stiffnesses, modeling of this effect becomes complicated and is beyond the scope of this text.

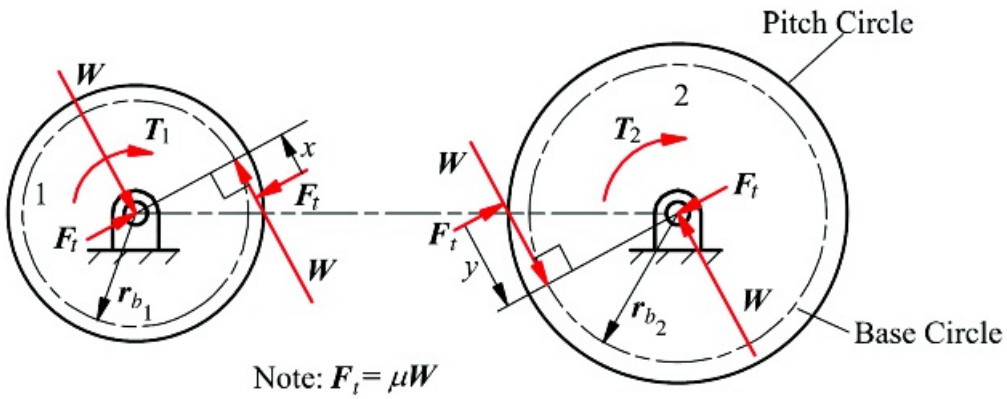


[Figure 14.34](#) Spur gears with friction.

14.11.2 Helical Gears

The teeth of an involute helical gear are similar in cross section to those of a spur gear. However, instead of being cut with their faces parallel to the gear axis, they are cut at an angle ψ to that axis where ψ is the helix angle of the gear. It is similar to the lead angle of a screw, except that the teeth of the helical gear are straight. That is, a straight line tangent to the pitch cylinder of the gear at its midplane can be drawn on the face of each tooth. The set of such lines from all teeth form the generators of a hyperboloid of one sheet. If this line is moved parallel to itself along an involute curve with the pitch circle radius equal to that of the pitch cylinder, it will generate the tooth face.

If friction is neglected, the force transmitted between contacting teeth is normal to the gear teeth at the point of contact. That is, it lies in the normal plane. It is inclined at angle ϕ_n to the cylinder tangent at the point of contact as shown in [Figure 14.35](#). Here, ϕ_n is the pressure angle for the hob used to cut the gear. Resolving the contact force W into the plane normal to the gear tooth gives

$$W_r = W \sin \phi_n$$

and

$$W_x = W \cos \phi_n$$

Resolving W_x in the plane tangent to the pitch cylinder

$$W_z = W_x \cos \psi = W \cos \phi_n \cos \psi$$

and

$$W_a = W_x \sin \psi = W \cos \phi_n \sin \psi$$

Also, from [Figure 14.35](#),

$$W_r = W_x \tan \phi_n = W_x \cos \psi \tan \phi_n$$

and

$$\tan \phi_t = \frac{\tan \phi_n}{\cos \psi} \quad (14.29)$$

Hence

$$\frac{W_r}{W_t} = \frac{\sin \phi_n}{\cos \phi_n \cos \psi} = \frac{\tan \phi_n}{\cos \psi} = \tan \phi_t$$

or

$$W_r = W_t \tan \phi_t \quad (14.30)$$

$$\frac{W_a}{W_t} = \tan \psi$$

or

$$W_a = W_t \tan \psi \quad (14.31)$$

The torque acting on the gear is represented in the free-body diagram in [Figure 14.36](#). From the figure,

$$T = W_t r_p \quad (14.32)$$

where r_p is the radius of the pitch circle. Using these relationships, the components W_p , W_a , and W_r can be computed in terms of the torque T .

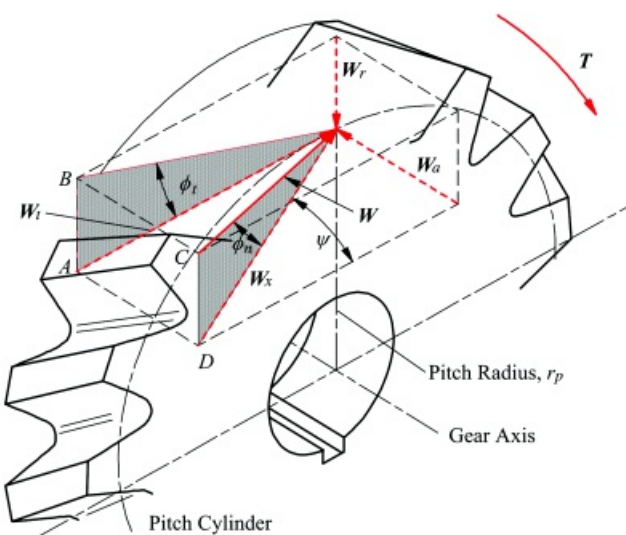


[Figure 14.35](#) Resolution of the contact force acting on a tooth of a helical gear. W is the contact force acting along the pitch line. W_r is the radial component of W . W_x is the component of W that is orthogonal to W_r . W_x is tangent to the pitch cylinder of the gear. W , W_r , and W_x lie in a plane normal to the gear tooth face at the point of contact. ψ is the helix angle of the teeth. W_a is parallel to the gear axis of rotation, and W_t is directed along the tangent to the pitch cylinder normal to W_a and passing through the pitch point.

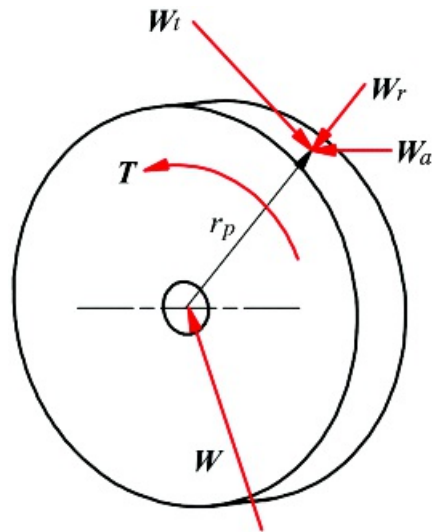


[Figure 14.36](#) The free-body diagram of the gear. The only component of the contact force W that exerts a moment about the gear axis is W_t .

Note that the axial thrust W_a also produces a couple tending to rotate the gear in the plane of the shaft axis. This produces an asymmetry in the bearing loads. The couple has magnitude

$$Y_a = W_a r_p = W_i r_p \tan \psi \quad (14.33)$$



Example 14.10 Analysis of Helical Gear

A helical gear is cut with a standard 25° pressure angle, diametral pitch 4 spur-gear cutter at a helix angle of 30° . If the gear has 40 teeth and transmits 100 hp at a speed of 500 rpm, calculate the radial and thrust loads to be carried by the mounting bearings. Also compute the couple due to the axial component. If the shaft bearings are to be 6 in apart, compute the additional radial bearing load from this source.

Solution

To solve the problem, we must determine the tangential component, W_t , of the normal force, and from this we can determine the other components. Using [Equation 14.32](#), the relationship between W_t , the power P , and the angular velocity, ω , of the gear is

$$W_t = \frac{P}{r_p} = \frac{P}{\omega r_p} \quad (14.36)$$

We can compute the pitch radius from the number of teeth and the diametral pitch. That is

$$r_p = \frac{N}{2P} = \frac{40}{2(4)} = 5 \text{ in}$$

Because the power is given in hp, r_p in inches, and ω in rpm, [Equation 14.36](#) becomes

$$W_t = \frac{(33,000)(12)(100)}{2\pi\omega r_p} = \frac{63,025(100)}{(500)3} = 2,520 \text{ lb}$$

From [Equations 14.29](#) and [14.30](#)

$$W_r = W_t \tan \phi_t = W_t \frac{\tan \phi_h}{\cos \psi} = 2520 \frac{\tan 25^\circ}{\cos 30^\circ} = 1360 \text{ lbs}$$

And from [Equation 14.31](#)

$$W_a = W_t \tan \psi = 2520 \tan 30^\circ = 1460 \text{ lbs}$$

The couple due to the axial load is given by [Equation 14.31](#) as

$$T_a = W_a r_p = W_t r_p \tan \psi = 2520(5) \tan 30^\circ = 7280 \text{ in-lbs}$$

The shaft bearings must produce a couple that will react with this couple to place the shaft in static equilibrium. The couple produced by the bearings is $6F$, so the *increase* in the reaction forces to support the couple produced by the axial load is

$$F_b = \frac{7230}{6} = 1210 \text{ lbs}$$

14.11.3 Worm Gears

Worm gears are a special case of crossed-helical gears, and the forces on the worm from the gear are usually resolved as shown in [Figure 14.37](#). The force equations are similar to those for helical gears except that in the case of worm gears, the lead angle, λ , is usually used instead of the helix angle. With worm gears, the worm is almost always the driver because in most cases friction makes it impossible to drive the worm from the gear. Referring to [Figure 14.37](#), the force component equations for the worm can be written as

$$W_t = \frac{T}{r_p}$$

where r_p is the pitch radius and T is the input torque on the worm.

$$W_a = \frac{W_t}{\tan \lambda}$$

$$W_r = W_t \frac{\tan \phi_t}{\tan \lambda}$$

and

$$W = \sqrt{W_a^2 + W_r^2 + W_t^2}$$

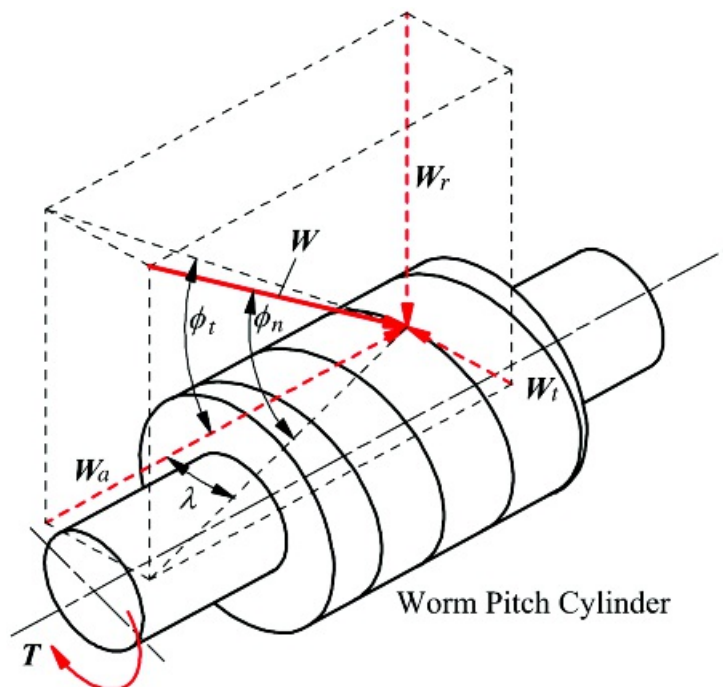


[Figure 14.37](#) The forces on a worm gear.

In most worm gear drives, the gear axis is at right angles to that of the worm. Because of this, W_a for the worm becomes W_t for the gear, and W_t for the worm becomes W_a for the gear. The radial component is the same for both the worm and the gear.

For typical values for λ and ϕ , the magnitude of W is much larger than the magnitude of W_r . This makes worm gears somewhat inefficient, because even small values of the coefficient of friction will produce large friction forces compared with W_r . This makes the equations in this section somewhat approximate for design purposes. For accurate designs, the contribution of friction must be included in the force calculations. If the friction is not included in the analysis, the effect of friction must be accounted for through a safety factor for the gearbox.

It is also necessary to account for the frictional losses by providing a means for cooling the gearbox. This is commonly done by providing fins on the gearbox to improve convective heat transfer. In extreme cases, the oil is cooled separately. In general, most of the frictional losses will be converted to heat, and if the design does not properly account for this heat load, the oil temperature will rise and the gearbox will fail prematurely.

14.11.4 Straight Bevel Gears

In computing the tooth forces on bevel gears, it is necessary to estimate the point of application of the force. It is typical to assume that the contact force acts at the middle of the tooth face. In practice, it is probably somewhat farther toward the thick end of the tooth because the tooth is stiffer in that direction. However, the error in assuming that the force contacts the middle of the tooth is small, and this will generally give slightly conservative results. In the absence of friction, the contact force, W , will be normal to the tooth, and as indicated in [Figure 14.38](#), the force can be resolved into three components. The tangential component, W_p , is the component that generates the shaft torque, and it is given by

$$W_p = W \cos \phi$$

where ϕ is the pressure angle. The force component in the plane of the gear shaft is

$$W_y = W \sin \phi$$

and this component can be used to compute the radial and axial components. These are

$$W_r = W_y \cos \gamma = W \sin \phi \cos \gamma$$

$$W_a = W_y \sin \gamma = W \sin \phi \sin \gamma$$

where γ is the cone angle for the gear. The torque, T , transmitted by the gear is given by

$$T = W_p r_{ave}$$

where r_{ave} is the average radius of the gear pitch cone. Note that as in the case of a helical gear, the force component W_a produces a time-varying couple on the shaft, and the couple must be resisted by the bearings.

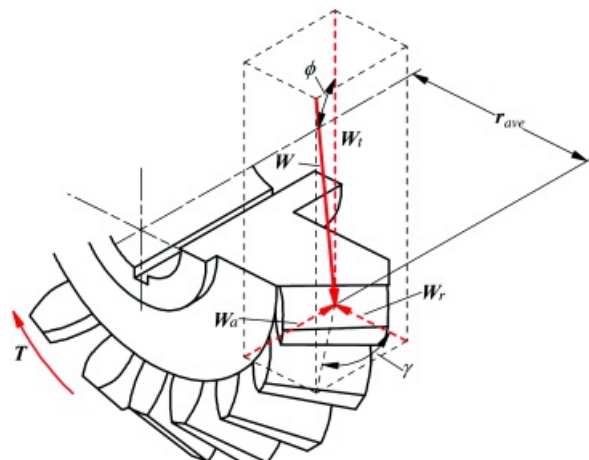
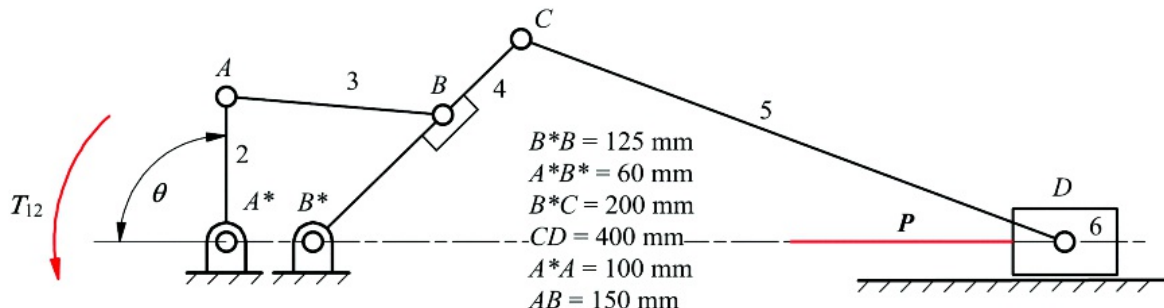


Figure 14.38 The force components for a straight-toothed bevel gear.

Problems

Free-Body Diagrams

- 14.1 In the mechanism shown in [Figure P14.1](#), sketch a free-body diagram of each link, and determine the force P that is necessary for equilibrium if $T_{12} = 90 \text{ N-m CCW}$ and $\theta = 90^\circ$.



[Figure P14.1](#) Mechanism for Problem 14.1.

- 14.2 Draw a free-body diagram for each of the members of the mechanism shown in [Figure P14.2](#), and find the magnitude and direction of all the forces and moments. Compute the torque applied to link 2 to maintain static equilibrium. Link 2 is horizontal. Use free-body diagrams.

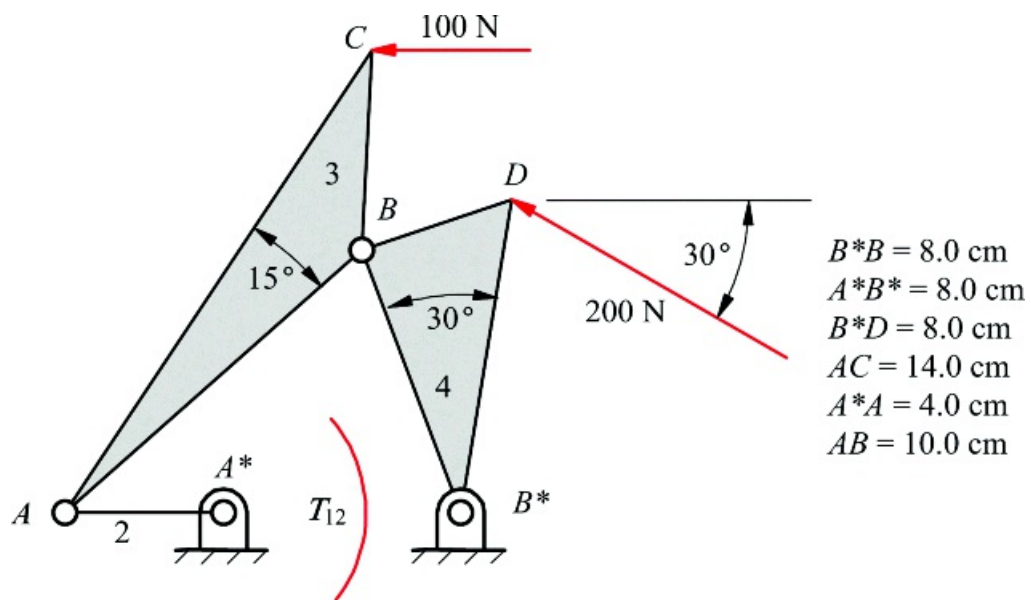


[Figure P14.2](#) Mechanism for Problem 14.2.

- 14.3 If a force of 1000 lb is applied to the slider as shown in [Figure P14.3](#), determine the force P required for static equilibrium. Use free-body diagrams.

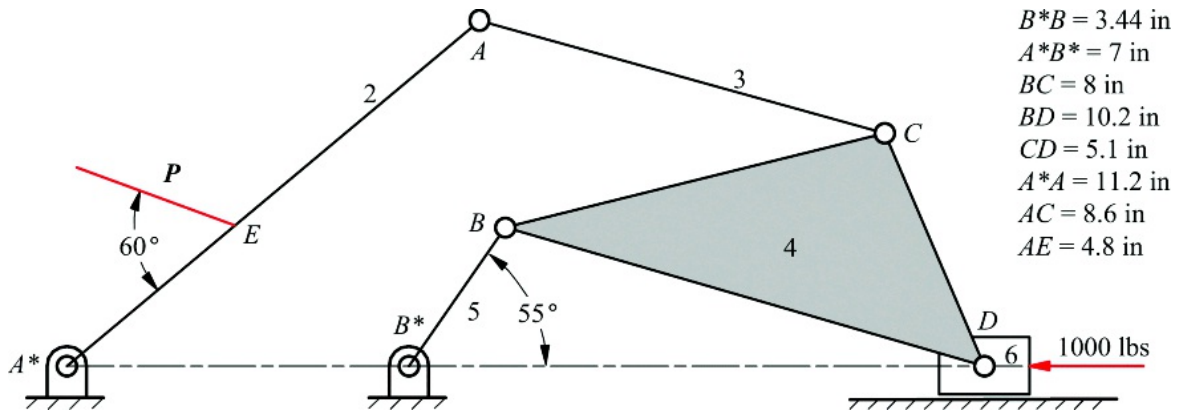


Figure P14.3 Mechanism for Problem 14.3.

14.4 For the mechanism and data given in Figure P14.4, determine the cam torque, T_{12} , and the forces on the frame at points A^* and B^* (F_{21} and F_{31}). Assume that there is friction between the cam and follower only.

$T_{13} = 50 \text{ in-lb}$	$W_2 = 16.1 \text{ lb}$
$\mu = 0.13$	$W_3 = 32.2 \text{ lb}$

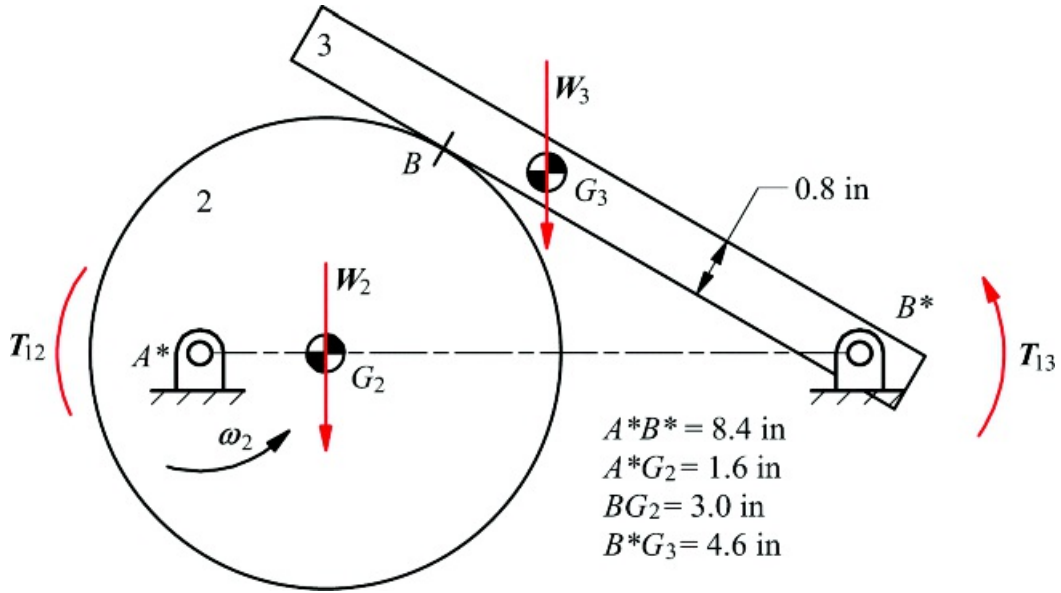
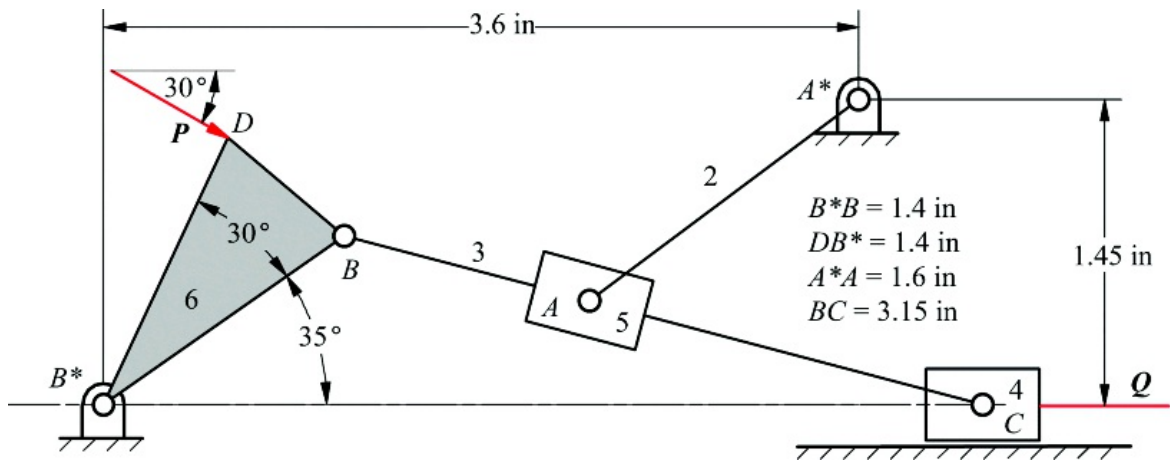


Figure P14.4 Mechanism for Problem 14.4.

Energy Methods

14.5 In the mechanism shown in Figure P14.5, $P = 100 \text{ lb}$. Find the value of the force Q on the block for equilibrium. Use energy methods.



[Figure P14.5](#) Mechanism for Problem 14.5.

14.6 If T_{12} is 1 in-lb in [Figure P14.6](#), find P_{16} using energy methods.

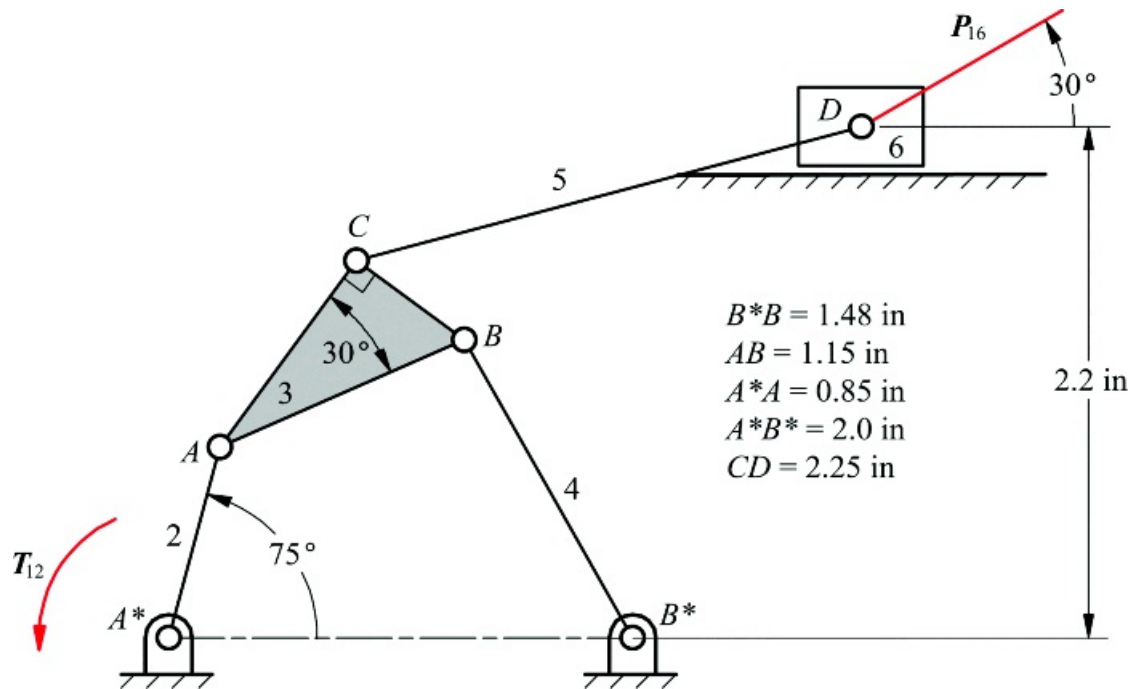


[Figure P14.6](#) Mechanism for Problem 14.6.

14.7 Assume that the force P is 10 lb in the direction shown in [Figure P14.7](#). Use energy methods to find the torque T_{12} required for equilibrium.

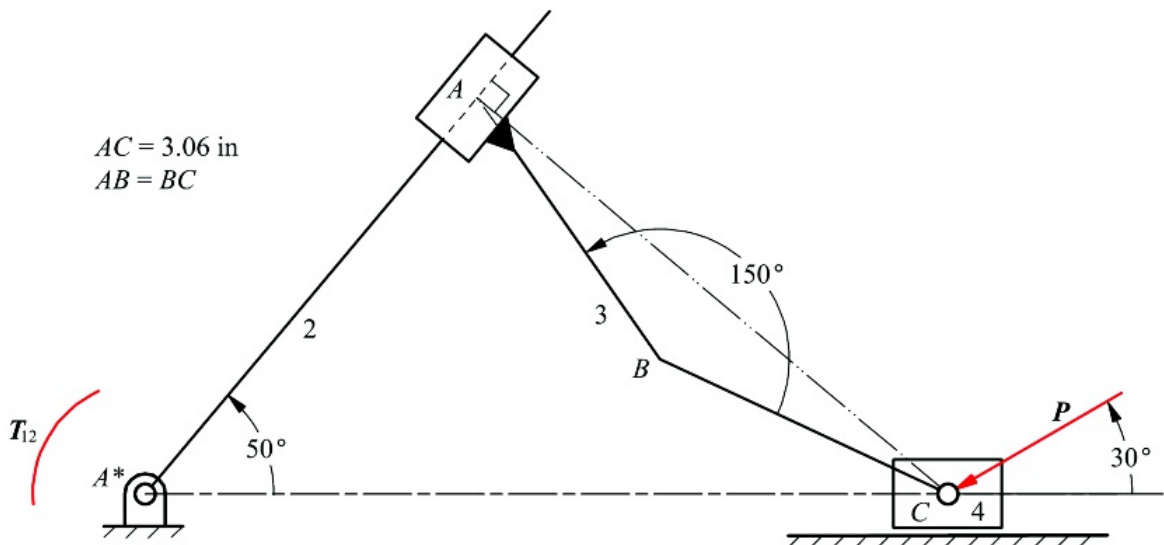


[Figure P14.7](#) Mechanism for Problem 14.7.

14.8 In the four-bar linkage shown in [Figure P14.8](#), the force P is 100 lb and horizontal. Use energy methods to find the torque T_{12} required for equilibrium.

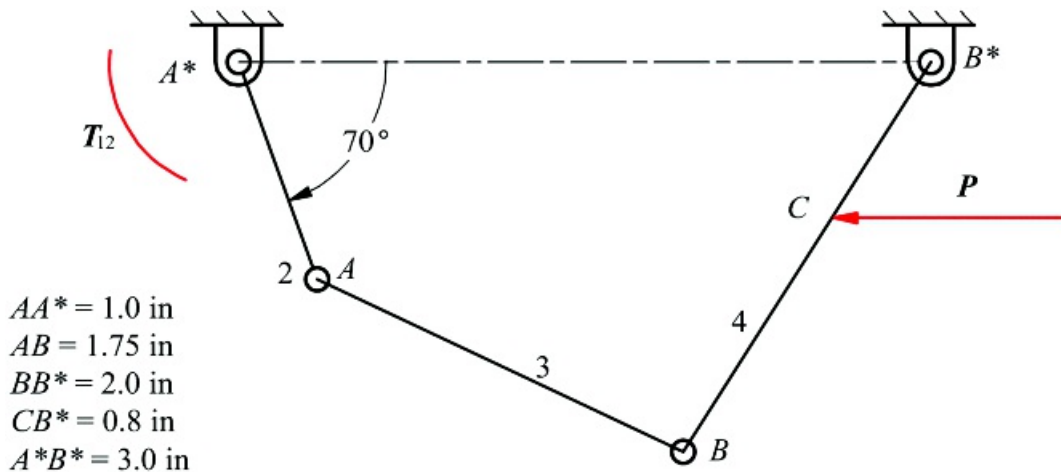


[Figure P14.8](#) Mechanism for Problem 14.8.

14.9 If F_{14} is 100 lb in [Figure P14.9](#), find the force F_{12} required for static equilibrium.

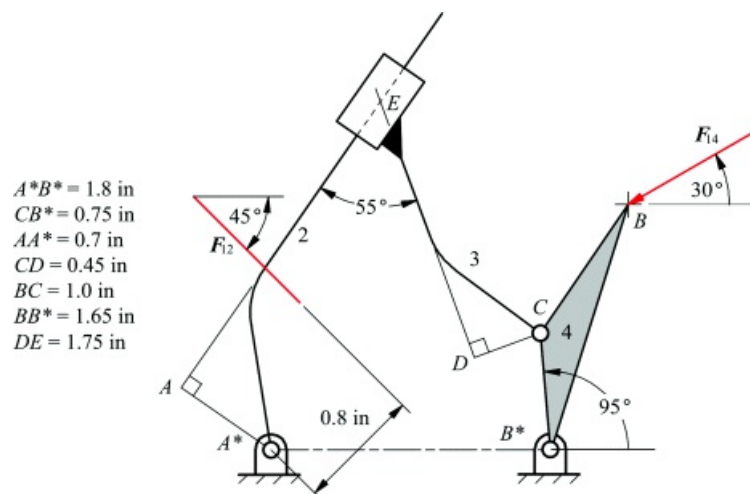


[Figure P14.9](#) Mechanism for Problem 14.9.

14.10 In the eight-link mechanism, most of the linkage is contained in the black box and some of the instant centers are located as shown in [Figure P14.10](#). The force P is 100 lb and is applied to point C on link 8. If $v_{A_2} = 100$ in/s in the direction shown in [Figure P14.10](#), compute the velocity of point B_8 and determine the torque T_{12} necessary for equilibrium.

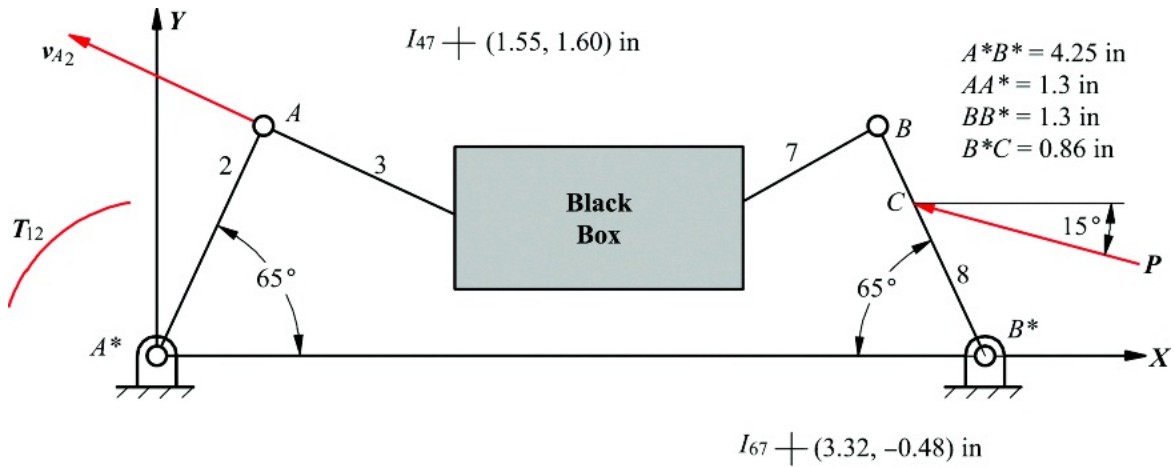


[Figure P14.10](#) Mechanism for Problem 14.10.

14.11 The mechanism in [Figure P14.11](#) is called a vice grip because a very high force at C can be generated with a relatively small force at D when points A^*A and B are collinear (toggle position). In the position shown, determine the ratio F_{14}/F_{13} . Use energy methods.

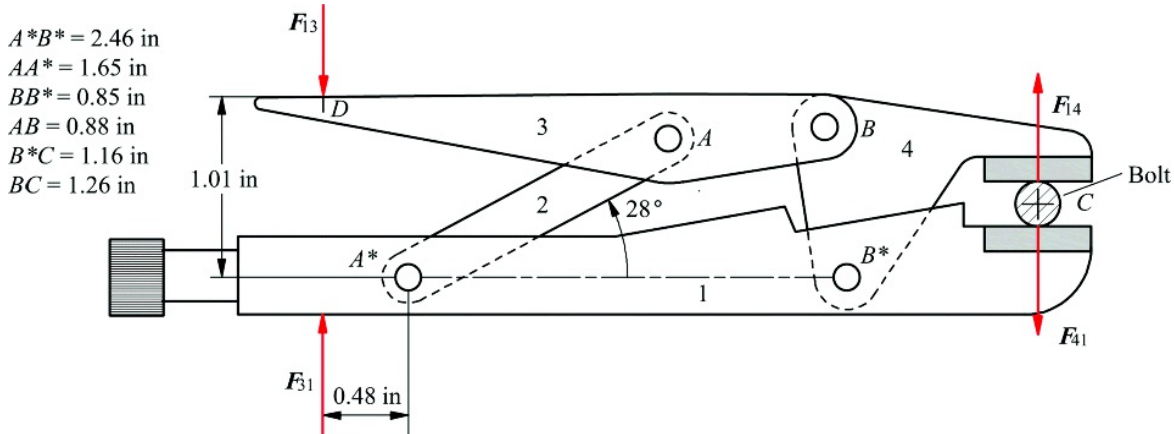


[Figure P14.11](#) Mechanism for Problem 14.11.

14.12 If Q is 100 lb in the direction shown in [Figure P14.12](#), use energy methods to find the torque T_{12} required for equilibrium. In the position considered, link 4 is horizontal.

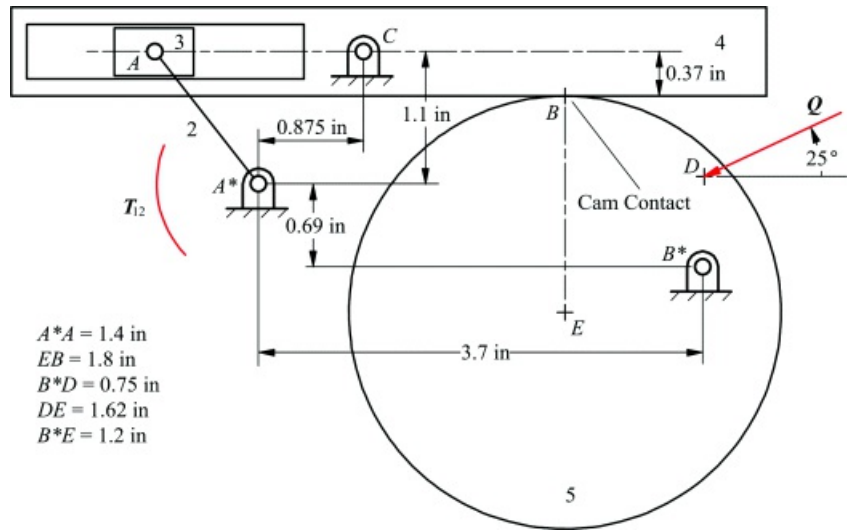


Figure P14.12 Mechanism for Problem 14.12.

14.13 If Q is 100 lb in the direction shown in Figure P14.13, use energy methods to find T_{12} . Use energy methods.

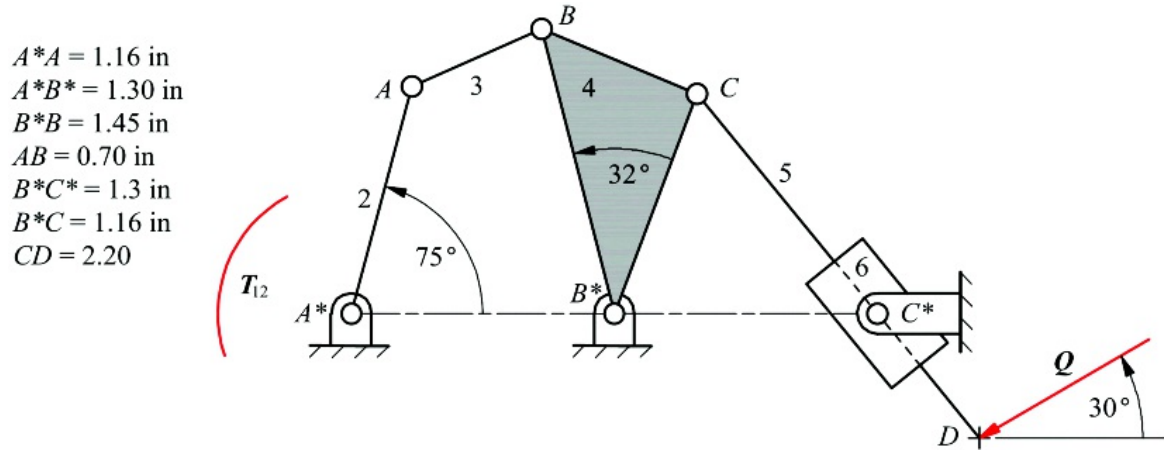
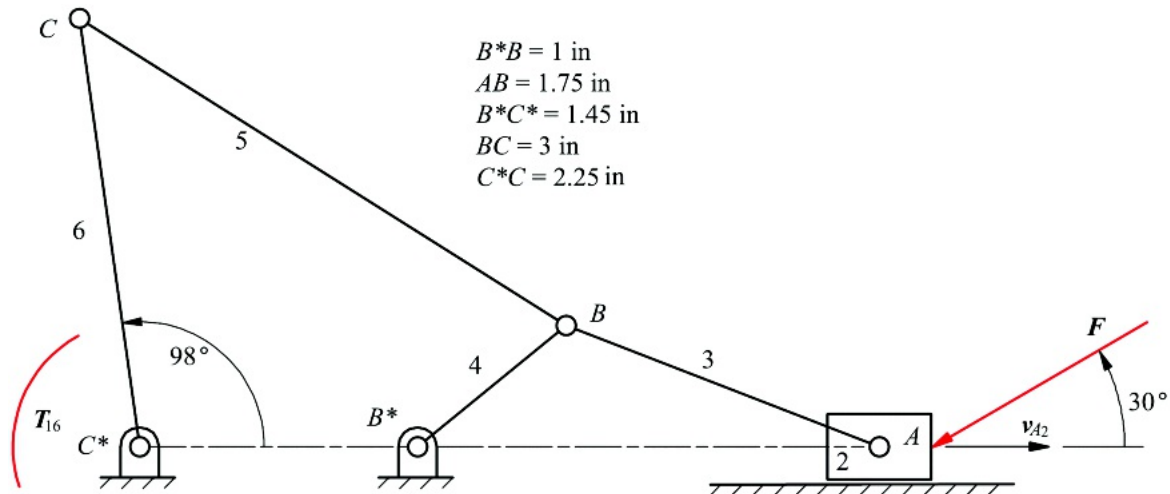


Figure P14.13 Mechanism for Problem 14.13.

14.14 If the velocity of link 2 is 10 in/s to the right, and the force on link 2 is 100 lb in the direction shown in Figure P14.14, find the torque on link 6 required to maintain equilibrium in the mechanism. Use energy methods.



[Figure P14.14](#) Mechanism for Problem 14.14.

14.15 In the mechanism shown in [Figure P14.15](#), point *C* is a swivel at the midpoint of Link 3 that carries link 5. The motion of the four-bar linkage causes arm 6 to oscillate. If link 2 rotates CCW at 12 rad/s and is driven by a torque of 20 ft-lb, determine the resisting torque on link 6 required for equilibrium. Use energy methods. In the position considered, link 2 is horizontal.

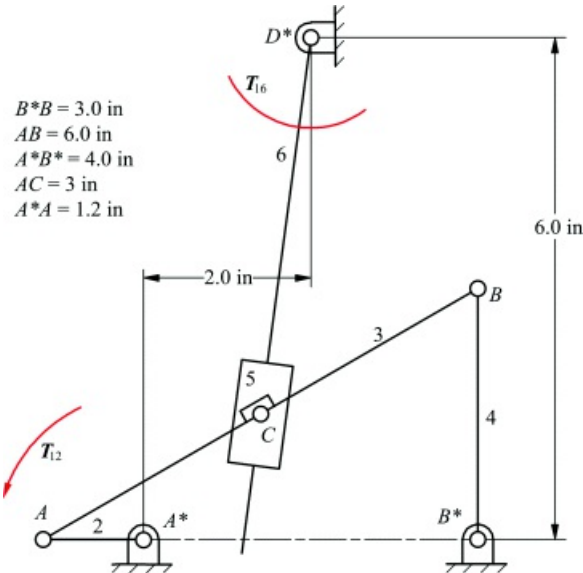


[Figure P14.15](#) Mechanism for Problem 14.15.

Pin Friction

14.16 Find the torque T_{12} in [Figure P14.16](#) for a coefficient of friction μ of 0.0 and 0.2. Assume that the radius of each pin is 1 in, and consider both pin and slider friction. Link 2 rotates CW.

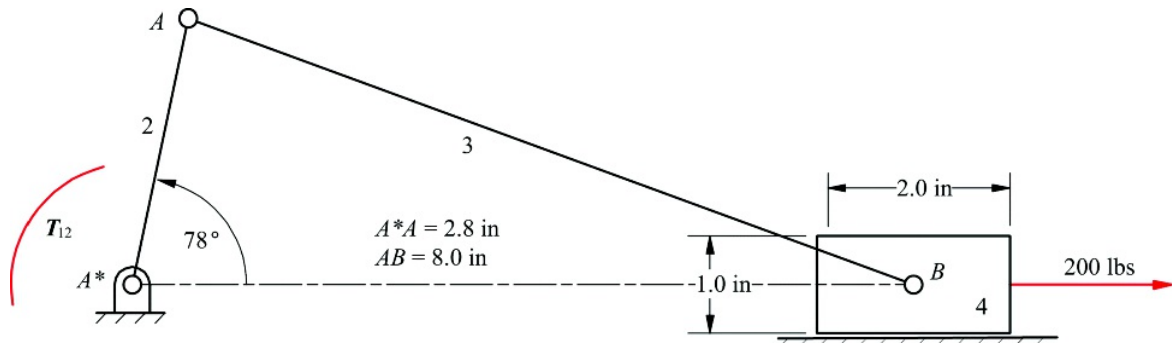


[Figure P14.16](#) Mechanism for Problem 14.16.

14.17 For the position given for the slider crank mechanism in [Figure P14.17](#), find the torque T_{12} required for equilibrium. The radius of each pin is 1 in, and the friction coefficient at the pin between links 3 and 4 and between the block and the frame is 0.3. Elsewhere, the coefficient of friction is 0. Link 2 rotates CCW.

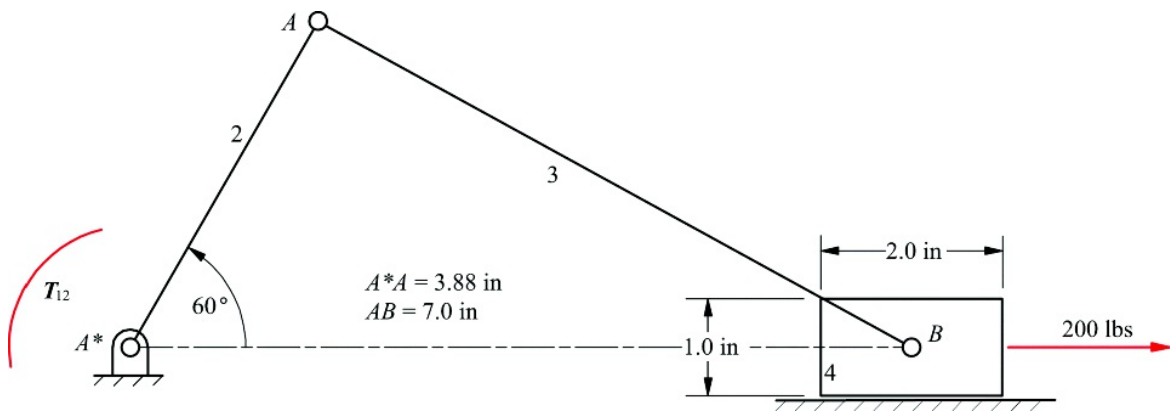


Figure P14.17 Mechanism for Problem 14.17.

14.18 If the radius of each pin is 0.9 in and the coefficient of friction at all joints is 0.15, find the torque T_{12} required for equilibrium in the position shown in [Figure P14.18](#). Link 2 rotates CCW.

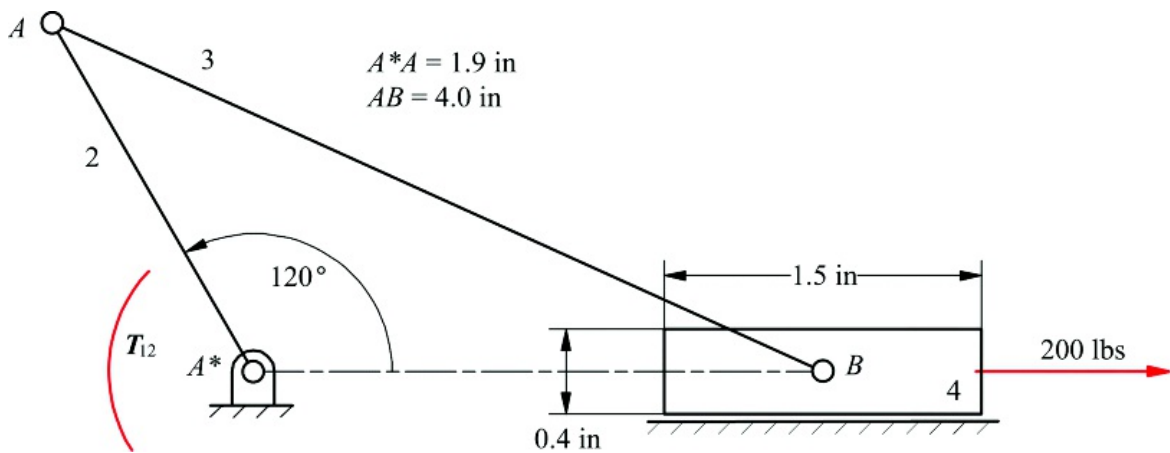


Figure P14.18 Mechanism for Problem 14.18.

14.19 In [Figure P14.19](#), if the coefficient of friction is 0.4 at each pin and each pin radius is 1 in, determine the force F required for equilibrium. Link 2 rotates CCW.

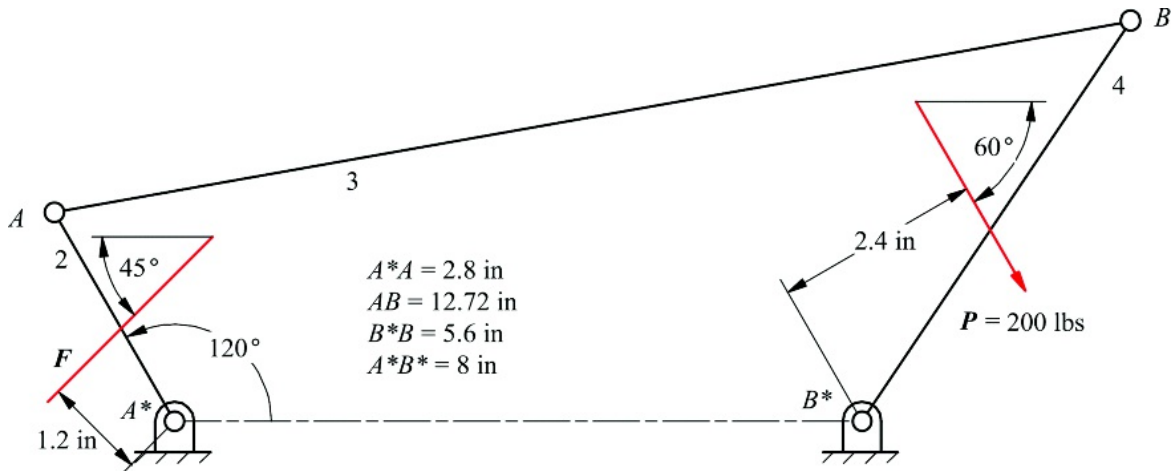
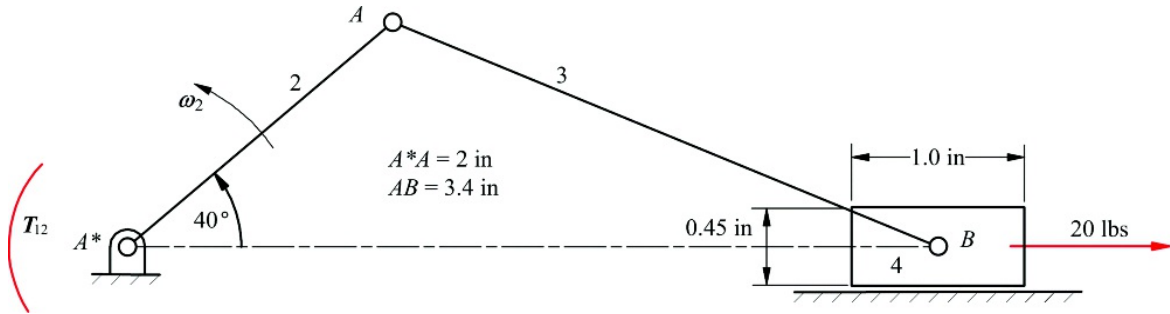


Figure P14.19 Mechanism for Problem 14.19.

14.20 Find the torque T_{12} in [Figure P14.20](#) for a coefficients of friction μ of 0.0 and 0.2. Consider friction at the slider only and neglect the masses of the links.



[Figure P14.20](#) Mechanism for Problem 14.20.

Out-of-Plane Forces

[14.21](#) The linkage shown in [Figure P14.21](#) is a type I double-rocker four-bar linkage in which the two coupler pivots, A and B have been replaced by spherical joints. It moves in the *horizontal* plane and is used to guide and support a heavy door that is hung from the coupler. The vertical crank shafts are each supported on a tapered roller bearing that supports both radial and thrust loads. The centers of these bearings are 1.5 in below the horizontal plane in which the spherical joint centers lie. The crank shafts are also supported by ball bearings that support only radial loads. The central plane of the ball bearings is 2 in above the plane of the spherical joint centers. The door weighs 500 lb, including the weight of the coupler, and its center of mass is directly below the mid-point of the coupler. Each of the cranks AB and CD weighs 30 lb and can be modeled as a uniform rod. Find the radial loads carried by the ball bearings and the radial and thrust loads carried by the tapered roller bearings when the linkage is in the position shown in [Figure P14.21](#).

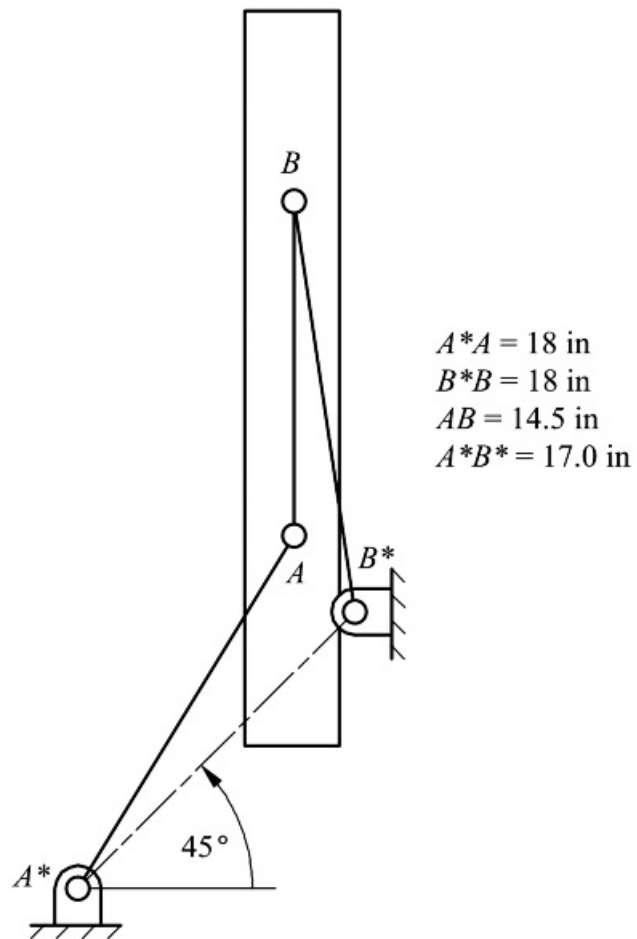


[Figure P14.21](#) Mechanism for Problem 14.21.

[14.22](#) The robot of Example 14.8 is positioned so that the angle between links 2 and 3 is 45° , and the payload

is 30 lb located on the axis of joint 3. Calculate the loads on links 2 and 3 in this position.

Gear Loads

14.23 A pair of spur gears with 31 and 57 teeth is cut to standard 20° pressure angle dimensions with diametral pitch 16. The wheel carries a load torque of 500 lb ft. Find the reaction loads carried by the bearings on which the gears turn.

14.24 A helical gear is cut with a standard 25° pressure angle, diametral pitch 8 spur gear cutter at a helix angle of 30° . The gear has 50 teeth and transmits 150 hp at a speed of 1500 rpm. Calculate the radial and thrust loads that must be carried by the mounting bearings. Also, compute the couple due to the axial component of the tooth loads. If the shaft bearings are to be 5 in apart, compute the additional radial bearing load from this source.

Project Problem

14.25 [Figure P14.25](#) shows a mechanical balance similar to those used in doctors' offices to weigh patients. The patient stands on a platform at the bottom of the picture. Weights are moved along the balance beam until the arm is in equilibrium. The positions of those weights are read on scales to read the patient's weight. The entire mechanism is a mechanical linkage that transfers the patient's weight force from the underside of the platform, up the column to the left side of the balance beam, with a mechanical advantage that allows the small sliding weights on the beam to balance the much larger weight of the patient.



[Figure P14.25](#) Balance scale for Problem 14.25.

Design a suitable linkage to effect this transfer of the weight force with the appropriate mechanical advantage. Can you find a mechanism in [Chapter 8](#) that would be useful in constraining the motion of the platform?

The balance beam consists of two rails, rigidly connected together, on which the weights slide. The primary balance weight slides on the lower of the two rails. It weighs two pounds, and moves two inches to the right of the zero point to balance 100 pounds. The rider, or light balance weight slides on the upper rail. It moves 3.5 inches to the right of the zero point to balance 10 pounds. What must be the weight of the rider? The fulcrum, or balance point, of the beam is in the white housing about five inches to the left of the column axis. The linkage transferring the patient's weight from the platform also connects to the beam inside this housing. The black weight on the left end of the beam is a counterbalance allowing the zero point to be several inches to the right of the fulcrum on which the beam balances. Its position can be adjusted with a screwdriver to ensure the beam is balanced at zero weight.

15

DYNAMIC FORCE ANALYSIS OF MECHANISMS

Prerequisite Knowledge Needed for Chapter 15

A basic knowledge of statics and dynamics from a course on applied mechanics.



15.1 Introduction

In machine dynamics, we bring together *kinematics*, the study of motion and geometry, with *kinetics*, the study of the relationship between force and motion, to derive information on the forces and torques active in moving machinery. This information is, in turn, essential to the computation of the stresses internal to the members of a machine and the elastic deflections of the members. Because two major failure modes of machine members are deformation or fracture due to excessive stress and vibration and interference due to excessive elastic deflection, this information is obviously crucial for the purposes of machine design.

Thus, we make use of the full power of methods described in [Chapters 1](#) through [14](#) of this book to calculate the accelerations and angular accelerations to which machine members are subjected. These are related to the loads acting on those members using Newton's second law.

The computation of stresses and deflections in machine members is beyond the scope of this book. It is covered in texts on strength of materials, stress analysis, and design of machine elements. There are powerful computer tools such as finite-element analysis codes that can be used for this purpose. However, the input to such a program must include a complete description of the forces acting on the member. This includes both forces of reaction against the base or other members and active forces and torques produced by self-weight, by loads, including dynamic body forces such as centrifugal force, and by actuators or prime movers powering the machine. Powerful computational tools are available for simulation and analysis of such situations, but it is necessary to understand the dynamic effects to ensure that the software models prepared for use in such systems are correct.

The relationship between force and motion that is central to the study of kinetics is Newton's second law

$$\boxed{\mathbf{F} = m\mathbf{a}} \quad (15.1)$$

where F is the force acting on a particle, m is its mass, and a is its acceleration.

Since this relationship refers to only a single particle and the machine members we want to deal with are bodies with distributed mass, it is necessary to derive appropriate equations relating force and torque for a rigid body with distributed mass from Newton's second law and the rigidity assumption. This results in the *Newton-Euler* equations describing the motion of a rigid body. The description of the motion of the *center of mass* of the body has exactly the same form as [Equation 15.1](#). That is, the center of mass moves as though the entire mass of the body were condensed into a particle at that point

$$\boxed{\mathbf{F} = m\mathbf{a}_G} \quad (15.2)$$

where a_G is the acceleration of the center of mass.

Rotary motion of the body is described by Euler's equation

$$\boxed{\mathbf{\dot{M}}_G = I_G \boldsymbol{\alpha}} \quad (15.3)$$

where ΣM_G is the resultant moment of the force system acting on the body *about the center of mass*, I_G is the inertia matrix based on fixed coordinate axes with origin at the center of mass, and $\boldsymbol{\alpha}$ is the angular acceleration of the body relative to that same fixed frame. Alternatively, if the body is rotating about a fixed point, P , moments may be taken about that point and the inertia matrix expressed in the same fixed coordinate frame with origin at P . Euler's equation then becomes

$$\boxed{\mathbf{\dot{M}}_P = I_P \boldsymbol{\alpha}} \quad (15.4)$$

It is important to note that this special case, rotation about a fixed point, is the *only case* in which the inertia matrix may be based on a point other than the center of mass.

In practice for any case, except rotation of a symmetric body about a fixed axis of symmetry, it is much more convenient to express the inertia matrix about a coordinate frame *fixed in the moving body*. There is always a set of three orthogonal axes, fixed in the body, for which the inertia matrix becomes a diagonal matrix. These axes are called the *principal axes of inertia*. If the inertia matrix, I_G , is expressed in the principal axes, and the angular velocity, ω , and angular acceleration, α , are expressed in the same frame, [Equation 15.3](#) becomes

$$\sum M_G = I_G \alpha + \omega \times I_G \omega \quad (15.5)$$

This is the form of Euler's equation that is most useful for spatial motion.

The methodology of dynamics problems is to use [Equations 15.2–15.5](#) applied to each free body in the system in a manner exactly analogous to the use of static equilibrium equations in analyzing a structure. If the right-hand sides of [Equations 15.2](#) and [15.3](#) are set to zero, they become identical to the static equilibrium equations [Equations 14.5](#) and [14.6](#). This is why [Equations 15.2](#) and [15.3](#) are often called *dynamic equilibrium equations*.

Of course, the presence of the inertia terms on the right-hand sides of the dynamic equilibrium equations complicates their solution. Most dynamic problems in engineering fall into one of two classes. In the first of these, the motion of each body in the system is known. Therefore the acceleration of the center of mass and the angular acceleration of each member are known or can be computed by the use of kinematic techniques. Thus the right-hand sides of the dynamic equilibrium equations can be treated as known quantities, and the equations can be solved algebraically in a manner exactly analogous to the solution of the static equilibrium equations.

In the second class of dynamics problems, the motion of each body is not known a priori, and it is necessary to treat the accelerations on the right-hand sides of the equations as the second derivatives of position variables. The forces and moments acting on the member, which appear on the left-hand sides of the equations, must then also be related to the position variables to produce a set of differential equations in those position variables. These equations are called the *equations of motion* of the system. Description of the motion of the system then requires solution of the equations of motion.

In many machine-design problems the motion of some input element is specified and dynamic analysis of these systems falls into the first of the two classes described above. These problems may be called *machine dynamics problems*. In this book, we will confine ourselves to this class of dynamic problems.

Dynamic problems that must be solved by solution of the differential equations of motion are treated in courses and texts on vibrations or system dynamics. Another class of such problems is treated in the area of multi-body system dynamics.



15.2 Problems Solvable Using Particle Kinetics

Some machine design problems require only [Equation 15.1](#) or the energy and momentum relationships derived from it for solution. That is, it is not necessary to use rotary inertia. Effectively, the inertias can be modeled as particles with adequate accuracy. The reader has probably encountered simple problems of this type in applied mechanics courses.

15.2.1 Dynamic Equilibrium of Systems of Particles

First, it is necessary to relate the positions of the concentrated masses of the system kinematically to find their accelerations. In principle, this requires first relating their positions, then their velocities and accelerations. The way this works out is illustrated by the following examples.



Example 15.1

Vehicle Acceleration and Braking

An automobile has a total weight $W = 4000$ lb. As shown in [Figure 15.1](#), its wheelbase (distance between the front and rear axle centers) is $b + c = 90$ in, and its center of mass is $b = 40$ in behind the front axle center. When it is parked on a level surface, the center of mass is $h = 25$ in above the ground. The wheel radius is $r = 14.5$ in, and on a good surface, the coefficient of friction between the tires and the road is $\mu = 0.8$. If the weights and moments of inertia of the wheels are neglected, estimate the ratio of the maximum acceleration that the vehicle can achieve to the gravitational acceleration, g , if it is driven by

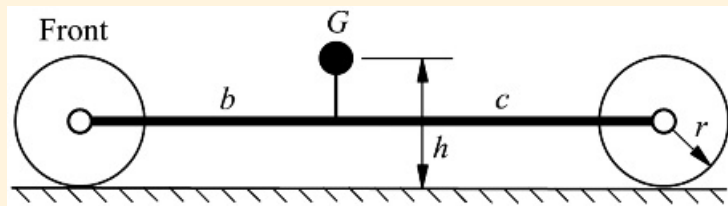


[Figure 15.1](#) The vehicle model for Example 15.1.

1. The rear wheels
2. The front wheels
3. Find also the maximum deceleration that can be achieved if the braking effort is optimally apportioned between front and rear wheels. What is the percentage of the braking force at the front wheels?

Solution

In this instance, the kinematic part of the solution is trivial. Since the wheel inertia is neglected, it is not even necessary to develop expressions for the angular velocities and angular accelerations of the wheels. We therefore start with the first case, when the rear wheels are driving.

1. Since the wheel weight and inertia will not be considered separately, we start with a free-body diagram of the whole vehicle shown as [Figure 15.2](#).

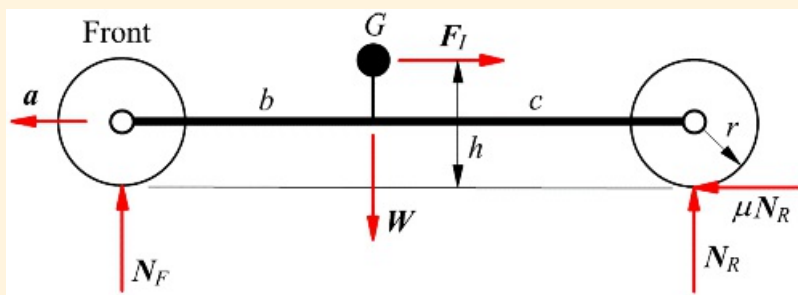


[Figure 15.2](#) Free-body diagram when vehicle is driven via the rear wheels.

There is no rotation of the vehicle mass, so the angular acceleration is zero. Therefore, the inertia torque term ($I_G \ddot{\alpha}$) in [Equation 15.3](#) is zero.

The term ma_G in [Equation 15.2](#) can be computed and treated as a known force. If we move the term to the left-hand side of the equation, we can treat it as an applied force and solve the problem as a statics problem. As will be discussed in more detail later, when we treat the term, ma_G , in this way, it is called an inertia force, F_I , and it is in the direction opposite to that of the acceleration. The magnitude of F_I is given by

$$F_I = \frac{Wg}{\mu g}$$

where a is the magnitude of the acceleration a , which is positive in the forward direction, and W is the magnitude of the weight, W . That is, the mass of the vehicle is W/g .

The dynamic equilibrium equations are

$$\sum F_x = 0 : \quad F_I + \mu N_R = 0 \quad (a)$$

$$\sum F_y = 0 : \quad W = N_R + N_F \quad (b)$$

$$\sum M_G = 0 : \quad cN_R = bN_F + h\mu N_R \quad (c)$$

Moments are conveniently taken about G to eliminate W and a from the moment equation (their lines of action pass through G).

Using Equation a together with the expression for F_I gives

$$N_R = \frac{Wg}{\mu g}$$

Applying this to Equation b,

$$N_F = W \left(1 - \frac{a}{\mu g} \right)$$

Substitution of these expressions into Equation c gives, after some rearrangement,

$$\frac{a}{g} \left(\frac{b+c}{\mu} - h \right) = b$$

or

$$A = \frac{a}{g} = \frac{\mu b}{b + c - \mu h}$$

where A is the required ratio of the acceleration to the gravitational acceleration. Substitution of the values of μ , b , c , and h given in the problem statement results in

$$A = 0.457$$

That is, the maximum acceleration that can be achieved by the vehicle is 45.7 percent of the

gravitational acceleration.

2. The free-body diagram for front-wheel drive is as shown in [Figure 15.3](#).

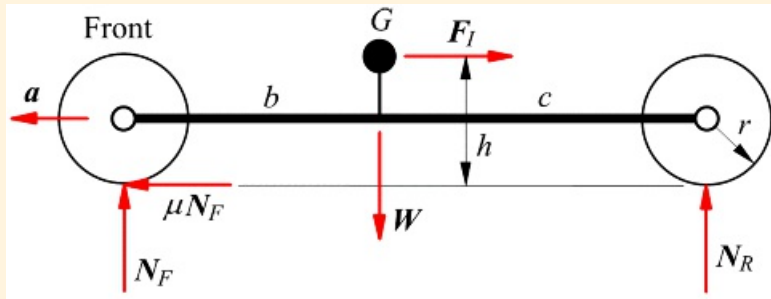


[Figure 15.3](#) The free-body diagram when the vehicle is driven via the front wheels.

The dynamic equilibrium equations are

$$\sum F_x = 0 : -F_I + \mu N_F = 0 \quad (d)$$

$$\sum F_y = 0 : W = N_R + N_F \quad (e)$$

$$\sum M_G = 0 : -cN_R = bN_F + b\mu N_F \quad (f)$$

Substitution for F_I in Equation d gives

$$N_F = \frac{Wc}{\mu g}$$

Substitution in Equation e gives

$$N_R = W \left(1 - \frac{\alpha}{\mu g} \right)$$

Substitution of these values into Equation f, after rearrangement, gives

$$\frac{\alpha}{g} \left(\frac{b - c}{a} + b \right) = c$$

Hence

$$\alpha = \frac{g}{\beta} = \frac{\mu g}{b + c + ab}$$

Substitution of the given values yields

$$A = 0.364$$

As can be seen, for the values given, the acceleration that can be achieved with front-wheel drive is significantly lower than with rear-wheel drive.

3. The free-body diagram for braking is as shown in [Figure 15.4](#).

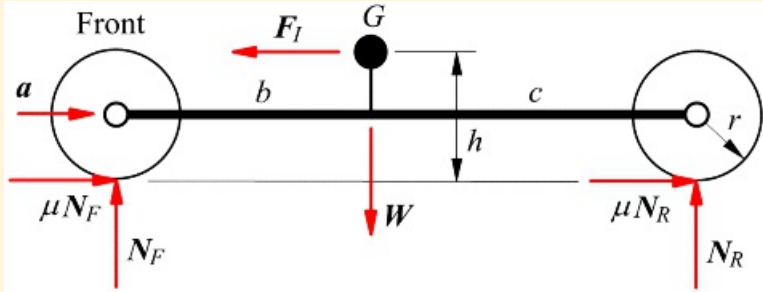


[Figure 15.4](#) The free-body diagram during braking.

In this case the inertia force is directed forward. The dynamic equilibrium equations are, in this instance,

$$\sum F_x = 0 : \quad F_I - \mu(N_F + N_R) = 0 \quad (g)$$

$$\sum F_y = 0 : \quad W = N_R + N_F \quad (h)$$

$$\sum M_G = 0 : \quad cN_F + b\mu(N_F + N_R) = bN_F \quad (i)$$

Substitution from Equation *h* into Equation *g*, together with substitution for F_I gives

$$\frac{W\alpha}{\varepsilon} = \mu W$$

or $A = \mu$. For the values given, $A = 0.8$.

Substitution from Equation *h* into Equation *i* gives

$$N_F(b + c) = (c + b\mu)W$$

or

$$N_F = W \frac{c + b\mu}{b + c}$$

For the values given

$$N_F = 0.773 W \text{ and } N_R = 0.222 W$$

Therefore, 77.8 percent of the braking effort is at the front wheels, which is why the front brakes of automotive vehicles are usually much bigger than the rear brakes.

Notice also that, for this configuration, the deceleration available through optimal braking is considerably greater than the maximum possible acceleration.



Example 15.2 Flyball Governor

A flyball governor is arranged as shown in [Figure 15.5](#) to allow adjustment of the governed speed by adjusting the preload in the spring. As the weights swing outward under the influence of centrifugal force, the spring is compressed.

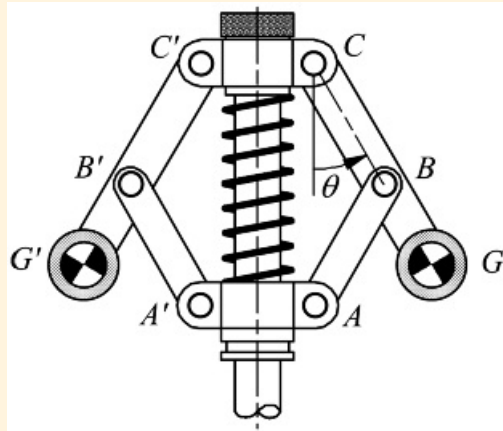


[Figure 15.5](#) The flyball governor discussed in Example 15.2. The dimensions are $AB = BC = A'B' = B'C' = 1.5$ in, $CG = C'G' = 2.438$ in, $CC' = 1.25$ in. G and G' are the effective centers of mass of the arms.

The governor operates a throttle valve to control the speed of an engine. The valve is fully closed when the angle θ is 75° . Compute the speed at which the valve is closed if the effective centers of mass of the arms are in the locations G and G' shown and other inertias can be neglected. The weight of each arm is 0.25 lb. The adjusting nut is set so that the spring is at its natural or free length when $\theta = 5^\circ$. The stiffness of the spring is 20 lb/in. The lengths of the links are as indicated in the figure caption.

Solution

The radius of rotation of the center of mass of each arm is

$$r = 2.438 \sin 75^\circ + 0.625 = 2.979 \text{ in}$$

Hence the centrifugal acceleration of the point G is

$$a_C = r\omega^2 = (2.979/12)\omega^2 = 0.248\omega^2$$

The magnitude of the inertia force is

$$F_I = m a_C = (0.25/32.2) \times 0.248\omega^2 = 0.00198\omega^2$$

Free-body diagrams of links AB and BC are shown in [Figure 15.6](#). Since AB is a two-force member, the forces at A and B are equal, opposite, and collinear. For link BC

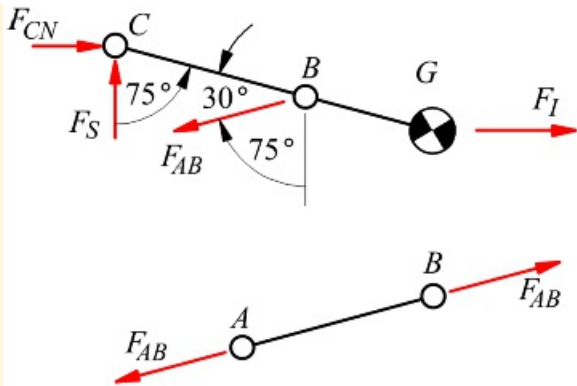


Figure 15.6 Free-body diagrams of links AB and BC used in the solution of Example 15.2.

$$\sum F_x = 0 : \quad F_{CN} + F_I - F_{AS} \sin 75^\circ = 0 \quad (\text{a})$$

$$\sum F_y = 0 : \quad F_S - F_{AS} \cos 75^\circ = 0 \quad (\text{b})$$

where F_S is half the force from the spring.

Taking moments about point C in the free-body diagram for link BC

$$\sum M_C = 0 : \quad F_{AS}BC \sin 30^\circ - F_S CC \sin 15^\circ = 0 = F_{AS} 1.5 \sin 30^\circ - F_S 2.438 \sin 15^\circ \quad (\text{c})$$

The distance AC in this position is

$$AC = 2 \times 1.5 \cos 75^\circ = 0.776 \text{ in}$$

When the spring is at its natural length

$$AC = 2 \times 1.5 \cos 5^\circ = 2.989 \text{ in}$$

Hence the spring is compressed the distance

$$x = 2.989 - 0.776 = 2.212 \text{ in}$$

and the spring force for half the governor is given by

$$2F_S = 20 \times 2.212 = 44.24 \text{ lb}$$

or

$$F_S = 22.12 \text{ lb}$$

Hence, from Equation b

$$F_{AB} = F_3 / \cos 75^\circ = 22.12 / \cos 75^\circ = 85.47 \text{ lb}$$

Using Equation c

$$F_I = \frac{1.5 \sin 30^\circ}{2.438 \sin 15^\circ} F_{AB} = \frac{1.5 \sin 30^\circ}{2.438 \sin 15^\circ} 85.47 = 101.58 \text{ lb}$$

Therefore

$$\omega^2 = F_I / 0.00193 = 101.58 / 0.00193$$

or

$$\omega = 229.4 \text{ rad/s}$$

or

$$\omega = 2,191 \text{ rpm}$$

This is the speed at which the governor will cause the throttle valve to close.

15.2.2 Conservation of Energy

Conservation of energy is useful in mechanism problems in which there is interchange between kinetic and potential energy. Most often the potential energy is either gravitational potential energy or strain energy. If the total energy in the system can be calculated in some position of the system and the system has mobility one, then the kinetic energy and hence the velocity can be calculated in any other position of the system, provided joint friction can be neglected. This type of calculation is usually much more efficient than pursuing the same result via dynamic equilibrium. Conservation of energy provides only information on the variables that determine the system energy. Thus, although positions and velocities can be related in this way, the method will yield no information on accelerations.

Conservation of energy can often be used in association with conservation of momentum to solve problems in which energy is stored in a spring, a raised weight, or a flywheel and then rapidly released, as in punching and stamping machines, jackhammers, and similar types of mechanisms.

15.2.3 Conservation of Momentum

Conservation of momentum is particularly useful in mechanism problems that involve impacts or other short-period, impulsive events. The methodology is to compare the momentum of the system immediately before and immediately after the impulsive event. In problems involving one-dimensional motion, only conservation of linear momentum is required. In problems involving two- or three-dimensional rigid-body motion, conservation of angular momentum is also required.

The general methodology of problems involving conservation of energy and conservation of momentum is illustrated in the following example.



Example 15.3 Hydraulic Impactor

A hydraulic impactor (jackhammer) uses a rotary hydraulic motor to turn a cylindrical cam, as shown in [Figure 15.7](#). The cam has a ramp, which causes the follower to extend a spring, and a step, which releases the follower and allows the spring to contract, accelerating a hammer. At the end of the stroke, the hammer strikes the impactor bit, driving it into the ground. If it is assumed that the impact between the hammer and the bit is perfectly elastic (no loss of energy), find the velocity and kinetic energy of the bit immediately after it is struck by the hammer. The bit weighs 20 lb, and the hammer weighs 17.5 lb. The spring has a rate of 2000 lb/in, and the cam lift is 2 in. At the end of the stroke, when the hammer strikes the bit, the spring is compressed 0.5 in. Also estimate the hydraulic power needed to drive the device if it delivers 5 strokes per second.

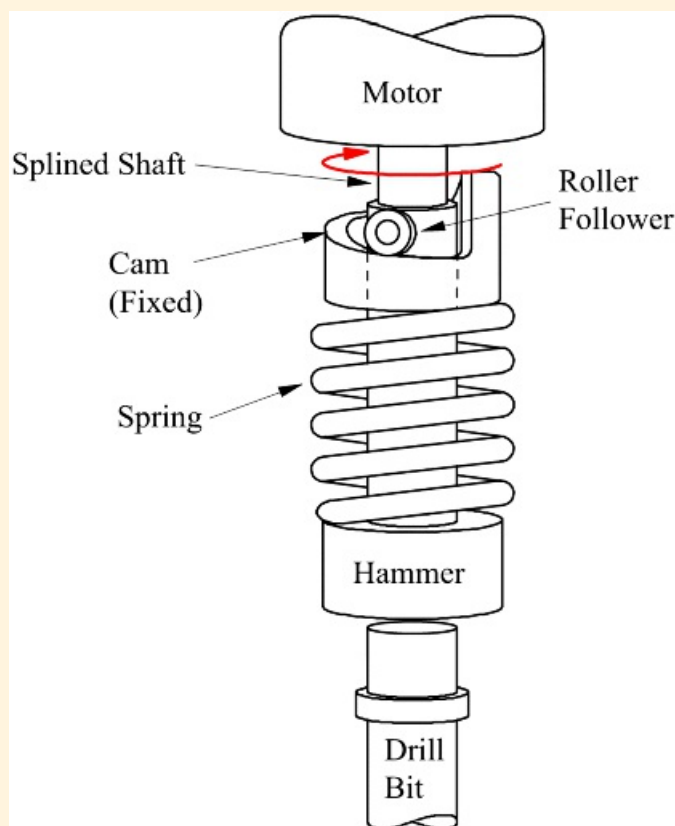


[Figure 15.7](#) The drive mechanism of the hydraulic impactor discussed in Example 15.3.

Solution

The critical position and velocity parameters for this problem are shown in [Figure 15.8](#). We first use conservation of energy to find the velocity of the hammer at the instant of impact.

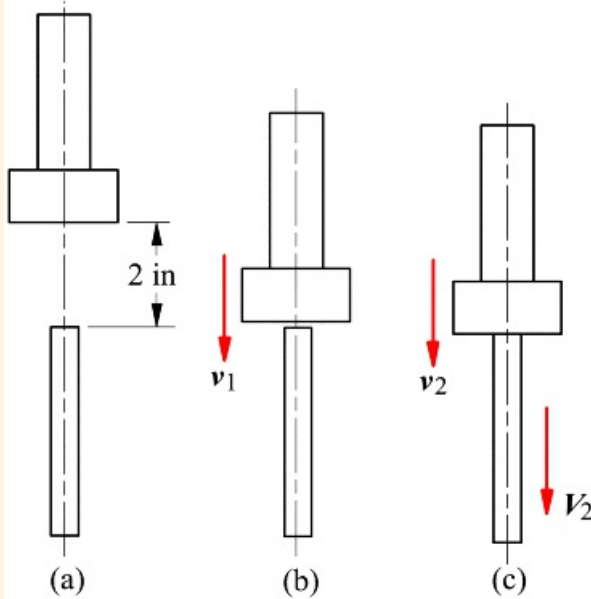


[Figure 15.8](#) Three critical configurations of the system: (a) with the hammer fully raised and both hammer and bit at rest; (b) at the instant before impact with the hammer at velocity v_1 and the bit at rest; and (c) at the instant after impact with both hammer and bit moving, the hammer at velocity v_2 and the bit at velocity V_2 .

When the hammer is in the fully raised position as in [Figure 15.8\(a\)](#), the hammer and bit are at rest so kinetic energy is

$$K_0 = 0$$

The strain energy is

$$E_{\text{str}} = \frac{1}{2} \times 2000 \times 2.5^2 = 6250 \text{ in-lb} = 520.8 \text{ ft-lb}$$

Here 2.5 in is used because that is the total extension of the spring in this position. Note that the spring is extended 0.5 in even when the cam follower is in its lowest position.

If the position at which the hammer strikes the bit is taken as the zero reference, the gravitational potential energy of the hammer is

$$E_{\text{pot}} = 17.5 \times 2/1.2 = 2.9 \text{ ft-lb}$$

Hence the total mechanical energy of the system when the hammer is fully raised is

$$U_0 = K_0 + E_{\text{str}} + E_{\text{pot}} = 523.7 \text{ ft-lb}$$

Now consider the instant immediately before the impact of the hammer on the bit that is illustrated by [Figure 15.8\(b\)](#).

If the velocity of the hammer is v_1 , the kinetic energy of the system is

$$K_1 = \frac{1}{2} \times \frac{17.5}{32.2} \times v_1^2 = 0.272 v_1^2 \text{ ft-lb}$$

The strain energy is now

$$P_{1S} = \frac{1}{2} \times 2000 \times 0.5^2 = 250 \text{ in-lb} = 20.8 \text{ ft-lb}$$

and the gravitational potential energy is zero.

Therefore, the total mechanical energy is

$$U_1 = K_1 + P_{1S} = 0.272 v_1^2 + 20.8 \text{ ft-lb}$$

Equating this expression to the system energy when the hammer is fully raised gives

$$U_1 = U_0 = 0.272 v_1^2 + 20.8 = 523.7 \text{ ft-lb}$$

Hence, solving for v_1 ,

$$v_1 = 43.0 \text{ ft/s}$$

and

$$K_1 = 523.7 - 20.8 = 502.9 \text{ ft-lb}$$

We now use both conservation of momentum and conservation of energy to determine the velocities of hammer and bit immediately after the impact, which is the condition shown in [Figure 15.8\(c\)](#).

Let v_2 be the velocity of the hammer immediately after impact, and let V_2 be the velocity of the bit at that instant. Both are taken to be positive in the downward direction. The momentum of the system immediately before impact is

$$g_1 = \frac{17.5}{32.2} \times 43.0 = 23.4 \text{ lb-s}$$

Immediately after impact, the momentum is

$$g_2 = \frac{20}{32.2} \times V_2 + \frac{17.5}{32.2} \times v_2$$

Equating g_1 and g_2 gives

$$23.4 = \frac{20}{32.2} \times V_2 + \frac{17.5}{32.2} \times v_2$$

or

$$V_2 + 0.875v_2 = 37.63 \quad (\text{a})$$

The kinetic energy of the system immediately after the impact is

$$K_2 = \frac{1}{2} \times \frac{20}{32.2} V_2^2 + \frac{1}{2} \times \frac{17.5}{32.2} v_2^2$$

Since the impact is elastic, K_1 and K_2 can be equated

$$502.5 = \frac{1}{2} \times \frac{20}{32.2} V_2^2 + \frac{1}{2} \times \frac{17.5}{32.2} v_2^2$$

or

$$1619 = V_2^2 + 0.875 v_2^2 \quad (\text{b})$$

Substitution for V_2 from Equation *a* into Equation *b* gives

$$1619 = (37.63 - 0.875v_2)^2 + 0.875v_2^2$$

Expansion and simplification of this equation give

$$v_2 = 43.0 \text{ and } v_2 = -2.875 \text{ ft/s}$$

Solution of this quadratic equation in v_2 gives the following values

$$v_2 = 43.0 \text{ and } v_2 = -2.875 \text{ ft/s}$$

The first of these values is the velocity of the hammer before impact. That must be a solution because the values before impact give the same energy and momentum, but the second value is then the correct solution for the velocity of the hammer after impact. The negative value indicates that the hammer rebounds slightly in the upward direction.

Substitution back into Equation *a* gives

$$V_2 = 37.63 - 0.875(-2.875) = 40.1 \text{ ft/s}$$

The kinetic energy of the bit at this instant is

$$K_2 = \frac{1}{2} \times \frac{20}{32.2} \times 40.1^2 = 499 \text{ ft-lb}$$

The strain energy put into the spring by each rotation of the cam is

$$E_{32} - E_{13} = 520.8 - 20.8 = 500 \text{ ft-lb}$$

The gravitational potential energy put in by raising the hammer is

$$E_{GG} = 2.9 \text{ ft-lb}$$

Hence the energy put in on each rotation of the cam is

$$w = 502.9 \text{ ft-lb}$$

If the cam rotates 5 times per second, the power put in is

$$P = 5 \times 502.9 = 2510 \text{ ft-lb/s} = 2510/550 = 4.57 \text{ hp}$$

This completes the solution of the problem.



15.3 Dynamic Equilibrium of Systems of Rigid Bodies

[Equation 15.3](#) is applicable for general spatial motion. The matrix I_G is a symmetric, 3×3 matrix.

In the present work, we will restrict consideration to planar motion with one of the principal axes normal to the plane of motion. In this case, [Equation 15.3](#) becomes

$$\sum M_G \cdot k = I_G \alpha \quad (15.6)$$

where I_G is a scalar quantity, being the moment of inertia of the body about an axis through the center of mass normal to the plane of motion, k is a unit vector normal to the plane of motion, and α is the angular acceleration, taken to be positive in the k direction. That is

$$\alpha = \alpha k \quad (15.7)$$

We make this restriction because the vast majority of machine dynamics problems are planar motion problems. Solutions of problems involving general spatial motion follow the same lines as the examples studied below, but require use of the general forms of Euler's equation: [Equation 15.3](#) or [Equation 15.5](#).

If a body is in motion, the sum of the forces acting on it is equal to its mass multiplied by the acceleration of its center of mass. That is

$$\sum F = m a_G \quad (15.8)$$

If we introduce a force, F_I , such that

$$F_I = -m a_G \quad (15.9)$$

called the inertia force, which is applied on a line passing through the center of mass, and a couple, M_I

$$M_I = -I_G \alpha \quad (15.10)$$

called the inertia torque, and treat these in the same way as any other external force and torque, then the dynamic equilibrium equations assume the same form as the static equilibrium equations

$$\sum F = 0 \quad (15.11)$$

$$\sum M_O = 0 \quad (15.12)$$

where O is any point in the plane about which moments are taken. Notice that, since all moment vectors are normal to the plane of motion, the moment equation may be treated as a scalar equation. The summation of the forces $\sum F$ now includes F_I , and $\sum M_O$ includes M_I . Note that the point of application of the inertia force is defined to be the center of mass and that the moment of inertia used in computing the inertia couple is that about the

center of mass, whether or not the moments are taken about the center of mass.

The replacement of the $-ma_G$ term with the inertia force, and replacement of $-I_G\alpha$ with the inertia torque to convert the dynamic equilibrium equations into the same form as the static equilibrium equations is known as D'Alembert's principle. The general procedure for solving a dynamic equilibrium problem in machine dynamics is the following:

1. Solve the position, velocity, and acceleration kinematics of the system using the procedures of [Chapters 4, 5](#), or [7](#) to obtain the accelerations of all bodies with significant mass and the angular accelerations of all bodies with significant inertia.
2. Compute the inertia force and couple acting on each body according to D'Alembert's principle.
3. Apply the inertia force and couple as an external force and torque to each member. The line of action of the inertia force passes through the center of mass of each member.
4. Draw a free-body diagram of each member including all external forces acting on that member and all reaction forces from other members to which it is connected.
5. Write three force and moment equilibrium equations for each member.
6. Solve the equations for the unknown forces.

It may be seen that the last three steps in the process are identical to the solution of a static equilibrium problem.



Example 15.4

Dynamic Force Analysis

The members of the mechanism of Example 4.4 and [Figure 4.16](#) in [Chapter 4](#) have the inertial properties tabulated below and indicated in [Figure 15.9](#). Find the driving torque that must be applied to the crank, member 2, to maintain the constant angular velocity of 60 rpm in the clockwise direction. Friction in all joints (including the prismatic joint) and the mass and moment of inertia of link 5 may be neglected. The mechanism moves in the horizontal plane. Therefore, only dynamic forces need to be considered. In the data below, k_3 and k_6 are the radii of gyration for links 3 and 6, respectively.

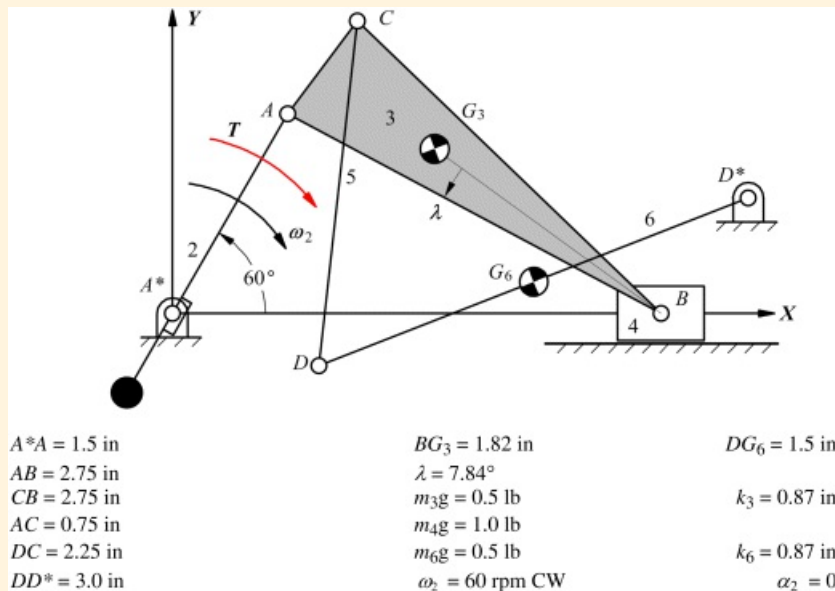


[Figure 15.9](#) The mechanism of Example 15.4 (and of Example 4.4 in [Chapter 4](#)).

Since the geometry and velocity and acceleration are identical to those of Example 4.4 in [Chapter 4](#), that solution can be used for parts 1 and 2 of the solution procedure, with one modification. It is necessary to find the accelerations of points G_3 and G_6 .

In both cases the acceleration image is used. G_6 is at the midpoint of DD^* . Since point D^* is a fixed point, it maps into point o' on the acceleration polygon, and hence the image of DD^* is $d'o'$. Next g_6' is located at the midpoint of $d'o'$, and the acceleration a_{G6} is the vector $o'g_6'$.

Similarly, point g_3' can be located on the image $a'b'c'$ of ABC by constructing $\angle a'b'g_3'$ equal to $\angle ABG_3 = \lambda$, and making

$$\frac{g_3'}{g_3} = \frac{BG_3}{AB}$$

The accelerations of these two points can now be scaled from the acceleration diagram in [Figure 15.10](#).

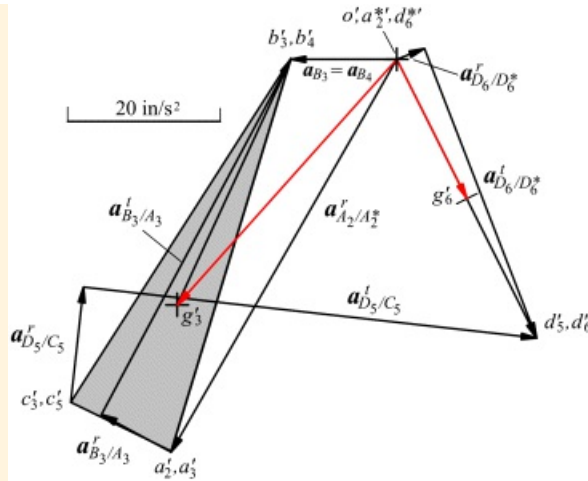


Figure 15.10 The acceleration diagram of [Figure 4.17](#) in [Chapter 4](#): modified to allow computation of the acceleration of points G_3 and G_6 . The acceleration image is used. It is necessary only to construct the position of point g'_3 such that $\angle ab'g'_3 = \lambda$ and $fb'g'_3/a'b' = BG_3/AB$, and of point g'_6 at the midpoint of $o'd'$.

$$a_{G_3} = 1.00 \times 20 = 20.0 \text{ in/s}^2 \text{ at } -63^\circ \text{ to the x axis}$$

$$a_{G_6} = 2.16 \times 20 = 43.2 \text{ in/s}^2 \text{ at } -132^\circ \text{ to the x axis}$$

Scaling $a_{B3/A3}^r$ from [Figure 15.10](#) gives

$$a_3 = \frac{a_{B3/A3}^r}{BA} = \frac{2.63 \times 20}{2.75} = 19.1 \text{ rad/s}^2 \text{ CCW}$$

In addition, we need the angular acceleration information that was derived in Example 4.4 of [Chapter 4](#):

$$\alpha_C = 40/3.0 = 13.3 \text{ rad/s}^2 \text{ CCW}$$

$$\alpha_S = 14.9 \text{ in/s}^2 \text{ (to the left)}$$

It may be noted that we have not attempted to find the acceleration of the center of mass of link 2, and in fact there is not sufficient information to find it. This is because it is not needed as long as we are seeking only the torque, T , and not the reaction force at point A , and as long as the angular velocity of member 2 is constant.

Step 3 in the procedure given above can now be addressed. The free-body diagrams for the mechanism are shown in [Figure 15.11](#).

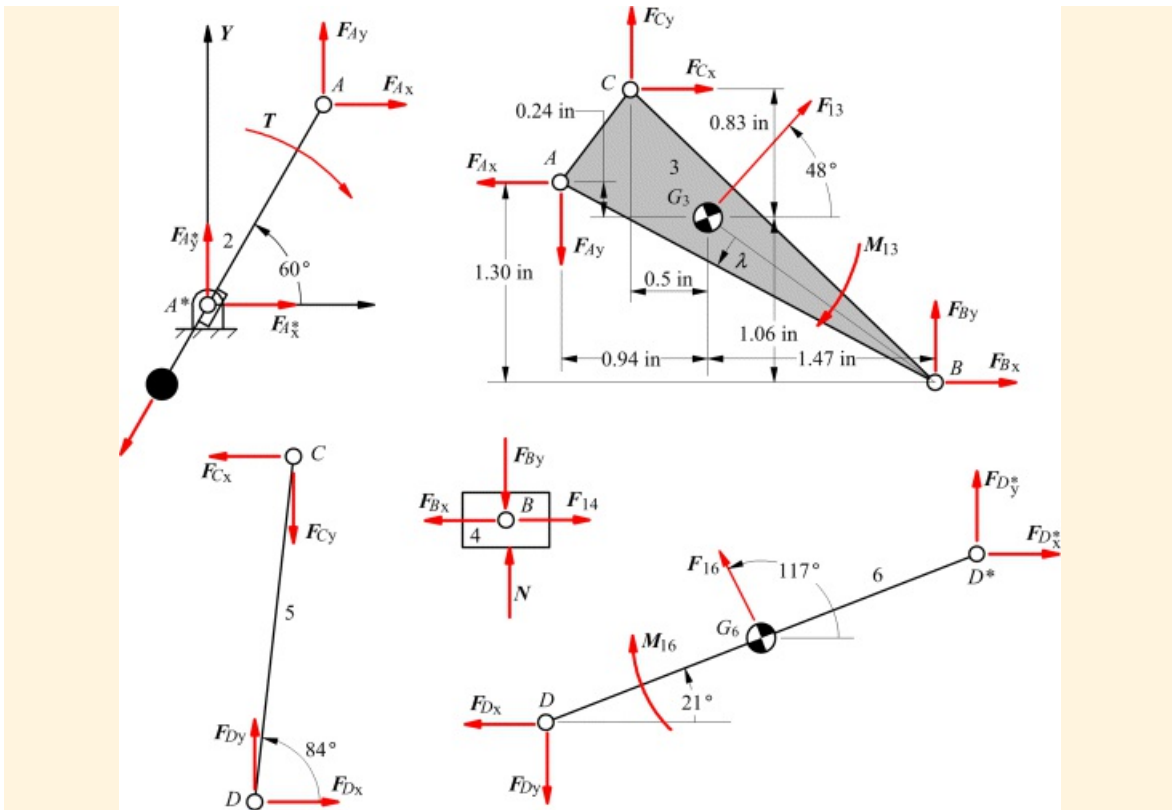


Figure 15.11 Free-body diagrams for Example 15.4.

The inertia force acting at G_3 is calculated as follows

$$F_{I3} = -m_3 \ddot{x}_{G_3} = \frac{0.5}{32.2} \times \frac{43.2}{12} = 0.056 \text{ lb at } 48^\circ \text{ to the } x \text{ axis}$$

Notice that the direction of F_B is determined by simply adding 180° to the direction of α_{G_3} .

Similarly, the inertia force acting at G_6 is calculated

$$F_{I6} = -m_6 \ddot{x}_{G_6} = \frac{0.5}{32.2} \times \frac{20.0}{12} = 0.026 \text{ lb at } 117^\circ \text{ to the } x \text{ axis}$$

The inertia force acting on the translating mass 4 is

$$F_{I4} = -m_4 \ddot{x}_{G_4} = \frac{1.0}{32.2} \times \frac{13.9}{12} = 0.036 \text{ lb along the } x \text{ axis}$$

The inertia couple acting on member 3 is calculated as follows

$$M_{I3} = -I_3 \alpha_3 = -m_3 k_3^2 \alpha_3 = \frac{0.5}{32.2} \times \left(\frac{0.87}{12} \right)^2 \times 19.1 = 0.00156 \text{ ft-lb} = 0.0187 \text{ in-lb CW}$$

The inertia couple acting on member 6 is

$$M_{I6} = -J_S \ddot{x}_S = -m_S k_S^2 \ddot{x}_S = \frac{0.5}{32.2} \times \left(\frac{0.87}{12} \right)^2 \times 13.3 = 0.00109 \text{ ft-lb} = 0.0130 \text{ in-lb CW}$$

Step 4 in the procedure is the drawing of free-body diagrams of all members.

Step 5 of the solution procedure is writing dynamic equilibrium equations for each free-body diagram. Starting with member 2

$$\sum M_{A^*} = 0 : F + F_{A_x} \times 1.5 \sin 60^\circ = F_{A_y} \times 1.5 \cos 60^\circ$$

Here we have chosen to take moments about point A^* because doing so eliminates the components of F_{A^*} and also F_D . Force equilibrium would, in this case, give two equations that could ultimately be solved for the components of F_{A^*} . Since we are not interested in F_{A^*} , the components are not written out.

Moving to member 3

$$\begin{aligned} \sum F_x &= 0 : F_{C_2} - F_{B_3} + 0.036 \cos 48^\circ = F_{A_x} \\ \sum F_y &= 0 : F_{C_2} + F_{B_3} + 0.036 \sin 48^\circ = F_{A_y} \\ \sum M_{G_3} &= 0 : F_{C_2} \times 0.83 + F_{C_2} \times 0.5 + 0.0187 = F_{A_x} \times 0.24 + F_{A_y} \times 0.94 + F_{B_3} \times 1.06 + F_{B_3} \times 1.47 \end{aligned}$$

Here the choice of the point about which to take moments makes little difference. Use of G_3 slightly simplifies the equation since it eliminates F_{B_3} .

Continuing with member 4

$$\sum F_x = 0 : \quad F_{D_4} = 0.036 \delta = F_{B_2}$$

$$\sum F_y = 0 : \quad N = F_{B_2}$$

No moment equation is written because this member is restrained from rotation.

Member 5 is a two-force member because its mass and moment of inertia are neglected. This implies both that $F_C = F_D$ and that both forces are aligned and opposed along the axis of the member. The alignment along the axis is required by the moment equation. Consequently

$$\sum F_x = 0 : \quad F_{C_5} = F_{D_5}$$

$$\sum F_y = 0 : \quad F_{C_5} = F_{D_5}$$

$$\sum M_D = 0 : \quad F_{C_5} \times 2.25 \cos 84^\circ = F_{C_5} \times 2.25 \sin 84^\circ$$

or

$$F_{C_7} = F_{D_x} \tan 84^\circ \text{ and } F_{D_y} = F_{D_x} \tan 84^\circ$$

Finally, for member 6

$$\rightarrow M_{S^*} = 0 : 0.0130 + F_{D_x} \times 3 \sin 21^\circ + 0.026 \times 1.5 \sin 96^\circ = F_{D_y} \times 3 \cos 21^\circ$$

The force equilibrium equations would yield only expressions for the components of F_{D^*} . Since we are not interested in F_{D^*} and can eliminate it by taking moments about point D^* , the force equilibrium equations are not needed. Substitution of the previous relationship between F_{D_x} and F_{D_y} into this equation gives

$$0.0130 - F_{D_x} \times 3 \sin 21^\circ + 0.026 \times 1.5 \sin 96^\circ = F_{D_x} \tan 84^\circ \times 3 \cos 21^\circ$$

or

$$F_{C_7} = F_{D_x} = 0.0020 \text{ kN}$$

Then

$$F_{C_7} = F_{D_y} = 0.0020 \times \tan 84^\circ = 0.0193 \text{ kN}$$

Substitution of these values into the force equilibrium equations of member 3 gives

$$F_{A_c} = 0.0395 + F_{B_c} = 0.0395 - 0.036 = 0.0755$$

$$F_{A_y} = 0.0615 + F_{B_y}$$

Substitution into the rotation equations gives

$$\begin{aligned} 0.0300 &= 0.24 F_{A_x} + 0.94 F_{A_y} + 1.06 F_{B_x} + 1.47 F_{B_y} \\ &= 0.24 \times 0.0755 + 0.94 F_{A_y} + 1.06 \times 0.036 + 1.47 F_{B_y} \end{aligned}$$

or

$$0 = 0.0263 + 0.94 F_{A_y} + 1.47 F_{B_y}$$

Elimination of F_{B_y} gives

$$0 = 0.0263 + 0.94 F_{A_y} + 1.47(F_{A_y} - 0.0009)$$

or

$$\bar{F}_{A_y} = 0.0262 \text{ lb}$$

The values obtained for F_{B_x} and F_{B_y} can be substituted into the moment equation of member 2 to give

$$T = 0.0755 \times 1.5 \sin 60^\circ - 0.0262 \times 1.5 \cos 60^\circ$$

or

$$T = -0.078 \text{ in-lb}$$

Therefore, when passing through this position a torque of 0.078 in-lb in the CCW direction is needed to prevent member 2 from accelerating and to maintain its constant speed of rotation.

Further examples of dynamic equilibrium of systems of rigid bodies may be found in [Chapter 16](#) in the context of balancing reciprocating machines. See Examples 16.4 and 16.5.



15.4 Flywheels

Flywheels are used to store energy and to smooth speed fluctuations during a machine cycle. They serve a function similar to that of a capacitor in an electric circuit or an accumulator in a hydraulic circuit. In a typical situation where a flywheel is required, a machine that needs to operate at near-constant speed must be matched to one that produces significant torque fluctuations. For example, an electric motor that works best at near-constant speed may need to drive a punch press or reciprocating compressor that produces a strongly fluctuating load torque. Conversely, an internal combustion engine that produces strong torque fluctuations may be required to drive a load shaft at close to constant velocity.

Actually, a flywheel is an essential component of an internal combustion engine because the cycle includes strokes in which air is being compressed in the cylinder, so the engine is then absorbing energy rather than producing it. The flywheel allows energy to be stored during the power stroke when the charge is burning and expanding and returned to the piston when it is compressing the charge. This is also a reason for the use of engines with multiple cylinders, since the torque fluctuations for different cylinders can be evenly distributed over the engine cycle, reducing the output torque fluctuations and reducing the size of the requisite flywheel.

If the machine-induced energy fluctuations are known and the allowable speed fluctuation is specified, the requisite flywheel inertia is readily calculated. The coefficient of speed fluctuation, c_3 , is defined as

$$c_3 = \frac{\omega_2 - \omega_1}{\bar{\omega}} \quad (15.13)$$

where ω_2 is the maximum flywheel angular velocity, ω_1 is the minimum flywheel angular velocity, and $\bar{\omega}$ is the average flywheel velocity. The allowable fluctuation coefficient varies by application, from 0.05 or more for agricultural and mining machinery down to about 0.003 for alternating-current generators. Values appropriate to given applications may be found in machine design handbooks.

If the moment of inertia of the flywheel is I_w , the change in flywheel energy is

$$\Delta E = \frac{I_w}{2} (\omega_2^2 - \omega_1^2) \quad (15.14)$$

Although speed may fluctuate asymmetrically over the cycle, it is often adequate to approximate the average angular velocity as the mean of ω_2 and ω_1

$$\bar{\omega} = \frac{\omega_2 + \omega_1}{2}$$

Because $2\bar{\omega} = \omega_2 + \omega_1$ and $c_3\bar{\omega} = \omega_2 - \omega_1$

$$\omega_2^2 - \omega_1^2 = 2c_3\bar{\omega}^2$$

Then

$$I_w = \frac{\Delta E}{c_3\bar{\omega}^2} \quad (15.15)$$

can be used to estimate the required flywheel inertia.

The following example illustrates the way in which a flywheel can be sized for a particular application.



Example 15.5 Punch Press

A machine used to punch holes in a metal plate is to be driven by an induction motor with rated speed 1700 rpm. The allowable drop in motor speed is 15 percent. The machine will be required to punch holes of up to 1 in diameter in a steel plate that is up to 0.5 in thick with shear strength of 50,000 psi. The holes are to be punched at a rate of one every 2.5 s. Find the requisite motor power and flywheel inertia.

Solution

The maximum punch force is approximately

$$F = \pi d t \tau$$

where $\tau = 50,000$ psi is the shear strength of the material, d is the diameter of the hole, and t is the plate thickness. That is, the maximum punch force is simply the shear area multiplied by the shear strength. The force profile as the punch penetrates is irregular with the peak force occurring at a penetration distance of about 3/8 of plate thickness. A typical profile is sketched in [Figure 15.12](#).

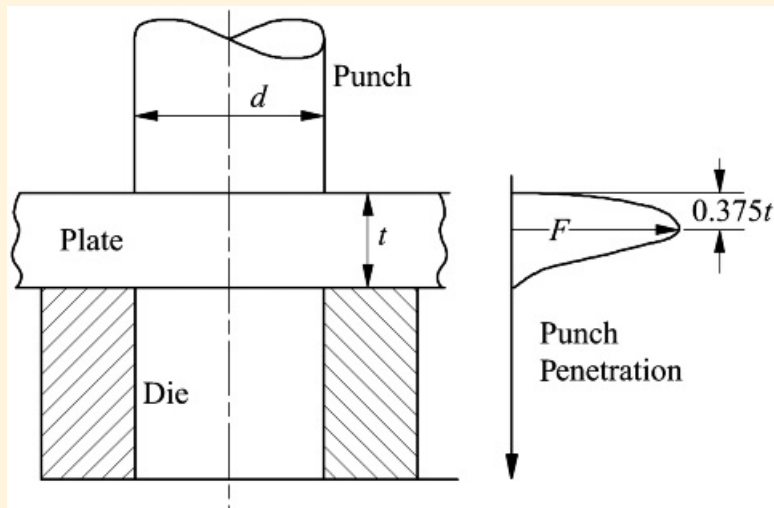


[Figure 15.12](#) Punch force as a function of depth of penetration. The peak force, F , occurs at a penetration depth of about $0.375t$, where t is the plate thickness.

The area under the curve of punch force versus depth of penetration is the energy used in the punching operation. It can be measured experimentally, but the punch force profile can be roughly approximated as a triangle. Therefore

$$\Delta E = \frac{F_0}{2} \cdot 0.375t \quad (15.16)$$

is a frequently used approximation. In the present instance

$$F = \pi \times 1.0 \times 0.5 \times 50,000 = 78,540 \text{ lb}$$

so

$$\Delta F = 78,540 \times 0.5 / 2 = 19,620 \text{ lb-in} = 1,640 \text{ ft-lb}$$

At a punching rate of one hole once every 2.5 s, the average power required is

$$P = 1640 / 2.5 = 656 \text{ ft-lb/s} = 1.12 \text{ hp}$$

This is the power for which the motor should be sized.

Now, if the rated motor speed is 1700 rpm we can assume that the maximum motor speed will be this value so

$$\omega_2 = \frac{1,700 \times 2\pi}{60} = 178 \text{ rad/s}$$

Also, we can assume that the motor speed quickly drops to its minimum value during the punch stroke and that it is then built back up approximately uniformly to the maximum value in the remainder of the cycle time. Therefore

$$\bar{\omega} = \frac{\omega_1 + \omega_2}{2}$$

is an adequate approximation to the average motor speed, $\bar{\omega}$.

Since the allowable motor speed variation is 15 percent, $c_0 = 0.15$ and so, applying [Equation 15.13](#),

$$0.15 = \frac{\omega_2 - \omega_1}{\bar{\omega}} = \frac{2(\omega_2 - \omega_1)}{\omega_2 + \omega_1}$$

Substitution of $\omega_2 = 178$ gives

$$0.075(178 + \omega_1) = 178 - \omega_1$$

or

$$\omega_1 = 153 \text{ rad/s}$$

Also, applying [Equation 15.14](#)

$$1,640 = \frac{\rho}{2} (178^2 - 153^2)$$

or

$$J_g = 0.396 \text{ ft-lb s}^2$$

Sizing of a flywheel for an internal combustion engine starts with the pressure-volume chart of the engine's combustion cycle. Multiplication of the pressure by the piston area produces the piston force. Force analysis of the slider-crank mechanism of the engine with the piston force as input produces the crankshaft torque as a function of crank angle. The flywheel is then sized to bring the speed fluctuations produced by the torque variation within acceptable limits. Although this process is beyond the scope of this book, it is fully explained in texts on the dynamics of reciprocating machinery.



Problems

15.1 The four-wheeled vehicle shown in [Figure P15.1](#) slides down a steep slope with its rear wheels locked (not moving relative to the body) and its front wheels rolling freely. If M is the mass of the vehicle, h the normal distance from its center of mass, G , to the ground, r the wheel radius, and $2c$ the distance between the axles, find the acceleration of the vehicle. The angle of the slope is θ , and the coefficient of friction between the wheels and the ground is μ . The mass and moment of inertia of each wheel about its axle may be neglected. What is the largest value for the angle θ at which the vehicle will not slide?

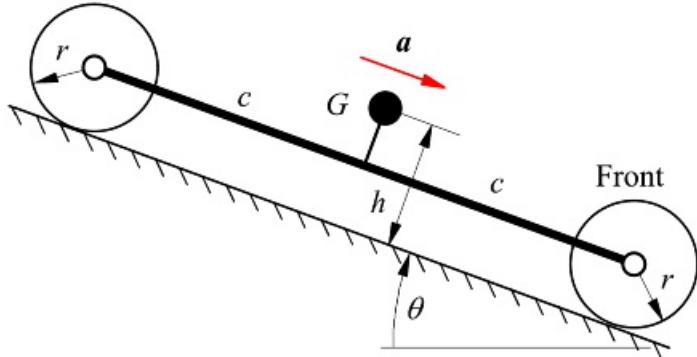


[Figure P15.1](#) Device for Problem 15.1.

15.2 The flyball governor shown in [Figure P15.2](#) is started from rest and accelerated slowly about the axis of rotation. At what speed of rotation will it be in the position shown? Friction may be neglected. Ignore the masses of the four links. Use the following dimensions

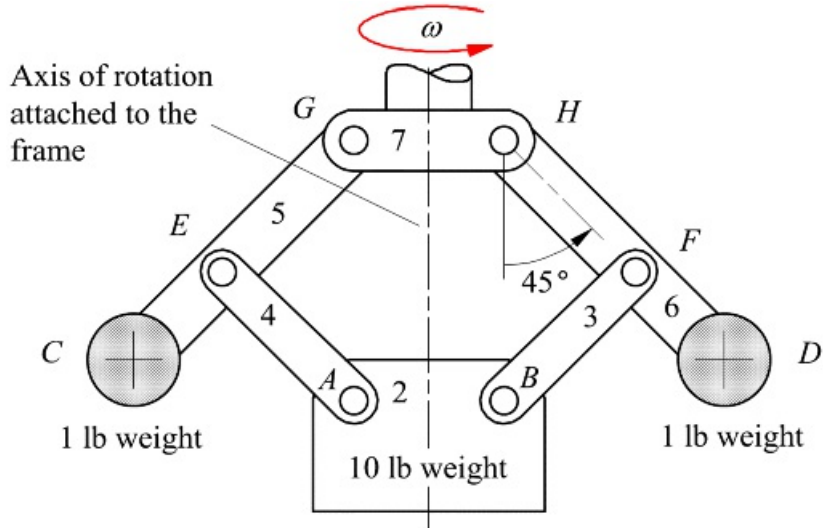


[Figure P15.2](#) Mechanism for Problem 15.2.

$$AG = CG = 2.50 \text{ in} \quad BG = DH = 3.75 \text{ in} \quad CG = DH = 5.54 \text{ in} \quad AB = BF = 3.75 \text{ in}$$

15.3 Solve Problem 15.2 assuming a coefficient of friction of 0.3 at each of the six pin joints. The diameter of each joint is 0.8 in.

15.4 A wheel, of mass m and radius r , rolls without slipping on a horizontal plane. It hits a step of height h . If the velocity of the center of the wheel before striking the step is V , directed as shown in [Figure P15.4](#), find:

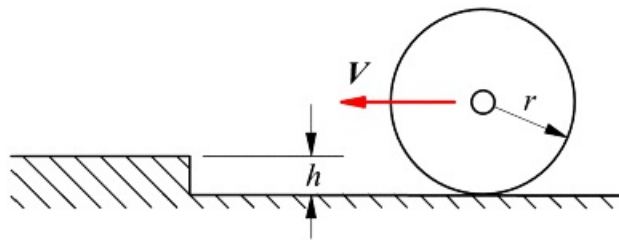


[Figure P15.4](#) Mechanism for Problem 15.4.

1. The magnitude and direction of the velocity of the center of the wheel immediately after the impact
2. The minimum value of V for which the wheel surmounts the step
3. The impulse exerted on the wheel by the edge of the step at impact

The impact may be considered to take place over a vanishingly small time interval. The wheel is assumed to remain in contact with the edge of the step after the impact. The wheel may be considered to have its moment of inertia about its center in the direction of rotation to be $I = mr^2$.

[15.5](#) In [Figure P15.5](#), link 2 rotates at an angular velocity of 20 rad/s (CW) and angular acceleration of 140 rad/s² (CW). Find the torque that must be applied to link 2 to maintain equilibrium. Link 2 is balanced so that its center of mass is at the pivot A^* . The center of mass of link 3 is at A , and the mechanism moves in the horizontal plane. Friction may be neglected.

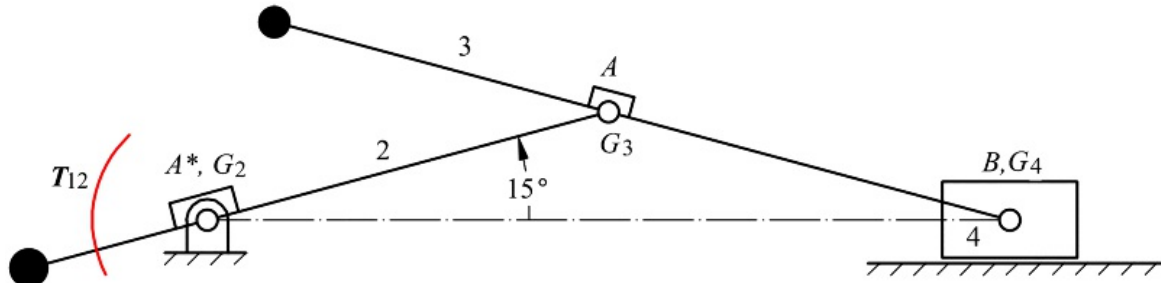


[Figure P15.5](#) Mechanism for Problem 15.5.

$A_1^*A_1 = AB = 100 \text{ mm}$	$m_3 = 0.74 \text{ kg}$	$m_4 = 0.32 \text{ kg}$
$I_{G2} = .00205 \text{ N-s}^2\text{-m}$	$I_{G3} = .0062 \text{ N-s}^2\text{-m}$	

[15.6](#) Find the external torque (T_{12}) that must be applied to link 2 of the mechanism illustrated in [Figure P15.6](#) to drive it at $\omega_2 = 1,800 \text{ rad/s CCW}$ and $a_2 = 0 \text{ rad/s}^2$. Link 2 is in a horizontal position, and it is balanced so that its center of mass is at the pivot O_2 . The mechanism moves in the horizontal plane, and friction may be neglected.

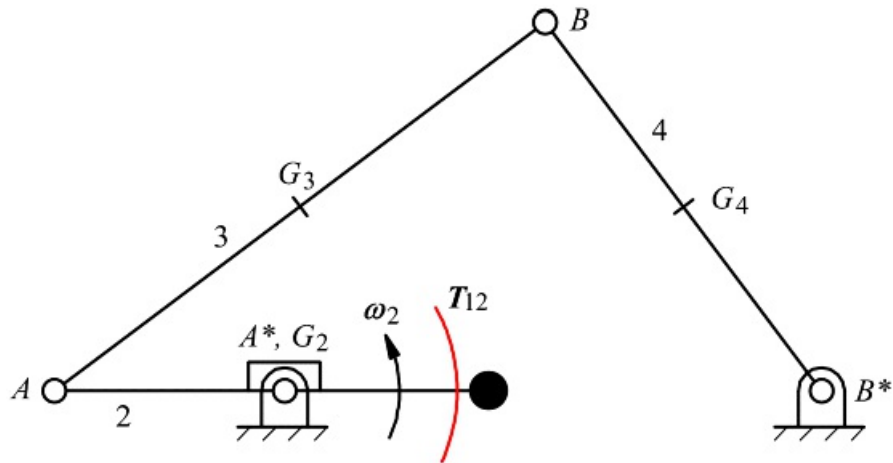


[Figure P15.6](#) Mechanism for Problem 15.6.

$$W_3 = 0.708 \text{ lb} \quad I_{G_3} = 0.0154 \text{ lb-s}^2\text{-in} \quad W_4 = 0.780 \text{ lb} \quad I_{G_4} = 0.0112 \text{ lb-s}^2\text{-in}$$

$$A^*A = 3.0 \text{ in} \quad AB = 8.0 \text{ in} \quad B^*B = 6.0 \text{ in} \quad A^*B^* = 7.0 \text{ in} \quad AG_3 = 4.0 \text{ in} \quad BG_4 = 3.0 \text{ in}$$

15.7 Find the external torque (T_{12}) that must be applied to link 2 of the mechanism in [Figure P15.7](#) to drive it at $\omega_2 = 210 \text{ rad/s}$ CCW and $a_2 = 0 \text{ rad/s}^2$. Link 2 is balanced so that its center of mass is at the pivot A^* . The mechanism moves in the horizontal plane and friction may be neglected.

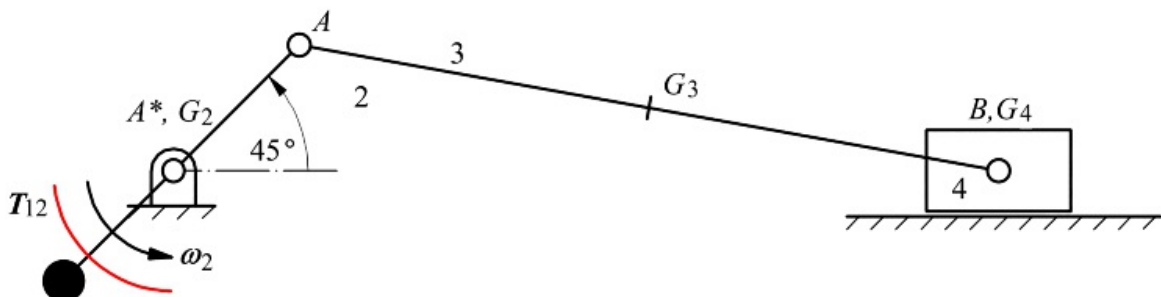


[Figure P15.7](#) Mechanism for Problem 15.7.

$$W_3 = 3.4 \text{ lb} \quad I_{G_3} = 0.1035 \text{ lb-s}^2\text{-in} \quad W_4 = 2.86 \text{ lb}$$

$$A^*A = 3.0 \text{ in} \quad AB = 12.0 \text{ in} \quad BG_3 = 6.0 \text{ in}$$

15.8 In the mechanism shown in [Figure P15.8](#), the center of mass of link 3 is at G_3 , which is located at the center of link 3. The mass of link 3 is 0.5 kg. Its moment of inertia about G_3 is 0.0012 N-s²-m. The weights and moments of inertia of members 2 and 4 may be neglected. Link 2 is driven at a constant angular velocity of 50 rad/s CW by the torque applied to link 2. The mechanism moves in the horizontal plane, and friction may be neglected.

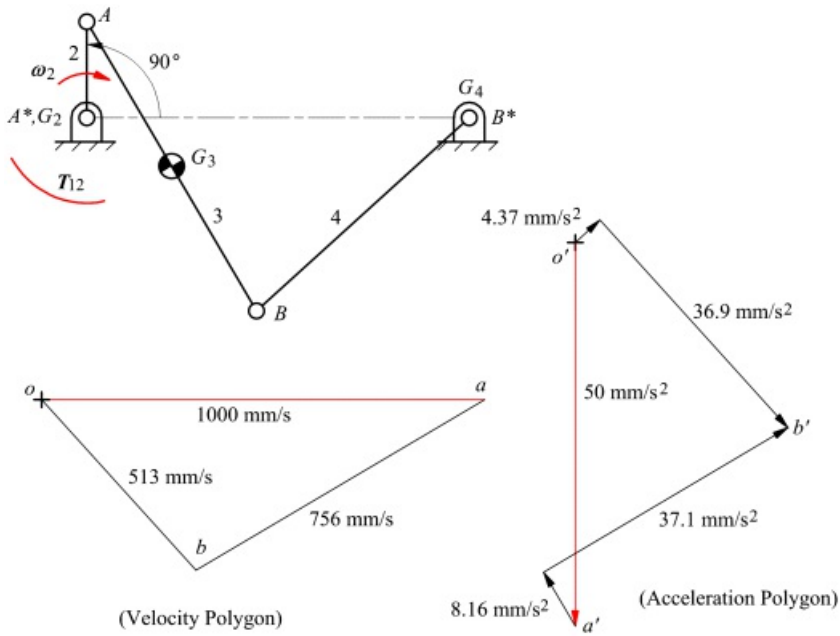


[Figure P15.8](#) Mechanism for Problem 15.8.

1. Find the magnitudes and directions of the inertia force and inertia torque acting on link 3.
2. Find the magnitudes and directions of the forces exerted on link 3 by link 2 at *A* and by link 4 at *B*.

$$A^*A = 20 \text{ mm} \quad AB = 70 \text{ mm} \quad B^*B = 60 \text{ mm} \quad A^*B^* = 80 \text{ mm}$$

15.9 Link *AB* of the geared five-bar linkage shown in [Figure P15.9](#) drives CCW against a load torque $T_{15} = 25 \text{ in-lb}$. If $\omega_2 = 0.001 \text{ rpm CW}$, find the driving torque T_{12} . The mechanism moves in the horizontal plane, and friction may be neglected. The gears 2 and 3 are represented by their pitch circles. Both gears turn on bearings supported by the tie link, 4. The weight of link 2 is small and can be neglected. Gear 3 is 0.2 in thick and may be treated as a solid disk. The weight of gear 3 is 0.235 lb, and $\theta = 135^\circ$.

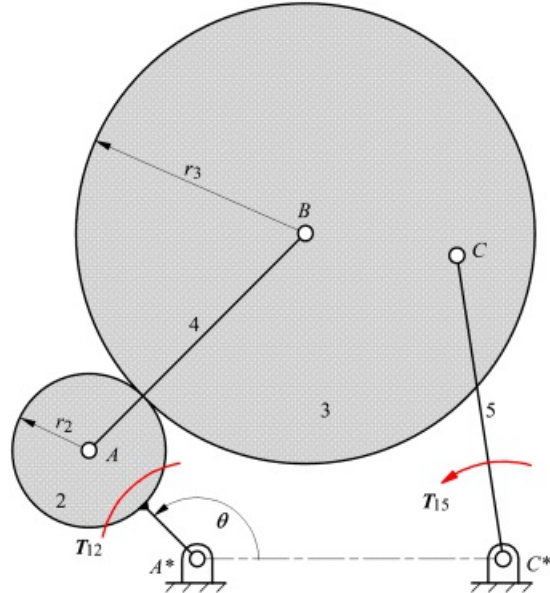


[Figure P15.9](#) Mechanism for Problem 15.9.

$$A^*A = 1.0 \text{ in} \quad AR = 2.0 \text{ in} \quad BC = 1.0 \text{ in} \quad C^*C = 2.0 \text{ in} \quad A^*C^* = 2.0 \text{ in} \quad r_2 = 0.5 \text{ in} \quad r_3 = 1.5 \text{ in}$$

15.10 A punch press similar to that of Example 15.5 is to punch holes of diameter up to 0.75 in through steel plate up to 0.375 in thick. The shear strength of the steel will range up to 60,000 psi. The rated speed of the motor is 1500 rpm, and a 10 percent drop in motor speed is allowable. If holes are to be punched at a maximum rate of 1 per second, find the requisite motor power and flywheel inertia.

15.11 A uniform rectangular plate is suspended from a rail by means of two bogies as shown in [Figure P15.11](#). The plate is connected to the bogies by means of frictionless hinge joints at A and at B . At time $t = 0$ the pin of joint B breaks, allowing the plate to swing downward. Write the equations of motion of the plate as it starts to move. Hence find its initial angular acceleration and the initial linear acceleration of point A .

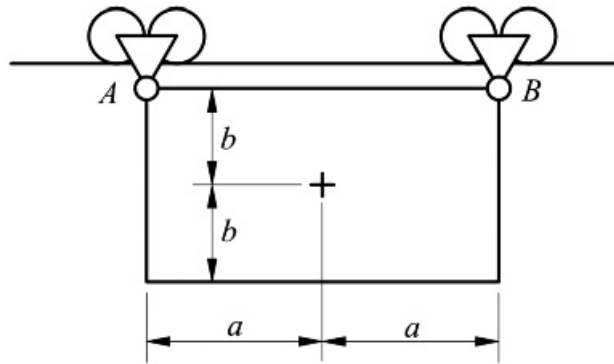


[Figure P15.11](#) Device for Problem 15.11.

You may assume that the rollers that support point A are frictionless and that they remain in contact with the rail. You may also assume that the angular displacement from the initial position is small. The moment of inertia of a uniform rectangular plate with sides $2a$ and $2b$ about an axis normal to its plane passing through its centroid is $m[(2a)^2 + (2b)^2]/12$, where m is the mass of the plate.

16

STATIC AND DYNAMIC BALANCING

Prerequisite Knowledge Needed for Chapter 16

This chapter depends on material presented in [Chapter 15](#).



16.1 Introduction

Fast-moving machinery with rotating or reciprocating masses is a significant source of vibration excitation. A major theme in machine dynamics and machine design is seeking to minimize the fluctuating forces that such machinery applies to its environment via its mounts. Rapidly rotating masses such as those in electric motors and generators, steam and gas turbines, vehicle wheels, and many other machines can generate significant fluctuating forces with even tiny amounts of unbalance. Combinations of rotating and reciprocating masses are found in internal combustion engines, pumps, compressors, and many other types of machinery. They are strong generators of fluctuating forces, but those forces can be at least partially balanced by appropriately placed weights. It is necessary to discuss the procedures used for balancing in these somewhat diverse types of systems.

When any mechanism is operated at high speeds, two types of forces must be considered. These are externally applied forces and inertial forces. Inertial forces arise when the individual members are subjected to large accelerations. In general, the inertial force system acting on a given member can be represented as an inertia force acting on a line through the center of mass, together with an inertia torque, as was described in Section 15.2. The force is given by $-ma$ and the couple by $I\alpha$, where m is the mass of the member, I is the mass moment of inertia about the center of mass, a is the linear acceleration of the center of mass, and α is the angular acceleration of the member. In high-speed machinery, the inertial forces may be larger in magnitude than the external forces. Consequently, when the mechanism is designed, both types of forces must be taken into account.

In general, the external forces will be associated with the useful function that the mechanism is to perform and with driving the mechanism. There is often little that can be done to alter their magnitudes. On the other hand, the inertial forces are due entirely to the mass and motion characteristics of the machine members. Therefore, prudent design practice dictates that the inertial forces be minimized. This can be done either by reducing the masses and moments of inertia of the moving members or by reducing the linear and angular accelerations. The masses may be reduced by using lighter materials and optimal geometries. For a given kinematic geometry, the angular accelerations cannot be reduced. However, the linear accelerations of the centers of mass can be reduced by moving the centers of mass toward points of zero acceleration. The way this is often done is to add mass in the form of balance weights to move the overall center of mass of a given member to a location of reduced acceleration. For a single rotor, this means moving the center of mass onto the axis of rotation. More complicated systems require some ingenuity to cause the inertial forces on different members to counteract each other, at least in part.



16.2 Single-Plane (Static) Balancing

In spite of all the care that may be taken in the design and manufacture of a rotating part, whether the part is completely machined, cast, or forged or is assembled from various parts as in the case of the armature of an electric motor, it rarely runs smoothly, particularly if the operating speed is high. Variations in dimensions due to machining, variations in homogeneity of the material, variations in the methods of assembly, and eccentricity of bearing surfaces all contribute to offsetting the center of mass from the axis of rotation.

The curve in [Figure 16.1](#) emphasizes the effect of a small amount of unbalance at high speeds. The curve shows the centrifugal force produced by an inch-ounce (in-oz) of unbalance at various angular speeds. (An in-oz is defined as 1 ounce of weight at 1 inch from the axis of rotation.) The centrifugal force due to 1 in-oz at 1000 rpm is 1.76 lb. At 10,000 rpm, it is 176 lb. That is, it increases as the square of the speed. It is evident that the centrifugal force produced on a large rotor can be very large, even if the center of gravity is displaced only a small amount from the axis of rotation, and consequently large shaking forces will be produced on the structure. For example, consider the rotor of an aircraft gas turbine weighing 400 lb that operates at 16,000 rpm and suppose the center of mass is 0.001 in from the axis of rotation. The 6.4 in-oz of unbalance would cause a centrifugal force of

$$F = mE\omega^2 = \left(\frac{400}{32.2}\right) \left(\frac{0.001}{12}\right) \left(\frac{(2\pi)16,000}{60}\right)^2 = 2924 \text{ lb}$$

Such a force could cause considerable damage to the machine. Since it is usually impossible to manufacture the rotor of a machine so that the center of gravity will lie within 0.001 in of the axis of rotation, the part must be balanced after manufacture, and the balancing is done experimentally.

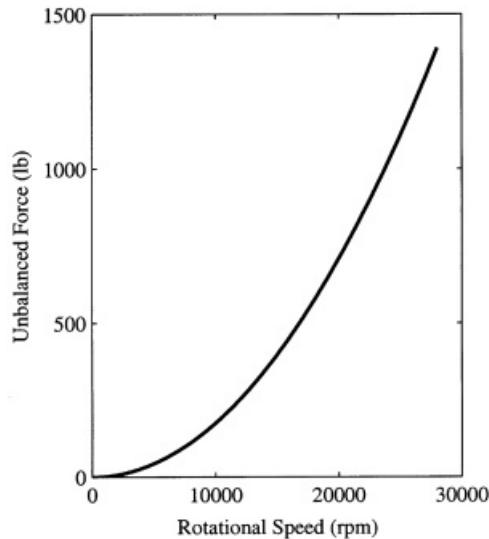


[Figure 16.1](#) Effect of 1 in-oz of unbalance.

To illustrate the principles that are involved in balancing a rotating mass, we will first consider a rod rotating at a constant angular velocity ω to which is attached a single concentrated mass of weight W at radius r . Let W_e be the weight (called the counterbalance weight) that must be added at some radius r_e to produce equilibrium as shown in [Figure 16.2](#). Static balance will be produced if the sum of the moments of the weights about the axis of rotation is zero. That is

$$-Wr \cos \theta + W_e r_e \cos \theta = 0$$

or

$$W_e r_e = W r \quad (16.1)$$

If the value of r_e is arbitrarily chosen, then the value of W_e can be found from [Equation 16.1](#). When the system is statically balanced, the shaft will not have any tendency to rotate in its bearings under the influence of gravity regardless of the position to which it is rotated. If the system is rotated with angular velocity ω , the static balance condition also ensures that the sum of the inertia forces is zero, as illustrated in [Figure 16.2](#). That is,

$$\frac{W}{g} r \omega^2 - \frac{W_e}{g} r_e \omega^2 = 0$$

or

$$W_e r_e = W r$$

which is identical to [Equation 16.1](#).

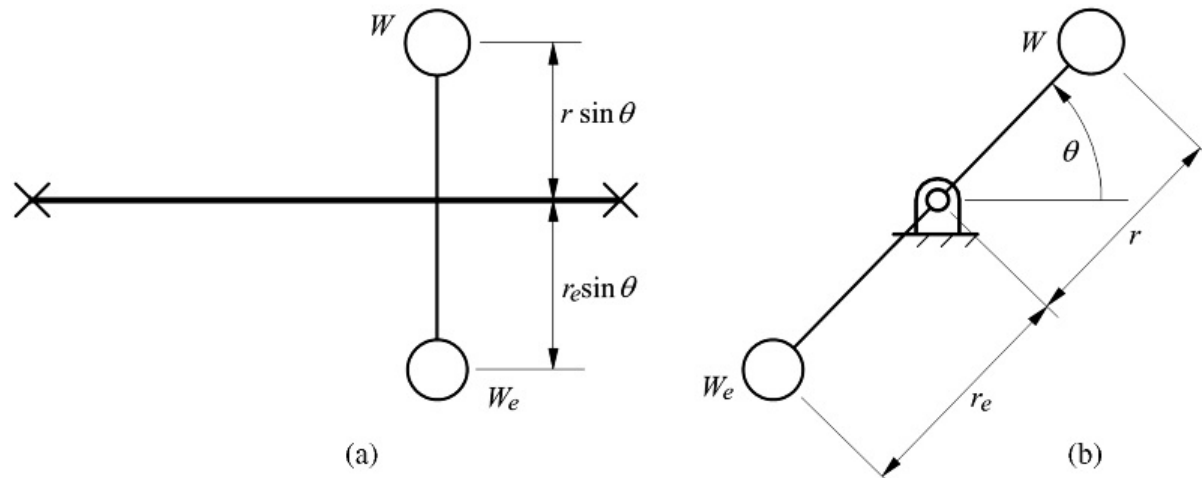


[Figure 16.2](#) A single rotating mass.

The simplest situation is a single rotor that can be regarded as rotating in a single plane, such as that just considered. This type of balancing is called static balancing because a static-type balance procedure in which the measurements are made on the rotor while it is stationary can be used. If the rotor cannot be regarded as spinning in a single plane, the balance procedure involves measurements while the rotor is spinning. This situation is discussed in Section 16.3. The procedure is called dynamic balancing.

There are situations in which an eccentric mass is deliberately spun to produce a rotating force vector. Example 16.1 concerns an eccentric rotor used to excite vibratory motion of a screen used to sort material particles by size.



Example 16.1 Eccentric Mass Out of Balance

An eccentric mass is rotated on a shaft mounted on the frame of a vibrating screen used to sort iron ore into different sizes. The mass is shaped as a circular sector as shown in [Figure 16.3](#). The mass weighs 20 lb, and its mass center is 4 in from the shaft axis. If it is rotated at 600 rpm, what is the force that it exerts on the shaft and hence on the frame of the screen?

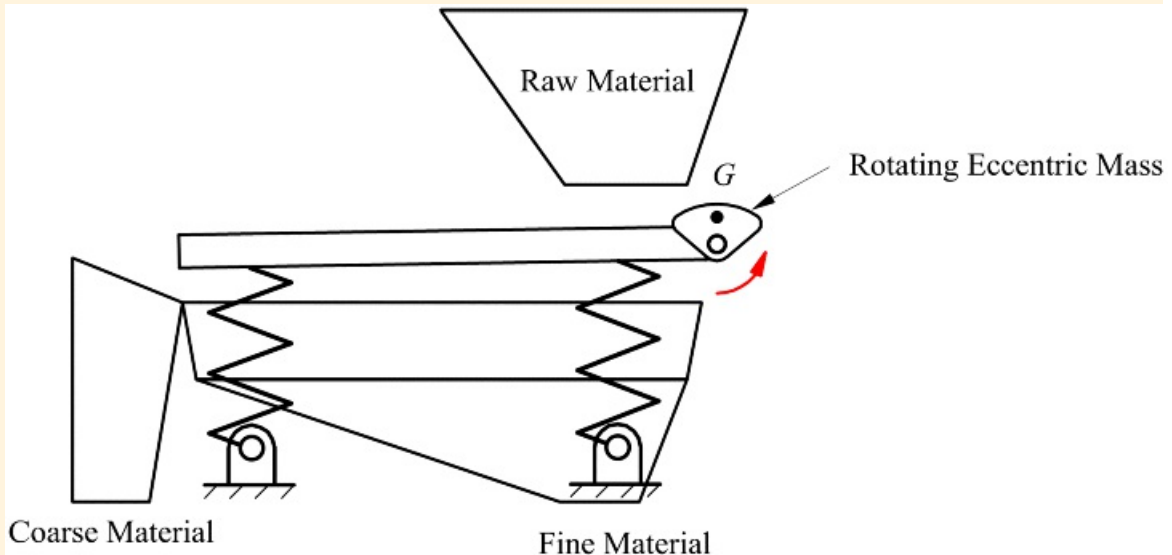


[Figure 16.3](#) The vibrating screen arrangement discussed in Example 16.1. G is the center of mass of the rotor.

Solution

The exciting force here is simply the centrifugal force of the rotating mass. The magnitude of the angular velocity is

$$\omega = 600 \times 2\pi / 60 = 62.83 \text{ rad/s}$$

so the magnitude of the acceleration of the center of mass is

$$a = r\omega^2 = (4/12) \times 62.83^2 = 131.6 \text{ ft/s}^2$$

Therefore, the magnitude of the rotating force is

$$F = ma = (20/32.2) \times 131.6 = 817 \text{ lb}$$

The product of the mass of a rotor and the distance from its center of mass to the shaft axis is called the *unbalance*. An unbalance of a given magnitude may be removed by adding a mass 180° out of phase with it or by subtracting mass with the same unbalance in phase with it. Referring to [Figure 16.4](#), if the mass of the rotor is m_A and is located at point A , then its unbalance is $m_A r_A$. If a balancing mass is to be placed at point B directly opposite point

A , then its mass must be m_B such that $m_B r_B = m_A r_A$. Similarly, balance can also be achieved by removing mass m_C at point C on the same line with A and the shaft axis provided $m_C r_C = m_A r_A$.

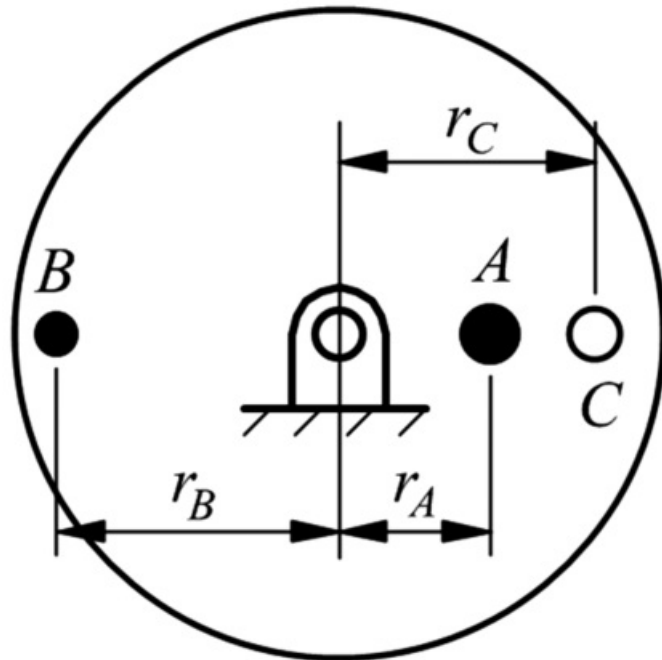


[Figure 16.4](#) A rotor with an eccentric mass with mass center at point A . The unbalance can be removed by placing a mass at point B or removing a mass at point C .



Example 16.2 Static Balancing

A factory producing gear sets statically balances spur gear wheels using the following procedure ([Figure 16.5](#)).

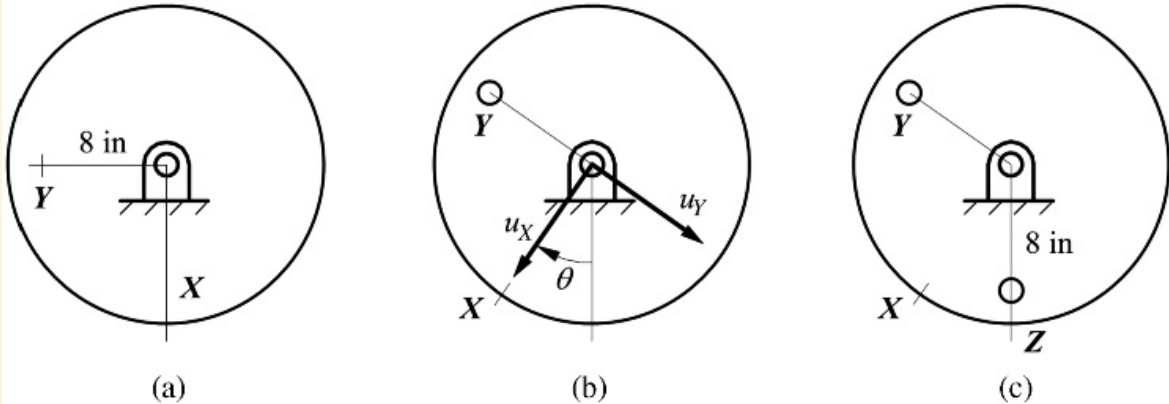


[Figure 16.5](#) The static-balance procedure used in Example 16.2. Three stages in the process are shown from left to right.

The wheel is mounted on a spindle that turns in very low friction bearings. The wheel is allowed to turn freely under gravity until it comes to rest. The low point, X , is marked. A small, known mass, m_Y , is next removed from the wheel at point Y , which is 90° clockwise from X and at a set radius, r_Y . The wheel is then replaced on the spindle and comes to rest with point Z at its lowest point. A calculated mass, m_Z , is then drilled out at a specified radius, r_Z , on the radial line through Z to balance the wheel.

If the mass drilled out of a given wheel at point Y weighs 0.1 lb at radius 8 in and the angle, θ , between the radial lines through X and Z is 35° , find the weight of the mass to be removed at Z if it is also drilled out at a radius of 8 in.

Solution

Let the initial unbalance be u_X . The unbalance of the trial mass at point Y is

$$w_Y = 0.1 \times 8 = 0.8 \text{ in-lb}$$

Now, when the wheel is in equilibrium after the trial mass is removed

$$w_Y \sin \theta = w_Y \cos \theta$$

Note that the unbalance is in the *opposite* direction to Y since mass was removed at Y , not added

$$w_Y = 0.8 \cot 35^\circ = 1.143 \text{ in-lb}$$

The total unbalance is then

$$w_Z = w_Y \cos \theta + w_Y \sin \theta = 1.143 \cos 35^\circ + 0.8 \sin 35^\circ = 1.394 \text{ in-lb}$$

Hence the weight of the mass to be removed at Z is

$$m_Z = 1394/\pi = 0.174 \text{ kg}$$



16.3 Multi-Plane (Dynamic) Balancing

If the inertial mass distribution of the rotor cannot be regarded as planar, fluctuating moments will be generated about axes normal to the axis of rotation in addition to the radial forces. Although the system may be statically balanced by eliminating the resultant radial forces, the shaking moments produced can still be potent sources of vibration excitation. Multi-plane or dynamic balancing techniques allow elimination of both radial unbalance forces and moments.

To see how this works, consider the system shown in [Figure 16.6](#). The shaft shown has two rotors mounted on it, each with an unbalance. The shaft turns in two bearings, as shown. First calculate the unbalance forces, F_A and F_C , exerted on the shaft by the bearings.

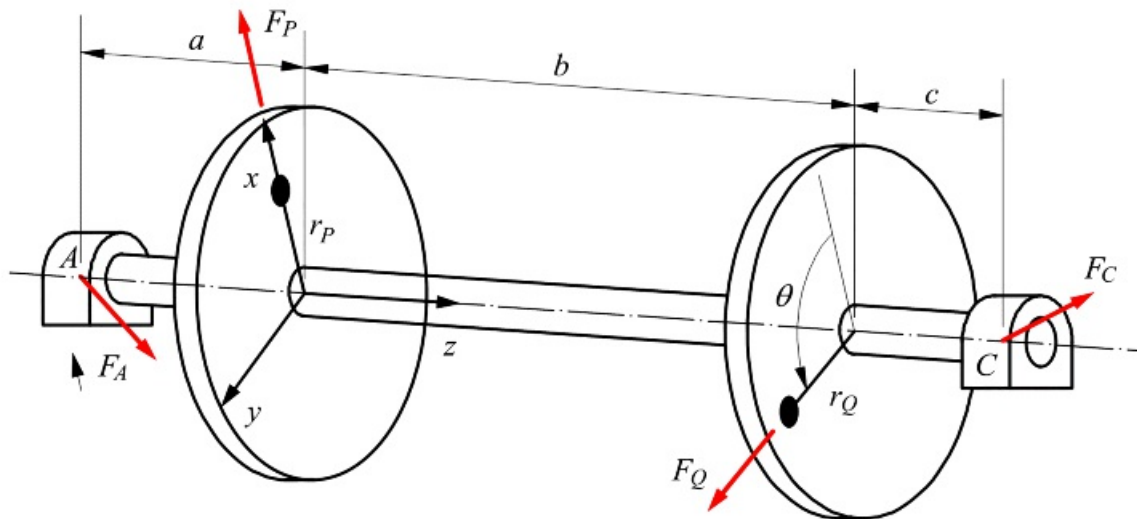


[Figure 16.6](#) A shaft with two rotors, both of which have unbalances. The left rotor plane is designated by P and the right by Q .

The unbalance of the left-hand rotor is

$$m_p = m_p r_p^2$$

where m_p is the mass of the left-hand rotor and r_p is the eccentricity of its center of mass. Hence, at a constant rotation speed ω , the unbalance force magnitude is

$$F_p = m_p \omega^2 r_p$$

Similarly, at the right-hand rotor, the unbalance is

$$m_Q = m_Q r_Q^2$$

where m_Q is the mass of the right-hand rotor and r_Q is the eccentricity of its center of mass. Hence, the unbalance force magnitude is

$$F_Q = m_Q \omega^2 r_Q$$

Using a reference frame fixed to the left-hand rotor as shown in [Figure 16.6](#) with the z axis along the shaft axis and the x axis aligned with the direction of the unbalance u_P , we can write the following force equilibrium equations

$$\sum F_z = 0 : \quad F_P + F_Q \cos \theta + F_{Ax} - F_{Cx} = 0 \quad (16.2)$$

$$\sum F_y = 0 : \quad F_Q \sin \theta + F_{Ay} + F_{Cy} = 0 \quad (16.3)$$

It is convenient to take moments about an axis through A and parallel to y because then F_C is the only unknown force appearing in the equations

$$\sum M_A = 0 : \quad a\hat{k} \times F_P i + (a+b)\hat{k} \times F_Q (\cos \theta i + \sin \theta j) + (a+b+c)\hat{k} \times (F_{Cx} i + F_{Cy} j) = 0$$

or

$$aF_P j + (a+b)F_Q (\cos \theta j - \sin \theta i) + (a+b+c)(F_{Cx} j - F_{Cy} i) = 0$$

Separating the component equations

$$-(a+b)F_Q \sin \theta - (a+b+c)F_{Cy} = 0 \quad (16.4)$$

$$aF_P + (a+b)F_Q \cos \theta + (a+b+c)F_{Cx} = 0 \quad (16.5)$$

We can solve for the components of F_C from [Equations 16.4](#) and [16.5](#) and then solve for the components of F_A from [Equations 16.2](#) and [16.3](#). From [Equation 16.4](#)

$$F_{Cy} = -\frac{(a+b)F_Q \sin \theta}{a+b+c}$$

and from [Equation 16.5](#)

$$F_{Cx} = -\frac{aF_P + (a+b)F_Q \cos \theta}{a+b+c}$$

From [Equation 16.2](#)

$$F_{Ax} = -F_P - F_Q \cos \theta - F_{Cx} = -F_P - F_Q \cos \theta + \frac{aF_P + (a+b)F_Q \cos \theta}{a+b+c}$$

or

$$F_{Ax} = -\frac{(b+c)F_P + cF_Q \cos \theta}{a+b+c}$$

From [Equation 16.3](#)

$$F_{Ay} = -F_Q \sin \theta + \frac{(a+b)F_Q \sin \theta}{a+b+c}$$

or

$$F_{Ay} = -\frac{cF_Q \sin \theta}{a+b+c}$$

Thus the forces applied to the bearings by the shaft are

$$F_A' = -F_A = \frac{\{(b+c)F_P + cF_Q \cos \theta\}i + cF_Q \sin \theta j}{a+b+c}$$

and

$$F_C' = -F_C = \frac{\{aF_P + (a+b)F_Q \cos \theta\}i + (a+b)F_Q \sin \theta j}{a+b+c}$$

These forces rotate with the shaft, so they fluctuate sinusoidally in any given direction.

If the system is statically balanced by adding a balance weight in the plane P , the required unbalance is

$$w = -m_P - m_C = -m_P i - m_C (\cos \theta i + \sin \theta j)$$

Addition of an unbalance of this magnitude and direction in plane P adds a force $\bar{F} = w^2 w = -F_P - F_Q$ to the system. The dynamic equilibrium equations become

$$\sum F_x = 0 : -F_P - F_Q \cos \theta + F_P + F_Q \cos \theta + F_{Ax} + F_{Cx} = 0 \quad (16.6)$$

$$\sum F_y = 0 : -F_Q \sin \theta + F_Q \sin \theta + F_{Ay} - F_{Cy} - F_{Ay} - F_{Cy} = 0 \quad (16.7)$$

Once again, taking moments about an axis through A and parallel to y

$$\sum M_A = 0 : -a\dot{\theta} \times \{F_P i + F_Q (\cos \theta i + \sin \theta j)\} + a\dot{\theta} \times F_P i + (a+b)\dot{\theta} \times F_Q (\cos \theta i + \sin \theta j) + (a+b+c)\dot{\theta} \times (F_{Cx} i + F_{Cy} j) = 0$$

or

$$bF_Q(\cos \theta j - \sin \theta i) + (a+b+c)(F_{Cx}j - F_{Cy}i) = 0$$

Therefore

$$F_{Cx} = -\frac{bF_Q \cos \theta}{a+b+c}$$

$$F_{Cy} = -\frac{bF_Q \sin \theta}{a+b+c}$$

and from [Equations 16.6](#) and [16.7](#)

$$F_{Ax} = -F_{Cx} = \frac{bF_Q \cos \theta}{a+b+c}$$

$$F_{Ay} = -F_{Cy} = \frac{bF_Q \sin \theta}{a+b+c}$$

As may be seen, although the system is now statically balanced (the resultant radial force is zero), the forces exerted on the bearings are not zero, and so a vibration excitation effect is still present. Since $F_A = -F_C$, the bearing forces form a couple with moment

$$M = (a+b+c)k \times (F_{Ax}i + F_{Ay}j) = (a+b+c)(F_{Ax}j - F_{Ay}i) = (a+b+c)F_Q(\cos \theta j - \sin \theta i)$$

This couple rotates with the shaft.



Example 16.3 Two-Plane Balance

A small gas turbine rotor carries four blade disks positioned in planes A , B , C , D as shown in [Figure 16.7](#). The shaft turns in bearings in planes P and Q . Relative to the reference frame shown, the unbalances of the blade disks are, respectively

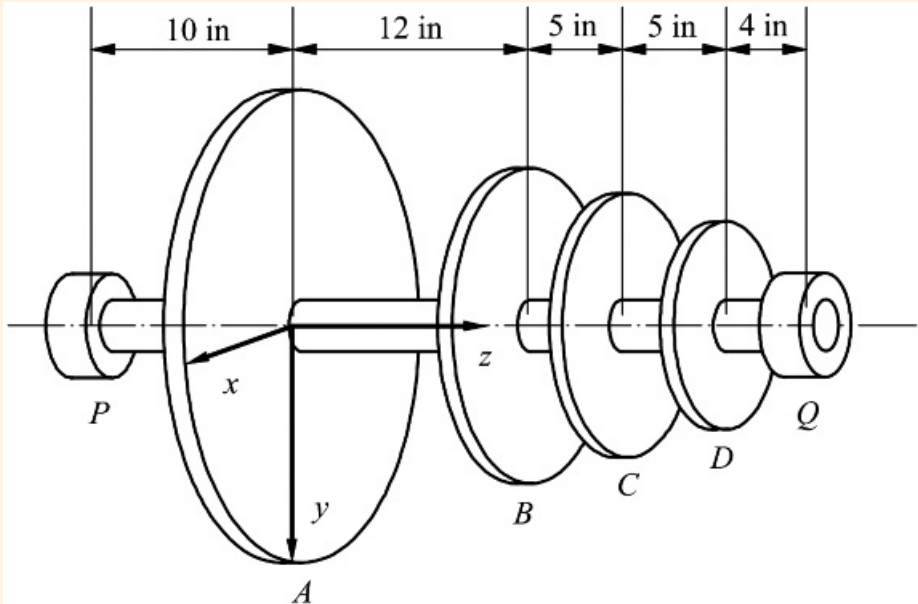


[Figure 16.7](#) The turbine rotor whose balance is analyzed in Example 16.3.

$$u_A = 0.08 \text{ in-lb at } 0^\circ; u_B = 0.03 \text{ in-lb at } 70^\circ; u_C = 0.04 \text{ in-lb at } -115^\circ; u_D = 0.03 \text{ in-lb at } 160^\circ$$

1. Compute the rotating radial forces that the rotor would apply to the bearings when spinning at the engine's normal operating speed of 15,000 rpm.
2. The rotor is to be balanced by removing material from disk A at radius 3.5 in and from disk D at radius 2.0 in. Calculate the mass that must be removed at each location and the angular position at which it must be removed.

Solution

1. $\omega = 15,000 \times 2\pi/60 = 1571 \text{ rad/s}$. Therefore, the unbalance forces at the respective blade disks are

$$\begin{aligned} F_P &= \frac{0.08 \times 1571^2}{32.2 \times 12} = 511 \text{ lb } \angle 0^\circ \\ F_B &= \frac{0.03 \times 1571^2}{32.2 \times 12} = 192 \text{ lb } \angle 70^\circ \\ F_C &= \frac{0.04 \times 1571^2}{32.2 \times 12} = 233 \text{ lb } \angle -115^\circ \\ F_D &= \frac{0.03 \times 1571^2}{32.2 \times 12} = 192 \text{ lb } \angle 160^\circ \end{aligned}$$

Let $F_P = F_{Px}i + F_{Py}j$ be the force exerted on the shaft by the bearing at P , and let $F_Q = F_{Qx}i + F_{Qy}j$ be the force exerted on the shaft by the bearing at Q . The force equilibrium equations are

$$\sum F_x = 0 : \quad F_{P_x} + F_{Q_x} + F_A \cos C^\circ + F_B \cos 70^\circ + F_C \cos(-115^\circ) + F_D \cos 160^\circ = 0$$

or

$$F_{P_x} + F_{Q_x} - 511 + 192 \cos 70^\circ + 255 \cos(-115^\circ) + 192 \cos 160^\circ = 0$$

giving

$$F_{P_x} + F_{Q_x} = -288 \text{ lb} \quad (16.8)$$

$$\sum F_y = 0 : \quad F_{P_y} + F_{Q_y} - F_A \sin C^\circ - F_B \sin 70^\circ + F_C \sin(-115^\circ) - F_D \sin 160^\circ = 0$$

or

$$F_{P_y} + F_{Q_y} + 192 \sin 70^\circ + 255 \sin(-115^\circ) - 192 \sin 160^\circ = 0$$

giving

$$F_{P_y} + F_{Q_y} = -15 \text{ lb} \quad (16.9)$$

Taking moments about P

$$\begin{aligned} \sum M_P = 0 : \\ 10k \times 5110 + 22k \times (65.7i + 180j) + 27k \times (-107.8i - 23.1j) + 32k \times (-180i + 65.7j) \\ + 36k \times (F_{Q_x}i + F_{Q_y}j) = 0 \end{aligned}$$

Therefore

$$\begin{aligned} F_{Q_x} &= \frac{1}{36}(-3960 - 6237 - 2102) = 4.9 \text{ lb} \\ F_{Q_y} &= -\frac{1}{36}(5110 + 1445 - 2911 - 5760) = 58.8 \text{ lb} \end{aligned}$$

and substitution back into Equations 16.8 and 16.9 gives

$$\begin{aligned} F_{P_x} &= -288 - 59 = -347 \text{ lb} \\ F_{P_y} &= -15 - 5 = -20 \text{ lb} \end{aligned}$$

Consequently, the magnitude and direction of the bearing force at P is

$$F_P = \sqrt{347^2 + 20^2} = 348 \text{ lb} \angle 183.3^\circ$$

Similarly, the bearing force at Q is

$$F_Q = \sqrt{4.9^2 + 58.8^2} = 59 \text{ lb} / 4.8^\circ$$

2. Since the unbalance force is simply the unbalance multiplied by ω^2 and has the same direction as the unbalance, it is convenient to simply work with the unbalances. u_A is the required unbalance to be added to disk A, and u_D is the unbalance to be added to disk D. If the rotor is fully dynamically balanced, the forces at the bearings P and Q are both zero. The x direction force equilibrium equation gives

$$x_{A_x} + 0.03 + 0.03 \cos 70^\circ + 0.04 \cos(-115^\circ) + 0.03 \cos 160^\circ + x_{D_x} = 0$$

The y direction equation is

$$x_{A_y} + 0 + 0.03 \sin 70^\circ + 0.04 \sin(-115^\circ) + 0.03 \sin 160^\circ + x_{D_y} = 0$$

These equations give

$$x_{A_x} + x_{D_x} = -0.0452 \text{ in-lb} \quad (16.10)$$

$$x_{A_y} + x_{D_y} = -0.0022 \text{ in-lb} \quad (16.11)$$

Since the bearing forces are zero, it is better to take moments about an axis through A, so only the components of u_D appear as unknowns in the moment equations. Hence

$$12k \times (0.03 \cos 70^\circ + 0.03 \sin 70^\circ) + 17k \times (0.04 \cos(-115^\circ)) + 0.04 \sin(-115^\circ) \\ + 22k \times ((0.03 \cos 160^\circ + u_{D_x})i + (0.03 \sin 160^\circ + u_{D_y})j) = 0$$

This reduces to

$$\begin{aligned} 0.0523 - 22u_{D_y} &= 0 \\ -0.7345 + 22u_{D_x} &= 0 \end{aligned}$$

or

$$\begin{aligned} u_{D_x} &= 0.0357 \text{ in-lb} \\ u_{D_y} &= 0.0024 \text{ in-lb} \end{aligned}$$

so the magnitude of the required additional unbalance at disk D is

$$u_D = \sqrt{0.0357^2 + 0.0024^2} = 0.0358 \text{ in-lb}$$

and its direction is

$$\angle \omega_D = \tan^{-1}(0.0024/0.0357) = 3.8^\circ \text{ relative to the } x \text{ axis}$$

Substitution back into [Equations 16.10](#) and [16.11](#) gives

$$\begin{aligned} w_{A_x} &= -0.0452 - 0.0357 = -0.0809 \text{ in-lb} \\ w_{A_y} &= -0.0022 - 0.0024 = -0.0046 \text{ in-lb} \end{aligned}$$

so the magnitude of the required additional unbalance at disk A is

$$w_A = \sqrt{0.0809^2 + 0.0046^2} = 0.0810 \text{ in-lb}$$

and its direction is

$$\angle \omega_A = 180^\circ + \tan^{-1}(0.0046/0.0809) = 183.3^\circ \text{ relative to the } x \text{ axis}$$

Now the unbalance at A is to be created by *removing* mass at the radius 3.5 in. The weight of the mass to be removed is

$$m_A = 0.0810/3.5 = 0.023 \text{ lb}$$

Since the material will be removed, it should be removed at the angle $180^\circ + 183.3^\circ = 363.3^\circ$, that is, at angle 3.3° to the x axis in the positive rotation direction about the z axis.

Similarly, at disk D the material is to be removed at the radius 2.0 in. The weight to be removed is

$$m_D = 0.0358/2.0 = 0.0179 \text{ lb}$$

and it must be removed at the angle $180^\circ + 3.8^\circ = 183.8^\circ$ measured from the positive x axis direction.



16.4 Balancing Reciprocating Masses

A second major source of vibration excitation in machinery is the presence of masses that perform oscillatory motions. The classic case is the reciprocating piston mass in an internal combustion engine, or a reciprocating pump or compressor.

Although the motion of the reciprocating mass in one of these machines is not strictly harmonic, it is customary to treat it as being so for the purposes of trying to reduce the tendency of the machine to excite vibration. There are several reasons for making this approximation. One is that a simple harmonic oscillation is easy to model and conceptualize. Another is that the fundamental frequency of oscillation is really most important. If we imagine the oscillatory acceleration decomposed into harmonic components, there will be a large-amplitude fundamental with the period of the overall oscillation, and a train of higher harmonics with much smaller amplitudes. Not only are these harmonics less effective in exciting vibration because of their smaller amplitudes, but their frequencies are much higher than the fundamental. Since higher frequency vibrations are much more effectively damped out in most structures, the fundamental frequency tends to dominate the transmitted vibration.

Another approximation that is commonly used when dynamically modeling reciprocating machines is to model the mass of the connecting rod as two equivalent masses, one located on the crank pin axis and the other at the wrist pin axis. That is, the distributed mass of the connecting rod is split into a reciprocating point mass at the wrist pin and a pure rotating point mass at the crank pin. The reciprocating component then simply becomes a part of the piston mass, and the rotating component becomes a part of the mass of the crank pin.

This decomposition can be done to preserve the correct location of the center of mass of the connecting rod. However, the moment of inertia of the two mass elements about that center of mass will not be exactly the same as that of the connecting rod. The error introduced in this manner is minimal in most analyses.

16.4.1 Lumped Mass Distribution

To develop an expression for discretizing the distribution of the masses of the crank and connecting rod, consider the slider-crank mechanism shown in [Figure 16.8](#). The crank is assumed to rotate with a constant angular speed ω . Points A and B are the crank pin and wrist pin, respectively, and G_2 and G_3 are the centers of mass of links 2 and 3, respectively. The sum of the weights of the crank and crank pin is m_2g , and the centrifugal force acts outward along line G_2A as shown in [Figure 16.8\(b\)](#). In [Figure 16.8\(c\)](#), the masses of the crank and crank pin have been replaced by a concentrated mass m_A located at A such that the centrifugal forces shown in [Figures 16.8\(b\)](#) and (c) will be equal. Thus

$$m_A \omega^2 = m_2 \omega^2$$

or

$$m_A = \frac{m_2}{\omega^2} \quad (16.12)$$

Note that in [Equation 16.12](#) it is assumed that the center of mass of the crank and point A are on the same side of the rotation axis. If G_2 is on the opposite side, the effective mass of the crank will be *negative*. This is because the inertial force due to G_2 will be in the opposite direction from that due to a mass at A .

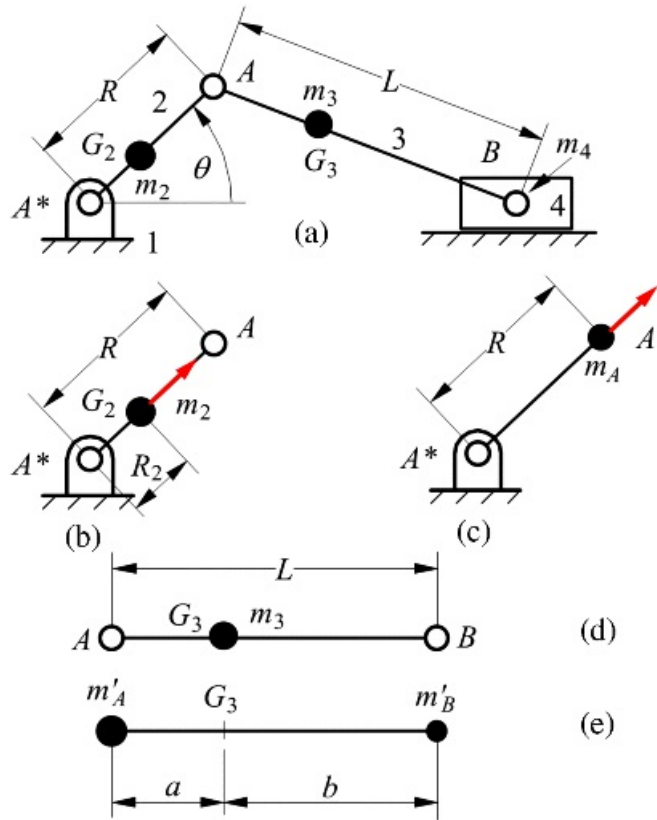


Figure 16.8 A slider-crank mechanism: Replacement of connecting rod and crank pin inertias by approximately equivalent lumped masses located at points A and B .

The connecting rod of mass m_3 in [Figure 16.8\(d\)](#) can be approximated by the system shown in [Figure 16.8\(e\)](#), which consists of the two concentrated weights m'_A and m'_B connected by a weightless rod. For the center of mass of the substitute masses m'_A and m'_B to remain at G_3

$$m'_S(a + b) = (m'_A + m'_B)a$$

or

$$m'_S = \frac{m_3 a}{a + b} = \frac{m_3 a}{L} \quad (16.13)$$

where $m_3 = (m'_A + m'_B)$ is the mass of the connecting rod, b is the distance from the center of mass of the connecting rod to the center of the piston pin, and a is the distance from the center of mass of the connecting rod to the center of the crank pin. Similarly

$$m'_A = \frac{m_3 b}{a + b} = \frac{m_3 b}{L} \quad (16.14)$$

The replacement system in [Figure 16.8\(e\)](#) will have the same inertia forces as the actual connecting rod but its inertia torque will be somewhat different. The total equivalent masses at A and B can be represented by

$$\tilde{m}_A = m'_A + m_A \quad (16.15)$$

and

$$\tilde{m}_B = m'_B + m_4 \quad (16.16)$$

where m_4 is the mass of the piston.

It should be noted that this replacement is an approximation. It almost always increases the effective moment of inertia of the connecting rod about its mass center. This is because the radius of gyration of the central bar portion of the member is actually relatively small ($L/\sqrt{12}$) if the bar is uniform. Modeling it as lumped masses at its ends always increases the effective moment of inertia.

The shaking forces generated by the reciprocating and rotating masses of a reciprocating machine can now be estimated as in the following example.



Example 16.4 Shaking-Force Calculation

A single-cylinder reciprocating air compressor has a piston that weighs 2.5 lb and a connecting rod of length 12 in weighing 2.0 lb, with its center of mass 4 in from the center of the crank pin. The crank radius is 3 in with a counterbalance weight 4.0 lb and center of mass 2 in on the reverse side of the crankshaft axis.

Estimate the shaking force for a constant crank angular velocity of 300 rpm (CW) at 30° after top dead center (TDC).

Solution

Figure 16.9 shows the linkage geometry in the specified position, together with the corresponding velocity and acceleration diagrams.

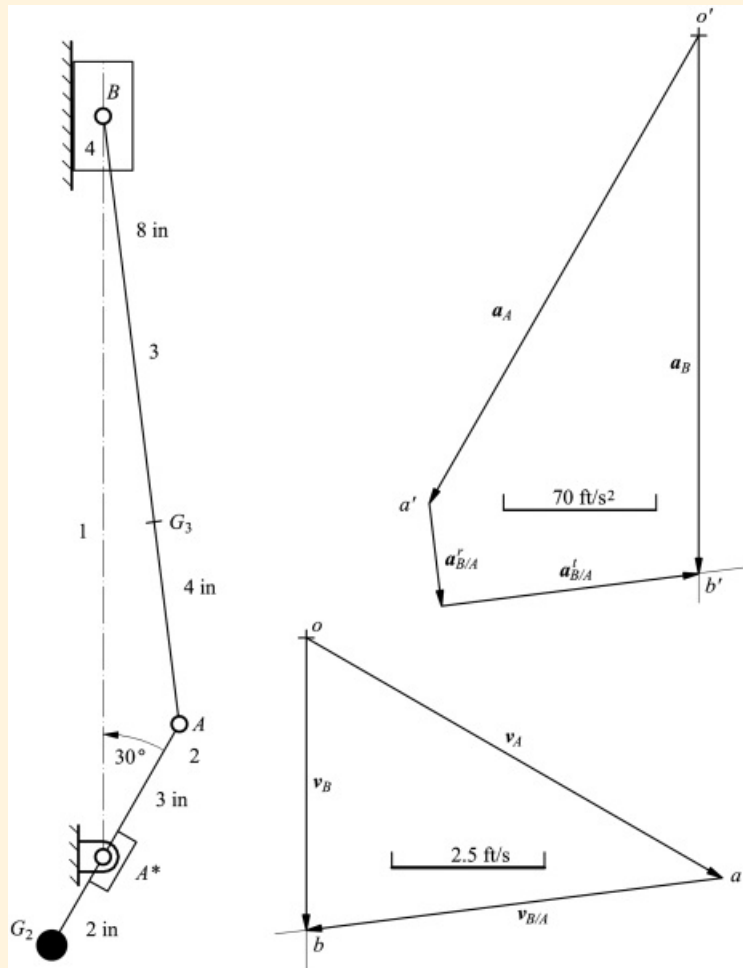


Figure 16.9 Position, velocity, and acceleration diagrams for the air compressor mechanism of Example 16.4.

The angular velocity of the crank (member 2) is

$$\omega_2 = 300 \times 2\pi / 60 = 31.42 \text{ rad/s CW}$$

Hence the velocity of point *A* is

$$v_A = 0.25 \times 31.42 = 7.85 \text{ ft/s} \angle -30^\circ$$

which is plotted as oa on the velocity diagram. The velocity of point B is given by $v_B = v_A + v_{B/A}$. The directions of both v_A and $v_{B/A}$ are known. Completion of the triangle by drawing ob parallel to the slide and ab normal to AB gives

$$v_{B/A} = ab = 6.87 \text{ ft/s} \text{ in the direction shown}$$

Hence, the angular velocity of the connecting rod, member 3, is

$$\omega_3 = \frac{ab}{AB} = \frac{6.87}{1.0} = 6.87 \text{ rad/s CCW}$$

Since the angular velocity of member 2 is constant

$$a_A = a_A^r = 0.25 \times 31.42^2 = 246.8 \text{ ft/s}^2 \angle -120^\circ$$

This is plotted on the acceleration diagram as $o'a'$. The acceleration of B is given by $a_B = a_A + a_{B/A} = a_A + a_{B/A}^r + a_{B/A}^t$. The radial component $a_{B/A}^r$ can be calculated and plotted

$$a_{B/A}^r = 1.0 \times 6.87^2 = 47.20 \text{ ft/s}^2$$

parallel to BA as shown in the figure. The direction of $a_{B/A}^t$ can now be plotted through the tip of this arrow. Its intersection with the direction of a_B , parallel to the slide, gives the point b' and completes the polygon. Scaling from the diagram gives

$$a_B = 243 \text{ ft/s}^2 \text{ (down)}$$

This is actually all the acceleration information needed to solve the problem, because the distributed mass of the connecting rod will be approximated by lumped masses at points A and B .

Applying Equations 16.13 and 16.14, the equivalent weights for the connecting rod are

$$m'_A = (8/12)2.0 = 1.333 \text{ lb}$$

$$m'_B = (4/12)2.0 = 0.667 \text{ lb}$$

Therefore, the total effective weight at point B is

$$\bar{m}_B = 0.667 + 2.5 = 3.167 \text{ lb}$$

The reciprocating shaking force component is, therefore

$$F_B = -\bar{m}_B a_B = 243 \times 3.167 / 32.2 = 24.4 \text{ lb (up)}$$

The rotating mass at A in [Figure 16.10](#) will be the sum of \bar{m}_A and the effective mass m_A of the crank referred to point A . Note that points A and G_2 are on opposite sides of the rotation axis. Therefore, the effective mass of the crank alone will be negative. From [Equation 16.12](#) the effective mass m_A of the crank is given by

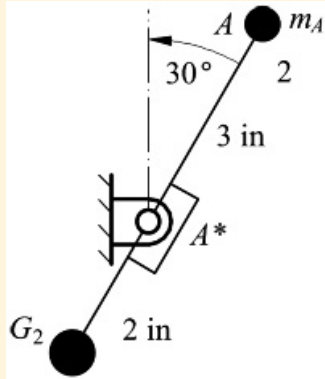


[Figure 16.10](#) Effective mass distribution of the continuously rotating crank of Example 16.4. The mass m_A is the equivalent rotating mass of the connecting rod.

$$\bar{m}_A = \frac{\rho_2}{\rho_1} m_2 = -\frac{2}{3} 4.0 = -2.667 \text{ lb}$$

The total equivalent mass at A is given by [Equation 16.15](#) as

$$\bar{m}_A = \bar{m}_A' + m_A = 1.333 - 2.666 = -1.333 \text{ lb}$$

Therefore, the center of gravity for m_A is on the same side of the rotation axis as G_2 . Consequently, the inertia force due to the effective rotating mass is

$$F_A = \bar{m}_A R \omega^2 = -\frac{1.333(3)(31.42)^2}{12 \times 32.2} = -10.22 \text{ lb} \angle 60^\circ$$

The inertial force at A could also be written as $+10.22 \text{ lb}$ at an angle of -120° with the horizontal axis. In this system, the rotating masses contribute very little. The reciprocating masses are dominant in the generation of the shaking force.

16.4.2 Balancing a Slider-Crank Mechanism

As already discussed, the inertia of the connecting rod can be approximated by two concentrated masses, one at the crank pin and the other at the wrist pin. The slider-crank system then becomes a combination of a mass assumed to be rotating at constant angular velocity (the crank mass together with the equivalent mass at the crank pin from the connecting rod) and a reciprocating mass (the piston and wrist pin mass, together with the equivalent mass from the connecting rod concentrated at the wrist pin). To a first approximation, the piston motion can be regarded as a simple harmonic motion. This is equivalent to replacing a Fourier series by its fundamental term; it is an approximation, but a useful one. The inertia force from the reciprocating mass is then a simple harmonic force acting along the cylinder axis. The inertia force from the rotating mass rotates with the crank. Its component along the cylinder axis is also harmonic, with the same period as the inertia force from the reciprocating mass. The rotating inertia force can be completely removed by counterweighting the crank so that the center of mass of the equivalent mass system is at the crankshaft axis. The inertia force of the reciprocating mass cannot be completely removed. However, it can be offset by increasing the mass of the counterweight on the

crank so that the axial component of the crank inertia force opposes the inertia force from the reciprocating mass. This reduces the magnitude of the axial inertia force from the reciprocating mass, but at the cost of reintroducing a lateral shaking force from the counterweighted crank. A popular arrangement for single-cylinder engines is to use a crank counterweight that is large enough to halve the amplitude of the reciprocating inertia force. This results in a rotating inertia force of half the amplitude of the original reciprocating unbalance. The resultant inertia force rotates in the *opposite* direction to the crank. If one is willing to tolerate the extra complexity of arranging a counter rotating counterweight on the crankshaft axis, this remaining unbalance force can also be removed.

The *shaking force* is the *resultant of all the forces acting on the frame of a mechanism due to inertia forces only*. Thus, if the resultant of all the forces due to inertia effects acting on the frame is zero, there is no shaking force. There may, nevertheless, be a *shaking couple* present. Balancing a mechanism consists of eliminating the shaking force and shaking couple. In some instances, but not all, we can accomplish both. We shall discover that in most mechanisms, by adding appropriate balancing weights, we can reduce the shaking force and shaking couple, but it is usually not practical to provide a means of completely eliminating them.

Since the slider-crank mechanism is so widely used in such machines as internal combustion engines and compressors, considerable work has been done on the development of techniques for balancing these mechanisms. The approach to balance the slider-crank mechanism will use the approximate mass distribution developed in Section 16.4.1 along with an approximation for the acceleration of point *B* at the piston. An expression for the acceleration of the piston is developed in the following section.

Approximate Expression for Piston Acceleration

If the crank moves with constant angular speed ω , the acceleration of any point on the crank is given by

$$a_c = r\omega^2 \quad (16.17)$$

where r is the distance from A^* to the point of interest. In Figure 16.11, point *A* is the primary point of interest. If the lumped-mass model is used for the connecting rod, the only other point of interest is point *B* at the wrist pin. The acceleration of this point can be determined using Figure 16.11. A local x, y coordinate system is located at point A^* as shown such that the x axis is along the line A^*B .

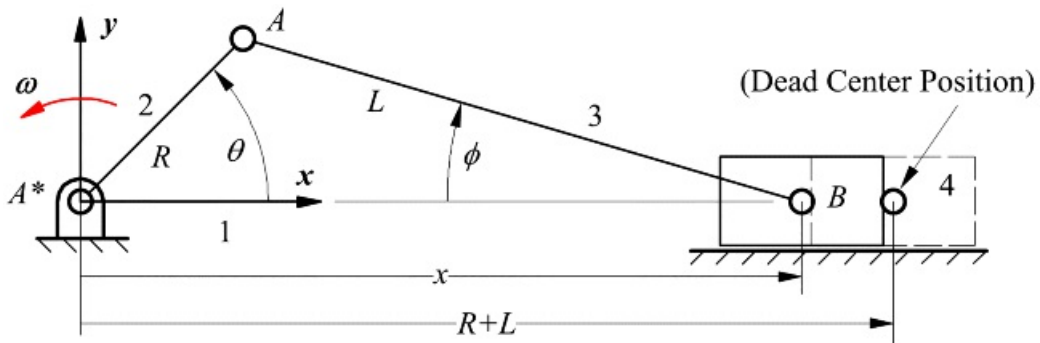


Figure 16.11 Slider-crank mechanism coordinate system.

The position of the point *B* relative to A^* , the origin of the x and y coordinate axes, is represented by x . Link 2 is at an angle θ from the x axis for the position shown. The connecting rod makes an angle of ϕ with the x -axis. The distance x may be represented by the sum of the projection of the crank and connecting rod on the x axis:

$$x = R \cos \theta + L \cos \phi \quad (16.18)$$

It is desirable to represent x as a function of R , L , and ϕ . To do this, θ may be eliminated by noting that the vertical projections of R and L are equal, or

$$R \sin \theta = L \sin \phi$$

or

$$\sin \phi = (R/L) \sin \theta \quad (16.19)$$

but

$$\cos \phi = \sqrt{1 - (\sin \phi)^2} \quad (16.20)$$

Therefore, substitution of [Equation 16.19](#) into [Equation 16.20](#) gives

$$\cos \phi = \sqrt{1 - [(R/L) \sin \theta]^2} \quad (16.21)$$

Substitute [Equation 16.21](#) into [Equation 16.18](#) to get

$$x = R \cos \theta + L \sqrt{1 - [(R/L) \sin \theta]^2} \quad (16.22)$$

[Equation 16.22](#) is an exact expression for the location of the piston relative to the center of the crank bearing.

The expression for the velocity may be obtained by differentiating x with respect to t . Noting that $d\theta/dt = \omega$, the linear speed of the piston after simplification is

$$v_B = \frac{dx}{dt} = -R\omega \left[\sin \theta + \frac{R}{2L} \sin 2\theta / \sqrt{1 - \left(\frac{R}{L} \sin \theta \right)^2} \right] \quad (16.23)$$

The expression for the acceleration of the piston may be obtained by differentiating v_B with respect to t and remembering that ω , the angular speed of the crank, is constant. Then

$$a_x = \frac{dv_B}{dt} = -R\omega^2 \left[\cos \theta + \frac{\frac{R}{L} \cos 2\theta \left\{ 1 + \left(\frac{R}{L} \right)^2 \right\} + \left(\frac{R}{L} \right)^3 \sin^4 \theta}{\left\{ 1 - \left(\frac{R}{L} \sin \theta \right)^2 \right\}^{3/2}} \right] \quad (16.24)$$

If the velocity or acceleration is negative, it is directed from the piston to the crank bearing. The angular velocity of the crank is positive if it is counterclockwise.

For most practical engines, the value of R/L will be less than 1/4 so that $(R/L)^2$ will be small compared with 1. With this approximation, the expression for the acceleration can be simplified with little loss of accuracy to

$$a_x = -R\omega^2 \left(\cos \theta + \frac{R}{L} \cos 2\theta \right) \quad (16.25)$$

The maximum error in the approximate expressions above is around 0.5 percent of the maximum values for $R/L \sim 1/4$. Therefore, because of the form for the equations, the approximate expressions are sometimes used in analytical work. However, when a computer is used, the simplification is not necessary because it is only slightly more difficult to compute the exact value for the acceleration of the piston.



16.5 Expressions for Inertial Forces

We can represent the inertia forces as the vectors

$$\vec{f}_A = -\bar{m}_A \ddot{\theta} A = \bar{m}_A R \omega^2 \angle \theta \quad (16.26)$$

and

$$\vec{f}_B = -\bar{m}_B \ddot{\theta} B \cong \bar{m}_B R \omega^2 \left(\cos \theta + \frac{R}{L} \cos 2\theta \right) \angle \theta^c \quad (16.27)$$

Therefore, in terms of x and y components, the total shaking force would be

$$f_s = f_A + f_B = R \omega^2 \left[(\bar{m}_A + \bar{m}_B) \cos \theta + \bar{m}_B \left(\frac{R}{L} \right) \cos 2\theta \right] i + R \omega^2 (\bar{m}_A \sin \theta) j \quad (16.28)$$

If a counterbalance mass is added to the crank, the mass would be added to the side of the crank that is opposite A . As discussed in Section 16.2, this is equivalent to subtracting mass from the side of the crank where A is located. Regardless of whether we add or subtract mass, it is convenient to represent the “added” mass as an equivalent mass at A by using [Equation 16.12](#). If the counterbalance mass is \bar{m}_{cb} , at a distance R_c from the crank axis, the equivalent mass \bar{m}_{eq} at point A would be

$$\bar{m}_{eq} = \frac{R_c}{R} \bar{m}_{cb}$$

The total inertial force at point A would then be

$$\vec{f}_A = (\bar{m}_A - \bar{m}_{eq}) R \omega^2 \angle \theta$$

and [Equation 16.28](#) can be rewritten as

$$f_s = f_A + f_B = R \omega^2 \left[(\bar{m}_A + \bar{m}_B - \bar{m}_{eq}) \cos \theta + \bar{m}_B \left(\frac{R}{L} \right) \cos 2\theta \right] i + R \omega^2 (\bar{m}_A - \bar{m}_{eq}) \sin \theta j \quad (16.29)$$

The results are shown schematically in [Figure 16.12](#). [Equation 16.29](#) can be easily programmed using MATLAB. This permits the user to compute the shaking force as a function of θ and to determine the best choice of counterbalance weight to minimize the maximum value for the shaking force. The program *ShakeAnalysis* in *KinDAP.m*, which is included in the accompanying material of this book, performs the necessary calculations and plots the results.

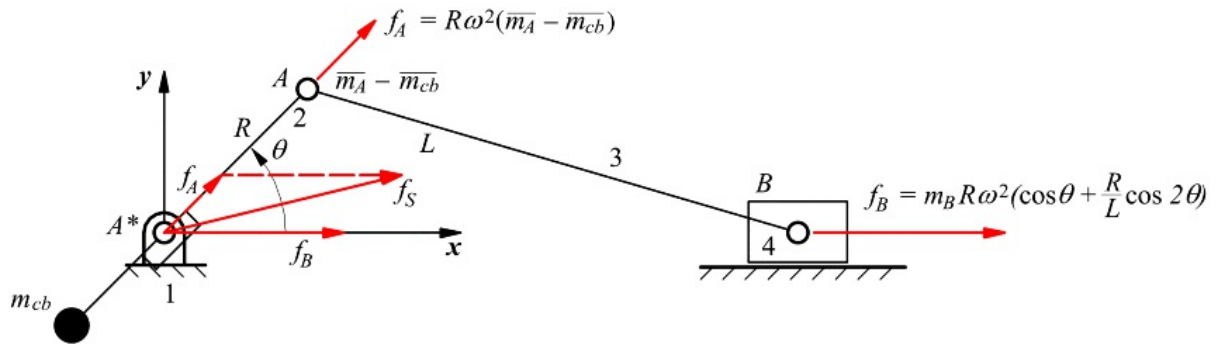


Figure 16.12 Equivalent slider-crank mechanism with inertial forces (ω = constant).

Notice that m_{cb} appears in both components of f_S . The objective of the balancing procedure is to adjust m_{cb} to reduce the magnitude of f_S that varies directly with θ and in part with 2θ . It is customary to refer to the portion of the force occurring at the circular frequency ω rad/s as the primary inertia force and the portion occurring at 2ω rad/s as the secondary inertia force. We note that the vertical component has only a primary part and that it therefore varies directly with the crankshaft speed. On the other hand, the horizontal component, which is in the direction of the cylinder axis, has a primary part varying directly with the crankshaft speed and a secondary part that varies at twice the crankshaft speed.

Note also that the equations derived are in terms of mass. In general, we will measure directly the weights for the crank and connecting rod and not the mass. However, as used in the earlier examples, the mass can be conveniently determined from the weight by dividing the weight by the acceleration of gravity.



Example 16.5

Balancing a Slider-Crank Mechanism

The purpose of this example is to introduce the student to a numerical technique for balancing a model of a slider-crank mechanism and gives an example of the use of a computer program for balancing a slider-crank mechanism. The computer program *ShakeAnalysis.m* will be used to determine the “optimum” counterbalance value for a slider-crank mechanism that might be used in a small engine.

The program computes the maximum value of the shaking force for a specified value of the counterbalance weight (assumed to be located at a distance equal to the crank radius). The program also computes the maximum shaking-force value for no counterbalance weight and for the optimum counterbalance weight. The maximum value is found through a simple search over the crank angle range of 0° to 360° . Given the counterbalance weight W_{cb} , the program increments the crank angle θ in 1° increments. The shaking force is computed at each of these θ values, and the maximum value is selected.

For the analysis, assume that the following data have been recorded

Piston	$W_4 = 20 \text{ lb}$
Rod	$L = 14 \text{ in}$
	$W_A = 24.28 \text{ lb}$
	$W_B = 9.72 \text{ lb}$
Crank	$R = 4.0 \text{ in}$
	$W_A = 3.75 \text{ lb}$
Rotation speed	1000 rpm
Gravity	$g = 386 \text{ in/s}^2$

Use the program *ShakeAnalysis* in *KinDAP.m* given in the supporting material of this book to find the optimum counterbalance weight for the mechanism. Note that the weights of the crank and the connecting rod mentioned are already referred to the crank pin and the piston pin. The value for the crank corresponds to a weight of 1.875 lb at a center of gravity location of 2 in from the crank pivot. The value for the coupler corresponds to a weight of 34 lbs at a distance of 4 in from the crank pin at A .

Solution

Begin the optimization with an initial value for the counterbalance mass as $\bar{m}_{cb} = \bar{m}_A + 2\bar{m}_B/3$. This value is often suggested as the optimum counterbalance mass. The counterbalance weight corresponding to this mass is

$$W_{cb} = (W_A + W_B) + 2(W_B + W_A)/3 = (3.75 + 24.28) + 2(9.72 + 20)/3 = 47.84 \text{ lb}$$

The program *ShakeAnalysis* was run with three values for the counterbalance force. The first value was the given value (47.85 lb), the second value was no counterbalance force, and the third value was the optimum value (45.87 lb) determined by the program. The corresponding maximum shaking-force values are given in [Table 16.1](#). The program also plots the corresponding shaking force for each of the values of the counterbalance force. These are shown in [Figure 16.13](#). Notice that the shaking force can be reduced by almost 70 percent by the addition of the simple counterbalance weights.

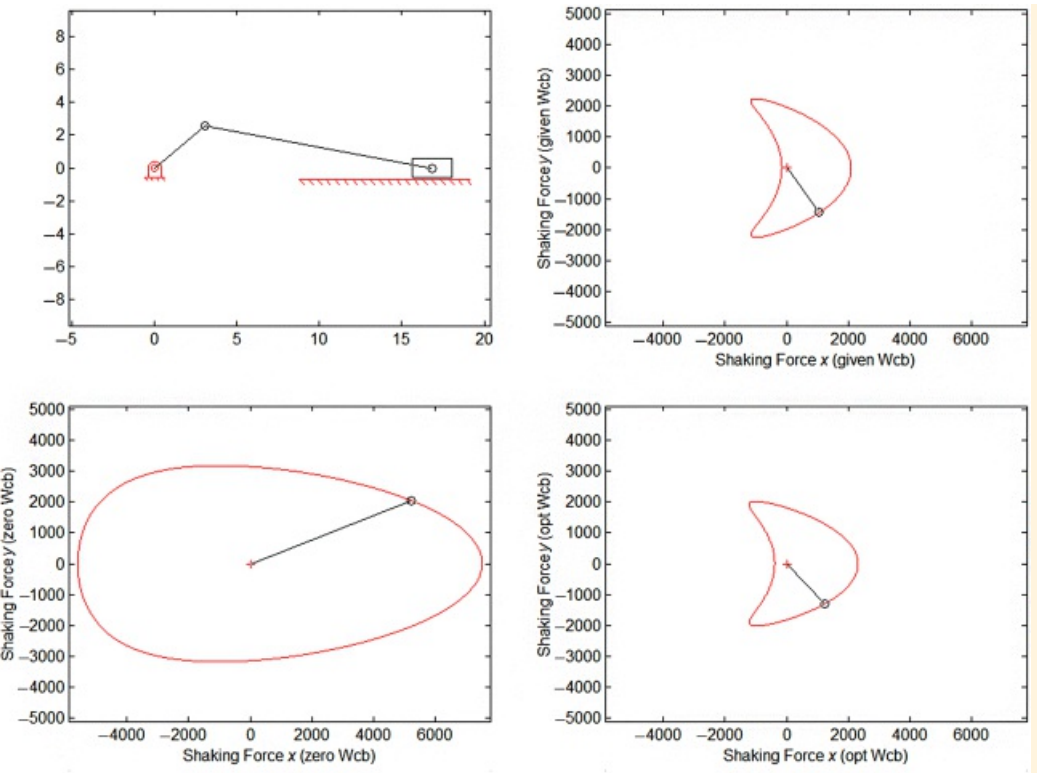


Figure 16.13 Shaking-force diagrams for Example 16.5. The top right diagram is for the given counterbalance weight. The bottom left diagram is for no counterbalance weight, and the bottom right diagram is for the optimum counterbalance weight.

Table 16.1 Summary of Shaking-Force Values for Example 16.5

Counterbalance Weight (lb)	Maximum Shaking Force (lb)	Crank Angle
0	7527.4	0°
47.85	2495.4	262.7°
45.86	2316.0	100.0°



16.6 Balancing Multi-Cylinder Machines

The approximation of the connecting rod and crank pin masses used above is also routinely used when discussing multi-cylinder engine balancing. Because of these approximations and manufacturing variations, even a perfectly balanced multi-cylinder engine, pump, or compressor will generate some residual vibration. For this reason, vibration-isolating mounts are always necessary. In many situations, it is necessary to trade off the complexity involved in achieving a higher level of balance against using a simpler scheme relying on vibration mounts to further reduce the remaining vibration.

Balance is not the only constraint when selecting an automotive engine configuration. An even firing sequence of the cylinders is preferred, although digital ignition has loosened that constraint resulting in “odd fire” engines. Engine designers try to optimize the firing sequence to minimize the elastic windup of the crankshaft. Two-stroke and diesel engines, which fire every piston stroke, require different crankshaft geometries and balance arrangements than four-stroke engines that fire every second piston stroke.

In multi-cylinder engines and compressors, the weight of the crankshaft and the part of the weight of the connecting rod that is concentrated at the crank pin can be counterbalanced exactly using the dynamic balancing procedures discussed earlier. Therefore, only the balancing of the reciprocating weights will be considered here.

If we have n cylinders, the inertial force associated with each piston is in the direction of the piston travel and is given by

$$f_{S_i} = \overline{m}_{S_i} R_i \omega^2 \left[\cos(\theta + \phi_i - \psi_i) + \frac{R_i}{L_i} \cos 2(\theta + \phi_i - \psi_i) \right], \quad i = 1, 2, \dots, n \quad (16.30)$$

where \overline{m}_{S_i} , R_i , L_i , and ϕ_i are the reciprocating mass, the crank radius, the connecting rod length, and the phase angle, respectively, for the i th cylinder. The angle θ gives the position of the piston axis for cylinder 1 relative to the x axis, and each cylinder axis is oriented at an angle of ψ_i relative to the axis of cylinder 1. If the first crank starts in the direction of the x axis, the angle θ is equal to the crank angular velocity multiplied by the time. In most engines and compressors, \overline{m}_{S_i} , R_i , and L_i will be the same for all cylinders. Therefore, the subscript i must be maintained for the angles ϕ_i and ψ_i only. The phase angle ϕ_i gives the angle from crank 1 to crank i as shown in [Figure 16.14](#). Both $\phi_1 = 0$ and $\psi_1 = 0$, although both angles are usually included in the equations for symmetry.

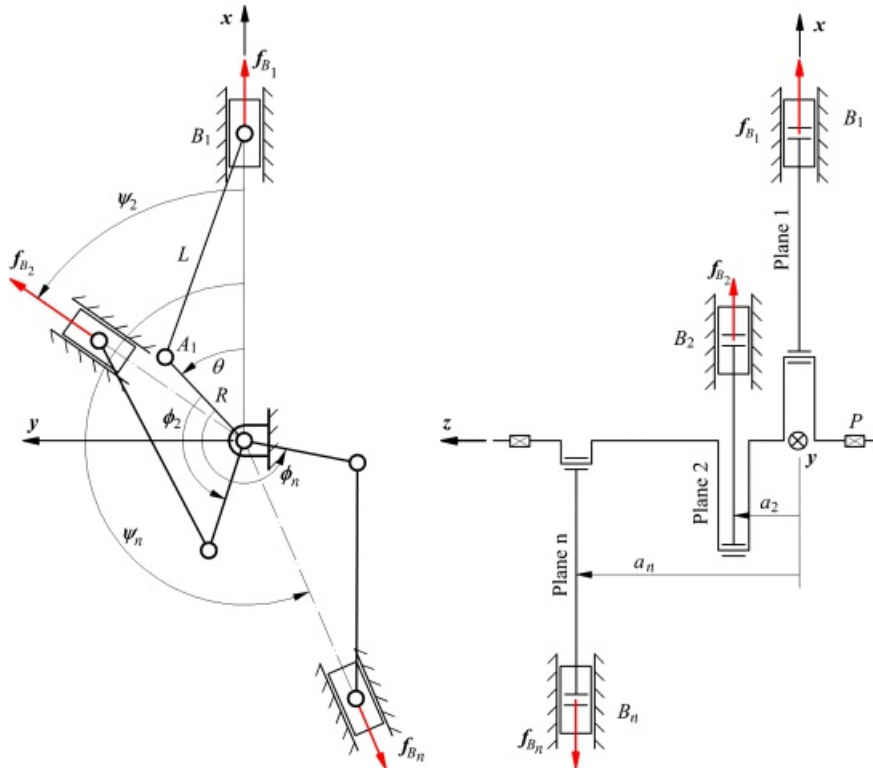


Figure 16.14 Schematic diagram of shaking forces in a multi-cylinder engine.

The total shaking force will be the vector sum of the forces from all of the cylinders. For the analysis, the coordinate axes will be oriented as shown in [Figure 16.14](#). The z axis is along the rotation axis of the crankshaft, the x axis is in the direction of the piston travel of the first cylinder, and the y axis is defined such that a right-handed coordinate system results. Then, the x component of the shaking force from the cylinder is

$$f_{S_x} = f_S \cos \psi_i = \bar{m}_S R \omega^2 \left[\cos(\theta + \phi_i - \psi_i) + \frac{R}{L} \cos 2(\theta + \phi_i - \psi_i) \right] \cos \psi_i \quad (16.31)$$

and the y component is

$$f_{S_y} = f_S \sin \psi_i = \bar{m}_S R \omega^2 \left[\cos(\theta + \phi_i - \psi_i) + \frac{R}{L} \cos 2(\theta + \phi_i - \psi_i) \right] \sin \psi_i \quad (16.32)$$

The total inertial force vector due to the reciprocating masses is given by summing the vector contribution from each cylinder. It is convenient to sum the x and y components separately when doing this. The result is

$$f_x = m_S R \omega^2 \left[\sum_{i=1}^n \cos(\theta + \phi_i - \psi_i) \cos \psi_i + \frac{R}{L} \sum_{i=1}^n \cos 2(\theta + \phi_i - \psi_i) \cos \psi_i \right] \quad (16.33)$$

and

$$f_y = m_S R \omega^2 \left[\sum_{i=1}^n \cos(\theta + \phi_i - \psi_i) \sin \psi_i + \frac{R}{L} \sum_{i=1}^n \cos 2(\theta + \phi_i - \psi_i) \sin \psi_i \right] \quad (16.34)$$

[Equations 16.33](#) and [16.34](#) can be expanded to separate the fixed components from those dependent on ϕ using the following trigonometric identities

$$\cos(\theta + \phi_i - \psi_i) = \cos \theta \cos(\phi_i - \psi_i) - \sin \theta \sin(\phi_i - \psi_i) \quad (16.35)$$

and

$$\cos 2(\theta + \phi_i - \psi_i) = \cos 2\theta \cos 2(\phi_i - \psi_i) - \sin 2\theta \sin 2(\phi_i - \psi_i) \quad (16.36)$$

Then

$$f_x = m_3 R \omega^2 \left[\cos \theta \sum_{i=1}^n \cos(\phi_i - \psi_i) \cos \psi_i - \sin \theta \sum_{i=1}^n \sin(\phi_i - \psi_i) \cos \psi_i \right. \\ \left. + \frac{R}{L} \cos 2\theta \sum_{i=1}^n \cos 2(\phi_i - \psi_i) \cos \psi_i - \frac{R}{L} \sin 2\theta \sum_{i=1}^n \sin 2(\phi_i - \psi_i) \cos \psi_i \right] \quad (16.37)$$

and

$$f_y = m_3 R \omega^2 \left[\cos \theta \sum_{i=1}^n \cos(\phi_i - \psi_i) \sin \psi_i - \sin \theta \sum_{i=1}^n \sin(\phi_i - \psi_i) \sin \psi_i \right. \\ \left. - \frac{R}{L} \cos 2\theta \sum_{i=1}^n \cos 2(\phi_i - \psi_i) \sin \psi_i - \frac{R}{L} \sin 2\theta \sum_{i=1}^n \sin 2(\phi_i - \psi_i) \sin \psi_i \right] \quad (16.38)$$

To balance the forces, it is necessary for f_x and f_y to be zero. This can be achieved by making the resultant of the terms on the right hand side of [Equations 16.37](#) and [16.38](#) equal to zero. This occurs for all values of ϕ when

$$\sum_{i=1}^n \cos(\phi_i - \psi_i) \cos \psi_i = 0 \quad (16.39)$$

$$\sum_{i=1}^n \cos(\phi_i - \psi_i) \sin \psi_i = 0 \quad (16.40)$$

$$\sum_{i=1}^n \sin(\phi_i - \psi_i) \sin \psi_i = 0 \quad (16.41)$$

$$\sum_{i=1}^n \sin(\phi_i - \psi_i) \cos \psi_i = 0 \quad (16.42)$$

$$\sum_{i=1}^n \cos 2(\phi_i - \psi_i) \cos \psi_i = 0 \quad (16.43)$$

$$\sum_{i=1}^n \cos 2(\phi_i - \psi_i) \sin \psi_i = 0 \quad (16.44)$$

$$\sum_{i=1}^n \sin 2(\phi_i - \psi_i) \cos \psi_i = 0 \quad (16.45)$$

$$\sum_{i=1}^n \sin 2(\phi_i - \psi_i) \sin \psi_i = 0 \quad (16.46)$$

[Equations 16.39–16.42](#) are necessary to balance the primary shaking forces, and [Equations 16.43–16.46](#) are necessary to balance the secondary shaking forces. In some crank arrangements, it will be possible to satisfy all eight equations. In other cases, it may be possible to satisfy either [Equations 16.39–16.42](#) or [Equations 16.43–16.46](#). If there is a choice, it is generally more important to balance the primary shaking forces rather than the secondary shaking forces because the factor (R/L) will always be less than 1, making the primary shaking forces larger than the secondary shaking forces.

In most cases, the cylinders will be offset along the z axis. Therefore, the individual shaking forces will not be in a single plane, and there is a possibility of a shaking moment. The components of the shaking moment can be determined by summing moments about the x and y axes in the plane of cylinder 1. This will give two components of the shaking moment. If a_i is the distance from the plane of cylinder 1 to the plane of cylinder i ($a_1 = 0$), the x component of the moment is given by

$$\begin{aligned} M_x &= -\sum_{i=1}^n f_{x_i} a_i \\ &= \bar{m}_p R \omega^2 \left[\cos \theta \sum_{i=1}^n a_i \cos(\phi_i - \psi_i) \sin \psi_i - \sin \theta \sum_{i=1}^n a_i \sin(\phi_i - \psi_i) \sin \psi_i \right. \\ &\quad \left. + \frac{R}{L} \cos 2\theta \sum_{i=1}^n a_i \cos 2(\phi_i - \psi_i) \sin \psi_i - \frac{R}{L} \sin 2\theta \sum_{i=1}^n a_i \sin 2(\phi_i - \psi_i) \sin \psi_i \right] \end{aligned} \quad (16.47)$$

and the y component is given by

$$\begin{aligned} M_y &= -\sum_{i=1}^n f_{y_i} a_i = \\ &= \bar{m}_p R \omega^2 \left[\cos \theta \sum_{i=1}^n a_i \cos(\phi_i - \psi_i) \cos \psi_i - \sin \theta \sum_{i=1}^n a_i \sin(\phi_i - \psi_i) \cos \psi_i \right. \\ &\quad \left. + \frac{R}{L} \cos 2\theta \sum_{i=1}^n a_i \cos 2(\phi_i - \psi_i) \cos \psi_i - \frac{R}{L} \sin 2\theta \sum_{i=1}^n a_i \sin 2(\phi_i - \psi_i) \cos \psi_i \right] \end{aligned} \quad (16.48)$$

For dynamic balance, it is important to balance both the shaking force and the shaking moment. Both will cause undesirable vibrations at the engine base. To balance the shaking moment, we want the moment components in

[Equations 16.47](#) and [16.48](#) to be zero. This occurs when

$$\sum_{i=1}^n a_i \cos(\phi_i - \psi_i) \cos \psi_i = 0 \quad (16.49)$$

$$\sum_{i=1}^n a_i \cos(\phi_i - \psi_i) \sin \psi_i = 0 \quad (16.50)$$

$$\sum_{i=1}^n a_i \sin(\phi_i - \psi_i) \sin \psi_i = 0 \quad (16.51)$$

$$\sum_{i=1}^n a_i \sin(\phi_i - \psi_i) \cos \psi_i = 0 \quad (16.52)$$

$$\sum_{i=1}^n a_i \cos 2(\phi_i - \psi_i) \cos \psi_i = 0 \quad (16.53)$$

$$\sum_{i=1}^n a_i \cos 2(\phi_i - \psi_i) \sin \psi_i = 0 \quad (16.54)$$

$$\sum_{i=1}^n a_i \sin 2(\phi_i - \psi_i) \sin \psi_i = 0 \quad (16.55)$$

$$\sum_{i=1}^n a_i \sin 2(\phi_i - \psi_i) \cos \psi_i = 0 \quad (16.56)$$

As in the case of the shaking force, satisfaction of [Equations 16.49–16.52](#) is necessary to balance the primary shaking moments, and satisfaction of [Equations 16.53–16.56](#) is necessary to balance the secondary shaking moments.

Notice that it may be possible to reduce the shaking forces using counterweights even though [Equations 16.39–16.46](#) and [16.49–16.56](#) are not satisfied. However, it is much more efficient if the shaking forces can be internally balanced by a careful design of the crank phase angles. Even in cases in which it is not possible to balance the shaking forces perfectly by satisfying all of the equations directly, if the equations are satisfied approximately, the shaking forces and moments will be reduced, and the sizes of any additional counterbalance weights will also be reduced.

To illustrate the use of the equations, we will investigate two examples. For a more extensive consideration of the topic, see the work by Holowenko [1].

16.6.1 Balancing a Three-Cylinder In-Line Engine

Three-cylinder in-line engines are commonly used in small utility tractors. An example of this cylinder arrangement is shown in [Figure 16.15](#). Notice that ψ_i is zero for each cylinder, and the crank phase angles are distributed symmetrically about the crankshaft axis. Because $\psi_i \approx 0$, $\sin \psi_i \approx 0$, and $\cos \psi_i \approx 1$. Therefore, [Equations 16.40](#), [16.41](#) and [16.45](#) and [Equations 16.50](#), [16.51](#) and [16.55](#) are satisfied identically. The left-hand sides of the remaining equations are given in the following

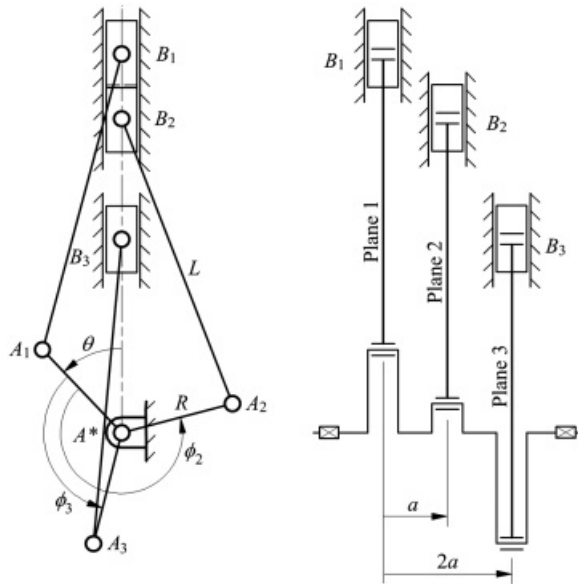


[Figure 16.15](#) Schematic diagram of a three-cylinder in-line engine.

$$\begin{aligned}
 \sum_{i=1}^3 \cos \phi_i &= 1 + \cos 240^\circ + \cos 120^\circ = 1 - \frac{1}{2} - \frac{1}{2} = 0 \\
 \sum_{i=1}^3 \sin \phi_i &= 0 + \sin 240^\circ + \sin 120^\circ = 0 - \frac{\sqrt{3}}{2} + \frac{\sqrt{3}}{2} = 0 \\
 \sum_{i=1}^3 \cos 2\phi_i &= 1 + \cos 480^\circ + \cos 240^\circ = 1 - \frac{1}{2} - \frac{1}{2} = 0 \\
 \sum_{i=1}^3 \sin 2\phi_i &= 0 + \sin 480^\circ + \sin 240^\circ = 0 + \frac{\sqrt{3}}{2} - \frac{\sqrt{3}}{2} = 0 \\
 \sum_{i=1}^3 a_i \cos \phi_i &= 0 + a \cos 240^\circ + 2a \cos 120^\circ = 0 - \frac{a}{2} - \frac{2a}{2} = -\frac{3a}{2} \\
 \sum_{i=1}^3 a_i \sin \phi_i &= 0 + a \sin 240^\circ + 2a \sin 120^\circ = 0 - \frac{a\sqrt{3}}{2} + \frac{2a\sqrt{3}}{2} = \frac{a\sqrt{3}}{2} \\
 \sum_{i=1}^3 a_i \cos 2\phi_i &= 0 + a \cos 480^\circ + 2a \cos 240^\circ = 0 - \frac{a}{2} - \frac{2a}{2} = -\frac{3a}{2} \\
 \sum_{i=1}^3 a_i \sin 2\phi_i &= 0 + a \sin 480^\circ + 2a \sin 240^\circ = 0 + \frac{a\sqrt{3}}{2} - \frac{2a\sqrt{3}}{2} = -\frac{a\sqrt{3}}{2}
 \end{aligned}$$

In this engine, the shaking forces are balanced exactly, but the primary and secondary moments are not balanced. The moments form a shaking couple on the engine. The magnitude of the couple is given by [Equation 16.48](#) as

$$M = m_2 R \omega^2 \left[-\frac{3a}{2} \cos \theta - \frac{a\sqrt{3}}{2} \sin \theta - \frac{R}{L} \frac{3a}{2} \cos 2\theta - \frac{R}{L} \frac{a\sqrt{3}}{2} \sin 2\theta \right] \quad (16.57)$$

This equation can be simplified by the trigonometric relationship

$$p \cos \beta + q \sin \beta = \sqrt{p^2 + q^2} \sin(\beta + \gamma) \quad (16.58)$$

where $\tan \gamma = p/q$. Equation 16.57 can then be written as

$$M = \frac{m_2 R \omega^2}{2} \left[-2\sqrt{3} \sin(\theta + 60^\circ) - 2 \frac{R}{L} \sqrt{3} \sin(2\theta - 60^\circ) \right] \quad (16.59)$$

The first term is the primary shaking moment and the second term is the secondary shaking moment. The primary shaking moment can be balanced by counterweights that rotate at the engine speed but are out of phase with the first crank by positive 60°. The secondary shaking moment can be balanced by counterweights that rotate at two times the engine speed and are out of phase with the first crank by negative 60°. Figure 16.16 shows one balancing scheme for the shaking moments. The mass of the counterbalances for the primary moment is [1]

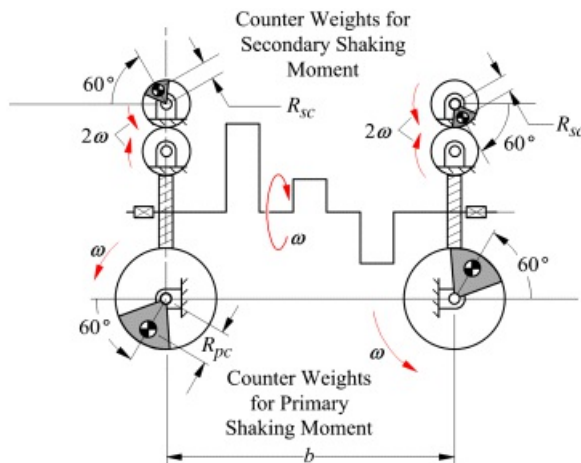


Figure 16.16 Arrangements to balance primary and secondary shaking moments. The counterbalance weights are shown for the position when $\theta = 0$.

$$m_{C2, \text{primary}} = 2\sqrt{3}m_2 \frac{R}{R_{pc}} \frac{a}{b}$$

and for the secondary moment

$$m_{C2, \text{secondary}} = \frac{3}{4}m_2 \frac{R}{R_{sc}} \frac{a}{b}$$

where R_{pc} is the radial location of the center of mass of the counterweights for the primary shaking moment, R_{sc} is the radial location of the center of mass of the counterweights for the secondary shaking moment, and b is the distance between the rotation axes of the counterweights. The counterweights for the primary shaking moment rotate at the same velocity as the crankshaft, and the counterweights for the secondary shaking moment rotate at

twice the velocity of the crankshaft.

16.6.2 Balancing an Eight-Cylinder V Engine

Eight-cylinder V engines (V-8) are commonly used in high-performance automobiles. An example of this cylinder arrangement is shown in [Figure 16.17](#). The engine shown is assumed to have the cylinder banks oriented at 90° to each other. Cylinders 1 and 5, 2 and 6, 3 and 7, and 4 and 8 are symmetrically located relative to the vertical axis. Then ψ_i is 90° for cylinders 5, 6, 7, and 8 and 0° for cylinders 1, 2, 3, and 4. The phase angles are $\phi_1 = \phi_5 = 0^\circ$, $\phi_2 = \phi_6 = 90^\circ$, $\phi_3 = \phi_7 = 270^\circ$, and $\phi_4 = \phi_8 = 180^\circ$. Substitution of the known angles into [Equations 16.39–16.46](#) and [16.53–16.56](#) will show that the shaking-force equations and the secondary shaking-moment equations are satisfied. However, the primary shaking-moment equations are not satisfied. The left-hand sides of [Equations 16.49–16.52](#) give

$$\begin{aligned} \sum_{i=1}^8 a_i \cos(\phi_i - \psi_i) \cos \psi_i &= -3a, & \sum_{i=1}^8 a_i \cos(\phi_i - \psi_i) \sin \psi_i &= -a \\ \sum_{i=1}^8 a_i \sin(\phi_i - \psi_i) \sin \psi_i &= 3a, & \sum_{i=1}^8 a_i \sin(\phi_i - \psi_i) \cos \psi_i &= -a \end{aligned}$$

The x component of the shaking moment is given by [Equation 16.47](#). Substitution of numbers into that equation gives

$$\begin{aligned} M_x &= -m_g R \omega^2 \left[\cos \theta \sum_{i=1}^8 a_i \cos(\phi_i - \psi_i) \sin \psi_i - \sin \theta \sum_{i=1}^8 a_i \sin(\phi_i - \psi_i) \sin \psi_i \right. \\ &\quad \left. + \frac{R}{L} \cos 2\theta \sum_{i=1}^8 a_i \cos 2(\phi_i - \psi_i) \sin \psi_i - \frac{R}{L} \sin 2\theta \sum_{i=1}^8 a_i \sin 2(\phi_i - \psi_i) \sin \psi_i \right] \\ &= -\overline{m}_g R \omega^2 a [\cos \theta + 3 \sin \theta] \end{aligned}$$

or using [Equation 16.58](#) with the trigonometric identity $\sin \theta = \cos(\theta - 90^\circ)$

$$M_x = \sqrt{1.0 \overline{m}_g R \omega^2 a} \cos(\theta - 71.56^\circ) \quad (16.60)$$

The y component of the shaking force is given by [Equation 16.48](#). Substitution of numbers into that equation gives

$$\begin{aligned} M_y &= -m_g R \omega^2 \left[\cos \theta \sum_{i=1}^8 a_i \cos(\phi_i - \psi_i) \cos \psi_i - \sin \theta \sum_{i=1}^8 a_i \sin(\phi_i - \psi_i) \cos \psi_i \right. \\ &\quad \left. + \frac{R}{L} \cos 2\theta \sum_{i=1}^8 a_i \cos 2(\phi_i - \psi_i) \cos \psi_i - \frac{R}{L} \sin 2\theta \sum_{i=1}^8 a_i \sin 2(\phi_i - \psi_i) \cos \psi_i \right] \\ &= -\overline{m}_g R \omega^2 a [-3 \cos \theta + \sin \theta] \end{aligned}$$

or using [Equation 16.58](#),

$$M_y = \sqrt{1.0 \overline{m}_g R \omega^2 a} \sin(\theta - 71.56^\circ)$$

The x and y components of the shaking moment can be combined vectorially to form the vector

$$M = \sqrt{10m_B R \omega^2 a} [\cos(\theta - 71.56^\circ) \hat{i} + \sin(\theta - 71.56^\circ) \hat{j}]$$

Therefore, the shaking moment is of constant magnitude and can be balanced by the couple formed by rotating counterweights. The magnitude of the couple must be equal to $\sqrt{10m_B R \omega^2 a}$. A possible counterweight arrangement for the crankshaft position corresponding to $\theta = 0$ is given in [Figure 16.18](#).

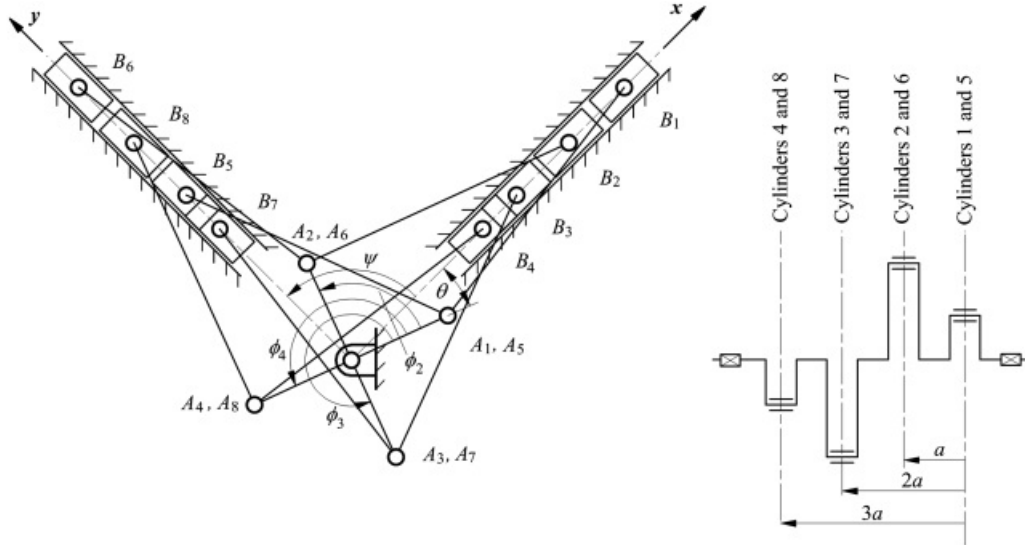


[Figure 16.17](#) Eight-cylinder engine with 90° V.

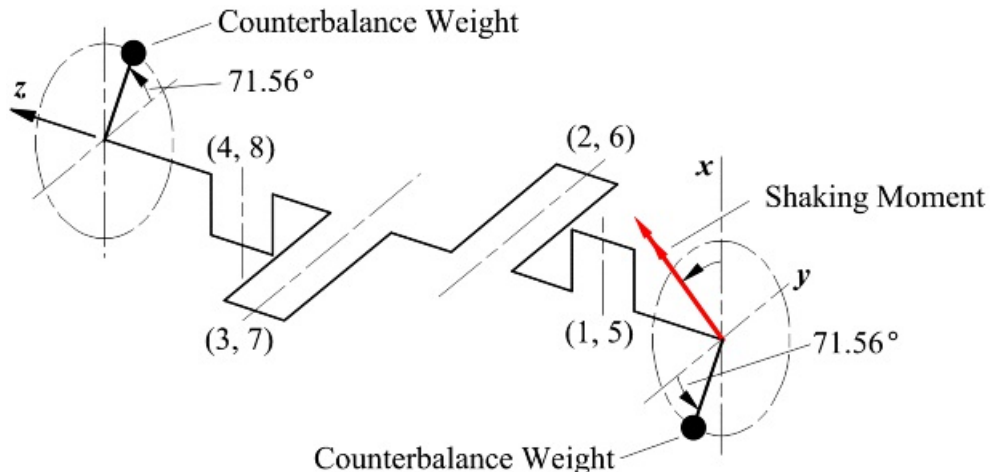


[Figure 16.18](#) Rotating counterweights used to balance shaking forces in an eight-cylinder V engine.



16.7 Static Balancing of Mechanisms

So far we have considered only rotors and reciprocating machines. However, all mechanisms require external forces and torques to keep them in equilibrium under the effects of gravity. These external forces and torques that are required to keep the system in equilibrium will, in general, vary with the configuration of the mechanism. However, it is possible to design a system so that it remains statically balanced in all configurations of the mechanism. It may be advantageous to develop machinery with this property of static balancing because the actuators will then be needed only to dynamically move the system around the equilibrium position, thereby decreasing the need for large and costly motors. Some common applications of statically balanced mechanisms that we see in our daily life include study desk lamps, ceiling-mounted medical equipment in doctor's offices, machines for lifting heavy machinery, and others.

Gravity balancing can be analyzed systematically if one analytically describes the total potential energy V of the system at a configuration $q = (q_1, q_2, \dots, q_n)$ of the mechanism, where q is a set of independent coordinates or the *generalized coordinates* for the system. The common contributors to the potential energy of a mechanical system are gravity and springs. In general, we can write the potential energy as $V(q)$ to label that the potential energy changes as the mechanism takes different configurations. If $r_i(q_1, q_2, \dots, q_n)$ are the torques/forces applied at the generalized coordinates to keep the system in equilibrium under the influence of gravity and/or springs, these are given by the following expression

$$r_i(q) = \frac{\partial V(q_1, q_2, \dots, q_n)}{\partial q_i}, \quad i = 1, \dots, n. \quad (16.61)$$

The potential energy $V(q)$ of a system in a configuration q can be analytically obtained by adding up the potential energy contributions from each of the M bodies that make up the system, that is

$$V(q) = \sum_{i=1}^M V_i(q) \quad (16.62)$$

where $V_i(q)$ is the potential energy contributed by the i th body of the system. If the potential energy becomes invariant with configuration, then

$$r_i(q) = \frac{\partial V(q_1, q_2, \dots, q_n)}{\partial q_i} = 0$$

that is, external torques/forces need not be applied to the system to keep it in equilibrium. We can further break down the potential energy $V(q) = V_g(q) + V_s(q)$, where $V_g(q)$ is the potential energy due to gravity and $V_s(q)$ is the potential energy due to springs within the system. In general, $V_g(q)$ depends on the mass distribution within the system and the kinematic design of the mechanism. Hence, there may be less flexibility to alter $V_g(q)$ through design. However, $V_s(q)$ is the potential energy due to springs and it can be altered by introducing suitable springs within the mechanism. Section 16.7.1 gives examples of planar-open and closed-chain mechanisms to illustrate the gravity balancing method. In addition, a practical design of a gravity balancing orthosis (GBO) that was tested on healthy human subjects is provided in Section 16.7.2.

16.7.1 Gravity Balancing of Planar Mechanisms: Examples

Single Link with an R-Joint

Consider a rigid link of length l which can turn around a fixed hinge in the vertical plane. This link has a mass m

and its orientation is described with respect to the horizontal line by the angle θ , as shown in [Figure 16.19](#) (left). Its center of mass is at l' . The potential energy of this link is

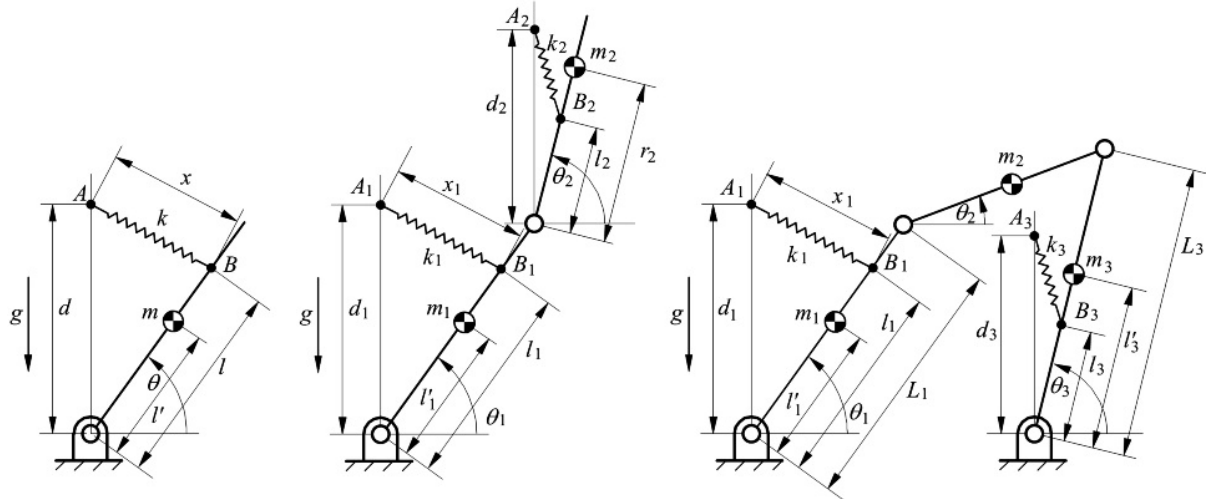


[Figure 16.19](#) (Left) gravity-balanced one-link hinged mechanism; (Center) gravity balanced two-link open-chain mechanism; (Right) gravity-balanced three-link closed-chain planar mechanism.

$$V_g(\theta) = mg^2 \sin \theta$$

A linear spring of stiffness k is added such that one end of the spring lies on the vertical line passing through the hinge at a distance d while the other end is attached to the moving link at a distance l from the hinge. It is assumed that the spring has *zero-free length*. That is, the force in the spring is kx , where x is the distance between the two attachment points A and B , in the fixed frame and on the moving link, respectively. Note that zero-free length springs can be made with commonly available commercial springs and off-the-shelf steel wire so that the spring extension is given by the distance $|AB|$. The potential energy due to the spring is given by

$$V_s(\theta) = \frac{1}{2}k(l^2 + d^2 - 2ld \sin \theta) \quad (16.63)$$

The total potential energy $V(\theta)$ is the sum of $V_g(\theta)$ and $V_s(\theta)$ and its expression can be simplified to be

$$V(\theta) = \frac{1}{2}k(l^2 + d^2) + (mg^2 - kd^2) \sin \theta \quad (16.64)$$

If the parameters of the spring satisfy the relationship $mg^2 = kld$, the potential energy $V(\theta)$ becomes constant and, according to [Equation 16.61](#), will not require an external torque at the hinge to keep it in equilibrium. With this choice of the spring, the mechanism becomes gravity balanced in every configuration of the link.

Two-Link Open-Chain Mechanism

Consider a two-rigid link open chain with lengths l_1 and l_2 moving in the vertical plane. The links have masses m_1 and m_2 and their orientations are described with respect to the horizontal line by angles θ_1 and θ_2 , respectively, as shown in [Figure 16.19](#) (Center). The center of masses are at lengths l'_1 and l'_2 from their respective hinges. The potential energy for the system is

$$V_g(\theta) = m_1 g l'_1 \sin \theta_1 + m_2 g (l'_1 \sin \theta_1 + l'_2 \sin \theta_2)$$

Linear zero-free length springs with stiffness k_1 and k_2 are added at distances d_1 and d_2 as shown in the figure, through lines which pass through the two joints and remain parallel to the vertical line. Note that this could be achieved via a parallelogram linkage. The other ends of the two springs attach to the links at distances l_1 and l_2 , respectively. The potential energy due to the springs is given as

$$V_s(\theta) = \frac{1}{2}k_1(l_1^2 + d_1^2 - 2l_1d_1\sin\theta_1) + \frac{1}{2}k_2(l_2^2 + d_2^2 - 2l_2d_2\sin\theta_2) \quad (16.65)$$

The total potential energy $V(\theta)$ is the sum of $V_g(\theta)$ and $V_s(\theta)$ and its expression can be simplified to be

$$V(\theta) = \frac{1}{2}k_1(l_1^2 + d_1^2) + \frac{1}{2}k_2(l_2^2 + d_2^2) + \sin\theta_1(m_1g\vec{l}_1 + m_2g\vec{l}_1 - k_1l_1d_1) + \sin\theta_2(m_2g\vec{l}_2 - k_2l_2d_2) \quad (16.66)$$

If the parameters of the springs satisfy the relationships

$$k_1l_1d_1 = m_1g\vec{l}_1 + m_2g\vec{l}_1$$

and

$$k_2l_2d_2 = m_2g\vec{l}_2$$

the potential energy $V(\theta)$ becomes constant and the mechanism will not require torques at the joints to keep it in equilibrium. With these choices of the springs, the mechanism becomes gravity balanced in every configuration. Please note that this is only one of the many configurations in which the springs can be used to gravity balance the system.

Four-Bar Mechanism

Consider a four-bar linkage with link lengths L_1 , L_2 , and L_3 moving in the vertical plane as shown in [Figure 16.19](#) (Right). The links have masses m_1 , m_2 , and m_3 their orientations are described with respect to the horizontal line by the angles θ_1 , θ_2 , and θ_3 respectively, as shown in [Figure 16.19](#) (Right). The center of masses are at lengths \vec{l}_1 , \vec{l}_2 , and \vec{l}_3 from their respective hinges. The potential energy for the system is

$$V_g(\theta) = m_1g\vec{l}_1\sin\theta_1 + m_2g(L_1\sin\theta_1 + \vec{l}_2\sin\theta_2) + m_3g\vec{l}_3\sin\theta_3$$

Linear zero-free length springs with stiffness k_1 and k_3 are added at distances d_1 and d_3 , as shown in the figure, through lines which pass through the joints and remain parallel to the vertical line. The other ends of the two springs attach to the links at distances l_1 and l_3 , respectively. The potential energy due to the springs is given by

$$V_s(\theta) = \frac{1}{2}k_1(l_1^2 + d_1^2 - 2l_1d_1\sin\theta_1) + \frac{1}{2}k_3(l_3^2 + d_3^2 - 2l_3d_3\sin\theta_3) \quad (16.67)$$

The total potential energy $V(\theta)$ is the sum of $V_g(\theta)$ and $V_s(\theta)$ and its expression can be simplified to be

$$V(\theta) = \frac{1}{2}k_1(l_1^2 + d_1^2) + \frac{1}{2}k_3(l_3^2 + d_3^2) + \sin\theta_1(m_1g\vec{l}_1 + m_2gL_1 - k_1l_1d_1) + \sin\theta_2m_2g\vec{l}_2 + \sin\theta_3(m_3g\vec{l}_3 - k_3l_3d_3) \quad (16.68)$$

Note that having the parameters of the two springs satisfy the relationships

$$k_1 \dot{\theta}_1 = m_1 g \dot{\theta}_1 + m_2 g \dot{\theta}_2$$

and

$$k_2 \dot{\theta}_2 = m_2 g \dot{\theta}_2$$

is not enough to make the potential energy $V(\theta)$ become constant. However, due to the loop closure, the angles θ_1 , θ_2 , and θ_3 satisfy additional constraints, one of which is

$$\dot{\theta}_1 \sin \theta_1 + \dot{\theta}_2 \sin \theta_2 = \dot{\theta}_3 \sin \theta_3 \quad (16.69)$$

This constraint can be used to substitute the expression

$$\sin \theta_2 = \frac{L_3}{L_2} \sin \theta_3 - \frac{L_1}{L_2} \sin \theta_1$$

in [Equation 16.68](#) to obtain the following expression for the potential energy

$$V(\theta) = \frac{1}{2} k_1 (\dot{\theta}_1^2 + \dot{\theta}_1^2) + \frac{1}{2} k_3 (\dot{\theta}_3^2 + \dot{\theta}_3^2) + \sin \theta_1 \left(m_1 g \dot{\theta}_1^2 + m_2 g L_1 - k_1 \dot{\theta}_1 \dot{\theta}_1 - m_2 g \dot{\theta}_2 \frac{L_1}{L_2} \right) + \sin \theta_3 \left(m_3 g \dot{\theta}_3^2 - k_3 \dot{\theta}_3 \dot{\theta}_3 + m_2 g \dot{\theta}_2 \frac{L_3}{L_2} \right) \quad (16.70)$$

The parameters for the two springs can now be chosen to satisfy the relationships

$$k_1 \dot{\theta}_1 \dot{\theta}_1 = m_1 g \dot{\theta}_1^2 - m_2 g \dot{\theta}_1 \dot{\theta}_1 - m_2 g \dot{\theta}_2 \frac{L_1}{L_2}$$

and

$$k_3 \dot{\theta}_3 \dot{\theta}_3 = m_3 g \dot{\theta}_3^2 - m_2 g \dot{\theta}_2 \frac{L_3}{L_2}$$

to obtain a balanced system. Please note that this design uses two springs to gravity balance the system and other configurations of the springs may also exist to achieve the same goal.

16.7.2 Gravity-Balancing Orthosis

A vast number of people suffer from profound muscle weakness. In addition, subjects with neurological injuries have severe movement limitations. For example, survivors of stroke often show hemiparesis (i.e., one-sided weakness of the body). This results in both spatial and temporal asymmetry in their gait between healthy and the affected legs. One of the aims of rehabilitation after stroke is to improve their walking function. The goal of the gravity-balancing orthosis (GBO) design was to assist persons with hemiparesis to improve their gait by progressively changing the level of gravity on their limbs. The design was expected to be able to dial in a level of gravity between no gravity and full gravity. In the beginning, the stroke survivor will walk with 100 percent

gravity assistance from the GBO and this assistance will be decreased over six weeks of training with the device [2]. Some of the salient features of GBO are: (1) it is passive, that is, it does not need motors or actuators, but is only composed of rigid members and springs; and (2) it has a simple human–machine interface to accommodate variability in geometry and inertia of the users.

[Figure 16.20](#) shows the architecture of the GBO. It uses three cuffs to strap the orthosis to the pelvis, thigh, and shank segments. An adjustable parallelogram mechanism is used in the design to identify the combined system center of mass of the human and orthosis. Two zero-free-length springs are used in the design so that the combined potential energy of the human leg and GBO becomes configuration invariant. The attachment point of the spring on the human pelvis is calibrated to attain the desired level of partial gravity balancing of the human user. Additional details of this design are provided in reference [3].

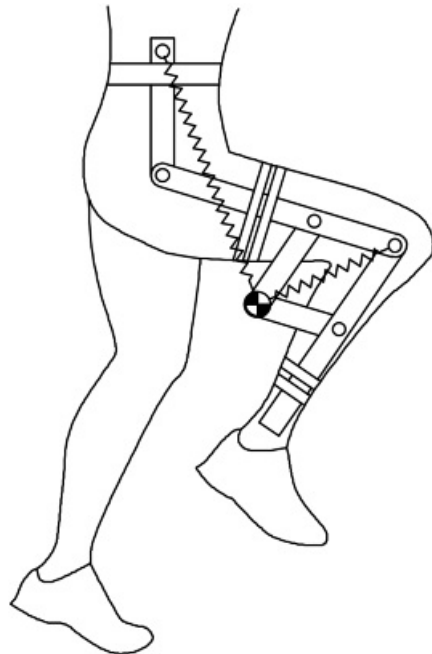


[Figure 16.20](#) Schematic of a gravity-balancing orthosis for a human subject consisting of five rigid members and two springs [3].

Before a long-term pilot study on stroke survivors, the performance of the device was quantitatively evaluated using electromyographic (EMG) data of the key muscle groups within the human body that are involved in the motion of the leg. Experiments on tasks that involve leg raising and walking were performed. The results showed that the EMG activity from rectus femoris and hamstring muscles with the device reduced by up to 75 percent when the leg was raised and kept stationary in a new configuration. In the walking experiments, stroke patients showed an increased range of motion by 45 percent at the hip joint and by 85 percent at the knee joint.



16.8 Reactionless Mechanisms

As we saw earlier in this chapter, as a mechanism moves, it creates reaction forces on its supporting base. As a result, often machines have to be mounted on floors that minimize the transmission of these reaction forces on the surrounding environment. In critical applications, such as in space, where a robot arm may be mounted on a freely moving base station, the reaction forces due to the motion of the arm may destabilize the base, if left uncorrected. Additional fuel must be spent by the thrusters on the base station to correct for these disturbance forces. This motivates the question if one can design general open- or closed-chain mechanisms which are reactionless (i.e., these do not apply any reaction forces on its supporting base).

We can answer this question using the Newton's laws applied to a collection of rigid bodies that make up an interconnected system. The relationship between the force system and the motion of the mechanism is described by the Newton–Euler relationships ([Equations 15.2](#) and [15.5](#)). From these relationships, it is clear that the resultant external force is zero if and only if the acceleration of the system center of mass is zero. If the system is connected to the ground at a single point and it is reactionless, the point at which it is connected must be the system center of mass. If the system is connected to the ground at multiple points, one of which is the system center of mass, then the sum total of the reaction force vectors at the attachment points must be zero.

In addition, the Newton–Euler law states that the rate of change of angular momentum of the system about the system center of mass is equal to the net external moment applied about the system center of mass.

If the system is connected to the ground at only one point (i.e., at the system center of mass), and it does not transmit any moment to the base then this connection must be through a passive rotational joint. In this case, the motion of the system will be such that the system angular momentum will remain constant. If the system is passively connected to the ground at multiple points, and the motion of the system is chosen so that the angular momentum is a constant, then the net moment it exerts on the ground will be zero.

The above conditions lay the foundations for design of reactionless mechanisms and were used to design a reactionless three-link planar open-chain mechanism. The center of mass of the chain was located using a series of parallelograms with the knowledge of the geometry and mass of the links. Based on the arguments of the preceding paragraphs, the system was connected to the base at the center of mass using a passive joint. While detailed calculations are not presented in the book, the readers are encouraged to look at the reference [4].



References

1. Holowenko, A.R. (1955). *Dynamics of Machinery*. New York, NY: New York, NY.
2. Krishnamoorthy, V., et al. (2008). "Gait Training Following Stroke: A Pilot Study Combining a Gravity-Balanced Orthosis Device, Functional Electrical Stimulation and Visual Feedback." *Journal of Neurologic Physical Therapy*, Vol. 232, pp. 192–202, December.
3. Banala, S., et al. (2006). "Gravity Balancing Leg Orthosis and Its Performance Evaluation." *IEEE Trans. on Robotics*, Vol. 22, No. 6, pp. 1228–1237.
4. Agrawal, S. K., and Fattah, A. (2004). "Reaction-Less Space and Ground Robots: Novel Designs and Concept Studies." *Mechanisms and Machine Theory*, Vol. 39, pp. 25–40.

Problems

Rotary Balance

16.1 [Figure P16.1](#) shows a system with two weights, W_A and W_B , that have been found to balance a system of weights (not shown) on the shaft. The weights for W_A and W_B are 4 and 8 lb, respectively, and the radii, r_A and r_B , are both 6 inches. Later, it is decided to replace W_A and W_B by two weights, W_C and W_D , where the planes for the two weights are as shown. What are the magnitudes and angular locations of W_C and W_D if the radius of the center of gravity for both links is 5 in?

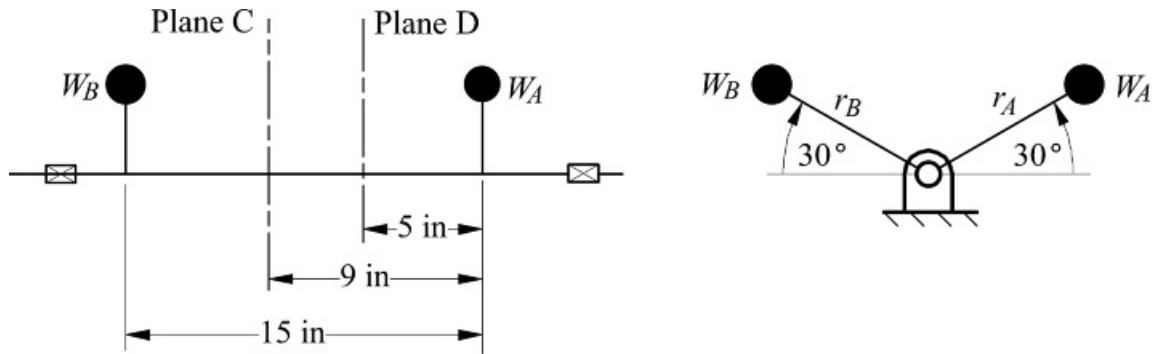


[Figure P16.1](#) Weights for Problem 16.1.

16.2 [Figure P16.2](#) shows a system with two weights, W_A and W_B , that have been found to balance a system of weights (not shown) on the shaft. The weights for W_A and W_B are 6 and 8 lb, respectively, and the radii, r_A and r_B , are both 5 inches. It is decided to replace W_A and W_B by two weights, W_C and W_D , where the planes for the two weights are as shown. What are the magnitudes and angular locations of W_C and W_D if the radius of the center of gravity for both links is 6 in?

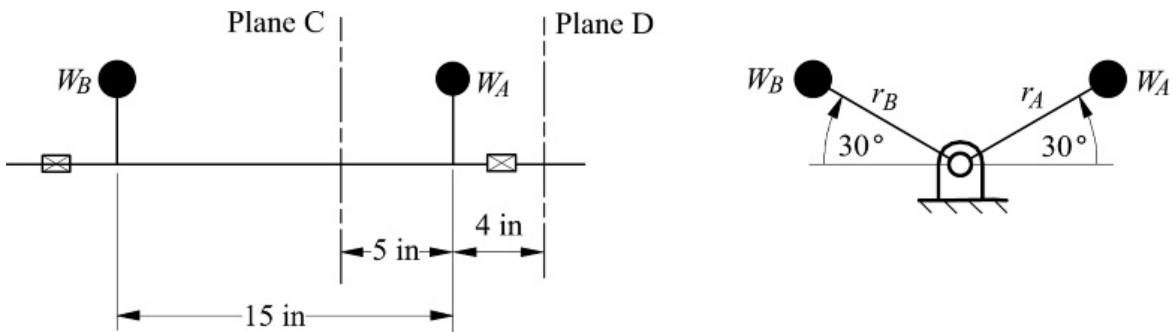


[Figure P16.2](#) Weights for Problem 16.2.

16.3 Three rotating weights W_1 , W_2 , W_3 are to be balanced by two weights W_A and W_B in planes A and B , as shown in [Figure P16.3](#). Determine the magnitude and angular locations of the counterbalance weights necessary to balance the rotating weights.

$W_1 = 12 \text{ lb}$	$r_1 = 2.5 \text{ in}$	$\theta_1 = 30^\circ$	$z_1 = 4 \text{ in}$
$W_2 = 9 \text{ lb}$	$r_2 = 2.5 \text{ in}$	$\theta_2 = 150^\circ$	$z_2 = 16 \text{ in}$
$W_3 = 8 \text{ lb}$	$r_3 = 2.5 \text{ in}$	$\theta_3 = 270^\circ$	
$r_A = 2.5 \text{ in}$	$r_B = 2.5 \text{ in}$		

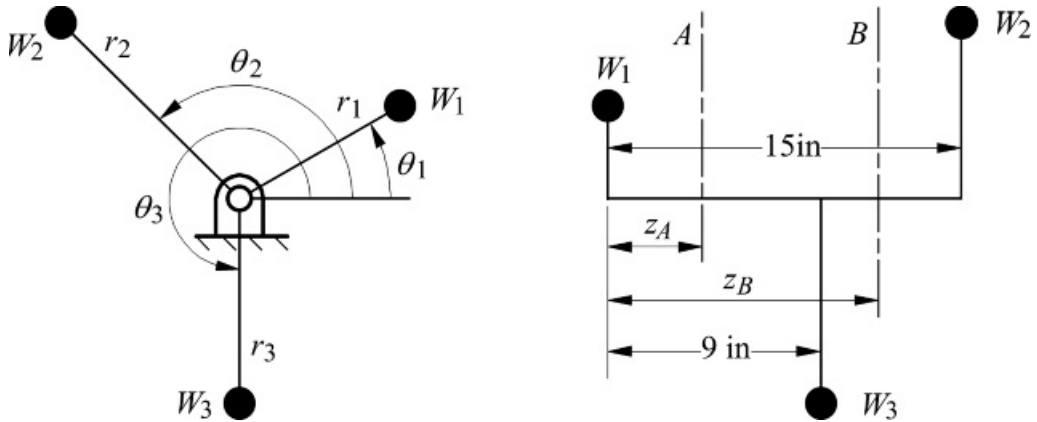


[Figure P16.3](#) Weights for Problem 16.3.

16.4 Solve Problem 16.3 if z_A and z_B are 4.5 in and 12 in, respectively.

16.5 Four weights, W_1 , W_2 , W_3 , and W_4 are all rotating in a single plane, as shown in [Figure P16.5](#).

Determine the magnitude and angular location of the single weight necessary to balance the four rotating weights. Assume that the radius to the center of gravity of the balancing weight is 9 in. The shaft is rotating at 1800 rpm.

$W_1 = 12 \text{ lb}$	$r_1 = 9 \text{ in}$	$\theta_1 = 30^\circ$
$W_2 = 9 \text{ lb}$	$r_2 = 12 \text{ in}$	$\theta_2 = 133^\circ$
$W_3 = 8 \text{ lb}$	$r_3 = 10 \text{ in}$	$\theta_3 = 270^\circ$
$W_4 = 5 \text{ lb}$	$r_4 = 8 \text{ in}$	$\theta_4 = 315^\circ$

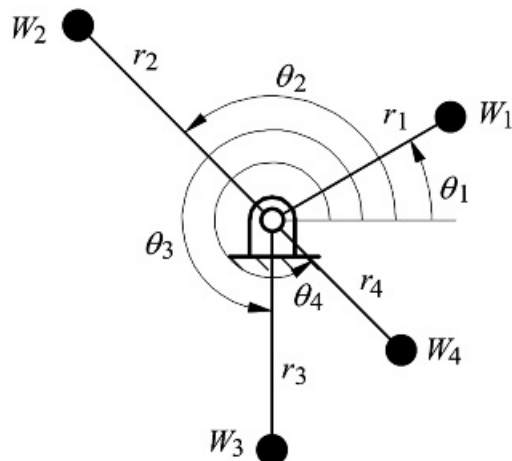


[Figure P16.5](#) Weights for Problem 16.5.

16.6 Solve Problem 16.5 for the following set of data:

$W_1 = 20 \text{ lb}$	$r_1 = 4 \text{ in}$	$\theta_1 = 45^\circ$
$W_2 = 10 \text{ lb}$	$r_2 = 12 \text{ in}$	$\theta_2 = 133^\circ$
$W_3 = 8 \text{ lb}$	$r_3 = 12 \text{ in}$	$\theta_3 = 180^\circ$
$W_4 = 6 \text{ lb}$	$r_4 = 10 \text{ in}$	$\theta_4 = 270^\circ$

Shaking Forces

16.7 Using [Figure P16.7](#), determine the magnitude and location of the shaking force acting on the frame. Determine the location with respect to point A . Also find the magnitude of the reaction force at point A and

at point C. Assume that $W_3 \gg W_2$ and W_4 . Use $W_3 = 2.0 \text{ lb}$, $I_3 = 0.1 \text{ lb-s}^2\text{-in}$, and $\omega_2 = 6.28 \text{ rad/s CCW}$ (constant).

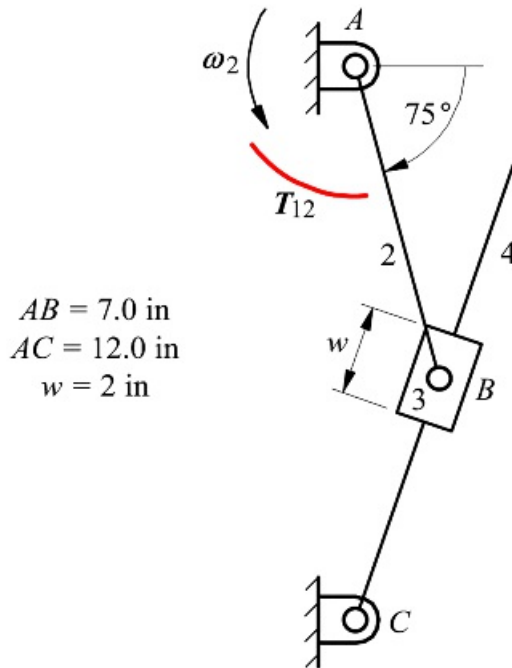


Figure P16.7 Mechanism for Problem 16.7.

16.8 For the mechanism and data given in Figure P16.8, determine the shaking force and its location relative to point A. Draw the shaking force vector on the figure. The force F_B is 10 lb in the direction shown. For the moments of inertia of link 3, use $g = 386 \text{ in/s}^2$ and $I_G = m l^2 / 12$.

$A^*A = 3 \text{ in}$	$AB = 12$	$A^*G_2 = 1.2 \text{ in}$	$AG_3 = 3.6 \text{ in}$
$\omega_2 = 160 \text{ rad/s CCW}$	$\alpha_2 = 0 \text{ rad/s}^2$	$W_2 = 0.95 \text{ lb}$	$W_3 = 3.5 \text{ lb}$
		$W_4 = 2.5 \text{ lb}$	$I_{G_3} = 0.00369 \text{ lb-s}^2\text{-in}$

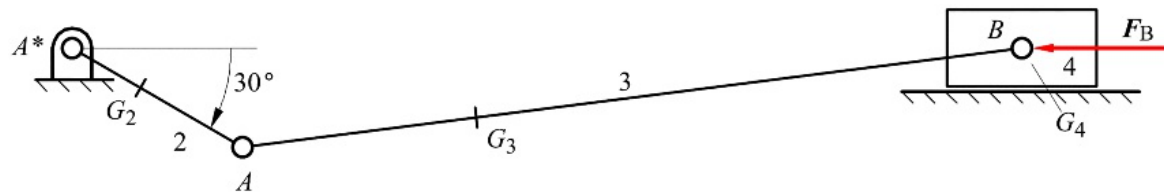
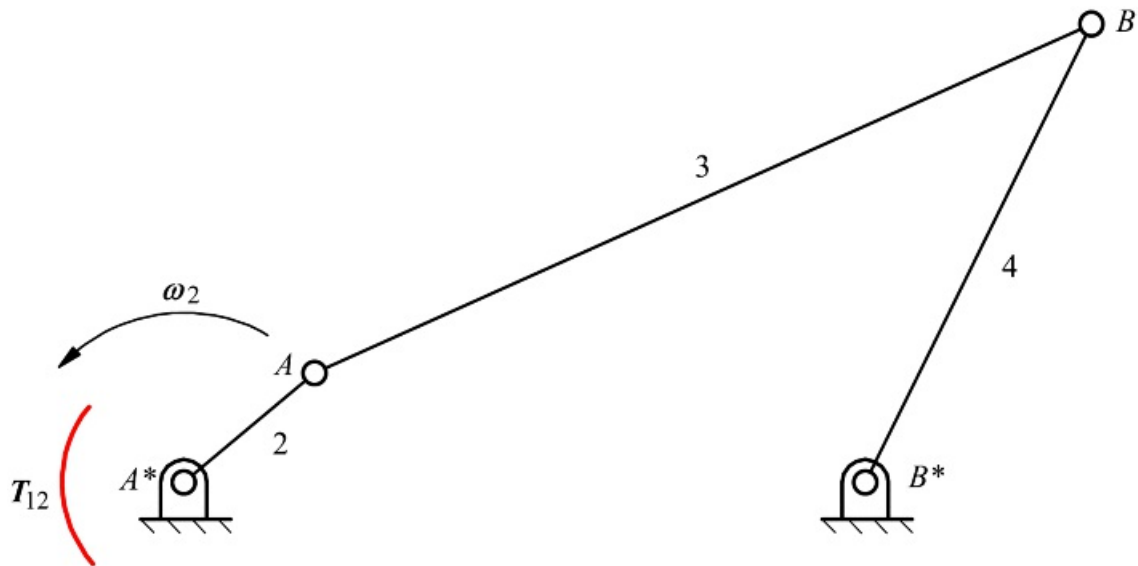


Figure P16.8 Mechanism for Problem 16.8.

16.9 For the mechanism shown in Figure P16.9, determine the magnitude and location of the shaking force acting on the frame. Determine the location with respect to point A^* if the weight of each link is uniformly distributed along its length. Draw the shaking force vector on the figure.

$\omega_2 = 12 \text{ rad/s CCW}$	$\alpha_2 = 0$	$W_2 = 0.5 \text{ N}$	$W_3 = 2.5 \text{ N}$	$W_4 = 1.5 \text{ N}$
$A^*A = 10 \text{ cm}$	$AB = 50 \text{ cm}$	$B^*B = 30 \text{ cm}$	$A^*B^* = 40 \text{ cm}$	

For the moments of inertia for the links, use $g = 9.81 \text{ m/s}^2$ and $I_G = ml^2/12$.



[Figure P16.9](#) Mechanism for Problem 16.9.

16.10 For the mechanism in [Figure P16.10](#), assume that ω_2 is 200 rad/s CCW (constant) and link 2 is balanced so that its center of mass is located at the pivot at point A^* . Also assume that I_{G2} is small enough to be neglected. For the data given, determine the shaking force and its location relative to point A^* . Draw the shaking force vector on the figure.

$$J_{G_2} = 0.0106 \text{ lb s}^2 \text{ in} \quad W_2 = 2.69 \text{ lb} \quad I_{G_4} = 0.0631 \text{ lb s}^2 \text{ in} \quad W_4 = 6.72 \text{ lb} \quad AC_3 = 8.8 \text{ in} \quad BC_4 = 4.0 \text{ in} \\ A^*A = 2.2 \text{ in} \quad AB = 17.6 \text{ in} \quad B^*B = 8.0 \text{ in} \quad A^*B^* = 13.5 \text{ in}$$

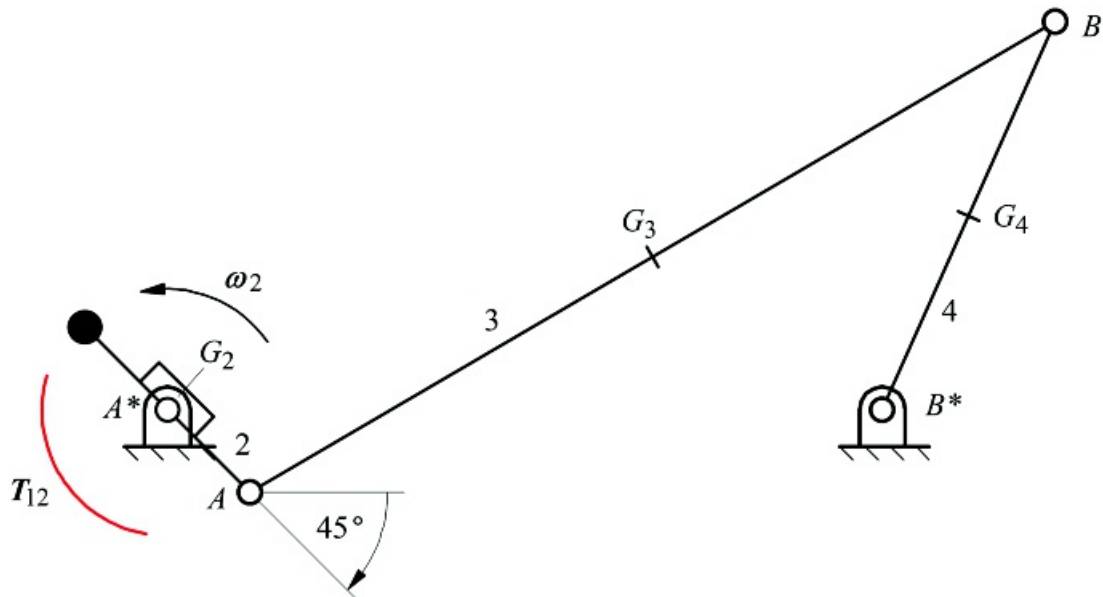


[Figure P16.10](#) Mechanism for Problem 16.10.

Reciprocating Balance

16.11 A single-cylinder engine, shown in [Figure P16.11](#), is mounted so that the crankshaft is horizontal. The engine is characterized by the following data:

Rotational speed (constant)	1200 rpm
Equivalent unbalanced weight of crank at A	6 lb

Weight of piston	7 lb
Weight of connecting rod	15 lb

Determine the magnitude of the shaking force when the crank angle is 120° if there is no counterbalance weight. Then determine the shaking force at the crank location if a counterbalancing weight is added that is equal to $\bar{m}_{G_3} - \bar{m}_A + 2\bar{m}_B/3$. Use $A^*A = 3$ in, $AB = 12$ in, and $AG_3 = 6$ in.

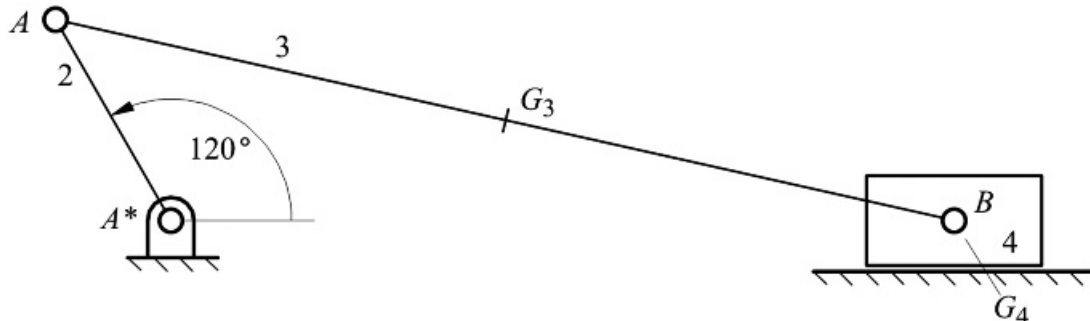


Figure P16.11 Mechanism for Problem 16.11.

16.12 Solve Problem 16.11 if the crank length is 2 in (stroke is 4 in), the engine speed is 1800 rpm, and the equivalent unbalanced weight of the crank at A is 5 lb.

16.13 For the mechanism and data given in Figure P16.13, determine the shaking force and its location relative to point A^* . Draw the shaking force vector on the figure.

$\omega_2 = 210 \text{ rad/s CCW}$	$\alpha_2 = 0 \text{ rad/s}^2$	$W_2 = 3.40 \text{ lb}$	$J_{G_3} = 0.1065 \text{ lb s}^2 \text{ in}$	$W_3 = 3.40 \text{ lb}$	$W_4 = 2.85 \text{ lb}$
$A^*A = 3 \text{ in}$	$AB = 12 \text{ in}$	$AG_3 = 6 \text{ in}$			

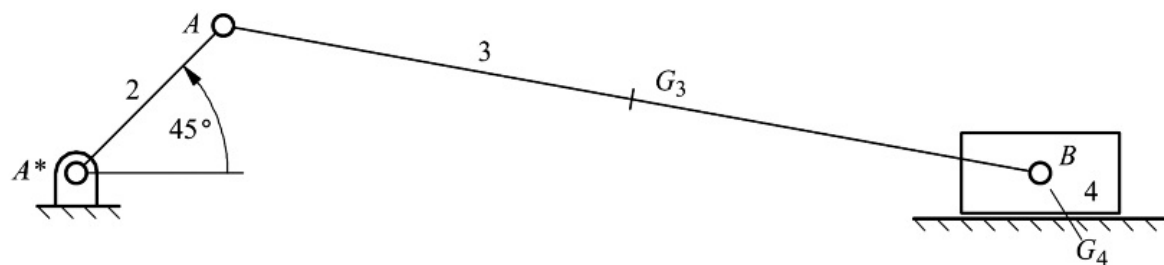


Figure P16.13 Mechanism for Problem 16.13.

16.14 For the engine given in Problem 16.11, use the procedure in Section 16.4.1 to determine the equivalent masses for the connecting rod. Lump the weight of the connecting rod at the crank pin and piston pin and draw the polar shaking-force diagram for the following three cases:

- No counterbalancing weights
- A counterbalancing weight equal to the sum of the crank weight at the crank radius, the part of the connecting rod weight assumed to be concentrated at the crank pin, the weight of the piston, and the part of the connecting rod weight concentrated at the piston pin.
- A counterbalancing weight equal to the sum of the crank weight at the crank radius, the part of the connecting rod weight assumed to be concentrated at the crank pin, and half of the weight concentrated at the piston pin (weight of the piston and part of the connecting rod weight concentrated at the piston pin).

16.15 For the engine given in Problem 16.11, use the procedure in Section 16.4.1 to determine the equivalent masses for the connecting rod. Lump the weight of the connecting rod at the crank pin and piston pin and locate the counterbalancing weight at the crank radius. Determine the optimum counterbalancing weight that will give

a. The smallest horizontal shaking force

b. The smallest vertical shaking force

Reciprocating Balance of Multi-Cylinder Engines

16.16 The two-cylinder engine shown in [Figure P16.16](#) has identical cranks, connecting rods, and pistons. The rotary masses are perfectly balanced. Derive an expression for the shaking forces and shaking moments using the symbols indicated if $\phi_2 = 90^\circ$. Are the primary or secondary shaking forces balanced? What about the primary and secondary shaking moments?

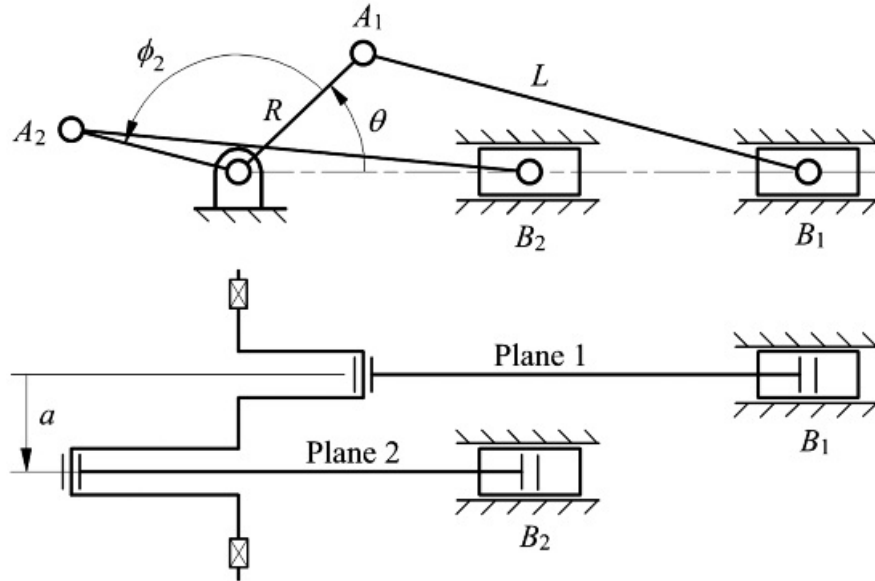


[Figure P16.16](#) Schematic diagram for engine for Problem 16.16.

16.17 Solve Problem 16.16 when $\phi_2 = 180^\circ$.

16.18 The four-cylinder engine shown in [Figure P16.18](#) has identical cranks, connecting rods, and pistons. The rotary masses are perfectly balanced. Derive an expression for the shaking forces and shaking moments for the angles and offset values indicated. Are the primary or secondary shaking forces balanced? What about the primary and secondary shaking moments?

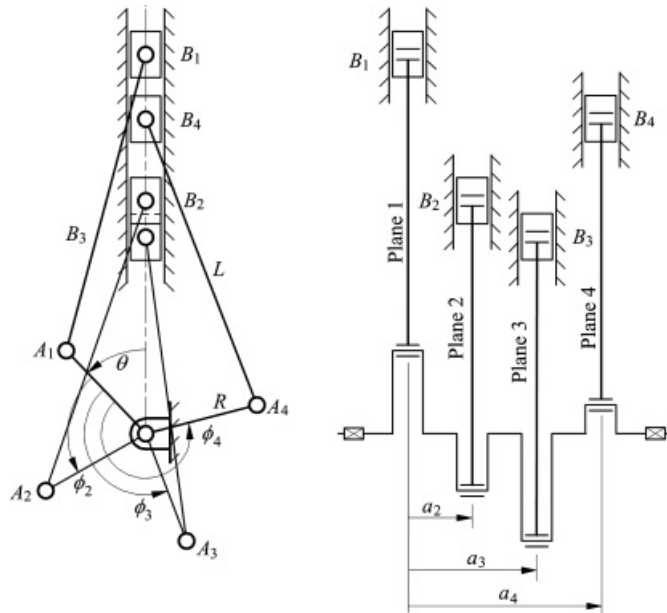


[Figure P16.18](#) Schematic diagram for engine for Problem 16.18.

16.19 Solve Problem 16.18 for the following values for the phase angles and offset distances:

$$\begin{array}{llll} \phi_1 = 0^\circ & \phi_2 = 90^\circ & \phi_3 = 270^\circ & \phi_4 = 180^\circ \\ a_1 = 0 & a_2 = a & a_3 = 2a & a_4 = 3a \end{array}$$

16.20 Solve Problem 16.18 for the following values of the phase angles and offset distances:

$$\begin{array}{llll} \phi_1 = 0^\circ & \phi_2 = 130^\circ & \phi_3 = 90^\circ & \phi_4 = 270^\circ \\ a_1 = 0 & a_2 = a & a_3 = 2a & a_4 = 3a \end{array}$$

16.21 The six-cylinder engine shown in [Figure P16.21](#) has identical cranks, connecting rods, and pistons. The rotary masses are perfectly balanced. Derive an expression for the shaking forces and shaking moments for the angles and offset values indicated. Are the primary or secondary shaking forces balanced? What about the primary and secondary shaking moments?

$$\begin{array}{llllll} \phi_1 = 0^\circ & \phi_2 = 240^\circ & \phi_3 = 120^\circ & \phi_4 = 120^\circ & \phi_5 = 240^\circ & \phi_6 = 0^\circ \\ a_1 = 0 & a_2 = a & a_3 = 2a & a_4 = 3a & a_5 = 4a & a_6 = 5a \end{array}$$

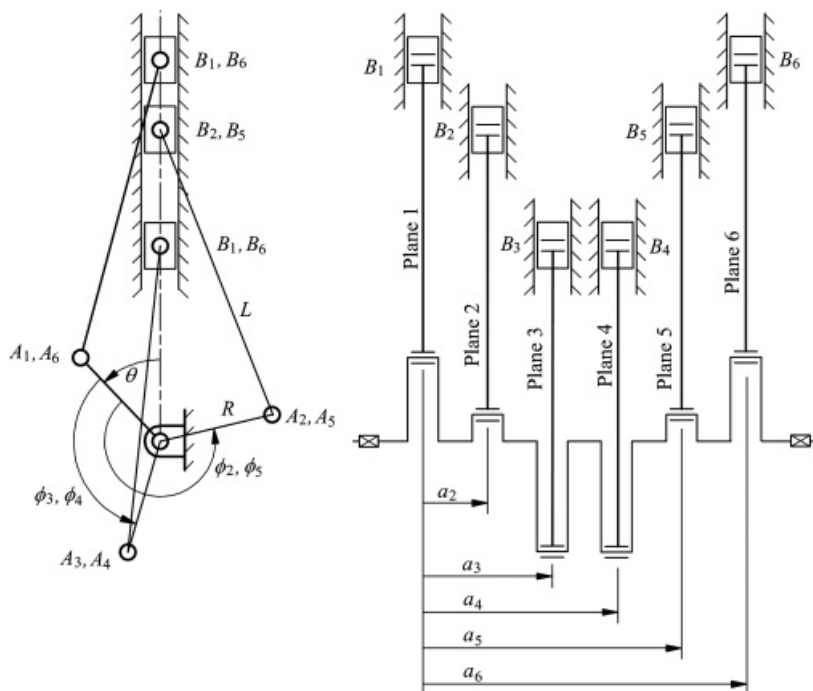


[Figure P16.21](#) Schematic diagram for engine for Problem 16.21

16.22 Solve Problem 16.21 for the following values for the phase angles and offset distances:

$$\begin{array}{llllll} \phi_1 = 0^\circ & \phi_2 = 120^\circ & \phi_3 = 240^\circ & \phi_4 = 60^\circ & \phi_5 = 300^\circ & \phi_6 = 180^\circ \\ a_1 = 0 & a_2 = a & a_3 = 2a & a_4 = 3a & a_5 = 4a & a_6 = 5a \end{array}$$

16.23 The two-cylinder V engine in [Figure P16.23](#) has identical cranks, connecting rods, and pistons. The rotary masses are perfectly balanced. Derive an expression for the shaking forces and shaking moments for the angles and offset values indicated. The V angle is $\psi = 60^\circ$, and the phase angle is $\phi_2 = 90^\circ$. Are the primary or secondary shaking forces balanced? What about the primary and secondary shaking moments?

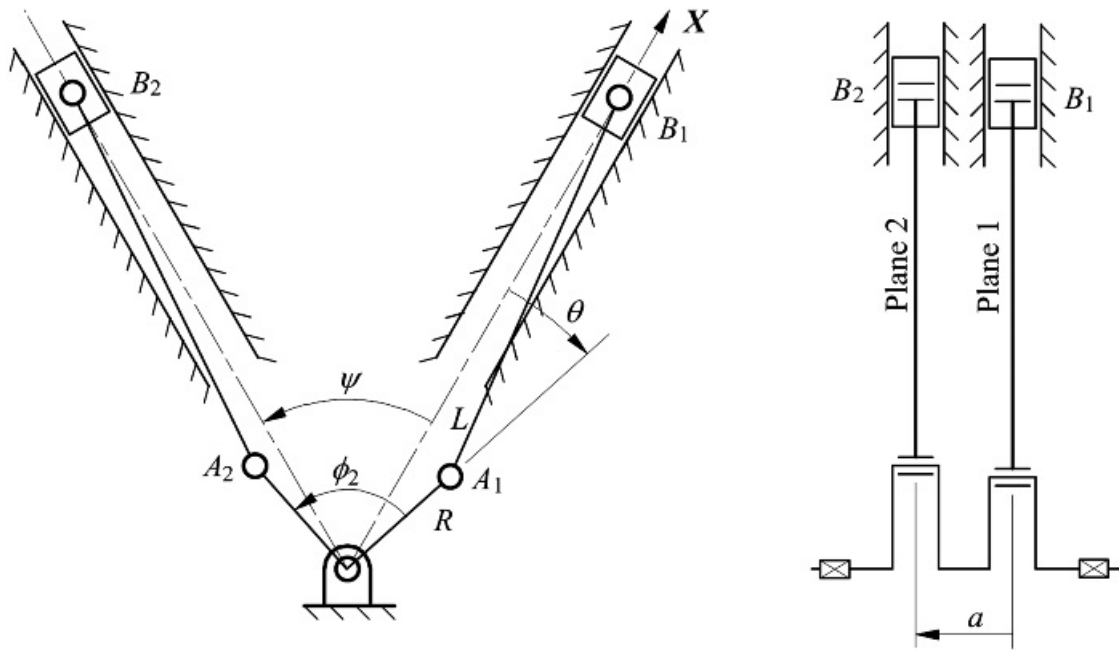


[Figure P16.23](#) Schematic diagram for engine for Problem 16.23.

16.24 Solve Problem 16.23 if $\psi = 180^\circ$ and $\phi_2 = 180^\circ$.

16.25 The six-cylinder V engine shown in [Figure P16.25](#) has identical cranks, connecting rods, and pistons. The rotary masses are perfectly balanced. Derive an expression for the shaking forces and shaking moments for the angles and offset values indicated. The V angle is $\psi = 60^\circ$, and the phase angles ϕ_1 , ϕ_2 , and ϕ_3 are 0° , 120° , and 240° , respectively. Are the primary or secondary shaking forces balanced? What about the primary and secondary shaking moments?

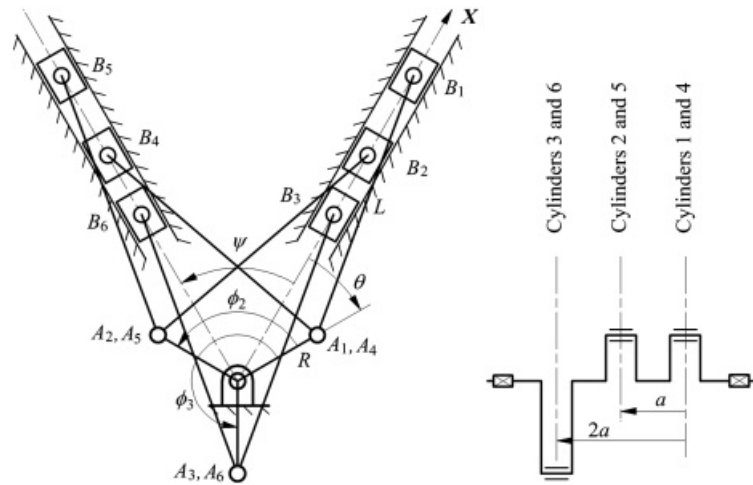


[Figure P16.25](#) Schematic diagram for engine for Problem 16.25.

Project Problems

16.26 Six-cylinder engines with a V configuration are very commonly used in automobiles and trucks when a compact, mid-sized engine is needed. They can be thought of as two of the three cylinder engines discussed in Section 16.6.1 coupled together by a common crankshaft with their cylinders in different planes. Different engine designers have tried various angles between the cylinder planes. Arrangements with the angle 60° or 120° have natural advantages. However, most modern V6 engines have a 90° angle between the cylinder planes.

An engine that will be perceived to run smoothly needs both to be well balanced and to have even firing intervals between successive cylinders. One automobile company decided to build a V6 engine by simply

removing two cylinders from one end of their successful V8 engine, similar to that discussed in Section 16.6.2. The only difference was that the three crank throws would be at 120° to each other, rather than 90° as on the V8. The connecting rods of one cylinder from each bank connected to each of the three crank throws. This arrangement allowed many parts to be common between the V6 and V8 engines, and facilitated their production on the same assembly line.

The resulting V6 engine was perceived to run roughly at some speeds, but the manufacturing advantages were such that the company did persevere with it for a number of years. Analyze the balance of the 90° V6 engine and the firing order to identify the feature that resulted in the roughness. Can you suggest a change to the engine that would have fixed the problem?

16.27 Katie is a big fan of Lampxar movies. She would like to create the Lampxar animated lamp, shown in [Figure P16.27](#), in real life. She can easily make a lamp but she would like it to move using the smallest motors possible. To do this she would like to use passive elements to support the gravitational load so the motors just need to move the inertia. For now we will just look at the distal link (the one attached to the head) and assume the other is fixed.

- (a) Where should the springs be located (L_5) if the only mass is in the head of the lamp, and what should their stiffness and pre-load be for the shown configuration? Use the formulation in Section 16.7 to derive the potential energy for the system and check if the spring parameters and placements can be chosen so that the system can be gravity balanced.
- (b) If she plans to use two motors, one for each planar degree of freedom, and each motor can provide a maximum torque T , what is the acceleration of the center of mass M_h of the lamp head? Hint: You would need to derive the dynamic equations of motion for the two degree of freedom system in order to answer this question. Assume that the base mass M_b is much larger compared to M_h .

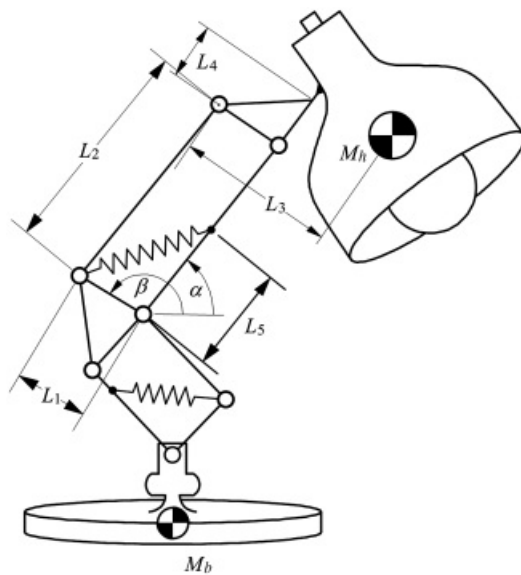


[Figure P16.27](#) Schematic diagram for engine for Problem 16.27.

Prerequisite Knowledge Needed for Chapter 17

A basic knowledge of the use of electrical motors, mechanism design, and control.



17.1 Introduction

Linkages and mechanisms are used to transfer mechanical work from a generating site to a site at which it produces a useful effect. An actuator is a motor or other device that generates mechanical work in a controlled manner. Traditionally, machines for complex operations involving many sub-functions, such as printing or packaging, were powered by a single motor, referred to as the *prime mover*, with all of the sub-functions being performed by linkages of various types. The prime mover was sometimes a large electric motor, but could equally be an internal combustion engine, a steam engine, or a water turbine. Once the system was tuned, timing was not an issue since everything was powered in lockstep off the same power train. This type of machine can achieve rapid cycle rates, and hence high productivity. It is an appropriate design when motors are expensive and inflexible in their operation. It is still the best configuration for very high production rates as when producing beverage cans or loading tissues into a package.

Improvements in actuator technologies have resulted in relatively compact and inexpensive devices that can be controlled with precision. Combining these with digital control technology has made it possible to replace mechanical coordination via linkages with digital coordination. This has several potential advantages. Production and other machinery can be much more flexible in its operation. It is no longer necessary to design and build a machine specifically to fill, cap, and label bottles of a particular shape. Rather, the same machine can be reprogrammed to fill a different type of bottle. The only mechanical changes needed are relatively minor tooling articles. Likewise, a production line can accommodate several different models of automobile, and many options on each, by use of digital reconfiguration for each model and option.

The purpose of this chapter is to introduce the essential elements to (a) drive a particular linkage that they have designed using actuators under computer control, (b) tune the performance of the system using simple knowledge about feedback control, (c) choose different actuators, and (d) share experience with the design of a hands-on machine-design laboratory.



17.2 Computer Control of the Linkage Motion

In general, a linkage is powered by as many actuators, typically electric motors, as the degrees of freedom of the mechanism. *Electric motors* work by virtue of the force experienced by a conductor carrying a current in the presence of a magnetic field. The field interacts with the conductors in a second winding to produce torque. Electric motors produce a very modest torque in proportion to their weight and operate at a very high speed. These characteristics mean that, if reduction of weight or bulk is important, the output of the electric motor must be reduced in speed, and proportionately increased in torque, by means of a mechanical transmission, very often a gear train of one of the types discussed in [Chapter 13](#).

Typically, a computer controls the current delivered to a motor that regulates its output torque. Since computers provide signals digitally (i.e., trains of bits that represent zeros and ones), these are converted to continuous signals, in analog form, using a *digital to analog (D-A) convertor*. Digital computers operate at very low power levels, whereas actuators must provide the muscle to run the machine. Therefore, the output of the digital to analog convertor is fed into a *power amplifier* that provides an output proportional to the signal, but at the voltage and level required by the actuator.

As a motor moves, built in potentiometers or encoders measure the angular orientation of the shaft.

Potentiometers typically provide the angular information as a continuous voltage signal while encoders provide this same information in a digital form. These built-in *sensors* provide information about the state of the mechanical system and motion of the system. The desired motion of a motor, or the intended motion of the system as a whole, is then compared with the sensed motion of the motor or the intended motion of the whole system. The errors in the motor motion, or of the overall system motion, are used in *closed-loop feedback control* to alter the motion of the individual motors so that these errors exponentially or asymptotically converge to zero.

[Figure 17.1](#) provides a broad summary of computer control of motion of the linkage, but there are specific details that need to be explored. If the system has a single degree of freedom, as in the case of a four-bar linkage or a slider-crank linkage, the electric motor will be coupled to the driving crank. The electric motor will then control the position or speed of the crank, and subsequently the motion of the entire mechanism will follow based on the geometry of the linkage. However, if the system has multiple degrees of freedom, the motion of the individual motors will have to be coordinated to get the output motion of a reference point on the system to follow a desired motion. The input-output kinematics of such a multi-degree-of-freedom system was outlined in [Chapter 9](#). These kinematic equations need to be solved to compute the input joint angle trajectories, which will then be given to the controller of the motor.

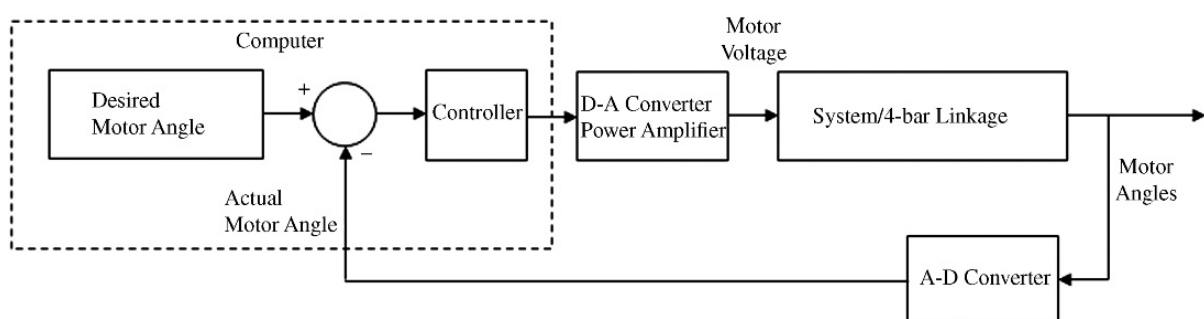


[Figure 17.1](#) Schematic of computer control of a four-bar linkage using electrical motors, sensors, and controller designs.

Since each motor controls a moving joint, the reflected dynamics of the moving linkage on that specific joint affect its performance. As a result, each motor within the system may have to be tuned separately to achieve a desired level of performance for the system as a whole. These aspects of feedback control will be discussed in more detail in Section 17.3.

Another important issue in the design of a computer-controlled system is the choice of actuators that could be electric, pneumatic, or hydraulic. Also, it is important to size the motors to meet the desired load and speed

characteristics. These issues are discussed in some detail in Section 17.4. Section 17.5 provides an example of a hands-on design laboratory where students can use the knowledge gained in a course to design linkage systems, program these using computers, and demonstrate the tasks for the design that was intended.

As was indicated earlier, some sensors, such as potentiometers, tachometers, resolvers, strain gauges, and so forth, produce continuous signals, while others, such as incremental or absolute encoders, produce pulse trains, or digital words. If an integrated computer controller is to be used, at some point every continuous signal must be digitized. This results in quantization errors. The size of these errors depends on the dynamic range and the length of the digital word into which the signal is translated. Thus, if the range of the signal is 0 to 5 volts and it is digitized to an 8-bit word, each step length is $5/256 = 0.0195$ volts. Since for a given digital level there is no way of telling where the corresponding analog value was on the step, the quantization error is $\pm 0.0195/2$, or ± 0.0098 volts. When dealing with digital data, the quantization error is determined by the lowest digital resolution in the system. For example, if an incremental encoder produces 720 pulses per resolution and it is coupled to an embedded computer with a 16-bit data bus width, the quantization error will be ± 0.25 degrees since $2^{16} = 65,536$, which is much greater than 720. On the other hand, if the encoder has 10-bit resolution, it produces $2^{10} = 1024$ pulses per revolution, and if it is coupled to a processor with an 8-bit bus width, $2^8 = 256$, so the quantization error will be $\pm \Delta/(2 \times 256)$, where Δ is the dynamic range of the signal.



17.3 The Basics of Feedback Control

[Figure 17.1](#) provides an intuitive way to describe *feedback control*. If the sensed motor angle is smaller than the desired motor angle at a specific time, one needs to accelerate the motor so that it can catch up to the desired motor angle. This can be achieved by instantly increasing the torque supplied by the motor in proportion to the error. Similarly, if the motor angle is ahead of its desired motion profile, it needs to slow down. However, a motor is a dynamic system (i.e., a change in motor torque does not instantaneously change the motor position).

Mathematically, this input-output motion is described by a differential equation with torque as the input and the joint angle as an output. The goal of a *feedback controller* is to continuously modulate the torque input based on the current joint error to achieve the desired joint motion response, both in the transient and steady state stages.

The most common control law, applied to a physical system described by a linear differential equation, has a structure in which the motor applied torque is a linear combination of the error and its higher derivatives

$$u = k_0 \varepsilon + k_1 \dot{\varepsilon} \quad (17.1)$$

where u is the input to the system, ε is the error between the desired and sensed output, and k_0, k_1, k_2 are positive constants. Let us see this equation in the context of a rotating link. Let θ be the angle from a reference and ω the applied torque at the joint along the same direction of increasing angle. We assume that this link has moment of inertia, I , about the rotating joint axis. We also assume that the link is connected to the ground by a torsional stiffness of $\kappa_2 > 0$ and a rotary dashpot of coefficient $\zeta_1 > 0$. The dynamics of this system is described by the differential equation

$$I\ddot{\theta} + \zeta_1\dot{\theta} + \kappa_2\theta = u \quad (17.2)$$

On defining the error $\varepsilon = \theta_d - \theta$ and a control law using the structure of [Equation 17.1](#)

$$u = k_0(\theta_d - \theta) + k_1(\dot{\theta}_d - \dot{\theta}) \quad (17.3)$$

the resulting closed-loop equation becomes

$$I\ddot{\theta} + \zeta_1\dot{\theta} + \kappa_2\theta = k_0(\theta_d - \theta) + k_1(\dot{\theta}_d - \dot{\theta}) \quad (17.4)$$

This equation can be simplified to

$$I\ddot{\theta} + (\zeta_1 + k_1)\dot{\theta} + (\kappa_2 + k_0)\theta = k_0\theta_d - k_1\dot{\theta}_d \quad (17.5)$$

If the goal of the controller is to change the angular position of the link to θ_d and stay there at rest, then $\dot{\theta}_d = 0$. With this choice, the final equation becomes

$$I\ddot{\theta} + (\zeta_1 + k_1)\dot{\theta} + (\kappa_2 + k_0)\theta = k_0\theta_d \quad (17.6)$$

One can immediately recognize that the above equation represents a spring-mass-damper system with a positive stiffness of $\kappa_2 + k_0$ and damping coefficient of $\zeta_1 + k_1$. This equation represents a stable system. This can be confirmed visually by making a simple experiment where a mass is attached to a spring and a dashpot. When

perturbed from an initial condition, the system will oscillate and come back to the rest configuration. The stability of the system implies that the oscillations would not grow uncontrollably over time after the initial perturbation.

[Equation 17.6](#) requires that at steady state, the system will come to rest at $\dot{\theta} = k_0 \theta_d / \omega_2 + k_3$. One can choose the control gain k_3 to achieve a desired steady state error, but it cannot be zero. One should also note that before settling down at rest, the system will exhibit a transient response that is correlated with the choice of the gains k_3 and k_1 . One can characterize the transient response in terms of two quantities: (i) the natural frequency $\omega_n = \sqrt{\omega_2 + k_0}/\zeta$, and (ii) damping $\zeta = 1/2\omega_1 + k_1/\sqrt{(\omega_2 + k_0)}$. Here, ω_n relates to the speed of response and ζ characterizes the number of oscillations to approach the steady state behavior.

Such a structure of the controller, applied to a second-order system with $k_1 = 0$, is referred to as a *Proportional (P)* controller. If both $k_0 \neq 0$ and $k_1 \neq 0$, the controller is labeled as a *Proportional Derivative (PD)* controller. Often, one adds an integral component to the control law $u = k_0(\theta_d - \theta) + k_1(\dot{\theta}_d - \dot{\theta}) + k_2 \int(\theta_d - \theta) d\tau$ to reduce the steady-state error, and this is labeled as *Proportional Integral Derivative (PID)* controller. Even though we described the structure of this controller quite intuitively with the example of a linear second-order differential equation with a single input and output, the underlying concept can be expanded to more complex linear systems. The details are outside the scope of this chapter. Students are encouraged to read about this topic from specialized textbooks on controls.

In our application, one needs to control the motion of a linkage with a motor. Once an electric motor is added to a joint of a four-bar linkage, the dynamics of the motor and the linkage become coupled. Due to the inherent kinematic nonlinearity within the system, the coupled dynamic system is no longer described by linear differential equations. Systematic control design techniques for non-linear dynamic systems are quite limited and beyond the scope of this book. However, it can be shown that simple joint level *P*, *PD*, and *PID* control techniques work well for linkage systems driven by electric motors and provide stable control response. The difference now is that the controller gains k_0 , k_1 , k_2 have to be tuned for different regions of the workspace and are usually listed in a look-up table.



17.4 Actuator Selection and Types

A useful way of characterizing the behavior of an actuator is to plot force, for a linear actuator, or torque, for a rotary actuator, against speed. The shape of this characteristic curve, and its relationship to the corresponding characteristic of the load, has important implications for the behavior of the actuator under load. Consider the torque-speed curve shown in [Figure 17.2](#). The torque-speed demand curve of a typical load is also shown in that figure. In many applications, but not all, load increases with speed. Since the actuator torque is equal to the load torque at point A , the system will tend to settle into that combination of torque and speed, called the *operating point*. If the speed increases above ω_A , the load torque will exceed the actuator torque and the system will tend to decelerate back to speed ω_A . Conversely, if the speed decreases below ω_A , the actuator torque will exceed the load torque and the system will tend to accelerate back to point A . This is an example of stable operation. Note also that this actuator has a finite maximum speed, which is the speed, ω_0 , at which the actuator torque drops to zero. ω_0 is called the *no-load speed*. Similarly, the actuator torque at zero speed, T_{\max} , is called the *stall torque*.

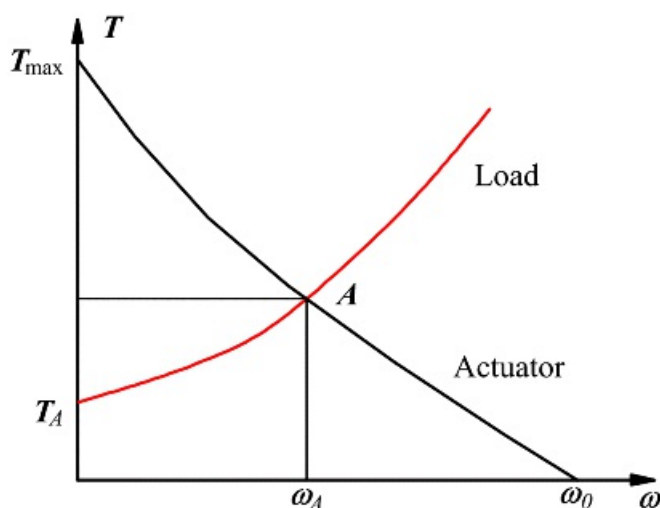


[Figure 17.2](#) Torque-speed characteristics of actuator and load for stable operation.

Consider now the situation depicted in [Figure 17.3](#). Here the actuator torque-speed characteristic increases in torque with increasing speed. The load torque does not increase as rapidly as the actuator torque with speed. The operating point at which the actuator torque is equal to the load is point B . If the system is operating at point B , and the speed fluctuates even slightly higher than ω_B , the actuator torque will exceed the load torque and the system will accelerate to an even higher speed. The speed will continue to increase without bound and the system will *run away*, possibly resulting in catastrophic failure. Conversely, if the speed fluctuates even slightly below ω_B , the load torque will exceed the actuator torque and the system will decelerate further. Very quickly the speed will drop to zero and the system will *stall*. It is not possible for the system to operate at point B . This is an example of an unstable operating point.

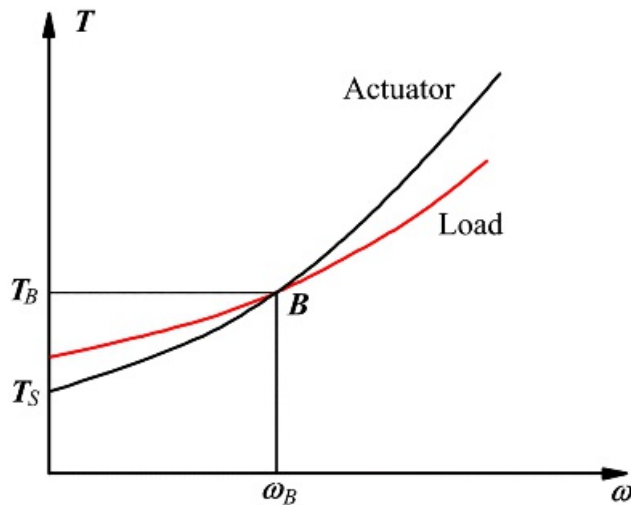


Figure 17.3 Torque-speed characteristics of actuator and load in unstable operation.

Some actuators display torque-speed curves that climb to a peak and then decline to zero with increasing speed. With a given load they may display both stable and unstable operating points. An internal combustion engine is a good example. A change gearbox is necessary in an automobile to keep the operating point on the declining side of the torque-speed curve. If the operating point shifts to the opposite side of the peak of the characteristic curve, the engine will stall.

17.4.1 Electric Actuation

There is a truly bewildering variety of electrical actuators on the market today. The use of new technologies, such as solid-state power switching technologies, has allowed the introduction of new architectures and new uses for traditional architectures. New permanent magnet technologies have resulted in greatly improved performance for some classes of electrical actuators.

Electric motors work by virtue of the force experienced by a conductor carrying a current in the presence of a magnetic field. The field interacts with the conductors in a second winding to produce torque. The mechanically fixed structure is called the stator. The rotating structure is called the rotor. If the rotor carries windings it is also called an armature. To produce a continuous torque, the electric field must typically rotate relative to the structure that generates it so that it maintains a fixed relationship to the magnetic field. If motor size and weight is not a problem, a motor with a very large frame size and a large number of poles may be used. The speed of an electric motor is inversely proportional to the number of poles used in the field winding. It is easier to accommodate a large number of poles in a larger frame size. Consequently, smaller motors tend to have higher operating speeds.

Commutated Motors

A commutator is a mechanical switch that is used to switch the current-carrying coils in the motor armature so that the torque produced is always in the same direction. The armature is the switched winding of the motor. A mechanical commutator is formed with a number of conducting segments mounted to form a cylindrical surface on the rotor, against which two or more "brushes" bear. The current is passed between the brush and whatever segment it is in contact with. Brushes eventually wear out and must be replaced. There may also be arcing between the brushes and the commutator segments, producing radio interference and other problems. To avoid this, commutation may be done by means of solid-state electronic switching. Hall effect sensors are used to trigger the switches at the appropriate times. At the same time, the rotor and stator are reversed, with the field being on the rotor.

The use of permanent magnets, rather than field windings, avoids the need for any electrical connections to the rotor. The rotor magnets are commonly made from rare earth materials that can maintain higher field strengths than traditional ferrous magnets. The result is a brushless direct current motor that works like a commutated motor, but is mechanically simpler, more rugged, and more reliable. There are differences in the performance characteristics of mechanically commutated DC motors depending on the connectivity relationship between the

field and armature windings. The field may be excited by an external source, in which case the motor is called externally excited. More often, the field is excited by the same source as the current in the armature. If the field and armature windings are connected in parallel, the motor is called a *shunt wound* motor. If the torque produced by the motor is plotted against rotation speed, a shunt wound motor will have a characteristic performance curve like that shown in [Figure 17.4](#). It will have relatively constant torque over its typical operating range. The torque will eventually decline with speed, and there will be a finite maximum speed at which the torque becomes zero.

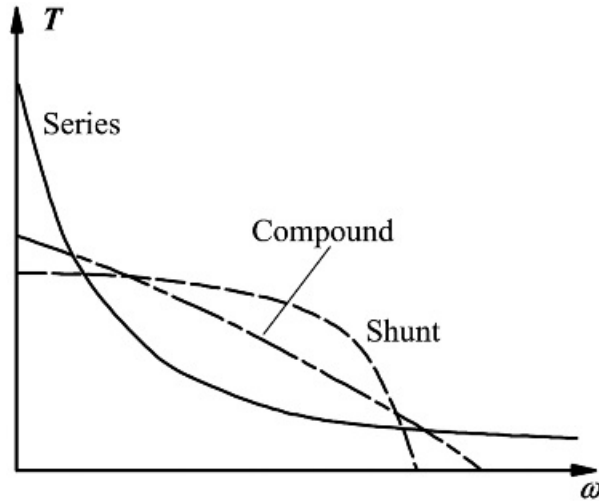


[Figure 17.4](#) Torque-speed characteristics typical of DC motors of the shunt wound, series wound, and compound types.

If the field windings are connected in series with the armature windings, the machine is called a *series wound* motor. This results in somewhat different performance characteristics as shown in [Figure 17.4](#). The torque at stall or low speed is very high, with a sharp initial drop-off with increasing speed. Ideally the torque never drops to zero. The motor continues to produce some torque even at very high speed. Consequently, operation is unstable at no load. It should also be pointed out that most electric motors cannot be run continuously at *stall*, which is zero speed, or at very low speeds. If the motor is held at, or near, stall for an appreciable length of time, heat will typically build up until it damages the motor. The ability of the motor to operate near stall may be seen to be a matter of heat transfer. If the motor is sufficiently well-cooled to be able to dissipate the heat generated at stall without a damaging rise in temperature, it may be operated in that regime. That is important for some classes of machine, including industrial robots. Motors that can be operated at or near stall are called torque motors.

Non-Commuted Motors

There are also several types of electric motor that do not use commutators. The most commonly used type is the induction motor. In this type of alternating current motor, the armature has a simple “squirrel cage” configuration. The armature current necessary to produce torque is induced by the alternating current in the stator winding. Induction motors have torque-speed characteristics like that shown in [Figure 17.5](#). For stable operation, it is necessary to operate the motor on the high-speed side of the hump in the torque-speed curve so that a decrease in speed produces an increase in torque. In contrast to the other types of electric motor we have discussed, the torque is typically not at its highest at stall.

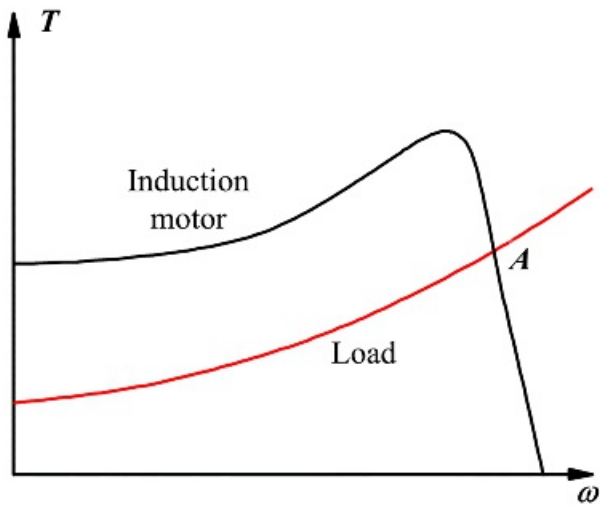


[Figure 17.5](#) Torque-speed characteristics of induction motors. With the load characteristics shown, the motor is self-starting and will operate stably at Point A.

Another type of motor that does not use a commutator is commonly referred to as a *stepping motor*. In this type of motor, the torque is generated magnetically, rather than electromagnetically, as in other types of motor. The motor has a number of discrete, equally spaced stable positions. Feeding a voltage pulse to it causes it to rotate to the next stable position. Consequently, stepping motors are very useful for indexing. It is not necessary to provide a means of keeping track of position since the position of the motor is known simply by counting the number of pulses supplied to it.

Solenoid

A solenoid is a simple, cylindrical winding that, when energized by a direct current, creates a strong magnetic field and draws a ferromagnetic core into itself. Solenoids are used as simple, two-state, linear actuators. Typically, they have two stable positions. Solenoids are not suited to providing variable force or stroke. Electric linear actuators for long or controllable stroke are compound devices using rotary motors in combination with power screws, racks and pinions, or similar rotary to linear convertor mechanisms. They are readily controlled to produce desired motion outputs, but when used on their own, do not do well if a controllable force is desired. Driving a linear actuator in series with a compliant element—a spring—provides controllable force.

Speed Control

The advent of solid-state power switching devices has revolutionized electric actuator control. Pulse-width modulators and phase-controlled rectifiers make it possible to control DC motors without the energy losses inherent in earlier methods, which basically used potentiometer configurations. DC devices typically respond to the *average* supply voltage. Pulse width modulation controls that average by chopping a constant voltage DC input into a train of pulses with controlled widths, thereby controlling the *average* voltage going to the motor.

These developments have allowed controlled actuators, or servo-motors, to be made much simpler, more compact, and more rugged than in the past. However, the cost and complexity has shifted to the control electronics from which the motor is supplied. When selecting electric actuators, it is important to remember that the power control unit may cost as much or more than the motor. It is instructional to take a look inside the controller of a hybrid vehicle if you get the chance. The sizes of the conductors and complexity of the circuits are impressive.



Example 17.1

Rollers of a conveyor belt used to convey material up a gradient have the torque-speed curve shown as curve X on [Figure 17.6](#). Here the abscissa is the rotational speed of the belt rollers in rpm, and the ordinate is the driving torque in in-lb. This is an example of a load that decreases with speed since material is loaded onto the belt from a hopper that limits the rate of deposition. Since the rate of deposition is constant, if the belt is driven faster there will be less material on the belt to be lifted, causing the load to decrease.

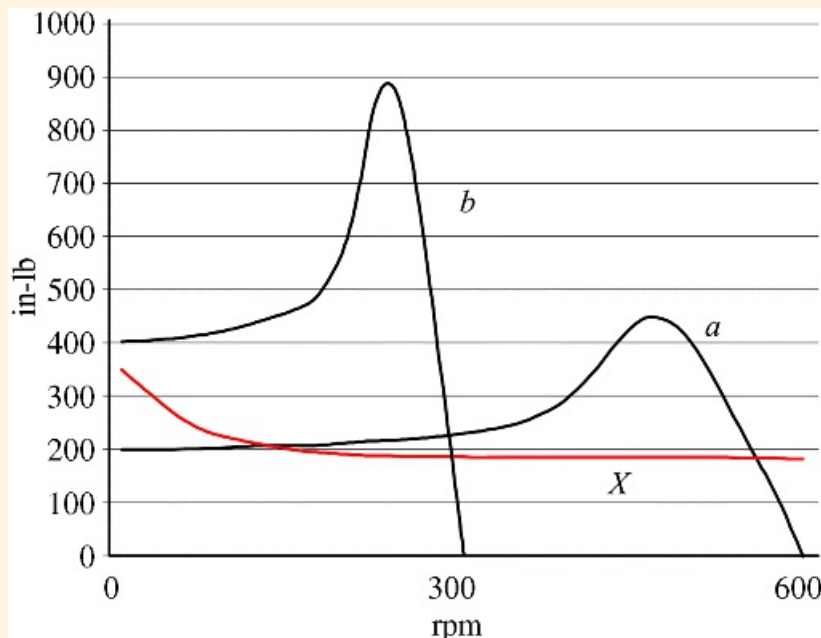


[Figure 17.6](#) (a) Torque-speed curves for an induction motor direct driving a load and (b) with a speed reduction of 2.0. The torque-speed requirement of the load is curve X .

The belt drive roller is to be driven at a speed as near as possible to 300 rpm. The motor to be used is an induction motor. Its torque-speed curve is curve (a) in [Figure 17.6](#).

A gearbox suitable for use with this motor and load is available with a reduction ratio of 2.0. Naturally it would be preferred to couple the motor directly to the head pulley of the belt, without the extra expense and complication of a gearbox. The torque-speed curves of the motor directly coupled to (a) and in combination with the gearbox (b) are shown. Which configuration would you select, and why?

Solution

This problem is typical of mechanical drive problems in requiring relatively low rotational speeds as compared to the no-load speeds of available electric motors. As shown by curve a , the motor has quite low torque, but has a high no-load speed. This suggests use of a step-down gearbox. This will have the effect of dividing the motor speed by the reduction ratio, while multiplying the output torque by the same ratio, producing the curve b for the motor-gearbox combination.

By inspection of those curves we reach the following conclusions:

- The intersection of this curve with the load curve produces both an unstable and a stable operating point. Installation of a clutch between the motor and the head pulley would be necessary to allow the motor to be run up to speed before applying the load. The stable operating point occurs at a considerably faster speed than that at which it is desired to run the belt.
- With the gearbox only a stable operating point occurs. The motor can be started from rest under load.

The resulting speed is close to that desired for the belt.

17.4.2 Hydraulic Actuation

An alternative to electric actuation is the use of a fluid-power system. This term encompasses both hydraulic and pneumatic actuation systems. In a hydraulic system, energy is transmitted via a flowing liquid. Liquid at high pressure is provided by a pump that might be driven by an electric motor, as is the case in the hydraulic actuation systems used on some industrial robots, or directly by the engine in the case of the hydraulic systems used in construction machinery. Hydraulic actuators provide much higher force or torque per unit weight than electric actuators. For this reason, they seldom require speed-reducing transmissions. Hydraulic actuation is often the system type of choice in heavy-duty applications, particularly when light weight and/or compactness are desired. Hydraulic cylinders are widely used as linear actuators, particularly when loads are large and strokes are long.

There are several different types of hydraulic power transmission systems in use. One common type uses a pressure regulated supply pump to provide a near constant supply pressure difference over the pressure of the reservoir. The pressure to each of several actuators in the system is then tailored to that needed to support the load by means of a control valve. Another type of hydraulic transmission is a displacement-controlled system. This is a hydrostatic system in which the flow of fluid to the actuator is controlled by means of a variable displacement pump. This configuration requires the use of a separate variable displacement pump for each actuator. It is a much more efficient type of system than the valve controlled configuration, but tends to be less compact. On the other hand, a displacement controlled hydraulic system does not require a large reservoir for heat rejection like a valved system does.

A typical hydraulic actuator is a simple cylinder, with the piston carrying the load. One end of the cylinder is fed with high-pressure oil from a supply pump. The other end is connected to a reservoir at atmospheric pressure. The high-pressure oil tends to force the piston to move to expand the high-pressure chamber, causing the piston to apply force to the load. [Figure 17.7](#) shows the schematic representation of a hydraulic circuit. The pump raises the pressure of fluid from the reservoir to a constant high-pressure value. Fluid passes through the control valves to the actuators. Actuator 1 is being driven to the right against a load. Actuator 2 is driven to the left. The control valves are depicted as being closed center valves, meaning that when the valve spool is in its central position both the high pressure and return lines are blocked, locking the actuator in place. Thus, Actuator 3 can support a load in either direction, but cannot move. Force is approximately the cross-sectional area of the cylinder times the pressure differential that can be applied across it. It is not quite as simple as that since the piston rod significantly reduces the active area on one side of the piston, and there may be significant seal friction to be overcome before the piston can move the load. There is a set of conventions that allow hydraulic circuits to be drawn schematically much like electric circuits. [Figure 17.7](#) shows a valved hydraulic power system operating three actuators under variable control.

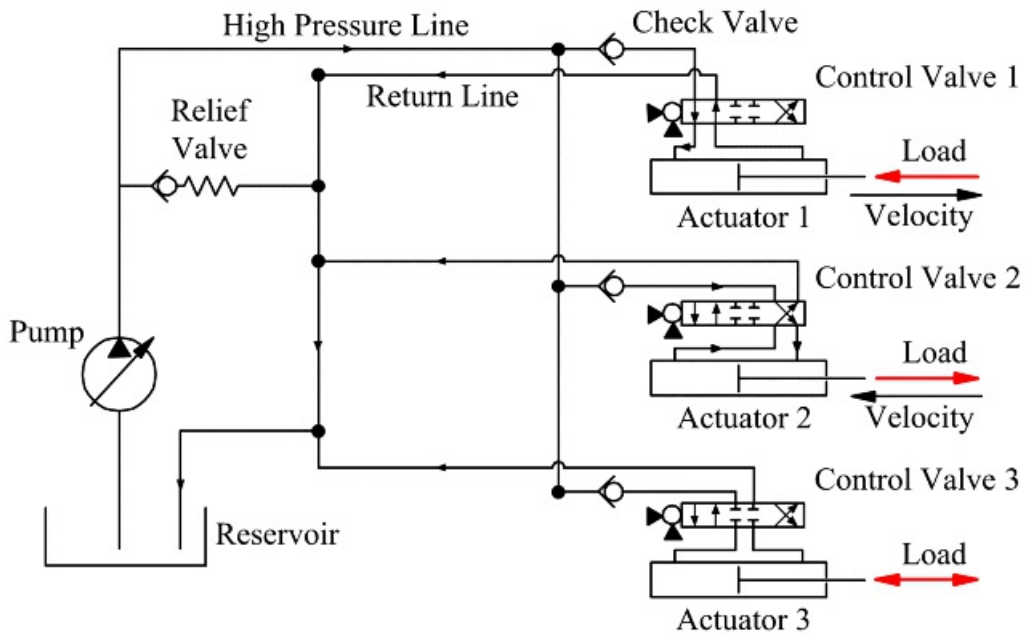


[Figure 17.7](#) A schematic representation of a hydraulic circuit.

17.4.3 Pneumatic Actuation

Pneumatic systems are inexpensive and have long been a staple of fixed automation systems in factories. Physically, they very much resemble hydraulic systems. They operate on the same principles except the working fluid is air, rather than oil. It is, however, considerably more difficult to implement sophisticated controls on pneumatic systems. The primary reason is that the working fluid, air, is quite compressible compared to hydraulic fluid.

Pneumatic systems operate at pressures that are an order of magnitude lower than those typical of hydraulic systems. Consequently, a pneumatic actuator must be much larger than a hydraulic actuator to deliver equivalent force. The main reason is that it is much harder to seal air chambers than those filled with viscous hydraulic fluid. The very low viscosity of air makes it difficult to keep it trapped in a chamber.



17.5 Hands-On Machine-Design Laboratory

This section gives an example of a laboratory set-up and class projects within a machine-design class. The goals of this laboratory are three-fold: (1) to use the knowledge of this book to design a functional mechanism, (2) to create a functional prototype using either traditional machining or 3D printing, and (3) to demonstrate and control the working prototype for the intended task. This section provides a quick description of the required components and hardware to achieve goal 3, while we assume that such a laboratory has access to a machining or 3D printing facility.

We expect that the laboratory will have multiple stations and each station will have the required hardware and electronics to control, in closed-loop, up to four DC servomotors given to a student group. Our example station uses the following components along with a host computer: (1) a single-board computer, NI SB-Rio with four analog outputs (AO), 16 analog inputs (AI), and 100 digital pins that can serve as inputs or outputs (DIO); (2) a Maxon Escon 70/10 motor driver that takes pulse width modulated (PWM) signals as the inputs and varies the amount of current supplied to the motor to get a desired torque or speed; (3) four Pittman GM9236S027-R1-SP brushed DC geared motors; (4) a power supply that uses a 120V AC power source and converts to 24V DC power supplied to the controller and drivers; and (5) joint encoders integrated within the Pittman motors. It is expected that these five components may be substituted by other components performing similar functions within different laboratories.

At the minimum, a programming interface must be developed so that a student group can easily play back a desired motor-angle trajectory that they computed using the kinematics of the design. The software could consist of two separate programs: one running on a host computer, while the other runs on the single board computer. The program on the host computer would read the motor trajectory data and send those to the single board computer. The program running on the single board computer will take the desired and current angles of the motors as inputs and send output command voltages to the motor drivers. Real-time data, such as desired and current motor angles, time, and voltage, can be displayed in graphs and saved in text files.

A sample program interface is shown in [Figure 17.8](#) with motor enabler buttons to turn the motors on and off and to reset the encoders. There are also buttons that can move the motors in small increments so that the motors can be brought to their home positions, as required to set the encoders. The desired motor angles can be provided to a PID controller in two different modes. The “time-based” mode provides angles at a fixed frequency to the PID controller while the “error-based” mode provides the next angle once the error is reduced below specified values. The two different modes can be used depending on whether speed or accuracy is more desirable.

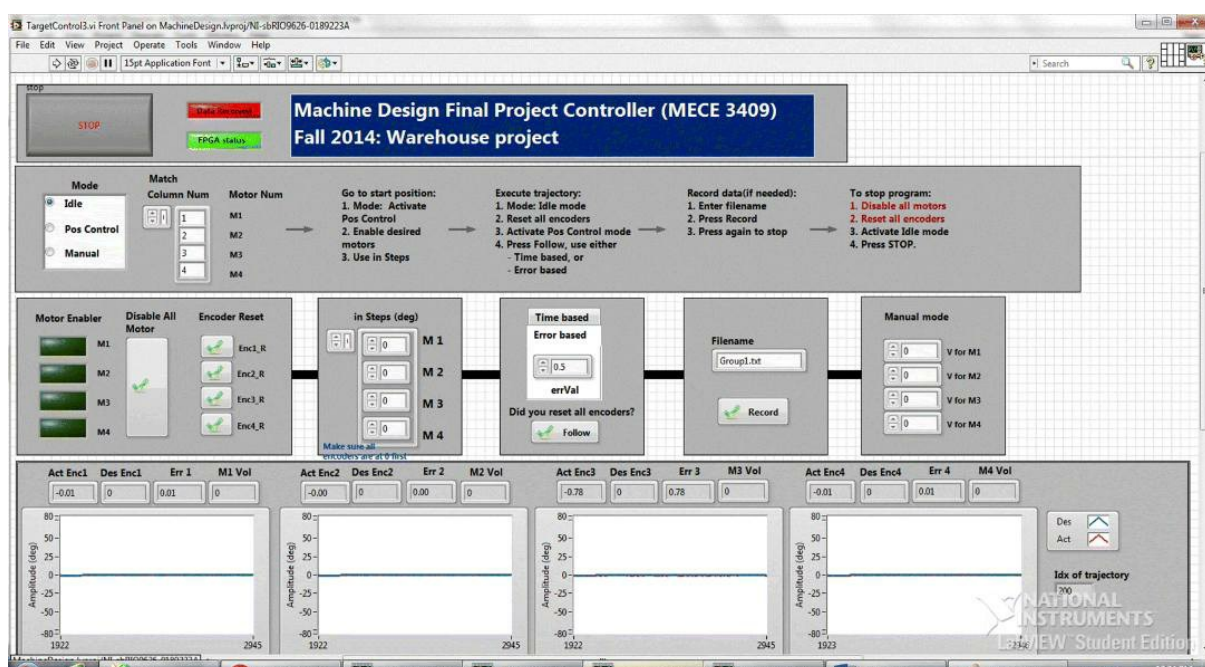


[Figure 17.8](#) Program interface for a hands-on machine-design laboratory.

17.5.1 Examples of Class Projects

The class projects were chosen to motivate students to come up with innovative design solutions using the knowledge of mechanisms and kinematics that they have learned. Each group was asked to perform the following major tasks: (1) create a fully functional design to achieve a motion as specified in the goals of the project; (2) use the DC servomotors as actuators within their design; (3) use the machine shop to turn, mill, laser cut, and/or 3D print at least one part in their design; (4) have a small budget to order small parts to complete the assembly of their design; (5) solve the kinematics of their system to compute the motor commands to achieve a target motion; and (6) implement and test the performance of their system. Specifically, we discuss two such class projects.

Rodent Gait Trainer

The goal of this project was to design a robot that can move a mock rodent leg through a prescribed path during locomotion, [Figure 17.9](#) (Left). The physical motivation for this project comes from the emerging field of rehabilitation robotics where patients with stroke or spinal cord injury use a robotic exoskeleton to retrain the gait of neurally impaired individuals [1,2]. It is expected that gait-training strategies on rodents can provide insights into how these could be performed optimally on humans.

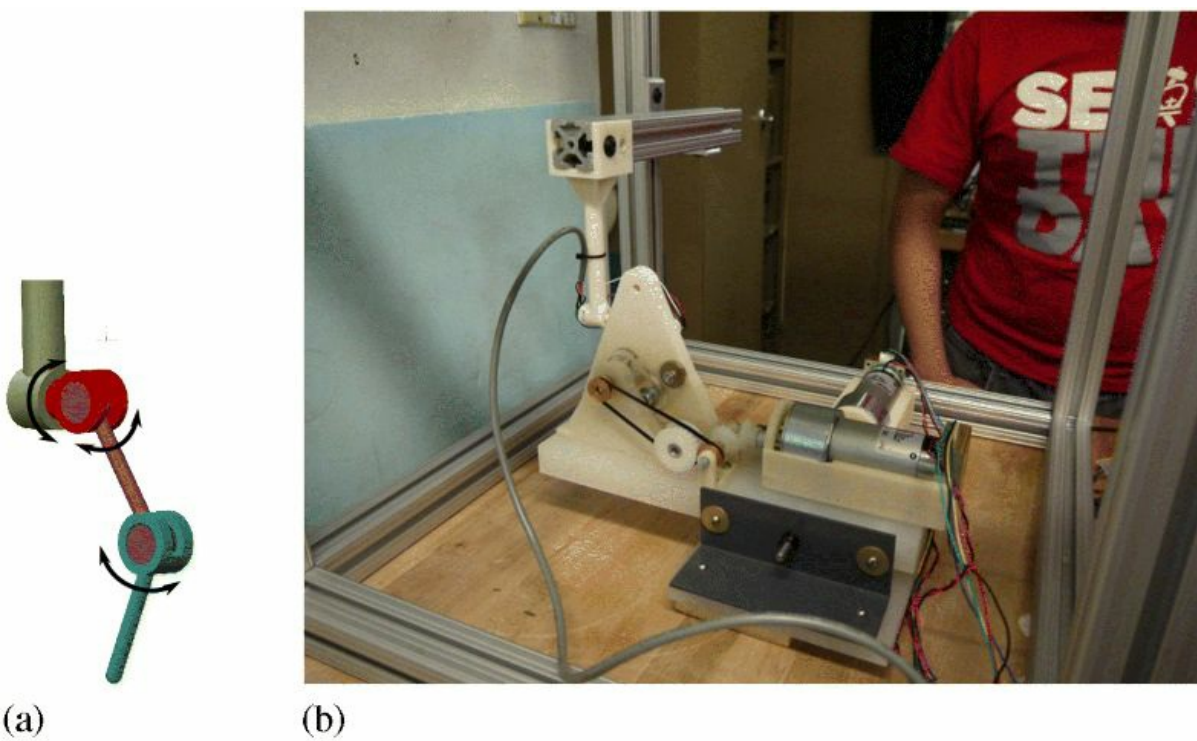


[Figure 17.9](#) (Left) CAD model of a rodent leg, (Right) student prototype that uses the motors to achieve the rodent leg motion.

Each group was given a 3D printed model of a mock rodent leg, on which all joints were instrumented with potentiometers to sense the motion of the joints. The rodent leg was mounted on a metal cube with rails, as shown in [Figure 17.9](#) (Right). Each group was asked to create a fully functional design that moves the end-effector of the rodent leg on a prescribed three-dimensional periodic path. To achieve this, they had to design a prototype that coupled to the rodent leg and was driven by the given motors. Based on the specific kinematic design, they had to compute the appropriate motor angles to achieve the path and provide these to the controller. The programming interface then moved their design through the angles provided. [Figure 17.9](#) (Right) shows an example of a design that uses a belt-driven four-bar linkage to provide the sagittal plane motion of the leg (i.e., forward and backward, up and down), while a prismatic joint driven by a lead screw achieved the motion normal to the sagittal plane.

Laparoscope

The goal of this project was to design a robot that can automate the motion of a laparoscope to perform a surgical task, [Figure 17.10](#) (Left). The physical motivation of this project comes from the emerging field of surgical robotics where patients are operated on by robots. The project is motivated by abdominal surgery in which the laparoscope is inserted into the abdomen. The surgeon controls the handle of the tool while the tool tip remains inside the patient. Since the tool is inserted through the abdominal wall, the skin and soft tissues will provide a “fulcrum” effect (i.e., when the surgeon’s hand moves up, the tool tip moves down). In addition, only two-dimensional camera views of the tool tip will be available to the surgeon during the operation. These issues make such surgery difficult and not all surgeons are proficient at minimally invasive surgery. The project groups were asked to execute a suturing task with their design. They needed to insert a circular needle into a surface, then move the robot tip to the other side of it, without hitting the surface, and pull the needle out. The needle was to be inserted along a circular path having the same radius of curvature as the needle to minimize tissue damage.

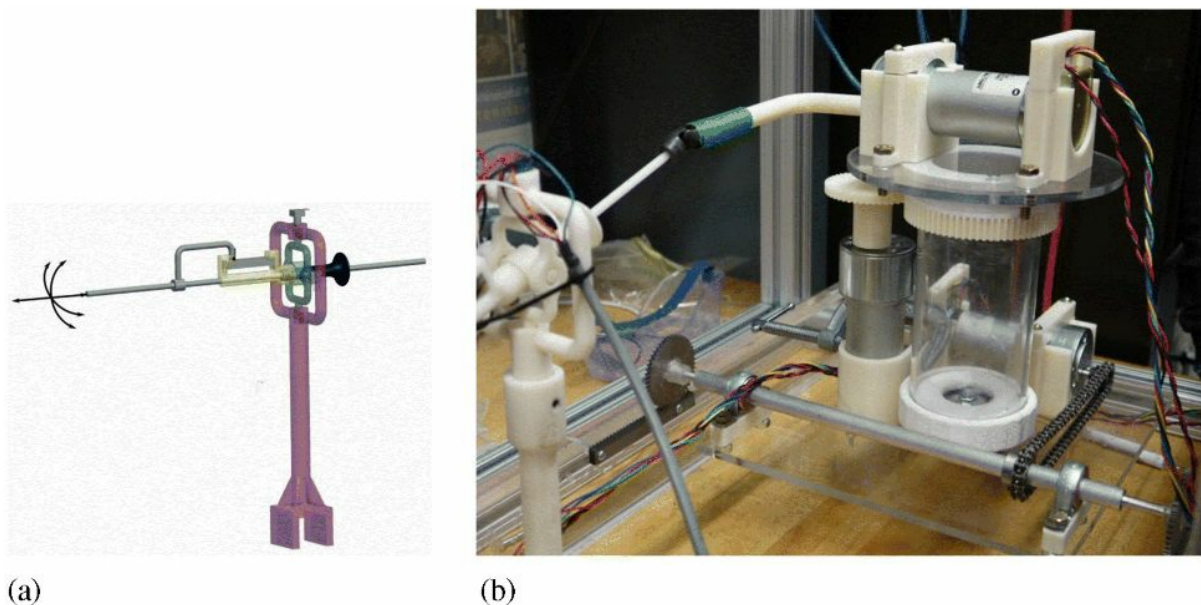


[Figure 17.10](#) (a) CAD model of a laparoscope and (b) student prototype that uses the motors to achieve the laparoscope motion.

Each group was given a 3D printed model of a laparoscope, in which all joints were instrumented with potentiometers to sense the motion of the joints. The laparoscope was mounted on a metal cube with rails as shown in [Figure 17.10](#) (Right). Each group was asked to create a fully functional design that moves the tip of the laparoscope on a prescribed 3D periodic path. To achieve this, they had to design a prototype that coupled to the laparoscope and was driven by the motors supplied. Based on the specific kinematic design, they had to compute the appropriate motor angles to achieve the path and provide these to the controller. The controller then moved their design through the angles programmed. [Figure 17.10](#) (Right) shows an example of a design that used a chain-driven rack and pinion system to provide forward and backward motion, a geared revolute joint to provide side-to-side motion, and a directly driven arm to provide vertical motion.



References

1. Banala, S. K., Kim, S. H., Agrawal, S. K., and Scholz, J. P. (2009). "Robot Assisted Gait Training with Active Leg Exoskeleton (ALEX)." *IEEE Transactions on Neural Systems and Rehabilitation Engineering*, Vol. 17, No. 1, pp. 2–8.
2. Srivastava, S., et al. (2014). "Assist-as-Needed Robot-Aided Gait Training Improves Walking Function in Individuals Following Stroke." *IEEE Transactions on Neural Systems and Rehabilitation Engineering*, pp. 84–92.



Problems

17.1 A tachometer produces a continuous (analog) signal covering the range -5.0 to + 5.0 volts. The signal is processed by an analog to digital convertor with a sixteen-bit word length. Calculate the magnitude of the quantization error that results from this operation.

17.2 A magnetic encoder produces 72 evenly spaced pulses over each revolution. The signal is fed to an integrated processor with an eight-bit data bus width. Calculate the magnitude of the quantization error for this signal.

17.3 A sensor produces a continuous signal in the range 0.0 to 3.0 volts. It is processed by an analog to digital convertor with a twelve-bit word length. Calculate the magnitude of the resulting quantization error.

17.4 The motor of Example 17.1 is to be used to power a large industrial fan. The load torque from the fan is closely approximated by the expression $T = 150 + 16 \times 10^{-4} \Omega^2$ where T is torque in in-lb and Ω is rotational speed in rpm. Plot curve a of Figure 17.6 and this load curve on the same graph. What operating points do you see? Are they stable, or unstable? Is it viable to drive the fan directly with this motor?

The torque-speed values from which curve a was plotted are shown in the following table:

Ω rpm	0	50	100	150	200	250	300	350	400	450	500	550	600
T in-lb	200	202	204	207	212	220	229	245	298	440	410	210	0

17.5 The motor of Example 17.1 and Problem 17.4 is to be used to power a hoist with a winch drum of radius 1 ft. The motor will be coupled to the drum via a gearbox. The maximum load to be lifted is 4500 lb and the load is independent of speed. Applying a 20 percent factor of safety (i.e., designing for a maximum load of 5400 lb), what reduction ratio must be supplied by the gearbox? Estimate the speed at the operating point and calculate the lifting speed.

17.6 The torque-speed relationship of an internal combustion engine used to power light aircraft is approximated by the expression

$$T = \omega(10.83 - 0.04137\omega)$$

where T is engine torque in ft-lb, ω is engine speed in rad/s.

This engine is mated to a propeller that has a torque-speed requirement modeled by the expression

$$T_p = 0.04138\omega^2$$

with T_p in ft-lb and ω in rad/s.

Estimate the operating point speed in rpm of the engine directly coupled to the propeller. Is this a stable operating point?

17.7 Consider a link of mass m that is uniformly distributed over its length l . It is rotating in a horizontal plane hinged at one end, acted on by an external torque τ . A control system needs to be designed to move the link from its initial angle $\theta = 0^\circ$ to $\theta = \theta^*$.

- Derive the equations of motion of the system.
- Choose a P-controller of the form $\tau = k_p(\theta^* - \theta)$. What is the motion of the link?
- Does the link settle down at the desired angle θ^* ?

17.8 For the system described in Problem 17.7, choose a PD controller of the form $\tau = k_p(\theta^* - \theta) - k_d\dot{\theta}$ with $k_p > 0$ and $k_d > 0$.

- i. What are the governing equations of motion for this system under PD control?
- ii. What is the system response $\theta(t)$? Will the link settle down at the desired θ^* ? Will there be a steady state error?
- iii. What are the natural frequency ω_n and damping ζ for this controlled system? How does ω_n depend on the gain K_p ? Can you increase the speed of response of this system by changing K_p ?
- iv. What will happen to the response as you increase ζ , possibly by choosing larger K_d ?
- v. Plot the response of this system for $m = 1 \text{ Kg}$, $J = 1 \text{ m}$, $K_p = 3 \text{ Nm/rad}$, and $K_d = 1 \text{ Nm-s/rad}$.
- vi. Plot the response of this system for three different values of $K_d = 3, 6, 9 \text{ Nm-s/rad}$. How does the response change as you increase K_d ?
- vii. Plot the response of this system for $m = 1 \text{ Kg}$, $J = 1 \text{ m}$, $K_p = -3 \text{ Nm/rad}$, and $K_d = 1 \text{ Nm-s/rad}$. Does this system show a stable response?

INDEX

A

acceleration
 angular
 centrifugal
 centripetal
 chain rule for
 computational representation
 Coriolis component
 four-bar linkage
 general coincident points in analysis for
 graphical analysis for
 of coupler point
 piston
 polygon
 radial component of
 special cases of
 tangential component of
acceleration equations
 for four-bar linkage
 general
 for slider-crank
 special cases
acceleration image theorem
Ackermann steering linkage
actuation
 electric
 hydraulic
 pneumatic
actuators
 control electronics
 linear
 rotary
 selection of
ADAMS
adaptive suspension vehicle
addendum circle
addendum of a gear tooth

American Gear Manufacturer's Association (AGMA)
analog computer
analysis of cam follower-displacement functions
 cycloidal motion
 general polynomial motion
 harmonic motion
 parabolic motion
 uniform motion
analysis of planetary gear trains
 equations
 superposition
 tabular method
analysis techniques
analytix
angular acceleration
angular bevel gears
animation
annotation
approximate piston acceleration
approximate straight-line mechanisms
armature
Aronhold, S.H.
Artobolevsky, I.I.
assembly configurations
assembly modes
assembly order
autodesk inventor
automotive engine
automotive steering mechanisms
auxiliary point technique
axial joint

B

backhoe
balancing
 multi-cylinder machines
 reciprocating masses
 rotors, dynamic
 rotors, static
 slider-crank
ball bearing
Banala, S.K.
base circle of an involute
base member
base pitch
bearing
 ball bushing
 hydrodynamic
 hydrostatic
 roller on rail
 rolling element
 solid contact
Bennett linkage
Bernoulli, J.
bevel gears
 addendum angle
 back cone
 dedendum angle
 face cone
 pitch cone
 pitch diameter
 root cone
Tredgold's approximation
binary link
body-fixed coordinates
body reference frame
Bricard's exact straight-line linkage
brushes
bushing

C

cam contact

cam and follower

base circle

pitch curve

pitch points

pressure angle

prime circle

cam-follower systems

cylindrical cam

cylindrical-faced oscillating follower

cylindrical faced translating follower

face cam

frog cam

heart cam

knife-edged follower

offset flat-faced translating follower

radial flat-faced translating follower

roller follower

wedge cam

yoke cam

cam mechanisms

cam profile generation

analytical generation

graphical layout

oscillating cylindrical follower

oscillating flat-faced follower

radius of curvature

translating flat-faced follower

Cardan joint

center of mass

centrifugal acceleration

centrigugal force

centripetal component of acceleration

centrodes

chain drive

chain rule for positions, velocities and accelerations

change of branch
change gearbox
Chasles, M.
Chebyshev
Chebyshev's circle mechanism
Chebyshev's straight-line mechanism
 cognates
Chen, F.Y.
Chen, T.W.
Chironis, N.P.
Churchill, F.T.
circle diagram
circle mechanisms
circle of sliders
circle point
circular pitch
closed chain
closed-loop feedback control
closure equations
 for compound mechanisms
 displacement
 of four-bar linkages
 mechanisms with higher pairs
 of spatial mechanisms
closures
cognate linkages
coincidence (GCP)
collinear (GCP)
common normal, between joint axes
commutator
compact gear box
complex number method
compound joint
compressor
computational analysis of linkages
computational representations
 acceleration
 position

velocity
computer numerical control (CNC) machining
coordinate transformation operators
computer control of linkage motion
computer graphics
concatenation of transformations
conjugate cam
conjugate gear profile
connecting rod
crank pin
wrist pin
connectivity
conservation of energy
conservation of momentum
constant velocity couplings
geometric requirements
practical implementation
constant velocity ratio gears
constant-width cam
constraint analysis
constraint criterion
constraint manager
construction machinery
contact ratio
continuously rotatable joint
controller
proportional (P)
proportional derivative (PD)
proportional integral derivative (PID)
control valve, hydraulic
coordinates of gear tooth generated by a rack
coriolis component of acceleration
counterbalance mass
counterweight
couple
coupler
coupler-driven linkages
crank

crank-rocker
crank-rocker design (graphical)
crankshaft
crank-shaper mechanism
crossed helical gears
crown bevel gear
cycle rate
cycloid
cylindrical follower
cylindrical joint

D

damping ratio

Davidson, J.K.

dedendum circle

dedendum of a gear tooth

degrees of freedom

Delone's circle mechanism

delrin

Denavit, J.

dependent equations

derivative of a vector of constant magnitude

design of a six-link dwell mechanism using coupler curve

design of a six-link mechanism for a double oscillation

design of mechanisms

design of six-bar linkages using coupler curves

design, practical considerations

Dhande, S. G.

diametral pitch

diesel engine

digital coordination

digital to analog convertor

dimension lock (GCP)

Diophantine equation

direct kinematics problem

 direct position kinematics problem

 direct rate kinematics problem

 serial chain

displacement pole

double-crank

double-lever mechanism

double-rocker problem

Double-rocker design

drafting mode

drag-link

drawing a four-bar linkage (GCP)

drawing a slider-crank linkage (GCP)

drawing layer

driven dimension
driving dimension
dual complex numbers
dual quaternions
Dudley, D.W.
dwell mechanism
dynamic balance
dynamic equilibrium
equations
systems of rigid bodies
dynamic force analysis
dynamics

E

eccentric mass

Einstein, A.

electric linear actuator

electric motor

brushless

compound wound

externally excited

induction motor

non-commutated

series wound

servo-motor

shunt wound

speed control

stepping motor

electronically coordinated

elliptic trammel

encoder

absolute

incremental

end effector

equality (GCP)

equation (GCP)

equation for motion of body given motion variables of two points

equations of motion

equations for slider-crank linkage

equivalent linkages

equivalent masses

Euclid

Euler's equation

Evans straight-line linkage no. 1

Evans straight-line linkage no. 2

exact straight-line mechanisms

external forces

F

face gear
Farley, D.M.
Fattah, A.
feedback control
five-bar cognate Linkages
fixed automation system
fixed pivotff
fluctuating forces
fluid-power system
flywheels
follower bounce of cams
force
force system
in-plane
out-of-plane
FourbarAnalysis
four-bar cognate linkages
four-bar linkage
 acceleration analysis
 position analysis
 velocity analysis
four-bar mechanism
 with revolute and prismatic joints
four-revolute linkageff
four-stroke engine
Fourier series
frame
frame size of electric motor
free-body diagram
friction
 angle
 in cam contact
 drive
 in revolute joints
 in slider joints
front-end loader

function generation problem

fundamental law of gearing

G

GCP for Rigid-Body Guidance

four positions

three positions

three positions for a slider crank

gear equations

gear fouling

gear generating cutter

gear hobbing

gear interference and undercutting

gear loads

helical gears

spur gears

straight bevel gears

worm gears

gear manufacture

gear shaper cutter

gear standards

gear tooth thickness

gear train

compound

concentric

planetary

reversing mechanism

rotation direction

simple

general coincident points

in acceleration analysis

in velocity analysis

general cylinder

generalized coordinates

generally overconstrained linkage

generating curve

Geneva mechanisms

geometric constraint programmingff,

for finding instant centers

geometry of motion

general velocity and acceleration equations

gimbals

Goodman, T.P.

graphical acceleration analysis

graphical analysis

of a four-bar mechanism

of a slider-crank mechanism

graphical position analysis

graphical program

graphical velocity analysis

Grashof neutral linkage

Grashof type 1 linkage

Grashof type 2 linkage

Grashof's inequality

Grashof's rules

gravitational potential energy

gravity balancing of planar mechanisms

gravity balancing orthosis (GBO)

ground pivots

H

Hain, K.
Hall, A.
Hall effect sensor
hands-on machine design laboratory
Hanson, R.S.
harmonic components
harmonic fundamental
harmonic drive
flexspline
rigid circular spline
wave generator
hart
exact straight-line linkage
Hartenberg, R.S.
helical gear
axial pitch
contact ratio
formulas
helix angle
manufacturing
minimum tooth number
normal diametral pitch
normal pitch
normal plane
normal pressure angle
parallel shafts
transverse diametral pitch
transverse pitch
transverse plane
transverse pressure angle
velocity ratio and center distance
helical joint
herringbone gears
Hertzian stresses
higher pair
Hirschhorn, J.

Hoeken linkage
Holowenko, A.R.
homogeneous coordinates
homogeneous transformation
Hooke joint
horizontal (GCP)
hr_crankrocker.m
hr_slidercrank.m
Hrones and Nelson coupler-curve atlas
Hunt, K.H.
hybrid graphical-numerical methods
hydraulic actuator
hydraulic circuit
hydraulic cylinder
hydraulic jack
hydraulic power transmission
 displacement controlled system
 valve-controlled system
hydrodynamic lubrication
hydrostatic power transmission
hyperboloid of revolution
hypoid gears

I

idle degrees of freedom
indexing mechanisms
inertia matrix
inertia torque
inertial forces
inertial reference frame
initial setup for GCP
in-line engine
input rocker
input-output function
instant center
 of a curved slider
 of a general cam-pair contact
 of a prismatic joint
 at a revolute joint
 of a rolling contact pair
instant centers of velocity
internal gears
instant center of relative motion
instant centers of velocity
interference
internal combustion engine
inverse kinematics problem
inversion
 inverse position kinematics
 inverse rate kinematics problem
 serial chain
involute
involute function
involutometry
isosceles slider-crank exact straight-line mechanism

J

Jacobian matrix

jerk

joints

journal

K

Kennedy, A.B.W.

Kennedy-Aronhold theorem

KinDAP

kinematics

analysis

equivalence

joint

of mechanisms

synthesis

kinetic energy

kinetics

KINSYN

Krishnamoorthy, V.

Kutzbach criterion

L

lamina

layers

Leonardo da Vinci

level-luffing crane

limitations of GCP

LINCAGES

line color

line of action of a gear mesh

line type

link

linkage synthesisff

linkage

linkages that cannot be analyzed by classical means

Linkage synthesis

of a crank with chosen fixed pivots

of Crank-Rocker Linkages

of slider cranks and elliptic trammels

for three positions with selected moving pivots

for two positions of a moving lamina

Liu, C.H.

locally overconstrained linkage

location of instant center

loop

lower pair

lubricant

graphite

grease

molybdenum di-sulphide

oil

lubrication

boundary

hydrodynamic

hydrostatic

lumped mass approximation, balancing reciprocating machines

M

Mabie, H.H.

machine dynamics problem

machine

mass moment of inertia *see* [moment of inertia](#)

MATLAB

matrix transformations

mechanical transmission

mechanically coordinated

mechanism design

mechanism

mechanisms with revolute joints and fixed slides

members

merge (GCP)

Merritt, H.E.

midpoint (GCP)

Mitchiner, R.G.

miter gears

mobility criterion, uses of

mobility

module of a gear

moment

moment of inertia

motion generation

for parallel motion using coupler curves

motion limits

motion platform

motion program

motion, irregular

mount

moving pivot

moving reference frames

moving sliders

multi-plane balance *see* [dynamic balance](#)

N

natural frequency

Newton-Euler equations

Newton's laws of motion

second law

third law

no-load speed

nonlinear equation solver

nonlinear system

nonstandard gearing

Norden bomb sight

notational differences: vectors and complex numbers

numerical optimization

numerical solution

nylon

O

Ocvirk, F.W.
odd-fire engine
Oldham coupling
operating point
 stable
 unstable
order of the design positions
order problem
origin of the acceleration polygon
origin of the velocity polygon
ornithopter
orthogonal matrix
overconstrained linkage

P

pantograph
planar collinear
skew
parallelism(GCP)
parallelogram circle mechanism
parallelogram linkage
parametric design programs
particle kinetics
path generation problemff
path of contact
path-angle problem
Peaucellier's exact straight-line linkage
performance specification
perpendicularity (GCP)
physical model
Pieper, D.L.
ping-pong table mechanism
pin-in-a-slot joint
pin-in-a-slot linkage, inversions of
pinion
pitch cylinder
pitch point
Pitman arm
pitch circle of a gear
pitch diameter
planar joint
plane of motion
planetary gear systems
planetary gear nomenclature
internal ring gear
planet carrier
planet gears
sun gear
planar linkage, planar mechanism
points not on vector loops
pole

displacement
of electric motor
image
polycentric hinge
position lock (GCP)
potential energy
potentiometer
power amplifier
power train
precision position
pressure angle of a gear pair
preventive maintenance
prime mover
principal axes of inertia
prismatic joint
profile cam
 dwell
 returns
 rises
profile curve
projective geometry
prototyping kit
PTC Creo
pump

Q

quantization error

quaternary link

quick return mechanism

quick return shaper machine

R

rack
rack-and-pinion steering mechanism
radial component of acceleration
radius of gyration
rapson slide
rare earth metal
reactionless mechanisms
reciprocating mass balance
reciprocating mass
RECSYN
reference frames
Reinholtz, C.F.
resolver
Reuleaux, F.
revolute joint
right circular cylinder
rigid-body guidance
Roberts'
linkage
theorem
robotic mechanisms
actuated in parallel
manipulator
serial chains
rocker
rocker-amplitude problem
roller bearing
rolling and sliding contacts
rolling contact
rotating mass
rotating sliding joints
rotating-radius method
rotation about a fixed point
rotation equations of a spatial mechanism
rotor
Roth, B.

Rothbart, H.A.

RPRP mechanism

RRPP mechanism

run-away

S

SAM

Sandor and Freudenstein

Sarrus, P.F.

Sarrus' exact straight-line mechanism

scale factor

scaling of velocity polygons

Slater, N.

Scotch yoke

self-conjugate cam

sensor

ShakeAnalysis.m

shaking couple

shaking force

primary

secondary

shaking moment

primary

secondary

serial chain

Shigley, J.E.

single plane balancing see [static balancing](#)

singular position

sixbar.m

skeleton of a binary link

sketch mode

slider-crank

acceleration equations

solution of position equations when crank-driven

solution when coupler-driven

solution when slider-driven

velocity equations

slider-crank linkage

inversions of

motionlimits

slider-hinge link

sliding joint, jamming

Smith, M.R.
snapping feature
solenoid
solidedge
solid-modeling program
solid-state power switching
solidworks
solution branches
solution of closure equations for four-bar linkages
 coupler-driven
 crank-driven
spalling
spatial mechanism
closed-loop spatial mechanisms
 lower-pair joints in
 velocity and acceleration relationships
special cases for the velocity and acceleration equations
special mechanisms
 planar mechanisms
spherical joint
spherical linkage
 four-bar loop
 Grashof inequality
 position analysis
spiral bevel gears
spring-mass-damper system
spur gears
spur gear formulas
Srivastava, S.
stability of a system
stall
stall torque
statically determinate
statically indeterminate
static balance
 mechanisms
 rotors
static equilibrium

problems
static force analysis
statics
stator
steam engine
Stephenson linkage
Stephenson six-bar chain
Stewart-Gough Platform
 direct position problem
 inverse position problem
straight line mechanisms
strain energy
strain gage
stresses
structure
superscript notation
suspension mechanism, automotive
 roll center
surface grinding of cams
synthesis
 dimensional
 type
synthesis of cam motion programs
system of particles

T

tachometer

tangency (GCP)

tangential component of acceleration

teflon

ternary link

three-dimensional printing

three-two-one motion platform

time ratio

timing belt

topological interference

topology

torque-speed characteristic

Townsend, D.P.

transient response

translation equations

transmission angle

trial mass

triangle inequality

tribology

Troubleshooting Graphical Programs

turning block linkages

turning link

twist angle, between joint axes

two points are instantaneously coincident

two points fixed in a moving body

two points instantaneously coincident and in rolling contact

two-dimensional drawing mode

two-position double-rocker design

two-stroke engine

type 1 double-rocker

type 2 double-rocker

U

unbalance

uniform rectilinear translation

uniform rotation

unintended constraints

universal joint

automotive drive shaft

dual universal joints

velocity ratio fluctuation

unscaling

using GCP for

to find cognate linkages

pathsynthesis

to design a double dwell mechanism

V

variable displacement pump
vector loop
vector polygon
velocity
velocity and acceleration of coupler point
velocity equations
four-bar linkages
velocity image theorem
velocity polygon
velocity ratio
gears
V-engine
vertical (GCP)
vibration excitation
Vijayakar, S.
virtual linkage
virtual work
viscous resistance
visualization

W

walking toy

water turbine

WATT

Watt, James

Watt six-bar chain

Watt's approximate straight-line mechanism

wear

Whitney, D.E.

whole depth of gear tooth

WorkingModel

worm gears

double enveloping

nonenveloping

single enveloping

worm gear terminology

axial pitch

lead

pitch diameter

worm gear formulas

Wu, L.I.

Z

zero1 bevel gears

Zhonge, Y.

WILEY END USER LICENSE AGREEMENT

Go to www.wiley.com/go/eula to access Wiley's ebook EULA.